INTRODUCTION TO

Autogyros, Helicopters, and Other V/STOL Aircraft

Volume I:
OVERVIEW and AUTOGYROS

Franklin D. Harris

Franklin D. Harris

Piedmont, Oklahoma

National Aeronautics and
Space Administration
Ames Research Center
Moffett Field, California 94035-1000
May 2011

Prepared for Monterey Technology, Inc.
under NASA Contract NNA07BB01C
Subcontract 200703.NNA07BB01C
Task Order 01C-38
ISBN: 978-0-615-47845-6

Available from:

NASA Center for AeroSpace Information
7115 Standard Drive
Hanover, MD 21076-1320
(301) 621-0390

National Technical Information Service
5285 Port Royal Road
Springfield, VA 22161
(703) 487-4650

DEDICATION

To my parents, Lieutenant Colonel Glenn John Harris and Mary Catherine Van Buren Harris, and my mother-in-law, Mrs. Dorothy E. Bullis, shown after her first helicopter ride, November 8, 1982. Assistance by author.

"Helicopters remain a remarkable innovation to many. But if they have the opportunity to experience flight firsthand,

their reaction is one of total jubilation."

As quoted by my wife, Susan Bullis Harris,

May 16, 2004.

And to Sue. Whenever I asked her if she thought I would finish this book, she'd reply, with conservative New England reserve, "Eventually."

TABLE OF CONTENTS

PREFACE

This introduction to rotorcraft and their technology begins with a broad review of several types of rotorcraft. The evolution of these unique aircraft, from autogyros to helicopters to high-speed configurations, has spawned a major industry and an associated technology. The history of rotorcraft, beginning with very early concepts and modelhelicopters, has been well recorded in the popular literature. On the other hand, the evolutionof the technology resides in literally thousands of technical publications.

I have tried to bring together the popular history of rotorcraft evolution and the parallel, major technical steps made by its pioneers. Tying the engineering explanations andanalyses to configuration evolution provides the reader with two foundations. The firstfoundation is a more complete appreciation of what has been accomplished in

creating therotorcraft industry. The second foundation is a clear and simple introduction to (1) physicaland mechanical aspects, (2) basic nomenclature, (3) engineering symbols, and(4) fundamental equations . As you will see, the early pioneers encountered and solved a number of problems simply by cut-and-try methods. More often than not, the dynamics, aerodynamics, structural, and other associated analytical technologies actually followed successful demonstration that the problem had been understood and solved.

In bringing these two branches of history and technology together, I have found the occasional use of first-person pronouns to be a more natural and comfortable style to adopt.

ACKNOWLEDGMENTS

This three-volume book has come to be published because of four men who have given me not just their encouragement and personal support but all of the resources they had at their command. I owe an enormous debt of gratitude to Bill Warmbrodt, Chief of the Aeromechanics Branch at NASA Ames Research Center; Wayne Johnson of the Aeromechanics Branch; Barry Lakinsmith, Deputy Director of the U.S. Army Aeroflight- dynamics Directorate (AFDD) at Ames; and Mike Scully, Chief Design Engineer of AFDD . These men are friends, and they never hesitated to correct my work or gently chide me to hurry up. Most importantly, they convinced me that, given the scope of the book, three volumes were the only practical way to go.

Upon reading parts of my draft, Wayne and Mike made it very clear that I needed an exceptionally good editor. Thanks to Bill Warmbrodt, I was steered to Charlotte Barton at NASA Ames who put my work in the expert hands of Cathy Dow. Cathy showed me how technical writing should read.

I am particularly grateful to Kathy Ponce, a NASA Ames Librarian, who tracked down so many long-forgotten reports, and to Gerardo Nunez, one of Mike Scully's cohorts, who made copies of these reports for me.

As you will read, Wayne Johnson used his CAMRAD II analysis to add a modern comparison to several early rotorcraft analyses. He also contributed a great deal to correcting my discussions of unsteady aerodynamics and ground resonance.

There are a number of perhaps unwitting contributors who helped round out this book. A simple recording of their names is really insufficient thanks for their freely given thoughts and comments relative to many technical aspects and historical facts. My thanks go to:

Mahendra Bhagwat
Dick Carlson
Charles Crawford
Anubhav Datta
John Davis
Mark Dreier
Ron Gormont

Dewey Hodges
Jack Landgrebe
Gordon Leishman

Finally, this book only

Bernie Lindenbaum Todd
Quackenbush Jim McCroskey
Marilyn Smith Bob McKillip
Chee Tung Gerardo Nunez
Harold Ulisnick Susan O
Dan Wachpress Bob Ormiston
Wayne Wiesner Rick Peyran
Tom Wood Mark Potsdam
Hyeonsoo Yeo John Preston
Larry Young Ray Prouty

exists because of the pioneers who brought the rotorcraft

industry to life and the untold thousands who carried the early work forward. Because of them, I have had a most enjoyable career just trying to be a good engineer.

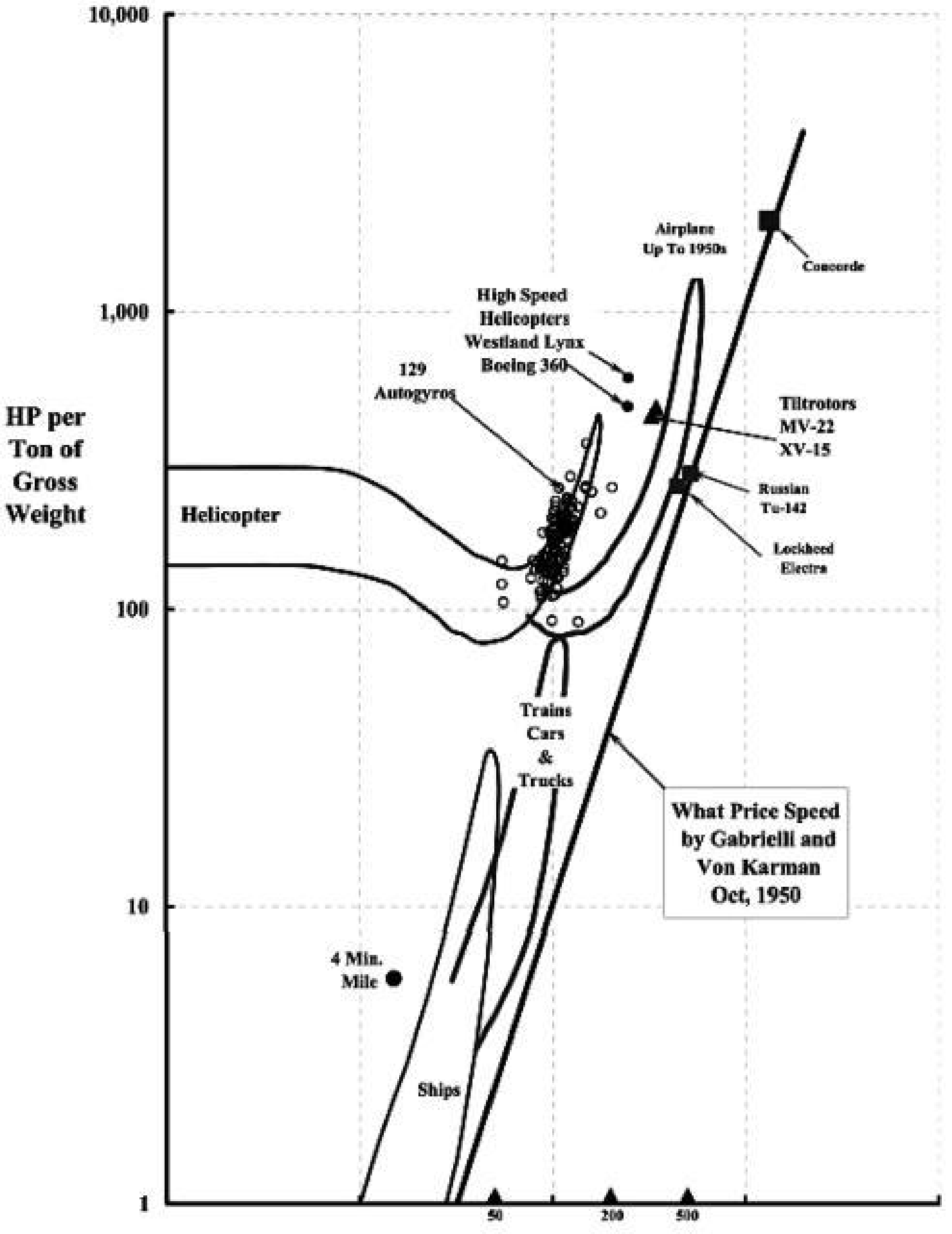
10,000
1,000
100
10
1
HP per Ton of Gross Weight
Helicopter
129 Autogyros
High Speed Helicopters
Westland Lynx
Boeing 360
Airplane Up To 1950s
Concorde
Tiltrotors
MV-22
XV-15
Russian Tu-142
Lockheed Electra
Trains Cars & Trucks
Ships
4 Min. Mile
What Price Speed by Gabrielli and Von Karman Oct, 1950
50
200
500

1 10 100 1,000 10,000

Speed (mph)

Rotorcraft enjoy a unique position in the transportation industry.

1 OVERVIEW

Rotorcraft, both low- and high-speed classes, enjoy a unique position in the field of transportation. Today, the helicopter is the most well-known example of a low-speed rotorcraft, but during the 1920s to the early 1940s the autogyro was the dominant rotorcraft in production. The autogyro, however, was not designed to hover. When the helicopter proved feasible in the late 1930s, further development of the autogyro was curtailed. Industry capitalized on the efficient hovering ability of the helicopter by incorporating the evolution of the gas turbine engine in the mid- 1950s . Together, these two features

resulted in the most favorable ratio of horsepower to gross weight of any vertical takeoff and landing aircraft in widespread use as the preface figure clearly shows [1].

If the helicopter has inherent shortcomings, it now appears to be in providing high forward speed and range commensurate with its hovering ability. This impression, created by comparisons such as the preface figure, shows the helicopter to be about 100 to 300 miles per hour slower than other aircraft in its power-to-weight-ratio class. On the horizon you can now see at least one high-speed rotorcraft, the tiltrotor. This configuration has demonstrated efficient hovering, the transition from helicopter to airplane flight, and efficient forward flight to 300 knots. It is this latest evolution that has been the goal of virtually every rotorcraft inventor since the industry began.

There are no less than four very clear milestones for an industry that began, perhaps you could say, as early as 1785 with a rudimentary helicopter model . There are, of course, any number of "firsts" in any industry that grows. For the rotorcraft industry, I have selected the four that seem to me to have the broadest and most far reaching effects.

The first milestone was reached by Juan de la Cierva with his successful demonstration of the autogyro. This first successful rotorcraft was developed through a series of trials and errors that began with an idea in 1919 [2] . After trying three distinct configurations, Cierva succeeded, as he relates in references [3-5] with his Type 4 autogyro shown in Fig. 1-1 . This rotorcraft "was ready to be used in real flight, and on 17th January 1923, it flew [piloted by Cavalry Lieutenant Alejandro Gomez Spencer] right

across the aerodrome at Getafe [Spain] at a height of several meters."

The Type 4 underwent considerable modifications and evolved into the Model C.6A . In October 1925, Cierva concluded 3 weeks of flight demonstrations of his Model C.6A at Farnborough, England, with a resounding success. This rudimentary rotorcraft required a total of 32 different experimental steps as Cierva struggled with the technical fundamentals of rotor system design, but with his strong engineering background, he was able to lay the theoretical foundation for the rotorcraft industry today.

1. OVERVIEW

Cierva, with help from co-author Don

Rose, wrote a more popular narrative of his work entitled *Wings of Tomorrow* [6], which was published in 1931. This book is fascinating from two points of view. First, it explains the more technical side of his aircraft in laymen terms, and second, it is clearly marketing the product. The capabilities to invent, develop, produce, and sell are not often found in one person. You can appreciate the contributions Cierva made even further by reading an up-to-date, detailed, and well-researched history such as *Cierva Autogiros—The Development of Rotary-Wing Flight* written by Peter Brooks [7].

Autogyro development flourished not only in England but also in the United States, principally around the Philadelphia, Pennsylvania area, which became a veritable hot bed of rotorcraft activity. In early 1929, Harold F. Pitcairn acquired the U.S. rights to the Cierva Autogiro and became president of

the Pitcairn-Cierva Autogiro Company of America, Inc. The Kellett Aircraft Corporation acquired a license from Pitcairn in 1931 and autogyro development really took off. Even with Cierva's untimely death on December 9, 1936, the success of the rotorcraft industry was ensured.

Fig. 1-1. On January 17, 1923, the Cierva Autogiro Type 4 laid the foundation for the rotorcraft industry today [3].

The second milestone I would suggest is the demonstration of a truly practical helicopter. E . H. Henrich Focke accomplished this milestone with his model F. 61. His side- by-side configuration is shown in Fig. 1-2. The F. 61 astounded the world with its stability, control, and performance just prior to the beginning of World War II. The pilot, Ewald Rohlfs, made the first flight of 28 seconds on June 26, 1936. Focke, in relating his story [8, 9] set the number-one design requirement to provide the "possibility of a forced landing in case of engine failure." He records [10] that "on 10th May 1937 he [E. Rohlfs] performed the very first auto-rotational landing, with engine off; a perfect 3-point, tail-down landing." Focke set five additional design criteria "in the order of their importance":

- Controllability and stability
- General safety in operation

- Simplicity of the piloting maneuvers •

Acceptable performance

- Reasonable servicing

These design criteria were just as important to Cierva and remain a top priority today.

Fig. 1-2. The Focke F. 61 helicopter

astounded the world in June 1936 and ushered in
the first growth step of the industry [9].

1. OVERVIEW

One statement Focke makes in giving the Fifth Cierva Memorial Lecture [10] is particularly interesting. He writes that

"The licence agreement with Cierva did not give the author's firm the right to theoretical information, so that a copy of Cierva's *Engineering Theory of the Autogiro* was not made available to my company. It was asserted by some that to make a helicopter it was necessary only to modify slightly an Autogiro. In reality, with the help of the Reports and Memoranda of Glauert and Lock it was necessary to reconstruct again all the technical knowledge concerning the blades, the rotor-head, the controls, and further, during 1932 to 1936, to make special application of all this knowledge to the helicopter."

The copy of Cierva's *Engineering Theory of the Autogiro* [11] that Focke refers to does not appear to have been widely circulated. However, the two notebooks were edited by Dr. James A. J. Bennett, and a copy came into the hands of Dr. Richard Carlson in the mid-1970s. Dr. Carlson made three copies, forwarded one to the American Helicopter Society, and gave me one . The engineering theory is in one volume and the *Theory of Stresses on Autogiro Rotor Blades* [12] is in the second volume . Even a quick review of Cierva's notes shows just how advanced his engineering analysis was as he developed his Autogiro.[1]

Focke also refers to the Reports and Memoranda of Glauert's first study [13] published in November 1926, which was followed quickly by Lock's report [14] published in March 1927 . Together, these

reports set the formative standards for technical work that exist even to this day. The R&Ms were, and still are, published by the Aeronautical Research Committee of Great Britain. These early theoretical reports, along with the extensive licensing arrangements that Cierva entered into, spread autogyro technology around the world.

The Henrich Focke helicopter development program was accompanied by "more than 2,000 wind tunnel measurements," testing of "a free flight flying model with a small engine of 0.7 hp and an all-up weight of 9 pounds," and lengthy whirl stand testing on a special ground test rig. "A 50-hours-of-endurance test was made, and after disassembly, inspection, and reassembly, 10 more hours were run." Focke thus added to the theoretical foundation. Just as importantly, he set the precedent for what constitutes a satisfactory supporting test program for

rotorcraft development within the industry. He seems to offhandedly pass all this work off (in his Cierva Lecture) with the thought that: "By and by, the whole theoretical foundation of the behaviour of the rotor was established."

The 2,100-pound-gross-weight F. 61 went on to establish record levels of performance on June 26th and 27th of 1937. Test pilot Ewald Rohlfs demonstrated a 62-mile flight at an average speed of 77 miles per hour. He took the rotorcraft to 7,800 feet, which was some 7,300 feet above the previous record. As you will read later, the German government placed production orders for the follow-on design, the much larger Model Fa 223 with a takeoff gross weight over 8,000 pounds.

[1] Peter Brooks [7] states in note 2, pg. 357, that the word Autogiro was a Cierva Company trademark, to be spelled with a capital A and with the "i." He further says the generic term is autogyro, spelled with a lowercase "a" and a "y." Others have noted that autogiro is Spanish for autogyro in some dictionaries.

1. OVERVIEW

The history of the helicopter has been told (and retold) many times with new and marvelous stories still coming to light. A history I found particularly satisfying was published in 1982 by Jean Boulet in his *History of the Helicopter as Told by its Pioneers* [15]. From this history, it becomes even clearer that the Focke success inspired companies in both England and the United States. In England, Gand J. Weir, Ltd carried on with two rotorcraft based on the Focke design. This step ultimately led to today's Westland Helicopters

Ltd. In the U.S.A., the Platt-LePage Aircraft Company was formed. This company won the first U.S . Army Air Corps helicopter design competition on April 15, 1940, with a configuration patterned after the Focke F. 61. The Army assigned this rotorcraft the model number XR-1. This step ultimately led to the Piasecki Helicopter Corporation[2] and to today's Helicopter Division of the Boeing Company, which produces the modern tandem rotor helicopter.

The third milestone I have selected was accomplished by Igor Sikorsky with his Model VS-300. He pioneered the single main rotor (with anti-torque and directional control provided by a tail rotor) configuration shown in Fig. 1-3. Sikorsky's interest in the helicopter is frequently traced back to his first unsuccessful attempts to build a coaxial helicopter in Russia in the early 1900s . However, it is the progressive development of the more modern,

single main rotor configuration over the period from late 1938 to the end of December 1941 that stands out. Sikorsky, supported by United Aircraft, achieved a 10-second first flight with the initial VS-300 on September 14, 1939. The rotorcraft was nearly uncontrollable because the pilot's (Igor Sikorsky himself) stick was about 60 degrees out of phase with the necessary rotor motion. This caused a normal fore and aft stick movement to produce more helicopter roll motion than the desired pitch motion. I found this initial effort by Sikorsky somewhat surprising in view of the theory and data available at the time, but, in retrospect, history does not show that lessons learned are always readily interchanged and heeded. This initial VS-300 crashed on December 9, 1939, and the direct control system of the main rotor with collective and cyclic pitch was abandoned for two years. During those two years, a number of small tail rotors were added to control pitch, roll, and yaw. As control was improved, these

additional tail rotors were selectively removed. Finally, on December 8, 1941, the prototype of what most people accept as the modern day, single-rotor helicopter was successfully flown. Sikorsky had returned to direct control of the main rotor (with correct phasing), and only one tail rotor, used for anti-torque and yaw control, was needed. Along the way, Sikorsky captured the world endurance record with a 1-hour, 32-minute (and 26. 1-second) hover flight. The VS-300 continued flight research until it was retired in October 1943. These efforts supported development of the XR-4 that was to become the first production helicopter obtained in quantity by the U.S. Army Air Corps. (The XR-2 and XR-3 were assigned to the Kellett Autogiro Corp.)

---

[2] In 1955, at the start of my senior year at Rensselear Polytechnic Institute, I interviewed for any "job" with the Piasecki Aircraft Corp. When I actually hired on (June 1956), the company had become the Vertol Aircraft Corporation, and I missed the opportunity to work for

(well, at least in the same building with) Frank Piasecki himself. That is my only regret about my career with an industry that has given me so much downright fun and to which I owe so much.

1. OVERVIEW

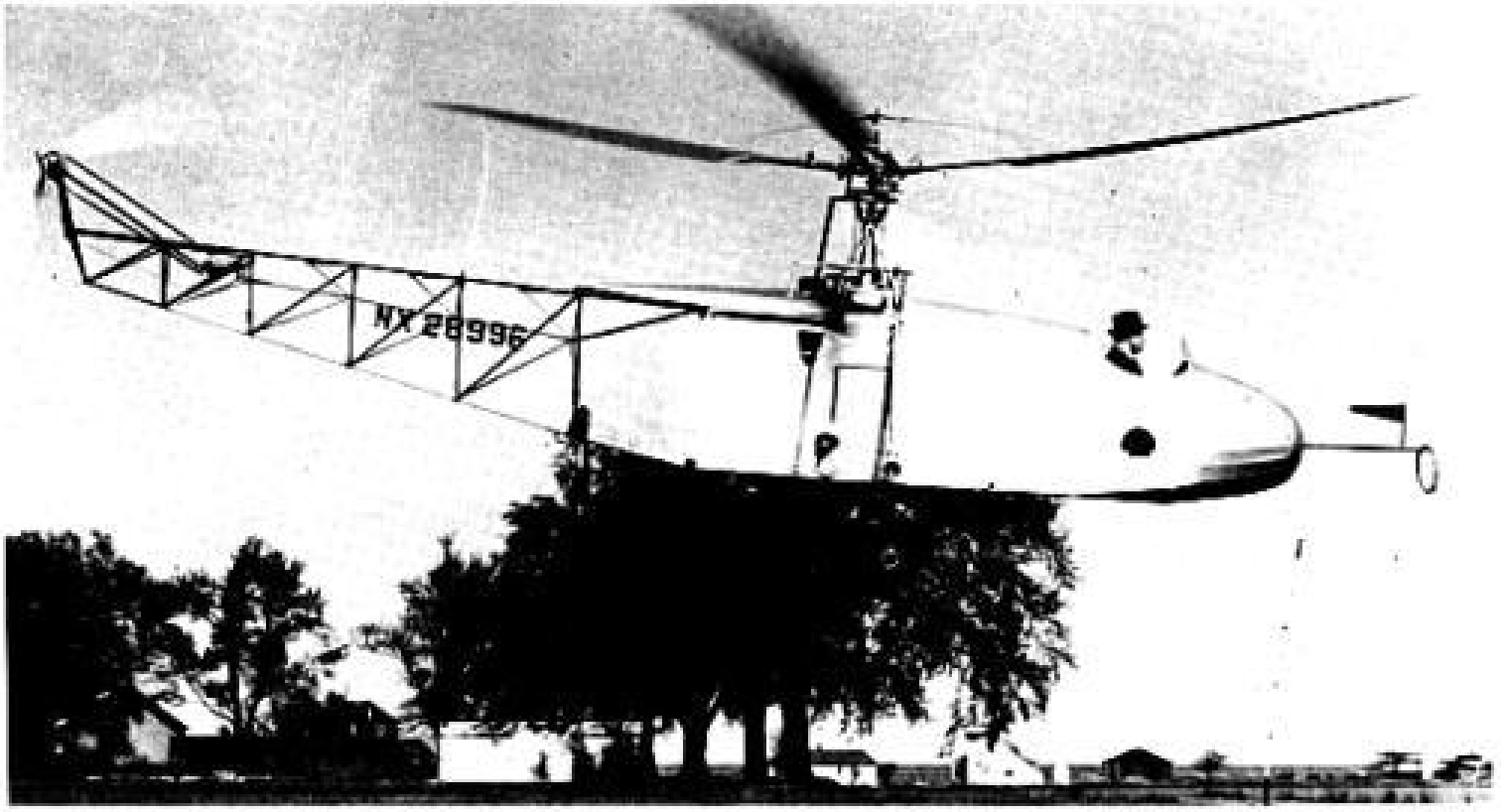

Fig. 1-3. The Sikorsky VS-300 established the modern helicopter, single main rotor configuration in December 1941 (photo from author's collection).

You can follow the development of the VS-300 in Sikorsky's own words. His reports of the 1941 and 1942 period [1 6-21] are fascinating. A nephew of Igor Sikorsky wrote a somewhat more technical overview of the development of the VS-300 [22] . In 1998 William Hunt wrote an excellent, very technically oriented story [23] . The book written by Sikorsky's chief test pilot, Charles Morris [24], and the one by Col. Franklin Gregory [25] bring the story home with the most important view—the user. You will also find excellent accounts of rotary wing history recorded by the Air Corps [26, 27].

In selecting just two helicopter-related milestones for this overview, I have not intended to dismiss the enormous efforts that came before or after. Rather, I have brought many of these accomplishments to light in Volume

II—Helicopters. The number of books available about the helicopter (its history, the many companies that have come and gone, and the several "family trees" of production helicopters today) will let you peruse the past as thoroughly as you like. I have always enjoyed each new view that has been published and continue to learn a great deal.

Before going on to discuss the fourth rotorcraft milestone I have selected, a little more must be said about the helicopter and its rotor system.

1. OVERVIEW

The helicopter rotor system is fundamental to its hovering efficiency. The rotor system is also the reason for the slower speed

of the helicopter relative to fixed-wing aircraft, as shown in the preface figure. As the primary lifting and propelling device, the rotor system permits installation of a minimum horsepower engine for hovering, but with power available set by hovering requirements, airplane-like speeds have yet to be commonly achieved. Finally, the rotor system blades and hub aerodynamic drag at high speed is, today, two to three times that of the equivalent fixed-wing airplane.

Helicopter development and rotor system technology is still in its infancy. Chronologically, airplane or fixed-wing development leads rotorcraft by 30 to 40 years. To illustrate this point, the principles of helicopter flight and control were convincingly demonstrated by 1940 in contrast to the accomplishments of the Wright brothers and others in the fixed-wing industry by 1910. As another example, the rotorcraft industry

adopted the retractable landing gear for helicopters in the late 1970s, but this feature was incorporated on airplanes in the mid-1930s. Higher cruising speed made the reduced drag worthwhile despite the extra weight and mechanical complications. On balance, however, the helicopter is well suited to a diverse group of tasks because of its broad range in operating speeds. However, the helicopter breakthrough that parallels the swept-wing and gas turbine engine combination of the airplane is still awaiting full-rate production. Since Cierva's Autogiro burst on the scene, there has been a continual search for a high-speed rotorcraft to compliment the helicopter.

This brings me to the fourth milestone I have selected for this introduction to rotorcraft. Today, the search for a configuration that combines both helicopter and airplane capabilities has yielded the tiltrotor. This vertical takeoff and landing

aircraft (VTOL) is illustrated in Fig. 1-4. The Bell–Boeing V-22 tiltrotor is in production for the U.S. Marines. The V-22 was preceded by the Bell XV-15, the first practical tiltrotor, which reached 300 knots at 16,000-feet altitude on June 17, 1980. While perhaps not as familiar to you as the helicopter, the tiltrotor has already demonstrated speeds above 300 knots at over 15,000-feet altitude, and with its large diameter rotors, the hovering efficiency of the tiltrotor approaches that of the helicopter.

This most recent step, as impressive as it is, is not the fourth milestone I have in mind. Milestone number four is, in fact, not a product. Rather it is the outgrowth from a technical meeting held in the United States at Philadelphia, Pennsylvania, on December 9, 1949. The occasion was the First Convertible Aircraft Congress. This meeting was sponsored by the Philadelphia Sections of the American Helicopter Society (a relatively new

group founded in 1943 by a small group of Sikorsky Aircraft employees) and the Institute of the Aeronautical Sciences (now the AIAA). The chairman for the 1-day meeting was E. Burke Wilford and proceedings were published [28]. The morning session had five papers and was chaired by Richard H. Prewitt, by then president of his own company. Laurence LePage chaired the afternoon session and six papers were presented. Over 200 pioneers attended this "Congress."[3]

[3] This first Convertible Aircraft Congress was followed by a second in Dec. 1952 [29], a third in Nov. 1955 [30], and a fourth in Dec. 1958 [31].

1. OVERVIEW

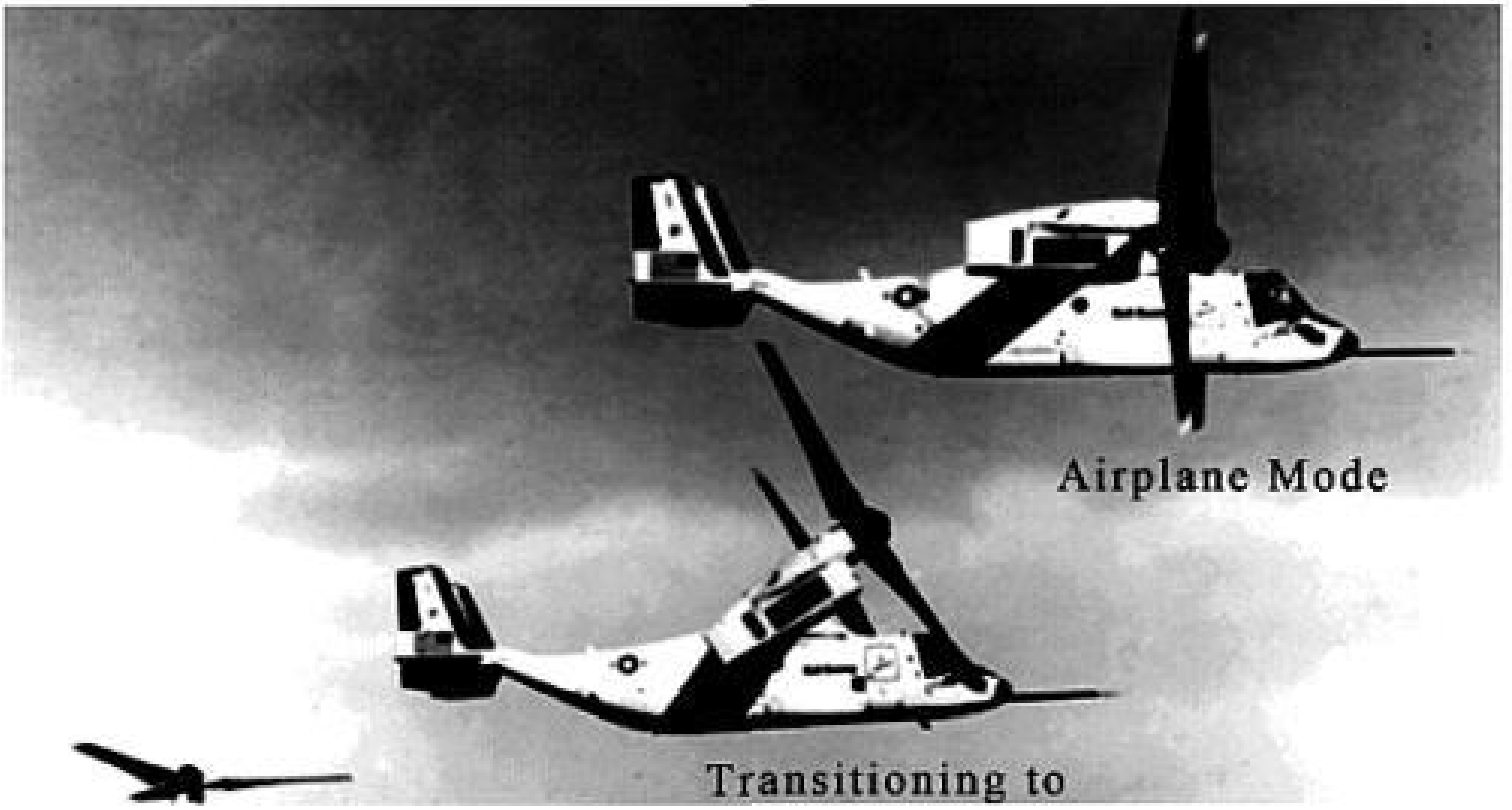

Fig. 1-4. The Bell–Boeing V-22 is the first

practical tiltrotor to reach production (photo courtesy of Bell Helicopter Textron).

At that time, late 1949, there was only one demonstrated suggestion of a convertible aircraft. This rotorcraft, the HV-2A[4] shown in Fig. 1-5, was championed by Gerard P. Herrick. The HV-2A was patterned after the autogyro, however the top "wing" could be started and stopped in flight. Its predecessor, the HV-1 that began fixed-wing flying on November 6, 193 1, was destroyed when a blade struck the vertical stabilizer during a rotor start-up from the fixed, biplane mode.

The HV-2A, piloted by George Townson, completed the first of about 100 "conversions" from fixed to rotary wing towards the end of July 1937 . A very interesting article [32] appeared in early 1991 that provides more detail of this first successful step towards a practical VTOL.

Gerard Herrick presented the first paper in the afternoon session of the First Convertible Aircraft Congress . He showed a movie of past efforts and then discussed his newest design, the HC-6D.

The foreword to the proceedings of the First Convertible Aircraft Congress is a proper conclusion to this discussion of milestone four. The words that appear over the signature of Chairman Wilford read as follows:

---

[4] The H stood for Herrick, of course, and the V stood for Vertoplane. All manner of names for a "convertible aircraft" can be found in the literature. We seem to have settled today on VTOL, short for Vertical Takeoff and Landing, to capture the capability still being sought.

Fig. 1-5. The Herrick, HV-2A stoppable rotor autogyro completed 100 conversions from fixed to rotating wing in the 1939–1940 period (photo from author's collection).

"Eleven years have passed since the First Rotary Wing Aircraft Congress at [The] Franklin Institute paved the way for the modern conception of the Helicopter. At that time Sikorsky had not flown his famous test ship, Arthur Young was working on his models in his barn at Paoli [Penn.], and Frank Piasecki was just finishing his course in aeronautical engineering under Dr. Klemin. Pitcairn, Kellett, Dr. Myers, Herrick and others had spent large sums of money and better than a decade of their lives to lay the foundation for Rotary Wing and Convertible Aircraft.

History often repeats. The proceedings of this [First Convertible Aircraft] Congress will be read and will attract many new minds and hearts to the final solution of useful flight for humanity. We want to thank the members of the general committee and the Philadelphia Section of the Institute of the Aeronautical Sciences for their help. We all hope that something of great use to the U.S.A. and the citizens of the world will come to pass.

The work is only begun. Let us all remember that saying of Dr. Johnson of London in the 18th century:

'The Power of Invention is conferred by nature upon the few, but the labor of working out the Science of an Invention is more than can be easily endured.' "

Shortly after this milestone meeting, the search for a VTOL aircraft began in earnest. This intense period started in the United States with a U.S . Army- and Air Force-sponsored research program that led to the McDonnell Aircraft Corp. XV-1 Convertiplane and the Bell Helicopter XV-3 tiltrotor of the mid-1950s.

The intense period seems destined to continue as successful high-speed rotorcraft such as the XV-15 and its larger derivative, the V-22 (currently in low-rate production), are demonstrated. Koch [33], Schneider [34], and more recently Rogers [35] report nearly 50 configurations that have been built and flown to date, and the search continues. How influential this meeting—this First Convertible Aircraft Congress—was in initiating the VTOL era is, of course, open to conjecture. To me, it was a milestone of the first order.

1. OVERVIEW

To summarize this overview, consider the progress made in this industry by just the sheer numbers of rotorcraft developed. Fig. 1-6 gives a thumbnail sketch of this progress. In its

growth from the early 1900s, the rotorcraft industry has seen basic technology evolve first with the creation, development, and production of nearly 500 autogyros . Many lessons learned from this relatively low-speed rotorcraft were then applied to achieve successful prototypes of modern helicopters in the late 1930s and early 1940s. The helicopter quickly replaced the autogyro and, by 1950, formed the production base for the industry that exists today. The number of helicopters produced is in the tens of thousands. So far, a seven-decade search has yielded the tiltrotor as the most promising configuration with which to expand the industry a third time.

This overview, concluding with Fig. 1-6, provides a background to discuss the rotorcraft industry and the associated evolution of technology that made the industry possible. Consider first Volume I—Autogyros; second, Volume II—Helicopters; and then other vertical

and short takeoff and landing (V/STOL) aircraft, Volume III.

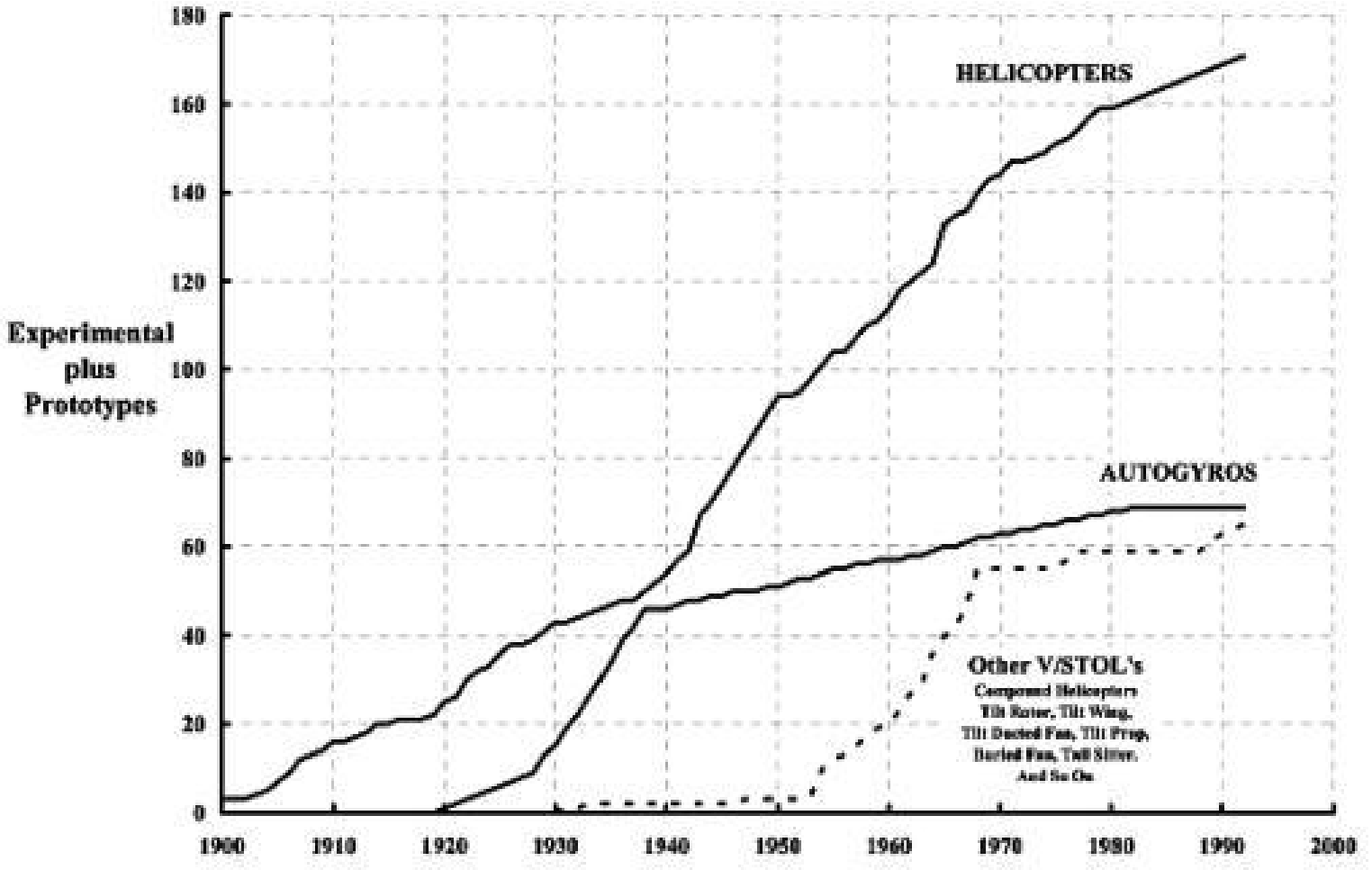

Fig. 1-6. V/STOL aircraft development has been continuous over the past nine decades.

2 AUTOGYROS

The autogyro was conceived by Juan de la Cierva [3], a Spaniard, in 1919, and his concept was patented in Spain, November 15, 1922 (No. 81,406) . The initial developments borrowed heavily from existing biplane aircraft in that the upper wing was replaced by a free-wheeling "horizontal airscrew." The fuselage, lower wing, engine, and forward thrusting propeller, etc., were more or less retained. Brooks [7] provides an excellent historical summary of Cierva's rotary wing flight development. Brooks is able to trace the concept of a gliding windmill (to coin a term) or—more precisely—an autorotating rotary wing back to the Middle Ages. Be that as it may, Cierva's jump from idea to formal demonstrations outside Spain took 5 years. His early work did not go unnoticed [36] . In October 1925 he concluded 3 weeks of flight

demonstrations and tests [37] of his Model C. 6A in Farnborough, England with a paper presented to the Royal Aeronautical Society [3] . He ended this lecture with the words: "Type 6 has been completely remodeled twice, which gives a total number of 32 distinct machines built and tested in order to arrive at the results demonstrated earlier in this week before many of those present tonight."

The door that Cierva opened up was perceived by members of the Society to be "one of the most wonderful inventions since the original invention of the aeroplane itself." As Fig. 1-6 shows, the number of experimental and developmental autogyros grew rapidly as the aeronautical community around the world became familiar with the technology breakthrough Cierva had made. By 1933 Cierva had developed the Model C.30, and this configuration was the production leader. Brooks [7] estimates that out of the roughly 500

autogyros made by 1945, about 180 were the Model C.30 illustrated in Fig. 2-1.

Fig. 2-1. Over 180 Model C.30 Cierva Autogiros were produced by 1945.

2. AUTOGYROS

Cierva described [3] the fundamental rotor system problem inherent to his concept as follows: "The chief difficulty was now the asymmetry of lift on the [rotary] wings, for

the wings rotating against and with the relative wind would have their average velocities through the air respectively increased or decreased, with a corresponding asymmetry of lift and a displacement of their resultant lift from the vertical, leading to a sideways movement and ending probably in a sideslip." He was obviously quite certain that "a lifting windmill" would turn "provided the axis [about which the blades rotated] was slightly inclined backwards from the vertical." It was the rolling moment caused by asymmetrical lift between the advancing blade side of the rotor disc and the retreating blade side of the disc that had to be reduced.

His first approach to overcoming this fundamental problem was to stack two rotors coaxially. The top rotor was set to turn clockwise, and the lower rotor was set to turn counterclockwise. After several taxi tests, this first solution proved unsatisfactory and

was abandoned because the lower rotor autorotated at two-thirds the RPM of the top rotor. Using "the blade element theory of airscrews," he designed his second configuration with a single rotor system "with the cantilever blades capable of being set at varying incidence by the pilot, who could thus displace the resultant lift to right or left at will." This second autogyro was "reconstructed nine times." But, after identifying "[in]sufficient torsional rigidity to withstand twist and consequent change of effective incidence [of the blades] caused by a shift of the [airfoil] centre of pressure," the second approach was abandoned. His third approach "had a lifting windmill of five rigid blades, [with] lateral [rolling moment] control being obtained by the differential effect of a large elevator divided into two parts, right and left. The fuselage was designed to take the resulting torsional couple." This third autogyro "was damaged and rebuilt four times in the course of these

experiments." This third approach was finally abandoned as well.

It was with his fourth design that Cierva finally achieved success by incorporating what is referred to today as a flapping hinge into his rotor system. Appendix A provides the patent Cierva obtained first in Spain on April 18, 1922, and then in the United Kingdom on June 30, 1924. The patent illustrates the early approaches and explains the flapping hinge with patent figure 4.

2.1 ROLLING MOMENT

The first, second, and third Cierva prototypes used rotor blades virtually cantilevered from the hub and with additional wire bracing. These aircraft were not successful

although the rotors did begin to windmill as forward speed was built up. Cierva does not say how many times the prototypes rolled over on takeoff, but one can imagine a number of near flights before the rotor blades began to create a show-stopping problem. By then he must have fully understood the inherent root cause of the rolling moment problem.

Understanding the rolling moment problem Cierva encountered, and how he solved it, is fundamental to understanding rotorcraft.

Cierva traced the rolling moment problem to the cantilevered "wings" which were rotating against, and with, the relative wind as illustrated in Fig. 2-2. In this figure, the rotor blades are shown at the instant of rotation when one blade is advancing with the aircraft while its pair is retreating. In rotorcraft terminology, rotation is measured

with an azimuth angle denoted by the Greek letter psi (ψ). The common reference for $\psi = 0$ is when the master blade is trailing downwind, which generally places the master blade over the rotorcraft fuselage and pointing toward the tail. In Fig. 2-2, the master blade is shown after a quarter of a revolution so that $\psi = 90$ degrees. The blades are rotating at a speed of (Ω) so the peripheral speed at the blade tip is $V_t = \Omega R$, the blade radius being denoted by (R). The tip of the advancing blade experiences the maximum relative velocity of $V_t + V$ while the tip of the retreating blade sees the least relative velocity of $V_t - V$. In fact, the relative velocity at any radial station (r), measured outwardly along the blade from the center of rotation and with the master blade at any azimuth point (ψ), is described by

$$(2.1) \quad V_{r,\psi} = \Omega r + V \sin \psi \, .$$

This is the most fundamental equation in rotor

system technology.

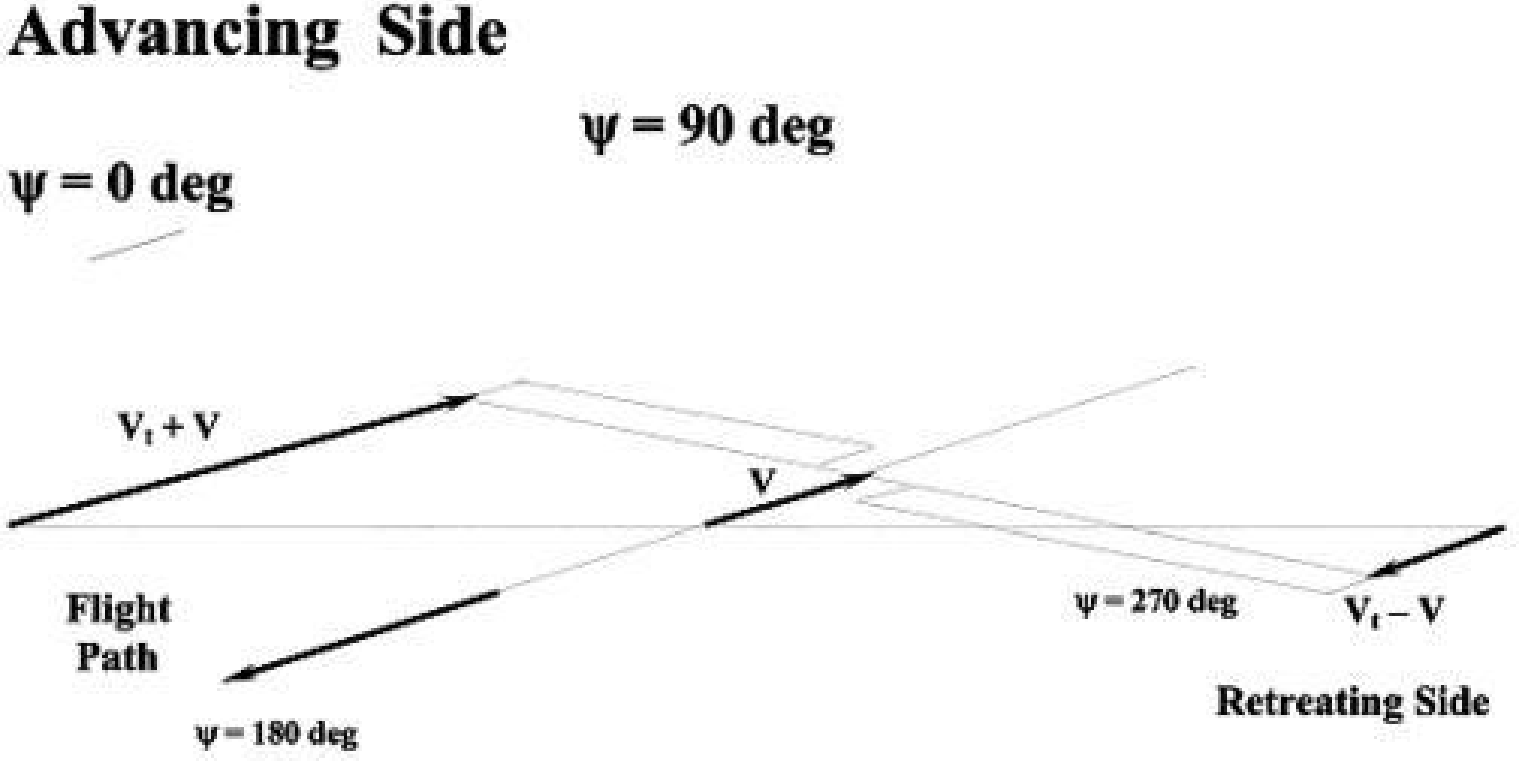

Fig. 2-2. Forward speed creates a lateral velocity asymmetry across the rotor disc.

2.1 ROLLING MOMENT

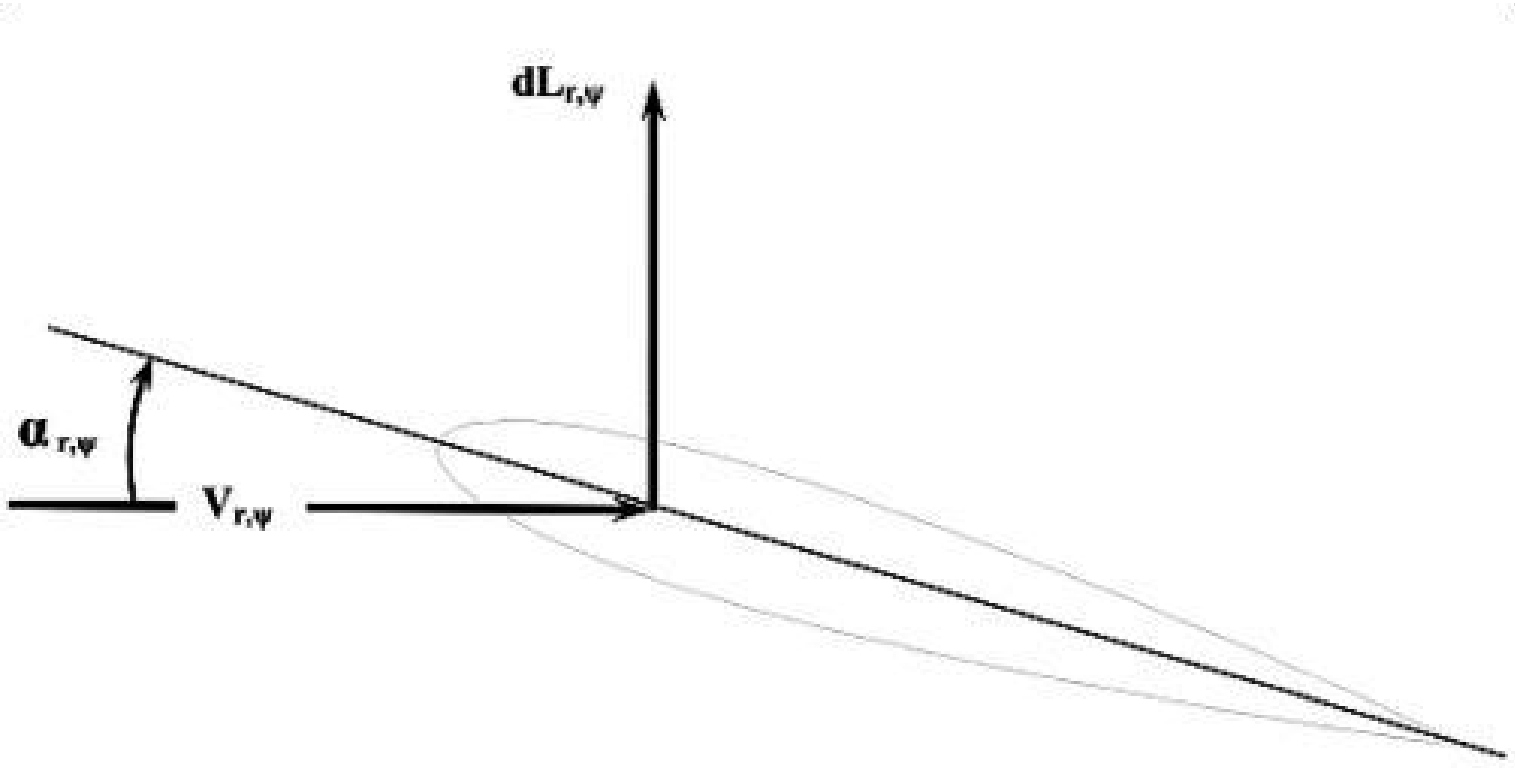

Fig. 2-3. Blade element aerodynamics.

Cierva related the radius and azimuth varying relative velocity to an asymmetry in lift using "the blade element theory of airscrews." The concept of a blade element is also fundamental to rotor technology. A blade element is a small-cross section of the blade located at any given blade radius station (r) as shown in Fig. 2-3 . A blade element has a planform area defined as chord times elemental radius (c dr). Its cross-sectional shape is that of an airfoil.

The blade element can carry an element of lift (dL) as shown in Fig. 2-3, and this elemental lift can be calculated with simple aerodynamics (see Appendix B) as

(2.2)

$$dL_{r,\psi} = \frac{1}{2}\rho(\Omega r + V\sin\psi)^2\left(a_\infty \alpha_{r,\psi}\right)(c\,dr).$$

In Eq. (2.2), ρ is the density of air (0.002378 slugs/ft^3 at sea level), $\alpha_{r,\psi}$ is the airfoil angle of attack, and a_∞ is the lift-curve slope of the airfoil (nominally 0.1 per degree of angle of attack).

Calculation of rotor lift for Cierva aircraft is rather simple and illustrates some additional basics of rotor system technology. The first step is to obtain the total blade lift when the blade is at any given azimuth angle

(ψ). Mathematically this is done by integrating over the blade radius assuming that (1) the blade element angle of attack is the geometric pitch angle (θ), and (2) both the blade chord and the geometric pitch are constant over the span. The results are:

$$L_\psi = \int_0^R \tfrac{1}{2}\rho(\Omega r + V\sin\psi)^2 \left(a_\infty \alpha_{r,\psi}\right)(c\,dr)$$

(2.3)

$$= \frac{\rho a_\infty cR\theta}{6}\left[(\Omega R)^2 + 3(\Omega R)V\sin\psi + 3V^2\sin^2\psi\right]$$

.

$$= \frac{\rho a_\infty cR\theta}{6}\left[(\Omega R)^2 + \frac{3}{2}V^2 + 3(\Omega R)V\sin\psi - \frac{3}{2}V^2\cos 2\psi\right]$$

2.1 ROLLING MOMENT

Now the total lift of one blade is seen to vary around the azimuth. It is the average or steady value of this azimuth-varying lift over one revolution that defines the force called rotor lift. The averaging mathematics is quite straight forward, as follows:

$$\text{Rotor Lift} \equiv b\left[\frac{1}{2\pi}\int_0^{2\pi} L_\psi d\psi\right]$$

(2.4)

$$= \frac{b}{2\pi}\int_0^{2\pi} \frac{\rho a_\infty cR\theta}{6}\left[(\Omega R)^2 + \frac{3}{2}V^2 + 3(\Omega R)V\sin\psi - \frac{3}{2}V^2\cos 2\psi\right]d\psi.$$

$$= b\frac{\rho a_\infty cR}{6}\left[(\Omega R)^2 + \frac{3}{2}V^2\right]\theta = b\frac{\rho a_\infty cRV_t^2}{6}\left[1 + \frac{3}{2}\left(\frac{V}{V_t}\right)^2\right]\theta$$

In Eq. (2.4), the lift from all blades (b) is

introduced to give the total rotor system capability. Remember that $V_t = \Omega R$.

Cierva was quite satisfied that his rotor would windmill up to some tip speed (V_t) once the aircraft gained forward speed (V) . But it was the sum of all the blade element lifts (dL)— acting at a moment arm (r sin ψ) about the longitudinal aircraft axis—that created a substantial rolling moment on early Cierva aircraft. In his early configurations, the blades were cantilevered from the hub and could, therefore, introduce an elemental rolling moment of

(2.5) Elemental Rolling Moment $\equiv dMR_{r,\psi} = -(r \sin \psi) dL_{r,\psi}$.

The same integrations that calculated rotor lift show immediately that the magnitude of the rolling moment about the longitudinal axis of the aircraft is

(2.6)

$$\text{Rolling Moment} = -b\frac{\rho a_\infty c R^2}{6}\left[(\Omega R)V\right]\theta = -b\frac{\rho a_\infty c R^2 V_t^2}{6}\left[\frac{V}{V_t}\right]\theta.$$

In Eqs. (2.5) and (2.6), the minus sign says that the rolling moment raises the "starboard wing" if the rotor is rotating counterclockwise when viewed from above.

As Cierva noted, the asymmetry in blade element velocity leads to "a corresponding asymmetry of lift and a displacement of their resultant lift from the vertical [centerline of rotation]." The amount of displacement of the lift from the shaft is obtained by substituting Eq. (2.4) into Eq. (2.6), which shows that

(2.7)

$$\text{Rolling Moment} = -\left[\frac{V/V_t}{1+\frac{3}{2}(V/V_t)^2}\right] R\,(\text{Rotor Lift}).$$

2.1 ROLLING MOMENT

Since V/V_t had to be about 0.2 for the rotor system to generate enough lift for takeoff, the effect was that the lift, equal to the gross weight of the aircraft, was, approximately, acting 0.2R to the starboard side of the aircraft. Even large ailerons would have a tough time counteracting a rolling moment of this magnitude at such low speed! Cierva's successful autogyros cruised at V/V_t from 0.4 to 0.6, so things might have gotten even worse had the aircraft taken off and the flight path speed increased.

It is very interesting to note that Cierva designed his second configuration with a single rotor system "with the cantilever blades capable of being set at varying incidence by the pilot, who could thus displace the resultant lift to right or left at will." Cierva appears to have introduced the capability to vary the blade pitch angle (θ) (or warp the blade twist) as the blade was turning. If this is the case, then the lift of the advancing blade could be reduced while the lift of the retreating blade could be increased, which could reduce the rolling moment to zero . A number of mechanisms could be designed which would vary blade pitch angle in a sinusoidal matter such that

$$\theta_{\psi} = \theta_{o} - B_{1C} \sin \psi \tag{2.8}$$

where θ_o is a mean or average blade pitch angle common to all blades and B_{1C} is the amplitude of the oscillating or cyclic pitch

angle. Cierva suggests that the pilot could control B_{1C} in some fashion. Both the preceding rotor lift and rolling moment expressions can be rederived assuming the varying blade pitch angle of Eq. (2.8) with the results that

(2.9)

$$\text{Rotor Lift} = b\frac{\rho a_\infty cRV_t^2}{6}\left\{\left[1+\frac{3}{2}\left(\frac{V}{V_t}\right)^2\right]\theta_o - \frac{3}{2}\frac{V}{V_t}B_{1C}\right\}$$

and

$$\text{(2.10)}\quad \text{Rolling Moment} = -b\frac{\rho a_\infty cR^2V_t^2}{6}\left\{\frac{V}{V_t}\theta_o - \frac{3}{8}\left[1+\frac{3}{2}\left(\frac{V}{V_t}\right)^2\right]B_{1C}\right\}.$$

Suppose now that that rolling moment must always be zero. Then Eq. (2.10) can be used to find what cyclic pitch angle (B_{1C}) must be applied to zero-out rolling moment. With this requirement, the pilot would be making a cyclic pitch control input of

(2.11) $$B_{1C} = \frac{\frac{8}{3}\frac{V}{V_t}\theta_o}{1+\frac{3}{2}\left(\frac{V}{V_t}\right)^2} \quad \text{for Rolling Moment} = 0.$$

Cierva rebuilt this second prototype nine times. Ultimately he identified "[in]sufficient torsional rigidity to withstand twist and consequent change of effective incidence [of the blades] caused by a shift of the [airfoil] centre of pressure" as a significant impediment. This observation suggests that blade element airfoil aerodynamics were twisting the torsionally limber blade in a very counterproductive way.

2.1 ROLLING MOMENT

The second prototype was abandoned and, with his third prototype, Cierva tried to control rolling moment from five rigid blades "by the differential effect of a large elevator

divided into two parts, right and left. The fuselage was designed to take the resulting torsional couple." This third autogyro "was damaged and rebuilt four times in the course of these experiments." This third approach was finally abandoned as well . The fourth Cierva prototype was successful because he stopped trying to overcome the powerful rolling moment of cantilevered rotor blades with weak, fixed-wing aerodynamics. Instead he inserted a hinge near the blade-root end so that all integrated blade loads were forced to act at a very small moment arm. This hinge was called a flapping hinge.

2.2 FLAPPING HINGE

The Cierva flapping hinge solution to asymmetrical rotor system lift and associated

rolling moment is shown in Fig. 2-4, which is reproduced from the late-1924 paper, *An Introduction to the Helicopter* [38] by Alexander Klemin. Professor Klemin's paper laid a strong foundation for rotorcraft and was later published as NACA TM 340. The Cierva flapping hinge approach centered the centrifugal force of the blade above the hinge. His objective for this vertical offset appears to ensure that the rotor would track in a plane nearly normal to the shaft. That is, the centrifugal force moment about the hinge would tend to droop the blade-tip down and this would oppose the tip-up moment created by blade lift. This design was applied to the Cierva C.4 Autogiro, shown in Fig. 2-5, which demonstrated success on January 17, 1923.

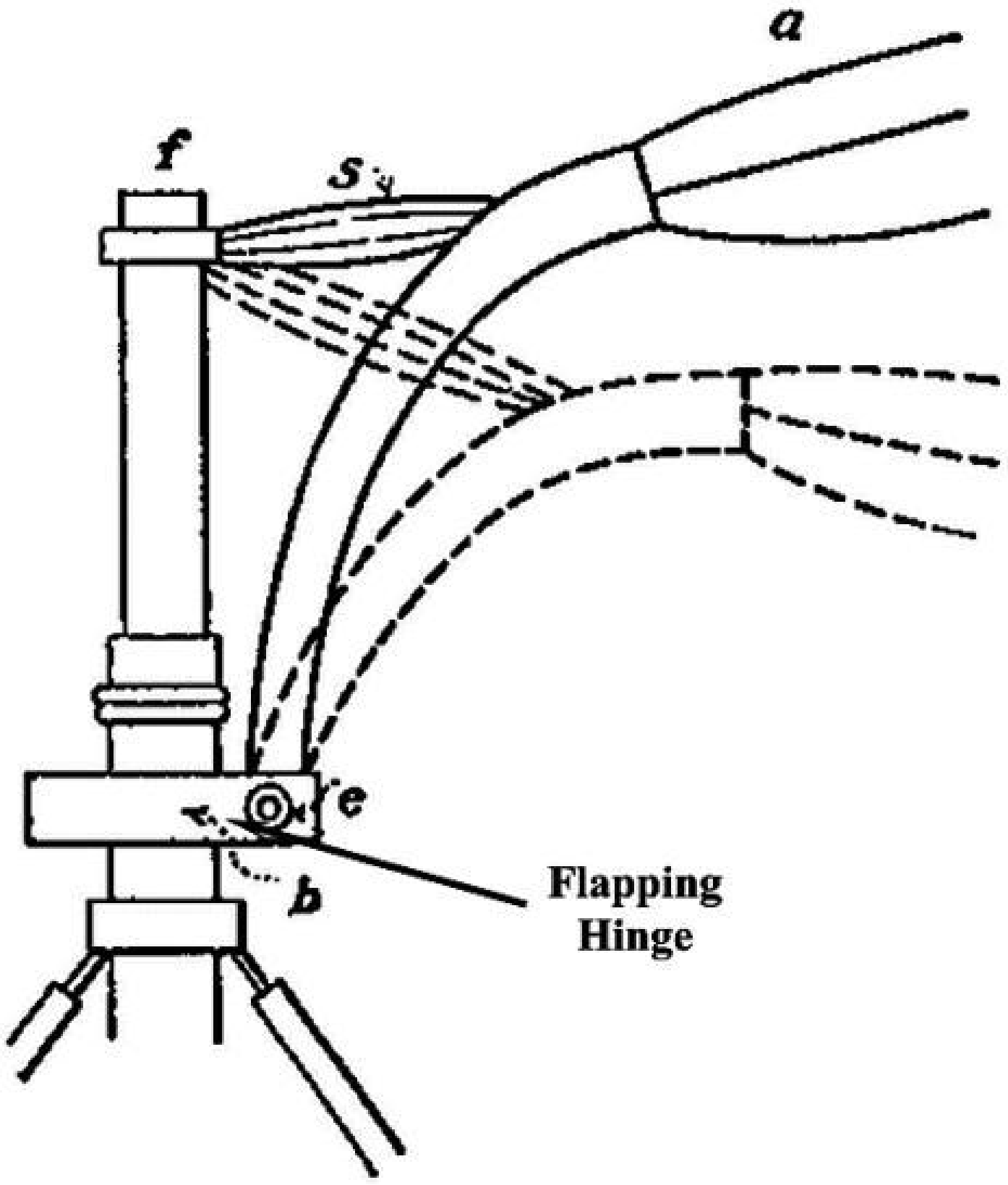

FIG. 6 PRINCIPLE OF LA CIERVA'S AUTOGIRO

(The wings are fixed to a piece *b*, by means of hinges *e*, so that they are free to move as shown in the diagram. The piece *b* turns freely about the axis *f*. *S* are elastic shock absorbers limiting the downward motion of the wings.)

Fig. 2-4. Cierva patented his flapping hinge in Spain in late 1922 (see Appendix A).

2.2 FLAPPING HINGE

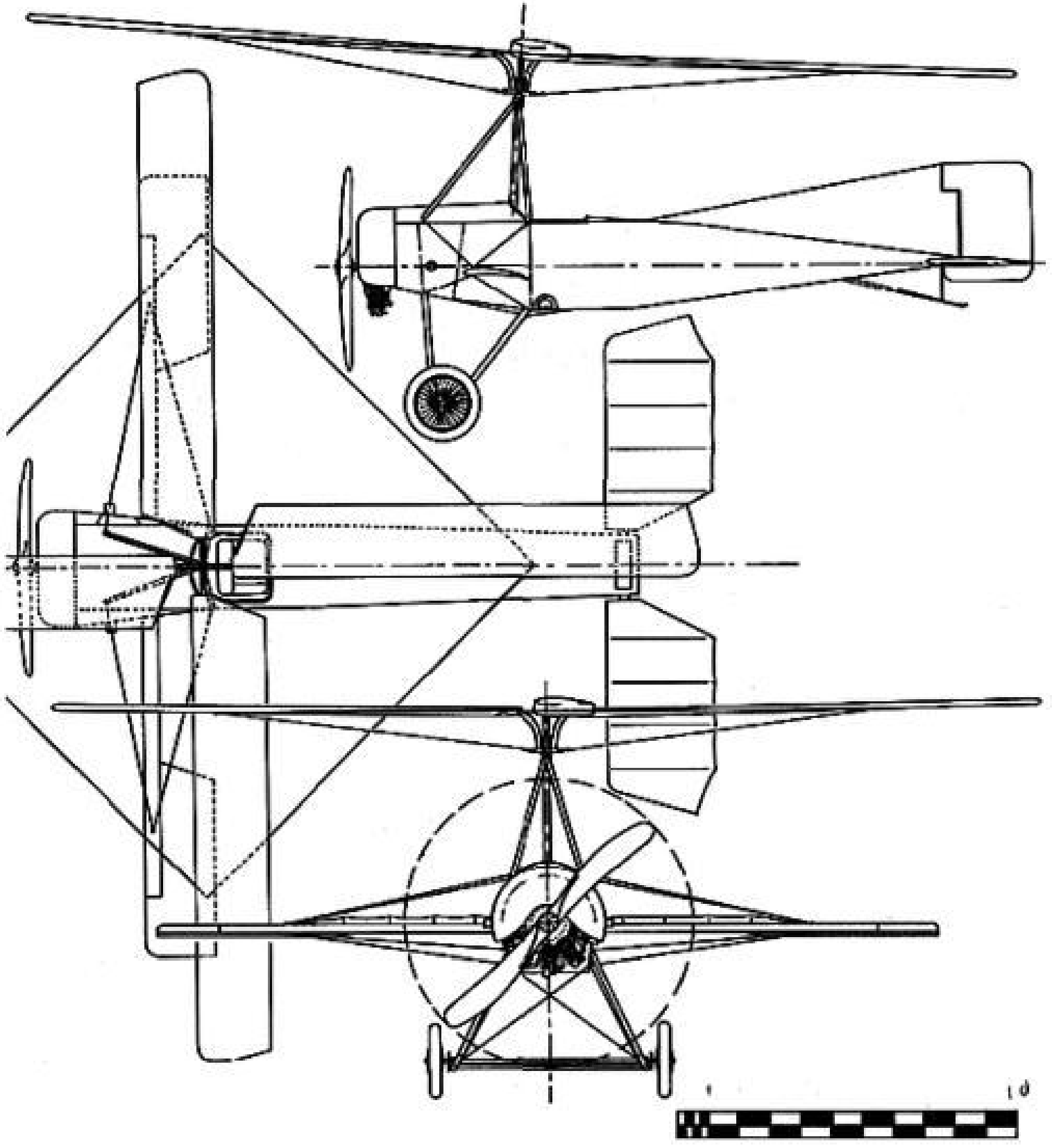

Fig. 2-5. The Cierva C.4—the first truly

successful rotorcraft [7].

(Gross weight 1,200 lbs, weight empty 925 lbs, diameter 26 ft 3 in., rotor speed 140 rpm, LeRone 9C 80 hp, speed range 35 to 55 mph.)

The success with the C.4 led to the C.5, a two seater with a 3-bladed, nearly 38-foot-diameter rotor, more than a 10-foot increase in diameter relative to the C.4. Unfortunately, a blade fatigue failure stopped development of the C.5. Cierva then designed the C.6, which had a 4-bladed rotor and diameter of just under 33 feet. The C.6, with additional development, was so successful that Cierva took the rotorcraft to England for a 3-week demonstration during October 1925 . Following the demonstration, and at the invitation of the Royal

Aeronautical Society, Cierva gave a lecture explaining much of what led up to the C.6. This lecture was later published in the Journal of the Royal Aeronautical Society [3].

As has been pointed out many times, the concept of a flapping hinge was first suggested by Charles Renard in 1904 and patented in 1908 by Louis Bréguet who then used the idea for his own helicopters.[5] An excellent photo of a vintage 1909, 3-bladed propeller with flapping hinges is provided by Rosen [41] on page 25 of his history of the propeller. Otto and Richard Baumgärtel also patented the use of hinges to reduce rotor system loads in Germany in March 1908. Their configuration, as applied to a propeller (Fig. 2-6), included a hinge that allowed inplane lead-lag motion as well as out-of-plane flapping motion. Attaching the blade with, in effect, a universal joint was a step that Cierva later took,

and I will discuss shortly. It is generally believed that Cierva developed his flapping hinge solution without knowledge of Renard or Baumgärtel patents.

To grasp the importance of the flapping hinge and rotorcraft technology at any level, Fig. 2-7 must be fully understood at the onset. The rotor blade shown in this figure (when the system is viewed from the top) is rotating counterclockwise at an angular velocity (Ω), which is normally expressed in radians per second. The blade, one of a set, is attached to the hub arm by the flapping hinge. All of the blade lift is concentrated at the hinge point. By keeping the hinge point as close to the center of rotation as structurally possible, the moment introduced from any given blade is reduced to the blade lift (L_b) times the hinge offset distance (r_β). The

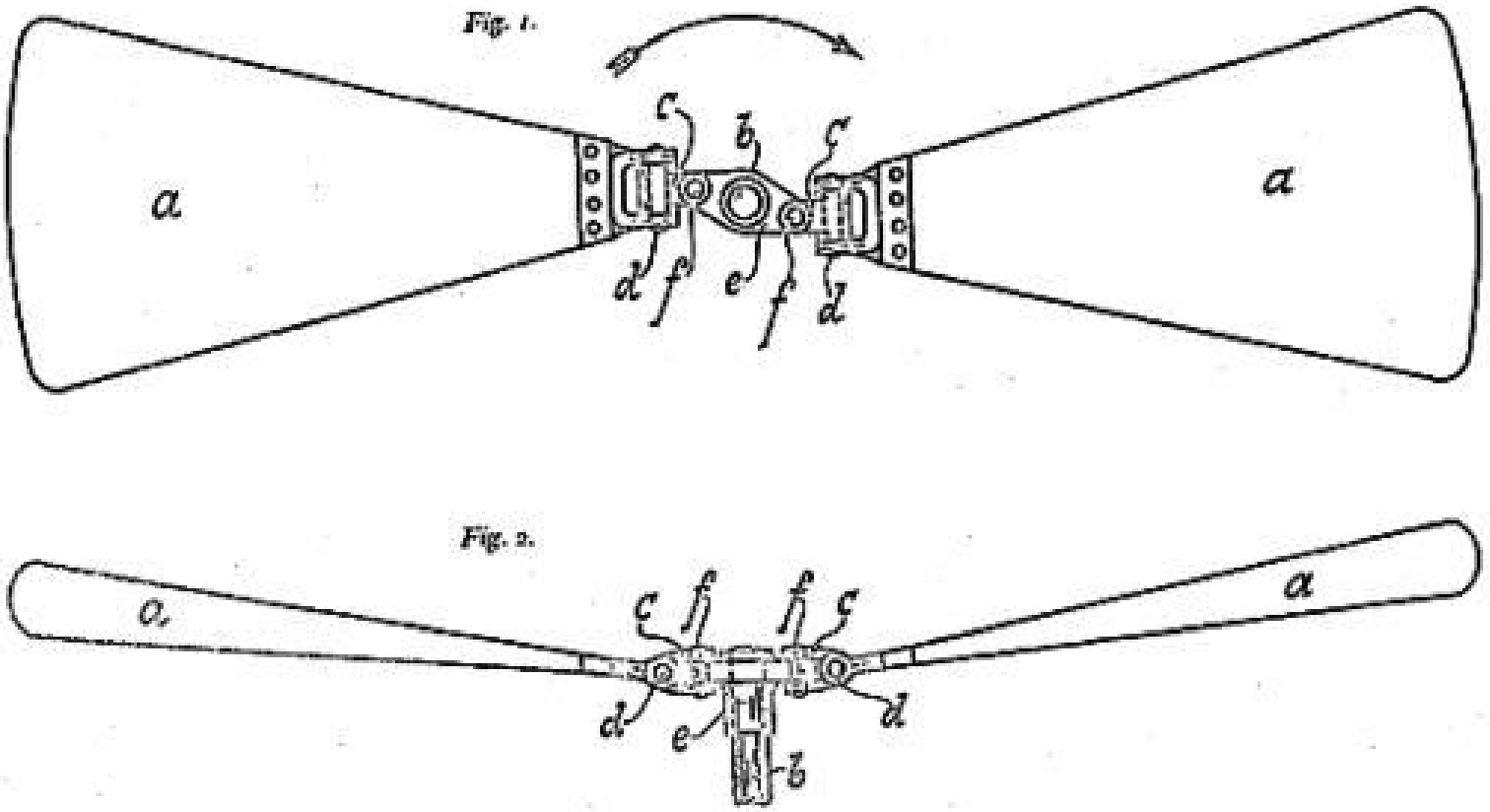

Fig. 2-6. The 1908 Baumgärtel patent for blade attachment with articulation.

---

[5] Bréguet's fame in the world of aeronautics is well known. He describes his helicopter work in references [39] and [40]. His 1935 coaxial helicopter was the world leader at the time Focke came forward with his F.61.

2.2 FLAPPING HINGE

early hinge assemblies were made up of ball bearings and a hinge pin, and were grease lubricated. Modern configurations remain similar. The attachment is designed primarily by centrifugal force, which varies between 10,000 and 100,000 pounds depending on the size of the rotorcraft.

The hub and shaft assembly shown in Fig. 2-7 is inclined slightly aft of vertical and gliding with a flight path velocity (V_{FP}). Thus, the hub and its arms trace out a plane that is at a slight positive angle of attack denoted as (α_{hp}). The up-flow through the rotor ($V_{FP} \sin \alpha_{hp}$) is the velocity component that acts on the blades to turn the rotor system and create lift. If the hub plane angle of attack were 90 degrees, the rotorcraft would be in vertical descent and might well be called a windmill . In fact, most autogyros rarely descended at more than 45-degrees angle of attack until the last 10

to 15 feet of altitude.

A standard rotor reference axis system has evolved over the years, which defines the blade position during rotation by the azimuth angle (ψ). The azimuth angle can be expressed in time as $\psi = \Omega t$ or in radians or degrees from some zero reference angle. The zero angle for blade azimuth is most commonly set by when the reference blade is trailing aft over the fuselage or is aligned downwind. In Fig. 2-7, the reference blade is shown having completed about three-quarters of a revolution so (ψ) is approximately 270 degrees. The second key reference angle is the blade incidence or pitch angle (θ). This angle defines the inclination of an airfoil to the hub plane. In Cierva's time the reference airfoil was taken at the two-thirds radius station (i.e., about two-thirds of the distance from the center of rotation to the tip of the blade). Since the airfoils in favor during the early 1920s had flat bottom surfaces,

attaching the blade to the hub arm at the "optimum" fixed-pitch angle of 2 or 3 degrees was a relatively simple matter.

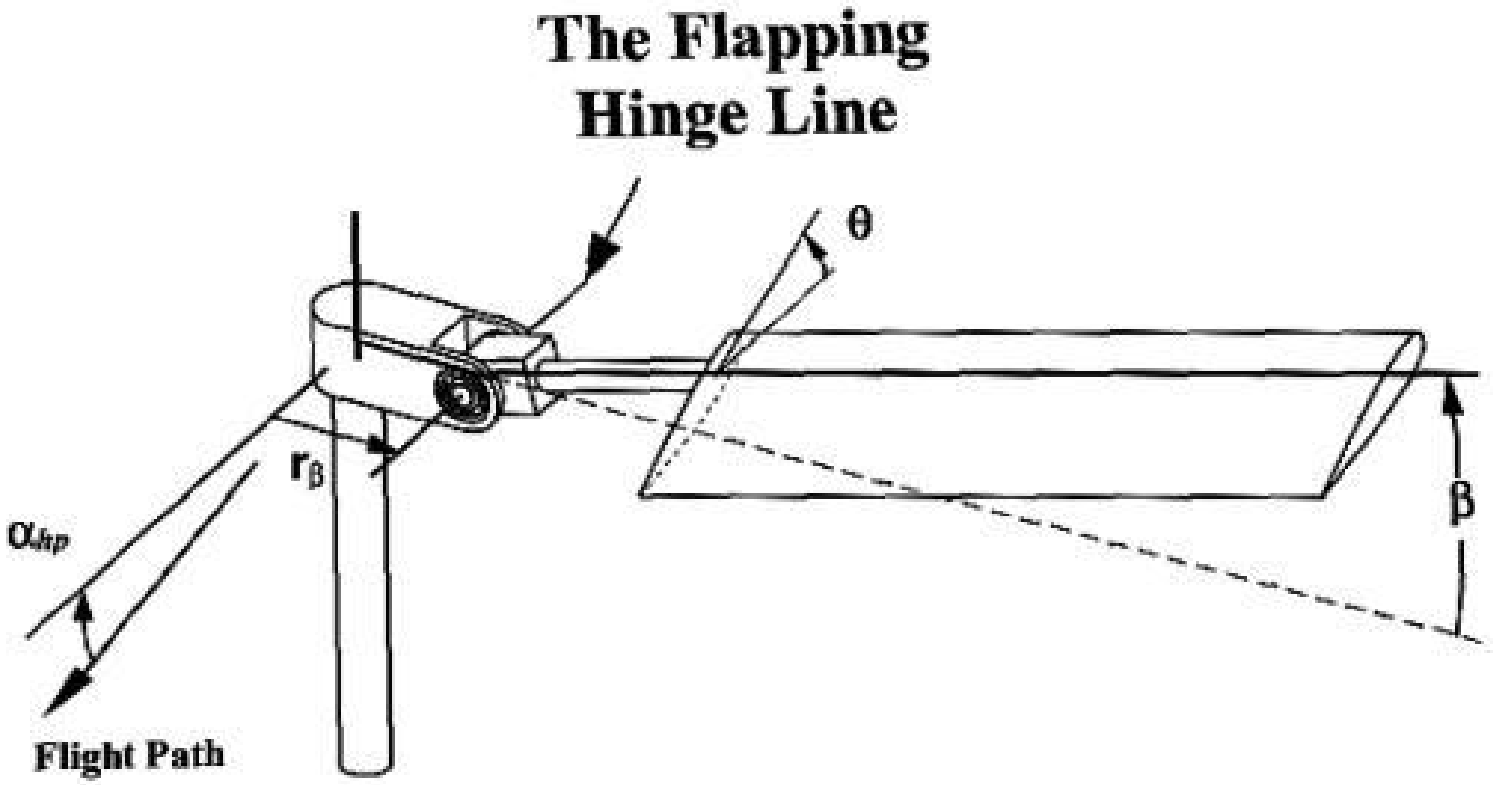

Fig. 2-7. The modern schematic of the flapping hinge (drawing by Rick Peyran).

The third key reference angle is the flapping angle (β). This angle is one measure of the rotation of the blade or deflection out of the plane of rotation. The flapping angle is not constant in the general case. The blade rises and falls in a well-behaved manner as it completes each revolution. Now consider the Cierva Model C.30 as an example. This autogyro had a 37-foot-diameter rotor that turned at about 190 to 210 rpm (say 20 rad/sec) when flying at a normal cruise speed of 85 to 90 mph (130 ft/sec). Thus, the blade tip had a peripheral or tip speed (V_t) on the order of $\Omega R = 20 \times 37/2 = 370$ ft/sec. One revolution was completed in roughly one-third of a second. When the blade advanced from $\psi = 0$ to $\psi = 90$ degrees, the apparent or resultant velocity (V_R) at the blade tip increased from $V_R = V_t = 370$ ft/sec at $\psi = 0$ degrees to a maximum of $V_R = V_t + V = 500$ ft/sec at $\psi = 90$ degrees. When the blade reached an upwind

azimuth of $\psi = 180$ degrees, the resultant tip velocity dropped back to $V_R = V_t = 370$ ft/sec, identical to the downwind or $\psi = 0$-degree azimuth position. Then, as the blade reached $\psi = 270$ degrees on the retreating portion of its revolution, the resultant velocity was reduced to $V_R = V_t - V = 240$ ft/sec. This resultant velocity pattern is, of course, periodic or harmonic in character and described simply by $V_R = V_t + V \sin \psi$ for the blade tip. The more general description for all radial distances (r) along the blade, including the tip where $r = R$, is conventionally written as

$$(2.1) \quad V_{r,\psi} = r\,\Omega + V \sin \psi$$

where the subscripts to V, (r) and (ψ), are used to reinforce the physical point that the resultant velocity varies with both radius station along the blade and blade azimuth (and thus with time since $\psi = \Omega\, t$).

The flapping motion of the blade (β_ψ) and the physics behind the motion are quite simple to understand if the overall requirement for rolling moment equilibrium is kept in mind, as Cierva did. With the freedom to flap, a blade has the inherent capability to self- correct its lift distribution due to the varying resultant blade element velocity ($V_{r,\psi}$) it sees in forward flight. The self-correcting velocity that does this is an angular flapping velocity, which takes the assumed form (actually an educated guess) of

$$(2.12) \quad d\beta/dt = \Omega \left(a_{1S} \sin\psi - \ b_{1S} \cos\psi \right).$$

The coefficient (a_{1S}) in Eq. (2. 12) is referred to as the first harmonic, longitudinal flapping coefficient. The coefficient (b_{1S}) is the first harmonic lateral flapping coefficient. In the first harmonic, the subscript 1 implies a Fourier series and refers the coefficients to

sin 1ψ or cos 1ψ as opposed to, say, sin 2ψ or some higher harmonic. The subscript S keys the motion to the shaft, hub plane, or the axis about which the blades rotate.

A linear velocity all along the blade is created by the flapping motion. This velocity—out of the rotational plane—varies linearly from blade root to tip and is simply

$$(2.13) \quad r\,d\beta/dt = r\left[\Omega\left(a_{1S}\sin\psi - b_{1S}\cos\psi\right)\right].$$

2.2 FLAPPING HINGE

$$dL_{R,90}$$

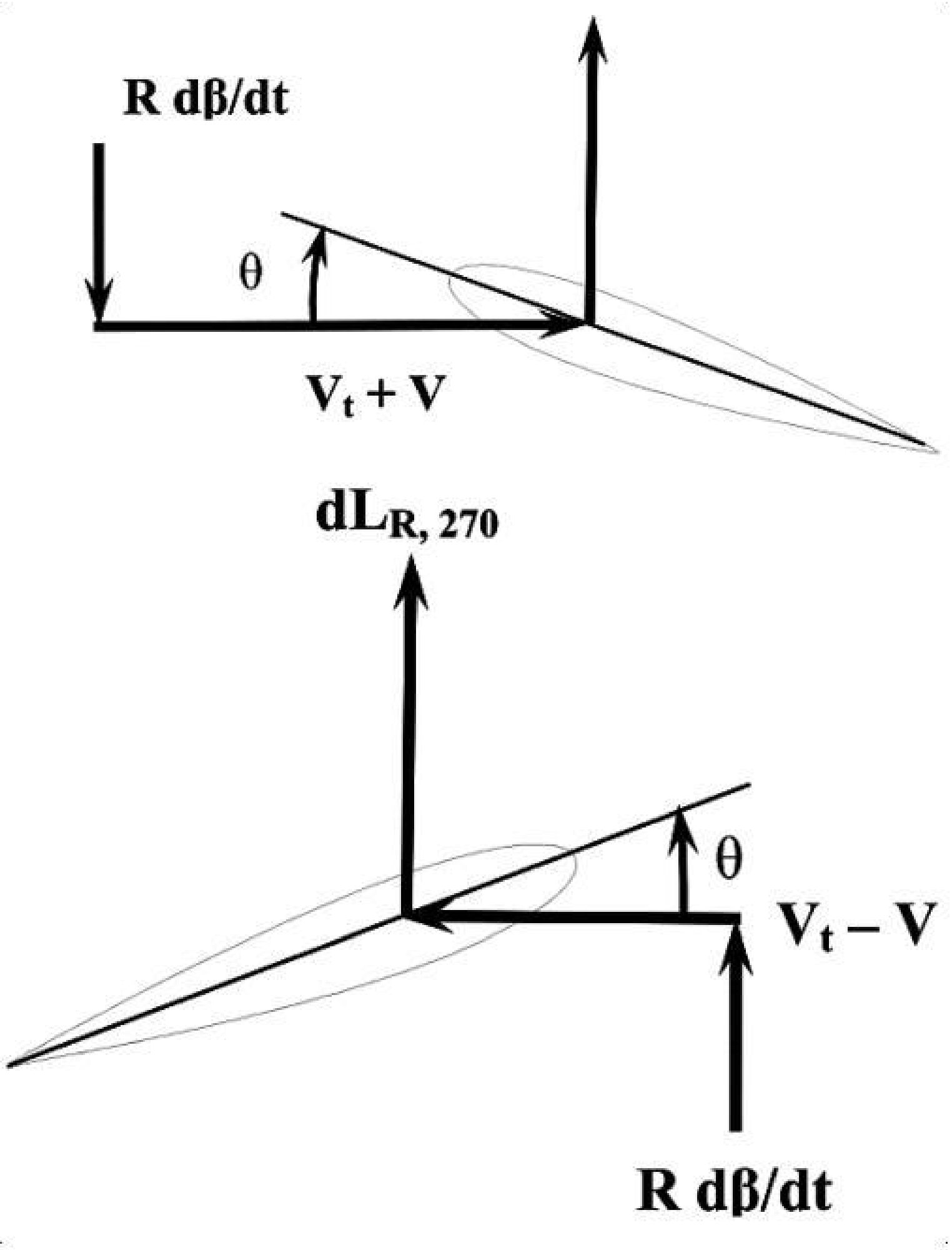
R dβ/dt
θ
$V_t + V$
$dL_{R,\,270}$
θ
$V_t - V$
R dβ/dt

Fig. 2-8. The blade element environment is quite different between 90- and 270-degree azimuths.

Since the resultant velocity is symmetrical when the blade is at $\psi = 0$ degrees and at $\psi = 180$ degrees (i.e., $V_{r,0} = V_{r,180} = r\,\Omega$), the lift distribution along the blade radius from root to tip is symmetrical between these two azimuths. In this fore and aft situation, the blade sees no cause to do any flapping. Therefore, the flapping velocity is zero (i.e., $d\beta/dt$ is zero and thus b_{1S} is zero to the first approximation). However, when the blade is at $\psi = 90$ and 270 degrees, the blade element sees two very different resultant velocity distributions and potentially two very different lift distributions . A simple illustration of this velocity distribution laterally across the rotor disc was shown in Fig.

2-2. The blade, with its flapping degree of freedom to create another velocity (r d β/dt), nearly equalizes the lift between advancing and retreating portions of the revolution. The near equalizing of lift between $\psi = 90$ and 270 degrees becomes clearer by looking at Fig. 2-8. The blade tip is shown here as an airfoil in cross-section. The velocities, angles, and lift forces acting on the blade tip at both azimuth positions are also shown.

The lift at a blade tip is found from the simplest aerodynamic theory for an airfoil. This basic, linear, aerodynamic theory states that an element of lift (dL) depends on an element of blade area, the dynamic pressure at the blade element, the angle of attack of the blade element, and the lift-curve slope of the airfoil. Thus,

$$(2.14) \quad dL_{R,\psi} = (c\ dr)\left(0.5\rho V_{R,\psi}^2\right)\left(a_\infty \alpha_{R,\psi}\right)$$

where (c) is the chord or local width of the blade, (dr) is the element of blade span, (ρ) is the density of air, ($V_{R,\psi}$) is the local velocity, and ($\alpha_{R,\psi}$) is the airfoil angle of attack. In linear aerodynamic theory, the airfoil lift coefficient is given as $C_l = a\,\alpha$ where the lift-curve slope is denoted by (a or a_∞), as discussed in Appendix B. From Fig. 2-8 you can see, on the advancing side of the disc where $\psi = 90$ degrees, that the blade-tip lift becomes

(2.15) $dL_{R,90} = 0.5\rho a_\infty (c\,dr) V_{R,90}^2 \alpha_{R,90} = K(V_t + V)^2 \alpha_{R,90}$ and, because $Rd\beta/dt = -R(\Omega a_{1S})$ in accordance with Eq. (2.13), it

follows that (2.16) $\alpha_{R,90} = \theta - \Omega R a_{1S}/(V_t + V)$.

Similarly, on the retreating side of the disc where $\psi = 270$ degrees, (2.17) $dL_{R,270} = K(V_t - V)^2 \alpha_{R,270}$

where

(2.18) $\alpha_{R,270} = \theta + \Omega R a_{1S}/(V_t - V)$.

The first order magnitude of the flapping velocity (a_{1S}) can easily be found by balancing advancing and retreating blade-tip lifts. This is the first approximation to balancing the rotor system in rolling moment. Thus, you let

(2.19) $dL_{R,90} = dL_{R,270}$

and therefore

(2.20) $K(V_t + V)^2\left[\theta - \Omega R a_{1S}/(V_t + V)\right]$

$= K(V_t - V)^2\left[\theta + \Omega R a_{1S}/(V_t - V)\right]$. With a

little algebra, you find that

(2.21) $a_{1S} \equiv 2\theta V/V_t$.

This approximation for (a_{1S}) can be substituted into Eq. (2.12) to give

(2.22) $d\beta/dt = \Omega\ a_{1S} \sin\psi = 2\,\Omega\ V\ \theta \sin\psi/V_t$.

Integrating the flapping angular velocity of Eq. (2.22) once with respect to time, while including the lateral flapping velocity term ($b_{1S} \cos\psi$), gives the flapping deflection more generally as

(2.23) $\beta_\psi = \text{constant} - a_{1S} \cos\psi - b_{1S} \sin\psi$ $= \beta_0 - a_{1S} \cos\psi - b_{1S} \sin\psi$. The integration constant, (β_0) in Eq. (2.23), is generally referred to as the blade coning angle. This angle is physically the steady deflected slope of the blade and represents the balance between total blade lift (L_b) and total blade centrifugal force (F_C). To the first order, (2.24) $\beta_0 = L_b/F_C$.

The lift of one blade (L_b) is, of course, nothing more then the total rotor lift divided by the number of blades (b). To a first approximation, blade lift would be the rotorcraft gross weight (W) divided by (b). The centrifugal force (F_C) is on the order of ten times the aircraft weight divided by the number of blades or roughly 10,000 to 100,000 pounds. The steady coning angle is generally about 4 to 6 degrees or 0.1 radian.

2.2 FLAPPING HINGE

The solution to the rolling moment problem that Cierva achieved with the flapping hinge is described by Eq. (2.23). Physically, the reasoning is quite simple.

Whenever the blade element dynamic pressure ($0.5\rho V_{r,\psi}^2$) is large, the blade flaps to lower the local blade element angle of attack ($\alpha_{r,\psi}$). This blade response, primarily in the first harmonic of blade motion (i.e., at sin ψ and out of the rotational plane), provides the dominate velocity to control blade element angle of attack and equalize blade element lift. While you may not see the velocity at work, you can definitely see the resulting flap angle displacement given by Eq. (2.23).

The flapping motion or slope given by Eq. (2.23) is seen more clearly by looking in at the rotor system from the $\psi = 270$-degree side view. As shown in Fig. 2-9, this view lets you think of the autorotating or gliding rotor as a lifting wing. The rotor shaft is inclined slightly aft of vertical to obtain autorotation as Cierva stated. A blade in the downwind position has a flap angle of ($\beta_0 - a_{1S}$) since $\psi = 0$ degrees. When the blade rotates to the upwind azimuth

of $\psi = 180$ degrees, the flap angle increases to a maximum of $(\beta_0 + a_{1S})$. The longitudinal line joining the blade tips in this side view defines the tip path plane (tpp). The angle between the tip path plane and the forward velocity is then defined as the tip-path-plane angle of attack (α_{tpp}).

With the introduction of the flapping hinge, Cierva reduced the steady hub moments that the rotor could apply to his autogyro. To a first approximation, the pitching moment (M_P), acting about the aircraft lateral axis, became simply

$$M_P = \frac{F_C \, r_\beta \, b}{2} a_{1S} . \tag{2.25}$$

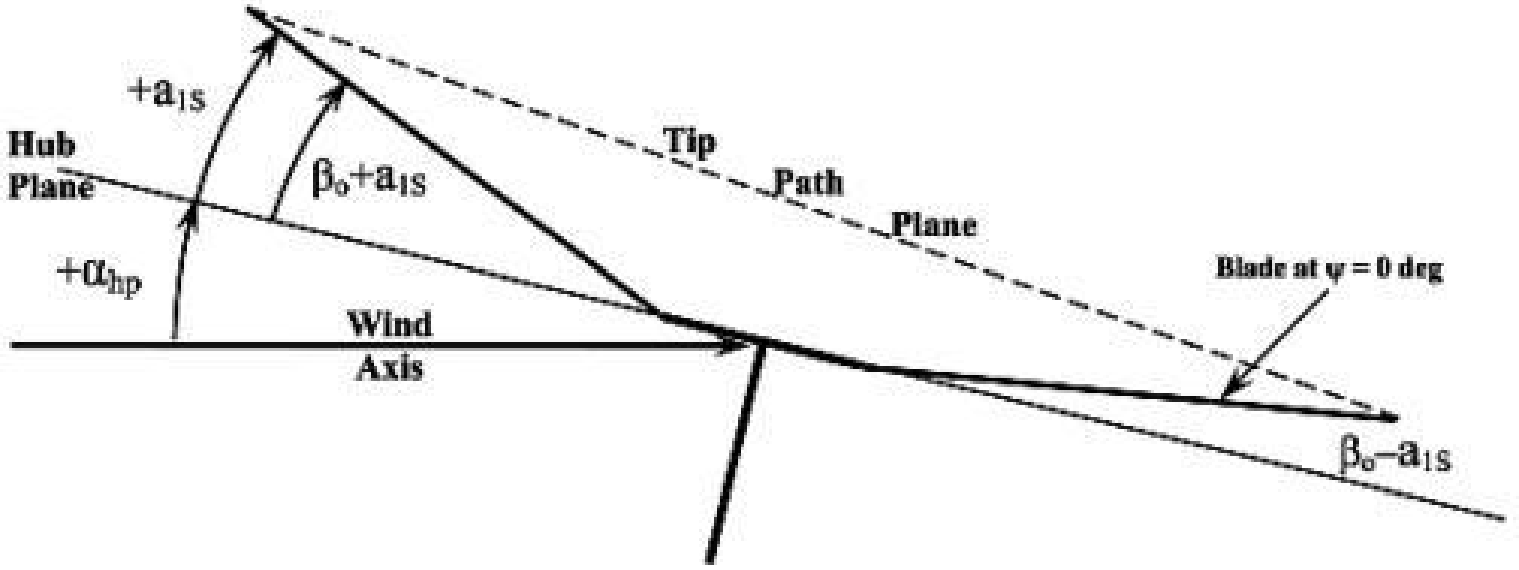

Fig. 2-9. The tip path plane (tpp) has an angle of attack much like a fixed wing.

Thus, $\alpha_{tpp} = \alpha_{hp} + a_{1S}$.

2.2 FLAPPING HINGE

This pitching moment was small enough that the normal-size horizontal elevator provided quite adequate longitudinal stability and control . Cierva did find, however, that a

residual rolling moment (M_R) still remained. This moment was caused by a small amount of lateral flapping (b_{1S}) and was of magnitude

$$(2.26) \quad M_R = \frac{F_C \, r_\beta \, b}{2} b_{1S} \, .$$

To balance this rolling moment, Cierva inclined the rotor shaft to one side. Early autogyros then flew with a slight list that varied from 1 to 3 degrees depending on flight condition. Small, auxiliary wings were also retained until a more direct control of the rotor hub plane was achieved.

It is worth taking time out for a moment to define two key nondimensional rotorcraft parameters that have stood the test of time. These two very important velocity ratios were created from Fig. 2-9 . The first is advance ratio defined as

$$(2.27)\quad \mu_{hp} \equiv \frac{V_{FP} \cos \alpha_{hp}}{V_t}.$$

This velocity ratio establishes the flow condition parallel to the hub plane or perpendicular to the rotor shaft. The second parameter is the inflow velocity ratio defined as

$$(2.28)\quad \lambda_{hp} \equiv \frac{V_{FP} \sin \alpha_{hp} - v_i}{V_t}.$$

This parameter measures the flow through the rotor and parallel to the shaft. Throughout technical literature you will find a mix in sign convention for the inflow ratio (λ_{hp}). About half of the investigators have chosen inflow down through the rotor as positive; the other half have chosen flow up as positive . Since the lifting rotor creates a wake just like a lifting fixed wing, there is an averaged induced velocity (v_i) that also must be accounted for in the first

order definition of the inflow ratio. The rotor wake for positive rotor lift induces a downward flow, which I chose as negative inflow. Both advance ratio and inflow ratios can be related to the tip path plane (tpp) as well. In that case you have

$$(2.29)\quad \mu_{ttp} \equiv \frac{V_{FP} \cos \alpha_{ttp}}{V_t} \quad \text{and}$$

$$\lambda_{ttp} \equiv \frac{V_{FP} \sin \alpha_{ttp} - v_i}{V_t}.$$

These two velocity ratios are in very common use today.[6] In some studies you will find the subscripts vary. For example, μ_S and λ_S may appear as a reference to the shaft axis system. The shaft axis system and the hub plane really are the same when you think about it.

[6]As you can see from Eq. (2.28), I have chosen α_{hp} to be positive when the rotor shaft is inclined aft in the sense of a conventional lifting wing. This quite arbitrary selection makes the component of flight path speed (V) parallel to the shaft, that is (V sin α_{hp}), positive for upflow.

2.2 FLAPPING HINGE

The Cierva Model C.6A was so well received in England that Cierva moved his activities there. With enormous help from James G. Weir, the Cierva Autogyro Company Ltd. was established on March 24, 1926, with Weir as chairman and Cierva as technical director. An order for one C.6A to be built by A.V. Roe & Co. Ltd. was received from the British Air Ministry, and Cierva ordered one additional rotorcraft for test flying and further demonstrations.

2.3 LEAD-LAG HINGE

With Frank Courtney [42] as the pilot, Model C.6A development continued, without catastrophic incident, until February 7, 1927. On that day, Cierva had to deal with a very serious metal fatigue failure when a rotor blade simply snapped off near the root on his Model C.6C . The aircraft fell to the ground from about 250 feet, and at around 1 5 feet above the ground another blade came off. The aircraft was destroyed, but Courtney escaped serious injury. The British Air Ministry immediately grounded their autogyro.

Solving the structural fatigue problem Cierva encountered was akin to finding out how many times you can bend and unbend a paper clip before it breaks. On the Model C.6C, the

blade was cycling back and forth in the plane of rotation. There was no hinge to accommodate this motion, which induced one cycle of bending for every revolution of the blade. Considering a rotor speed of about 1 90 rpm and perhaps 25 hours of flight time, this would mean that only 300,000 bending cycles had occurred before the fatigue failure. By comparison, rotorcraft industry design standards today demand at least 2,000 to 10,000 hours of safe life, which is more on the order of 10-million fatigue cycles.

A degree of freedom that allowed the blade to lead and lag in the plane of rotation was the design improvement that Cierva incorporated on his Model C.6C, and this led to the Model C.6D . This additional hinge, shown in Fig. 2-10, was initially referred to as a drag hinge but is called a lead-lag hinge or just a lag hinge today. The inplane blade

motion this hinge allows is defined by the angle (ξ). The lag hinge is centered about a vertical pin in contrast to the flapping hinge, which can be thought of as a horizontal pin joint. Together, the two hinges act very much like a universal joint or like the ball-and-socket shoulder-to-arm joint of a human. The lag hinge was placed just outboard of the flapping hinge on the Cierva Model C.6D at a distance from the centerline of rotation (and toward the blade tip) defined as (r_ξ). The lag hinge relieved the substantial inplane bending moments that were, in fact, created by the flapping motion. But remember, the rotor needed flapping in the first place to avoid rolling moment, and it was rolling moment that caused Cierva so much trouble with his first three prototypes. Fixing one problem while creating two new ones is not an uncommon occurrence in the development of rotorcraft.

Lead-lag motion occurs primarily at

once per revolution and, as for the flapping motion, can be described most conveniently by a Fourier series because the motion is harmonic. Physically, the cause of the lead-lag motion is quite easy to understand. Whenever the rotor blade flaps away from its steady coning angle position (β_o), each blade element moves slightly closer to (or further from) the centerline of rotation. To conserve angular momentum, the blade must accelerate (or decelerate) relative to the rotor shaft steady rotational speed (Ω). Thus, the flapping motion creates a Coriolis force on each element of the blade. The sum of the elemental forces leads to a moment about the lag hinge. The moment is reacted by both inertia and centrifugal force terms. As you will see later, this is a relatively

2.3 LEAD-LAG HINGE

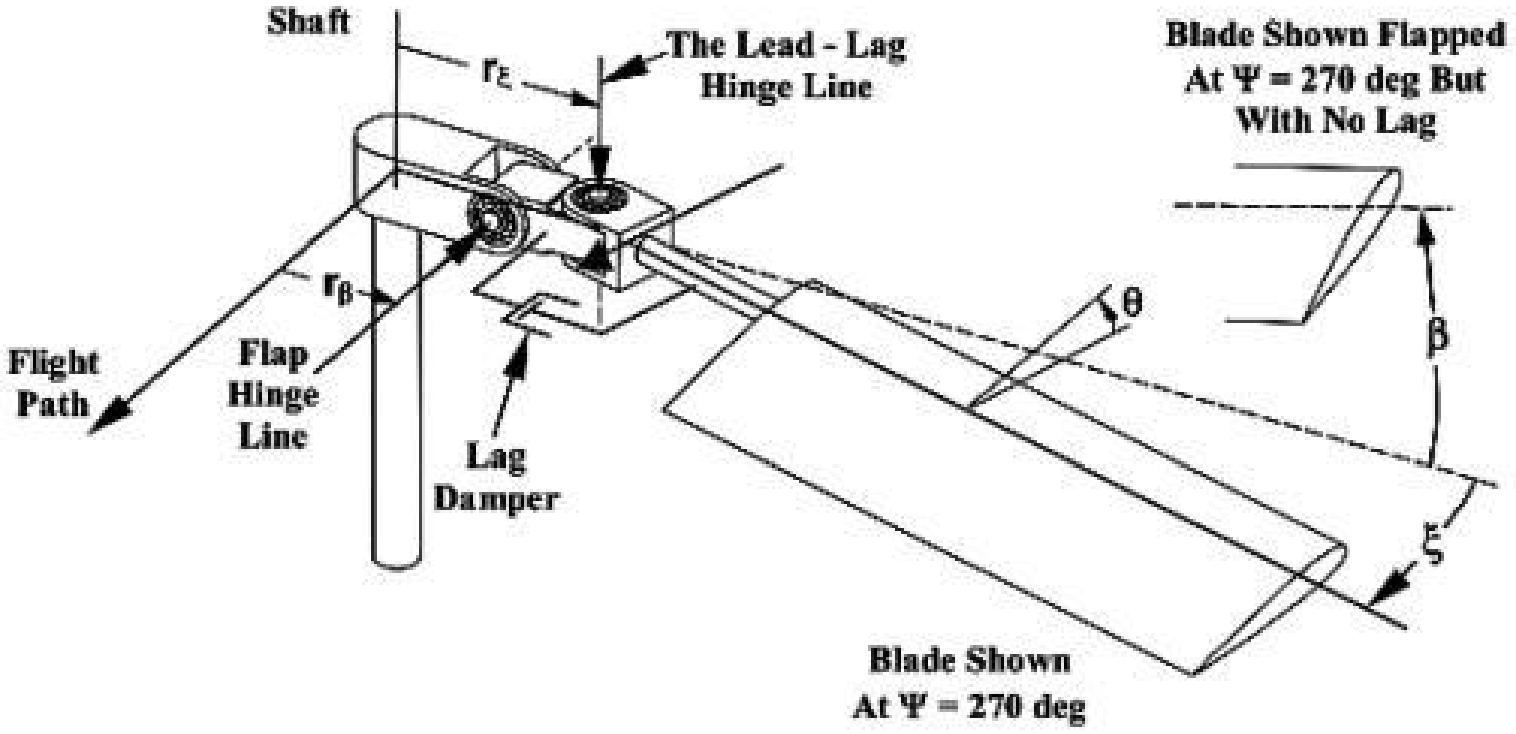

With Some Lag

But With No Flap

Fig. 2-10. The lead-lag hinge relieved blade-root inplane bending loads (drawing by Rick Peyran).

simple dynamics problem that shows the inplane lead-lag motion is out of phase with the flapping motion by 90 degrees . Cierva solved this engineering problem[7] (and many others), and today the lag motion is described to

the lead-lag first order as

$$(2.30) \quad \zeta_\psi = \zeta_0 - \left(1-\frac{3}{2}r_\xi - \frac{3}{2}r_\xi^2\right)\beta_0\left(a_{1S}\sin\psi - b_{1S}\cos\psi\right).$$

The steady lead-lag angle (ζ_0) for a given rotor system depends primarily on how much power (P) the system is absorbing. This angle is approximated by

$$(2.31) \quad \zeta_0 = \frac{P/b\Omega}{r_\xi F_C}.$$

In the early Cierva autogyros, the rotor system was unpowered and therefore the steady lead-lag angle was nominally zero. However, a power takeoff from the main engine was added to later autogyro models, which I will discuss

shortly. This power takeoff was first used to pre- spin the rotor up to near flight RPM so that taxi and takeoff distance could be reduced. Later, the pre-spin was fast enough for jump takeoffs. This gave the autogyro nearly vertical takeoff and landing capability.

---

[7] Brooks notes on pages 100 and 101 of *Cierva Autogiros—The Development of Rotary Wing Flight* that Cierva prepared two design analysis documents, but that they were never formally published. Fortunately, they have been preserved. Dr. J. A. J. Bennett undertook the task of editing the two volumes. Copies of the draft volumes were entrusted by Dr. Bennett to Dr. Richard M. Carlson who, in turn, made a copy for the American Helicopter Society library (and a copy for this author who is most grateful). The first volume is titled *Engineering Theory of the Autogiro* and dates from 1929. The second volume is titled *Theory of Stresses on Autogiro Rotor Blades* dating from 1934. Both volumes were originally provided courtesy of the Cierva Autogiro Co. Ltd.

2.3 LEAD-LAG HINGE

The addition of the lead-lag hinge solved one of the major blade structural-fatigue problems, but, as often happened, the solution created a new problem. This new problem became known as ground resonance and, as Brooks [7] (pages 235 to 237) notes, "recurred repeatedly throughout the development of rotor-wing aircraft." The culmination of incidents associated with the unexplained phenomena of ground resonance came in 1941 with the absolutely total destruction of the Kellett XR-2 autogyro "in less than five seconds." Brooks (page 235) records that the catastrophe occurred "during one of the first tests of a jump takeoff" and that the vibration "built up so rapidly that the aircraft broke up before anything could be done to stop it." The photograph Brooks shows on page 235

(reproduced here as Fig. 2-1 1) confirms what potential for disaster the lag hinge introduced.

The hardware fix for this potential mechanical instability was the lead-lag damper shown in Fig. 2-10 . At the Kellett Autogiro Company, Richard Prewitt, the chief engineer, developed what became the modern oil damper. He notes [43] that:

"We had diverged from the standard form of friction dampers on this model [the KD-1] and experienced considerable difficulty in making our self-centering oil dampers function properly. The difficulty proved to be one of obtaining proper arrangement and adjustment of the self- centering cam and of obtaining proper dampening in the oil plunger unit. This unit was finally corrected, when a unique orifice arrangement made the units self-filling. Their maintenance requirements are now substantially nil." [See Fig. 2-12.]

The standard form of friction damper, Fig. 2-13, that Prewitt refers to is the type both Cierva and Pitcairn used on their Autogiros.

This damper development at Pitcairn is describe in detail by Joseph Pecker [44], a mechanical engineer who consulted with the Pitcairn Autogiro Company on many of their hardware programs . Neither the Kellett oil damper nor the Pitcairn/Cierva friction type of lead-lag damper is readily apparent in any autogyro photographs I have seen because it was buried inside the spar and the lead-lag hinge, but a damper of some form was incorporated on all very successful autogyros.

The theory that explains ground resonance was, as is frequently the case, developed after the XR-2 disintegrated. Brooks [7] (page 237) notes that "Bob Wagner of Kellett and Robert Coleman of the National Advisory Committee on Aeronautics (N.A.C.A.) came up independently with mathematical solutions for the proper configuration and for damping to prevent ground resonance. This was a major step in the

development of rotary-wing aircraft. Paul Stanley of the Autogiro Company of America had also arrived at mathematical and engineering solutions to the problem with the result that Pitcairn Autogiros are claimed to have largely avoided ground resonance."

31 2.3 LEAD-LAG HINGE

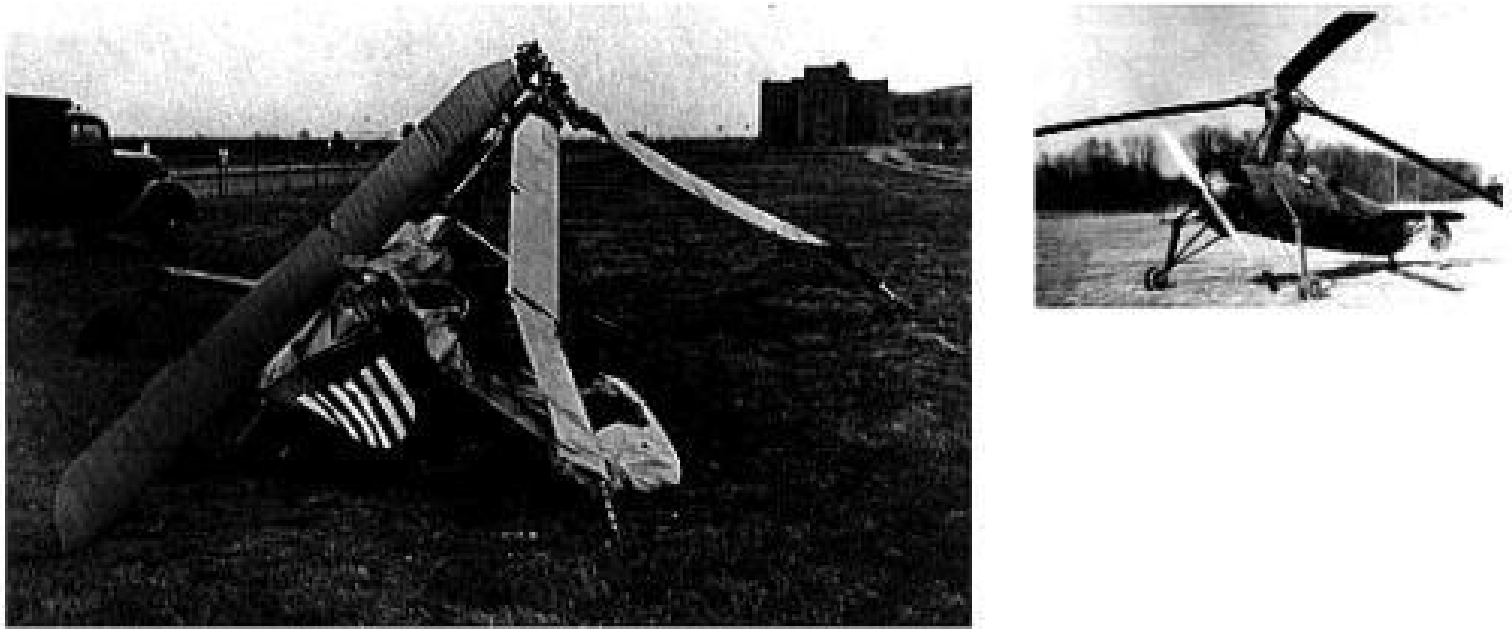

Fig. 2-11. The Kellett XR-2 autogyro before and after ground resonance in 1941 [7].

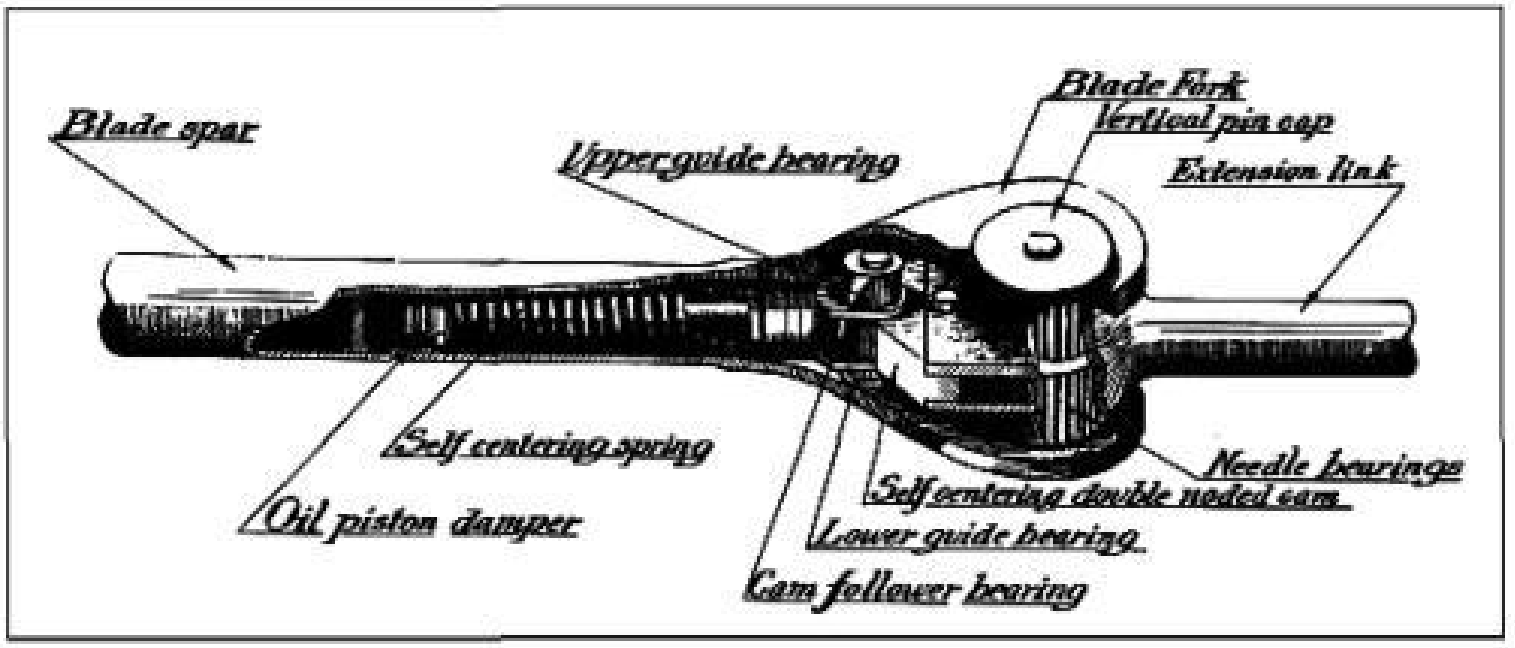

Fig. 2-12. The Kellett KD-1 oil piston lead-lag damper (figure courtesy of W. Wiesner).

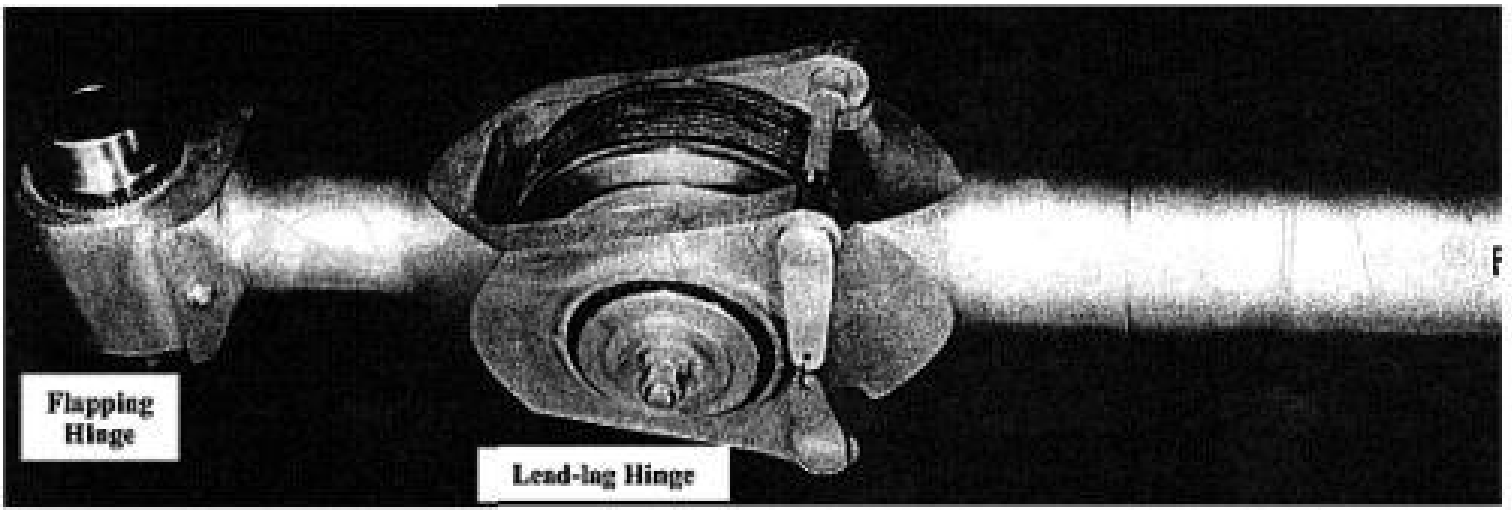

Fig. 2-13. The Cierva- and Pitcairn-style friction lead-lag damper [44].

2.3 LEAD-LAG HINGE

The ground resonance dynamics analysis is not one of the easier engineering problems to solve as you can see from Appendix C. However, George Townson, in his excellent book containing both history and engineering features of autogyros [45], has the clearest illustration of the ground resonance situation I have ever seen. His illustration from page 149 of his book is reproduced here as Fig. 2-14. The problem is basically a two-degrees-of-freedom vibration problem with damping included. One degree of freedom is the rotorcraft rocking on its landing gear. Since shock absorbers were standard equipment for all autogyros just for hard landings, this first degree of freedom was well damped. The second degree of freedom is the blade lead-lag motion, which, the inventors found out, definitely needed additional mechanical damping. The two motions of rotorcraft rocking and blade lead-lagging have the potential to couple

together such that one motion can feed the other. Without damping in both degrees of freedom, there can be real problems. Fortunately, theory to predict ground resonance was in place when practical helicopters began to evolve [46].

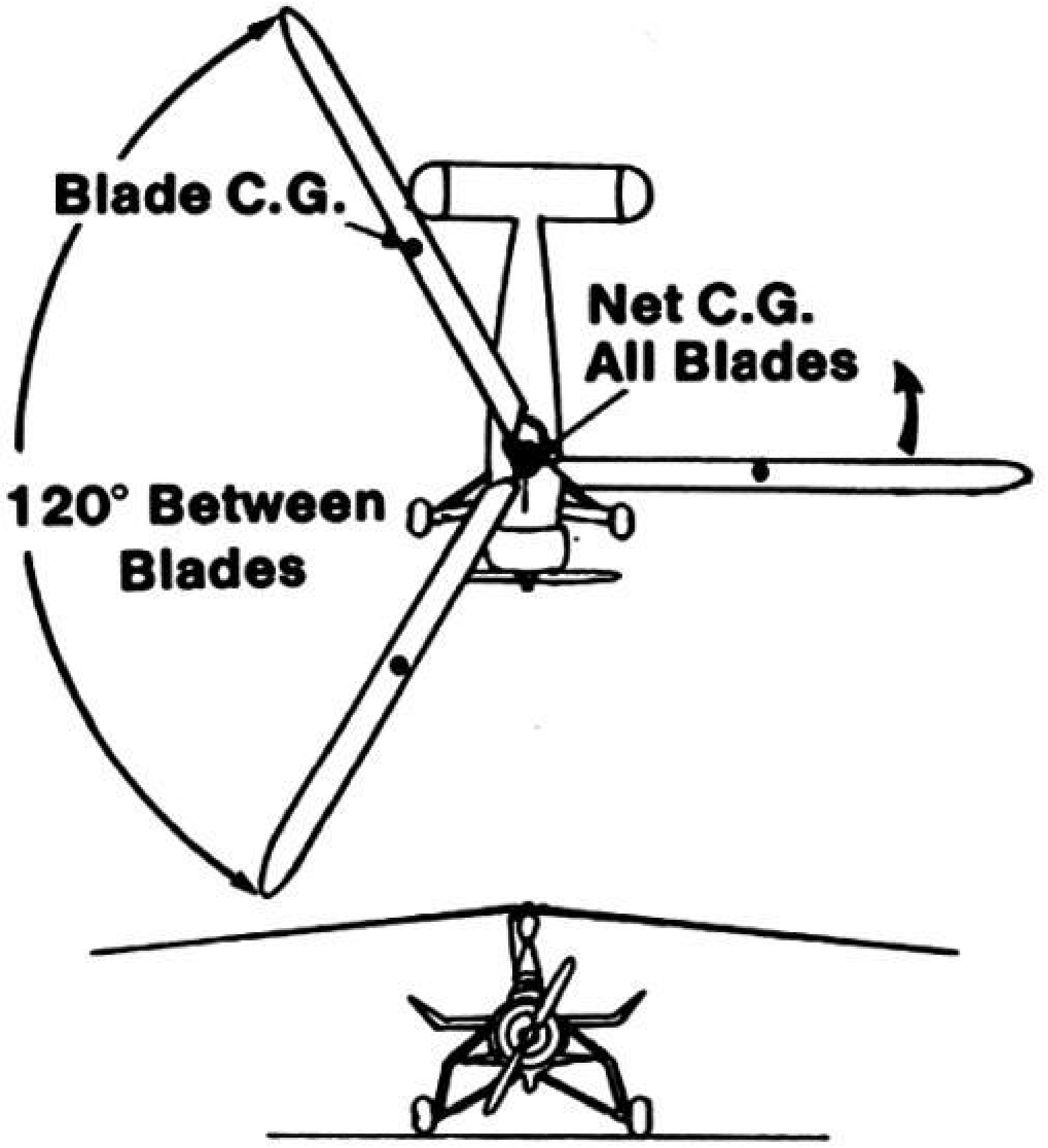
Blade C.G.
Net C.G.
All Blades
120° Between
Blades

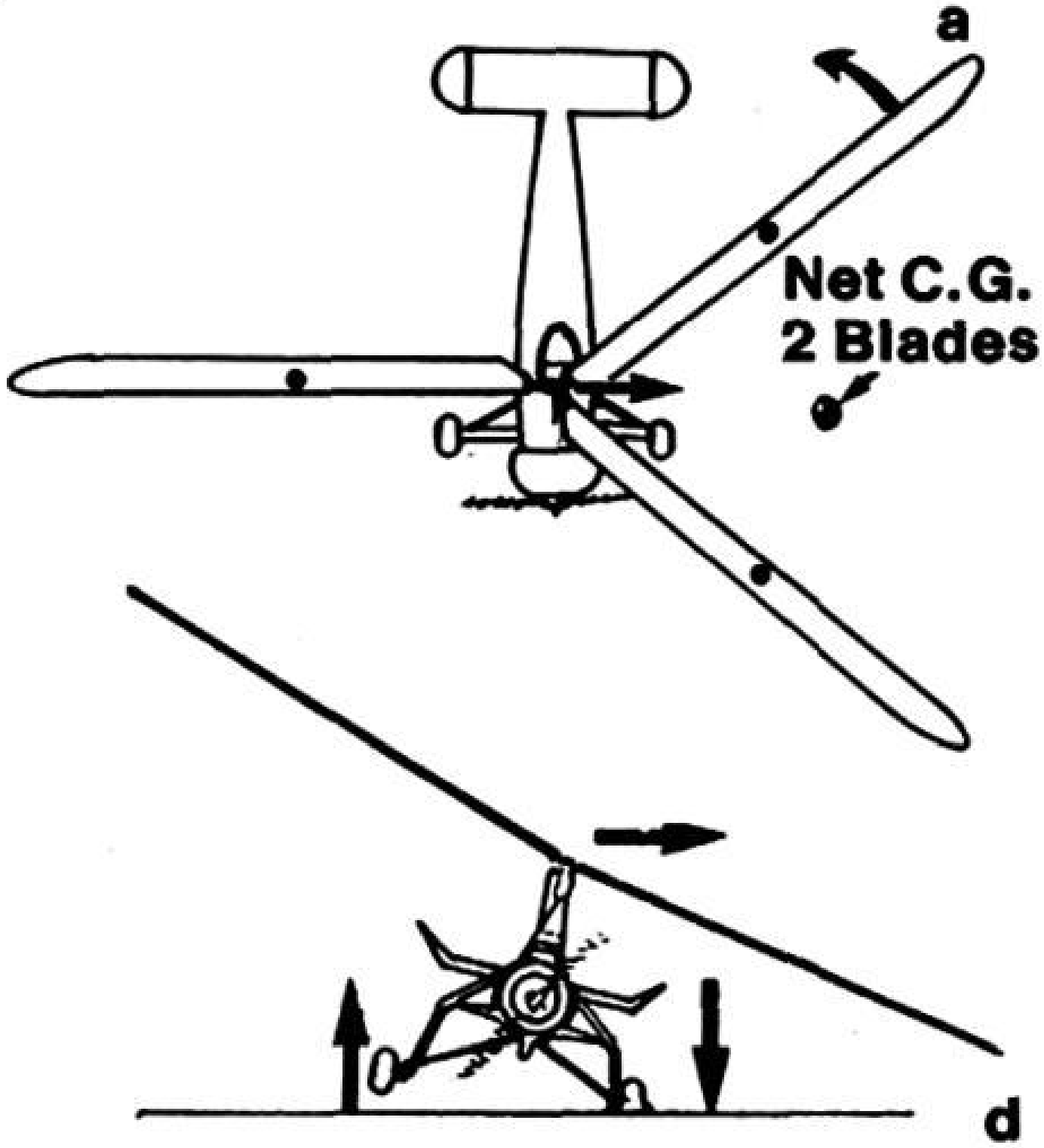

GROUND RESONANCE

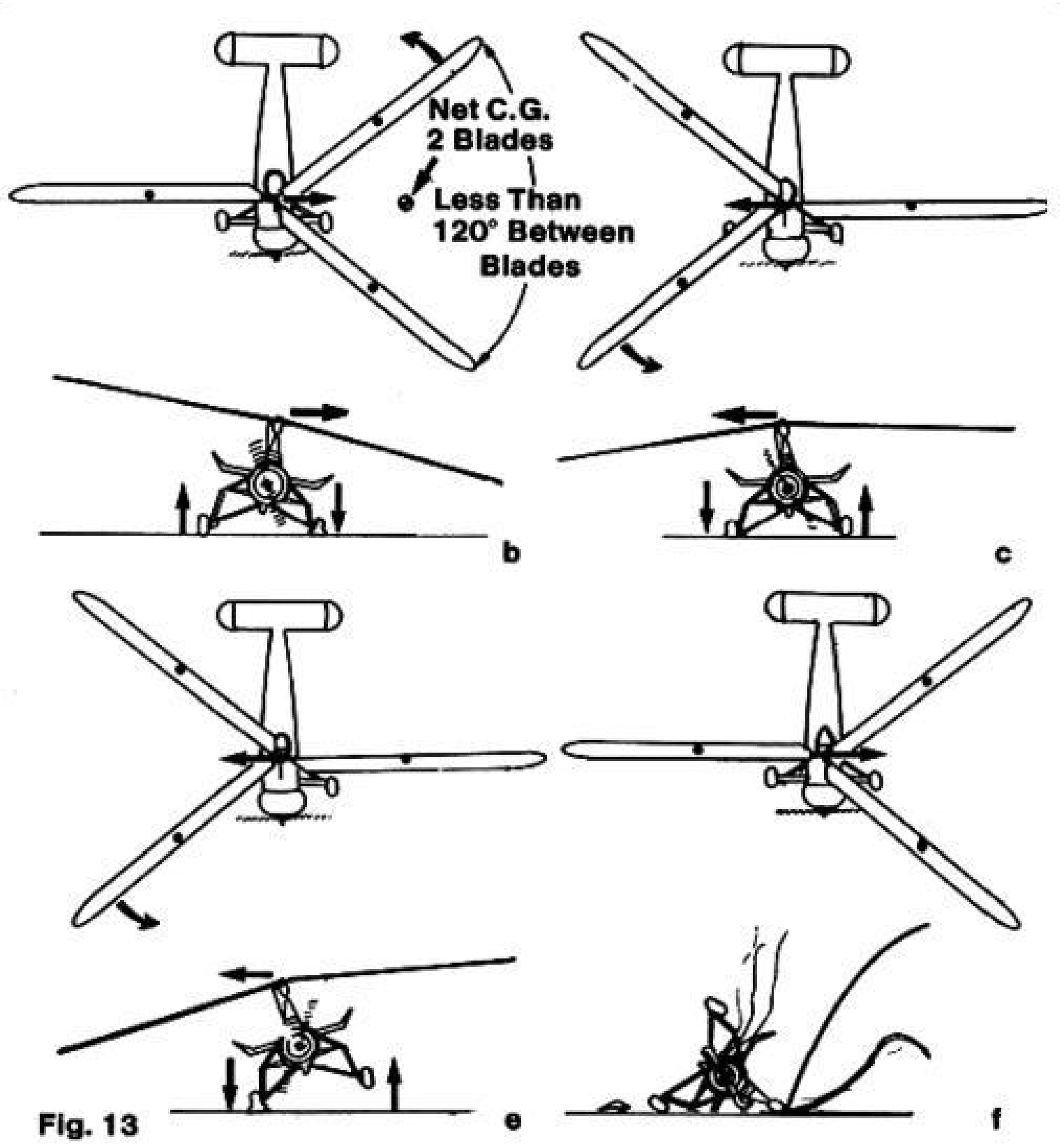

Fig. 13

Fig. 2-14. De-patterned blades in the lead-lag plane create a potentially destructive

force that can lead to ground resonance [45].

2.4 ROTOR STARTUP

Cierva was invited to present a second paper to the Royal Aeronautical Society on February 13, 1930. This lecture [4] gave him a chance to update his audience after 5 years of progress. By this time, his development efforts had taken him from the C.6, the autogyro they had first seen fly, up to the Cierva C.19 Mk. III, the first true production rotorcraft. He mentions the lead-lag hinge, points out improved blades and their smooth skin construction, hints about his vortex theory for vertical descent, and spends considerable time discussing his autogyro versus a comparable fixed-wing aircraft. Judging from the audience remarks [4], they were generally pleased with Cierva's progress, although they commented

that there was a lack of quantitative data in his presentation.

Audience members believed that the autogyro was safer than an airplane by virtue of its near vertical landing capability. Indeed, demonstrations continued to show vertical speed at touchdown in the 13- to 16-feet-per-second range with less than a 4-yard ground run. These rates of descent, equivalent to a free fall from 3 to 4 feet, are less than are found with a parachute whose diameter equals the rotor diameter.

The next problem that needed to be solved completely—according to remarks from the audience [4]—was to dramatically reduce the takeoff distance of the autogyro. Initially, the early autogyros used a rope or wire wound around pegs under the blades that was pulled by several men (or a horse or even a car) to pre-spin the rotor up to 30 to 50 rpm. Then, by

taxiing around the generally rough airfield at 20 to 30 miles per hour, rotor speed increased to the required takeoff of 130 to 150 rpm. Cierva quickly learned that taxiing alone did the trick, although several minutes were required. In short, the autogyro takeoff distance and takeoff time were considerably longer than those of an airplane.

The Cierva C.19 Mk. II, similar to Fig. 2-15, but with a 30-foot-diameter rotor, was flight tested at the Royal Aircraft Establishment in early 1930. Their report [47] showed that the "scorpion tail" (a name coined by Mr. Wimperis, the Director of Scientific Research at the British Air Ministry [4]) brought the "windmill speed" up to 90 rpm or about 50% of normal flight speed. At 50% rotor speed, "the run to unstick Gyroplane C.19" was 200 yards . Additional testing at 68% pre-spin reduced the lift-off distance to 150 yards, and at 95% pre- spin, the C.19 could get off the

ground in 1 10 yards. This performance was obtained with a takeoff gross weight of 1,400 pounds.

Cierva considered a power takeoff from the engine with shafting and gearing to the rotor, but thought that this approach added too much complexity and weight (165 pounds) . Instead, he took an aerodynamic approach that used the propeller slipstream. The biplane horizontal stabilizer was enlarged and included a pilot-selected, large, trailing-edges-up angle to turn the slipstream up through the aft portion of the rotor disc. The stabilizer took a nearly closed, venetian blind position for rotor startup as shown in Fig. 2-16. Cierva notes [4] that "sixty to seventy percent of the flying revolutions are obtained in no wind by this means."

2.4 ROTOR STARTUP

Fig. 2-15. The first production autogyro was the Cierva C.19 [7].

With the pre-spin, which took 45 to 60 seconds, the takeoff run was on the order of 100 to 200 feet. This solution was incorporated on the C.19 . (Frankly, it looks rather ungainly to me, but the two large rudders mask the stabilizer in most photos.) However, the "turned-up tail was considered the most promising of several approaches," one of which was rockets on the blade tips. Mr. Wimperis went on to say that he hoped the

up-turned tail would "reduce the length of the [takeoff] run to something that they were accustomed to with normal types of aircraft."

As it turned out, a satisfactory engine drive for rotor mechanical spin-up evolved quite quickly because Harold Pitcairn became convinced that autogyros were the safe aircraft he envisioned.

Harold Pitcairn was an aviation pioneer [48] . He built an airplane manufacturing company specializing in mail carrying airplanes in Bryn Athyn, a town just outside of Philadelphia, Pennsylvania, and, with the award of airmail delivery routes during the late 1920s, his company grew into Eastern Airlines . Pitcairn was a very strong advocate of safe airplanes. His chief engineer was Agnew Larsen, a close friend, who provided enormous talent in bringing autogyros to a budding industry. A more

technical story of autogyro development written by Larsen was included in the first-issued Journal of the American Helicopter Society [49]. When Pitcairn became aware of the success Cierva had in England, he and Larsen visited Cierva, bought a C.8, and brought it back to the United States. The C.8 was the first truly successful rotorcraft to fly in the U. S. In the spring of 1929, Pitcairn flew the C.8 to Langley Field, Virginia. Additional demonstrations followed with overwhelming press coverage and public interest.

2.4 ROTOR STARTUP

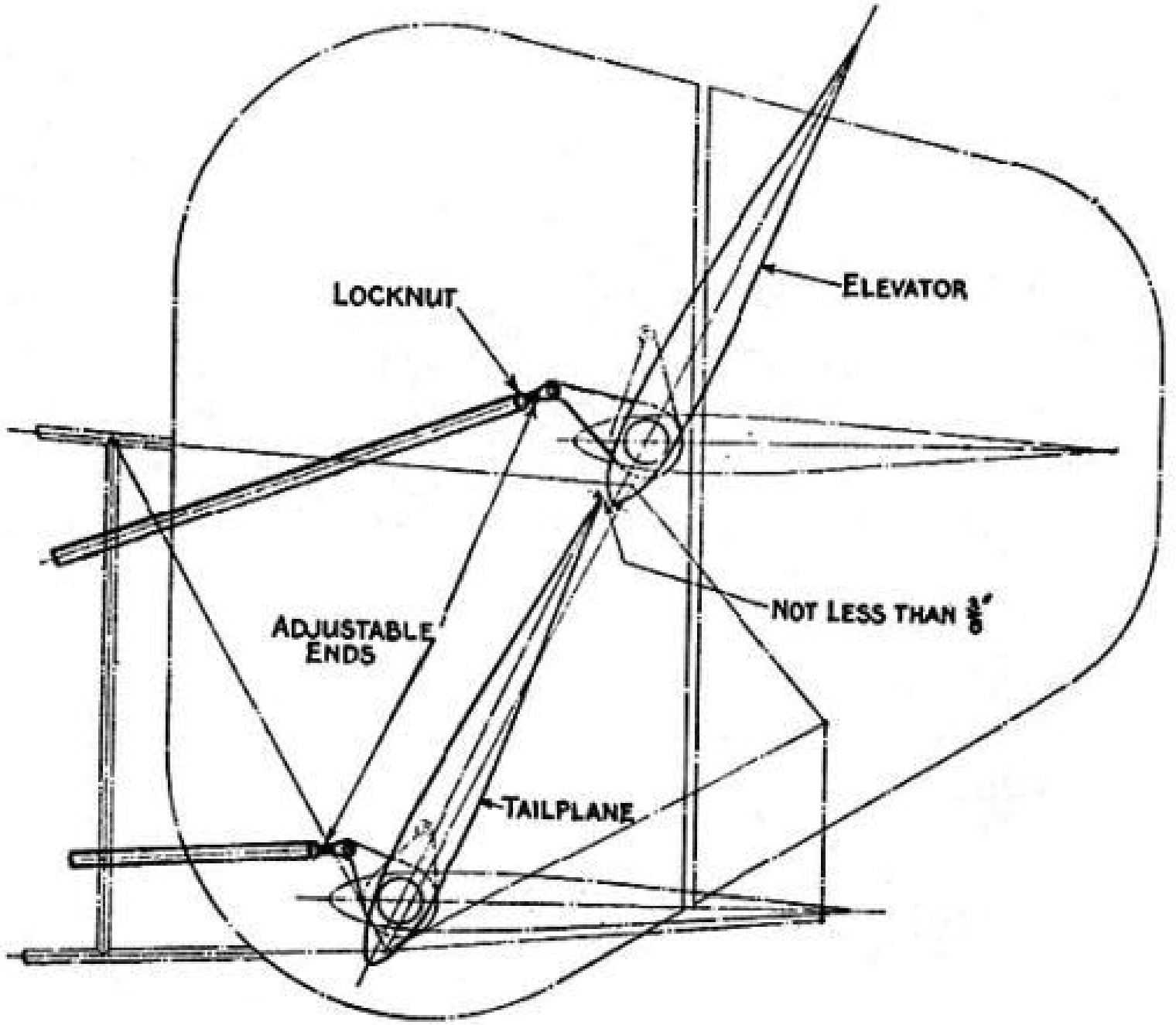

Fig. 2-16. The horizontal tail of the C.19 could be pilot-adjusted to deflect propeller slipstream up into the rotor for pre-spin [50].

In February 1929, after three

unsuccessful negotiating efforts, Pitcairn obtained the exclusive U.S. rights to inventions and patents from the Cierva Autogyro Company, Ltd. Almost immediately, he renamed Pitcairn Aeronautics, Inc . to the Autogiro Company of America, Inc., and a virtual partnership with Cierva in England was cemented. The Autogiro Company of America operated along the lines shown in Fig. 2-17. It became the licensing, technical, and business center for autogyro development in the United States . The company itself granted manufacturing licenses and did research, development, and engineering for its first licensee, the Pitcairn Autogiro Company. The second manufacturing license was granted to Wallace Kellett and the third to Lawrence Buhl.

When a fire destroyed his factory in mid-November 1929, Pitcairn moved his operations from Bryn Athyn to Willow Grove, Pennsylvania, and then bought additional land,

which became Pitcairn Field. (This facility was later taken over by the government during World War II and became Willow Grove Naval Air Station.) Then, in December 1929, Pitcairn bought a Cierva C.19 Mk. II with a "scorpion tail" pre-spin configuration. He and his engineering team (lead by Agnew Larsen) were not satisfied with the Cierva up-turned tail for rotor pre-spin. They got busy designing a unique clutch and gear train that was incorporated into the PCA-2. At the end of March 1930, his design team had the first PCA-2 flying. The PCA-2, Fig. 2-18, was created from PCA-1, -1A, and -1B developments during 1929 and 1930, and was the first autogyro sold in the United States. It received its Approved Type Certificate (ATC No. 410) on April 2,193 1, and became commercially successful.

37 2.4 ROTOR STARTUP

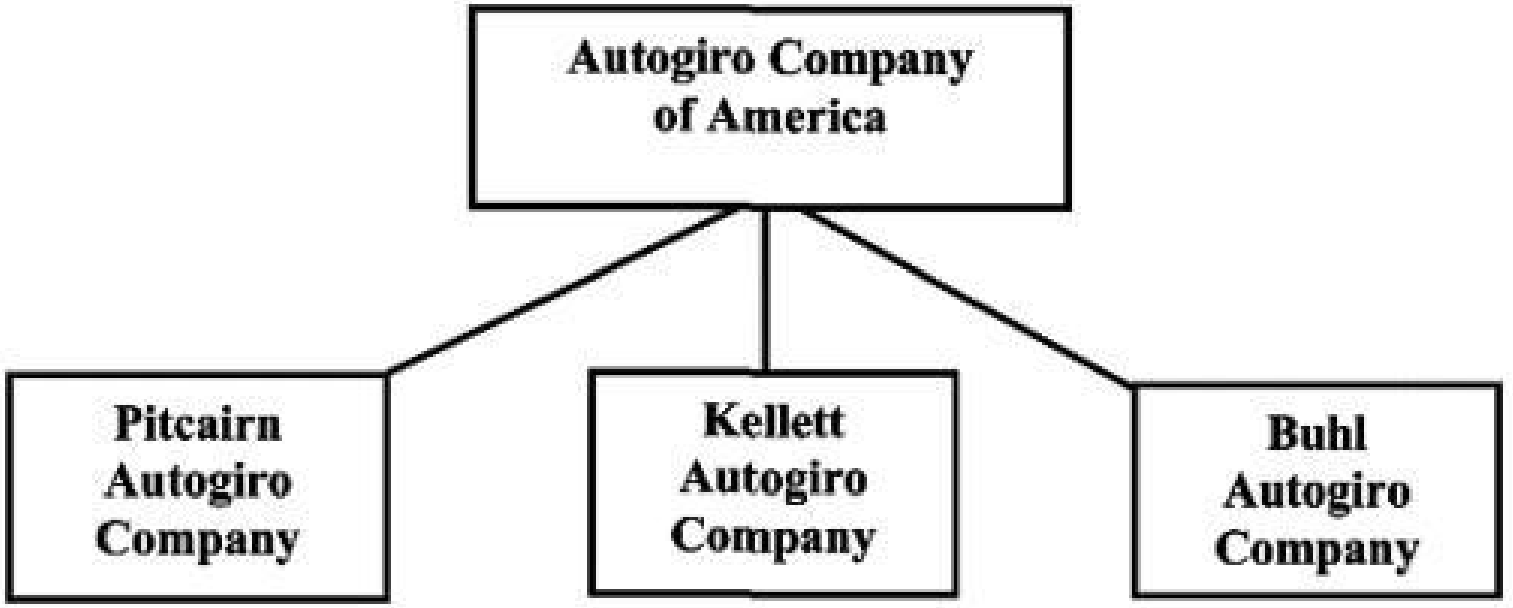

Fig. 2-17. Harold Pitcairn laid the foundation for the rotorcraft industry in the U.S.

Fig. 2-18. The first production autogyro certified in the United States was the Pitcairn PCA-2. This one was sold to the N.A.C.A. in 1931 [53].

The story of this mechanical rotor starter is well told by Agnew Larsen [49]. By way of background, he writes early in his paper (in studying the Cierva C.8 and applying the knowledge gained to the PCA-1) that:

2.4 ROTOR STARTUP

"The engineering personnel of the Pitcairn Aviation Company were essentially all airplane designers, with limited or no experience in mechanical engineering design and therefore not capable of refining the large and bulky rotor hub on the Cierva C-8 autogyro, or reducing its weight from 200 pounds to the 75 pounds that was considered a rational allocation for it. Consequently, the

services of the Machine and Tool Designing Company were called in soon after the completed negotiations with the Cierva Company to carry on this phase of the work. The first designs of rotor hubs as incorporated in the two original American autogiros [PCA-1 and -2], were marvels of light weight with great strength. This was accomplished through the employment of alloy steels, heat-treated to high physical properties. During this phase of the pioneering work, the highest authorities, such as metallurgists from Bethlehem Steel and the International Nickel Co., ball bearing experts from SKF, Norma–Hoffman, Fafnir and others were always consulted and followed. In this way, serious mishaps in the very early embryonic stages of our efforts were avoided while we learned and progressed."

Larsen next writes about setting specifications for a mechanical starter that "were liberalized in RPM's desired, but much stricter in weight allowance" and then recounts:

"The Machine and Tool Designing Company produced a beautiful, light weight, twin disc starting clutch and gear reduction unit, weighing only 48 lbs. This transmission was capable of delivering 15 to 20

horsepower, which was the maximum allowed by Wright Aeronautical, for delivery by the rear accessory drive shaft on their Whirlwind engine. This was sufficient to turn the 42 foot rotor at about 80 or 90 rpm, permitting stabilization of rotor speed in about 30 to 40 seconds and requiring only a short forward run for takeoff. Starting from this humble, light weight beginning, this very same design of rotor starter was gradually developed in the next three years up to an ultimate 55 horsepower, delivering 125 rpm on a large 50-foot diameter rotor."

Agnew Larsen, in telling this story of a major autogyro improvement, quietly omits his own leadership role in engineering the rotor startup assembly. Joseph Pecker [44] notes that "through the extensive research work conducted, under the supervision of Mr. Larsen, by Mr. Stanley, the writer [Pecker], and others of the Pitcairn Engineering Staff, a basically sound engineering foundation, dealing with hubs and starters, was established." All the details of the starting system and the hub are described with excellent engineering drawings in the patent awarded to Pecker [51].

Pecker applied for this patent in June of 1932, and he assigned the patent to the Autogiro Company of America when it was awarded on April 14, 1936.

Cierva incorporated the Pitcairn pre-spin drive system into his Mk. IV upgrade of the C.19 . It was a feature in all future autogyros, including the best-selling Cierva C.30. The C.30 mechanical starter is shown in Fig. 2-19.

Starting the rotor up in preparation for takeoff required some caution when the prevailing wind was blowing at more than 20 to 25 miles per hour. Autogyros were started facing downwind or with the wind on either the port or starboard sides. For example, Brie [52] notes that the C.30 Autogiro was certificated in Britain for operation in winds up to 30 miles per hour. He teaches that the rotorcraft should be started with the wind

coming on the starboard side (because the C.30 rotor rotated clockwise when viewed from the top). The rotor starter is engaged and the rotor is brought up to 100 rpm. Then the autogyro is taxied to an into-the-wind position. The rotor is then brought up to 185 rpm. At that point the takeoff is begun.

2.4 ROTOR STARTUP

The piloting technique addressed concern for flapping, which could become quite erratic in the 0- to 100-rpm range because centrifugal force was too low relative to blade lift. The possibility of blade-fuselage contact was real. You can see the situation from Eq. (2.21), which is repeated here for convenience as

(2.21) $a_{1S} = 2\theta V/V_t$.

At 100 rpm, the 37-foot-diameter C.30 rotor

had a tip speed of 194 ft/sec. The blade pitch angle (θ) of all blades, accounting for the airfoil angle of zero lift of –4 degrees, was 6.75 degrees . At 30 mph, 44 ft/sec, the flapping would be a reasonable 3 degrees. However, the flapping would behave inversely with RPM as

$$(2.32) \quad a_{1S} = 10.2 \frac{V_{mph}}{RPM} \text{ in degrees .}$$

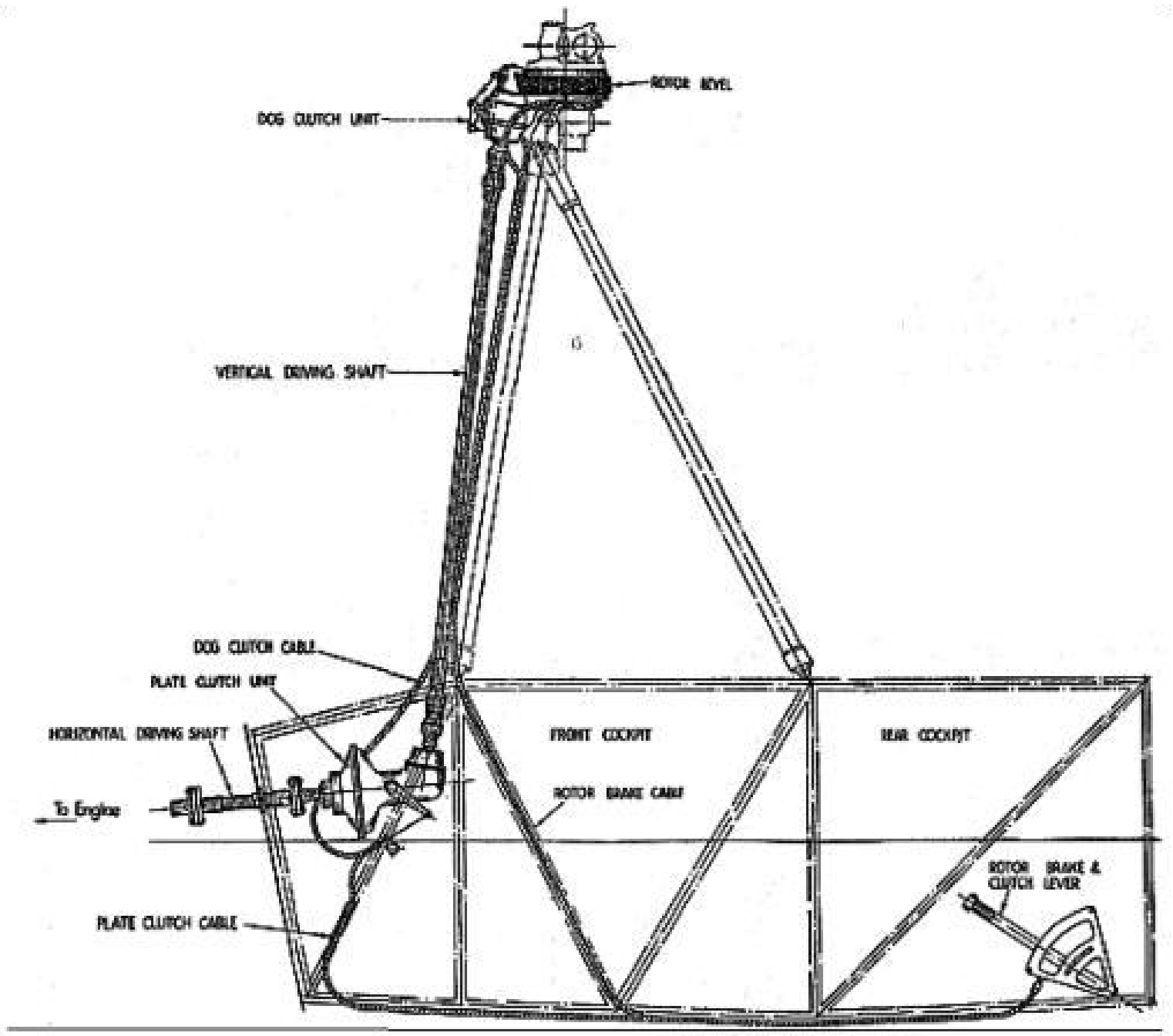

Fig. 2-19. The C.30 mechanical starter [52].

The C.30 did have limiting stops to flapping motion. The down-flapping stop was set to –4 degrees and the up-flapping stop was set at 30 degrees [52] . These angles were referenced to the hub plane. Roughly speaking then, a blade *might* contact the down stop at any RPM below 75 when the wind was 30 mph. (Banging the down stop created excessive blade-root-end stresses.) Since it took from 30 to 45 seconds for the mechanical starter to bring the rotor up to speed, the pilot had to take considerable care by following the advice from Brie [52] . By starting with the wind against the starboard side, the potentially large flapping would be high on the upwind, starboard side, and low on the port side. This minimized the chance of a blade striking the aft end of the fuselage (i.e., the vertical stabilizer).

By the end of 1931, over 100 autogyros

had been built and sold. Having started their own companies, Wallace Kellett and Lawrence Buhl were exercising their license from the Pitcairn Autogiro Company of America. The Kellett K-2 was certificated with ATC No. 437 on July 17, 1931. The Buhl Autogiro, the first autogyro with a pusher engine and propeller, made its first flight on December 15, 1931, and both Cierva C.19s and Pitcairn PAC-2s were performing well in the field. The next deficiency to overcome was control at low speed.

2.5 DIRECT CONTROL

In these early autogyros, the rotor hub spun on bearings attached to a short shaft fixed to the airframe. The assembly was called a spindle, and the shaft was frequently referred to as the axle. Control was simply the normal

airplane ailerons, rudder, and elevator. These surfaces were virtually useless at speeds below 25 miles per hour and in descent. Fortunately, the basic autogyro was stable enough in these flight regions, so landings—in calm wind—were generally successfully made by low-time or even first-time pilots . But, everyone, including
experienced pilots, was having trouble on windy days. As might be guessed, Cierva was already conceiving a way to give the pilot direct control of the rotor thrust vector.

Invited by Pitcairn, Cierva made his third visit to the United States, arriving just before Christmas 1931. It was to be a working vacation. Cierva presented his ideas for direct control to Pitcairn and a small group during January and early February 1932 at Pitcairn's Bryn Athyn, Pennsylvania home. The concept was quite simple as the schematic, provided

by Brie [52] for the Cierva C.30, shows (see Fig. 2-20). The spindle assembly would be mounted on a universal joint attached at the lower side to the airframe structure (i.e., the pylon struts). A control stick would hang down from the spindle into the cockpit. The pilot could pull aft on the stick handle, which, through an intermediate lever, tilted the spindle nose up and inclined rotor thrust rearward. Moving the stick handle right tilted the spindle to the right, which inclined the rotor thrust to starboard. Smith, in telling the Harold Pitcairn story [48], says that "Cierva's presentation, couched in mild bland tones, had a stunning effect [on the group] as he proceeded with a novel theory that he had developed in England." Smith writes later that "as he [Cierva] proceeded in an almost pedantic manner, the enormous significance of his thinking overwhelmed his audience."

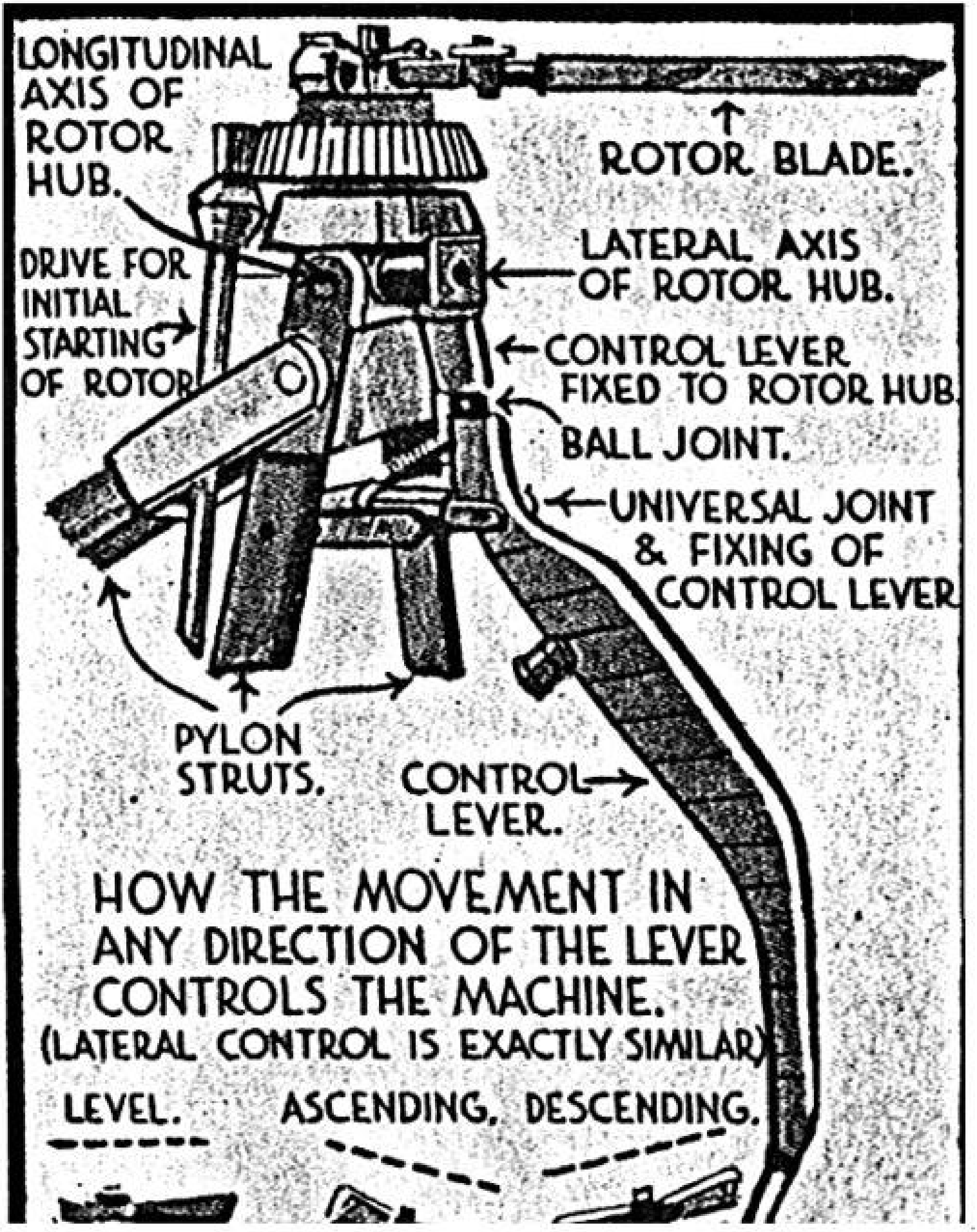
LONGITUDINAL AXIS OF ROTOR HUB.
ROTOR BLADE.
DRIVE FOR INITIAL STARTING OF ROTOR
LATERAL AXIS OF ROTOR HUB.
CONTROL LEVER FIXED TO ROTOR HUB.
BALL JOINT.
UNIVERSAL JOINT & FIXING OF CONTROL LEVER
PYLON STRUTS.
CONTROL LEVER.
HOW THE MOVEMENT IN ANY DIRECTION OF THE LEVER CONTROLS THE MACHINE.
(LATERAL CONTROL IS EXACTLY SIMILAR)
LEVEL.
ASCENDING.
DESCENDING.

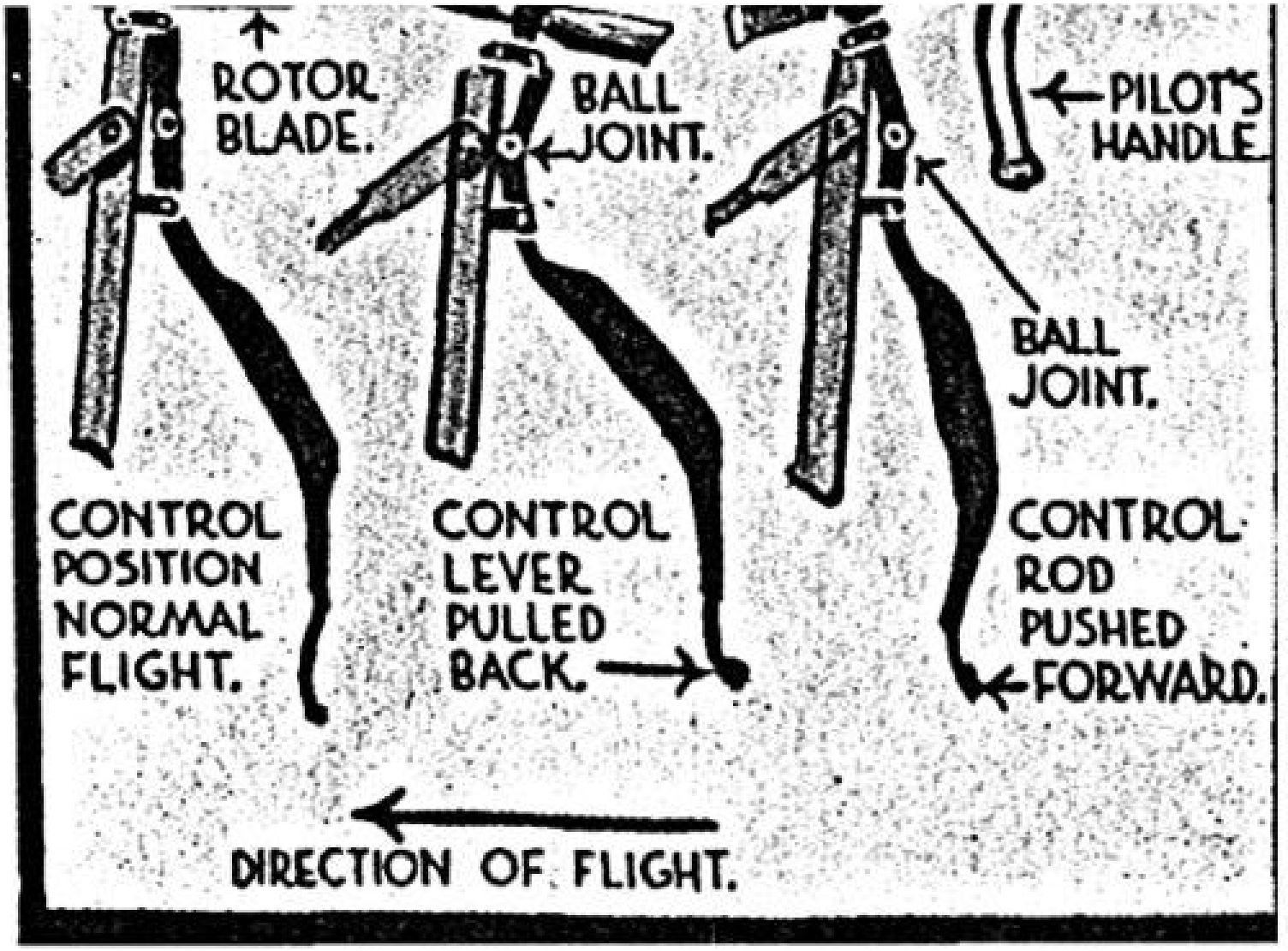

Fig. 2-20. The direct control system of the C.30 [52].

2.5 DIRECT CONTROL

Brooks [7] notes that "Cierva achieved a workable system of direct control in Britain in March 1932. Later that spring, the C.19 Mk V

with this improvement incorporated was demonstrated to Harold Pitcairn, Jim Ray [Pitcairn's chief pilot] and Agnew Larsen of the American Autogiro Company who had come to England specially to study this new development. Pitcairn and Ray later flew the C.19 Mk V. In April 1933, Cierva publicly demonstrated the direct control C.30 prototype. Early in 1934 the direct control Avro [A.V. Roe & Company, Cierva's manufacturer] C.30A entered full production in Manchester and deliveries stared in July [1934]."

The universal joint Cierva incorporated allowed the pilot direct control of the longitudinal incidence angle (i_{hp}) of the hub, relative to an aircraft station line. To define the hub angle of attack (α_{hp}) then required the sum of the autogyro waterline angle of attack (α_{wl}) and (α_{hp}). The hub could also be tilted left and right by an angle (i_{ϕ}).

These variable hub angles relative to the autogyro, (i_{hp}) and (i_{ϕ}), were governed by the kinematics of the pilot stick and linkage as Fig. 2-20 shows. Direct control gave pitch and roll control independent of flight path velocity and was a major improvement. Wings and ailerons came off, and rudder and elevator became fixed-stabilizer surfaces.

Pitcairn, Ray, and Larsen rushed home and immediately built a small prototype, the PA-22. Unfortunately, this autogyro experienced several development problems and took until mid-1933 before direct control was working satisfactorily. The PA-22 then became a test bed for many advanced concepts . In fact, Pitcairn did not produce a production direct control autogyro until 1941 (this was the Pitcairn PA-39). Efforts by Kellett were more successful, and they went into production with their KD-1, Fig. 2-21, which received its ATC (No. 712) in January 1935, with first delivery

in early 1935 . Kellett used a conventional "joy stick" mounted to the cockpit floor rather than the hanging stick used by Cierva and Pitcairn.

Unfortunately, direct control of the hub plane with a hanging stick did not appear feasible as larger-sized autogyros were studied. Experience up to the mid-1930s had shown that any appreciable dissimilarity in manufactured blades caused extreme feedback to the pilot's handle . These and other vibratory loads came on top of the normal steady loads created by rotor blade flapping. The magnitude of just the minimal loads at the pilot's handle is relatively easy to see because these minimal loads come primarily from hub moment due to flapping. Thus, the steady-hub pitching moment is

$$(2.25) \quad M_P = \frac{F_C \, r_\beta \, b}{2} a_{1S} .$$

Now, using Fig. 2-20 and data from the *Theory of Stresses on the Autogiro Rotor Blades* by Cierva [12], consider the three-bladed (b = 3) Cierva C.30 as an example. Cierva says "the blade can be assumed to be an 18.5-feet-long uniform beam weighing 41 pounds." This gives a running weight ($\bar{w}$) of 2.22 pounds per foot and, therefore, a running mass ($\bar{m}$) of 0.0689 slugs per foot based on a gravitational constant of 32.17 feet-per-second squared. At 210 rpm for normal flight, rotor speed is 22 radians per second, and the centrifugal force (F_C) is calculated as

Fig. 2-21. The first production direct control autogyro in the U.S. was the Kellett KD-1. The control stick was in the cockpit with control mechanization run up through the rotor support structure (photo courtesy of Jean-Pierre Harrison).

(2.33)

$$F_C = \int_0^R r\Omega^2 dm = \int_0^R r\Omega^2 \bar{m} dr = \frac{\bar{m}\Omega^2 R^2}{2} = 5,700 \text{ lbs}.$$

The flapping hinge offset (r_β) was located 1.75 inches from the rotor centerline, so r_β = 1.75 inches . Therefore, the rotor system could generate, following Eq. (2.25), roughly 15,000 inch-pounds of moment per radian of flapping, which translates into 260 inch-pounds per degree of flapping. With Fig. 2-20 as a guide, the first reaction to this moment is the end of "control lever fixed to rotor hub," which was about 11 inches long . Thus, the force on the "ball joint" would be about 24 pounds per degree of longitudinal flapping. The distance from the "ball joint" to the "universal joint and fixing of control lever" is approximately 3 inches; from "universal joint" to the pilot's grip is about 49 inches. These approximate dimensions, following Fig. 2-20, suggest the pilot had a 16-to-1 mechanical advantage, which would mean a longitudinal stick force of, say, 1.5 pounds per degree of longitudinal flapping (a_{1S}). (Note that these dimensions also

give about 3 inches of stick travel in an arc per 1 degree of hub plane tilt, or spindle tilt, if you prefer.)

2.5 DIRECT CONTROL

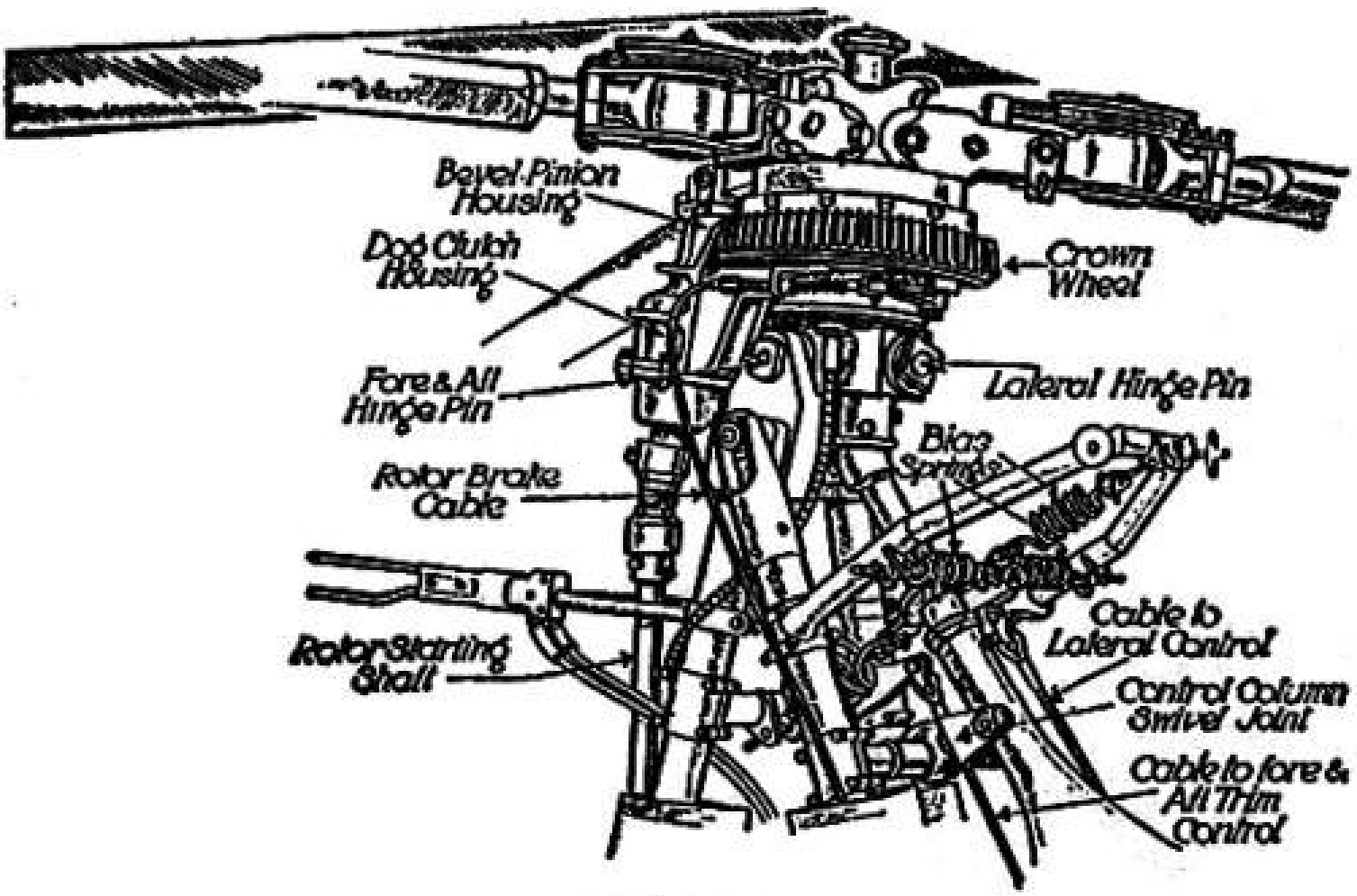

FIG. 3.

Fig. 2-22. Details of the Cierva C.30 upper control system [5].

A stick force of 1.5 pounds per degree of flapping might be acceptable if that was all the C.30 needed for trim, but, in fact, flapping could easily be 5 degrees at certain high-speed flight and center-of-gravity conditions. On the other hand, in low-speed flight, the rotor tip path plane remained virtually parallel to the hub plane, so the pilot was simply tilting the thrust vector without creating flapping. Therefore, Cierva added "bias springs" in the upper control system so the pilot had adjustments to bring his (or her) stick force to zero in high speed and to provide a force feel in low-speed flight. Details of the upper control bias spring system are shown in Fig. 2-22.

The book by Reginald Brie [52] on how to fly the Cierva C.30 explains, in Chapter VI,

several other facets of the "machine," which give considerable insight. I quote as follows:

The main number of control movements essential in any aircraft are three – longitudinal, lateral, and directional, and, whereas these are normally obtained on the aeroplane by the coordinated movement of the control column, rudder and throttle, for the first time they are obtained with the "direct control" method employed on the modern Autogiro by the movement of the control column and throttle only. Whilst these two controls are independent in themselves they are not independent in their action, as an analysis of their functioning will show –

(a) A movement of the control column laterally results in DIRECTIONAL control. In other words, although the machine tilts as it turns, it is actually turning because of the tilt produced by this lateral movement, rather than tilting as a result of the turn. An analogy is provided by the man who steers his bicycle "hands off" through the movements of his body only.

(b) A movement of the control column fore and aft results in SPEED control. Within the limits of minimum and maximum speeds in horizontal flight, and with a constant throttle setting, if the control column is eased forward there will be an increase in speed and if backward, a decrease.

(c) A movement of the throttle results in ALTITUDE control. Assuming the machine to be flying level at 60 m.p.h., if the throttle is opened there will be an increase in height, and if closed then a loss in height will result. It will thus be observed that there is a close relationship between (b) and (c), and it is necessary to appreciate how dependent each is for cause and effect upon the other, for once the minimum horizontal speed with full throttle stage is reached, there is a reversal in the results indicated in (b), as the control column then becomes the ALTITUDE control, and in order to gain height it must be eased FORWARD. The result of easing the control column backward at this stage (approximately 15–20 m.p.h.) would be to lose height, a situation fraught with an element of risk if practised at a low height with obstacles ahead, although

the machine itself is under perfect control.

Two examples will help to explain this

1. The most economical throttle setting for slow level flying is not that for the slowest minimum horizontal speed. For an indicated air speed of, say, 40 m.p.h. in the first case the throttle will be about two-thirds open, whereas in the latter case at 15 m.p.h. full throttle is required.

2. At full throttle one can achieve either maximum or minimum horizontal speeds in level flight.

In order that these facts may be fully appreciated an analysis of the "drag" [drag that propeller thrust overcomes] on the Autogiro gives the following approximate results

(a) Power [required by propeller to provide thrust that overcomes] losses due to friction [profile drag] on the rotor system which, owing to the continuous and uniform rotational speed within narrow limits of the rotor, are practically constant at all speeds.

(b) Power [required by propeller to provide thrust that overcomes] losses due to the displacement of air to ensure adequate lift [induced drag]. These losses are at a minimum at high speeds and at a maximum at slow speeds, due to the difference in the amount of air encountered by the rotor per second, which is dependent on the machine's speed.

(c) Power [required by propeller to provide thrust that overcomes] losses due to the resistance offered to a smooth air-flow by the fuselage and structure. The increase in drag from these sources alone being proportional to the square of the speed of the machine [parasite drag].

At high speeds, therefore, although the power losses on the rotor are less owing to the greater amount of air-flow dealt with per second by the disc, the drag from the fuselage, undercarriage, etc., considerably increases.

Conversely, at slow speeds a point is reached where the rotor ceases to act at its optimum efficiency for ensuring minimum horizontal flight with full throttle, and where the machine will definitely lose height.

2.5 DIRECT CONTROL

This, as stated previously, is at an indicated air speed of 15 to 20 m.p.h., and in order to climb the control column must be eased forward, the best climbing speed being at approximately 65 m.p.h.

Control Characteristics

The main essential of flight is motion, for without it there can be no lift. On the Autogiro this motion is obtained by the automatic self-rotation of the blades during flight, which provides all the necessary lift independently of any forward movement of the machine as a whole. In addition, as all normal control surfaces, such as ailerons, elevators and rudder are suppressed, all necessary control is obtained by tilting the rotor disc in any desired direction about the horizontal; the further practical result is that stability and control are also independent of any forward speed of the machine. The rotor being a stable surface, the directional and longitudinal stability of the Autogiro under all conditions

of flight is ensured by means of the fixed vertical and horizontal fins at the rear.

The lift on all blades being equal, the machine flies on an even keel, and the resultant lift force on the rotor is located in close proximity to the centre of rotation of the blades, and in a direction that is normal under all conditions to the plane of the disc. In consequence, any tilting of the rotor disc from a normal position by means of the control column results in a displacement of the total rotor lift force relative to the centre of gravity position, which in turn causes an immediate change in the attitude of the machine. In other words, the backward tilting of the rotor disc by the easing back of the control column causes the line of the lift force to advance in relation to the centre of gravity of the machine, and the nose to rise.

Conversely, the easing forward of the control column will result in the raising of the tail.

A movement of the control column to left or right will cause the machine to bank, and at the same time to turn, the latter additional change in direction occurring as a result of the sideslip produced by the bank, the resultant wind action produced on the inner side of

the machine acting on the fairly large fixed tail surface in much the same way as on a weathercock.

It is of importance that the reaction of the machine to any given movement of the hanging control column should be thoroughly understood, as the first impression might be that the result would be the reverse of normal practice. This is not so, as a link is provided between the control column and rotor head, and if a movement is made to left or right the machine will turn in that direction. It is impossible, however, to sideslip or yaw independently of a turn.

Very positive directional control of the machine on the ground is provided by means of a steerable tail wheel operated by conventional rudder bar. There being no rudder, the secondary sphere of usefulness of this control is as a "pilot's comforter" to those accustomed to conventional aircraft, who, through force of habit, would otherwise feel lost without something to do with their feet.

With the method of control employed on the "direct control" Autogiro there is normally no corresponding increase in the load felt on the control column with an increase in movement as experienced on a

fixed wing machine with ailerons and elevators; so, in order to give the pilot a corresponding "feel," a load or resistance is provided by artificial means, which consists of a bias gear in the form of coil springs attached to the top end of the control column.

2.5 DIRECT CONTROL

In addition to making control more flexible the bias tends to make the machine automatically stable in all directions, as by the method of adjustment provided the machine can be trimmed for high- or low-speed conditions of flight, and also for variations in load; a further feature being that the control column has not only a tendency to remain in the normal flying position, but also to return to it if deflected, as, for instance, by an air disturbance.

The discussion by Brie [52] is, of course, aimed at the general pilot and laymen. The overall tone is that the thrust vector is directed in space and the "machine" just

follows. He does not hint, rightly so, at hub moment or other forces involved in the direct control of a modern autogyro. Fortunately, an entirely different view of flying the Cierva C.30 is obtained from the comments of flight test pilots . This group of pilots has the responsibility to point out deficiencies and shortcomings in an aircraft, and they can be counted on to do so. In the C.30 investigation by the Air Ministry, a view from a test pilot is recorded in Appendix I of Reference [54]. The pilot, Squadron Leader H . P . Fraser, reports a number of shortcomings and at least one major deficiency (in my mind) that deserved notice. Some of them, which I have paraphrased, follow:

1. The hand moves in the same way as in an aeroplane, but the control column tilts in the opposite direction.

2. On takeoff and landing, the steering bar controls the tail wheel, which leads to an overwhelming desire to correct for drift by the steering bar rather than the

control column.

3. In the normal speed range the autogiro is very simple to handle, but

a. there is a good deal of lag in the fore and aft control, though practically none in the lateral control,

b. the control is rather heavy, especially in turns,

c. banking beyond 45 degrees can lead to a spiral dive of increasing speed with recovery possible only by leveling out the aircraft first,

d. with aft control column movement, the autogiro swings to the right as the nose rises; pushing forward, the autogiro swings to the left as the nose falls,

e. suddenly closing the throttle causes a nose left yaw, the reverse occurring when power is pulled,

f. even in still air the autogiro cannot be flown hands-off for any length of time, and in average bumps it is definitely unstable; but departures from a given attitude occur slowly so control corrections can be made in a leisurely fashion.

4. In flight above and below the normal speed range, the autogiro is not so easy to handle as might at first be expected, and

a. *up to 115 mph, the nose has to be forced down, but beyond that speed the autogiro becomes nose heavy. Beyond a certain speed it becomes very difficult, if not impossible, to recover from a dive.* [My italics because it is a major deficiency.]

b. in slow-speed flying there is a large time lag in the fore and aft control.

c. in slow-speed flying the control column cannot be pushed forward too quickly to increase speed or the autogiro will sink bodily onto the ground before it has had time to get the nose down and pick up speed.

d. the safe height for slow flying at full throttle in smooth air over level ground is above 5 feet, while in bumpy air, stay above 15 to 20 feet.

e. descents at glide angles below 45 degrees, with or without engine, present no peculiar difficulty,

2.5 DIRECT CONTROL

f. descents at gliding angles approaching 70 degrees are only possible by vigorous and skilful use of the controls, and the aircraft pitches and rolls considerably and is quite uncontrollable directionally.

5. The takeoff is accomplished in three stages:

a. Starting the rotor with the autogiro stationary.

b. Accelerating the whole aircraft with the rotor disc at minimum incidence (stick forward).

c. Establishing autorotation by increasing disc incidence, thus accelerating blades to the speed of rotation necessary to lift the autogiro off the ground.

6. Landing with the engine off necessitates two things:

a. Having a minimum gliding speed of 40 mph just before flattening out.

b. Having no drift when touching down.

7. Bad view downwards and ahead.

8. If it became necessary to make a parachute descent from a direct control autogiro, the present form of hanging control column would probably hinder the pilot from getting out of the cockpit. On one occasion, small splits developed in the trailing edges of two blades during flight, causing the control column to vibrate through an amplitude of about 12 inches at high and 6 inches at low speed.

9. Laterally, the autogiro rolls immediately [when] the control is applied, but there is a definite time lag before sideslip, which follows, has caused sufficient yaw to turn the aircraft.

10. The lack of a rudder is considered a serious drawback, particularly for correcting drift when landing.

11. It would be advantageous if [there were] some means of increasing control power to get the autogiro out of a dive. An elevator is suggested.

12. The simplicity of the direct control should make the autogiro an easy craft to fly in clouds and conditions of bad visibility, but the possibility of getting into a

dangerous dive makes blind flying definitely unsafe.

This partial list of test pilot observations did not keep the Cierva C.30 from receiving a commercial certification in Britain in December of 1933 . However, by United States helicopter standards created in 1952 [55], modified in 1962 [56], and used through 1995, the flying qualities of this aircraft would not be acceptable. Flying quality considerations such as aircraft trim, with associated control position and stick force, are key subjects that receive considerable attention by aircraft engineers.

2.6 LONGITUDINAL TRIM

Understanding how a direct control autogyro trims out aircraft pitching moment, and how the stick position influences this trim,

is a very important subject. It was brought to Cierva's attention with a quite unfortunate, fatal accident caused by a change in airfoils while designing the C.30 . Prior to the C.30, all rotorcraft used airfoils having virtually zero pitching moment (see Appendix B) . For the C.30, Cierva chose to use a highly cambered airfoil, the Göttingen 606, which was developed in Germany. The intention was to improve rotor performance . This airfoil may, indeed, have raised performance, but the blades responded to the airfoil pitching moment with several degrees of periodic elastic twisting, which took trim control away from the pilot at high speed. The outcome was that at high speed, the C.30 could not be recovered from a high-speed dive. This led to the first fatal autogyro accident in Britain on January 21, 1935. The Air Ministry grounded their C.30s and initiated efforts by the National Physical Laboratory and the Royal Aircraft Establishment that were reported in references

[54] and [57]. The maximum speed of the C.30 was placarded at 1.5 times 85 miles per hour (i.e., 127 mph) by the Air Ministry until a fix was found. Brooks provides many more details about the situation in reference [7], pages 192 to 194.

The trim situation and how periodic elastic twisting could cause a very serious, if not catastrophic, problem was examined by Cierva [12] who passed his notes to J. A. Beavan and C. N. H. Lock. They analyzed the C.30 situation in depth, reported their findings [57] (in what I consider a classic piece of engineering), and showed that airfoil pitching moment easily explained the C.30 accident. In the United States, Kellett also used the Göttingen 606 airfoil in developing their KD-1 Autogiro (Fig. 2-21), and ran into the same adverse longitudinal trim situation as the Cierva C.30. Richard Prewitt, the chief engineer at Kellett, along with his staff, developed a

short-term fix for the problem. Prewitt wrote [43]:

"Shortly after the first flight of this autogiro [the KD-1 on December, 1934], we found it to be longitudinally unstable above eighty m.p.h. We developed a theory of this instability, based on the assumption that the slightly unstable blade sections caused a negative pitching moment when operating on the advancing side of the rotor where the velocities are high. This theory proved to be correct when small turned-up trailing edge tabs were attached at the tips of the blades. In fact the pitching moment coefficient of the blade section was over corrected to the extent that the pilot reported it required a heavy forward load on the stick at high speed. This over-correction was rectified by successively cutting off the inboard end of the tab section until a desired longitudinal stability was obtained. Fortunately, the lateral stability was improved with the correction in longitudinal stability."

Later, the flying qualities of the Kellett KD-1s were studied at the N.A.C.A. in Langley, Virginia. John Wheatley, another pioneer in autogyro rotor technology, wrote a number of exceptional reports that I will

discuss later. References [58] and [59] deal with blade elastic twisting. He used data from the N.A.C.A. flight testing of the KD-1 to show how influential airfoil pitching moment characteristics were on the longitudinal trim of the direct control autogyro. Work from Lock, Beavan, and Wheatley led to the Göttingen 606 airfoil being replaced by the NACA 23012 airfoil.

2.6 LONGITUDINAL TRIM

2.6.1 Fundamentals

Studying longitudinal trim, as Beavan and Lock did in reference [57], requires only the simplest force and moment diagram, which is provided in Fig. 2-23.

Beavan and Lock wrote only one longitudinal trim equation to analyze the C.30 accident as you can see in Appendix II of their report [57] . Their equation, Eq. (2.34) in more up-to-date symbols, was an aircraft pitching-moment equation written in the body axis system. The body axis system follows the conventional aircraft waterline and station line references used by draftsmen to layout, for example, the side view shown in Fig. 2-23 . Station lines are vertical lines that conventionally move from nose to tail. Station lines are perpendicular to water lines, which set vertical dimensions in the aircraft. The body axis reference system always rotates with the body, so that in Fig. 2-23, where the C.30 is shown landing nose up at the angle (Θ), this angle is measured between the gravity vector and a station line (or between the horizon and a waterline) . The aircraft angle of attack (α_{AC}) is measured between the flight path velocity ($V_{\text{Flight Path}} = V_{FP}$) and a

waterline.

(2.34) $\sum \text{Moments about c.g.} = 0 \approx M_p + \left(T_{hp}\, i_p + H_{hp}\right) a - T_{hp}\, c - L_t\, b \quad (+\text{Nose up})\,.$

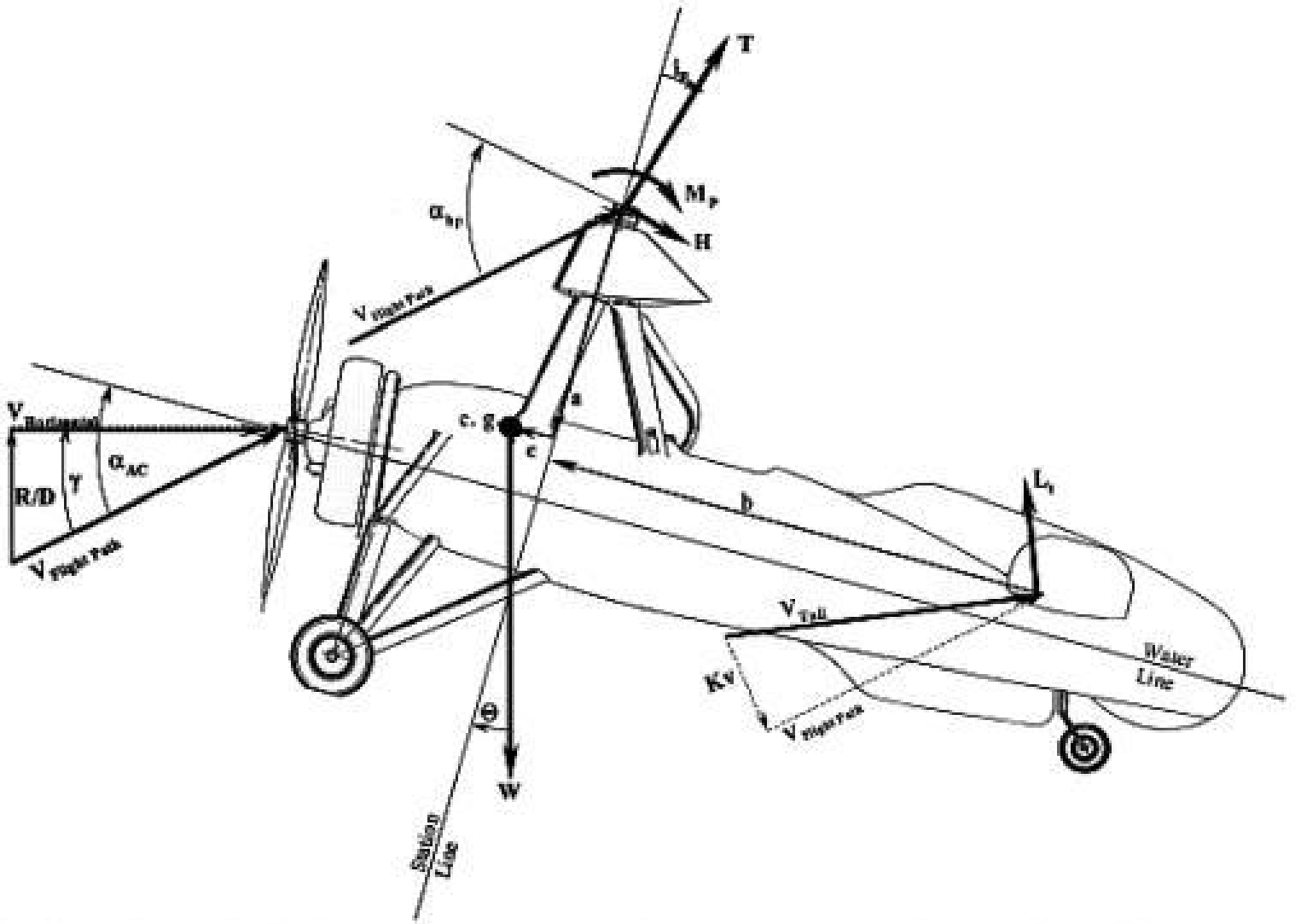

Fig. 2-23. The force and moment longitudinal trim diagram for the Cierva C.30 [52].

2.6 LONGITUDINAL TRIM

Beavan and Lock, in writing Eq. (2.34), accepted a number of assumptions in their aircraft pitching-moment trim analysis, including:

1. The C.30 was in level flight or only in a slight descent, so angles would be small, making sine of an angle equal to the angle (in radians) and cosine of an angle would be unity.
2. The propeller thrust acts as a force passing through the aircraft center of gravity (c.g.), and the propeller normal force and pitching moment would be zero. 3. The drag and lift forces of the fuselage (includes wheels, rotor support, etc.) act at 4.

the c.g.

The fuselage pitching moment without the horizontal stabilizer lift (L_t) would be zero.

5. The tail drag and pitching moment would be zero.
6. The rotor would induce a velocity on the horizontal tail.

Because of these assumptions, they did not worry about the force trim equations . They simply said that the propeller would provide thrust to overcome the drag of the C.30—whatever that might be—and they were satisfied with rotor thrust approximating the weight of the autogyro. However, for completeness here, the two force equations, written in the *flight path velocity coordinate system*, with many fewer assumptions, are

Parallel to the flight path velocity (positive is forward)

$$\sum F_X$$

$$= 0 = W \sin\gamma + T_{prop} \cos\left(\alpha_{AC} + i_{prop}\right) - H_{prop} \sin\left(\alpha_{AC}\right.$$

$$+i_{prop}) - D_{fuselage} \quad (2.35) \qquad - T_{hp} \sin \alpha_{hp}$$
$$- H_{hp} \cos \alpha_{hp} - L_{tail} \sin(\alpha_{AC} + i_{tail} - \alpha_{interference})$$
$$- D_{tail} \cos(\alpha_{AC} + i_{tail} - \alpha_{interference})$$

Perpendicular to the flight path velocity (positive is down)

$$\sum F_Z = 0 = W \cos \gamma - T_{prop} \sin(\alpha_{AC}$$
$$+i_{prop}) - H_{prop} \cos(\alpha_{AC} + i_{prop}) - L_{fuselage} \quad (2.36)$$
$$- T_{hp} \cos \alpha_{hp} + H_{hp} \sin \alpha_{hp} - L_{tail} \cos(\alpha_{AC}$$
$$+i_{tail} - \alpha_{interference}) - D_{tail} \sin(\alpha_{AC} + i_{tail} - \alpha_{interference})$$

While most of the symbols used in Eqs. (2.34), (2.35), and (2.36) are defined in Fig. 2-23, some additional information is needed. First of all, the propeller thrust (T_{prop}), which is not shown in Fig. 2-23 for clarity, acts perpendicular to the face of the propeller. The normal force of the propeller

(H_{prop}), also not shown, acts perpendicular to propeller thrust and is positive upwards. In addition, a propeller operating at angle of attack has a pitching moment (M_{prop}), also not shown, which is positive nose up. The face of the propeller need not be perpendicular to the aircraft waterline . In Fig. 2-23, I have shown the rotational axis of the propeller (i_{prop}) at a negative incidence because the C.30 propeller incidence was set to a nose- down angle of i_{prop} = –5 degrees.

2.6 LONGITUDINAL TRIM

The fuselage lift ($L_{fuselage}$), drag ($D_{fuselage}$), and pitching moment ($M_{fuselage}$) are not shown in Fig. 2-23 for the sake of clarity. These are conventional aerodynamic loads that generally are assumed to act at the aircraft center of gravity. These fuselage loads

follow conventional aircraft aerodynamics as described in any number of textbooks, for example, reference [60] . The horizontal stabilizer lift (L_{tail}) is shown in Fig. 2-23 because it is a major contributor to aircraft pitching moment, but neither stabilizer drag (D_{tail}) nor pitching moment (M_{tail}) is shown because they are generally small contributors to aircraft pitching moment. The horizontal stabilizer may not be installed parallel to a waterline. It can have some small angle of incidence (i_{tail}), which, in the case of the C.30, was i_{tail} = 2.0 degrees leading edge up. Loads from the vertical stabilizers are ignored completely in this study of the C.30 longitudinal trim.

The lifting rotor induces a downwash velocity (Kv) on the horizontal stabilizer. *This interference velocity is not small.* The immediate effect of this interference is to reduce the angle of attack of the stabilizer by

the angle ($\alpha_{interference}$), which Beavan and Lock [57] calculated "on the assumption that the rotor is equivalent to a monoplane aerofoil [wing] of the same lift and span with elliptical distribution of lift." This assumption defines the induced velocity (v)—*in rotorcraft aerodynamic terms*—as

$$v = \frac{T_{hp}}{2\rho\left(\pi R^2\right)V_{FP}}. \tag{2.37}$$

Actually, if Beavan and Lock had wanted to make calculations that included very low-speed flight including vertical descent, they had available the classical rotorcraft assumption from Glauert given in reference [13], which was

(2.38)

$$v = \frac{T_{hp}}{2\rho\left(\pi R^2\right)\sqrt{\left(V_{FP}\sin\alpha_{hp} - v\right)^2 + \left(V_{FP}\cos\alpha_{hp}\right)^2}}.$$

However, in their calculation of the interference angle ($\alpha_{interference}$), Beavan and Lock accepted (1) small angle assumptions; (2) simple wing theory applicable to reasonable flight path velocities; and (3) a value $K = 1.76$. They thus arrived at

$$(2.39)\quad \tan\alpha_{interference} \approx \alpha_{interference} \approx \frac{K\,v}{V_{FP}} = 1.76\left[\frac{T_{hp}}{2\rho\left(\pi R^2\right)V_{FP}^2}\right].$$

2.6.2 Blade Twisting Effect

Now let me return to the specific problem of why the Cierva C.30 Autogiro could not be pulled out of a high-speed dive. Beavan and Lock saw from their very simple aircraft pitching moment equation, Eq. (2.34),

that the rotor hub incidence (i_p) [and therefore the pilot longitudinal stick position (δ)] was explicitly given as

$$(2.40) \quad i_p = \frac{T_{hp}\, c - H_{hp}\, a + L_t b - M_p}{T_{hp}\, a}.$$

2.6 LONGITUDINAL TRIM

The solution task *only* required calculating rotor thrust (T_{hp}), rotor H-force (H_{hp}), hub pitching moment (M_p), and stabilizer lift (L_{tail}). Beavan and Lock calculated thrust, H-force, and hub moment using the simple equations Lock originally gave in reference [14], but with their addition of steady and cyclic elastic twisting. (Since the original work by Lock, several authors have revamped, extended,

changed notation, and otherwise adapted the equations as needed.)

Beavan and Lock did not bother to express their results in longitudinal stick position. Rather, the adverse C.30 longitudinal trim situation was clear enough once they had the hub incidence angle (i_p). However, for my purposes here, I will express the situation in longitudinal stick position ($\delta_{Long.}$). The C.30 longitudinal stick position was kinematically related to hub plane incidence (see discussion surrounding Fig. 2-20) as

(2.41) $\delta_{Long.} = (3\text{-in. long. stick per deg. hub incidence})\, i_p$.

The effect of the Göttingen 606 airfoil pitching moment coefficient ($C_m = -0.052$) must have been a real eye opener to these two engineers when they had their version of Fig. 2-24 in front

of them. What should have been a positive stick gradient requiring the pilot to move the stick forward to increase speed became dangerously adverse above 80 to 100 miles per hour. Their prediction of flight test data when blade elastic twist was included is impressive.

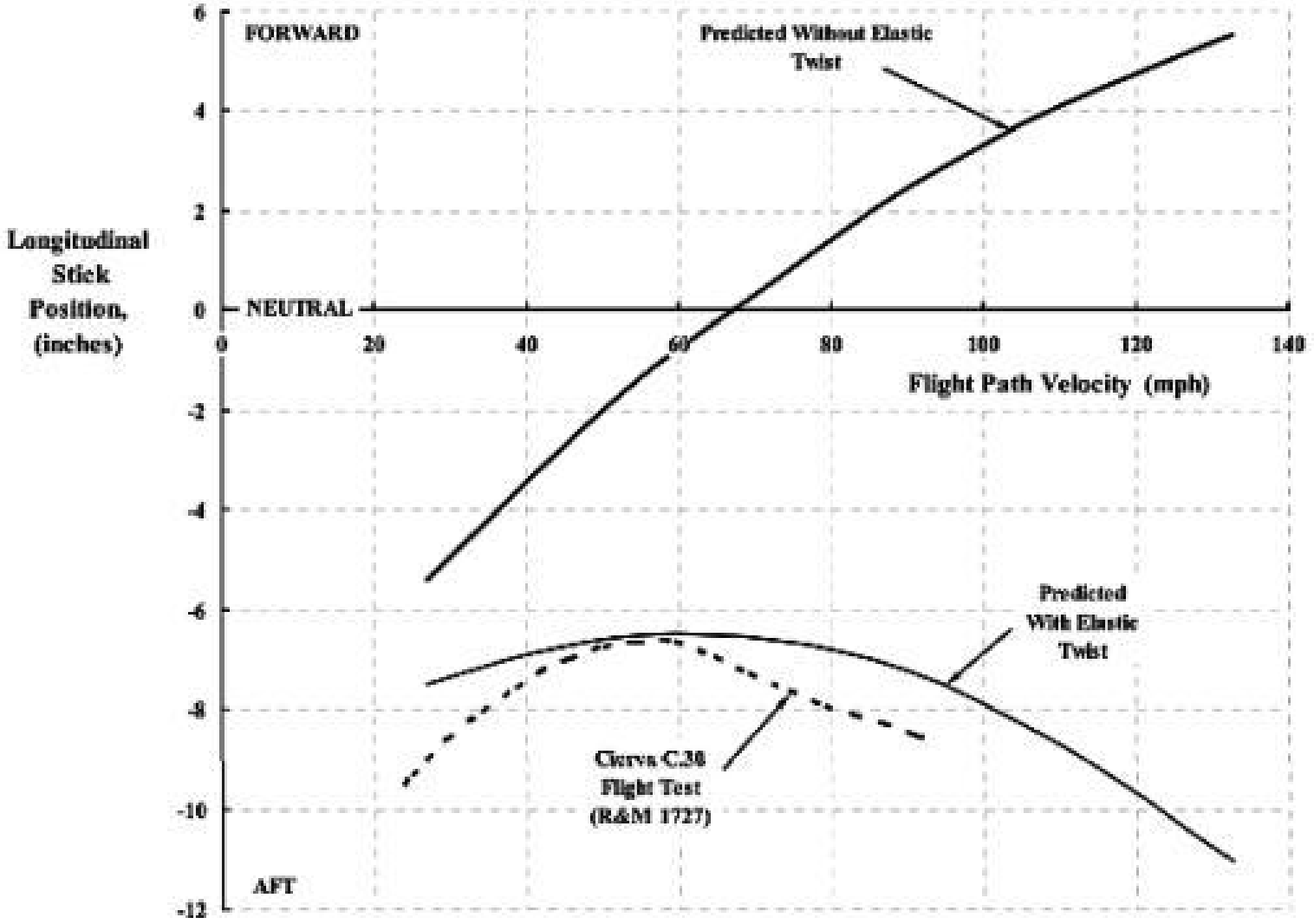

Fig. 2-24. Blade elastic twisting due to airfoil

pitching moment adversely affected the C.30 longitudinal trim.

2.6 LONGITUDINAL TRIM

Beavan and Lock satisfactorily traced the inability of a pilot to recover from a high-speed dive to longitudinal flapping (a_{1S}). What was happening was that the requirement for zero rotor rolling moment was being met by a combination of blade feathering, according to Eq. (2.1 1), and by flapping, according to Eq. (2.21). They found that, as speed increased with initial forward stick, elastic twisting tilted the rotor forward more than was required for trim, so the pilot was required to pull aft on the stick to bring the rotor tilt back. Unfortunately, the pilot ran out of aft stick margin, and from then on the autogyro began an outside loop! Brooks

recounts on pages 193 and 194 of reference [7] that a test pilot, Alan Marsh, flying a float-equipped military C.30, did recover from an outside loop situation by switching off the engine. Marsh landed on the water, restarted the engine, and taxied to shore. I can imagine Marsh wondering just who was flying the machine!

In analyzing the rotor behavior, Beavan and Lock improved the equations Lock gave in reference [14] with the addition of elastic twisting. First they derived a very reasonable equation estimating blade elastic twisting (see Appendix D), which they wrote (with a little of my rearranging) as

(2.42)

$$\text{Elastic } \theta_{x,\psi} \equiv E\theta_{x,\psi} = \left[\frac{A}{12}\left(4x - x^4\right) + \frac{\beta_o B}{6}\left(3x - x^3\right) + \left(\frac{A\mu_{hp}^2}{4} + \frac{C}{2}\right)\left(2x - x^2\right)\right]$$

$$+\frac{A\mu_{hp}}{3}\left(3x-x^3\right)\sin\psi-\frac{A\mu_{hp}^2}{4}\left(2x-x^2\right)\cos 2\psi$$

where the constants A, B, and C are

$$A=\frac{\rho c^2 R^4\Omega^2}{2GJ}C_m \qquad B=\frac{m x_{cg} R^3\Omega^2}{GJ}$$

$$C=\frac{m x_{cg} R^2 g}{GJ} \quad \text{and} \quad x=r/R.$$

They conveniently provided the needed C.30 rotor characteristics and operating conditions tabulated here:

Torsional stiffness, GJ	17,720 foot-pounds/radian per foot run of blade
Chord, c	0.917 feet
Radius, R	18.5 feet
Mass of blade per unit length, m	0.0615 slug per foot
Flapping hinge offset, r_0	1.75 inch (0.00788 R)
Spar axis behind airfoil leading edge	0.21091 feet (0.23 c)
Distance airfoil c.g. behind spar axis, x_{cg}	0.06 foot
Geometrical pitch at root, θ_{root}	0.0465 radians (2.664 degrees)
Weight moment, M_w	338.6 foot-pounds
Flapping inertia, I_{flap}	129.8 slugs per square foot
Air density, ρ	0.002378 slugs per cubic foot
Advance ratio, μ_{sp}	0.4 (Flight path velocity of 129 mph)
Rotor speed, Ω	25.65 rad/sec (245 rpm and tip speed of 474.6 fps)
Gravitational constant, g	32.17 feet-per-second squared
Airfoil angle of zero lift, α_o	–2.58 degrees (–0.04503 radians)
Blade coning angle, β_o	5.32 degrees (0.09285 radians)
Airfoil pitching moment, C_m	–0.052 (nose down is negative)

2.6 LONGITUDINAL TRIM

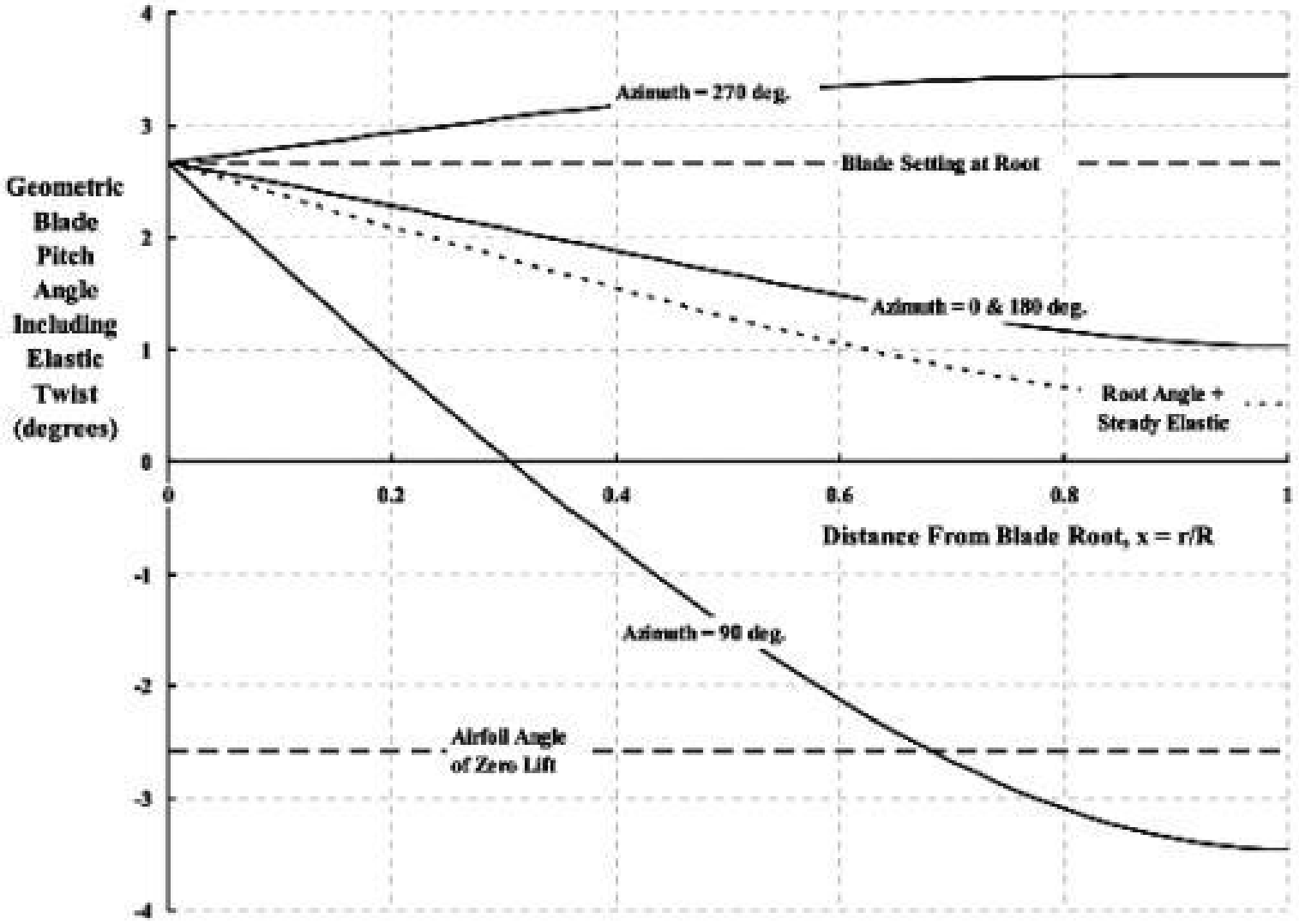

Fig. 2-25. C.30 blade elastic twisting due to airfoil pitching moment at high speed.

With the above information in hand, Beavan and Lock calculated blade elastic twist at four azimuth positions (ψ) for this high-speed point. They added the elastic twist to the blade-

root geometric pitch angle (θ_{root}) of 2.664 degrees . Their results, presented here as Fig. 2-25, show that at the blade tip (r = R) the cyclic elastic twist amounted to nearly ±3.5 degrees about a steady blade angle of 0.5 degrees. This newly found feathering angle behavior needed to be added into the rotor blade flapping equation.

In contrast to their rather accurate calculation of elastic twist, Beavan and Lock incorporated this elastic twisting into the rotor's contribution to longitudinal trim with a surprisingly crude approximation. They wrote that "In the first draft of the report [57] the approximate formula $\theta = \theta_o + \theta_1 \sin\psi$ was adopted, the values of θ_o and θ_1 being chosen to make θ coincide as nearly as possible with its value at 0.7R from the root, as given by the exact expression. This position was taken since, owing to the higher velocity there, the outer portions of the blades are much the most

important." Their revised equations for calculating rotor thrust (T_{hp}), rotor H-force (H_{hp}), hub pitching moment (M_p), and stabilizer lift (L_{tail}) were then rederived based on

(2.43)

$$\theta_\psi = \theta_{root} - \alpha_o + \left[0.213A + 0.293\beta_o B + 0.228A\mu_{hp}^2 + 0.455C\right] + 0.586A\mu_{hp}\sin\psi - 0.228A\mu_{hp}\cos 2\psi$$

2.6 LONGITUDINAL TRIM

The six rotor equations describing rotor behavior that Beavan and Lock wrote formed a classical foundation to rotorcraft rotor system technology.[8] In modern notation then, they first used advance ratio and inflow ratio as defined

earlier with Eq. (2.29), which is repeated here for convenience as

(2.29) $$\mu_{hp} = \frac{V_{FP}\cos\alpha_{hp}}{V_t} \qquad \text{and}$$

$$\lambda_{hp} = \frac{V_{FP}\sin\alpha_{hp} - v}{V_t}.$$

They ignored powers of advance ratio greater than squared and proceeded to assume simple first harmonic flapping (β) and first harmonic pitch angle (θ) of the form

(2.44)
$$\beta_\psi = \beta_o - a_{1S}\cos\psi - b_{1S}\sin\psi$$
$$\theta_\psi = \theta_o - B_{1C}\sin\psi$$

where they set $B_{1C} = -0.586\left(\frac{\rho c^2 R^4 \Omega^2}{2GJ}\right)C_m\mu_{hp}$.

Then, in the order needed for calculation, they

wrote (2.45)

$$\beta_o = \frac{\rho a c R^4}{2 I_{flap}} \left[\frac{1}{3}\lambda_{hp} + \frac{1}{4}\left(1+\mu_{hp}^2\right)\theta_o - \frac{1}{3}\mu_{hp} B_{1C} \right] - \frac{M_w}{I_{flap}\Omega^2}.$$

(Historically, it is worth noting that Lock introduced the notation $\gamma = \rho a c R^4 / I_{flap}$ in Part II of his March 1927 report, R&M 1127 [14]. At that time airfoil lift-curve slope (a) was taken as one-half of our modern lift-curve slope associated with $C_\ell = a\alpha$ where $a \approx 2\pi$. Thus, in 1927, when Lock wrote $\gamma = \rho(a \text{ in } 1927) c R^4 / I_{flap}$, he numerically meant our modern definition. Beavan and Lock adopted the modern definition for airfoil lift-curve slope in their April 1936 report [57], although they had a typographical error in their equation 11.)

$$(2.46)\quad b_{1S} = \frac{\frac{8}{3}\mu_{hp}\beta_o}{1+\frac{1}{2}\mu_{hp}^2} + A_{1C}\,.$$

$$(2.47)\quad a_{1S} = \frac{2\mu_{hp}\lambda_{hp} + \frac{8}{3}\mu_{hp}\theta_o - B_{1C}\left(1+\frac{3}{2}\mu_{hp}^2\right)}{1-\frac{1}{2}\mu_{hp}^2}\,.$$

They knew that the torque equation should reduce to zero for the autogyro autorotating rotor, so they wrote this key equation (updated to the modern form) as:

---

[8] The most elementary rotorcraft aerodynamic theory that derives six classical equations formulated by Lock is (in my mind) quite well explained in the book by Alfred Gessow and Garry Myers, *Aerodynamics of the Helicopter* [61]. This is a time-honored reference book that is still available and should be found in the library of

anyone interested in accumulating rotorcraft knowledge. Only the effect of blade elastic twisting (θ_e) in response to airfoil pitching moment (C_m) needs to be included, which I have done in Appendix E.

2.6 LONGITUDINAL TRIM

(2.48)

$$\frac{Q}{\rho b c R V_t^2 R} = \frac{C_{do}}{8}\left(1+\mu_{hp}^2\right) - \frac{a}{4}\left[\begin{array}{l} \lambda_{hp}^2 + \frac{2}{3}\theta_o\lambda_{hp} + \mu_{hp}\lambda_{hp}a_{1S} - \frac{1}{2}\mu_{hp}\lambda_{hp}B_{1C} + \frac{1}{2}\mu_{hp}^2\beta_o^2 - \frac{2}{3}\mu_{hp}\beta_o b_{1S} \\ + \frac{1}{4}\left(1+\frac{3}{2}\mu_{hp}^2\right)a_{1S}^2 + \frac{1}{4}\left(1-\frac{1}{2}\mu_{hp}^2\right)a_{1S}B_{1C} + \frac{1}{4}\left(1+\frac{1}{2}\mu_{hp}^2\right)b_{1S}^2 \\ + \frac{1}{3}\mu_{hp}\beta_o A_{1C} - \frac{1}{4}\left(1+\frac{1}{2}\mu_{hp}^2\right)b_{1S}A_{1C} \end{array}\right].$$

From just these first four equations, Beavan and Lock defined the autorotating rotor situation. They, with slide rule, pencil, and paper (or you, with a spreadsheet software like Microsoft® Excel®) first set values of rotor characteristics and operating conditions . This

gave them ρ, a, x_{cg}, c, R, M_W, I_{flap}, γ, θ_{root}, α_o, V_{FP}, rpm, $\mu_{hp} \approx V_{FP} / V_t$. They knew many of the blade input values "from measurements on the full scale blades made at the R.A.E." The Göttingen 606 airfoil characteristics, such as lift-curve slope (a), angle of zero lift (α_o), and pitching moment coefficient (C_m), were obtain from wind tunnel tests. Operating values, such as rotor speed (rpm), came from C.30 flight test data. All they had to do then was vary (λ_{hp}), recalculating all four equations until the torque equation became zero. They were searching for a positive inflow ratio, since only the positive root of the quadratic in Eq. (2.48) is applicable for an autorotating rotor. Now having the inflow ratio they could calculate rotor thrust (T_{hp}), H–Force (H_{hp}), and hub pitching moment (M_p)[9] from

(2.49)

$$\frac{T_{hp}}{\rho bcRV_t^2} = \frac{a}{2}\left[\frac{1}{2}\lambda_{hp} + \frac{1}{3}\left(1+\frac{3}{2}\mu_{hp}^2\right)\theta_o - \frac{1}{2}\mu_{hp}B_{1C}\right]$$

(2.50) $$\frac{H_{hp}}{\rho bcRV_t^2} = \frac{1}{4}\mu_{hp}C_{do} + \frac{a}{2}\left[\begin{array}{l}\lambda_{hp}\left(\frac{3}{4}a_{1S} - \frac{1}{2}\mu_{hp}\theta_o - \frac{1}{4}B_{1C}\right) + \beta_o\left(\frac{1}{4}\mu_{hp}a_{1S} - \frac{1}{6}b_{1S}\right) \\ a_{1S}\left(\frac{1}{4}\mu_{hp}a_{1S} + \frac{1}{3}\theta_o + \frac{1}{2}\mu_{hp}B_{1C}\right)\end{array}\right]$$

(2.51) $$M_P = \frac{F_C\, r_\beta\, b}{2} a_{1S}$$

The final steps were to calculate the hub plane angle of attack (α_{hp}) and, from the aircraft pitching moment equation, the hub plane incidence (i_p) using

(2.52) $$\tan\alpha_{hp} = \frac{\lambda_{hp}}{\mu_{hp}} + \frac{T_{hp}/\rho\pi R^2 V_t^2}{2\mu_{hp}\sqrt{\mu_{hp}^2 + \lambda_{hp}^2}}$$ and

$$(2.40)\quad i_p = \frac{T_{hp}\, c - H_{hp}\, a + L_t b - M_p}{T_{hp}\, a}.$$

---

[9] I have purposely left out a portion of the pitching moment caused by lateral flapping that arises when the flapping hinge is not at the center of rotation. Beavan and Lock correctly included the term even though it is quite small for the C.30 study they were doing. I will introduce the missing lateral flapping term later.

2.6 LONGITUDINAL TRIM

In Eqs. (2.49), (2.50), and (2.48), the thrust, H-Force, and torque coefficients are more commonly found today in coefficient form using a definition of solidity as the ratio of actual total blade area (bcR) to disc area (πR^2)—assuming a rectangular blade. Thus

$$\text{Solidity} \equiv \sigma = \frac{b\,c\,R}{\pi R^2} \quad \text{so} \quad b\,c\,R = \pi R^2 \sigma$$

(2.53)

$$\text{and therefore} \frac{C_{Thp}}{\sigma} = \frac{T_{hp}}{\rho\, bcR\, V_t^2}, \quad \frac{C_{Hhp}}{\sigma} = \frac{H_{hp}}{\rho\, bcR\, V_t^2}, \quad \text{and}$$

$$\frac{C_Q}{\sigma} = \frac{Q}{\rho\, bcR\, V_t^2 R}$$

There is more to be learned from the Beavan and Lock report [57] as Fig. 2-26 shows. The first computation these two engineers made was with a fixed collective pitch ($\theta = \theta_{root} - \alpha_o = 5.54$ deg) and no elastic twist. Their trim solution showed that thrust exceeded the C.30 flight test weight of

about 1,900 pounds, particularly at the higher speeds. This result is the top line in Fig. 2-26, where their calculated rotor thrust (T_{hp}) is shown next to the open- circle data points. I confirmed their longitudinal trim analysis results with simple spreadsheet software; then I recomputed the trim adjusting collective pitch so rotor thrust equaled weight AND aircraft pitching moment was zero.

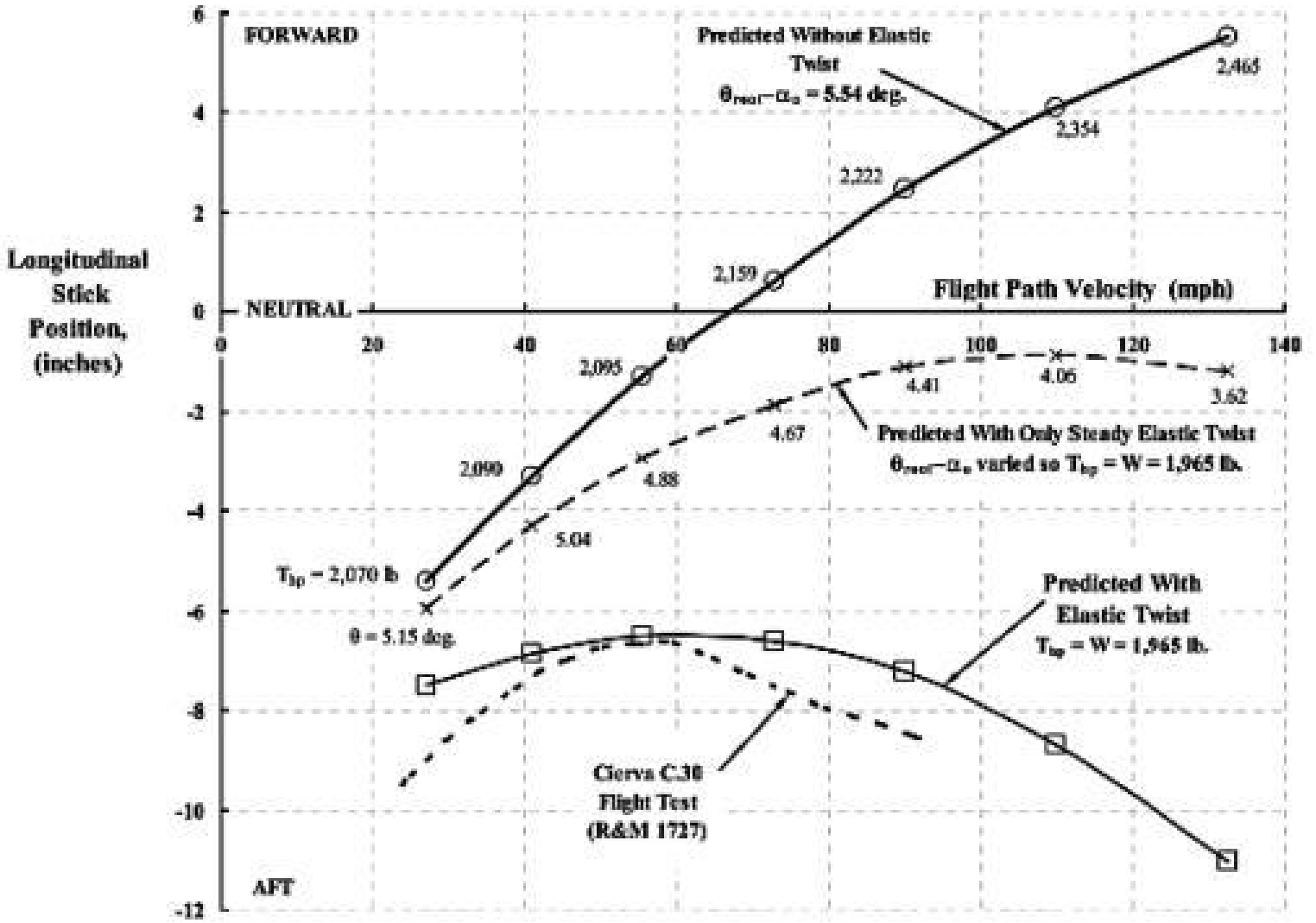

Fig. 2-26. C.30 longitudinal trim analysis.

2.6 LONGITUDINAL TRIM

My additional result is shown in Fig. 2-26 with the × symbols and a light dashed line. The collective pitch required is tabulated next to each × symbol . Clearly, elastic twisting, which reduces the mean collective pitch—the bracketed term in Eq. (2.43)—only accounts for about one-third of the C.30 adverse stick position characteristic . I suspect that if the flight- test-measured stick position trend with speed were no worse than my light dashed line, the C.30 would have been considered satisfactory. However, the periodic or cyclic elastic twisting created the dangerous characteristic of this Autogiro.

Beavan and Lock ended their report [57] with conclusions and "Further developments." Their opening sentence to conclusions was:

"The blades are found to twist to the extent of several degrees, in the sense that the mean pitch angle (at any radius) round the circle is decreased and that superimposed on this is a periodic variation."

They ended their conclusions with:

"[By] applying the results to the motion of a complete machine, much better agreement is now found with the experimental values obtained for incidence and stick position in gliding tests at the R.A.E., Farnborough. In particular, the somewhat anomalous reversal of stick position at the higher speeds is predicted."

Their recommendations for follow-on work have occupied the careers of more rotor system technology engineers than I could

possibly list. In April 1936, Beavan and Lock wrote:

"An attempt should be made on the more complex problem of the bending of the blades, where the inertia is not negligible as is the torsional moment of inertia of the [blade element] section.

In addition, further consideration may be needed with regard to the questions of tip loss and varying induced flow over the disc.

Wind tunnel measurements of the fuselage drag and rotor downwash on the tail are very desirable in order to make a more complete comparison of performance.

The question of longitudinal and lateral stability can also be attacked from the theoretical side."

2.6 LONGITUDINAL TRIM

2.6.3 Flapping and Feathering Interchangeability

The effect of cyclic torsional twisting was not the only key point Beavan and Lock made in their report [57] . They used C.30 experimental data to confirm the interchange between first harmonic pitch change (B_{1C}) and first harmonic longitudinal flapping (a_{1S}). They acknowledged, on page 1 3, "Cierva's conclusion that the [elastic] twist to some extent takes the place of [longitudinal] flapping." Further on they write that "this is in agreement with the theory of R & M 1127, Part I [14], where a non-twisting flapping rotor and a non-flapping blade whose pitch angle is varied sinusodially around the circle are compared."

The fact that either (B_{1C}) or (a_{1S}) can satisfy the zero rolling moment requirement was pointed out earlier with Eqs . (2.1 1) and

(2.21). The exact interchange as affected by longitudinal trim became clear with the Beavan and Lock analysis. A key point from their trim study is shown in Fig. 2-27. This figure points out that the rotor angle of attack as measured between the flight path velocity and the tip path plane (see Fig. 2-28) AND the aircraft angle of attack as measured between the flight path velocity and a waterline (see Fig. 2-23) are *nearly* independent of how the rotor zero rolling moment requirement is met—*provided the thrust equals weight in both cases*. Beavan and Lock proved this very important and useful point mathematically.

The proof that longitudinal flapping (a_{1S}) and cyclic pitch (B_{1C}) are interchangeable on a one-for-one basis starts with the assumption that flapping is a small angle and the statements that

(2.54) $\alpha_{hp} = \alpha_{tpp} - a_{1S}$ and therefore $\lambda_{hp} = \lambda_{tpp} - \mu_{tpp} a_{1S}$ and $\mu_{hp} = \mu_{tpp}$.

Then the hub plane inflow (λ_{hp}) can be replaced in the Beavan and Lock equation for flapping, Eq. (2.47), so that

$$a_{1S} = \frac{2\mu_{hp}\left(\lambda_{tpp} - \mu_{tpp}a_{1S}\right) + \frac{8}{3}\mu_{hp}\theta_o - B_{1C}\left(1 + \frac{3}{2}\mu_{hp}^2\right)}{1 - \frac{1}{2}\mu_{hp}^2}. \quad (2.55)$$

Now collecting terms gives

(2.56)

$$a_{1S}\left(1 - \tfrac{1}{2}\mu_{hp}^2\right) + a_{1S}\left(2\mu_{hp}^2\right) = a_{1S}\left(1 + \frac{3}{2}\mu_{hp}^2\right) = 2\mu_{hp}\lambda_{tpp} + \frac{8}{3}\mu_{hp}\theta_o - B_{1C}\left(1 + \frac{3}{2}\mu_{hp}^2\right)$$

and therefore, since the functions of advance ratio are the same for both longitudinal flapping (a_{1S}) and cyclic pitch (B_{1C}), you have

$$(2.57)\quad a_{1S} + B_{1C} = \frac{2\mu_{hp}\lambda_{tpp} + \frac{8}{3}\mu_{hp}\theta_o}{1 + \frac{3}{2}\mu_{hp}^2}.$$

2.6 LONGITUDINAL TRIM

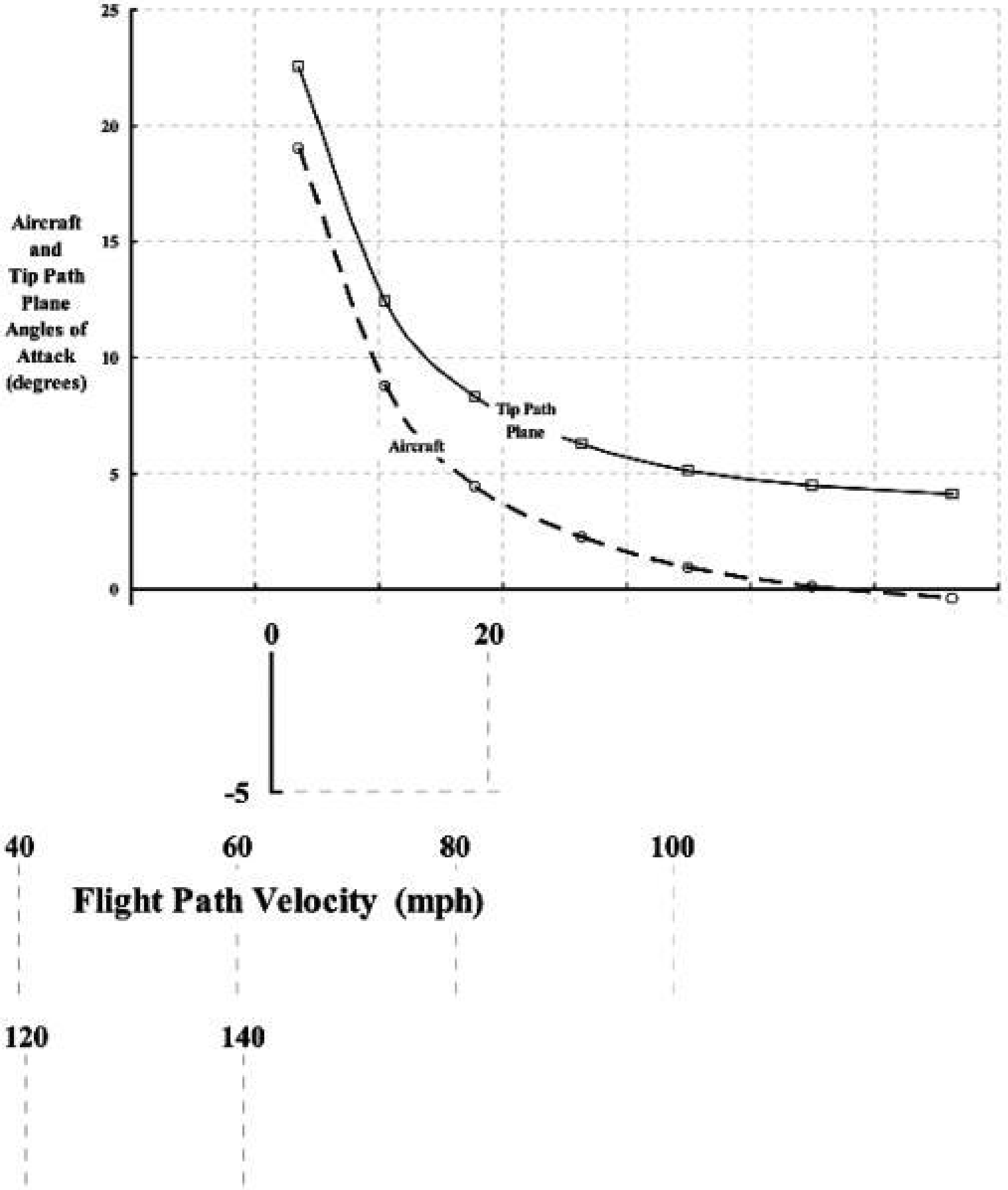

Fig. 2-27. Trimming with cyclic pitch *or*

longitudinal flapping result in nearly equal angles.

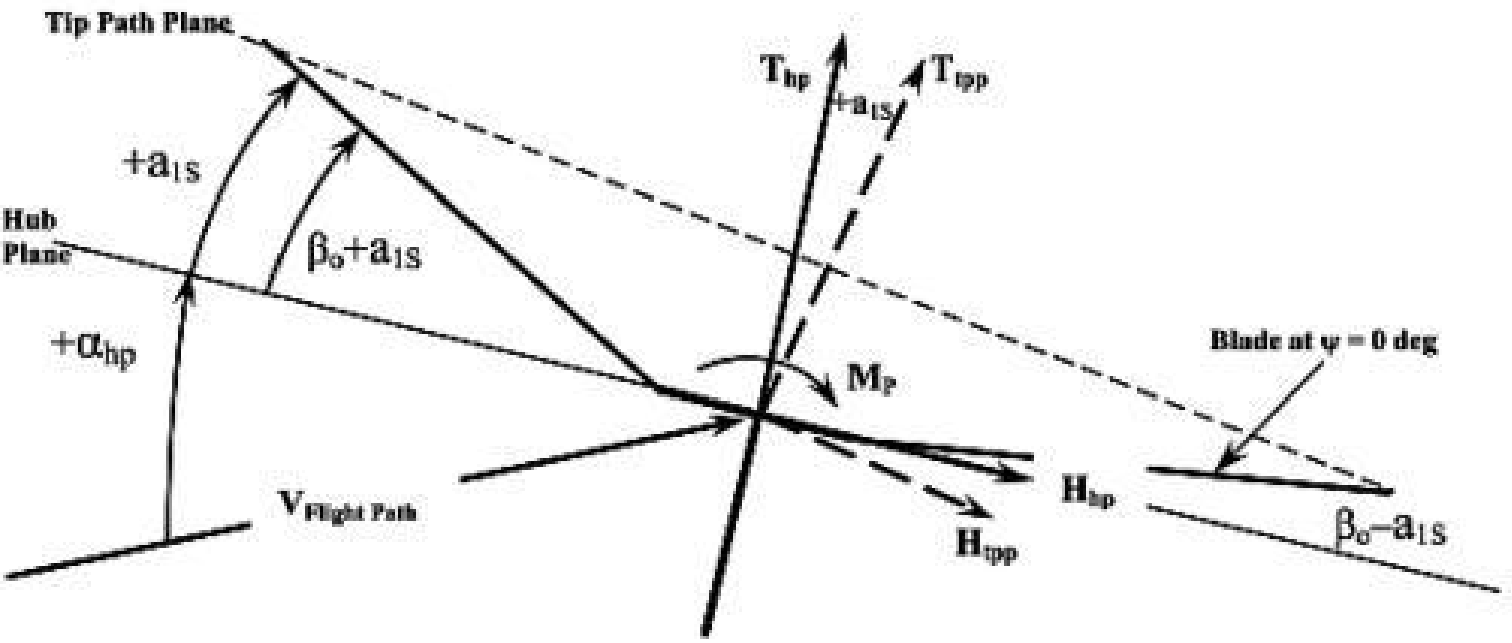

Fig. 2-28. The tip-path-plane angle of attack is the sum of the hub-plane angle of attack and the first harmonic longitudinal flapping, or $\alpha_{tpp} = \alpha_{hp} + a_{1S}$.

2.6 LONGITUDINAL TRIM

The longitudinal pitching moment trim

is *nearly* independent of whether the tip path finds its place in space with flapping (a_{1S}) or with cyclic pitch (B_{1C}). The reason *nearly* is italicized is because the hub pitching moment (M_p) depends directly on flapping (a_{1S}) according to

$$(2.51) \quad M_P = \frac{F_C \; r_\beta \; b}{2} a_{1S}$$

Therefore, if flapping is adjusted to zero with cyclic pitch according to

$$(2.58) \quad a_{1S} = \frac{2\mu_{hp}\lambda_{tpp} + \frac{8}{3}\mu_{hp}\theta_o}{1 + \frac{3}{2}\mu_{hp}^2} - B_{1C}$$

then the hub pitching moment will go to zero, and this will cause a change in the aircraft pitching moment solution. The change is very small in the case of the Cierva C.30 and hardly perceptible in Fig. 2-27. The reason for the small effect with the C.30 is that the flapping hinge offset (r_β) is only 1 .75 inches or 0.00788R. Thus, the aircraft pitching moment solution is driven much more by the rotor forces

(T_{hp} and H_{hp}) times their moment arms to the aircraft center of gravity, than by the hub pitching moment (M_p).

One other contribution Glauert [1 3], Lock [14], and Beavan and Lock [57] made must be mentioned before closing this discussion of longitudinal trim. They provided a much simpler way to solve for the torque (or power) that a rotor required to produce lift. Their original calculations were based on Eq. (2.48), repeated here for convenience as

(2.48)

$$\frac{Q}{\rho b c R V_t^2 R} = \frac{C_{do}}{8}\left(1+\mu_{hp}^2\right) - \frac{a}{4}\left[\begin{array}{l} \lambda_{hp}^2 + \frac{2}{3}\theta_o\lambda_{hp} + \mu_{hp}\lambda_{hp}a_{1S} - \frac{1}{2}\mu_{hp}\lambda_{hp}B_{1C} + \frac{1}{2}\mu_{hp}^2\beta_o^2 - \frac{2}{3}\mu_{hp}\beta_o b_{1S} \\ + \frac{1}{4}\left(1+\frac{3}{2}\mu_{hp}^2\right)a_{1S}^2 + \frac{1}{4}\left(1-\frac{1}{2}\mu_{hp}^2\right)a_{1S}B_{1C} + \frac{1}{4}\left(1+\frac{1}{2}\mu_{hp}^2\right)b_{1S}^2 \\ + \frac{1}{3}\mu_{hp}\beta_o A_{1C} - \frac{1}{4}\left(1+\frac{1}{2}\mu_{hp}^2\right)b_{1S}A_{1C} \end{array}\right].$$

Through a number of substitutions (plus

pencil, paper, and elbow grease), they proved that this cumbersome torque equation was nothing more than

(2.59)

$$\frac{C_Q}{\sigma}=\frac{C_P}{\sigma}=\frac{C_{do}}{8}\left(1+\mu_{hp}^2\right)-\lambda_{hp}\left(\frac{C_T}{\sigma}\right)_{hp}-\mu_{hp}\left(\frac{C_H}{\sigma}\right)_{hp}.$$

In fact, when the coefficient form was stripped away, things got even simpler because

(2.60)

$$\text{Power}=Q\Omega=T_{hp}v-\left(T_{hp}\sin\alpha_{hp}+H_{hp}\cos\alpha_{hp}\right)V_{FP}+\frac{\rho\left(\pi R^2\right)V_t^3\sigma C_{do}}{8}\left(1+3\mu_{hp}^2\right)$$

and furthermore $\left(T_{hp}\sin\alpha_{hp}+H_{hp}\cos\alpha_{hp}\right)$ is just rotor drag.

2.6.4 Stick Vibration

The addition of mechanical rotor startup and direct control, the removal of the wing, the installation of more power per pound of gross weight, and the correction of elastic twist effects on trim plus other improvements led the military of several countries to seriously consider autogyros for field evaluation. Problems with stick vibration [62] with direct control rotors, however, began to be openly talked about. In fact, Captain Franklin H. Gregory, who was championing rotary wing aircraft in the U.S. Army [25], commented about the stick shake shortcoming at the banquet following the Second Annual Rotating Wing Aircraft Meeting. This was the evening of December 1, 1939. The banquet toastmaster, Laurence Le Page, invited Captain Gregory to

say a few words, which were transcribed into the end of the meeting proceedings. After a pleasant joke, Gregory closed with two thoughts:

"The rotary winged aircraft, the present rotary winged aircraft, does land in a surprisingly small amount of space, and every time I fly one across the country—particularly with a head-wind, I get discouraged because you don't go fast, but, on the other hand, I always fly low because the head-winds are also smaller down low and I think it is great because if the engine stops any of those fields down below are possible landing spaces. That is a fact.

But, again, getting out on arriving at my destination I say 'Hello, Joe, how are you. ' (Making motion of hand quivering) Those of us that know anything of the present rotary winged aircraft know that the stick is directly connected to the rotor and there are certain vibrations transmitted to the stick and the stick does assume a periodic motion in the cockpit and, after flying a few hours you forget you haven't got that stick. So, to you engineers, I say, remove that shake and you have increased your popularity with the pilots tremendously."

Shortly thereafter, the Army Air Corps lent the N.A.C.A. a YG-1B (a military version of the Kellett KD-1 pictured in Fig. 2-21) to specifically investigate control stick vibration. F. J. Bailey reported the investigation results in reference [63] in June of 1940.

Bailey, who presented a paper at the Second Rotating Wing Aircraft Meeting (and presumably went to the banquet), begins his report introduction with:

"Conventional three-bladed direct-control autogiros of the tilting-hub type are generally regarded as unsuitable for extended cross-country flights, largely because of severe vibration of the control stick that appears at airspeeds above 80 miles per hour. The importance of the problem of stick vibration has been recognized by designers and several solutions have been proposed."

In the report summary, Bailey wrote that:

"The most important component of the variation in stick

force was found to have a frequency of three times the rotor speed and an amplitude that rose from negligible values at tip-speed ratios [V_{FP}/V_t] below 0.20 to ± 5.2 pounds longitudinal and ± 3.2 pounds lateral at tip-speed ratios of 0.35 . Variations in stick force at all other frequencies were small in comparison with those at three times the rotor speed."

2.6 LONGITUDINAL TRIM

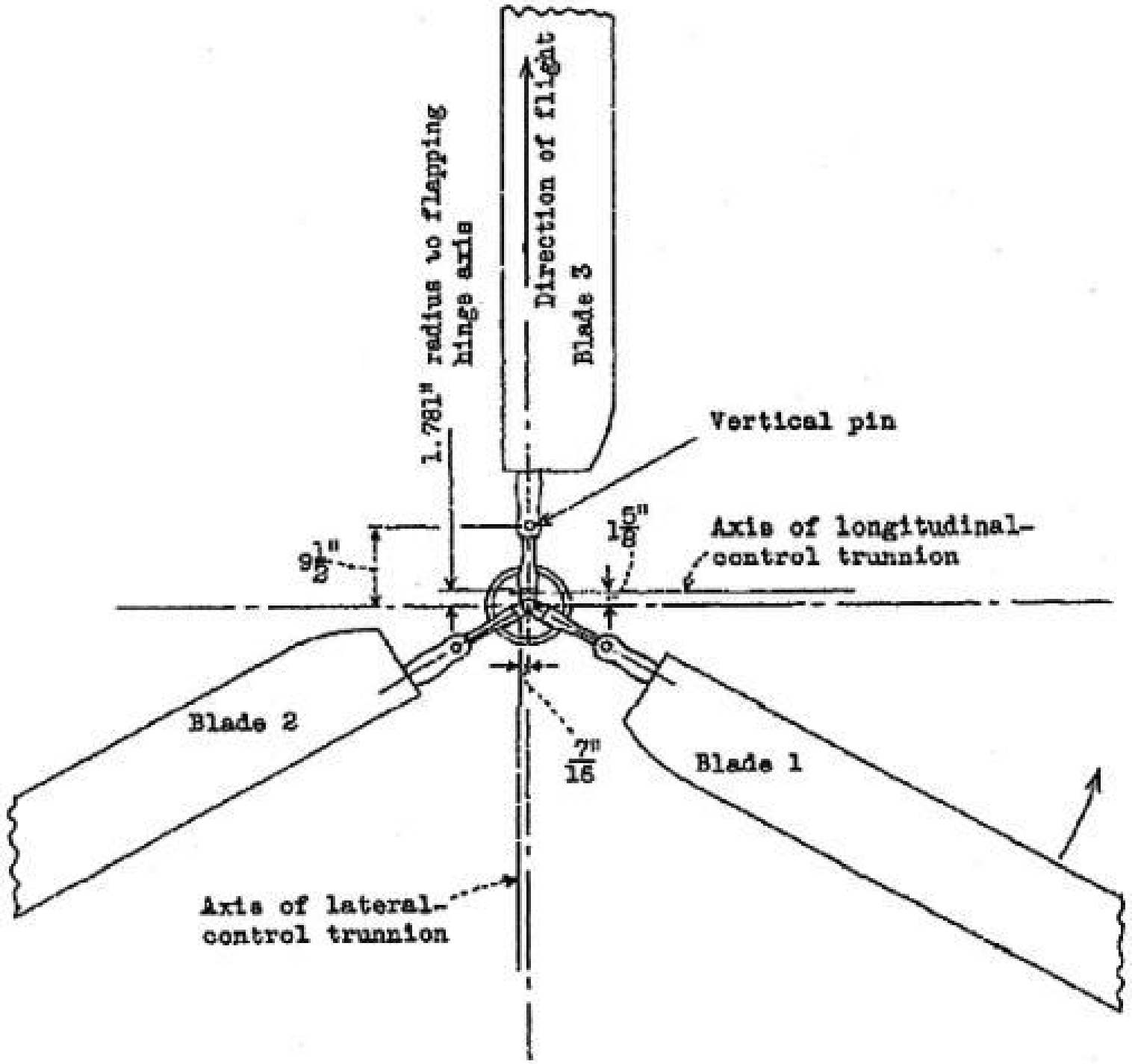

Fig. 2-29. The Kellett YG-1B rotor system [63].

The report Bailey presented contained a sketch of the Kellett YG-1B rotor system, Fig. 2-29, which was 40 feet in diameter and

rotated counterclockwise when viewed from above. The blade chord was 12 inches, but he noted that "over the outboard portion of the blades, between 72 and 93 percent of the radius, the chord was extended 1 inch by a trailing- edge tab. The tab was reflexed [bent up] approximately 10° to counteract the unstable center- of-pressure travel of the Göttingen 606 [airfoil] section." The sketch Bailey included shows that the hub pitched fore and aft about an axis 1-5/8 inches ahead of the rotor rotational axle; the hub rolled left and right about an axis 7/16 inches to port of the rotor rotational axle. Both of these "trunnions" were located in a plane 2-3/4 inches below the plane of the flapping hinges.

A "control-force recording stick" was calibrated by loads acting about 1.9 feet above "a flexible, elastic section located near its lower end" that allowed deflection to be recorded on film. The calibration expressed

moments about the trunnions in terms of stick force. The

calibration figures given were: 7.3 foot-pounds of longitudinal trunnion moment per 1 pound of longitudinal stick force, and 10 foot-pounds of lateral trunnion moment per 1 pound of longitudinal stick force. Bailey gave no other information about the control system.

Bailey gives representative example waveforms of the "control-force recording stick" marked on the film. A tick mark on the film was made by a once-per-revolution counter, so that zero azimuth could be defined. The waveform, a Y versus azimuth trace, was then measured every 10 degrees by

ruler to obtain a tabulated set of longitudinal and lateral moments versus azimuth. Then a 12-harmonic Fourier series was calculated that best fit the waveform. The "control-force recording stick" had a natural frequency of 3 1 cycles per second, so each harmonic of the recorded data was corrected for the instrument's dynamic amplification. The resulting waveform was so dominated by three cycles per rotor revolution and six cycles per rotor revolution, that Bailey used just the following simple Fourier series to present the final results:

(2.61) $\Delta M_{\psi} = A_3 \cos 3\psi + B_3 \sin 3\psi + A_6 \cos 6\psi + B_6 \sin 6\psi$.

He removed the steady moment and tabulated the coefficients A_3 through B_6 for both longitudinal and lateral moments at the nine speeds where measurements were obtained. His reasoning for not including the

steady was that the steady only "indicated failure to trim out the average stick forces [to zero] with the bungee."

Longitudinal moment about the hub pitch axis, Fig. 2-30, and lateral moment about the hub roll axis, Fig. 2-31, illustrate the 3-per-rev character of the control loads at 97 miles per hour. In these 2 figures, I have shown the Bailey 12-harmonic Fourier series fit to the recorded data, which are shown with the symbols. The waveform after correction for the dynamic response is also shown. This corrected moment waveform, *when expressed as a stick shake in pounds*, is described mathematically as

(2.62) $\text{Long. Stick Force} = 1.712\cos 3\psi + 3.740\sin 3\psi + 0.014\cos 6\psi + 0.904\sin 6\psi$

(2.63) $\text{Lateral Stick Force} = -2.50\cos 3\psi + 1.50\sin 3\psi - 0.45\cos 6\psi - 1.30\sin 6\psi$.

A very informative view of stick shake is shown in Fig. 2-32. Rather than waveforms plotted versus azimuth, the vibratory longitudinal stick force, Eq. (2.62), is plotted versus the vibratory lateral stick force, Eq. (2.63), in Fig. 2-32. As you look at this graph, keep in mind that your hand is being shaken three times per revolution and in a somewhat diagonal sense. You would feel a vibration at roughly 10 cycles per second, which is a very fast pounding. Bailey noted that stick vibration at low speed was "negligible." This would correspond to the flight path speed of 62 miles per hour, which is the smallest ellipse shown on the figure. He also noted in his report's introduction that "severe vibration of the control stick appears at air speeds above 80 miles per hour." That vibration level is the one next to the smallest ellipse on Fig. 2-32. One can only guess about the comments from the pilot regarding stick shake at the 108-miles-per-hour

test point!

67 2.6 LONGITUDINAL TRIM

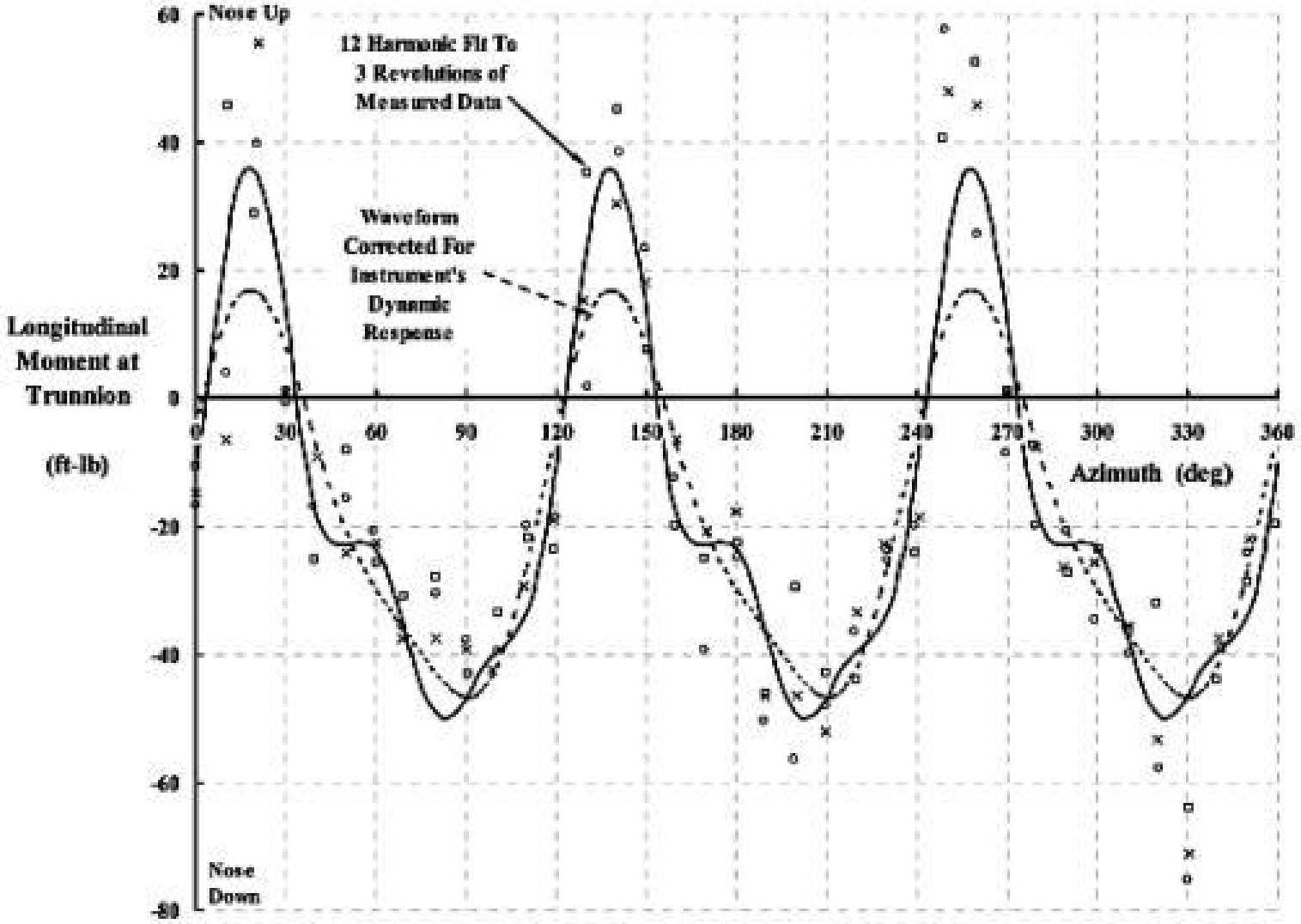

Fig. 2-30. Longitudinal moment at the hub pitch trunnion at 97 mph [63].

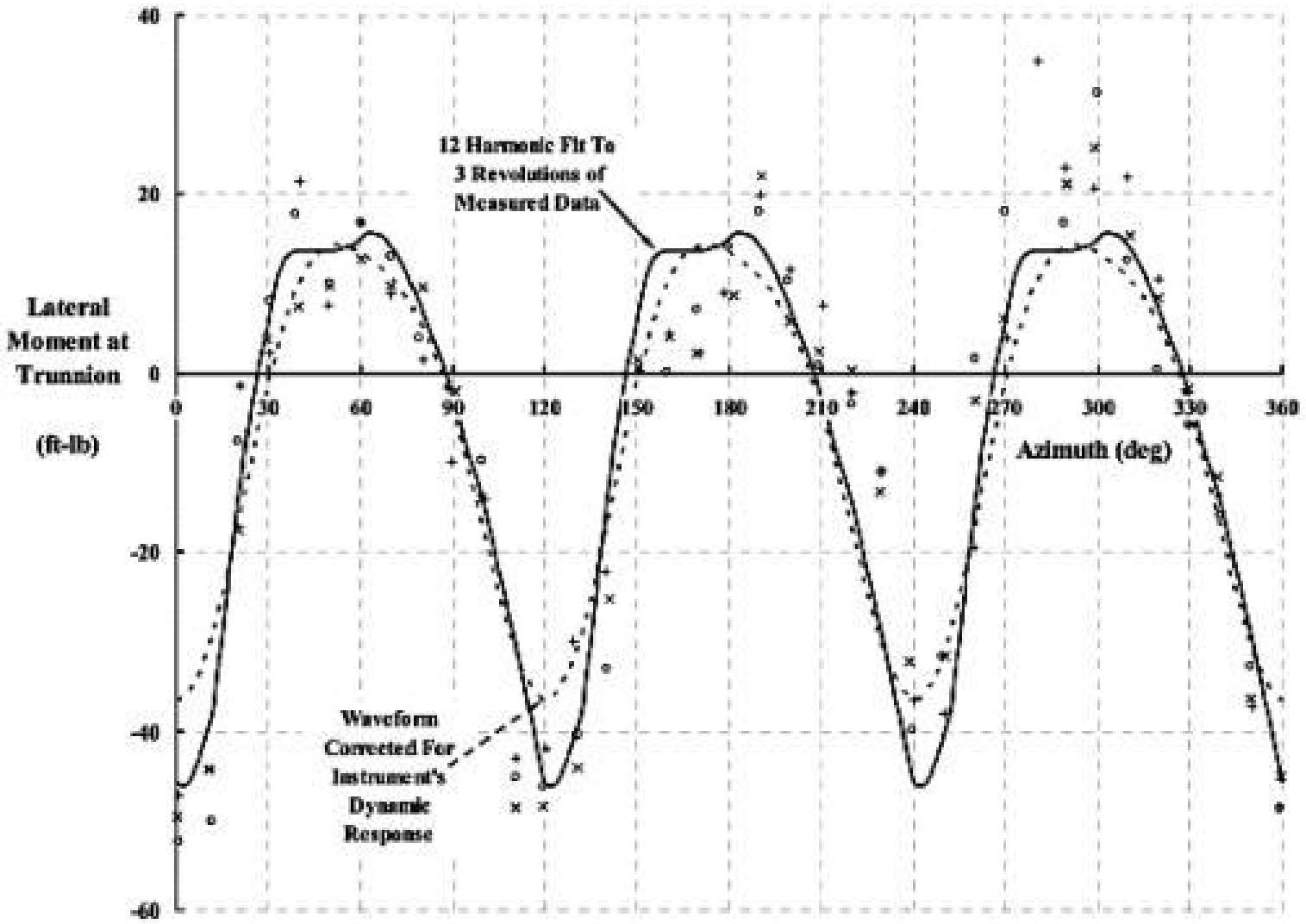

Fig. 2-31. Lateral moment at the hub roll trunnion at 97 mph [63].

2.6 LONGITUDINAL TRIM

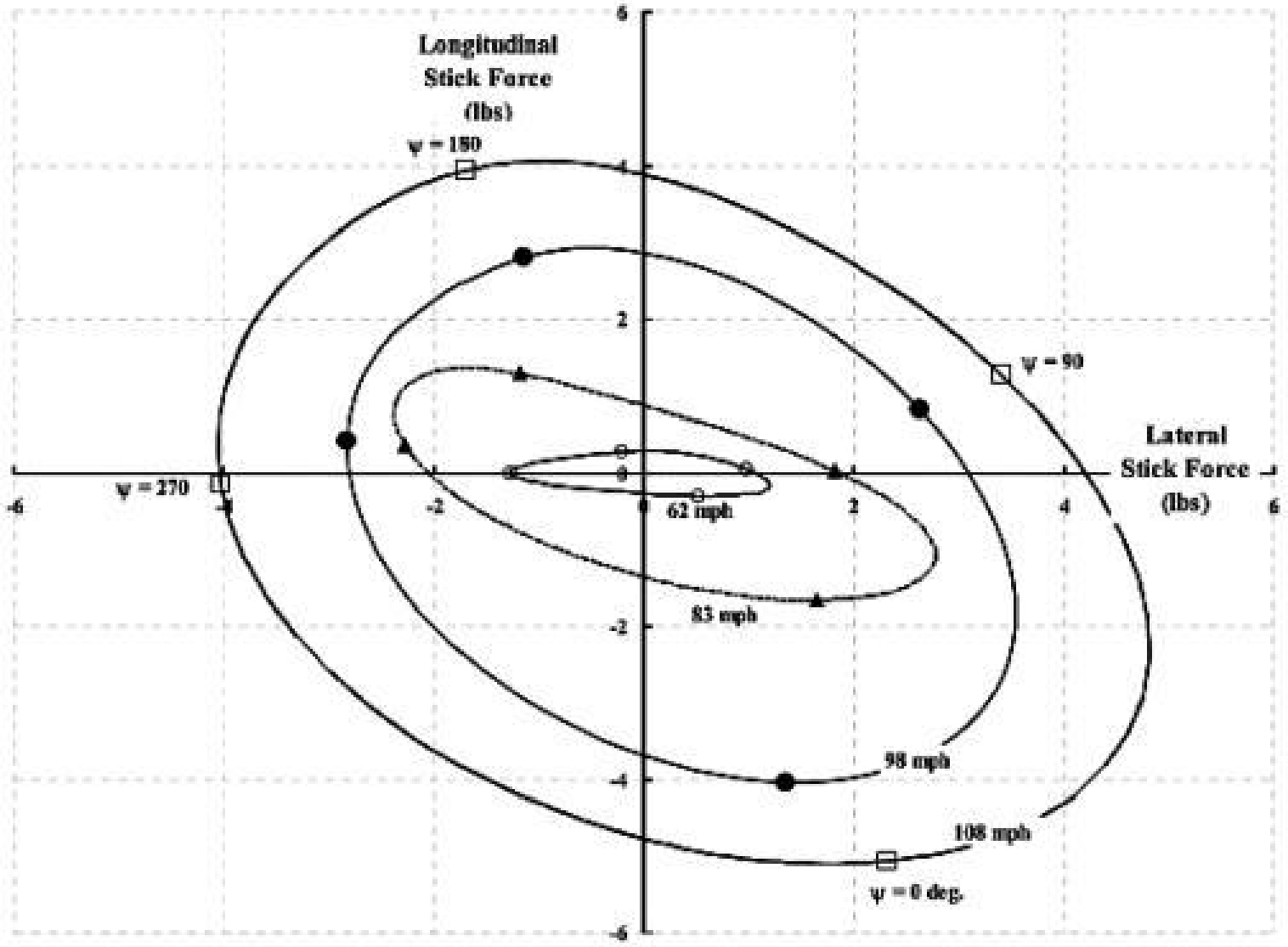

Fig. 2-32. The YG-1B stick vibration increased with speed [63].

Calculating control loads and stick forces—even in the year 2010 with the best of theories and computers—is "iffy" at best. The problem can be addressed, but without

including blade bending (over and above flapping), twisting, and lead-lagging, no meaningful estimates can be made . Even Cierva [12] was just beginning to scratch the surface of the problem in the early 1930s.

There is, however, something to be learned without knowing all the details of the problem. Consider this question arising from the Bailey report: Why were the stick forces dominated by the three-per-rev waveform and, to a lesser extent, six-per-rev harmonics? The answer begins with the simplest view given in Fig. 2-33 . Suppose only one force, a vertical force, is acting at the flapping hinge . Assume there is no flapping moment at the hinge. This is not correct because the hinge uses bearings and the friction from a bearing creates a moment, which Pecker [44] shows is not insignificant. Now, thinking of the Bailey planform view, Fig. 2-29, the vertical force ($F_{Blade\ 1}$) creates a nose-down moment about the longitudinal

control trunnion located a distance (a = 1-5/8 inches) ahead of the rotor axis. The moment arm of this vertical force must include the flapping hinge offset r_β = 1.781 inches. Therefore, the moment contribution from Blade 1 is

2.6 LONGITUDINAL TRIM

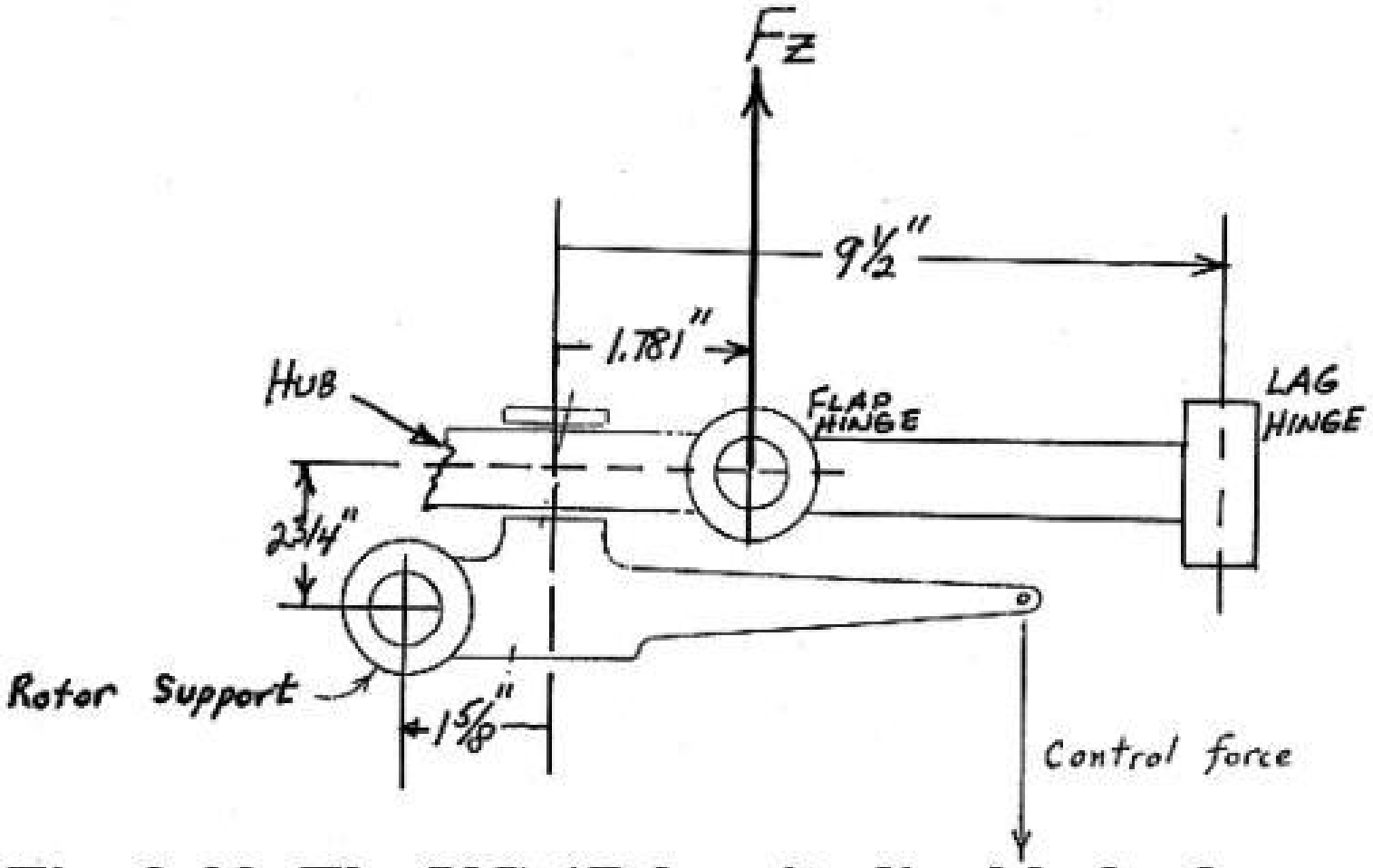

Fig. 2-33. The YG-1B longitudinal hub plane

tilting geometry. The hub is in the rotating system and the blade is shown at ψ = 0 degrees. The nonrotating longitudinal control trunnion is 1-5/8 inches forward of the rotor hub axle.

(2.64) $\text{Blade 1 Moment} = -\left(a + r_\beta \cos\psi\right) F_{\text{Blade1}}$.

Blade 2, following Bailey's sketch, Fig. 2-29, trails behind Blade 1 by 120 degrees, so it puts in a nose-down moment of

(2.65)

$$\text{Blade 2 Moment} = -\left[a + r_\beta \cos\left(\psi - 120^\circ\right)\right] F_{\text{Blade2}} .$$

Blade 3, following Bailey's sketch, trails Blade 1 by 240 degrees, so it puts in a nose-up moment about the trunnion of

(2.66)

$$\text{Blade 3 Moment} = -\left[a + r_\beta \cos\left(\psi - 240^\circ\right)\right] F_{\text{Blade3}} .$$

Now think about the total moment created by the sum of each blades' contribution.

The three blade moments, when added together (and after a little trigonometry is applied), give a pitching moment about the longitudinal control trunnion of (2.67)

$$\text{Trunnion Moment} = -a(F_1+F_2+F_3)+\frac{\sqrt{3}}{2}r_\beta(F_3-F_2)\sin\psi+\frac{1}{2}r_\beta(F_3+F_2-2F_1)\cos\psi.$$

2.6 LONGITUDINAL TRIM

Now imagine that the vertical force of blade 1 varies periodically with azimuth and can be approximated by a Fourier series of the form

(2.68) $F_1 = F_o + F_{1S}\sin\psi + F_{1C}\cos\psi + F_{2S}$

$\sin 2\psi + F_{2C}\cos 2\psi + F_{3S}\sin 3\psi + \text{etc.}$

If the other two blades are a perfect match with

blade 1, then their vertical force becomes

$$(2.69)\quad F_2 = F_o + F_{1S}\sin(\psi-120^\circ) + F_{1C}\cos(\psi-120^\circ) + F_{2S}\sin 2(\psi-120^\circ) + F_{2C}\cos 2(\psi-120^\circ) + \text{etc.}$$

$$(2.70)\quad F_3 = F_o + F_{1S}\sin(\psi-240^\circ) + F_{1C}\cos(\psi-240^\circ) + F_{2S}\sin 2(\psi-240^\circ) + \text{etc.}$$

It is a simple matter to make the substitutions of the force equations (2.68), (2.69), and (2.70) into the trunnion moment Eq. (2.67). After you do the substitution and tackle the trigonometry, you get

Trunnion

$$\text{Moment} = -a\left[(3F_o) + (3F_{3S})\sin 3\psi + (3F_{3C})\cos 3\psi\right]$$

(2.71)

$$-\frac{r_\beta}{2}\left\{(3F_{1C})+\left[(3F_{2S})+(3F_{4S})\right]\sin 3\psi+\left[(3F_{2C})+(3F_{4C})\right]\cos 3\psi\right\}$$

There are three things you should notice about this result:

1. All the force harmonics that appear in Eq. (2.71) have been multiplied by 3, which is the number of blades (b).

2. The force sum ($F_1+F_2+F_3$) acting at the arm (a) only has a steady component ($3F_o$) and the three-per-rev components ($3F_{3S}$) and ($3F_{3C}$). This shows the other harmonics have cancelled out in going from the rotating system (i.e., the hub) to the nonrotating system (i.e., the trunnion). The next harmonic in the pattern would be a six per rev. Note that ($3F_o$) is the rotor thrust (T_{hp}).

3. The hub moment terms, those containing

the hinge offset (r_β), involve the force harmonics that are one less than the blade number (b) and one more than the blade number (b). This means moments translate from the rotating to the nonrotating system at harmonic frequencies of (b –1) and (b+1). The next harmonics in the pattern would be at six per rev and involve (F_5) and (F_7).

The reason Bailey saw control load waveforms that were dominated by three per rev and, to a much less extent, six per rev, was because the Kellett YG-1B Autogiro had three blades— *that were nearly perfectly matched.* If the blades had been mismatched to any greater extent, the canceling of certain force harmonics would not occur, and the control load required to balance the trunnion moment would have severely shaken the pilot stick even more.

Gessow and Myers [61] provide a short

chapter at the end of their classic book that will introduce you to other vibration problems.

2.7 SWASHPLATE CONTROL

While Cierva and Pitcairn continued to equip their Autogiros with direct control rotors into the early 1 930s, others (notably Raoul Hafner and David Kay in England, and E. Burke Wilford and Richard Prewitt at Kellett in the United States) made a practical design for the pilot to directly control the blade incidence or pitch angle (θ) shown fixed in Fig. 2-7 and Fig. 2-10. The Wilford design is particularly noteworthy. He successfully developed what he referred to as a "gyroplane," Fig. 2-34, that first flew in August 193 1 . He intended to compete directly with Cierva, Pitcairn, and Kellett, using a very different rotor system and

control system. The Wilford rotor system, about 40 years ahead of its time, had neither flap nor lead- lag hinges, and, in terminology used today, was clearly a "hingeless" rotor system. You should recall that Cierva apparently tried some form of this control system on his second prototype as noted earlier in the rolling moment discussion, Section 2.1 . Wilford incorporated a blade incidence control system, Fig. 2-35, that made use of Eq. (2.57). He based his design, in part, on the inventions patented, and the prototype built, by Rieseler and Kreiser in Germany in 1926 [64-66] . The successful application by Wilford, Kay, Hafner, and Kellett was to become the key element in helicopter control and stability.

Fig. 2-34. The first E. Burke Wilford "gyroplane" after some modifications

on August 5, 1932 (photo courtesy of Wayne Wiesner).

D = 32, A = 804, bcR = 72, Chord = 1.125 feet = 13.5 inches, RPM = 170, S_w = 100, V_{cr} = 85 mph, V_{land} = 26 mph, GW = 1800, Jacobs = 160 hp, DL = 2.24. First flight without wing on October 1, 1932.

2.7 SWASHPLATE CONTROL

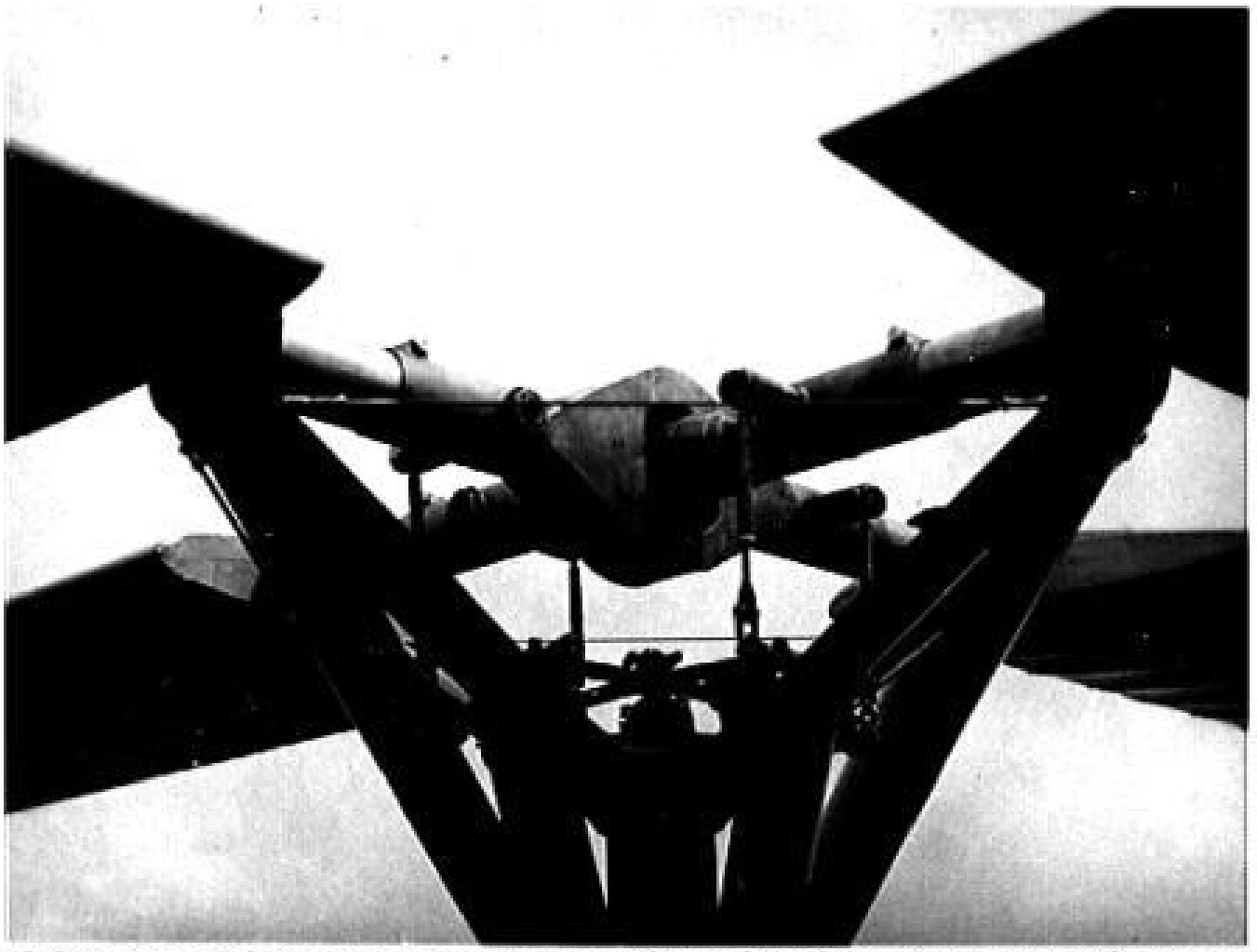

Fig. 2-35. The Wilford rotor system had neither flapping nor lead-lag hinges. Instead, blade feathering followed Eq. (2.57) to zero the rolling moment (photo courtesy of Wayne Wiesner).

2.7.1 The E. Burke Wilford Rotor System

The details of the Wilford rotor system are shown in Fig. 2-35 and, in my very rough sketch, Fig. 2-36, which follows shortly. There were neither flapping nor lead-lag hinges. The centrifugal force of one blade was exactly counteracted by its pair, which is a very light structural arrangement for blade retention. The four blades, grouped in counteracting pairs, were all fixed at the same root collective pitch angle (θ_o). Each blade pair could change pitch cyclically (that is, they followed $\theta_\psi = \theta_o - B_{1C} \sin\psi - A_{1C} \cos\psi$) because of the feathering

bearings located just inboard of where the blade airfoil contour ends. Each blade in a pair had its cyclic pitch controlled by a pitch link. The bottom end of each pitch link was controlled by one arm of a "spider," an early version of what is called a swashplate today. The four-arm spider rotated with the blades about its own ball bearing. The inner race of the spider bearing was attached to a nonrotating rod and

ball assembly that could tilt the spider about the ball just below the spider. Thus, the plane of the four-arm spider could be inclined relative to the rotational axis of the blades. This created up and down travel of the bottom of each pitch link, which changed the blade pair incidence in a sinusoidal manner as the blades rotated. In essence, these upper controls acted like a simple, variable-amplitude cam, which the pilot could control.

2.7 SWASHPLATE CONTROL

In contrast to the Cierva C.30 with its tightly packed, 1.75-inch flapping hinge offset (r_β = 0.00788R) retaining 3 blades of 1 8.5-feet radius, Wilford blade spars flexed about a point some 15 inches from the rotor centerline, and the blades were only 16-foot

radius (r_β = 0.078R). Therefore, according to Eq. (2.5 1), the Wilford rotor system was capable of generating very large hub pitching and rolling moments (about 10 times the hub moment of the C.30) to trim his "gyroplane" in flight.

E. Burke Wilford, who was very well known, liked, and respected in the rotorcraft industry, told his story [67] about the development of "feathering control" at what became the first Rotating Wing Aircraft Meeting. This historic meeting was held at The Franklin Institute in Philadelphia, Pennsylvania, on Friday and Saturday, October 28 and 29, 1938 . The meeting was sponsored by the Philadelphia Chapter of the Institute of the Aeronautical Sciences, later to become the A.I.A.A. All the papers presented were made available in a bound volume; I have included the index to the volume in Appendix F. E. Burke Wilford, president of the Pennsylvania Aircraft

Syndicate Ltd., was the I.A.S Philadelphia chapter president and general chairman of what we call today, an annual American Helicopter Society Forum. The meeting began with Wilford welcoming the large group of rotorcraft enthusiasts[10] and thanking the committee of very prominent figures in the field who helped put the four-session event together:

Mr. Agnew E. Larsen, chief engineer of the Pitcairn Autogiro Company
Mr. Wynn Laurence LePage, educator, editor, columnist, and prominent rotary wing aircraft engineer Mr. Richard H. Prewitt, chief engineer at Kellett Autogiro Corporation
Mr. James G. Ray, chief pilot for the Pitcairn Autogiro Company
Mr. Ralph H. McClarren, director of the Aeronautics section at The Franklin Institute

He then went on, saying:

"As this is probably the first rotary wing aircraft conference occurring in the world, we hope to make a little history here, and the only way that we can do that is for everyone to say what he thinks. Don't be afraid of

hurting anybody's feelings, or departing from conventional procedure. That's what this meeting is for, and we hope that it will be the start of a real boom in the rotary wing aircraft industry. We hope to see that within the next ten years, there will be at least 10,000 men working in this industry. To all you young men that are here, why, this is the line to work in, because it is going places."

Dr. Alexander Klemin[1] [1] of the Guggenheim School of Aeronautics at New York University was the chairman of the first session. Burke Wilford's paper [67] was the last paper presented in the first session. In his lecture, Wilford first showed a 7-minute film of the "development of feathering control, which I [Wilford] believe was the first rotor control which was ever flown in the world—the rigid blade adaptation to a rotor that flew without hinges, which Cierva said was impossible." He further notes that "ground resonance is still unsolved in all other types of rotary wing aircraft, this one doesn't seem to

have it. But it is only fair, also, to say that this one hasn't had much flying, and it is now in the hands of the

---

[10] In Appendix I of the proceedings, Ralph McClarren, the meeting secretary, notes that 242 people registered at this first Rotating Wing Aircraft Meeting (1938), but no list of attendees is included.

[11] Dr. Klemin gave a special lecture titled *Principles of Rotary Aircraft* [68] at the regular meeting of the Franklin Institute at 8:15 p.m. on Thursday, October 27th, the night before the forum started.

2.7 SWASHPLATE CONTROL

N.A.C.A., and I hope they will give it a lot of flying." A portion of the film appears to have dealt with Cierva activities in 1928 in England, which made Wilford "realize that rotor control was an absolute necessity; to that end I [Wilford] got [Walter] Rieseler and [Walter]

Kreiser, who were two men who started in Germany without knowledge of Cierva, to come to America; and in Professor Klemin's wind tunnel we made the first wind tunnel tests on rotor [blade feathering] control."

The wind tunnel tests of rotor control plus early flights of the first Wilford gyroplane [69] on August 5, 1 93 1 , with subsequent modifications over the following year (including wings off), led to a quite acceptable autogyro, Fig. 2-34 . In discussing the configuration development in his paper, Wilford makes a very significant technical point. He says:

"I think one of the most interesting things which Elliott Daland [engineer] and Paul Hovgard [pilot and engineer] contributed in this particular year was the leading of the control to offset gyroscopic couple. Many people thought, may I say, semi-rigid blades were impossible, due to gyroscopic torque, but he [Daland, I think] led the control by the system of cut and try by 40 degrees. I believe Bleeker had done the same thing in his

helicopter, and it appears necessary in any kind of feathering control. I think they also use it [lead the control] in the Hafner type, where they have hinges. You will notice the little ball stick in the middle. That was the cam [spider or swashplate upper control, see Fig. 2-35], and it was effective for both longitudinal and lateral control. The angles of movement are exceptionally small—I think only a degree and a half on the blades."

Wilford was highlighting the control geometry between the spider (i.e., swashplate) and the rotor response so that fore and aft pilot stick motion gave the aircraft pure longitudinal pitch displacement; and lateral stick movement only produced roll response. He also passes on the information that the cyclic pitch amplitude was on the order of "only a degree and a half on the blades." Wilford pointed out several times during the forum that his blades were definitely not rigid and, in fact, the behavior of his rotor system was not caused by gyroscopic forces. At one moment in the forum he questioned whether a truly rigid, propeller-like rotor blade could be made.

It is relatively easy to understand how the "feathering, semi-rigid" rotor blades Wilford designed were able to control his "gyroplane" given (a) further discussion and expansion of basic equations already introduced, and (b) review of Fig. 2-36. To get orientated, reconsider the two equations for first harmonic flapping and feathering

$$\beta_\psi = \beta_o - a_{1S}\cos\psi - b_{1S}\sin\psi \tag{2.72}$$

$$\theta_\psi = \theta_o - B_{1C}\sin\psi - A_{1C}\cos\psi\,. \tag{2.73}$$

The sign convention and symbols used in Eqs. (2.72) and (2.73) have persisted for decades. They have been used by virtually all authors until the arrival, beginning in the 1980s, of advanced technical papers and newer text books, such as references [70] and [71], which assume the flapping and feathering

motions are represented by more mathematically familiar positive Fourier series. The original equations grew out of autogyro analyses and were guided by some physical intuition about rotor system behavior. As you learned from the earlier discussion about flapping in Section 2.2, a rotor blade responds to an airload roughly 90 degrees later in azimuth. Thus, a reduction in pitch angle at $\psi = 90$ degrees (i.e., a positive

control input of $+ B_{1C}$) leads to a nose-down input to the aircraft and an increase in aircraft speed, which is positive. The logic sequence is:

a. the pilot pushes forward on the cyclic stick, which is positive ($+\delta_{long}$) b. the swashplate tilts

to produce only a ($+ B_{1C}$) and no (A_{1C})

c. the blade element angle of attack at 90-degrees azimuth is reduced d. the blade lift at 90-degrees azimuth, say at the tip, is reduced

e. the blade gets a negative flap velocity, ($d\beta/dt = \Omega a_{1S} \sin\psi$) because ($a_{1S}$) is negative

f. the flapping velocity integrates to ($\beta = \beta_o - a_{1S} \cos\psi$), which gives the 90-degree later response that some might call a gyroscopic response

g. the rotor flaps down at 180-degrees azimuth to $(\beta_o - a_{1S})$ and up at 0-degrees azimuth to $(\beta_o + a_{1S})$

h. the rotor tip path plane tilts forward from trim by (a_{1S}) and the rotorcraft pitches nose down

i. the rotor thrust vector is tilted forward

j. an increment of positive propulsive force, $[-T(-a_{1S})]$, is created k. the rotorcraft is accelerated forward which is positive

speed stability $\left(+\Delta V_{FP} / +\Delta \delta_{long}\right)$.

2.7.2 Pitch-Roll Coupling With the Wilford System

The Wilford rotor system introduced the equivalent of a flapping hinge far removed from the centerline of rotation. As noted above, the Cierva C.30 physical flapping hinge was offset to $r_\beta = 0.00788R$; Wilford blade spars flexed with $r_\beta = 0.078R$. This difference caused a significant change in the rotor flapping response. The altered flapping behavior changed how pure stick movements must be coupled to blade feathering.

Flapping hinge offset (r_β) causes cross coupling between (a_{1S}) and (b_{1S}). The basic equations defining the hub pitching moment (M_P) and rolling moment (M_R) do not change,

of course, which is to say

$$(2.74)\quad M_P = \frac{F_C\ r_\beta\ b}{2} a_{1S} \qquad \text{and} \qquad (2.75)$$

$$M_R = -\frac{F_C\ r_\beta\ b}{2} b_{1S}$$

but the first harmonic longitudinal flapping (a_{1S}) and lateral flapping (b_{1S}) expressions—including the influence of flapping hinge offset—now become

$$(2.76)\quad a_{1S} = \frac{\left[2\mu_{hp}\lambda_{hp} + \frac{8}{3}\mu_{hp}\theta_o - \left(1+\frac{3}{2}\mu_{hp}^2\right)B_{1C}\right] + \left[\frac{12r_\beta}{\gamma(R-r_\beta)}\right]b_{1S}}{1-\frac{1}{2}\mu_{hp}^2}$$

2.7 SWASHPLATE CONTROL

$$(2.77)\quad b_{1S}=\frac{\frac{4}{3}\mu_{hp}\beta_o-\left[\frac{12r_\beta}{\gamma(R-r_\beta)}\right]a_{1S}}{1+\frac{1}{2}\mu_{hp}^2}+A_{1C}.$$

To see the coupling introduced by flapping hinge offset, consider a simplification where the advance ratio is low enough to ignore (i.e., $\mu_{hp}^2\approx 0$). Then Eqs. (2.76) and (2.77) can easily be solved simultaneously for the flapping coefficients to obtain

$$(2.78)\quad a_{1S}=\frac{1}{\left[\frac{12r_\beta}{\gamma(R-r_\beta)}\right]^2}\left\{-B_{1C}+\left[\frac{12r_\beta}{\gamma(R-r_\beta)}\right]A_{1C}\right\}$$

$$(2.79)\quad b_{1S}=\frac{1}{\left[\frac{12r_\beta}{\gamma(R-r_\beta)}\right]^2}\left\{A_{1C}+\left[\frac{12r_\beta}{\gamma(R-r_\beta)}\right]B_{1C}\right\}.$$

Then it follows that the hub moments are reduced to

$$(2.80)\quad M_P = \frac{F_C\, r_\beta\, b}{2}\frac{1}{\left[\dfrac{12r_\beta}{\gamma(R-r_\beta)}\right]^2}\left\{-B_{1C}+\left[\frac{12r_\beta}{\gamma(R-r_\beta)}\right]A_{1C}\right\}$$

for pitch, and for roll,

$$(2.81)\quad M_R = -\frac{F_C\, r_\beta\, b}{2}\frac{1}{\left[\dfrac{12r_\beta}{\gamma(R-r_\beta)}\right]^2}\left\{A_{1C}+\left[\frac{12r_\beta}{\gamma(R-r_\beta)}\right]B_{1C}\right\}.$$

Remember that (γ) is the number Lock used in his equation where $\left(\gamma=\rho a c R^4/I_{flap}\right)$ as discussed on page 58.

From Eqs. (2.80) and (2.8 1) you can see that in order to obtain a pure, uncoupled pitching moment (M_P), a forward longitudinal stick movement must introduce both longitudinal cyclic (B_{1C}) and lateral cyclic (A_{1C}). The proportions must be such that the rolling moment comes out zero; and, from Eq. (2.81), that means the term

$$\left\{A_{1C}+\left[\frac{12r_\beta}{\gamma\left(R-r_\beta\right)}\right]B_{1C}\right\}$$

must be zero. Therefore, if the forward stick motion (say 1 inch) produces 1 degree of longitudinal cyclic (i.e., $B_{1C} = 1$ deg), then the same 1 inch of forward stick motion must produce a lateral cyclic amounting to

$$A_{1C}=-\left[\frac{12r_\beta}{\gamma\left(R-r_\beta\right)}\right]B_{1C}.$$

Accept, for the sake of discussion, that the Wilford gyroplane had an "equivalent flapping hinge" of $r_\beta = 0.078R$ and a Lock number of γ

= 5. Then A_{1C} would need to be –0.2 degrees for every 1 degree of B_{1C}. This represents a phase angle shift in azimuth of 11.6 degrees where the maximum resultant cyclic occurs.

Now, with the preceding equations in mind, take a look at Fig. 2-36 where I have taken a schematic guess about how the feathering control and hingeless rotor system that Wilford designed worked. For the sake of simplicity, the master blade, blade 1, is shown at the 90-degree azimuth position, which, according to Eq. (2.73), is the azimuth position for maximum longitudinal cyclic (B_{1C}). The blades are numbered in the direction of rotation, so blade 4 is at the 0-azimuth position on Fig. 2-36 . This orientation helps in the discussion of pitching moment. Wilford wrote in his paper that Elliott Daland and Paul Hovgard "led the control *by the system of cut and try* [my italics] by 40 degrees." Frankly, while I do understand "cut and try,"

I do not quite understand the words "led the control" or the magnitude of "40 degrees." But, with modern knowledge, we know what Daland and Hovgard were doing. Their objective was to get the fore and aft stick motion from the pilot to give a pure longitudinal pitching response without some lateral response, such as aircraft rolling. The same uncoupling statement applies to lateral stick movement.

Based on Fig. 2-35 and Fig. 2-36, the "system of cut and try" appears to have begun with a rotating, four-arm spider (or swashplate, if you prefer) placed below the blade spar feathering axis. I assume the spider is mounted at the top end of a nonrotating control rod with a bearing. This control rod, I imagine, extends from the fuselage interior, up the rotor pylon support, through the centering ball, and ends at the inner race of the bearing holding the spider. The lower end of the control rod can

be moved to the right by the pilot pushing on his stick (or moved left by the pilot pulling on his stick), given the simple linkage shown in Fig. 2-36.

The outboard end of each spider arm is attached with a rod end bearing, somewhere along the length of a pitch control lever. One end of the pitch control lever is fixed to the rotating blade support arms . The other end of the pitch control lever connects to the lower end of a pitch link. The upper end of the pitch link connects to the outboard end of the pitch arm. The inboard end of the pitch arm is rigidly attached to the blade spar.

2.7 SWASHPLATE CONTROL

Now suppose the bottom of the control

rod is pulled to the right by the pilot pushing forward on his stick, which would be a positive stick displacement ($+\delta_{long}$) . The spider plane would tilt to the left about its longitudinal axis by an angle (χ) . The spider-arm-to-blade-1 pitch control lever would rise an amount ($h = \chi c$). Because the pitch control lever pivots about its pinned end, the bottom of the pitch link would rise a distance [blade 1 $H = (d+e)(h/e)$] . Upward movement of the pitch link would feather the blade nose down because of the trailing pitch arm. This would be a positive longitudinal cyclic in the amount ($+B_{1C} = H/b$), but this is not all that would be going on. Because of the longitudinal cyclic input, an increment of forward (negative) longitudinal flapping given by Eq. (2.76) would be created. This longitudinal flapping would give rise to an increment of rotor hub rolling moment.

Now you can see that the pilot, with just

forward stick motion, would be creating both pitching and rolling moments . With the control system coupled both mechanically and aerodynamically (do not forget a_{1S} and b_{1S} in the previous two equations), we can fully appreciate the acknowledgement by E. Burke Wilford of the lengthy trial and error search by Daland and Hovgard—and admire their success in obtaining uncoupled "gyroplane" response.

It is impossible to conclude this discussion about the E . Burke Wilford "gyroplane" and its hingeless rotor controlled by feathering without recognizing John Brooks Wheatley. John B . Wheatley was the first of a number of outstanding engineers at the N.A.C.A. to tackle rotorcraft problems head on. He, along with Glauert, Lock, Beavan, and others in England, single-handedly laid the foundation for a practical aerodynamic theory of rotors. In support of the "gyroplane"

approach Wilford was offering, Wheatley published [72] an aerodynamic analysis showing that "the aerodynamic principles of the gyroplane are sound, and further research on this wing system is justified." The N.A.C.A. management clearly supported Wheatley's view because a 10-foot-diameter, 4-bladed model rotor was built and tested in the N.A.C.A. Langley 20-foot wind tunnel. Wheatley reported the 4-bladed results [73] and included 2-bladed results as well. The primary results covered an advance ratio range from 0 to 0.8 and hub plane angles of attack from 0 to 90 degrees. He also provided data for the "idling rotor" case (he suggests an advance ratio of 1.5) covering angles of attack from 0 to 5 degrees at several collective pitch settings. As you read on, the name John Wheatley comes up quite frequently, and you will gain an appreciation of what he, his cohorts, and those who followed—supported by the N.A.C.A. (and later NASA)

management—did for the rotorcraft industry.

The demonstration by E . Burke Wilford that a nonflapping, feathering rotor system was quite feasible opened the door to our modern swashplate configuration. The first one through this door was Raoul Hafner.

2.7 SWASHPLATE CONTROL

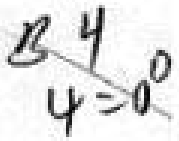

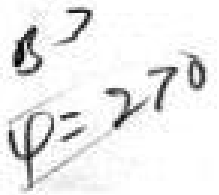

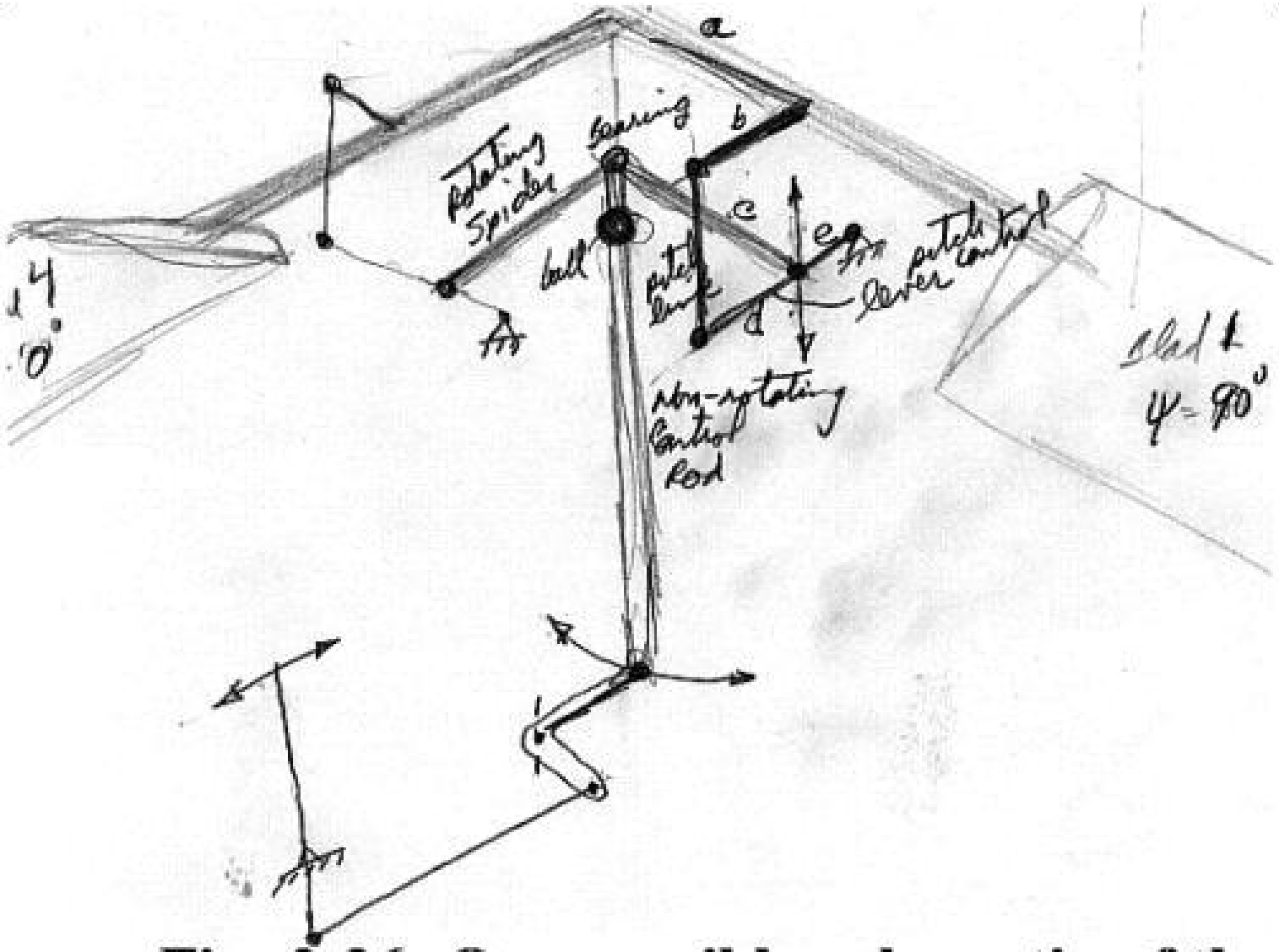

Fig. 2-36. One possible schematic of the Wilford feathering rotor.

2.7.3 The Raoul Hafner Rotor System—Part I

Raoul Hafner [74], who immigrated from Austria to England in 1932, used his

early efforts with helicopters as an "opportunity to discover many of the peculiarities of rotors." He quickly found that rotor control, not rotor lift and drag, was where he should focus his engineering attention. In 1934–1935 he completed design of the A.R. III gyroplane[12] which then "made its first flight at Heston in September, 1935, piloted by Captain V. H. Baker. Further development work was carried out during the following year, and in its final form the machine [see Fig 2-37 and Fig. 2-38], to which we give the type No. A.R. III, had its first public demonstration when Flying Officer A. E. Clouston, R.A.F.O., flew it at the Society's garden party on May 9th of this year [1937]."

---

[12] Hafner notes that he used the word gyroplane for his A.R. III because it was "the official British class-name for a windmill plane."

2.7 SWASHPLATE CONTROL

Hafner read a lecture before the Royal Aeronautical Society on October 14, 1937. His excellent lecture, along with the very interesting discussion that followed, were published in the February 1938 issue of the Royal Aeronautical Society Journal [74]. The published paper is 35 pages long and the discussion that followed occupies another 16 pages. Hafner went into great design detail about his A.R. III and then continued with a detailed theoretical rotor analysis. He concluded the paper with an excellent control load analysis of what was to be a prototype of the modern swashplate control system.

The description of the A.R. III autogyro by Raoul Hafner is accompanied by rather poor engineering photos but excellent

drawings. In his introduction of the aircraft, he mentions that his two early machines (helicopters R. I and R. II) had neither flapping nor lag hinges and used only feathering for control. In this regard, Hafner started down the Wilford path at about the same time, but Hafner soon gave up because the rotor shaft of the R. II was too rigid and the blades created "unpleasant forces" which proved to be "unsurmountable." He was thus led "to the adoption of freely hinged rotor blades." The Hafner A.R. III demonstrator was more than comparable to the Cierva C.30 or both Pitcairn and Kellett autogyros in the United States. For example, the A.R. III featured:

a. a conventional welded tubular fuselage

b. a cambered elevator arranged to counteract engine torque (flat surface to starboard,

cambered surface to port)

c. pilot trimable elevator positions over a very wide incidence angle

d. a cocked rudder hinge (forward at the top) so it was effective in descent

e. airplane-like cockpit controls, albeit with a hanging stick

f. pedal control of rudder and tail wheel

g. pedal operated brakes

h. a collective pitch lever mounted on the left-hand-side of the pilot

i. a rotor startup drive and an overriding clutch

j. a rotor brake

k. flapping hinges on the rotor centerline ($r_\beta = 0$) with three blades

l. lead-lag hinges with friction dampers

m. blade retention with a long tie rod (i.e., tension-torsion assembly) plus fail-safe

secondary retention

n. the lowest solidity rotor of the era for performance ($\sigma = 0.0237$)

o. zero pitching moment airfoil for blade sections

p. high-inertia blades

On top of this impressive list, Hafner successfully incorporated jump takeoff capability (discussed in the next section), which Cierva, Pitcairn, and Kellett were still perfecting.

2.7 SWASHPLATE CONTROL

Fig. 2-37. Raoul Hafner publicly demonstrated the prototype of our modern swashplate control system with his A.R. III on May 9, 1937 [74].

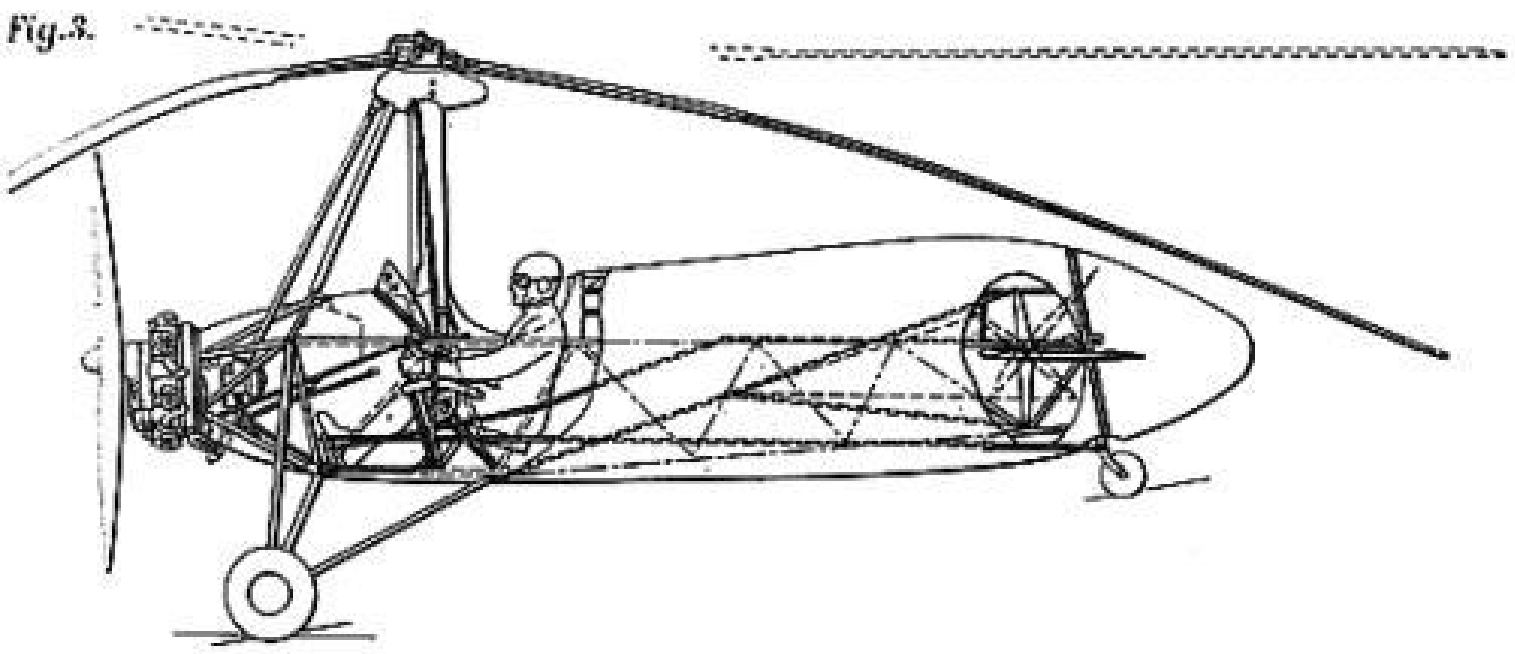

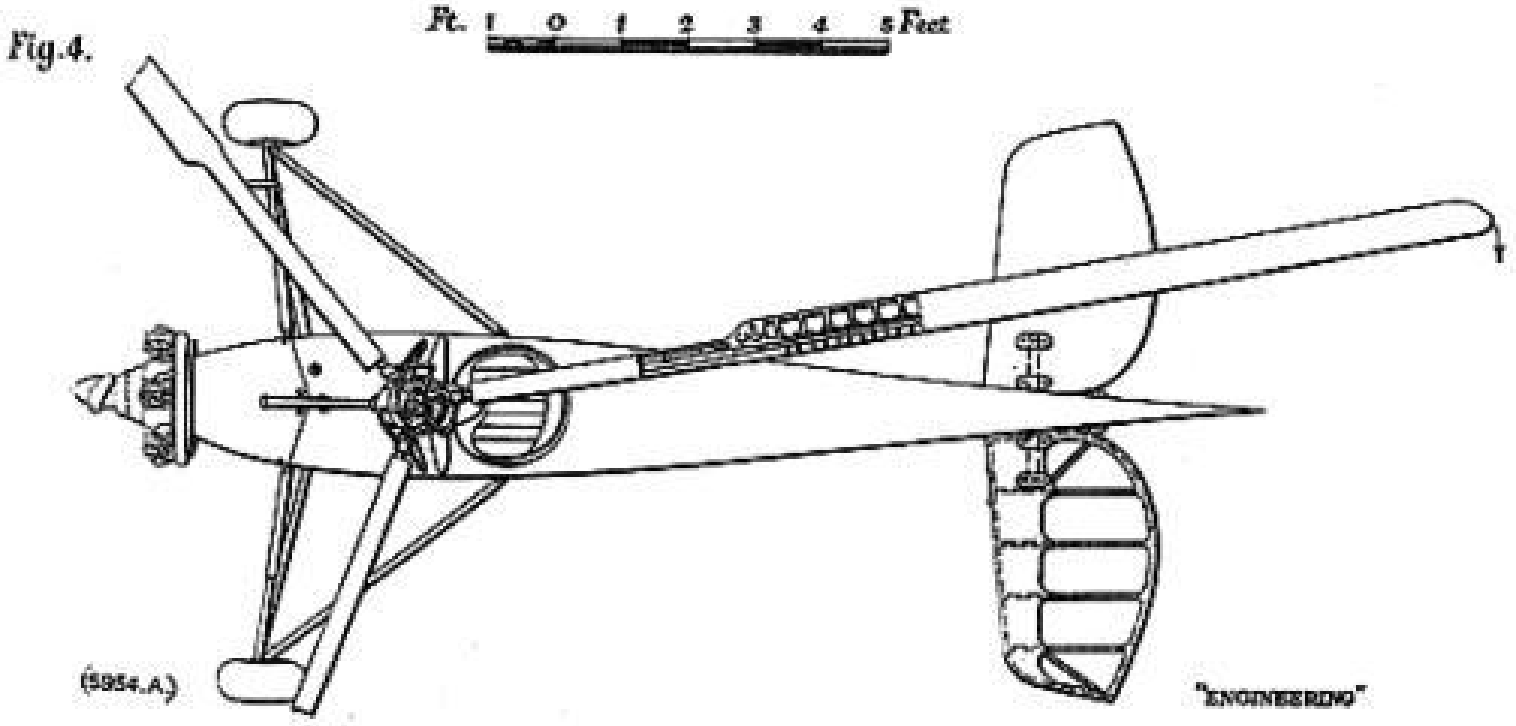

Fig. 2-38. The Hafner autogyro had a 33-foot-diameter rotor, an 84-hp Pobjoy engine, and a takeoff gross weight of 890 pounds. Rotor solidity was 0.0237 [74].

2.7 SWASHPLATE CONTROL

The upper control system of the Hafner A.R. III is quite clearly conveyed with two figures he included in his paper. I have reproduced them here as Fig. 2-39 and Fig. 2-40. The key to the system is the upper end of the pilot "joystick" which passes through the spherical bearing located at the point Hafner refers to as the "focus point." This long nonrotating control tube houses a rod that carries the inner races of the two tapered bearings. The outer races of the two bearings support the three-arm spider. The three arms of the spider are bent downward at their outer ends so as to lay in the flapping hinge plane for the nominal collective pitch setting. The cyclic stick input from the pilot tilts the upper control shaft about the focus point, which tilts the spider (i.e., swashplate plane). The ends of the spider arms are ball jointed to the pitch arm of each blade. The pitch arms, unlike the approach Wilford took with trailing pitch arms

shown in Fig. 2-35, are leading the blade spar axis.

The collective pitch input to the Hafner control system was quite simple. The rod, sliding within the spider control tube, simply raised and lowered the two tapered bearings and spider assembly. This up and down travel of the rod was controlled by the pilot "lift" lever. Today the "lift" lever is referred to as the collective pitch control.

The planform view of the Hafner A.R. III rotor head, shown in Fig. 2-41, indicates that the blades rotate clockwise when viewed from above. The flapping hinges for all blades are at the centerline of rotation. The ball joint connection between the tip of the spider arm and the free end of the pitch arm *does not* lie on the flapping hinge line. If it did, the pitch arm would be considerably longer and the 3-arm spider would be indexed roughly another 30

degrees in the direction of blade rotation. If you say that blade 1 is the master blade and that this blade is at the 0-degree azimuth position, the spider arm is advanced from the blade 1 span axis by approximately 60 degrees.

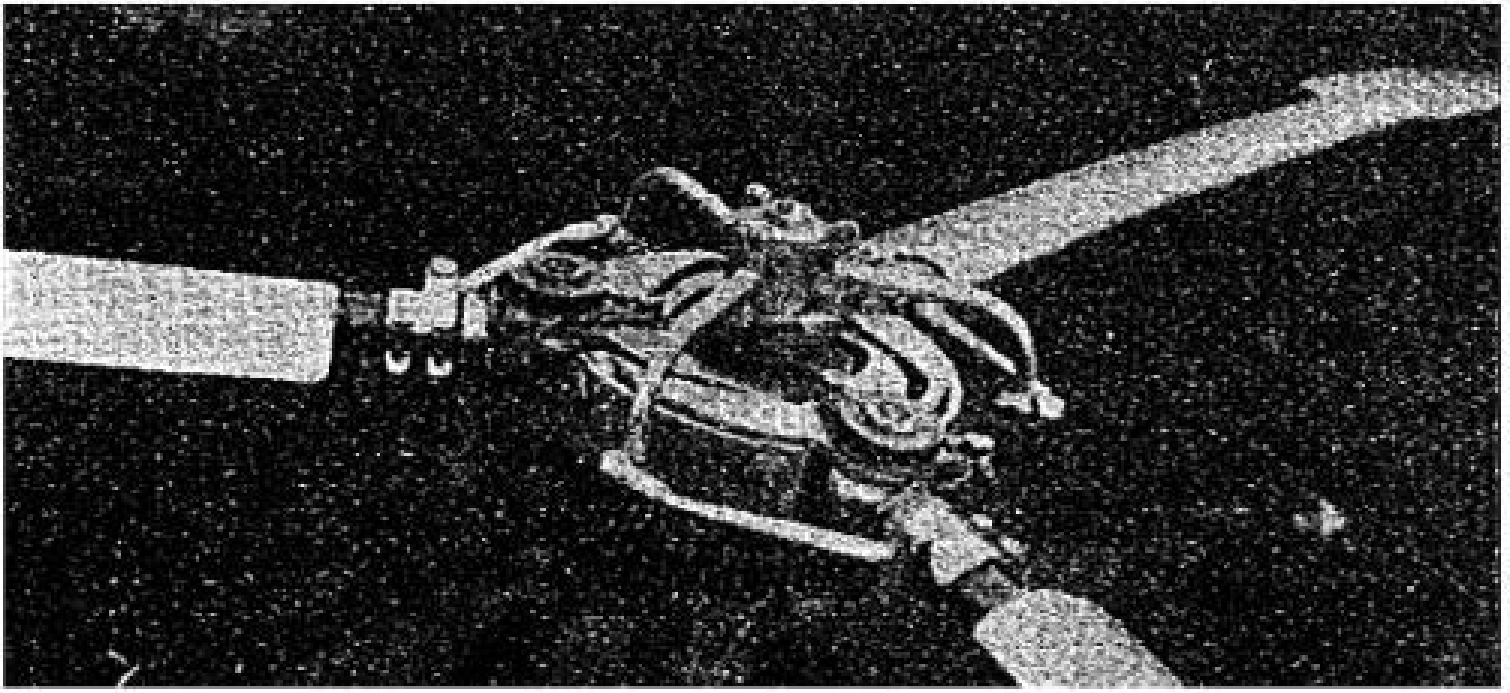

Fig. 2-39. The Raoul Hafner A.R. III rotor head in 1937 [74].

2.7 SWASHPLATE CONTROL

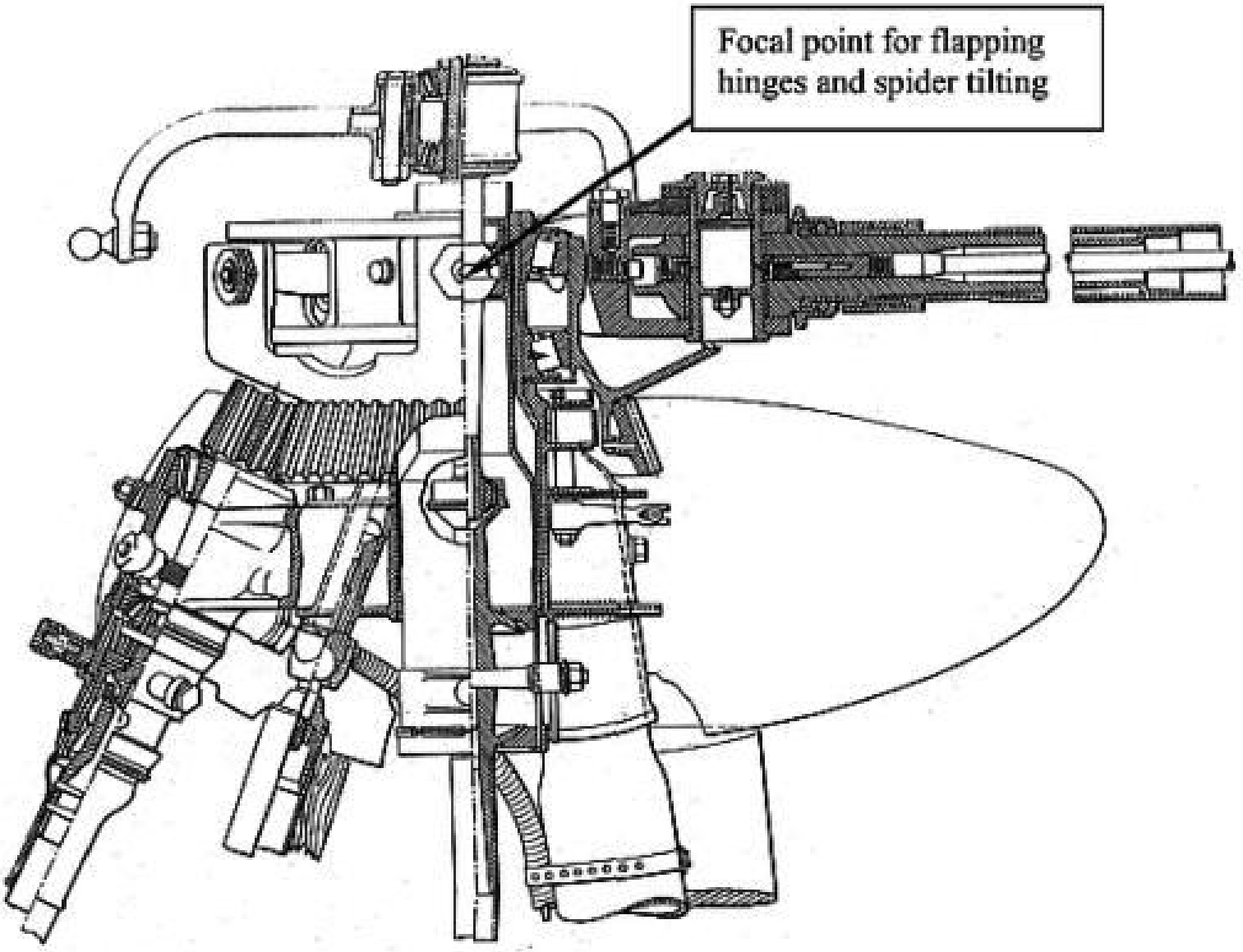

Fig. 2-40. Layout details of the Hafner A.R. III rotor head [74].

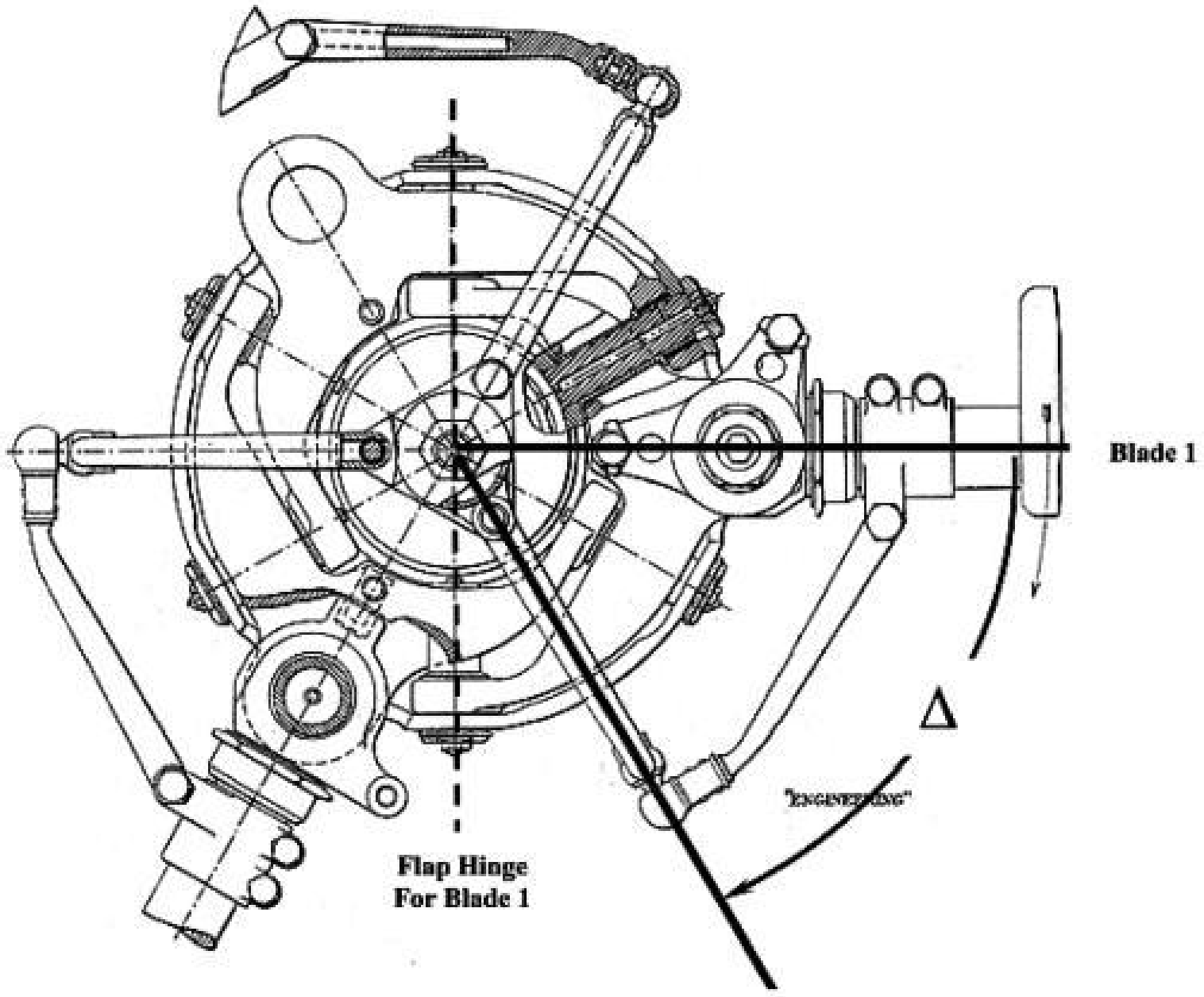

Fig. 2-41. The Hafner spider control system introduced coupling between flapping and feathering because of the control advance angle, Δ [74].

2.7 SWASHPLATE CONTROL

The identification of flapping and feathering coupling with the pitch arm extending ahead (or behind) in azimuth of the blade span axis is quite significant to rotor system behavior. The primary influence is on pilot control and the secondary influence is on aircraft stability and gust response. Hafner determined the amount of pitch (θ) coupling with flap (β) using "the control advance angle" (Δ). He measured (Δ) as a positive angle when it was ahead of the blade in azimuth as shown in Fig. 2-41 . Were the pitch arms trailing the blade, that would be a negative (Δ). You can see from Fig. 2-41 that if, in the Hafner design, the spider arm stays perpendicular to the rotor shaft (i.e., in the plane of the paper) then the ball joint at the end of the pitch arm must stay in the spider control plane . But now, if the blade flaps up (i.e., comes out of the paper) its

feathering or pitch angle will be reduced. Just folding a rectangular piece of paper on a diagonal illustrates the flap-up/feather-down kinematics. The universally accepted sign convention for this flap-up/feather-down coupling is *negative* coupling. The coupling, as Hafner used it, is defined as

$$(2.82) \quad \frac{\Delta\theta}{\Delta\beta} = -\text{cotangent } \Delta$$

and with the Hafner design, (Δ = 60 degrees), which means that $\Delta\theta/\beta = -0.5773$. Of course, if the pitch arm/spider arm ball joint extended around to the flapping hinge line (Δ = 90 degrees), there would be no pitch-flap coupling.[13]

The influence of pitch-flap coupling through the "the control advance angle" can be very large. While the fundamental flapping

equation, Eq. (2.72), remains unchanged, the blade pitch definition from Eq. (2.73) must now contain a term reflecting the coupling. That is, the flapping equation remains

(2.72) $$\beta_\psi = \beta_o - a_{1S}\cos\psi - b_{1S}\sin\psi$$

but the feathering equation becomes

(2.83)

$$\theta_\psi = \theta_o - B_{1C}\sin\psi - A_{1C}\cos\psi + \frac{\Delta\theta}{\Delta\beta}\beta_\psi .$$

A general solution approach, such as Wheatley provided [75],[14] to solve for the thrust ($2C_T/\sigma a$), the coning (β_o), the longitudinal flapping (a_{1S}), and the lateral flapping (b_{1S}) yields

(2.84)

$$\frac{2C_T}{\sigma a} = \frac{1}{2}\lambda_{hp} + \left(\frac{1}{3} + \frac{1}{2}\mu_{hp}^2\right)\theta_o - \frac{1}{2}\mu_{hp}B_{1C} + \left[\left(\frac{1}{3} + \frac{1}{2}\mu_{hp}^2\right)\beta_o - \frac{1}{2}\mu_{hp}b_{1S}\right]\frac{\Delta\theta}{\Delta\beta}$$

---

[13] The modern angle notation for this pitch-flap coupling is δ_3 which is equal to $90^o - \Delta$. The modern definition is therefore $\Delta\theta/\Delta\beta = -\tan\delta_3$.

[14] The John Wheatley classic 1934 NACA technical report [75] provides the simplest derivation of the blade flapping motions, rotor forces, and rotor moments I could recommend. Many authors have extended his original work, but no one, in my opinion, has improved upon his clarity.

2.7 SWASHPLATE CONTROL

(2.85)
$$\beta_o = \frac{\frac{\gamma}{2}\left[\frac{1}{3}\lambda_{hp} + \frac{1}{4}\left(1+\mu_{hp}^2\right)\theta_o - \frac{1}{3}\mu_{hp}B_{1C} - \frac{1}{3}\mu_{hp}\frac{\Delta\theta}{\Delta\beta}b_{1S}\right]}{1 + \frac{3r_\beta}{2\left(R-r_\beta\right)} - \frac{\gamma}{8}\left(1+\mu_{hp}^2\right)\frac{\Delta\theta}{\Delta\beta}} - \frac{M_W}{I_{flap}\Omega^2}$$

$$(2.86)\quad a_{1S} = \frac{\left[2\mu_{hp}\lambda_{hp} + \frac{8}{3}\mu_{hp}\theta_o - \left(1+\frac{3}{2}\mu_{hp}^2\right)B_{1C}\right] + \left[\frac{12r_\beta}{\gamma(R-r_\beta)} - \left(1+\frac{3}{2}\mu_{hp}^2\right)\frac{\Delta\theta}{\Delta\beta}\right]b_{1S} + \left[\frac{8}{3}\mu_{hp}\frac{\Delta\theta}{\Delta\beta}\right]\beta_o}{1-\frac{1}{2}\mu_{hp}^2}$$

$$(2.87)\quad b_{1S} = \frac{\frac{4}{3}\mu_{hp}\beta_o - \left[\frac{12r_\beta}{\gamma(R-r_\beta)} - \left(1+\frac{1}{2}\mu_{hp}^2\right)\frac{\Delta\theta}{\Delta\beta}\right]a_{1S}}{1+\frac{1}{2}\mu_{hp}^2} + A_{1C}.$$

I have written these four equations in their coupled form so that the effect of flapping hinge offset (r_β) and the pitch-flap coupling ($\Delta\theta/\Delta\beta$) are clear. These equations are, of course, four linear equations. A simultaneous solution of the three blade motion equations (β_o, a_{1S}, and b_{1S}) is required before the flapping and blade pitch waveforms can be seen and the thrust can be calculated.

Pilot control is the fundamental design aspect affected by pitch-flap coupling. To see the potentially adverse control situation, simply think of the Hafner A.R. III in vertical descent where advance ratio (μ_{hp}) is, for practical

purposes, zero. Because the Hafner rotor hub and blades were designed with the flapping hinge at the centerline of rotation ($r_\beta = 0$), the
preceding blade motion equations reduce, with $\mu_{hp} = 0$, to

$$\beta_o = \frac{\frac{\gamma}{2}\left[\frac{1}{3}\lambda_{hp} + \frac{1}{4}\theta_o\right]}{1 - \frac{\gamma}{8}\frac{\Delta\theta}{\Delta\beta}} \qquad \text{for } r_\beta = 0 \text{ and } \mu_{hp} = 0 \tag{2.88}$$

$$a_{1S} = -B_{1C} - \frac{\Delta\theta}{\Delta\beta} b_{1S} \qquad \text{for } r_\beta = 0 \text{ and } \mu_{hp} = 0 \tag{2.89}$$

$$b_{1S} = A_{1C} + \frac{\Delta\theta}{\Delta\beta} a_{1S} \qquad \text{for } r_\beta = 0 \text{ and } \mu_{hp} = 0 . \tag{2.90}$$

The first harmonic flapping coefficients, found by simultaneously, are

solving Eqs. (2.89) and (2.90)

2.7 SWASHPLATE CONTROL

(2.91) $$a_{1S} = \frac{-B_{1C} - \frac{\Delta\theta}{\Delta\beta} A_{1C}}{1 + \left(\frac{\Delta\theta}{\Delta\beta}\right)^2} \qquad b_{1S} = \frac{A_{1C} - \frac{\Delta\theta}{\Delta\beta} B_{1C}}{1 + \left(\frac{\Delta\theta}{\Delta\beta}\right)^2} \quad .$$

Note here that pitch-flap coupling is squared in the denominator, which means that coupling of either sign reduces flapping motion—*for a rotor in axial flight*. This is not true for a rotor in edgewise flight.

Now consider how the pilot's stick motion affects longitudinal and lateral flapping. Suppose the pilot pushes the grip of the hanging "joystick" directly forward 3 or 4 inches, say a distance (δ_{long}). This will (with the reversing linkage Hafner mentions) cause the spindle to tilt nose down an angle (φ) in the autogyro plane of symmetry. The amount of forward spindle tilt is dependent on the mechanical gear ratio between the stick movement and the spindle . Hafner gives virtually zero information about this gear ratio ($\Delta\varphi/\Delta\delta_{long}$), but I would estimate, from Fig. 2-38

and Fig. 2-40, that 1 inch of grip travel gave 1.5 degrees of spindle tilt. Therefore let $\varphi = (\Delta\varphi/\Delta\delta_{long})\delta_{long}$. Now, with a tilted spindle, the spider will travel in a plane inclined to the rotor hub axis. Therefore, the ball joint at the pitch-arm-to-spider-arm junction will travel up and down a height ($h_{ball\ joint}$) relative to its mean position. This height is simply

(2.92) $h_{ball\ joint} = (\text{spider arm length})\left[\varphi\cos(\psi+\Delta)\right]$.

Keep in mind that the azimuth angle (ψ) is keyed to the master blade, which, in Fig. 2-41, I have taken as zero degrees. Now, the master blade feathering angle (or more commonly, the pitch angle) will be, assuming small angles,

(2.93)

$$\theta_\psi = \frac{h_{\text{ball joint}}}{\text{pitch arm length}} = \left(\frac{\text{spider arm length}}{\text{pitch arm length}}\right)\left[\frac{\Delta\varphi}{\Delta\delta_{\text{long}}}\delta_{\text{long}}\cos(\psi+\Delta)\right].$$

From Fig. 2-38 (and with thanks to the 5-foot scale Hafner included), the spider arm length (s.a.l) measures 7.5 inches. That is, s.a.l. = 7.5. Furthermore, the ball joint is 6.625 inches measured perpendicular to the blade span axis, which defines the pitch arm length as p.a.l. = 6.625. Note that knowing the individual spider arm and pitch arm lengths (s.a.l. and p.a.l. respectively) really does not matter according to Eq. (2.93). All that counts is the ratio of the lengths, which, in the Hafner design, is quite adequately measured from Fig. 2-41 as $2.15/1.86 = 1.155$. In fact, the ratio (s.a.l./p.a.l.) is identical to $1/\sin\Delta$ with the Hafner spider control system.

The master blade pitch angle, Eq. (2.93), takes a more familiar form by

expanding its cosine function to give

2.7 SWASHPLATE CONTROL

$$\theta_\psi = \left\{\frac{\text{s.a.l.}}{\text{p.a.l.}}\cos\Delta\right\}\frac{\Delta\varphi}{\Delta\delta_{\text{long}}}\delta_{\text{long}}\cos\psi - \left\{\frac{\text{s.a.l.}}{\text{p.a.l.}}\sin\Delta\right\}\frac{\Delta\varphi}{\Delta\delta_{\text{long}}}\delta_{\text{long}}\sin\psi$$

(2.94)

$$= \left\{\frac{1}{\sin\Delta}\cos\Delta\right\}\frac{\Delta\varphi}{\Delta\delta_{\text{long}}}\delta_{\text{long}}\cos\psi - \left\{\frac{1}{\sin\Delta}\sin\Delta\right\}\frac{\Delta\varphi}{\Delta\delta_{\text{long}}}\delta_{\text{long}}\sin\psi$$

$$= -\left\{\frac{\Delta\theta}{\Delta\beta}\right\}\frac{\Delta\varphi}{\Delta\delta_{\text{long}}}\delta_{\text{long}}\cos\psi - \frac{\Delta\varphi}{\Delta\delta_{\text{long}}}\delta_{\text{long}}\sin\psi$$

because $\dfrac{\Delta\theta}{\Delta\beta} = -\text{cotangent}\,\Delta$

You can immediately see that the forward movement of the pilot "joystick" grip introduces both longitudinal and lateral cyclic pitch to the blades. That is, because $\theta_\psi = -A_{1C}\cos\psi - B_{1C}\sin\psi$, the pilot forward longitudinal stick input with the Hafner spider

control system is really giving the rotor

$$(2.95)\quad A_{1C} = \left\{\frac{\Delta\theta}{\Delta\beta}\right\}\frac{\Delta\varphi}{\Delta\delta_{long}}\delta_{long} \qquad \text{and}$$

$$B_{1C} = \frac{\Delta\varphi}{\Delta\delta_{long}}\delta_{long}\,.$$

These kinematics can be substituted into Eq. (2.91), and the A.R. III blade flapping motion responds to a longitudinal stick input in vertical

descent as

$$(2.96)\quad a_{1S} = -\frac{\Delta\varphi}{\Delta\delta_{long}}\delta_{long} \qquad b_{1S} = 0$$

This is really a beautiful result. Of course, this result might have been deduced directly from Eq. (2.91) because if lateral flapping is to be zero (i.e., $b_{1S} = 0$), then Eq. (2.91) says lateral feathering (A_{1C}) must equal pitch-flap coupling ($\Delta\theta/\Delta\beta$) times longitudinal feathering (B_{1C}) . Therefore, longitudinal flapping (a_{1S}) will equal negative longitudinal feathering . The Hafner control system design yielded uncoupled response to a fore and aft longitudinal stick motion in a vertical descent, and the same is true for lateral stick motion. Furthermore, the coupling was minimized in steady-level flight. Of course, if the flapping hinge offset were other than zero, then there would have been some coupling. The Hafner

paper [74] has a lengthy section dealing with the theory of the rotor. The control system design plus engineering analysis shows that he knew exactly what he was doing.

2.7.4 Gust Response With Hafner Rotor System

As I stated earlier, pilot control is the fundamental design aspect affected by pitch-flap coupling. Hafner clearly ensured that the pilot would have no surprises in this regard. The second most important aspect is aircraft response due to a disturbance. A good example of a disturbance is a gust.

Imagine that the A.R. III, while flying in trim at 115 miles per hour, encounters a 20-foot-per-second updraft. The pilot takes no corrective action so his control-inputs to blade-feathering remain fixed. Assume the autogyro

is trimmed with zero longitudinal and lateral flapping before the updraft is encountered. The question is: What does the rotor do? This question is answered by comparing the two columns in Table 2-1, which were calculated

using Eqs. (2.84), (2.85), (2.86), and (2.87).[15] The first column shows the trim conditions prior to the gust. The second column of Table 2-1 shows that the 20-foot-per-second gust immediately increases rotor thrust by nearly 60 percent. This is an increase in load factor from 1 g to 1.56 g and a very noticeable bump to the pilot. Additionally, the rotor flaps aft 0.94 degrees from its 0-degree trimmed state. This causes the autogyro to pitch nose up, since the rotor thrust vector is now inclined aft of its trimmed orientation. The rotor also flaps

laterally 0.45 degrees. This tilts the thrust vector slightly, which introduces a rolling moment to port because Hafner chose clockwise rotor rotation when viewed from above. Fig. 2-42 shows the calculated waveforms.

You can see that the Hafner control system design for his A.R. III gave the pilot uncoupled control and minimized aircraft response to disturbances . His control system was easily on par with modern standards.

Table 2-1. The Hafner A.R. III Response to a 20-fps Vertical Gust With Control Advance Angle of *Positive* 60 Degrees, $\Delta\theta/\Delta\beta = -0.578$

Input Parameter	Trimmed	20-fps Gust
Flight Speed, V (mph)	115	Same
Rotor Speed (rpm)	270	Same
Hub Plane Angle of Attack, α_{hp} (deg)	+5.5	+12.3
Advance Ratio, μ_{hp}	0.36	Same
Induced Velocity, v (fps)	1.33	Same
Inflow Ratio, λ_{hp}	+0.0320	+0.0751
Pilot Input to Blade Pitch		
Collective Pitch, θ_o (deg)	+5.19	Same
Longitudinal Cyclic, B_{1C} (deg)	+3.29	Same
Lateral Cyclic, A_{1C} (deg)	–1.95	Same
Results		
Rotor Thrust, T_{hp} (lbs)	900	1,300
Coning, β_o (deg)	+5.45	+7.64
Longitudinal Flapping, a_{1S} (deg)	0	+0.94
Lateral Flapping, b_{1S} (deg)	0	+0.45
Flapping Amplitude (deg)	0	+1.04

[15] Hafner provides virtually no A.R. III dimensional data in his Society lecture [74]. He does give the rotor area as 846 square feet from which the diameter is 32.82 feet. The three blades are quoted as having an area of 20.04 square feet, which makes solidity 0.02369 and an average blade chord of 0.4071 feet. Fortunately, his Flight magazine article [76] is more helpful . This article gives a flight weight of 900 pounds and a

blade centrifugal force of 3,400 pounds. I guessed a normal rotor speed of 270 rpm and, therefore, a uniform blade

section mass of 0.031 slugs-per-foot to give 3,400 pounds of centrifugal force. The flapping second moment of inertia calculates as 45.66 slug-ft^2 and, therefore, the Lock number comes out at 8.8. The flight path speed of

1 15 miles per hour plus an estimated hub plane trim angle of 5.5 degrees nose-up seemed to give reasonable results. Brooks [7] provides some information about gross weight and speed.

2.7 SWASHPLATE CONTROL

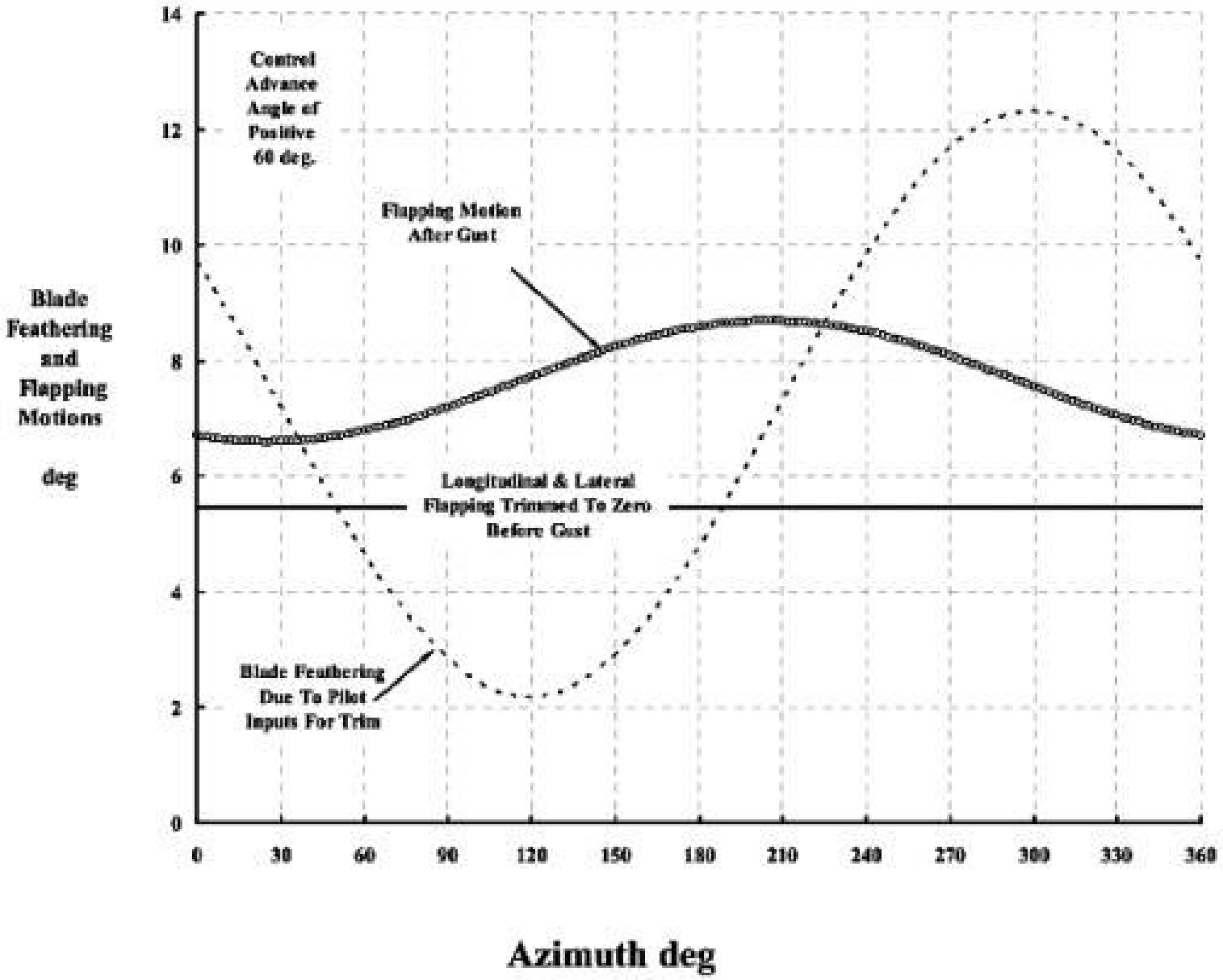

Fig. 2-42. Rotor trim upset due to a 20-fps vertical gust at 115 mph.

An appropriate question to ask about the Hafner control system design decision at this point is "Why not have a trailing pitch arm where the control advance angle would be $\Delta =$

–60 degrees? Or, for that matter, why not have zero pitch-flap coupling (i.e., $\Delta = 90$ degrees)? After all, Eq. (2.96) shows that the pilot inputs would be uncoupled." This question is answered with Table 2-2. Clearly, the flapping response is reduced as long as $\Delta\theta/\Delta\beta$ is negative. Conversely, positive $\Delta\theta/\Delta\beta$ values where flap up increases pitch are clearly to be avoided. Excessive lateral flapping alone would create a dangerous aircraft.

Table 2-2. Response to a 20-fps Vertical Gust With Various Values of $\Delta\theta/\Delta\beta$ Pitch-Flap Couplings

Parameter	Trim	$\Delta\theta/\Delta\beta$ 0	$\Delta\theta/\Delta\beta$ –0.578	$\Delta\theta/\Delta\beta$ –1.0	$\Delta\theta/\Delta\beta$ –1.732	$\Delta\theta/\Delta\beta$ 1.0	$\Delta\theta/\Delta\beta$ 0.578
Hafner Control Advance Angle, Δ (deg)		90	60	45	30	–45	–60
Delta 3, δ_3 (deg)	Variable	0	30	45	60	135	150
Rotor Thrust, T_{hp} (lbs)	900	1,535	1,300	1,214	1,138	5,960	2,151
Coning, β_o (deg)	5.45	9.07	7.64	7.12	6.66	36.70	12.92
Longitudinal Flap, a_{1S} (deg)	0	1.91	0.94	0.51	0.20	7.04	2.71
Lateral Flap, b_{1S} (deg)	0	1.64	0.45	0.25	0.20	21.19	4.95
Flap Amplitude (deg)	0	2.52	1.04	0.56	0.28	22.33	5.64

2.7 SWASHPLATE CONTROL

You should take careful notice of the last two columns in Table 2-2. These results suggest that the more positive $\Delta\theta/\Delta\beta$ becomes, the greater the gust response. In fact, there is a value of positive $\Delta\theta/\Delta\beta$ where flapping motion is completely divergent. In simple mathematical terms, this means that there is no simultaneous solution to Eqs. (2.85), (2.86), and (2.87). Therefore, longitudinal flapping (a_{1S}), lateral flapping (b_{1S}), and coning (β_o) are indefinable. In terms of the dynamic equation of flapping motion as explained by Johnson, starting on page 602 of reference [70], the flap frequency is reduced from once per revolution to zero. A simple equation estimating this critical pitch-flap coupling to absolutely avoid is

$$(2.97)\quad \frac{\Delta\theta}{\Delta\beta}=\frac{8}{\gamma}\left(\frac{1+\frac{1}{2}\left(\frac{r_\beta}{R}\right)}{1-\left(\frac{r_\beta}{R}\right)}\right)\left(1+1.803\mu_{hp}^2+2.594\mu_{hp}^4\right)\ .$$

2.7.5 The Raoul Hafner Rotor System—Part II

Hafner [74] summarizes the control system noting that "it is in fact due to the smoothness and precision of this control that the pilot is able to carry out the various flying manœuvers with accuracy and confidence, of which the aviation correspondent of a leading London newspaper, when describing the demonstration at this Society's Garden Party, stated that 'No flying machine ever built is so manœuvrable as the Hafner gyroplane,[16] for in effect the whole of the sustaining member [the rotor] is also a control surface, infinitely and instantly responsive.'" To

substantiate his claim, Hafner tells the Royal Aeronautical Society members that "the fundamental difference between the two rotors [other autogyro control systems like the Cierva C.30 tilting hub direct control and his design] lies in the fact that the hub of the Hafner rotor rotates about a rigid axle through which all the flying loads are carried direct to the fuselage, which the variation of incidence is achieved by a separate control linkage which enables the rotor to be controlled by light loads on the control column, which, as is shown in the mathematical analysis of control and as has been proved in flight, is free from all parasite loads and vibrations." Recalling the earlier discussion (Section 2.6.4) of vibratory control loads measured by Wheatley [62] from the N.A.C.A. with the Pitcairn YG-2, and Bailey [63] with the Kellett YG-1B, the words Hafner spoke would have been music to the ears of Captain Frank Gregory.

Hafner included his control load analysis near the end of his lecture . He reminded the audience that the blade was retained to the hub with a long tie rod, which I have shown here in Fig. 2-43. One feathering bearing is clearly shown just outboard of the lag hinge in his drawing. He states that:

"The blades produce no [torsional] moments about their longitudinal [spanwise] or pitch change axes due to

---

16 When I read that the "aviation correspondent of a leading London newspaper" wrote that in his column, I believe the fixed-wing community would have hotly disputed the claim. Certainly, the Cierva Autogiro Company was quick to take issue as you will read shortly.

(a) aerodynamic forces, because the blades

are fitted with aerofoil sections, the centre of pressures of which lie always on a straight line coinciding with the pitch change axis; and

(b) weight and centrifugal forces, because the centre of gravity of each blade lies also in this [pitch change] axis."

This frees him to first calculate control loads only due to twisting the tie rods. He assumes that the feathering motion is periodic as given by Eqs. (2.83) and (2.72) combined so that

$$\theta_\psi = \theta_o - B_{1C}\sin\psi - A_{1C}\cos\psi + \frac{\Delta\theta}{\Delta\beta}(\beta_o - a_{1S}\cos\psi - b_{1S}\sin\psi)$$

(2.98)

$$= \left(\theta_o + \frac{\Delta\theta}{\Delta\beta}\beta_o\right) - \left(B_{1C} + \frac{\Delta\theta}{\Delta\beta}b_{1S}\right)\sin\psi - \left(A_{1C} + \frac{\Delta\theta}{\Delta\beta}a_{1S}\right)\cos\psi$$

Tie-rod attachment in rotor blade.

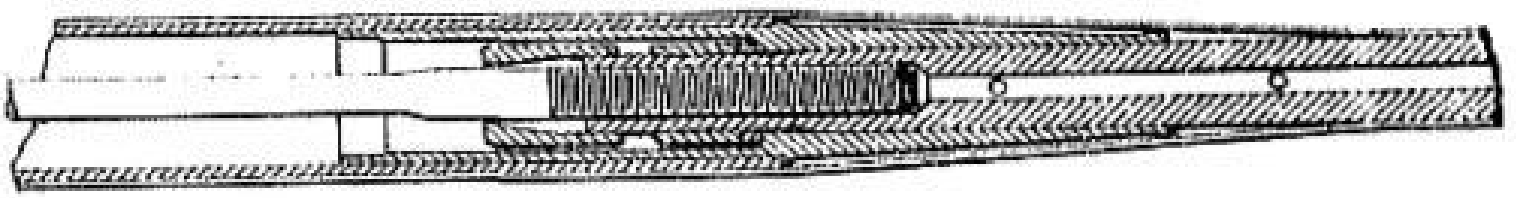

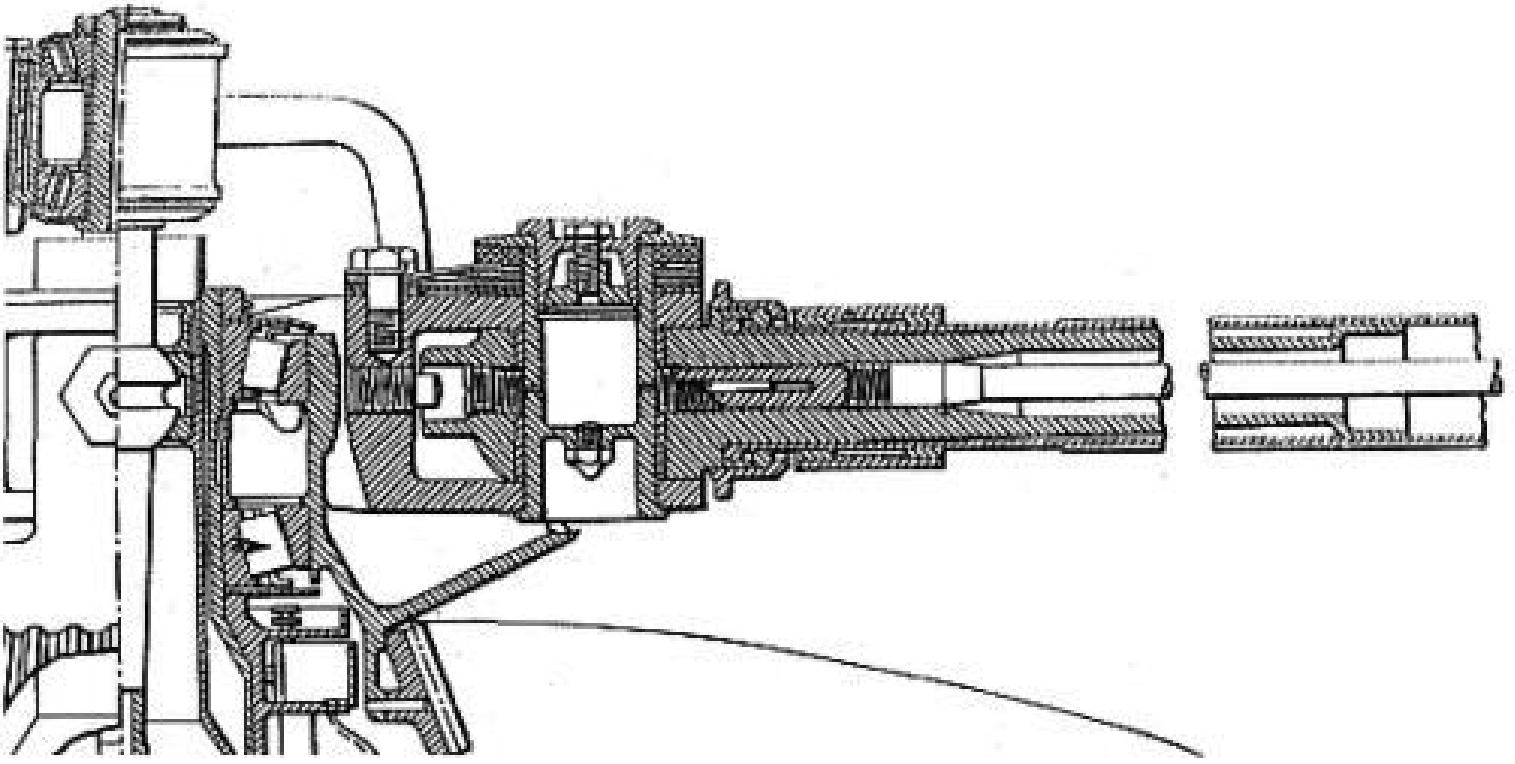

Fig. 2-43. Each A.R. III blade was retained by a tie rod [74].

2.7 SWASHPLATE CONTROL

The control loads depend on the forces required to twist the tie rods under a centrifugal force. Assume a tie rod was made of spring steel. Perhaps Hafner used classical

torsion theory of the era, provided, for example, by the second edition of *Mechanical Engineer's Handbook* [77] by Marks. In this 1925 handbook, the torsional stiffness of the tie rod (in modern notation) is

$$(2.99) \quad \text{Torsion Moment} = GJ\frac{\theta}{L}.$$

Hafner does not give the tie rod dimensions in his Society lecture [74], but in a later Flight magazine article [76] he states that 91.4 inch-pounds of moment twists the assembly 5.5 degrees. This information says that the torsional spring constant, (GJ/L) in Eq. (2.99), equals 635 inch-pounds per radian. Fig. 2-38 shows that the tie rod was about 50 inches long, and from the Marks handbook, Section 5, spring steel has a sheer modulus of elasticity (G) of 12,000,000 pounds per square inch. These estimates suggest the tie rod polar moment of inertia ($J = \pi d^4/32$) was 0.002644 inches,^{4} and therefore the tie rod diameter

was about 0.40 inch. Hafner notes that his preliminary stress analysis was favorable, and then goes on to say:

"but in view of the importance of this member one of these rods was given a very thorough test for possible fatigue effects due to the torsional oscillation. A tensile load four times the normal operating load was applied to one end through a large roller bearing, the other end being rigidly held. A torsional oscillation was applied to the free end with an amplitude more than twice the maximum possible in the aircraft, and with a frequency approximately four times that occurring in flight. The tie-rod underwent about three million reversals (equivalent to about 300 flying hours) without showing any sign of fatigue or strain, although one bearing failed in the course of the test."

Hafner appears satisfied that the tie rods can be designed based only on centrifugal force considerations saying "the proportions of the tie-rods are such that from a stressing point of view, the twisting causes only a very small increase in the stress intensity due to the centrifugal load...."

In fact, the tie rod was rather highly stressed and was, therefore, probably made of nickel chromium steel with a Brinell hardness over 250. Assuming it had an 0.40-inch diameter, the tie rod area was 0.1289 square inches. Hafner writes that he tested it in torsional oscillations with "a tensile load four times the normal operating load." He gives the normal centrifugal force as 3,400 pounds [76], which means the tie rod was being tested at a tensile stress ($S_{tensile} = 4$ CF/A) of about 106,000 pounds per square inch. The Marks 1925 handbook suggests, on pages 480/481, that the tie rod probably would not have yielded (i.e., take a permanent set) until the stress reached 20 to 50 percent higher depending on the exact composition of steel—*and any manufacturing defects*. I suspect that the threaded lengths of the tie rod, even though of larger diameter as shown by Fig. 2-43, was of much greater concern.

One thing seems clearly apparent about the tie rod design. Hafner made sure that the rotor could be over-sped by at least a factor of 1.5 for jump takeoff and, perhaps, even to twice normal rotor speed. Secondly, he refers to his concept [76] as "the torsionally flexible member described in my patents Nos. 418,212 and 418,698 published in October 1934." Presumably these are British patents.

2.7 SWASHPLATE CONTROL

Now, having some rough idea about the tie rod properties, let me go on to the pilot control loads. The blade is feathered by twisting the tie rod. The tie rod is twisted nose-up by a force acting up at the spider-arm-to-pitch-arm ball joint ($F_{ball\ joint}$) as Fig. 2-40 shows. The pitch arm length (p.a.l.) was taken earlier as

6.625 inches, which means that the ball joint force is 360 pounds per radian of pitch or about 6.3 pounds per degree of feathering (θ_ψ). This force for one blade, say the master blade, is resolved into the spider nonrotating spindle roll and pitch axis system by the spider arm length (s.a.l.) simply as

(2.100)

$$\text{Spindle Roll Moment} = RM_{spindle} = \left[\frac{GJ}{L(\text{p.a.l.})}\theta_\psi\right]\left[(\text{s.a.l.})\sin(\psi+\Delta)\right]$$

and

(2.101)

$$\text{Spindle Pitch Moment} = PM_{spindle} = \left[\frac{GJ}{L(\text{p.a.l.})}\theta_\psi\right]\left[(\text{s.a.l.})\cos(\psi+\Delta)\right].$$

As noted earlier, the ratio of spider arm and pitch arm lengths is (s.a.l./p.a.l. = 1/sin Δ). Then, substituting the periodic feathering, Eq. (2.98), into the spindle moment equations

gives the blade 1 contribution to the spindle moments as

(2.102)

$$\text{Blade 1 RM}_{\text{spindle}} = \frac{GJ}{L \sin\Delta}\left[\left(\theta_o + \frac{\Delta\theta}{\Delta\beta}\beta_o\right) - \left(B_{1C} + \frac{\Delta\theta}{\Delta\beta}b_{1S}\right)\sin\psi_1 - \left(A_{1C} + \frac{\Delta\theta}{\Delta\beta}a_{1S}\right)\cos\psi_1\right]\left[\sin(\psi_1 + \Delta)\right]$$

and

(2.103)

$$\text{Blade 1 PM}_{\text{spindle}} = \frac{GJ}{L \sin\Delta}\left[\left(\theta_o + \frac{\Delta\theta}{\Delta\beta}\beta_o\right) - \left(B_{1C} + \frac{\Delta\theta}{\Delta\beta}b_{1S}\right)\sin\psi_1 - \left(A_{1C} + \frac{\Delta\theta}{\Delta\beta}a_{1S}\right)\cos\psi_1\right]\left[\cos(\psi_1 + \Delta)\right].$$

Of course, the contributions from blade 2 and blade 3 must be added. This is done by repeating Eqs . (2.102) and (2.103), but with a blade 2 azimuth of $\psi_2 = \psi_1 + 120^\circ$ and a blade 3 azimuth of $\psi_3 = \psi_1 + 240^\circ$. The trigonometry is somewhat tedious, but the result is simplicity itself.

The resulting spindle roll and pitch moments for the Hafner three-bladed rotor are only steady moments—*there are no vibratory components*—given by

(2.104)

$$RM_{spindle} = -\frac{3}{2}\left(\frac{GJ}{L}\right)\left[\left(A_{1C} + \frac{\Delta\theta}{\Delta\beta}a_{1S}\right) + \left(B_{1C} + \frac{\Delta\theta}{\Delta\beta}b_{1S}\right)\cot\Lambda\right]$$

and

(2.105)

$$PM_{spindle} = \frac{3}{2}\left(\frac{GJ}{L}\right)\left[\left(B_{1C} + \frac{\Delta\theta}{\Delta\beta}b_{1S}\right) - \left(A_{1C} + \frac{\Delta\theta}{\Delta\beta}a_{1S}\right)\cot\Lambda\right].$$

There is, of course, a vertical spindle load that the pilot must apply with the "lift" lever to increase the collective pitch of the three blades simultaneously. This load amounts to (2.106)

$$\text{Spider Lift Force} = 3\left(\frac{GJ}{L}\right)\left(\theta_o + \frac{\Delta\theta}{\Delta\beta}\beta_o - \theta_{install}\right) + 3\left(I_\theta\Omega^2 R\right)\left(\theta_o + \frac{\Delta\theta}{\Delta\beta}\beta_o\right).$$

2.7 SWASHPLATE CONTROL

The second vertical load in Eq. (2.106) comes from operating the blade at any pitch angle (other than zero) in a centrifugal force field. This force is somewhat akin to sitting on a swing, twisting the swing, then letting go and the swing untwisting. The force depends on the polar moment of inertia (I_θ) of the airfoil-shaped blade section. However, if the blade section were cylindrical, this force would be zero. With respect to this vertical force, Hafner installed the tie rods at the angle expected for flight ($\theta_{install}$) to give the tie rods a centering position and reduce the "lift" lever load to near zero in flight. Note that the 3 in the preceding equations denotes the three blades, so the equations can be used for any number of blades (b) by simply replacing the 3.

To get the pilot forces at the "joystick" grip, Hafner gives the information [76] that the

resultant spindle moment

$$\sqrt{\left(RM_{spindle}\right)^2+\left(PM_{spindle}\right)^2}$$ for 5.5 degrees of feathering "and

including friction on the pitch change bearing and ball joint due to control loads = 91.4 lb. in." Additional friction in the "control mechanism" adds 2.27 inch-pounds so that together the "total moment, 94.12 inch-pounds [there must be a little more somewhere] gives a stick load of 2.51 pounds." This information implies an equivalent mechanical gear ratio of 37.5 to 1.

From the little sketch below, the pilot grip force (P) is related to the nonrotating spindle moment as

$$(2.107)\quad P=\frac{b}{a\,c}\left(\text{Spindle Moment}\right).$$

Fig. 2-39 indicates the lengths (a) and (b) are about equal, which makes c = 37.5 inches for the Hafner A.R. III.

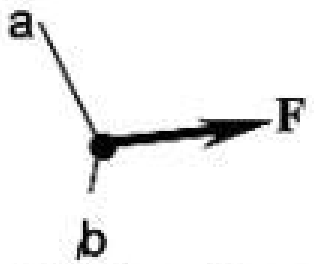

Hafner closes his analysis of control loads [74] by addressing

"Control Load Due to Moment of Inertia of Blade about Pitch Change Axis." The half page derivation is ill advised, in my opinion, because he leaves a distinctly wrong impression. However, in his "Summary of Mathematical Analysis" he says "The analysis further shows that if the plane of rotation of the rotor [i.e., the tip path plane, Fig. 2-9] coincides with that of the hub [giving zero flapping], which arrangement is to be preferred, then the inertia of the blades with respect to the pitch change axis acts exactly in the opposite sense to the action of the tie- rods, thus very fortunately, reducing still more the loads in the joystick." His statement, written as a single degree of freedom vibration problem in modern notation, becomes

(2.108)

$$\text{Torsion Moment} = I_\theta \frac{d^2\theta_\psi}{dt^2} + \left(\frac{GJ}{L} + I_\theta \Omega^2 \right) \theta_\psi .$$

Since the feathering motion is simple harmonic, $d^2\theta_\psi / dt^2 = -\Omega^2 \left(\theta_\psi - \theta_o \right)$, the inertial once-per-revolution torsional moment about the pitch change axis is cancelled, which reduces the torsion moment equation to the static problem Hafner solved. In effect, the blade is near resonance when feathered at once per revolution, and the torsion moment depends primarily on the tie rod spring constant (GJ/L). It is precisely this fact that makes the Hafner control

system design so attractive—and so feasible, particularly for larger machines—a point that Hafner drives home in his Flight magazine article [76].

Before leaving the Hafner story of swashplate control development, there was some very interesting discussion that followed his Royal Aeronautical Society lecture [74]. The chairman, Lieutenant Colonel J. T. C. Moore-Brabazon, a past president of the Society, opened the discussion by immediately saying that in a hundred years' time people would be saying "What wonderful engineers they had in those days, what marvelous machines they designed, but what poor photographs they took of them." Brabazon

took Hafner to task and suggested "to the young workers present who were trying out new things that they would do well to be really careful about their first photographs." Hafner, in his turn, apologized and added that the film "represented the first effort of an amateur."

Chairman Moore-Brabazon then asked Captain Frank Courtney [42] to say a few words. Courtney reminded the group that even though he had been in America the past few years, he had stayed close to "rotative-wing aircraft and still believed these rotating wings were the solution of the problem of safety in flight." He did include the statement that because the autogyro "had not leapt suddenly into tremendous success right at the start, people had regarded it as being, while very interesting, neat, and even beautiful, not particularly reliable."

Dr. A. P. Thurston was asked to

speak next and he began by saying that "it was difficult for him to realise that when he first met Herr Hafner he could hardly speak a word of English, but he had delivered his lecture that evening as one who was perfect in the language." Thurston went on to remind the audience that Major Jack Coats' [late of the RAF] generosity helped Hafner through the "development and building of the present machine and its forerunner." Major Coats first met Hafner in Vienna in 1930 and was so impressed he agreed to "set aside a certain sum of money for the building of machines [these were probably the R. I and R. II helicopters] and their further development." Hafner responded that he was grateful for the reference Dr. Thurston made to Major Coats, because to him "is due a great deal of credit for anything I have been able to achieve."

The third audience member to speak was another pilot, Reginald Brie [52] who

wanted to keep his remarks short so that "as much time as possible should be allowed to the unconverted." Brie noted that he had known Herr Hafner since 1932 and thought that he "was imbued with an infectious enthusiasm such as seemed to grip all those associated with rotative-wing flying."

Dr. H . C . H. Townend, the next audience member to speak, apparently had absorbed all of the Hafner engineering analysis, had seen the Garden Party flight demonstration, and chose to raise a very significant point. He was puzzled about "the difference in performance, particularly in controllability between the de la Cierva autogiro and the Hafner aircraft." Townend saw that rotor control by tilting the hub or by swashplate was aerodynamically the same and that it therefore "seemed to him inadequate to account for the difference in controllability [between the two control systems]." Hafner, in

his response, said, "There is very little difference aerodynamically between the Cierva autogiro and the Hafner gyroplane.

2.7 SWASHPLATE CONTROL

The extra controllability of the latter [spider control] is mainly due to the fact that the control is free from parasitic loads, and together with a low gear ratio to the joystick, which is possible in such a case, enables the pilot to carry out the various flying manœuvers quickly, effortlessly, accurately and with confidence."

The next several audience members who spoke touched on several subjects which I will briefly summarize as follows:

Dr. Watts: Now that lifting and controllability are

demonstrated, what about performance?

Mr. Reder: As a member of the Cierva Autogiro Company he thought it was too soon to make any comparison with different types of rotative-wing aircraft and that he hoped "they all got what they wanted to see, which was a machine that could carry out taxi flights from house to house."

Mr. Forman: From his experience of the work in America, he thought "they [Pitcairn and Kellett] were having about the same amount of success over there as was attained in Europe by Herr Hafner and Senior de la Cierva." He said that "when high speeds were achieved he thought the whole problem would be solved."

Mr. Kronfeld: "Why had Herr Hafner given up—he hoped only for the time being—the idea of going up into the sky absolutely vertically?"

Mr. Norman: The machines were coming along he could see, but what about "places from which such aircraft could be operated, in the centre of cities, and that would involve the question of flying in air much more turbulent than that experienced on the aerodromes where tests were at present carried out."

Mr. Radcliffe: "Up to the present, gyroplanes have not

shown a very good ratio of gross weight to tare weight [weight empty] and could Herr Hafner indicate what this ratio might be when the all-up weight [takeoff gross weight] is 9,000 pounds."

The discussion part of the paper Hafner published [74] ends with a 6-1/2-page communication from Dr. J. A. J. Bennett. Keep in mind that at the time of the Hafner lecture (October 1937), Dr. Bennett had stepped forward to fill Cierva's position as technical director of the Cierva Autogiro Company because of Cierva's death on December 9, 1936 . One can imagine that Bennett was disappointed in not attending the lecture—or, if he was there, he chose not to speak, preferring a written discussion. At any rate, Bennett's 6-1/2 pages gave Herr Hafner a thorough lesson sprinkled with some very pointed remarks.

Apparently a "controversy," as stated

by Hafner, was in full roar. The chronology of the situation seems to have begun when (if not before) the Hafner A.R. III performed at the Royal Aeronautical Society Garden Party on May 9, 1937. Clearly the press gave the demonstration, which included jump takeoffs, a glowing report as did the many people who saw the "gyroplane" fly. That event led to Hafner giving his lecture to the Society on October 14, 1937 . Then Bennett wrote an article about Hafner's lecture for Flight magazine [78], which was published on October 28, 1937, just two weeks after the lecture. The article Bennett wrote set the mood of the Cierva Autogiro Company. Hafner replied in detail to the article by Bennett in the November 1 1, 1937, issue of Flight [76] . At this point the Flight magazine editor intervened with:

"The arguments pro and con could obviously go on indefinitely. While *Flight* has been very pleased to give the hospitality of its columns to Dr. Bennett and Mr. Hafner we do suggest that the discussion should now be continued in the Journal of the R.Ae.S–Ed."

After that exchange, the Hafner lecture was published in the February 1938 issue of the Royal Aeronautical Society Journal. It included the communication by Bennett, which, as Hafner saw it (and as I thought when I read both), was "on the whole a repetition of an article published by him [Bennett] in Flight of October 28th 1937, where he opened a controversy on my paper."

An opening facet of the "controversy" was that Bennett continually referred to the Hafner hub and control system as a "false hub." Hafner, in his published paper, really took issue with that description saying, "Dr. Bennett considers the general use of the phrase

'direct feathering' to describe the A.R. III control as misleading terminology, since bodily tilting of the hub also produces feathering, and moreover he prefers to describe the former [Hafner's system] as a 'false hub' control. I cannot agree with this nomenclature which confuses means with ends." Bennett, after a couple of engineering pages, does equate the spider plane to "the false hub." Fortunately, both Hafner and Bennett were at least in agreement that both systems achieved control by tilting the rotor thrust vector relative to the aircraft center of gravity. However, they both went to enormous mathematical length to state that flapping and feathering were equivalent, [see Eq. (2.57)], when the objective was to reorient the tip path plane.

Bennett, in his communications, does congratulate Hafner "on designing such a neat and spectacular machine ....." But very pointedly refers to several Cierva British

Patent Specifications that covered every important aspect of the Hafner design. Specifically, Bennett refers to

- B.P.S. No. 410532—November 1932, Spider
- B.P.S. No. 264753—November 1925, Delta-3
- B.P.S. No. 393976—December 1931, Benefit of focus point

Furthermore, Bennett made sure everyone knew that "the word Autogiro is the registered trade mark of the Cierva Autogiro Co." To me, many parts of the Bennett communication sound as if the Cierva Autogiro Company was preparing to take Hafner to court. And yet, Peter Brooks, on page 21 of reference [7], suggests that "Hafner is believed to have made use of several Cierva patents with Cierva's knowledge and permission." Of course, by the time of this "controversy" Cierva had, unfortunately, been dead nearly a year.

However, I think the real heart of the "controversy" was twofold. First, the Hafner swashplate design plus tie rod blade retention reduced control loads, both steady and vibratory, in comparison to the Cierva C.30. Bennett acknowledged this point, but blamed the characteristics of the C.30 on the cambered airfoil. Secondly, the jump takeoff capability of the A.R. III was enhanced by the pilot having a "lift" lever, which Bennett said Cierva felt was an unwanted cockpit control because the "consistent use of the control in the most effective manner is probably beyond the capacity even of an expert pilot." (I doubt the pilots took *that* comment to heart!) It took Bennett and Otto Reder completing the C.40 (under development at the time Cierva died) before the Cierva Autogiro Company had, by August

1938, an Autogiro that compared to what the Hafner A.R. III gyroplane demonstrated a year earlier. I will return to this "controversy" again when the subject of jump takeoff is addressed.[17]

While all this progress (and controversy) was going on in England, the swashplate control efforts of Raoul Hafner were carried forward by Richard Prewitt, chief engineer at the Kellett Autogiro Company in the United States. The Prewitt design came closest to what we think of today as the modern swashplate control system.

2.7.6 Closing Remarks

The modern version of a blade pitch

control system is shown schematically in Fig. 2-44 . The swashplate, really a large ball bearing as Fig. 2-44 suggests, is the bridge between the nonrotating environment of the pilot and the rotating world of a blade . The inner ring of the swashplate is nonrotating and is ball-mounted to a slider. The slider permits the swashplate to travel up and down the rotor shaft a short distance of only several inches. The ball allows the swashplate to tilt left or right, and fore or aft, in response to pilot input. Maximum angles of swashplate tilt today are on the order of 15 to 25 degrees. The pilot dictates the swashplate rise and fall (i.e., the linear travel of the swashplate along the rotor shaft) with a "collective stick." He or she (or even some form of autopilot) controls the swashplate tilt in any direction with a "cyclic stick."

The physical connections between the collective and cyclic sticks used by the pilot,

and the nonrotating ring of the swashplate, have been made in any number of ways as new technology evolved. The Hafner hanging stick gave way to cables, pulleys, tubes, and bell cranks such as Kellett used in their XR-3 and XR-60. Today, hydraulic actuators combined with electronics and computers provide extremely reliable control for modern rotorcraft.

The ball bearing feature of the swashplate bridges the gap from nonrotating to rotating systems . The rotating ring of the swashplate is forced to rotate with the shaft by a "scissors" assembly (not shown), which allows swashplate tilting. Pitch links then make the connection from the swashplate rotating ring to each blade pitch arm. The pitch arm is rigidly attached to the blade-root end.

---

[17] The Raoul Hafner paper [74] contains even more worthwhile material than I have touched on here. One

thing is for sure, the discussions following a lecture to the Royal Aeronautical Society were very well recorded. They make reading historically significant engineering absolutely fascinating for me.

2.7 SWASHPLATE CONTROL

The Feathering

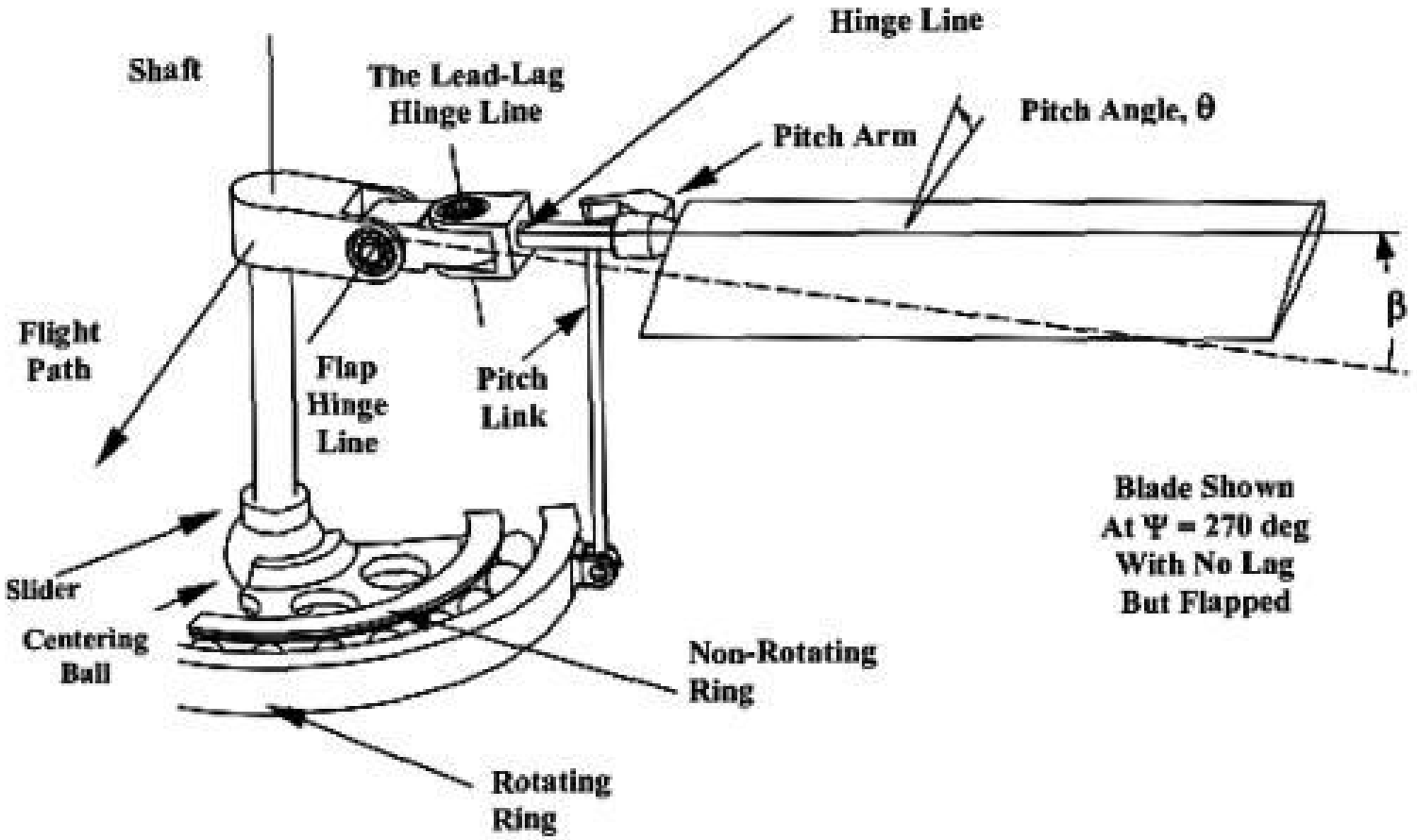

Fig. 2-44. Blade feathering and a modern

swashplate gave the pilot complete control (drawing by Rick Peyran).

The blade-root end is generally of circular shape and is attached to the hub with two feathering bearings and a "tension-torsion strap," which, in the Hafner blade retention assembly, was a long tie rod. The two feathering bearings react flap and lead-lag bending moments created by all blade loads. The tension-torsion strap restrains the blade against centrifugal force, but is designed to be quite easy to twist. Very little centrifugal force is loaded onto the two bearings. The total control system—from the pilot stick to blade-root end—requires only a small pilot force to vary blade pitch when the rotor system is at rest. The stick forces, without some power assist or force-balancing springs, can, for large rotorcraft, become very large in flight as you will see later.

The mathematical description of the control system, shown in Fig. 2-44, needs one other term added to what you have read so far. The term accounts for pitch (θ) – lag (ξ) coupling so that the blade feathering equation now appears as

(2.109)

$$\theta_\psi = \theta_0 - B_{1C}\sin\psi - A_{1C}\cos\psi + \frac{\Delta\theta}{\Delta\beta}\beta_\psi + \frac{\Delta\theta}{\Delta\xi}\xi_\psi .$$

2.7 SWASHPLATE CONTROL

The step that added collective pitch to what began as the Wilford "feathering blade" rotor system was made by Raoul Hafner with his A.R. III and David Kay[18] with his Kay Gyroplane in

England, and by Kellett and his chief engineer, Richard Prewitt, with the XR-3 in the United States in 1941.[19] The objective in the 1930s and early 1940s was to produce a machine that could do a jump takeoff.

---

[18] Unfortunately, I have yet to find much detail about the Kay hub and control system. The 1938 Jane's All The World's Aircraft [79] volume states on page (53c) that he had a patented hub, "in which blades are hinged on bushes are keyed to eccentrically mounted Z spindles. By rocking the Z spindles, the bushes are rotated and also oscillated about a transverse axis. This gives control over 8 degrees of the rotor blade incidence in the air. The same motion is used to tilt the rotor head for lateral control."

[19] Brooks notes on page 237 of reference [7] that "the rotor hub in the XR–3 was of completely new design, having a fixed spindle [hub] with collective and cyclic pitch control instead of the tilting direct-control head.

2.8 JUMP TAKEOFF

By the end of 1933 the autogyro industry had begun serious research and development of ways to give their aircraft jump takeoff capability. At that time the industry had (1) a configuration that could land in a very small area, (2) a rotor system that could be pre-spun up to near takeoff rotor speed, and (3) direct control of the aircraft throughout its flight envelope. But the true coming of the helicopter could already be seen because Louis Bréguet, assisted by René Dorand, was only 2-1/2 years away from first flight [39].[20] The view of the autogyro advocate was that if their rotorcraft could takeoff from the same small area in which it landed, then the autogyro had every benefit of the helicopter—except true hover—with considerably less complexity.

The autogyro pioneers all tackled the problem from the same starting point. Because the mechanical drive for rotor startup worked

well, that drive, with strengthening, could be used to over speed the rotor to 125 to 175 percent of normal flight RPM while the autogyro was on the ground. Any anti-torque the aircraft required would come from wheel-to-ground contact. The rotor would be over-sped at virtual zero collective pitch and, presumably, near zero thrust, so the full weight of the autogyro would be on the wheels. The rotor would store up an excess of kinetic energy. To release this energy, the pilot would declutch the startup drive and *something* would increase collective pitch from zero to the flight setting of 4 to 6 degrees. The autogyro would get an initial burst of thrust far in excess of its weight, and the leap upward would begin. The trajectory was not necessarily straight up because the propeller thrust would already be accelerating the autogyro up to speed so normal slow-speed forward flight would be obtained quite quickly. The flight could then be continued as if from a normal takeoff.

Each band of engineers appears to have agreed on the physics of how to do a jump takeoff. The differences were in just what would be the mechanical *something* that would raise collective pitch from zero to the flight setting. It is not clear if the height to which the autogyro should jump was initially a design objective. The early efforts appear to have resulted in 0 (i.e., failure) to 15 feet. With improvements over an 8-year period, jump heights ranged from 25 to 35 feet, depending on the prevailing wind. But then U.S. Army Air Force Captain Gregory [25] cleared things up in the United States by stating that the military requirement was to clear a 50-foot obstacle with no forward speed, whether landing or taking off.[21]

---

[20] As it turned out, the helicopter also arrived in the United States (the Platt-LePage XR-1 and the Sikorsky XR-4) and the autogyro advocates were virtually out of

business by 1943 or, like Kellett, had converted their configuration to the helicopter.

[21] I believe this one requirement said that only a helicopter would satisfy the U.S. Army. In my opinion, this statement by Gregory spelled doom for the autogyro.

2.8 JUMP TAKEOFF

The fact that jump takeoff was not fully developed until the very early 1940s should not diminish technical interest in the engineering approach to moving collective pitch from zero degrees to 4 to 6 degrees with a flick of the pilot's wrist. Cierva, Pitcairn Kellett, and Hafner each made their mechanical system work. Some details are a little sketchy, but let me describe each approach in turn.

2.8.1 Cierva's Approach

Cierva began efforts in August 1933 when, according to Brooks [7], "the first jump takeoffs had been achieved with the C.30 prototype, G-ACFI [British registration designation], fitted with a special rotor head." Apparently the early efforts were kept out of the public eye because Cierva did not announce the successful development of "direct takeoff" until his lecture before the Royal Aeronautical Society on March 15, 1935 [5]. Even then, he was quite tentative because he said,

"I want to make perfectly clear that the results obtained, only a few feet high jump, while absolutely conclusive are still experimental, and prudence forces me to refrain from making any forecast as to how soon they will be obtainable in a practical way. The eighteen months of development have given us a thorough insight into the theoretical aerodynamics of the new effect, together with a considerable experience of its practical side."

Then, Cierva goes on with

"All our conclusions will be incorporated in a new experimental machine [this was to be the C.40], which not only should show a very improved performance but which ought to be free from the secondary imperfections of the first one [ground resonance tendency and vibration]. Until the new machine has been thoroughly tested, nothing more can be said about this development. I will only mention that the mechanism used for the pitch change involves no addition whatsoever to the existing element of normal direct control autogiros, *consisting substantially in a tilt of the drag hinge in a vertical plane containing the axis of the blade, and that it operates automatically by the mere application of the starting torque in the usual way* [my italics] . Also, the actual manœuvre from the pilot's point of view is a very simple one, easier and more pleasant than an ordinary takeoff."

The details were described in depth by Dr. James A. J. Bennett. Dr. Bennett met Cierva in 1930, became a leading member of the autogyro community, and carried on as technical director at the Cierva Autogiro Company after Cierva died.[22] In 1960, the Royal Aeronautical Society established the

Cierva Memorial Lecture series when the Helicopter Association of Great Britain merged with the Society. Dr. Bennett had the enormous honor of giving the first lecture [80][23] . His recollections about working with Cierva provide insight into Cierva—both the man and the engineer. By custom, there was no discussion at a Memorial Lecture, but Wing Commander Reginald Brie [52] was asked to say a few words about Cierva, which give

---

[22] Señor Juan de la Cierva Codorníu was killed on December 9, 1936, when the DC–2 he was on crashed. Brooks describes the unfortunate circumstances surrounding the accident on page 248 of his book [7].

[23] In January 1939, Harold F. Pitcairn published a wonderful, unsurpassed tribute to Cierva [81] . A long-time friend, Wayne Wiesner, gave me his copy of the tribute. A Cierva Memorial Fellowship was started at New York University and Brooks [7] notes that there were 45 sponsors . Wallace Kellett became chairman of the Fellowship Committee. In the spring of 1940, Wayne Wiesner was one of the first recipients of the Cierva Fellowship.

even more insight into the man himself. The evening ended by Brie saying that "there was nobody better qualified [than Bennett] to present an appreciation of Cierva's life and work." Brie closed by proposing "a hearty vote of thanks to Professor Bennett for delivering this First Cierva Memorial Lecture."

In his lecture, Bennett includes a rather detailed discussion of the Cierva method to mechanically adjust collective pitch from 0 to the 4-to-6 degrees needed for a burst of thrust that initiates jump takeoff. He describes "a tilt of the drag hinge in a vertical plane containing the axis of the blade" and how "it operates automatically by the mere application of the

starting torque." The figure Bennett uses to illustrate the hinge geometry is shown here as Fig. 2-45.

The technical aspects of Cierva's idea are rather interesting when you think about it. He tried the approach with the C.30 prototype and the aircraft jumped up "a few feet." The flight rotor speed of the C.30 was nominally 245 rpm (25.65 radians per second or a tip speed of 475 feet per second for the C.30 blade radius of 18.5 feet), so the over-speed at zero collective pitch might have been, I will guess for this example, equal to 125 percent (32.06 radians per second) . Because thrust is zero and advance ratio is zero, the horsepower and torque at this condition is easily estimated from Eq. (2.60) as

(2.110)

$$\text{Power} = Q\Omega = \frac{\rho\left(\pi R^2\right) V_t^3 \sigma C_{do}}{8} = \frac{0.002378(1075)(1.25\times 475)^3 (0.047)(0.01)}{8}$$

which works out to about 31,500 foot-pounds per second (57 hp) and a torque of 980 foot-pounds. A simple first question to answer is this: How long does it take for the rotor to slow down from 32.06 to 25.65 radians per second if the collective pitch stays at 0 degrees? The answer to this question gives some idea about how long the aircraft can take to get up to flight speed.

To answer the question I have posed only requires the angular deceleration equation, which is

(2.111)

$$I\frac{d^2\psi}{dt^2} = I\frac{d\Omega}{dt} = Q = \rho A V_t^2 R C_Q = \left[\rho\left(\pi R^2\right)R^3 C_Q\right]\Omega^2 = -0.954\Omega^2 .$$

Note that while power is being drawn from the engine, the torque coefficient (C_Q) is positive.

However when declutched, the torque coefficient goes immediately from positive to negative ($C_Q = -\sigma C_{do}/8$) and the rotor draws energy from the over-sped RPM. Now integrate, assuming that the torque coefficient is constant over the integration interval, and that at time equals zero, rotor speed equals the initial 125 percent value (Ω_o = 32.06 radians per second). The result is that rotor speed bleeds off as

2.8 JUMP TAKEOFF

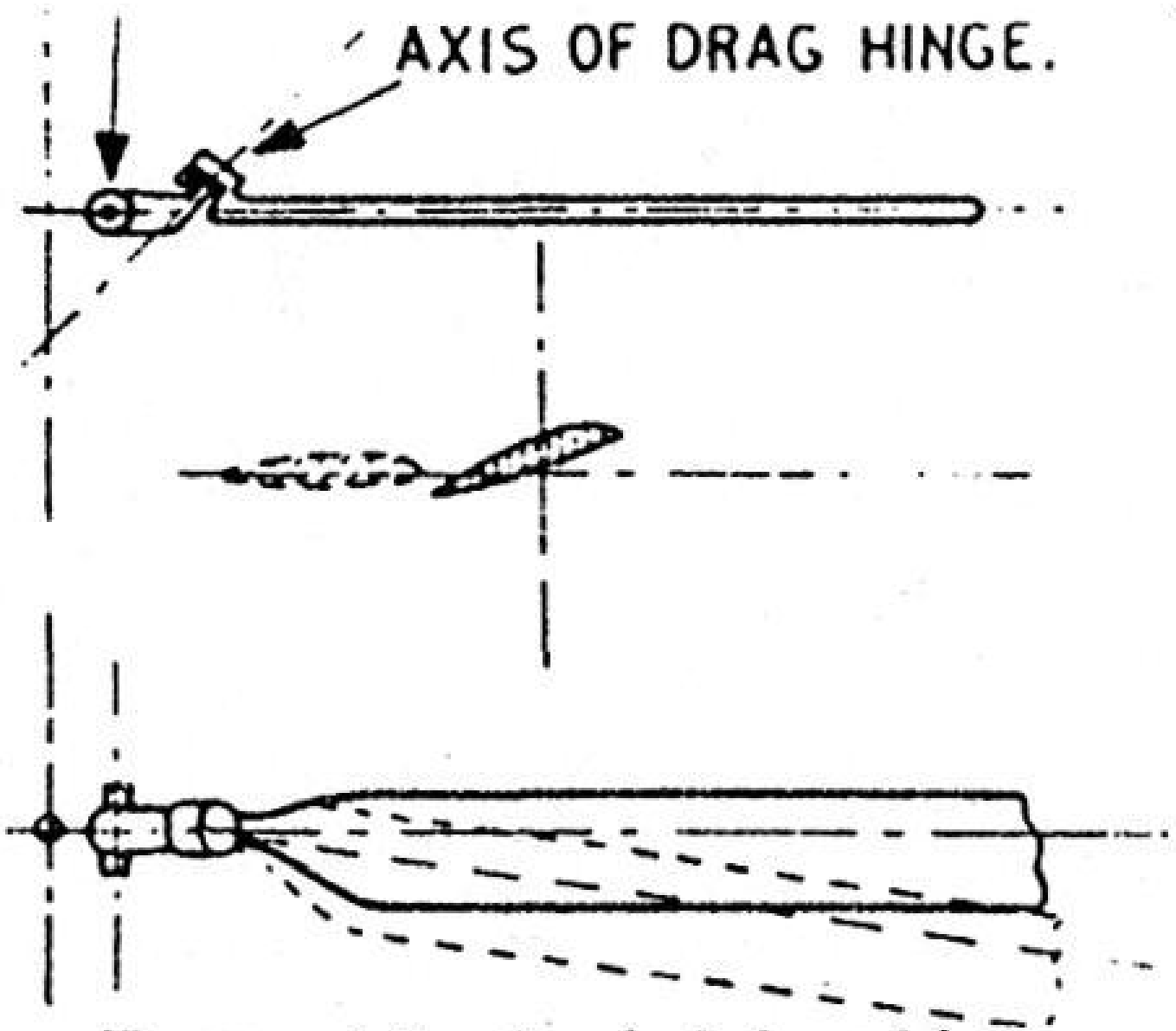

FIGURE 15. Angled drag hinge.

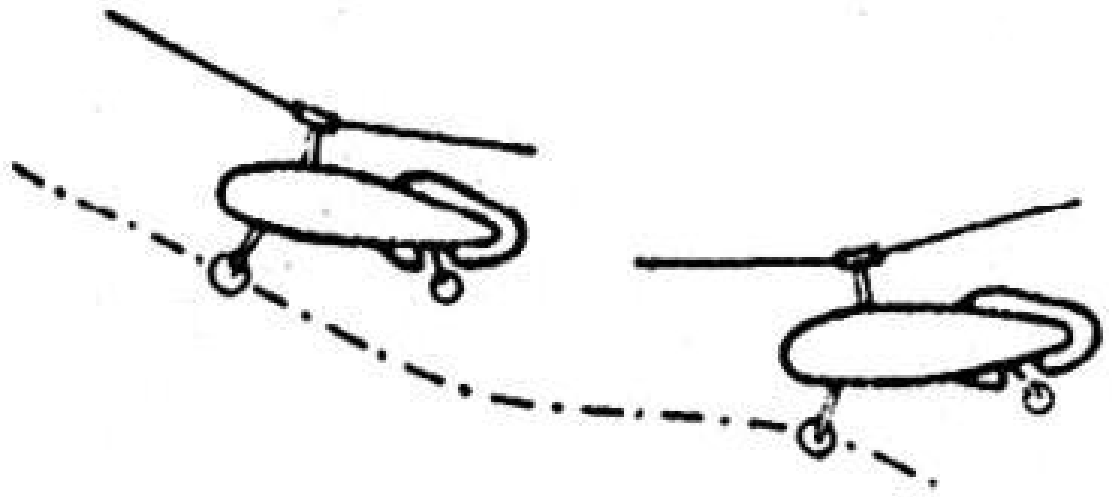

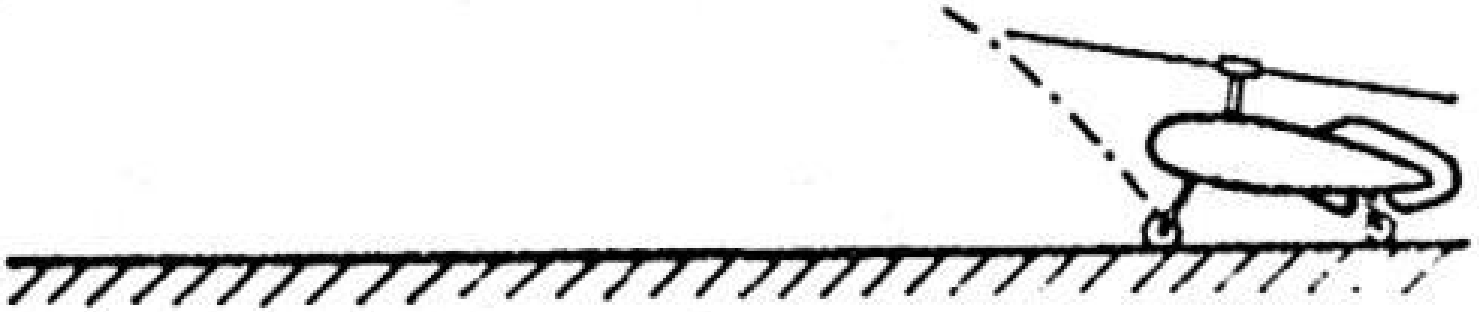

FIGURE 16. Path of machine during direct take-off.

Fig. 2-45. The inclined lead-lag hinge Cierva used to decrease blade pitch during rotor over-speeding prior to a jump (i.e., direct) takeoff [80].

$$(2.112)\quad \Omega_t = \frac{\Omega_o}{1-\left[\frac{\rho(\pi R^2)R^3 C_Q}{I}\right]\Omega_o t} = \frac{\Omega_o}{1-kt} = \frac{32.06}{1+0.0785t}.$$

Keep in mind that I arrived at Eq. (2.112) by assuming that the torque coefficient (C_Q) was constant over the integration interval and that ($C_Q = -\sigma C_{do}/8$). This result, applied to the C.30 Autogiro where the polar moment of inertia (I) for all blades is ($I = 3\times128.8$ slug-feet^2), shows that after 3.2 seconds the rotor speed will have dropped from 32.06 to 25.65 radians per

second, the normal rotor speed.

Looking at the problem from an energy point of view is also interesting. The exchange of energy behaves as

(2.113)

$$\text{Kinetic Energy per unit of time} = I\Omega\frac{d\Omega}{dt} = \text{power} = \left[\rho\left(\pi R^2\right)R^3 C_P\right]\Omega^3$$

2.8 JUMP TAKEOFF

which, *upon integrating with a constant power coefficient* (C_P) and decaying rotor speed defined by Eq. (2.112), gives

(2.114)

$$\frac{1}{2}I\left(\Omega_o^2 - \Omega_T^2\right) = \int_0^T \left[\rho\left(\pi R^2\right)R^3 C_P\right]\Omega^3\,dt = \rho\left(\pi R^2\right)R^3 C_P \int_0^T \left[\frac{\Omega_o}{1-kt}\right]^3 dt$$

$$= \frac{1}{2}\left[\rho\left(\pi R^2\right)R^3 C_P\right]\left[\frac{2-kT}{(1-kT)^2}\right]\Omega_o^3 \quad \text{where } k = \frac{\rho\pi R^5 C_Q \Omega_o}{I}$$

The kinetic energy given up to slowing the rotor down from 32.06 to 25.65 radians per second is 72,000 foot-pounds at zero thrust. If this same amount of kinetic energy were, instead, all applied to lifting the 1,450 pound C.30, the Autogiro would have jumped 50 feet above the ground instead of the "only a few feet high jump" which Cierva obtained in his first trials. The difference, of course, is that when the collective pitch goes from 0 to 4-to-6 degrees, the burst of thrust is accompanied by a very large increase in power required, which dissipates the kinetic energy even more quickly than the example above suggests.

Now consider the blade motion coupling Cierva used to make jump takeoff work. The application of 57 horsepower to the prototype C.30 yielding a 125-percent over-speed creates a steady lag angle (ξ_o) as Eq. (2.3 1) shows. This lag angle, under power with zero blade pitch, amounts to

(2.31) $\zeta_o =$

$$\frac{P/b\Omega}{r_\xi F_C} = \frac{(550)(57)}{3(32.06)(1)(5,200)} = 0.063 \text{ radians} = 3.6 \text{ degrees}.$$

Then, when the engine is declutched, the blade returns to a straight-out position and the flight collective pitch increases to about 6 degrees as Bennett suggests in Fig. 2-45 . This pitch-lag coupling is determined quite simply by

(2.115) $\Delta\theta = \Delta\xi \tan\alpha_1$ so that

$$\alpha_1 = \text{arc}\tan\left(\frac{\Delta\theta}{\Delta\xi}\right)$$

where (α_1) is the lead-lag hinge inclination from vertical.[24] For the C.30 prototype, this inclination is roughly 60 degrees, which is somewhat more than Bennett suggests in Fig.

2-45.

While the basic approach worked on the three-bladed C.30, the lead-lag dampers impeded the return of the blade to straight out from the 3.6-degree lag position at the over-sped rpm condition. The lag damping was reduced but then ground resonance became an issue. As Brooks [7] relates the story,

---

[24] Bennett [80] provides an excellent discussion of some 1 5 flapping and lead-lag hinge geometries that were tested on the Cierva C.30 Autogyro. In his figures 18, 19, and 20 in reference [80], he shows the mechanical layout of each one. With figure 17, he explains hinge angles such as delta-3 . Furthermore, he notes that the lead- lag hinge, when inclined fore and aft from vertical, couples flapping to lead-lag motion, which provides enough damping in the lead-lag motion that lag dampers can be removed. His nomenclature has been handed down through the decades. This makes the First Cierva Memorial Lecture absolutely required reading.

2.8 JUMP TAKEOFF

"The main drawback to this elegantly simple system lay in the fact that unrestricted movement of the blades in the drag plane, required for the jump, meant that it was not possible to provide adequate drag hinge damping to prevent ground resonance. Because of this, the system was found to be only practical [at that moment] for two-blade rotors and, even then, vibration levels were high. Even with two blades, to avoid resonance, it was found that the blades had to be held in flat pitch against the forward stops, instead of being simply allowed to lag during the spin-up. This design was a feature of the Autodynamic rotor which first publicly demonstrated jump takeoffs [to over 20 feet] on June 23, 1936."

An account by Bennett [80] is also very interesting. He writes that,

"only a two-bladed rotor having been free from 'ground resonance' when Cierva's inclined drag hinges were operated without dampers, and the two-bladed rotor having had inherent vibration of twice rotor frequency and of unpleasant amplitude throughout the

entire speed range, it was necessary to find a solution to this difficulty before the jump takeoff technique developed by Cierva could be applied to an aircraft suitable for production. The three-bladed rotor system of the C.40 was relatively free from vibration and the 'ground resonance' *difficulty was overcome by the provision of drag dampers which damped the motion of the blades with respect to each other but which allowed the symmetrical oscillation of the three blades with respect to the hub to remain undamped* [my italics] . This configuration, which proved to be most successful, brought the Autogiro once more to the production stage."

The Cierva C.40 (Fig. 2-46) jumped to about 12 feet in height by over-speeding the rotor to 285 rpm versus its normal flight rotor speed of 1 80 rpm, which is an over-speed of 58 percent.

As it turned out, the C.40 was the last of the Cierva Autogiros . Bennett writes that "a batch of five C.40 Autogiros was supplied to the Royal Air Force shortly before the Second World War and they were used by the British Expeditionary Force in France in 1940."

2.8.2 Pitcairn's Approach

Pitcairn engineers demonstrated a collective pitch mechanism for jump takeoff with their P-22 research aircraft. Rather than try to accomplish the change from flat pitch to 4 to 6 degrees through hinge geometry, they used the excessive centrifugal force in a much different way. The details are a little sketchy, but Agnew Larsen, chief engineer at Pitcairn, writes [49]

"While Cierva initiated this important new development in England by employing large inclinations of the lead-lag hinge in the rotor blade span axis, the approach in this country was different. The mechanical principle employed by the Autogiro Company of America was to permit the blades to increase their pitch by a four or five degree rotation on a steep pitch multithreaded shank in the blade root. The source of energy to effect this was the powerful centrifugal pull on the blades, causing them to momentarily move outward, away from the hub center. This motion was minute and

was, of course, confined between positive stops, one for minimum pitch and one for maximum. The means of control was hydraulic pressure which held the blades in the position of minimum pitch and, upon the sudden release of pressure, simultaneously with the declutching of the power torque, the blades were all equally free to shift outward and upward to the aerostational pitch [flight setting] of approximately 4-3/4 degrees where they remained throughout the entire flight regime. There could be no flutter of the blades, because the pitch on the sextuple thread was so steep that the powerful centrifugal pull on that angle virtually locked it there. This system was first tried out on the PA-22 flying mock-up, and later it was thoroughly applied in the more advanced PA-36 all-metal cabin,

2.8 JUMP TAKEOFF

jump-takeoff, and roadable autogiro, and later in the PA-39 conversions of the older PA-18 autogiros under contract for the British Air Ministry. The system worked very well and proved eminently successful in every way. It was remarkably free from any bugs, its automatic

functioning being virtually fool-proof; smooth, sure and positive."

Thus, with the Pitcairn approach, the blades were drawn inward, by a hydraulic cylinder, to a minutely smaller radius, and the blade was then in flat pitch. The rotor was then over-sped. At the pilot's command, engine power to the rotor was removed, hydraulic pressure was released, and centrifugal force took over. As soon as the hydraulic pressure was turned off, the blades slid outward along a very course thread, which increased pitch to 4.75 degrees. I like the part where Larsen says: "It was remarkably free from any bugs, its automatic functioning being virtually fool-proof; smooth, sure and positive."

The Pitcairn P-22 (which led to the P-36, in its ninth research configuration) over-sped the rotor to about 150 percent and, as Townson [45] states, "When the meteorological

conditions were right a vertical jump to eight to ten feet was not unusual." The P-36 (Fig. 2-47) did better, reaching some 35-foot-high jumps.

2.8.3 Hafner and Kellett's Approach

Both Hafner, with his A.R. III, and Kellett, with their XR-3, used a swashplate configuration, as I have already discussed. This gave the pilot control of collective pitch for the jump takeoff maneuver and was independent of centrifugal force.

Each chief engineer, as you can see, found a way to nearly instantaneously change blade collective pitch from flat pitch to flight setting by a flick of the pilot's wrist. The Cierva and Bennett approach required no additional hardware to the direct control rotor system. Larsen, at Pitcairn, added hydraulics to the

aircraft systems and kept the Cierva direct control system. Hafner, in England, and Prewitt, at Kellett, introduced the modern swashplate control system, which reduced control loads and vibration—and gave the pilot complete control of the jump takeoff maneuver.

Now let me return to the Raoul Hafner lecture [74] and its "controversy" for a moment. Giving a pilot (even an "expert pilot") control of rotor system collective pitch with a "lift" lever was not something that either Cierva or Bennett favored, as you will recall reading in Section 2.7. On top of this, Hafner created discord with Bennett and the Cierva Autogiro Company regarding the jump takeoff maneuver. In his lecture, Hafner showed a comparison between two jump takeoff trajectories. He used a diagram, reproduced here as Fig. 2-48, to say that his gyroplane could perform a "towering" jump takeoff and implied that all other autogyros were taking

off along the "jumping" path. The film that he showed during his lecture must have included both trajectories because he answered a question from Dr. Townend by saying:

109 2.8 JUMP TAKEOFF

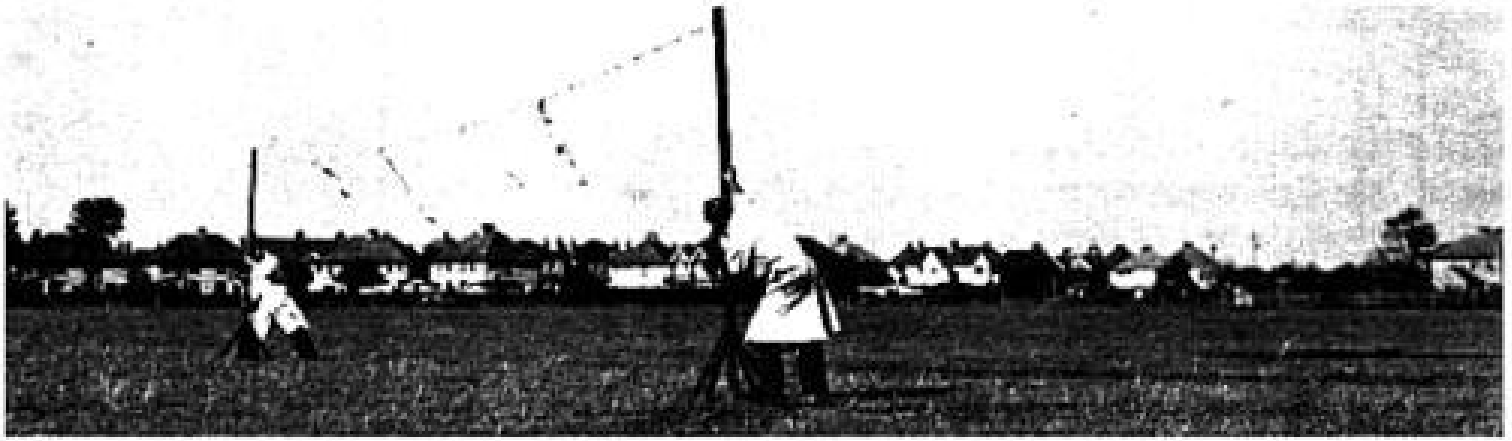

Fig. 2-46. The Cierva C.40 performing a jump takeoff not too long after first flight in February 1938 (photo courtesy of Gordon Leishman).

Fig. 2-47. The Pitcairn P-36 publicly demonstrated jump takeoffs in July 1940 [45].

"The diagram which Dr. Townend mentioned showing the contrast between jumping and towering takeoffs of the A.R. III was obtained from film records [the numbers are actual times in seconds] and is in agreement with calculations. It was drawn to scale. In both cases wind conditions and initial rotor revolutions were identical, and it serves, therefore, as a good comparison. The towering takeoff in question was shown later in the film. On one or two occasions when an extreme jump takeoff was carried out the aircraft in the subsequent sink actually touched the ground."

Hafner suggests that the "towering" takeoff is preferable and is only possible because of the superior controllability provided by his A.R. III spider control system. Of course, Bennett [78] immediately took issue with this outlook saying:

"the kinetic energy is most efficiently converted into potential energy the more sudden the change in pitch, and in the type of jump takeoff demonstrated last year by the 'Autogiro' and filmed by *Flight* the machine 'towered' right from the top of the jump. That the change of pitch is effected automatically does not necessarily mean that the change of pitch is sudden. In fact, de la

Cierva intended that the rate of change of pitch should be controlled so that any quality of direct takeoff from 'towering' to pure vertical 'jumping' could be achieved and he patented suitable means for obtaining this result in January, 1935 . It is considered that multiplication of manual controls is a retrograde step and that a manual control for effecting pitch change for takeoffs is undesirable, as consistent use of the control in the most effective manner is probably beyond the capacity even of an expert pilot."

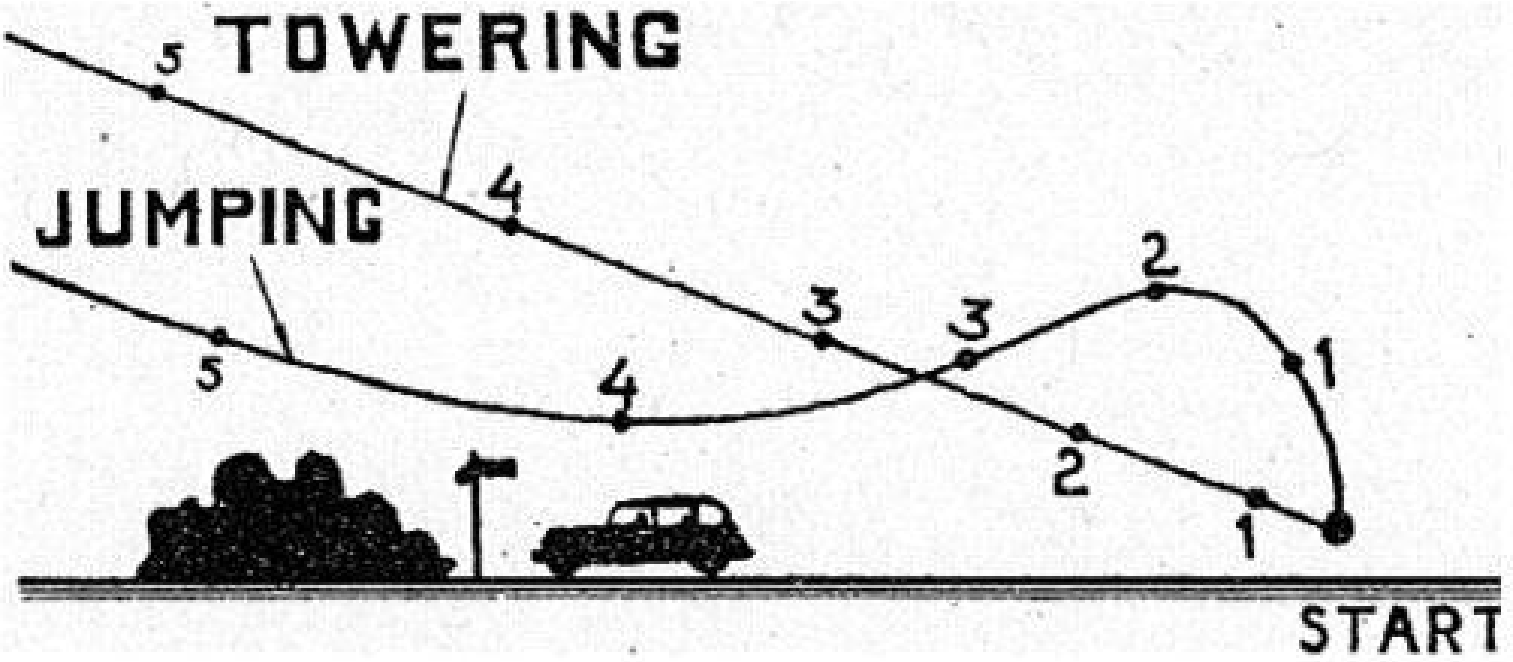

Fig. 2-48. The Hafner view of the benefits to a pilot-controlled jump takeoff [74].

2.8 JUMP TAKEOFF

Hafner immediately took advantage of *Flight* magazine, which was "pleased to give the hospitality of its columns" to pros and cons—up to a point. Regarding jump starts, Hafner wrote [76] that, yes,

"de la Cierva patented various elaborate mechanisms in order to delay the rate of change [of pitch] and obtain takeoffs varying from the direct jump. The lift lever of the A.R. III is a simple mechanism, and its use during a direct takeoff is in effect analogous to the fore-and-aft movement of the joystick in an orthodox aircraft during a running takeoff, and anyone who can be trusted with a joystick is safe to handle it, since the worst misuse of it would be a very crude jerk, which would produce a jump takeoff."

A little further on Hafner says, "I fail to see how any automatic device could improve on

the performance of even a mediocre pilot."

Personally, I doubt that Hafner was particularly concerned about (1) Bennett's criticism of the A.R. III spider swashplate, (2) his criticism of giving a pilot the "lift" lever, (3) his view of jump takeoff trajectories, or even (4) about what to call autogyros. I believe Hafner was ready to return to designing helicopters . The helicopter, I think he knew, was going to require his control system.

2.8.4 Kellett's Predictions

The jump takeoff maneuver, applicable to both autogyros and helicopters, is a very interesting problem in F = ma and energy use. Before discussing the 1934 theoretical and model experimental study by John Wheatley of the N.A.C.A. [82], let me first discuss the simpler, 1938 Richard Prewitt

analysis of the problem [83], which used the energy method.

Richard Prewitt, chief engineer of the Kellett Autogiro Corporation, presented a paper at the Rotary Wing Session during the Sixth Annual Meeting of the Institute of Aeronautical Sciences (later to become the A.I.A.A.). This meeting was held on January 25, 1938, and the paper by Prewitt was titled *Possibilities of the Jump-Off Autogiro* . At that time, Kellett was responding to U.S . Army Air Force field use of its YG-1/1A/1B autogyro, which had direct control—not swashplate control—and no jump takeoff capability. He also was in the midst of developing the XR-2 with the jump takeoff feature when it encountered ground resonance (see Fig. 2-11).

In his paper, Prewitt [83] first answers the question about how much power is "required for sustentation [hovering]"

as a reference point. He develops a "simple plot of power loading *vs* . disc loading" based on the 1920 view by E. P. Warner [84] of the "theoretical optimum values of horsepower required based on rotor diameter, rotor r.p.m., power loading, and disc loading." Prewitt confirms the view held by Warner with experimental data from eight helicopters provided by R. N. Liptrot [85] during an April 1930 lecture to the Royal Aeronautical Society. This historically significant graph is reproduced here as Fig. 2-49. The solid line that Prewitt chose to represent the hovering power required by an "actual helicopter" was computed as

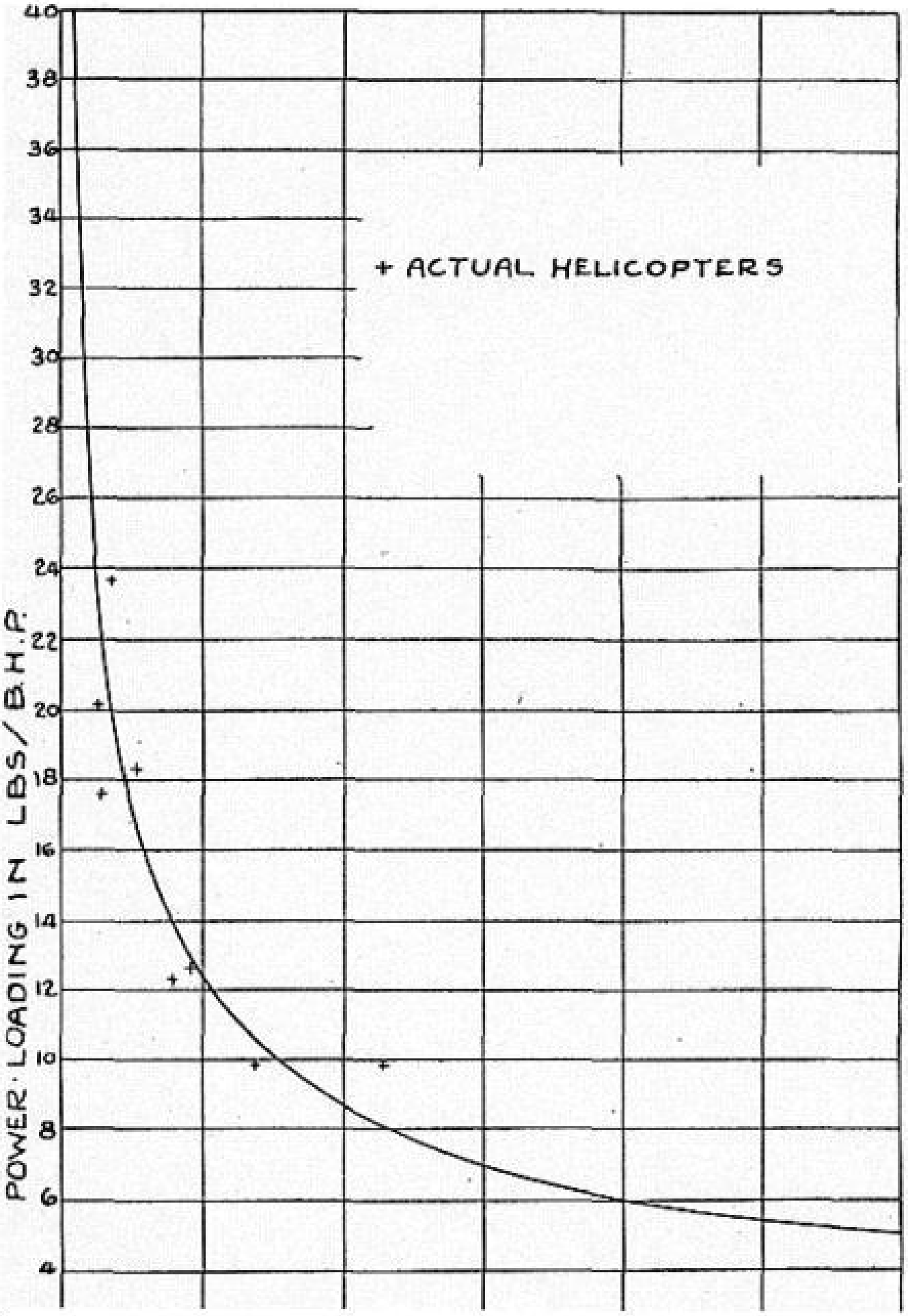
40
38
36
34
32
30
28
26
24
22
20
18
16
14
12
10
8
6
4
+ ACTUAL HELICOPTERS
POWER LOADING IN LBS / B.H.P.

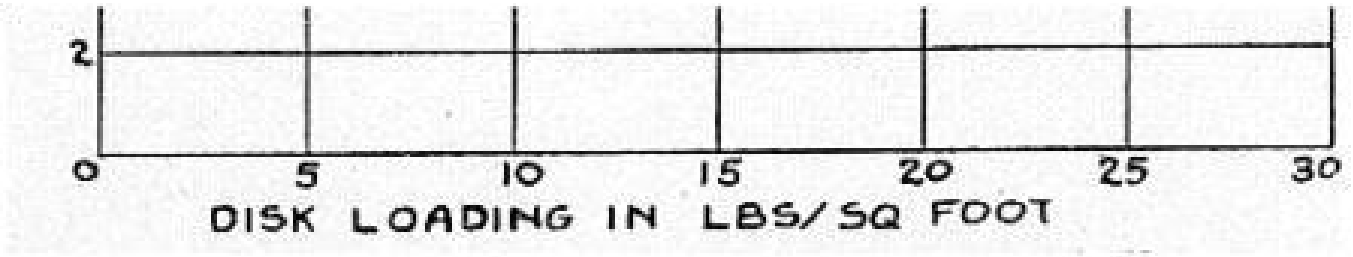

Fig. 2-49. The Prewitt view of hovering helicopter performance in January 1938 [83].

$$(2.116)\quad \frac{W}{HP}=\left[\frac{550}{\sqrt{W/2\rho A}}\right]FM$$

where (W) is weight in pounds, (HP) is the brake horsepower of the reciprocating engine, (ρ) is the density of air, and the rotor, or rotors as the case may be, have an area (A). The constant (FM) is referred to today as Figure of Merit. Were the helicopters 100 percent efficient, their Figure of Merit would be 1.0. The line Prewitt shows in Fig. 2-49 assumes the Figure of Merit is 0.7. Thus, his opinion was that the helicopter rotor would produce 30 percent less thrust per horsepower than what should be expected from the ideal rotor.

Prewitt gave the very simplest

approach to analyzing the jump takeoff by extending the energy approach described in Eq. (2.113) to include potential energy. Following his thought, but with modern notation, he wrote

$$I\Omega\frac{d\Omega}{dt} = P + W\frac{dh}{dt}. \tag{2.117}$$

This equation can be easily integrated, assuming power is constant, to give

2.8 JUMP TAKEOFF

$$\frac{I}{2}\left(\Omega_o^2 - \Omega_t^2\right) = (550\,HP)\,t + Wh \tag{2.118}$$

and this result can be solved for the jump takeoff height (h), which is simply (2.119)

$$h = \frac{I}{2W}\left(\Omega_o^2 - \Omega_t^2\right) - \frac{550}{W/HP}t\,.$$

This result can be used to approximate the jump height for an autogyro, say the Cierva C.30. Suppose the initial rotor speed (Ω_o) is 75 percent higher than the C.30's normal low rotor speed of 180 revolutions per second (i.e., $\Omega_o = 1.75 \times 19$ radians per second). The C.30 rotor system polar moment of inertia (I) is 390 slug-feet^2, its takeoff gross weight is about 1,900 pounds, and its rotor diameter is 37 feet, which is an area of 1,075 square feet. From Eq. (2.1 16), with the C.30 disc loading (W/A) of 1.77 pounds per square foot, and assuming a sea-level density (ρ) of 0.002378 slugs per cubic foot, the power loading (W/HP) comes out 20 pounds per horsepower. Now, assume the jump takeoff is completed within 1.75 seconds (see Fig. 2-48) and that the rotor speed decays to ($\Omega_{t\,=\,1.75}$ = 19 radians per second) or 180 revolutions per second. From Eq. (2.1 19), the jump height is 27 feet. This is, of course, an optimistic result.

There is one major reason the preceding example yields the optimistic result of 27 feet. If the rotor thrust only equals the autogyro weight then there is no excess rotor thrust to climb, and the autogyro would simply be "hovering" for 1.75 seconds with its wheels just off the ground. Prewitt recognized the introductory nature of Eq. (2.1 19) and offered several realistic engineering equations (and a step-by-step solution method using the equations) to obtain a more realistic jump height. The equations and method Prewitt used, which parallel the more exact method given by Wheatley [82] that I will discuss next, yielded results for four cases that he tabulated as follows:

Table 2-3. The Prewitt View of Possible Jump Takeoff Performance

Ship	Propeller Type	Rotor Blade Angle, deg	Jump Height, feet	Horizontal Distance, feet	Time, sec	Initial Acceleration, ft/sec^2
1	Fixed	0 to 5	Normal takeoff			
2	Fixed	0 to 15	40	25	2.5	35
3	Controllable	0 to 20	75	34	3.8	40
4	Controllable	0 to 30	225	55	4.2	60

Along with this table, Prewitt gives the jump takeoff paths shown here as Fig. 2-50 and offers two conclusions:

"(1) It appears that all-purpose autogiros can be built to 'jump-off' up to 100 feet and that for special purposes, autogiros can be made to 'jump-off' 200 feet. In the former case, the gross weight of the ships will be increased less than 5 per cent to account for the increase in blade weight and extra mechanism involved and in the latter case, the gross weight will be increased less than 15 per cent for the same items.

(2) The available kinetic energy in the rotor system for 'jump-off' is directly proportional to the weight of the blades and to the square of the rotational speed of the rotor. Thus, with a

2.8 JUMP TAKEOFF

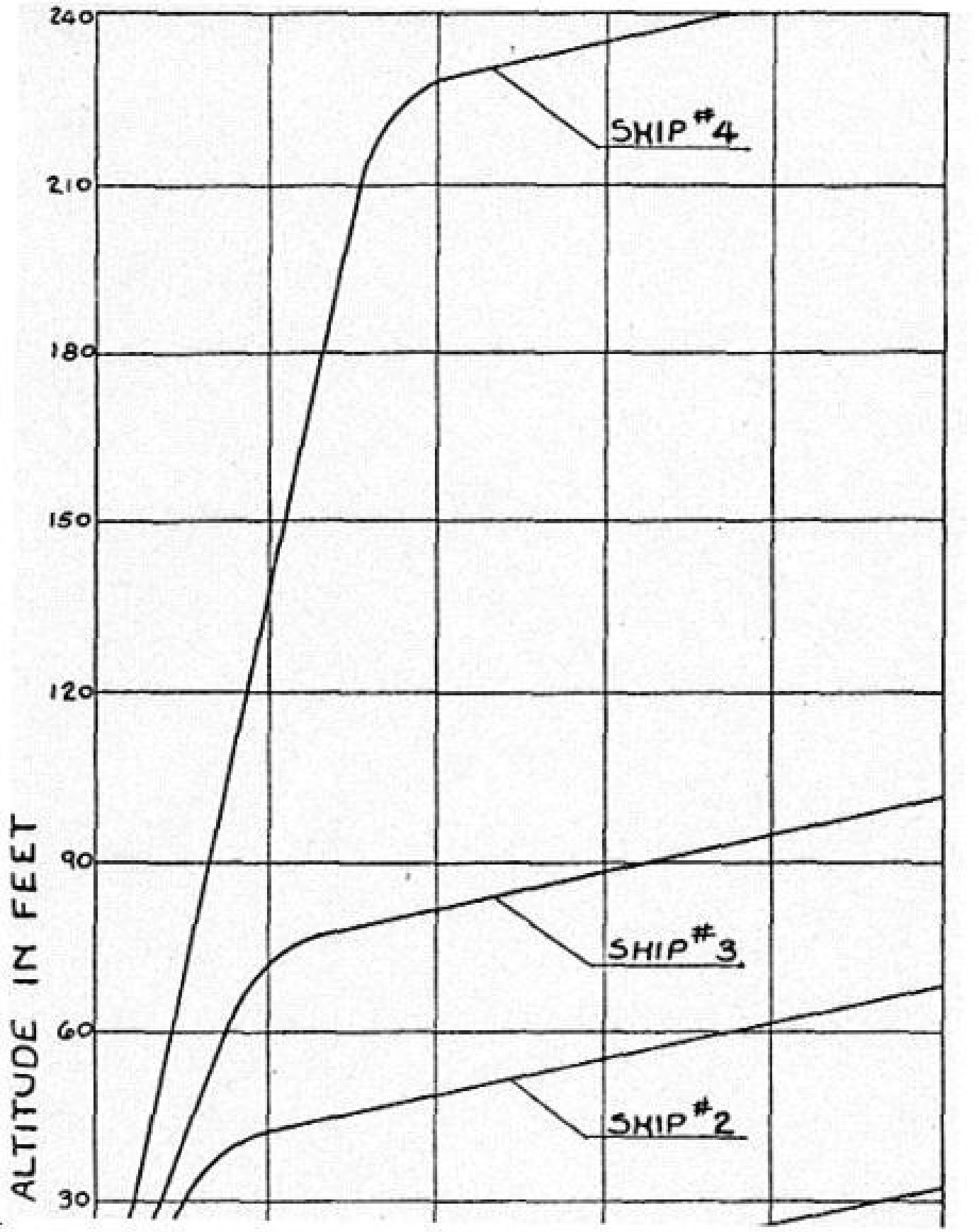

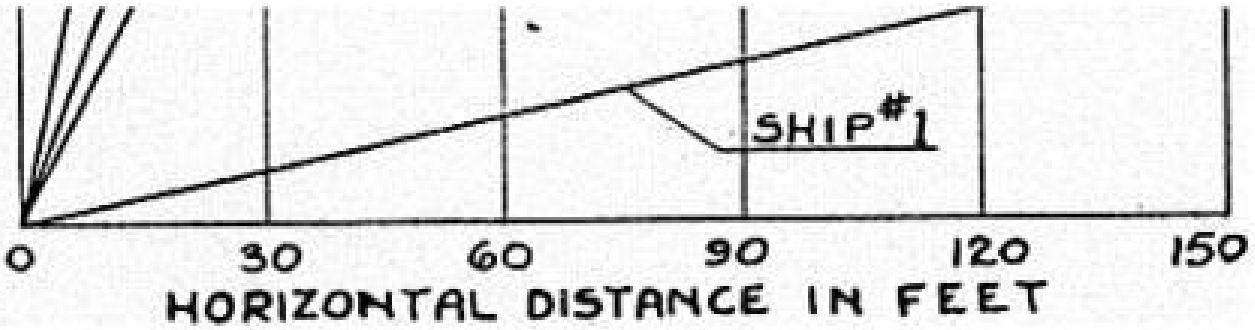

Fig. 2-50. The Prewitt calculated jump takeoff trajectories [83].

given autogiro having the weight of blades fixed, the height of 'jump-off' is dependent upon the horsepower available for accelerating the rotor. This in turn, is dependent upon the pitch setting of the propeller which, for relatively high jumps, would have to be of controllable [pitch] type to provide adequate power for the rotor and yet hold down the engine r.p.m. at top speed."

The potential for autogyro jump takeoff that Prewitt suggested must have been well received by aircraft advocates. However, at this point in time the Henrich Focke side-by-side German helicopter, Fig. 1-2, had already astounded the world in 1936 and this first industry growth step was about to be taken in the United States. Clearly, the

capability Prewitt predicted did not meet the U.S. military objective of a *vertical* takeoff to 50 feet height—but it did come close.

2.8.5 Wheatley's Research

Concluding discussion of jump takeoff at this point would dismiss the contribution John Wheatley made to this aspect of rotorcraft technology. In October of 1936, Wheatley [82] published a thorough analysis, supported with 10-foot-diameter model testing, which gave predicted jump takeoff performance a real foundation. He began with the statement that

vertical acceleration (d^2h/dt^2) depended on the

difference between excess rotor thrust (T) and aircraft weight (W). He wrote the F = ma physics as

$$(2.120) \quad \frac{W}{g}\frac{d^2h}{dt^2} = T - W$$

and proceeded to methodically integrate from acceleration to vertical velocity (dh/dt) to vertical height (h). The problem, of course, requires knowing how thrust varies over the integration interval . Thrust depends upon vertical velocity and the decaying rotor speed, and rotor speed depends on deceleration torque, which itself depends on vertical velocity. The exact solution is readily obtained, given some auxiliary equations, by doing numerical integration on a computer. However, Wheatley found that the problem could be linearized with engineering accuracy. His solution provided answers in closed

form, which is—I believe—always the most useful form.

The variation of thrust and torque with vertical velocity and rotor speed is obtained from Eqs. (2.48) and (2.49). These equations are simplified for the vertical jump takeoff problem because advance ratio (μ_{hp}) is zero. Because advance ratio is zero and the pilot intends to go straight up, both longitudinal and lateral feathering (B_{1C} and A_{1C}) are zero and there is no flapping (i.e., a_{1S} and b_{1S} both equal zero). The general equations for thrust and torque therefore reduce, with slight rearranging to make rotor speed (Ω) and solidity (σ) more visible, to

$$(2.121)\quad C_{Thp} = \frac{T_{hp}}{\rho \pi R^4 \Omega^2} = \frac{\sigma a}{2}\left[\frac{1}{2}\lambda_{hp} + \frac{1}{3}\theta_o\right]$$

and

(2.122)

$$C_Q = \frac{Q}{\rho \pi R^5 \Omega^2} = \frac{\sigma C_{do}}{8} - \frac{\sigma a}{4}\left[\lambda_{hp}^2 + \frac{2}{3}\lambda_{hp}\theta_o\right]$$

$$\text{or} \quad C_Q = \frac{\sigma C_{do}}{8} - \lambda_{hp} C_{Thp} .$$

Now the inflow (λ_{hp}) to the rotor depends primarily on the flight path velocity (V_{FP}) and the angle of attack of the hub plane (α_{hp}) as Eq. (2.28) shows. In the jump takeoff case, the velocity is the vertical climb speed (V_{FP} = dh/dt) and the hub plane is at -90 degrees angle of attack. Thus, the rotor inflow becomes

(2.123) $$\lambda_{hp} = \frac{-\frac{dh}{dt} - v_i}{V_t} .$$

For all intents and purposes, the vertical jump takeoff is exactly equivalent to the horizontal

takeoff of a fixed-wing aircraft. This allows the induced velocity (v_i), defined by Eq. (2.38), to be simplified to

$$(2.124)\quad v_i = \frac{T_{hp}}{2\rho(\pi R^2)\sqrt{\left(-\frac{dh}{dt} - v_i\right)^2}} \quad \text{or} \quad \frac{v_i}{V_t} = \frac{C_{Thp}}{2\sqrt{\left(-\frac{dh/dt}{V_t} - \frac{v_i}{V_t}\right)^2}}.$$

2.8 JUMP TAKEOFF

Note that the induced velocity equation, (2.124), is a quadratic which gives the induced velocity directly as

(2.125)

$$\frac{v_i}{V_t} = \frac{1}{2}\sqrt{2C_{Thp} + \left(\frac{dh/dt}{V_t}\right)^2} - \frac{1}{2}\left(\frac{dh/dt}{V_t}\right).$$

The explicit equation for thrust coefficient [obtained by substituting Eq. (2.125) into Eq. (2.123) and substituting the result into Eq. (2.121), which can then be solved for (C_{Thp})] is

$$(2.126)\quad C_{Thp}=\frac{T_{hp}}{\rho\pi R^4\Omega^2}=\frac{\sigma^2a^2}{8}\left[\frac{1}{8}+\frac{4}{3}\left(\frac{\theta}{\sigma a}\right)-\left(\frac{dh/dt}{\sigma aV_t}\right)-\sqrt{\frac{1}{64}+\frac{1}{3}\left(\frac{\theta}{\sigma a}\right)-\frac{1}{4}\left(\frac{dh/dt}{\sigma aV_t}\right)+\left(\frac{dh/dt}{\sigma aV_t}\right)^2}\right]$$

With rotor thrust known, the decelerating torque [obtained by substituting Eq. (2.125) into Eq. (2.123) and substituting the result into Eq. (2.122)] is

$$(2.127)\quad \text{Decel } C_Q=-\frac{Q}{\rho\pi R^5\Omega^2}=-\frac{\sigma C_{do}}{8}-\frac{\sigma^3a^3}{2}\left[\left(\frac{dh/dt}{\sigma aV_t}\right)+\sqrt{\left(\frac{dh/dt}{\sigma aV_t}\right)^2+2\frac{C_{Thp}}{\sigma^2a^2}}\right]\frac{C_{Thp}}{\sigma^2a^2}.$$

The variation of thrust and decelerating torque coefficients, Eqs. (2.126) and (2.127), with the nondimensional climb velocity $\left(\frac{dh/dt}{V_t}\right)$, is illustrated in Fig. 2-51. I chose a rotor solidity (σ)

of 0.1, assumed the airfoil lift-curve slope (a) to be 5.73 per radian and its drag coefficient (C_{do}) to be 0.012, and set collective pitch (θ) to 10 degrees (0. 1745 radians) . These constants correspond to one of Wheatley's experimental points. As Fig. 2-51 shows, the torque coefficient Wheatley measured was somewhat higher (i.e., more decelerating torque) than that computed by Eq. (2.127). He included a table showing test data versus his calculated results. I have included his comparison here, but I cannot reproduce his calculated torque coefficients.

Table 2-4. The Wheatley 10-Foot-Diameter Model Rotor Static Torque Coefficient Comparison

Pitch Angle θ_o, deg	Measured $d(1/\Omega)/dt$ sec/rad per sec	Measured C_Q	Calculated C_Q
10	0.00525	–0.000726	–0.000587
14	0.00812	–0.001122	–0.009690
18	0.01273	–0.001760	–0.001460

2.8 JUMP TAKEOFF

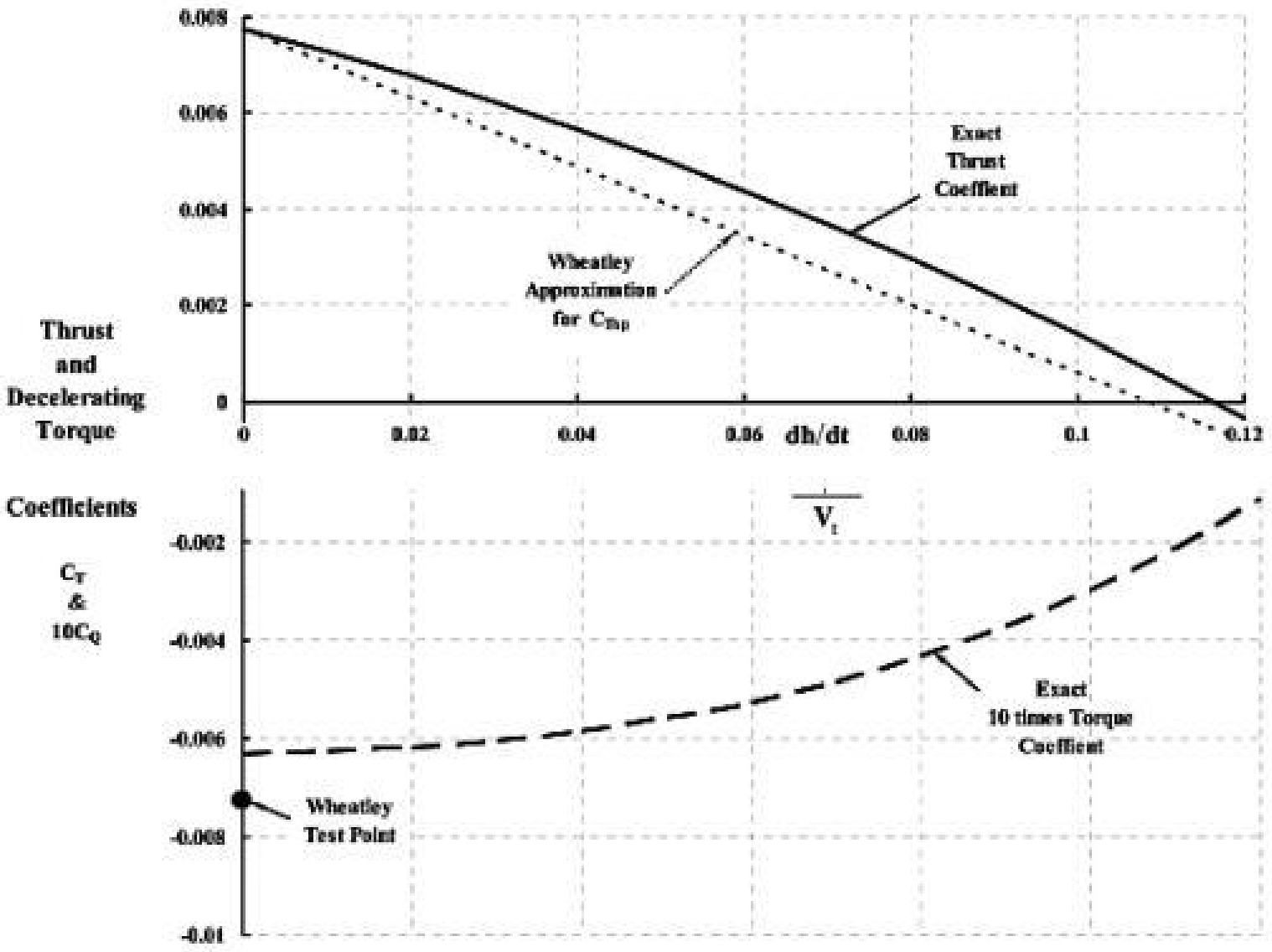

Fig. 2-51. Thrust and torque coefficient trend with vertical climb ratio.

Fig. 2-51 also shows the linear approximation to the thrust coefficient versus nondimensional climb velocity that Wheatley accepted. He took a somewhat roundabout way to arrive at

(2.128)

$$C_{Thp} = \frac{T_{hp}}{\rho \pi R^4 \Omega^2} = \text{Initial } C_{Thp} - \frac{\sigma a}{8} \frac{dh/dt}{V_t} .$$

Wheatley, ever the practical engineer,[25] chose to assume that the torque coefficient *did not* vary with the nondimensional climb velocity. This is clearly a *very* first approximation to the exact trend shown in Fig. 2-51, but he had a reasonable rational saying

"It is proposed that C_Q be assumed independent

of $\dot{h}/\Omega R$ at all pitches less than 16°; the error introduced by the approximation is greater in figure 2 [refer to Fig. 2-51] where the solidity is 0.10 but is still reasonably small for the lower values of $\dot{h}/\Omega R$. Experimental justification for this assumption will subsequently be presented."

---

[25] My opinion: A practical engineer is one who can get 90 percent of the right answer in 10 percent of the time.

2.8 JUMP TAKEOFF

The "experimental justification" Wheatley used, which I will discuss in more detail in a moment, came from tests of a 4-blade, 10-foot-diameter model. The rotor had a solidity (σ) of 0.10. The rectangular blades were untwisted. His test setup allowed the rotor to

be spun up, released to climb up vertically, and then caught by a safety harness. Time histories of several "jumps" showed that $1/\Omega$ varied nearly linear with time.

To begin integrating Eq. (2.120), an approximation is first required for how rotor speed (Ω) varies with time (t). Since the decelerating torque coefficient is assumed constant at its initial value, Eq. (2.112) is directly useable. For convenience, that equation is repeated here as

$$\Omega_t = \frac{\Omega_o}{1 - \left[\frac{\rho\left(\pi R^2\right) R^3 C_Q}{I}\right] \Omega_o t} \quad (2.112)$$

Note that the reciprocal of rotor speed (Ω_t) is a simple linear equation, which Wheatley found characteristic during his model testing.

Knowing how rotor speed varies with time from its initial value (Ω_o) means that thrust is known; then the F = ma problem can be restated with the linear thrust coefficient assumption Wheatley used as

(2.129)

$$\frac{W}{g}\frac{d^2h}{dt^2} = \left(\rho\pi R^4\Omega_t^2\right)\left(\text{Initial } C_{Thp}\right) - \left(\rho\pi R^4\Omega_t^2\right)\frac{\sigma a}{8}\frac{dh/dt}{R\Omega_t} - W.$$

This equation is a linear second-order differential equation, which becomes clearer after the time-varying rotor speed from Eq. (2.1 12) is substituted into Eq. (2.129). Thus, after some simplification, the problem Wheatley solved is

(2.130)
$$\frac{d^2h}{dt^2} = \frac{g}{W}\frac{\left(\rho\pi R^4\Omega_o^2\right)\left(\text{Initial } C_{Thp}\right)}{\left[1-\frac{\rho\pi R^5\Omega_o C_Q}{I}t\right]^2} - \frac{1}{8}\frac{g}{W}\left[\frac{\rho\pi R^3\Omega_o\sigma a}{1-\frac{\rho\pi R^5\Omega_o C_Q}{I}t}\right]\frac{dh}{dt} - g.$$

Keep in mind that the torque coefficient (C_Q) in Eq. (2.130) is that value at time equals zero and that it is a deceleration torque coefficient

where the vertical velocity is zero. That is, for this problem

(2.131)

$$C_Q = -\frac{\sigma C_{do}}{8} - \frac{\sigma^3 a^3}{2}\sqrt{2\frac{C_{Thp}}{\sigma^2 a^2}}\frac{C_{Thp}}{\sigma^2 a^2} = -\frac{\sigma C_{do}}{8} - \frac{\sqrt{2}\,\sigma^3 a^3}{2}\left(\frac{C_{Thp}}{\sigma^2 a^2}\right)^{\frac{3}{2}}.$$

There are three constants involved in the vertical acceleration equation. Therefore, to avoid an unwieldy mess, Wheatley defined

2.8 JUMP TAKEOFF

(2.132)

$$K_1 = \frac{1}{8}\frac{g}{W}\left(\rho\pi R^3 \Omega_o \sigma a\right) \qquad K_2 = -\frac{\rho\pi R^5 \Omega_o C_Q}{I}$$

$$K_3 = \frac{g}{W}\left(\rho\pi R^4 \Omega_0^2\right)\left(\text{Initial } C_{Thp}\right) = \frac{\text{Initial } T_{hp}}{W} g$$

and then the vertical acceleration is abbreviated to

(2.133) $$\frac{d^2h}{dt^2}+\frac{K_1}{1+K_2t}\frac{dh}{dt}=\frac{K_3}{(1+K_2t)^2}-g.$$

This equation, as Wheatley notes, "can be integrated quite easily. Reference to a text on differential equations establishes that" the vertical velocity is

(2.134)

$$\frac{dh}{dt}=\frac{K_3}{(K_1-K_2)(1+K_2t)}-\frac{g(1+K_2t)}{(K_1+K_2)}+\frac{C_1}{(1+K_2t)^{\frac{K_1}{K_2}}}.$$

The time history of vertical height (h) follows immediately as

(2.135) $$h=\frac{K_3}{K_2(K_1-K_2)}\log(1+K_2t)-\frac{g\left(t+\frac{1}{2}K_2t^2\right)}{(K_1+K_2)}+\frac{C_1}{(K_1-K_2)}\left[1-\frac{1}{(1+K_2t)^{\frac{K_1}{K_2}-1}}\right]$$

where the integration constant (C_1) is

$$(2.136)\quad C_1 = \frac{g(K_1 - K_2) - K_3(K_1 + K_2)}{K_1^2 - K_2^2}.$$

Wheatley made comparisons of his linear jump takeoff theory to the test data acquired with the experimental setup shown in Fig. 2-52. The rotor was spun up to as high as 725 revolutions per minute by a 25-horsepower electric motor. He makes no statement about the ballast spinning, and I would guess that it did not because he would have mentioned its polar moment of inertia. Wheatley was quite concerned about the safety harness tension, which lowered the actual weight being lifted. He made cable tension a test variable but concluded that the actual tension during a jump was about one-third of the static tension. Test data from 160 vertical jumps was given in tabular form.

A moving picture, taken up from below, gave rotor speed, and the rotor dragged a cord up as it went, which gave the height of the jump.

The 10-foot-diameter, 3-blade rotor used in the experiment had a polar moment of inertia (I) of 3.23 slug-feet^2. The blade chord (c) was 0.523 feet and the solidity (σ) was 0.10. The constant chord blades were untwisted and the airfoil was the NACA 0018, which is uncambered. The collective pitch was ground adjustable and remained "fixed while the rotor was being brought up to speed and jumped." The tests were conducted in the return section of the N.A.C.A. Langley large wind tunnel, which provided an enclosed space about 50 feet by 200 feet, and 70 feet high.

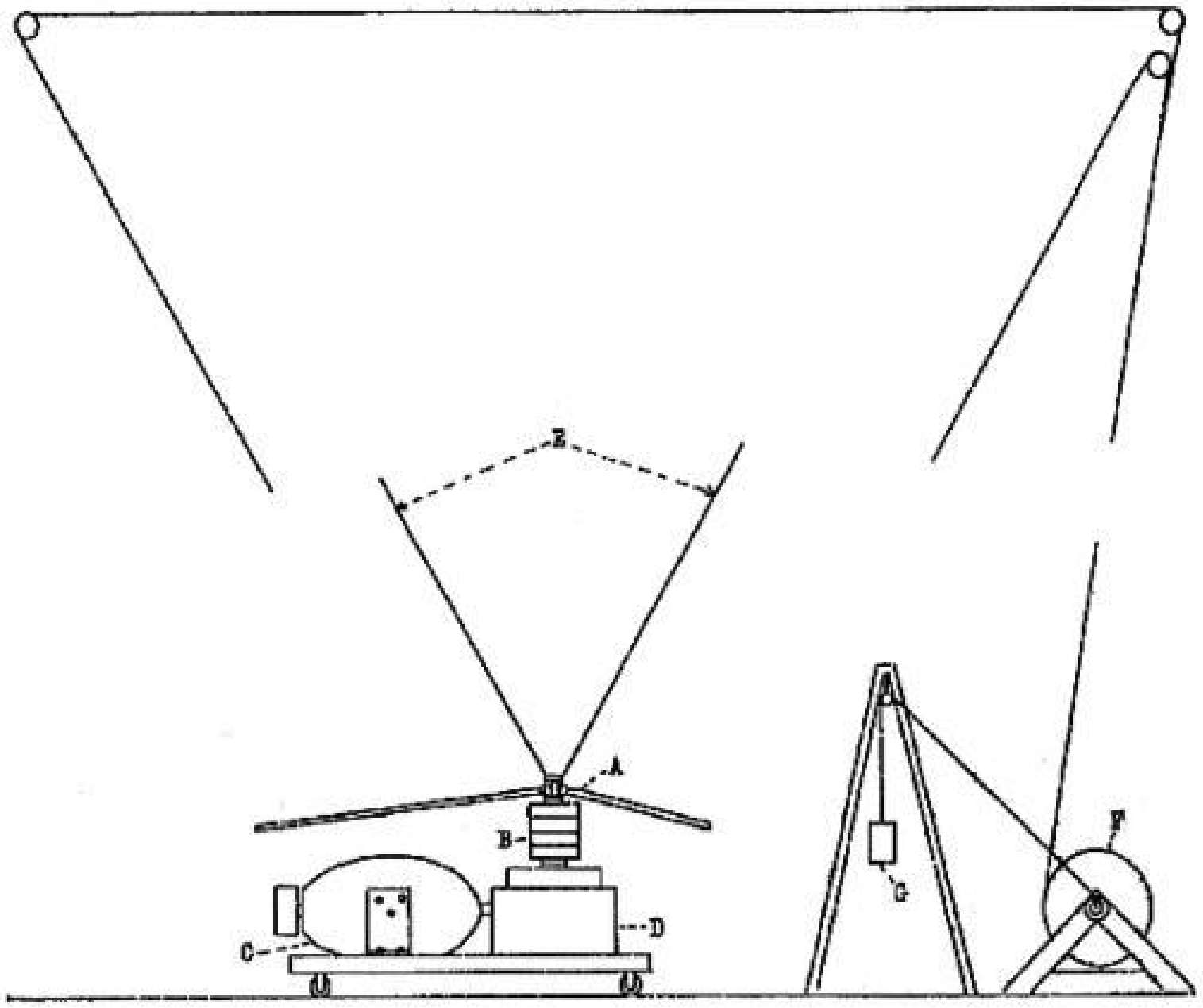

Fig. 2-52. The Wheatley jump takeoff test with a 10-foot-diameter rotor [82].

Wheatley provided the bulk of the 160 test results in tabular form giving only collective pitch, disc loading, initial rotor speed, cable tension (T_C), and maximum height attained. His report [82] compares

theory to test for only 3 of the 160 jump takeoff time histories, 2 of which are shown here as Fig. 2-53 and Fig. 2-54. The theory, Eq. (2.135), shown on the two figures is as given in the preceding discussion. However, the equations I have written for thrust coefficient, Eq. (2.126), and torque coefficient, Eq. (2.13 1), are slightly more optimistic than what Wheatley actually used. Wheatley states that "the influence of the cable tension on the jumps was uncertain." Therefore, both Fig. 2-53 and Fig. 2-54 show theory for the influence of initial torque and cable tension.

The two preceding examples illustrate several points that disturbed Wheatley. These points were:

1. "The figures establish that the allowance that should be made for the cable tension is considerably less than the nominal value of this variable." Wheatley felt, for example, that the nominal cable tension of 12.5 pounds should really be closer to 3 pounds. As it turns

out, the broader issue deals with the accurate calculation of initial thrust and torque.

2.8 JUMP TAKEOFF

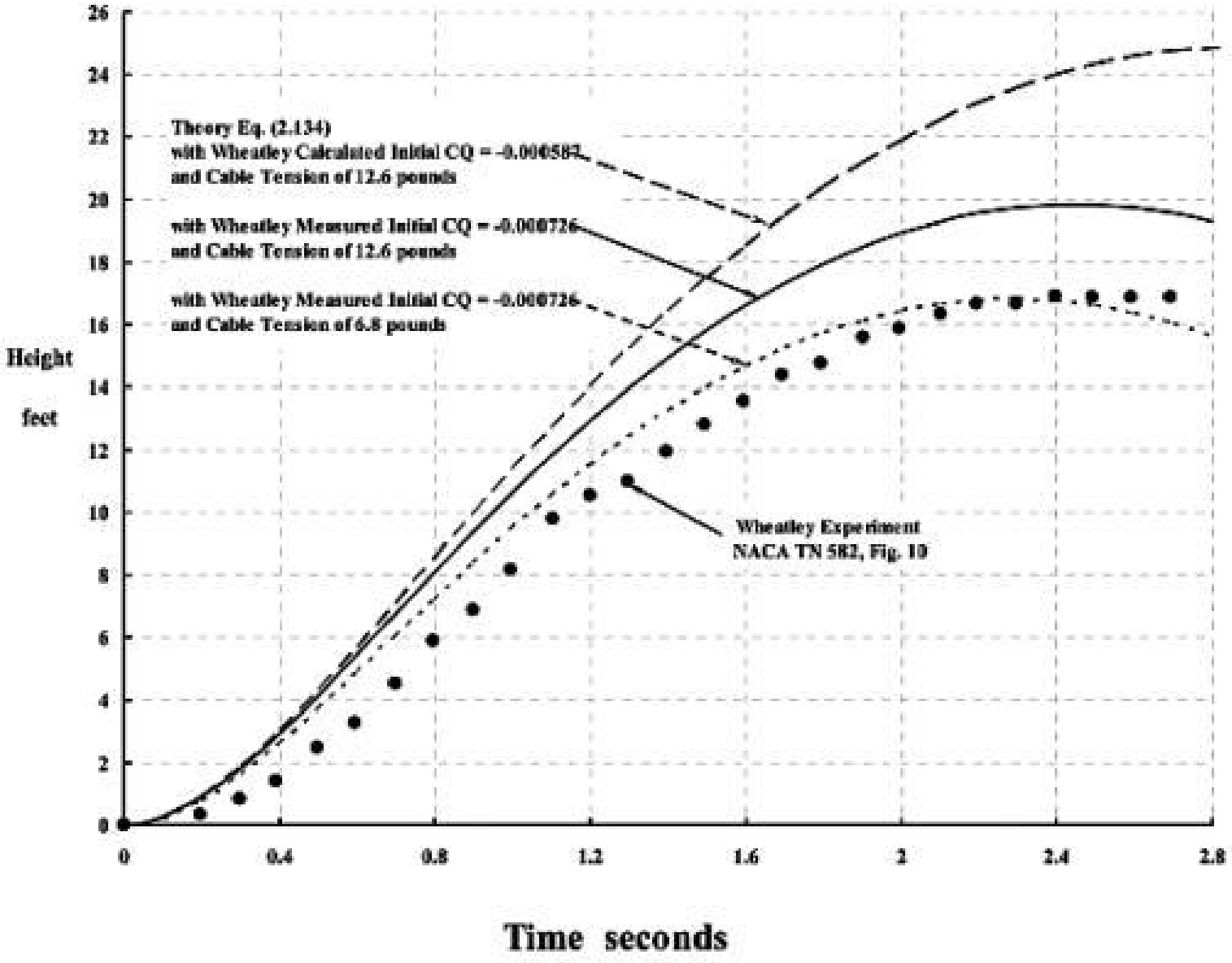

Fig. 2-53. Theory vs. test: W = 83.3 lbs, θ = 10°, initial RPM = 700.

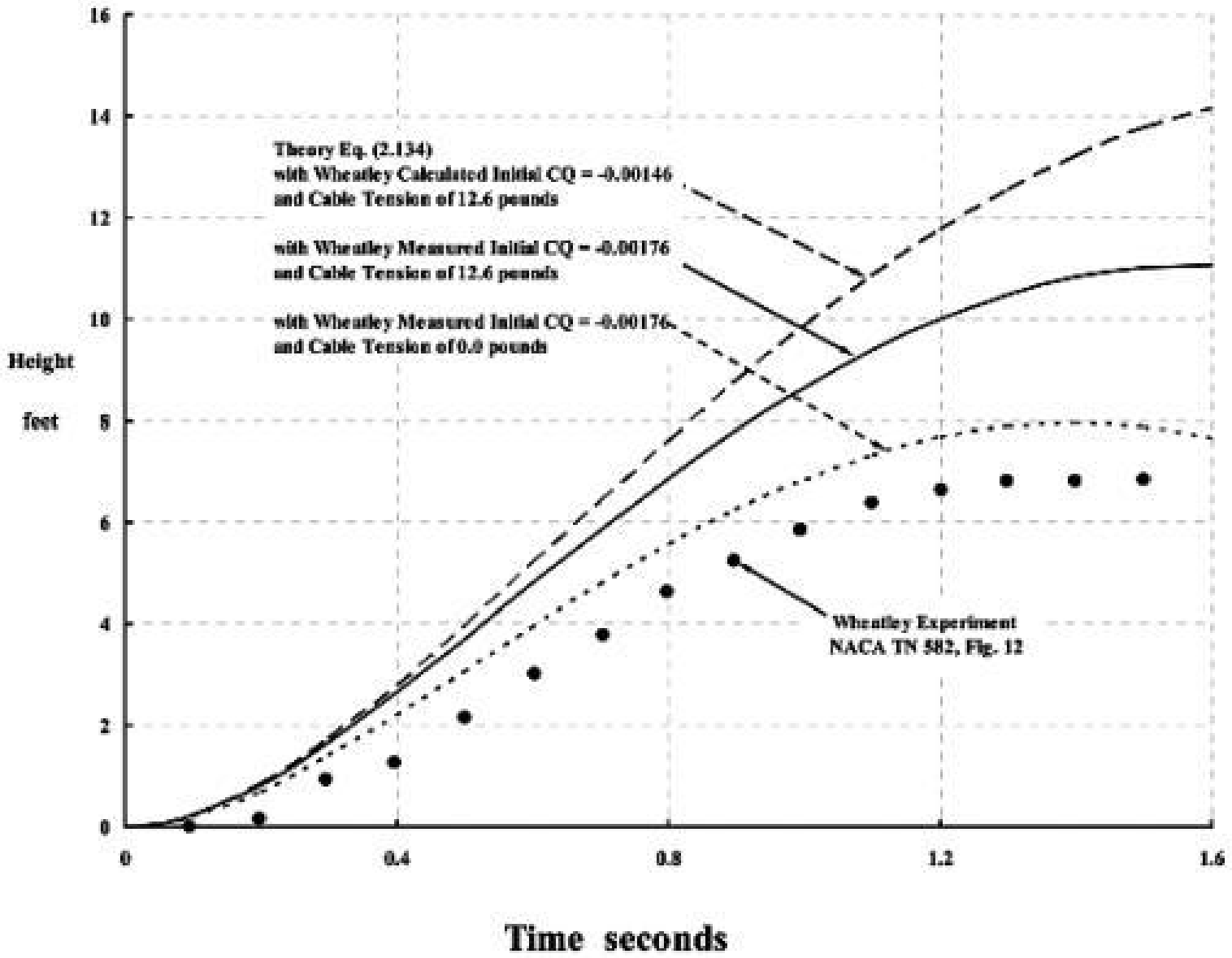

Fig. 2-54. Theory vs. test: W = 130.3 lbs, θ = 18°, initial RPM = 600.

2. "It will be noted in table III [see Table 2-4 herein] that the experimental and calculated torque coefficients differ by an appreciable amount." He added that if "the rotor pitch angle increased slightly because of the dynamic twist of the rotor blades; while this twist should be quite small, a twist of approximately 1° would explain most of the discrepancies between the torque coefficients of table III."

3 . "It is considered possible that the source of compensating error is the ground effect, which would tend to increase the thrust of the rotor when it was near the ground plane at no additional cost in torque."

4. "The analysis is not as exact at a pitch angle of 18° as at one of 10°."

He concluded that the experiment "served a useful purpose in attesting to the validity of the mathematical analysis, which can be used with more confidence than would have been justified without experimental verification."

The larger body of data from the Wheatley jump takeoff experiment gives just the maximum height reached (along with collective pitch, disc loading, initial rotor speed, and cable tension) and is also of considerable value . Maximum height reached (h_{max}) is determined by only a few physical facts. While Wheatley did not extend his theory in this direction, a quite simple approximation is easily obtained.

An estimate of maximum height reached in a jump takeoff depends on when the vertical velocity is zero. Thus, by setting (dh/dt = 0) in Eq. (2.134), an estimate of time to reach maximum height is

(2.137) Approximate time to max. height $= t_{max} \approx \dfrac{K_2 - K_1 + \sqrt{\dfrac{K_3}{g}\left(K_1^2 - K_2^2\right)}}{K_2\left(K_1 - K_2\right)}$.

The rotor speed will decay to

(2.112) $$\Omega_t = \frac{\Omega_o}{1 - \left[\frac{\rho(\pi R^2) R^3 C_Q}{I}\right] \Omega_o t_{max}}$$

and the corresponding maximum height is simply approximated as

(2.138)

$$h_{max} \approx \left(\frac{4I}{\rho \pi R^4 \sigma a}\right)\left[\ln\left(\frac{T_o}{W}\right) + \frac{W}{T_o} - 1\right]\left[\frac{C_{T_o}}{-C_{Q_o}}\right].$$

All 160 maximum height test points Wheatley tabulated are compared in Fig. 2-55 to the maximum height predicted by Eq. (2.138) . At the lower collective pitches, the prediction of maximum height by Eq. (2.138) is optimistic . The deterioration in accuracy as collective pitch is increased above 12 degrees is also quite evident. This leads me to the calculation of initial thrust and torque. As you can see from Eq. (2.138), maximum height

depends on three parameters. The constant term depends on just rotor physical properties and the density of air (ρ). This constant is hardly a source of major error since it is nothing more than the ratio of blade density to air density. The second parameter is the ratio of initial thrust (T_o) to weight (W). Both Fig. 2-53 and Fig. 2-54 suggest that this ratio is too large. The third parameter is

the ratio of initial thrust coefficient (C_{To}) to initial torque coefficient (C_{Qo}). It is the inaccurate prediction of initial (i.e., static) thrust coefficient by Eq. (2.126) and, as Wheatley tabulated, torque coefficient by Eq. (2.127) that drives Eq. (2.138) to its optimistic result.

You might think that the fixed-wing industry would have known all about static thrust and torque calculations from their propeller design work. However, the calculation of propeller static thrust and the torque required to produce that thrust was not, surprisingly, a burning issue for the fixed-wing industry. Their concentration was on designing fixed-pitch propellers for maximum efficiency in cruise and at maximum speed, as early NACA reports by Dr. William Durand and Professor E. Lesley [86] and [87] illustrate. In 1917 and 1918, they accumulated test data from nearly 100 model propellers in "the aerodynamic laboratory of the Leland Stanford Junior University." The school was named by Stanford for his son; hence the Junior. At that time, Dr. Durand was Chairman of the N.A.C.A.

When the controllable pitch, constant speed (rpm) propeller came on the scene [41],

propeller blades were still designed for high speed. With variable pitch propellers, collective pitch was simply adjusted to maximize takeoff performance. And so it was left to the rotorcraft industry to maximize the thrust-to-torque ratio for autogyro jump takeoff performance. At the same time, the ground work was being laid to maximize the thrust-to- horsepower ratio for the hovering helicopter.

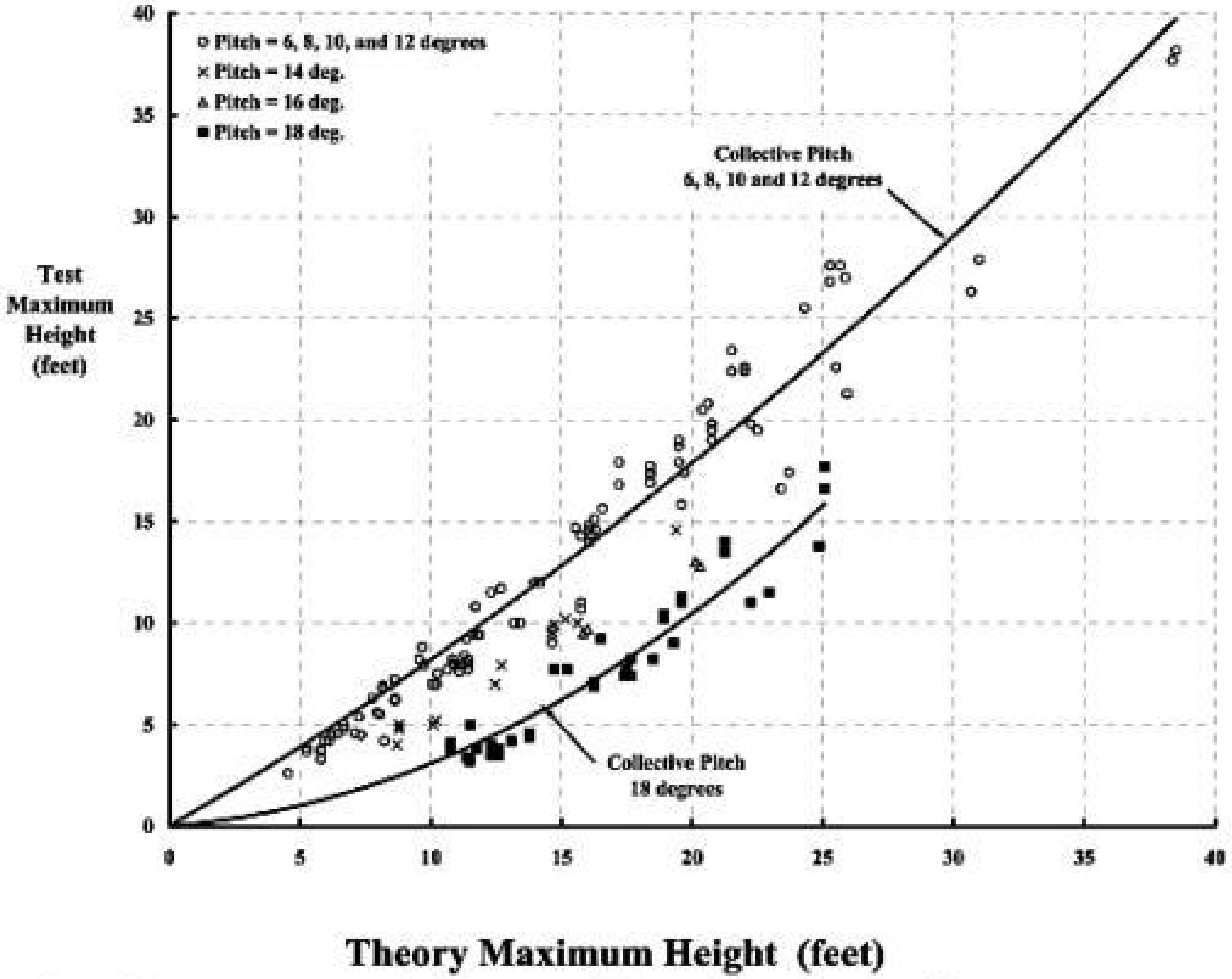

Fig. 2-55. Prediction of jump takeoff maximum height.

2.8.6 Static Thrust and Torque

A milestone step in understanding rotor static performance was completed by Montgomery Knight and Ralph Hefner at the Georgia School of Technology in December of 1937 [88].[26] Their initial theoretical and experimental work was timely for the autogyro jump takeoff performance problem and, of course, just as applicable to the helicopter, which clearly was becoming the second-generation product of the rotorcraft industry. Knight and Hefner carefully documented application of what is called blade element momentum theory.[27] Their experimental work gathered thrust and torque for rotors having two, three, four, and five blades, which led them to prove that the fundamental way to account for solidity (σ) was by scaling thrust coefficient by the square of solidity, and torque coefficient by the cube of solidity.

This very fundamental point appears to have been lost somewhere during the seven decades that followed publication of their report. You can regain an appreciation of its importance, however, by just rewriting the autogyro maximum jump takeoff height equation as

(2.139)

$$h_{max} \approx \left(\frac{4I}{\rho\pi R^4}\right)\left[\ln\left(\frac{T_o}{W}\right)+\frac{W}{T_o}-1\right]\left[\frac{C_{T_o}/(\sigma a)^2}{-C_{Q_o}/(\sigma a)^3}\right]$$

or rewriting the static thrust coefficient, Eq. (2.126), letting vertical velocity (dh/dt) equal zero, which leads to

(2.140)

$$\frac{C_{Thp}}{\sigma^2 a^2}=\frac{T_{hp}}{\rho\pi R^4\Omega^2\sigma^2 a^2}=\frac{1}{8}\left[\frac{1}{8}+\frac{4}{3}\left(\frac{\theta}{\sigma a}\right)-\sqrt{\frac{1}{64}+\frac{1}{3}\left(\frac{\theta}{\sigma a}\right)}\right]$$

or, rather than thinking of decelerating torque, think of a powered helicopter rotor in hover, in which case Eq. (2.127), becomes

(2.141)

$$\frac{C_Q - \frac{\sigma C_{do}}{8}}{\sigma^3 a^3} = \frac{Q}{\rho \pi R^5 \Omega^2 \sigma^3 a^3} = \frac{\sqrt{2}}{2}\left(\frac{C_{Thp}}{\sigma^2 a^2}\right)^{\frac{3}{2}} .$$

Knight and Hefner focused their work on rectangular, untwisted blades having a 2.5-foot radius and a 2-inch chord. Their blades used the NACA 0015 airfoil and were carefully balanced so the section center of gravity was at the airfoil 1/4-chord point. They noted in their report that "five blades and three hubs were used. The blades were identical and interchangeable, thus making possible the four rotor combinations." The 2-inch chord was constant from "the tip to a radius of 5 inches." Moving inboard, the airfoil

transitioned to a circular cross section (3/4-inch diameter) at the 1 .5-inch radius station. A flapping hinge was installed at the 1-inch radius station. Their test results were provided in tables as well as

---

[26] Montgomery Knight presented a paper at the first Rotating Wing Aircraft Meeting held at the Franklin Institute in late October of 1938 [see Appendix F]. His session dealt with Research Programs and he spoke in depth about "Research at Georgia Tech."

[27] A more up-to-date explanation of blade element momentum theory is given by Alfred Gessow and Garry Myers in their classic book, *Aerodynamics of the Helicopter* [61].

2.8 JUMP TAKEOFF

figures. The agreement between their equations for thrust and torque, derived from

blade- element momentum theory, was quite impressive.

The key results from the 1937 ground-breaking work by Knight and Hefner begin with Fig. 2-56. With 35 data points from their 4 separate rotors, they developed the relationship that if collective pitch (θ) is scaled as

$$\Theta = \frac{16}{a}\left(\frac{\theta}{\sigma}\right) \quad \text{in radians} \tag{2.142}$$

then

$$\frac{C_T}{\sigma^2} = \frac{a^2}{32}\left[\frac{1}{2} + \frac{1}{3}\Theta + \frac{(1-3\Theta)(1+2\Theta)^{3/2} - 1}{15\Theta^2}\right]. \tag{2.143}$$

When you read the Knight and Hefner report you will see that I have altered the structure of their equations to be consistent with the structure used in this discussion.[28]

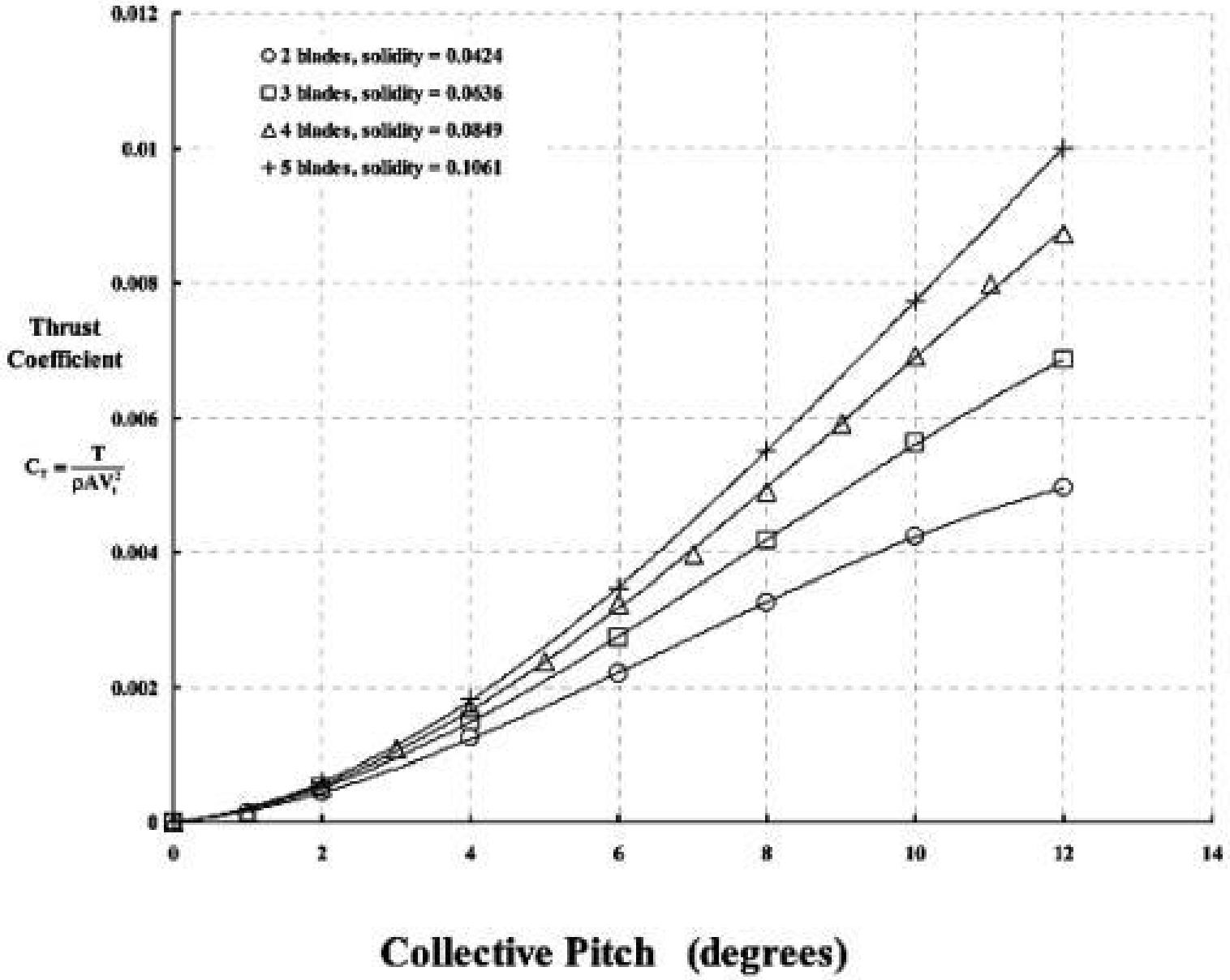

Fig. 2-56. Knight and Hefner model test results from 1937 [88].

---

[28] There are a few typographical errors in the Knight and Hefner equations [88], however their numerical comparisons are quite correct. In sorting out these errors, I chose a somewhat simpler form to use here.

2.8 JUMP TAKEOFF

The thrust coefficient versus collective pitch data for the four different solidity rotors shown in Fig. 2-56 can be "collapsed" to one line when graphed as

$$\frac{C_T}{\sigma^2} \text{ versus } \frac{\theta}{\sigma}.$$

This is done in Fig . 2-57 assuming, as their airfoil data showed, that the airfoil lift-curve slope (a) is 5.73 per radian for the NACA 0015. As you can see, the form that Knight and Hefner found theoretically is well supported by their simple experiment. Fig. 2-57 also includes Wheatley's thrust approximation, Eq. (2.140), for the sake of completeness . Either equations from Wheatley or Knight and Hefner

are adequate for the prediction of thrust coefficient.

On the other hand, prediction of torque coefficient with Eq. (2.141) is totally inadequate. In analyzing the torque coefficient, Knight and Hefner wrote, "The torque may be divided into three parts analogous to the partition of drag on an airfoil [i.e., wing]." In the somewhat more commonly used terminology today, total torque is the sum of:

1. Induced torque.
2. Minimum profile torque.
3. Delta profile torque.

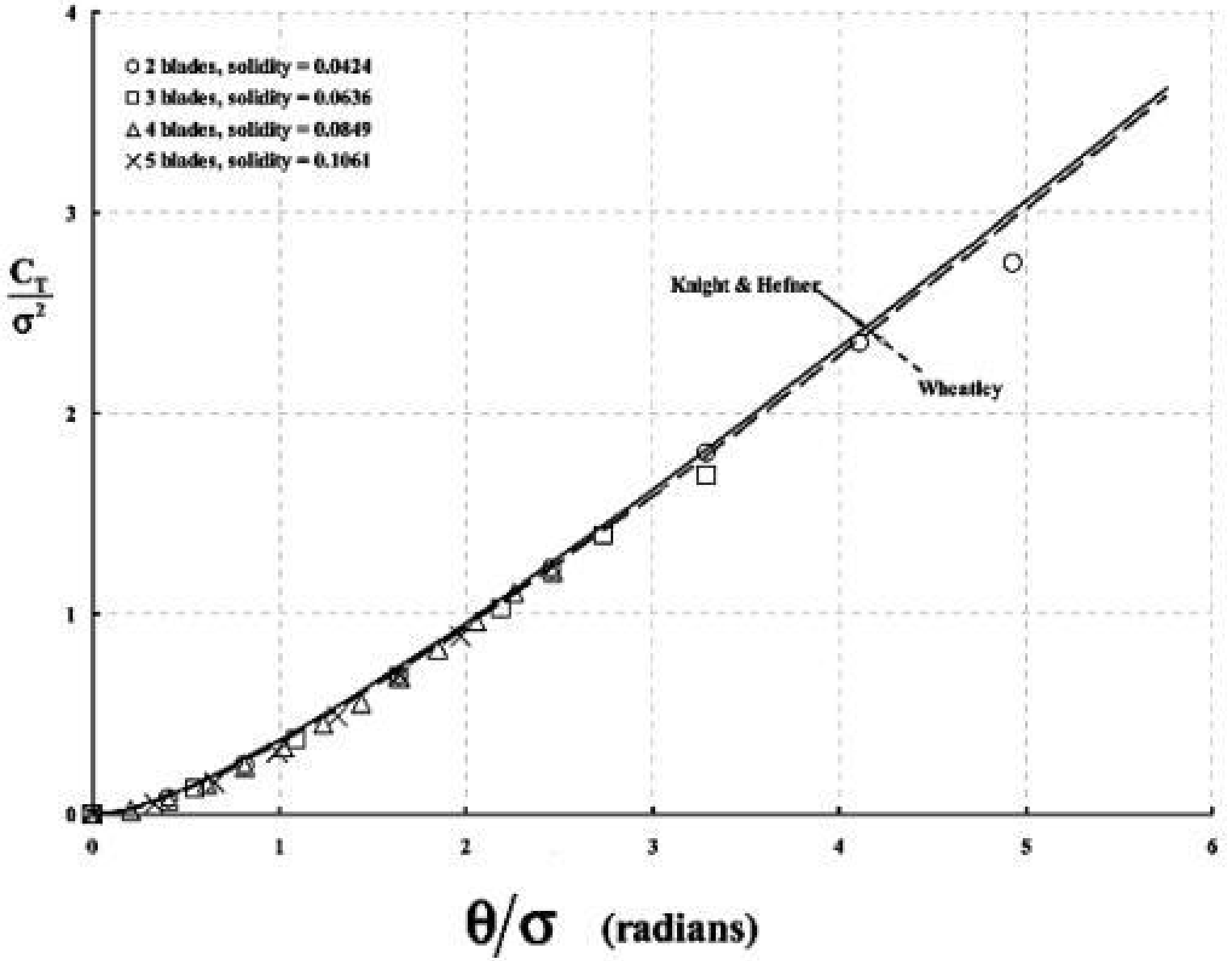

Fig. 2-57. Accounting for solidity when calculating thrust coefficient [88].

2.8 JUMP TAKEOFF

Then, using blade element momentum theory, they proceeded to arrive at the following equations:

(2.144)

$$\text{Induced } \frac{C_Q}{\sigma^3} = \frac{a^3}{3,584}\left[(1+2\Theta)^{3/2} - 1 - 3\Theta - \frac{384}{a^2}\left(\frac{C_T}{\sigma^2}\right)\right]$$

(2.145) $$\text{Min. Profile } \frac{C_Q}{\sigma^3} = \frac{C_{do}}{8\sigma^2}$$

(2.146)

$$\text{Delta Profile } \frac{C_Q}{\sigma^3} = \frac{\delta}{512}\left[1 + \frac{4}{3}\Theta + \frac{1}{4}\Theta^2 + \frac{7(1+2\Theta)^{3/2} - 3(1+2\Theta)^{7/2} - 4}{42\Theta^2}\right]$$

where, again, $\Theta = \frac{16}{a}\left(\frac{\theta}{\sigma}\right)$ in radians. Knight and Hefner acknowledged that there is some

delta profile torque due to the increase of airfoil drag coefficient with airfoil lift coefficient, a component that Wheatley ignored in his jump takeoff study. Knight and Hefner, from their airfoil experiment, chose to account for this airfoil drag rise as

(2.147)

$$C_d = C_{do} + \varepsilon\alpha^2 = C_{do} + \varepsilon\left(\frac{C_\ell}{a}\right)^2 = C_{do} + \delta C_\ell^2 .$$

From their torque equations, they were immediately able to see that induced and delta profile torque were both dependent on collective pitch. They therefore concluded that subtracting minimum profile torque from total torque would yield the sum of induced and delta profile torques, a torque that could be scaled by solidity cubed. Thus, the experimental data should be examined in the form

$$\frac{C_Q - \frac{\sigma C_o}{8}}{\sigma^3} \text{ versus } \frac{\theta}{\sigma}.$$

Fig. 2-58 shows that the blade element momentum theory had led them toward the right conclusion. They compared two values of airfoil drag rise constant (δ) and finally satisfied themselves that a (δ) of 0.038 was quite reasonable considering the small scale of their model. I have included the result Wheatley obtained from Eq. (2.141) in Fig. 2-58, as well as his data from Table 2-4 based on the Knight and Hefner minimum airfoil drag coefficient (C_{do}) of 0.0113.

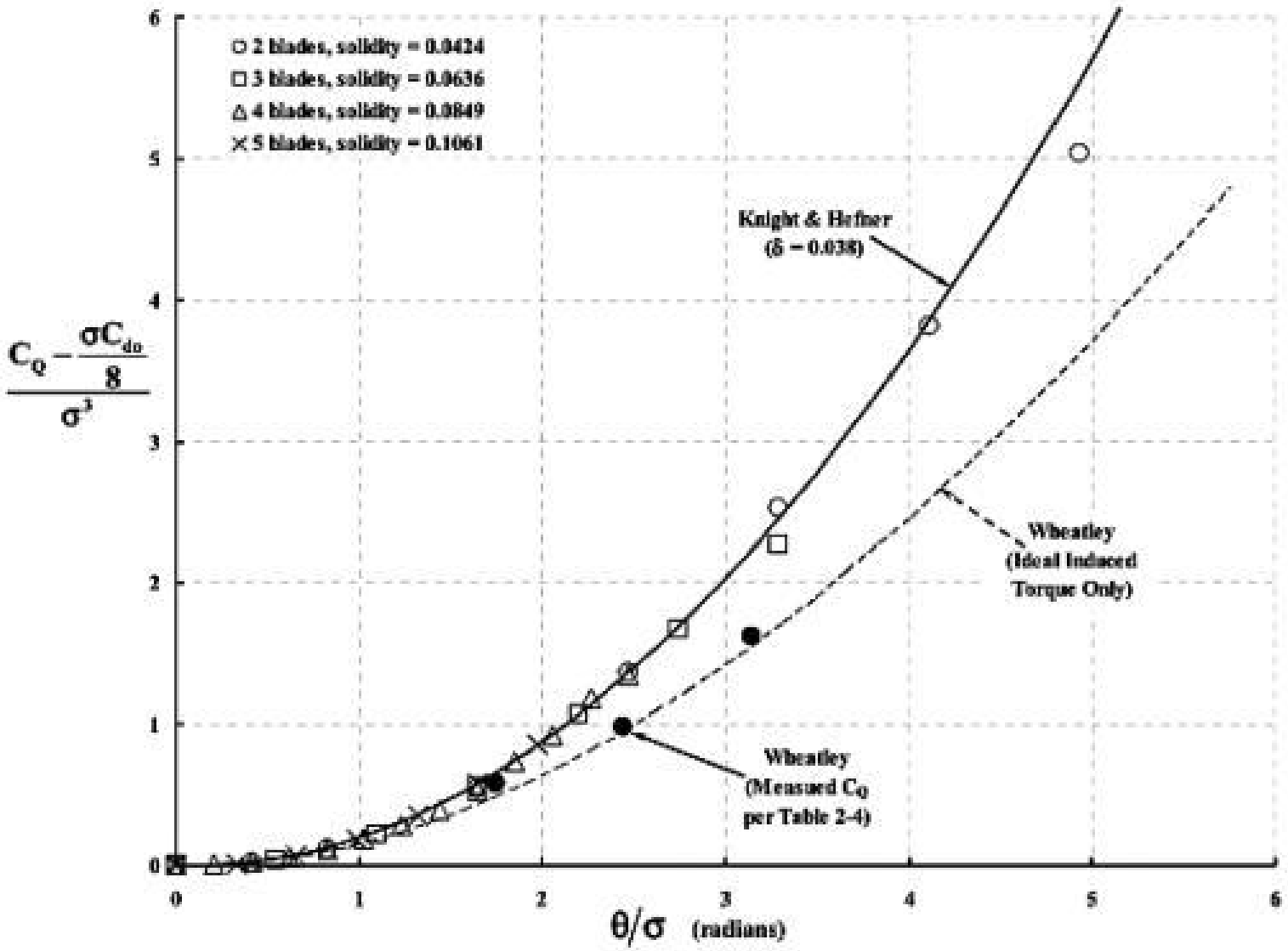

Fig. 2-58. Accounting for solidity when calculating torque coefficient [88].

2.8.7 Ground Effect

Wheatley, you will recall, raised a question about how "ground effect" might

have influenced his jump takeoff experiment. He wrote [82]:

"It is considered possible that the source of compensating error is the ground effect, which would tend to increase the thrust of the rotor when it was near the ground plane at no additional cost in torque."

The subject of ground effect on rotor thrust and torque coefficients was the second task Knight and Hefner took on as part of their "research program at Georgia Tech." They introduced their report [89] on ground effect with:

"Proximity to the ground has a pronounced effect on the aerodynamic characteristics of the lifting airscrew. Ground effect is therefore of importance in the study of the landing and the takeoff qualities of gyroplanes and helicopters. No comprehensive attack on this problem has thus far been found by the writers although it has been mentioned occasionally in the literature (references 1, 2, and 3), and an approximate mathematical analysis has been made by Betz (reference 4)."[29]

[29] References from Knight and Hefner are included here as references [90], [8], [91], and [92] respectively.

2.8 JUMP TAKEOFF

Knight and Hefner gave their own mathematical analysis of ground effect, which they supported with 5-foot-diameter model experiments . The models were from their early work [88], but this time they only used two-, three-, and four-bladed configurations. They tabulated their experimental results in the coordinates of

$$\frac{C_T}{\sigma^2} \text{ versus } \frac{\theta}{\sigma} \quad \text{and} \quad \frac{C_Q - \frac{\sigma C_o}{8}}{\sigma^3} \text{ versus } \frac{\theta}{\sigma}.$$

Based on the work by Knight and Hefner, Fig. 2-59 shows that Wheatley did

have reason to wonder about how ground effect might be influencing his jump takeoff experimental results because his 10-foot-diameter model began its jump takeoff at a height (Z)-to-diameter (D) ratio of about 0.35 [Fig . 2-52] . Wheatley, in writing that thrust would increase at "no additional cost in torque," clearly anticipated the experimental trend Knight and Hefner reported [89] some 5 years later.

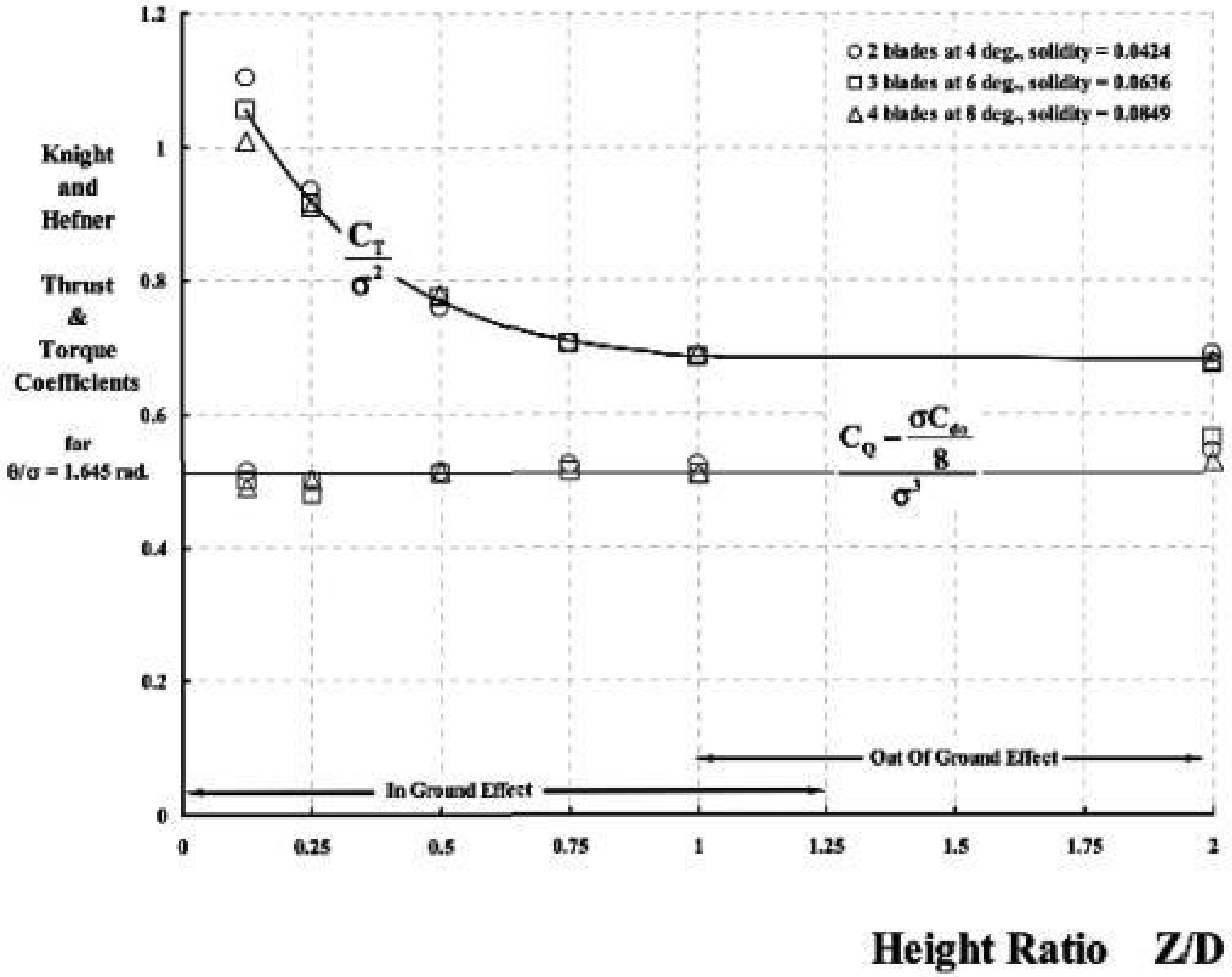

Fig. 2-59. At equal collective pitch/solidity ratio, thrust increases as the rotor approaches the ground, but power is unaffected.

Knight and Hefner give a power required calculation method based on their theoretically derived correction factor. I have revised their approach slightly so that

(2.148) IGE

$$C_Q = \frac{\sigma C_{do}}{8} + \left(\text{Delta } C_Q\right)_{OGE} + \tanh\left[\frac{11}{8}\ln\left(1+2\frac{Z}{D}\right)\right]\left(\text{Induced } C_Q\right)_{OGE}.$$

The initials IGE and OGE stand for in and out of ground effect, respectively.

Using Eq. (2.148) is relatively simple. The rotor geometry and flight condition are used to calculate the ratio of thrust coefficient to solidity squared. With (C_T/σ^2) known, Eq. (2.143) is used to find the collective pitch parameter (Θ) . Then, Eq. (2.146) is used to calculate delta profile torque OGE, and Eq. (2.144) is used to calculate

induced torque OGE. These steps provide the information to calculate IGE torque (or power, since $C_Q = C_P$). Applying this approach to all of the experimental data from Knight and Hefner [88, 89] yielded the correlation of test and theory shown in Fig. 2-60. The inverse problem of predicting the increase in thrust as the ground is approached at equal power is, of course, equally simple using the same four equations. It is just a matter of finding the collective pitch parameter (Θ) that makes Eq. (2.148) constant, even though the ratio of height above the ground (Z) to rotor diameter (D) is decreasing . Each value of (Z/D) yields a (Θ), which is used to calculate thrust with Eq. (2.143) with results such as those shown in Fig. 2-59.[30]

Despite the theoretical work by Knight, Hefner, and Betz, rotor power in ground effect—for a given thrust—was strictly an empirical-to-semiempirical engineering art.

It was an art then and still is today, unfortunately. However, as I will discuss later, enough additional experimental data in and out of ground effect was acquired to create a fairly reliable, empirical, power-required correction [93, 94].

2.8.8 Thrust Overshoot

Besides ground effect, there is another facet of jump takeoff that Wheatley did not address in his experiment. Cierva, Pitcairn, Hafner, and Kellett autogyros increased collective pitch from flat pitch (i.e., a near-zero-thrust collective-pitch setting used for over-speeding the rotor) to a normal flight setting. Wheatley powered his 10-foot-diameter model rotor up to over-speed with collective pitch already set at 6 to 18 degrees. He then sprung a release, and the model rose. This is the simple "toy Chinese top" problem, and relatively simple equations

can be used to estimate maximum height. With full-scale autogyros, the rapid increase in collective pitch from zero to some value, (either by the pilot as Hafner and Kellett chose or by centrifugal force as Cierva and Pitcairn chose), raises a question about how thrust varies with a transient change in collective pitch. This question was answered by Carpenter and Fridovich at the N.A.C.A. in 1953 [95].

---

[30] I have used Microsoft® Excel® spreadsheet software for this and nearly every other calculation and figure in this book. Personally, I think this software is wasted on accountants. Of course, the equations included can be easily programmed in any other computer language.

2.8 JUMP TAKEOFF

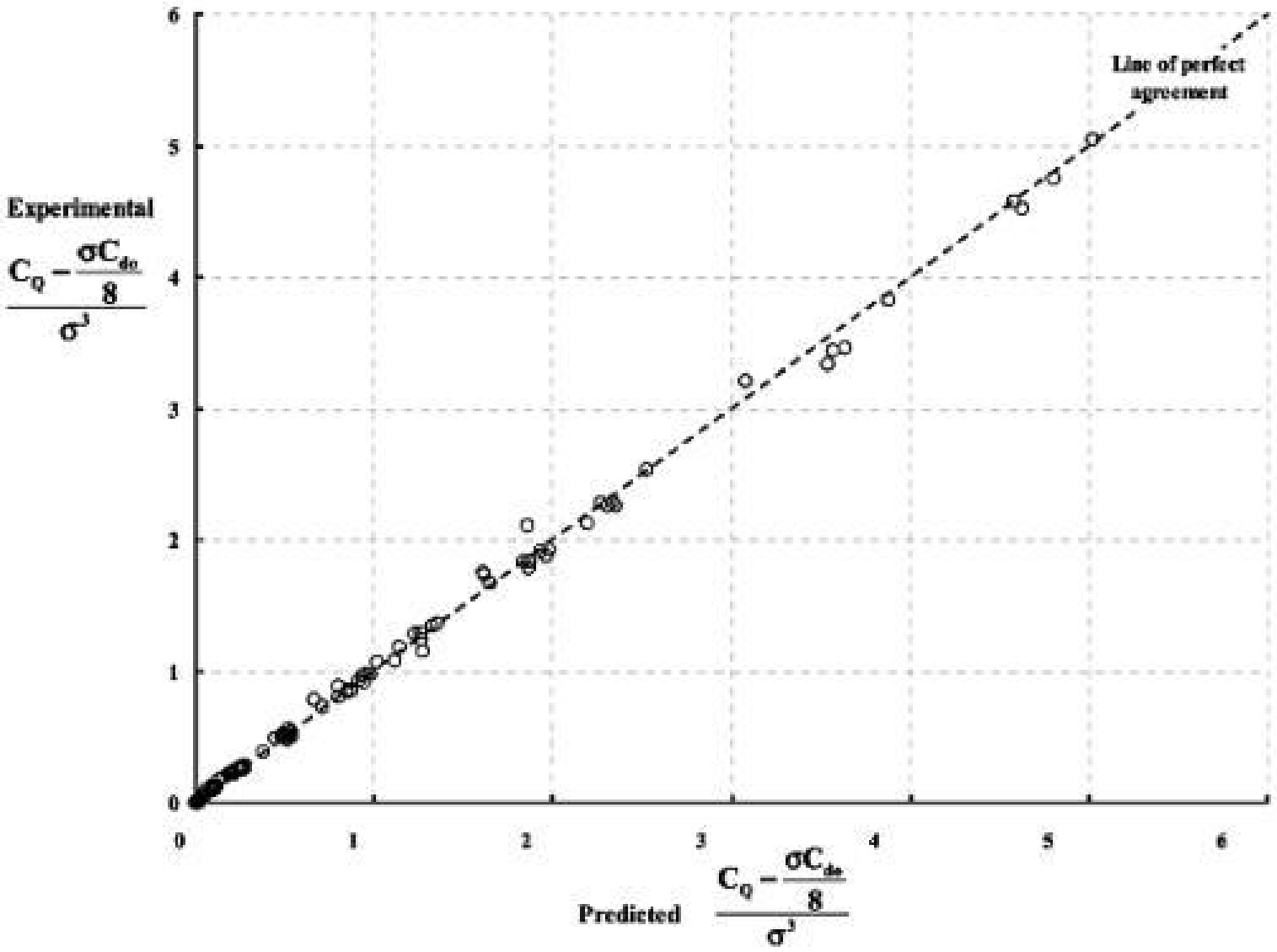

Fig. 2-60. Knight and Hefner model rotor experimental OGE data [88] and IGE data [89] predicted with Eqs. (2.144) and (2.146), assuming $\delta = 0.0447$.

You might be surprised that this question was still unanswered nearly two decades after the Wheatley experiment [82]—and with helicopters well into production. The introduction to the report by

Carpenter and Fridovich provides the answer:

"One of the methods currently used to get an overloaded helicopter airborne is the maneuver commonly referred to as the "jump takeoff" or "engine over speed takeoff." This maneuver is a takeoff with a flight path initially vertical, effected by the release of excess kinetic energy stored in the rotor. The rotor is initially accelerated at or near a blade pitch angle of 0° to a rotor speed greater than its normal speed. At this over speed condition, the blade pitch is suddenly increased to its normal value or higher and the consequent rotor thrust, being greater than the weight of the machine, lifts it vertically from the ground. During the takeoff, the rotor decelerates, the thrust returns to its normal value, and the pilot must gain sufficient forward speed to stay airborne with the power available."

Helicopters flying in 1953 were all powered by reciprocating piston engines. These engines were, as you will read later in Volume II—Helicopters, quite underpowered for their weight (even with supercharging) and did not give early production helicopters much performance. In fact, the U.S.

Army Air Corps' first helicopter, the Sikorsky R-4, could only hover in ground effect when loaded to *normal* gross weight.

2.8 JUMP TAKEOFF

Carpenter and Fridovich used the N.A.C.A. "Langley helicopter test tower" and a three-bladed rotor to conduct their experiments . This "apparatus" was built between 1946 and 1947 and first used in 1948. The whirl tower, as this type of test facility came to be commonly called, was described in detail by Carpenter [96] . The rotor hub was approximately 40 feet above the ground, which placed the 38-foot-diameter rotor nearly out of ground effect. At that time, the N.A.C.A. had two sets of full-scale rotor blades available. Sikorsky provided these blade sets in support of flight research on the R-4 conducted by the

The objective for the 1953 Carpenter and Fridovich test [95] with the three-bladed, 38-foot-diameter, 0.042-solidity rotor was to measure the time history of thrust for several rates of pitch change from zero to maximum collective pitch. Their results quantified the "overshoot" in thrust, which accompanied an induced velocity that could not keep up with collective pitch change . They obtained the behavior of the induced velocity during the transient period "by measuring the drag of balsa-wood paddles (approximately 4 inches square) mounted on a horizontal bar about 2 feet below the rotor blades. The paddles were mounted on strain-gage beams and their response to a change in induced velocity was recorded by an oscillograph." The Carpenter and Fridovich data showed that the Knight and Hefner basic thrust equation, Eq. (2.143) repeated here for convenience, was

inadequate.

(2.143)

$$\frac{C_T}{\sigma^2} = \frac{a^2}{32}\left[\frac{1}{2} + \frac{1}{3}\Theta + \frac{(1-3\Theta)(1+2\Theta)^{3/2} - 1}{15\Theta^2}\right].$$

Carpenter and Fridovich measured "thrust over shoot" during pitch change rates of 6 to 200 degrees per second. The collective pitch was increased from 0 to a maximum of 3, 6, 9, and 12 degrees. Their data summary chart is reproduced here as Fig. 2-61 . At the highest rate, probably typical of Cierva and Pitcairn Autogiros, the rotor was quite capable of a maximum thrust coefficient ($C_{T\,max}$) nearly twice that of the final, steady-state thrust coefficient ($C_{T\,final}$).

An example of the Carpenter and

Fridovich experimental time history results is shown in Fig. 2-62 and Fig. 2-63. I chose this particular test case because, as they said,

"For a pitch rate of 48° per second [see Fig. 2-62] which is thought to be the maximum rate at which a pilot can move the controls (based on unpublished CAA and NACA tests), the time lag between full induced velocity is approximately 0.7 second, whereas at still a slower rate of 20° per second the time lag is about 0.4 second. For the most rapid rate of blade-pitch increase [200 degrees per second], the blade inertia accounts for about 38 percent of the total maximum thrust and decreases to about 2 percent of the total maximum thrust for the slowest rate of blade-pitch increase [6 degrees per second]."

2.8 JUMP TAKEOFF

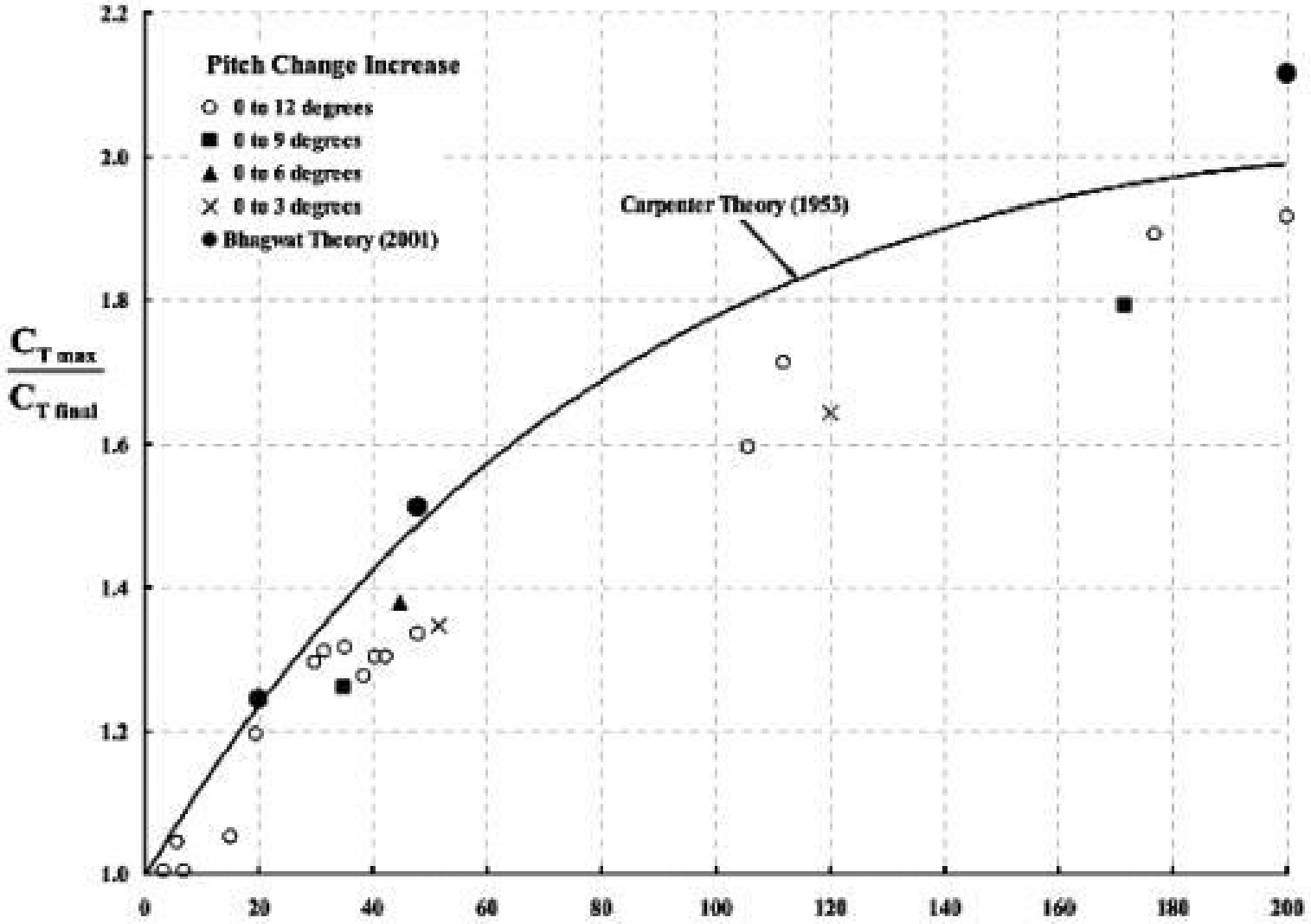

Fig. 2-61. The Carpenter and Fridovich test showing the effect of rapid collective pitch changes on maximum thrust [95].

The rotor thrust coefficient (C_T) variation with time, in response to the collective pitch increase from 0 to 12 degrees at a

48-degrees-per-second rate for one-fourth of a second, is shown in Fig. 2-63 . Thrust "overshoots" the final steady-state thrust for about one-fourth of a second and reaches a maximum of 1.35 times the final steady value. I have not reproduced the blade coning time history Carpenter and Fridovich provided because it follows thrust almost exactly. The induced velocity exhibits no "overshoot" as Fig. 2-62 shows. This behavior was characteristic of the induced velocity time history regardless of the pitch change rates.

Carpenter and Fridovich present a very simple theory to explain the experimental results shown in Fig. 2-61 , Fig. 2-62, and Fig. 2-63. The key assumption of their theory is that there is an "apparent additional mass of air influenced by the rotor disc." This mass of air must be accelerated from zero velocity, and this additional force must be included in the blade element momentum

theory. Based on work by Max Munk [97], Carpenter and Fridovich defined the apparent air mass as

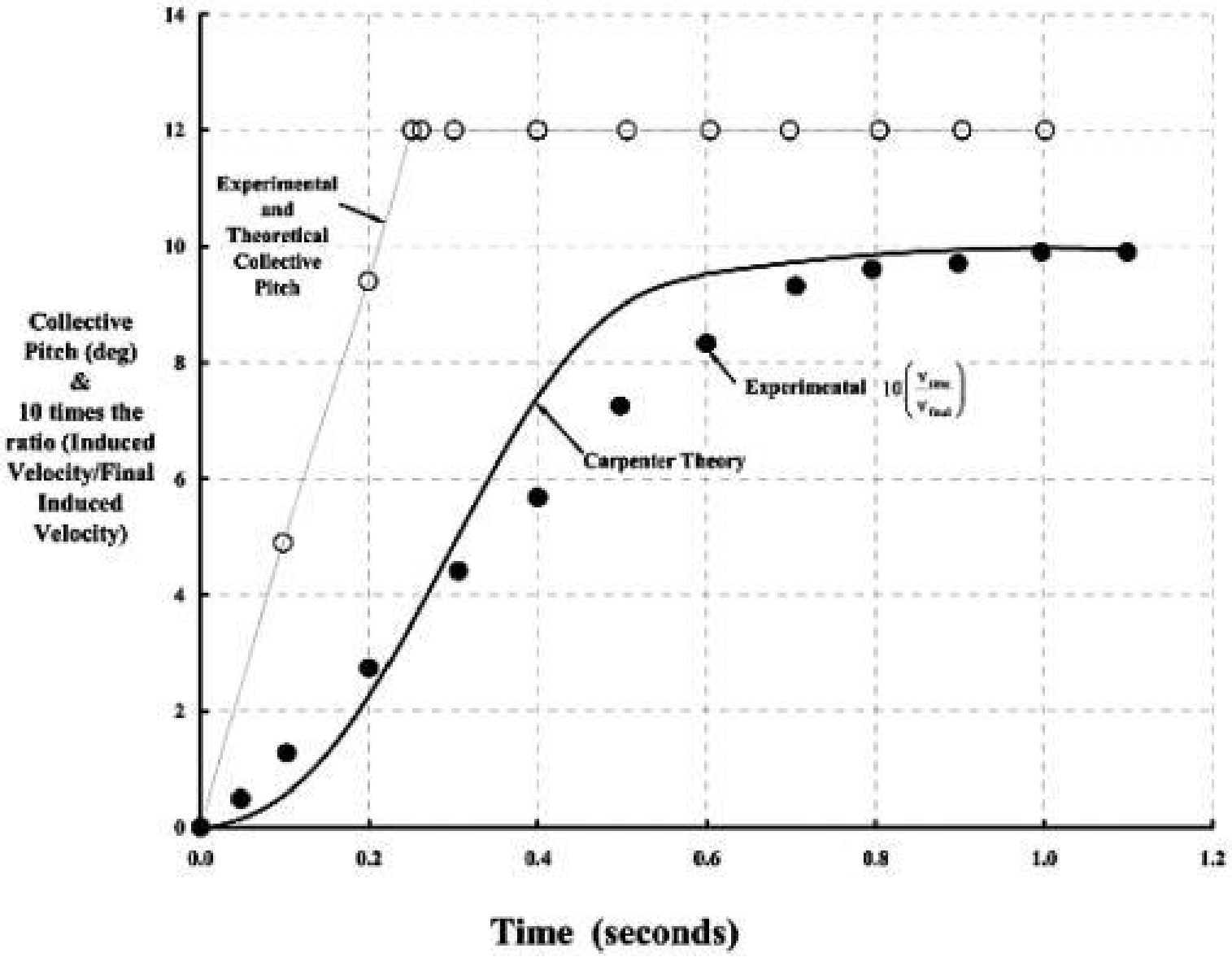

Fig. 2-62. Collective pitch change at 48 degrees per second for 0.25 seconds and induced velocity response.

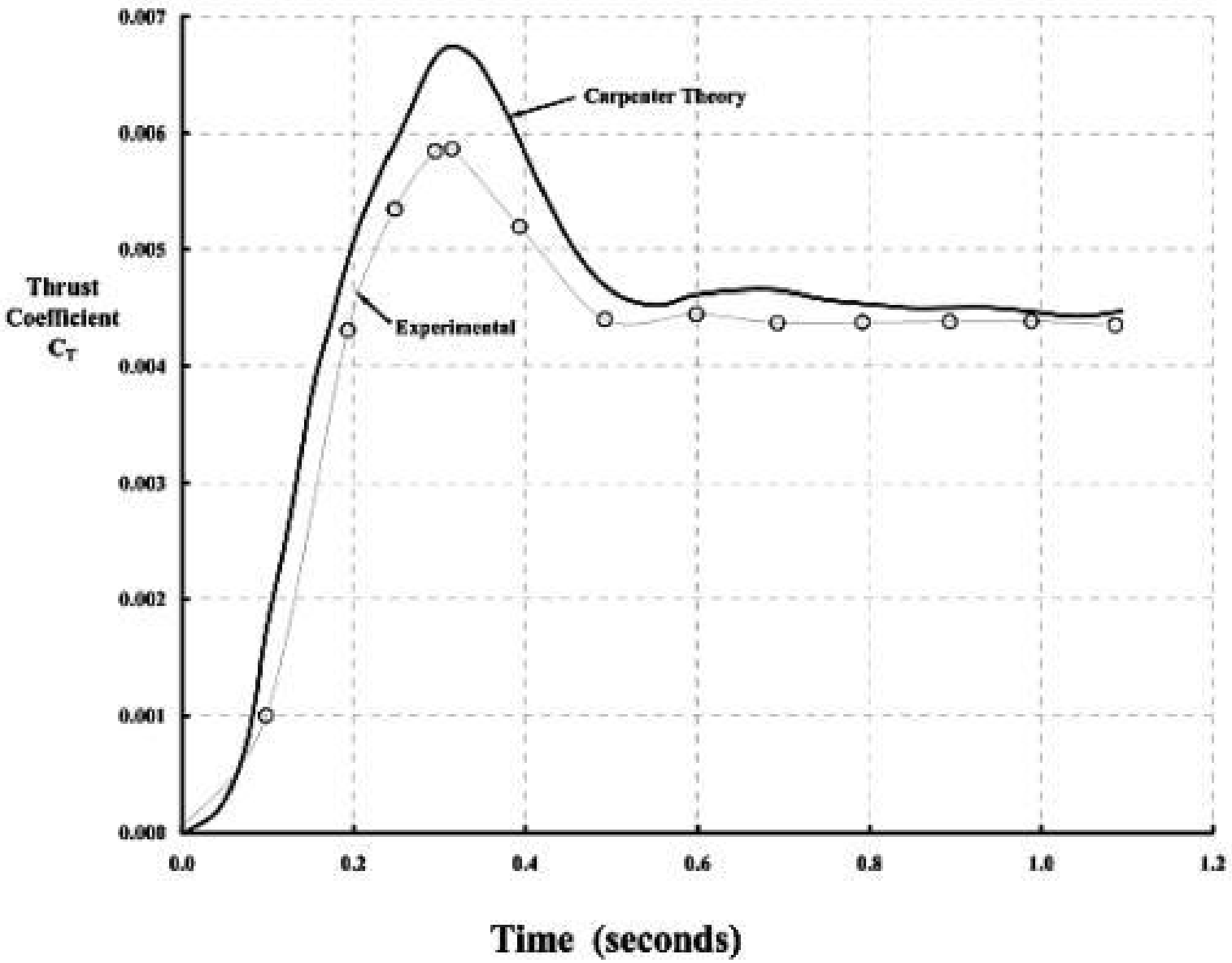

Fig. 2-63. Rotor thrust overshoot lasted for about 0.25 seconds.

2.8 JUMP TAKEOFF

(2.149)

$$\text{Apparent Mass} \equiv m_{air} = 0.637\rho\left(\frac{4}{3}\pi R^3\right) \text{ in slugs}$$

and then wrote the blade element momentum theory for induced velocity (v) as

(2.150)

$$m_{air}\frac{dv}{dt} + 2\pi\rho R^2\left[v\left(v + \frac{2R}{3}\frac{d\beta}{dt}\right)\right] = \frac{1}{6}\left(bcaRV_t^2\right)\left(\theta_{time} - \frac{3}{2}\frac{v}{V_t} - \frac{1}{\Omega}\frac{d\beta}{dt}\right).$$

Because the rotor blades were attached to the hub with a flapping hinge, Carpenter and Fridovich needed to include the effect of

flapping velocity ($d\beta/dt$) on the blade element angle of attack. (When you read their report [95], you will see that I have reduced his basic equation to a rectangular blade and assumed the induced velocity to be uniform over the whole rotor disc.)

The Carpenter and Fridovich theory required the flapping velocity. To calculate this velocity, they wrote the classic, second-order differential equation for flapping as

(2.151)

$$I_{flap}\frac{d^2\beta}{dt^2}+I_{flap}\Omega^2\beta=\frac{1}{8}(\rho acR^4)\left(\theta_{time}-\frac{4}{3V_t}v-\frac{1}{\Omega}\frac{d\beta}{dt}\right)-M_W$$

where I have again assumed a rectangular blade and uniform induced velocity.

The simultaneous solution posed by Eqs. (2.150) and (2.151) was, in 1953, solved by an analog computer; they used "the Bell Telephone Laboratories X-66744 relay computer at the Langley Laboratory." They used a time step of 0.02 seconds. Today, powerful digital computers, coupled with any one of the numerical integration schemes available [98], make short work of the problem Carpenter and Fridovich faced.

Once the time histories of induced velocity (v) and coning (β) were obtained, they computed the vertical hub force (T_{hub}) measured by the whirl tower balance as

(2.152)

$$T_{hub} = m_{air}\frac{dv}{dt} + 2\pi\rho R^2\left[v\left(v + \frac{2R}{3}\frac{d\beta}{dt}\right)\right] - bm_{blade}\frac{R}{2}\frac{d^2\beta}{dt^2}$$

and then converted this force to a thrust coefficient by

$$(2.153) \quad C_T = \frac{T_{hub}}{\rho \pi R^2 V_t^2}.$$

Based on my literature survey, the test and analysis by Carpenter and Fridovich received very little immediate follow-on attention from others in the rotorcraft industry. Nearly 20 years passed before their problem was studied again. But then, in the early 1970s, Peters [99] extended the concept of "apparent mass" to help explain rotor behavior during other transient conditions. Peters' explanatory efforts were quite successful and his work came to be known as the "dynamic inflow" theory. Most recently, Bhagwat [100] published his Ph.D . thesis dealing with an advanced free-wake theory programmed on a powerful digital

computer. This modern analysis brought a half-century of accumulated theoretical and computer power to bear on what may appear as a simple problem. As part of his thesis, Bhagwat studied the Carpenter and Fridovich problem in some detail . His quite modern theory prediction of thrust "overshoot" is shown in Fig. 2-61 . The modern theory hardly differs from the Carpenter and Fridovich result of 1953; however, Bhagwat [101] concludes that their apparent mass approach, while in good agreement with observed behavior, is not the source of the dynamic overshoot. The correct source is the complex wake springing from behind each blade, the induced velocity field about the rotor caused by this wake, and the actual lift of each blade

section airfoil.

2.8.9 Closing Remarks

As you can see, prediction of jump takeoff trajectories involves several important variables that influence the initial thrust and decelerating torque . Rotor over-speed, rotor inertia, ground effect, and thrust "overshoot" are just the beginning. I have found no comprehensive study of the autogyro's real limits to performing jump takeoffs . However, analytical capability does exist today to investigate the problem—should the need arise.

Jump takeoff capability, even to heights of 35 feet as demonstrated by late model autogyros, did not add enough capability to this first generation of rotorcraft. The autogyro quickly faded in the face of competition offered by even underpowered

helicopters . In fact, the autogyro is still frequently referred to as a short takeoff and landing (STOL) aircraft, when fuel efficient vertical takeoff and landing (VTOL) aircraft with modern jet aircraft cruise speed remains the goal.

Of course, the autogyro pioneers did lay the foundation that the helicopter pioneers needed in order to expand the rotorcraft industry. A perfect example of this foundation is the development of rotor blades during the autogyro era.

2.9 BLADES

The evolution of rotor blades during the autogyro era is a fascinating story. On one

hand, you see the story unfold by studying the many aircraft photos and three view drawings that exist in popular literature. But these two sources give only a feeling about the number of blades and their external geometry such as span or radius (R) and width or chord (c). On the other hand, it is the technical reports and papers that provide the facts and figures that bring the accomplishments of the autogyro pioneers into true focus.

In a simplistic sense, a rotor blade is a rotating wing. In a structural dynamics sense, a rotor blade is nothing more than a centrifugally stiffened rotating beam—with a cross section shaped like an airfoil. However, the planform variations among rotor blades, even during the autogyro era, are quite interesting. In January 1923 the C.4, the first successful Cierva Autogiro, had four rectangular planform blades (see Fig. 2-5). The blades had a very wide chord for their radius as you can see

from Table 2-5 . Then Cierva developed the C.6A, a slightly expanded C.4, which he demonstrated in England in 1925. With the introduction of the C.6A, the budding rotorcraft community almost immediately adopted the term "solidity" to describe aerodynamic planform geometry. The term solidity that Cierva introduced accounted for two reference areas that might be used in studying rotors—one being the swept disc area (πR^2) and the other being the physical blade planform area (bcR) for a rectangular blade, where (b) is blade number. These two areas were formed into a ratio referred to as solidity (σ) . This descriptive parameter remains in use today, so you should remember that

(2.154)

$$\text{Solidity} \equiv \sigma \equiv \frac{bcR}{\pi R^2} = \frac{bc}{\pi R} = \frac{b}{\pi(R/c)}$$

for rectangular blade

The ratio of blade radius (R) to blade chord (c) is, of course, blade aspect ratio.

The influence of solidity on rotor performance was the basis of early criticism of the autogyro. While Cierva enjoyed the praise of the overwhelming majority of those who saw his C.6 fly in England, he got little encouragement from one of the most highly respected fixed- wing aeronautical engineers of the era. The critic was Herbert Glauert. In November 1 926, about a year after Cierva demonstrated the C.6, H. Glauert published a landmark analysis [13] entitled *A General Theory of the Autogyro*, released as Aeronautical Research Committee, Reports and Memoranda, Number 1111 (R&M 1111). This appears to be the first formally published study of autogyro rotor system performance. The

report by Glauert laid a firm cornerstone for all future rotorcraft performance analysis and may well be one of the most referenced documents in the technical world of the rotorcraft industry.

2.9 BLADES

Table 2-5. Rotor Solidity Was Greatly Reduced in Less Than 10 Years

General									
Model	C. 4	C. 6A	C. 19 Mk. III	PCA-2	C.19 Mk. IV	C.30 P&A	KD-1	A.R. III	PA-36
Year	1923	1925	1929	1930	1931	1933	1934	1936	1939
Gross Weight (lb) (lbs)	1,200	2100	1450	2940	1450	1800	2100	890	1,800
Installed Power (hp) (hp)	80	110	105	300	105	140	225	84	175
GW/hp	15.0	19.1	14.8	9.8	14.8	12.9	9.3	10.6	10.3
Rotor									
Blades	4	4	4	4	3	3	3	3	3
Diameter (ft)	32	36	35	45	34	37	40	32.82	43
Chord (in.)	28	30	18.6	22	18.6 (est.)	11	12	4.9	17 to 11
Disc Area (sq ft)	803	1,018	962	1,588	908	1,075	1,257	846	1,452
R/c	6.86	7.20	11.3	12.3	11.0	20.2	20.0	40.2	17.2
Solidity	0.189	0.1768	0.1107	0.0976	0.084	0.0470	0.0478	0.0237	0.0444
Tip Speed (ft/sec)	234	260	230	340	320	370	420	464	450
Blade Airfoil	Eiffel 106	Gött. 429	Gött. 429	Gött. 429	RAF 34	Gött. 606	Gött. 606	Sym.	NACA 23012
Wing									
Span (ft)	None	None	20.5	30.33	20.5	None	None	None	None
Chord-Root (ft)	na	na	2.53	4.33	2.53	na	na	na	na
Projected Area (sq ft)	na	na	45	101	45	na	na	na	na

In R&M 1 1 11, Glauert captures the essence of Cierva's aerodynamic theory, but when you read beyond the technical work, you will find that he included several rather pessimistic statements about rotary wing performance. For instance, in the general discussion part of his report, he states:

"The maximum lift drag ratio of rotating wings is poor compared with that of ordinary fixed wings; its ordinary value is approximately 6 and it is unlikely to exceed 8 in any practical case. It occurs at a small value of lift coefficient [using disc area, πR^2, as the fundamental area

and the forward speed as fundamental speed] in the neighbourhood of 0.05 and so at a speed approximately three times the stalling speed. .....The important conclusion is reached that as the maximum speed of the gyroplane is increased, the loading must also be increased in order to maintain a sufficient ratio of tip speed to forward speed; and there is a corresponding increase of the stalling [speed] .....*Thus, the principal merit of a gyroplane, its low landing speed, inevitably disappears when high speed of level flight is required, and there remains only the absence of a sudden stall to counter-balance the very poor efficiency as compared with an aeroplane.*" [My italics]

Glauert based his numerical examples and statements on an autogyro rotor having four blades of 17.5-foot radius and 2.75-foot chord, or a solidity of 0.20. His comment at the end of Appendix II of his R&M is particularly interesting because he noted:

" A reduction of the solidity leads to improved speed of horizontal flight since the power taken by the windmill is reduced. Also the best loading falls more rapidly than the maximum lift coefficient and hence the higher

top speed is accompanied by a lower stalling speed. *The limiting condition for this method of [L/D] improvement is clearly the impossibility of making very thin [narrow chord with thin airfoil] blades of large radius and is a matter of structural strength."* [My italics]

2.9 BLADES

What Glauert failed to consider was Cierva's, Pitcairn's, Kellett's, and Hafner's resourcefulness. In 4 years, as Table 2-5 shows, solidity was halved and, 4 years later, solidity was halved again. The Hafner A.R. III, with a rotor solidity of 0.0237, made it quite clear that Glauert's use of the word "impossibility" was hardly visionary. However, Glauert's view that the maximum rotor lift-to-drag ratio was "unlikely to exceed 8" was more correct as you will read later.

Cierva used his models C.6 through C.18 to evaluate several planform geometries before selecting the production configuration used on the C.19 . *Cierva Autogiros—The Development of Rotary Wing Flight* by Peter Brooks [7] contains a photographic chronology of the blade planform study. In his *Engineering Theory of the Autogiro* [11], Cierva discusses the aerodynamic merits of several planforms . I have reproduced a few of his sketches in Fig. 2-64, Fig. 2-65, and Fig. 2-66. While Cierva investigated the effect of blade twist in flight, Fig. 2-64, he made no attempt to calculate performance for other than untwisted rectangular blades. However, in Part IV of his *Engineering Theory* he says that:

"It is quite certain that a certain degree of [aerodynamic] improvement can be obtained by (a) giving the blades a wash-in in pitch angle, which diminishes the stalling of certain [radial airfoil] sections and (b) tapering the tips, with a decrease of the profile losses in that region, which is little useful for lift and (c) decreasing the chord

near the root, where stalling is more pronounced and the trailing and leading edges change places in horizontal flight." [See Fig. 2-2.]

Cierva goes on to say that "but, in every case, there is a possibility of impairing the efficiency by overdoing (a), (b), or (c)." He then concludes with:

"My results, so far, are that not a great degree of [aerodynamic] improvement is obtained, either by (a), (b), or (c), but, by using shapes such as the types RB 53 [see Fig. 2-66] and RB 55 [see Fig. 2-65] with a considerable parallel (constant chord) portion in the optimum region, the best results are obtained. The types F 1017 and F 1038 are not so good, probably on account of the very long tapering and thick tip, and the F 1038 (modified) [see Fig. 2-64] was slightly worse than the F 1038 because of the increased tapering and the decrease of the wash-in."

Cierva did not give theoretical results for twisted blades with arbitrary planform. Instead, he seems confident in using the blade-tip pitch angle as the reference angle (θ =

θ_{tip}) in his rectangular, untwisted blade equations . With respect to planform, he recommends his basic equations, but with a solidity he defines as (σ_{shape}). In effect, he defines an average chord equivalent to a rectangular blade chord. For nonrectangular planforms he writes

$$(2.155)\quad \sigma_{shape} = \frac{b}{\pi R}\left\{\frac{\int_0^R c_r r\sqrt{R^2-r^2}\,dr}{R^3/3}\right\} \quad \text{for nonrectangular planform}$$

where (c_r) is the chord variation with radius. Cierva performed the integration required by Eq. (2.155) graphically for all but the simplest planforms.

2.9 BLADES

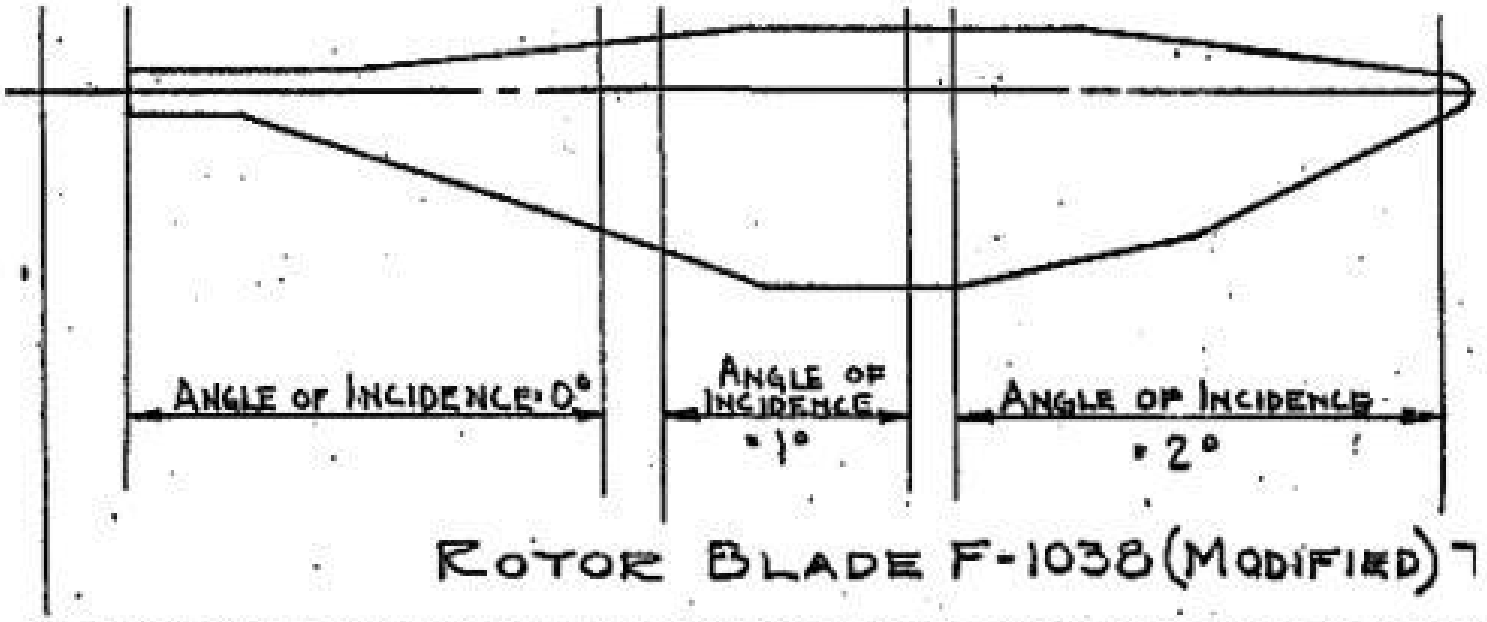

Fig. 2-64. Cierva rotor blade type F-1038 (modified). Equivalent rectangular blade solidity of 0.19 [11].

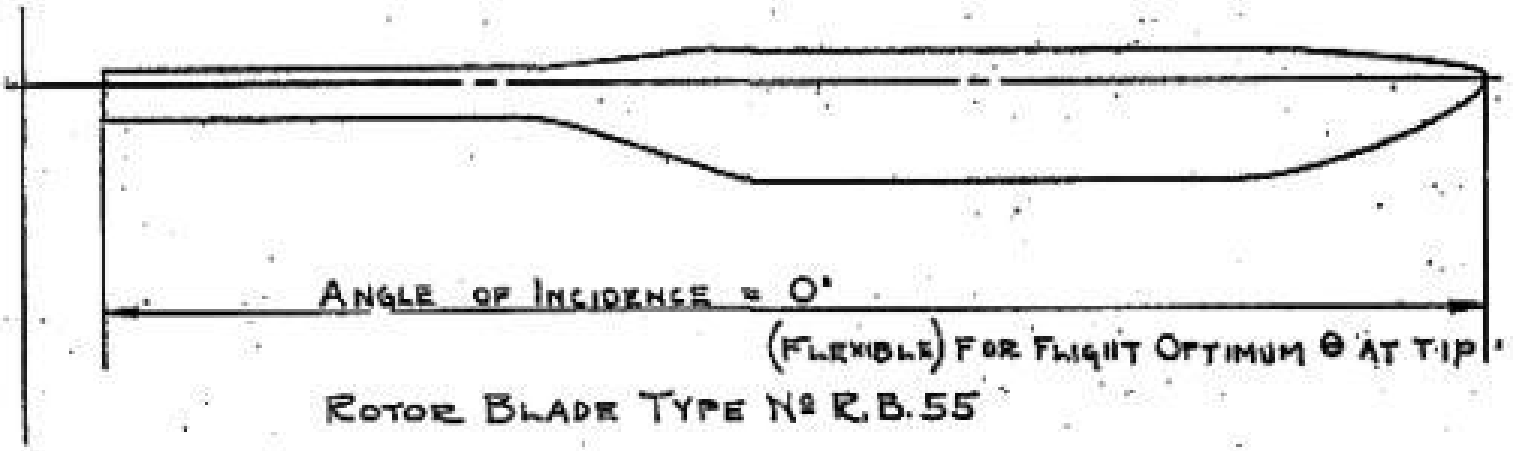

Fig. 2-65. Cierva rotor blade type R.B. 55. Equivalent rectangular blade solidity of 0.088 [11].

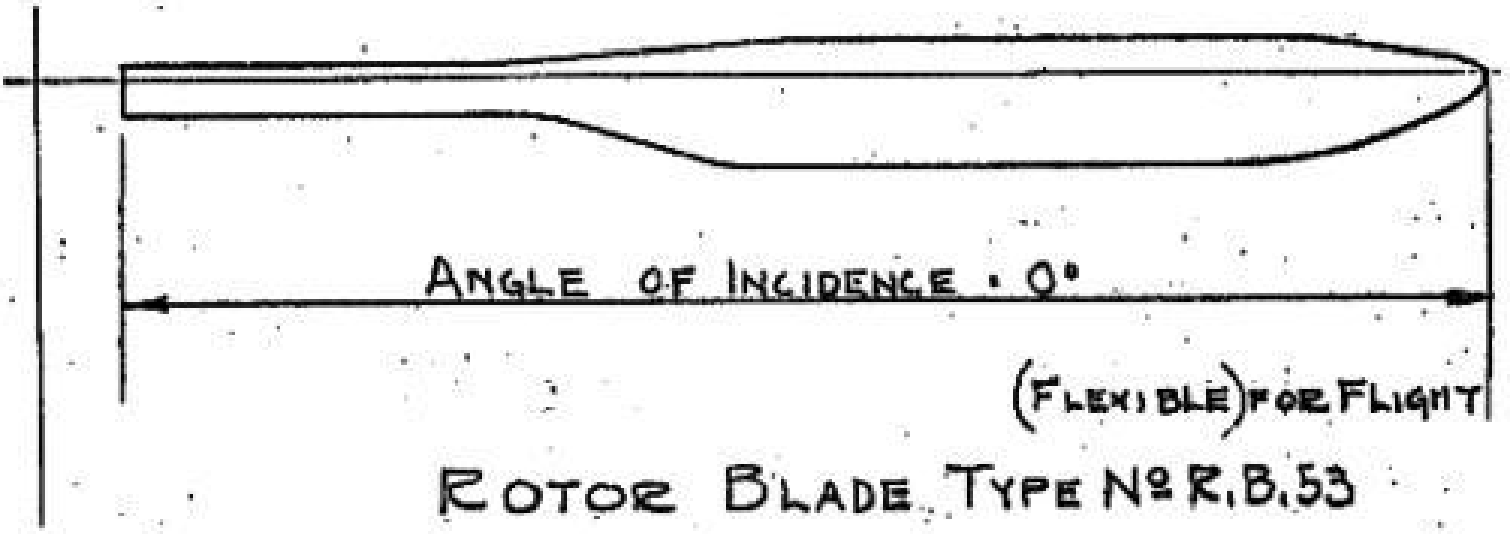

Fig. 2-66. Cierva rotor blade type R.B. 53. Equivalent rectangular blade solidity of 0.090 [11].

2.9 BLADES

The concept of an equivalent rectangular blade solidity for any nonrectangular planform has altered slightly over the decades. Today, in technical literature [61] you will find an equivalent chord leading to

a thrust-weighted solidity, which is what Cierva had in mind. This solidity is calculated as

(2.156) Thrust weighted $\sigma_T \equiv \frac{b}{\pi R}\left\{\frac{\int_0^R c_r r^2 dr}{R^3/3}\right\}$ for nonrectangular planform.

In addition, an equivalent chord leading to a torque- or power-weighted solidity is used occasionally and is calculated as

(2.157) Torque weighted $\sigma_Q \equiv \frac{b}{\pi R}\left\{\frac{\int_0^R c_r r^3 dr}{R^4/4}\right\}$ for nonrectangular planform.

When Cierva went into production it was with the C.19 shown in Fig. 2-67 and Fig. 2-68. The blade planform, as the top view shows, certainly appears to be a derivative of the Cierva Type R.B. 53 shown in Fig. 2-66. Photos by Brooks [7] of early Pitcairn, Kellett, and Buhl machines all show the stamp of the Cierva production blade planform.

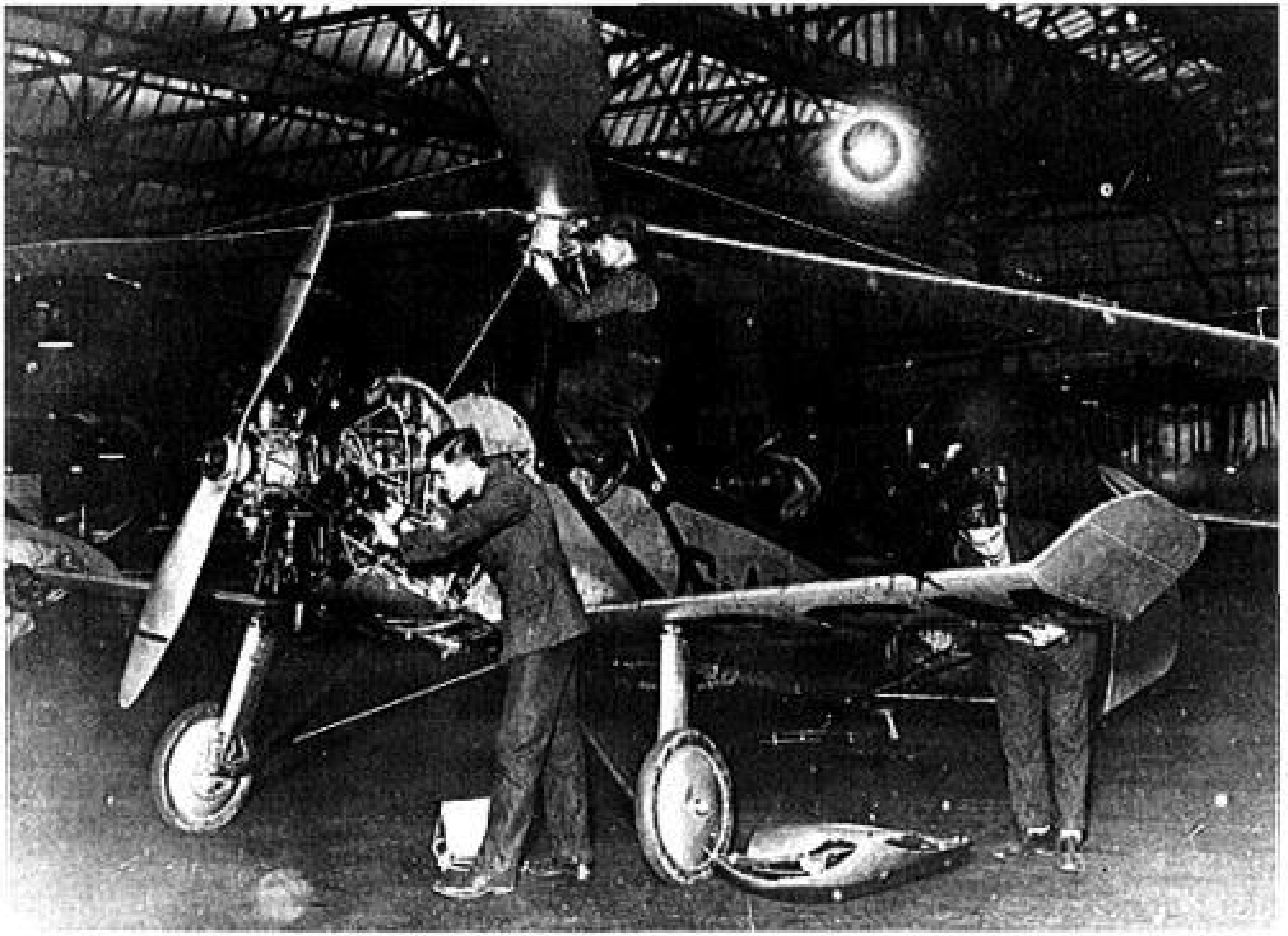

Fig. 2-67. A Cierva C.19 Mk. III in final assembly [7].

2.9 BLADES

2.9.1 Structural Details

Looking closely at Fig. 2-68, you can almost guess the basic blade design from the artist rendition. The leading edge of each blade is solid white back to about the 30-percent chord point. Beyond that to the trailing edge there are closely spaced lines that represent airfoil ribs—some 65 per blade by my count.

Considerably more detail about the C.19 blades is shown in Fig. 2-69 and Fig. 2-70. These informative sketches are from *The Book of the C.19 Autogiro* [50]. The foreword states, "The authors of the book [Mr. Sanders, in charge of the design staff, and Mr. A. H. Rawson, test pilot] are those who have been most closely in touch with Senor Don Juan de la Cierva, the inventor of the Autogiro, during the development of the principle, and in particular of the type of machine explained and illustrated."

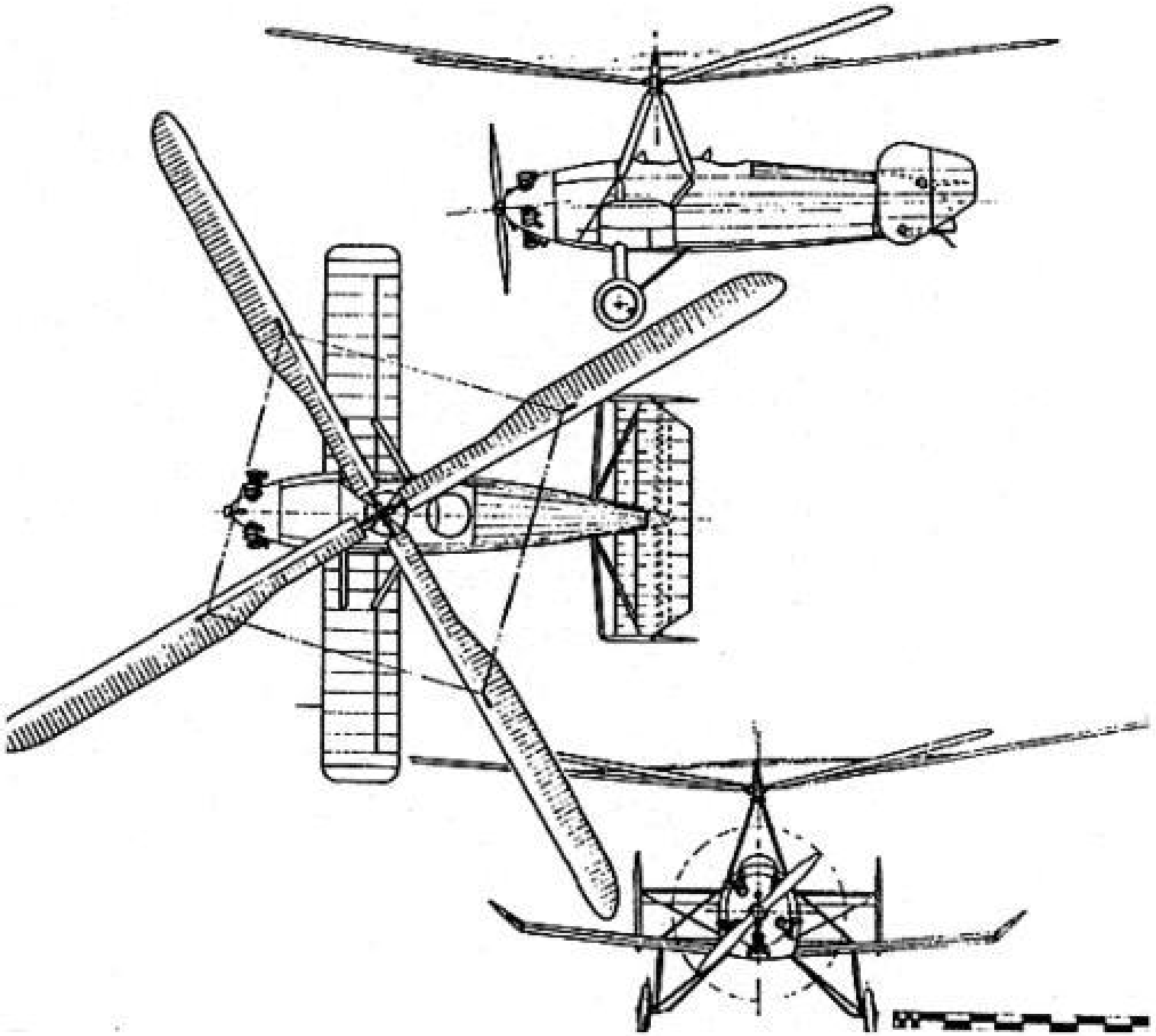

Fig. 2-68. The Cierva C.19 Mk. III [7].

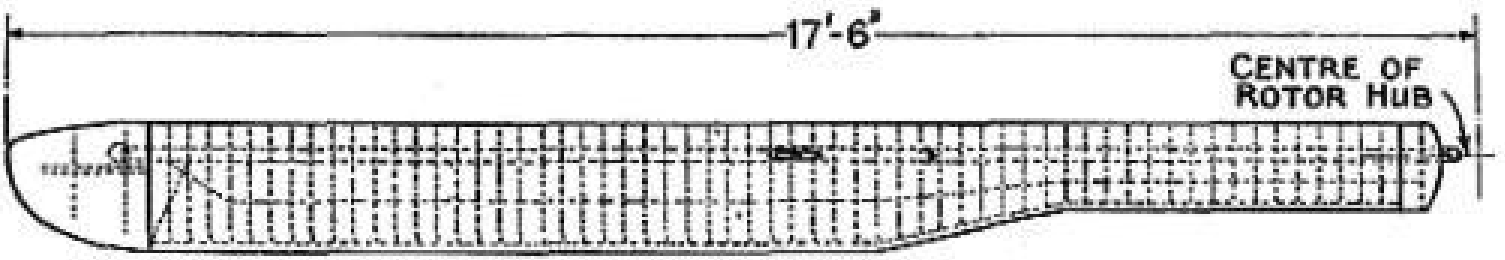

FIG. 4. PLAN VIEW OF ROTOR BLADE

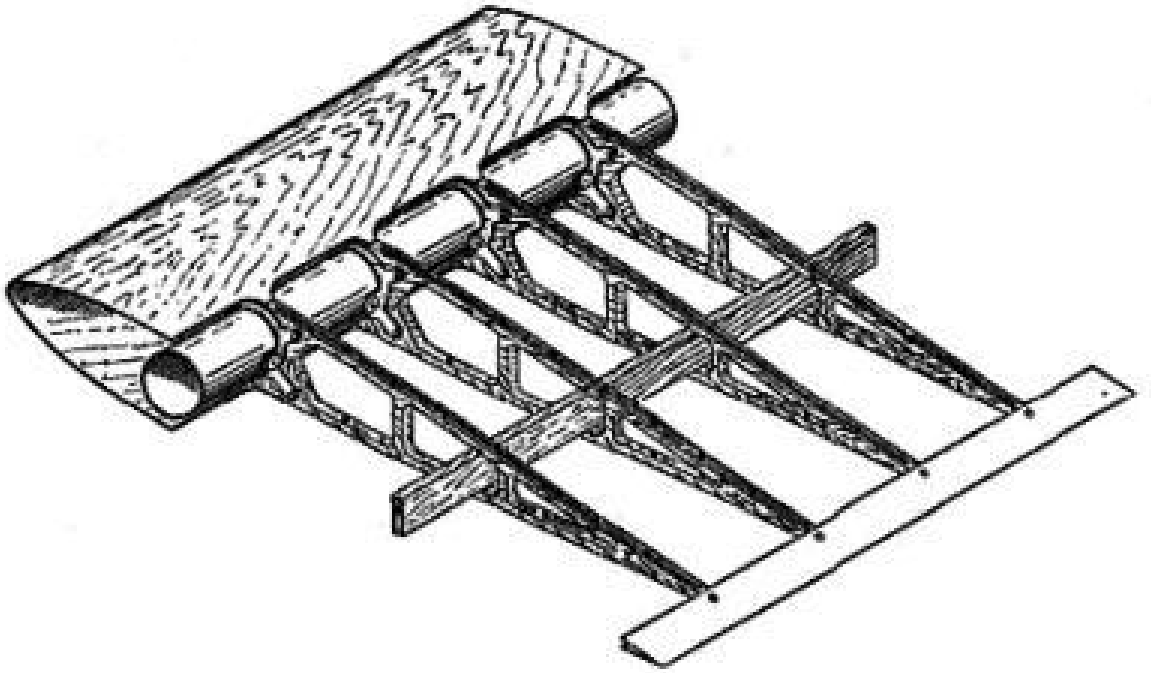

Fig. 2-69. The Cierva C.19 Mk. III blade with 18.6-inch chord [50].

The description of the C.19 blade that Sanders gives is quite complete for a book addressed to the uninitiated autogyro enthusiast. He writes:

"The rotor blades, which are the chief components of the Autogiro, are designed to give the

necessary lift to the machine. These are of wood and metal construction. Each blade is 17 ft. 6 in. long with a chord of 18.6 inches (along the main portion) and is of "Göttingen 429" section, set at an angle of incidence of 2°10' [Fig. 2-69].

The main spar is of high tensile steel tube, 1-3/4 in. diameter by 20 S.W.G. This spar runs the length of the blade (except at the extreme tip) at 0.25 of the chord from the leading edge. The ribs are of wood, consisting of a mahogany core 5/32 in. thick, faced on each side with 1/16 three-ply [Fig. 2-69]. Each rib is grooved along its top and bottom edges and drilled to take the sewing string fixing the fabric covering. The ribs are very closely spaced (3 in. apart) and each one is riveted to a flanged clip which is sweated to the main spar. In addition, every third rib is bolted to the spar. Owing to the close spacing of the ribs the load carried by each is very small.

To stiffen the blade in a horizontal plane an auxiliary spar is fitted at approximately midway between the main spar and the trailing edge, starting from the root end, and continuing to the outer end of the main spar. This auxiliary spar is of 1/4 in. thick spruce, approximately 7/8 in. deep, and is glued and bradded to each rib. The trailing edge is a strip of 26 G.

duralumin, 2-1/2 in. wide, doubled back over the ribs and riveted to each.

2.9 BLADES

The nose portion of the blade is covered with 1/16 in. 3-ply extending back to the centre of the main spar. The whole blade is fabric covered, and the outer end of the blade, known as the rotor blade tip, is a 22 S.W.G. aluminum fairing, which is made in halves and riveted. To stiffen this fairing two duralumin ribs and two channel pieces are fitted inside. One of these ribs is bolted to the end of the main spar as a means of attachment to the blade. In addition the inner edge of the tip is doubled back and screwed to a special thick rib at the end of the main portion of the blade. At the root end of the blade is another aluminum fairing, stiffened with a spruce former, and screwed to the end rib [Fig. 2-70].

Provision is made for draining any moisture that may get into the blade by means of six drain eyelets spaced at intervals along the bottom surface near the

trailing edge.

A machined fork end is bolted and sweated in the root end of the main spar, forming an attachment to the articulation joints in the rotor hub [Fig. 2-70].

On assembly the rotor blades are inter-braced with 1 5 cwt. cable, the ends of which are attached to friction dampers on the main spar. Turnbuckles are provided in this bracing for adjustment.

The friction dampers [Fig. 2-71] work somewhat on the principle of the shock absorbers used on cars, and the friction between the steel plates and cork disc can be adjusted to give the required stiffness. The crank arms of the dampers are designed so as to have a certain degree of free movement in a vertical plane, thus enabling them to adjust themselves to the rise and fall of the blades. The friction dampers are fitted at 8 ft. 3-1/2 in. from the centre line of the rotor hub.

A 20 cwt. suspension cable is fitted from the top of the rotor hub to a bracket on the main spar at 6 ft. 6-1/2 in. from the centre line of the rotor hub. This cable is of such a length that a relax angle of 8° is allowed. Provision for adjustment is also made in this bracing by

means of turnbuckles.

Each blade is balanced to a standard weight so that all blades of the same type are interchangeable, provision being made for correcting weight at the outer end of the main spar."

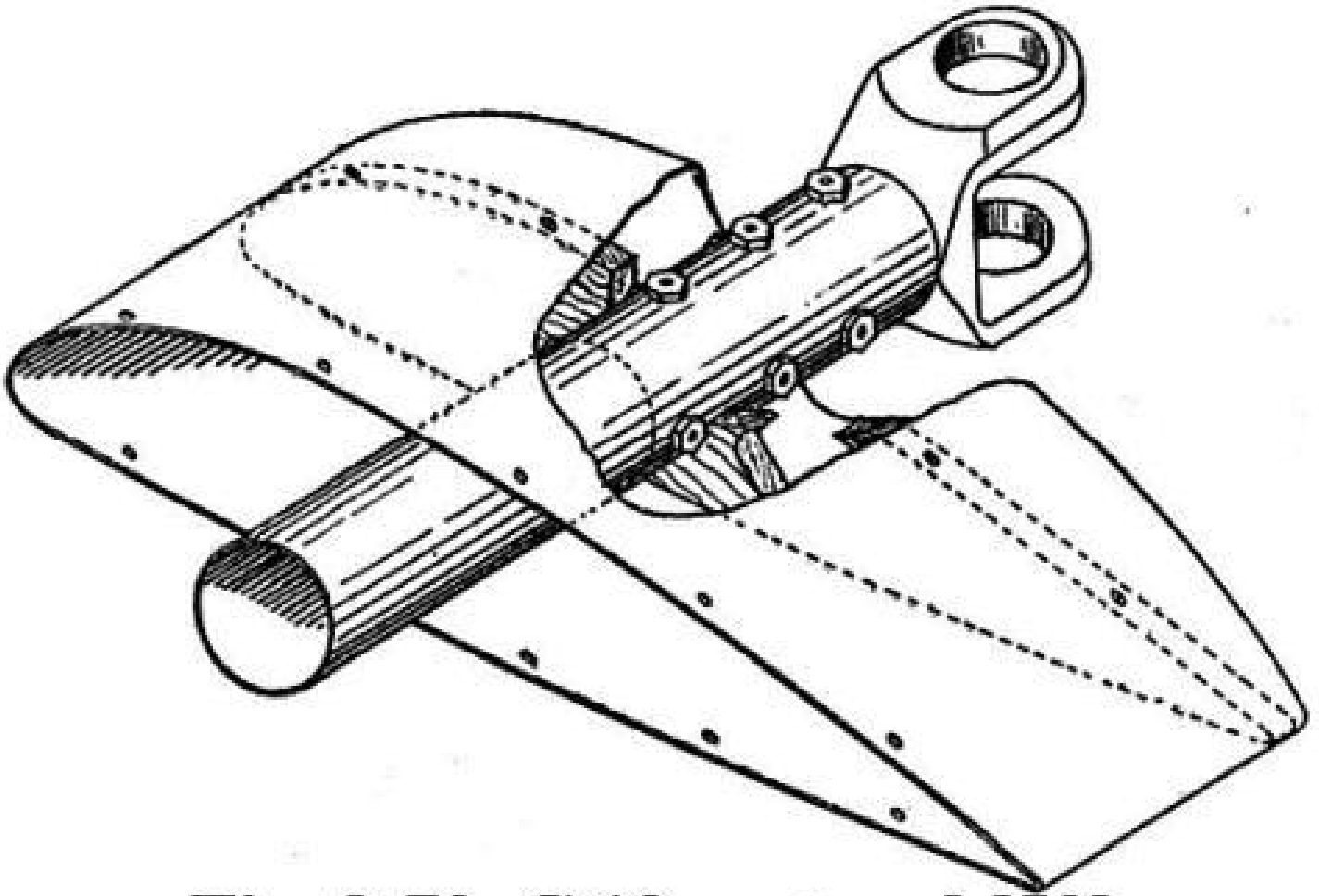

Fig. 2-70. C.19 root end [50].

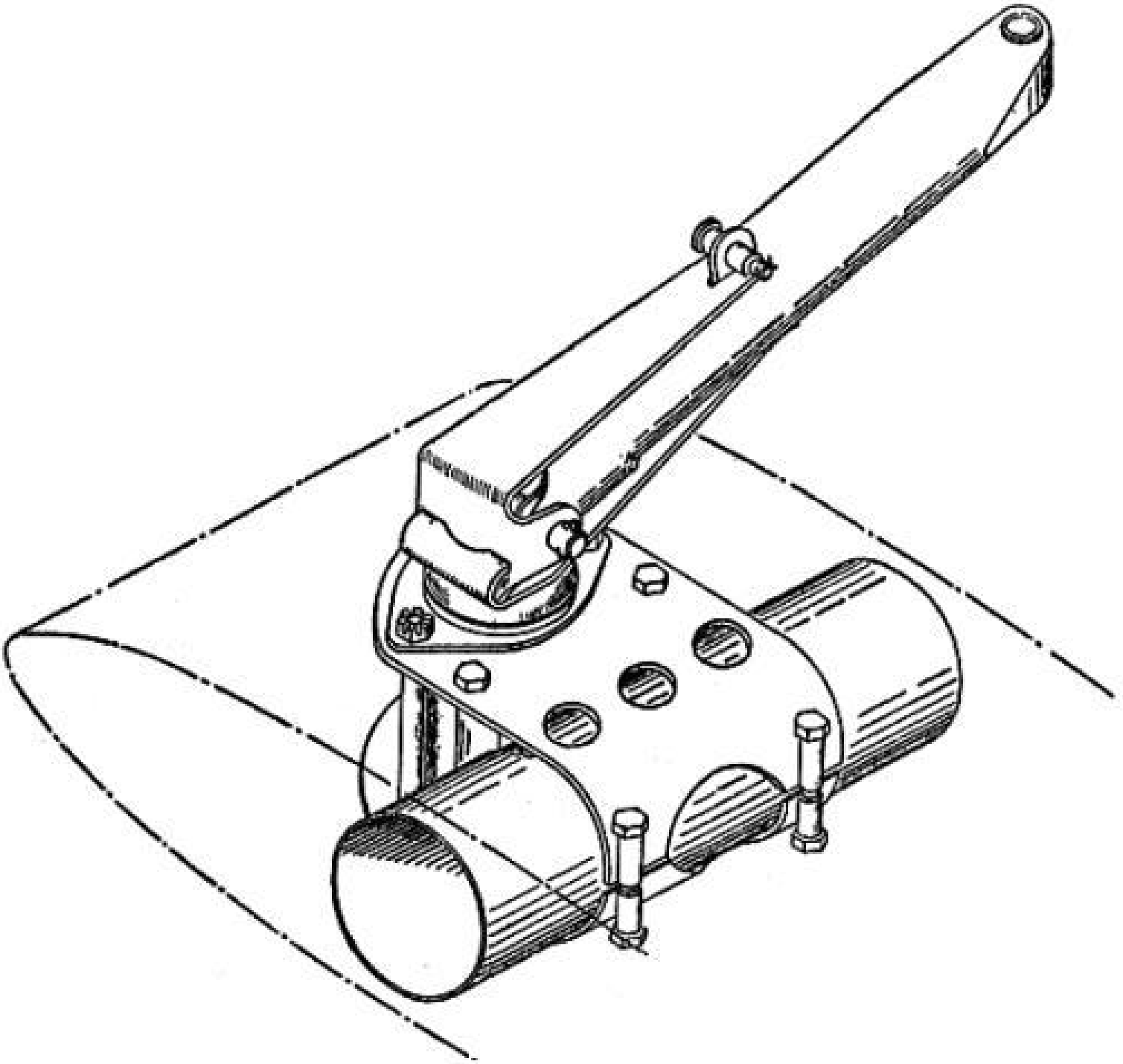

Fig. 2-71. Lag damper [50].

2.9 BLADES

Sanders [50] points out that cables carried damper loads from one blade to another. Thus, the blades were free to lead-lag as a group, but motion relative to each other was restricted. Furthermore, cables were used to hold the blades up when they were stationary. These cables were referred to as "droop" cables . These cables were soon to be removed, as I will discuss shortly.

The main load member for these early blades was a constant diameter, constant wall thickness, high-strength steel tube . This tube is referred to as the blade spar. The "forked" extension to the spar, used to capture the lead-lag hinge pin, was also high-strength steel. This fitting was "sweated and bolted" to the main spar. Sanders [50] indicates "every third rib is bolted to the spar." Apparently,

3/16-inch-diameter holes were drilled into the spar. The holes were drilled on the inplane or chordwise axis of the spar. Even with the stress rise correction factors Cierva applied, this deliberate damage to such a critical load-carrying member would never be considered today.

Very interesting information about the Pitcairn PCA-2 blade was included by George Townson in his technically oriented book [45]. He provides a photograph of a blade before covering, shown here in Fig. 2-72.

On page 23 of his terrific book, Townson gives an unmatched detailed description of the PCA-2 blade, writing:

"The rotor blades were generally rectangular in plan form. The chord of the blade was of two widths; the one outboard being larger than the inboard. Transitional section of increasingly longer ribs faired the inner, narrow

chord to the wider outer chord. The tip was curved with its thickness tapering into a rather sharp edge at the tip. Drain holes were provided at several places along the trailing edge of the blade to ventilate the inside to expel any moisture that was present as the result of condensation. These holes also prevented air pressure being built up from the centrifugal pumping caused by the rotation of the blade. The outer chord width was 22 inches; the inboard 5-3/4 feet had a chord of only 14-25/32 inches, the transition required three feet from inner to outer. The main member was a round tube of 4130 steel, 2-1/8 inches in diameter straightened to a close tolerance, heat treated and hand polished. Approximately fifty plywood ribs, an average of three inches apart, formed the airfoil. A Pitcairn #4 airfoil was developed. It was a modification of the Göttingen 429. Ribs were routed from five-ply wood having alternate layers of mahogany and birch and were one quarter of an inch thick.

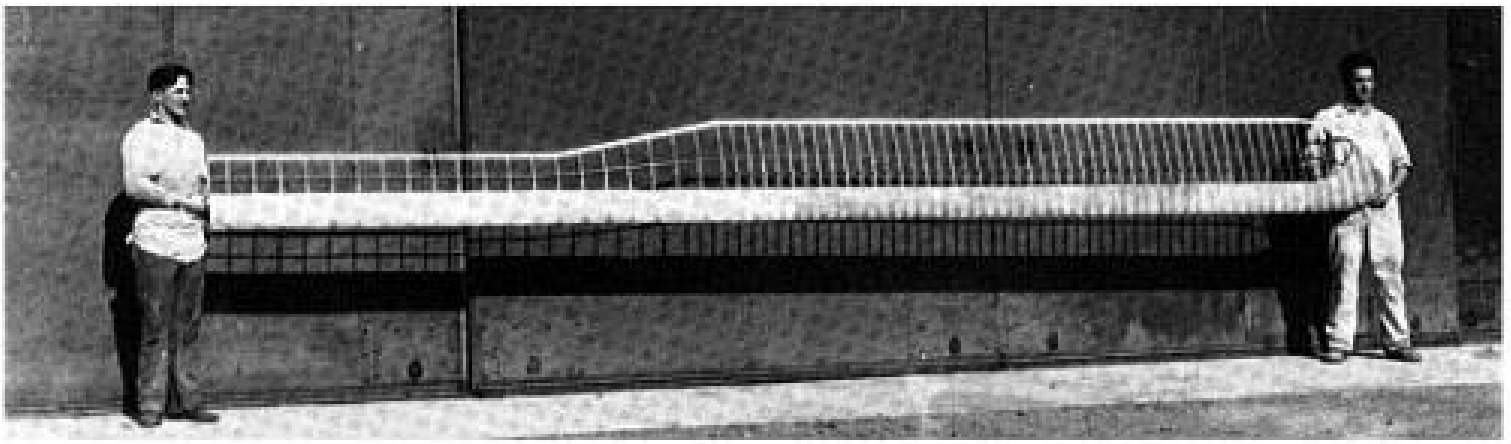

Fig. 2-72. Pitcairn PCA-2 blade before covering [45]

(do not let the shadows confuse you).

2.9 BLADES

Each rib had a stainless steel collar riveted onto one side, and these in turn were fastened to the steel spar. Some of the early blades had these collars soldered to the spar, but this was later changed to spot welding. The welding process was especially developed by Pitcairn engineers so that the maximum strength in the weld could be developed without reducing the strength of the spar tube in the process. The blade was covered to a point just aft of the spar tube with thin plywood that had been preformed to the leading edge shape. The trailing edge was formed into a stainless steel "vee" of thin sheet which was nailed to the ribs on earlier models. Later a steel tail was formed for each rib and the wood rib cut off blunt about three inches from the end of the rib. The stainless steel trailing edge was provided with slip joints so that

one section of the trailing edge telescoped into the other if the blade flexed fore and aft. As the entire blade was finished in doped fabric, the slip joints were covered with small leather patches so as not to wear out the trailing edge fabric. The fabric was held down to the ribs by rib stitching in the same manner as an airplane wing."

Two very important components, used by early developmental autogyros and the first production models, were "droop" cables and blade-to-blade lead-lag limit cables . These cables, clearly visible on the Cierva C.19 while stationary (Fig. 2-73), are frequently invisible to the eye when studying photographs of autogyros in flight. The purpose of the "droop" cables is, of course, obvious. With the flapping hinged blade, some limits to both minimum and maximum flap angles are required. On early autogyros, these limits were rubber pads on the hub spaced below and above the blade spar, which allowed for nearly a 30-degree range in flapping. The

blade-to-blade lead-lag cables were designed to keep the blades from depatterning in relative azimuth, which could lead to ground resonance (recall Fig. 2-14).

The design requirements for both "droop" and lead-lag cables was carefully explained by Cierva in Part V of his *Engineering Theory* [11] . Part V is titled "Kinematics and Dynamics of the Rotary Blades" and covers rotor speed and motions about both flap and lag hinges. With respect to flapping, he concludes, from three possible flight situations, that a "sudden increase in speed without change of incidence, such as occurs at top speed in strong gusts" will create maximum flap-up angles ranging from 13 to 21 degrees and minimum flap angles around –10 degrees . In an abbreviated analysis, Cierva concludes that the lead-lag angle will range from ±2.15 to ±5.2 degrees, but an increase of 50 to 100 percent on these angles "should be

allowed for abnormal conditions [such as] sudden accelerations, bumpy air, etc." He further notes that "the restrictive interbracing should give a perfect freedom between consecutive blades of about 0.5 to 1 degree, and the restriction should be absolute for an angle equal to $0.5 + \beta_o a_{1s}$ in order to prevent the stops, limiting the movement at the hinge, from taking any loads when starting or stopping the blades." Cierva is very emphatic about the lead-lag cables saying, "If any elastic interbracing is used, great care should be taken to have it sufficiently slack to not restrict the motion in flight, since resonant conditions can easily be reached, with the subsequent vibration and risk of [blade] failure."

Fig. 2-73. Cierva C.19 Mk. III showing "droop" and lead-lag cables [7].

While the Cierva C.19 Mk. III sold in limited quantities, it clearly had several imperfections. The "droop" and lead-lag cables were right at the top of the list. At this time, the rotor startup problem had been solved, but direct control had yet to be invented. This period does not receive much attention in the popular literature, but it deserves, in my opinion, a great deal of attention. During this interval, roughly between November 1930 and June 193 1, Cierva developed the low-solidity, three-bladed rotor system having no cables.[31] Brooks [7] recounts the period, writing:

"While he was in the United States, Cierva had also been analyzing Autogiro rotor performance and had satisfied himself about the considerable potential increase in efficiency that would result if the parasite drag of blade suspension and inter-blade bracing cables and friction damper arms could be eliminated. Tests were conducted at Willow Grove on a C.19 in which damping was by means of felt blocks at the [rotating] wing roots. Inter-blade cables were eliminated. Short flights were made with both four-blade and two-blade rotors with this arrangement."

Cierva returned to Europe, via Paris, to attend the First Congress on Air Safety (December 10–23, 1930) and then went home to Spain. In March 193 1 he arrived back in England and immediately began development of what was called the "cantilevered" blade. The use of cantilevered only meant that a "droop stop," projecting out from the hub, provided a resting spot for the blade flapping hinge assembly (and thus the blade spar) when not rotating.

As Fig. 2-74 shows, the droop stops, despite the blade bending or elastically drooping, provided ample clearance between the blade and the aft fuselage. Note that the two rudders were removed, and the single, conventional rudder was enlarged. Brooks [7] quotes the maximum speed of the C.19 Mk. IV as 100 to 102 miles per hour, an increase of some 10 miles per hour over the C.19 Mk. III (82 to 95 miles per hour). Minimum speed remained at 25 miles per hour.

---

[31] It is at this point, circa June 1931, that I think the modern rotor system was born. The modern control system of cyclic and collective pitch came later with the Hafner A.R. III.

2.9 BLADES

Fig. 2-74. Cierva C.19 Mk. IV with "cantilevered" blades circa June 1931 [7].

The importance of rotor blade droop is not always appreciated in rotor blade design. Flapwise bending stiffness (EI_{flap}) in pound-feet squared, running weight (w_b) in pounds per foot, running mass (m_b) in slugs per foot, and blade radius (R) in feet are, of course, key parameters defining droop of a "cantilevered" beam.[32] But these four key structural parameters, along with rotor speed (Ω) in radians per second, also define the natural vibrating frequencies of the rotating, pin-ended (i.e., flapping hinged) beam and, of course,

vibratory loads and stresses. There is little published evidence that the autogyro pioneers saw the connection. However, I have run across comments here and there about aircraft vibration with the three "cantilevered" blade rotor system, which never appeared about autogyros with four- bladed, cable-supported rotor blades.

Cierva progressed from a four-bladed, high-solidity, cabled rotor to a three-bladed, low-solidity, "cantilevered" blade rotor using the same basic airframe, as Fig. 2-73 and Fig . 2-74 show. His calculated performance improvement was obtained, so it is natural to wonder about the structural dynamics of the two rotor systems.

The structural dynamic behavior of a rotating beam subjected to airloads is, to many engineers, the most interesting applied mathematical problem that rotorcraft offer.

Fortunately for my discussion here, early autogyro blades were constructed as uniform beams, so an introduction to rotor blade structural dynamics is relatively simple. To begin with, think just about the blade deflection when the autogyro is stationary, and the blades are not rotating. The

---

[32] The units of many rotor blade parameters are frequently NOT given in the pound, slug, foot, second, system. For example, structural engineers will quote flapwise stiffness in pound-inches squared and dynamic engineers denote mass in slugs. In the exchange of data between the two groups, a 12 or 32.174 has quite often been misplaced, generally to the embarrassment of members from both groups. So, remember that weight, in pounds, equals mass, in slugs, times 32.174 feet-per-second squared.

C.19 Mk. III and Mk. IV provide two distinct examples as Fig. 2-73 and Fig. 2-74 show. In both configurations, Cierva appears to allow the same minimum clearance of about 12 inches between a blade and the airframe. With the Mk. III, the "droop" cables (according to Sanders) were adjusted by turnbuckles to give a blade-root slope of –8 degrees. Assuming first that there is no elastic bending, the *blade tip* would therefore be hanging some 28 or 29 inches below a straight-out reference line as Fig. 2-75 shows.

This rigid blade deflection (rigid Z_r) in feet, at any radius station (r) in feet, is calculated simply as

(2.158)

$$\text{rigid } Z_r = (\text{root slope})\, r = \frac{8^\circ}{57.3 \text{ degrees/radian}}\, r .$$

Note here that degrees are converted to radians

by the factor $180/\pi$ or 57.3 . Elastic bending increases this deflection all along the radius . In the Mk. IV case, the elastic bending deflection of the uniform beam (elastic Z_r) in feet, from any strength-of-materials textbook [102], is

(2.159)

$$\text{elastic } Z_r = \frac{w_b}{EI_{flap}}\left(\frac{R^2}{4}r^2 - \frac{R}{6}r^3 + \frac{1}{24}r^4\right) = \left(\frac{w_b R^4}{EI_{flap}}\right)\left(\frac{x^2}{4} - \frac{x^3}{6} + \frac{x^4}{24}\right)$$

where (EI_{flap}) is the flapwise bending stiffness in pound-feet squared and (w_b) is the running weight in pounds per foot. The blade radius (R) is measured in feet, and the nondimensional radius (x) is the ratio (r/R).

The elastic bending depends solely on the beam parameter (w_bR^4/EI_{flap}) or its reciprocal (EI_{flap}/w_bR^4), which is occasionally encountered in structural dynamic work. *Note that the beam parameter is not unitless; it has the units of feet.* This parameter is a major

factor in designing a blade free of resonance vibration behavior, as you will learn shortly.

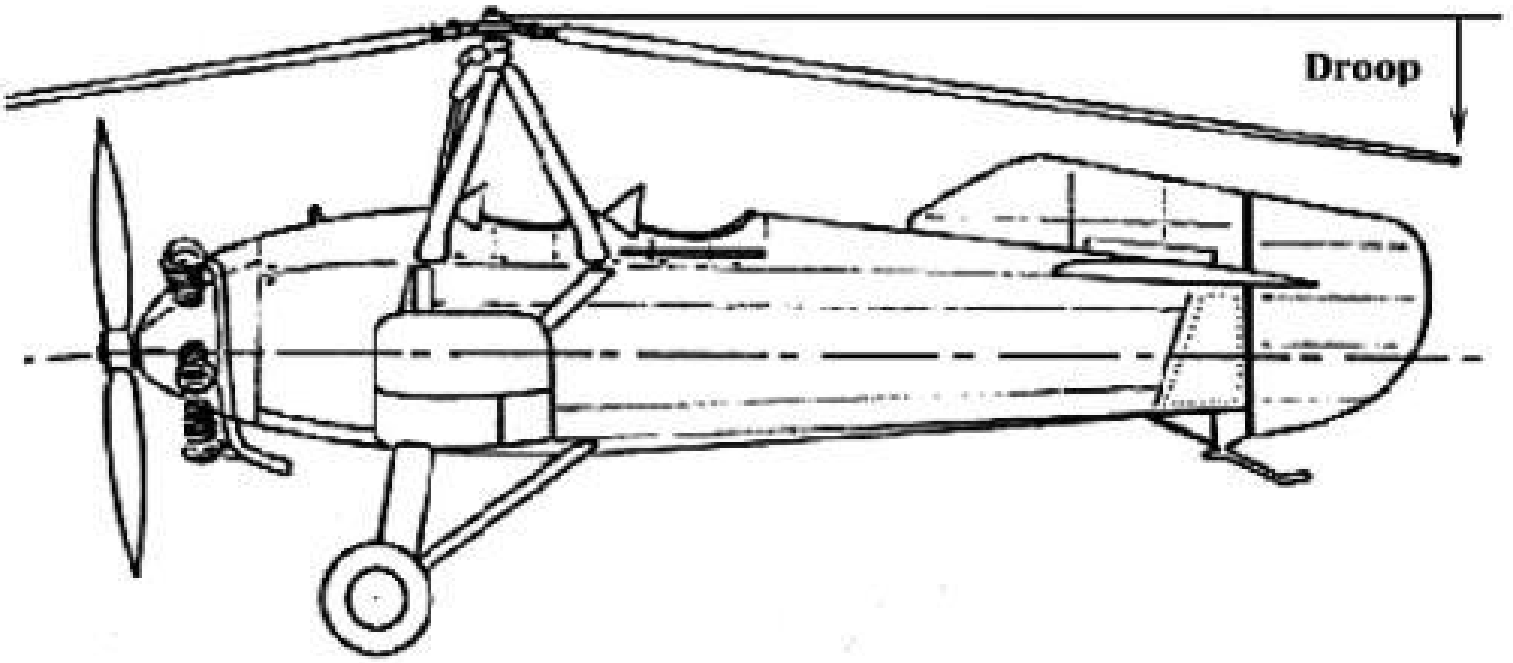

Fig. 2-75. Cierva C.19 Mk. IV "cantilevered" blades drooped [7].

2.9 BLADES

The beam parameter ($w_b R^4/EI_{flap}$) can be estimated first for the C.19 Mk. III, and then inferred for the Mk. IV, based on information that Sanders and Rawson [50] and Cierva [11,

12] have provided. According to Sanders, the Mk. III "main spar is a high tensile steel tube, 1-3/4 in. diameter by 20 S.W.G." High tensile steel has an elastic modulus (E) of 29,000,000 pounds per square inch and weighs about 520 pounds per cubic foot [77]. Sanders gives the "tube" outside diameter as 1-3/4 inches . He quotes the wall thickness as "20 S.W.G.," which is British Imperial standard wire gage equating to 0.036 inches [77]. This makes the spar inside diameter (ID) equal to 1.678 inches. The spar cross-sectional moment of inertia (I_{flap}) is, therefore,

(2.160) spar $I_{flap} = \frac{\pi}{64}\left(OD^4 - ID^4\right) = 0.07122$ inches^4

and so the flapwise stiffness is about

(2.161)

spar $EI_{flap} = (29{,}000{,}000)(0.07122)\left(\frac{1}{12^2}\right) = 14{,}340$ pound$-$feet^2.

Cierva, in his detailed calculations of the C.30A blade including comparisons to bench test results [12], finds that the wooden and other parts increase the spar bending stiffness by 40 percent. Therefore,

(2.162) blade $EI_{flap} = 1.4(14,340) = 20,080$ pound – feet^2.

The cross-sectional area of the spar is 0.1938 square inches, so the running spar weight is

(2.163)

$$w_{spar} = \frac{\pi}{4}\left(OD^2 - ID^2\right)(\text{density}) = (0.1938)(520)\left(\frac{1}{12^2}\right) = 0.7 \text{ pounds / foot}.$$

Cierva [11, 12] states that for the C.30A, the wood and other parts of the blade weigh about 85 percent of the spar, so

(2.164) blade $w_b = 1.85\, w_{spar} = 1.295$ pounds / foot.

On this basis, considering the radius as 17.5 feet, the C.19 Mk. III beam parameter is (2.165)

C.19 Mk.III

$$\frac{w_b R^4}{EI_{flap}} = \frac{(1.295)(17.5)^4}{20,080} = 6.049 \text{ feet}.$$

Given the beam parameter, the elastic deflection of the C.19 Mk. III blade—*without the "droop" cable*—would be, from Eq. (2.159), on the order of

(2.166)

$$\text{elastic } Z_{tip} = \left(\frac{w_b R^4}{EI_{flap}}\right)\left(\frac{1}{8}\right) = 0.756 \text{ feet} = 9 \text{ inches}.$$

(Actually, because of the vertical component of cable support tension, the elastic deflection is only about 5 inches.)

2.9 BLADES

By my estimate, the C.19 Mk. III blade weight, neglecting the "forked" root-end extension, lag damper, etc., is on the order of 22.7 pounds . The centrifugal force (F_c) at the blade-root end for the Mk. III normal rotor speed of 125 rpm, or 13.1 radians per second, is about

(2.167)

$$F_C \text{ at root} = \frac{1}{2}\frac{w_b}{g}R^2\Omega^2 = \frac{1}{2}\left(\frac{1.295}{32.174}\right)(17.5)^2(13.1)^2 = 1,060 \text{ pounds}.$$

This makes the spar tensile stress

(2.168)

$$F_C \text{ stress at root} = \frac{F_C}{A_{spar}} = \frac{1,060}{0.1938} = 5,460 \text{ pounds per inch}^2.$$

Now consider the step from the Mk. III to the Mk. IV. With reduced solidity, the three-bladed rotor operated at a higher rotor speed of 180 rpm or 18.9 radians per second. Assuming no other changes, this higher rotor speed raises the centrifugal force to 2,060 pounds and more than doubles the tensile stress due to centrifugal force. It seems most likely to me that Cierva would have accepted the higher stress during this 6-month prototype phase . Going to a thicker-walled tube does not reduce the centrifugal force stress appreciably because the centrifugal force goes up in proportion to area as the preceding equations show. Therefore, he would have needed to reduce wood part weight. Brooks [7] provides some evidence that this redesign did happen, however, saying:

"The three blades of the revolutionary new cantilevered rotor, like those of the previously cabled-braced type were manufactured at Hamble [England] using techniques developed by Avros. They had tubular steel spars at about [the] quarter chord. Initially, light spruce ribs were bolted to the spar by steel clips ("scrivits"). There was an ash leading edge member and a much lighter spruce strip at the trailing edge. The blades were fabric covered. By late 193 1 , however, Cierva had decided on a solid balsa wood fairing to the tubular spar with a spruce core, the whole assembly being covered with fabric. This type of blade remained in use until the introduction of the C.30 direct control Autogiro which reverted to built-up blades with spruce ribs and plywood covering."

Brooks' recounting leads me to believe that Cierva made only minor modifications to MK. III blades for the prototype Mk. IV, namely reducing the radius from 17.5 feet to 17 feet. Accepting this view means that the Mk. IV had a beam parameter of about

(2.169) C.19 Mk.IV

$$\frac{w_b R^4}{EI_{flap}} = \frac{(1.295)(17.0)^4}{20,080} = 5.386 \text{ feet}.$$

The rotor blade parameter can also be established for both the Cierva C.30 and the Hafner A.R. III . As Brooks notes above, the next Cierva production Autogiro was the C.30A, and the blade for this Autogiro followed the built-up design he used on the C.19 Mk. III. Cierva provides quite detailed technical data about the C.30A blade in his *Theory of Stresses on Autogiro Rotor Blades* [12]. Measurements of blade flapwise stiffness and mass were made and recorded. Using the Cierva data, the blade flapwise stiffness (EI_{flap}) is 3,650,000 pound- inches squared, and the blade weight per inch is based on 41 pounds for a 222-inch radius or

0.1847 pounds per inch (2.216 pounds per foot). Therefore, with great confidence you can determine the C.30 had a rotor blade parameter, (2.170), of about

(2.170) C.30A

$$\frac{w_b R^4}{EI_{flap}} = \frac{(2.216)(18.5)^4}{3,650,000/12^2} = 10.241 \text{ feet}.$$

An estimate of the Hafner A.R. III blade parameter is obtained from the blade-tip droop, seen quite pronounced in Fig. 2-38. From this figure, the droop stop measures about –10 degrees and the rigid blade deflection is 33 inches . I measured the elastic tip deflection as approximately 23 inches giving a total tip deflection of some 56 inches. From Eq.

(2.159), the maximum elastic droop is a direct measure of the blade parameter. That is, since

$$(2.171) \quad \text{elastic } Z_{tip} = \left(\frac{w_b R^4}{EI_{flap}} \right) \left(\frac{1}{8} \right)$$

it follows that, for the Hafner machine,

(2.172) A.R. III

$$\frac{w_b R^4}{EI_{flap}} = 8\left(\text{elastic } Z_{tip}\right) = 8(23/12) = 15.333 \text{ feet}.$$

Earlier calculations leading to a centrifugal force of 3,400 pounds at 270 rpm rotor speed (see footnote, page 90) gave the Hafner blade a running mass of 0.03158 slugs per foot, which is 1.016 pounds per foot. With a radius of 16.405 feet, the blade flapwise bending stiffness (EI_{flap}) was probably on the order of

4,800 pound-feet squared or 691,100 pound-inches squared.

2.9.2 Vibration Frequencies

Given this background about rotor blade structural parameters, let me proceed to the very important subject of vibrating beams. This subject bears directly on vibratory loads and the shaking forces transmitted through the airframe to the pilot or other occupants and even to critical components of the machine, such as instruments.

A rotor blade vibrates just like any structural beam. Imagine a blade hanging by its flapping hinge. If the blade is "plucked" or hit with a mallet, it responds by vibrating in several shapes, some of which are clearly visible. Each shape has an associated frequency. The shapes are called normal modes

of vibration. Simply shaking one end of a telephone cord can reproduce a good example of this vibration and the associated normal modes. The first mode of the telephone cord is simply a straight line from the telephone to your hand. When you move your end up and down very, very, slowly, the cord will remain a straight line. The second mode will appear if you shake the cord rather slowly. At just the right rate of up and down motion, the cord will vibrate between a concaved shape on the low side and a convexed shape on the high side. If you look at the telephone cord from the side, it appears just like a jump rope being turned by two children, one at each end. If you shake the telephone cord much faster, it will appear to divide itself into two jumping ropes with the middle standing quite still . This is the third mode. In the telephone cord examples, the shaking you have

selected is an up-and-down motion having the natural frequency (cycles per second) of a *very* limber "beam." When a rotor blade is struck, all normal modes respond, but it takes special sensors to record detailed data that you see so clearly with a telephone cord.

If the rotating rotor blade is forced to vibrate by an airload, then the responding vibratory shape is dictated, in part, by the airload distribution along the rotor radius. All natural mode shapes will be excited, though not in equal proportions. The proportion each mode contributes depends on the airload frequency and amplitude.

A crucial rotor blade design question arises when the blade has a natural mode

frequency (ω_M), in radians per second, that corresponds to an airload forcing frequency. Airloads are powerful forces, but, in simple cases, they act at integers of rotor speed. That is, airloads are periodic (harmonic) forces which load the blade at once per revolution, twice per revolution, and so on. An example of this type of harmonic airload is a blade element of lift ($dL_{r,\psi}$) written as

$$(2.173)\quad dL_{r,\psi} = L_o + L_{1S}\sin\psi + L_{1C}\cos\psi + L_{2S}\sin 2\psi + L_{2C}\cos 2\psi + L_{3S}\sin 3\psi + \text{etc.}$$

where rotor azimuth (ψ) is in radians and, you will recall, is equal to rotor speed (Ω) in radians per second times time (t) in seconds. Should the blade have a mode frequency (ω_M) equal to any integer (n = 1, 2, 3, etc.) times rotor speed (i.e., $n\Omega$), then the airload will shake the blade at the blade's natural frequency. This, of course, is the case of

resonance, which must be avoided since it can lead to excessive vibratory blade bending and premature blade failure due to fatigue if there is little or no damping.[33]

The calculation of rotor blade frequencies and mode shapes is quite simple in two specific cases . The first case corresponds to the situation where the blade is not rotating ($\Omega = 0$). The second case corresponds to the situation where the blade is rotating but has no flapwise stiffness ($EI_{flap} = 0$). This second case is, in effect, just a rotating chain. Unfortunately, from the point of view of a theoretician, real rotor blades fall between these two extremes . As you might assume, Cierva, in his *Theory of Stresses on Autogiro Rotor Blades*[12], gives an engineering equation to calculate the natural frequency of the most critical flapwise mode. This critical mode is the *second* mode of a flapping hinged, rotating blade, because it falls,

for practical blades, above 2.5 per rev and below 3.5 per rev. Thus, in a poor design, the second mode might have its natural frequency right on 3 per rev giving a chance for resonance. The equation Cierva derived, using beam theory of the day, is

$$(2.174) \quad \omega_2 = \Omega \sqrt{6.4 + 373 \frac{EI_{flap}}{m_b R^4 \Omega^2}} \, .$$

---

[33] I feel certain that Cierva, with his structural engineering background, was quite knowledgeable about vibrating beams and fatigue failure. My reference [103], which dates back to 1928, deals with the subject as part of vibrations of elastic bodies. Unfortunately, a centrifugally loaded beam, with one end pinned and the other free, does not have a simple solution in elementary functions such as sine, cosine, or any hyperbolic functions as do the classic beam problems discussed in textbooks.

2.9 BLADES

You should immediately notice in Eq. (2.174) that the rotating blade natural frequency depends on the same beam properties as the nonrotating elastic deflection or droop.

All flapwise frequencies *of uniform beams hinged at one end and free at the other end*, such as early autogyro blades with zero or near-zero flapping hinge offset, can be estimated quite closely with Eq. (2.175).[34] Modes are numbered from $M = 1$ to however high you want to go, but most studies stop at $M = 5$. The first mode, $M = 1$, is called the rigid-body mode, which has a natural frequency of rotor speed (i.e., $\omega_1 = \Omega$). In the first mode, the blade vibrates without any bending and simply flaps up and down as a rigid blade. Rigid blade flapping motion is

completely determined by damping provided by the airloads. This is the only mode that acts this way. All higher modes (M = 2, 3, 4, etc.) have elastic bending. Equation (2.175) can be used to calculate the natural frequency of each mode.

$$\left(\frac{m_b R^4}{EI_{flap}}\right)\omega_M^2 = \left[\frac{\pi}{4}(4M-3)\right]^4 + M(2M-1)\left(\frac{m_b R^4}{EI_{flap}}\right)\Omega^2$$

(2.175)

$$+\frac{2}{\pi}\left[\frac{\pi}{4}(4M-3)\right]^4 \arctan\left\{\frac{M}{12}(4M-5)(M-1)\ln\left[1+\frac{1}{\left[\frac{\pi}{4}(4M-3)\right]^4}\left(\frac{m_b R^4}{EI_{flap}}\right)\Omega^2\right]\right\}.$$

where M = mode number = $2, 3, 4 \cdots \infty$

Again, notice in Eq. (2.175) that the rotating blade mode frequencies depend on the same beam properties as the nonrotating elastic deflection or droop . This very important fact

means that the blade frequency parameter $[(m_b R^4/EI_{flap})\Omega^2]$ is related to the beam parameter $(w_b R^4/EI_{flap})$ as

$$(2.176)\quad \frac{m_b R^4}{EI_{flap}}\Omega^2 = \frac{\Omega^2}{g}\left(\frac{w_b R^4}{EI_{flap}}\right).$$

Because rotor speed (Ω) is in radians per second and the gravity constant (g) equals 32.174 feet-per-second squared, the blade frequency parameter has no units. Furthermore, $\left[\left(m_b R^4/EI_{flap}\right)\omega_M^2\right]$ also has no units because the natural frequency (ω_M) is in radians per

second.

The natural frequency in the two limiting cases, ($\Omega = 0$ and $EI_{flap} = 0$), are directly given by Eq. (2.175). They are

$$(2.177)\quad \omega_M^2 = \left[\frac{\pi}{4}(4M-3)\right]^4\left(\frac{EI_{flap}}{m_b R^4}\right)$$

for $\Omega = 0$ (a nonrotating blade)

[34] I created this frequency approximation for flapping hinged blades in the mid-1970s after being inspired by the Dave Peters frequency approximation for a rotating beam cantilevered at the root [104].

and

$$(2.178)\quad \omega_M^2 = M(2M-1)\Omega^2 \quad \text{for } EI_{flap} = 0$$

(a chain).

Given the several blade structural properties and the ability to estimate the natural frequency of a blade from Eq. (2.175), it is helpful to summarize the information about the four autogyro blades under

discussion. Table 2-6 shows the progress made by the autogyro pioneers developing blades. This autogyro blade property summary shows that as solidity was reduced, tip speed increased. Blade static elastic deflection, or droop, increased, and no natural frequency ratio was *exactly* at an integer of rotor speed, although several are too close by modern standards . That is, the frequency ratio (ω_M/Ω) does not *exactly* equal 1, 2, 3, 4, 5, etc. Remember, the airloads are periodic as Eq. (2.173) suggests, and if an airload harmonic, say L_{3S} sin 3ψ, is large (which it is as you will see shortly), then the blade having a natural frequency ratio of 3 will experience excessive bending, perhaps to the point of early fatigue failure.

There is, of course, an additional concern. As you learned from the discussion about stick shake with the three-bladed Kellett autogyro (recall Fig. 2-30 and Fig. 2-3 1), a

three- bladed rotor passes 3-per-revolution vertical vibration to the airframe. Therefore, amplification of 3-per-revolution airloads (because the blade has a natural frequency ratio too close to 3) will mean the airframe is subjected to just that much higher vibratory loads. A very important frequency ratio trend from Table 2-6 is, in fact, the second mode (i.e., M = 2 or the first elastic mode) dropping from comfortably above 3 times rotor speed ($\omega_2/\Omega > 3$) to uncomfortably close to 3 per rev to reasonably below 3 per rev.[35]

The blade natural frequencies (ω_M) or frequency ratios (ω_M/Ω) can be presented graphically. I prefer the frequency ratio (ω_M/Ω) form, which is shown in Fig. 2-76.[36] Equation (2.175), for uniform beams, gives the lines in this figure, and the data points are from Table 2-6. For the sake of completeness, Cierva's recommended frequency from Eq. (2.174) is also shown. When a specific

configuration is selected, say the Cierva C.30A, I prefer plotting the frequency ratio versus rotor speed, in revolutions per minute, to an expanded scale as shown in Fig. 2-77.

---

[35] Rotorcraft engineers rarely say "3 per revolution" or "3 times rotor speed." They use the shorthand "3 per rev" or "N per rev" or write "N/rev" because so many conversations deal with vibration and vibratory loads. Everyone "just knows" that the blade airloads—in most cases—are harmonic integers of rotor speed, and so the most asked structural dynamic question is, "What part of the aircraft is responding to what airload harmonic, and do we have a resonance situation?"

[36] The reason the frequency ratio format appeals to me is because the proximity to an airload integer, particularly 3 per rev on a three-bladed rotor, is immediately read on an engineering scale.

2.9 BLADES

Fig. 2-77 raises the question about rotor speed operating range. The C.30A, according to Cierva's *Theory of Stresses on Autogiro Rotor Blades*, was designed for the rotor speed range of 180 to 210 revolutions per minute. The higher rotor speed was associated with low-speed forward flight at altitude; the lower rotor speed was expected during takeoff at sea level. Fig. 2-77 shows that the second mode is rather close to 3 per rev (by modern standards) while the third mode could easily be *exactly* at 6 per rev. Since a three-bladed rotor can pass 6-per-rev vibratory loads (as well as 3-per-rev loads) to the airframe, this high frequency vibration might have been noticed by a pilot as a buzz. The third way natural frequencies are presented (Fig. 2-78) is the one most often seen in technical material.

Table 2-6. Early Autogyro Blade Properties

Parameter	Model			
	C. 19 Mk. III	C.19 Mk. IV	C.30A	A.R. III
Year	1929	1931	1933	1936
Gross Weight (lb)	1,450	1,450	1,800	890
Number of Blades	4	3	3	3
Radius (ft)	17.5	17	18.5	16.41
Chord (in.)	18.6	18.6 (est.)	11	4.9
Disc Area (sq ft)	962	908	1,075	846
Solidity	0.1107	0.084	0.0470	0.0237
Tip Speed (ft/sec)	230	320	407	464
Rotor Speed (rad/sec)	13.14	18.82	22.00	28.28
Blade Airfoil	Gött. 429	RAF 34	Gött. 606	Sym.
Running Weight (lb/ft)	1.295	1.295	2.216	1.017
Flapwise Stiffness (lb-ft^2)	20,080	20,080	25,350	4,800
Running Mass (slug/ft)	0.04025	0.04025	0.06888	0.03161
Blade Weight (lb)	23	22.342	41.000	16.7
Centrifugal Force (lb)	1,060	2,060	5,700	3,400
Weight Moment (ft-lb)	198	187	379	137
Second Moment of Inertia (slug-ft^2)	71.90	65.92	145.37	45.66
Lock Number (at sea level)	27.5	26.75	10.06	8.83
w_bR^4/EI_{flap} (ft)	6.049	5.386	10.241	15.333
$(m_bR^4/EI_{flap})\Omega^2$	32.462	59.292	154.057	381.137
Frequency Ratio Mode 1 ω_1/Ω	1.0	1.0	1.0	1.0
Frequency Ratio Mode 2 ω_2/Ω	3.69	3.21	2.79	2.61
Frequency Ratio Mode 3 ω_3/Ω	9.70	7.70	5.77	4.84

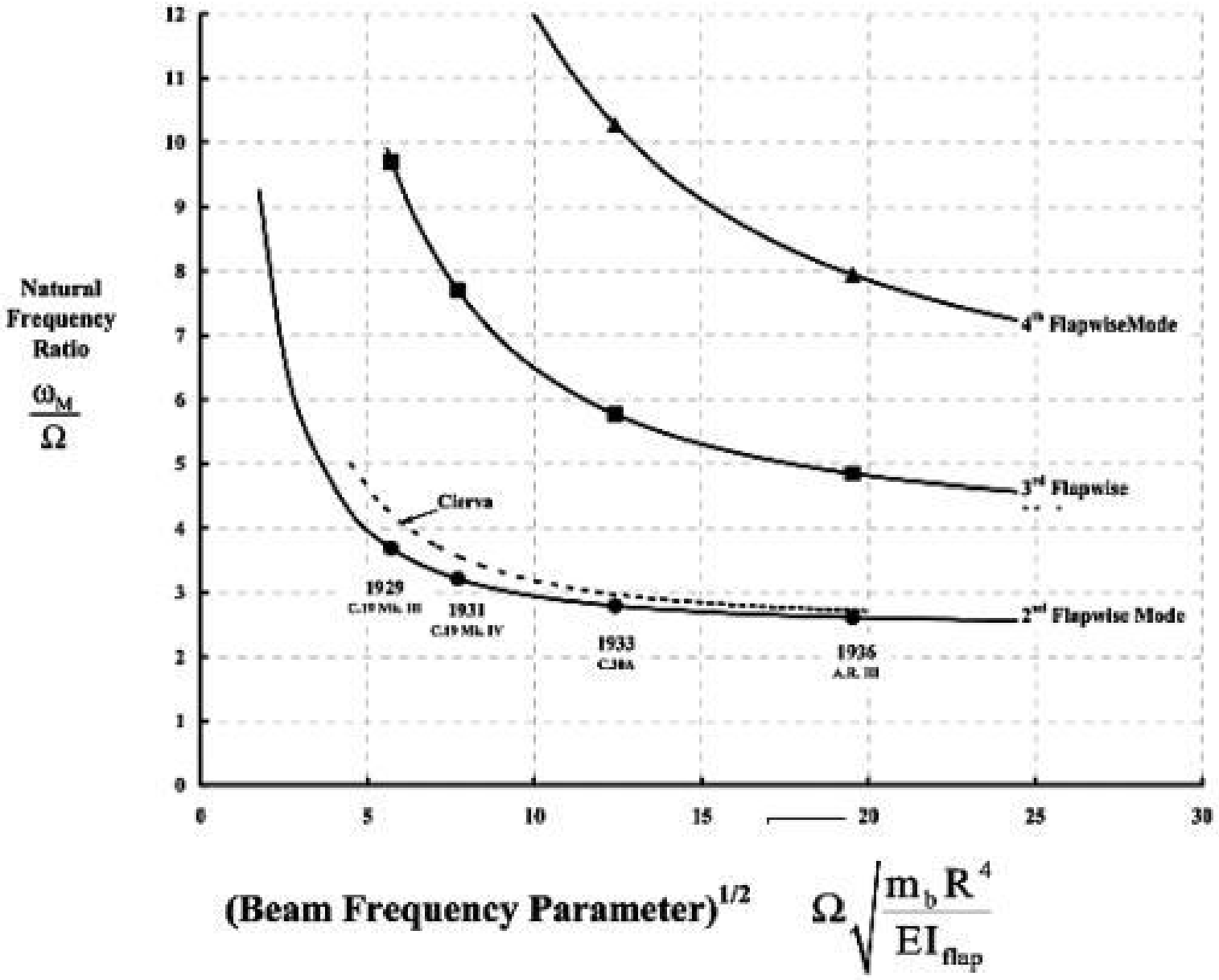

Fig. 2-76. Rotor blade flapwise natural frequency ratios for a uniform beam.

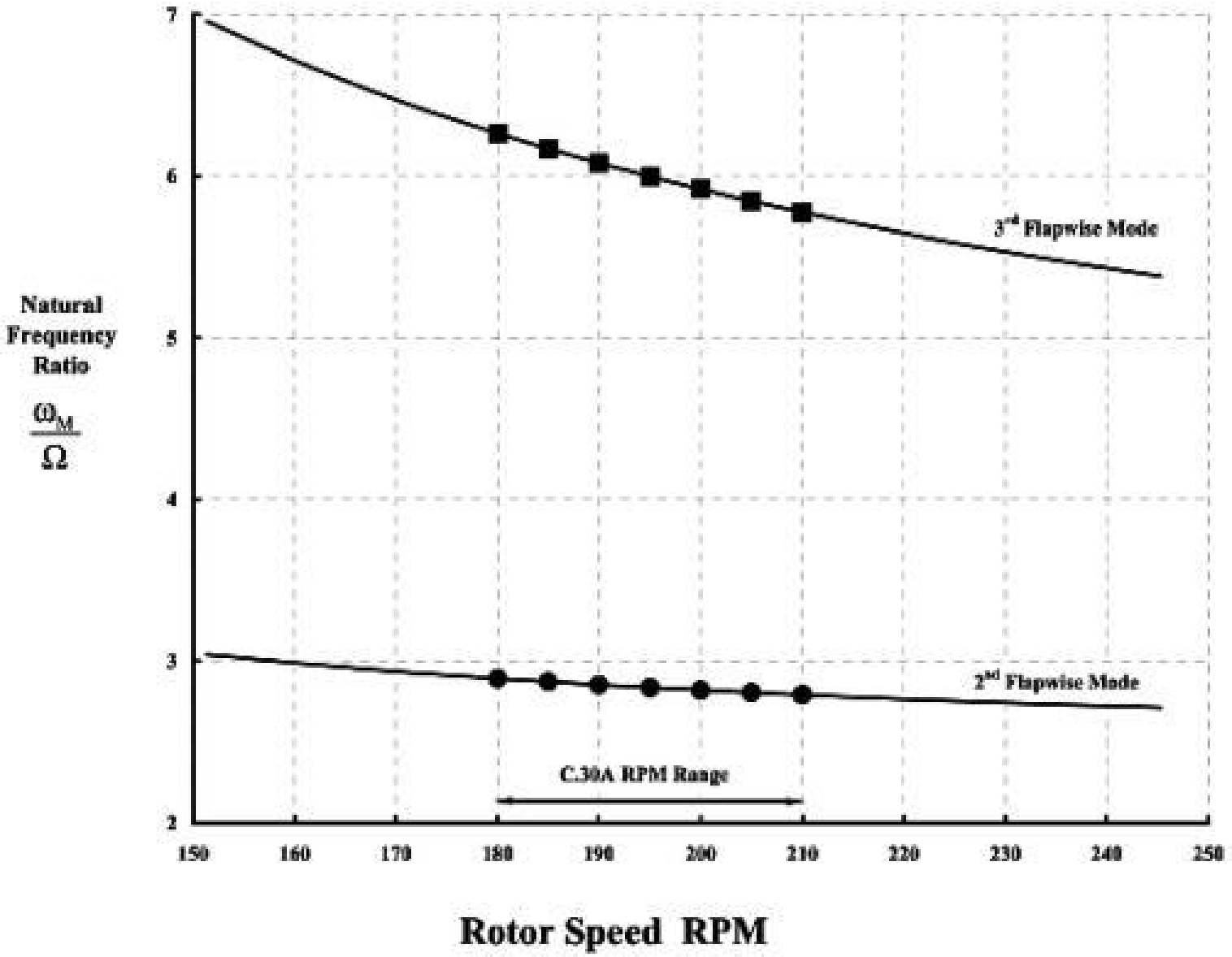

Fig. 2-77. Cierva C.30A blade natural frequency ratios.

2.9 BLADES

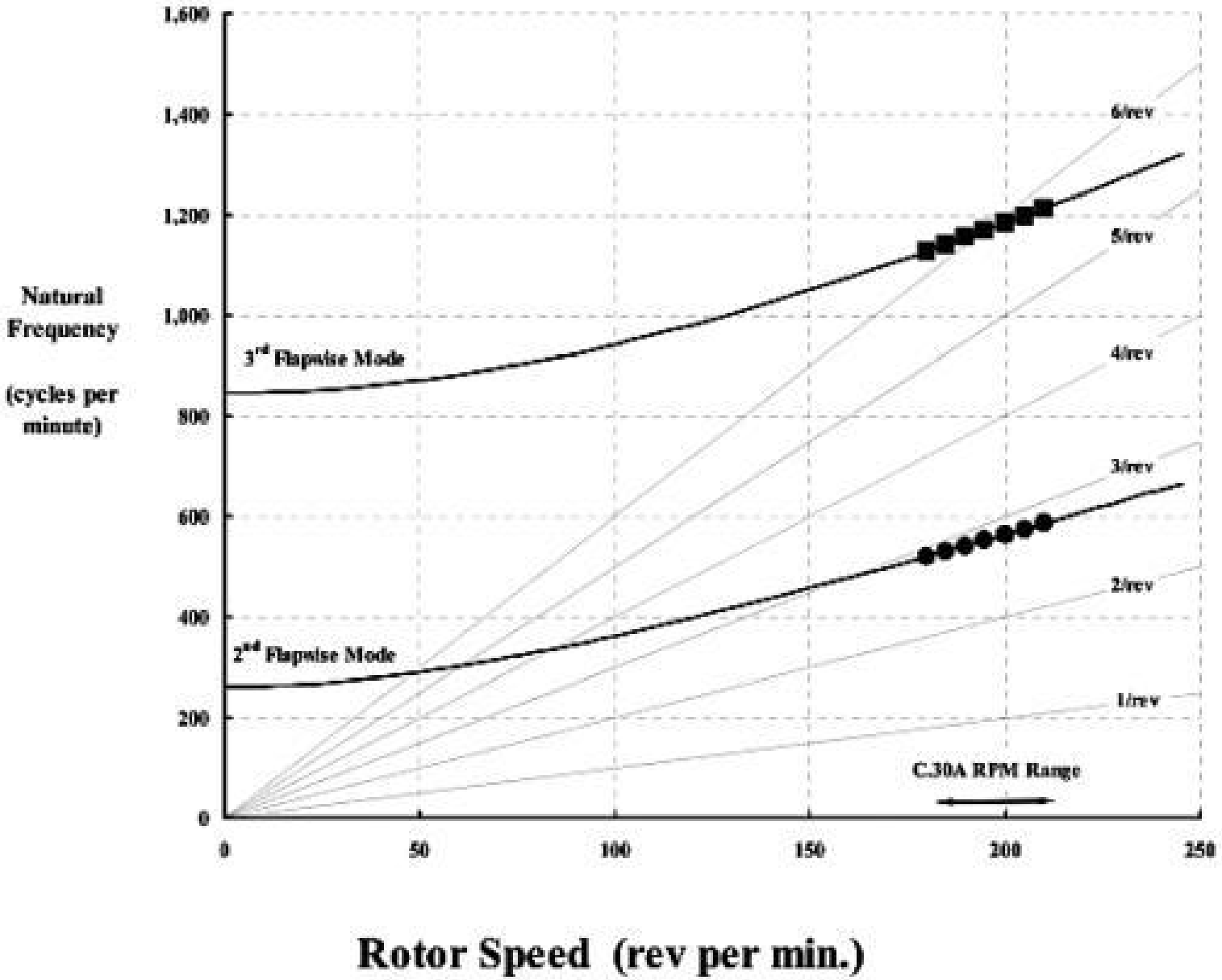

Fig. 2-78. Cierva C.30A blade natural frequencies.

2.9.3 Mode Shapes

The mode shapes I have mentioned several times are simply graphs of flapwise

deflection (Z_r), divided by radius (R), and normalized to 1.0 at the blade tip. They are plotted versus nondimensional radius station (x = r/R). Both of the limiting cases have mode shapes calculable from simple equations. The mode shapes for a nonrotating blade ($\Omega = 0$) are calculated, using hyperbolic and trigometric sine, as

$$\left(\frac{Z_r}{R}\right)_{M=1} = x$$

and then for $M = 2, 3, 4,$ etc. and $\Omega = 0$

(2.179)

$$\left(\frac{Z_r}{R}\right)_M = \frac{\sinh\left(F^{1/4}x\right)}{2\sinh\left(F^{1/4}\right)} + \frac{\sin\left(F^{1/4}x\right)}{2\sin\left(F^{1/4}\right)}$$

$$F^{1/4} = \left[\left(\frac{m_b R^4}{EI_{flap}}\right)\omega_M^2\right]^{1/4} = \frac{\pi}{4}(4M-3)$$

The mode shapes for the case of a rotating chain ($EI_{flap} = 0$) are even simpler because they are Legendre polynomials (the odd ones), so that for

the first several modes

$$\left(\frac{Z_r}{R}\right)_{M=1} = x, \qquad \left(\frac{Z_r}{R}\right)_{M=2} = \frac{5}{2}x^3 - \frac{3}{2}x, \qquad \left(\frac{Z_r}{R}\right)_{M=3} = \frac{63}{8}x^5 - \frac{70}{8}x^3 + \frac{15}{8}x$$

$$\left(\frac{Z_r}{R}\right)_{M=4} = \frac{429}{16}x^7 - \frac{693}{16}x^5 + \frac{315}{16}x^3 - \frac{35}{16}x \quad \text{for } EI_{flap} = 0 \tag{2.180}$$

Graphs of these two limiting cases are provided in Fig. 2-79 for the second and third modes. Autogyro blades, as Fig. 2-80 shows, fall between the two limiting cases. (Appendix G provides the methodology I used to calculate these mode shapes and the corresponding frequencies given in Table 2-6.)

The flapwise axis is, of course, not the only axis about which a blade has natural frequencies and mode shapes. Both chordwise (i.e., inplane or lead-lag) and torsion axis are, if anything, even more important than the flapwise axis . This is because, unlike the

flapwise modes, these lag modes have next to zero damping to protect the blade from resonance response.

The chordwise natural frequencies are quite dependent on the root-end restraint. Cierva, in his *Theory* [12], provides no frequency equation and only devotes 1 page (out of 149 main body pages) to this subject. This one page discusses root restraints such as lead-lag dampers of various types. He does note that "when plain bearings are used on the drag hinge, it is advisable to calculate the additional frictional restraint due to centrifugal force [and] a frictional coefficient of 0.15 is recommended." He does express the view that "in the general case, where the superstructure has a very high moment of inertia in the direction considered, the bending on the spar will be negligible at all points except at the root and close to it." This statement says that chordwise stiffness (EI_{chord}) contributed by the

trailing edge and skin leads to a chordwise stiffness about (in my experience) 10 to 20 times the flapwise stiffness. If the blade lead-lag hinge is similar to the flapwise hinge, and there is no lag damper, the chordwise natural frequencies of each mode can be estimated to the first order with

$$\left(\frac{m_b R^4}{EI_{chord}}\right)\omega_M^2 = \left[\frac{\pi}{4}(4M-3)\right]^4 + M(2M-1)\left(\frac{m_b R^4}{EI_{chord}}\right)\Omega^2 - \left(\frac{m_b R^4}{EI_{chord}}\right)\Omega^2$$

(2.181)

$$+\frac{2}{\pi}\left[\frac{\pi}{4}(4M-3)\right]^4 \arctan\left\{\frac{M}{12}(4M-5)(M-1)\ln\left[1+\frac{1}{\left[\frac{\pi}{4}(4M-3)\right]^4}\left(\frac{m_b R^4}{EI_{chord}}\right)\Omega^2\right]\right\},$$

where M = mode number = $2,3,4\cdots\infty$

The chordwise mode shapes, in this fundamental pinned-free, no-damper beam case, are quite similar to the flapwise mode shapes . Designing a blade so that chordwise frequency placement is between integers of

rotor speed is not easy. Many a rotorcraft has experienced broken trailing edges. Unfortunately, the total subject is beyond the scope of this volume.

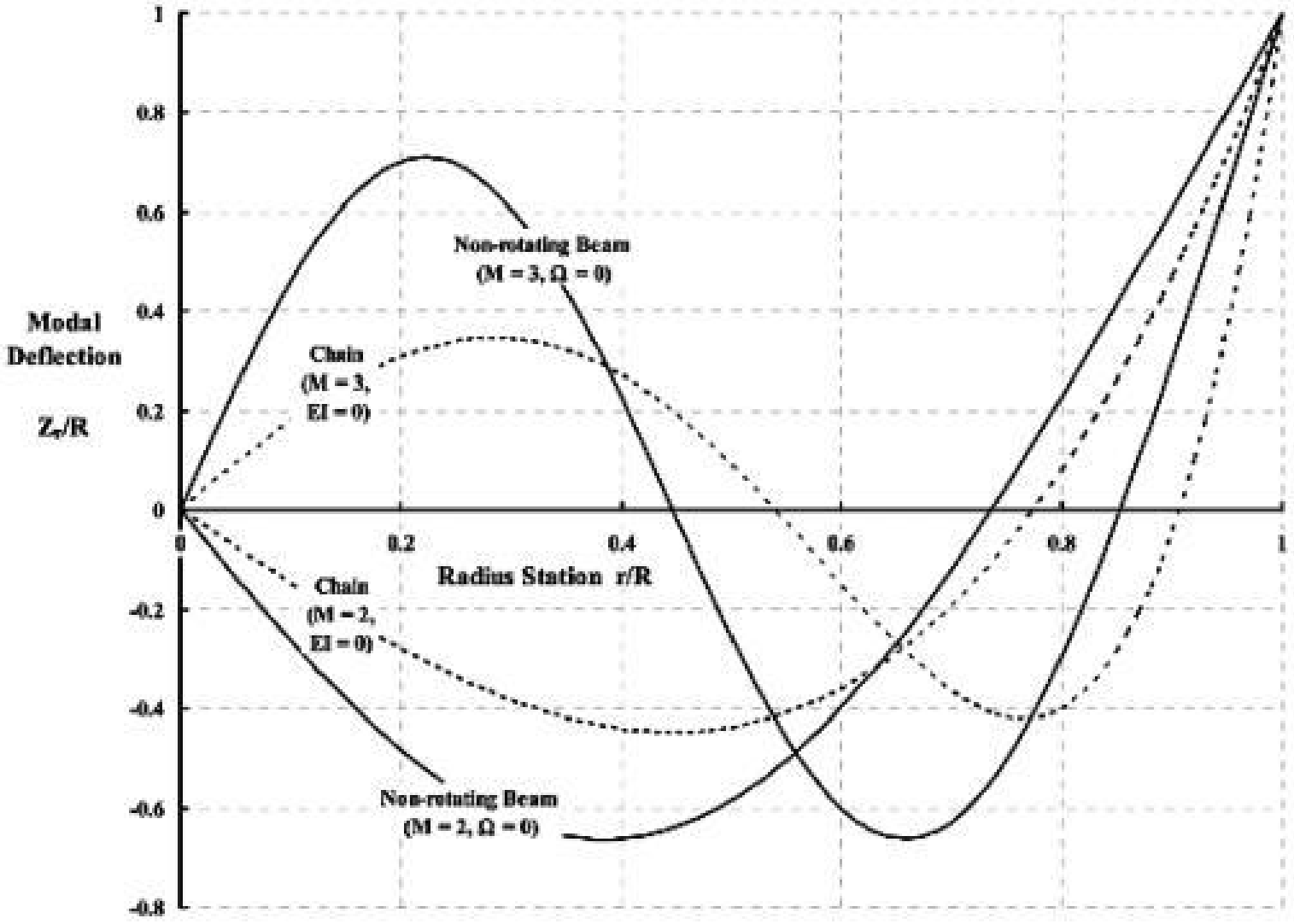

Fig. 2-79. Mode shapes two and three for

nonrotating beam and rotating chain.

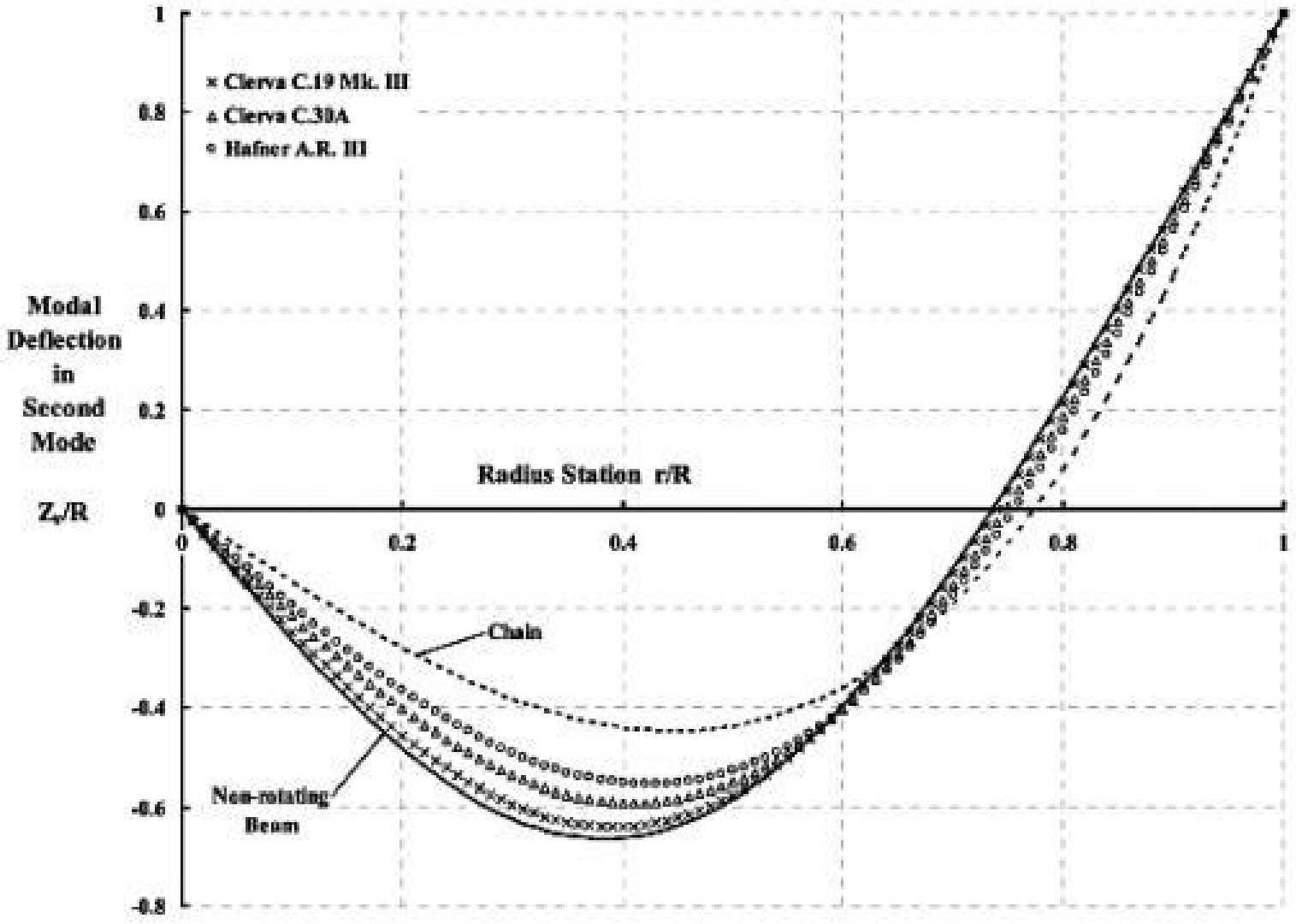

Fig. 2-80. Autogyro blade second mode shape is closer to nonrotating beam. 162

2.9 BLADES

The torsion natural frequencies are

also dependent on the root restraint. The direct control rotor systems that Cierva, Pitcairn, and Kellett pioneered used a very rigid fixing of the blade root to maintain blade collective pitch. On the other hand, when Hafner and Kellett introduced the swashplate, the blade root was, in effect, connected by a reasonably stiff spring, but a spring nonetheless. For example, the Hafner A.R. III (Fig. 2-39) spider arms were hardly a rigid connection for a blade's pitch arm.

The fascinating thing about the torsional vibratory modes is that the first mode, assuming the root is *not* restrained, has a natural frequency of 1 per rev, and there is no elastic twisting from blade root to tip. Because this is a resonance condition ($\omega_1 = \Omega$), the blade can be oscillated about its torsion axis with zero force. In the Hafner spider design, the spider arms are just gently guiding the blade to feather at once per revolution. Hafner

recognized this fact and designed the control system for just the loads required to twist the torsion rod. The fact that cyclic pitch, in and of itself, creates no control system loads is quite remarkable—and rotorcraft have no size restraint in this regard. Of course, both flapwise and chordwise deflections can—and do—affect torsion natural frequencies because of the coupling. However, for the uncoupled case with a *rigid root* condition, the natural frequencies are found from

$$(2.182)\quad \omega_M^2 = \Omega^2 + \left[(2M-1)\frac{\pi}{2}\right]^2 \left(\frac{GJ}{I_\theta R^2}\right)$$

for $M = 1, 2, 3, \text{etc.}$

where the blade element torsional stiffness (GJ) is in pound-feet squared per radian per foot of blade, the second moment of inertia (I_θ) is in

slug-feet squared per foot of blade, and the torsion natural frequency (ω_M) is in radians per second as is rotor speed (Ω).

In Eq. (2.182), the second term is the nonrotating blade torsional natural frequency. This frequency is classically obtained by assuming mode shapes of the form

$$(2.183) \quad \left(\frac{\theta_x}{\theta_{tip}}\right)_M = \sin\left[(2M-1)\frac{\pi}{2}x\right]$$

for $M = 1, 2, 3,$ etc.

where the blade radial station (x) equals (r/R), and the elastic twist (θ_x) is normalized to one unit of the tip torsional deflection (θ_{tip}).

Cierva, in analyzing the torsion axis [12], derives the first mode nonrotating

frequency by summing potential energy with kinetic energy. He calculates both energies assuming an approximate first mode shape of

$$\frac{\theta_x}{\theta_{tip}} = \frac{r}{R} = x \qquad (2.184)$$

rather than the more rigorous $\sin(\pi x/2)$. This gives him the first torsion mode natural frequency as

2.9 BLADES

$$\omega_1^2 = \Omega^2 + \frac{3}{2}\left(\frac{GJ}{I_\theta R^2}\right) \qquad (2.185)$$

versus

$$\omega_1^2 = \Omega^2 + \frac{\pi^2}{4}\left(\frac{GJ}{I_\theta R^2}\right).$$

Cierva analyzed four causes of elastic twisting and was satisfied that elastic twisting would be governed by 1-per-rev and 2-per-rev loads, and "so, if the blade has a natural frequency of oscillation in torsion not less than 3 or 4 per revolution, dynamic effects can be neglected." He then sets an "arbitrary" design criteria for the lowest torsion mode frequency as

(2.186) $$\sqrt{\frac{3}{2}\left(\frac{GJ}{I_\theta R^2}\right)} \geq 3\Omega_{max}.$$

This criteria means that at the maximum rotor speed (Ω_{max}), the first mode rotating frequency divided by rotor speed would be at least $\sqrt{10}$=3.16 per rev, and at lower rotor speeds

the frequency ratio would, of course, be higher.

Cierva uses the C.30A blade as a numerical example of the torsion natural frequency calculation. He found, for example, that the "wooden superstructure" increased the spar-tube- alone torsional stiffness by 1.25 or 25 percent. That is, his bench tests show the 1 8.5-foot-long blade had a blade element torsional stiffness of 2,700,000 pound-inches squared (1 8,750 pound-feet squared). He calculates the spar torsional stiffness using a "chrome-nickel steel"

modulus (G) of 12,000,000 pounds per square inch and a polar moment of inertia (J) of 0.18 inch^4, which gives a spar-alone torsional stiffness of 2,160,000 pound-inches squared. Cierva recommends that the second moment of inertia (I_θ) be calculated for the total blade as

(2.187)

$$\text{Total blade } I_\theta = (\text{mass of tube})(\text{tube radius})^2$$

$$+0.15(\text{mass of superstructure})(\text{blade chord})^2.$$

The C.30A dimensions he gives are that the "tube" (the spar) is 1.5 inches in diameter, the spar weight is 2 1 .1 pounds, the "wooden superstructure" weighs 17.9 pounds, and the blade chord is 1 1 inches. With these properties, he calculates that

(2.188)

$$\text{Total blade } I_\theta = \left(\frac{21.1}{32.174}\right)\left(\frac{1.5/2}{12}\right)^2 + 0.15\left(\frac{17.9}{32.174}\right)\left(\frac{11}{12}\right)^2 = 0.0727 \text{ slug} - \text{ft}^2$$

which gives, on a per-foot basis, a second moment of inertia (I_θ) of 0.00393.

With respect to rotor speed, Cierva designed the C.30A for a "maximum" rotor speed of 294 revolutions or 30.8 radians per second. Based on the preceding data and the design maximum rotor speed versus his criteria,

he calculates that

$$\sqrt{\frac{3}{2}\left(\frac{GJ}{I_0R^2}\right)}=\sqrt{\frac{3}{2}\left(\frac{18,750}{0.00393(18.5)^2}\right)}=145\geq 3(30.8)=93 \quad (2.189)$$

which shows the C.30A blade having a satisfactory and significant torsional natural frequency margin.

It is worth noting that the engineering approach Cierva took was conservative. Had he used the classic frequency solution, the 3/2 in Eq. (2.1 89) would change to $\pi^2/4 = 2.47$ and rather than 145, he would have arrived at 1 85. Through my study and use of two Cierva design manuals [1 1 , 1 2] I found many more conservative engineering approximations.

2.9.4 Bending Moments and Stresses

The design of rotor blades is, of course, not complete by achieving nonresonance frequency placement. The real criterion is "*Thou shall not break.*" This criteria means designing to calculated blade bending moments and forces and, most importantly, stresses. Cierva, in Part VIII of his *Engineering Theory* [1 1][37], devotes 25 pages and several figures to "Stresses on the Rotor Blade." This 1929 design manual addresses every component in the blade and a number of design conditions, such as on ground, during landing, when the rotor brake is applied, and, of course, in normal flight. Cierva writes, for example, that

"a load factor of 6 on the combined centrifugal tension and torsion at the root, in normal flight at sea level, should be sufficient, in my opinion, for machines with ceilings less than 22,000 feet, the worst possible case being an increase of 50% on the speed of rotation at the ceiling, which means an increase in centrifugal force of about 400% while torsion will only increase 125%,

leaving still a factor of safety greater than 1.25.

These stresses are taken exclusively by the central spar of the blade, but combined forces along the blade can be distributed between the spar and the covering, especially when the blades are covered by metal, plywood or timber planking.

In any case, a load factor of 6 on whichever normal flight case is worse, should cover any momentary increase in load and the fatigue due to periodical changes in the bending."

As might be expected, this first-ever rotor blade loads and stress analysis includes many "rules of thumb." Cierva just simply lacked blade airloads and the blade response that airloads create. His second volume, *Theory of Stresses on Autogiro Rotor Blades*, was, I will guess, first printed sometime in 1934. It was more polished than the first volume and stood on a less empirical foundation. This second volume was much more than a theory of stresses; in my opinion it was closer to being a

very comprehensive design manual. This later volume includes four appendices of quite noteworthy engineering information.

---

[37] Several figures in this first volume are dated November 1929 and signed by Cierva.

2.9 BLADES

Fig. 2-81. The first blade flapwise bending stresses were measured on the Pitcairn

PAA-1 in January 1931 [photo courtesy of NASA Images].

The first appendix contains measured "extensometer"[38] data giving "alternating fiber stresses on the upper fiber of the tubular spar, the known centrifugal stress having been deducted in every case." The Pitcairn Autogiro Company of America obtained this data, at four radius stations, during a series of tests in January 1931. Cierva notes that "special recording extensometers weighing only a few ounces were designed and supplied by Mr. A.V. de Forest and under his guidance a series of flights were done." Brooks [7] records that the test, along with bench fatigue tests, were done "to obtain useful information as to the proper and safe location of spot welds on Autogiro rotor blade spars." The test aircraft was the Pitcairn PAA-1, shown in Fig. 2-81.

The first appendix gives the PAA-1

test weight as 1,550 pounds, the radius as 18.5 feet, the chord as 18.6 inches, the airfoil as the Göttingen 429, the rotor speed as 145 revolutions per second, the airspeed as 90 to 95 miles per hour, the altitude as sea level, and the probable in-flight blade pitch at the tip as 4 degrees. From the measured flapwise bending stress waveforms, Cierva tabulates the maximum and minimum stresses (in pounds per square inch and with the stress due to centrifugal force removed) from two flights. Cierva concludes the first appendix to his *Theory of Stresses on Autogiro Rotor Blades* by providing blade property data, writing that

> "The weight of each blade, uniformly distributed, was of approximately 40 lbs. But a friction damper of 3.2 lbs. weight, was attached at about 0.45 of the radius. The tubular spar of 1 .75 inch outside diameter, high properties steel, had a moment of inertia, in a normal section, equal to 0.11046 inches^4 [I_{flap}]. The effect of the superstructure, partially three-ply wood and

[38] The extensometer came before the strain gage [105]. The strain movement was mechanically amplified and a scribe scratched a metal plate. The result was similar to an oscillograph trace or, in the case of the Pitcairn PAA-1, the flapwise bending stress waveform.

fabric, was to increase the rigidity [EI_{flap}] of the tube alone by about 20%. Fig. 8 represents graphically the distribution of upper fiber stresses along the radius, corresponding to the relative maximums given before.

An application of the theory to this blade and comparison with the above [experimental] results is given in Appendix II."

The figure 8 Cierva refers to is reproduced here as Fig. 2-82, with measurements tabulated in Table 2-7. The data is for an advance ratio of 0.5. I believe this figure is the first graph of experimental flap

bending stresses the rotorcraft industry ever saw. Finally, Cierva had some stress data at the outermost fiber of the spar. The figure shows that stress at the

1/3-radius station, not counting stress due to centrifugal force, varied between "compression of +23,000 lbs/inch^2 [blade-tip bent up] and tension of –7,500 lbs/inch^2 during a rotor revolution."

Table 2-7. Blade Flap Bending Stresses Measured on the PAA-1

Flight	Radius	Maximum	Minimum
1	0.333R	22,650	–6,750
	0.491R	20,600	–8,700
	0.724R	14,800	–8,100
	0.875R	5,300	–2,700
2	0.491R	25,500	–13,600
	0.724R	17,650	–10,950

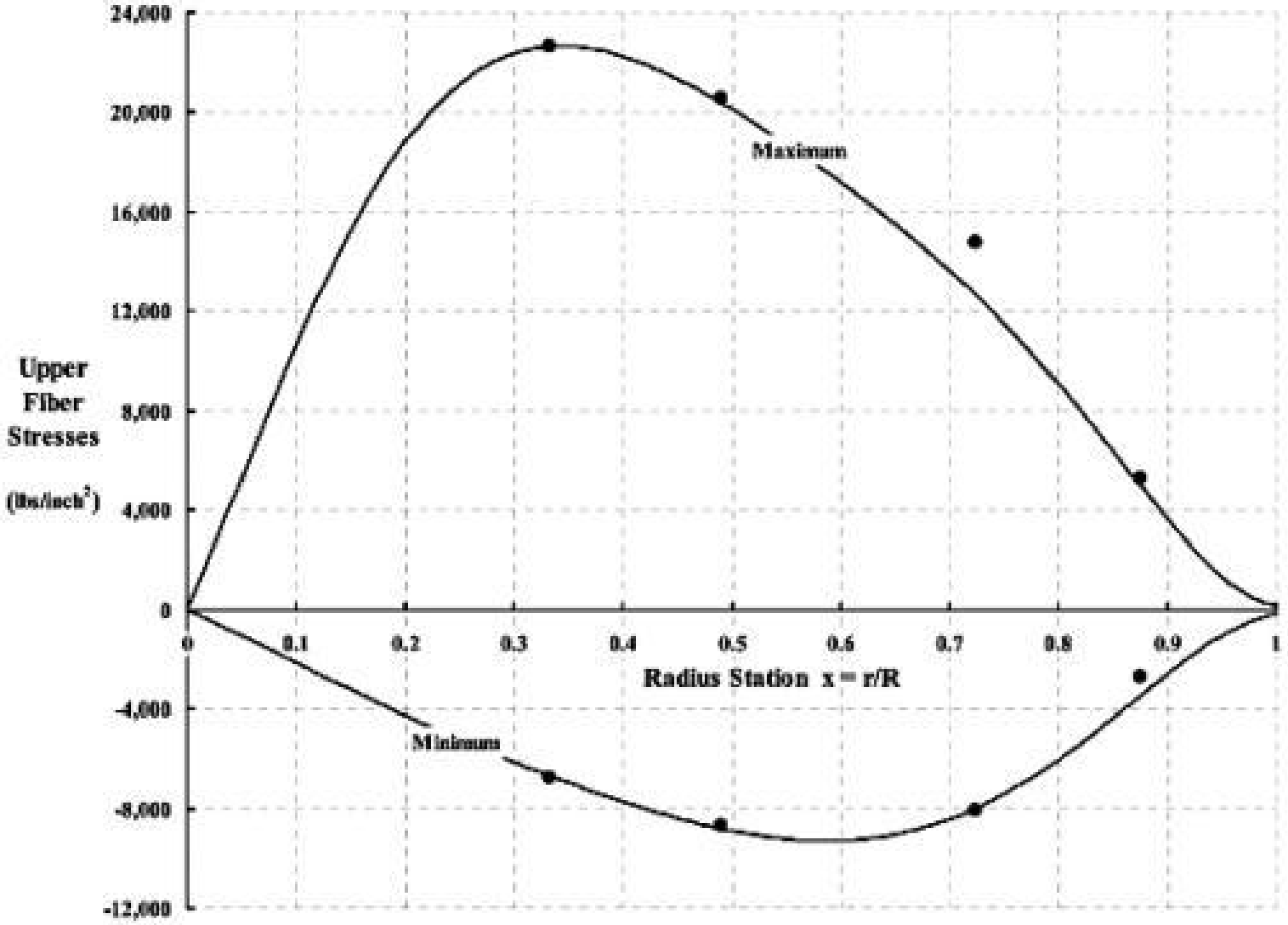

Fig. 2-82. Blade flap bending stresses measured on the PAA-1 [12].

2.9 BLADES

In the second appendix, Cierva compares his flap bending theory with the test data obtained with the PAA-1 from the first appendix. He begins with the blade properties, which I have converted to the convention used in this discussion, as

$$EI_{flap} = 1.2(29,000,000)(0.11046) = 3,850,000 \text{ lb/in}^2 = 27,740 \text{lb/ft}^2$$

$$m_b = \frac{40}{(32.174)(18.5)} = 0.0672 \text{ slug/ft}$$

$$\Omega = \frac{145}{60}(2\pi) = 15.18 \text{ rad/sec}.$$

$$\frac{m_b R^4}{EI_{flap}} \Omega^2 = 65.42$$

With these parameters at hand, Cierva

calculates the spanwise distribution of maximum and minimum stresses for a worst-case condition and for "normal" conditions. From these two cases, he defines the design to "values to be taken for fatigue stressing, in accordance with the theory, [which] are the averages between the worse case and normal values." He tabulates and graphs the results, and I have included his figure here as Fig. 2-83. By mid-1931, Cierva is satisfied that his theory of 1929 gives him design methodology to calculate fatigue stresses that are "in excess of the real ones [test data], proving that the assumptions made are on the safe side."

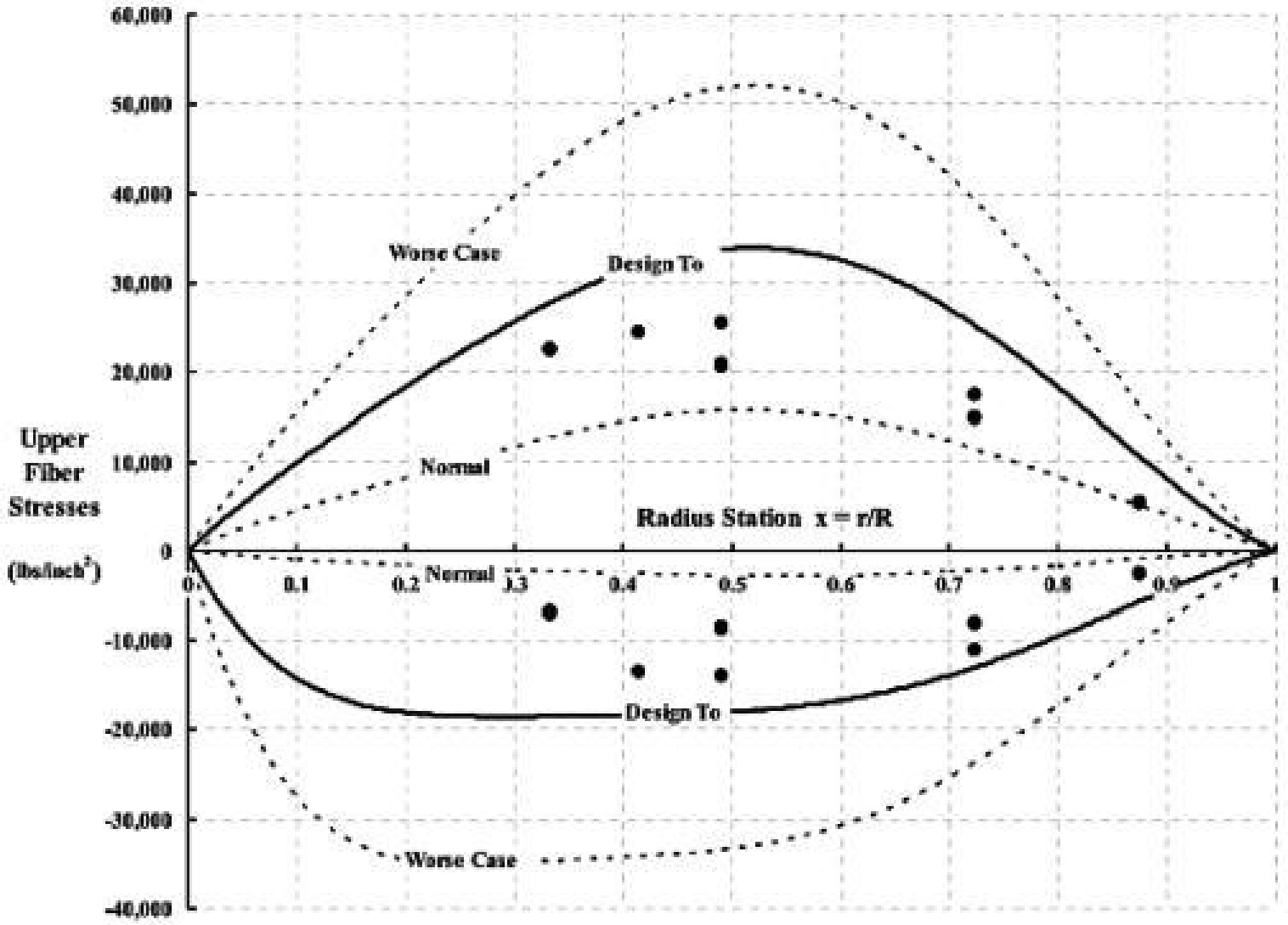

Fig. 2-83. PAA-1 test data fell below the flapwise stress parameters of the Cierva theory of design [12].

Cierva clearly shows that he is well aware of the fatigue loading that his "design to" stresses imply. In the body of *Theory of Stresses on Autogiro Rotor Blades*, he gives the equations for steady and alternating stress, written here in modern notation, as

$$\text{Steady stress} = \frac{S_{max} + S_{min}}{2}$$
$$\text{Alternating stress} = \frac{S_{max} - S_{min}}{2} \quad (2.190)$$

Furthermore, he closes the second appendix with a brief discussion of the "Periodicity of Bending Moment." An enlarged photograph of one of the extensometer records is provided for the 0.333R radius station. The data was recorded in smooth air, normal flying conditions. Cierva then does a Fourier analysis out to 3 per rev, compares it to what he has calculated for 0.4R, and concludes that "the resemblance is marked."

The third appendix included in the *Theory of Stresses on Autogiro Rotor Blades*

is titled "On Fatigue Stresses of Steel." From two German papers published in 1931–1932, Cierva concludes that for the proportions of steady and alternating stresses on his blade, the allowable alternating stress for his chrome-nickel steel spar should be no higher than one-third of the static ultimate tensile stress of the material. For chrome-nickel steel, this static stress can range from 100,000 to 150,000 pounds per square inch [77] . The specific value depends on proportions of ingredients used to produce the steel and the surface finish. Cierva used 145,000 pounds per square inch, which means that alternating stresses below ±50,000 pounds per square inch would indicate a reasonable design. Fig. 2-83 clearly shows that Cierva evaluated the PAA-1 blades as satisfactory because the highest alternating stress was about ±26,000 pounds per square inch.

In the fourth and last appendix, Cierva

provides a step-by-step analysis of the C.30A blade. By any standard, the 22 pages of calculations and tables, plus 8 figures, are quite thorough. The summation of all stresses in combination, then multiplied by four additional safety factors, gives a maximum critical fiber ultimate stress (at the 0.2R radius station) of 158,000 pounds per square inch for a short portion of the blade . This calculated absolute total stress exceeded the 145,000 pounds per square inch he felt comfortable with. Cierva, while accepting the C.30A blade, says that "it is recommended to lengthen the tapered part of the spar to about 0.25R (for similar blades) which, as can readily be appreciated in figure 8, would result in an almost uniform distribution of stresses over the first quarter of the tube [length]."

With all the preceding background, you might now be wondering how to calculate loads and stresses for a rotor blade

in flight. The flapwise bending moment calculation requires solving the problem presented in Fig. 2-84. The equation to solve is simply:

2.9 BLADES

(2.191) Flapwise $M_{r,t}$

$$= \int_r^R (\eta - r)\, d\left(L_{\eta,t}\right) - \int_r^R \left(Z_{\eta,t} - Z_{r,t}\right) d\left(CF_{\eta,t}\right) - \int_r^R (\eta - r)\, d\left(I_{\eta,t}\right).$$

Equation (2.191), born when propellers burst on the scene, has occupied rotorcraft engineers for at least seven decades . I have absolutely no doubt that 1,000 man-decades, if not more, have been spent in obtaining, slowly but surely, increasingly accurate

approximate solutions to this equation. The equation does not look too formidable until you insert the definitions of blade element lift (dL), centrifugal force (dCF) and inertia (dI). Then you begin to see the impending complexities because

(2.192)

$$FM_{r,t} = \int_r^R (\eta - r)\left(\frac{dL_{\eta,t}}{d\eta}\right)d\eta - \int_r^R (Z_{\eta,t} - Z_{r,t})(m_\eta \Omega^2 \eta)d\eta - \int_r^R (\eta - r)(m_\eta)\left(\frac{\partial^2 Z_{\eta,t}}{\partial t^2}\right)d\eta$$

$$FM_{r,t} = (EI_{flap})_r \left(\frac{\partial^2 Z_{r,t}}{\partial r^2}\right)$$

This is a differential-integral equation, which uses the dummy variable, η.

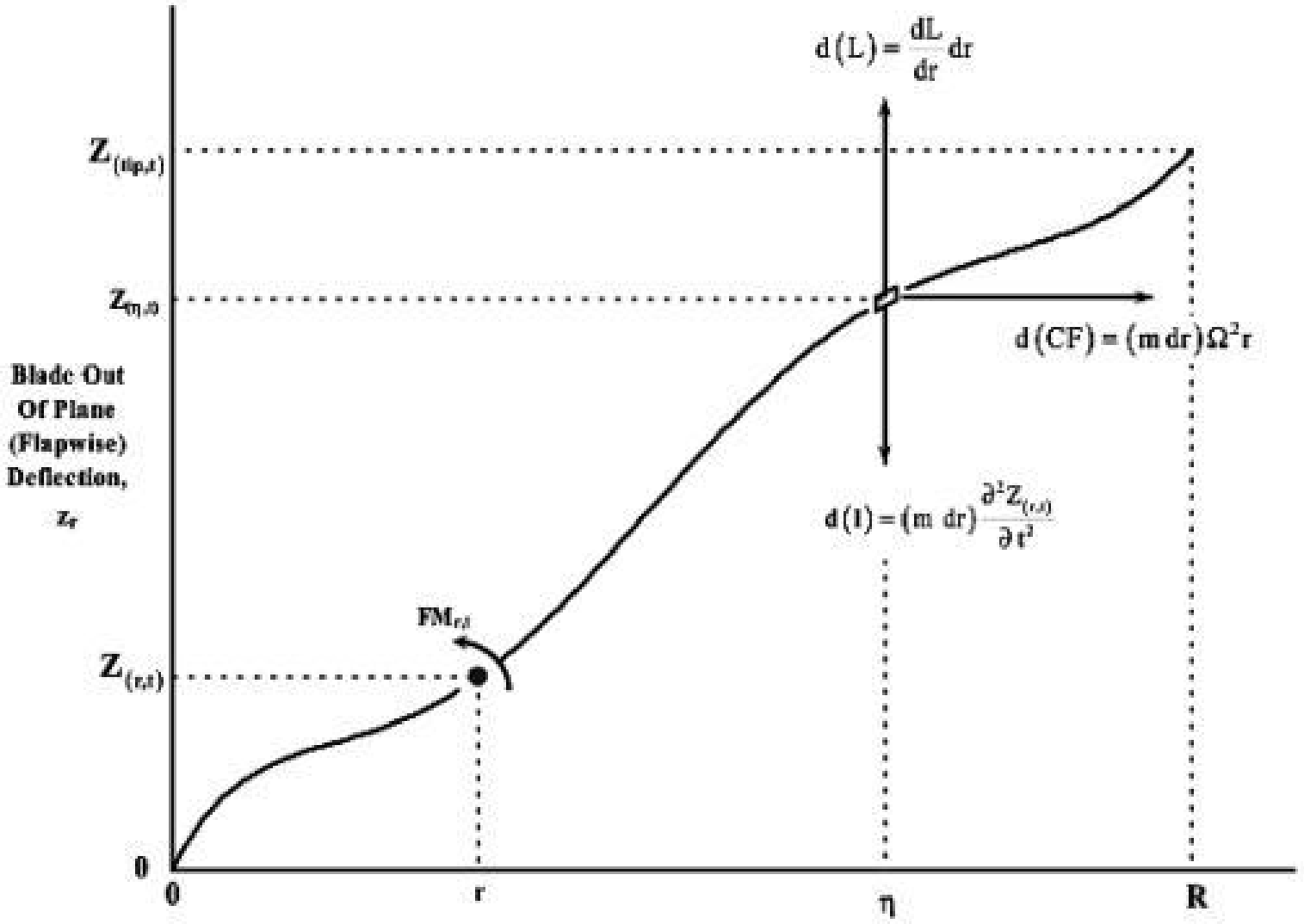

Radius Station, r

Fig. 2-84. Flapwise forces and bending moment on a rotating rotor blade.

You can see from Fig. 2-84 and Eq. (2.192) that the flapwise bending moment at any radius station (r) depends on the sum of all moments outboard of the station you are interested in. Furthermore, this moment ($FM_{r,t}$) depends on the deflected shape ($Z_{r,t}$) of the blade whose value varies with both radius and time, which introduces the centrifugal stiffening in the second integral of this classic equation. On top of this, a third integral is included that accounts for the inertial loads due to acceleration. If that were not bad enough, the solution depends on airloads, which, you can see, also depend on knowing the deflection of the blade.

I often wonder if Cierva had this bending moment figure and equation in front of him when he was conceiving, designing, building, and trying to get his first Autogiro (Fig. 2-85) off the ground.

Cierva did not stop to solve Eq. (2.192) while designing his blades. In fact, I do not think that he even bothered to try. The only thing he wanted from the formidable flapwise bending moment problem was the *critical* fatigue stresses the blade would be subjected to. He knew that the blade would flex during a revolution and, at some point in the revolution, the blade would be bent, tip up, a maximum. Then, somewhere else in the revolution, the blade would be bent, tip down, a maximum. Therefore, for his purposes, Equation (2.192) only needed to be solved for the peak values of moment. From the positive and negative peak moments, he could calculate steady and alternating stresses according to Eq. (2.190).

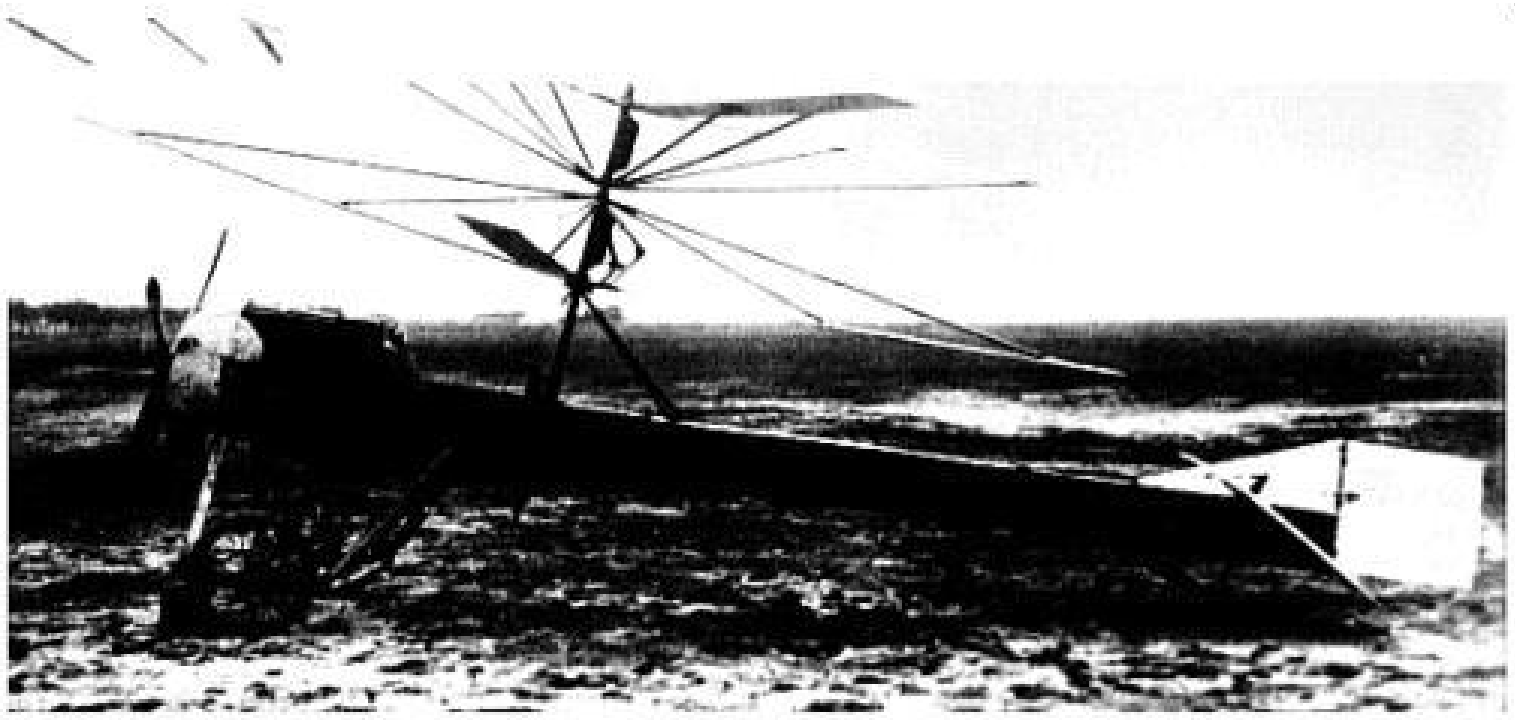

Fig. 2-85. The Cierva C.1, his earliest full-size experimental machine [3, 106].

2.9 BLADES

The details of the Cierva engineering solution for flap moments became available to close associates when his *Theory of Stresses on Autogiro Rotor Blades* was printed. Cierva then shared his approach to using Eq. (2.192)

with a larger audience when he gave a third lecture before the Royal Aeronautical Society on Friday, March 15, 1935 . A much larger group was able to read about his approach in the published paper [5]. This paper gives real insight into Autogiro development. After discussing the Aerodynamical Progress, he goes on to Dynamical Problems, beginning with:

"Perhaps the most irritating of the secondary difficulties met with in the autogiro developments have been those of a dynamical nature. The dis-symmetry of speeds on both sides of the rotor produces periodical variation in the lift and drag and in lift and drag moments on each blade. The articulations which allow the blades to flap, correct the dis-symmetry of the lift moments as far as their average value at any rate, and an equivalent reason makes practically essential a second articulation which permits the blades a certain freedom in their relative angular distances from each other. But, while the flapping motions are strongly damped by the variations in lift they entail, there is no appreciable damping in the horizontal oscillations, and this can produce important resonant phenomena and unpleasant free oscillations of relatively large amplitude following any impulsion – a bump for instance."

He adds more detail about what is today called ground and air resonance, and he notes that lag damping between each blade and the hub is a better solution than blade-to-blade interbracing or blade-to-blade damper connections with cables.

In the next section of the paper, The Engineering Technique, Cierva begins discussing the flap bending problem. He writes that

"considerable progress has been made in the knowledge of the strength requirements of the blades. Their proper study involves what for a long time appeared to be insurmountable difficulties. The tensile stresses due to centrifugal force can, of course, be very easily estimated, and the torsional stresses (if proper precautions to avoid torsional resonances are taken) can be minimised to the point where they can be neglected, but secondary bending moments of a periodic nature are present in the vertical [flapwise] plane."

After several more background paragraphs, he begins describing his approach to "bending moments in the vertical plane." (I have included all that he wrote.)

"An analysis of the influence of the several parameters affecting the bending moments permits to determine the maximum values which any extreme maneuvers is likely to produce. That extreme maneuver is assumed to be similar to the one which would suddenly increase the incidence of the wing of an aeroplane to the angle corresponding to the maximum lift coefficient.

Once the bending moments are calculated on the assumption that the blade is absolutely rigid, the differential equation representing the deflected shape of the blade axis can be established, if the elastic characteristics of the blade are given. If that equation could be integrated, the radius of curvature at any point could be calculated, and from it the true bending moment. Unfortunately this is not the case, and I have been obliged to devise an approximate method consisting in integrating the differential equation on the assumption that the blade is perfectly flexible by making the product of the moment of inertia of the section by the elongation coefficient, or $I \times E$, equal to zero. The

equation is immediately integrable and the radius of curvature of the perfectly flexible blade can be calculated. Multiplying it by the I × E product, an auxiliary bending moment is found. Calling it BM_f, and the bending moment for the same point of the blade assumed perfectly rigid BM_r, it can be shown that the expression $BM_r\ BM_f\ /(BM_f+BM_r)$ graphically represented in Fig. 4 gives a very close approximation to

the true bending moment, particularly for its maximum values. The magnification [amplification] factor due to dynamic effects can be calculated by estimating the period of free oscillation of the blade when deflected in the approximate shape it adopts under the action of the bending moments, the aerodynamical damping introduced and, finally, by expanding the periodical bending moment, with time as the independent variable, into a Fourier series. The magnification factor corresponding to the amplitude of each harmonic can then be immediately calculated and also the difference of phase of the forced oscillation in

that harmonic.

A graphical summation of the harmonics of the forced vibration gives a representation of the final bending moments, and the ratios of the positive and negative maximums to those calculated in the static assumption are the corresponding magnification factors.

This process is of course exceedingly elaborate, and a number of simplifying assumptions have to be made which are not of a nature that could substantially alter the results. Of particular difficulty is the calculation of the harmonics of the periodic bending moment with any degree of accuracy, since the third and even fourth harmonics are of importance but this can he done at least in the case corresponding to maximum stresses under the limiting maneuvers mentioned.

The most interesting conclusions of this study are that maximum bending stresses are almost independent of the weight of the machine, being a definite characteristic of each design of blade, and that they are also almost independent of the moment of inertia of the blade spar.

Measures in flight by means of extra light extensometers made by M. de Forest especially for the Autogiro Company of America, have substantially confirmed the conclusions of my theoretical analysis."

These several paragraphs from the 1935 Cierva paper do not do justice to the nearly 100 pages of assumptions, inferences, simplifications, logic paths, and equations documented in his *Theory of Stresses on Autogiro Rotor Blades*. His solution technique follows the Rayleigh–Ritz method, better known to some as the energy method.

2.9.5 C.30A Flapwise Bending Analysis

As fascinating as the Cierva method of calculating flapwise bending moments is,[39] it is even more interesting to compare the results of modern day methods to the C.30A results Cierva gives in the fourth appendix of his

Theory of Stresses on Autogiro Rotor Blades. (This will take several pages!)

The first step Cierva took to predicting the flapwise bending stresses of the C.30A blade, shown in Fig. 2-86 (and which includes a modern theory result I will discuss shortly), was to define the operating condition. Cierva was a pilot; in fact, he was one of a very small group of autogyro test pilots. Therefore, he selected an operating condition well outside of the normal flight envelope. He first established the rotor speed (Ω) and advance ratio (μ) design condition for the *one point* where he was going to do the calculations. (He was not joking

---

[39] Reading, interpreting, and understanding Cierva's work was slow going. First off, I had to translate his symbols to those that I have grown up with. For example, he uses Ω for tip speed. On the plus side, his slide rule was quite accurate. Most fascinating was his ability to accurately infer loads (both radially and azimuthally) from

very fundamental equations; but his logic was difficult—very difficult at times—to follow. Even today, I do not think I could fully explain his application of Lord Rayleigh's methodology.

2.9 BLADES

when he said in his lecture that the "process is of course exceedingly elaborate.") He determines first that, for a collective pitch of 6.25 degrees, the low rotor speed would be 19.6 radians per second at a light weight of 1,500 pounds and 110 miles per hour at sea level, which is an advance ratio of 0.445 . The high rotor speed at a weight of 1 ,800 pounds (at sea level with the same collective pitch) and "in turns or pull ups was obtained before as equal to 30.8 [radians per second]." From figures relating bending moment amplification in terms of damping

coefficient ($\rho cR/m_b$) and the blade frequency parameter, he concludes that the design point should be

$$\frac{m_b \Omega^2 R^4}{EI_{flap}} = 0.004 \quad (2.193)$$

which, he assumes, is representative of a worst case. Since the flapwise stiffness (EI_{flap}) of the C.30A blade is 25,350 pound-feet squared, and the running mass (m_b) is 0.06888 slugs per foot, the rotor speed derived from Eq. (2.193) is 28 radians per second. This is a tip speed (V_t) of 518 feet per second making the advance ratio, at 110 miles per hour, equal to 0.311. The Cierva design tables and figures go out to an advance ratio of 0.5 and beyond, so he selects the worst case as $\mu = 0.5$. This becomes the design point he uses as the example in his fourth appendix.

The design advance ratio of 0.5 at a

design tip speed of 518 feet per second implies a design flight speed of 176 miles per hour. This speed could only be reached in a dive. How many "g's" might be pulled during the recovery from this dive is open to question. However, an estimate of the ratio of rotor thrust coefficient to solidity (i.e., the blade loading constant, C_T/σ) at the onset of retreating blade stall is[40]

(2.194)

$$\left(\frac{C_T}{\sigma}\right)_{\substack{\text{blade}\\ \text{stall}\\ \text{onset}}} = \frac{C_{\ell\max}}{6}\left[\frac{1-\mu^2-\frac{4}{3\pi}\mu^3+\frac{25}{24}\mu^4-\frac{46}{15\pi}\mu^5-\frac{5}{16}\mu^6+\frac{1}{90\pi}\mu^7}{1+\frac{8}{3}\mu+\frac{3}{2}\mu^2+\left(\frac{32}{45\pi}-\frac{5}{24}\right)\mu^4}\right].$$

Cierva chose the Göttingen 429 with an airfoil maximum lift coefficient of 1.40, so for a 0.5 advance ratio, the blade loading coefficient (C_T/σ) at stall onset is 0.0626. The rotor thrust is, therefore, *at least*

$$T = \rho\left(\pi R^2\right) V_t^2 \sigma \left(\frac{C_T}{\sigma}\right)_{\substack{\text{blade} \\ \text{stall} \\ \text{onset}}} \tag{2.195}$$

$$= (0.002378)\left(\pi 18.5^2\right)\left(518^2\right)(0.047)(0.0626)$$

$$= 2,030 \text{ pounds}$$

which gives a load factor of 1.35 g. This is a very mild pull-out from a dive at the weight of 1,500 pounds and does not compare to the 2- or 3-g pull-outs modern rotorcraft can be subjected to and are designed for.

---

[40] Eq. (2.194) is an update to the low advance ratio expression I included in a 1987 paper [107].

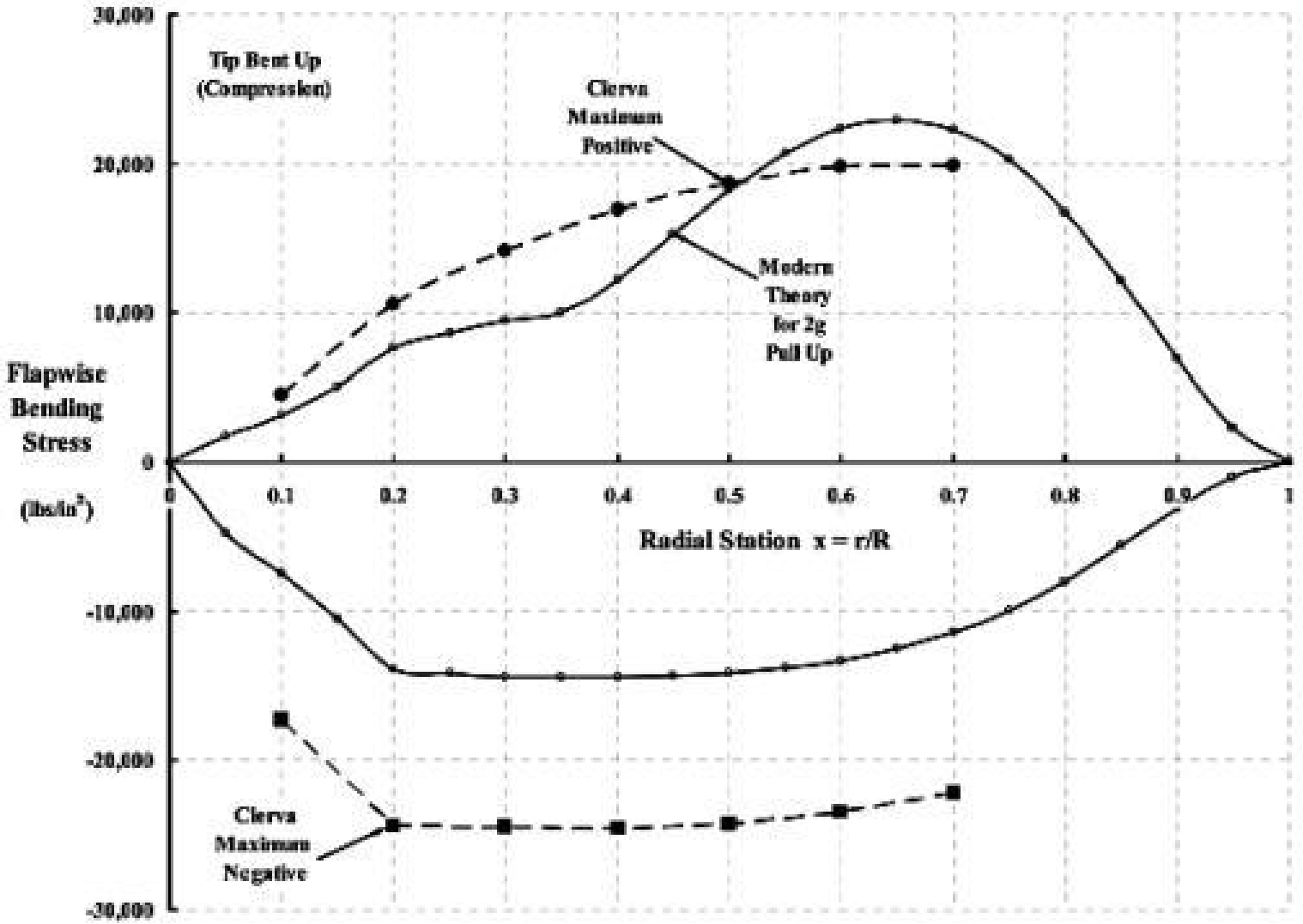

Fig. 2-86. Estimated C.30A blade flapwise bending stresses at $\mu = 0.5$ [12].

Now with the design condition selected, consider a modern day theory solution of Eq. (2.192) leading to the prediction included in Fig. 2-86 . Since the bending is

known to be periodic (i.e., harmonic), Eq. (2.192) can be rewritten in terms of azimuth with the substitutions $\psi = \Omega t$ or $\frac{1}{dt^2} = \Omega^2 \frac{1}{d\psi^2}$ to give

$$FM_{r,\psi} = (EI_{\eta\eta})_r \left(\frac{\partial^2 Z_{r,\psi}}{\partial r^2}\right) = \int_r^R (\eta - r)\left(\frac{dL_{\eta,\psi}}{d\eta}\right) d\eta - \int_r^R (Z_{\eta,\psi} - Z_{r,\psi})(m_\eta \Omega^2 \eta) d\eta - \int_r^R (\eta - r)(m_\eta)\Omega^2 \left(\frac{\partial^2 Z_{\eta,\psi}}{\partial \psi^2}\right) d\eta \quad (2.196)$$

Solving this equation requires some reasonable estimate of the running airload ($dL_{\eta,\psi}/d\eta$). It is, of course, simple enough to write the blade element statement that

$$\frac{dL_{\eta,\psi}}{d\eta} = \left(\frac{1}{2}\rho V_{\eta,\psi}^2\right) c_\eta C_{\ell\eta,\psi} \quad (2.197)$$

and then say the blade has uniform running mass (m_b), the blade has constant chord (c), the blade element velocity ($V_{\eta,\psi}$) is approximately $\Omega\eta + V_{FP}\sin\psi$, and finally to invoke linear

2.9 BLADES

aerodynamics where the airfoil lift coefficient ($C_{\ell\eta,\psi}$) equals the lift-curve slope (a) times the blade element angle of attack ($\alpha_{\eta,\psi}$) . These assumptions do simplify the problem somewhat because now you have the problem stated as

$$\left(EI_{flap}\right)_r\left(\frac{\partial^2 Z_{r,\psi}}{\partial r^2}\right)=\tfrac{1}{2}\rho ac\int_r^R(\eta-r)\left(\Omega\eta+V_{FP}\sin\psi\right)^2\alpha_{\eta,\psi}d\eta$$

(2.198)

$$-m_b\Omega^2\left\{\int_r^R\left(Z_{\eta,\psi}-Z_{r,\psi}\right)(\eta)d\eta+\int_r^R(\eta-r)\left(\frac{\partial^2 Z_{\eta,\psi}}{\partial\psi^2}\right)d\eta\right\}$$

No further significant progress can be made without some reasonable estimate of the blade element angle of attack.

The classic expression for the blade element angle of attack (available for decades) is derived in several rotorcraft technology reports [75] and reference books [70], so you can write immediately that

$$\alpha_{\eta,\psi} = \theta_{\eta,\psi} + \frac{V_{FP}\cos\psi - v_{\eta,\psi} - \Omega\dfrac{\partial Z_{\eta,\psi}}{\partial\psi} - V_{FP}\sin\psi\dfrac{\partial Z_{\eta,\psi}}{\partial\eta}\cos\psi}{\Omega\eta + V_{FP}\sin\psi}. \tag{2.199}$$

The increase in the complexity of the flap bending problem should be all too clear now. The angle of attack, which gives the airload that the blade responds to with deflection (Z), depends on the rate of deflection ($\Omega\ \partial Z_{\eta,\psi}/\partial\psi = \partial Z_{\eta,\psi}/\partial t$) and the slope of the bending blade ($\partial Z_{\eta,\psi}/\partial\eta$). Furthermore, the blade pitch angle ($\theta_{\eta,\psi}$) has its own elastic response, which means the solution of the real problem requires solving a blade torsion equation at the

same time blade bending is being calculated. On top of this growing list of inner dependence (i.e., coupling) between airload and deflection, lies the fact that the velocity induced on the blade element ($v_{\eta,\psi}$) by the trailing wake of the lifting rotor is not constant. No wonder Cierva sought—and fortunately found—an engineering solution that a very small group of engineers could tackle with a slide rule!

As I mentioned earlier, the blade flapwise bending problem has been "solved" by quite a few engineers and mathematicians over the past seven decades. In Appendix H, I have included one example of a numerical solution using an implicit, finite difference integrating scheme.[41] The solution is obtained by solving the fourth order, partial differential equation

---

[41] This method was first constructed by Mark Dreier of Bell Helicopter in the early 1980s. He did the original

work for the fun of it, in response to a challenge I proposed. Mark never published the work despite my encouraging words. Then in 1 992/1 993, after I grasped the approach and had a fast, large computer, I "programmed" an embellished version of Mark's creation on a Microsoft® Excel® spreadsheet. This version used 25 beam elements. In 2002, Anubhav Datta, then a graduate student at the University of Maryland, inquired about "my" Excel flapwise only, beam bending solver. I sent my notes and the spreadsheet file to Anu and he wrote a Fortran code that could handle up to 100 beam elements. With his code, Anu compared the finite difference approach to his much more comprehensive, fully coupled (i.e., flap, lag, torsion) blade bending solver and confirmed that with 80 beam elements, the solution was stable and accurate.

form of the moment equation. This fourth order equation is obtained by differentiating Eq. (2.192) twice and putting it in

nondimensional form. Then, because the beam is assumed to have constant running mass (m_b) in slugs per foot, constant stiffness (EI_{flap}) in pound-feet squared, and constant chord (c) in feet, you have

(2.200)

$$\left(\frac{EI_{flap}}{m_b\Omega^2R^4}\right)\frac{\partial^4(Z/R)_{x,\psi}}{\partial x^4}+x\frac{\partial(Z/R)_{x,\psi}}{\partial x}-\frac{1-x^2}{2}\frac{\partial^2(Z/R)_{x,\psi}}{\partial x^2}+\frac{\partial^2(Z/R)_{x,\psi}}{\partial\psi^2}=\frac{1}{m_b\Omega^2R^2}\frac{\partial L_{x,\psi}}{\partial x}$$

where, assuming linear aerodynamics of the blade element airfoil, the lift loading is

$$\frac{1}{m_b\Omega^2R^2}\frac{\partial L_{x,\psi}}{\partial x}=\frac{1}{2}\left(\frac{\rho acR}{m_b}\right)\left(x+\mu\sin\psi\right)^2\alpha_{x,\psi}$$

(2.201)

$$\text{and } \alpha_{x,\psi} = \theta_{x,\psi} + \frac{\left(\lambda_{hp}\right)_{x,\psi} - \dfrac{\partial\left(Z/R\right)_{x,\psi}}{\partial\psi} - \mu_{hp}\dfrac{\partial\left(Z/R\right)_{x,\psi}}{\partial x}\cos\psi}{x + \mu_{hp}\sin\psi}.$$

You should immediately notice that Eqs. (2.200) and (2.201) are completely nondimensional . Just as important, the solution depends on the reciprocal of the blade frequency parameter $\left(m_b\Omega^2R^4/EI_{flap}\right)$, which Cierva set equal to 0.004 in his analysis of the

C.30A blade "vertical bending." The parameter $\left(\rho acR/m_b\right)$ depends, of course, on the ratio

of air density to blade density and is, therefore, sensitive to altitude.

Cierva, in his *Theory*, used the nondimensional parameters to construct 33 pages of tables and some 60 figures to

facilitate the *rapid* computation of vertical bending fatigue stresses. He provides ways to account for nonconstant mass and stiffness, including additions of point masses, and ways to account for nonconstant chord blades. In subsequent historical information that I will discuss shortly, it took "six men and a boy" to deal with this problem, but I have found no elapsed times quoted.

In contrast to the Cierva approach in the 1930s with tables, charts, figures, 6 men, 1 boy, and slide rules, Appendix H, programmed in my personal computer, provides converged flapwise bending moments in 5 minutes doing 4 rotor blade revolutions in 2-degree increments while keeping track of 25 radial stations, albeit for uniform blade properties.

Now consider the results, shown in Fig. 2-86, when modern day tools are applied to

Cierva's specific design condition. Equations (2.200) and (2.201) were solved by the finite difference scheme from Appendix H, for the conditions shown in Table 2-8, using C.30A blade properties:

2.9 BLADES

Table 2-8. C.30A Design Conditions

Parameter	Value		Parameter	Value
Flight Speed (ft/sec)	177		Flapwise Stiffness (lb-ft^2)	25,350
Tip Speed (ft/sec)	518		Running Mass (slug/ft)	0.06888
Density (slug/ft^3)	0.002378		Hinge Offset (ft)	0
Blade Number	3		Collective Pitch (deg)	6.5
Radius (ft)	18.5		Cyclic Pitch (deg)	0
Chord (in.)	11.0		Hub Plane α (deg)	7.2
Blade Twist (deg)	0		Frequency Parameter	0.00400

Cierva did not quote a hub plane angle of

attack (α_{hp}) for these inputs. However, he did explain that the rotor would have as many blade elements operating at the airfoil maximum lift coefficient of 1.4 as possible for the design condition. I chose the hub plane angle of attack of 7.2 degrees as reasonable for a nonaerobatic aircraft. At these conditions, the rotor produced a calculated thrust of 3,000 pounds, which means the 1,500-pound C.30A is experiencing a 2-g pull-up.

The bending moments get converted to spar stresses, conventionally, as

(2.202)

$$\text{Spar } S_{x,\psi} = \left(FM_{x,\psi}\right)\frac{(\text{Spar OD}/2)}{\text{Spar I}_{flap}} = \left\{\frac{EI_{flap}}{R}\left[\frac{\partial^2 (Z/R)_{x,\psi}}{\partial x^2}\right]\right\}\frac{(\text{Spar OD}/2)}{\text{Spar I}_{flap}}$$

Cierva uses the elastic modulus (E) as 29,000,000 pounds per square inch and the spar thickness as its outside diameter (OD), a constant 1.5 inches. Using blade radius (R) in

inches gives the spar stress in pounds per square inch, which makes structural engineers happy. In addition, Cierva gives the details that inboard of radial station 0.1R, the spar moment of inertia (I_{flap}) is 0.1306 inches,[4] and outboard of radial station 0.2R, the spar moment of inertia is 0.09 inches[4]. The variation is linear between 0.1R and 0.2R. He further makes the point in his *Theory* that

"in most practical cases, the structure is composed of a main spar and some sort of superstructure. In this case, the total EI_{flap}, which is the sum of EI for all structural elements, should be taken for K [a curvature multiplying constant] but the individual values of E and d [OD/2] should be used in order to calculate the fiber stresses on each element .....In the ordinary type of [blade] construction now in use, EI_{flap} is approximately 20 to 40 % greater than [the spar's EI] so that it can be seen that the spar receives no real relief from the superstructure."

The preceding pages lead to the calculated flapwise bending stress at the 0.65 radial station varying with azimuth as shown in Fig. 2-87. The maximum positive stress, which occurs at 260 degrees, and the maximum negative stress are two of the

points plotted on Fig. 2-86.

2.9 BLADES

The solid line on Fig . 2-87 has been calculated using Appendix H methodology built from Eqs. (2.200) and (2.201), however several much more comprehensive theories have, of course, become available in the last several decades. The pace of these progressively improving theories has been keyed to bigger, faster, digital computers. One such theory, CAMRAD, was initially created by Wayne Johnson in 1980 and began with a calculation of the induced velocity ($v_{x,\psi}$) acting at each blade element based on wake geometry provided by Scully [108] in 1965. Over time, Johnson incorporated several improvements to his program, and in 1993 he

introduced CAMRAD II [109].

The induced velocity is assumed constant (i.e., uniform over the rotor disc) and the airfoil is linear in lift versus angle of attack in the Appendix H solution to Eq. (2.201) . Johnson's more comprehensive calculation of bending moment, including what is commonly called nonuniform downwash (i.e., $v_{x,\psi}$) and nonlinear airfoil lift and drag properties that allow stall, is shown with the dashed line in Fig. 2-87. While the maximum positive and negative peaks are of similar values between the two solutions of the beam problem, nonuniform downwash and blade stall clearly create several higher harmonic loads and stresses . The accurate calculation of these higher harmonic loads is very important to rotorcraft vibration, as you will learn shortly.

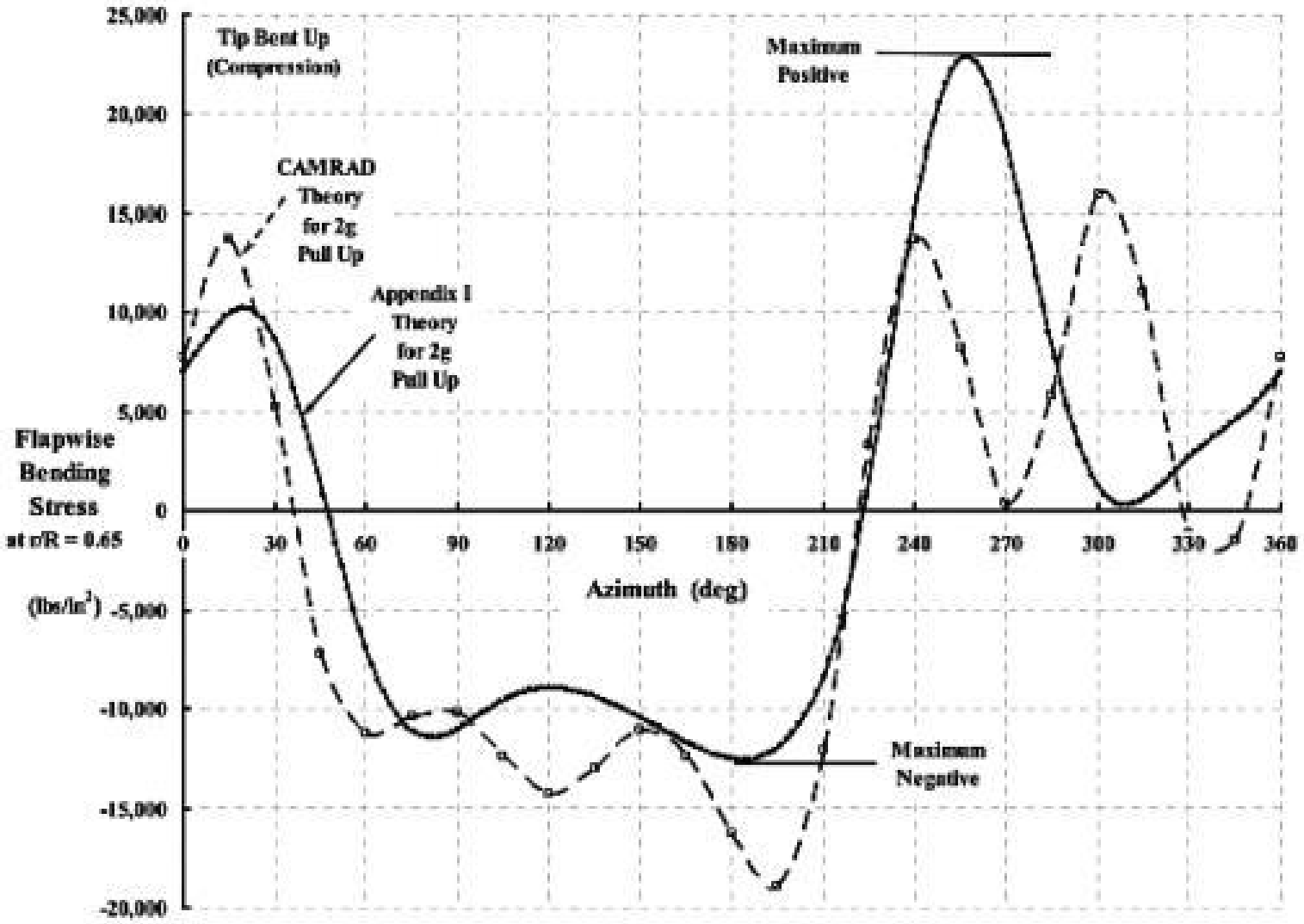

Fig. 2-87. Estimated C.30A blade flapwise bending stresses at r/R = 0.65, μ = 0.5.

Cierva clearly was the first to study rotor blade bending in "the vertical plane." J. B. B. Owen was the second man to tackle the flapwise bending problem and obtain visible results, which were published in 1938 [1 10]. Later, on October 6, 1951, at an all-day meeting of the Helicopter Association of Great Britain, Owen presented a discussion [111] of bending moments in both vertical and horizontal planes. Interestingly, in 1968, Westland Helicopters Limited published a book titled *A History of British Rotorcraft, 1866–1965* [1 12], and Owen contributed a short discussion about rotor blade research from 1933 to 1939. Owen's first- person summary of 1968 is quite interesting. In the opening paragraphs he writes:

"My first contact [1933] with Autogiros came when I joined Mr. H. A. Mettam who was then working in this field with Messrs. A. V. Roe at Manchester [England] . The blades of these machines were then occasionally failing at the root fittings [see Fig. 2-70], due probably to corrosion fatigue associated with the

swetting on of the ends, and I became interested in the strength problems associated with this type of aircraft. I had access to what I remember as 'black and green' volumes, which had been written by Cierva. These if I remember correctly, included the bending moment rule which he eventually published in the December 1935 [Royal Aeronautical] Journal. This rule is reproduced in equation (36) of R & M 1875 [1 10], where I demonstrated that it is very satisfactory except in the regions of the blade tip where bending moments are not usually important.

The contribution of R & M 1875 was that it shed physical light on what was happening in the bending of Autogiro blades and demonstrated the very large reduction in the transverse bending moment on a blade, due to the centrifugal forces present. Up to this time, this had not been generally accepted.....In this and later reports I drew attention to the lack of knowledge of the aerodynamic loads on blades....."

The Owen R & M 1875 report from 1938 was a catalyst to the small rotorcraft industry. Owen, of course, had identified the real problem—"the lack of knowledge of the aerodynamic loads on blades." In 1964 the first

bit of "knowledge" finally became available. In the mid- 1960s, a Sikorsky H-34 was instrumented with differential pressure transducers on one of its four blades and data was obtained—in flight—by NASA . The long-awaited data was published by Scheiman [1 13] in 1964. The heavily instrumented rotor was then removed from the H-34 helicopter and tested in the NASA Ames Full-Scale Wind Tunnel. Results from that "rotor alone" test were published by Rabbott in 1966 [1 14]. You will learn more about this acquisition of "knowledge" in Volume II—Helicopters.

A significant question grew out of Cierva's and Owen's work. The question, rather simply stated, is this: Are the flapwise bending *stresses* lower with a low flapwise stiffness blade (in the limit, a chain or $EI_{flap} = 0$) or with a high stiffness blade (in the limit, completely rigid or $EI_{flap} = \infty$)? This question is worth answering before leaving vertical

plane (flap) bending and going on to horizontal plane (chord) bending. Let me use the flap bending calculator in Appendix H to give you an answer. Suppose the C.30A blade is the reference point with (a) the spar outside diameter constant at 1 .5 inches, and (b) the superstructure remaining constant. The only variable then is the wall thickness of the spar. The bench testing by Cierva showed that the experimental value of flapwise stiffness was 3,650,000 pound- inches squared. The tubular spar accounts for 2,600,000 pound-inches squared of the total,

leaving the "superstructure" as 1,050,000 pound-inches squared or 7,290 pound-feet squared. (Frankly, the units of pounds and

inches preferred by structural engineers are handier for this illustration.) Therefore, in this example, the blade element flapwise stiffness (EI_{flap}) varies with tube-wall thickness (in inches) as

$$(2.203)\quad EI_{flap} = EI_{spar} + 1{,}050{,}000 = 29{,}000{,}000\left[\frac{\pi}{64}\left(1.5^4 - ID^4\right)\right] + 1{,}050{,}000 \ \text{in lb} - \text{in}^2$$

where the spar inside diameter (ID) in inches equals the outside diameter (OD = 1.5 inches) less twice the wall thickness of the tube. For reference, the C.30A spar wall thickness is 0.08 inches. In a similar manner, the blade weight (W_b) in pounds varies with wall thickness as

(2.204)

$$W_b = \left\{\text{Density}\left[\frac{\pi}{4}\left(OD^2 - ID^2\right)R\right] + 18.83\right\} = \left\{0.3\left[\frac{\pi}{4}\left(OD^2 - ID^2\right)(222)\right] + 18.83\right\}$$

where the density of steel is taken as 520 pounds per cubic foot or 0.3 pounds per cubic

inch. For reference, the C.30A radius of 18.5 feet equals 222 inches.

The Appendix H bending moment calculator uses flapwise stiffness in pound-feet squared and needs the running mass—not total blade weight, which means a conversion of

$$(2.205)\quad EI_{flap} = \frac{EI_{flap}\ \text{in lb}-\text{in}^2}{12^2}\ \text{in lb}-\text{ft}^2$$

$$m_b = \frac{W_b}{gR} = \frac{W_b}{(32.174)(18.5)}\ \text{in slugs/ft}.$$

For this example, the input to Appendix H, using the C.30A design condition from Table 2-8, is given in Table 2-9. Keep in mind that the radius, chord, rotor speed, spar outside diameter, and "superstructure" remain constant,

and the thrust is set to 3,000 pounds.

The influence of spar wall thickness, the only variable in this example, is shown in Fig. 2-88 and Fig. 2-89. Notice in Fig. 2-88 that while the flapwise bending moment waveform changes substantially, the magnitude of the fatigue moment (i.e., the peak-to-peak divided by 2) as seen in Fig. 2-89 is relatively independent of the large range in blade stiffness. Therefore, the fatigue flapwise bending stress increases as the second moment of inertia of the spar becomes smaller, as Eq. (2.202) dictates. I imagine Cierva performed a "vertical bending" trade study similar to Table 2-9 to arrive at the C.30A spar and "superstructure."

2.9 BLADES

Table 2-9. Spar Wall Thickness Study

Parameter	S.W.G. 25	S.W.G. 19	S.W.G. 14	S.W.G. 10	S.W.G. 3	S.W.G. 0000000
Wall Thickness (in.)	0.020	0.040	0.080	0.128	0.252	0.500
Inside Diameter (in.)	1.460	1.420	1.340	1.244	0.996	0.500
Flap Stiffness (lb-in.^{2})	1,771,591	2,451,826	3,650,000	4,830,554	6,838,836	8,150,759
Running Mass (slug/ft)	0.04208	0.05223	0.07170	0.09356	0.14253	0.20794
Spar 2nd Moment (in.^{4})	0.02547	0.04892	0.09024	0.13095	0.20020	0.24544
Lock Number	16.47	13.27	9.67	7.41	4.86	3.33
$m_b\Omega^2R^4/EI_{flap}$	314.09	281.72	259.76	256.14	275.61	337.37
Mode 2 Frequency Ratio	2.636	2.654	2.669	2.671	2.658	2.625
Mode 3 Frequency Ratio	4.994	5.087	5.162	5.176	5.107	4.936
EI_{flap}/R (in.-lb)	7,980	11,044	16,441	21,759	30,806	36,715
OD/2I (1/in.^{3})	29.45	15.33	8.31	5.73	3.75	3.06
Fatigue Moment (in.-lb)	27,124	27,274	25,745	26,130	26,208	22,684
Fatigue Stress (lb/in.^{2})	66,570	34,843	17,831	12,472	8,182	5,776
Blade Weight (lbs)	25.0	31.1	42.7	55.7	84.8	123.8

2.9.6 C.30A Chordwise Bending Analysis

Now let me proceed to the chordwise axis . Cierva, of course, considered spanwise bending moments and stresses in the horizontal, or inplane, or chordwise plane as well. However, in contrast to the considerable number of pages devoted to flapwise bending moments and stresses, he deals with

inplane moments and stresses in less than five pages . With respect to chordwise loads and stresses in forward flight, he writes in his *Theory* that:

"The only bending moment which can be of any importance is the alternat[ing] one which appears when there is any restraint to the free motion of the blade, either in relation to the others or to the hub. In the general case it is imposed by a damper, more commonly a frictional one.

In certain cases there will be no appreciable restraint for the small motion of the order of 1° to 2° 30' either side of the central position, which the blades perform in any condition of flight. In other cases, on the contrary, the restraint will be obtained even for very small motions.

If the restraint is of the frictional type, it will be constant and independent of both rotational speed and the amplitude of the motion, but there may be other cases, such as friction dependent on centrifugal force or hydraulic dampers, where the restraint will increase with either centrifugal force or angular speed of the oscillatory motion, which will depend directly, everything

else equal, on the angular speed of rotation. Each case will have to be treated on its merits, but it will be convenient in any case to assume a constant restraining torque equal to the maximum which normally can be applied and consider it for fatigue stressing. In certain systems, where high exceptional values might be attained, this case should also be considered, not as a fatigue case.

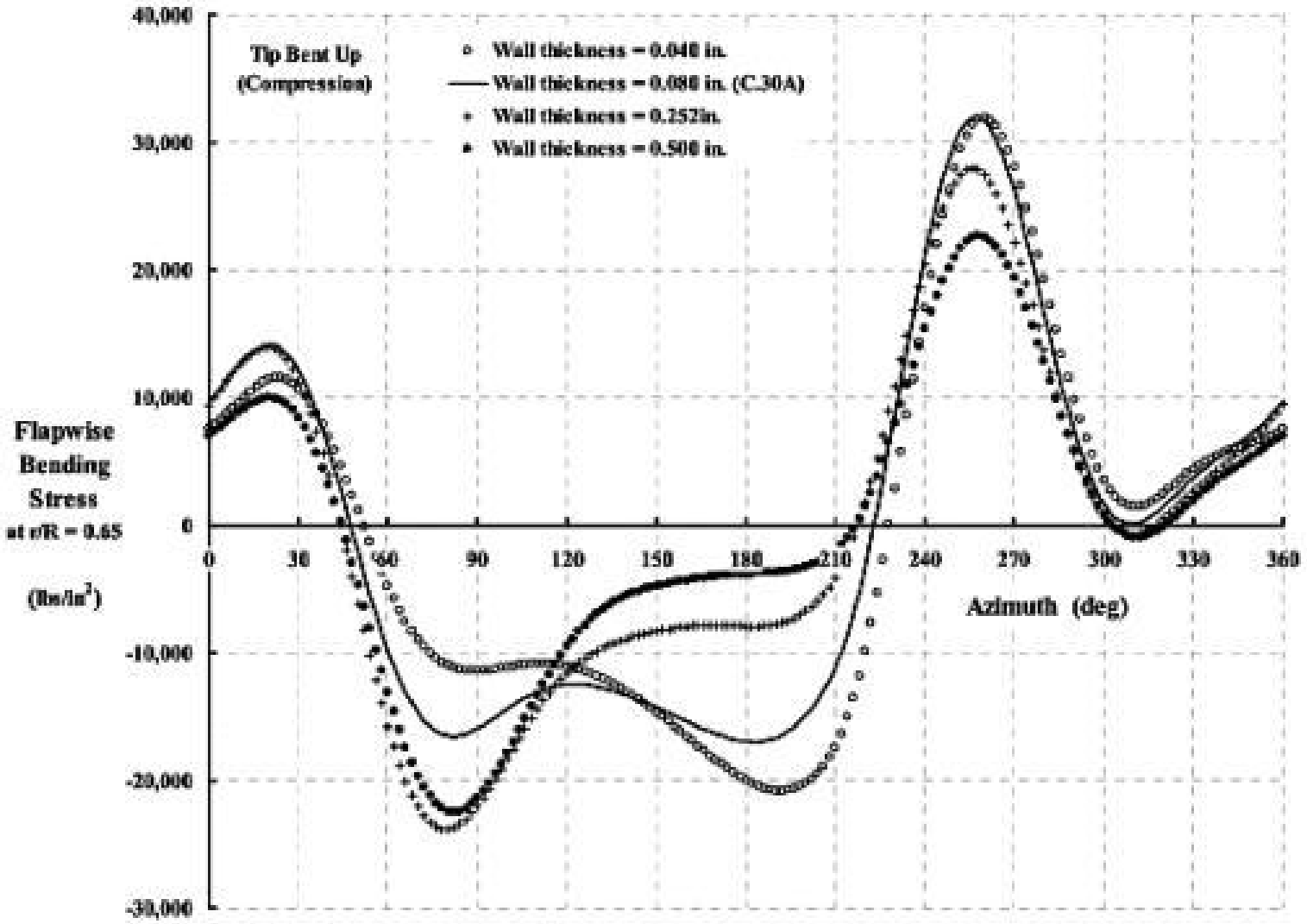

Fig. 2-88. Flapwise bending moment at μ = 0.5 for several wall thicknesses.

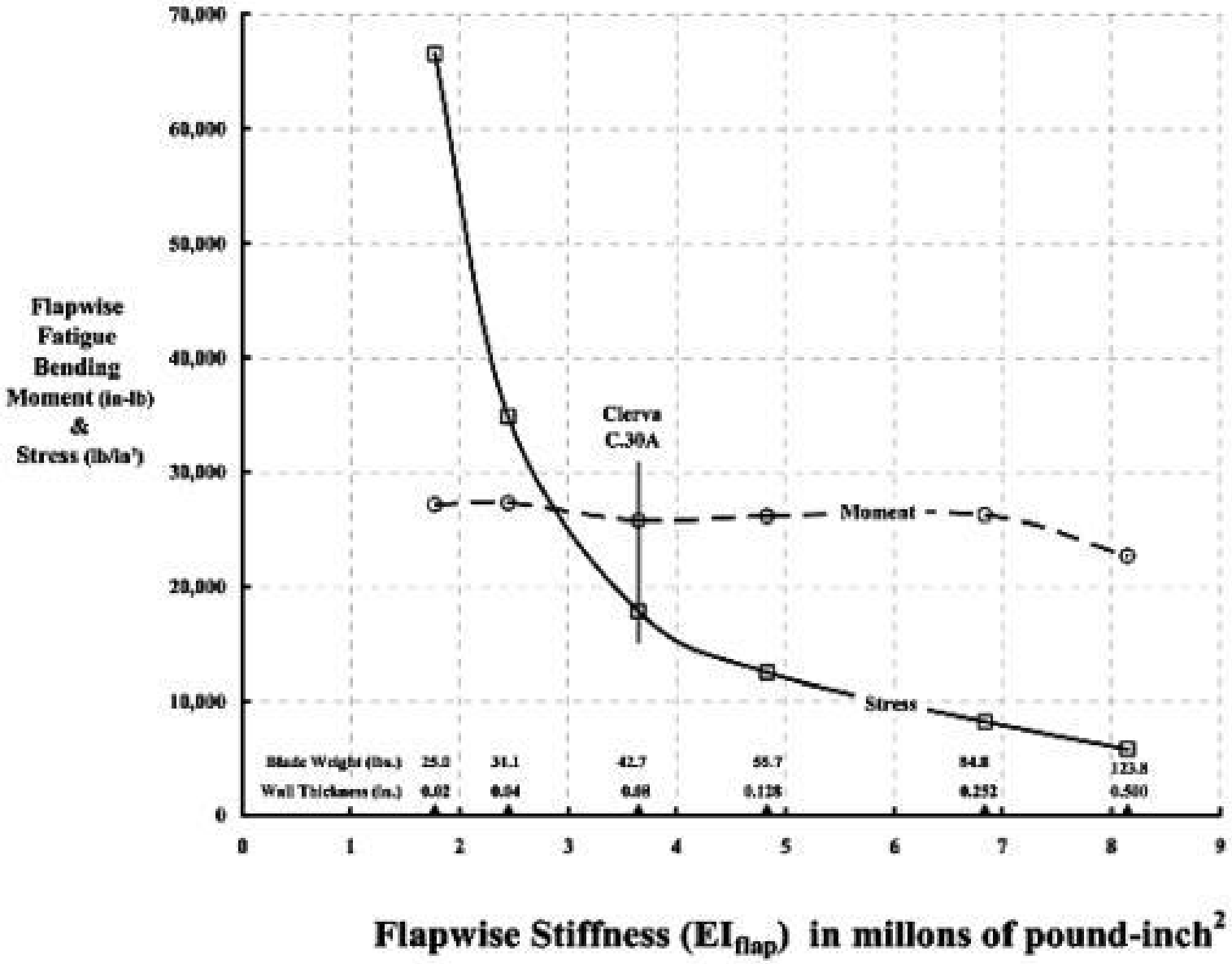

Fig. 2-89. Fatigue moment and stress at μ = 0.5 for several wall thicknesses.

2.9 BLADES

The distribution along the radius can be

calculated by equation (1) and (2) (Part I, (2) (b)). All said there [in Part I] applies to this case. In the general case, where the superstructure has a very high moment of inertia in the direction considered [inplane], the bending on the spar will be negligible at all points except at the root and close to it. In the case of ordinary blade construction, it is reasonable to assume that the stresses on the spar become negligible at a distance from the first rib equal to about 0.1 of the radius. A linear law may be assumed for the change.

When plain bearings are used on the drag hinge, it is advisable to calculate the additional frictional restraint to centrifugal force. A frictional coefficient of 0.15 is recommended."

Part I, (2) (b) of his *Theory* that Cierva refers to addresses "Stresses On Ground"; subset (2) (b) is "Bending in [the] Plane of Rotation" during starting.

The Cierva approach to chordwise bending moments and stresses is quite interesting. The only loads of interest in forward

flight are those loads created by the lead-lag damper and the frictional moment caused by the plain bearings of the lag hinge . In the fourth appendix of his *Theory* Cierva gives the C.30A example along with the explanation that:

"The blades are restrained in their motions relative to the tube by friction dampers, which are never adjusted to a torque superior to 15 [pounds force] × 200 [inches for moment arm] = 3,000 lbs-inches. In addition, however, the friction due to centrifugal force on the drag pin [pin through the lead-lag hinge], which has a plain bearing, will have to be considered.

The maximum centrifugal force in any condition of flight considered will be, at the vertical drag pin equal to

$$(F_C)_{max} = 0.5\left(\frac{41}{32.2}\right)(18.5)(30.8)^2 = 11,200 \text{ lbs}$$

The pin diameter is 1-5/8 inch = 1 .625 inch, so that assuming a coefficient of friction equal to 0.15, greater than any value that can reasonably be expected, the centrifugal friction torque will be equal to 11200 × 0.15 × 1.625/2 = 1380 lbs-inches.

The total maximum horizontal BM [bending moment] at the root will be taken as 3000 + 1360 = 4360 lbs-inches. It will be considered as an alternative one, changing once a revolution from + 4360 to – 4360 lbs-inches."

Using the planform view of the C.30A blade, Fig. 2-90, he assumes the ±4,360 fatigue moment is transferred from the spar to the superstructure in a linear manner. At the 0.1 radial station, the spar takes the full moment; at the 0.3 radial station, the superstructure takes the full moment. Then he calculates the spar chordwise stresses over the root end out to a radius station of 0.3R and tabulates the results shown in Table 2-10 .

Table 2-10. The Cierva C.30A Spar Chordwise Fatigue Stress Analysis [12]

Parameter	Point A to r/R = 0.1	r/R = 0.15	r/R = 0.20	r/R = 0.25	r/R = 0.30
Moment (in.-lbs)	±4,360	±3,270	±2,180	±1,090	0
Z ($in.^3$)	0.1741	0.1426	0.1199	0.1199	0.1199
Fatigues Stress ($lb/in.^2$)	±25,000	±23,000	±18,150	±9,075	0

2.9 BLADES

The symbol Z in this table is frequently used by structural engineers. It is the ratio of the second moment of inertia (I), in inches^4, to the distance (d), in inches, from the cross-section neutral axis to the outermost fiber being stressed. Thus, Z = I/d, and so moment in inch-pounds divided by Z is stress in pounds per square inch, in this case, fatigue stress.

When you look closely at the C.30A planform sketch, Fig. 2-90, you will see that the basic spar starts out (point A on the sketch) as British Imperial S.W.G. number 10 which means a tube having a 0.128-inch wall thickness. The outside diameter is 1.5 inches. At 20 inches *inboard* of point B, a tapering-in wall thickness begins so that at point B the tube

is still 1.5 inches in outside diameter but has become S.W.G. 14, a wall thickness of 0.080 inches. This movement to a spar having a tapered wall thickness was considerably refined in the autogyro era.

It is fascinating to me that Cierva, in his *Theory,* never discusses stresses in the "superstructure" and, in particular, the trailing edge. Apparently, he was more than satisfied that "the rigidity of the superstructure in a horizontal plane is very great" and, therefore, the stresses must be quite low. Any thought that a chordwise resonance condition might occur is conspicuously absent in his design manual. I think this confidence must have been obtained from other calculations and data suggested by Fig. 2-89, which shows that high stiffness results in very low flapwise fatigue stresses.

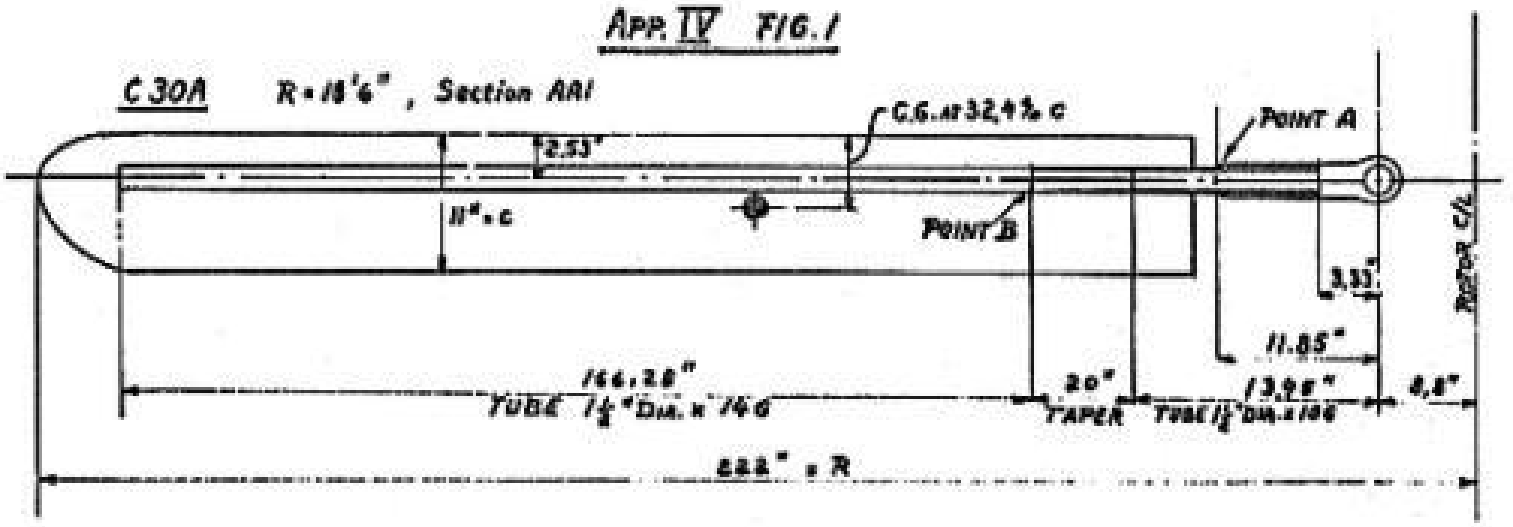

WEIGHTS: SPAR 21.1 LBS

SUPERSTRUCTURE 17.9 LBS

(FORKEND NOT INCLUDED)

TUBE	A in^2	I in^4	Z =
1½" x 16G	0.8517	0.1306	0.1741
1½" x 14G	0.3569	0.0900	0.1199

Fig. 2-90. A sketch of the C.30A blade drawn by Cierva and included in his *Theory*.

2.9 BLADES

2.9.7 C.30A Torsional Bending Analysis

Cierva provides considerable guidance about loads and stresses in the torsion axis. In his *Theory*, Part II, Stresses in Flight, Section 6, Torsional Stresses, he lists the possible sources of torsional stresses as

"(1) Transverse offset between the [blade element airfoil] lift and inertia forces acting on the blade
(2) Pitching moments due to camber of the aerofoil
(3) Transverse offset between the vertical shear due to bending in a vertical plane and the elastic central axis of the blade
(4) Secondary torsion induced by bending in a horizontal plane combined with deformations in bending in a vertical plane."

and proceeds to derive simple equations for each contributor to torsional stresses.

The first contributor is referred to today in shorthand as c.g.–a.c . offset. Fig. 2-90 shows that the blade element center of gravity is located chordwise 32.4 percent of chord (i.e., 3.564 inches) *behind* the airfoil leading edge . Since the airfoil lift acts, nominally, at the 1/4-chord point (2.75 inches), that is to say at 25 percent of chord behind the airfoil leading edge, a positive blade element lift tends to twist the blade nose up. You will recall that Hafner [74] was very careful to keep the "superstructure" light so that the blade element center of gravity was placed at the 1/4-chord point. Hafner specifically intended to reduce this torsional moment component to zero . The C.30A blade, with its aft c.g., introduced a nose-up torsional moment (T_x) along the blade, which Cierva calculates (in modern notation) as

(2.206) c.g.–a.c. offset

$$T_x = \frac{3}{16}\left(\text{c.g.offset} - \tfrac{1}{4}c\right)\rho C_{\ell max} c R^3 \Omega_{max}^2 \left(1 - x^2\right).$$

This moment, in foot-pounds, depends on the c.g. offset in feet behind the airfoil 1/4-chord point (i.e., the airfoil aerodynamic center, a.c.) in feet, on the air density (ρ) in slugs per cubic foot, on blade chord (c) in feet, on blade radius (R) in feet, and, following Cierva's worst-case assumption, on the maximum design rotor speed (Ω_{max}) in radians per second. He assumes that in forward flight the blade could be operating at the airfoil maximum lift coefficient ($C\ell_{max}$) over the full span. The nondimensional radial station is ($x = r/R$).

Cierva argues, correctly to the first approximation, that the torsion moment due to c.g.–a.c. offset will "in the case of the extreme manœuvre, oscillate between zero and the value given by Eq. (2.206)."

The next torsion moment Cierva considers is due to the airfoil pitching moment coefficient (C_m). Beavan and Lock [57] tackled this moment in 1936 when they sought to explain the adverse stick gradient of the C.30, as you learned in Section 2.6. They credited Cierva's notes for starting them in the right direction. In 1937, Wheatley [59] gave an even more in-depth analysis at the N.A.C.A. of both c.g.–a.c. offset and pitching moment loads in the torsion axis. But in the early 1930s, Cierva calculated this airfoil pitching-moment- dependent torsional moment, in foot-pounds, from

(2.207) pitching moment T_x

$$= \rho C_m c^2 R^3 \Omega^2 \left[\tfrac{1}{3}\left(1-x^3\right)+\mu\left(1-x^2\right)+\mu^2\left(1-x\right)\right].$$

The airfoil pitching moment coefficient (see Appendix B) is taken about the airfoil 1/4-chord point. In his torsion analysis [12] Cierva includes the situation where the blade might have two different airfoils in separate span segments of the blade.

The third torsion moment considered deals with the coupling between the vertical shear due to flapwise bending and torsion. He writes:

"The shear force studied in (4) will be situated, transversely [the chordwise direction] to the blade, at ¼ c from the leading edge. If the neutral elastic axis of the blade (the axis of the tubular spar in the general case) is at a distance d_s from the leading edge, it will produce a torsional moment equal to

$$(\tau_3)_x = S_x \left(d_s - \tfrac{1}{4}c\right)$$

By using equation (156) in conjunction with (146), (147), (148) and (149), the values of (τ_3) for any point (r/R) or those at the root (maximum), can be obtained.

The maximum value (absolute) will be for $(S_+)_o$ which corresponds, as said in ((4)(h)), to $\psi = 3\pi/2$ and the absolute maximum of opposite sign will be for $(S_-)_o$, corresponding to $\psi = 0$ and $\psi = \pi$."

The fourth torsional moment, due to simultaneous bending in vertical and horizontal planes (he later calls this "torsion due to double bending"), causes Cierva to write a very clear 2-1/2-page dissertation on the *real* coupled bending/torsion deflection and loads he sees with rotor blades. He relies on the assumption that there will be no inplane bending—if there is no lead-lag damper and the lag hinge is frictionless—and gives the fascinating approximation that the maximum *fatigue* torsional moment due to "double bending" will be

(2.208)

$$\text{maximum flap-lag } T_x = \pm\left[-\frac{1}{9}\left(\frac{1-4\mu}{1+\frac{4}{3}\mu}\right)+\frac{2}{3}\mu^2\right]\left(\frac{\rho cR}{m_b}\right)\left(\frac{C_{\ell max}}{2}\right)Q_R(1-x)$$

where the restraining torque at the drag hinge (Q_R) is that value found from the chordwise stress analysis summarized in Table 2-10 (i.e., $Q_R = 4{,}360$ foot-pounds).

To arrive at the total fatigue moments in torsion, Cierva simply adds up the four contributors. He assumes no dynamic amplification and then distributes the torsion between spar and superstructure saying, "the [spar's] relief due to superstructure will be taken into consideration by multiplying the values above by (1-1/2)." Then he writes, "we have finally" the table (reproduced here as Table 2-11) where (J) is the spar polar moment of inertia about the spar neutral axis. The torsion

stress is calculated in the conventional manner [102] as

(2.209) Torsion shear stress

$$\tau_x = \frac{(\text{Torsion Moment})(\text{Distance to outermost fiber})}{J}.$$

2.9 BLADES

Table 2-11. The Cierva C.30A Spar Torsion Fatigue Stress Analysis [12]

Parameter	Point A r/R = 0.093	Point B r/R = 0.186	r/R = 0.3	r/R = 0.4	r/R = 0.5	r/R = 0.6	r/R = 0.7
Max + Moment (in.-lbs)	1,880	1,720	1,500	1,290	1,070	845	620
Max – Moment (in.-lbs)	–2,400	–2,190	–1,910	–1,660	–1,400	–1,120	–810
Spar J ($in.^4$)	0.261	0.18	0.18	0.18	0.18	0.18	0.18
Max + Shear Stress ($lb/in.^2$)	5,400	7,150	6,250	5,400	4,500	3,520	2,580
Max – Shear Stress ($lb/in.^2$)	–6,900	–9,110	–7,950	–6,900	–5,830	–4,650	–3,370

2.9.8 C.30A Total Blade Stresses

The concluding steps in the Cierva stress analysis of the spar are reasonably conventional, but he does take the most conservative path. The resultant flapwise and chordwise stresses are first determined "assuming alternate maximums occur simultaneously." To this table of plus and minus maximum stresses, he adds in the steady stress due to centrifugal force calculated at the maximum design rotor speed of 30.8 radians per second and accounts for the torsion stress (which is minor).

There is an end to the process Cierva described as "exceedingly elaborate" and where "a number of simplifying assumptions have to be made which are not of a nature that could substantially alter the results." The *conclusion to the process* begins with the final summary (Table 2-12) of the steady and alternating (fatigue) stresses [see Eq. (2.190)].

Table 2-12. The Cierva Summary of C.30A Spar Steady and Fatigue Stresses [12]

Parameter	Point A r/R = 0.093	Point B r/R = 0.186	r/R = 0.3	r/R = 0.4	r/R = 0.5	r/R = 0.6	r/R = 0.7
Steady Stress (lb/in.^{2})	20,390	35,300	34,025	30,200	26,525	22,125	16,350
Fatigue Stress (lb/in.^{2})	±30,650	±27,600	±19,825	±20,900	±21,825	±21,925	±22,150

Now Cierva's thoroughness really comes to the forefront. He completes the stress analysis by introducing four factors that raise the stresses summarized in Table 2-12. In paragraph 4 of the example from Appendix IV used for the C.30A blade [12], he writes [my comments are in brackets]:

"Fatigue Factor K_1. Appendix III gives for nickel-chrome steels with a final stress of 85 tons [British tons of 2,200 pounds per ton] (by extrapolation) a ratio of $P_f/P_s = 0.46$ [fatigue stress to steady stress]. As the ratio P_y/P_s [yield stress over ultimate stress, in British tons] is taken as $65/85 = 0.765$, the factor $K_1 = 0.765/0.46 = 1.66$." [This factor accounts for the damage fatigue can do when the alternating stress is occurring around a high steady stress.]

"Form Factor K_2. There are holes well spaced, 3/16 [inch in] diameter, in the [spar] horizontal plane. They represent a decrease in section [moment of inertia] of about 8 %. For BM [bending moment] in a horizontal plane, they represent a decrease in the Z [see Table 2-10] of the section of about 25 %. As the centrifugal tension represents about 50 % of the stress and the BM are in planes oblique to the horizontal, a reasonable assumption is to take a drop of strength of about 15 % (as done in the case of stresses on the ground). As fatigue stresses are very important, however, a factor K_2 = 1.3 will be taken." [Each hole creates local stress risers that cannot be ignored.]

"Safety or Material Factor K_3. It will be taken, as stated, as equal to 1.5, since the material is consider as reliable." [Material imperfections and manufacturing defects are a very real consideration.]

"Load Factor K_4. Taken equal to 1."

[Cierva has calculated loads at an extreme point in the flight envelope, which makes 1 reasonable in my opinion.]

With these reasonable factors in hand, Cierva applies the factors to see if the sum of steady and fatigue stresses exceed the maximum allowable stress (65 British tons per square inch or 145,000 pounds per square inch). He calculates this absolute maximum stress as

(2.210) $\text{Absolute maximum stress} = K_2 \times K_3 \times [\text{Steady} + K_1 \times \text{Fatigue}] \times K_4$ and gives the results tabulated and also graphed, as shown in Fig. 2-91.

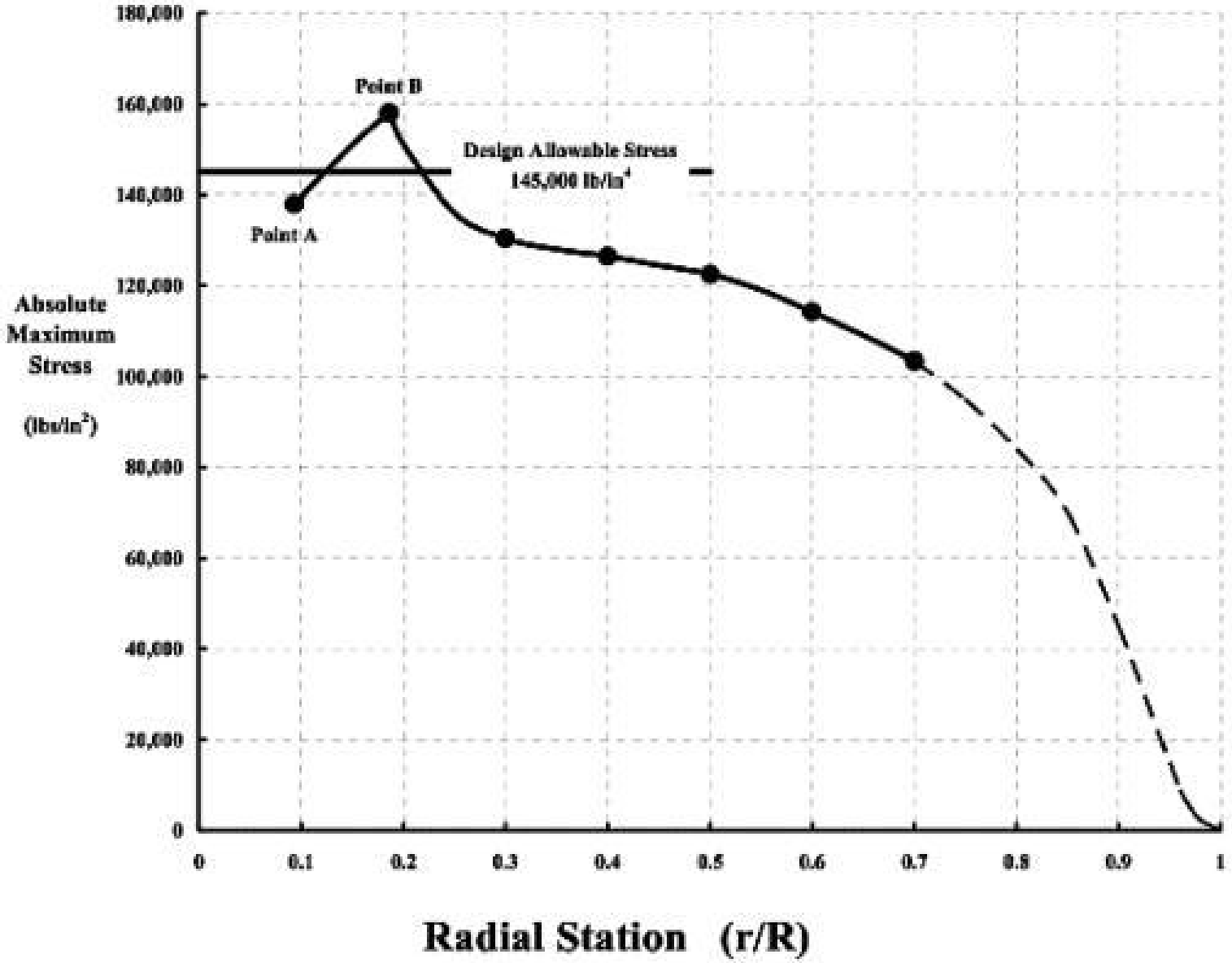

Fig. 2-91. The maximum absolute stress results Cierva included in his *Theory*.

2.9 BLADES

In reviewing this summarizing result, Cierva writes of the C.30A blade analysis that:

"It will be observed [from Fig. 2-91] that for a short length about Point B the factored stress exceeds the value P_y = 1 45000 lbs/in^2 so that, strictly speaking, the blade is under strength by the criterion laid down in the Theory [12]. As, however, the maximum value of V/V_t in horizontal flight, fully loaded, is very appreciably less than the value V/V_t = 0.5 maximum for which the assumptions of the Theory hold, and as the stresses below that value [μ = 0.5] decrease very appreciably, the final factor of 0.92 [a negative margin of calculated stress divided by P_y, the yield stress] can be accepted as satisfactory, but in new designs it is recommended to lengthen the tapered part of the spar to about 0.25 R (for similar blades) which, as can readily be appreciated in Fig. 2-91, would result in an almost uniform distribution of stresses over the first quarter of the tube."

2.9.9 Closing Remarks

The Cierva rotor blade loads and stress

analysis has come down through the decades. Perhaps not in the "black and green volumes" that Owen recalled [112] or in the somewhat illegible two volumes edited by James Bennett that Dick Carlson gave me. But with the very abbreviated preceding discussion, I believe you will agree that Juan de la Cierva knew exactly what he was doing in the engineering world, not just in the world of invention, building, flying, licensing, and selling his own Autogiros.

I can think of no better way to conclude this introduction to rotor blades than with those words written by the Pitcairn chief engineer, Agnew Larsen, in his historical recollections [49] published in the first volume of the Journal of the American Helicopter Society. He passes on two thoughts, the first of which reads as follows:

"At the very start of the American autogiro engineering efforts of both Pitcairn and Kellett, it became apparent that little could be done without some working

knowledge of a "theory" for the whole procedure. Consequently, early in the Spring of 1929, a hurried trip was made to England by Harold Pitcairn, the author [Larsen], and Jean Nicol, the clever designer of the M & T Design Co., to acquire this basic design information. At this time Mr. Pitcairn urged Cierva to direct his efforts toward the accumulation and collating of his vast supply of technical data for condensation into a workable volume, The [Engineering] Theory of the Autogiro [11]. Later in the fall of 1929, when Cierva made his first trip to this country, he spent much time on it, with Paul Stanley as his assistant. The momentous work was compiled and copyrighted, and privately published for the benefit of licensees like Kellett, Pitcairn's manufacturing company, and for the use of proper personnel of the Department of Commerce, NACA, Air Force, and Bureau of Aeronautics. Without this authoritative guide, no progress could have been made, nor could the government authorities have granted type certificates required for manufacture of autogiros. The Autogiro Company of America's recommendations for Approved Type Certification were endorsed by them."

Mr. Larsen could easily have added praise for Cierva's second volume, *Theory of Stresses on Autogiro Rotor Blades*.

2.9 BLADES

The second thought from Agnew Larsen is even more important because he wrote:

"The direct control of all the original smaller models, up to a gross weight of approximately 2500 lbs., as in the Kellett KD-1, KD-1B and KD-2, proved to work very well indeed. In the still smaller models, like the Pitcairn PA-22, the British Cierva C-30, and the French LePere jobs, this direct control was, if anything, even better. The chief difficulties in all of these direct control ships, however, was an uncomfortable characteristic vertical bouncing, or a three-per- rev vibration of the whole aircraft, to a greater or lesser degree. This was a new and most disturbing annoyance which grew out of the more rigid, though hinged, [three] rotor blades owing to the absence of the droop support cables. The final solution of this problem required some two or three dozen different, direct-control rotors (tested internationally in England, France, and America) and between three to four years, before ultimate satisfactory

solution. The cue to this solution lay in the fact that this bouncing fault was virtually non-existent in the two most flexible rotors, out of a total of twenty-six that were methodically analyzed. This led to step-tapered steel spars and the ultimate elimination of bouncing in all rotors where proper considerations of bending flexibility were applied."

Clearly, a solution to autogyro vibrations—caused by the more advanced, three-bladed rotor system—was found by trial and error.

191

192

2.10 VIBRATION

Vibration has been, and unfortunately continues to be, a very detracting feature of rotorcraft. The magnitude of vibration, say at the pilot seat, is an immediate question asked of a test pilot at the end of a first forward flight of

a prototype. After first flight, there has always been (at least in my experience) a vigorous effort to reduce vibration throughout the machine, until, finally, the first acceptable production aircraft is ready for delivery. Thereafter, incremental product improvement frequently includes a program aimed at reducing vibration even further. In retrospect, autogyro vibration or "vertical bouncing" as Agnew Larsen called it, was a relatively minor vibration problem compared to what many modern rotorcraft have encountered. Cierva wrote in his 1935 paper [5] that:

"Perhaps the most irritating of the secondary difficulties met with in the autogiro developments have been those of a dynamical [vibration] nature."

I believe that a large number of rotorcraft engineers would agree that Cierva's words are a considerable understatement.

The Agnew Larsen recollection [49]

that vertical vibration "was virtually eliminated" with "the two most flexible rotors" is a direct indication of how important it is to tune the blades of a three-bladed rotor system well away from a 3-per-rev natural frequency. As you learned in the section on blades and can see from Fig. 2-93, the early four-bladed rotor systems, with their cable support for droop, were "rigid" or "stiff." Later, three-bladed systems were, as Larsen says, "flexible." I have put quotes around the words *rigid, stiff,* and *flexible* because they are extremely inexact engineering terms with which to describe blades— or fuselages. These words, *rigid, stiff,* and *flexible* have no place in the study of vibration.

Vibration depends on the proximity of natural frequencies to the frequency of the applied forces and moments, and the magnitude of the applied forces and moments. To illustrate this point, remember the classic dynamics problem given in the first chapter of any text book [115] used to study vibration. The fundamental single-degree-of-freedom problem, Fig. 2-92, shows a mass (m), in

slugs, hanging on a spring attached to an overhead beam (A). The spring stiffness is (k) in pounds per foot. The mass is also attached to the beam with a dashpot (a damper). The units of the damping constant (c) are pounds per foot per second. The system is acted on by an oscillating force ($P_o \sin \omega t$) or, more generally, ($F_S \sin \omega t + F_C \cos \omega t$). The mass shakes up and down a vertical distance (x) governed by the classic F = ma equation:

$$(2.211) \quad m\frac{d^2x}{dt^2} + c\frac{dx}{dt} + kx = F_s \sin \omega t + F_C \cos \omega t .$$

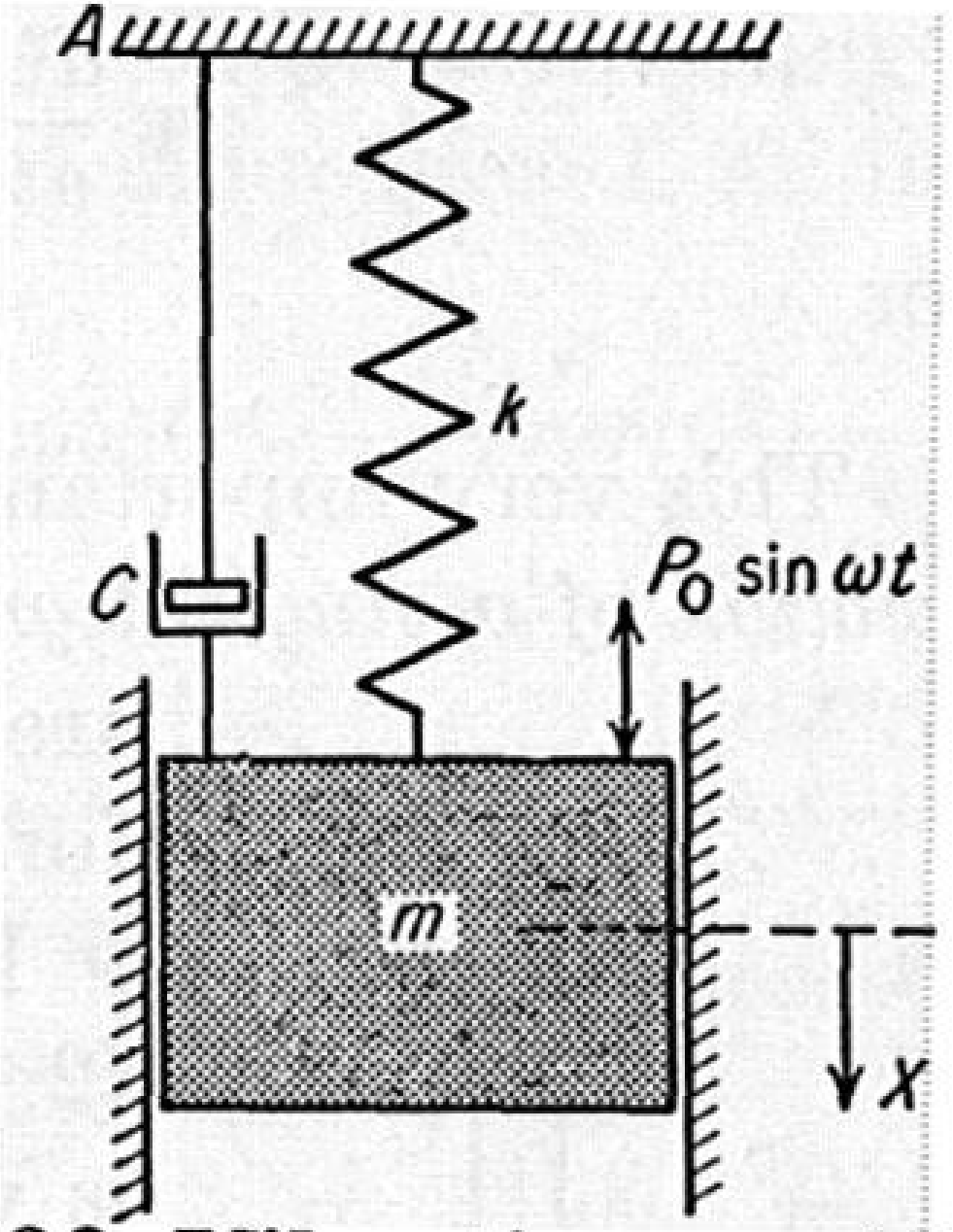

Fig. 2-92. Vibration problem.

2.10 VIBRATION

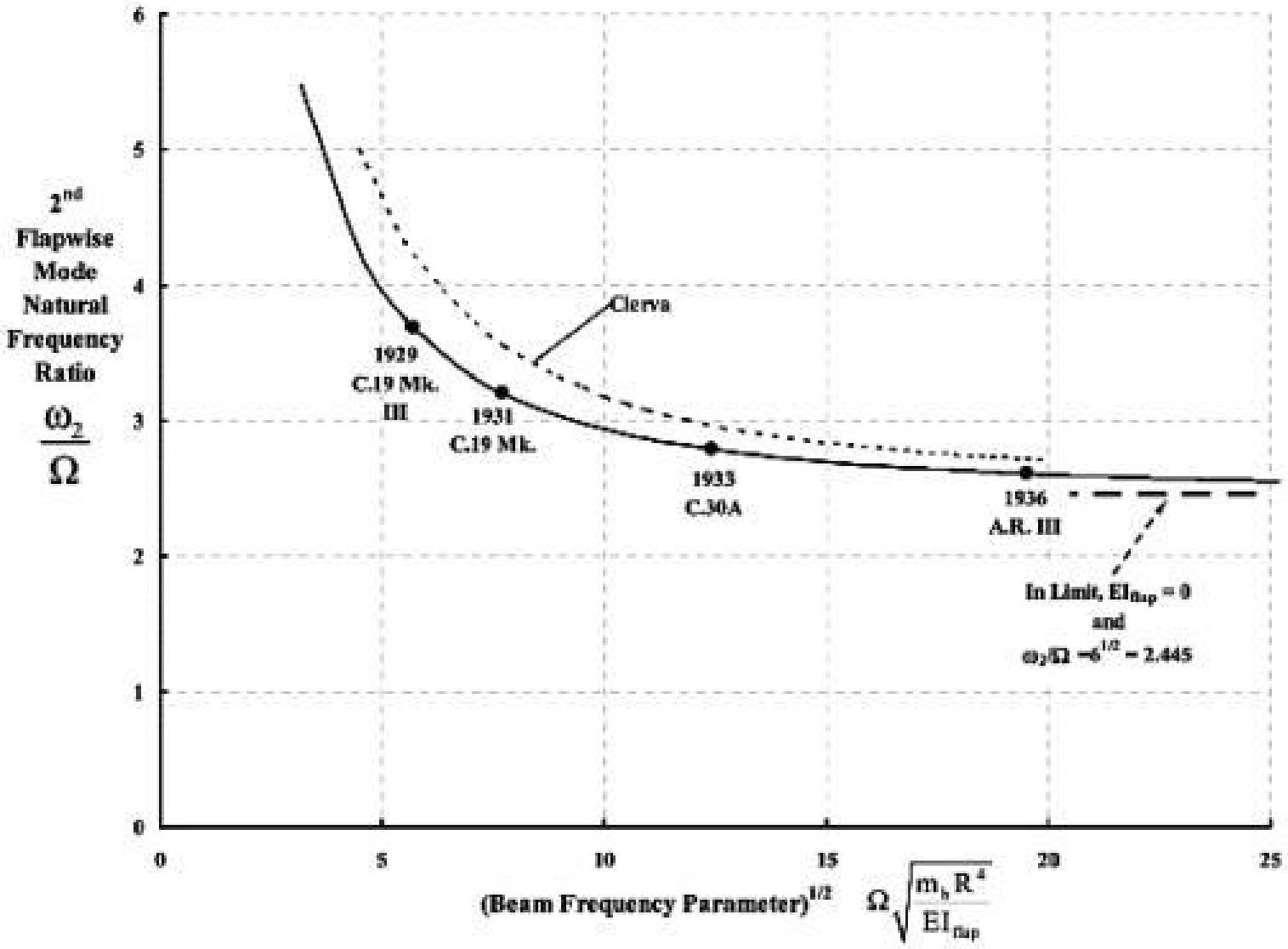

Fig. 2-93. Frequency ratio for the second flapwise mode of a uniform beam.

The classic solution to this second-order differential equation gives mass displacement (x) in feet as a function of time (t) in seconds.

The solution is, quite simply

$$(2.212)\quad x_t = \left[\frac{F_S\left(k-m\omega^2\right)+F_C\left(c\omega\right)}{\left(k-m\omega^2\right)^2+\left(c\omega\right)^2}\right]\sin\omega t+\left[\frac{F_C\left(k-m\omega^2\right)-F_S\left(c\omega\right)}{\left(k-m\omega^2\right)^2+\left(c\omega\right)^2}\right]\cos\omega t\,.$$

The mass experiences an acceleration that varies with time. This acceleration, which is the second derivative of displacement with respect to time, is

$$(2.213)\quad \left(\frac{d^2x}{dt^2}\right)_t = -\omega^2 x_t$$

$$= -\omega^2\left\{\left[\frac{F_S\left(k-m\omega^2\right)+F_C\left(c\omega\right)}{\left(k-m\omega^2\right)^2+\left(c\omega\right)^2}\right]\sin\omega t+\left[\frac{F_C\left(k-m\omega^2\right)-F_S\left(c\omega\right)}{\left(k-m\omega^2\right)^2+\left(c\omega\right)^2}\right]\cos\omega t\right\}.$$

At some point in time, the acceleration will be a maximum, either positive or negative. The magnitude of this maximum acceleration is

$$(2.214)\quad \left(\frac{d^2x}{dt^2}\right)_{max} = \pm\frac{\omega^2\sqrt{F_s^2+F_c^2}}{\sqrt{\left(k-m\omega^2\right)^2+(c\omega)^2}}.$$

Now, suppose you are sitting on the mass, seat belt on, but assume your mass is trivial compared to the mass of the block (m) you are sitting on. Then your body will feel a maximum force (F_{max}) equal to

$$(2.215)\quad \text{Max. body force} = F_{max} = \frac{W_{body}}{g}\left(\frac{d^2x}{dt^2}\right)_{max} = \frac{W_{body}}{g}\left[\pm\frac{\omega^2\sqrt{F_s^2+F_c^2}}{\sqrt{\left(k-m\omega^2\right)^2+(c\omega)^2}}\right].$$

This maximum body force is a vibratory force and is a fraction of your weight (W_{body}) and, therefore, a fraction of the gravity constant (g). You could, therefore, express your vibratory environment as

$$(2.216)\quad \frac{F_{max}}{W_{body}} = \frac{1}{g}\left(\frac{d^2x}{dt^2}\right)_{max} = \frac{1}{g}\left[\pm\frac{\omega^2\sqrt{F_s^2+F_c^2}}{\sqrt{\left(k-m\omega^2\right)^2+(c\omega)^2}}\right].$$

For example, suppose the vibration is due to 3-per-rev rotor loads. Assume a rotor speed (say for the Cierva C.30A) of 180 revolutions per minute, which is 3 revolutions, or cycles, per second. Then the 3-per-rev rotor vibratory load is oscillating at 9 cycles per second or 18π radians per second. For this

example then, $\omega=18\pi$.

Now imagine the block you are sitting on is really the Cierva C.30A Autogiro weighing 1,500 pounds, which is a mass (m) of 46.62 slugs. Suppose the rotor shaking force is one-tenth of the gross weight (i.e., $F_S = F_C = 150$ pounds), and assume that the spring has a spring constant (k) of 43,750 pounds per foot. For the sake of discussion, assume there is no damping (i.e., $c = 0$). Using Eq. (2.216) with this information you calculate that

$$\frac{F_{max}}{W_{body}} = \frac{1}{g}\left[\pm\frac{(18\pi)^2\sqrt{150^2+150^2}}{\sqrt{\left(43{,}750-46.62(18\pi)^2\right)^2+(0\times 18\pi)^2}}\right] = \frac{6.4348\ \text{ft/sec}^2}{32.174\ \text{ft/sec}^2} = 0.2g. \quad (2.217)$$

Note that resonance occurs in this classic dynamics problem when (2.218)

$$\left(k-m\omega^2\right)\equiv 0 \quad \text{or} \quad \sqrt{\frac{k}{m}}=\omega.$$

For this example

$$\sqrt{\frac{k}{m}} = \sqrt{\frac{43,750}{46.62}} = 932 \gg \omega = 18\pi . \quad (2.219)$$

2.10 VIBRATION

The conclusion from this example is that you are experiencing a 0.2g vibration at 3 per rev, which, by the way, is much worse than a "most disturbing annoyance" as Agnew Larsen described. In fact, many rotorcraft test pilots have returned from their first forward flight of a new prototype with much more forceful words, such as "intolerable," "totally unacceptable," "couldn't read the instruments," "everything is a blur," "won't sell," and "we've got one hell

of a vibration problem." To a chief engineer (like Cierva), a test pilot might be less restrained. Of course, when seen in print, Cierva's words "most irritating" might be very appropriate.

Keep in mind that the pilot is not the only one that is unhappy in this example. The beam is reacting to the two forces shown in Fig. 2-92 . The spring force is the spring constant times the displacement (x), and the damper force is (c dx/dt). Taken together, the beam is providing a reacting force (R_t) in pounds that amounts to

$$R_t = \left\{\frac{F_S\left[k\left(k-m\omega^2\right)+(c\omega)^2\right]+F_C\left[cm\omega^3\right]}{\left(k-m\omega^2\right)^2+(c\omega)^2}\right\}\sin\omega t + \left\{\frac{F_C\left[k\left(k-m\omega^2\right)+(c\omega)^2\right]-F_S\left[cm\omega^3\right]}{\left(k-m\omega^2\right)^2+(c\omega)^2}\right\}\cos\omega t \quad (2.220)$$

This reactive force, at some point in time, will reach a maximum, either positive or negative, of

(2.221) $$R_t = \pm\sqrt{\frac{\left(k^2 + c^2\omega^2\right)\left(F_s^2 + F_c^2\right)}{\left(k - m\omega^2\right)^2 + \left(c\omega\right)^2}}.$$

Using the parameter values from the preceding example, you will calculate that the reactive force is slightly greater than ±500 pounds. This vibrating force, at 3 per rev, requires careful attention to the structure because significant fatigue damage will occur over the life of the aircraft. Just consider the fact that 25 years—or longer—is not uncommon for a service life. Rotorcraft, say on average, fly 500 hours a year. This means 12,500 hours will be accumulated on the structure over a typical service life. With a rotor speed of 180 revolutions per minute, a 1-hour flight accumulates 10,800 cycles per hour at one per rev. However, this ±500-pound load is occurring at 3 per rev, which means 32,400 cycles per flight hour are accumulated. After 25 years, portions of the airframe will have accumulated (32,400 times 12,500 equals) 400 million cycles (i.e., 400×10^6 cycles) and each cycle could be at ±500 pounds on the

1,500-pound-gross-weight Cierva C.30A.[42]

---

[42] Many rotorcraft structural elements can be designed to withstand a million to 10-million cycles, but I, personally, do not believe any material is suitable for 400-million cycles of fatigue loading. It is simply a question of how many times can you bend a paperclip before it cracks or breaks.

2.10 VIBRATION

2.10.1 C.30 Vibration Background

The preceding example adapts the classic single-degree-of-freedom vibration problem to the world of autogyros. In many ways, the example is somewhat extreme. Consider the more practical vibration problem presented in Fig. 2-94 . To keep things reasonably simple, I have assumed that the C.30

three-bladed rotor system only applies a vertical vibratory force (F_Z), and a fore and aft, or longitudinal, vibratory force (F_X) . Both forces are in pounds and are applied at the rotor hub . Following Fig. 2-23, the vertical force acts behind the aircraft center of gravity (c.g.), a distance (c) in feet; the longitudinal force acts above the c.g., a distance (a) in feet. The pilot sits in the aft cockpit in a seat located (d) feet behind the c.g.

The vertical force will not only shake the aircraft up and down, but this vibratory force will also pitch the aircraft nose up and nose down because this force acts behind the aircraft c.g. The longitudinal force will shake the aircraft fore and aft (which I will ignore) and also pitch the aircraft because it acts above the c.g. The pilot will feel the combination of vertical displacement (Z_{cg}) of the c.g. and angular displacement (Θ_{cg}) about the c.g. Because he sits behind the c.g. a distance (d), his vertical

displacement (Z_{pilot}) will be

$$Z_{pilot} = Z_{cg} - d(\Theta_{cg}) \tag{2.222}$$

where a positive vertical displacement is upwards, and a positive angular displacement is nose up. The pilot will, therefore, feel an acceleration of

$$\frac{d^2 Z_{pilot}}{dt^2} = \frac{d^2 Z_{cg}}{dt^2} - d\frac{d^2 \Theta_{cg}}{dt^2}. \tag{2.223}$$

Now, think in terms of $F = ma$, and include in your thinking $I\ d^2\theta/dt^2 = M$, because there is a rotation. In this case, the moment of inertia (I) is the aircraft moment of inertia (I_{AC}) about the center of gravity and is in slug-feet squared. Consider Fig . 2-94 for the autogyro versus the classic vibration problem of Fig. 2-92. First off, there is no

obvious spring. Any up and down motion of the aircraft c.g. will mean that the hub goes up and down an equal amount because the autogyro structure is, for all intents and purposes, "rigid." Therefore, vertical displacement will create a vertical velocity and vertical acceleration that each blade feels. This is also true for pitching motion.

Similarly, there is no obvious damper to include in the autogyro problem. Thus, any spring or damper must appear in the rotor blade forces and moments behavior. This means that any spring or damper is included in the vibratory forces acting at the hub (i.e., F_Z and F_X). With this logic, the linear and angular accelerations at the aircraft c.g. become simply

$$\frac{d^2 Z_{cg}}{dt^2} = \frac{F_Z}{m_{AC}} \tag{2.224}$$

and $$\frac{d^2\Theta_{cg}}{dt^2} = \frac{-cF_Z + aF_X}{I_{AC}}$$

Note that in Eq. (2.224), I have assumed the vertical force to be positive upwards and that a positive longitudinal force is aft. The acceleration that the pilot feels is now known in terms of the two forces acting at the rotor hub because

2.10 VIBRATION

(2.225)

$$\frac{d^2Z_{pilot}}{dt^2} = \frac{F_Z}{m_{AC}} - d\left(\frac{-cF_Z + aF_X}{I_{AC}}\right) = F_Z\left(\frac{1}{m_{AC}} + \frac{dc}{I_{AC}}\right) - F_X\left(\frac{da}{I_{AC}}\right)$$

You can see here that a vertical shaking force

will amplify the acceleration that the pilot feels because the nose-down motion of the aircraft will raise the pilot just as the linear vertical motion does. At this point, it is not clear whether an upward vertical force will be accompanied by a longitudinal force in the forward or aft direction. With a longitudinal force of the right magnitude acting aft, the pilot might feel a rocking motion rather than a "vertical bounce."

There is a little more that can be deduced about three-bladed autogyro vibration before you (and the pioneers) become stymied. The step is to assume the vertical and longitudinal forces to be

$$F_Z = F_{ZS} \sin \omega t + F_{ZC} \cos \omega t$$
$$F_X = F_{XS} \sin \omega t + F_{XC} \cos \omega t \tag{2.226}$$

and, therefore, the acceleration at the pilot seat,

in feet-per-second squared, becomes (2.227)

$$\frac{d^2 Z_{pilot}}{dt^2} = \left[\frac{F_{ZS}}{m_{AC}} - d\left(\frac{-cF_{ZS} + aF_{XS}}{I_{AC}}\right)\right]\sin \omega t + \left[\frac{F_{ZC}}{m_{AC}} - d\left(\frac{-cF_{ZC} + aF_{XC}}{I_{AC}}\right)\right]\cos \omega t \ .$$

Let me now repeat the vibration calculation. From the approximate geometry, the rotor longitudinal force acts 4 feet above the c.g., so a = + 4; the vertical force acts 0.5 feet behind the c.g., so c = + 0.5; and the pilot seat is 3.5 feet behind the aircraft c.g., so d = + 3.5. The C.30A second moment of inertia in pitch (I will guess) is roughly 1,000 slug-feet squared, so I_{AC} = 1,000, and at a gross weight of 1,500 pounds, the aircraft mass (m_{AC}) is 46.62 slugs. As in the classic problem, assume that the rotor hub forces act at 3 per rev, so $\omega = 18\pi$ radians per second. With no knowledge about the forces at this time, I will assume that

$$F_{ZS} = F_{ZC} = 150 \text{ lbs} \quad \text{and} \quad F_{XS} = F_{XC} = 15 \text{ lbs}$$

which leads to the result that

(2.228)

$$\frac{d^2Z_{pilot}}{dt^2} = \left[3.22 - (-0.0525)\right]\sin \omega t + \left[3.22 - (-0.0525)\right]\cos \omega t$$

The pilot will feel a maximum vibratory acceleration of (2.229)

$$\left(\frac{d^2Z_{pilot}}{dt^2}\right)_{max} = \pm\sqrt{3.28^2 + 3.28^2} = \pm 4.64 \ \text{ft/sec}^2 = \pm 0.14\text{g} \ .$$

The crux of the "vertical bounce" problem Agnew Larsen referred to lies, of course, in predicting the hub forces (and moments).[43]

---

[43] In the Cierva C.30, the flapping hinge, located a the 0.00788R radial station, permits hub moments to be ignored in this discussion.

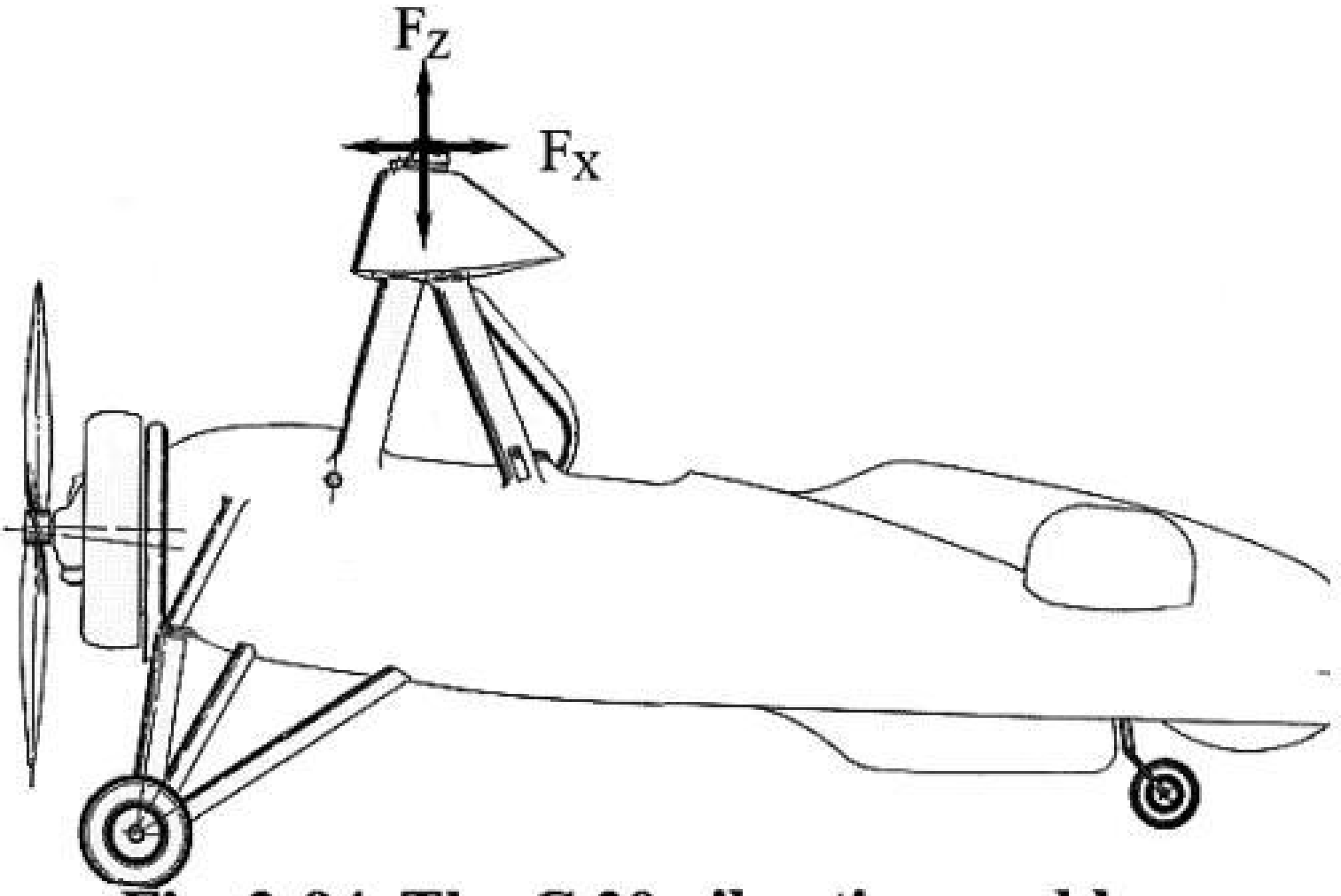

Fig. 2-94. The C.30 vibration problem.

2.10.2 C.30 Vibratory Hub Loads

Consider first the vertical force (F_Z) acting at the flapping hinge. From Fig. 2-84 you can see that centrifugal force cannot create a vertical force. Therefore, only the

blade lift elements (dL) and blade inertia elements (dI) need be considered. Then, the vertical force for one blade is simply

(2.230)

$$\text{One blade } F_Z = \int_0^R d\left(L_{\eta,t}\right) - \int_0^R d\left(I_{\eta,t}\right) = \int_0^R \left(\frac{dL_{\eta,t}}{d\eta}\right) d\eta - \int_0^R \left(m_\eta\right)\left(\frac{\partial^2 Z_{\eta,t}}{\partial t^2}\right) d\eta .$$

Since the blade element loads are known to be periodic (i.e., harmonic), Eq.(2.230) can be rewritten in terms of azimuth with the substitutions $\psi = \Omega t$ or $\frac{1}{dt^2} = \Omega^2 \frac{1}{d\psi^2}$ to give

(2.231) One blade

$$F_Z = \int_0^R \left(\frac{dL_{\eta,\psi}}{d\eta}\right) d\eta - \int_0^R \left(m_\eta\right)\Omega^2\left(\frac{\partial^2 Z_{\eta,\psi}}{\partial \psi^2}\right) d\eta .$$

A solution to the flapwise bending moment problem, Eqs. (2.196) through (2.201), provides all the information needed to calculate the vibratory vertical force at the hub for one blade.

2.10 VIBRATION

The discussion of blades, Section 2.9, included an example of flapwise bending moments calculated with two modern theories. One theory is contained in Appendix H; the other, more comprehensive theory, is embodied in the computer program called CAMRAD [109]. The flapwise bending stress calculated with the two solution methods led to Fig. 2-87. Those two solutions at Cierva's design condition also provide the comparison of vibratory, vertical force (F_Z) at the hub for *one blade*, which follows:

$$\text{Appendix H} \quad F_Z = 991 - 687\cos\psi - 322\sin\psi - 147\cos 2\psi - 56\sin 2\psi$$

$$-51\cos 3\psi - 5 \qquad (2.232)$$

$\sin 3\psi - 32\cos 4\psi - 17\sin 4\psi$

$-20\cos 5\psi + 5\sin 5\psi - 9\cos 6\psi + 1\sin 6\psi$

and

CAMRAD $F_z = 984 - 880\cos\psi - 1260\sin\psi - 170\cos 2\psi + 214\sin 2\psi$

(2.233) $-76\cos 3\psi - 45\sin 3\psi - 9\cos 4\psi - 12\sin 4\psi$.

$-0\cos 5\psi + 14\sin 5\psi + 17\cos 6\psi + 9\sin 6\psi$

These two results show just how large the difference between predicted vibratory vertical hub loads can be . The vertical vibratory load amplitudes of the first six harmonics are shown in Fig. 2-95 . The amplitudes are calculated in the conventional manner as

(2.234) Amplitude $F_n = \sqrt{F_{nC}^2 + F_{nS}^2}$

Note that I have used a semilog scale to display the amplitudes in Fig. 2-95. An extremely rough rule of thumb is that the amplitude decreases as the harmonic (n per rev) squared. The contrast, when shown graphically as in Fig. 2-95, is a clear indication of just how difficult a vibration problem the autogyro pioneers were facing and how little could be learned from theory of the era.

The vibratory vertical hub load for one blade is not the whole story, of course . The total hub load for three blades is the answer sought. The total vertical force created by three blades was discussed earlier in Section 2.8. The process of adding the vertical forces from three blades together is quite simple. All that is required is the assumption that each blade in the set has the identical one-blade vertical vibratory

force description in a Fourier series. This means the total three-bladed vertical hub load is computed from

$$(2.235)\quad F_Z = F_{Z\ \text{Blade 1}}(\text{calculated at } \psi) + F_{Z\ \text{Blade 1}}(\text{cal. at } \psi + 120^\circ) + F_{Z\ \text{Blade 1}}(\text{cal. at } \psi + 240^\circ)$$

and the very explicit result of the trigonometry is

$$(2.236)\quad F_Z = 3\left[F_o + F_{Z3C} \cos 3\psi + F_{Z3S} \sin 3\psi + F_{Z6C} \cos 6\psi + F_{Z6S} \sin 6\psi + \text{etc}\right].$$

Using Appendix H and the CAMRAD

Fourier series for one blade ($F_{Z\ \text{Blade}\ 1}$) from Eqs. (2.232) and (2.233), the immediate results for the Appendix H solution are

(2.237)

$$\text{Appendix H}\quad F_Z = 3[991 - 51\cos 3\psi - 5\sin 3\psi - 9\cos 6\psi + 1\sin 6\psi]$$
$$= 2{,}973 - 153\cos 3\psi - 15\sin 3\psi - 27\cos 6\psi + 3\sin 6\psi$$

and similarly, for the CAMRAD solution

(2.238) $\text{CAMRAD}\quad F_Z = 2{,}952 - 228\cos 3\psi - 135\sin 3\psi + 51\cos 6\psi + 27\sin 6\psi$.

It is customary when conveying vibratory forces and moments to remove the steady force (the zero harmonic, F_o in this example) from the final results. Therefore, in Fig. 2-96 you see a comparison of the two modern-theory views about the vertical

vibratory hub load for the 1,500-pound-gross-weight C.30 Autogiro at an advance ratio of 0.5 during a 2-g pull-up.

With this background in hand, let me proceed to a more practical example. I say more practical because vibration during a 2-g pull-out at an advance ratio of 0.5 (i.e., the extreme flight condition Cierva chose for stressing the rotor system) can be expected to exceed vibration in cruise flight. Therefore, consider the cruise situation where the flight speed is 110 miles per hour, and the rotor speed is 200 revolutions per minute. Assume the C.30A is at a gross weight of 1,500 pounds. For this example, CAMRAD II [109], a most modern theory, is far superior to the calculator provided in Appendix H. Therefore, CAMRAD II is the source of the calculated vibratory forces (F_Z and F_X) shown in Fig. 2-94, tabulated by harmonic in Table 2-13, and required by Eq. (2.225), which is repeated here for convenience

(2.225)

$$\frac{d^2 Z_{pilot}}{dt^2} = \frac{F_Z}{m_{AC}} - d\left(\frac{-cF_Z + aF_X}{I_{AC}}\right) = F_Z\left(\frac{1}{m_{AC}} + \frac{dc}{I_{AC}}\right) - F_X\left(\frac{da}{I_{AC}}\right)$$

where, again for the Cierva C.30A autogyro, the rotor longitudinal force (F_X) acts 4 feet above the c.g., so a = + 4; The vertical force (F_Z) acts 0.5 feet behind the c.g., so c = + 0.5; and the pilot seat is 3.5 feet behind the aircraft c.g., so d = + 3.5 . The C.30A second moment of inertia in pitch is roughly 1,000 slug-feet squared, so I_{AC} = 1,000, and at a gross weight of 1,500 pounds, the aircraft mass (m_{AC}) is 46.62 slugs.

2.10 VIBRATION

10,000

Appendix I
CAMRAD

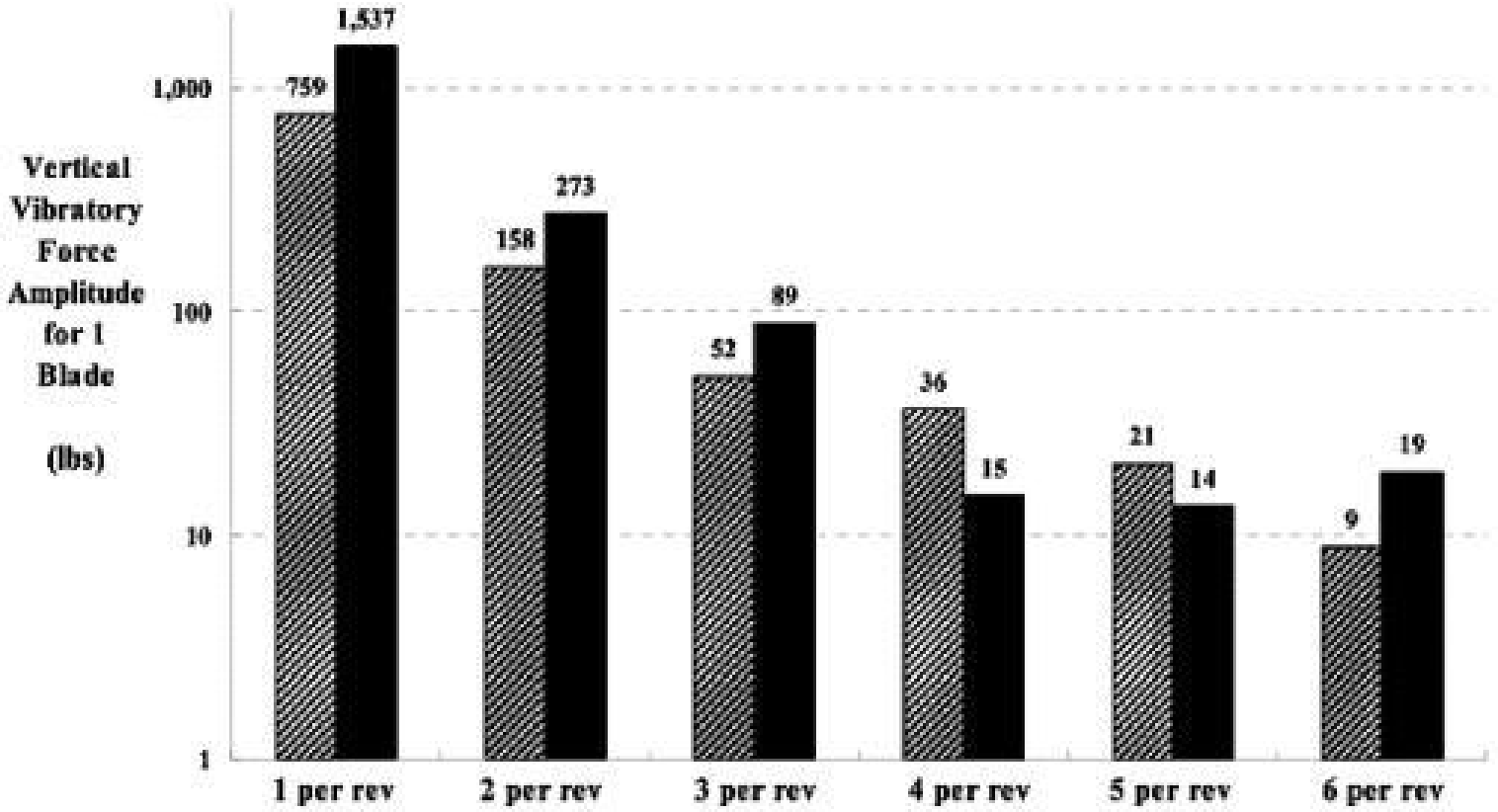

Fig. 2-95. The vertical vibratory force of one blade in a three-bladed rotor system.

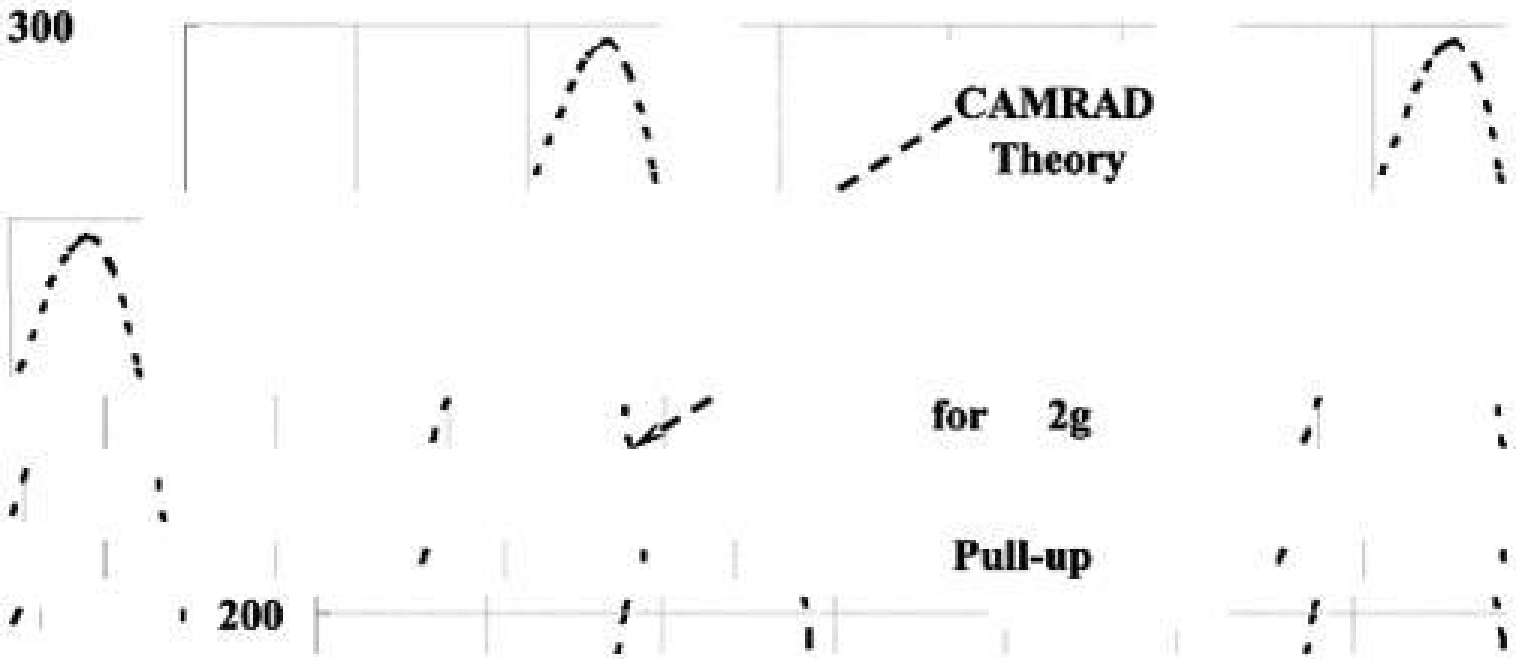

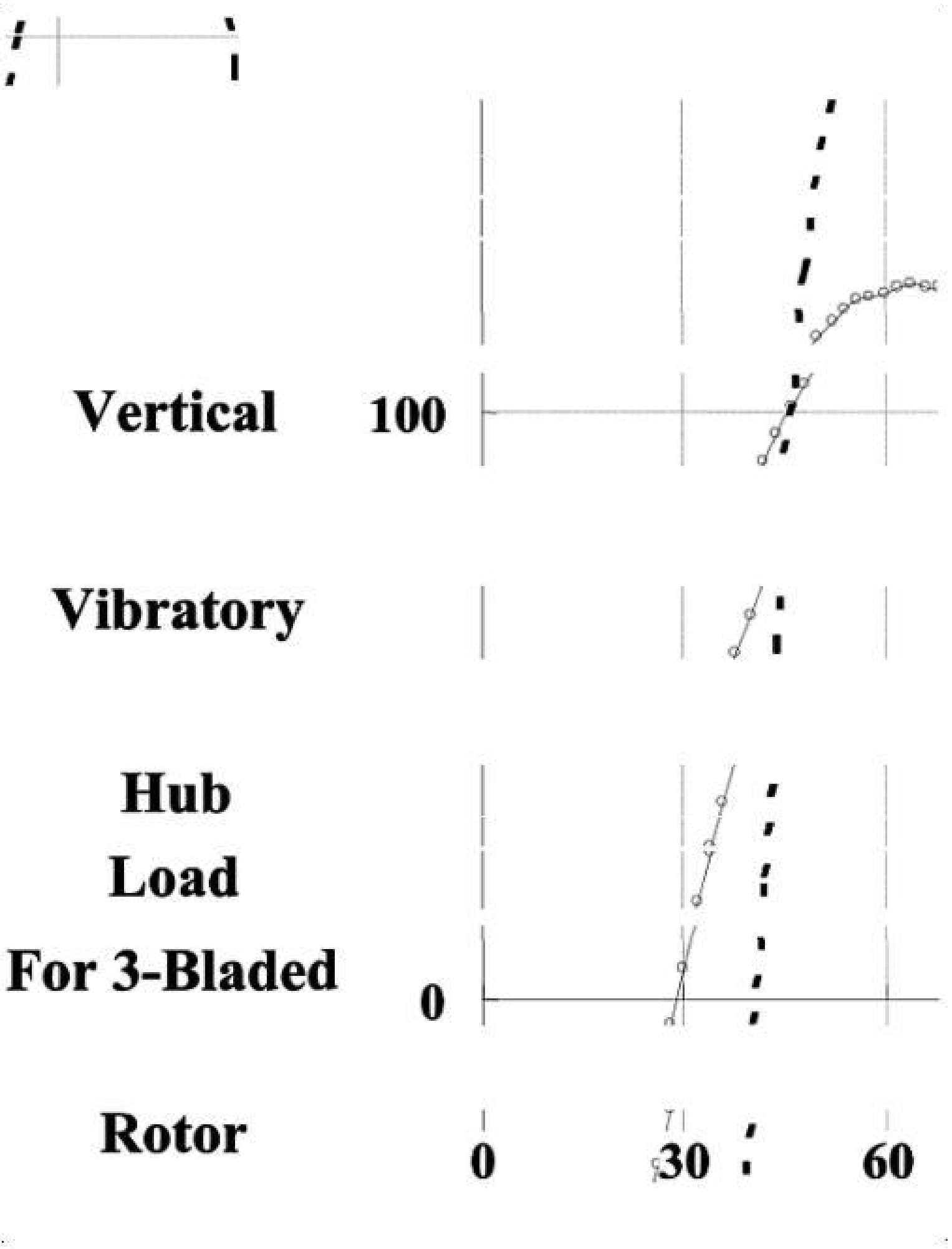
Vertical
100
Vibratory
Hub
Load
For 3-Bladed
0
Rotor
0
30
60

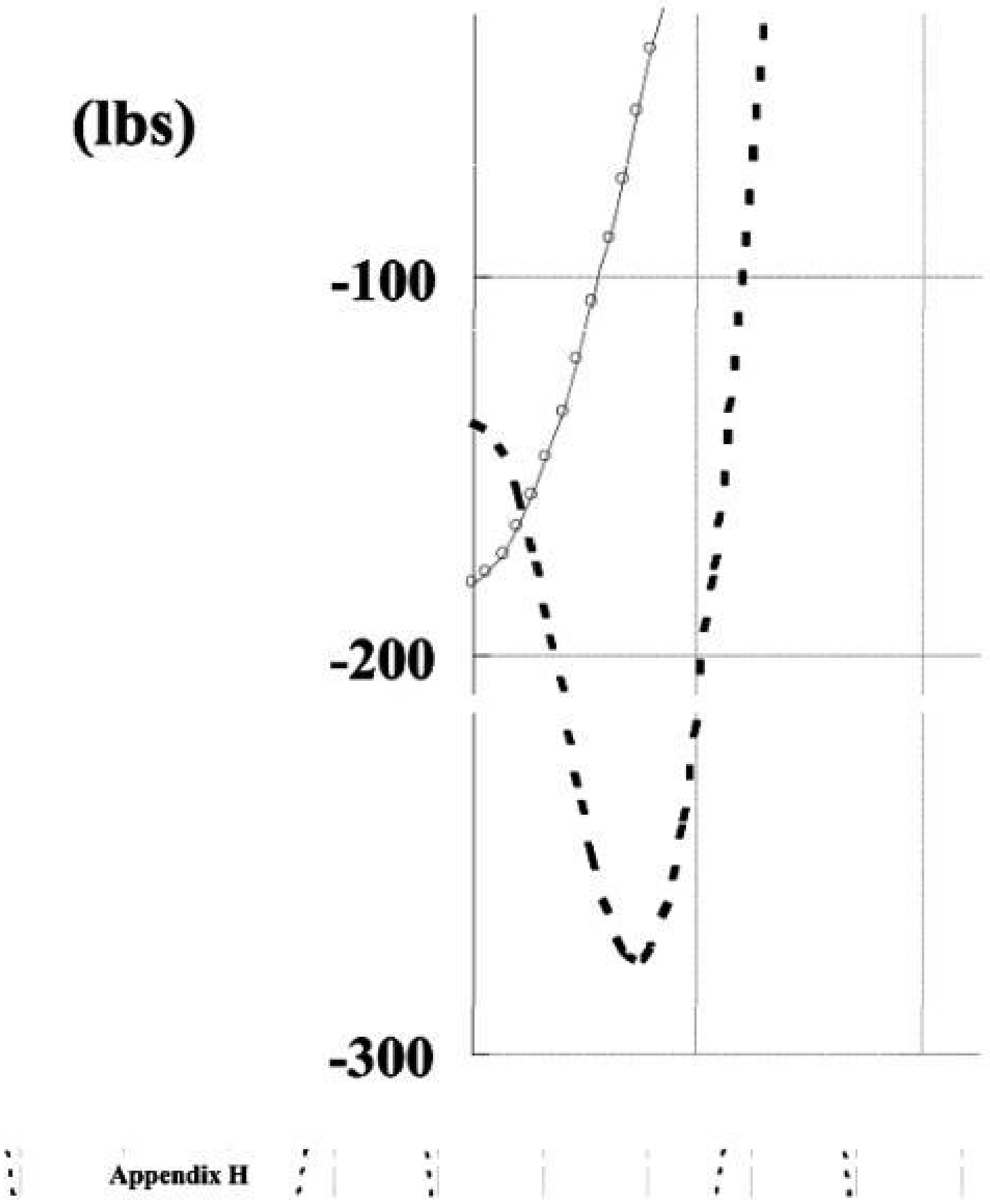
(lbs)
-100
-200
-300

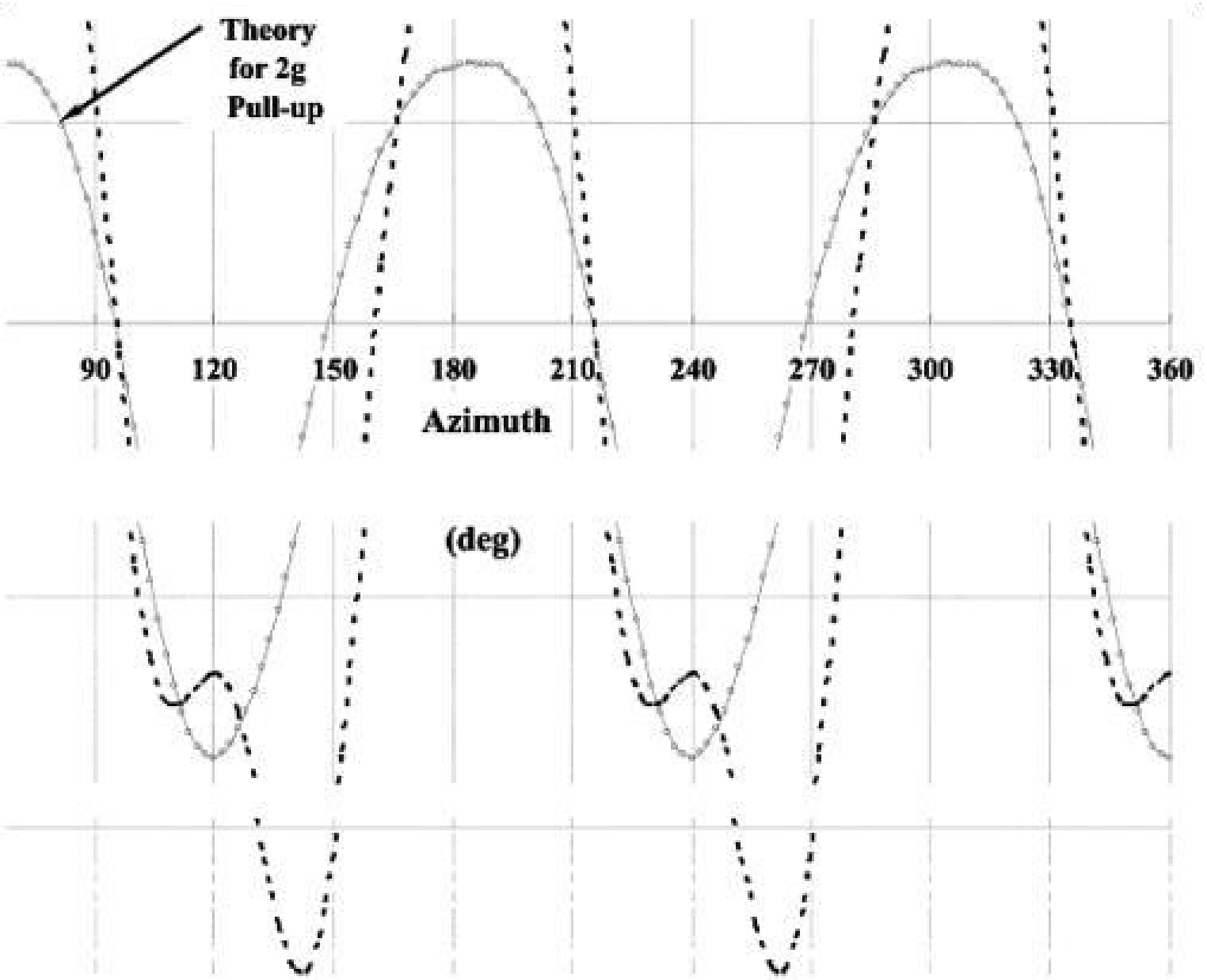

Fig. 2-96. Estimates of vertical hub load for a three-bladed rotor system, μ = 0.5. 202

Table 2-13. Vibratory Hub Loads for the

C.30A in Cruise as Predicted by CAMRAD II

Harmonic	F_Z (pounds)	F_X (pounds)
Mean	1,500	81
Cos 3ψ	–58	–4
Sin 3ψ	–18	+14
Cos 6ψ	–16	–3
Sin 6ψ	–2	–3
Cos 9ψ	–1	+2
Sin 9ψ	+1	–2

The calculation of vertical vibration at the pilot seat (d^2Z_{pilot}/dt^2) is now, of course, quite straightforward. The "vertical bounce," as Larsen described it, is quantified with Fig. 2-97 . Vibration at the pilot seat is about ±0.05 g's in cruise flight, which is close to imperceptible, but during the pull-out at high speed, the pilot could easily experience ±0.13 to ±0.14 g's. At this vibration level, pilots today would definitely express dissatisfaction in no uncertain terms.

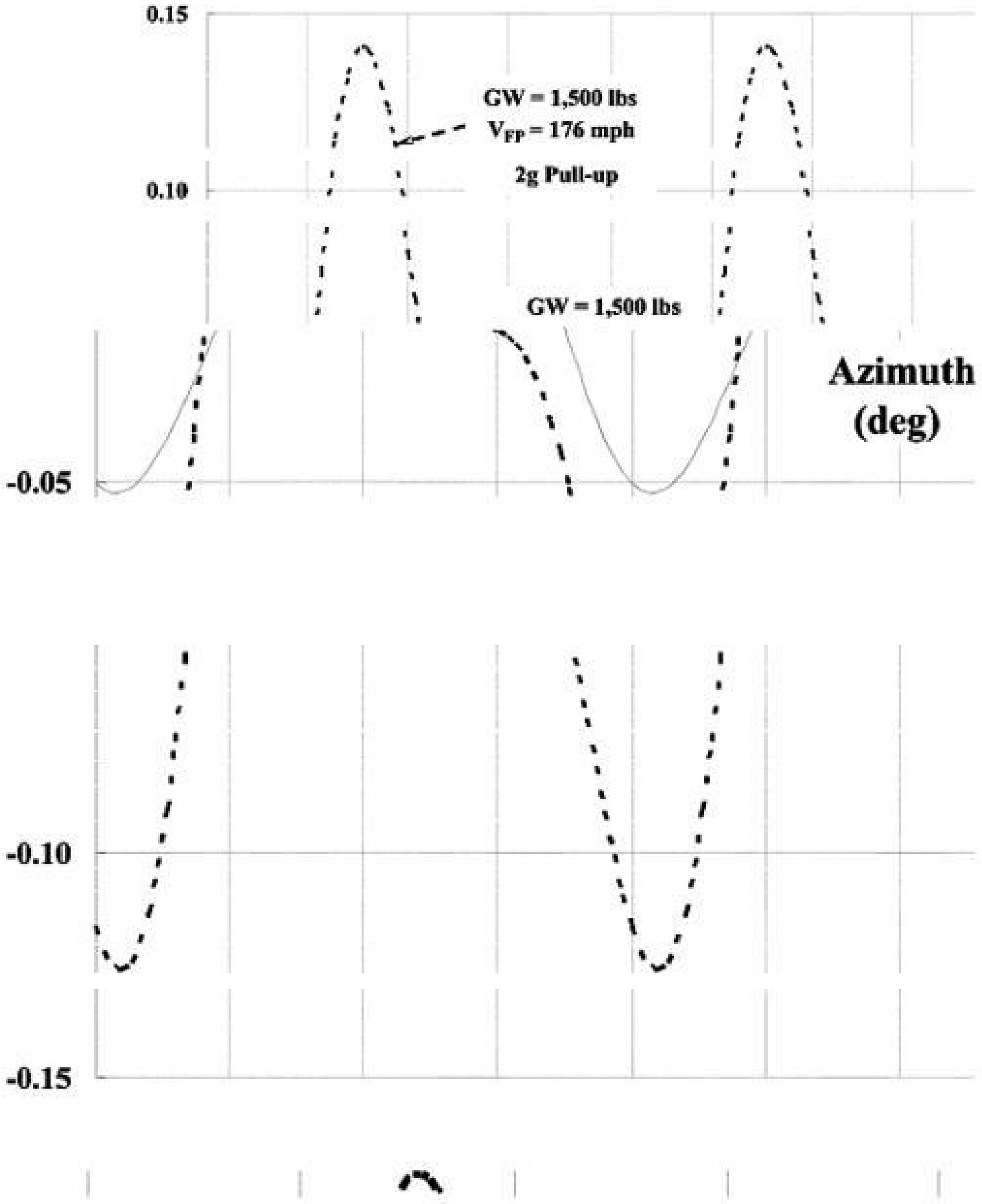
0.15
0.10
-0.05
-0.10
-0.15
GW = 1,500 lbs
V_{FP} = 176 mph
2g Pull-up
GW = 1,500 lbs
Azimuth
(deg)

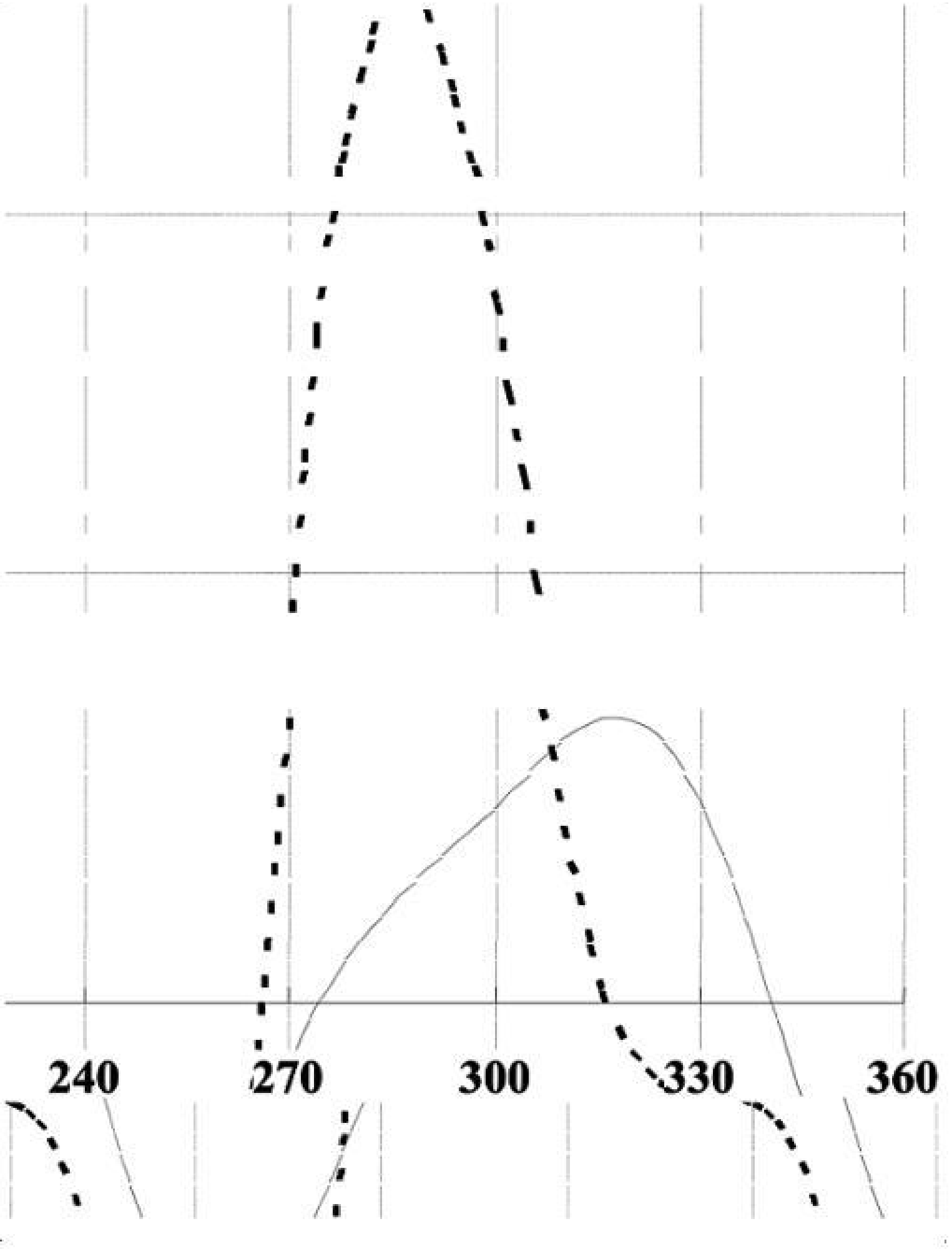
240
270
300
330
360

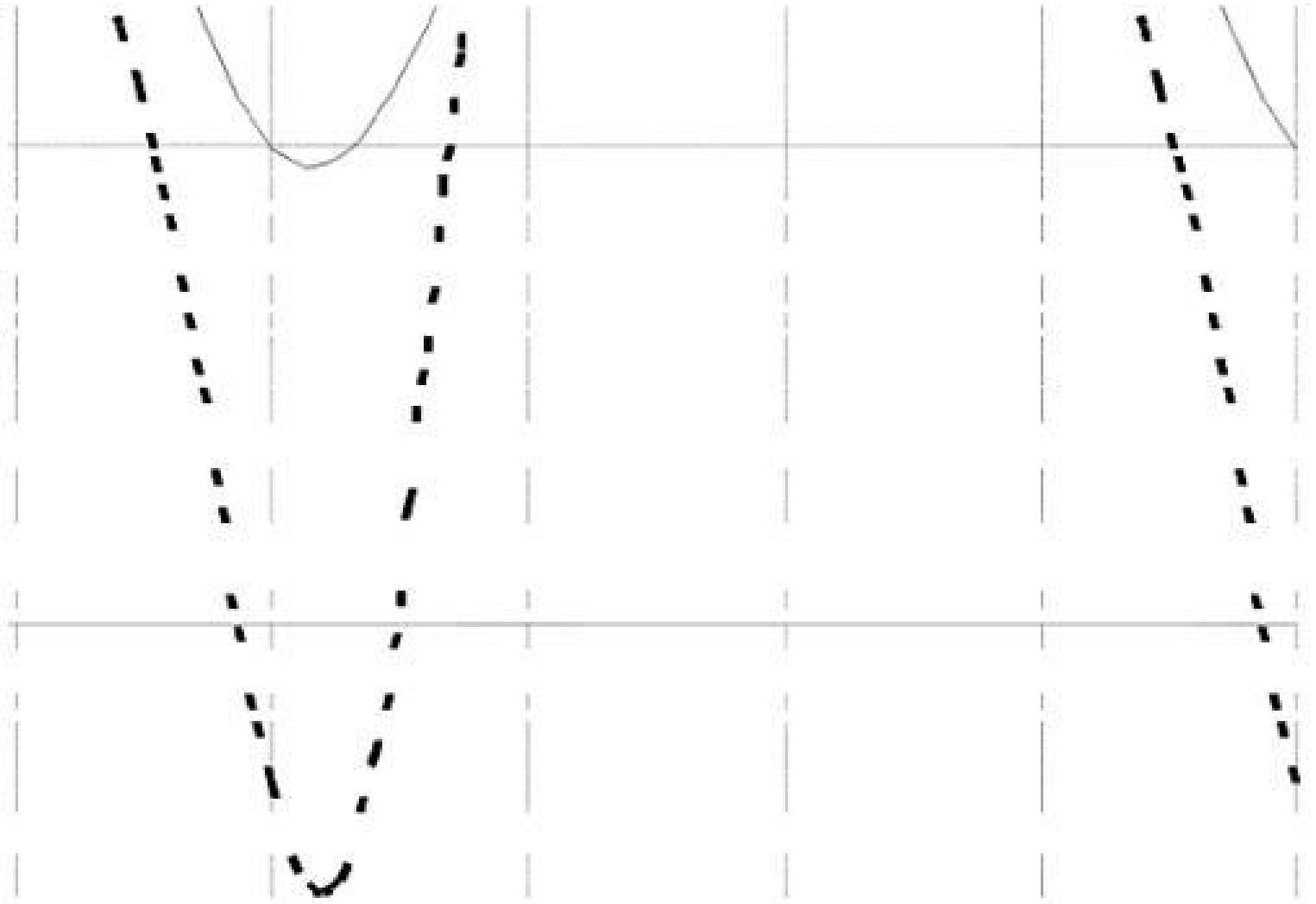

Fig. 2-97. Estimated C.30A vertical vibration at the pilot seat.

2.10 VIBRATION

This simple introduction to vibration created by n per rev (n being 3, 6, and 9 in this

C.30A example) has only scratched the surface of the most vexing rotorcraft problem. The rotor system can produce moments and other forces that shake the machine, and the fuselage will respond with bending over and above rigid body deflections. Engines and propellers simply add to the vibration problem. Vibration caused by airflow interaction between the rotor and the airframe can be the most vexing of them all.

2.10.3 C.30 Once-per-Revolution Vibration

There is a second potential vibration source that needs to be discussed. This is the likelihood of a once-per-revolution vibration. A primary source of this vibration is mismatched blades. You will recall in the discussion about blades, Section 2.9, Sanders and Rawson wrote in *The Book of the C. 19 Autogiro* [50] that

"Each blade is balanced to a standard weight so that all blades of the same type are interchangeable, provision being made for correcting weight at the outer end of the main spar."

This balancing only deals with the requirement met when balancing, for example, an automobile tire . It does not address blade mismatching due to blade element airfoil differences or blades of different twist. Despite tight tolerances called out on an engineering drawing, it is unrealistic to expect that manufacturing, even with the most skillful craftsmen, will produce "interchangeable" blades . Furthermore, there is little guarantee that a set of blades will remain identical over any extended period of service. Blades of the autogyro era absorbed moisture and warped, and frequent rebalancing was often required.

To appreciate this point about 1-per-rev

vibration, consider three blades having, for some reason, different vertical force harmonics. That is, assume

$$F_{Z1} = F_o + (F_{1S} + \Delta F1_{1S})\sin\psi + (F_{1C} + \Delta F1_{1C})\cos\psi$$

(2.239) $$F_{Z2} = F_o + (F_{1S} + \Delta F2_{1S})\sin\psi + (F_{1C} + \Delta F2_{1C})\cos\psi .$$

$$F_{Z3} = F_o + (F_{1S} + \Delta F3_{1S})\sin\psi + (F_{1C} + \Delta F3_{1C})\cos\psi$$

In Eq. (2.239), the incremental forces ($\Delta F1$, $\Delta F2$, and $\Delta F3$) represent differences of each blade from some master blade. An engineering drawing or, more likely, some average blade from the collection of blades produced by manufacturing could define this master blade. Now the vertical force sum of the three blades is

$$F_Z = 3F_o + (F_{1S} + \Delta F1_{1S})\sin\psi_1 + (F_{1C} + \Delta F1_{1C})\cos\psi_1$$

$$+ (F_{1S} + \Delta F2_{1S})\sin(\psi_1 + 120) + (F_{1C} + \Delta F2_{1C})\cos(\psi_1 + 120) \quad (2.240)$$

$$+ (F_{1S} + \Delta F3_{1S})\sin(\psi_1 + 240) + (F_{1C} + \Delta F3_{1C})\cos(\psi_1 + 240)$$

which, with some trigonometry, becomes

$$F_Z = 3F_o + \left[\Delta F1_{1S} - \frac{1}{2}(\Delta F2_{1S} + \Delta F3_{1S}) - \frac{\sqrt{3}}{2}(\Delta F2_{1C} - \Delta F3_{1C})\right]\sin\psi_1 + \left[\Delta F1_{1C} - \frac{1}{2}(\Delta F2_{1C} + \Delta F3_{1C}) + \frac{\sqrt{3}}{2}(\Delta F2_{1S} - \Delta F3_{1S})\right]\cos\psi_1 \quad (2.241)$$

Notice immediately that there will be, in the practical world, a once-per-revolution vibration for any combination of incremental forces other than the perfect case where all incremental forces equal zero. The only practical questions are what the level of 1-per-rev vibration will be, and will the pilot notice it?

A very real example of unmatched blades is seen when the blades have unmatched twist. Cierva was quite satisfied with the performance of zero twisted blades, but I believe that autogyro era blades would have been lucky to match twist to within plus or minus one degree about zero . However, no quantitative data appears to exist. To correct the behavior of each blade in an unmatched set—at least during a ground run-up—the autogyro pioneers developed a tracking procedure. This procedure consisted of

chalking the tips of each blade in the set. Each blade tip was chalked a different color. The rotor was run up and a ground engineer would let the blade tips touch a strip of cloth stretched along a tall pole (Fig. 2-98). The ground engineer allowed the blade tips to just "kiss" the cloth so that a colored chalk mark was made. He could then tell if all blades were tracking in the same plane. If, say, the blue blade was tracking high relative to the green and red blades, the autogyro would be shut down, and the root-end pitch of the blue blade would be adjusted to a lower pitch setting. When all blade chalk marks were superimposed, the effects of all sources of blade
mismatching were *deemed* removed. Tracking and balancing a set of blades could be a lengthy process, although the art was improved with experience over time.

The premise of on-ground tracking is that

if the tip displacement (a measure of blade coning angle) is equal for each blade in an unmatched set, then that is good enough. Unfortunately, the premise does not hold once forward flight is begun. The adverse effect of unmatched twist becomes more pronounced as forward speed is increased. To see this, consider the basic equations associated with the tracking procedure.

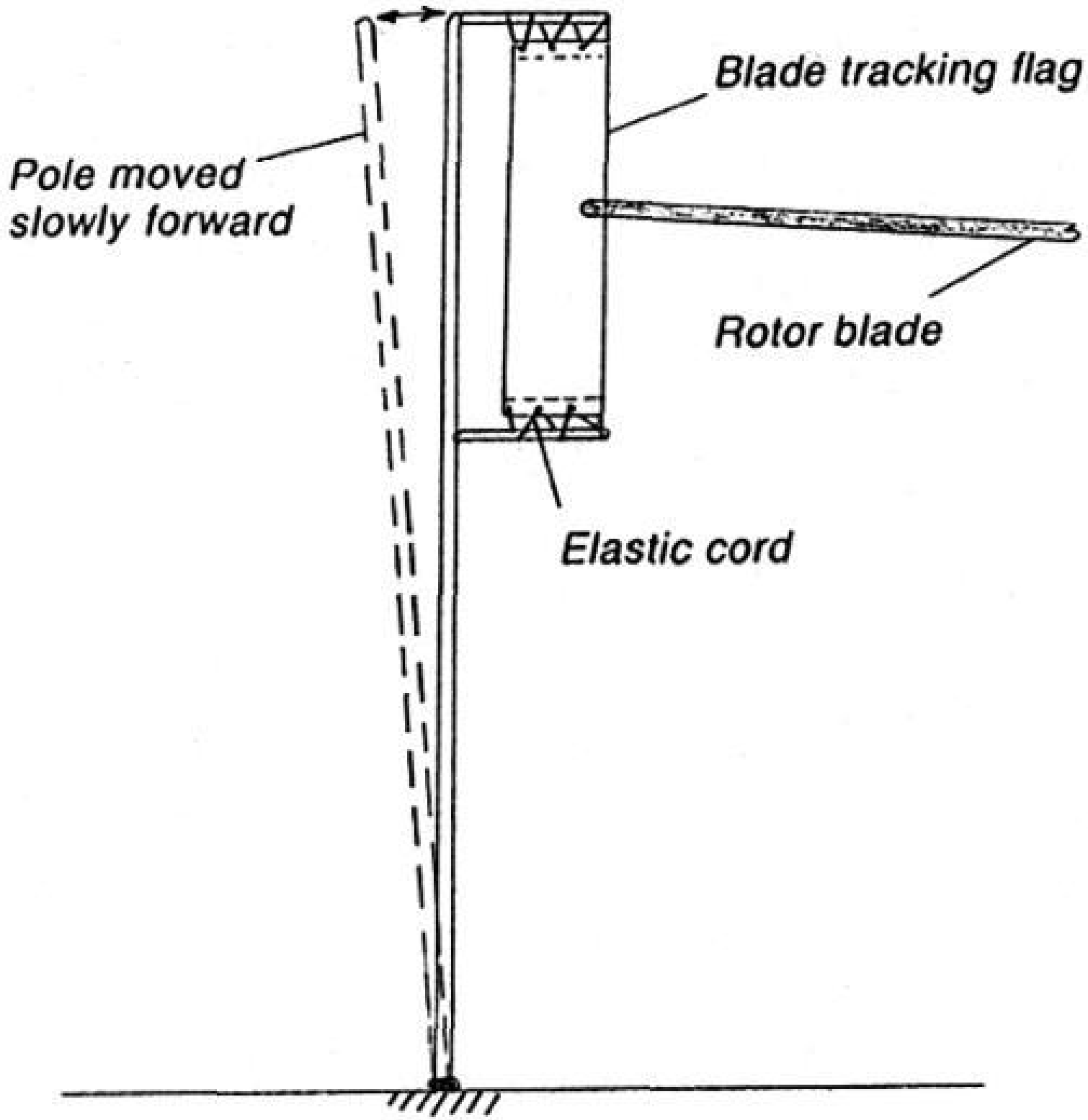

Fig. 2-98. Blade tracking flag [23].

To begin with, imagine three Cierva C.30A blades perfectly balanced but differing in twist. Each blade should have zero twist, but, unfortunately, blade 1 has a 1-degree *washout* (i.e., the tip pitch angle is nose up 1 degree relative to the root reference pitch angle). Blade 2 has 0.5 degrees of washout, and blade 3 has 1 degree of *wash in*. Assume the *deviation* of twist from zero increases linearly from the blade root to the tip. To analyze this situation, the fundamental blade feathering equation, Eq. (2.73), must now be generalized to include a radial variation of pitch angle, so that

$$\theta_{x,\psi} = \theta_o + x\theta_t - B_{1C}\sin\psi - A_{1C}\cos\psi . \tag{2.242}$$

Relative to this blade pitch equation, blade 1 twist (θ_{t1}) is + 1.0 degrees, blade 2 twist (θ_{t2}) is + 0.5 degrees, and blade 3 twist (θ_{t3}) is – 1.0 degrees. Remember that ($x = r/R$).

Now, following Wheatley [75], the coning angle (β_o) is approximated as

(2.243)

$$\beta_o = \frac{\gamma}{2}\left[\frac{1}{3}\lambda_{hp} + \frac{1}{4}\theta_o\left(1+\mu_{hp}^2\right) + \frac{1}{5}\theta_t\left(1+\frac{5}{6}\mu_{hp}^2\right) - \frac{1}{3}\mu_{hp}B_{1C}\right].$$

The previous longitudinal flapping angle expression [see Eq. (2.76)] must also include the effect of twist, but the lateral flapping angle [see Eq. (2.77)] remains unchanged, so that now

(2.244)
$$a_{1S} = \frac{\left[2\mu_{hp}\lambda_{hp} + \frac{8}{3}\mu_{hp}\theta_o + 2\mu_{hp}\theta_t - \left(1+\frac{3}{2}\mu_{hp}^2\right)B_{1C}\right] + \left[\frac{12r_\beta}{\gamma\left(R-r_\beta\right)}\right]b_{1S}}{1-\frac{1}{2}\mu_{hp}^2}$$

and

$$(2.245)\quad b_{1S} = \frac{\frac{4}{3}\mu_{hp}\beta_o - \left[\frac{12r_\beta}{\gamma\left(R - r_\beta\right)}\right]a_{1S}}{1 + \frac{1}{2}\mu_{hp}^2} + A_{1C}\,.$$

where all angles are in radians.

Next, assuming the blades are infinitely rigid, the tip deflection (Z_t) during a tracking ground run-up is simply

$$(2.246)\quad Z_t = R\beta_o\,.$$

Because each C.30A blade has a slightly different twist, the coning angle of each blade will be slightly different in turn. The assumptions here are, of course, that each blade is installed at the same root collective pitch (θ_o) and that the average inflow ratio (λ_{hp}) is applicable to all blades. Of course, advance ratio (μ_{hp}) is zero because the autogyro

is on the ground, and there is little, if any, wind.

Because, in this example, each blade has a twist error relative to the master blade, each blade will have a deviation in coning angle and blade tip deflection with the 222-inch radius (R) C.30A blades. From Table 2-6, the C.30A blade Lock number (γ) is 10.06. The situation facing the ground engineer is tabulated as

Deviation	Master	Blade 1	Blade 2	Blade 3
Twist (deg)	0	+ 1.0	+ 0.5	– 1.0
Coning (deg)	0	+ 1.0	+ 0.5	– 1.0
Longitudinal Flapping (deg)	0	0	0	0
Lateral Flapping (deg)	0	0	0	0
Tip Deflection (in.)	0	3.87 high	1.94 high	– 3.87 low

This is an excessive out-of-track situation. The ground engineer must adjust the root

collective pitch of each blade to correct the tip deflection caused by the twist deviation. If the relative coning angle is brought to zero on the ground (i.e., $\mu_{hp} = 0$), that means (2.247)

$$\frac{1}{4}\theta_o + \frac{1}{5}\theta_t = 0$$

so that the required $\Delta\theta_0 = -\frac{5}{4}(\theta_t \text{ deviation})$.

The ground engineer would make the root-end collective pitch change, do another tracking run (or more), and then the pilot could takeoff and check 1-per-rev vibration in flight. The rotor system as flown would then have the blade settings of

Deviation	Master	Blade 1	Blade 2	Blade 3
Twist (deg)	0	+ 1.0	+ 0.5	– 1.0
Collective Adjustment (deg)	0	– 1.25	– 0.5	+ 1.25
Master Collective (deg)	4.25	+ 4.25	+ 4.25	+ 4.25
Flight Collective (deg)	4.25	+ 3.0	+ 3.75	+ 5.5

Now calculate, according to Eqs. (2.243), (2.244), and (2.245), the flapping angles in forward flight, say at an advance ratio (μ_{hp}) of 0.35 with an inflow ratio (λ_{hp}) of + 0.02 . The results for each blade, provided in Table 2-14, are

Table 2-14. Flapping Differences Due to Mismatched Blade Twist

Parameter	Master	Blade 1	Blade 2	Blade 3
Twist (deg)	0	+ 1.0	+ 0.5	– 1.0
Flight Collective (deg)	4.25	+ 5.0	+ 5.75	+ 7.5
Ground Coning	0	0	0	0
Advance Ratio	0.35	0.35	0.35	0.35
Inflow Ratio	0.02	0.02	0.02	0.02
Longitudinal Flapping (deg)	5.08	4.58	4.96	5.58
Lateral Flapping (deg)	3.48	3.19	3.42	3.77
Flight Coning (deg)	7.92	7.26	7.77	8.58
Tip Deflection at 180-deg azimuth (in.)	50.37	45.87	49.32	54.86
Tip Path Plane Split at 180-deg azimuth (in.)	0	– 4.50	– 1.05	+ 4.49

2.10 VIBRATION

The results in Table 2-14 show that the three blades are no longer tracking in forward flight. The pilot would, in fact, readily see three distinct rotor tip planes when looking forward (i.e., the 180-deg azimuth position). However, it is not at all clear how much 1-per-rev vibration he would feel.

The amount of 1-per-rev vibration due only to the vertical force (F_Z) from one blade is found by solving

One blade

(2.248)

$$F_Z = \int_0^R \left(\frac{dL_{\eta,\psi}}{d\eta} \right) d\eta - \int_0^R (m_\eta) \Omega^2 \left(\frac{\partial^2 Z_{\eta,\psi}}{\partial \psi^2} \right) d\eta$$

$$= F_{Zo} + F_{Z1S} \sin\psi + F_{Z1C} \cos\psi + \text{etc.}$$

which, upon integration following Wheatley

[75], gives the 1-per-rev forces (F_{Z1S} and F_{Z1C}) in pounds as

(2.249)

$$F_{Z1S} = \frac{\rho acRV_t^2}{2}\left[\mu_{hp}\lambda_{hp} + \mu_{hp}\theta_o + \frac{2}{3}\mu_{hp}\theta_t - \frac{1}{3}\left(1 - \frac{3}{4}\mu_{hp}^2\right)a_{1S} - \frac{1}{3}\left(1 + \frac{9}{4}\mu_{hp}^2\right)B_{1C}\right] - \frac{m_b V_t^2}{2} b_{1S}$$

$$F_{Z1C} = \frac{\rho acRV_t^2}{2}\left[\frac{1}{3}\left(1 + \frac{3}{4}\mu_{hp}^2\right)(b_{1S} - A_{1C}) - \frac{1}{2}\mu_{hp}B_{1C}\right] - \frac{m_b V_t^2}{2} a_{1S}$$

These equations are applied to each blade. The results, calculated using the C.30A as an example, are shown in Table 2-15 . The C.30A is assumed to be cruising at sea level ($\rho = 0.002378$ slug/ft^3) at 1 10 miles per hour with a rotor speed of 200 revolutions per minute. The airfoil lift-curve slope (a) is 5.73 per radian, and the blade running mass (m_b) from Table 2-6 is 0.06888 slugs per foot. Remember that the C.30A was a direct control rotor system, so both longitudinal and lateral cyclic angles are zero (i.e., B_{1C} and A_{1C} =

0).

Table 2-15. Vertical 1-per-rev Vibration Due to Mismatched Blade Twist

Parameter	Master	Blade 1	Blade 2	Blade 3
Twist (θ_t in deg)	0	+1.0	+0.5	−1.0
Flight Collective (θ_o in deg)	4.25	+5.0	+5.75	+7.5
Longitudinal Cyclic (B1C in deg)	0	0	0	0
Lateral Cyclic (A1C in deg)	0	0	0	0
Advance Ratio (μ_{hp})	0.35	0.35	0.35	0.35
Inflow Ratio (λ_{hp})	0.02	0.02	0.02	0.02
Longitudinal Flapping (a_{1S} in deg)	5.08	4.58	4.96	5.58
Lateral Flapping (b_{1S} in deg)	3.48	3.19	3.42	3.77
Coning (β_o in deg)	7.92	7.26	7.77	8.58
Vertical Force Sine (F_{Z1S} in lbs)	−208.1	−198.3	−208.3	−217.9
Vertical Force Cosine (F_{Z1C} in lbs)	−494.3	−446.4	−482.4	−542.1
Deviation Force Sine (ΔF_{1S} in lbs)	0	−16.25	−6.27	+16.25
Deviation Force Cosine (ΔF_{1C} in lbs)	0	+2.97	+0.69	−2.97

2.10 VIBRATION

With the sine and cosine components of the deviation forces ($\Delta F1_{1S}$ through $\Delta F3_{1C}$) in-hand from the last two rows of Table 2-15,

and following Eq. (2.241), the 1-per-rev vertical vibratory force is

(2.250) $$F_Z = 3F_o + [-36.9]\sin\psi_1 + [+74.0]\cos\psi_1 .$$

This is the vertical vibratory 1-per-rev force that is transmitted from the rotor hub to the autogyro . The magnitude of the pilot seat vibration (in feet-per-second squared) is found from Eq. (2.227). The C.30A geometry is, again, a = + 4 feet, c = + 0.5 feet, d = + 3.5 feet, I_{AC} = 1,000 slug-feet squared, and m_{AC} = 46.62 slugs . I have only considered the vertical vibratory force (F_Z), so the horizontal vibratory force (F_X) is taken as zero . The net results are that

(2.251)

$$\frac{d^2 Z_{pilot}}{dt^2} = [-0.86]\sin\Omega t + [+1.72]\cos\Omega t$$

Note here that the frequency of the vibration (ω) is once per rev, which means the frequency

equals rotor speed (Ω) in radians per second. Finally, the maximum amplitude of the 1-per-rev vibration that the pilot feels is then simply

(2.252)

$$\frac{d^2 Z_{pilot}}{dt^2} = \pm\sqrt{(-0.86)^2 + (1.72)^2} = \pm 1.92$$

$$ft/sec^2 = \pm 0.06g\,.$$

This is a quite *unacceptable* level of 1/rev vibration by today's standards.

This illustration (using the simplest of theory) of how once-per-rev vibration due to mismatched blades comes about is, unfortunately, quite optimistic. A comparable calculation using modern advance methodology such as the Johnson CAMRAD II [109] gives

(2.253) $F_Z = 3F_o + [+48.3]\sin\psi_1$

$+[+127.3]\cos\psi_1$.

The magnitude of the pilot seat vibration (in feet-per-second squared) is again found from Eq. (2.227) with the result that

(2.254)

$$\frac{d^2Z_{pilot}}{dt^2} = [+1.12]\sin\Omega t + [+2.95]\cos\Omega t$$

Finally, the maximum amplitude of the 1-per-rev vibration that the pilot feels is then simply

(2.255)

$$\frac{d^2Z_{pilot}}{dt^2} = \pm\sqrt{(+1.12)^2 + (2.95)^2} = \pm 3.16$$

$$\text{ft/sec}^2 = \pm 0.098\text{g}.$$

This 1-per-rev vibration level based on hub vibratory loads predicted with an up-to-date comprehensive theory is, of course, totally unacceptable. Rotorcraft industry today

demands considerably tighter tolerances relative to blade mismatching, with a considerable increase in manufacturing costs.

209

2.10 VIBRATION

2.10.4 Closing Remarks

This introductory discussion of vibration barely touches the surface of what Cierva described as the "most irritating of the secondary difficulties" and Larsen classified as "vertical bouncing." As you will learn in Volume II—Helicopters, the rotorcraft industry has continually battled this problem with each new machine it has developed.

210

2.11 PERFORMANCE

The subject of aircraft performance is a very dear topic to those engaged in aeronautics . Cierva, with his invention and demonstration of the autogyro, simply added a whole new branch to the subject. His efforts in expanding the branch while "selling" his aircraft and its performance are easily traced using the three papers he presented to the Royal Aeronautical Society and the discussions that followed his presentations [3-5] . The three papers were presented in 5-year intervals and form, when supplemented with some equations and figures, a very interesting view of autogyro performance (and safety) versus what airplanes of the era offered. The views expressed by both supporters and critics make the birth of the rotorcraft industry a fascinating technology story.[44]

2.11.1 Descent and Landing

Cierva presented his first paper before the Royal Aeronautical Society in October 1925. It was published, along with audience discussion, in the January 1926 issue of the Society's Journal [3]. Cierva's paper, you will recall, followed the demonstration of his Model C.6A (shown in Fig. 2-99) at Farnborough, England, which many in the audience had seen. Cierva made it clear in the first three paragraphs of his paper that the autogyro was developed to solve the one shortcoming of the airplane—stalling at low speed. He notes that he and his brother, during 1911 glider experiments, "had some rather dangerous falls due to loss of flying speed, the most prolific cause of accidents to aeroplanes in their present form." Cierva continued, saying,

"In 1918 I had constructed a large biplane with three engines which, after most satisfactory trial flights, was

wrecked precisely by losing flying speed. The accident diverted all my energies to the solution of the problem of eliminating this danger; for the possibility of losing flying speed and the uncertainties of landing are, in fact, the only faults with which we can reproach the aeroplane, which otherwise is practically perfect in point of speed and manœuvrability."

From Cierva's point of view, his aircraft was created to improve aviation safety.

The first questions asked of Cierva at the conclusion of the paper came from Mr. C. N. H. Lock (who, along with Glauert and Wheatley, laid the technology foundation for rotorcraft) . Lock, after beginning with several complimentary remarks, posed five very direct questions, asking,

"First of all .....are there any conditions which may occur in flight which might stop the windmill from rotating? Secondly. .....might there possibility be a danger of the rotating wings stopping if the machine dived very rapidly at a high speed and then checked itself by raising the elevators as in an ordinary aeroplane

when diving and flattening out? Thirdly, what would be the actual velocity of descent in a very steep glide? Fourthly, would it be possible for the machine to descend absolutely vertically at a safe speed apart from considerations of stability?

---

[44] In October 1925, Cierva spoke very little English, and his paper was read to the Society by the Chairman, Sir Sefton Brancker. Throughout this first paper, Cierva's machine is referred to as an autogyro or Autogyro. In the second and third papers, the spelling became autogiro and, occasionally, Autogiro.

2.11 PERFORMANCE

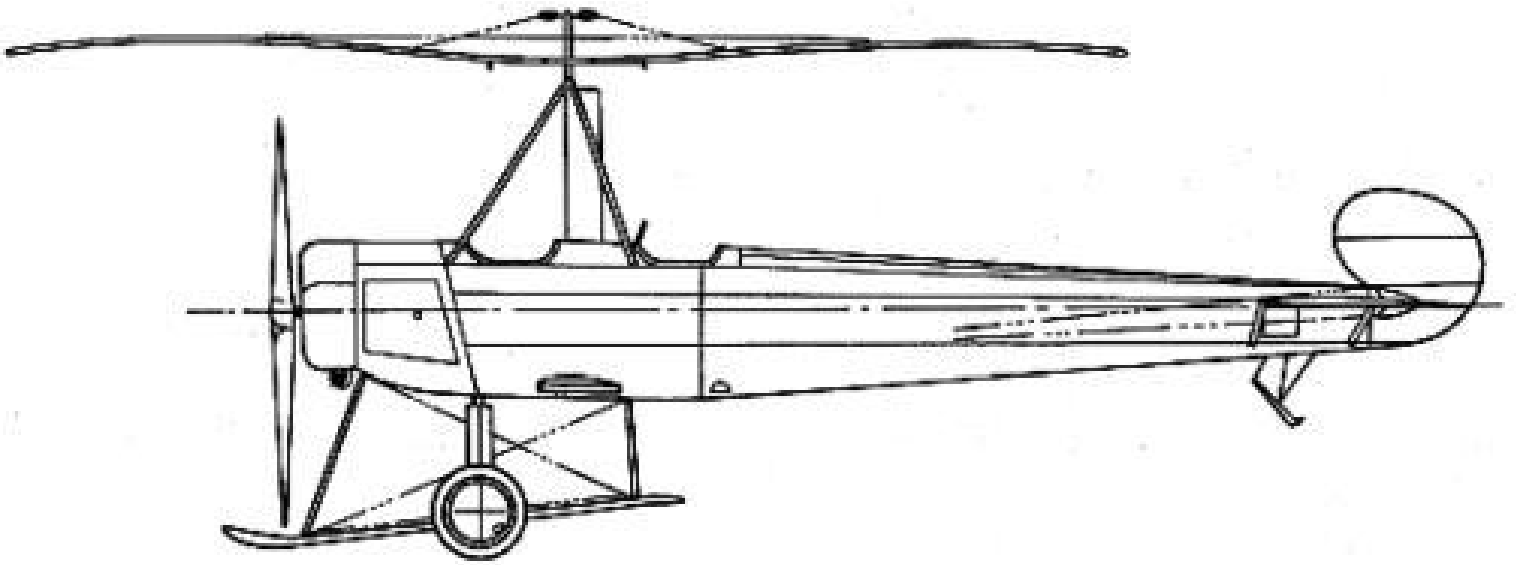

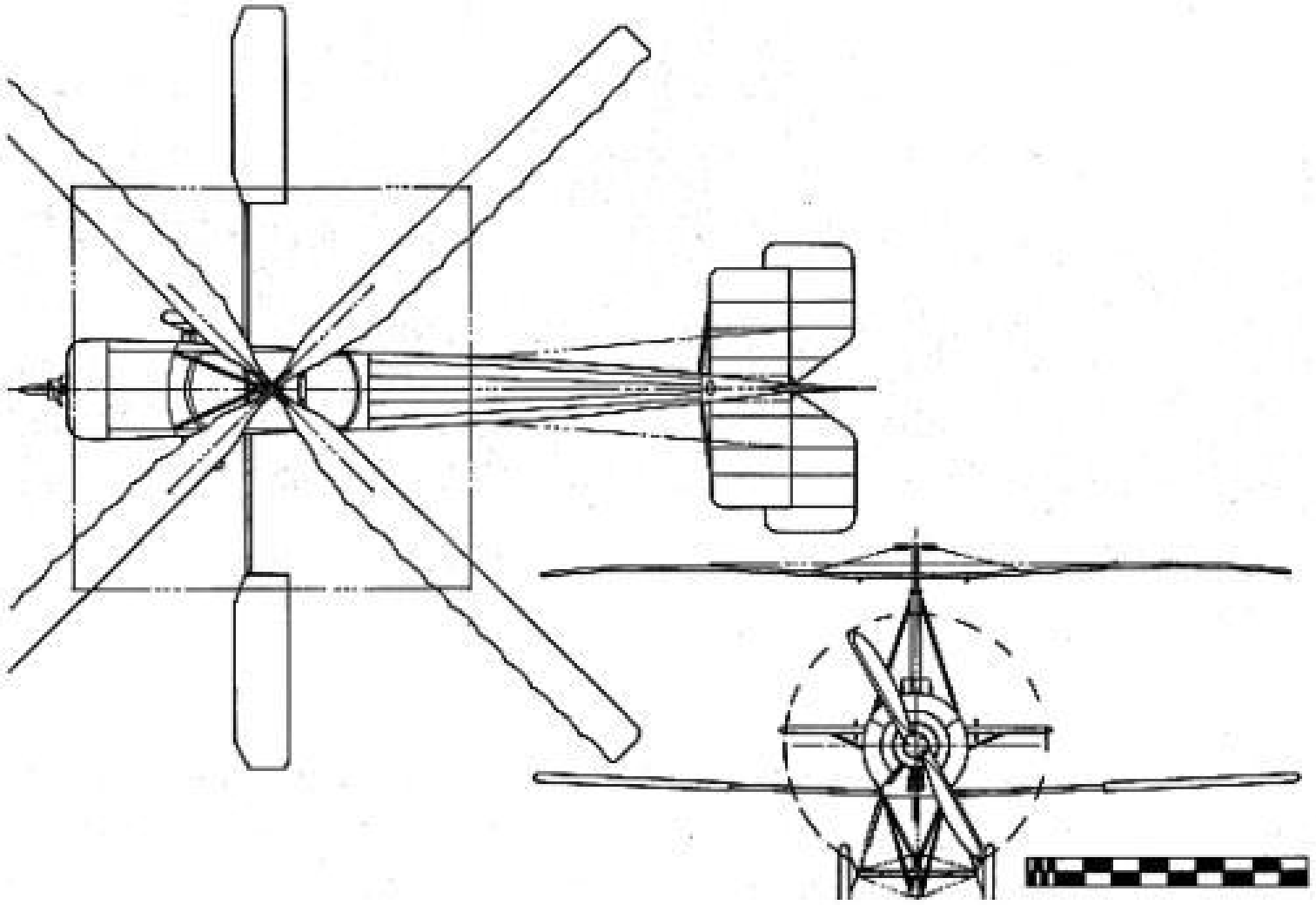

Fig. 2-99. The Cierva Model C.6A as demonstrated at Farnborough, England in October 1925 [7].

It was the fifth question that Lock asked which raised considerable speculation and various opinions about the landing performance of the autogyro. Lock asked Cierva

"whether he anticipated that the resistance of the Autogyro, in falling vertically, would be very much greater than that of a parachute of area equal to the disc area of the Autogyro, since a simple calculation indicates that a parachute having the same area and loading as the Autogyro would fall at a velocity of between 30 and 40 feet per second."

Cierva, responding to Lock, said that "in vertical descent the speed was about 3 to 4 meters per second (about 9.8 to 13 feet per second); the disc being nearly perpendicular to the vertical path." Cierva also added that "the landing speed with descent at 30° was about 4 m./s. [13 feet per second] horizontal, 2 m./s. [6.6 feet per second] vertical; the disc being nearly

horizontal and therefore about 30° to the flight path." Furthermore, Cierva, "in answer to the general queries as to area, rotational speed and loading of windmill blades, by nearly every speaker," gave the following data for the Model C. 6A,

"Blade area = $5.5 \times 0.75 \times 4 = 16.5$ m.^{2}
Total mass 900 kg.
Blades $40 \times 4 = 160$ kg.
Loading = 900/16.5 = 54.5 kg. /m.^{2}
Available power 90 h.p."

In English units, the four blades had a diameter (D) of 36.09 feet and blade chord (c) was 29.53 inches. The rotor solidity (σ) was 0. 1736. The flight weight (GW) was 1,980 pounds, and each blade weighed 88.2 pounds. The disc area ($A = \pi R^2$) was 1,023 square feet, making the disc loading (GW/A) 1 .94 pounds per square foot. Cierva further noted that "the

angular velocity remains about constant at about 130 r.p.m." This is a tip speed (V_t) of 245 feet per second.

The fact that Lock chose to compare the autogyro vertical descent performance to a parachute is, of course, not surprising. After all, the parachute was the only aerodynamic device the aeronautical world had in 1925 that descended in the manner many in the audience had seen demonstrated by the C.6A. Parachutes of the day achieved a measured drag coefficient ($C_D = D/qS$) on the order of 1.2, to perhaps 1.4,[45] which leads to a descent velocity (R/D) equation of

$$(2.256) \quad R/D = \sqrt{\frac{2W}{\rho C_D S}}.$$

A parachute, having an inflated diameter of 36.09 feet (equal to the C.6A rotor diameter, so

S = 1,023 square feet) with a drag coefficient (C_D) of 1.2 and carrying a weight of 1,980 pounds, has a rate of descent of 36.8 feet per second at sea level where the air density (ρ) is 0.002378 slugs per cubic foot. Lock said, "a parachute having the same area and loading as the [C.6A] Autogyro would fall at a velocity of between 30 and 40 feet per second." The fifth question Lock asked in regards to the first Cierva paper [4] inferred that the C.6A actual rate of descent of 10 to 13 feet per second—which few in the audience would debate having seen the flight demonstrations—meant that the C.6A rotor had a drag coefficient of 9.6 to 16.3!

When Lock asked his fifth question he had experimental data for vertically descending model rotors in hand. This data came from France [117], the United States [118], and his own tests in England [119]. (Lock had completed his work prior to the Cierva demonstration

of the C.6A, but his formal report came later.) These data generally confirmed that a rotor would descend at about the same speed as a parachute of equal diameter, carrying the same load. Just as importantly, the descending rotor did not follow the Glauert theory for an airplane propeller, which acted in a "normal state." This early work [117-120] (as the titles state) was aimed not at an autogyro, but rather at the helicopter and specifically at the vertical descent

---

[45] The drag coefficient of a parachute is rather dependent on the porosity of the material as pointed out by Hoerner [116].

performance of the helicopter following loss of power. What this meant to the rotorcraft

pioneers of the era was that autorotating rotor thrust in vertical descent (α_{hp} = 90 degrees) would be calculated as

(2.257) $$T_{hp} = \frac{1}{2}\rho(R/D)^2(\pi R^2)C_D$$

and that Glauert's suggestion for the rotor-induced velocity [Eq. (2.38) repeated her for convenience]

(2.258)

$$v = \frac{T_{hp}}{2\rho(\pi R^2)\sqrt{(V_{FP}\sin\alpha_{hp} - v)^2 + (V_{FP}\cos\alpha_{hp})^2}}$$

had serious limitations when the hub plane angle of attack (α_{hp}) was positive, and the flight path velocity (V_{FP}) was of certain magnitudes.

Before completing the discussion of

vertical descent, it is worth taking a moment to examine Glauert's suggestion [Eq. (2.258)]. Glauert's equation is a quartic in induced velocity (v) and therefore has four roots, not all roots being meaningful. The quartic is

$$\left\{v\sqrt{\left(V_{FP}\sin\alpha_{hp}-v\right)^2+\left(V_{FP}\cos\alpha_{hp}\right)^2}\right\}^2=\left[\frac{T_{hp}}{2\rho\left(\pi R^2\right)}\right]^2=\left(\sqrt{\frac{T_{hp}}{2\rho\left(\pi R^2\right)}}\right)^4 \tag{2.259}$$

which expands to

$$v^4-\left(2V_{FP}\sin\alpha_{hp}\right)v^3+\left(V_{FP}^2\right)v^2-\left(v_h\right)^4=0. \tag{2.260}$$

The solution is generalized by defining $v_h=\sqrt{\frac{T_{hp}}{2\rho\left(\pi R^2\right)}}$ as the reference velocity and then dividing through by this reference velocity raised to the fourth power. The result is a quartic of the form

(2.261)

$$\left(\frac{v}{v_h}\right)^4 - \left[2\frac{V_{FP}}{v_h}\sin\alpha_{hp}\right]\left(\frac{v}{v_h}\right)^3 + \left(\frac{V_{FP}}{v_h}\right)^2\left(\frac{v}{v_h}\right)^2 - 1 = 0$$

and the solution to this quartic for the most applicable root for autogyros (and helicopters) is given in Appendix I and seen visually in Fig. 2-100.

Now consider the autorotating rotor in the general sense. The autorotating rotor operates with no shaft power input. Therefore, from Eq. (2.60), you can write

(2.262)

$$\text{Power} \equiv 0 = T_{hp}v - \left(T_{hp}\sin\alpha_{hp} + H_{hp}\cos\alpha_{hp}\right)V_{FP} + \frac{\rho\left(\pi R^2\right)V_t^3\sigma C_{do}}{8}\left(1+3\mu_{hp}^2\right).$$

2.11 PERFORMANCE

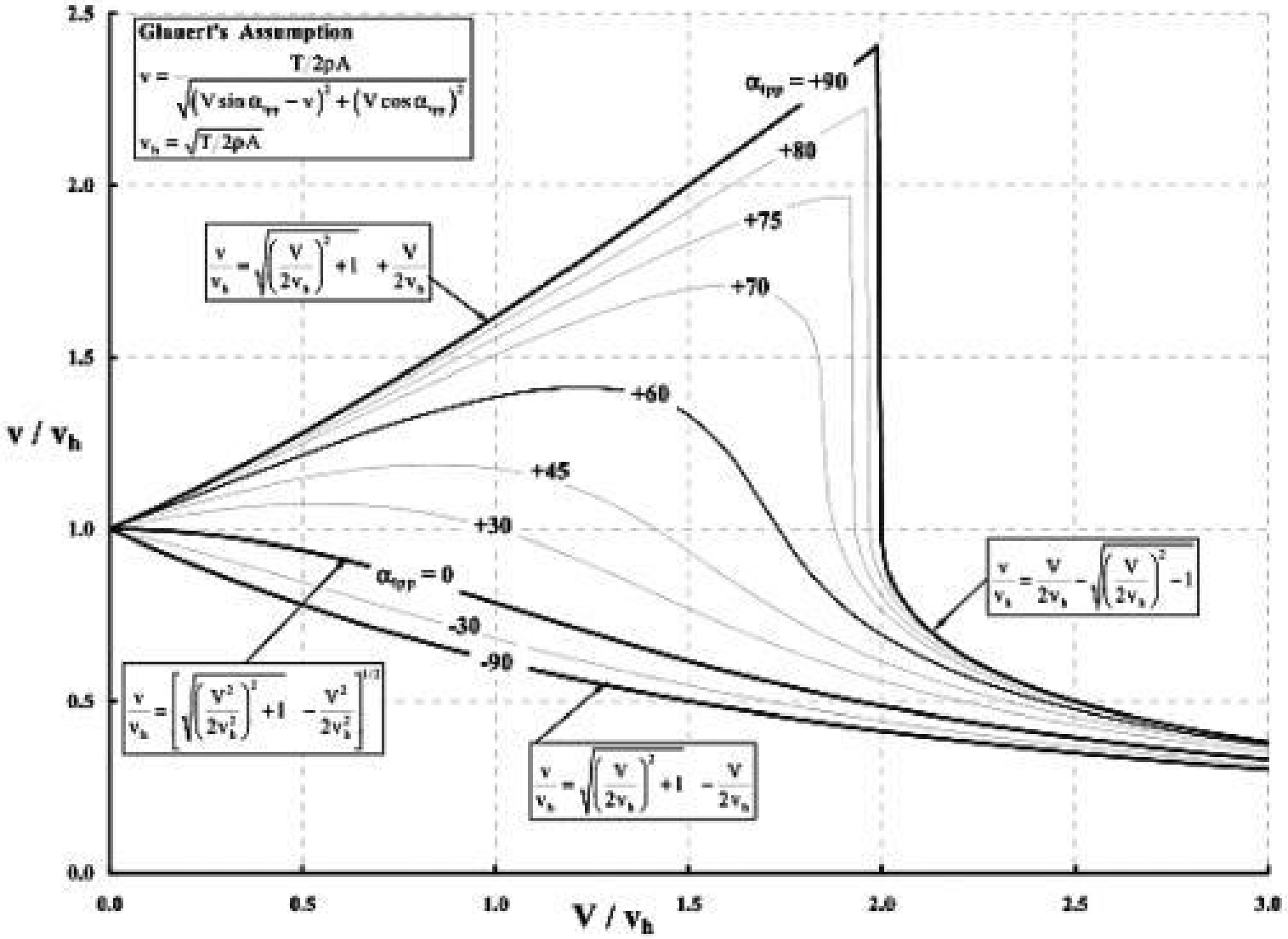

Fig. 2-100. The Glauert theory to calculate induced velocity.

In vertical descent, the hub plane angle of attack (α_{hp}) is 90 degrees, the hub plane advance ratio (μ_{hp}) is zero, and the flight path velocity (V_{FP}) becomes a rate of descent (R/D),

in which case Eq. (2.262) reduces to

(2.263)

$$\text{Power} \equiv 0 = T_{hp} v - \left(T_{hp}\right) V_{FP} + \frac{\rho\left(\pi R^2\right) V_t^3 \sigma C_{do}}{8}$$

and the rate of descent is calculated as (2.264)

$$V_{FP} = R/D = v + \frac{\rho\left(\pi R^2\right) V_t^3 \sigma C_{do}}{8 T_{hp}}.$$

The second term in Eq. (2.264), the profile power per pound of thrust (a velocity), can be partially evaluated based on the dimensions Cierva quoted. That is

$$\frac{\rho\left(\pi R^2\right) V_t^3 \sigma C_{do}}{8 T_{hp}} = \frac{(0.002378)(1{,}023)(245)^3 (0.1736)}{8(1{,}980)} (C_{do}) = 392 (C_{do}).$$

As you can see, the rate of descent required to just overcome the blade drag depends on the airfoil drag coefficient (C_{do}), which, as a minimum, is on the order of 0.01 1.[46] On this basis, no less than 4 feet per second of descent velocity is required to maintain rotor speed at 130 revolutions per minute during steady-state vertical descent with the rotor providing 1,980 pounds of thrust, as in the case of the Cierva C.6A.

The descent rate must also provide energy to create rotor thrust. In the ideal case of zero airfoil drag (i.e., $C_{do} = 0$), the rate of descent required is simply $V_{FP} = R/D = v$. This is where the Glauert theory fails. A quick look at Eq. (2.261) shows that if $V_{FP} = v$ and hub plane angle of attack is 90 degrees, the quartic returns $-1 = 0$, and no solution exists. To overcome this

situation, Lock and others turned to experiment and empirical methods to obtain the autogyro induced velocity in vertical descent. The parallel to a parachute was the beginning.

When an autorotating rotor is in steady vertical descent, little, if any, net flow goes through the rotor disc just as in a parachute. That is, the rotor vertical descent velocity is directly opposed by the mean induced velocity (i.e., $V_{FP} - v \approx 0$). Accepting this approximation means that the rate of descent, following Eq. (2.256) and assuming a parachute drag coefficient (C_D) of 1.2, is calculated as

(2.265)

$$V_{FP} = R/D = \sqrt{\frac{2W}{\rho C_D S}} = 1.29\sqrt{\frac{W}{\rho(\pi R^2)}}$$

and the induced velocity (v) is approximated from Eq. (2.264) as

$$v = R/D - \frac{\rho(\pi R^2) V_t^3 \sigma C_{do}}{8 T_{hp}}. \quad (2.266)$$

Using the Cierva C.6A data, the rate of descent is 36.8 feet per second, 4 feet per second of which is used to turn the rotor against its own drag. Thus, the mean induced velocity (v) is about 32.8 feet per second.

This derived point can be placed on the Glauert induced velocity graph, Fig. 2-100, by calculating the reference velocity (v_h), so that

(2.267)

$$v_h = \sqrt{\frac{T_{hp}}{2\rho(\pi R^2)}} = \sqrt{\frac{1,980}{2(0.002378)(1,023)}} = 20 \text{ ft/sec}$$

and it follows that

---

[46] Lock, in a very thorough manner, tested the Cierva C.6A rotor blade airfoil. The experimental aerodynamic properties of this airfoil, the Göttingen 429, were reported [121] in November 1926. The testing covered the Reynolds number range from 64,000 to 960,000 using 4-inch and 18-inch chord models. The full-scale C.6A rotor blade had a chord of 29.53 inches. At a tip speed of 245 feet per second, the Reynolds number of the tip airfoil is on the order of 3,855,000.

(2.268) $$\frac{V}{V_h} = \frac{32.8}{20} = 1.64$$

at $$\frac{V_{FP}}{V_h} = \frac{36.8}{20} = 1.84\,.$$

This point is shown in Fig. 2-101 as the large, solid black circle.

The Cierva C.6A demonstration—of what many though was vertical descent at a rate slower than a parachute—provided a research challenge to Glauert and Lock. They, along with Bateman, Townend, Caygill, and Nutt, immediately began an experimental program [119-124] in search of explanations for the difference between the descent rates Cierva quoted and model results. By the end of 1926, Caygill and Nutt [124], based on drop tests of 2.2-foot- diameter and 10-foot-diameter

models, drew the conclusion that "no evidence has been found of the very high value [of equivalent parachute drag coefficient] indicated by the full scale [C.6A] demonstration flights." Caygill and Nutt also wrote that "no further dropping tests are proposed. Further wind tunnel tests are being made by the National Physical Laboratory, and further full scale tests will be made by the Royal Aircraft Establishment." In short, truly vertical autorotation testing with models consistently led to a parachute-like drag coefficient of 1.2. No theoretical or experimental explanation was found for the vertical descent rates that Cierva quoted, and the researchers wanted more flight test data and more wind tunnel tests.

Model rotor testing in vertical descent did not end in 1926. In fact, it was not until 1951, when Castles and Gray at Georgia Tech in the U.S.A. provided definitive wind tunnel test results [125], that the researchers could,

with some confidence, empirically describe rotor performance in vertical descent. They followed the Lock experimental approach [1 19], but only a portion of the Glauert analysis approach [122] . Castles' and Gray's models were powered and their tests were conducted in an open-throat wind tunnel, a much closer approximation to free-air testing than the closed-throat wind tunnel Lock used. The Castles and Gray models were powered (as were Lock's) because their tests encompassed helicopters descending at partial power. Fortunately, they investigated autorotation and extended their investigation into the windmill regime where a rotor absorbs energy from the wind.

Castles and Gray, with very careful measurements of key parameters, were able to establish an experimentally defined trend for the induced velocity ratio (v/v_h) as a function of the flight path velocity ratio (V_{FP}/v_h) for the

90-degree hub plane angle of attack (α_{hp}). To obtain this trend, they used the Glauert [122] simple blade element momentum theory for thrust, a refinement to Eq. (2.49), to solve for induced velocity. That is, they let

(2.269)

$$\frac{C_T}{\sigma}=\frac{T_{hp}}{\rho bcRV_t^2}=\frac{a}{2}\left[\frac{1}{2}\lambda_{hp}\left(1-x_c^2\right)+\frac{1}{3}\left(1+\frac{3}{2}\mu_{hp}^2\right)\theta_o\left(1-x_c^3\right)-\frac{1}{2}\mu_{hp}B_{1C}\left(1-x_c^2\right)\right]$$

where the refinement was to account for the actual blade length. The airfoil portion of most blades was not apparent until some distance out from the centerline of rotation. This radial distance was called the root cutout radius ($r_c = x_cR$).

Glauert, and Castles and Gray, solved Eq. (2.269) for inflow ratio (λ_{hp}) with the advance ratio (μ_{hp}) set to zero (i.e., vertical descent), so that

2.11 PERFORMANCE

$$(2.270)\quad \lambda_{hp} = \frac{V_{FP} - v}{V_t} = \frac{\frac{4C_T}{a\sigma} - \frac{2}{3}\theta_o\left(1 - x_c^3\right)}{\left(1 - x_c^2\right)}$$

and the induced velocity ratioed to tip speed (V_t) is then defined as

$$(2.271)\quad \frac{v}{V_t} = \frac{V_{FP}}{V_t} - \lambda_{hp}\,.$$

At this point, the analysis by Castles and Gray departed from the Glauert and Lock approach of 1925.[47] From the measured rotor thrust, Castles and Gray calculated the reference velocity (v_h) and its ratio to tip speed (V_t) as

(2.272)

$$\frac{v_h}{V_t} = \frac{1}{V_t}\sqrt{\frac{T_{hp}}{2\rho(\pi R^2)}} = \sqrt{\frac{T_{hp}}{2\rho(\pi R^2)V_t^2}} = \sqrt{\frac{C_T}{2}}$$

and this leads directly to the nondimensional form of

$$\frac{v}{v_h} = \frac{V_{FP}}{v_h} - \frac{\lambda_{hp}}{\sqrt{C_T/2}}. \quad (2.273)$$

This approach to solving backwards for induced velocity was successful because (1) the collective pitch (θ_o) for the untwisted, rectangular blades was accurately measured; (2) the test conditions of wind tunnel speed (V_{FP}), tip speed (V_t), and density (ρ) were controlled in the open-throat wind tunnel; and (3) thrust and torque were accurately recorded from a balance . Blades for the Castle and Gray models were built with the NACA 0015 airfoil, and airfoil test results gave the

lift-curve slope (a) as 5.73 per radian. The results of data reduction from the Castles and Gray 4- and 6-foot-diameter models (NACA TN 2474) are shown with the open-circle points in Fig. 2-101.

Based on the empirical results shown in Fig. 2-101, two equations are needed to estimate vertical descending rotor performance. These two equations allow power required to be calculated over a very large range in the flight path velocity (i.e., rate of descent). Using Eq. (2.263) as a basis, when $0 \leq \frac{V_{FP}}{V_h} \leq 1.5$

---

[47] Glauert and Lock, in an effort to adapt their propeller theory of the era to vertically descending rotors, introduced two empirical parameters, (1/f) and (1/F) that, politely said, were really confusing, at least to me. In 1947 [126] Lock tried to clarify their early work, but many rotorcraft engineers had come to the conclusion that their experiments and analysis from 1925 were inadequate or, more probably, just plain wrong. Their primary experiment, R&M 1014, was with a two-bladed, 3-foot-diameter rotor in a 7- by 7-foot, closed-throat

wind tunnel. This was too much rotor for such a small tunnel, and no reliable tunnel corrections were known, which cast considerable doubt on the experimental data. My analysis of R&M 1014 data following Castle and Gray— but making a 1-degree change in collective pitch—is shown in Fig. 2-101 with the × symbol. I believe that Glauert and Lock did obtain a little meaningful data, but their data reduction and analysis led to considerable confusion in the decades that followed. I also re-analyzed Munk's NACA TN 22 1 [1 18] and found that this early test (1922) was quite acceptable as the solid black squares in Fig. 2-101 show.

2.11 PERFORMANCE

$$\text{(2.274)}\quad \text{Power} = T_{hp} v_h \left\{ 1.05 + 0.95\left(\frac{V_{FP}}{v_h}\right) + .05\left(\frac{V_{FP}}{v_h}\right)^2 \right\} - \left(T_{hp}\right) V_{FP} + \frac{\rho\left(\pi R^2\right) V_t^3 \sigma C_{do}}{8},$$

and when $1.5 \le \frac{V_{FP}}{v_h} \le 3.0$

(2.275)

$$\text{Power} = T_{hp} v_h \left\{ 6.063 \left(\frac{V_{FP}}{v_h} \right)^{-2.1} \right\} - \left(T_{hp} \right) V_{FP} + \frac{\rho \left(\pi R^2 \right) V_t^3 \sigma C_{do}}{8}.$$

Fig. 2-101, in one form or another, is one of the classic curves that all rotorcraft engineers encounter. It is frequently used to define a region of vertical descent (approximately $V_{FP}/v_h = 0$ to 1.7) where the descending rotor becomes increasingly immersed in its own turbulent wake. This region is commonly referred to as the vortex ring state. The vortex ring state is a very important *avoid region* for helicopters, particularly when pilots attempt to descend vertically from a hover by reducing power (a subject I will discuss more completely later). Of course, the autogyro is always flying outside the vortex ring state (i.e., $V_{FP}/v_h > 1.7$), in the region commonly called the windmill brake state.

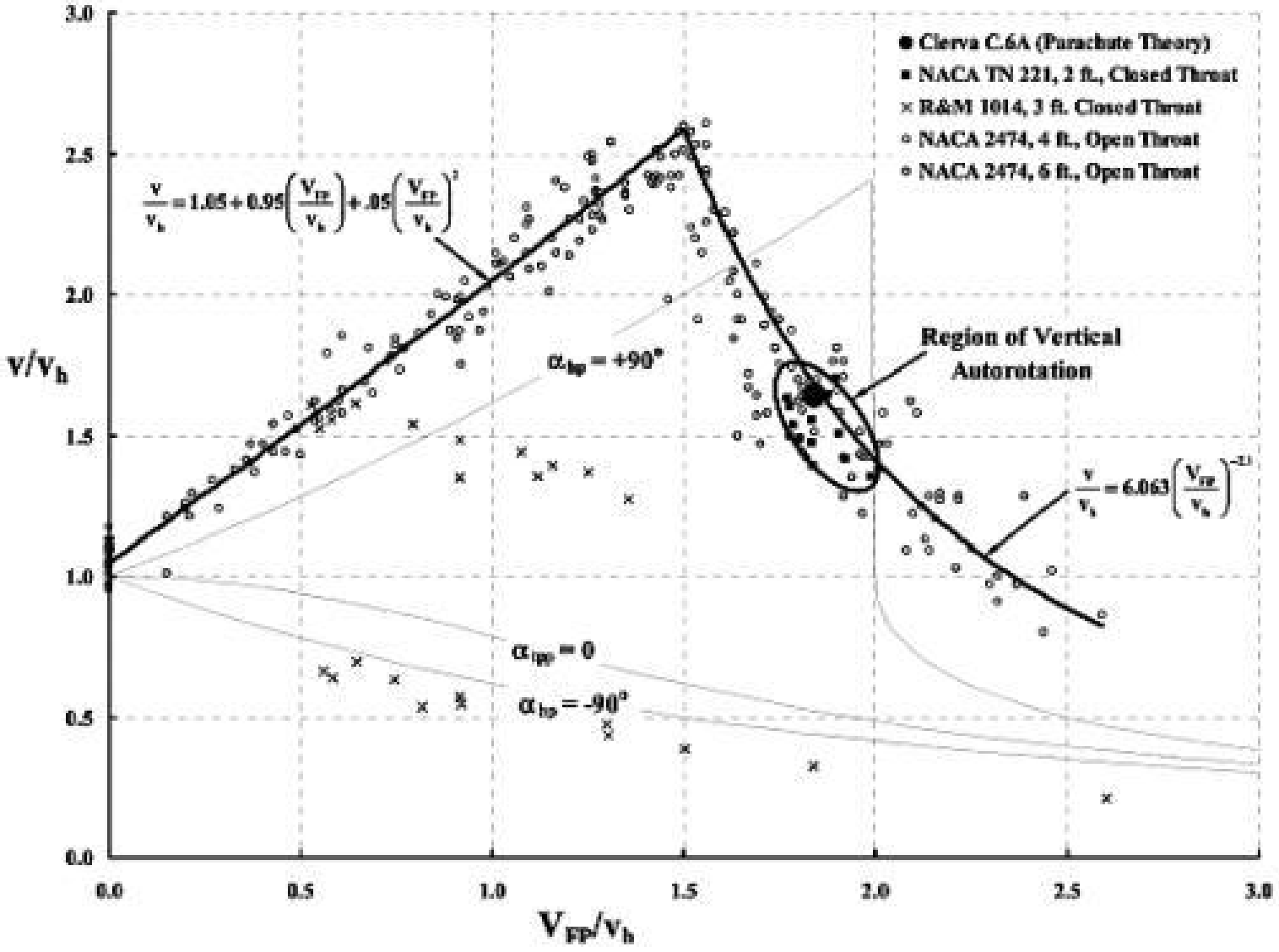

Fig. 2-101. Induced velocity of a rotor in vertical descent.

2.11 PERFORMANCE

The preceding, somewhat lengthy, introduction to the Glauert quartic equation, the efforts to overcome its shortcomings with empirical trends [Fig. 2-101], and then applying results to estimate induced velocity (v) in all regimes of flight [see Eq. (2.262)] is still an evolving story. However, autogyro (and helicopter) development and flight testing was not delayed at all while Glauert, Lock, and many others pursued their research.

Now let me leave the discussion of the Glauert induced velocity equation and return to the main story about performance.

2.11.2 Gliding and Landing

Cierva presented his second paper before the Royal Aeronautical Society on February 13, 1930 . It was published in the Society's Journal in November 1930 [4].

Introducing Cierva (who then had an excellent command of English), the Chairman noted that "of the fourteen types which had been produced recently in this and other countries, the inventor and designer, Senor de la Cierva, had himself made all the first tests; so he at least had absolute confidence in his own invention." When Cierva took the podium, he addressed two topics—product development and research—saying (my comments are in brackets)

"Today, taking advantage of your kind invitation, I come before you to tell you of how the crude experimental autogiros of 1925 [the C.6A,] have been developed into practical flying machines [the C.19, Fig. 2-15, and the Pitcairn PCA-2, Fig. 2-18]. I will also deal with a number of theoretical points in justification of the assertions I have often made about the qualities of the autogiro and in answer to the criticisms of which my system has been made the object from time to time."

With respect to product development, Cierva showed two slides of the C.19 and

pointed out some new features, all in four paragraphs of an eight-page paper! Then he began to "deal with a number of theoretical points." First, he restated a reasonable view (in my opinion) of the growing competition between autogyros and airplanes of the era, saying

"The autogiros lately produced [the C.19 and the PCA-2] have no better performance than the equivalent conventional aeroplanes ...[and] ...the comparison in performance between existing autogiros of several types and best equivalent aeroplanes can be summed up as follow:–Top speed, five to ten per cent less. Rate of climb, twenty per cent less. Steepness of climb, fifty percent more. Minimum horizontal speed, fifty per cent less. .....If they [autogyros] fall a little short of the best aeroplanes in that rather vague quality which is called "performance" they have a performance of their own, which is *utility* and *safety*."

He then alerted the audience about the still current landing and vertical descent issue, saying

"The landing qualities are so well known that it is hardly necessary for me to mention them. In any case, I want to state that the present autogiro can, with proper handling, be landed in perfectly still air with no run at all after touching the ground. In steep descent of about forty-five degrees the vertical speed of the latest machines is not more than 12 to 13 feet per second. I will deal later in this paper with the theory of the purely vertical descent, one of the more discussed performances of the autogiro."

Finally, he addressed the general topic of autogyro aerodynamics, saying

2.11 PERFORMANCE

"The aerodynamics of the autogiro is one of the most complex problems that can be imagined. A considerable number of parameters, both mechanical and aerodynamical, make it really awkward to handle from a purely theoretical point of view. On the other hand, scale effect being astonishingly great, wind channel experiments [such as reported by Lock in R&M 1154] are

of little use to check any approximate theory. Together with this, the extraordinary sensitiveness of the autogiro to changes in certain parameters, such as pitch and profile drag, explains why both eminent mathematicians [for instance, Glauert] and experimenters [for instance, Lock] have conservatively fixed the best lift-on-drag ratio of the autogiro [rotor alone] somewhere near seven (in some wind channel experiments it was only three point five), its maximum lift coefficient around point five [0.5] and its maximum thrust coefficient at about point seven [0.7], referred to the disc area.

I must say that some of the machines I produced in the course of the experimental development were not much better than what could be expected from those conclusions [recall the quite negative views Glauert expressed in R&M 1111]. I took more than one false step.

To continue this discussion of performance, let me address the three points somewhat out of order. I will continue with landing, then move to lift and drag of rotor blades alone, and conclude with autogyro performance compared to airplane performance in the period around 1930.

One of the reasons Cierva could say that "the landing qualities are so well known that it is hardly necessary for me to mention them" is because of *The Book of the Autogiro,* written by Sanders and Rawson [50]. In the chapter about how to fly the C.19 Autogiro, they include three topics: gliding and vertical descent, approach to landing, and landing. Their instructions, with some highlighting (italics) and notes by me, read as follows:

Gliding and Vertical Descent.

The machine will glide at 55 to 60 miles per hour like the normal aircraft. If the "stick" is pulled back the forward speed drops and the angle of descent increases until the condition, which is popularly termed "vertical descent," is reached. With the "stick" hard back and throttle shut the machine takes up a nearly horizontal position and descends at a steep angle on an even keel somewhat like a parachute. *The horizontal forward speed as registered on the air speed indicator in this condition of flight is 25 miles per hour,*

but in actual fact it is considerably less. Turns can be made with impunity in this condition of flight, the machine taking its own bank, but the response to controls, with the exception of the elevator, is necessarily somewhat sluggish.

Approach to Land.

The approach to land is normally made by gliding in at a rather steeper angle with relation to the ground than that taken by a normal aircraft, though actually the angle of the machine with relation to the horizontal is rather flat. If this angle is correctly judged the air speed indicator should register 35–40 miles per hour. If undershooting the landing mark, ease the "stick" forward so as to give the machine an increased speed and a flatter angle of glide, and if overshooting, bring the "stick" back so as to lose height by decreasing forward speed and making a more "vertical descent," *but do not make the latter manoeuvre as a general rule if the machine is less than 50 feet from the ground.* There is no need to perform an "S" turn in order to land on a mark.

2.11 PERFORMANCE

Landing.

Land as near as possible into wind, as any drift is greatly accentuated at the low, forward speed with which the machine touches the earth. *When 5 to 20 feet from the ground, pull the "stick" back smoothly but fairly quickly. The machine will hang against the wind and parachute gently on to the ground on an even keel,* [This is called a flare, which keeps the rotor speed up and decelerates the autogyro] *provided it is kept straight with the rudder, though it is not as liable to veer as a normal aircraft. The landing will be light or heavy according to the judgment exercised in gauging the height from the ground from which the machine is allowed to drop, a 5-feet drop being the optimum condition.*

" Vertical descent " right on to the ground should only be used for landing in case of emergency as, though the undercarriage is designed to withstand the shock if occasion demands, it is unnecessary to submit it repeatedly to the abnormal stresses imposed by a landing of this sort. If the wind speed is from 25–40 miles per hour, it is necessary to land in the manner of a

normal aircraft to avoid touching the ground with a *reversed ground speed.* Above 40 miles per hour wind speed a landing party will be necessary to hold the machine on the ground when landing, unless the machine is flown close to the ground in the lee of a building or other wind-break available.

Clearly, vertical descents were not encouraged in landing the C.19, despite Cierva's position that the rate of descent would be about 15 feet per second. In his second paper Cierva did not include any measured data that supported his position, and he was somewhat taken-to-task by several members of the Society.

The first quantitative picture about autogyro gliding performance became public when John Wheatley's test report on the Pitcairn PCA-2 was published by the N.A.C.A. in the United States [127]. Wheatley tested the PCA-2 at a gross weight (GW) of 2,940 pounds. Its rotor diameter (D) was 45 feet and, with four blades of 22-inch chord (c), the

PCA-2 rotor had a solidity (σ) of 0.0976. The disc loading (GW/A) was nominally 1.85 . The rotor area (A) was 1,588 square feet, and the wing area (S_w) was 101 square feet. The gliding performance of the PCA-2, as obtained by Wheatley and described in terms of vertical descent speed versus horizontal speed, is shown in Fig. 2-102.

The flight test data Wheatley carefully obtained illustrates that the resultant of vertical and horizontal velocity is constant after the descent angle reaches 45 degrees—a very useful trend. Thus, the resultant force in slow speed gliding is *nearly* constant for 45 to 90 degrees of descent angle. The constant is, as we know today, the vertical rate of descent equivalent to a parachute. Stated more precisely, low speed "gliding" performance at descent angles greater than 45 degrees is described simply by the relationship

$$(2.276)\quad (R/D)^2 + (V_{horizontal})^2 = \frac{T_{hp}}{\frac{1}{2}\rho C_D (\pi R^2)}$$

where the "parachutal" drag coefficient (C_D) is reasonably taken as 1.2.

You will notice two additional sets of data in Fig. 2-102—one set shown with open triangles and the other with solid squares. These data are measured speeds at touchdown

during landing of the Pitcairn PCA-2 by an average pilot in generally low wind conditions. It is interesting how this test program came

about. Shortly after the Wheatley flight research program [127], the Bureau of Air Commerce (within the U. S. Department of Commerce) requested that the N.A.C.A. conduct "an investigation to determine the rate of descent, the horizontal velocity, and the attitude at contact of an autogiro in landings." The Bureau wanted data to examine the strength and shock absorption requirement for an autogyro. The Pitcairn PCA-2 was the test aircraft. The flight testing was done at the N.A.C.A. Langley and reported by Peck [128], who wrote that the results

"disclosed that the maximum rate of descent at contact with the ground (10.6 feet per second) was less than the minimum rate of descent attainable in a steady glide (15.8 feet per second); that the rates of descent at contact were of the same order of magnitude as those experienced by conventional airplanes in landings; that flared landings resulted in very low horizontal velocities at contact; and that unexpectedly high lift and drag force coefficients were developed in the latter stages of the flared landings."

Peck drew the conclusion that the rate of descent at touchdown was quite dependent on *when* the pilot began leveling off or flaring. The *when* was measured by that height above the ground when the stick was pulled back and elevator input appeared [Fig. 2-103].

A key point that emerged from the PCA-2 landing tests was that rotor speed remained in the range of 129 to 136 revolutions, which was only slightly below the normal flight rotor speed of 140 revolutions per minute. Peck wrote that

"the reasons for the constant rotor speeds during the accelerated portions of the landing approaches and the unexpectedly high forces coefficients [C_L about 2.1, C_D about 1.8 based on flight path velocity and rotor swept area] prevailing during the flared landings are impossible to explain owing to lack of development of autogiro theory covering accelerated flight and the influence of ground effect on the effective angle of attack. It is believed, however, that a major contributing factor toward the high force coefficients is a relatively large ground

effect at the large angles of attack [about 45 degrees] and low airspeeds attained in the abruptly flared landings."

The ability of the pilot to flare and not stall—while not predictable at the time—was a distinct advantage to lowering forward speed and rate of descent at touchdown.

Cierva made it quite clear in his second paper to the Royal Aeronautical Society that "real vertical descents are difficult, since, by construction, the center of gravity of the machine is placed in front of the axis of the rotor, so that a purely vertical descent can only be obtained during a short period....." However, he devoted nearly two pages to his theory of vertical descent trying to construct the trailing vortex wake structure of the vertically descending rotor. He based his theory on the flow visualization data available at the time [123, 124, 129] . The more knowledgeable audience members did not buy his views, and

the subject seems to have been dropped. Arguments about vertical descents not withstanding, the landing of an autogyro was unquestionably simple.

A fitting way to close this discussion of the autogyro gliding and landing performance comes from the chairman (president of the Society) of the meeting on February 13, 1930, when Cierva completed his talk. To open the discussion, he said that

2.11 PERFORMANCE

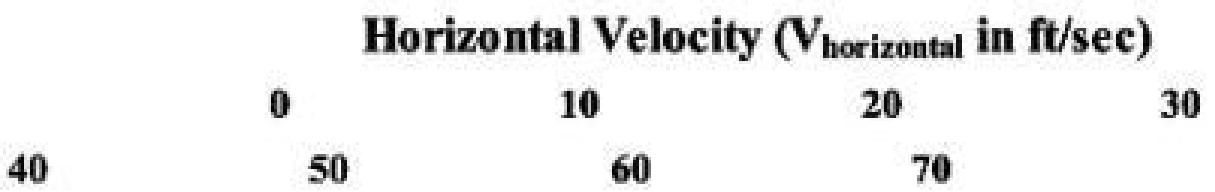

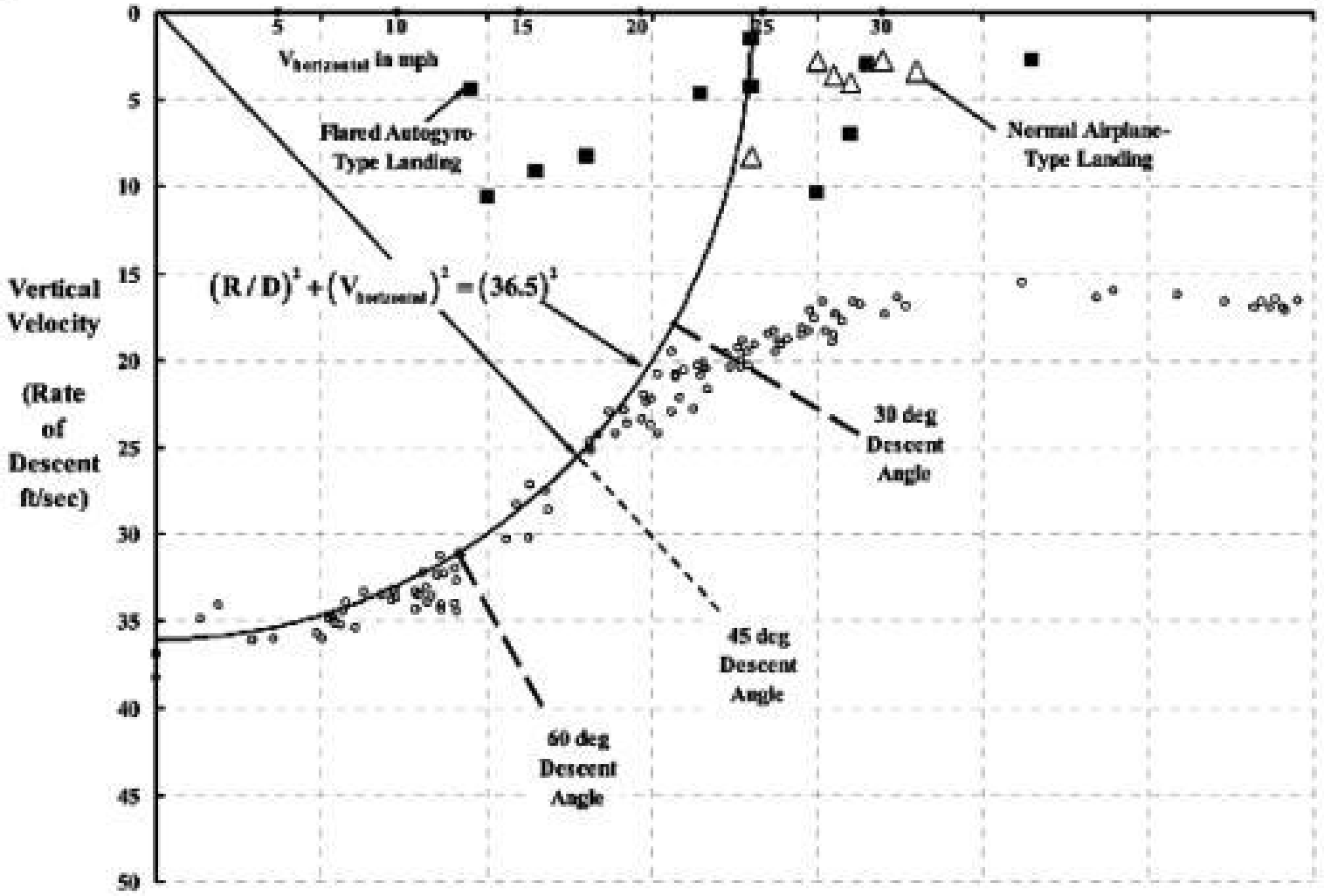

Fig. 2-102. Gliding and landing performance of the PCA-2 [127, 128].

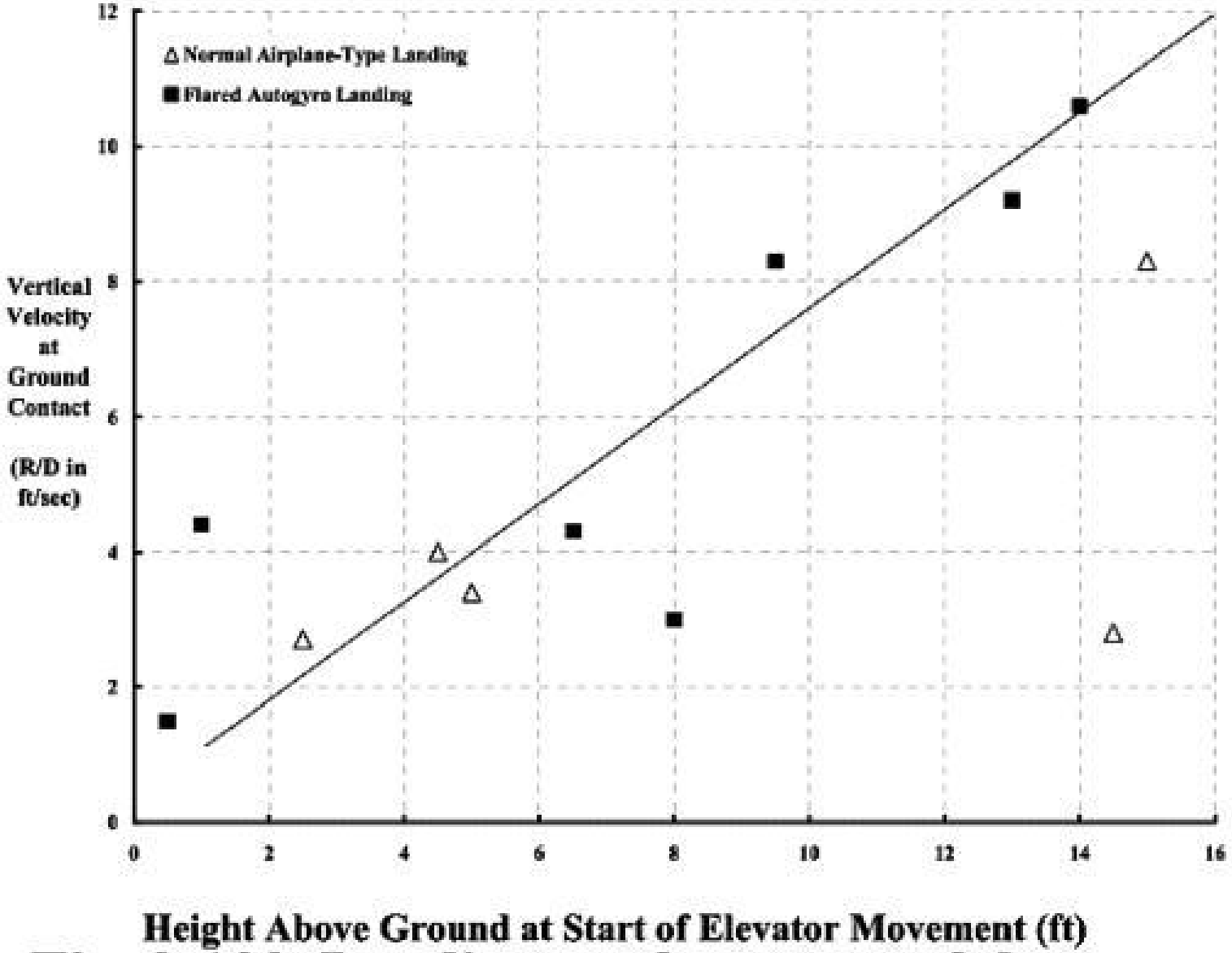

Fig. 2-103. Landing performance of the PCA-2 by an average pilot [128].

2.11 PERFORMANCE

"he had been fortunate enough to be flying one of the

later models [probably a C.19] on several occasions, and he had been amazed at the performance of the machine in the air. When one arrived over the aerodrome, say at 1,000 feet, and one found merely by casually shutting off the engine that the machine would ultimately arrive on the ground without doing anything else at all, it did take one a little time, if one were accustomed to flying the ordinary machine [an airplane], to get used to sitting perfectly still and admiring the surrounding scenery. But that was undoubtedly what happened. The ground simply came up in a gentle fashion, as the machine approached it at somewhere round 15 ft. per second, which the under-carriage was capable of coping with."

2.11.3 Maximum L/D

Cierva, in his second paper [4] presented before the Royal Aeronautical Society on February 13, 1930, addressed the subject of autogyro rotor aerodynamics, which is, he said, "one of the most complex problems that can be imagined." This technical subject, along with vertical descent, appears to have escalated an engineering difference of opinion

(between Cierva on the one side, and Glauert and Lock on the other) that began, I will guess, in the autumn of 1 926. Peter Brooks recounted the situation in his book [7] as follows:

"As a result of the British Air Ministry's sponsorship of Autogiro development,[48] the Royal Aircraft Establishment also undertook numerous investigations into the Autogiro's characteristics. This work was notably done by H. Glauert, C.N.H. Lock, J.A. Beavan, P.A. Tufton, J.B.B. Owen, and a number of others, their findings being fully written-up in official RAE and Aeronautical Research Committee R & M reports . On January 20, 1927, Glauert also read an important paper before the Royal Aeronautical Society on the theory of the gyroplane. Despite the fact that this paper correctly defined the mechanism, performance, and fundamental limitations of rotors with flapping blades, Cierva publicly took strong exception to almost every point Glauert made. He rather unfortunately gave the impression that he resented other investigators in the field he had made his own. This attitude, in its turn, probably contributed to the antagonism toward the Autogiro which seems to have existed in certain official circles and in at least part of

the British technical press – specifically in *The Aeroplane*, under its controversial and astringent editor, the formidable C.G. Grey."

Brooks' recounting of the January 20, 1927 presentation that Glauert made to the Royal Aeronautical Society, and the reaction Cierva had to it, does not convey the magnitude of the controversy that was stirred up . (I can only recommend that you read Glauert's published paper [131], and particularly the discussion that followed, for yourself.) First of all, Cierva did not attend the meeting. Instead, he sent a letter asking that it be read "after the lecture." In fact, Colonel Semple, Chairman of the Society, who presided at the meeting concluded his introduction of Glauert (who "needs no introduction to you. His reputation in aerodynamics is international as you well know") saying

"The papers which have been handed round are copies of a letter sent to me by Senior de la Cierva as his

contribution to the discussion. He excuses himself from coming to speak in person on the grounds of his difficulty in speaking English. [Cierva had also written "owing to the uncertainty of my being in London on the date arrange."] I have had these copies circulated so that you may appreciate his views and so that time during the discussion may be saved."

---

[48] Cierva was very fortunate to have the support of the Air Ministry. Mr. H. E. Wimperis, Director of Scientific Research at the Ministry, was instrumental in getting Cierva to come to England and was enthusiastic from the onset [130]. He remained a staunch supporter of rotorcraft.

2.11 PERFORMANCE

When Handley Page[49] spoke during the discussion, he must have captured the mood of the audience when he said,

"I think one of the most interesting things about this paper [Glauert's lecture] is the extraordinary divergence of opinion among the experts. ..... When

the next paper comes I hope it will be a paper from Senior de la Cierva, but I suppose it will be replied to by letter from Mr. Glauert, who will be unable to be present. I do hope, however, that then we shall have the facts of the whole thing." [The next paper was Cierva's lecture of February 13, 1930, and there was no response by Glauert.]

Handley Page was, I think, even more disgusted than his full discussion remarks imply. He had come to Glauert's January 1927 lecture expecting to see theory developed and compared to available test data. Glauert presented not one shred of evidence along those lines. Three years later, when Cierva responded to Glauert with his second lecture [4] in February 1930, Handley Page, if he was there (no discussion by him is included), would have been even more disgusted. Cierva presented absolutely no information about his theory and no test data. He simply said,

"My engineering theories, all based on energy equations since 1924 and very similar in general lines to

that developed later by Mr. C. N. H. Lock, and published by the Air Ministry in the R. & M. 1127 in 1927, were not a useful guide to me until, in 1928, I succeeded in finding an analytical method of integrating the frictional losses of energy, when the aerofoil used is the Göttingen 429, which gives the average profile drag in any conditions and for any value of the parameters defining a rotor. The theory [1 1] completed in this manner has allowed me to produce autogiros with the correct proportions [recall the reduction in rotor solidity shown in Table 2-5] and I can safely say that the present results check with amazing accuracy the simple assumptions which form the basis of my theory." [Cierva also did not give one equation or theory versus test data comparison to support this statement!]

The dominant issue in the Cierva–Glauert standoff was the current and future performance of the autogyro and—quite specifically—the maximum lift-to-drag ratio of a rotor. Glauert gave his initial pessimistic view in November 1926 with R&M No. 1111. Then Glauert used the lecture before the Royal Aeronautical Society on January 20, 1927 to further put Cierva's invention in its place.

Understandably, Cierva did not like it.

Cierva, in the second paragraph of his letter, which the chairman had distributed before Glauert began his lecture, writes:

"In the first place I must, with respect, record my protest against the manner in which Mr. Glauert has made assertions in an almost axiomatic form, from which the evident conclusion must be drawn that the autogiro is, in effect useless. Such assertions are based only on very incomplete and uncertain calculations which I am able to state are not at all in agreement with the experimental results."

Cierva became even more emphatic as his letter went on! In his turn following the general discussion, Glauert responded to Cierva's letter saying

---

[49] Handley Page pioneered the development of wing trailing-edge flaps and leading-edge slots. These high-lift features for a wing lowered airplane landing speeds without detracting from high-speed potential. He died in 1962.

2.11 PERFORMANCE

"It is rather difficult for me to reply to Senor de la Cierva's contribution because on the whole it is a simple statement of disagreement and I am not acquainted with the particular experiments to which he refers. All the experimental evidence which I have seen, both model and full scale, indicates that the lift/drag ratio of an autogyro and the performance of the aircraft is rather less favorable than I should estimate theoretically. I hope, however, that I have not given the impression that the autogiro is 'useless'. I believe that it is less economical than an aeroplane, but that it has very considerable advantages as regard safety and ease of landing."

In retrospect, at this point in the development of rotorcraft aerodynamics (i.e., 1925 to 1930), neither Cierva, Glauert, Lock, or anybody else for that matter, had (in my opinion) a solid basis for arguing anything. Handley Page,

clearly a cool head in the unfortunate dispute, was quite correct to say that there was "an extraordinary divergence of opinion among the experts."

Calculating autogyro rotor drag for a given lift in 1930 was, in fact, rather simple, but only because the real details necessary for an accurate calculation could not be included with just a slide rule, pencil, and paper. The power required (P_{req}) by a rotor is correctly defined from energy considerations as you learned earlier with Eq. (2.60). In its basic form, the governing equation is

$$\text{Power} = P_{req} = Q_{req}\Omega = \frac{1}{2\pi}\int_0^{2\pi}\int_a^R v_{r,\psi}\,dT_{r,\psi} - \left(T_{hp}\sin\alpha_{hp} + H_{hp}\cos\alpha_{hp}\right)V_{FP} + \frac{\rho b}{2}\frac{1}{2\pi}\int_0^{2\pi}\int_a^R c_r\left(V_{RE}\right)^3 C_d\,dr\,d\psi \tag{2.277}$$

In the autorotating rotor configuration used by Cierva where power required is zero, the rotor drag force (D_R), that is, the force that the autogyro propeller thrust (T_P) must overcome, is defined as

(2.278) Rotor drag $= D_R = \left(T_{hp} \sin \alpha_{hp} + H_{hp} \cos \alpha_{hp} \right)$.

Notice here that when the rotor hub plane angle of attack (α_{hp}) approaches 90 degrees (i.e., vertical descent), rotor drag becomes rotor thrust (T_{hp}).

Now, in the autorotating rotor, power required is zero so, from Eq. (2.277), it follows that

(2.279)

$$D_R = \frac{1}{V_{FP}} \left\{ \frac{1}{2\pi} \int_0^{2\pi} \int_0^R v_{r,\psi} dT_{r,\psi} + \frac{\rho b}{2} \frac{1}{2\pi} \int_0^{2\pi} \int_0^R c_r \left(V_{BE} \right)^3 C_d \, dr \, d\psi \right\}$$

which brings me to the hard part—performing the integrals called for in Eq. (2.279). The first integral gives the rotor-induced power that,

when divided by the flight path velocity (V_{FP}), is the rotor-induced drag. Both Cierva and Glauert knew that the induced velocity ($v_{r,\psi}$) was not a constant value. That is, the induced velocity varied at every radial station (r) along the blade and varied at every azimuthal station (ψ) as the blade rotated. However, neither pioneer had the computational tools to obtain the nonuniform distribution of this velocity. Glauert recommended and Cierva—among many, many others down through the decades—agreed

2.11 PERFORMANCE

that, until further notice, the induced velocity would be assumed constant as given by Eq. (2.38), which is repeated here for convenience,

(2.38)

$$v_{r,\psi} = v = \frac{T_{hp}}{2\rho(\pi R^2)\sqrt{(V_{FP}\sin\alpha_{hp} - v)^2 + (V_{FP}\cos\alpha_{hp})^2}}.$$

Moving induced velocity outside the integral sign as a constant leaves just the integral of elemental thrust ($dT_{r,\psi}$), which is total rotor thrust (T_{hp}). With an assumed constant induced velocity, calculating rotor drag is therefore reduced to

(2.280)

$$D_R = \frac{T_{hp} v}{V_{FP}} + \frac{1}{V_{FP}} \frac{\rho b}{2} \left\{ \frac{1}{2\pi} \int_0^{2\pi} \int_0^R c_r (V_{BE})^3 C_d \, dr \, d\psi \right\}.$$

The remaining integral calculates the profile power (that Cierva called "the frictional losses of energy") due to airfoil drag. Dividing profile

power by flight path velocity (V_{FP}) establishes the rotor profile drag. This integral, as written, assumes that the blade chord (c_r) need not be constant from blade root to blade tip (i.e., r = R). The velocity acting at a blade element (V_{BE}) *in its simplest and lowest value form* follows Eq. (2.1), so that

$$V_{BE} = V_{r,\psi} = \Omega r + \left(V_{FP} \cos \alpha_{hp} \right) \sin \psi \,. \tag{2.281}$$

Airfoil drag coefficients (C_d) for symmetrical airfoils such as the Göttingen 429 [121] are well known to behave, below stall, approximately as

$$C_d = C_{d\,min} + \delta C_\ell^2 \,. \tag{2.282}$$

At this point you can guess the next step to handling the profile drag integral. The blade will have a constant chord (i.e., $c_r = c$), the lowest blade element velocity given by Eq. (2.281) will be assumed, and the airfoil drag coefficient will be no greater than its minimum value (i.e., $\delta = 0$), which, it will be

assumed, does not vary with radius or azimuth. Then the profile drag integral is readily performed, and the rotor drag (D_R) is simply

(2.283)

$$D_R = \frac{T_{hp} v}{V_{FP}} + \frac{1}{V_{FP}} \frac{\rho b c}{2} C_{d\min} \left\{ \frac{1}{4} \Omega^3 R^4 + \frac{3}{4} \Omega R^2 \left(V_{FP} \cos \alpha_{hp} \right)^2 \right\}.$$

Eq. (2.283) is generally considered rather clumsy, so some factoring of rotor speed (Ω), in radians per second, and radius (R), in feet, is quickly done, and then

(2.284)

$$D_R = \frac{T_{hp} v}{V_{FP}} + \frac{1}{V_{FP}} \frac{\rho b c}{2} \left(\frac{\Omega^3 R^4}{4} \right) C_{d\min} \left\{ 1 + 3 \left(\frac{V_{FP} \cos \alpha_{hp}}{\Omega R} \right)^2 \right\}.$$

The final step to obtaining the traditional form of minimum rotor drag is to identify

the conventional parameters of

$$bcR = \left(\pi R^2\right)\sigma = A\sigma, \quad V_t = \Omega R,$$

$$\mu_{hp} = \frac{V_{FP}\cos\alpha_{hp}}{V_t}$$

and substitute these definitions into Eq. (2.284) to obtain

(2.285)

$$D_R = \frac{T_{hp}v}{V_{FP}} + \frac{1}{V_{FP}}\frac{\rho A\sigma V_t^3}{8}C_{d\min}\left(1+3\mu_{hp}^2\right).$$

In the debate that Cierva and Glauert were having, at least up to 1930, the rotor maximum lift-to-drag ratio was a key autogyro

performance parameter issue. While they did not agree—exactly—on rotor drag (I will discuss some differences shortly), they both agreed that rotor lift (L_R) would be calculated as

(2.286) Rotor lift $= L_R = \left(T_{hp} \cos \alpha_{hp} - H_{hp} \sin \alpha_{hp} \right)$.

Furthermore, Cierva and Glauert (and Lock) were willing to say that, in level forward flight, the rotor would be autorotating at a small value of hub plane angle of attack (α_{hp}). Accepting this small angle assumption brings considerable simplification because:

1. $\cos \alpha_{hp} \approx 1$ and $\sin \alpha_{hp} \approx \alpha_{hp}$

2. $T_{hp} \approx L_R$ and $H_{hp} \sin \alpha_{hp} \ll T_{hp}$

3. $V_{FP} \sin \alpha_{hp} - v \approx 0 \quad \text{so} \quad v \approx \dfrac{L_R}{2\rho A V_{FP} \cos \alpha_{hp}}$

or $v \approx \dfrac{L_R}{2\rho A V_{FP}}$.

This approach reduces the minimum rotor drag expression to

(2.287)

$$D_R = \frac{L_R^2}{2\rho A V_{FP}^2} + \frac{\rho A \sigma V_t^3}{8 V_{FP}} C_{d\min} \left(1 + 3\mu_{hp}^2\right)$$

Glauert Form .

One thing I should mention is that Cierva wrote [11] the minimum rotor drag equation in the slightly different form of

(2.288)

$$D_R = \frac{L_R^2}{2\rho A V_{FP}^2} + \frac{\rho A \sigma}{8} C_{d\min} \left\{ \frac{V_t^3}{V_{FP}} + 3 V_{FP} V_t \right\}$$

Cierva Form.

In their lectures to the Royal Aeronautical Society, neither Glauert (on January 20, 1927) or Cierva (on February 13, 1930) showed any test-versus-theory comparison, and many in the audience were disappointed. Handley Page, for one, wanted facts at Glauert's lecture and, while some odds and ends of experimental numbers were quoted, he hoped that Glauert would "at some time be able to add results of a corresponding [to Glauert's theory] full scale research work in flight." Personally, I think Glauert was premature in presenting his paper before Lock and Townend had finished the wind tunnel

testing of a 6-foot-diameter model of the C.6A rotor in forward flight [132]. This model test began in July 1927, with results reported in March 1928, so Glauert really did not have comprehensive data in hand. On the other hand, Cierva, in his second lecture some 3 years after Glauert's lecture, had the chance to show his theory in comparison to Lock's model test, but chose not to, apparently because he had little regard for the scale effects models introduced.

2.11 PERFORMANCE

Cierva and Glauert could have collaborated on a paper in mid-1928 showing Lock's and Townend's model results versus theory as given by either Eq. (2.287) or Eq. (2.288). Had they joined forces, they would have seen the comparisons shown in Fig. 2-104 and

Fig. 2-105. The baseline results of Fig. 2-104 are for four blades that modeled the Cierva C.6A rotor blades. Lock and Townend also tested two blades as shown in Fig. 2-105 because, as they wrote:

"In view of the success of the [Cierva] Autogyro Company in flying a 2-bladed autogyro, it was decided to test the present [4-bladed] model as a 2-blader by removing two of the blades. The experiment was conveniently made after the accident to the model in which one blade was damaged [I never was that lucky]. The experiments showed no special features except that as expected there was greatly increased vibration due to the periodic variation of the drag which necessitated additional damping in the drag balance. The vibration increased rapidly with decreasing incidence [higher speed] and the lowest incidence attained was 4°, which was hardly low enough to establish the maximum L/D."

The experimental data and the theory shown in Fig. 2-104 and Fig. 2-105 are for blades alone. The rotor test stand was built to accommodate a 10-foot-diameter model of the Cierva C.6A,

but those blades, which were scaled full scale including the spar, wooden ribs and fabric cover, were unsatisfactory. The testing proceeded with 6-foot-diameter, solid-wood blades. The drag of the hub and stub roots was measured as a tare, and then the drag of the assembled rotor system, less the tare, was tabulated as blades-alone drag.

In computing the rotor drag with Eq. (2.287), I set the operating parameters and rotor lift equal to the Lock and Townend data. For the minimum airfoil drag coefficient ($C_{d\ min}$), I selected 0.013 for the theory-versus-test comparisons. This is a somewhat arbitrary choice. Lock tested the Göttingen 429 airfoil [121] at both 4-inch and 18-inch chord sizes, each wing with an aspect ratio of 6. In the standard method of the era, this wing data was converted to infinite aspect ratio, which corresponds to the airfoil data required by blade element theory. The airfoil drag polar

behaved approximately as

$$C_d = C_{d\min}\left(1 + C_\ell^2\right)$$

and its minimum drag coefficient and maximum lift coefficient depended on the Reynolds number as given in Table 2-16. Lock also tested the airfoil with the trailing-edge first over a small angle-of-attack range. The drag coefficient for trailing-edge first was about double that of the leading-edge-first drag coefficient.

In both four- and two-bladed comparisons, I have shown a linear regression fit to the test-versus-theory data. Obviously, the drag of the four-bladed model is rather well predicted by Eq. (2.287). That is to say, the theory underestimates test drag by about 2 percent plus the offset of 0.25 pounds (possibly a tare). I would think that both Cierva and Glauert would have been very encouraged with this comparison. However, with the two-bladed

rotor test versus theory appearing so poorly correlated, that encouragement would have been short lived. *In fact, for the majority of two-bladed rotor data, the rotor was operating at high advance ratio with a great deal of retreating blade stall as you will learn shortly. The simple theory is quite inadequate if there is significant blade stalling.*

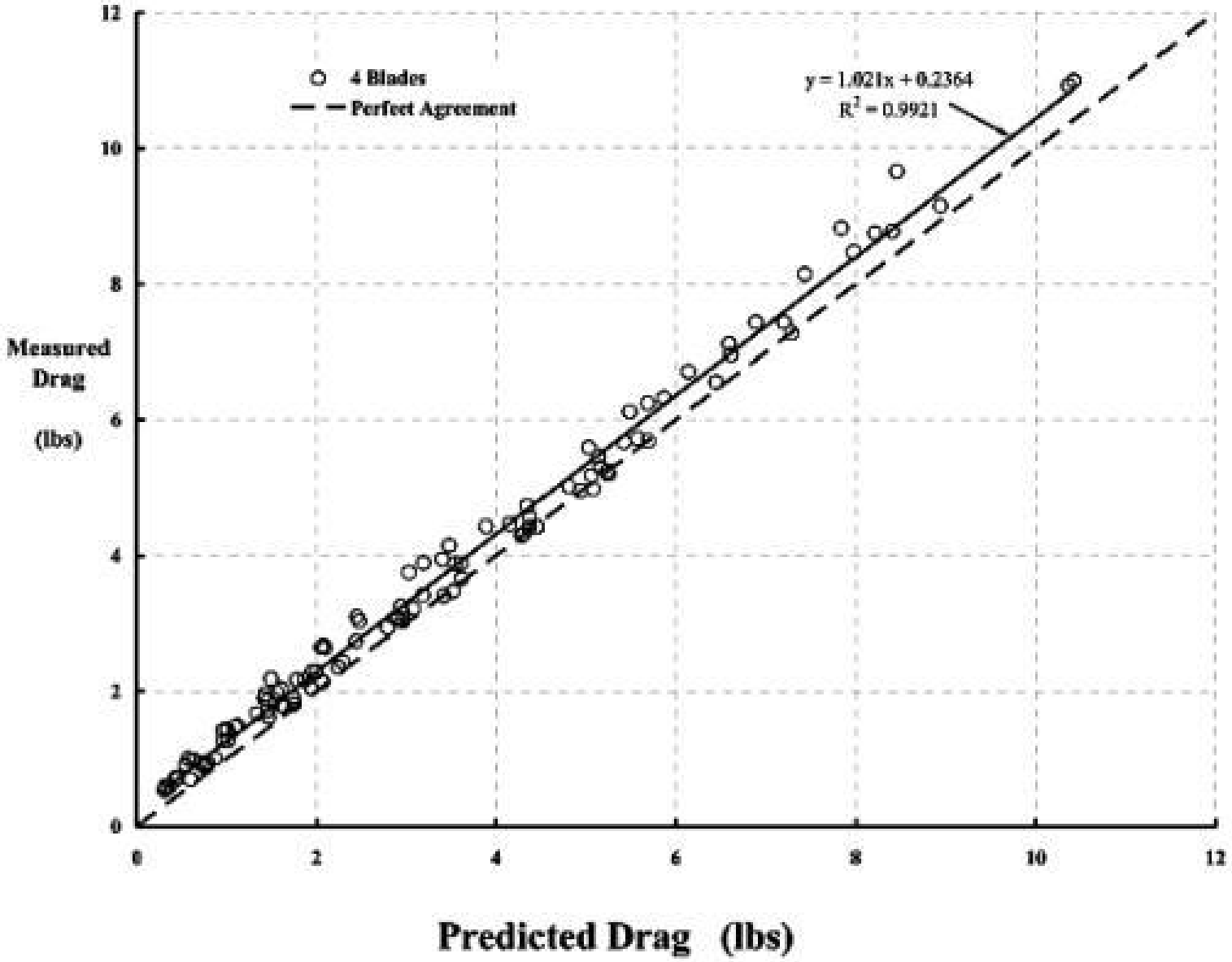

Fig. 2-104 Test versus theory for four blades (prediction with Eq. (2.287)).

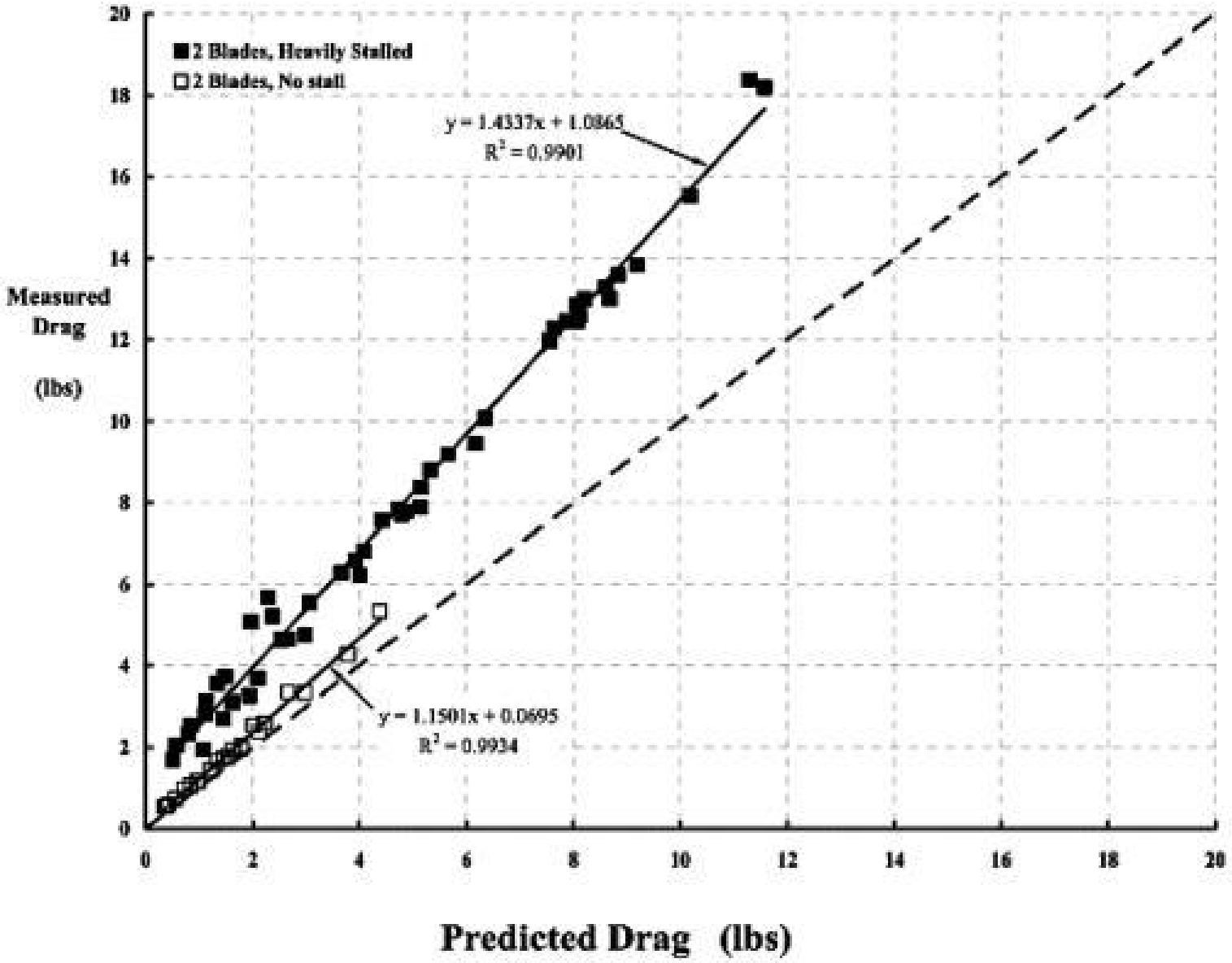

Fig. 2-105 Test versus theory for two blades (prediction with Eq. (2.287)).

2.11 PERFORMANCE

Table 2-16. Göttingen 429 Airfoil Data [121]

Reynolds Number	Minimum Drag Coefficient	Maximum Lift Coefficient
63,940	0.0160	
85,040	0.0154	
106,780	0.0146	
127,880	0.0137	0.88
148,980	0.0134	
287,720	0.0112	0.96
383,630	0.0108	1.00
575,450	0.0104	1.08
767,260	0.0102	1.16
959,080	0.0102	

Now let me address the subject of maximum rotor lift-to-drag ratio, a seriously debated subject between Cierva and Glauert. At this point, you might not view the simple expression for minimum drag, Eq. (2.287), as adequate; nevertheless, the rotor lift-drag ratio is approximated by

(2.289) $$\frac{L_R}{D_R} = \frac{L_R}{\frac{L_R^2}{2\rho A V_{FP}^2} + \frac{\rho A \sigma V_t^3}{8 V_{FP}} C_{d\min}\left(1+3\mu_{hp}^2\right)}.$$

The rotor lift (L_R) at which maximum rotor L/D occurs is found in the usual manner, so

(2.290) for maximum rotor L/D,

$$L_R = \frac{1}{2}\rho A V_t^2 \sqrt{\sigma \mu_{hp}\left(1+3\mu_{hp}^2\right) C_{d\min}}$$

or, in the nondimensional form,

(2.291) for maximum rotor L/D,

$$C_T \approx C_L = \frac{L_R}{\rho A V_t^2} = \frac{1}{2}\sqrt{\sigma \mu_{hp}\left(1+3\mu_{hp}^2\right) C_{d\min}}\ .$$

The rotor maximum L/D is, therefore, calculated simply as (2.292)

$$(L/D)_{Max} = 2\sqrt{\frac{\mu_{hp}^3}{\sigma\left(1+3\mu_{hp}^2\right) C_{d\min}}} = \frac{\mu_{hp}^2}{C_T \text{ for max. } L/D}.$$

This fundamental, very simplified theoretical result is compared to the Lock

and Townend 6-foot-diameter C.6A model test results in Fig. 2-106. Glauert's simple theory shows that maximum rotor L/D improves by reducing rotor solidity (σ). Halving the solidity from 0.1896, with four blades, to 0.0948, with two blades, is clearly beneficial as the experimental data shows.

As you can see, Fig. 2-106 leaves plenty of room to debate what the maximum lift-to-drag ratio of a rotor might be, at least beyond an advance ratio of 0.3. Glauert [13 1] made it quite clear when he replied to Cierva's letter that

"All the experimental evidence which I have seen, both model and full scale, indicates that the lift/drag ratio of an autogyro [rotor] and the performance of the aircraft is rather less favorable than I should estimate theoretically."

Certainly, the 6-foot-diameter-model rotor blades alone were not performing up to their calculated potential, never mind the rest of the aircraft. Cierva, on the other hand, made it quite clear that

"The autogyro, in spite of its extreme simplicity, is not at all an obvious [simple] problem, and any attempt to develop its theory as an extension of the aerofoil [wing or propeller] theory must perforce be regarded with very great diffidence owing to the fact that, in order to avoid almost insuperable complications, it is necessary to attempt simplification of the phenomena and perhaps also to neglect terms which might seem to be of the second order whereas in fact they may be, under certain most interesting conditions, of the first order."

So, each had made their case and, I will guess, neither man had conferred with the other with Fig. 2-106 in hand.

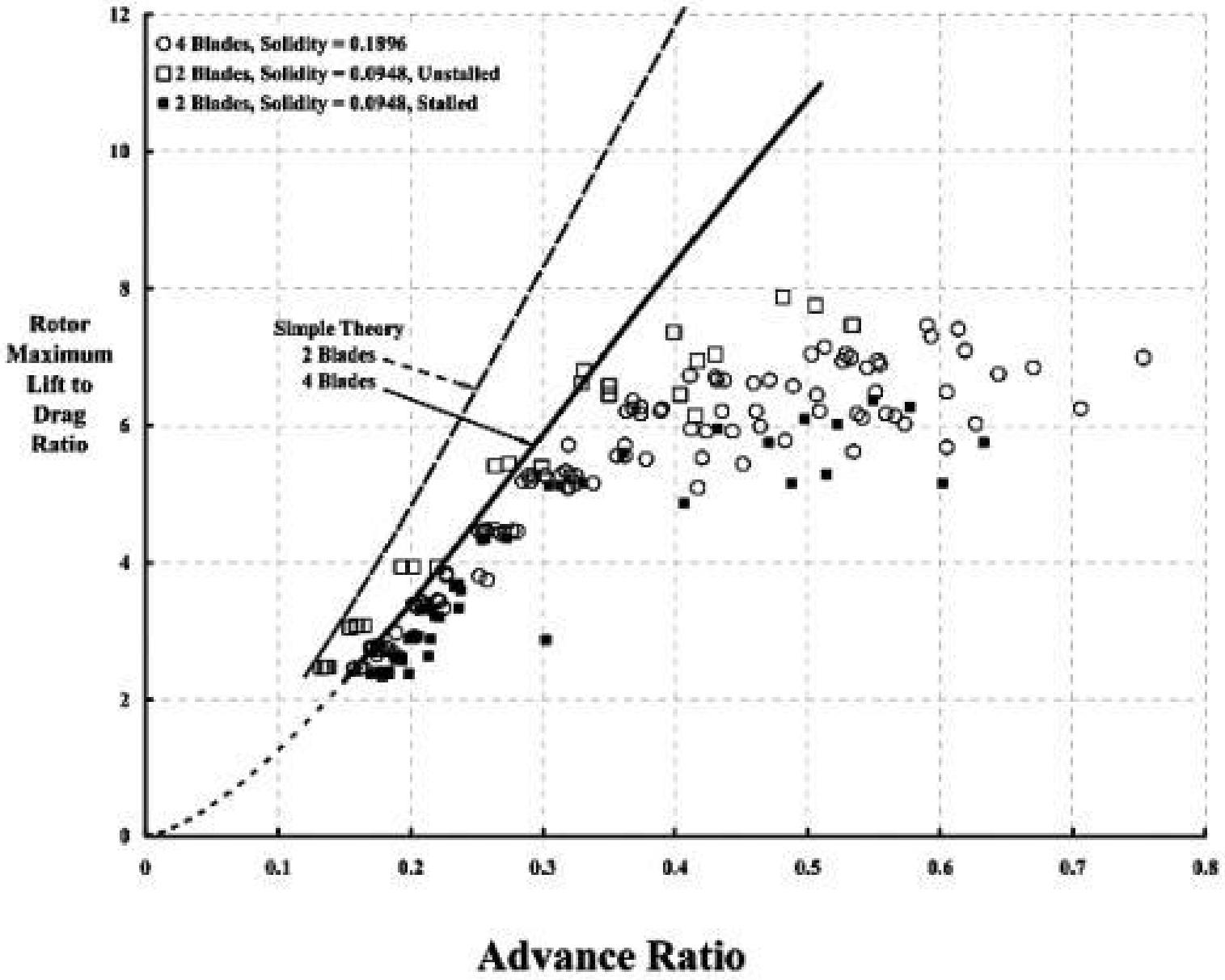

Fig. 2-106. Maximum rotor L/D theory versus test.

2.11 PERFORMANCE

A natural question when looking at Fig. 2-106 is, "Why did the model perform so poorly at high advance ratio, assuming the simple theory is approximately right?" A partial answer to this question lies within Fig. 2-107. To obtain lift-to-drag ratios well above 10 (which would be on-par with nonrotating biplane wings of the era), the 6-foot-diameter-model rotor should have been tested to much higher thrust coefficients . But the ability of the rotor to produce the necessarily high thrust—without many blade element airfoils stalling and creating very high drag—is not at all clear. Lock offered an opinion about blade stall [14] and noted that

"the order of magnitude of the effect of "[blade] stalling" could be determined in any particular case by evaluating graphically the integral in equation 29 [see Eq. (2.280)] on the basis of the performance data of the airfoil section."

It would take the rotorcraft industry three more decades (and the digital computer) before the

graphical integration Lock was suggesting could be done for just a few "particular cases."

However, a sense of just where, in relation to blade stall onset, the Lock and Townend 6-foot-diameter model was tested can be obtained from Eq.(2.194), repeated here as

(2.293)

$$\left(\frac{C_T}{\sigma}\right)_{\substack{\text{blade}\\ \text{stall}}} = \left(\frac{T_{hp}}{\rho bcRV_t^2}\right)_{\substack{\text{blade}\\ \text{stall}}} = \frac{C_{\ell max}}{6}\left[\frac{1-\mu^2-\frac{4}{3\pi}\mu^3+\frac{25}{24}\mu^4-\frac{46}{15\pi}\mu^5-\frac{5}{16}\mu^6+\frac{1}{90\pi}\mu^7}{1+\frac{8}{3}\mu+\frac{3}{2}\mu^2+\left(\frac{32}{45\pi}-\frac{5}{24}\right)\mu^4}\right].$$

onset onset

This estimate, along with the 1928 model test results for an autorotating rotor [132], is shown in Fig. 2-108. Clearly, the rotor, whether two bladed or four bladed, produces thrust well outside the estimated blade stall onset boundary suggested by Eq. (2.293). But this high thrust at high advance ratio is accompanied by a great deal of rotor drag and relatively poor rotor

lift-to-drag ratios as Fig. 2-106 shows. As you will read in Volume II—Helicopters, modern helicopter rotor blades have improved rotor maximum L/D, but they still do not achieve levels much above 10 in the 0.3 to 0.5 advance ratio range, primarily because both rotor solidity and tip speed were significantly increased over autogyro values.

2.11.4 Minimum Rotor Drag

It was immediately apparent that the simple theory used to predict rotor drag had one troublesome factor that bothered both Glauert and Cierva in 1928. The simple theory, Eq. (2.287), which I have repeated here

(2.287)

$$D_R = \frac{L_R^2}{2\rho A V_{FP}^2} + \frac{\rho A \sigma V_t^3}{8 V_{FP}} C_{d\,min}\left(1 + 3\mu_{hp}^2\right)$$

Glauert Form

raised an issue about the factor 3 in the $\left(1+3\mu_{hp}^2\right)$ term, which came, you recall, from the

simplified profile power integral. Glauert, in his first paper on autogyros [13], pointed out in

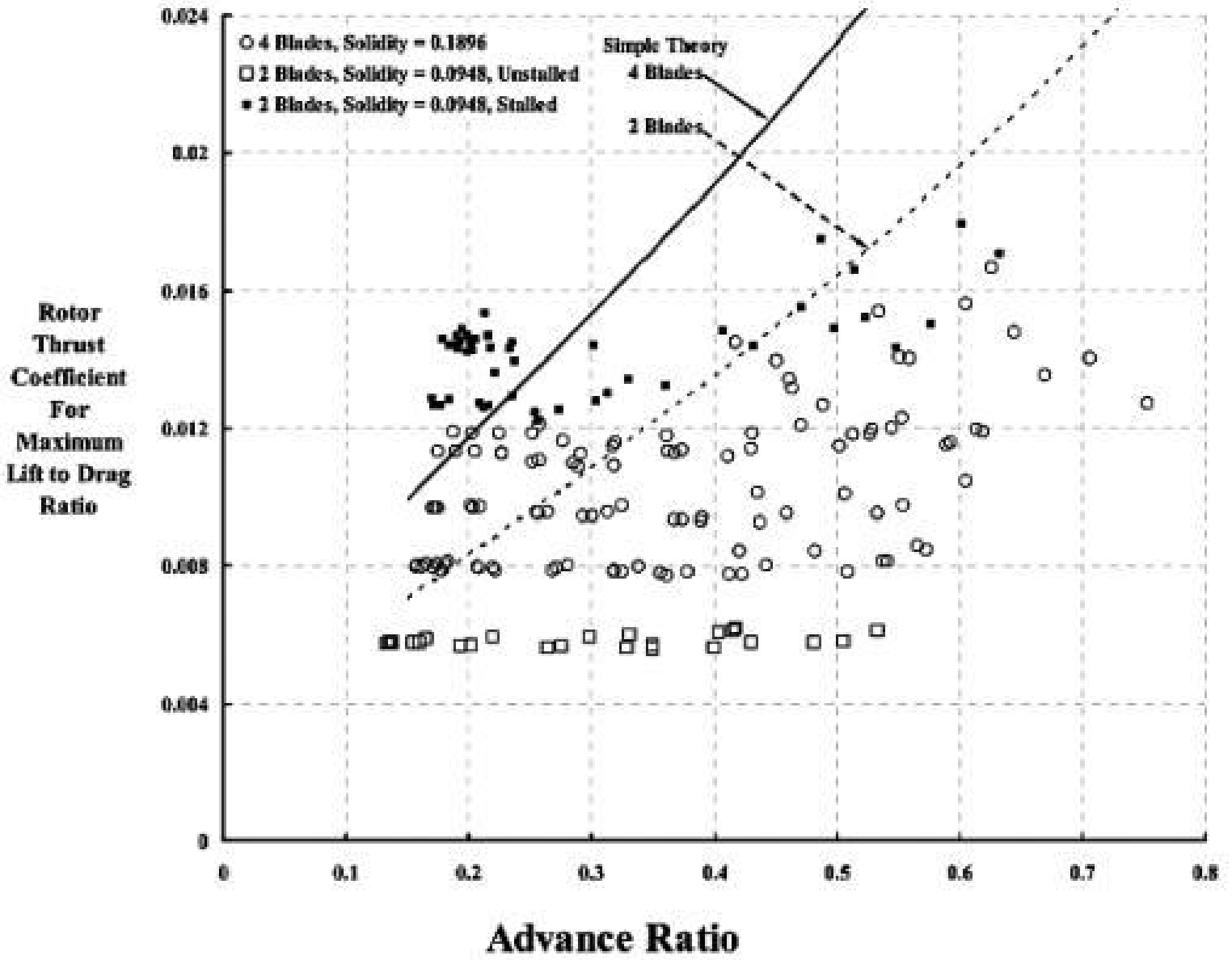

Fig. 2-107. Thrust coefficient for maximum rotor L/D—theory versus test.

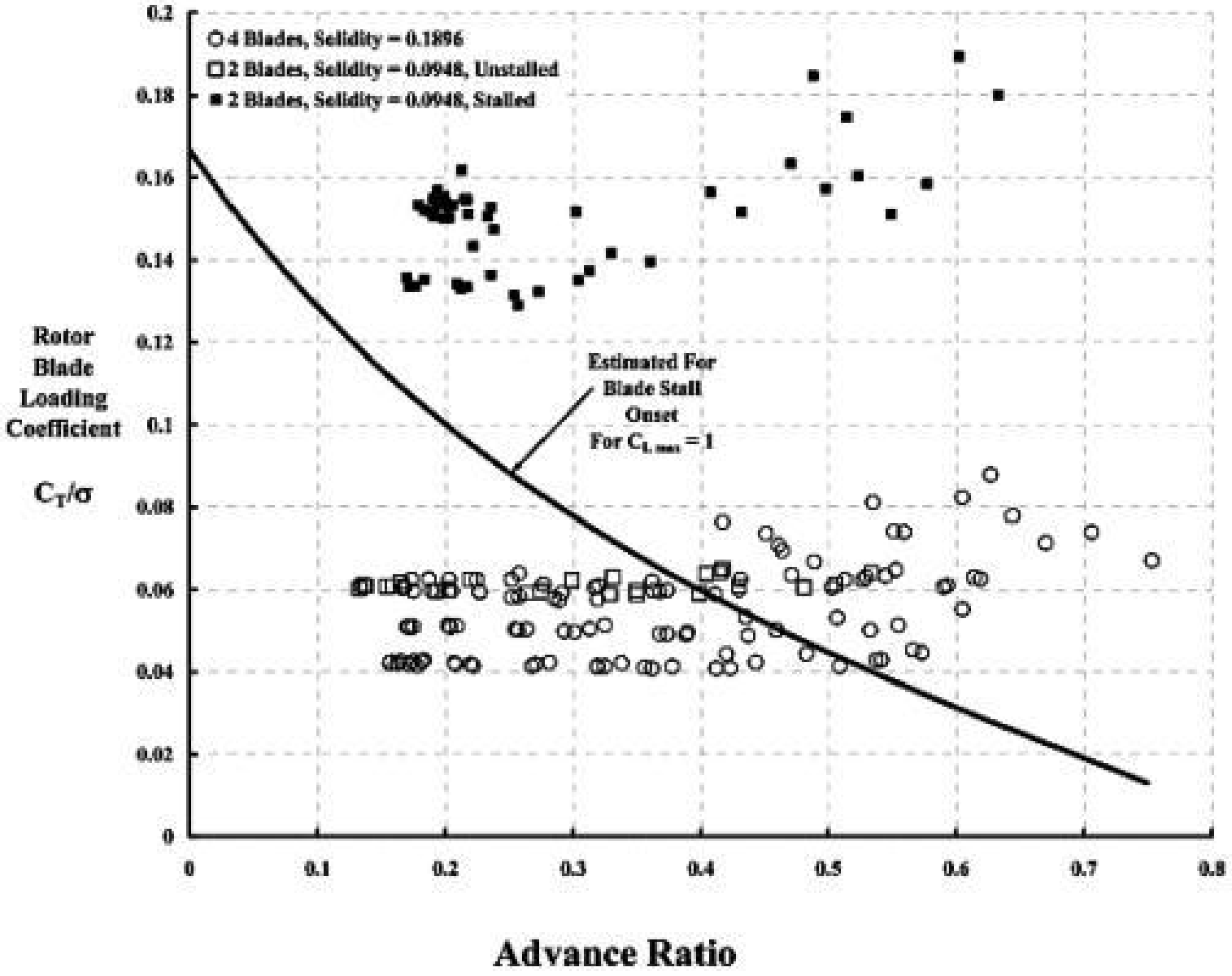

Fig. 2-108. Blade stall onset.

2.11 PERFORMANCE

an appendix of the paper that the blade element velocity (V_{BE}) should include the radial velocity component $\left(V_{FP}\cos\alpha_{hp}\right)\cos\psi$, as well as the tangential velocity component $\Omega r+\left(V_{FP}\cos\alpha_{hp}\right)\sin\psi$. That is, he recommended that

(2.294)

$$V_{BE}=V_{r,\psi}=\sqrt{\left[\Omega r+\left(V_{FP}\cos\alpha_{hp}\right)\sin\psi\right]^2+\left[\left(V_{FP}\cos\alpha_{hp}\right)\cos\psi\right]^2}$$

which compares to Eq. (2.28 1). This leads to a profile power integral that falls in the elliptical integral family. Appendix J includes a closed-form approximation to this problem. What was a constant 3 became a factor (n); but then (n) was itself a function of advance ratio. Glauert took a shortcut around the elliptical integral complication by providing a table.

The reproduced table, plus a comparison to $\left(1+3\mu_{hp}^2\right)$, is

Advance Ratio μ_{hp}	$\left(1+3\mu_{hp}^2\right)$	$\left(1+n\mu_{hp}^2\right)$	Glauert's n
0	1.00	1.00	4.5
0.30	1.27	1.43	4.73
0.40	1.48	1.78	4.87
0.50	1.75	2.26	5.03
0.60	2.08	2.88	5.22
0.75	2.69	4.11	5.53
1.00	4.00	7.13	6.13

Cierva, when his theory became available [1 1], agreed with Glauert that the blade element velocity should include the radial flow velocity and, with his own approximation, decided that it would be satisfactory to replace $\left(1+3\mu_{hp}^2\right)$ with $\left(1+4\mu_{hp}^2\right)$. It would be several decades (plus the advent of the digital computer and several full-scale helicopter rotor system wind tunnel tests) before a more accurate picture

began to emerge about this radial flow velocity. A review of this work [133] provided the approximation

(2.295) $1+4.65\mu_{hp}^2+4.15\mu_{hp}^4-\mu_{hp}^6$

which seemed to fit the experimental data up to an advance ratio of 1.0 and was, therefore, more realistic than $\left(1+3\mu_{hp}^2\right)$. On this basis, the rotor drag would be more accurately calculated as

(2.296)

$$D_R=\frac{L_R^2}{2\rho A V_{FP}^2}+\frac{\rho A\sigma V_t^3}{8V_{FP}}C_{d\,min}\left(1+4.65\mu_{hp}^2+4.15\mu_{hp}^4-\mu_{hp}^6\right).$$

A comparison of this somewhat refined rotor drag theory versus the Lock and Townend 6-foot-diameter-model data is shown in Fig. 2-109. I kept the airfoil minimum drag coefficient ($C_{d\ min}$) at 0.013, so this result can be compared to Fig. 2-104.

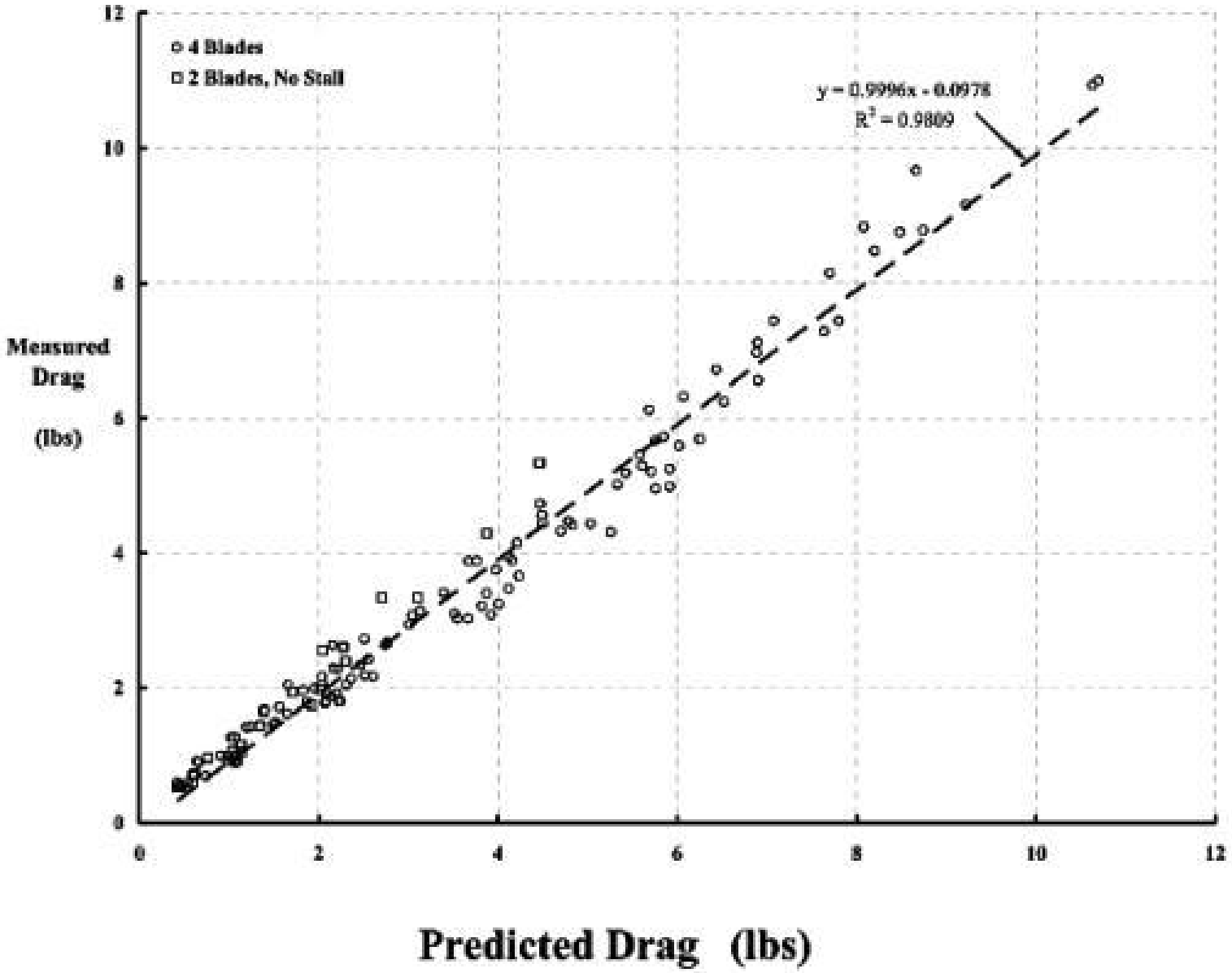

Fig. 2-109. Test versus theory for four and two blades (prediction with Eq. (2.296)).

2.11.5 Autogyro Versus Airplane

The fundamental issue of autogyro versus airplane performance in forward flight was not settled with Cierva's second lecture to the Royal Aeronautical Society on February 13, 1930. In this lecture, Cierva addressed his third point saying, you will recall, that

"the comparison in performance between existing autogiros of several types and best equivalent aeroplanes can be summed up as follow:–Top speed, five to ten per cent less. Rate of climb, twenty per cent less. Steepness of climb, fifty percent more. Minimum horizontal speed, fifty per cent less."

To Cierva, that was the current situation as he saw it. In his lecture, he showed his figure 3, which I have reproduced here as Fig. 2-110, to explain his views. (Major Green said during the discussion that "a diagram like Fig. 3 meant very little when there was no scale to it."). Of course, no one defined "best equivalent

aeroplane." With this figure displayed to the audience, Cierva made a number of points, some of which I have summarized as follows:

2.11 PERFORMANCE

1 . Figure 3 [Fig. 2-1 10] shows power required versus speed "for two normal equivalent machines."

a. Both aircraft are at equal weight.

b. The autogyro rotor diameter and airplane wing span are equal, so, at equal weight, the induced drags are equal. Since power is drag times velocity, induced powers are equal for both machines.

c. "Both machines have the same parasite drag." [Equal total drag of fuselage, landing gear, rudder and elevator, rotor

hub, etc.]

d. Therefore, "the required horse-power equations would differ only in the term corresponding to profile drag." [Profile power when drag is multiplied by speed.]

e. The airplane wing profile power increases as the cube of speed, but the autogyro rotor profile power rises "directly proportional to the speed within wide limits." [See Eq. (2.288).]

2. The airplane has its maximum efficiency in the middle speed range, "while the autogyro is at its best at both ends [of its speed range]."

3. The two distinct slopes of power required with speed (at high speed) show that the autogyro benefits by having does.

increased power available more than the airplane

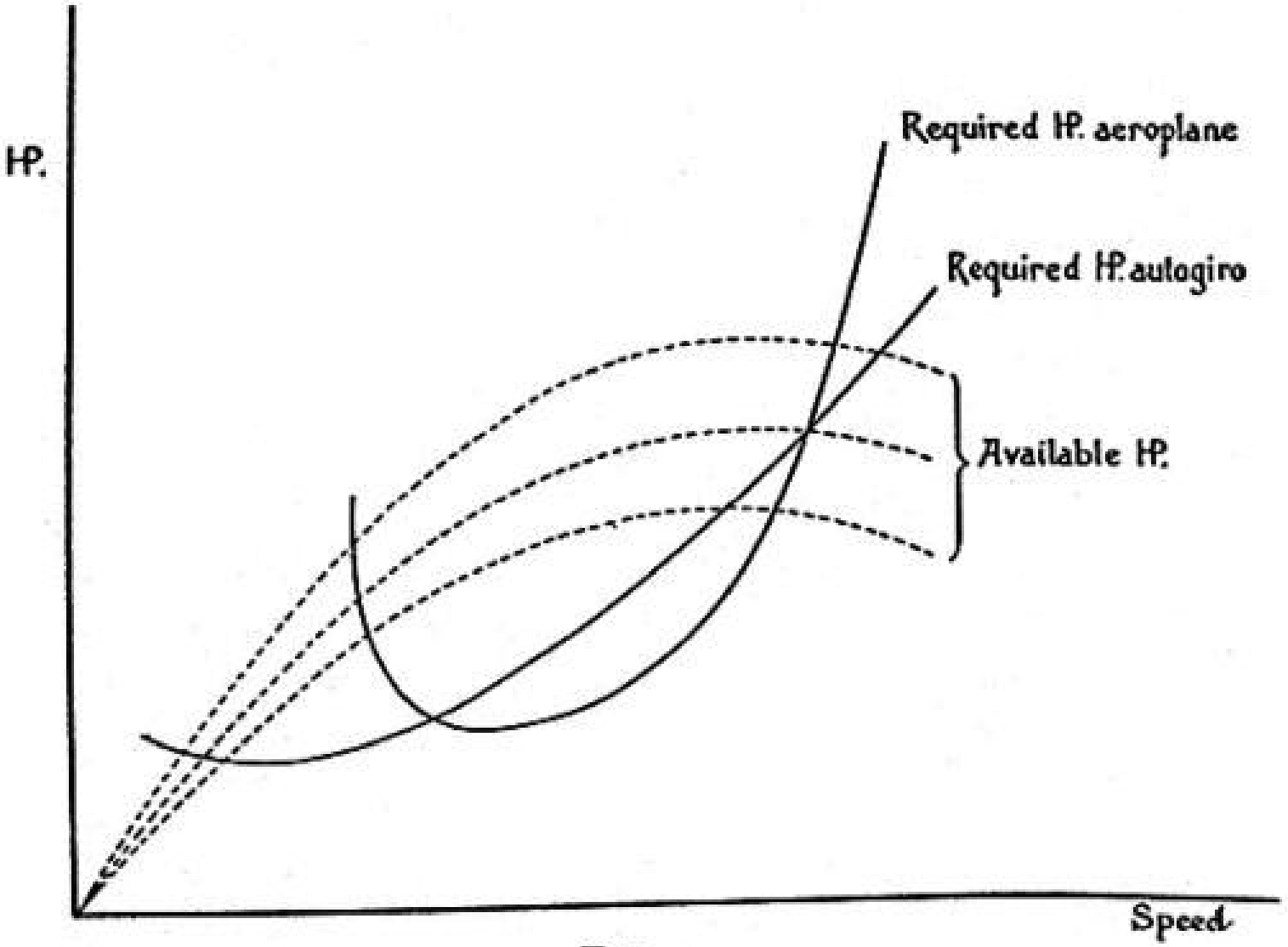

FIG. 3.

Fig. 2-110. Cierva's comparison of autogyro versus airplane performance [4].

Perhaps a word of explanation about the power available lines and their shape versus speed in Fig. 2-1 10 is in order before proceeding. During this era, propellers were fixed pitch. Rather than reflect propeller efficiency in power required to obtain engine power required (which can then be compared directly to engine power available), engine power available was reduced by propeller efficiency to define a thrust power available (which is then compared to thrust power required). That is, when you start with

(2.297) Prop Thrust Required = $T_{prop.req.}$ = Aircraft Total Drag = D_{AC}

then multiply by flight path velocity (V_{FP}) to get thrust horsepower required, you see

(2.298) Thrust Horsepower Required

$$HP_{thrust\,req.} = \frac{T_{prop} V_{FP}}{550} = \frac{D_{AC} V_{FP}}{550}.$$

But, the propeller is not 100 percent efficient. The propeller efficiency (η_P) was optimized for high speed during this era. Therefore, the total engine horsepower available ($HP_{eng.\ avail.}$) only provides available propeller thrust amounting to

(2.299)

$$\text{Available Propeller Thrust} = T_{prop\,avail.} = \left(\frac{550 HP_{eng.avail.}}{V_{FP}} \right) \eta_P$$

so the available thrust horsepower is only

(2.300)

$$\text{Available Thrust Horsepower } HP_{\text{thrust avail.}} = \frac{T_{\text{prop}} V_{FP}}{550} = \left(HP_{\text{eng.avail.}}\right)\eta_P .$$

Thus, the shape of a thrust horsepower available line mirrors the propeller efficiency because engine horsepower available is considered constant with airspeed. The helicopter pioneers did not follow this fixed-wing practice.

A comparison of the 1930s-era autogyro to the best equivalent airplane is very worthwhile because the debate over which machine is better is still going on today. To quantify the comparison, let me choose the 1930 Pitcairn PCA-2 as the representative autogyro and then present airplanes of that era in comparison. The performance of the PCA-2 was thoroughly

established by John Wheatley at the N.A.C.A. He published PCA-2 flight test results in NACA Report No. 434 in May 1932 [127]. Because he could not satisfactorily separate the rotor-blades-alone performance from the total autogyro performance, the full- scale, 45-foot-diameter rotor system was tested in the 30-foot by 60-foot wind tunnel at the N.A.C.A. Langley. Data from that test was reported in NACA Report No. 487 [75] in 1934. These two reports are an enormously valuable autogyro data base for the rotor-plus-wing configuration (including the Cierva C.19) before direct control autogyros (such as the Cierva C.30A) became available. Both reports provide all the experimental data in tables.

2.11 PERFORMANCE

Wheatley, in the introduction to NACA Report No. 434, wrote that

"The determination of lift and drag characteristics was decided upon as the initial step into an extensive program of research because of the lack of reliable full-scale information on the fundamental aerodynamic characteristics of the autogiro and the need to establish clearly a datum to which further work will be referred. The curves and data contained in the body of this report constitute, so far as is known, the first authentic full-scale information concerning autogiro characteristics that has been published."[50]

He goes on to describe the test apparatus (Fig. 2-1 1 1), and how aircraft lift and drag were obtained from a gliding test, shown in Fig. 2-1 12 . Wheatley included one adverse comment about the PCA-2 that affected the performance:

"The problem of control at the low air speeds and high angles of attack attainable in the autogiro demands attention [the direct control rotor was the response].

During glides at air speeds near the minimum value, corresponding to angles of attack from about 35° to 90°, lateral control was inadequate and the aircraft was unsteady. Elevator control, although sluggish, remained positive at all times, but ailerons and rudder often proved unable to check or delay a tendency of the autogiro to roll or yaw [many minor autogyro accidents occurred on landing because of this characteristic]."

Some evidence of controlling the aircraft in trim during a glide is, in fact, apparent. However, overall, the flight test data is as good, and probably better, than data acquired in a wind tunnel.

Rotor	Symbol	
Number of blades	b	4.
Profile of section		Göttingen 429.
Diameter	$2R$	45.0 ft.
Blade chord (outer straight portion)	c	1.833 ft.
Disk area	S_D	1,5888 sq. ft.
Solidity	Total blade area/ disk area	0.0976.

Wing		
Profile		Modified N.A.C.A.–M3.
Span		30 ft. 3-5/8 in.
Chord—root		4 ft. 4 in.
Area—projected	S_W	101 sq. ft.
Aspect ratio		9.1.
Incidence		1.7°.

General		
Total area	$S = S_D+S_W$	1,689 sq. ft.
Gross weight as flown	W	2,940 lb.
Wing loading	W/S	1.74 lb./sq. ft.
Engine		Wright R-975.
Power-rated		300 hp

Fig. 2-111. Pitcairn PCA-2 geometry tabulated by Wheatley [127].

---

[50] Wheatley was right; nothing had been published at the time he wrote NACA Report No. 434, but I believe that the Royal Aircraft Establishment in England acquired a great deal of technical data about Cierva Autogiros, specifically the C.6A [37] and the C.19 (I will bet). There are many references to unpublished T. numbered reports in the Aeronautical Research Committee R & M's.

If those old reports could be recovered, it would add a great deal of historical technology to the birth of the rotorcraft industry.

240

2.11 PERFORMANCE

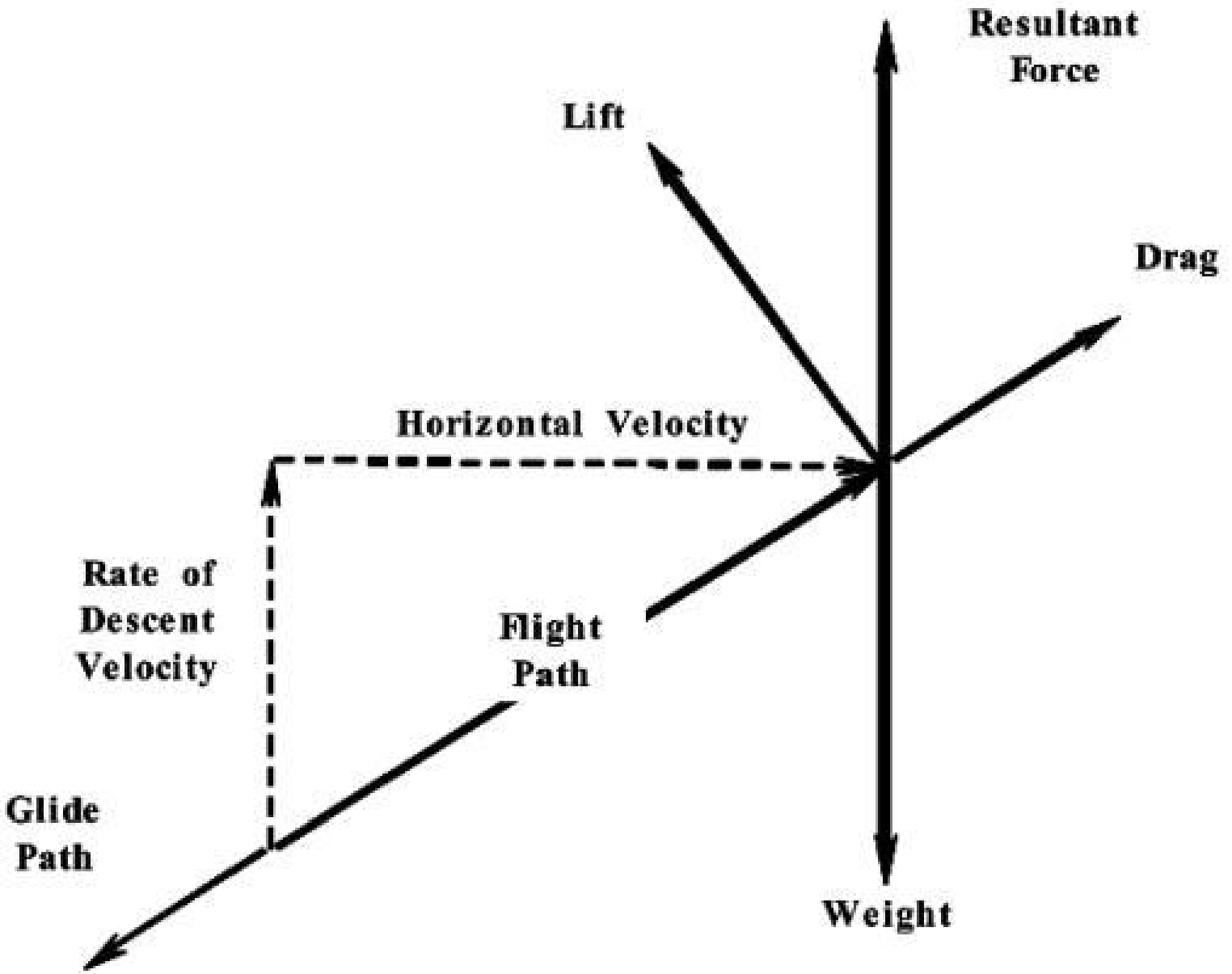

Fig. 2-112. Aircraft lift and drag obtained from gliding tests.

Wheatley obtained the PCA-2 lift and drag from gliding tests with the engine off and propeller stopped. One hundred and eighty-four separate glides were made in 22 flights . After each glide, the pilot restarted the engine, regained altitude, and started another glide. After each flight, the aircraft was refueled. The first glide in each flight began at about 2,900-pounds gross weight, and the last glide in that flight finished, on average, at about 2,760-pounds gross weight. Wheatley carefully accounted for the varying gross weight, which was caused by fuel burn off. The glide angle and flight path velocity were measured with a "trailing bomb," which was slung by a thin cable some 80 feet below the aircraft. Aircraft attitude was measured and the hub plane angle of attack was computed and

tabulated.

The lift and drag data that Wheatley obtained from this ground-breaking flight test is shown in Fig. 2-113. The accompanying hub plane angle of attack is shown in Fig. 2-114. In general, the PCA-2 remained nearly horizontal with only a moderate nose-down attitude—but still slightly positive angle of attack—to reach the higher speeds (over 100 feet per second). The rotor speed deviated very little from an average of 14.9 radians per second. Wheatley accounted for this slight rotor speed variation, as well as the hub plane angle of attack, to compute advance ratio. In calculations requiring air density, he used the density for each glide, but the average density was 0.002103 slugs per cubic foot. Some measurements of

performance with the engine and propeller at flight idled satisfied Wheatley that the drag of *this* stopped propeller was relatively unimportant.

Fig. 2-1 13 shows that in vertical descent, the flight path velocity (i.e., the rate of descent) was 35 feet per second. Additional analysis led Wheatley to conclude that "the minimum vertical velocity when gliding with the stopped propeller is 15 feet per second, at an airspeed of 36 miles per hour, and at a flight-path angle of -17°." He further noted that

"The maximum lift coefficient, based on the sum of wing and swept-disc area [1,689 square feet], is 0.895 [based on dynamic pressure, not tip speed] . The minimum drag coefficient with propeller stopped is 0.015, the maximum L/D with propeller stopped is 4.8, and the maximum resultant force coefficient is 1 .208 [based on

dynamic pressure and 1,689 square feet].

The fact that the maximum aircraft L/D was only 4.8 certainly could not have been very encouraging to autogyro advocates. Glauert and Lock had probably been getting comparable values with Cierva machines in England. In my opinion, Glauert's initial pessimism was warranted, but without the drive from Cierva (plus Pitcairn and Kellett)—and support from the Air Ministry in England, specifically from Mr. H . E . Wimperis—the rotorcraft industry could have easily died in 1930, along with the biplane.

Before bringing performance of comparable airplanes into the discussion, it is worthwhile to predict the PCA-2 drag using simple aerodynamic technology available in 1930. As Cierva pointed out, the propeller thrust must overcome the drag created by all components of the aircraft, not just the drag

created by the rotor blades alone. The rotor system hub and the exposed spars (commonly referred to as blade shanks) must be accounted for as well. Then, in the case of the PCA-2, the wing, which carries some lift, creates drag. And finally, the fuselage, wheels, vertical and horizontal stabilizer, engine, other protuberances, etc., must be added to the propeller load.

Now suppose all the drag from all the items—except the rotor blades alone—amounts to some equivalent parasite drag area (f_e) in square feet that varies with angle of attack. Then the aircraft drag (D_{AC}) is estimated simply as

(2.301)

$$T_{prop.req.} = D_{AC} = \frac{1}{2}\rho V_{FP}^2 \left(f_e\right)\left(1+K\alpha_{hp}^2\right)+D_R$$

with the autorotating rotor-blades-alone drag (D_R) estimate coming from Eq. (2.296). Thus, the aircraft drag is nothing more than

(2.302)

$$D_{AC} = \frac{1}{2}\rho V_{FP}^2 (f_e)\left(1 + K\alpha_{hp}^2\right) + \frac{W^2}{2\rho A V_{FP}^2 \cos\alpha_{hp}}$$

for autogyro.

$$+ \frac{\rho A \sigma V_t^3}{8 V_{FP}} C_{d\,min}\left(1 + 4.65\mu_{hp}^2 + 4.15\mu_{hp}^4 - \mu_{hp}^6\right)$$

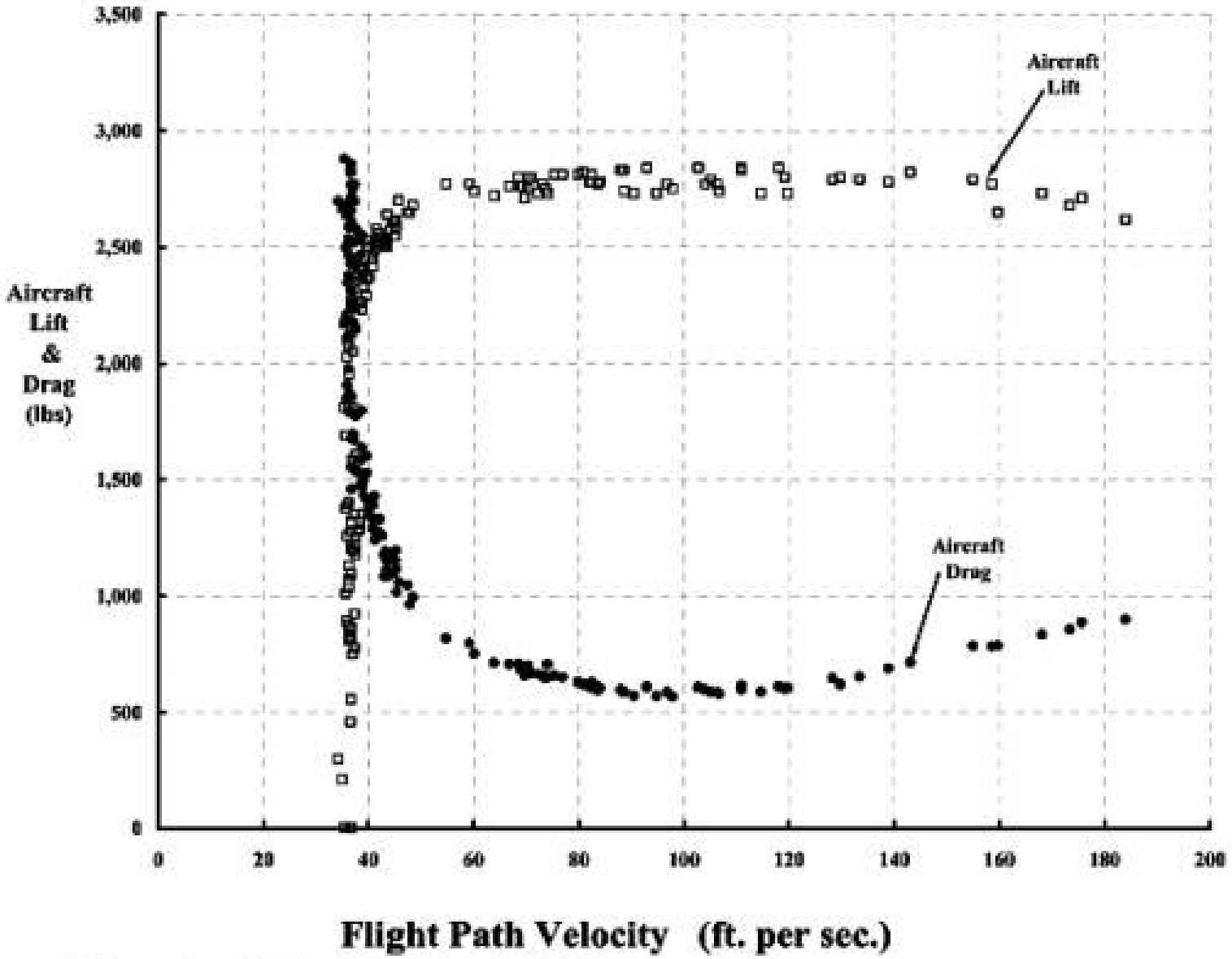

Fig. 2-113. PCA-2 lift and drag forces versus flight path velocity [127].

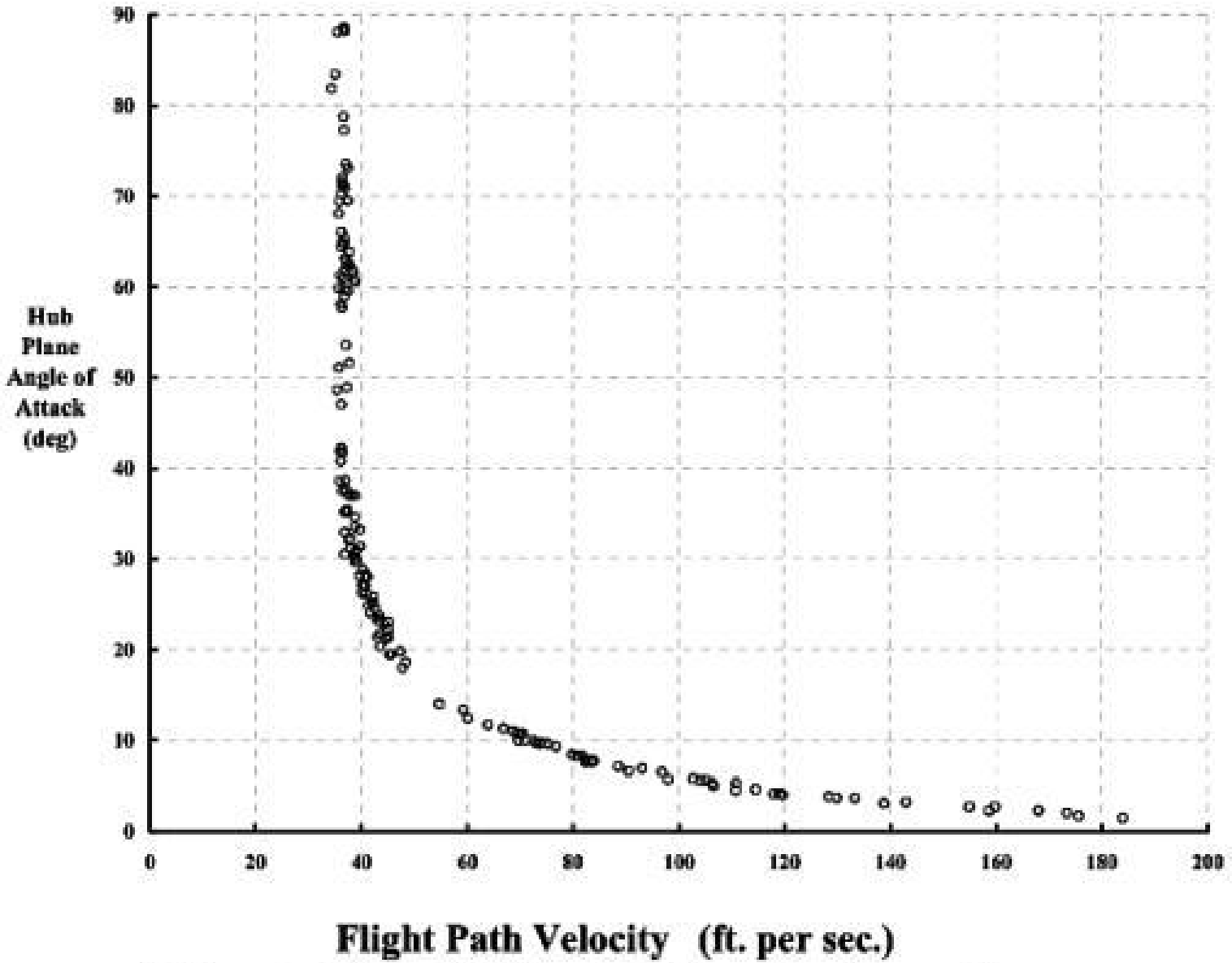

Fig. 2-114. PCA-2 trim during the Wheatley gliding tests [127].

2.11 PERFORMANCE

Notice in Eq. (2.302) that I assumed rotor lift (L_R) equal to aircraft weight (W), which implicitly says the wing operates at zero lift. Also notice that I have retained cosine α_{hp} in the denominator of the induced drag term, which extends the equation to higher angles of attack.

Given the PCA-2 configuration details and tabulated data of the flight parameters Wheatley provided, *you only have to estimate or guess* the equivalent parasite drag area (f_e), and its variation with angle of attack, to make the answer come out right (i.e., test and theory agree). It does help to adjust the airfoil minimum drag coefficient for the Göttingen 429 from the model value of 0.013 to 0.010 for the full scale. The specific data leading to the drag breakdown lines shown in Fig. 2-115 is:

Parameter	Value	Rational
Weight, lbs	2,825	Average for test
Rotor Speed, rad/sec	14.9	Average for test
Radius, ft	22.5	PCA-2
Tip Speed, ft/sec	varies	Average for test
Rotor Area, sq ft	1,588	PCA-2
Solidity	0.0976	PCA-2
Density, slug/cubic ft	0.002106	Average for test
$C_{d\ min}$	0.0100	Estimated full scale
Base Parasite Area, f_e, sq ft	19	Best guess
Parasite Area Constant, K, 1/sq rad	20	Best guess

Although rather semiempirically arrived at, the drag breakdown of Fig. 2-1 15 illustrates the fact that drag at high speed is dominated by base parasite drag area (f_e) of the configuration and, to a lesser extent, the profile drag of the rotor blades alone. Drag at low speed is dominated by rotor drag and mostly by rotor-induced drag.

Now consider, in Cierva's words, " a normal equivalent machine." Before Pitcairn got into the autogyro business, he and his

company were very prominent in the fixed-wing business. His airplane manufacturing side developed the "Mailwing" series, which refined his PA-5, -6, and -7 into the PA-8 shown in Fig. 2-1 16 . The PA-8 was certificated on September 19, 1930. Seven months later, the Pitcairn PCA-2 autogyro, shown in Fig. 2-1 17, was certificated. Consider then these five points:

1. both aircraft were built by a well established and very reputable company, 2. the two aircraft were certificated within 7 months of each other,
3. both aircraft used the same engine (Wright, 9 cylinders, J6 having 300 available horsepower),
4. the selling prices at the factory were close ($15,000 for the PCA-2 in 1931 versus $12,500 for the PA-8 in 1930), and
5. the chief engineer for both aircraft was Agnew Larsen.

I believe that the PA-8 is a satisfactory

example of an airplane equivalent to the PCA-2 autogyro. Of course, the PA-8 was quite well developed while the PCA-2 was the first in the series . Direct control and the lower solidity, three-bladed cantilevered rotor technology were yet to come, so the PCA-2 was not in the Cierva C.30A class.

2.11 PERFORMANCE

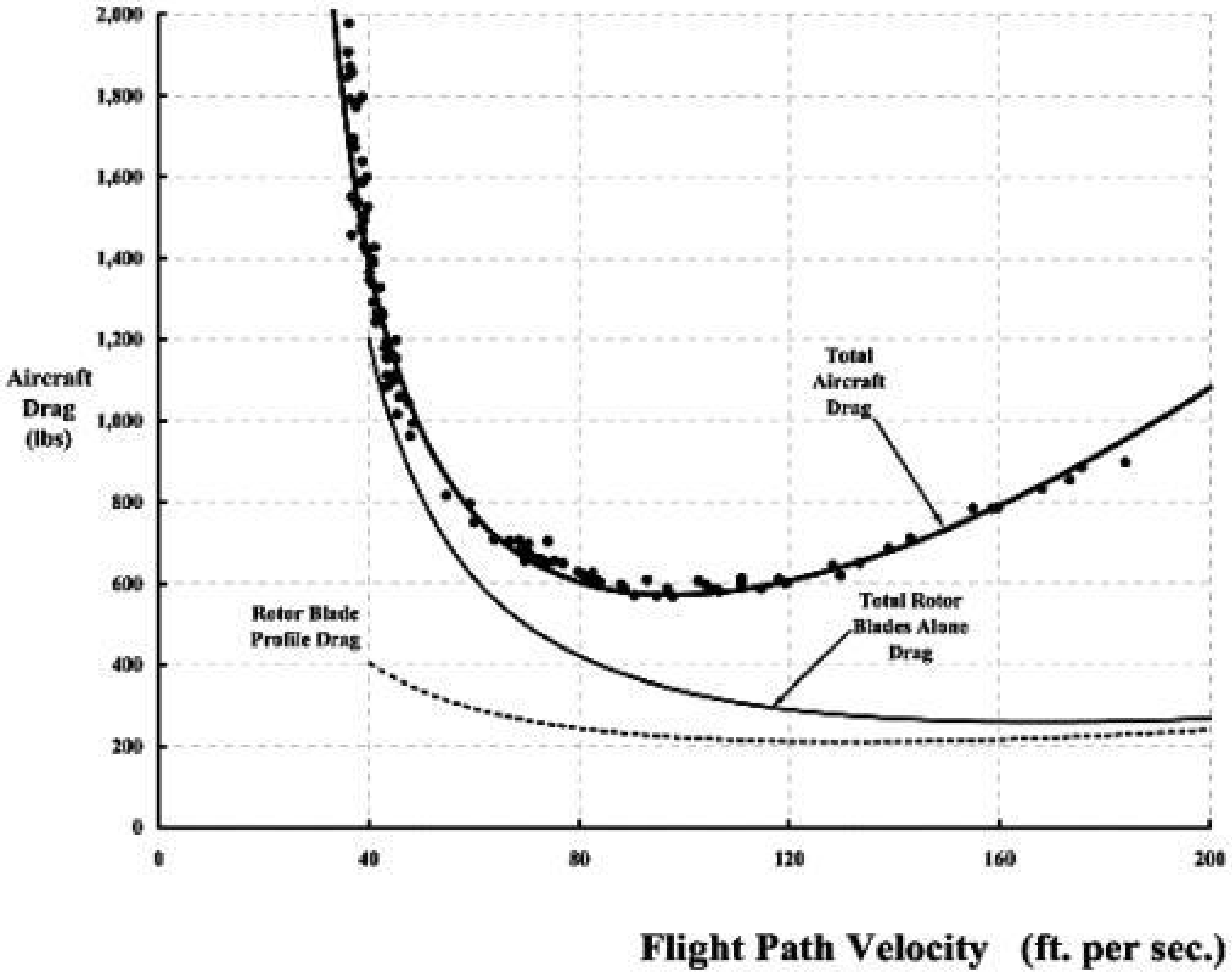

Fig. 2-115. Estimated PCA-2 drag breakdown.

The comparison of the two aircraft is shown in Table 2-17. I have used the summary data from two volumes of *U. S. Civil Aircraft Series* by Joseph P. Juptner [134, 135] as the

source for the comparison. There are, of course, some glaring differences that appear on Table 2-17 such as range, speed, and useful load. These differences cannot be assumed away as Cierva tried to do in his definition of "normal equivalent machines." He attempted to reduce the differences to just profile drag of the wing "which increases as the cube of flight path velocity" versus the rotor profile power which increases "directly proportional to the speed within wide limits." [4].

Cierva's view in February 1930 was that: "top speed, five to ten per cent less [than the airplane]." The tabulated comparison gives 1 18/145, which is more like 20 percent less. Cierva said, "rate of climb, twenty per cent less." My comparison shows 800/1,100, which is 21 percent less. Table 2-17 does not include Cierva's "steepness of climb, fifty percent more," but many photos support that view. Finally, Cierva stated "minimum horizontal

speed, fifty per cent less." Table 2-17 shows 20–25 versus 60-miles-per-hour landing speed, which is better than 50 percent. Glauert stated his belief that the autogyro "is less economical than an aeroplane, but that it has very considerable advantages as regard safety and ease of landing." Obviously, whether vertical descent was an issue or not, autogyro economics were not then, and I suspect Glauert thought they would never be, competitive with an "equivalent machine."

2.11 PERFORMANCE

Table 2-17 shows that the autogyro purchase price was only 20 percent more than the airplane . Furthermore, the PA-8 got roughly 600 miles out of 80 gallons of gas, or about 7.5 miles per gallon, while the PCA-2

got only 5.6 miles per gallon. Fuel economy certainly favored the airplane in 193 1. (Personally, I am glad that Glauert said he did not "think the autogyro was useless.")

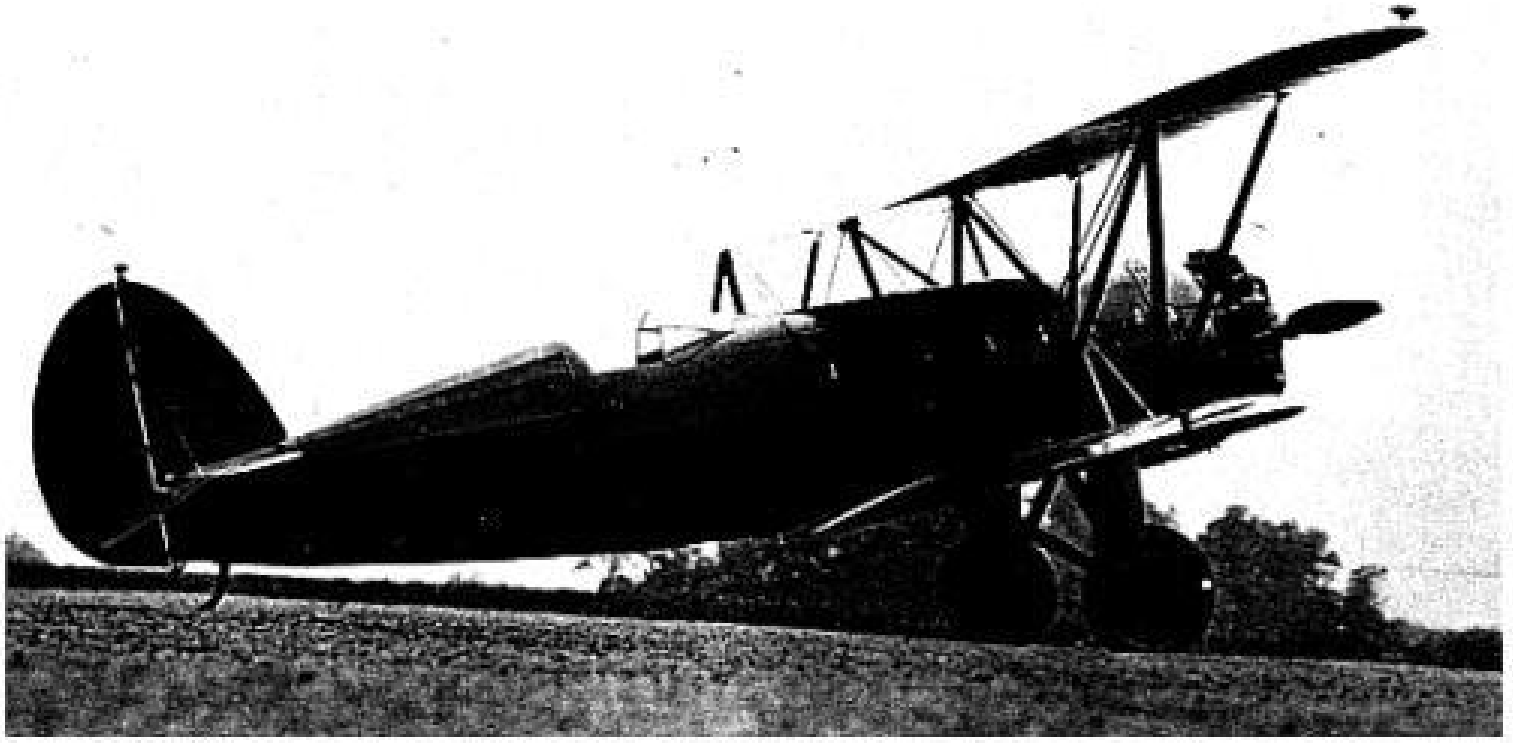

Fig. 2-116. The Pitcairn PA-8M "Super Mailwing," ATC No. 364, Sept. 19, 1930 [134].

Fig. 2-117. The Pitcairn PCA-2, ATC No. 410, April 2, 1931 [127].

Table 2-17. Autogyro Versus Airplane Comparison in the 1930/1931 Era

Parameter	PCA-2	PA-8
Engine	Wright J6	Wright J6
Horsepower available	300	300
Length overall	23 ft 1 in. (blades folded)	24 ft 10 in.
Height overall (tail down)	13 ft 0 in.	9 ft 9 in.
Rotor diameter	45 ft	
Rotor blade chord	22 in.	
Rotor blade area	159.5 sq ft	
Rotor blade airfoil	Göttingen 429	
Wing span upper		35 ft 0 in.
Wing span lower	30 ft 0 in.	31 ft 1 in.
Wing chord upper at root		58 in.
Wing chord upper at tip		58 in.
Wing chord lower at root	52 in.	52 in.
Wing chord lower at tip	30 in.	52 in.
Wing area upper		161 sq ft
Wing area lower	88 sq ft	117 sq ft
Total wing area	88 sq ft	278 sq ft
Wing airfoil	NACA M-3 modified	Pitcairn -2
Weight empty	2,093 lbs	2,294 lbs
Useful load	907 lbs	1,706 lbs
Payload with 52 gal. fuel	375 lbs	
Payload with 78 gal. fuel		1,008 lbs
Gross weight	3,000 lbs	4,000 lbs
Maximum speed @ sea level	118 mph	145 mph
Cruise speed @ sea level	98 mph	122 mph
Landing speed	20–25 mph	60 mph
Climb in one minute @ sea level	800 ft	1,100 ft
Climb after 10 minutes		7,500 ft
Ceiling	15,000 ft	16,000 ft
Gasoline capacity	52 gal.	80 gal.
Oil capacity	6.5 gal.	8 gal.
Cruising fuel flow	16 gal. /hr	15 gal. /hr
Range at cruising fuel flow	290 miles	600 miles
Price at factory field	$15,000 in 1931	$12,500 in 1930

Now let me examine the thrust horsepower required and thrust horsepower available comparison (recall Fig. 2-1 10) that Cierva presented to the Royal Aeronautical Society on February 13, 1930. To begin with, the PCA-2 aircraft drag (in pounds) from Fig. 2-115 becomes propeller thrust horsepower required simply by multiplying by flight path velocity (in feet per second) and dividing by 550, the conversion from foot-pounds per second to horsepower. The result of this rescaling is shown in Fig . 2-1 18 with flight velocity now given in miles per hour. The thrust horsepower available shown in the figure, following Eq. (2.300), is 300 horsepower times the propeller efficiency (η_P) . The propeller efficiency is somewhat of

an educated guess [136] for illustration purposes.[51] Note, however, that this guess must at least agree with the PCA-2 maximum and landing speeds quoted in Table 2-17.

The next step in the performance comparison is to obtain a thrust-horsepower-required line for the PA-8 airplane . The propeller thrust for airplanes is generally determined from the airplane parabolic drag polar. That is, the drag coefficient of an airplane is well approximated [60]—but only up to near stall—as

(2.303)

$$C_D = \frac{D}{qS_W} = C_{Do} + KC_L^2 + B\frac{C_L^2}{\pi AR} = \frac{f_e}{S_W} + \frac{B}{\pi S_W}\left(\frac{L}{qb_W}\right)^2$$

and therefore the airplane drag is simply

(2.304)

$$\text{Airplane Drag} = D_{AC} = qf_e + qS_W K C_L^2 + \frac{B}{\pi q}\left(\frac{L}{b_W}\right)^2$$

where dynamic pressure (q) equals $1/2\ \rho V^2$, (b_W) is the wing span, and K and B are constants.

Two estimates of PA-8 performance are included in Fig. 2-118. The parasite area (f_e) of 12.5 square feet gives a maximum speed at sea level of 145 miles per hour. If the PA-8 had the same parasite drag area as the PCA-2 (i.e., f_e = 19 square feet), the maximum speed would only be 125 miles per hour, which is not consistent with the certificated speed shown in Table 2-17. The Munk biplane theory [137] gives B = 0.83 for the PA-8 biplane gap-to-span ratio . Perkins

and Hage [60] suggest K = 0.012. The drag rise with stall is patterned after the Knight and Wenzinger experiments [138]. A maximum lift coefficient of about 1.4 set the landing speed at 60 miles per hour.

Viewing Fig. 2-118, it should be clear that Cierva took a great deal of liberty in comparing autogyros to airplanes (recall Fig. 2-110). In my opinion, I doubt that the more knowledgeable audience members bought his simplistic explanation. By assuming that "both machines have the same parasite drag," he completely dismissed hub and blade shank drag and tried to make his point based solely on blades-alone profile drag. Today, the rotorcraft industry is well aware that without reducing hub and blade shank drag, very high speeds will never be reached without a great deal more engine horsepower. Brooks [7] notes that the PCA-2 was given the larger Wright R-975 E2 engine having 420

horsepower, and the maximum speed only increased to 125 miles per hour. By extrapolation, the PCA-2 might have reached 145 miles per hour with another 120 horsepower. Perhaps Cierva had on his "marketing hat" when he gave his second lecture to the Royal Aeronautical Society on February 13, 1930.

---

[51] The applied aerodynamics text I have referred to here was taught in my first aero class at Rensselaer Polytechnic Institute in Troy, New York, in 1952. It is a small, thin, red-covered book—only 231 pages counting the index. It is also the best book on applied aero that I have read, and used, in 50 years. The only other comprehensive, applied aerodynamics text for airplanes that I have, which is of real value, is Perkins & Hage [60]. Of course, *Fluid-Dynamic Drag* by Hoerner [116] is indispensable.

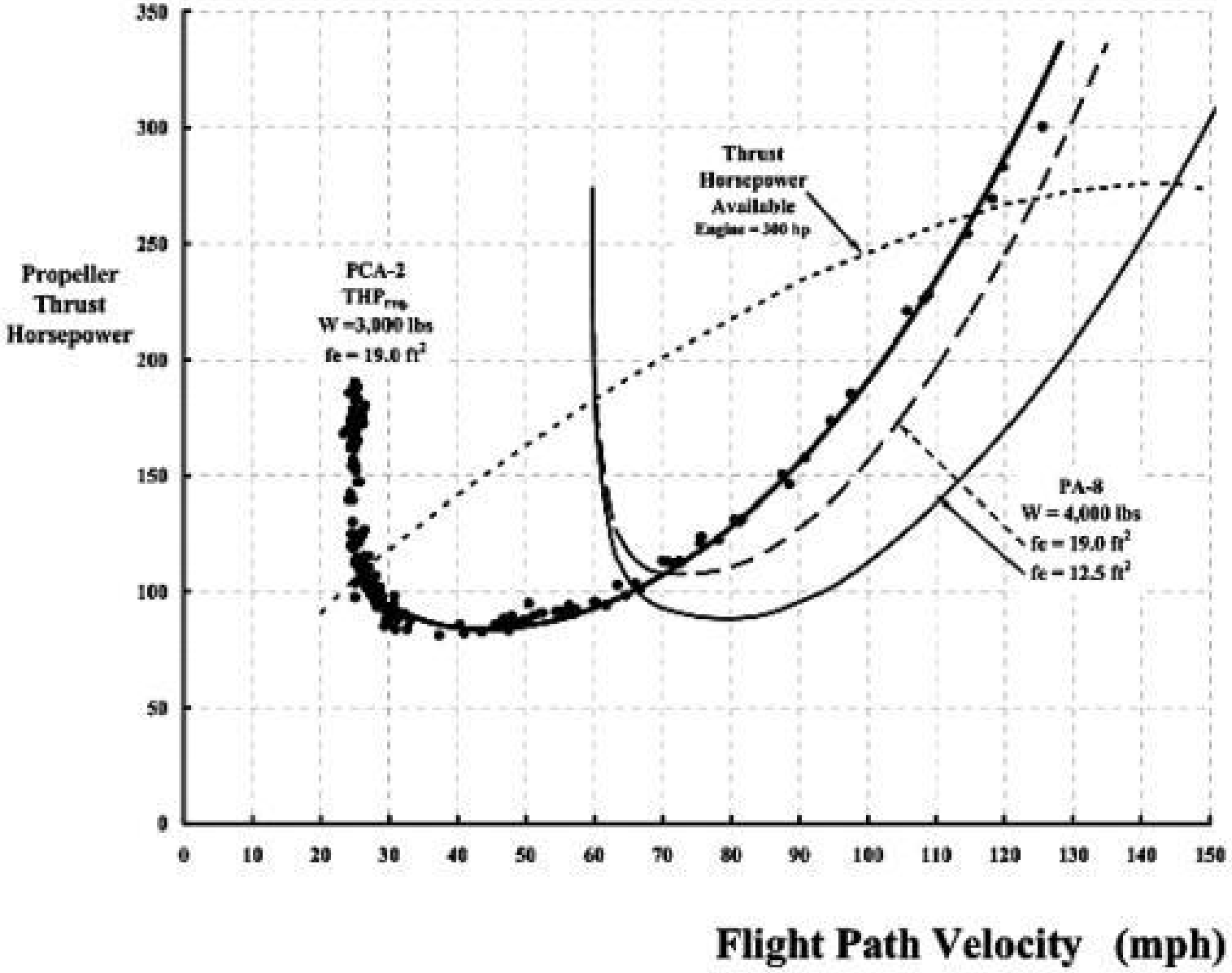

Fig. 2-118. PCA-2 and PA-8 performance curves.

2.11.6 Improvements

Cierva presented his third—and

last—lecture before the Royal Aeronautical Society on March 15, 1935. By this time his most advanced Autogiro, the C.30, was in low-rate production and doing well in the field. Rotor startup with power takeoff from the engine had replaced the "scorpion" tail. Direct control had significantly improved the C.19 and PAC-2 low-speed handling qualities, and the "cantilevered," low-solidity, three-bladed rotor system was improving performance. Cierva chose this 1935 opportunity to divulged the newest development progress [5]—jump takeoff.

Despite all of this development progress, Cierva began the lecture, after the introductory paragraph, with the following words:

"One of the characteristics of the development has been the great number of difficult secondary problems [ground resonance for one] . The very large number of parameters and the heterogeneity of the requirements,

some aerodynamical, some dynamical and some structural, make correct compromising–which is the secret of all successful engineering–an exceedingly delicate task.

2.11 PERFORMANCE

In many instances, sacrifices in one direction have to be made in order to improve some other point, until increased knowledge has permitted to redress the balance again. Simultaneous progress all along the line is only possible when a final formula is established, and the autogiro is only now arriving at that stage. Until then it [the autogyro] will necessarily lack that refinement of design which can only be attained by repeated steps in the same direction."

From this rather philosophical beginning, Cierva used the following two paragraphs to respond to his autogyro critics:[52]

"Let these considerations [the preceding two paragraphs] be my answer to those critics of the autogiro who ask, for example, why, after such a

relatively long development, we have failed to substantiate our early and repeated claims about the autogiro being capable of competing with the airplane in speed.

We are convinced of the potential truth of our claims and, if we had left aside the fundamental development, we feel we might have proved them by now. However, and we think wisely, we adopted the other course. Speed, which incidentally we do not consider to be the only criterion of utility of aircraft free from some of the limitations of the aeroplane [such as stalling and spinning], will come as the result of stabilisation of the general conception and of the concentrated efforts of a great number of engineers. So will useful load, and while we make no claim to superiority in every respect, we are convinced that we will not be far behind the aeroplane in what might be called aeroplane performance."

Cierva never said who "we" were. As it turned out, "we" were the rotorcraft industry, who, given Cierva's start, *and* "with the concentrated efforts of a great number of engineers [and many, many others]," developed the second-generation rotorcraft, the helicopter.

Of course, as you know now, utility, not speed, became the prime objective.

Let me now interject a remark Mr. Manning made during the discussion period that followed the second Cierva lecture in 1930 (which described the C.19 and dealt with aircraft maximum lift-to-drag ratios). Mr. Manning pointedly said,

"He thought the loss of top speed was important. The only excuse for the aeroplane was that its speed was greater than that of any other form of transportation. That was an advantage that must be pressed. With a good many light aeroplanes, if the conditions were slightly unfavorable, say a 20 miles per hour head wind, it was probably difficult for the machines with passengers and luggage to fly from London to Paris without landing to obtain further supplies of petrol. The expenditure of petrol in the case of the autogiro would be worse, and....."

In 1930, Manning was half wrong about light airplanes and all wrong about the growing civil

aviation transportation system.

The 1930 to 1935 period, when Cierva developed and brought the C.30 to market, saw Pitcairn and Kellett make considerable progress in the United States . The greatest strides in U.S. aeronautical research were made by John Wheatley at the N.A.C.A. at Langley Field in Virginia. After completing initial flight testing with the Pitcairn PCA-2 [127], Wheatley investigated the wing loading of the production PCA-2 [139] and then the influence of

---

[52] Hermann Glauert was not in the audience. He was killed in an accident at Farnborough, England, on August 4, 1934.

varying the load-sharing between rotor and wing [140].[53] But at this point, after having published a classic theory and test report [75], there was not much more that Wheatley could learn about the rotor system and its drag, without a wind tunnel test. In the introduction to *Full-Scale Wind-Tunnel Tests of a PCA-2 Autogiro Rotor* [141], he described the situation as follows:

"No quantitative evaluation of the interference of the remainder of the machine upon the rotor was possible [wing loading and interference on the rotor was established, but no more could be done], but the most serious fault with the results lay in the fact that the drag of the rotor, its most important characteristic, could not be found. In order to obtain complete and accurate information concerning the aerodynamic characteristics of the PCA-2 autogiro and to supply data applicable to an analysis of the sources of its drag, the rotor was removed from the machine and tested alone in the full-scale wind tunnel at Langley Field in December 1933."

The rotor system was installed in the 30- by 60-foot, open-throat wind tunnel. The entire supporting system beneath the rotor was shielded from the airstream to eliminate tare drag . The testing procedure was quite straightforward as Wheatley explained:

"The rotor was started by the air stream, no mechanical starting gear having been incorporated in the test set-up. The rotor was set at about 10° [hub plane] angle of attack, the wind tunnel was started slowly by jogging on and off the lowest speed switch point, and the air speed was gradually increased as the rotor picked up speed.

Force tests were made by the following procedure: The wind tunnel control was set for the lowest airspeed, the angle of attack was adjusted so the rotor operated steadily at a desired speed, and the necessary readings were taken. The angle of attack was then adjusted to give other desired rotor speeds, readings were again taken, and the process was repeated at other air speeds."

To ensure reasonably low vibration, Wheatley used a variation on the blade

tracking procedure you learned about earlier. He wrote:

"In order to check the track of the blades, the rotor was run [he does not say to what condition] and a paint brush was lowered onto the rotor from above until the high blades were marked. Indicated adjustments were then made and the process repeated until the rotor operated smoothly as indicated by the steadiness of the balance scales. When the rotor operation was considered satisfactory, the blade tips tracked to within 1-1/2 inches."

With tracked blades and a smooth rotor, Wheatley collected 89 data points with the production rotor, Table I, [141].[54] The points fall into 4 sets grouped reasonably close to rotor speeds of 100, 120, 140, and 150 revolutions per minute. All data were corrected for jet-boundary and blocking effects and "in addition, the drag of the rotor hub was measured with the blades removed and subtracted from the rotor [plus blades, droop cables, and lead-lag cables] data.

Wheatley presented rotor lift and drag in fixed-wing coefficient notation. That is

---

[53] Both of these reports provide data about the performance of what was to become a high-speed, compound helicopter. I will discuss these two reports in the third volume of this book, Other V/STOLs. [54] His report also includes some points where many of the droop and lead-lag cable end fittings were faired. He made the point though that "the results are of minor practical importance because of the current trend toward the use of cantilevered blades with no protuberances."

2.11 PERFORMANCE

(2.305) Rotor $C_L = \dfrac{L_R}{\left(\frac{1}{2}\rho V_{FP}^2\right)\left(\pi R^2\right)}$ and

$$\text{Rotor } C_D = \frac{D_R}{\left(\tfrac{1}{2}\rho V_{FP}^2\right)\left(\pi R^2\right)}.$$

With the hub plane angle of attack (α_{hp}) as his reference, he calculated advance ratio in the usual manner

$$(2.306) \quad \mu_{hp} = \frac{V_{FP}\cos\alpha_{hp}}{V_t}$$

and that became the measure of forward flight speed. Fig. 2-119 and Fig. 2-120 show the primary results Wheatley obtained.

All 89 data points shown in Fig. 2-119 and Fig. 2-120 were obtained with identical root collective pitch (θ_{root}). The variables are only wind tunnel speed and the approximate set of rotor speeds of 100, 120, 140, and 150 revolutions per minute. The approximate corresponding rotor lifts are 1,200, 1,700,

2,500, and 3,000 pounds . However, knowing that collective pitch at the blade tip (today we would use collective pitch at the 3/4-radius station) was a key parameter in the rotor equations, Wheatley was quite concerned about what he called "dynamic twist." Today dynamic twist is more commonly referred to as elastic windup. From PCA-2 flight testing, he "established the fact that the dynamic twist is about 0.89° at the tip for 1,000 pounds thrust." With the blades at rest, the collective pitch at the tip, measured with an inclinometer, was 1.9 degrees . But when rotating, Wheatley felt the more correct tip collective pitch would be 3 degrees for the 100-revolutions-per-minute data rising to 4 degrees when the rotor speed reached 150 revolutions per minute. I have made no distinction in Fig. 2-1 19 or Fig. 2-120 for rotor speed, thrust, or "dynamic pitch," but Wheatley does in his report.

The prediction of the PCA-2 rotor lift and drag requires only six equations . These equations, primarily given by Wheatley [75], are simply refinements to those equations you have encountered earlier. The following equations now account, approximately, for the reverse flow region as Wheatley derived. The radial velocity effect on profile drag is accounted for as suggested by Harris [133]. The blade flapping motion is described by

$$\beta_\psi = \beta_o - a_{1S}\cos\psi - b_{1S}\sin\psi \tag{2.307}$$

and the feathering, by

$$\theta_{x,\psi} = \theta_o + x\theta_t - B_{1C}\sin\psi - A_{1C}\cos\psi\,. \tag{2.308}$$

The rotor inflow ratio (λ_{hp}) and advance ratio (μ_{hp}) are defined relative to the rotor hub plane and calculated as

(2.309) $$\lambda_{hp} = \frac{V_{FP} \sin \alpha_{hp} - v}{V_t}$$

$$\mu_{hp} = \frac{V_{FP} \cos \alpha_{hp}}{V_t}$$

and, as a reasonable approximation in forward flight, the induced velocity (v) is taken as

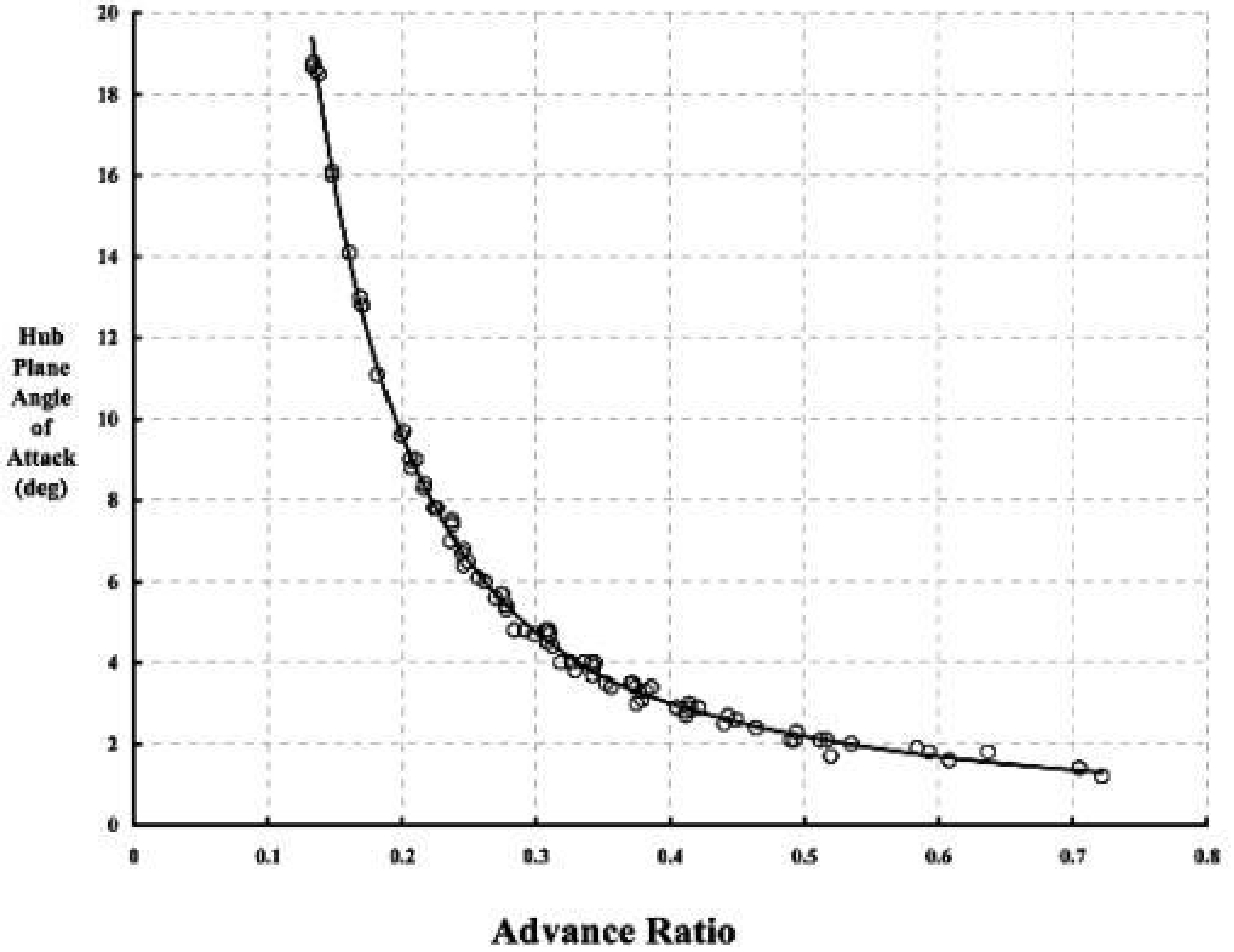

Fig. 2-119. PCA-2 blades-alone trim for autorotation.

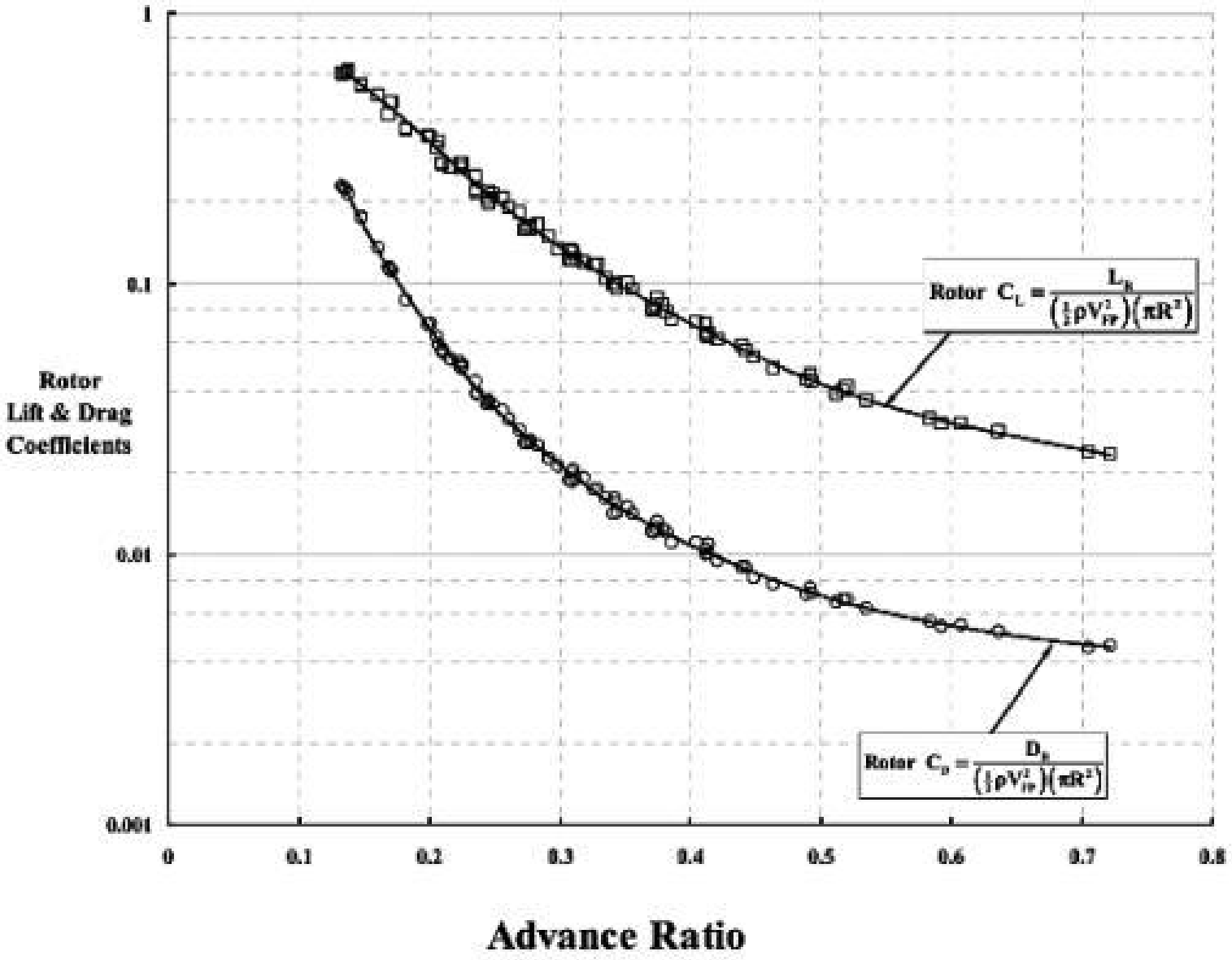

Fig. 2-120. PCA-2 blades-alone lift and drag performance in autorotation.

(2.310) $$v = \frac{T}{2\rho\left(\pi R^2\right) V_{FP} \cos\alpha_{hp}}.$$

The coning (β_o), longitudinal flapping (a_{1S}), and lateral flapping (b_{1S}) are calculated from

(2.311)

$$\beta_o = \frac{\gamma}{2}\left[\left(\frac{1}{3}+\frac{2}{25}\mu_{hp}^2\right)\lambda_{hp} + \left(\frac{1}{4}+\frac{1}{4}\mu_{hp}^2-\frac{1}{32}\mu_{hp}^4\right)\theta_o + \left(\frac{1}{5}+\frac{1}{6}\mu_{hp}^2\right)\theta_t - \frac{1}{3}\mu_{hp}B_{1C}\right]$$

(2.312)

$$a_{1S} = \frac{\left(2\mu_{hp}-\frac{1}{2}\mu_{hp}^3\right)\lambda_{hp} + \left(\frac{8}{3}\mu_{hp}+\frac{32}{45\pi}\mu_{hp}^4\right)\theta_o + \left(2\mu_{hp}+\frac{1}{12}\mu_{hp}^3\right)\theta_t}{1-\frac{1}{2}\mu_{hp}^2+\frac{7}{24}\mu_{hp}^4} - \frac{\left(\frac{1}{3}\mu_{hp}+\frac{1}{2}\mu_{hp}^3-\frac{5}{72}\mu_{hp}^5\right)B_{1C}}{1-\frac{1}{2}\mu_{hp}^2+\frac{7}{24}\mu_{hp}^4}$$

(2.313) $$b_{1S} = \frac{\frac{4}{3}\mu_{hp}\beta_o\left(1+\frac{4}{15\pi}\mu_{hp}^3\right)}{1+\frac{1}{2}\mu_{hp}^2-\frac{1}{24}\mu_{hp}^4} + A_{1C}.$$

The rotor thrust (T) is obtained from

$$\frac{2C_T}{\sigma a}=\left(\frac{1}{2}+\frac{1}{4}\mu_{hp}^2\right)\lambda_{hp}+\left(\frac{1}{3}+\frac{1}{2}\mu_{hp}^2-\frac{4}{9\pi}\mu_{hp}^3\right)\theta_o+\left(\frac{1}{4}+\frac{1}{4}\mu_{hp}^2-\frac{1}{32}\mu_{hp}^4\right)\theta_t$$
$$-\left(\frac{1}{2}\mu_{hp}+\frac{1}{8}\mu_{hp}^3\right)B_{1C}+\left(\frac{1}{8}\mu_{hp}^3\right)a_{1S} \tag{2.314}$$

and the rotor H-force (H) from

$$\frac{2C_H}{\sigma a}=\frac{C_{do}}{a}\left(0.776\mu_{hp}+1.1448\mu_{hp}^3-0.259\mu_{hp}^5\right)-\frac{1}{2}\mu_{hp}\lambda_{hp}^2+\frac{3}{4}\left(1-\frac{3}{4}\mu_{hp}^2\right)a_{1S}\lambda_{hp}$$
$$-\frac{1}{2}\left(\mu_{hp}-\frac{4}{3\pi}\mu_{hp}^2\right)\theta_o\lambda_{hp}+\frac{1}{6}\left(1+\frac{4}{15\pi}\mu_{hp}^3\right)\beta_o\left(A_{1C}-b_{1S}\right)$$
$$+\frac{1}{4}\left(\mu_{hp}-\frac{1}{4}\mu_{hp}^3\right)\left(\beta_o^2-\theta_t\lambda_{hp}-B_{1C}a_{1S}\right)+\frac{1}{4}\left(1+\frac{1}{8}\mu_{hp}^4\right)a_{1S}\theta_t$$
$$+\frac{1}{3}\left(1+\frac{2}{3\pi}\mu_{hp}^3\right)a_{1S}\theta_o+\frac{1}{4}\left(\mu_{hp}-\frac{3}{4}\mu_{hp}^3\right)a_{1S}^2+\frac{1}{4}\left(1+\frac{3}{4}\mu_{hp}^2\right)B_{1C}\lambda_{hp} \tag{2.315}$$

2.11 PERFORMANCE

The preceding five equations allow the rotor-power required or torque required to be

calculated simply as

(2.316)

$$C_P = \frac{P}{\rho(\pi R^2)V_t^3} = \frac{Q\Omega}{\rho(\pi R^2)(\Omega R)V_t^2} = \frac{Q}{\rho(\pi R^2)RV_t^2} = C_Q$$

$$= \frac{\sigma C_{do}}{8}\left(1 + 4.65\mu_{hp}^2 + 4.15\mu_{hp}^4 - \mu_{hp}^6\right) - C_T\lambda_{hp} - C_H\mu_{hp}$$

once the rotor solidity (σ), airfoil lift-curve slope (a), and airfoil drag coefficient (C_{do}) are established. The rotor lift (L_R) and drag (D_R) are, of course, easily calculated from

(2.317)
$$L_R = \left[\rho(\pi R^2)V_t^2\right]\left(C_T\cos\alpha_{hp} - C_H\sin\alpha_{hp}\right)$$
$$D_R = \left[\rho(\pi R^2)V_t^2\right]\left(C_T\sin\alpha_{hp} + C_H\cos\alpha_{hp}\right)$$

There is no doubt that the preceding

path to calculating rotor lift and drag represents early autogyro rotor performance technology applicable up to, perhaps, an advance ratio of 1.0 . However, given just a slide rule, pencil, and paper, the calculations are rather daunting; but keep in mind that rotorcraft pioneers were not put off by the task. The fact that reasonable engineering had led to equations worth the calculating effort (i.e., the elbow grease) was really quite a breakthrough. The fact that a comparison of this 1930s theory could be made to full-scale rotor performance data acquired in a very large wind tunnel must have made the work both fun and exciting.

The predictive capability (compared to Wheatley's experimental results) when using Eqs. (2.307) through (2.3 17) is illustrated by Fig. 2-121 for lift and Fig. 2-122 for drag. To obtain the rotor forces in pounds, I used the data Wheatley tabulated for rotor speed, hub

plane angle of attack, and advance ratio to determine flight path velocity (i.e., wind tunnel airspeed) in feet per second. Then, assuming the air density to be 0.002378 slugs per cubic foot, I calculated the dynamic pressure (q) . Wheatley gives the reference rotor area (πR^2) as 1,588 square feet, so with the tabulated lift and drag coefficients, it was an easy matter to convert coefficients back to pounds (thus, the experimental values shown in Fig. 2-121 for lift and Fig. 2-122 for drag).

The prediction of lift and drag for all 89 data points was easy after the performance equations were "programmed" onto a spreadsheet (I used Microsoft Excel). As input, I set the collective pitch (θ_o) to 1.9 degrees (but in radians), which Wheatley says was the tip pitch angle nonrotating . I assumed the blades were manufactured with zero twist, BUT allowed for the "dynamic twist" that Wheatley knew existed when the rotor was operating. The

airfoil lift- curve slope (a) was taken as 5.73 per radian. The rotor speed, hub plane angle of attack, and advance ratio were set to the values Wheatley tabulated for each point. Finally, at each point, the blade linear twist term (θ_t) was iterated to the value that zeroed torque, which satisfied the condition of autorotation. (I used the Goal Seek tool provided by Excel to do the iteration.)

2.11 PERFORMANCE

Using blade twist (θ_t) as the iteration parameter to obtain zero torque was a simple way to approximate "dynamic twist," the largest unknown that Wheatley addressed in his report [141] . The amount of blade twist required to zero torque varied from 1.4 degrees at low speed to −1.4 degrees at high speed. Wheatley used a figure of 0.8 degrees per 1,000

pounds of lift. However, guided by Eq. (2.42), it appears a more rigorous approximation found by linear regression analysis would be

$$(2.318)\quad \theta_t = -0.0000199\,V_t^2 + 0.00000729\,\beta_o V_t^2 - 0.0000263\,V_{FP}^2 .$$

In fact, the influence of elastic twisting (both steady and periodic) could be pursued more thoroughly by following Eq. (2.42) and studying the two Wheatley reports on the subject [58, 59] . But once the step towards including blade elastic twisting is taken, then blade bending both flapwise and chordwise should be included along with lead-lag motion. At that point, a much more comprehensive tool such as the Johnson CAMRAD computer program [109] is called for.

The capability of simple performance equations to approximate rotor drag is shown in

Fig. 2-122 . The average airfoil profile drag coefficient (C_{do}) used for the Göttingen 429 was 0.0127, which was increased from an estimate based on both British [121] and N.A.C.A. [142] data to account for droop and lead-lag cables (etc.).

John Wheatley's thorough flight testing of the Pitcairn PCA-2 Autogiro [127], followed by full-scale, rotor-alone wind tunnel testing [141], finally quantified practical autogyro performance as it existed before Cierva introduced the wingless, direct control C.30 . The performance situation is simply stated in Fig. 2-123 . The rotor blades alone (plus the droop and lead-lag cables, and associated fittings) were producing a maximum lift-to-drag ratio just under 7 . The PCA-2 aircraft reached a maximum lift-to-drag ratio slightly over 4.5 at an advance ratio of 0.3. By similarity, it is quite likely that the Cierva C.19 (see Fig. 2-15) reached maximum

lift-to-drag ratios comparable to the Pitcairn PCA-2 (Fig. 2-123), although I have no flight test data to confirm this statement.

Cierva makes the point in his 1935 lecture, his last, that

"The most efficient rotor produced so far has a maximum lift-drag ratio (excluding the drag of the hub) of the order of between 13 and 14. This represents an increase of some 40 percent on the best rotor of five years ago, and perhaps 80 percent on the early autogiro rotors. At the same time, the maximum lift coefficients have been materially increased. These results have been obtained by making the blades cantilevered, suppressing the suspension cables, replacing the cumbersome interblade bracing by non-reactive dampers at their root attachment, using more efficient aerofoil sections, replacing the fabric covering which constituted a relatively irregular and deformable surface by rigid superstructure, and by diminishing the solidity considerably."

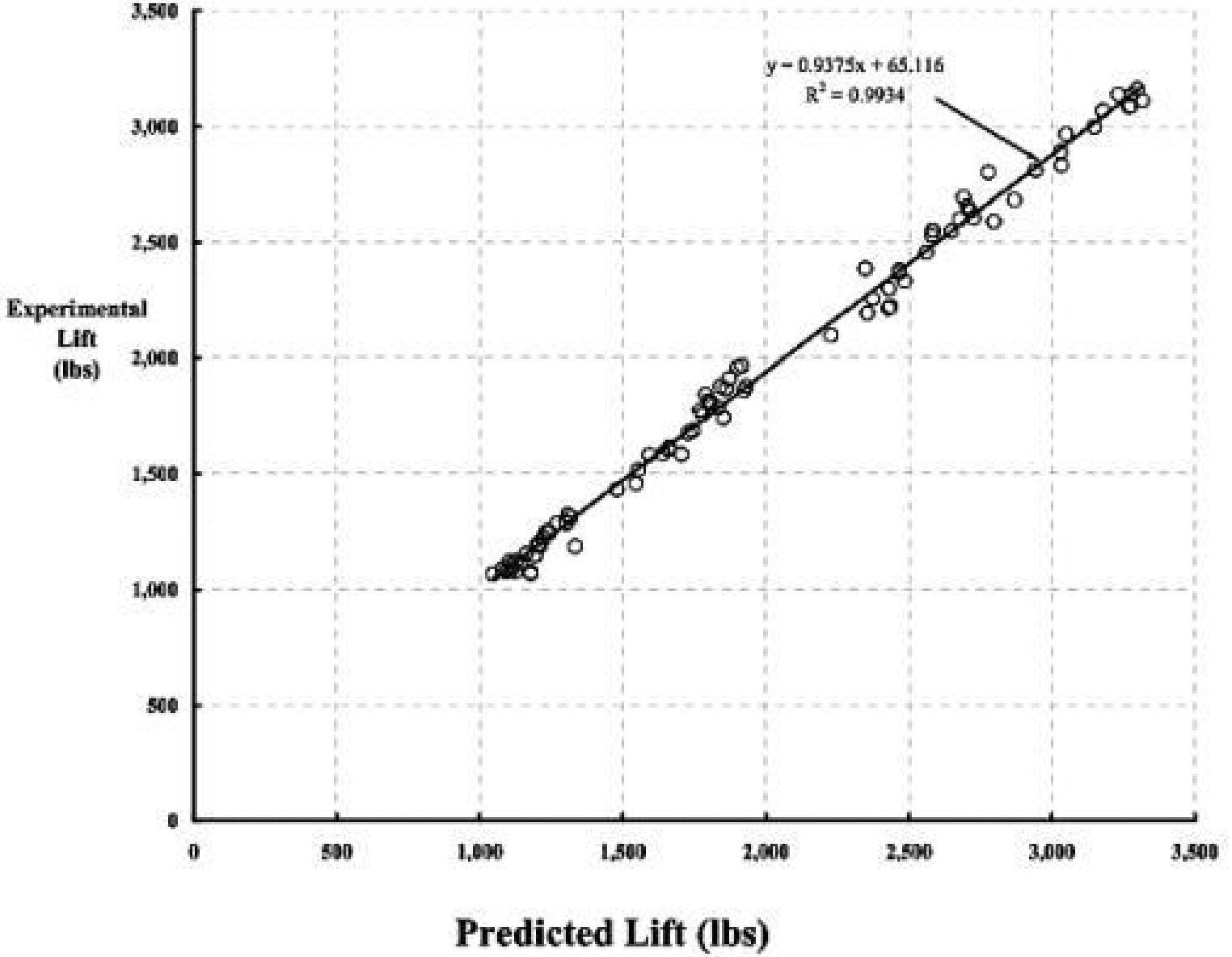

Fig. 2-121. Measured versus predicted lift for PCA-2 blades alone.

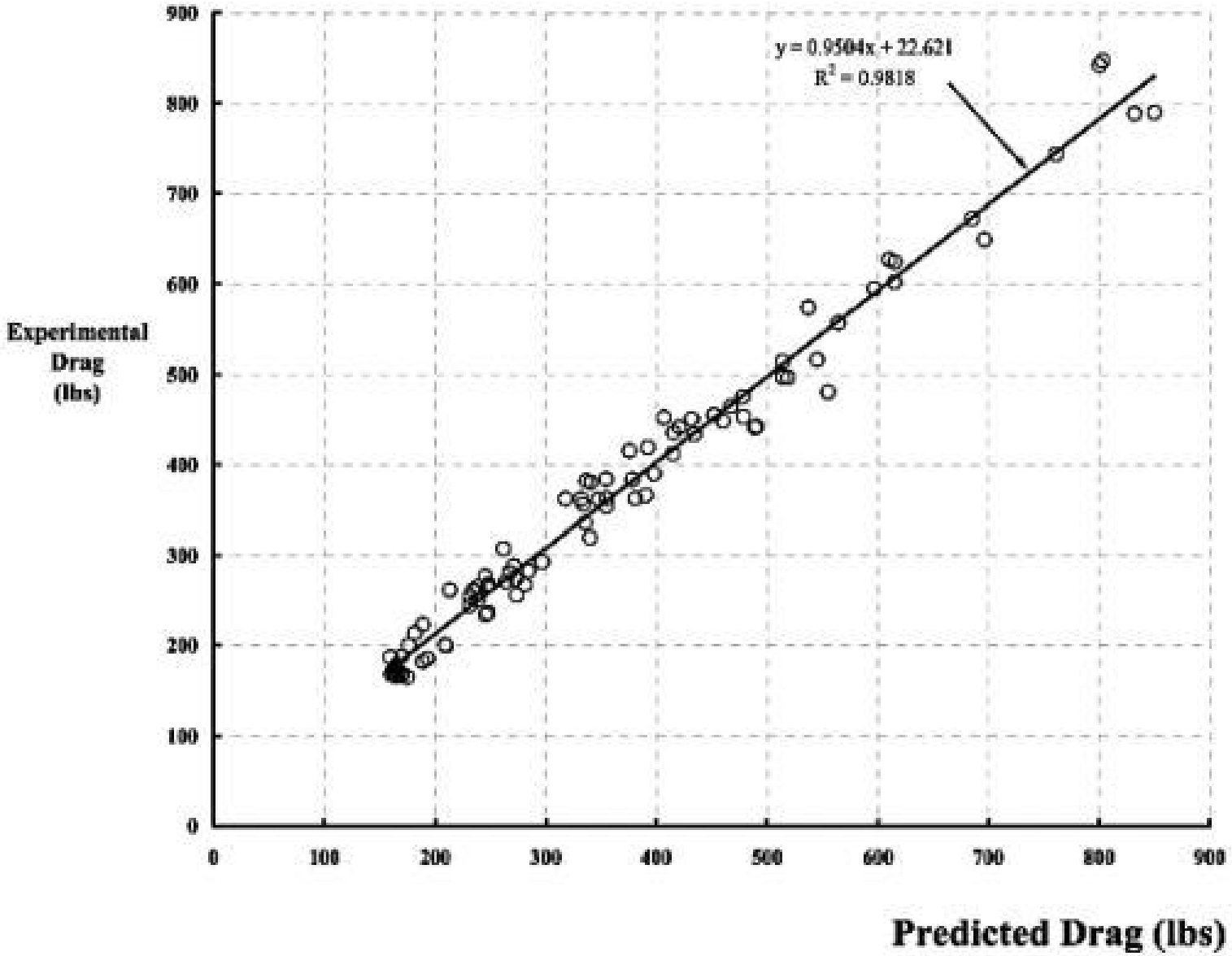

Fig. 2-122. Measured versus predicted drag for PCA-2 blades alone.

2.11 PERFORMANCE

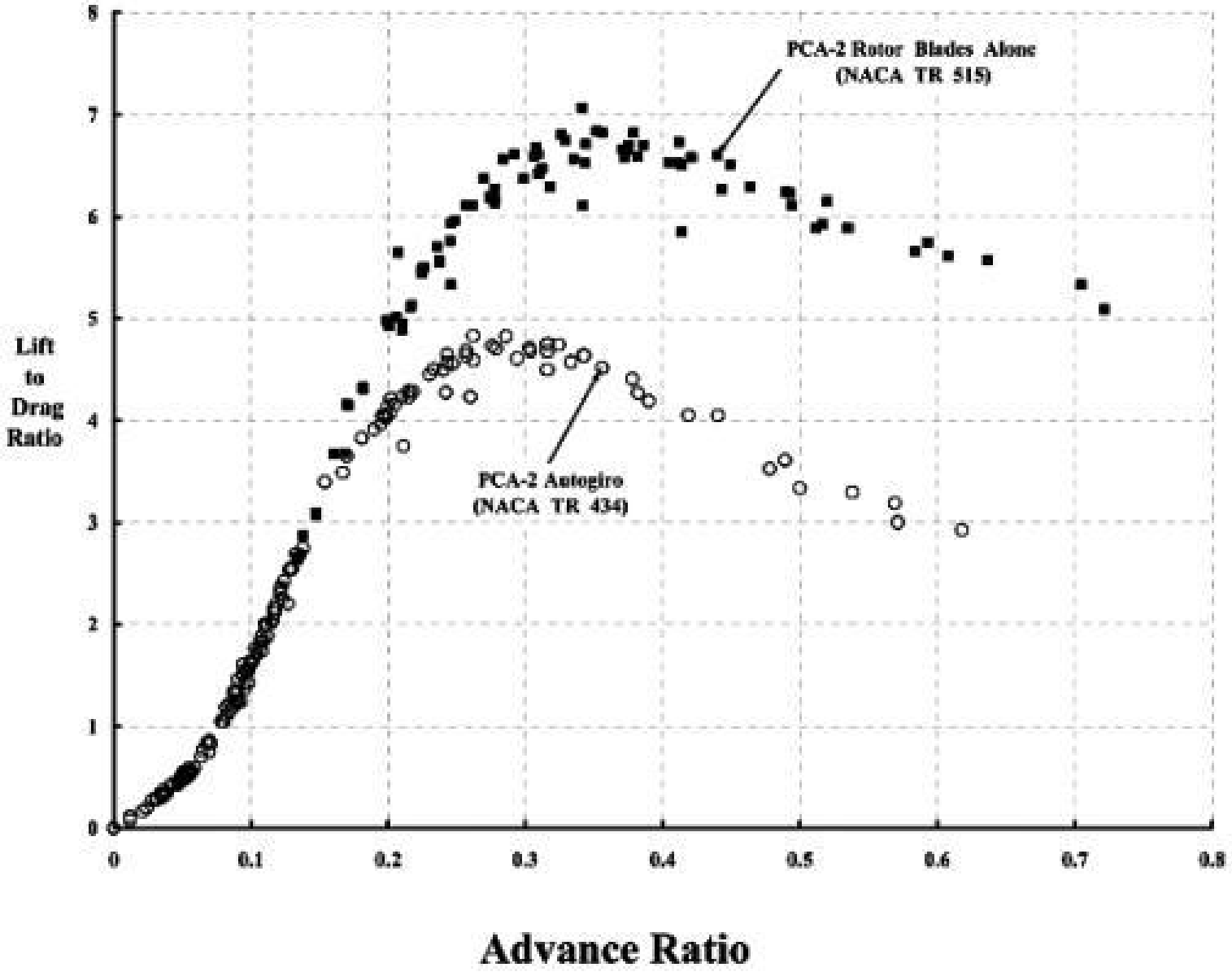

Fig. 2-123. PCA-2 blades alone and aircraft lift-to-drag ratios.

Cierva noted two additional performance points in his paper that are quite interesting. He writes first that "the symmetrical aerofoil makes a very poor autogiro blade." This may

be true, but the Göttingen 606 airfoil (which had a 0.17 thickness-to-chord ratio) he chose for the C.30 had a large nose-down pitching moment, which caused a fatality and a maximum speed restriction to be placed on the aircraft. Second, he was of the opinion that the introduction of direct control on the C.30 now meant that "a fixed wing in present machines [the PCA-2 and C.19] would certainly not pay for its extra weight."

When Cierva presented his March 15, 1935 paper, the Royal Aircraft Establishment (RAE) had finally (in 1934) obtained a C.30 to use to conduct an end-user evaluation. A report was ultimately published in March 1939 [54]. The RAE conducted gliding tests similar to those Wheatley did with the PCA-2 [127]. The C.30 demonstrated a lift-to-drag ratio that was only slightly better than the Pitcairn PCA-2, as Fig. 2-124 shows . And—most certainly— the performance of the C.30 fell far short of the

"best equivalent airplane." I cannot help but feel that Cierva knew—as he spoke to the Royal Aeronautical Society that Friday in 1935— that further rotor system improvements were not going to close the gap shown in Fig. 2-124. That was the position taken by the RAE [54] who concluded that

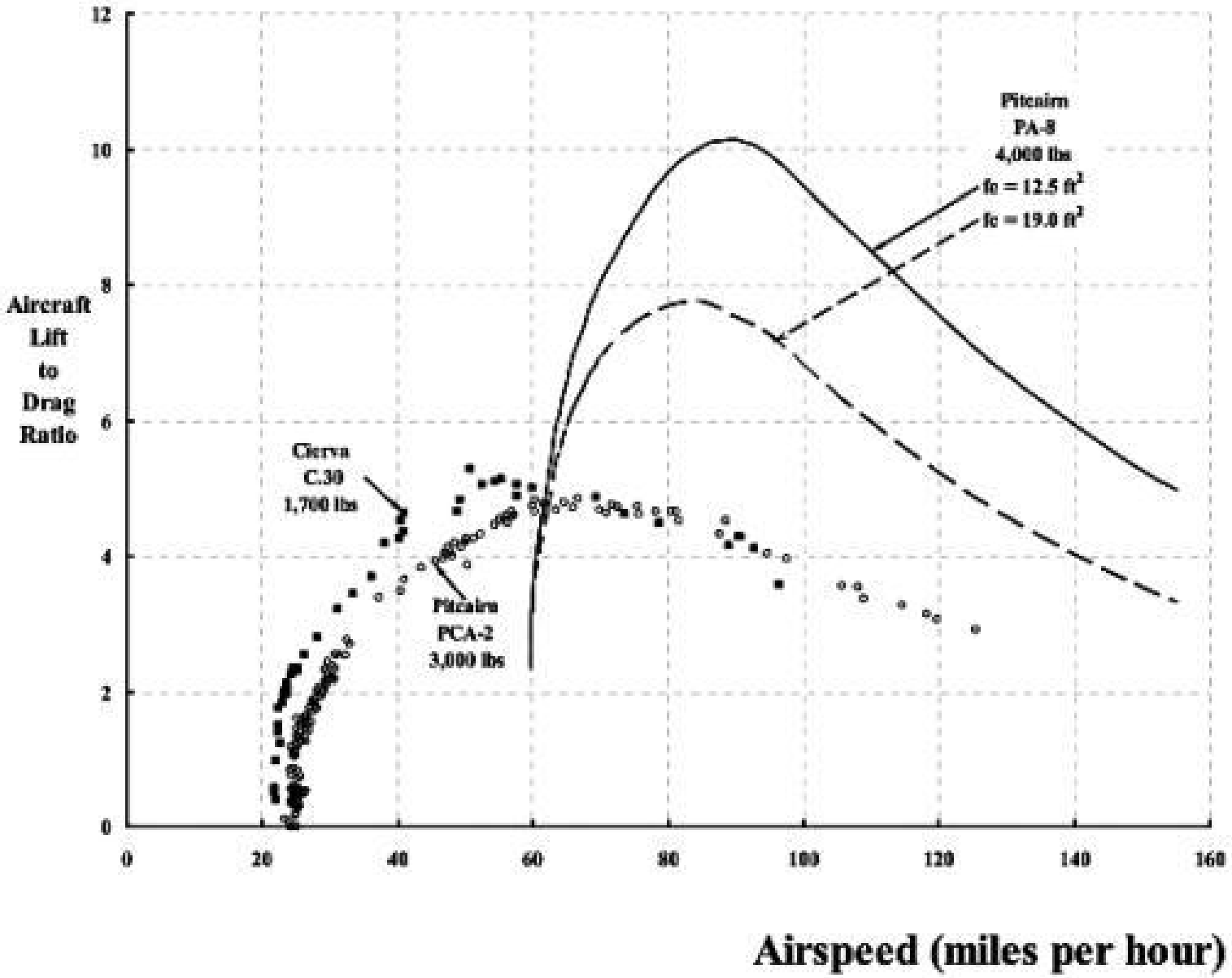

Fig. 2-124. Autogyro versus airplane lift-to-drag performance.

"the experiments do not suggest any very obvious method of improving performance of the aircraft [the C.30] except by reducing the parasitic drag of the fuselage. It has been estimated that the reduction of solidity and increase of blade angle as compared with the

C.6 autogiro has increased the L/D ratio of the rotor at top speed from 5.9 to 8.8 and it seems unlikely that much further improvement in the aerodynamic performance of the rotor can be obtained."

2.11.7 Drag Reduction

The view of the Royal Aircraft Establishment [54] that further autogyro performance improvements would come "by reducing the parasitic drag of the fuselage" was not a new thought in December 1936. Airplanes just after World War I[55] were not "things of beauty" from a drag point of view. John Anderson, in his superb book *A History of Aerodynamics* [143], credits the April 1922 Louis Bréguet paper [144] and, in particular, the 1929 Melvill Jones paper [145] as the catalysts for drag reduction and improving fixed-wing aircraft lift-to- drag ratios. Both Bréguet and Jones presented their views before audiences of the Royal Aeronautical

Society.

---

[55] By 1920, this war was generally referred to as "The Great War" or "The War to End All Wars." These were just working titles until we could give it a number.

2.11 PERFORMANCE

To point out just how important aircraft lift-to-drag ratio (L/D) was to air transport costs, Bréguet displayed the now-famous range equation. In modern notation, he showed the audience that

(2.319)

$$\text{Range} = 375 \frac{\eta_P}{\text{s.f.c.}} \frac{L}{D} \left[\ln \left(\frac{\text{Takeoff Wgt.}}{\text{Landing Wgt.}} \right) \right]$$

where range is in statute miles, propeller efficiency is (η_P), specific fuel (and oil) consumption (s.f.c.) of the engine is in pounds per horsepower per hour, and weights are in pounds. The constant, 375, is in statute miles per pound per horsepower per hour. The landing weight (W_L) is the takeoff weight (W_{TO}) less the weight of fuel (W_F) and oil (W_O) used. That is, $W_L = W_{TO} - (W_{Fuel} + W_{Oil})$. This quite well known equation applies here to propeller-driven aircraft using a reciprocating engine.[56]

Since fuel and oil weight used is generally 10 to 20 percent of the takeoff weight (the Lindbergh Spirit of St. Louis is one of several exceptions [146, 147]), Bréguet's range equation is easily simplified to

(2.320)

$$\text{Range} = 375 \frac{\eta_P}{\text{s.f.c.}} \frac{L}{D} \left[\frac{W_F + W_O}{W_{TO}} \right] \left[1 + \frac{1}{2} \left(\frac{W_F + W_O}{W_{TO}} \right) + \frac{1}{3} \left(\frac{W_F + W_O}{W_{TO}} \right)^2 + \cdots \right].$$

To simplify this further, aviation gasoline weighs about 6 pounds per U.S. gallon, and engine lubricating oil weighs about 7.4 pounds per U.S. gallon, so

(2.321)

$$\text{Range} \approx 375 \frac{\eta_P}{\text{s.f.c.}} \frac{L}{D} \left[\frac{6\,\text{Gal}_{\text{Fuel}} + 7.4\,\text{Gal}_{\text{Oil}}}{W_{TO}} \right] (1.05).$$

Now, oil consumption is about 1/10 of fuel consumption by gallon, so (2.322)

$$\text{Range} \approx 375 \frac{\eta_P}{\text{s.f.c.}} \frac{L}{D} \left[\frac{6.74\,\text{Gal}_{\text{Fuel}}}{W_{TO}} \right] (1.05)$$

which means that statute miles per gallon of fuel

is roughly (2.323)

$$\frac{\text{St.Miles}}{\text{Gal}_{\text{Fuel}}} \approx 2{,}650 \frac{\eta_P}{\text{s.f.c.}} \frac{L}{D}\left[\frac{1}{W_{TO}}\right].$$

The message Bréguet sent in 1922 was to get busy and (a) raise aircraft lift-to-drag ratio from 8.3 to 16.6; (b) raise propeller efficiency from 0.73 to 0.775; and (c) reduce engine fuel and oil consumption by 25 percent. Assuming a new design, these steps would nearly double the payload, and the "London to Paris passenger fares can then be brought down to some 450 or 500 francs—without profit for the company. Although very high, these last figures are more encouraging and nearly workable."

---

[56] Variations of the Bréguet equation, including its derivation, are available in references [60] and [136].

2.11 PERFORMANCE

Using the simplified Bréguet range expression, Eq. (2.323), autogyros, up to the Cierva C.30A, can be compared to light, civil airplanes produced and certificated by the United States fixed-wing industry in the era of 1927 through 1933 . This comparison is shown in Fig. 2-125 . The basic trend was confirmed—miles per gallon vary inversely with takeoff weight, and, just as Glauert maintained, autogyros were not "economical" when compared to either biplane or monoplane airplanes.

The over 500 data points shown in Fig. 2-125 come from the 9-volume *U. S. Civil Aircraft Series* by Joseph P. Juptner, 2 volumes of which were referenced earlier [134,

135] . This concise source provides maximum still air range (without reserves) in statute miles, and total fuel and oil capacity in U.S. gallons. The miles per gallon of gasoline were calculated from this data. Nearly 240 biplanes are shown with an × symbol in Fig. 2-125, and shaded circles denote an equal number of monoplanes . No seaplane or amphibian airplanes are shown. All the aircraft are single engine.

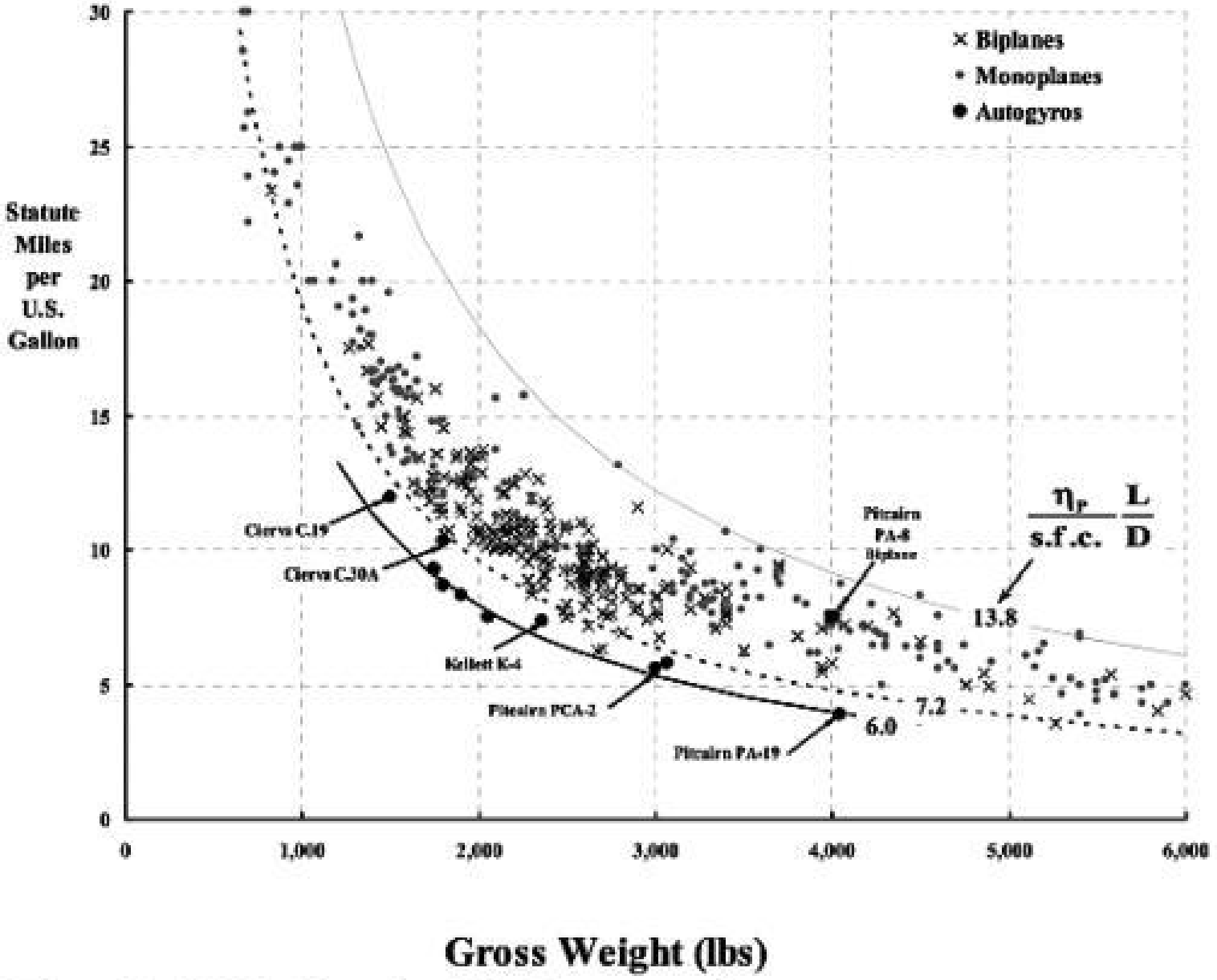

Fig. 2-125. Fuel efficiency of autogyros versus airplanes in 1927–1933.

2.11 PERFORMANCE

Fig. 2-125 shows three lines of aircraft performance as defined by the factor $\frac{\eta_p}{s.f.c.}\frac{L}{D}$

used in the Bréguet range equation. The lowest line, where the factor equals 6.0, suggests the position of the autogyro relative to the airplane as representative of the 1927 through 1933 era. The dashed line corresponds to relatively unstreamlined biplanes having a factor of 7.2 . The highest line shows the evolution of the monoplane through 1933, which is a factor of 13.8. Remember, the period from 1934 up to World War II was when the performance of the monoplane really improved. No data from that era is shown in Fig. 2-125.

Ignoring Cierva's position that autogyros would compete favorably with airplanes, I think that by the mid-1930s, biplanes were being replaced by monoplanes. As Fig. 2-125 shows, the monoplane was

more fuel efficient than the biplane at any takeoff weight. Monoplanes became the configuration of the future, and single-engine biplanes served primarily as light, one- or two-, or sometimes three-passenger sport planes . Airplane performance was improving by leaps and bounds through the 1930s, but real autogyro development was just getting started with the C.30. Still, many thought the autogyro was just another sport plane.

I think you will agree with John Anderson that motivation for fixed-wing aircraft performance improvement really did come from the 1929 Melvill Jones paper—once you have read Professor Jones' paper. His paper is titled *The Streamlined Aeroplane,* and it is the most entertaining aerodynamic performance paper I have ever read.[57] Furthermore, his logic is irrefutable. The Professor's position was that the "correct

aeroplane" should have no more drag than induced drag (because lift is required) plus skin friction drag (because an airplane has a surface.) He concedes that propeller efficiency of 0.75 "is practical on present-day craft, and efficiencies higher than say 85 to 90 per cent are unlikely to be achieved in the near future." His view on induced drag was that "although it is an important item in the power account at the lower cruising speeds, it is not the predominating factor at speeds above 90 m.p.h." With respect to skin friction drag, Jones concludes—after a very thorough discussion of flat plate and minimum airfoil drag—that airplanes of the era must have a turbulent boundary layer, not a laminar boundary layer.

Based on representative data for biplanes of the 1920s, Professor Jones used his assumptions for induced drag, skin friction drag, and propeller efficiency to calculated

engine brake horsepower per 1,000 pounds of weight for his ideal, streamlined aeroplane. Then he chose aircraft from the 1927 edition of *Jane's All The World's Aircraft* to see how close they came to his ideal.[58] He chose installed engine maximum brake horsepower as the reference power and top speed as the reference velocity, but remarked in a footnote that he was "aware that cruising speed is of more general interest than top speed, but I have used the top speed in computing these points because of the difficulty of estimating engine power at cruising

---

[57] Melvill Jones' opening sentence is: "Ever since I first began to study Aeronautics I have been annoyed by the vast gap which has existed between the power actually expended on mechanical flight and the power ultimately necessary for flight in a correctly shaped aeroplane." His paper just gets better.

[58] Professor Jones said, "I took the figures from Jane to avoid argument. Being, as I suppose, a makers' own figures, they are unlikely to be pessimistic as regards performance." (Now *that* is straightforward!)

speed." Fig. 2-126 is my reproduction of the performance assessment that Professor Jones presented to the fixed-wing industry in 1929. The figure shows that a sorry performance situation did indeed exist at the time . No wonder the aircraft industry was motivated to decrease drag and raise aircraft L/D . The progress just from 1927 through 1933 was certainly impressive, and development, as you know, did not stop then.

The performance of Cierva, Pitcairn, and Kellett autogyros compared to Professor Jones' perspective about "aeroplanes" is also shown in Fig. 2-126. In retrospect, it appears that Cierva was, in fact, improving

performance and reducing drag—at least relative to the first-generation autogyros and pre-1930 biplanes . Certainly retracting the landing gear would have been a big step forward. In fact, if Cierva had not died, he could have used his creative engineering ideas to further drag reduction, not of the rotor but of the rest of the machine. He would have had some very useful wind tunnel test results provided by the National Physical Laboratory to start with.

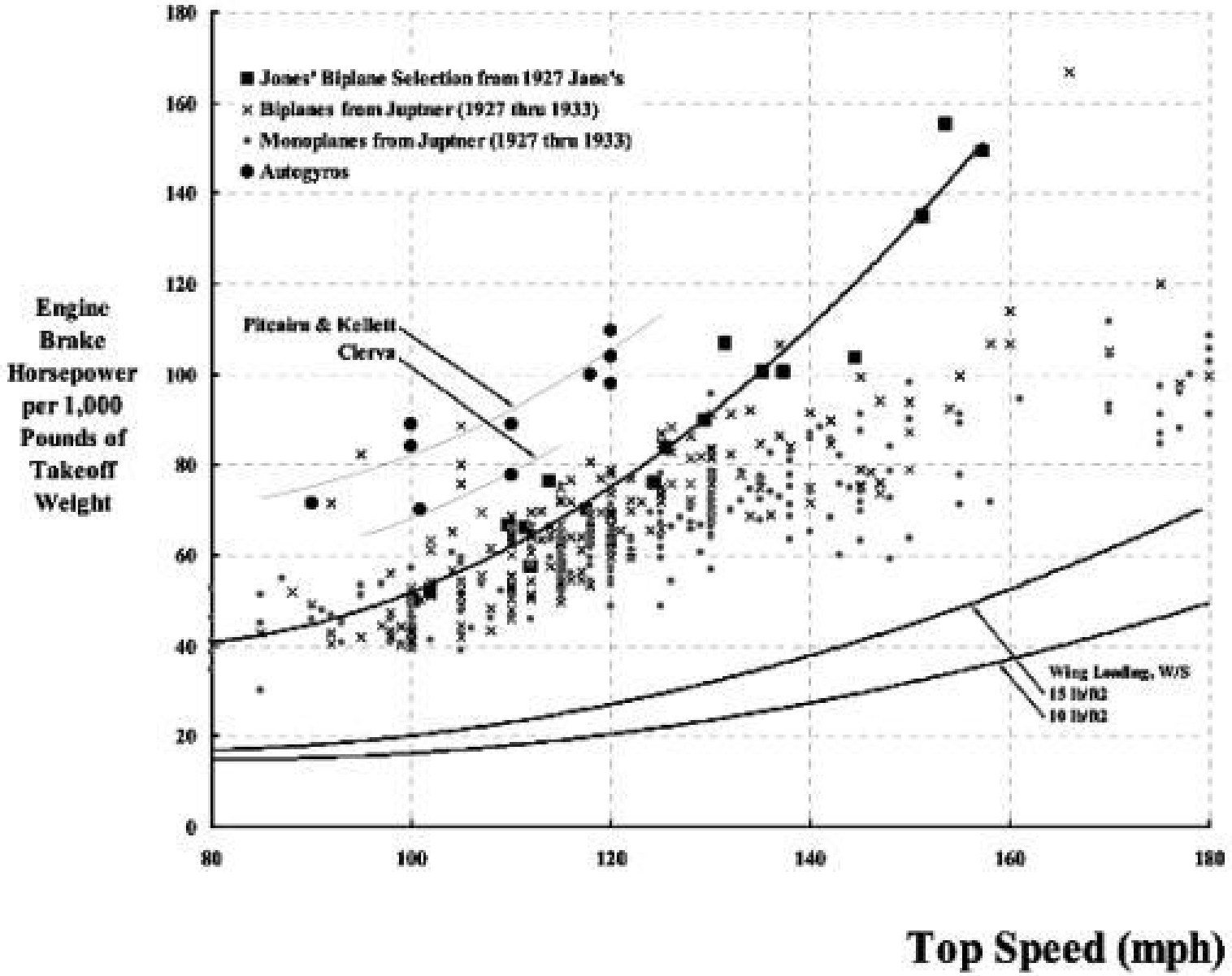

Fig. 2-126. Professor Jones' assessment of airplane performance in 1927 versus his ideal of the streamlined aeroplane [145].

2.11 PERFORMANCE

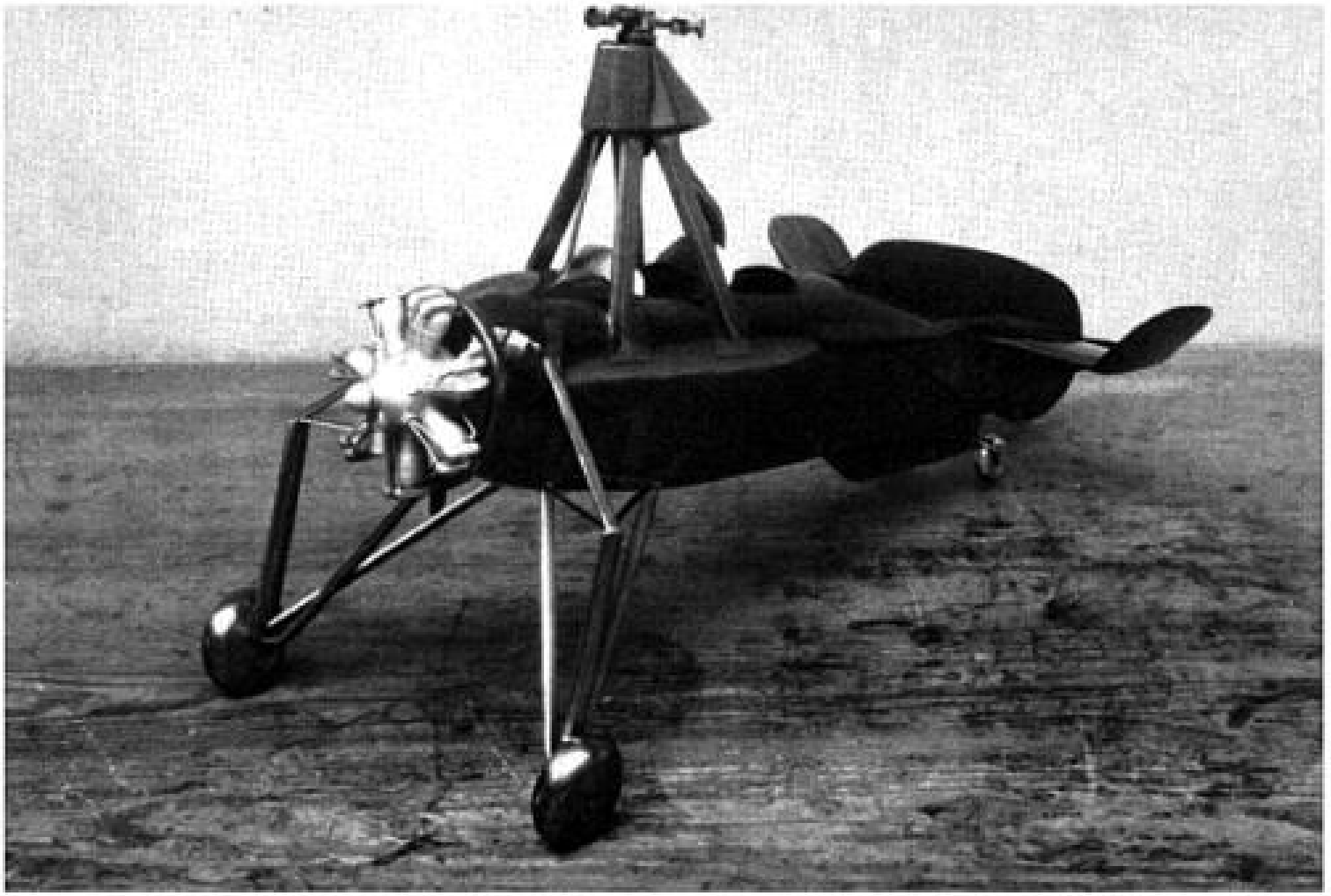

Fig. 2-127. The NPL performed wind tunnel tests on this C.30A 1/8-scale model [54].

The C.30 evaluation [54] by the Royal Aircraft Establishment and National Physical Laboratory contains a drag breakdown for a 1/8-scale model (Fig. 2-127) of the C.30A autogyro, shown in Table 2-18 . This C.30 parasite drag baseline was obtained from wind tunnel tests . The original data is

presented as drag in pounds at 100 feet per second, a common practice in that era. I have converted the data to the modern form of equivalent flat plate drag area (f_e) in square feet, which is drag divided by dynamic pressure (i.e., $f_e = D/q$). These data are for the fuselage at zero angle of attack. At a 26-degree angle of attack, the drag of the complete model was twice as high.

Table 2-18 shows the component drags of the Cierva C.30 Autogiro, but it just as easily could be relabeled as drag breakdown for an early biplane or, for that matter, any one of a number of monoplanes. In 1929, Professor Melvill Jones admonished the aircraft industry to reduce equivalent flat plate drag area (f_e)—the measurement of parasite drag. As you know, the aircraft industry has never stopped reaching for the Professor's ideal "streamlined aeroplane." To illustrate this point, consider Fig. 2-128. I constructed and

interpreted this parasite drag area chronology primarily from the enormously valuable technical survey titled *Quest For Performance* [148] by Laurence Loftin. Cierva, Pitcairn, and Kellett autogyros had, as you can see, considerable room for parasite drag reduction.

Table 2-18. C.30A Drag Breakdown Based on 1/8-Scale-Model Tests

Component	Drag at 100 fps (lbs)	Parasite Area (f_e in sq ft)	Percent
Undercarriage and its wheels	29	2.44	32
Engine and exhaust ring	17	1.43	18
Fuselage, with vertical fins	11	0.93	12
Pylon	10	0.84	11
Rotor hub	10	0.84	11
Tail plane	7	0.59	8
Windscreens	4.5	0.38	5
Tail wheel	1.5	0.13	2
Total	90	7.57	100

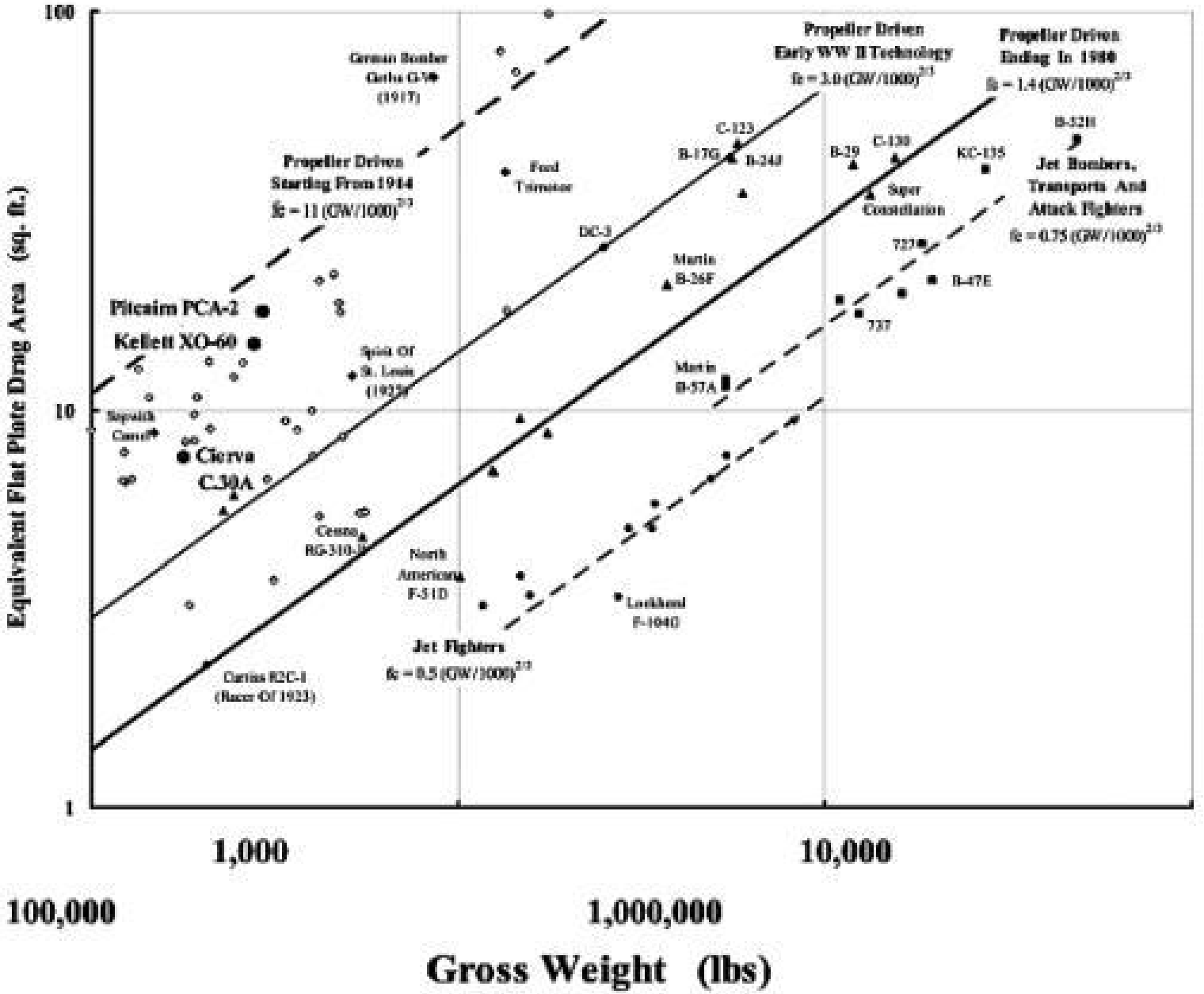

Fig. 2-128. The progress of the aircraft industry towards "the streamlined aeroplane."

2.11.8 Kellett YO-60 Predicted Performance

This introduction to autogyro performance would not be complete without an example of typical engine horsepower versus airspeed for a top-of-the-line autogyro. The complete performance of "modern" autogyros did not depend only on the rotor system L/D, of course. The drag of the fuselage, landing gear, hub, blade shanks, and other protuberances (i.e., everything but the blades) were quite important too. The propulsive efficiency of propellers was also a dominant factor in arriving at the total engine brake horsepower required to fly. The example I have chosen is the last Kellett autogyro.

2.11 PERFORMANCE

As Brooks notes on pages 238 and 239 of reference [7]: "The [one] XO-60 [and

seven] YO-60's were the last Autogiros delivered to the United States Army Air Forces. They were extensively tested after delivery but their higher initial cost and greater maintenance demands, as compared with fixed-wing liaison light aircraft, led to their rejection for army cooperation work." This last autogyro delivery was accompanied by a performance analysis [149] of the XO-60/YO-60 series.[59] I have taken some liberty in transposing the final data and results into 1990s terminology. The XO-60/YO-60 series, shown in Fig. 2-129, had the primary physical characteristics shown in Table 2-19.

The estimated XO-60 power required versus speed and data necessary to the estimate, based on [149], are shown in Fig. 2-130 to Fig. 2-133 . The standard method of relating power available and power required in the autogyro era was to reduce power available by propeller efficiency as discussed earlier. However, in

Fig. 2-130, I have chosen to increase power required by propeller efficiency so that engine brake horsepower required ($BHP_{req'd.}$) becomes

$$(2.324) \quad BHP_{req'd.} = \frac{D_{rotorcraft} V_{FP}}{550 \eta_{prop}} .$$

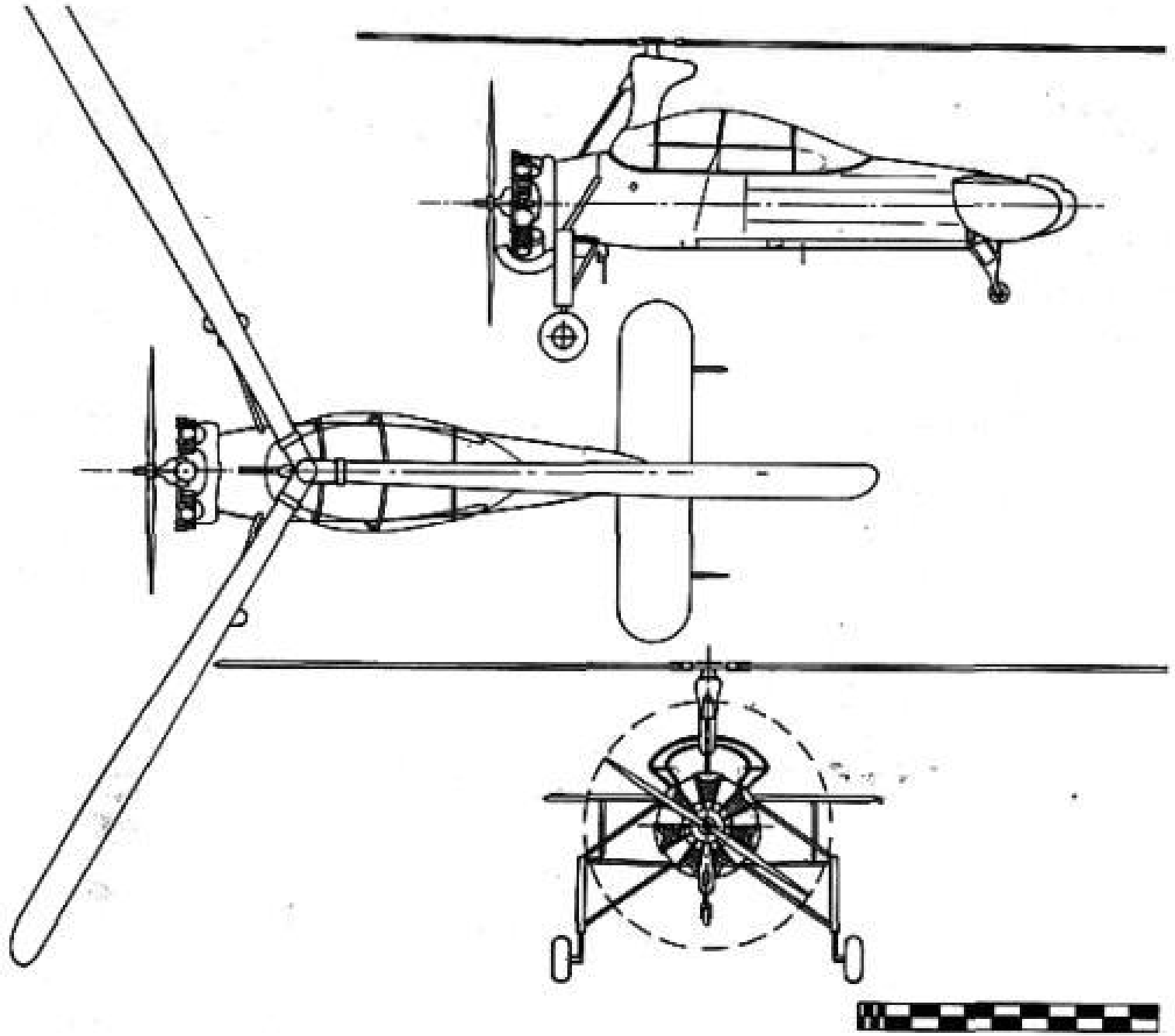

Fig. 2-129. The Kellett YO-60 [7].

[59] Wayne Wiesner, a longtime friend and a pioneer in his own right, sent me this reference in a private letter. In the early 1940s Wayne worked at Kellett under chief engineer Richard Prewitt. Wayne later joined Stan Hiller's innovative team as Jay Spenser notes in reference [150].

Table 2-19. XO-60 Physical Properties

Parameter	Value
Design Gross Weight	2,800 lbs
Operating Weight Empty	2,180 lbs
Normal Fuel	36 gal.
Main Rotor	3 blades
Diameter	43.2 ft
Chord at 70% radius	12.92 in.
Solidity	0.0476
Airfoil (root)	23016 NACA
Airfoil (tip)	23010 NACA
Rotor Speed at max speed at sea level	241 rpm
Rotor Speed at min speed at sea level	189 rpm
Horizontal Tail	
Span	10 ft
Chord	30 in.
Fuselage	
Number of Seats	2
Overall Length	21 ft 5 in.
Propeller	2 blades
Hamilton Standard, constant speed	2150 rpm
Hub Model	2B20
Blade Design	6135A-6
Diameter	8.5 ft
Engine	
Jacobs I-6MB-A rated at	300 hp
Operating Speed	2,150 rpm

The reason I have chosen this alternate form is to facilitate performance comparisons of the late-model autogyros to helicopters, as you will see later in Volume II—Helicopters. The rotorcraft drag ($D_{rotorcraft}$) is estimated at flight weight (W) by

(2.325)

$$D_{rotorcraft} = f_e\left(0.5\rho V_{FP}^2\right) + D_{rotor} = f_e\left(0.5\rho V_{FP}^2\right) + \frac{W}{(L/D)_{rotor}}.$$

The parasite drag area (f_e) varies with fuselage angle of attack (or, alternately, the hub plane angle of attack, α_{hp}) and, hence, with flight path velocity (V_{FP}). A longitudinal trim analysis must be completed to obtain the angles of attack. For the XO-60, this variation is shown in Fig. 2-13 1. Note the auxiliary scale giving flight path velocity.

The propeller efficiency for the Hamilton Standard constant speed propeller was obtained from Hamilton Standard and is shown in Fig. 2-132 . With previous Kellett flight test data available from the YG-1B, Wiesner was able to estimate the blades-alone drag for a gross weight of 2,800 pounds and altitudes of sea level, 5,000, and 10,000 feet. The blades-alone lift-to-drag ratio at sea level is shown in Fig. 2-133 . Rotor speed and hub plane angle of attack varied at each speed, which meant that advance ratio could not be based on one single defined tip speed.

2.11 PERFORMANCE

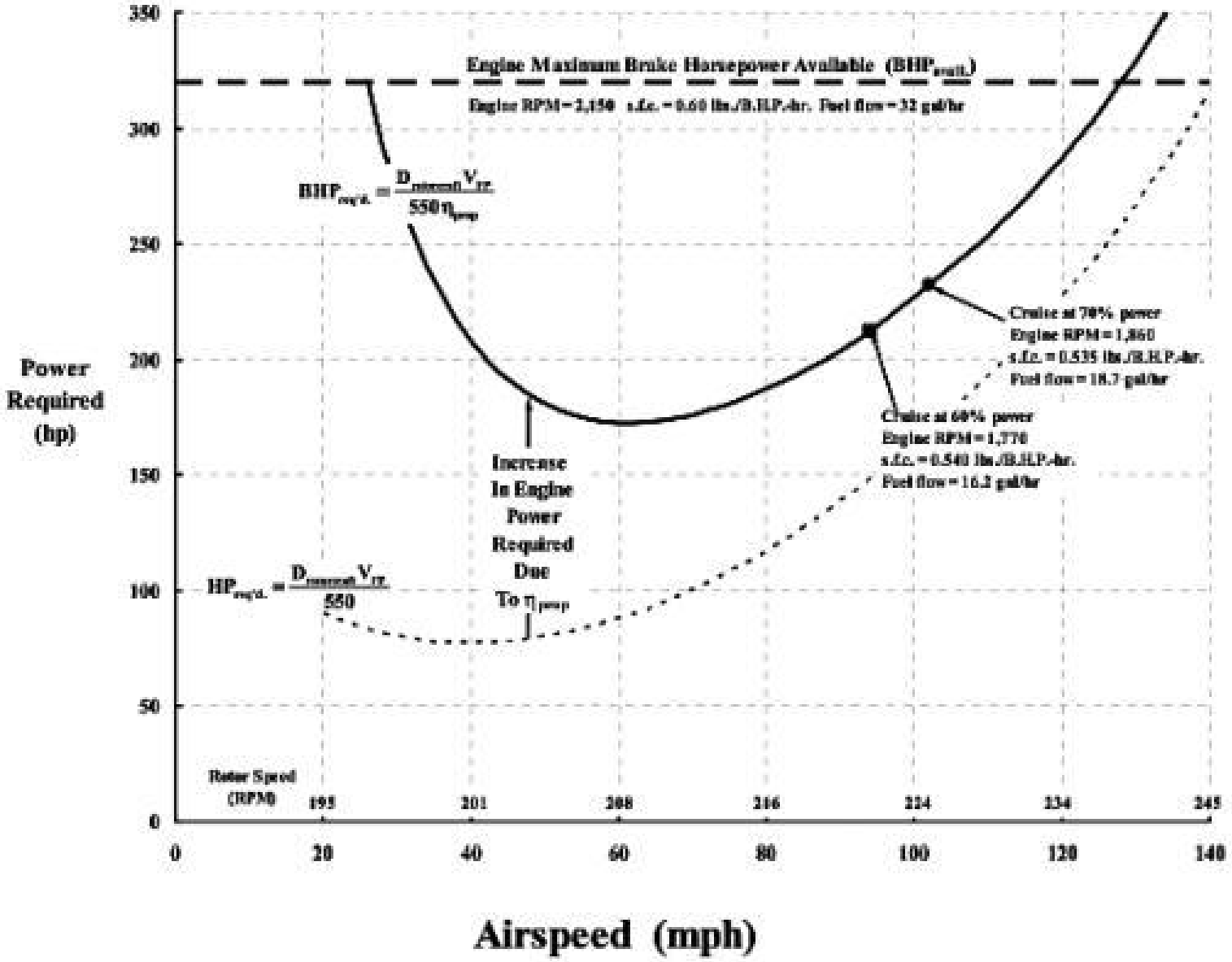

Fig. 2-130. The XO-60 did not have great performance, even at sea level.

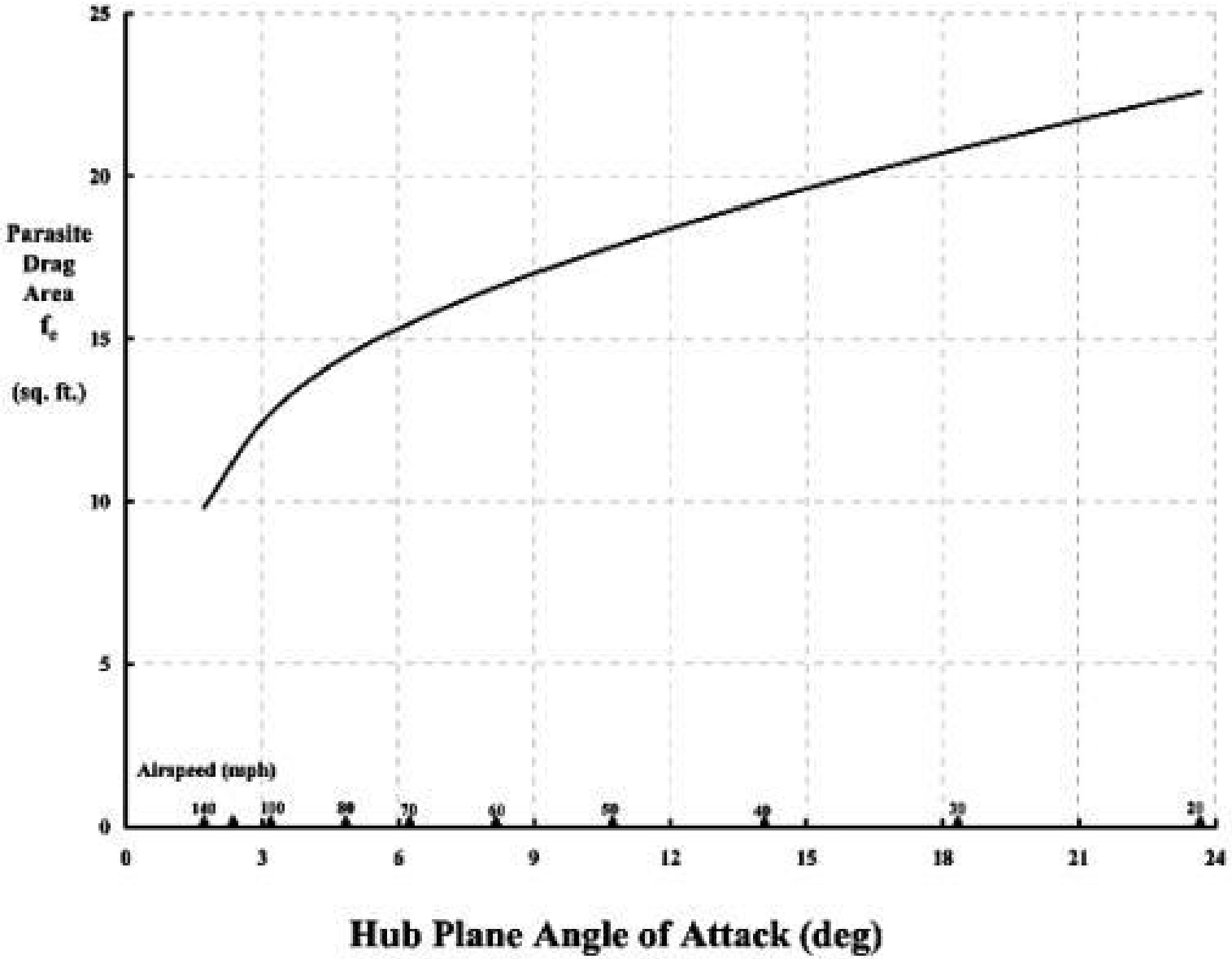

Fig. 2-131. The parasite drag area of "modern" autogyros was high.

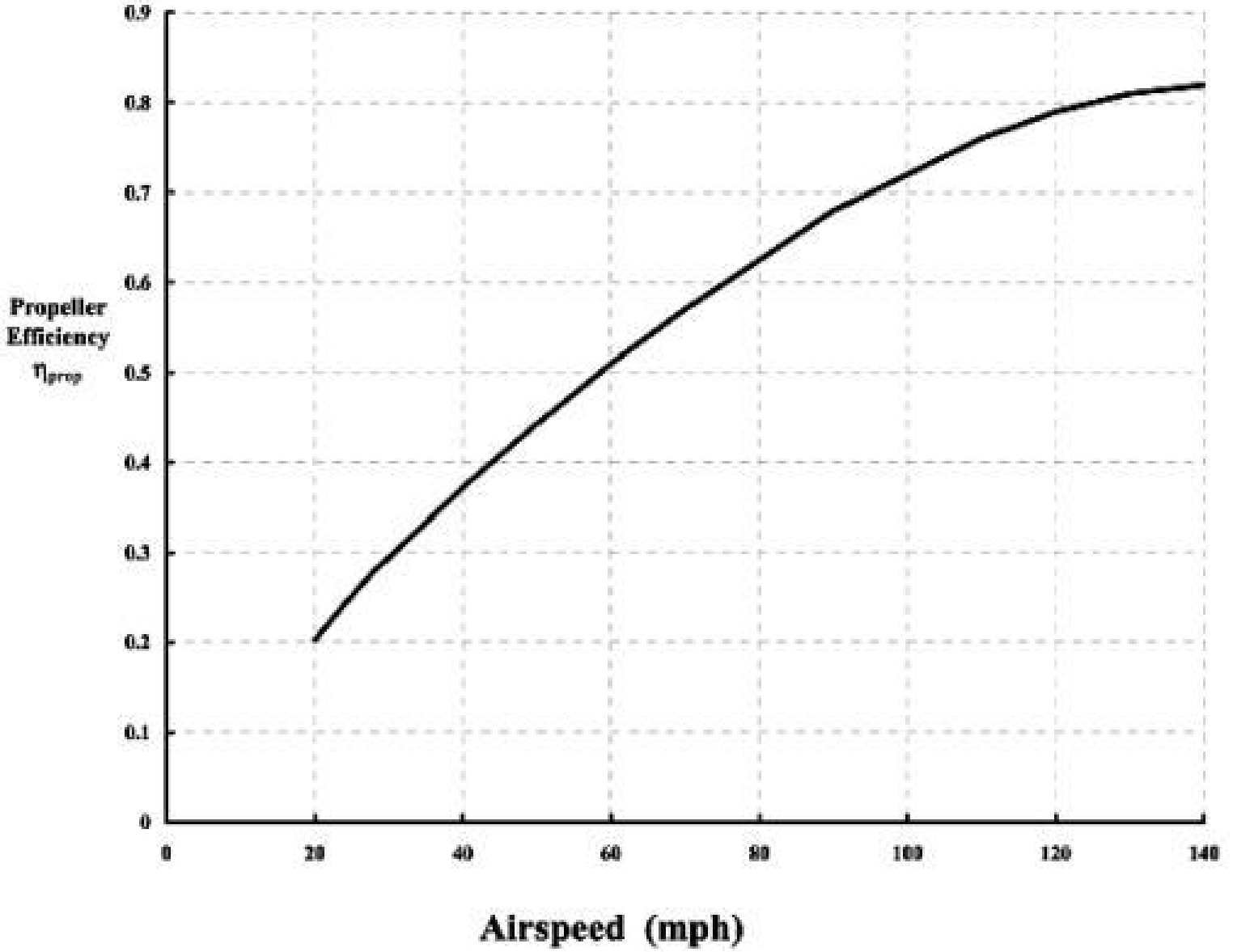

Fig. 2-132. The efficiency of the XO-60 variable-pitch propeller.

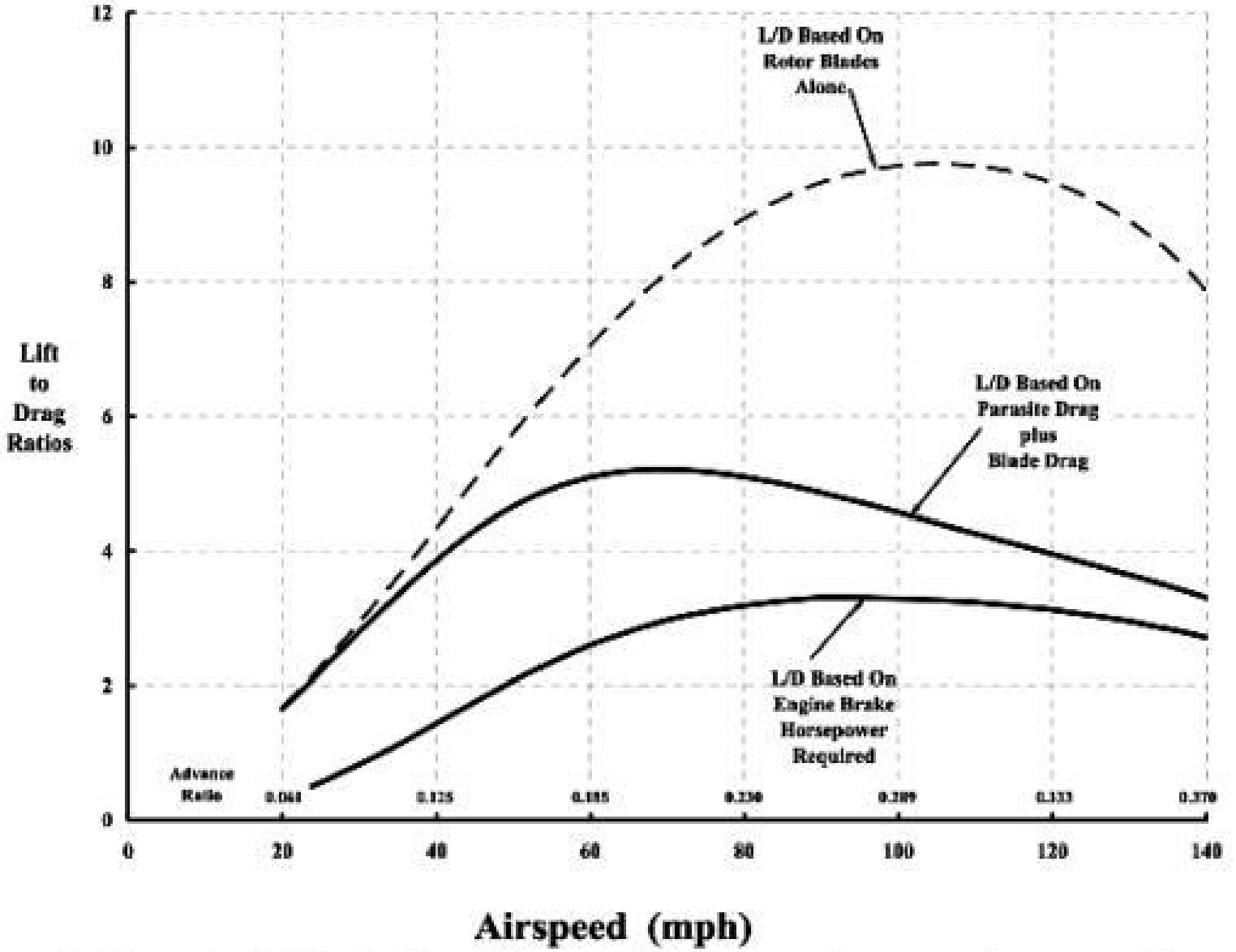

Fig. 2-133. The three L/D ratios estimated for the Kellett XO-60 in 1943.

2.11 PERFORMANCE

Table 2-20. Estimated and Guaranteed YO-60 Performance Parameters

Parameter	Value	Guaranteed
Gross Weight	2,800 lbs	
Design Altitude	Sea level	
Maximum Speed at Sea Level	134 mph	127
Minimum Speed	26 mph	30
Cruise Speed	70 to 94 mph	
Maximum Range with 36 gal.	210 statue miles	
Average Cruising Speed for Max Range	70 mph	
Endurance at 60% Power with 36 gal.	2.2 hours	2.0
Service Ceiling	13,750 ft	
Minimum Time to Climb to 10000 ft	16 min	
Takeoff Distance (to clear 50-ft obstacle)	247 ft	250
Landing Distance (to clear a 50-ft obstacle)	nil	
Maximum Permissible Diving Speed	154 mph	

You will note in Fig. 2-133 that there are three lift-to-drag ratios that can be quoted. The rotor-blades-alone L/D has been discussed at length earlier in this volume. The L/D based on parasite drag plus blade drag represents performance obtainable in a power-off glide. This is what Wheatley, for example, obtained with PCA-2 testing. The third L/D ratio

shown in Fig. 2- 133 is, I believe, the most meaningful because it is based on engine brake horsepower required ($EHP_{req'd.}$) in level flight. This third L/D ratio is defined here as

$$(2.326)\quad \left(\frac{L}{D}\right)_{EPR} = \frac{W\,V_{FP}}{550\,EHP_{req'd.}}.$$

Some typical summary performance data is provided in Table 2-20. Kellett actually based the final tabulated performance summary on 320 horsepower available from the engine and a gross weight of 2,800 pounds . The Kellett Autogiro Corporation guaranteed certain YO-60 performance parameters to the U.S . Army Air Force and those are also shown in Table 2-20.

The final power required versus airspeed performance displayed in Fig.

2-130 illustrates the penalty of having a propeller for forward thrust and a rotor for lift. Both devices incur a profile power loss. This represents a double loss in profile power. In fact, as you will see later, the rotor is quite capable of lifting and thrusting forward—very efficiently—as the helicopter has demonstrated. This aspect of wings, propellers, and rotors will be reopened in the discussion about high-speed rotorcraft.

2.11.9 Closing Remarks

Despite ongoing efforts by Cierva, Pitcairn, Kellett, and others, the autogyro never demonstrated airplane-like performance. In fact, the majority of autogyro improvements

dealt with the rotor system and its shortcomings, such as the vibration it transmitted to the airframe. The reduction in rotor solidity and the move to three cantilevered blades certainly helped, but hub and blade-shank drag reduction were never even addressed. Furthermore, no effort to retract landing gear was ever even discussed. Rotor-blades-alone maximum lift-to-drag ratios much above 10 were never realized, and the one attempt at utilizing an improved airfoil led to stability and control problems that caused a fatality. It almost seems to me that the mold was cast for all rotorcraft performance during the autogyro era.

As you will read in Volume II—Helicopters, preoccupation with the rotor system and its undesirable features permutated helicopter development.

2.12 MAINTENANCE

The autogyro matured with the addition of (1) direct rotor control (accompanied by the removal of the wings, ailerons, and rudder) and (2) auxiliary power drive to pre-spin the rotor prior to takeoff (leading to nearly vertical jump takeoffs) . Not incidentally, maintenance and safety generally improved as Cierva, Pitcairn, and Kellett, the industry leaders, developed new models. By the time the Cierva C.30 was fielded, Reginald Brie [52] was able to list rather specific maintenance requirements for this most produced autogyro model. Brie recommended that grease lubrication be periodically performed as shown here in Table 2-21.

Brie also prescribed that every 50 flying hours, the following points required lubrication:

a. Engine Controls and Petrol Control Rods
b. Clutch and Brake Controls in Cockpit
c. Actuating Gear for Bias Control in Cockpit
d. Levers for Bias Control on Pylon
e. Operating Controls and Pins for Dog and Plate
f. Clutch Controls
g. Casings in All Bowden Controls Are Well Packed With Vaseline and Should Receive Occasional Attention

Table 2-21. Lubrication Requirements of the Cierva C.30

- **Rotor System**
  1. Grease Flapping Articulation Pin Every 10 Flying Hours
  2. Drag [lead-lag] Articulation Pin, Grease Every Flying Day
  3. Grease Hub Every 20 Flying Hours
- **Control System**
  4. Grease Longitudinal Hinge Pin [hub pivot] Every 10 Flying Hours
  5. Grease Lateral Hinge Pin on Starboard Side Every 10 Flying Hours
  6. Ball Joint on Top of Control Column, [Grease] Every 10 Flying Hours
  7. Grease Hinge Fork Every 10 Flying Hours
  8. Center of Cross Shaft, Grease Every 10 Flying Hours
- **Pre-Spin Drive**
  9. Top Unit-Mechanical Starter [gear box], Grease Every 20 Flying Hours
  10. Grease Top Ball Joint Every 10 Flying Hours
  11. [Grease] Spline at Bottom of Transmission Shaft Every 10 Flying Hours
  12. Grease Bottom Ball Joint Every 10 Flying Hours
  13. Engine Clutch—Grease When Dismantling Only
- **Landing Gear**
  14. to 22. Eight Grease Points Done Every Flying Day

2.12 MAINTENANCE

Maintenance in the rotorcraft world today uses scheduled maintenance man-hour per flight hour as one contributor to operating cost per flight hour. Therefore, let me guess

from Reginald Brie's list that 2 man-hours would be scheduled for every 10 hours of flying plus 2 more hours for the 50-hour lubrication list. This gives 12 man-hours for 50 flying hours or about one-quarter of a man-hour for every flying hour. The cost of grease and the lubricant is not included.

What is left off of Brie's scheduled maintenance list is, of course, the 140-horsepower, Armstrong Siddeley Genet Major IA engine (military designation, the Civet I), the fuel system and, by the way, the propeller. Fortunately, a much more complete picture of the Cierva C.30 autogyro maintenance requirements is available . The AVRO Company delivered several military versions of the C.30 to the Royal Air Force . These aircraft were known as ROTA gyroplanes. Manuals [1 5 1-1 57] were provided for the autogyro.[60] It is from these manuals that I have constructed a much clearer picture of the C.30

aircraft and its maintenance.

The Royal Air Force version of the Cierva C.30, Fig. 2-134, is describe in Air Publication 1490, Volume I [1 52] as a two-seater, single engine gyroplane aimed at communication duty. Chapters I through VII of this primary volume give a specification-like description of the fuselage, undercarriage, tail units, rotor, controls, engine installation, flying equipment (i.e. instruments), and miscellaneous equipment. Rigging, Assembly, and Various Adjustments are covered in Chapter VIII, and Special Flying Notes are provided in Chapter IX.

Volume III of Air Publication 1490 [156] provides an index of assemblies by drawing number and the breakdown of parts in each assembly. This view of the ROTA is virtually a drawing tree, which I have summarized in table form along with a parts

count in Table 2-22 . Cierva and the AVRO Company organized the ROTA description into 25 assemblies and, by my count, about 2,800 parts defined by a drawing were required to build-up one ROTA. Of course, shop-floor supplies such as standard nuts, bolts, and washers, etc., added at least another 2,200 parts.

Once assembled, these parts required maintenance . The maintenance schedule [1 54] called for inspection between flights, and inspections (a) daily, (b) every 10 hours, (c) every 20 hours, (d) every 40 hours, and (e) every 120 hours . The Civet I engine and its "airscrew" required inspection as well, of course . The engine and propeller inspection intervals were identical to the airframe. The Air Ministry publication makes it quite clear that

"This schedule describes the technical detail of the maintenance and shows the routine which is considered to be necessary in normal circumstances. It is not to be

interpreted as absolving any persons concerned from the responsibility of acquainting themselves with or acting upon any circumstances indicating the necessity for additional [i.e., unscheduled maintenance] work."

---

[60] Miss Mary Jane Millare, Office Administrator of the Department of Research and Information Services at the Royal Air Force Museum in London, tracked down the original manuals and got me a copy. The rotorcraft industry, myself included, is extremely grateful.

2.12 MAINTENANCE

FRONTISPIECE

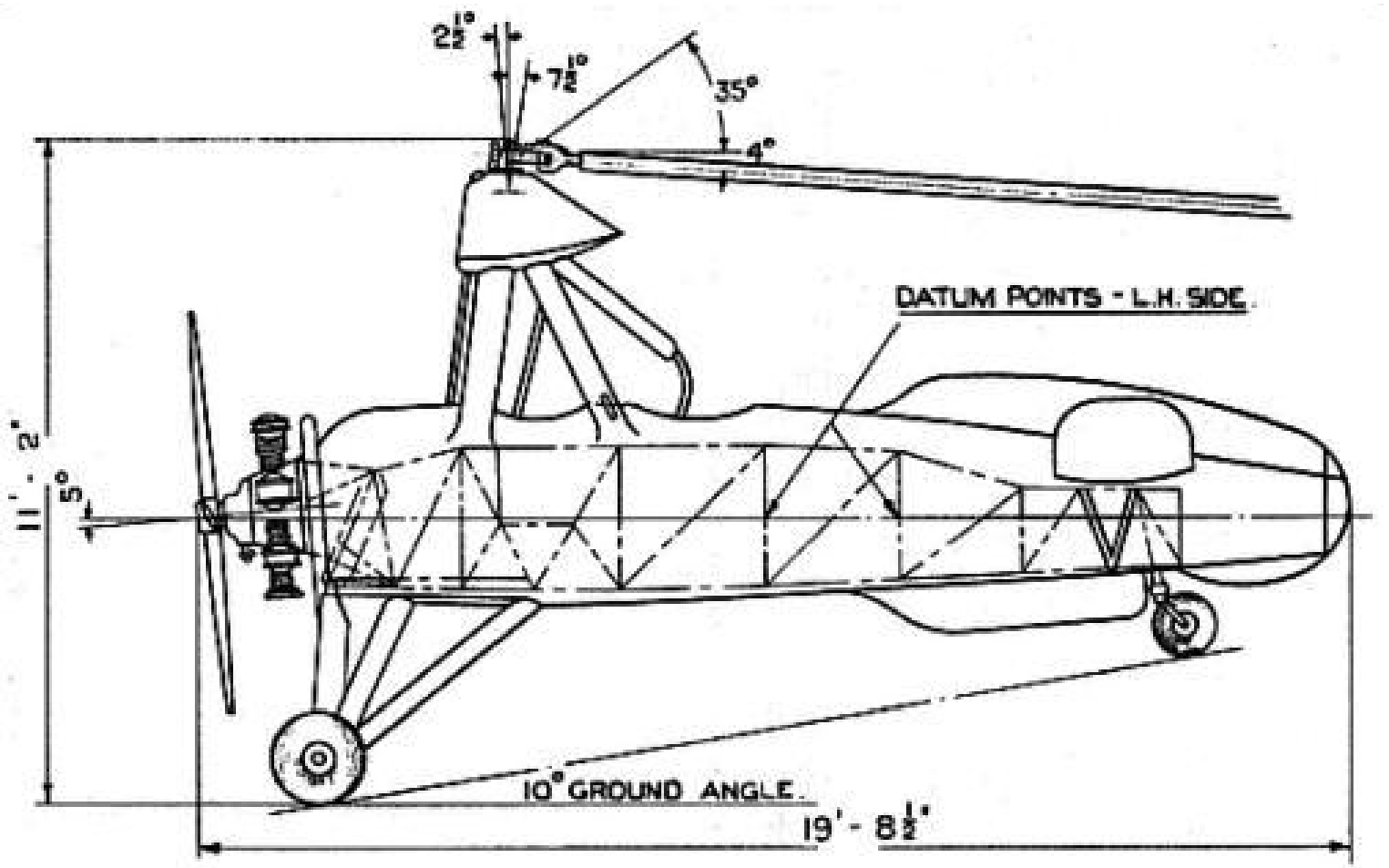
2½°
7½°
35°
4°
DATUM POINTS - L.H. SIDE.
11' - 2"
5°
10° GROUND ANGLE.
19' - 8½"

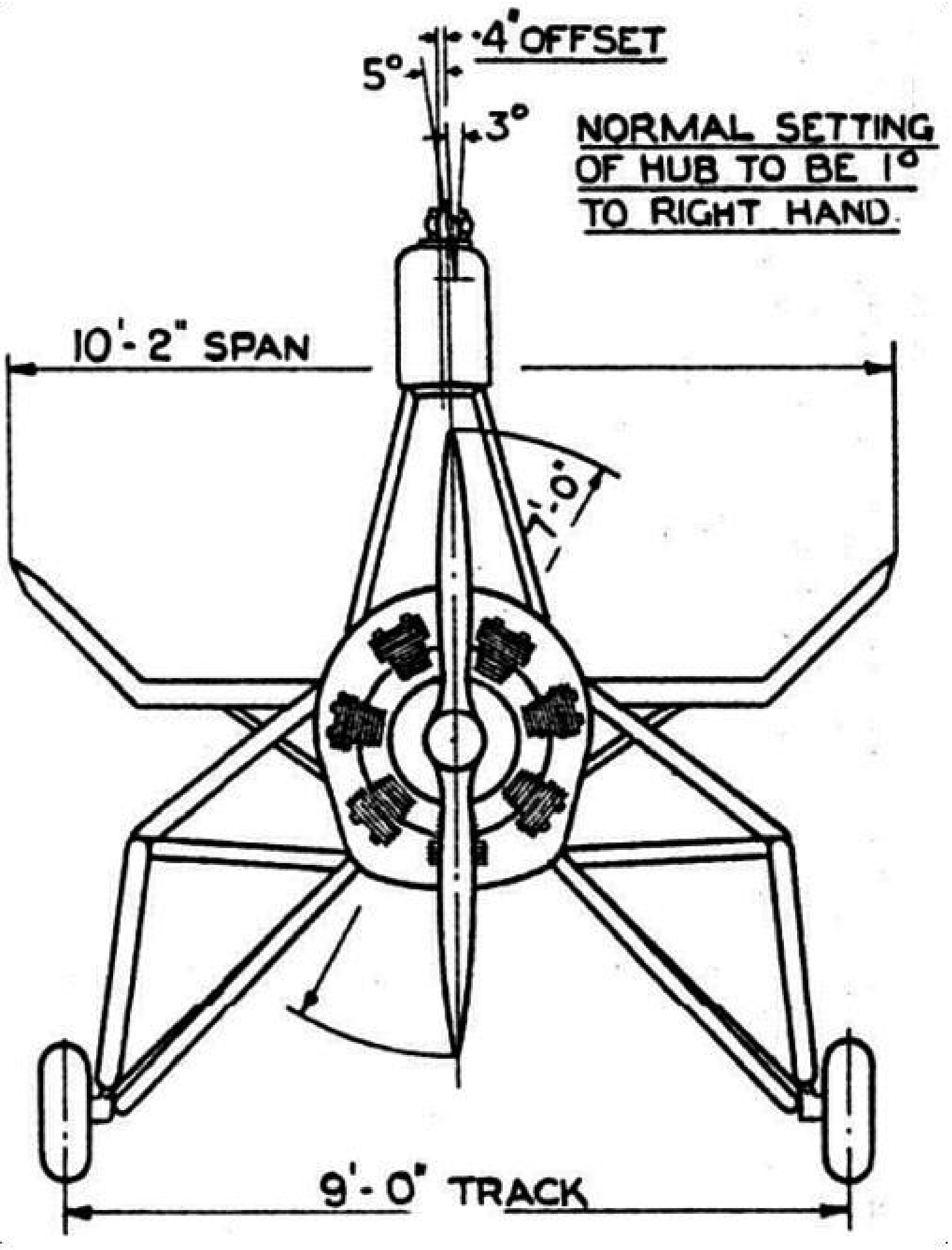
·4" OFFSET
5°
3°
NORMAL SETTING OF HUB TO BE 1° TO RIGHT HAND.
10'-2" SPAN
7'-0"
9'-0" TRACK

AREAS IN SQ. FT.

TAIL PLANE	15 · 6
UPTURNED TIP (BOTH)	8 · 55
UPPER FIN	12 · 9
LOWER FIN	3 · 38
ROTOR BLADES (EACH)	15 · 6
ROTOR BLADES {TOTAL OF 3 PER GYROPLANE}	46 · 8

"ROTA" GYROPLANE.

CIVET I ENGINE.

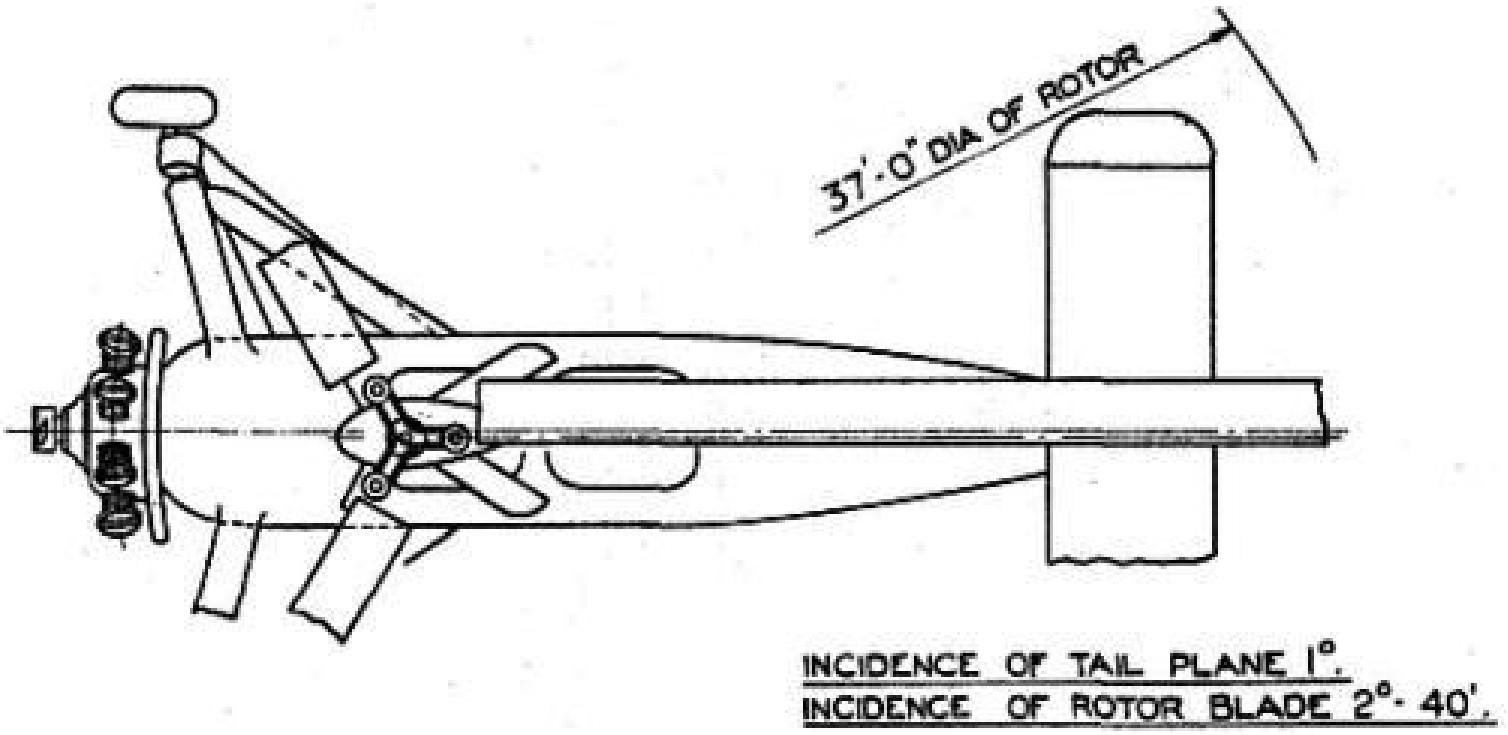

Fig. 2-134. The Royal Air Force C.30 was known as the ROTA Gyroplane.

Table 2-22. Index of Assemblies and Parts Count for the ROTA

Assembly	Drawing Number	Subassemblies Per Assembly	Drawing Parts Per Assembly	Shop Parts Per Assembly
Controls, Rotor Clutch and Brake, Wheel Brake	T556	8	79	86
Controls, Engine	O529	9	52	65
Controls, Machine	Not Given	8	191	128
Controls, Magneto Starting	O1938	1	16	45
Controls, Rotor (really rotor hub + transmission)	Not Given	21	435	297
Engine Cowling	E735	1	13	69
Engine Mounting	O535	1	65	36
Fuel System	P552	3	86	72
Fuselage, Bulkhead	O532	1	51	118
Fuselage, Clutch Mounting	C589	1	19	46
Fuselage, Fairings	E557	12	151	149
Fuselage, Flooring	D529	1	20	24
Fuselage, Joints	Not Given	0	0	0
Fuselage, Seating	N509	1	4	0
Fuselage, Skeleton	C576	10	80	0
Fuselage, Windscreens	M518	2	13	115
Instruments	Not Given	11	45	152
Miscellaneous	Not Given	5	59	44
Oil System	P546	3	39	55
Pylon Structure	J612	4	81	16
Rotor Blades	F699	3	1,056	516
Tail Plane	G550	2	41	0
Tail Struts	G544	5	26	38
Tail Wheel	K549	8	8	24
Alighting Gear (undercarriage)	K546	12	182	134
Airframe Grand Totals		**133**	**2,812**	**2,229**
Plus One Engine and One Prop	n/a	n/a	n/a	n/a

2.12 MAINTENANCE

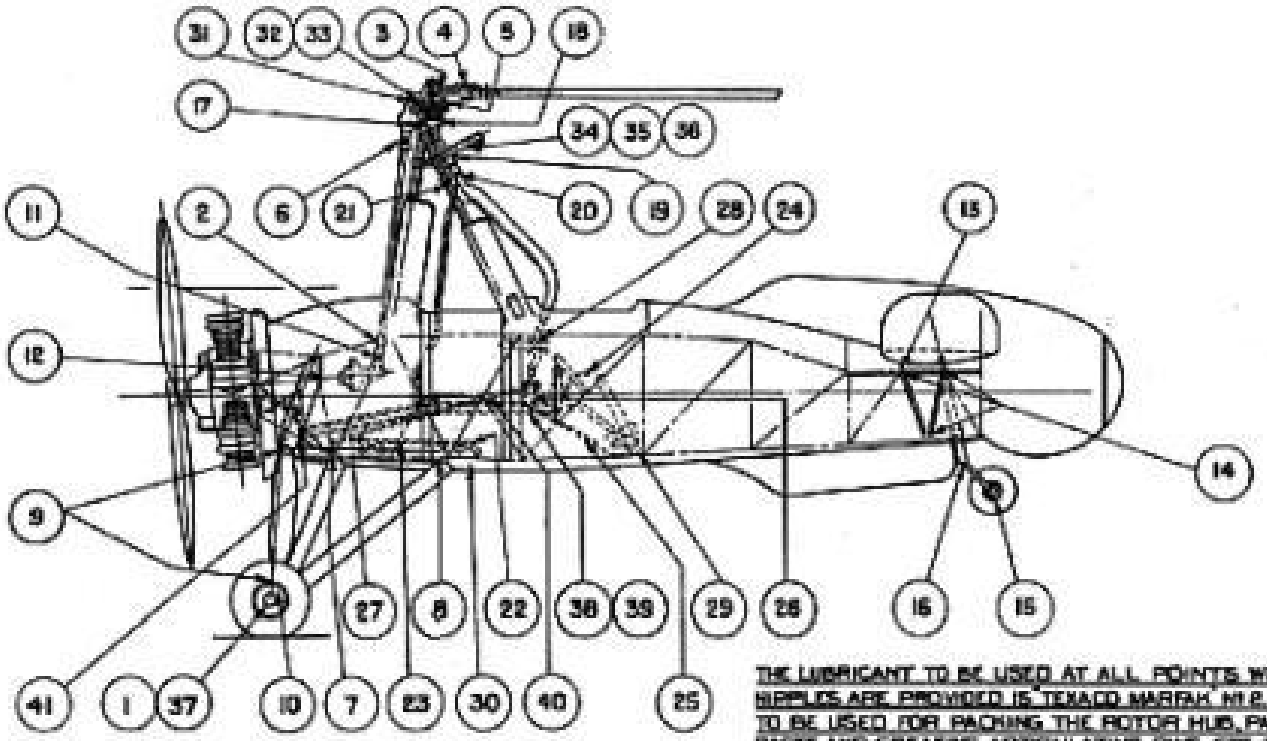

THE ITEMS MARKED * HAVE GREASE NIPPLES FITTED FOR THE USE OF A GREASE GUN.

THE LUBRICANT TO BE USED AT ALL POINTS WHERE GREASE NIPPLES ARE PROVIDED IS TEXACO MARFAK M.P. IT IS ALSO TO BE USED FOR PACKING THE ROTOR HUB, PACKING THE BALL RACES AND GREASING ARTICULATING PINS, ETC. THROUGHOUT THE ROTOR SYSTEM. WHEN RE-ASSEMBLING AFTER DISMANTLING. IN ALL OTHER CASES, THE TYPES OF LUBRICANT ARE LAID DOWN IN AP 1464A/D.E.D.

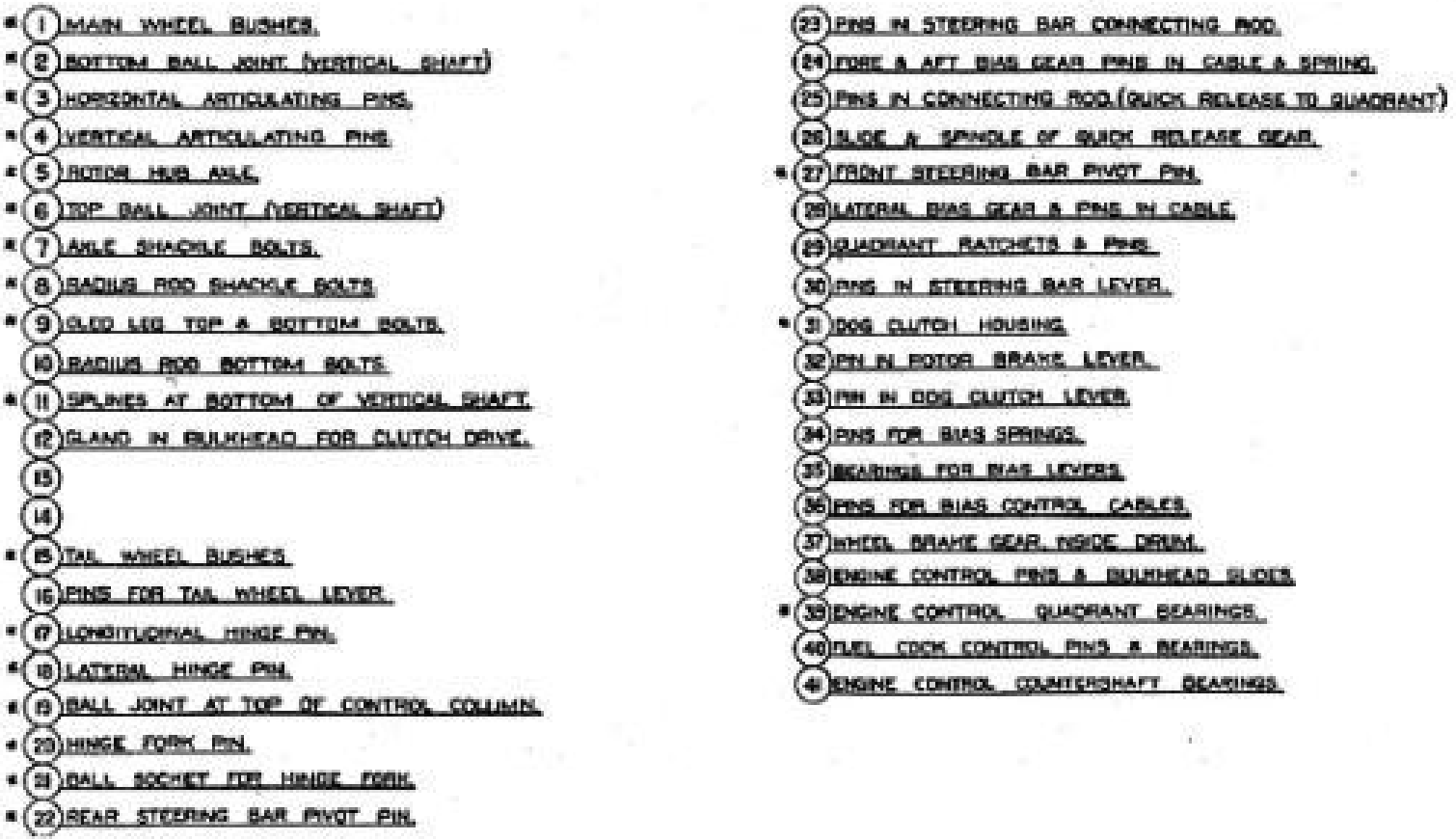

Fig. 2-135. The Royal Air Force C.30 lubrication diagram (the C.30 had 39 lubrication points).

For historical purposes, I have included both airframe and engine maintenance schedules in Appendix K. You will see that many of the maintenance items required lubrication. The lubrication diagram, Fig. 2-135, shows points that accepted grease and those that just got a squirt of oil.

So much for the practical subject of

maintenance. Now let me proceed to the most important autogyro aspect—safety.

277

278

2.13 SAFETY

The proponents of the autogyro argued that the first merit of the autogyro was its freedom from the dangers of fixed-wing stalling at low speed.[61] The lift performance at low speed was, in fact, better than fixed-wing aircraft, and this safety was carried over to the helicopter during power-off landings . You will recall that Henrich Focke, like Cierva, set the number one design criteria for his helicopter as safety following power failure. For the autogyro, the rotor was unpowered in flight so a transition from level to gliding flight following power failure was quite benign. The autogyro was virtually automatic in going

into a glide. The reasonable management (by the pilot) of potential and kinetic energies available from altitude, speed, and rotor inertia became the key to successful power-off landings, as you will read later.

By 1938 (about a 10-year span), Brooks [7] notes that five people had died in autogyro accidents: one in Britain, three in France, and one in the United States. By 1938, I estimate that

- Over 500 autogyros had been built, including nearly 50 prototypes
- More than 50 pilots had been trained
- At least 100 fixed-wing pilots had flown autogyros in the U. S. alone
- About 40,000 flight hours and over 2-1/2 million miles had been accumulated by the fleet.

Accepting these estimates leads to a statistic of 8,000 fleet hours flown for each fatality. The

fatality rate of the autogyro was, of course, at least twice as good as the fixed-wing industry was experiencing by 1938 [158]. That does not mean though that autogyro crashes were not happening. In his eleventh and twelfth appendices, Brooks [7] provides manufacturers' serial numbers . In his remarks' column, he notes that 30 "crashes" had happened, but lists no information about the 97 Kellett autogyros built by Japan. Therefore, on the basis of, say 400 autogyros, about 30 crashed. This would be an attrition rate of 7.5 percent, which actually is not too bad when compared to general aviation statistics.

Perhaps you will find this additional information about aviation safety useful [159]. The subject will come up again in the helicopter discussion presented in Volume II.

The gathering, analyzing, and reporting of aviation accident data has

played an important part in making air transportation safer. One of the earliest examples of this safety improvement activity took place in November 1921, at the Premier Congrés International de la Navigation Aérienne, held in Paris. During this conference, Albert Tete presented a review of the status of aerial transportation in France [160]. In addition, R. Mayo presented a paper entitled *Aviation and Insurance* [161], which discussed the "causes of the many accidents which account for the high insurance rates." Specifically, he stated:

---

61 The more optimistic of autogyro champions strongly suggested that forward flight efficiency comparable to the airplane would undoubtedly be achieved, however airplane development was already so far ahead that the lead held by the fixed-wing industry could not be overtaken.

"The frequent accidents to airplanes employed on air routes have been due to widely divergent causes. Probably 90% of them were due to carelessness and could have been avoided, had the necessary precautions been taken. The principal causes of accidents may be enumerated as follows:

1. Poor piloting;
2. Engine trouble;
3. Lack of system; [organization of personnel]
4. Poorly adapted airplanes;
5. Poor airdromes;
6. Unfavorable meteorological conditions."

With only minor changes, the Mayo paper presented in 1921 could be presented at any "aerial transportation" safety conference today.

In the United States, following World War I, the National Advisory Committee on

Aeronautics (N.A.C.A.), by request of the Assistant Secretaries for Aeronautics in the Departments of War, Navy, and Commerce, established a special commission "to prepare a basis for the classification and comparison of aircraft accidents, both civil and military." In NACA Report No. 308 [162], 13 classes of accidents, 4 classes of injuries, and 6 classes of damage to material were defined. Categories of immediate and underlying accident causes were established and an accident form was adopted. This approach was used to analyze 1,432 military and 1,400 civilian accidents that occurred before January 1929 [163] . In June 1936, a further refinement to definitions and methods of analysis was established with NACA Report No. 576 [164] . That report, entitled "Aircraft Accidents, Method of Analysis," became the standard United States reference on the subject and formed the foundation for current National Transportation Safety Board (NTSB) aviation accident

reporting.

There was an immediate payoff for the efforts of the N.A.C.A.-led committee. Analysis of the data revealed major shortcomings in aircraft design and pilot training (e.g., deficiencies in aircraft stability and control, and spin recognition and recovery) for which corrective actions were developed and implemented. It should be noted that solving these problems did not require computing accidents per flight hour or other ratios that are considered important measures of transportation safety today. The priority then, as now, was to put an end to accidents.

In October 1944, the U.S. Civil Aeronautics Administration (CAA), the predecessor to the Federal Aviation Administration (FAA), published the first "Statistical Handbook of Civil Aviation" [158].

This first of many CAA handbooks pointed out that reported accident statistics were based on definitions and classifications established by NACA Report No. 576 (although the Statistical Handbook incorrectly referenced the NACA report as "TR-567"). This document summarized aviation statistics dating back to 1926, including air carrier and private flying accident statistics compiled by the U.S. Civil Aeronautics Board (CAB), the predecessor to the NTSB. In the introduction, the CAA acknowledged that "there are some gaps in the early statistics because fact-gathering machinery had not been fully organized and it also was extremely difficult to obtain reliable figures from an industry still inchoate." With

respect to private flying, the CAA noted that, "Because of the dislocation caused by the War, statistics on the amount of private flying during the war years are incomplete." Despite these reservations, the 1944 CAA handbook provided early examples of detailed tables regarding such aircraft operating statistics as the number of hours flown, miles covered, and passengers carried. Many of the safety measures using these statistics are still used today.

Today, the NTSB investigates civil aviation accidents and has amassed a database of coded, as well as narrative, information. Over 32,000 aviation accidents, which have occurred since 1982, are summarized at the NTSB website (www.ntsb.gov) and at the FAA Office of System Safety (http://nasdac.faa.gov./asp/asy_ntsb.asp). The FAA Statistics and Forecast Branch publishes a yearly "Census Of U.S . Civil Aircraft." The

census provides details about the number and types of aircraft currently operating in the U.S. civil aviation fleet, along with other relevant data. Fleet-size data are obtained by extrapolating data from a survey questionnaire mailed to a sample of registered owners . The validity of this extrapolation has been questioned occasionally. Today there are approximately 350,000 U.S . civil registered aircraft, which makes updating and correcting the census and registration records a daunting task. Nevertheless, by combining data from the FAA and NTSB, such statistics as accidents per 100,000 operating hours for each civil aircraft grouping are prepared and widely distributed.

2.14 CONCLUDING REMARKS

The contributions made by Cierva before his tragic, untimely death (he was killed December 9, 1936 at the age of 50 in a Douglas DC-2 accident at Croydon Airport near London, England) cannot be restricted to just the preceding, technically oriented discussion. Just as importantly, Cierva spread rotorcraft technology worldwide—in the most direct way— by helping other companies get started in the autogyro business. Brooks [7] records that autogyros were manufactured in at least seven countries, which certainly hastened the arrival of a practical helicopter.

The autogyro era of the rotorcraft industry developed from the roots established by the Cierva Autogiro Company, Limited, as shown in Fig. 2-136. This initial industry base was created from the technology developed by Cierva and the business strength provided by the Weir brothers, in particular James Weir who

became chairman of the company. In effect, the Cierva Autogiro Company was the engineering department and business headquarters for the autogyro and its development. The A.V. Roe & Co., Ltd. became the manufacturing facility for the early contracts with the Air Ministry of Great Britain.

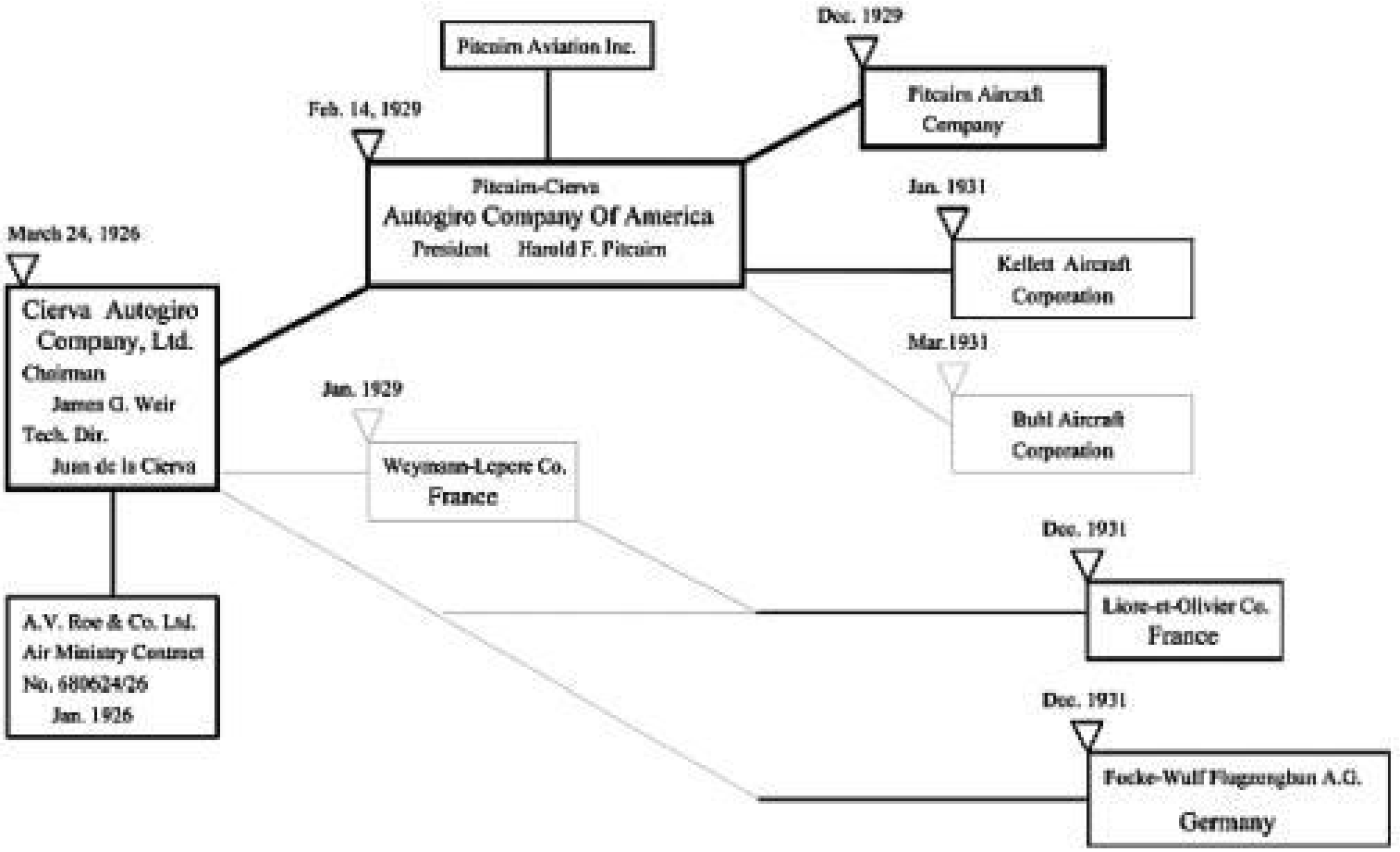

Fig. 2-136. In 5 years the autogyro industry spread to Europe and the U.S.

2.14 CONCLUDING REMARKS

As word of Cierva's success with the autogyro spread, Harold Pitcairn saw the potential in the United States and initiated a strong business tie with Cierva and Weir. This led to the Autogiro Company of America as a principal licensee. An immediate subsidiary, the Pitcairn Aircraft Company, was set up to design, develop, market, and produce its own line of autogyros. The Kellett brothers obtained a license from the Autogiro Company of America and became a competing firm with its own products.

In Europe, the initial license to the Weymann-Lepere Company passed on to the Liore-et-Olivier Company in France, and Henrich Focke brought the technology to

Germany.

The efforts of these pioneering companies, and TsAGI in Russia and Kayabe in Japan, were rewarded. Brooks [7] points out that the industry developed some 46 different autogyro types and delivered about 450 rotorcraft by the end of World War II. A summary of delivered production models shown in Fig. 2-137 confirms that the Cierva Model C.30 and its derivatives dominated the market.

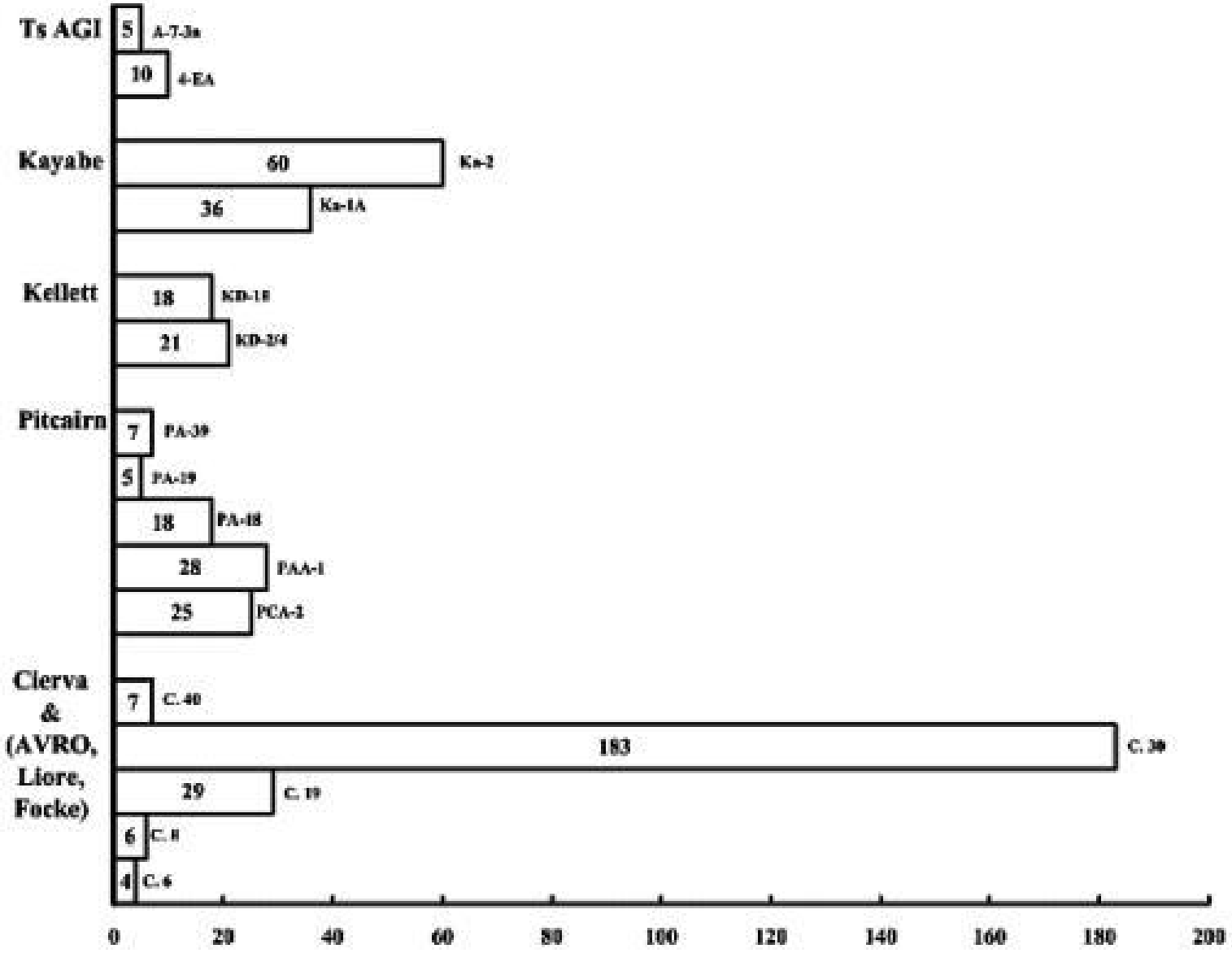

Fig. 2-137. A Summary of delivered production models (about 450 autogyros were delivered by the time the era ended).

Brooks also uncovered (and included in his excellent history) enough detailed data to construct several other summary charts, which capture the accomplishments during the autogyro era. For example, the industry demonstrated that it had a product at a reasonable price. Fig. 2-138 shows that in "back-then dollars" these early rotorcraft could be delivered for something on the order of $ 5.50 per pound of empty weight. The most produced model, the Cierva C.30, even approached $3.50 per pound. Updating these prices to 2010 dollars provides an estimate of about $50 to $77 per pound of empty weight.

The industry also made considerable progress in reducing the weight empty fraction of the autogyro over the two-decade period. This structural efficiency measure, the ratio of empty weight to maximum takeoff gross

weight, is shown in Fig. 2-139 . As the rotor systems improved and other components incorporated prevailing fixed-wing aircraft technology, the weight-empty fraction dropped from about 0.81 to 0.58 . Advanced configurations, on the drawing board as the era came to close, suggested that the structural efficiency would continue to improve and that empty weight would be less than half of the maximum takeoff gross weight.

These first successful rotorcraft certainly enjoyed a unique position in the transportation system of their day. With the wealth of technical data provided by Brooks [7], it is quite easy to incorporate the autogyro onto Gabrielli's and Von Karman's view shown in the front piece art of this volume. The future position of the practical helicopter that was yet to come is shown by the autogyro data in Fig. 2-140.

There is one last note I would like to make in closing this brief introduction to autogyros . In the early 1960s, the Royal Aeronautical Society established the Cierva Memorial Lecture honor. Dr. James A. J. Bennett, who carried on after Cierva's untimely death, had the privilege of giving the first lecture on February 16, 1961 [80]. Henrich Focke, in being honored for developing the first practical helicopter, gave the Fifth Cierva Memorial Lecture on October 23, 1964 [10]. In his introduction, Henrich Focke said,

"The author was brought to the task of making the first practical helicopter because de la Cierva did not do it himself."

2.14 CONCLUDING REMARKS

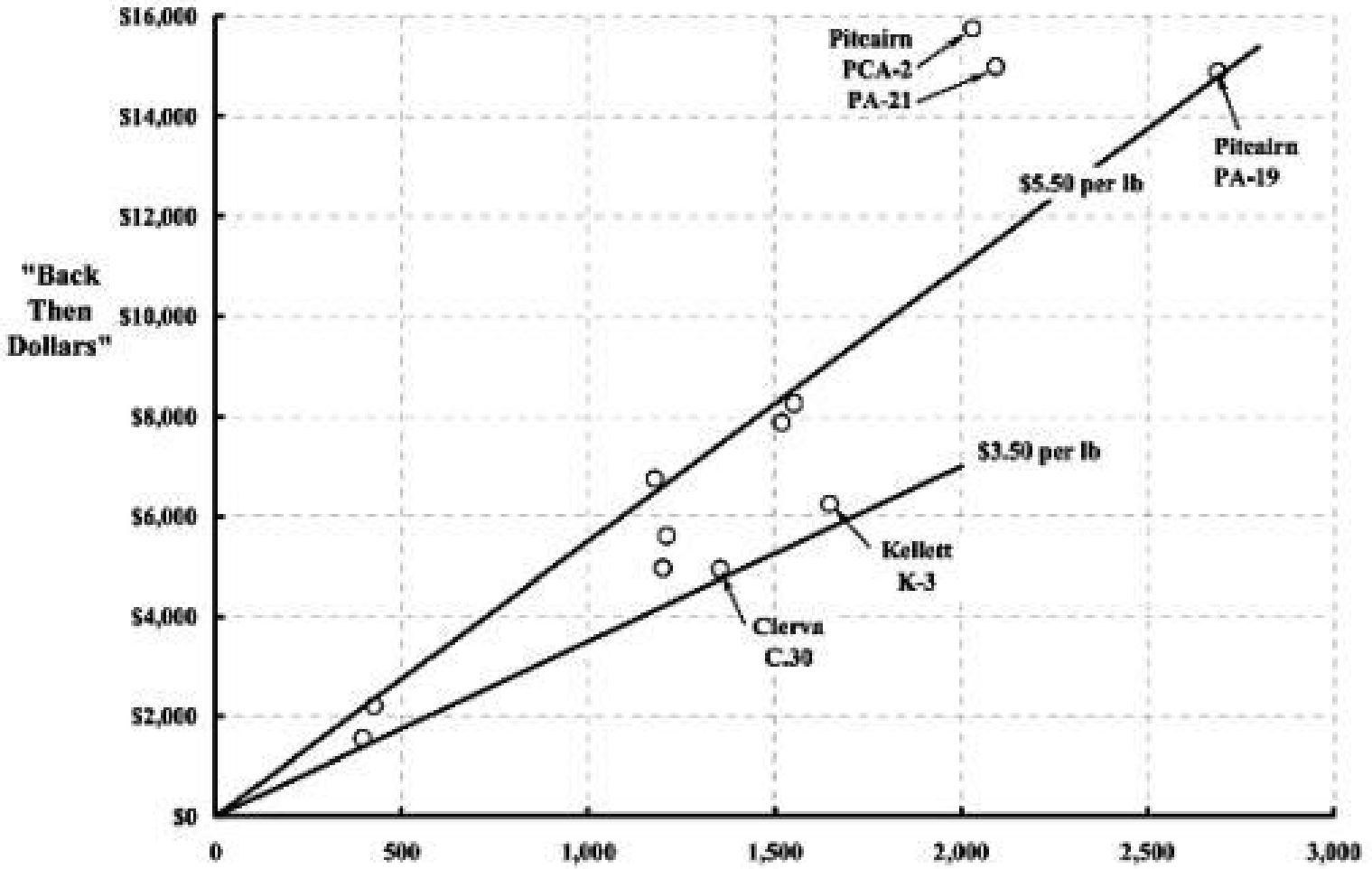

Fig. 2-138. Autogyros were not unreasonably expensive.

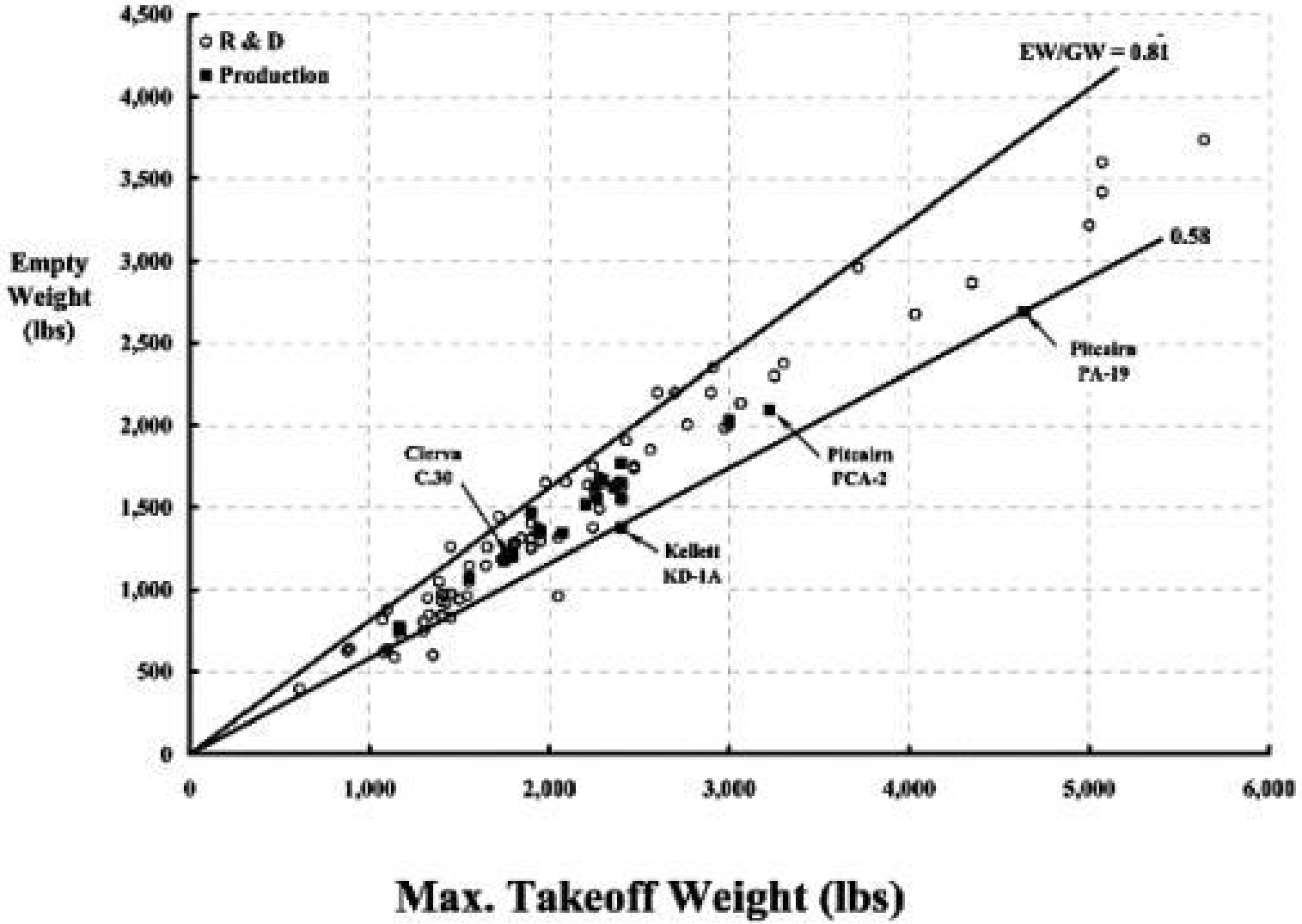

Fig. 2-139. The autogyro industry reduced the weight-empty fraction from 0.81 to 0.58 over two decades.

2.14 CONCLUDING REMARKS

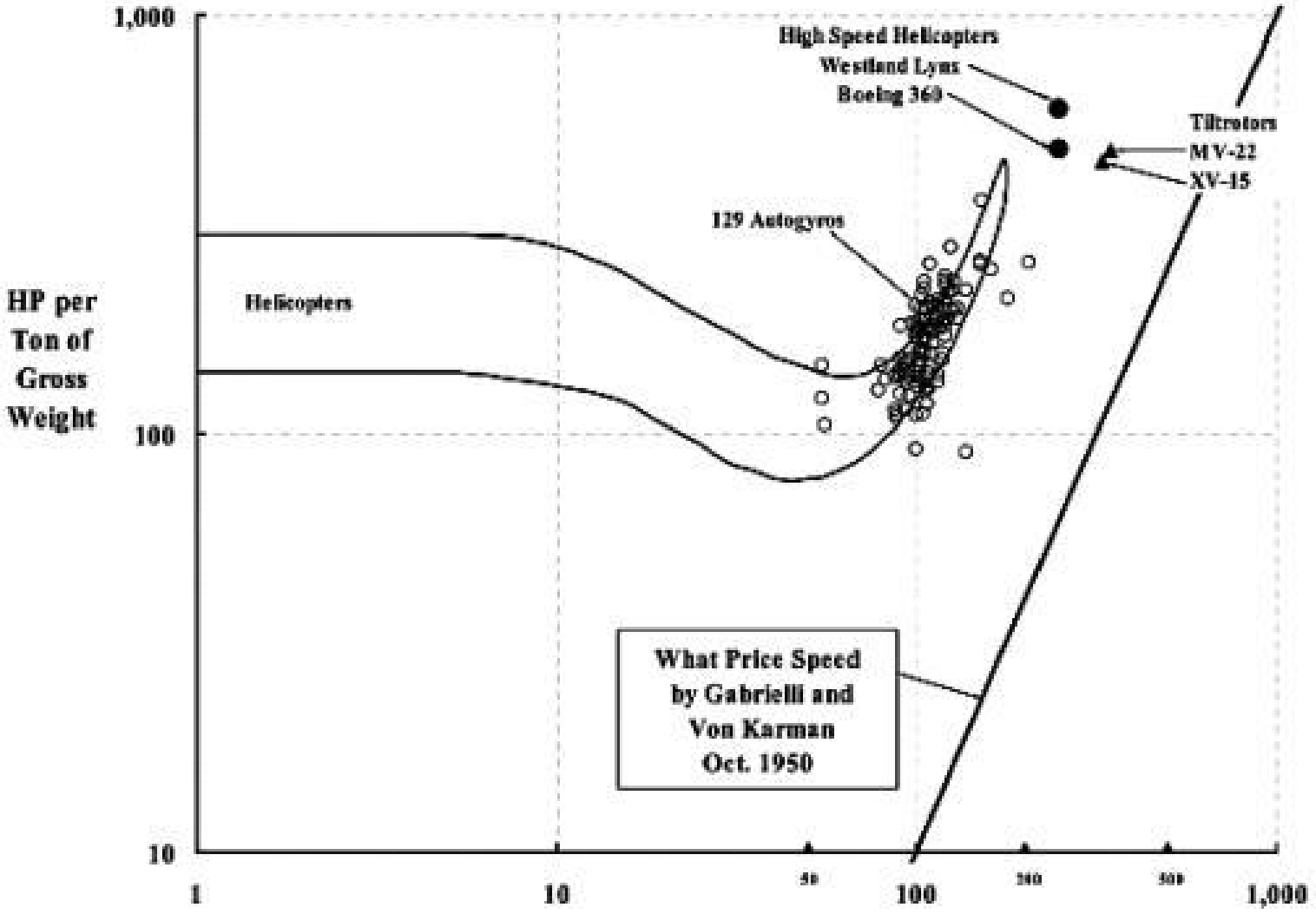

Fig. 2-140. Autogyros gave a hint as to where helicopters would place in the field of transportation.

2.15 REFERENCES

1. Gabrielli, G.; and von Karman, T.: What Price Speed. Mechanical Engineering, vol. 72, Oct. 1950.

2. Moreno-Caraciolo: The Autogiro. NACA TM No. 218, July 1923. 3. de la Cierva, J.: The Development of the Autogyro. J. Royal Aeronautical Society, vol. 30, no. 8, Jan. 1926.

4. de la Cierva, J.: The Autogyro. J. Royal Aeronautical Society, vol. 34, no. 8, Nov. 1930.

5. de la Cierva, J.: New Developments of the Autogyro. J. Royal Aeronautical Society, vol. 39, no. 8, Dec. 1935.

6. de la Cierva, J.; and Rose, D.: Wings of Tomorrow—The Story of the Autogiro. London, England: Brewer, Warren, and Putnam, 1931.

7. Brooks, P. W.: Cierva Autogiros—The Development of Rotary-Wing Flight.
Washington, D.C.: Smithsonian Institution Press, 1988.
8. Focke, H.: The Focke Helicopter. NACA TM No. 858, April 1938. 9. Focke, H.: The Focke Helicopter. J. Royal Aeronautical Society, vol. 42, no. 8, July
1938.
10. Focke, H.: German Thinking on Rotary-Wing Development. J. Royal Aeronautical
Society, vol. 69, no. 5, May 1965.
11. de la Cierva, J.: Engineering Theory of the Autogiro (original notes). Dr. J. A. J. Bennett
(Ed.): American Helicopter Society Library, 1929.
12. de la Cierva, J.: Theory of Stresses on Autogiro Rotor Blades (original notes). Dr. J. A.

J.
Bennet (Ed.): American Helicopter Society Library, 1934.
13. Glauert, H.: A General Theory of the Autogiro. Aeronautical Research Committee R&M
No. 1111, Nov. 1926.
14. Lock, C. N. H.: Further Developments of Autogiro Theory. Aeronautical Research
Committee R&M No. 1127, Mar. 1927.
15. Boulet, J.: History of the Helicopters—as Told by Its Pioneers. Paris, France: Empire,
1982.
16. Sikorsky, I. I.: Development of the VS-300 Helicopter. 9th Annual Mtg. of the Institute
of the Aeronautical Sciences, New York, N.Y., Jan. 1941.
17. Sikorsky, I. I.: Technical Development of the VS-300 Helicopter During 1941.

J. Aeronautical Sciences, vol. 9, no. 8, June 1942.

18. Sikorsky, I. I.: Progress of the Vought-Sikorsky Helicopter Program in 1942.

Aeronautical Engineering Review, vol. 2, no. 4, Apr. 1943.

19. Sikorsky, I. I.: Helicopters of Tomorrow. Aviation, Jan. 1942.

20. Sikorsky, I. I.: Recent Developments in Rotary-Wing Aircraft. 17th Annual Mtg. of the Institute of the Aeronautical Sciences, New York, N.Y., Jan. 1949. 21. Sikorsky, I. I.: The Story of the Winged-S. New York, N.Y.: Dodd, Mead & Co., 1967.

2.15 REFERENCES

22. Sikorsky, S. I.: The Search for a Solution—The Development of the VS-300. American

Institute of Aeronautics and Astronautics, vol. 78-3006, Jan. 1978. 23. Hunt, W. E.: "Heelicopter". London, England: Airlife Publishing Ltd., 1998. 24. Morris, C. L.: Pioneering the Helicopter. New York, N.Y.: McGraw Hill, 1945. 25. Gregory, H. F.: Anything a Horse Can Do. New York, N.Y.: Reynal & Hitchcock, 1944. 26. Butler, H. K.: Army Air Corps Airplanes and Observation (1935–1941). Saint Louis,

Mo.: Historical Office, United States Army Aviation Systems, 1990. 27. Butler, H. K.: A History of Army Aviation Logistics (1935–1961), Rotary-Winged

Aircraft and the Army (1939–1943). Saint Louis, Mo.: Historical Office, United States

Army Aviation Systems Command, 1990.
28. Anon.: Proc. of the First Convertible Aircraft Congress. Philadelphia Sections of the
American Helicopter Society and the Institute of the Aeronautical Sciences, The Franklin Institute, Philadelphia, Pa., Dec. 1949.
29. Anon.: Proc. of the Second Convertible Aircraft Congress. Philadelphia Sections of the
American Helicopter Society and the Institute of the Aeronautical Sciences, The Franklin Institute, Philadelphia, Pa., Dec. 1952.
30. Anon.: Proc. of the Third Convertible Aircraft Congress. Convertible Aircraft Pioneers
and the Franklin Institute, Philadelphia, Pa., Nov. 1955.
31. Anon.: Proc. of the Fourth Convertible

Aircraft Congress. Convertible Aircraft Pioneers
and the Franklin Institute, Philadelphia, Pa., Dec. 1958.
32. Levy, H.: Mr. Herrick's Convertiplane. Aeroplane Monthly, Feb. 1991. 33. Koch, J. J.: Summary of the VTOL State of the Art. American Helicopter Society
Newsletter, vol. 7, no. 9, Sept. 1961.
34. Schneider, J.: The History of V/STOL Aircraft. American Helicopter Society VertiFlite,
vol. 29, no. 3 and 4, March/April 1983.
35. Rogers, M.: VTOL Military Research Aircraft. New York, N.Y.: Crown Publishers, Inc.,
1989.
36. Seiferth, R.: Testing A Windmill Airplane ("Autogiro"). NACA TM No. 394, Nov. 1927. 37. Garner, A. M.: Flight Tests of the La Cierva

Autogyro. Royal Aircraft Establishment Report No. B. A. 555, November 18, 1925.
38. Klemin, A.: An Introduction to the Helicopter. Mechanical Engineering. (See also NACA TM No. 340), Nov. 1924.
39. Bréguet, L.: The Gyroplane. NACA TM No. 816, Jan. 1937.
40. Bréguet, L.: The Gyroplane. J. Royal Aeronautical Society, vol. 36, no. 8, Sept. 1937.
41. Rosen, G.: Thrusting Forward: A History of the Propeller. Hartford, Conn.: Hamilton Standard, Division of United Technologies, 1987.
42. Courtney, F. T.: The Eight Sea. New York, N.Y.: Doubleday & Company, Inc., 1972. 43. Prewitt, R. H.: The Autogiro. McClarren, R. H. (Ed.). Proc. of the First Rotating Wing Aircraft Mtg., The Franklin Institute, Philadelphia, Pa., Oct. 28–29, 1938.

2.15 REFERENCES

44. Pecker, J. S.: Mechanical Design in Rotary Aircraft. McClarren, R. H. (Ed.). Proc. of the Second Rotating Wing Aircraft Mtg., The Franklin Institute, Philadelphia, Penn., Nov. 30–Dec. 1, 1939.

45 . Townson, G.: Autogiro–The Story of the Windmill Plane. Fallbrook, Calif.: Aero Publishers, Inc., 1985.

46. Coleman, R. P.; and Feingold, A. M.: Theory of Self-Excited Mechanical Oscillations of Helicopter Rotors With Hinged Blades. NACA Report No. 1351, 1958.

47 . Anon.: Performance of Gyroplane C.19 Mk. II. Royal Aircraft Establishment Report No. B. A. 865, May 1930.

48 . Smith, F. K.: Legacy of Wings—The Harold F. Pitcairn Story. New York, N.Y.: Jason
Aronson, Inc., 1981.
49. Larsen, A. E.: American Autogiro, Gyroplane and Early Convertaplane Developments.
J. American Helicopter Society, vol. 1 , no. 1, Jan. 1956.
50. Sanders, C. J.; and Rawson, A. H.: The Book of the C.19 Autogiro. London, England:
Sir Isaac Pitman & Sons, Ltd., 1931.
5 1 . Pecker, J. S.: Aircraft With Rotary Sustaining Wings. Patent No. 2,037,433 issued by
Autogyro Company of America, USA, April 14, 1936.
52. Brie, R.: The Autogyro and How to Fly It. London, England: Sir Isaac Pitman & Sons,
Ltd., 1934.
53. Gustafson, F. B.: History of

NACA/NASA Rotating-Wing Aircraft Research, 1915–
1970 . American Helicopter Society VertiFlight, vol. VF-70, 1970. See also J. of the
American Helicopter Society, vol. 1, no. 1, Jan. 1956.
54. Hufton, P. A.; Nutt, A. E. W.; and Bigg, F. J.: General Investigation Into the
Characteristics of the C.30 Autogiro. Aeronautical Research Committee R&M No. 1859,
Mar. 1939.
55. Anon.: Military Specification Mil-H-850 1–Helicopter Flying and Ground Handling
Qualities: General Requirements for. Nov. 1952.
56. Anon.: Military Specification MIL-H-8501A–Helicopter Flying and Ground Handling

Qualities: General Requirements for. Sept. 1961; amended April 1962.
57. Beavan, J. A.; and Lock, C. N. H.: The Effect of Blade Twist on the Characteristics of the C.30 Autogiro. Aeronautical Research Committee R&M No. 1727, April 1936.
58 . Wheatley, J . B.: An Analytical and Experimental Study of the Effect of Periodic Blade Twist on the Thrust, Torque, and Flapping Motion of an Autogiro Rotor. NACA Report No. 591, Apr. 1937.
59. Wheatley, J . B.: An Analysis of the Factors That Determine the Periodic Twist of an Autogiro Rotor Blade, With a Comparison of Predicted and Measured Results. NACA Report No. 600, May 1937.
60. Perkins, C. D.; and Hage, R. E.: Airplane Peformance, Stability, and Control. New York,

N.Y.: John Wiley & Sons, Inc., 1949.
61 . Gessow, A.; and Myers, G. C . J.: Aerodynamics of the Helicopter. New York, N.Y.:
Frederick Ungar Publishing Co., 1967.

2.15 REFERENCES

62. Wheatley, J. B.: Control-Force Measurements in Flight of the Pitcairn YG-2 Autogiro.
NACA Confidential Memorandum Report for Army Air Corps (Langley Library,
1605.4, Pitcairn YG-2/1), Feb. 1936.
63. Bailey, F. J.: Flight Investigation of Control-Stick Vibration of the YG-1B Autogiro.

NACA TN No. 764, June 1940.
64. Anon.: The Wilford Gyroplane. Aero Digest, vol. 20, no. 2, Feb. 1932. 65. Hovgard, P. E.: Safety—With Performance. Aviation Engineering, Sept. 1932. 66. Klemin, A.: Notes on the Problems and Progress of Gyroplanes. Aero Digest, vol. 26,
no. 2, Feb. 1935.
67. Wilford, E. B.: The Gyroplane. Proc. of Rotating Wing Aircraft Meeting, Philadelphia,
Pa., Oct. 1938.
68. Klemin, A.: Principles of Rotary Aircraft. J. Franklin Institute, vol. 227, no. 2, Feb.
1939.
69. Klemin, A.; and Ruffner, B. P.: A New Type of Gyroplane. Aircraft Engineering, vol. 3,
no. 34, Dec. 1931.
70. Johnson, W.: Helicopter Theory. Princeton,

N.J.: Princeton University Press, 1980. 71. Leishman, J. G.: Principles of Helicopter Aerodynamics. Cambridge, England: Cambridge University Press, 2000.
72. Wheatley, J. B.: The Aerodynamic Analysis of the Gyroplane Rotating-Wing System. NACA TN No. 492, Mar. 1934.
73. Wheatley, J. B.: Wind-Tunnel Tests of a 10-Foot Diameter Gyroplane Rotor. NACA Report No. 536, Apr. 1934.
74. Hafner, R.: The Hafner Gyroplane. J. Royal Aeronautical Sciences, vol. XLII, no. 326, Feb. 1938.
75. Wheatley, J. B.: An Aerodynamic Analysis of the Autogiro Rotor With a Comparison Between Calculated and Experimental Results. NACA Report No. 487, Jan. 1934. 76.

Hafner, R.: Hafner and Cierva Gyroplanes. Flight, Nov. 11, 1937.
77. Marks, L. S. (Ed.): Mechanical Engineers' Handbook. New York, N.Y.: McGraw-Hill Book Company, Inc., 1924.
78. Bennett, D. J. A. J.: Gyroplane and Autogiro. The Aircraft Engineer (supplement to Flight), Oct. 28, 1937.
79. Grey, C. C.; and Bridgeman, L. (Eds.): Jane's All The World's Aircraft. London, England: Sampson Low, Marston & Company, Ltd., 1938.
80. Bennett, D. J. A. J.: The Era of the Autogiro. J. Royal Aeronautical Society, vol. 65, no. 610, Oct. 1961.
81. Pitcairn, H. F.: Juan de la Cierva. Philadelphia, Pa.: Autogiro Company of

America,
1939.
82. Wheatley, J. B.; and Carlton, B.: Analysis and Model Tests of Autogiro Jump Take-off. NACA TN No. 582, Oct. 1936.
83. Prewitt, R. H.: Possibilities of the Jump-off Autogiro. J. Aeronautical Sciences, vol. 6,
no. 1, Nov. 1938.

84. Warner, E. P.: The Problem of the Helicopter. NACA TN No. 4, May 1920. 85. Liptrot, R. N. C.: Modern Developments in the Helicopter. J. Royal Aeronautical
Society, vol. XLI, Aug. 1937.
86. Durand, W. F.; and Lesley, E. P.:

Experimental Research on Air Propellers, I. NACA
Report No. 14, 1917.
87. Durand, W. F.; and Lesley, E. P.: Experimental Research on Air Propellers, II. NACA
Report No. 30, 1918.
88. Knight, M.; and Hefner, R. A.: Static Thrust Analysis of the Lifting Airscrew. NACA TN
No. 626, Dec. 1937.
89. Knight, M.; and Hefner, R. A.: Analysis of Ground Effect on the Lifting Airscrew.
NACA TN No. 835, Dec. 1941.
90. Kussner, H. G.: Helicopter Problems. NACA TM No. 827, May 1937. 91. Platt, H. H.: The Helicopter: Propulsion and Torque. J. Aeronautical Sciences, vol. 3,
no. 11, Sept. 1936, pp. 398–405.
92. Betz, A.: The Ground Effect on Lifting

Propellers. NACA TM No. 836, Aug. 1937. 93. Zbrozek, J.: Ground Effect on the Lifting Rotor. Aeronautical Research Council R&M No. 2347, July 1941.
94. Hayden, J. S.: The Effect of the Ground on Helicopter Hovering Power Required.
American Helicopter Society 32nd Annual Forum, Washington, D.C., May 1976. 95. Carpenter, P. J.; and Fridovich, B.: Effect of a Rapid Blade-Pitch Increase on the Thrust and Induced-Velocity Response of a Full-Scale Helicopter Rotor. NACA TN No. 3044,
Nov. 1953.
96. Carpenter, P. J.: Effect of Wind Velocity on Performance of Helicopter Rotors as
Investigated With the Langley Helicopter Apparatus. NACA TN No. 3044, Oct.

1948. 97. Munk, M. M.: Some Tables of the Factors of Apparent Additional Mass. NACA TN
No. 197, July 1924.
98. Scarborough, J. B.: Numerical Mathematical Analysis. Baltimore, Md.: The John
Hopkins Press, 1966.
99. Peters, D. A.: Hingeless Rotor Frequency Response With Unsteady Inflow. AHS/NASA-
Ames Specialists' Meeting on Rotorcraft Dynamics, Moffett Field, Calif., Feb. 1974. 100. Bhagwat, M. J.: Transient Dynamics of Helicopter Rotor Wakes Using a Time-Accurate
Free-Vortex Method. Ph.D. Dissertation, University of Maryland, College Park, Md.,
Feb. 2001.
101. Bhagwat, M. J.; and Leishman, J. G.: Rotor Aerodynamics During Maneuvering

Flight
Using a Time-Accurate Free-Vortex
Wake. J. American Helicopter Society, vol.
48,
no. 3, July 2003.
102. Timoshenko, S.: Strength of Materials,
Part I—Elementary Theory and Problems. New
York, N.Y.: Robert E. Krieger Publishing
Co., 1976.
103. Timoshenko, S.: Vibration Problems in
Engineering. New York, N.Y.: D. Van Nostrand
Co., Inc., 1928.

2.15 REFERENCES

104. Peters, D. A.: An Approximate Solution
for the Free Vibrations of Rotating Uniform
Cantilever Beams. NASA TM X-62,299,

Sept. 1973.
105. Perry, C. C.; and Lissner, H. R.: The Strain Gage Primer. New York, N.Y.: McGraw-Hill Book Co., Inc., 1955.
106. Lunde, O . H.: Development and Operation of the Autogiro. Aeronautics, vol. II, no. 9, Oct. 30, 1940.
107 . Harris, F. D.: Rotary Wing Aerodynamics—Historical Perspective and Important Issues. National Specialist's Mtg. on Aerodynamic and Aeroacoustics, American Helicopter Society Southwest Region, Arlington, Tex., 1987.
108 . Scully, M.: Rotor Wakes. Thesis, MIT-Massachusetts Institute of Technology, Cambridge, Mass., 1965.
109. Johnson, W.: CAMRAD II Comprehensive Analytical Model for Rotorcraft

Aerodynamics and Dynamics-Theory Manual. Johnson Aeronautics Inc., Palo Alto, Calif., 1993.

1 10. Owen, J. B . B.: The Stressing of Gyroplane Blades in Steady Flight. Ames Research Center R&M No. 1875, April 1938.

111. Owen, J. B. B.: General Principles of the Structural Design of Helicopter Blades. Design and Construction of Rotor Blades Conf., Helicopter Assoc. of Great Britain, Library of the Royal Aeronautical Society, London, England, Oct. 1951.

1 12. Brie, R.: A History of British Rotorcraft, 1866–1965. Yeovil, Somerset, England: Westland Helicopters Ltd., 1968.

113. Schieman, J.: A Tabulation of Helicopter Rotor-Blade Differential Pressures, Stresses, and Motions as Measured in Flight. NASA TM X-952, Mar. 1964.

1 14. Rabbott, J. P. J.; Lizak, A. A.; and

Paglino, V. M.: A Presentation of Measured and
Calculated Full-Scale Rotor Blade Aerodynamic and Structural Loads. USAAVALABS
TR 66-31, July 1966.
1 15 . Den Hartog, J. P.: Mechanical Vibrations. New York, N.Y.: McGraw-Hill Book Co.,
Inc., 1956.
1 16. Hoerner, S . F.: Fluid-Dynamic Drag (2nd edition) . Brick Town, N.J.: published by
author, 1965.
117. Toussaint, A.: Drag or Negative Traction of Geared-Down Supporting Propellers in the
Downward Vertical Glide of a Helicopter. NACA TN No. 21, Sept. 1920.
1 18 . Munk, M. M.: Model Tests on the Economy and Effectiveness of Helicopter Propellers.
NACA TN No. 221, July 1925.

119. Lock, C. N. H.; Bateman, H.; and Townend, H. C. H.: An Extension of the Vortex Theory of Airscrews With Applications to Airscrews of Small Pitch, Including Experimental Results. Aeronautical Research Committee R&M No. 1014, June 1926.

120. Lock, C. N. H.; and Bateman, H.: Some Experiments on Airscrews at Zero Torque, With Applications to a Helicopter Descending With Engine "Off," and to the Design of Windmills. Aeronautical Research Committee R&M No. 885, Sept. 1923.

2.15 REFERENCES

121. Lock, C. N. H.; and Townend, H. C. H.:

Wind Tunnel Experiments on a Symmetrical Aerofoil (Göttingen 429 Section). Aeronautical Research Committee R&M No. 1066, Nov. 1926.

122 . Glauert, H.: The Analysis of Experimental Results in the Windmill Brake and Vortex Ring States of an Airscrew. Aeronautical Research Committee R&M No. 1026, Feb. 1926.

123. Lock, C. N. H.; and Townend, H. C. H.: Photographs of the Flow Round a Model Screw Working in Water, Especially in the "Vortex Ring State." Aeronautical Research Committee R&M No. 1043, May 1926.

124. Caygill, L. E.; and Nutt, A. E. W.: Wind Tunnel and Dropping Test of Autogyro Models. Aeronautical Research Committee R&M No. 1116, Nov. 1926.

125. Castles, W. J.; and Gray, R. B.: Empirical Relation Between Induced Velocity, Thrust,

and Rate of Descent of a Helicopter Rotor as Determined by Wind Tunnel Tests on Four Model Rotors. NACA TN No. 2474, Oct. 1951.

126. Lock, C . N . H.: Note on the Characteristic Curve for an Airscrew or Helicopter. Aeronautical Research Committee R&M No. 2673, June 1947.

127. Wheatley, J . B.: Lift and Drag Characteristics and Gliding Performance of an Autogiro as Determined in Flight. NACA Report No. 434, May 1932.

128. Peck, W. G.: Landing Characteristics of an Autogiro. NACA TN No. 508, Nov. 1934.

129. Lock, C. N. H.: Photographs of Streamers Illustrating the Flow Around an Airscrew in the "Vortex Ring State". Aeronautical Research Committee R&M No. 1167, Apr. 1928.

130. Wimperis, M. A.: The Rotating Wing In Aircraft. Aeronautical Research Committee

R&M No. 1108, Aug. 1926.
131. Glauert, H.: The Theory of the Autogyro. J. Royal Aeronautical Society, vol. 31,
no. 198, June 1927.
132. Lock, C. N. H.; and Townend, H. C. H.: Wind Tunnel Experiments on a Model Autogyro at Small Angles of Incidence. Aeronautical Research Committee R&M No. 1154, Mar.
1928.
133. Harris, F. D.: Preliminary Study of Radial Flow Effects on Rotor Blades. J. American Helicopter Society, vol. 11, no. 3, July 1966.
134. Juptner, J. P.: U. S. Civil Aircraft Series (vol. 4). Blue Ridge Summit, Pa.: TAB Aero, A Division of McGraw-Hill, Inc., 1993.
135. Juptner, J. P.: U. S. Civil Aircraft Series (vol. 5). Blue Ridge Summit, PA: TAB Aero, A Division of McGraw-Hill, Inc., 1993.
136. Hemke, P. E.: Elementary Applied

Aerodynamics . New York, N.Y.: Prentice-Hall, Inc.,
1946.
137 . Munk, M. M.: General Biplane Theory. NACA Report No. 151, 1932.
138. Knight, M.; and Wenzinger, C. J.: Wind Tunnel Tests on a Series of Wing Models
Through a Large Angle of Attack Range, Part I—Force Tests. NACA Report No. 317,
July 1928.
139 . Wheatley, J. B.: Wing Pressure Distribution and Rotor-Blade Motion of an Autogiro as
Determined in Flight. NACA Report No. 475, July 1933.

2.15 REFERENCES

140. Wheatley, J . B.: The Influence of Wing

Setting on the Wing Load and Rotor Speed of a PCA-2 Autogiro as Determined in Flight. NACA Report No. 523, Dec. 1934.
141 . Wheatley, J. B.; and Hood, M. J.: Full Scale Wind Tunnel Tests of a PCA-2 Autogiro Rotor. NACA Report No. 515, Oct. 1934.
142 . Pinkerton, R. M.; and Greenberg, H.: Aerodynamic Characteristics of a Large Number of Airfoils Tested in the Variable-Density Wind Tunnel. NACA Report No. 628, Oct. 1937.
143 . Anderson, J. D.: A History of Aerodynamics . Cambridge, England: Cambridge University Press, 1997.
144. Bréguet, L.: Aerodynamical Efficiency and the Reduction of Air Transport Costs. J. Royal Aeronautical Society, vol. 26, no. 307, Aug. 1922.
145. Jones, B. M.: The Streamlined Airplane. J. Royal Aeronautical Society, vol. 33, no. 221,

Aug. 1929.
146. Lindbergh, C . A.: The Spirit of St. Louis . New York, N.Y.: Charles Scribner's Sons,
1953.
147. Hall, D. H.: Technical Preparation of the Airplane "Spirit of St. Louis." NACA TN
No. 257, July 1927.
148 . Loftin, L.: Quest for Peformance. NASA SP-468, 1985.
149. Wiesner, W.: Performance Analysis of U.S. Army Air Force Model XO-60 Rotor
Aircraft Equipped With a Jacobs I-6MB-A Engine Rated at 300 H.P. and a Hamilton
Constant Speed Propeller. Report No. 130.8, Kellett Autogiro Corp., Upper Darby, Pa.,
May 1943.
150. Spenser, J.: Vertical Challenge, The Hiller Aircraft Story. Seattle, Wash.: University of
Washington Press, 1992.

151. Anon.: Notes on the Handling of the ROTA Gyroplane in the Air and Upon the Ground.
Air Ministry of Great Britain, July 1936.
152 . Anon.: Air Publication 1490, Volume I—The ROTA Gyroplane Civet 1 Aero-Engine.
Air Ministry of Great Britain, Dec. 1934.
153 . Anon.: Air Publication 1490, Volume II, Part 1—General Orders and Modifications. Air Ministry of Great Britain, Dec. 1934.
154. Anon.: Air Publication 1490, Volume II, Part 2—Maintenance Schedule [No. 42] ROTA with Civet I Engine . Air Ministry of Great Britain, Dec. 1934.
155. Anon.: Air Publication 1490, Volume II, Part 3—Instructions for Repair of ROTA Gyroplane . Air Ministry of Great Britain, Dec. 1934.
156. Anon.: Air Publication 1490 Volume III, Part 1—ROTA Aircraft, Provisional Schedule of Spare Parts. Air Ministry of Great

Britain, Dec. 1934.

157. Anon.: Instruction Book for the Siddeley Genet Major MK. IA Air Cooled Radial Aero Engine. Armstrong Siddeley Motors Ltd., Jan. 1936.

158. Anon.: Statistical Handbook of Civil Aviation. Civil Aeronautics Administration, Washington, D.C., 1944.

2.15 REFERENCES

159. Harris, F. D.; Kasper, E. F.; and Iseler, L. E.: U.S. Civil Rotorcraft Accidents, 1963 Through 1997. NASA TP-2000-209597, Dec. 2000.

160. Tete, A.: Organization and Exploitation of Regular Aerial Transportation Lines. NACA TM No. 83, May 1922.

161. Mayo, R. H.: Aviation and Insurance. NACA TM 93, May 1922.
162. Anon.: Aircraft Accidents, Method of Analysis. NACA Report No. 308, Aug. 1928.
163. Anon.: Aircraft Accidents, Method of Analysis. NACA Report No. 357, Jan. 1930.
164. Anon.: Aircraft Accidents, Method of Analysis. NACA Report No. 576, June 1936.

APPENDIX A

CIERVA'S PATENT

PATENT SPECIFICATION

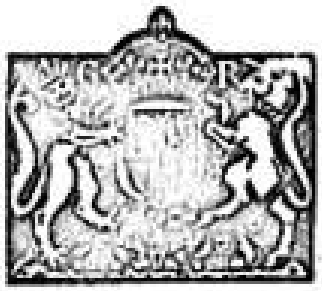

Convention Date (Spain): April 18, 1922. **196,594**
Application Date (In United Kingdom): March 29, 1923. No. 8955/23.
Complete Accepted: June 30, 1924.

COMPLETE SPECIFICATION.

I, JUAN DE LA CIERVA, Spanish subject, of 34, Alfonso XII, Madrid, Spain, Engineer, do hereby declare the nature of this invention and in what manner the same is to be performed, to be particularly described and ascertained in and by the following statement:—

An aeroplane with rotating wings as hitherto constructed consists essentially of an ordinary aeroplane provided with all the elements necessary for its progress and steering, such as motor, propeller, wheels for starting, rudder, *etc.*, in which however the wings, instead of remaining fixed relatively to it, as in the ordinary aeroplane, revolve freely by virtue of the supporting reaction of the wind, during forward movement upon them; round a shaft common to all of them and necessarily inclined backward.

In the accompanying drawings:—

Figs. 1 and 2 are illustrations of known forms of machine.

Figs. 3, 4 and 5 illustrate the present invention.

Figs. 1 and 2 illustrate two different types of said known apparatus. The main defect of this type of aeroplane lies in the lateral displacement of the centre of pressure in the assemblage of such rotating wings all moving in one direction, due to the want of symmetry in the velocities produced by the wind, an arrangement which necessitates the use of two groups of wings revolving in opposite directions, as in Fig. 1, accompanied by aerodynamic and structural disadvantages, or else the counteraction of such want of symmetry by producing a lift on the opposite side, which arrangement makes it necessary to arrange the wings with a suitable negative inclination with reference to the rotating shaft, and to construct them with wing sections of low aerodynamic power. The latter condition necessitates a very accurate calculation and a difficult and uncertain adjust-

ment, as well as a considerable increase of the wing surface, Fig. 2, and neither system does away with the structural difficulties inherent in the necessity of using shaft tubes capable of resisting great bending stresses and consequently of great weight and diameter, nor with problems of bracing the wings of the requisite length.

The improvement which forms the subject matter of this invention consists in arranging the rotating wings on a shaft tube, but without the aid of stays or angular bracing members, in such manner that they can move freely in a plane which passes through the axis of rotation, the joint being provided with two or more ball or roller bearings. The bearings required for all the wings are

fixed to a common armature or support which is itself capable of rotating freely on a radial, axial or ball bearing connected to the body of the apparatus which lies under it by means of some structural device, as for instance, a pyramid formed by four tubes. Fig. 3 shows this arrangement where monoplane wings are used, *e* being the joints of the two symmetrical wings *a a*, *r* the reinforcing braces of the wings, L the base or support of the wings which are mounted by bearings on the axis E supported on the tube pyramid *t*. The shaft Figs. 1 and 2, is dispensed with. Similar arrangement would apply to the employment of wings for biplanes or multiplanes.

The operation is as follows:—When the apparatus runs over the starting course, the system of wings acquires a speed of rotation, due to the reaction produced on the wing. The speed of rotation generates a centrifugal force F, Fig. 4, applied to the centre of gravity of each wing C directed perpendicularly to the axis, whilst the lifting reaction S is directed perpendicularly to the wing, and

APPENDIX A

2

196,594

both forces constantly balance each other, so that the resultant coincides with the straight line which connects the jointed shaft of the wing *e* with the point P of application of the lifting reaction, the consequence being that, under such conditions, the wing behaves as if it were rigidly connected with a central shaft tube. The joint *e* is arranged more or less below the wing, according to the type of each apparatus, in such manner that the angle α, which, aerodynamically, the wing must form with the axis of gyration (approximately a right angle) may be that which is suitable.

The advantages obtained are as follows:—

1. The centre of pressure and support is mechanical, and not aerodynamical, is automatically centered, as the system by reason of its construction cannot transmit moments which tend to tip the apparatus over. The aerodynamical lateral displacement of the centre of pressure gives rise to an inclination only of the means of rotation, Fig. 5, and consequently to the deviation of the lifting reaction coinciding therewith, by causing the apparatus to incline sightly, an effect which may be prevented by the twisting moment and which in any case is of no importance, considering the small angle β; and the means of using one group of wings only revolving in the same direction, without requiring any rigid stays or any calculations for the adjustment, or running any danger of the system getting out of order.

2. Dispensing with, owing to the absence of bending moments, the heavy shaft tube and its support by substituting a simple and light structural device.

3. Means of using wing sections of the highest efficiency without any negative inclination and with the reduction of the necessary wing surface resulting therefrom.

4. Absolutely automatic stability, not dynamical, instead of the conditions which obtain in aviation machines hitherto, inasmuch as the invention involves no displacement of the framework of the apparatus. The latter is in fact to a certain extent, supported by the joints of the wings which cause a temporary displacement of the central axis of rotation relatively to the remainder of the apparatus when a rolling motion place of the gyroscopic motion which occurs in apparatus with wings rigidly connected, which is obviously an advantage.

It is clear that the invention is capable of modifications in the details without altering its essential character which depends neither upon the aerodynamic features of the aeroplane with rotary wings, to which it is applied, nor upon the relative dimensions of the constituent elements of the joint, nor on the number of the latter.

Having now particularly described and ascertained the nature of my said invention and in what manner the same is to be performed, I declare that what I claim is:—

1. The use in aeroplanes with rotatory wings which revolve freely by virtue of the supporting reaction of the wind of a pair or a group of such wings, monoplane or multiplane, all revolving in the same direction, so mounted on a ring or the like or a shaft at the centre in a flexible manner, that they may move freely in a plane passing through the shaft, adopting at every moment the position required for the equilibrium between the centrifugal force produced by the speed of rotation and the lifting due to the reaction of the wind on the wing.

2. The method in aeroplanes with rotating wings which revolve freely by virtue of the supporting reaction of the wind whereby a flexible mounting for such wings is effected by means of a joint or the like between the wing and its means of rotation.

3. In an aeroplane with rotating wings or group of wings which revolve freely by virtue of the supporting reaction of the wind providing flexible elements on or about its relative centre such that the angle of the wings with relation to the axis may deflect during rotation.

4. The arrangement of the flexible means according to Claims 1, 2 or 3 of the wing below the centre of gravity of the same, in order to obtain an angle approximately a right angle between the shaft of rotation and the wing.

5. Rotating aeroplane wings constructed and operating substantially as described herein with relation to the drawings.

Dated this 20th day of March 1909.

of the aeroplane, would a rolling motion destroys the stability. The lift supplied according to said axis or shaft means of rotation produces moments opposed to the rolling motion. This effect takes the

dated this 30th day of March, 1923.

J. D. ROOTS & Co.,
Agents for the Applicant,
Thanet House, Temple Bar, London,
W.C. 2.

Redhill: Printed for His Majesty's Stationery Office, by Love & Malcomson, Ltd.—1924.

300

APPENDIX A

Fig 1.

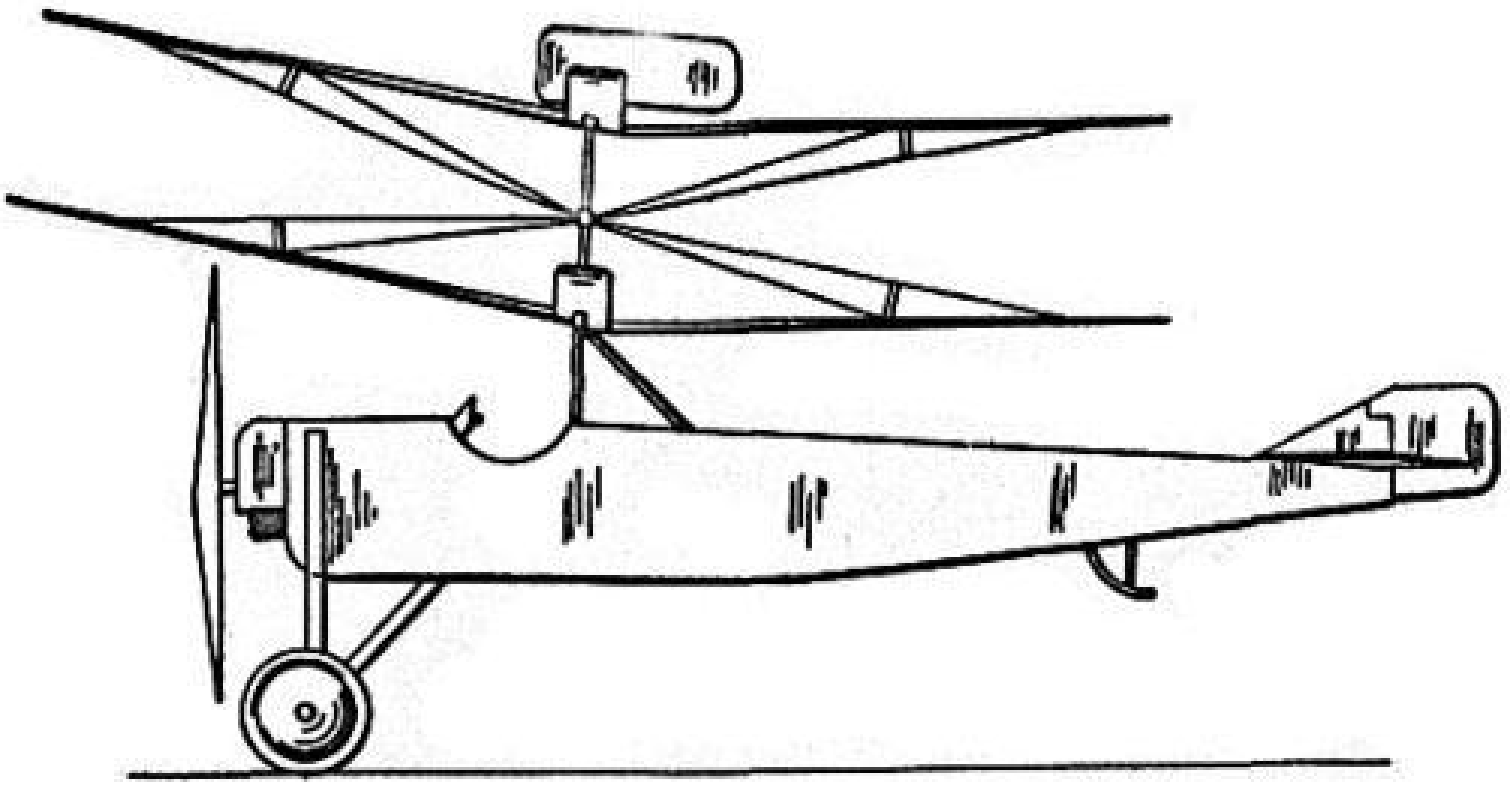

Fig. 2.

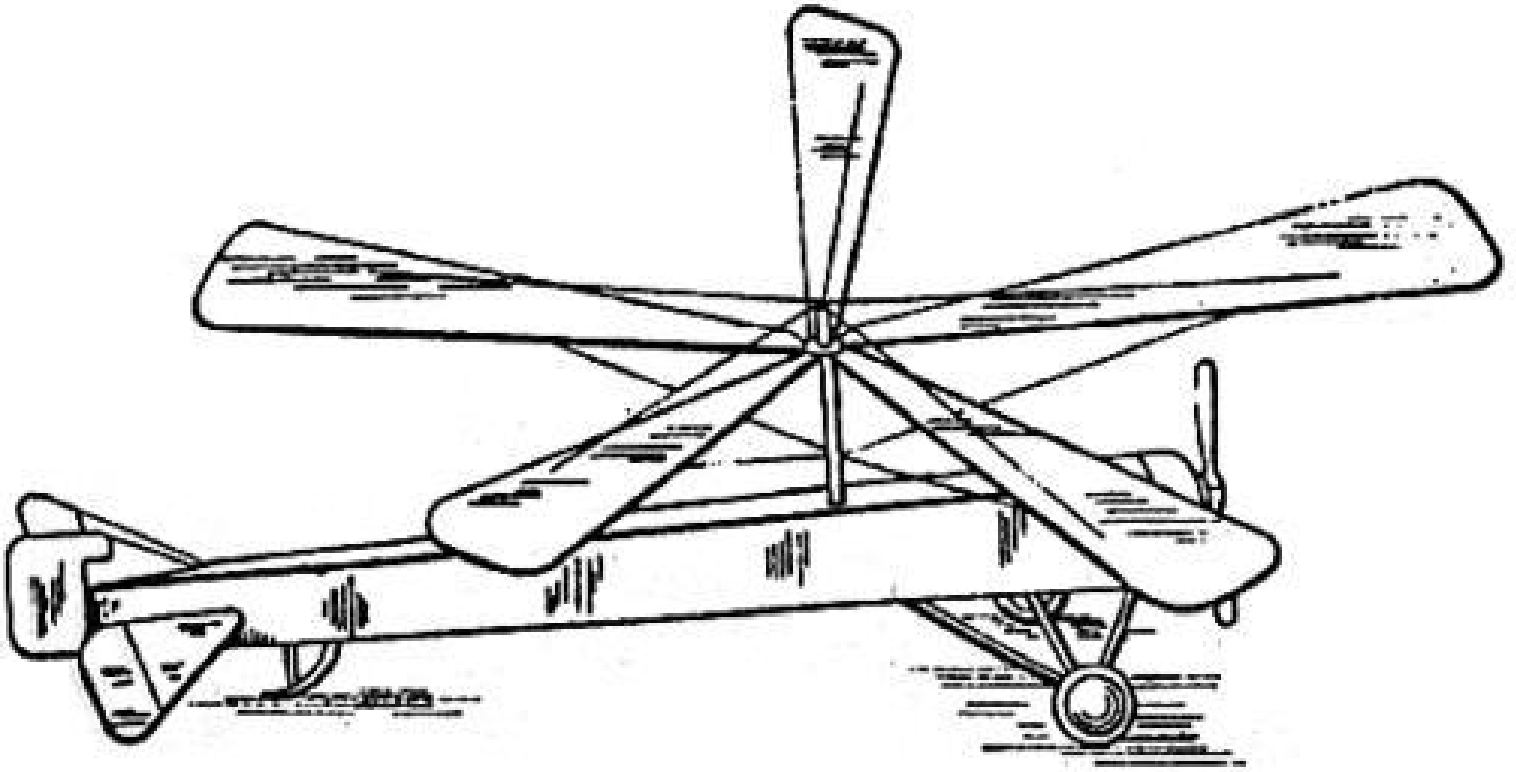

301 APPENDIX A

Fig. 3.

a

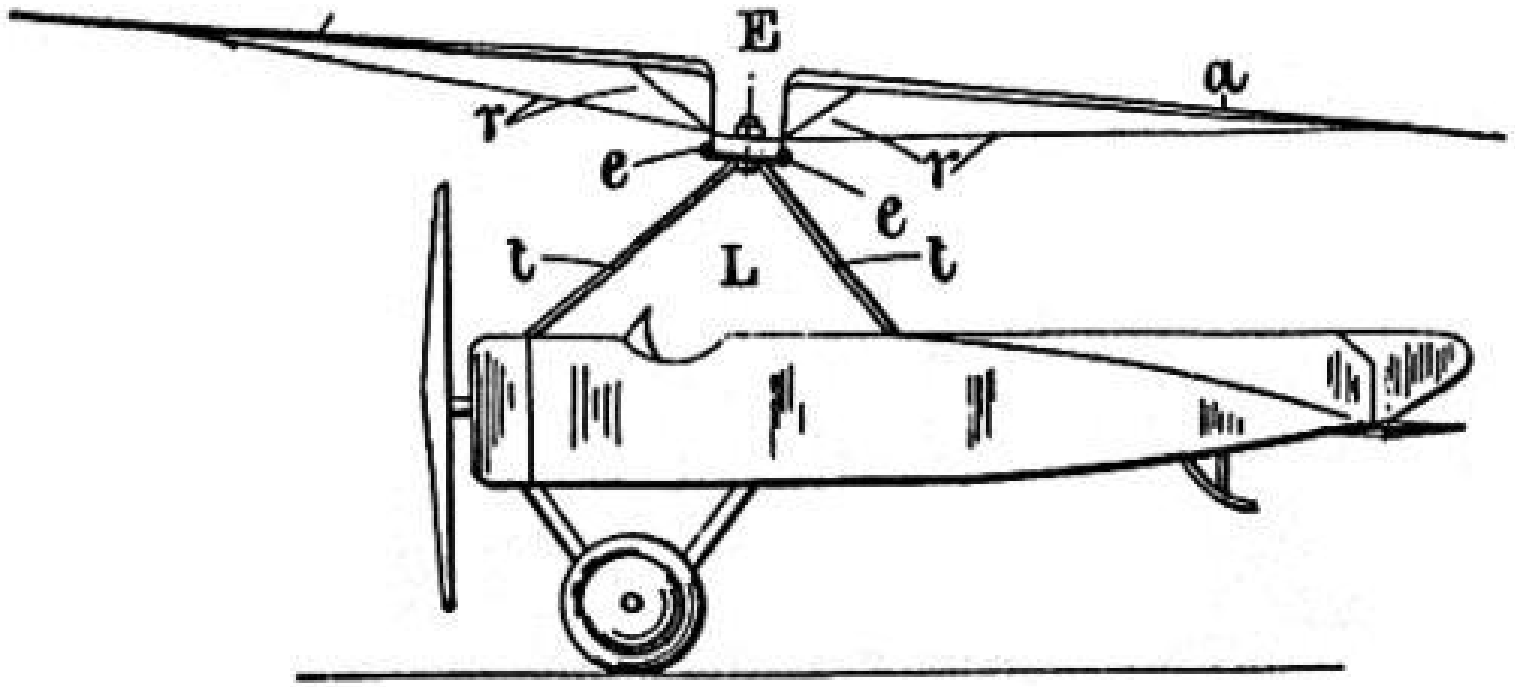

Fig. 4.

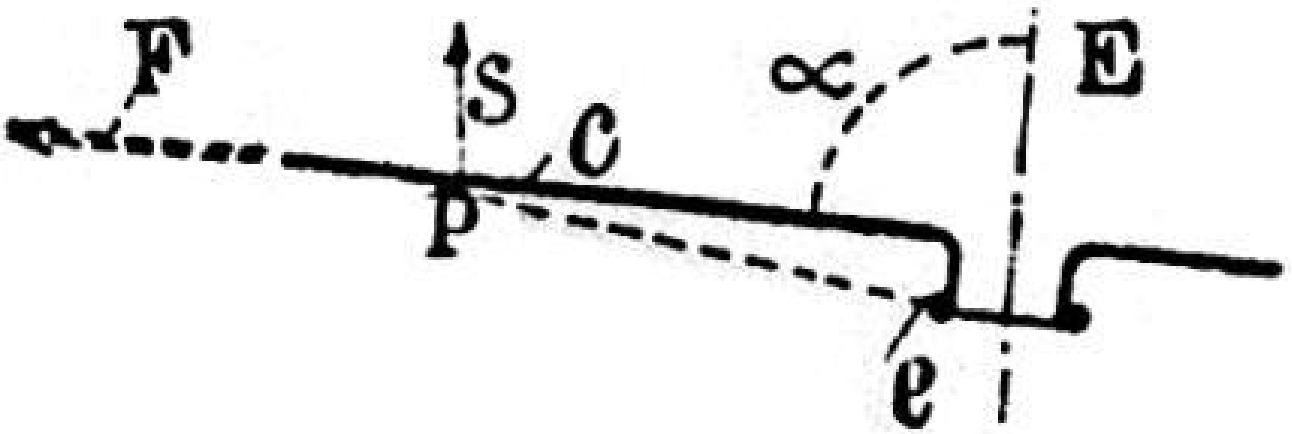

APPENDIX A

Fig. 5.

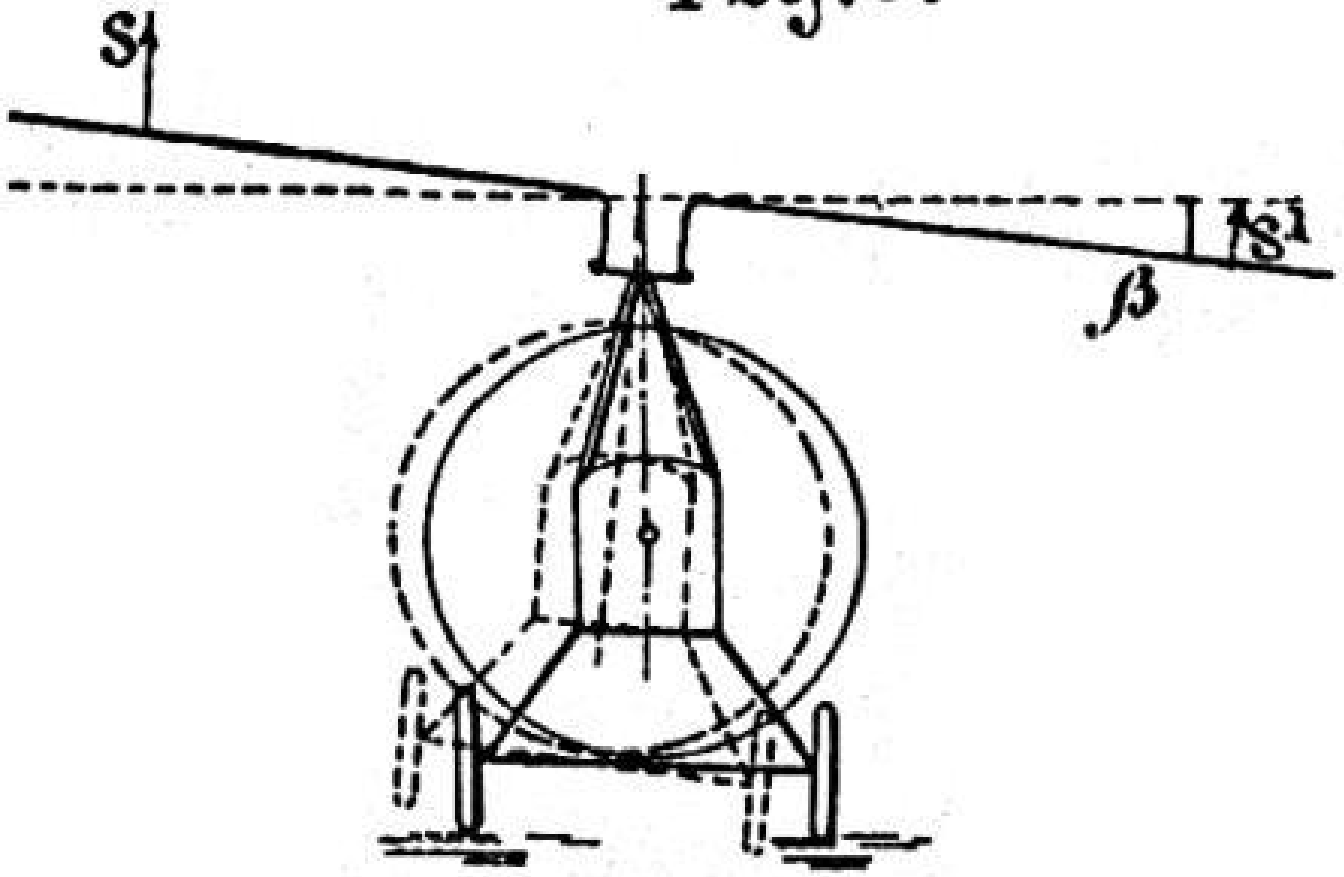

304

APPENDIX B

AIRFOIL LIFT AND PITCHING MOMENT

The aerodynamics of airfoils is a subject included in any number of textbooks studied by undergraduates. The subject has many degrees of complexity. For my purposes here, I have sought the least complex discussion and aimed for results, not derivations. To that end, I have turned to my early reference books[1,2,3] from which the fundamentals of lift and pitching moment of an airfoil in steady flow are crystal clear. However, an airfoil embedded in a rotor blade experiences unsteady flow, which means that this appendix must deal with an additional factor beyond introductory considerations. The effect of unsteady flow on airfoil lift and pitching moment is not found in many textbooks. My reference (Helicopter Theory by Wayne Johnson)[4] provides the theory using advanced mathematics, which I have reduced to elementary terms.

There are many sketches and photos showing how air flows around an airfoil. The

one I have selected for Fig. B-1 is from the thin book by L. Prandtl and O. G. Tietjens covering Applied Hydro-Aeromechanics. In this photo the airfoil is stationary, and streamlines of air are shown flowing about the airfoil. Fortunately, in studying fluid mechanics, it is only the relative motion between the air and the airfoil that matters.

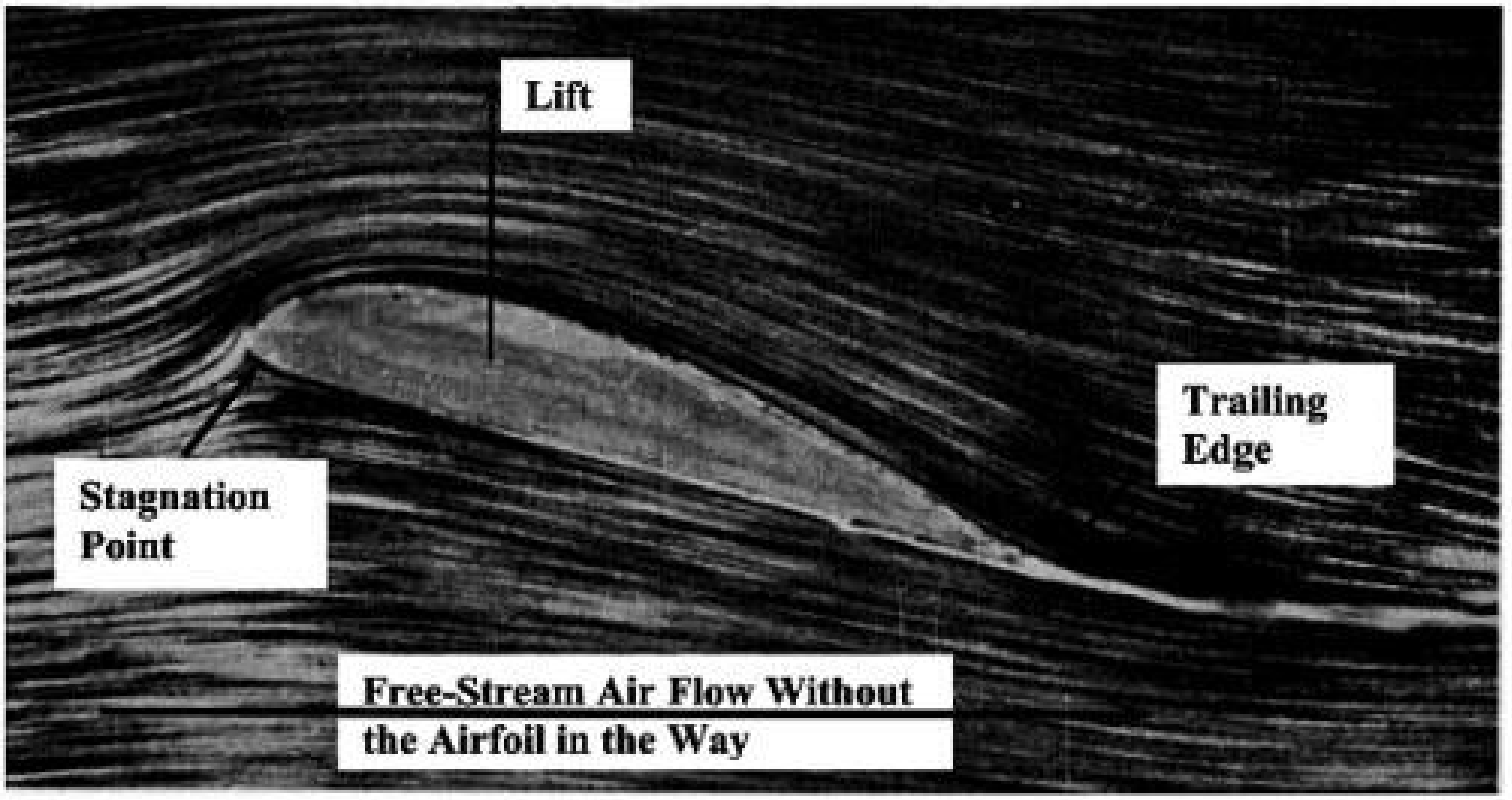

Fig. B-1. Air flow around a cambered airfoil set at positive angle of attack.

[1] L. Prandtl and O. G. Tietjens, *Fundamentals of Hydro- and Aeromechanics*, Dover Publications, Inc., New York.

[2] L. Prandtl and O. G. Tietjens, *Applied Hydro- and Aeromechanics*, Dover Publications, Inc., New York. [3] Paul E. Hemke, *Elementary Applied Aerodynamics*, Prentice-Hall, New York, 1946. [4] Wayne Johnson, *Helicopter Theory*, Princeton University Press, New Jersey, 1980.

APPENDIX B

That is, an airfoil flying in still air is exactly equivalent to an airfoil at rest in a moving air stream. The particles of air that pass over the upper surface of the airfoil travel faster than the particles passing along the lower surface of the airfoil. The difference in particle velocities between the upper and lower surface lead to a reduced pressure on the upper surface relative to the lower surface. In effect, the airfoil is sucked up—which is the force called lift.

The website http://en.wikipedia.org/wiki/Liftforce has a rather good, modern discussion of airfoil lift should you have the interest, but for this appendix it is the calculation of airfoil lift and pitching moment I intend to convey.

Thin Airfoil in Steady Flow

First imagine that an airfoil, shown as a dashed outline in Fig. B-2, is placed in a wind tunnel, and the tunnel velocity is (V). Following thin airfoil theory, imagine the airfoil is reduced in thickness so that it appears as a line. In thin airfoil aerodynamics this line is called the mean line, and it is upon this line that the actual airfoil shape is constructed. Figure B-2 shows this mean line to be straight, and the outlined airfoil is considered symmetrical about this straight mean line. However, the mean line can be curved to many

shapes in which case the airfoil is classed as cambered versus symmetrical (a cambered airfoil is shown in Fig. B-1). The aerodynamic properties of the cambered airfoil will be discussed shortly.

Physically, the airfoil mean line shown in Fig. B-2 can be thought of as a simple flat plate inclined in a wind tunnel to the relative wind (V) at angle of attack (α). Imagine this very thin airfoil to be an elemental portion of a wing that has an extremely large wing span. Assume the elemental span (dr) to be very small, and let the chord (c) of the airfoil times the elemental span define the elemental area (dS) of this portion of the wing (i.e., $dS = cdr$). Use the coordinate (x) to measure distance from the leading edge towards the trailing edge at which x then equals c. The pressures on the very thin airfoil produce an elemental normal force (dF_N/dr), an elemental chordwise force (dF_C/dr), and an elemental moment

about the leading edge (dM_{LE}/dr) . The resultant of the normal and chordwise forces is the airfoil elemental lift (dL/dr) . In aerodynamic theory, the lift force always acts perpendicular to the velocity as Fig. B-1 shows. In simple aerodynamic theory, airfoils of any type have no drag, so the lift force is computed as

$$\frac{dL}{dr} = \frac{dF_N/dr}{\cos\alpha}. \quad (1)$$

Imagine now two streams of air particles flowing along the velocity vector (V). The two streams strike the bottom of the dashed line airfoil at a point called the stagnation point, which is noted in Fig . B-1. At the stagnation point, the two streams separate. One stream flows along the airfoil surface: first forward, then around the airfoil nose, and then back to the airfoil trailing edge. The other stream leaves the stagnation point and travels directly

along the bottom surface of the airfoil to the trailing edge. The particles that traveled along the stream that traces out the upper surface move faster than the particles traveling in the stream that

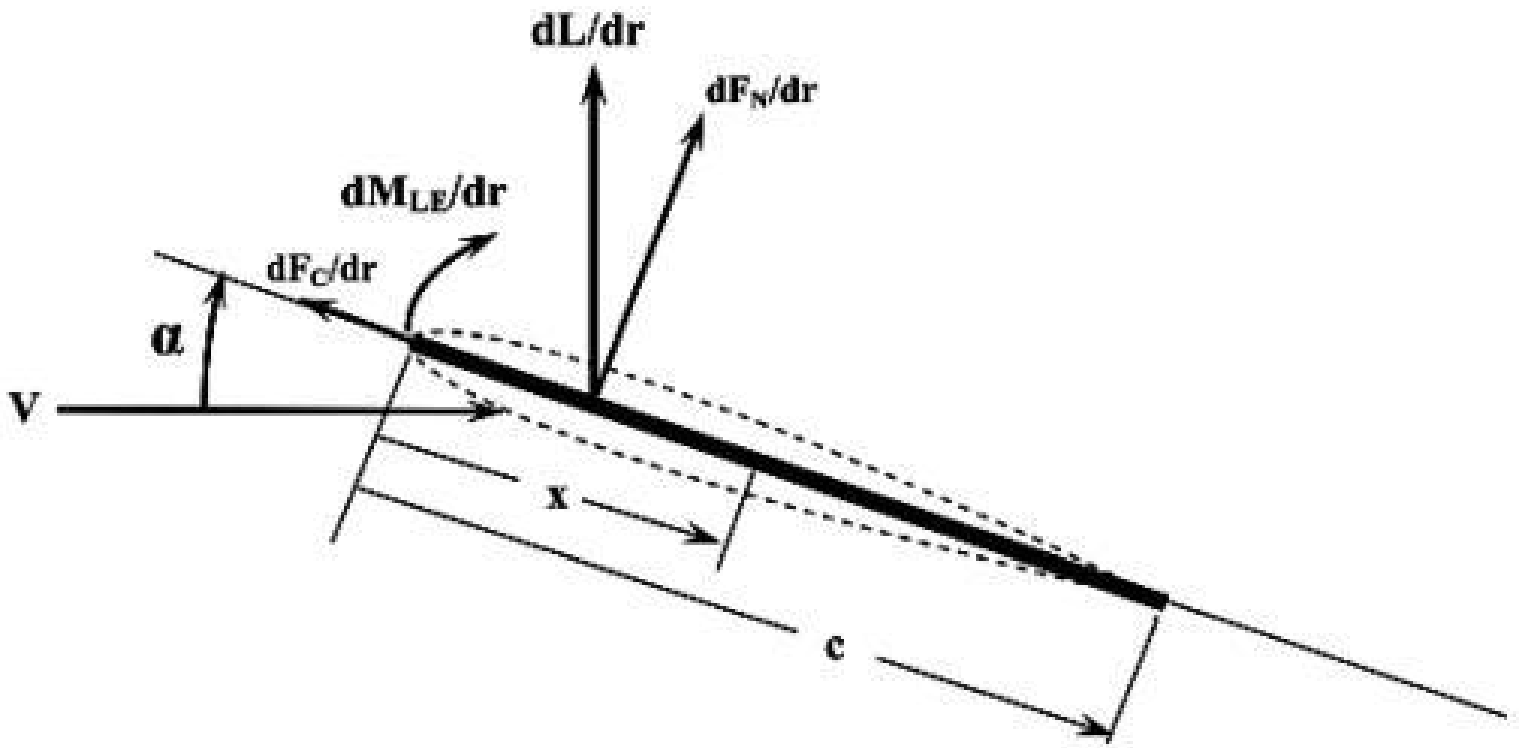

Fig. B-2. Forces and moment on an airfoil.

traces out the lower surface. This difference in

stream velocity creates a pressure vacuum on the upper surface and a higher pressure on the lower surface. In effect, the airfoil is lifted up by suction. The velocities of particles in the two streams are determined by[5] (2)

$$\text{Upper surface velocity} \equiv u_{upper} = V\left(\cos\alpha + \sin\alpha\sqrt{\frac{c-x}{x}}\right)$$

and

(3)

$$\text{Lower surface velocity} \equiv u_{lower} = V\left(\cos\alpha - \sin\alpha\sqrt{\frac{c-x}{x}}\right).$$

These two velocities create pressures on the very thin airfoil. The upper surface experiences a large suction relative to the lower surface because of the greater velocity of the particles. The two pressure distributions are calculated

using Bernoulli's law as

(4)

$$\text{Upper surface pressure} \equiv P_{upper} = P_o + \frac{1}{2}\rho V^2 - \frac{1}{2}\rho u_{upper}^2$$

and

(5)

$$\text{Lower surface pressure} \equiv P_{lower} = P_o + \frac{1}{2}\rho V^2 - \frac{1}{2}\rho u_{lower}^2 .$$

In these pressure equations, (P_o) is the barometric (or static) pressure of the air in which the airfoil is immersed. The second term ($1/2\rho V^2$) is commonly called the dynamic pressure and generally denoted by the letter (q).

---

[5]H. J. Stewart, *A Simplified Two-Dimensional Theory of Thin Airfoils*, J. of the Aeronautical Sciences, Oct. 1942.

APPENDIX B

It is the pressure difference between the lower and upper surface that creates a normal force on the airfoil. That is, $\Delta P = P_{lower} - P_{upper}$ and this pressure differential (ΔP) varies from leading edge to trailing edge as

$$\Delta P = \frac{1}{2}\rho V^2 \left(4 \sin\alpha \cos\alpha \sqrt{\frac{c-x}{x}} \right). \tag{6}$$

This pressure differential is frequently parameter ($q = 1/2\rho V^2$) to read as

nondimensionalized by the dynamic pressure

$$\frac{\Delta P}{\frac{1}{2}\rho V^2} = 4 \sin\alpha \cos\alpha \sqrt{\frac{c-x}{x}}. \tag{7}$$

The distribution of the differential

pressure (divided by the dynamic pressure) along the airfoil chord is shown in Fig. B-3. The computation offered by Eq. (7) is shown at 5- and 10-degree angles of attack. Note that this theoretical result—from what is called thin airfoil theory—shows that the differential pressure is infinite at the nose of the very thin airfoil when the airfoil thickness is theoretically zero. In practical cases the pressure differential can be very large, but is never infinite . This singularity reflects the behavior and velocity of the air particles that must go around the zero-thickness airfoil sharp leading edge with an infinite velocity. Real airfoils have a rounded leading edge, which is acted on by pressure, and this creates the chordwise force (dF_C/dr) shown in Fig. B-2 . This chordwise force is created primarily by leading-edge suction.

The differential pressures shown in Fig.

B-3 act perpendicular to the very thin airfoil surface. The pressure distribution acts as a suction, which creates an elemental normal force (dF_N/dr). This force is found by the integral (8)

$$\frac{dF_N}{dr} = \int_0^c \Delta P\, dx = \int_0^c \left[\frac{1}{2}\rho V^2 \left(4 \sin\alpha \cos\alpha \sqrt{\frac{c-x}{x}} \right) \right] dx$$

which, upon integration, gives the elemental normal force (9)

$$\frac{dF_N}{dr} = \left(\frac{1}{2}\rho V^2 \right)(c)(2\pi \sin\alpha \cos\alpha).$$

It then follows from Eq. (1) that the elemental lift is (10)

$$\frac{dL}{dr} = \frac{dF_N/dr}{\cos\alpha} = \left(\frac{1}{2}\rho V^2 \right)(c)(2\pi \sin\alpha).$$

Equation (10) is generally rearranged to appear as (11) $$\frac{dL}{\left(\frac{1}{2}\rho V^2\right)(c\,dr)} = (2\pi)\sin\alpha\,.$$

APPENDIX B

Then, by assigning dynamic pressure the symbol ($q = 1/2\rho V^2$) and taking the elemental area as ($dS = cdr$), airfoil lift from thin airfoil aerodynamic theory is most frequently seen in the lift coefficient (C_ℓ) form as

(12) $$C_\ell = \frac{dL}{q\,dS} = (2\pi)\sin\alpha \approx 2\pi\alpha\,.$$

The lift coefficient is now clearly seen as a lift curve slope (2π) times an angle of attack and, for small angles of attack, sin α is approximately α.

Thousands of airfoil experiments have been performed. The overwhelming conclusion from theory versus test comparisons is that the airfoil lift coefficient does vary in direct proportion to the angle of attack for angles of attack up to about 10 to 12 degrees. The experiments have shown, however, that the slope is not $dC_\ell/d\alpha = 2\pi = 6.28$ per radian as thin airfoil theory suggests; rather the slope is more on the order of 0.1 per degree or 5.73 per radian. As the experimental data began to accumulate, it became common to write $dC_\ell/d\alpha = a_\infty$. Even more common was the simple statement that

(13) $\quad C_\ell = a\alpha.$

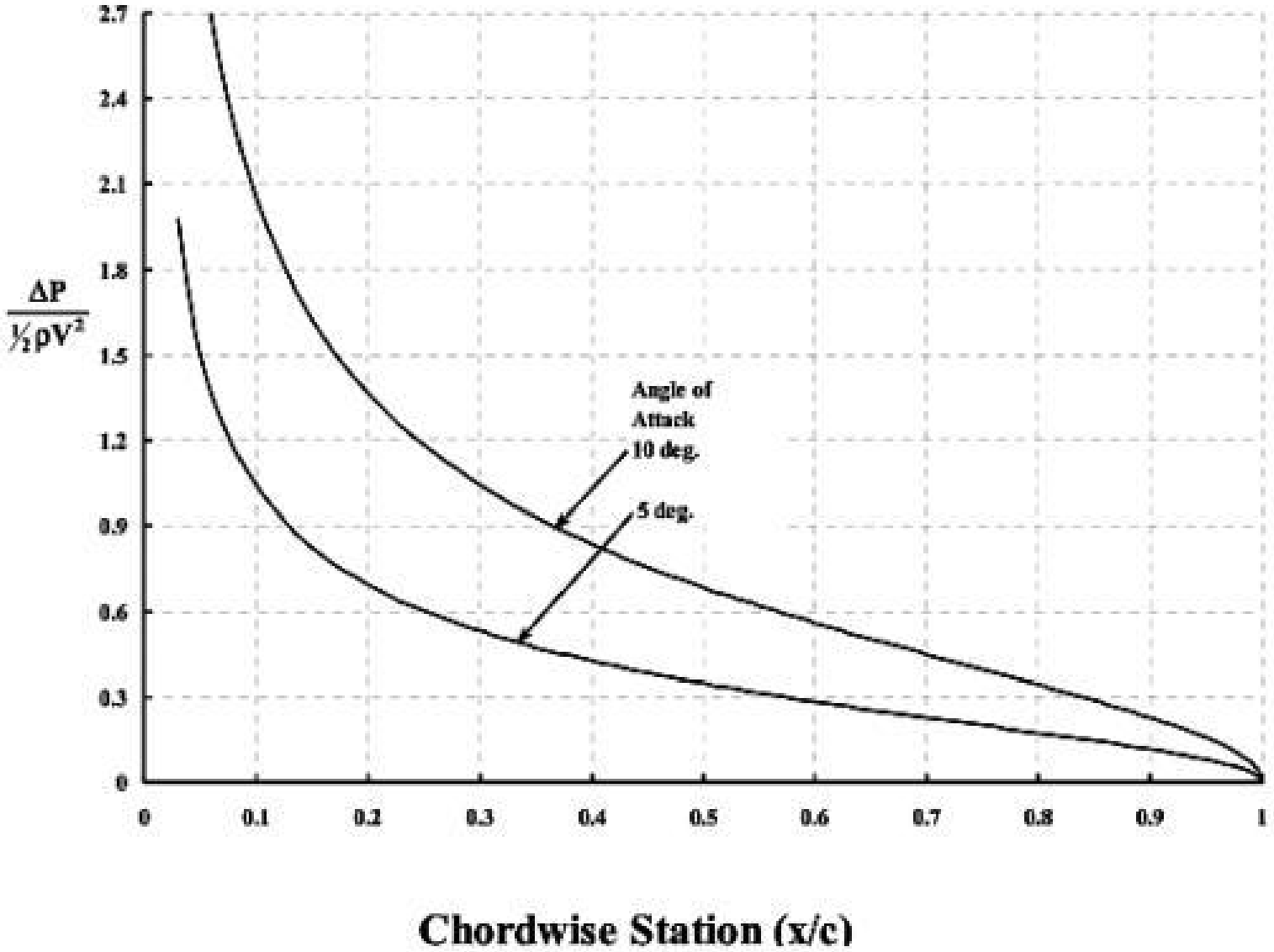

Fig. B-3. Differential pressure distribution over an airfoil from thin airfoil theory.

APPENDIX B

Now consider the elemental pitching

moment about the airfoil leading edge (dM_{LE}/dr). This elemental moment is calculated from the pressure distribution quite simply as

(14)

$$\frac{dM_{LE}}{dr} = -\int_0^c \Delta P\, x dx = -\int_0^c \left[\frac{1}{2}\rho V^2 \left(4\sin\alpha\cos\alpha\sqrt{\frac{c-x}{x}}\right)\right] x dx$$

which, upon integration, shows that

(15)

$$\frac{dM_{LE}}{dr} = -\int_0^c \Delta P\, x dx = -\left(\frac{c}{4}\right)\left[\left(\frac{1}{2}\rho V^2\right)(c)(2\pi\sin\alpha\cos\alpha)\right] = -\left(\frac{c}{4}\right)\left(\frac{dF_N}{dr}\right).$$

This result states immediately that the moment center of the pressure distribution is one- quarter of a chord length aft of the leading edge . That is, the elemental moment about the leading edge is simply the elemental

force (dF_N/dr) times the moment arm (c/4). The negative sign arises from the sign convention that a positive moment is nose-up.

It should be obvious that taking moments about the 1/4-chord point rather than the leading edge results in

$$\frac{dM_{c/4}}{dr} = 0. \tag{16}$$

This very important result leads to the oft quoted statement that an airfoil's center of pressure is extremely close to the quarter chord. Furthermore, thin airfoil theory finds that the center of pressure (i.e., the chordwise point at which the lift force acts) does not move as angle of attack and lift are changed. Advanced theories and experiments show these conclusions from thin airfoil theory are not quite correct as I will discuss shortly.

Cambered Airfoil in Steady Flow

Figure B-1 uses smoke to show streamlines of air particles flowing around a cambered airfoil, which is installed in a wind tunnel. The wind tunnel free-stream velocity is (V). Far ahead, and well above and below the airfoil, this velocity is parallel to the wind tunnel center line. However, air flow direction near the airfoil is increasingly influenced by the airfoil as the streamlines show.

A cambered airfoil has a shape built around a curved mean line. A typical example is shown in Fig. B-4. The mean line of a cambered airfoil is referenced to the trailing edge. The ordinate of the mean line is on the Y-axis. As Fig. B-4 shows, angle of attack (α_C) is measured as the angle between the free-stream chord line, which is the X-axis. The chord line geometrically connects the

leading edge to velocity and the chord line. The cambered airfoil adds two aerodynamic properties to a symmetrical airfoil. The first property is the addition of an angle (of attack) of zero lift (α_{0L}), which alters the elemental airfoil lift equation to

(17)

$$\frac{dL}{dr} = \left(\frac{1}{2}\rho V^2\right)(c)C_\ell = qc[2\pi\alpha] = qc\left[2\pi\left(\alpha_C + (-\alpha_{0L})\right)\right] = qc\left[2\pi(\alpha_C - \alpha_{0L})\right].$$

310

APPENDIX B

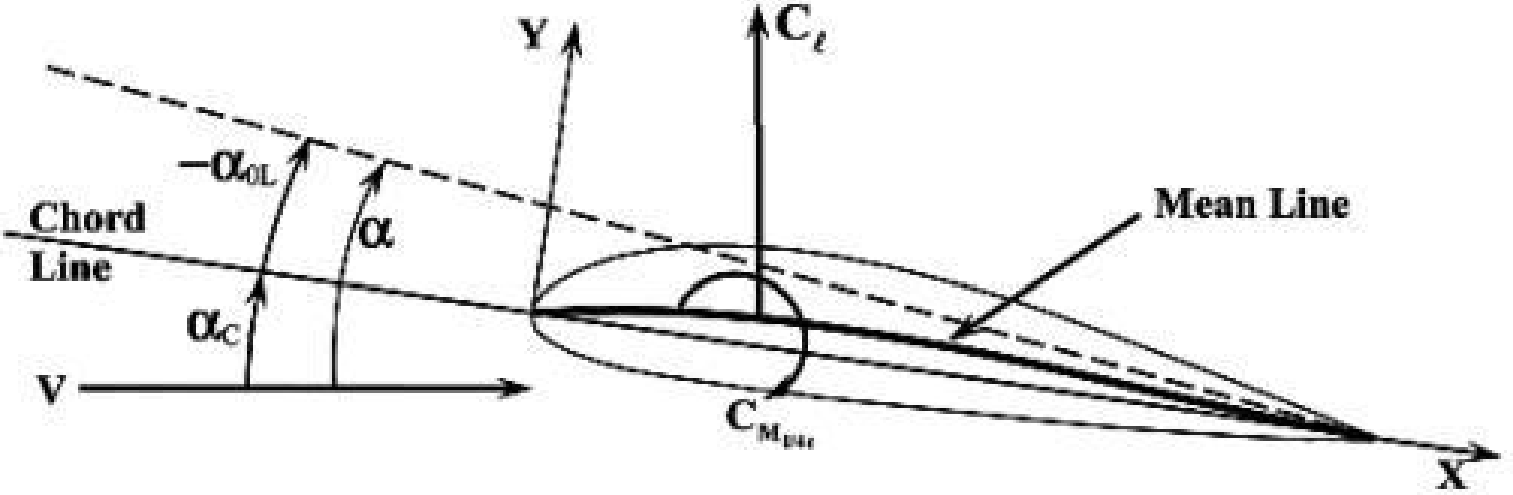

Fig. B-4. A cambered airfoil set at positive angle of attack, which is measured between the free-stream velocity and the chord line.

The reason I have expanded the angle of attack somewhat awkwardly is that the overwhelming number of cambered airfoils have a negative angle of zero lift.[6] That is, to produce zero lift the *chord line* angle of attack (α_C) must be equal to the angle of zero lift (α_{0L}) so that the total angle of attack (α) is zero.

The second property a cambered mean line adds is that the airfoil pitching moment coefficient about the 1/4-chord point ($C_{M_{1/4c}}$) is no longer zero as Eq. (16) shows is true for a symmetrical airfoil . That is, Eq. (16) now becomes

$$\frac{dM_{c/4}}{dr} = \left(\frac{1}{2}\rho V^2\right)\left(c^2\right)C_{M_{1/4c}} \tag{18}$$

and the airfoil pitching moment coefficient ($C_{M_{1/4c}}$) is *not necessarily* zero.

Thin airfoil theory gives relatively straightforward equations to calculate a cambered airfoil's angle of zero lift (in radians) and pitching moment coefficient about the 1/4-chord point. These integral equations are, for angle of zero lift (α_{0L}),

$$\alpha_{0L} = -\frac{1}{\pi}\int_0^1 \frac{y}{(1-x)\sqrt{x(1-x)}}dx \tag{19}$$

and for the pitching moment coefficient,

$$C_{M_{1/4c}} = \int_0^1 \frac{y\left(4x^2-6x+3/2\right)}{(1-x)\sqrt{x(1-x)}}dx \tag{20}$$

[6] Ira H. Abbott and Albert E. von Doenhoff, *Theory of Wing Sections*, Dover Publications, Inc., New York, 1959.

APPENDIX B

where the abscissa is a fraction of the chord; that is, $x = X/c$ and the ordinate is $y = Y/c$. A key to performing the integration is to define the camber as $y = (1-x)F_{(x)}$, which cancels the quantity (1-x) in the denominator and avoids a discontinuity at the trailing edge where $x = 1$. Since the mean line starts at $X = 0$, $Y = 0$, the function $F_{(x)}$ must be zero at $x = 0$ to avoid a discontinuity at the leading edge. One general construction of the mean line could be

(21)

$$y = (1-x)F_{(x)} = (1-x)\left[C_1 x + C_2 x^2 + C_3 x^3 + \cdots\cdots\right].$$

One of the earliest mean lines constructed assumed a general shape of

$$(22) \qquad y = (1-x)F_{(x)} = (1-x)\left[(C_1 x)(C_2 - x)\right].$$

When this shape is used in Eqs. (19) and (20), the angle of zero lift and the pitching moment coefficient become simply, for angle of zero lift (α_{0L}) in radians,

$$(23) \qquad \alpha_{0L} = -\frac{C_1}{8}(4C_2 - 3)$$

and for the pitching moment coefficient,

$$(24) \qquad C_{M_{1/4c}} = -\frac{\pi C_1}{32}(8C_2 - 7).$$

A practical example should help illustrate the properties of the cambered airfoil. You will recall from Section 2.6, which dealt with longitudinal trim, that Cierva used a

cambered airfoil for the rotor blade of his model C.30 Autogiro. Symmetrical airfoils had been used on all his previous models, but he sought an improvement in performance by using the German Göttingen 606 . The pitching moment coefficient of this airfoil was $C_{M_{1/4c}} = -0.052$ (see table

on page 56), and the result was severe blade twisting at high speeds . Of lesser concern was the experimental finding that the angle of zero lift was $\alpha_{0L} = -2.58$ degrees or –0.04503 radians (see table on page 56).

Having the answers to Eqs. (23) and (24) means that a rational guess of the Göttingen 606 mean line shape can be made. Thus,

$$(25) \qquad y = (1-x)\left[(0.190812x)(1.22198-x)\right].$$

The Göttingen 606 was quoted by Cierva as having a thickness ratio of t/c = 0.1 7. Therefore,

it seems reasonable (to me) to approximate the Göttingen 606 airfoil final shape with the NACA 0017 thickness[7] added to the mean line given by Eq. (25). This may be an adequate approximation to airfoil selection during the autogyro era. The result of this possibility is shown in Fig. B-5.

---

[7] From *Theory of Wing Sections* by Abbott and von Doenhoff (pg. 113), the symmetrical NACA 0017 thickness distribution is $\pm y_t = \frac{t}{0.20}\left(0.2969\sqrt{x} - 0.12600x - 0.35160x^2 + 0.28430x^3 0.10150x^4\right)$.

APPENDIX B

Note that a cambered airfoil having a zero pitching moment coefficient is quite

possible. Referring to Eq. (24), you can see that if $C_2 = 7/8$, then $C_{M_{1/4c}} = 0$. This mean line does not, however, mean that the angle of zero lift is zero, since, from Eq. (23), you have (26)

$$\alpha_{0L} = -\frac{C_1}{8}\left(4\frac{7}{8} - 3\right) = -\frac{C_1}{16}.$$

Maintaining the Göttingen 606 value of $C_1 = 0.190812$ leads to a reduction in angle of zero lift from –2.58 degrees to –0.683 degrees . A NACA 0017 airfoil thickness distribution added to a mean line shape of

(27) $$y = (1-x)\left[(0.190812x)(7/8-x)\right]$$

leads to the airfoil shown in Fig. B-6 as the dashed line, in contrast to the Göttingen 606 shown as the solid line. Notice that a slight curling-up near the trailing edge was sufficient to reduce pitching moment to zero.

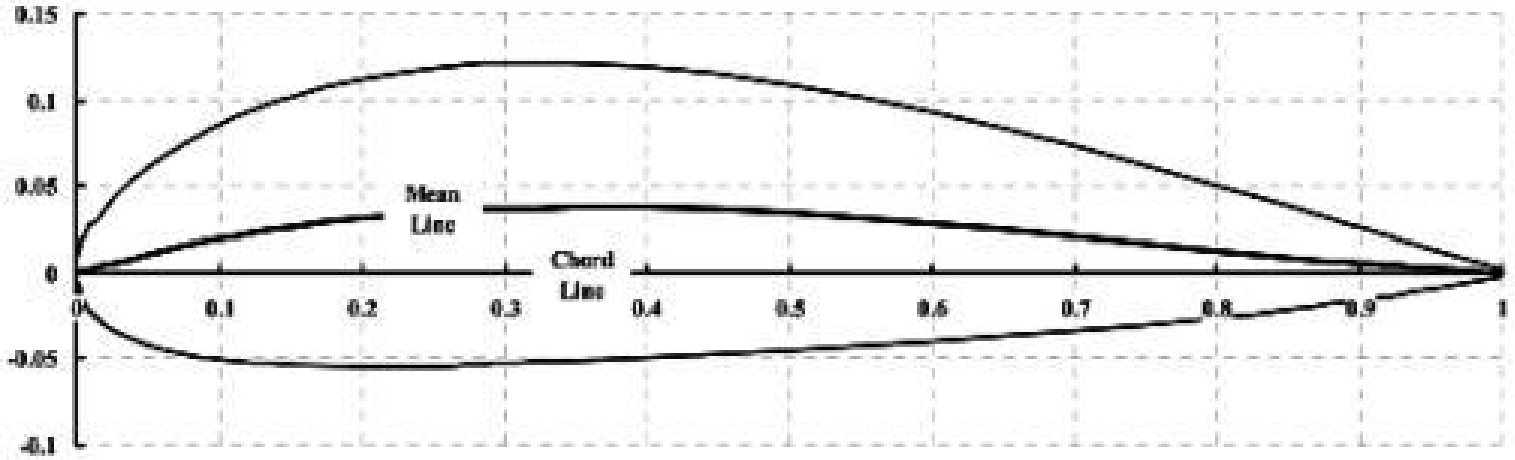

Fig. B-5. An estimate of the Göttingen 606 airfoil shape.

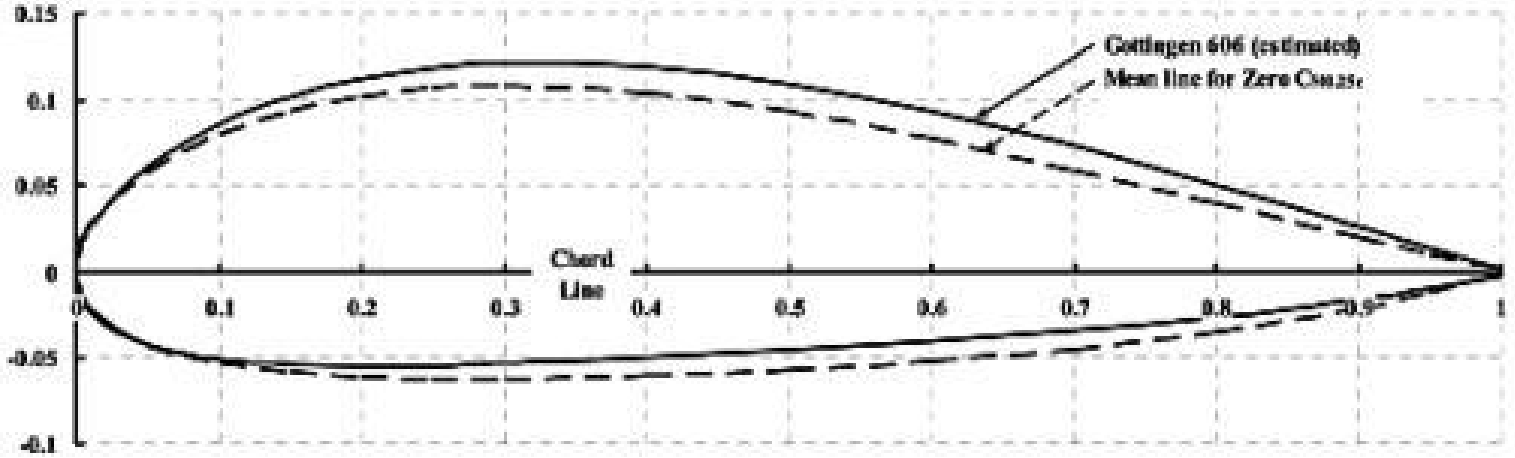

Fig. B-6. A revision of the Göttingen 606 airfoil shape to obtain zero pitching moment about the 1/4-chord point. Both shapes use a NACA 0017 airfoil thickness distribution.

APPENDIX B

As a final note, recall that Kellett also used the Göttingen 606 airfoil for their KD-1 rotor blades. Richard Prewitt, the chief engineer at Kellett, noted[8] that:

"Shortly after the first flight of this autogiro [the KD-1 on December, 1934], we found it to be longitudinally unstable above eighty m.p.h. We developed a theory of this instability, based on the assumption that the slightly unstable blade sections caused a negative pitching moment when operating on the advancing side of the rotor where the velocities are high. This theory proved to be correct when small turned-up trailing edge tabs were attached at the tips of the blades. In fact the pitching moment coefficient of the blade section was over corrected to the extent that the pilot reported it required a heavy forward load on the stick at high speed. This over-correction was rectified by successively cutting off the inboard end of the tab section until a desired longitudinal stability was obtained. Fortunately, the lateral stability was improved with the correction in longitudinal stability."

Thin, Uncambered Airfoil in Unsteady Flow

Even before the autogyro era began, fixed-wing aircraft quite frequently experienced a phenomena called flutter.[9] The flutter phenomena can be likened to a stop sign mounted on a torsionally soft pole where the stop sign can often be seen twisting back and forth in the wind. An aircraft wing can easily be twisted off the fuselage at high speed should flutter be encountered. An airplane wing lift and pitching moment can combine with inadequate structure in an adverse way, and the aeroelastic response can be quite catastrophic. The primary blame for flutter was traced to aerodynamic forces and moments that occurred during a wing's structural deflections. This structural deflection created an unsteady aerodynamic environment, which altered airfoil lift and pitching moment properties from those known at the time. In 1929, Glauert[10] published perhaps the first theory of airfoil lift and pitching moment during unsteady motion. Theodorsen[11] provided a more complete theory in 1935, and a very comprehensive book—truly a bible—about fixed-wing aeroelasticity was published in 1955.[12]

During the autogyro era, little effort was

made to transpose fixed-wing unsteady airfoil aerodynamics to the rotary wing problem. In fact, it took the demonstration of the helicopter to motivate a few researchers and mathematicians to seriously examine the unsteady flow experienced by an airfoil located somewhere along a rotor blade. Airfoils in a rotary wing environment experience an oscillating velocity, a varying pitching motion and, with flapping, a vertical rising and falling. Including all these unsteady motions seriously complicated even the relatively simple problem that Glauert solved in 1929. Several key reports, papers, and

---

[8] R. H. Prewitt, *The Autogiro*, Proceedings of the First Rotating Wing Aircraft Mtg., The Franklin Institute, Philadelphia, Pa., Oct. 28–29, 1938.

[9] A. R. Collar, *Aeroelasticity—Retrospect and Prospect*, J. of the Royal Aeronautical Society, vol. 63, no. 577, Jan. 1959.

[10] H. Glauert, *The Force and Moment on an Oscillating Aerofoil*, Aeronautical Research Committee R&M 1242,

1929.
[11] T. Theodorsen, *General Theory of Aerodynamic Instability and the Mechanism of Flutter*, NACA Report No. 496, 1935.
[12] Raymond L. Bisplinghoff, Holt Ashley, and Robert L. Halfman, *Aeroelasticity*, Addison-Wesley, Reading, Mass., 1955.

rotary wing books,[13,14,15,16,17] deal with the lift and pitching moment of an airfoil in a rotary wing environment.

There is no question that unsteady aerodynamics is a complicated subject. The theoretical derivation of equations that estimate just lift and moment of a flat plate requires advanced mathematical skills. The classical theoretical results leave the equations in a

world mixed with complex, imaginary, and real numbers . Furthermore, the theoreticians derive results using an axis system centered at the half chord point, so that the airfoil leading edge is placed at (–b) and the trailing edge is at (+b) . These notations and number mixing easily put off the practicing engineer. Therefore, what follows is a translation of rather advanced math to practical engineering equations for one example.

For this appendix, "useable" equations have been obtained. I have chosen Johnson's April 1980 one-page technical note[18] as the starting point for one simple example.

Suppose the airfoil is a thin, flat plate as shown in Fig. B-7. The airfoil has a chord (c) in feet. The chordwise dimension (x) in feet is measured positive aft starting from the leading edge. Now suppose the airstream (V) in feet per second is not constant, but is varying in a sinusoidal manner with time. This would be the case of an airfoil somewhere along a rotating rotor blade operating in forward flight.

Furthermore, suppose the airfoil is oscillating in pitch (α) in radians about some chordwise point (x_p) in a sinusoidal manner. This pitch angle is measured in radians . Assume for this example that the airfoil is *not* rising and falling (h), but stays in the same plane. This example assumes that the airfoil is one of many in a wing that has an infinitely long span, which is to say this example deals with two-dimensional, unsteady aerodynamics. Finally, assume that the sinusoidal motion of the airstream and the airfoil pitch oscillation are occurring at the same frequency (ω) in radians per second. Since the airfoil oscillates through one cycle in a time of $t = 2\pi/\omega$, it is common to note that $\psi = \omega t$. Thus, one oscillating cycle occurs as ψ goes from 0 to 2π radians, or, in degrees, ψ goes from 0 to 360 degrees.

Together, the preceding statements say, let:

---

[13] Wayne Johnson, *Helicopter Theory*, Princeton University Press, New Jersey, 1980.
[14] Rufus Isaacs, *Airfoil Theory for Flows of Variable Velocity*, J. of the Aeronautical Sciences, vol. 12, no. 1, Jan. 1945, pp. 113–118.
[15] J. Mayo Greenberg, *Airfoil in Sinusoidal Motion in a Pulsating Stream*, NACA TN No. 1326, June 1947.
[16] Arun I. Jose, et al., *Unsteady Aerodynamic Modeling with Time-Varying Free-Stream Mach Numbers*, J. of the American Helicopter Society, vol. 51, no. 4, Oct. 2006.
[17] J. Gordon Leishman, *Principles of Helicopter Aerodynamics*, Cambridge University Press, Cambridge, United Kingdom, 2000.
[18] Wayne Johnson, *Application of Unsteady Airfoil Theory to Rotary Wings*, AIAA J. of Aircraft, vol. 17, no. 4, April 1980.

APPENDIX B

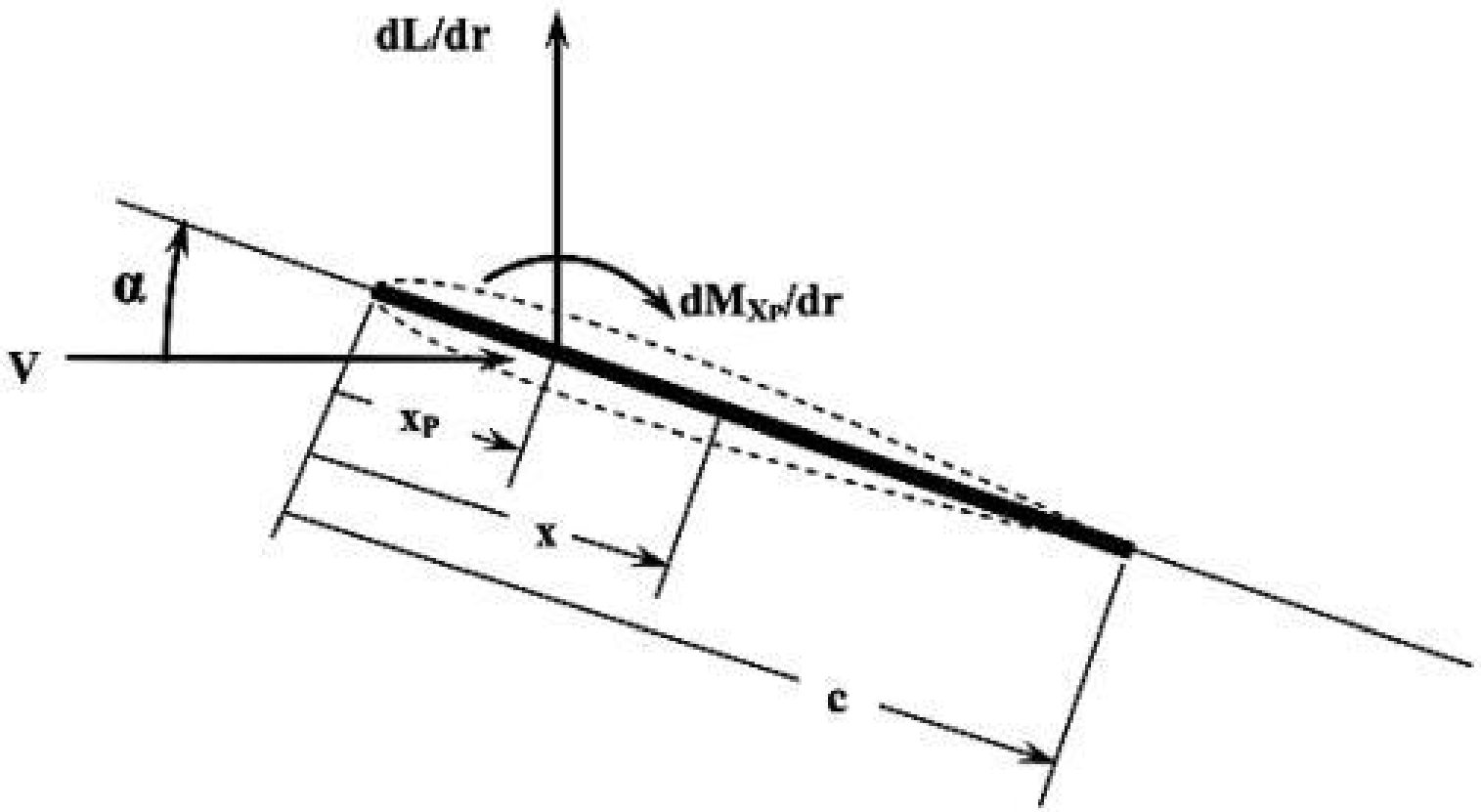

Fig. B-7. Geometry of a thin airfoil operating in unsteady flow.

$$V = V_0 + V_1 \sin(\omega t) \rightarrow \frac{dV}{dt} = \omega V_1 \cos(\omega t) \rightarrow \frac{d^2V}{dt^2} = -\omega^2 V_1 \sin(\omega t)$$

(28)

$$\alpha = \alpha_0 + \alpha_1 \sin(\omega t) \rightarrow \frac{d\alpha}{dt} = \omega\alpha_1 \cos(\omega t) \rightarrow \frac{d^2\alpha}{dt^2} = -\omega^2\alpha_1 \sin(\omega t) \ .$$

$$h = \text{constant} \rightarrow \frac{dh}{dt} = 0 \rightarrow \frac{d^2h}{dt^2} = 0$$

The general pitching moment and lift equations offered by Johnson are (after taking some poetic license) for an element of pitching moment about the chordwise point (x_p)

$$\frac{dM_{xp}}{dr}=\frac{\pi\rho c^2}{4}\left[\left(x_p-\frac{c}{2}\right)\left(\frac{d^2h}{dt^2}+V\frac{d\alpha}{dt}+\alpha\frac{dV}{dt}\right)-\frac{c}{4}V\frac{d\alpha}{dt}-\left(\frac{9c^2}{32}-cx_p+x_p^2\right)\frac{d^2\alpha}{dt^2}\right] \tag{29}$$
$$+\pi\rho\frac{c}{2}\left(x_p-\frac{c}{4}\right)V\left\{C_k\left[\frac{dh}{dt}+V\alpha+\left(\frac{3c}{4}-x_p\right)\frac{d\alpha}{dt}\right]\right\}$$

where the moment is positive nose-up. For an element of lift acting positive up at the point (x_p) on the flat plate,

$$\frac{dL_{xp}}{dr}=\frac{\pi\rho c^2}{4}\left[\frac{d^2h}{dt^2}+V\frac{d\alpha}{dt}+\alpha\frac{dV}{dt}+\left(\frac{c}{2}-x_p\right)\frac{d^2\alpha}{dt^2}\right] \tag{30}$$
$$+\pi c\rho V\left\{C_k\left[\frac{dh}{dt}+V\alpha+\left(\frac{3c}{4}-x_p\right)\frac{d\alpha}{dt}\right]\right\}$$

Now, say the airfoil is pitching about the 1/4-chord point (i.e., $x_p = \frac{1}{4}c$) and that the airfoil neither rises nor falls with time. These assumptions reduce the general equations somewhat so that you now have, for the elemental pitching moment in foot-pounds per foot acting positive nose-up at the 1/4-chord point,

(3 1)

$$\frac{dM_{\frac{1}{4}c}}{dr} = \frac{\pi \rho c^3}{16}\left[-\frac{3c}{8}\frac{d^2\alpha}{dt^2} - 2V\frac{d\alpha}{dt} - \alpha\frac{dV}{dt}\right]$$

and, for an element of lift in pounds per foot acting positive up at the 1/4-chord point on the flat plate,

(32)

$$\frac{dL_{\frac{1}{4}c}}{dr} = \frac{\pi \rho c^2}{4}\left[V\frac{d\alpha}{dt} + \alpha\frac{dV}{dt} + \frac{c}{4}\frac{d^2\alpha}{dt^2}\right] + \pi c \rho V\left\{C_\kappa\left[V\alpha + \frac{c}{2}\frac{d\alpha}{dt}\right]\right\}.$$

Finally, consider converting these pitching moment and lift equations into practical engineering equations that can be evaluated with any calculating tool (even a slide rule). Converting the { } term in the dL/dr expression, Eq. (32), will be discussed—just for the sake of completeness—after the results are given. The conversion is made by substituting the assumptions given by Eq. (28) into the moment and lift equations and then collecting the various sine and cosine terms. The process is tedious, but simple, with the result that, for the elemental pitching moment about the 1/4-chord point,

(33)

$$\frac{dM_{y_{qc}}}{dr} = \frac{\pi \rho c^3}{16}\left[-\left(\frac{3c}{8}\omega^2\alpha_1\right)\sin(\omega t) - (2\omega V_0\alpha_1 + \omega V_1\alpha_0)\cos(\omega t) - \left(\frac{3}{2}\omega V_1\alpha_1\right)\sin(2\omega t)\right]$$

and for the elemental lift, the more lengthy result is

$$\frac{dL}{dr}=\frac{\pi\rho c^2}{4}\left[\begin{array}{l}-\frac{c}{4}\omega^2\alpha_1\sin(\omega t)+(V_0\omega\alpha_1+V_1\omega\alpha_0)\cos(\omega t)\\+(V_1\omega\alpha_1)\sin(2\omega t)\end{array}\right]$$

$$+\pi c\rho(V_0+V_1\sin(\omega t))\left\{\begin{array}{l}\left(V_0\alpha_0+\frac{1}{2}V_1\alpha_1\right)F_1\\+\left[(V_0\alpha_1+V_1\alpha_0)F_1-\frac{c\omega}{2}\alpha_1G_1\right]\sin(\omega t)\\+\left[\frac{c}{2}\omega\alpha_1F_1+(V_0\alpha_1+V_1\alpha_0)G_1\right]\cos(\omega t)\\+\left(\frac{1}{2}V_1\alpha_1G_2\right)\sin(2\omega t)-\left(\frac{1}{2}V_1\alpha_1F_2\right)\cos(2\omega t)\end{array}\right\}. \quad (34)$$

The constants F_1, G_1, F_2, and G_2 are obtained accurately enough for engineering purposes from

$$F=1.0-1.88601019K+3.15193950K^2-1.95792310K^3 \quad (35)$$

$$G=-0.54533433K^{1/2}-0.72434519K+3.21608597K^{3/2}-2.15588120K^2$$

APPENDIX B

using the parameter (K) for F_1 and G_1 as $K_1 = c\omega/2V_0$, and for F_2 and G_2, $K_2 = 2K_1$. Equation (35) is satisfactory for calculating F and G constants as long as K is less than 0.60.

To illustrate this example, assume some parameters approximating the Cierva C.30 Autogiro such as

Parameter	Symbol	Unit	Value
Chord	c	feet	1.0
Density	ρ	slug/ft^3	0.0023769
Steady velocity	V_0	ft/sec	475
Oscillating velocity	V_1	ft/sec	190
Steady angle of attack	α_0	radians	$5(\pi/180) = 0.0872665$
Oscillating angle of attack	α_1	radians	$-4.5(\pi/180) = -0.0785398$
Frequency	ω	rad/sec	25.5

The input of values from this table into Eqs. (33) and (34) returns the results that, for elemental pitching moment

(36)

$$\frac{dM_{\frac{1}{4}c}}{dr} = +0.008938\sin(\omega t) + 0.690637\cos(\omega t) + 0.266389\sin(2\omega t)$$

and for elemental lift

(37)

$$\frac{dL_{\frac{1}{4}c}}{dr} = 100.668 - 29.186\sin(\omega t) + 3.401\cos(\omega t) + 3.507\sin(2\omega t) + 38.077\cos(2\omega t)$$

$$+4.804\sin(3\omega t) - 0.696\cos(3\omega t)$$

These results are illustrated graphically in Fig. B-8 for pitching moment and Fig. B-9 for lift. The moment and lift are plotted versus azimuth angle ($\psi = \omega t$) rather than time since only one cyclic is needed. With respect to moment, Fig. B-8, you can see that the first harmonic cosine and the second harmonic sine dominate the waveform in this example. Note that if the oscillating frequency were zero, Eq. (33) states that the moment would be zero throughout the

cycle, which is consistent with the known fact that a thin, flat plate has zero pitching moment about the 1/4-chord point, regardless of angle of attack.

The elemental lift versus azimuth, the solid line in Fig. B-9, shows that elemental lift is dominated by a steady lift, a first harmonic sine, and second harmonic cosine in this example. Throughout the autogyro era and on up to the late 1960s, unsteady aerodynamics was not included in rotary wing calculations . The assumption was that the oscillations in velocity and angle of attack were at a very low frequency. That is, everything went on in slow motion. Thus, ωt could be replaced by ψ and then ω could be set to zero. Under this nearly static situation K_1 and K_2 are zero, F_1 and F_2 equal 1.0, and G_1 and G_2 equal zero. These assumptions reduce Eq. (34) to

APPENDIX B

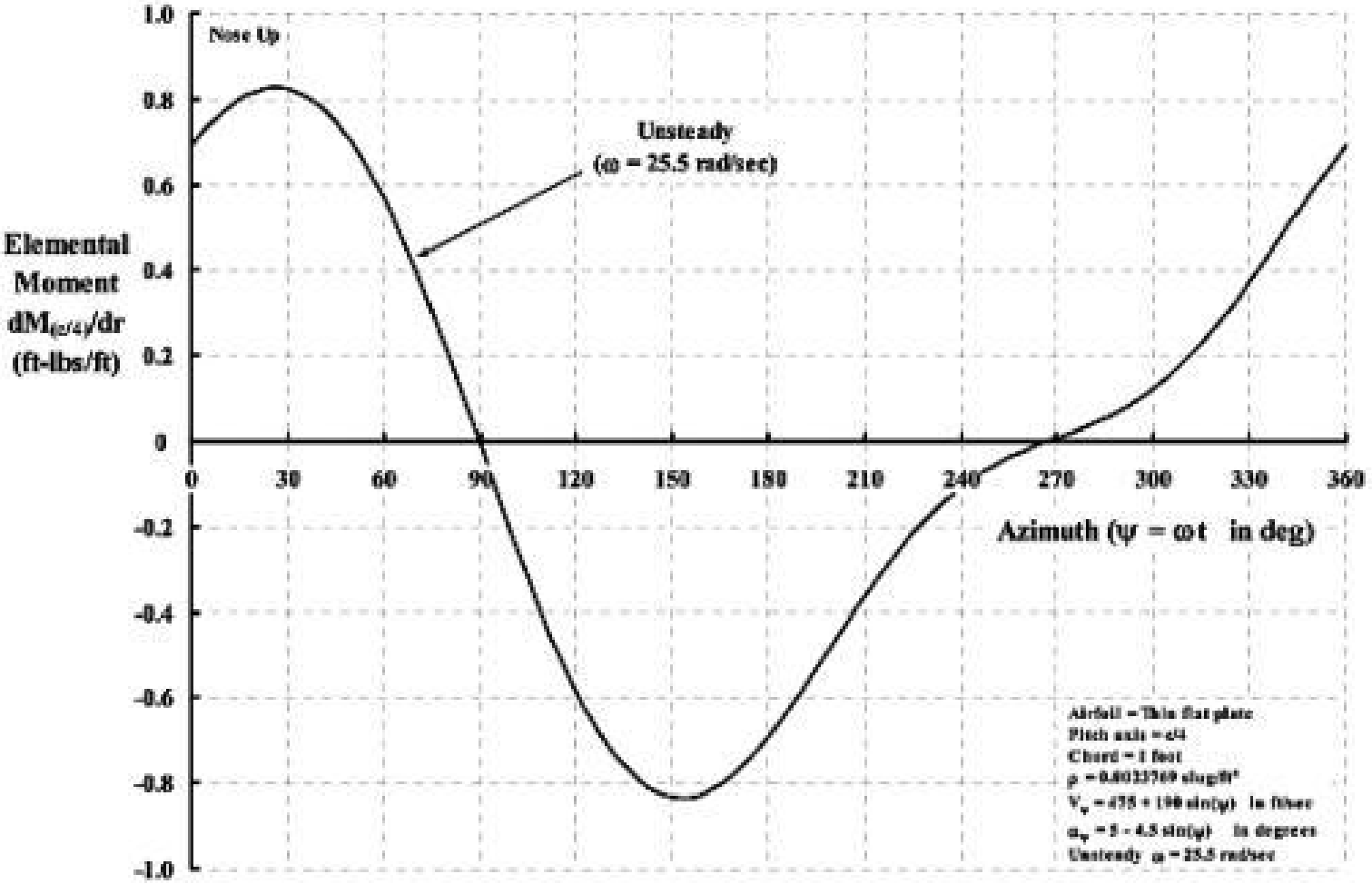

Fig. B-8. Elemental pitching moment for a thin, uncambered airfoil oscillating in angle of attack while the free stream is varying.

$$(38)\qquad \frac{dL}{dr}=\frac{\pi\rho c^2}{4}[0]+\pi c\rho(V_0+V_1\sin\psi)\left\{\begin{array}{l}\left(V_0\alpha_0+\frac{1}{2}V_1\alpha_1\right)+\left[(V_0\alpha_1+V_1\alpha_0)\right]\sin(\psi)\\ +[0]\cos(\omega t)-\left(\frac{1}{2}V_1\alpha_1\right)\cos(2\omega t)\end{array}\right\}$$

which is easily expanded with sine and cosine terms collected to yield

$$(39)\qquad \frac{dL}{dr}=\pi c\rho\left[\begin{array}{l}\left(\alpha_0V_0^2+V_0V_1\alpha_1+\frac{1}{2}V_1^2\alpha_0\right)+\left(\alpha_1V_0^2+2V_0V_1\alpha_0+\frac{3}{4}\alpha_1V_1^2\right)\sin\psi\\ -\left(V_0V_1\alpha_1+\frac{1}{2}\alpha_0V_1^2\right)\cos(2\psi)-\left(\frac{1}{4}\alpha_1V_1^2\right)\sin(3\psi)\end{array}\right].$$

Thus, for the numerical values of this example

(40)

$$\frac{dL_{1/4c}}{dr}=105.859-30.581\sin(\omega t)+41.167\cos(2\omega t)+5.293\sin(3\omega t)$$

which is the dashed line shown in Fig. B-9.

APPENDIX B

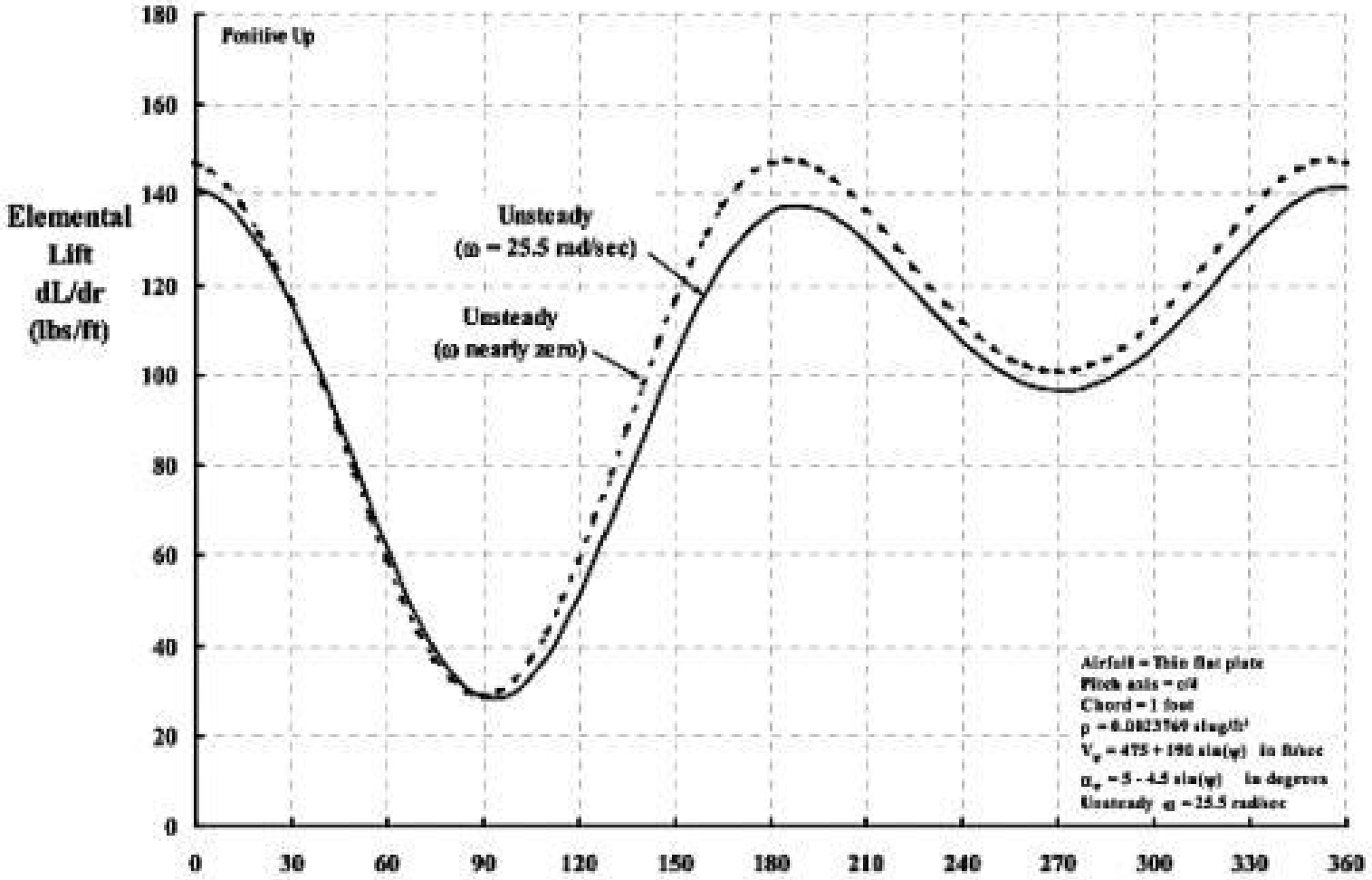

Fig. B-9. Elemental lift of a thin, uncambered airfoil oscillating in angle of attack while the free stream is varying.

The dimensional results shown in Figs. B-8 and B-9 are frequently seen in modern technical literature in some familiar coefficient form. The question is, "What do

two- dimensional airfoil coefficients, C_ℓ and $C_{M_{1/4c}}$, versus angle of attack look like?" The issue depends on how dynamic pressure (q) is defined. One possible approach (using this example) is to say that dynamic pressure is $q = \frac{1}{2} \rho \left(V_0 + V_1 \sin \psi\right)^2$ from which it follows from classical definitions that

(41)

$$C_\ell = \frac{dL/dr}{qc} = \frac{dL/dr}{\left[\frac{1}{2}\rho\left(V_0 + V_1 \sin\psi\right)^2\right]c} \text{ and } C_{M_{1/4c}} = \frac{dM_{1/4c}/dr}{\left[\frac{1}{2}\rho\left(V_0 + V_1 \sin\psi\right)^2\right]c^2}.$$

These two coefficients are shown as they vary with angle of attack in Fig. B-10. The immediate effect of including unsteady aerodynamics for an oscillating airfoil is to reduce the steady flow, aerodynamic, lift curve slope (2π) of the flat plate and create a small angle of zero lift much like a cambered plate. There is clearly a sliver of loops in the lift coefficient result, but one can argue that these

"hysteresis" loops are of rather secondary importance.

What is not of minor importance is the magnitude of the pitching moment coefficient shown with the dashed line in Fig. B-10. Recall that the angle of attack is varying as $\alpha_0 + \alpha_1 \sin(\omega t)$, and the first derivative with respect to time is $d\alpha/dt = \omega\alpha_1 \cos(\omega t)$. The moment coefficient appears to behave as

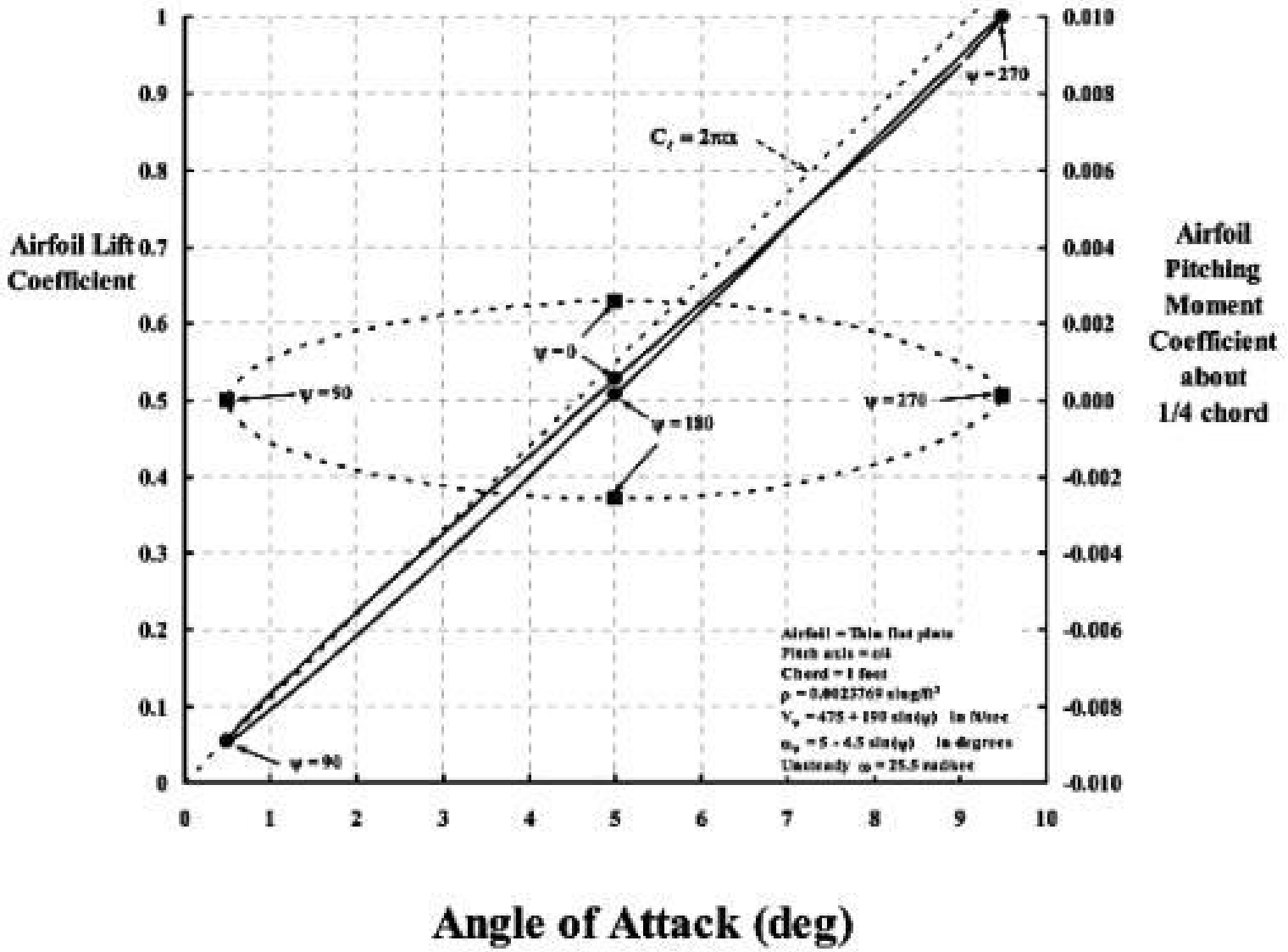

Fig. B-10. Lift and pitching moment coefficients of a thin, uncambered airfoil oscillating in angle of attack while the free stream is varying. Coefficients based on

$$q = \tfrac{1}{2}\rho\left(V_0 + V_1 \sin\psi\right)^2 .$$

$$(42) \qquad C_{M_{l/4c}} \approx -K\left[\omega\alpha_1 \cos(\omega t)\right]$$

in that the maximum and minimum moment coefficient occur at $\psi = \omega t = 0$ degrees and 180 degrees respectively.

Now, for the sake of completeness, let me outline how the { } term in Eq. (34) was obtained from

$$(43) \qquad \left\{C_K\left[V\alpha + \frac{c}{2}\frac{d\alpha}{dt}\right]\right\}.$$

To begin with, it would be a serious mistake for you to imagine that on my own I was able to transpose Eq. (43) from the world of imaginary and complex numbers to the practical engineering world. Having little residual math knowledge in this regard, I took advantage of Wayne Johnson's expertise and

patience. Wayne continuously guided me as I worked with pencil, paper, and MathCad 6.0. Thanks to his help, I can write the following:

1. The first thing to know is that imaginary numbers are identified by the letter (i).

The magnitude of "i" is $i = \sqrt{-1}$, and therefore $i^2 = -1$.

APPENDIX B

2 . A combination of real and imaginary numbers is written as a + ib, or, say, 10 + 4i.

This is a complex number. The letter i can be placed in front of the letter b or conversely with little resulting confusion. In fact, a complex number gives quite specific directions . A very simple interpretation of 10 + 4i would be: walk 10

miles East, stop, and then walk 4 miles North.

3. The transposing from imaginary numbers to real numbers depends on using Euler's relation, which is

$$e^{i\theta} = \cos\theta + i\sin\theta \quad \text{and} \quad e^{-i\theta} = \cos\theta - i\sin\theta .$$

4. Using Euler's relation, both the familiar trigonometric sine and cosine can be written in complex number form as

$$\sin\theta = \frac{1}{2i}\left(e^{i\theta} - e^{-i\theta}\right) = -\frac{i}{2}\left(e^{i\theta} - e^{-i\theta}\right)$$

$$\cos\theta = \frac{1}{2}\left(e^{i\theta} + e^{-i\theta}\right)$$

5. The coefficient (C_K) refers to Theodorson's function and is classically given as

$$C_K = F_K + iG_K .$$

6. The way the coefficient (C_K) is actually used is by knowing that

$$C_K e^{i\theta} = (F_K + iG_K)e^{i\theta}$$
$$C_K e^{-i\theta} = (F_K - iG_K)e^{-i\theta}.$$

7. It follows from points 4 and 6 that

$$C_K \sin\theta = F_K \sin\theta + G_K \cos\theta$$
$$C_K \cos\theta = F_K \cos\theta - G_K \sin\theta.$$

8. Alternately,

$$C_K \sin\theta = \sqrt{F_K^2 + G_K^2}\,\sin\left(\theta + \tan^{-1} G_K / F_K\right) = F_K \sin\theta + G_K \cos\theta$$

$$C_K \cos\theta = \sqrt{F_K^2 + G_K^2}\,\cos\left(\theta + \tan^{-1} G_K / F_K\right) = F_K \cos\theta - G_K \sin\theta.$$

9. There is a distinction and assumption about the shed wake created by an oscillating airfoil. If, for example, $\theta = \omega t$ then $K = c\omega/2V_0$, which implies $K_1 = 1(c\omega/2V_0)$.

In this situation $F_K = F_1$ and $G_K = G_1$.

When $\theta = 2\omega t$ then $K = 2(c\omega/2V_0)$, which means using $F_K = F_2$ and $G_K = G_2$.

10. After *all* multiplications are done, then throw away any imaginary numbers and use just real numbers!

APPENDIX B

The preceding ten points are enough to transpose $\left\{C_K\left[V\alpha+\frac{c}{2}\frac{d\alpha}{dt}\right]\right\}$ into what you see within the { } of Eq. (34). First make the substitutions for (V), (α), and (dα/dt) from Eq. (28) to obtain

(44)

$$\left\{C_K\left[V\alpha+\frac{c}{2}\frac{d\alpha}{dt}\right]\right\}=C_K\left[(V_0+V_1\sin(\omega t))(\alpha_0+\alpha_1\sin(\omega t))+\frac{c}{2}(\omega\alpha_1\cos(\omega t))\right].$$

Next, expand the trigonometry within the [ ]

of Eq. (44) to get

$$(45)\quad \left\{C_K\left[V\alpha+\frac{c}{2}\frac{d\alpha}{dt}\right]\right\}=C_K\left[\begin{array}{l}\left(V_0\alpha_0+\frac{1}{2}V_1\alpha_1\right)\\+(V_0\alpha_1+V_1\alpha_0)\sin(\omega t)+\left(\frac{c\omega\alpha_1}{2}\right)\cos(\omega t)\\-\left(\frac{1}{2}V_1\alpha_1\right)\cos(2\omega t)\end{array}\right].$$

Now take the multiplication one term at a time.

The first term is

(46)

$$C_K\left[\left(V_0\alpha_0+\frac{1}{2}V_1\alpha_1\right)\right]=(F+iG)\left(V_0\alpha_0+\frac{1}{2}V_1\alpha_1\right)=\left(V_0\alpha_0+\frac{1}{2}V_1\alpha_1\right)F_1$$

which is a case where the imaginary term is discarded.

The second term is written directly using point 7 or 8

(47) $C_K\left[(V_0\alpha_1+V_1\alpha_0)\sin(\omega t)\right]=(V_0\alpha_1+V_1\alpha_0)\left[G_1\cos(\omega t)+F_1\sin(\omega t)\right]$. The third term is

written directly using point 7 or 8

(48)

$$C_K\left[\left(\frac{c\omega\alpha_1}{2}\right)\cos(\omega t)\right]=\left(\frac{c\omega\alpha_1}{2}\right)\left[F_1\cos(\omega t)-G_1\sin(\omega t)\right],$$

and the fourth term is written directly using points 7 or 8 and 9; but note that with the frequency being at 2ω, $K = K_2$ so F and G must be subscripted by 2. Therefore (49)

$$C_K\left[-\left(\frac{1}{2}V_1\alpha_1\right)\cos(2\omega t)\right]=-\left(\frac{1}{2}V_1\alpha_1\right)\left[F_2\cos(2\omega t)-G_2\sin(2\omega t)\right].$$

When the four terms are added together and arranged in the conventional Fourier series format you obtain the { } term provided by Eq. (34). Note that this term, $\left\{C_K\left[V\alpha+\frac{c}{2}\frac{d\alpha}{dt}\right]\right\}$, not only appears in the elemental lift equation (30), but also in the

APPENDIX B

pitching moment equation (29) and would be included if the airfoil oscillated about any point other than the 1/4-chord point.

Thin, Cambered Airfoil in Unsteady Flow

The elemental lift and pitching moment for the thin, cambered airfoil in unsteady flow can be obtained by superposition and accounting for the angle of attack for zero lift. Thus, α_0 in Eqs. (33) and (34) is replaced by $\alpha_C - \alpha_{0L}$. Then the elemental pitching moment about the 1/4-chord point is simply

(50)

$$\frac{dM_{1/4}}{dr} = \frac{\pi\rho c^3}{16}\left[\left(\frac{3c}{8}\omega^2\alpha_1\right)\sin(\omega t) - \left(2\omega V_0\alpha_1 + \omega V_1(\alpha_C - \alpha_{0L})\right)\cos(\omega t) - \left(\frac{3}{2}\omega V_1\alpha_1\right)\sin(2\omega t)\right]$$

$$+\frac{\rho c^2}{2}\left(V_0 + V_1 \sin(\omega t)\right)^2 C_{M_{1/4c}}$$

and the elemental lift becomes

(51)

$$\frac{dL}{dr} = \pi c \rho \left[\begin{array}{l} \left(\alpha_0 V_0^2 + V_0 V_1 \alpha_1 + \frac{1}{2} V_1^2 (\alpha_C - \alpha_{0L})\right) + \left(\alpha_1 V_0^2 + 2 V_0 V_1 (\alpha_C - \alpha_{0L}) + \frac{3}{4}\alpha_1 V_1^2\right)\sin\psi \\ -\left(V_0 V_1 \alpha_1 + \frac{1}{2}(\alpha_C - \alpha_{0L}) V_1^2\right)\cos(2\psi) - \left(\frac{1}{4}\alpha_1 V_1^2\right)\sin(3\psi) \end{array} \right].$$

Results Using Modern Computational Fluid Dynamics (CFD)

This short discussion about airfoil lift and pitching moment would be incomplete without some very modern theoretical results compared to the thin airfoil, unsteady aerodynamics, discussed above . The modern theory I am referring to is called computational fluid dynamics and is simply

referred to as CFD by the current generation of practicing aerodynamists. With the enormous help of the digital computer, this generation has succeeded in solving two fundamental fluid dynamic equations that were derived more than 100 years ago. The second and most definitive equation accounted for viscous fluid forces and became known as the Navier–Stokes equation. Prandtl and Tietjens (see footnote 1) note on page 259 of *Fundamentals of Hydro-and Aeromechanics* that "The equation was first found by Navier in 1827 and Poisson in 1831. Their derivation was based on certain theories of intermolecular forces. Without using hypotheses of this kind, St. Venant in 1843 and Stokes in 1845 found the same equation on the assumptions that the normal and shear stresses are linear functions of the deformation velocities ... ." These four men finished the derivation of the fluid dynamic

equation for a fluid having no viscosity that was obtained by Leonhard Euler and published in 1752, 1753, an 1755.[19] It took another two centuries for experts in fluid mechanics and applied mathematics to first solve the Euler

equation, and still longer to solve the Navier–Stokes equation.

---

[19] John D. Anderson, *A History of Aerodynamics*, Cambridge University Press, Cambridge, United Kingdom, 1997.

APPENDIX B

In contrast to the incompressible thin airfoil theory developed by Ludwig Prandtl during World War I—which you are now familiar with—the Euler theory from the mid-1750s accounted for practical airfoils that are thick (e.g., a Göttingen 606) and for compressibility associated with Mach numbers greater than zero. However, the Euler theory assumes that the fluid has no viscosity. The Navier–Stokes equation, which came 90 years

later, improved upon the Euler equation because fluid viscosity effects were included. To obtain practical results from the Navier–Stokes equation required very advanced digital computer technology coupled with very creative numerical integration methodology.

Today, Euler and Navier–Stokes equations are solved using any one of several numerical integration schemes called computer codes. One of these codes is called OVERFLOW 2.[20,21] Two people that are experts in using this particular computer code are Marilyn Smith (a Professor at the Georgia Institute of Technology in Atlanta, Georgia) and Mark Potsdam (a member of the U.S. Army Aeroflightdynamics Directorate located at NASA Ames Research Center). I was extremely fortunate to have these two individuals collaborate on the CFD results presented herein. The question I posed to them was, "What does CFD think about my elemental lift and pitching moment curves shown in Figs. B-8 and B-9 using the following input?"

- The airfoil is a NACA 0012 with a 1-foot chord.
- The pitch axis is located at the 1/4 chord.
- Temperature and density are for sea level on a standard day. • Angle of attack varies as 5.0 –4.5 sin (ωt) in degrees. • Free-stream velocity varies as 475 +190 sin (ωt) in feet per second. • The oscillation frequency (ω) is 25.5 in radians per second.

This input is representative of a rotor blade element located at the 3/4 radius station of a rotor traveling at 190 feet per second (112 knots) with a tip speed of 633 feet per second, which would be an advance ratio (μ) of 0.40. The Reynolds number varies between 1 .82 million and 4.25 million, and the Mach number varies between 0.255 and 0.596, which correspond to the retreating blade azimuth ($\psi = \omega t = 270$ degrees) and the advancing blade azimuth ($\psi = \omega t = 90$ degrees),

respectively.

A comparison of predictions by thin airfoil theory, Euler theory, and Navier–Stokes theory for how elemental lift (dL/dr) varies with azimuth is shown in Fig. B-11. It is clear from this figure that all three theories capture the elemental lift, unsteady aerodynamic behavior for this example . The primary difference is the change of the average elemental lift over the cycle. To explain the differences is relatively simple . In the thin airfoil case, the average elemental lift has been computed with a basic airfoil steady lift curve slope of $a = 2\pi$ per radian and independent of Mach number, but reflecting Theodorsen F and G functions . The average elemental lift is 100.9 pounds per foot.

---

[20] Robert H. Nichols and Pieter G. Buning, *User's Manual for OVERFLOW 2.1–version 2.1t*, Aug. 4, 2008.
[21] Pieter G. Buning, et al., *CFD Approaches for Simulation of Wing-Body Stage Separation*, AIAA-2004-4838,

APPENDIX B

The solution of the Euler equation with the example input leads to the upper curve on Fig. B-11, which has an average elemental lift of 129.1 pounds per foot. The Euler solution always returns a lift curve slope that depends on Mach number as $2\pi/\sqrt{1-M^2}$ in steady aerodynamics up to Mach numbers where the flow is Mach 1 somewhere along the upper surface of the airfoil.[22] The average Mach number over the oscillation is 0.425, which means the thin airfoil average elemental lift (of 100.9 pounds per foot) should increase by no less than $1/\sqrt{1-0.425^2}=1.1$. The Euler equation, when solved with CFD, more accurately accounts for the shed wake, which is equivalent to more accurate F and G functions during the oscillation.

The unsteady aerodynamic results using the CFD solution to the Navier–Stokes equation is the middle line on Fig. B-11. The average elemental lift is 115.1 pounds per foot. The Navier–Stokes equation includes fluid viscosity and accurately predicts the typical airfoil lift curve slope of 5.73 per radian versus the Euler theory result of 2π per radian. Both compressibility and shed wake influences are accounted for in the Navier–Stokes and Euler theories. Therefore the Euler solution for average elemental lift of 129.1 pounds per foot should be reduced by approximately $5.73/2\pi = 0.91$, which is about the reduction that Fig. B-11 shows (i.e., 115.1/129.1 = 0.89).

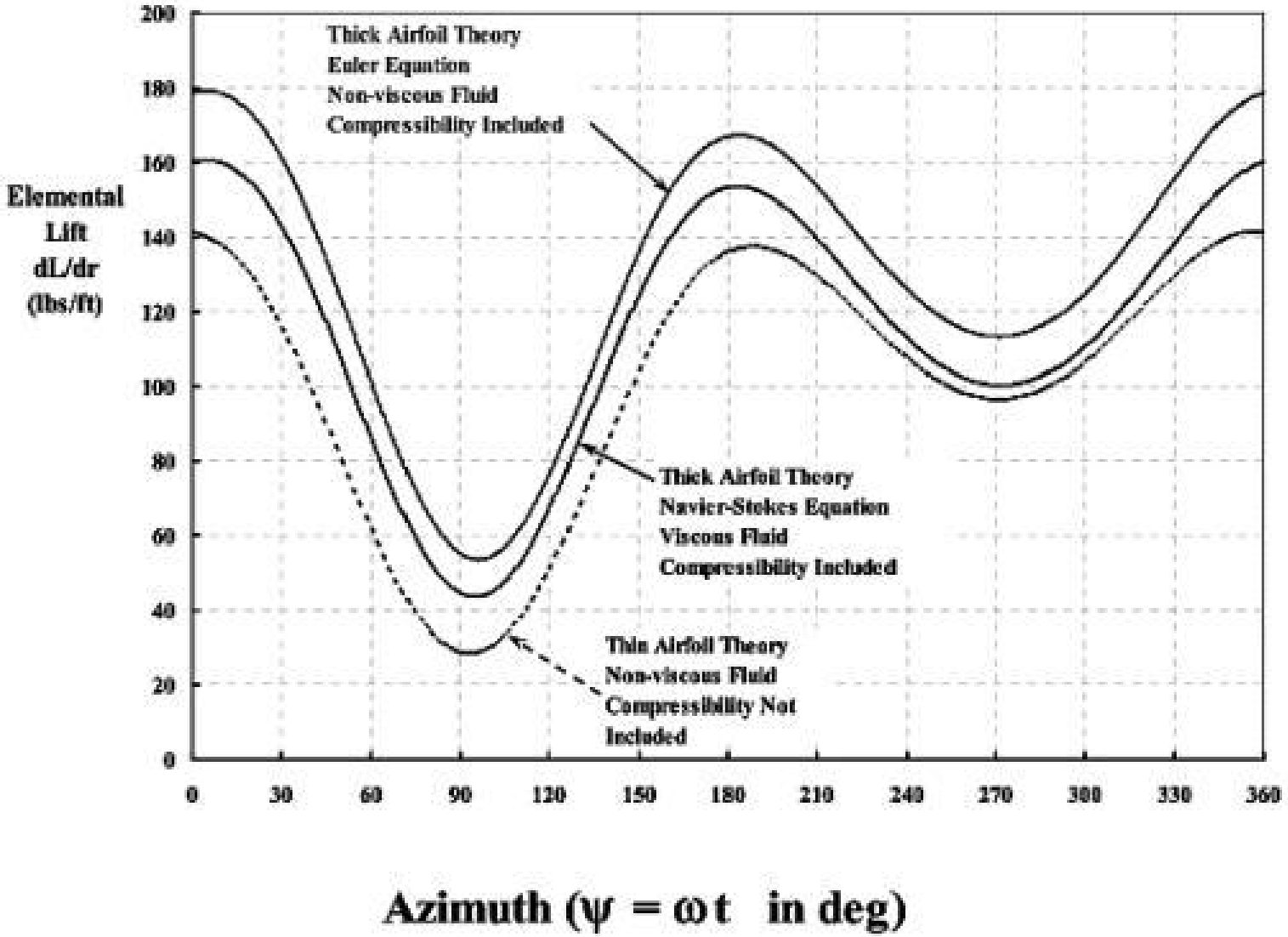

Fig. B-11. Thin airfoil theory versus CFD predictions for elemental lift.

---

[22] Hermann Glauert, *The Effects of Compressibility on the Lift of an Airfoil*, R&M no. 1135, 1927.

Now consider the elemental pitching moment comparison provided in Fig. B-12. With

thin airfoil theory, the moment at the 1/4-chord point does not vary with lift in steady flow. This result, however, is not supported by experimental data.[23] For the NACA 0012 airfoil, the

center of pressure moves forward from the 1/4-chord point as airfoil lift increases . In steady flow, the movement is not great but sufficient enough that the pitching moment about the 1/4-chord point is approximately

$$C_{M_{1/4c}} = 0.0065(C_L) + 0.0014(C_L)^2 \quad (52)$$

which says that the center of pressure is only at the 1/4-chord point when the airfoil lift is zero. To a first approximation then, the average elemental pitching moment about the 1/4-chord point should increase approximately as

$$(53) \qquad \left(\frac{dM_{1/4c}}{dr}\right)_{avg} \approx 0.0065(c)\left(\frac{dL}{dr}\right)_{avg} .$$

The average elemental pitching moment for the Navier–Stokes result in Fig. B-12 is 0.832 foot-pounds per foot, and the average elemental lift is 115.1 pounds per foot. Recall that a 1-foot chord was chosen for this example . Therefore, the computation of $dM_{1/4c}/dL$ as 0.832/115.1 = 0.00723 adequately explains the fact that the Navier–Stokes result lays above the thin airfoil curve in Fig. B-12.

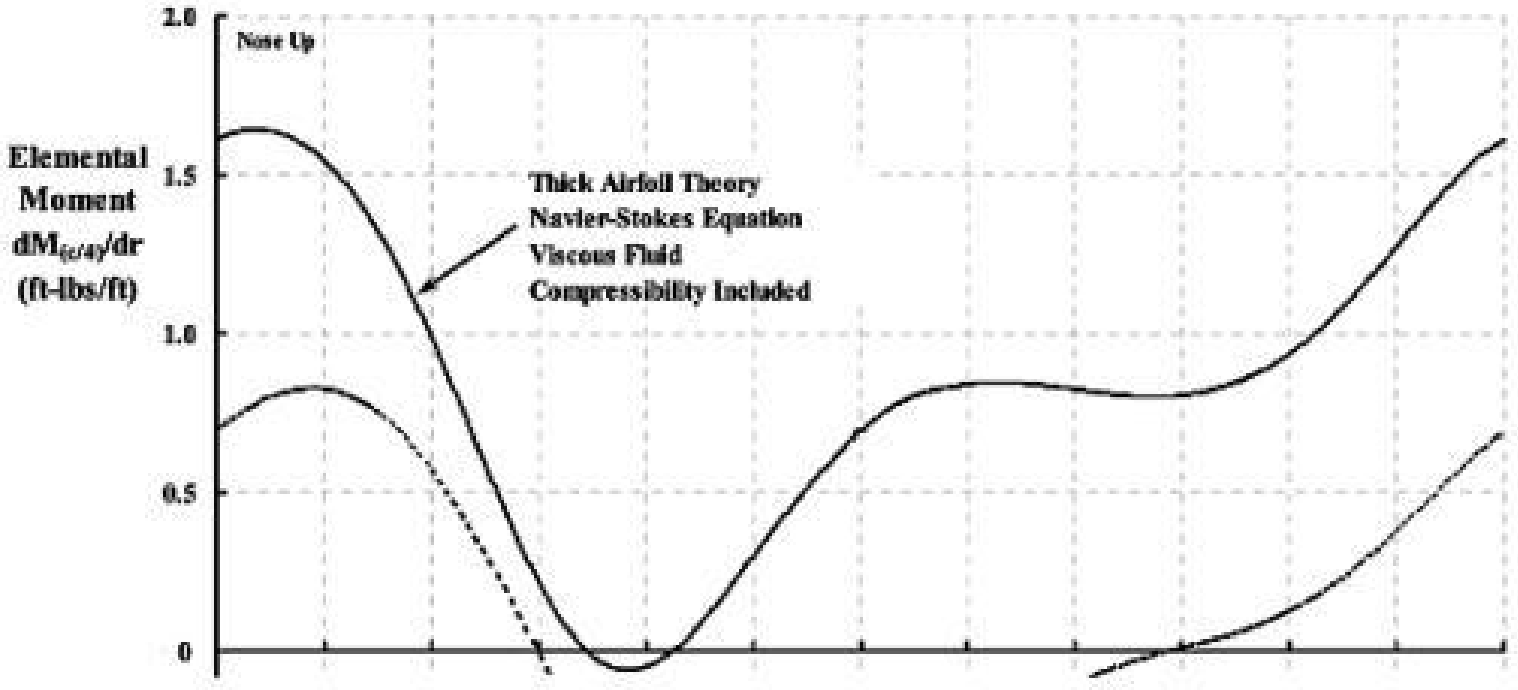

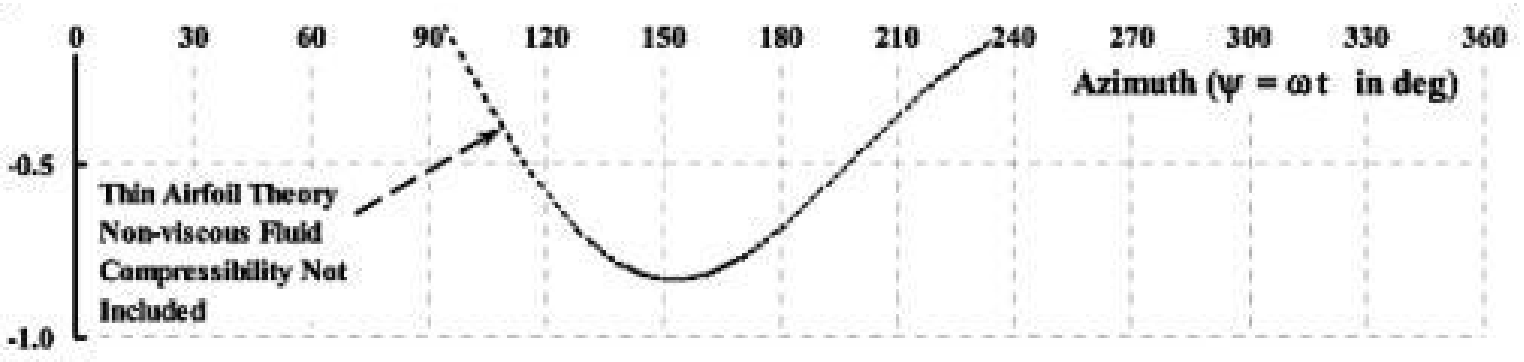

Fig. B-12. Thin airfoil theory versus CFD predictions for elemental moment.

---

[23] Charles D. Harris, *Two-Dimensional Aerodynamic Characteristics of the NACA 0012 Airfoil in the Langley 8-Foot Transonic Pressure Tunnel*, NASA TM 81927, April 1981.

APPENDIX B

What is not so easily explained is the approximately 30-degree azimuthal shift in the maximum and minimum peaks of the elemental moment that the Navier–Stokes equation reveals when compared to thin

airfoil theory. I know of no comparable wind tunnel experimental data where the free-stream velocity is varied, so a comparison of theory to test cannot be made as yet. The problem I posed falls in the category of rotor airload measurements . A definitive rotorcraft experiment in this regard had to wait for wide use of the helicopter.

A benefit of solving the Navier–Stokes equation by the OVERFLOW 2 code has been the prediction of elemental drag, which is shown for my example problem in Fig. B-13.

The results presented in Figs. B-1 1, B-12, and B-13 are completely dimensional for the example I chose. The more interesting graphs are seen when the loads and moment are presented in coefficient form. The coefficients are based on the local dynamic pressure computed as $q = \frac{1}{2}\rho\left(V_0 + V_1 \sin\psi\right)^2$.

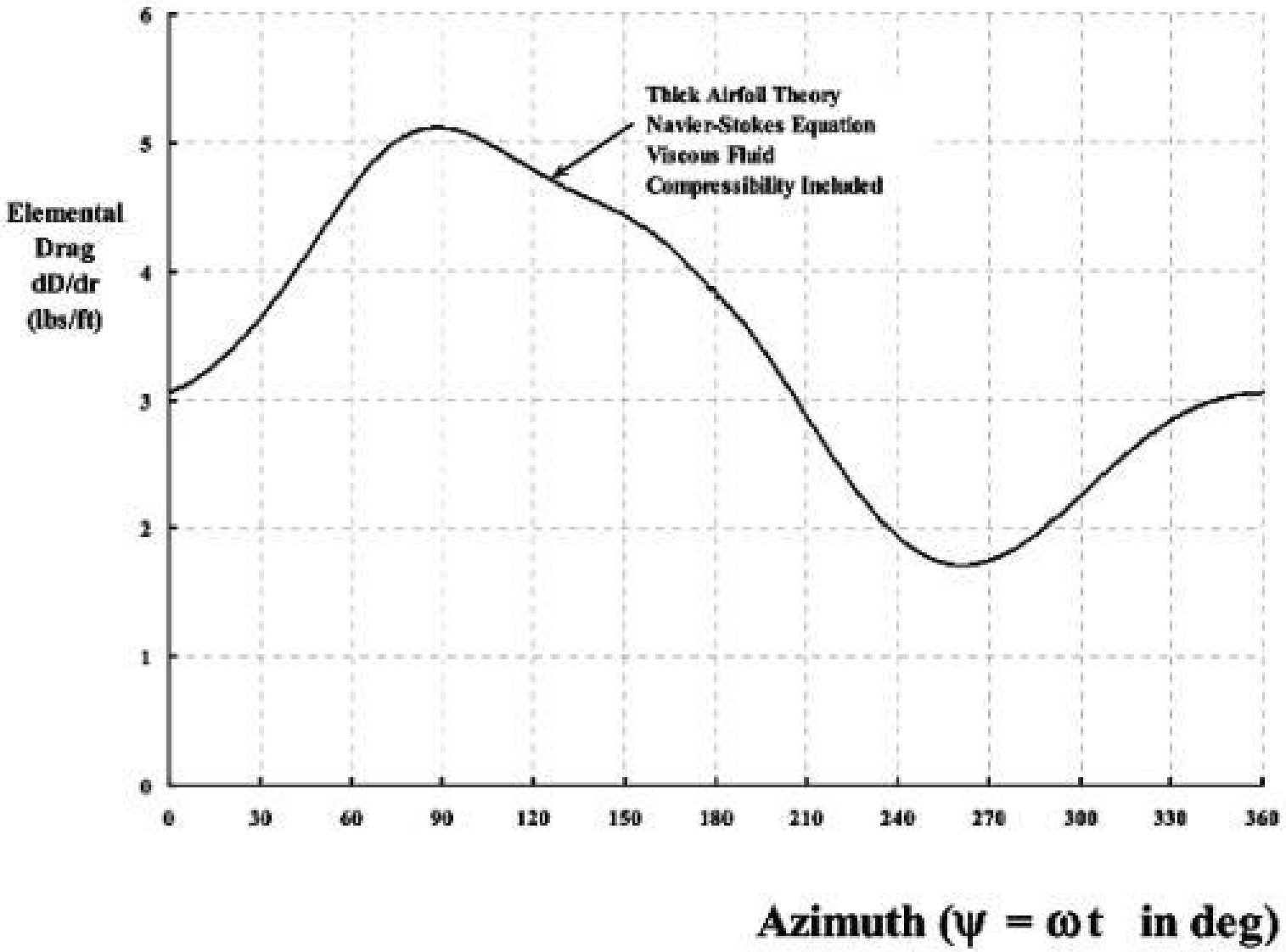

Fig. B-13. Only Navier–Stokes theory predicts elemental airfoil drag.

Figure B-14 shows that both the

elemental lift coefficient and the elemental pitching moment coefficient generally follow the oscillating angle of attack, which was given as $\alpha = 5.0 - 4.5 \sin(\psi)$ in degrees. Note the enlarged scale used for the moment coefficient because a pitching moment coefficient of 0.01 is rather large in the rotorcraft world. Rotor blades are long with narrow chord and quite torsionally limber, which means that the airloads can easily twist them.

Another way to examine the Navier–Stokes results frequently used by rotorcraft engineers is shown in Figs . B-15, B-16, and B-17 . The conventional lift coefficient versus angle of attack is provide in Fig. B-15. The slight hysteresis loops caused by unsteady aerodynamics are clearly comparable to thin airfoil theory as Fig. B-10 shows. I have added a reference quasi-steady lift coefficient versus angle of attack accounting

for an average Mach number of 0.425 and lift curve slope of 5.73 per radian (0.1 per degree).

The unsteady aerodynamic effects on pitching moment coefficient become clearer when plotted against lift coefficient as Fig. B-16 illustrates. The center of pressure moves forward of the 1/4-chord point with a CFD theory that includes fluid viscosity.

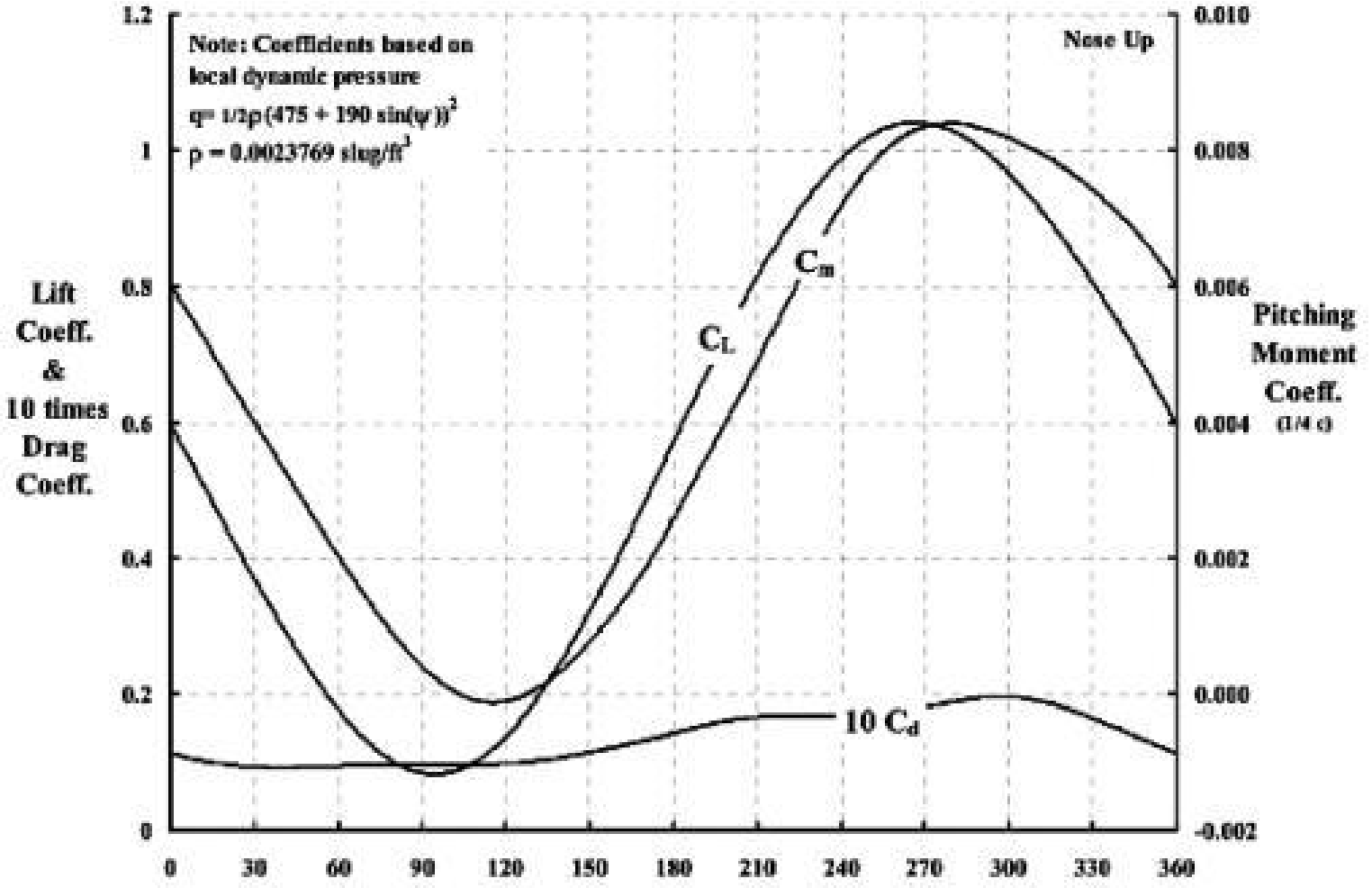

Azimuth ($\psi = \omega t$ in deg)

Fig. B-14. Solution results according to the Navier–Stokes equation for the example chosen.

APPENDIX B

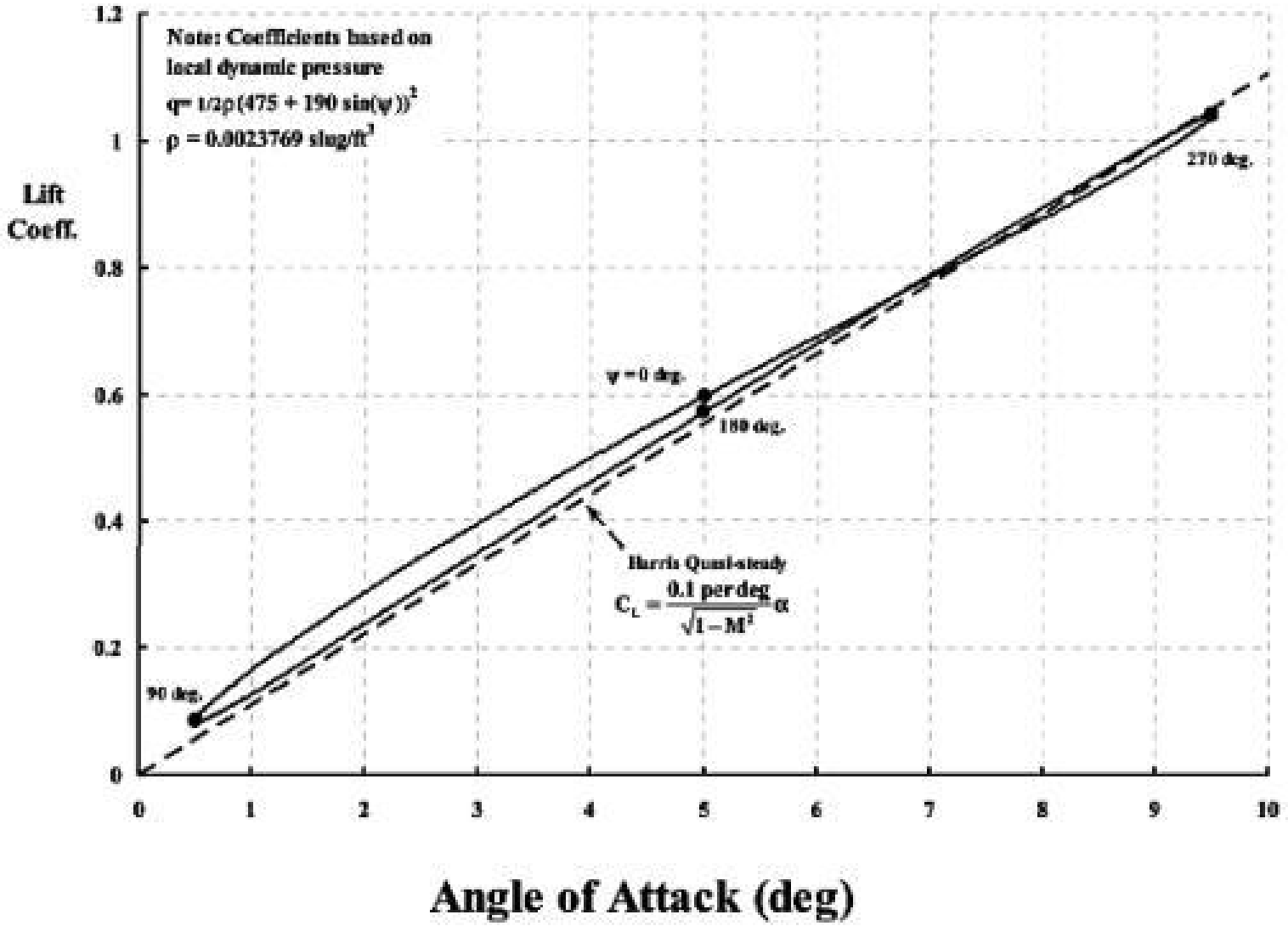

Fig. B-15. Hysteresis loops in lift coefficient versus angle of attack due to unsteady aerodynamics according to the Navier–Stokes equation for the example chosen.

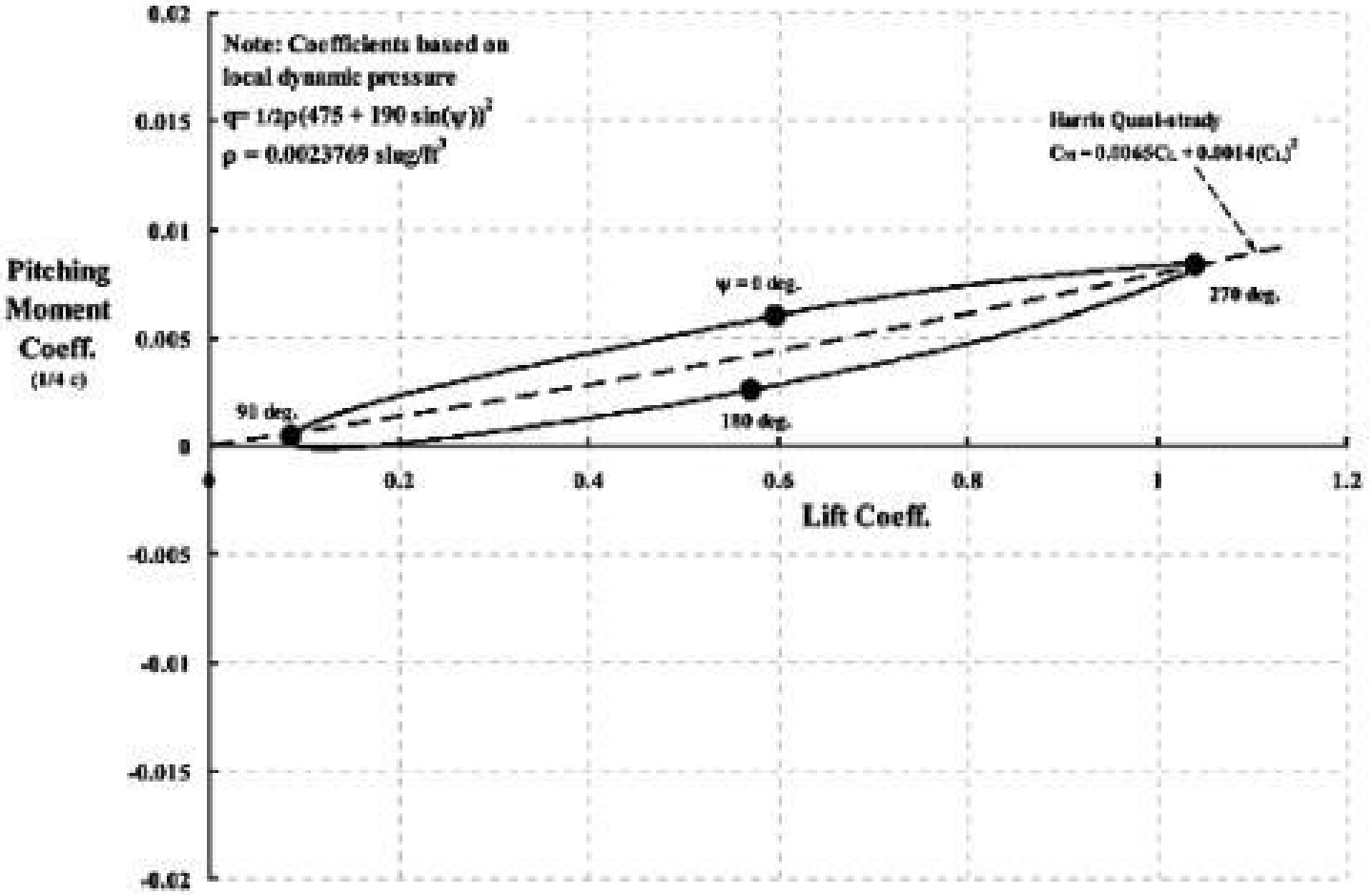

Fig. B-16. Hysteresis loops in moment coefficient versus lift coefficient due to unsteady aerodynamics according to the Navier–Stokes equation.

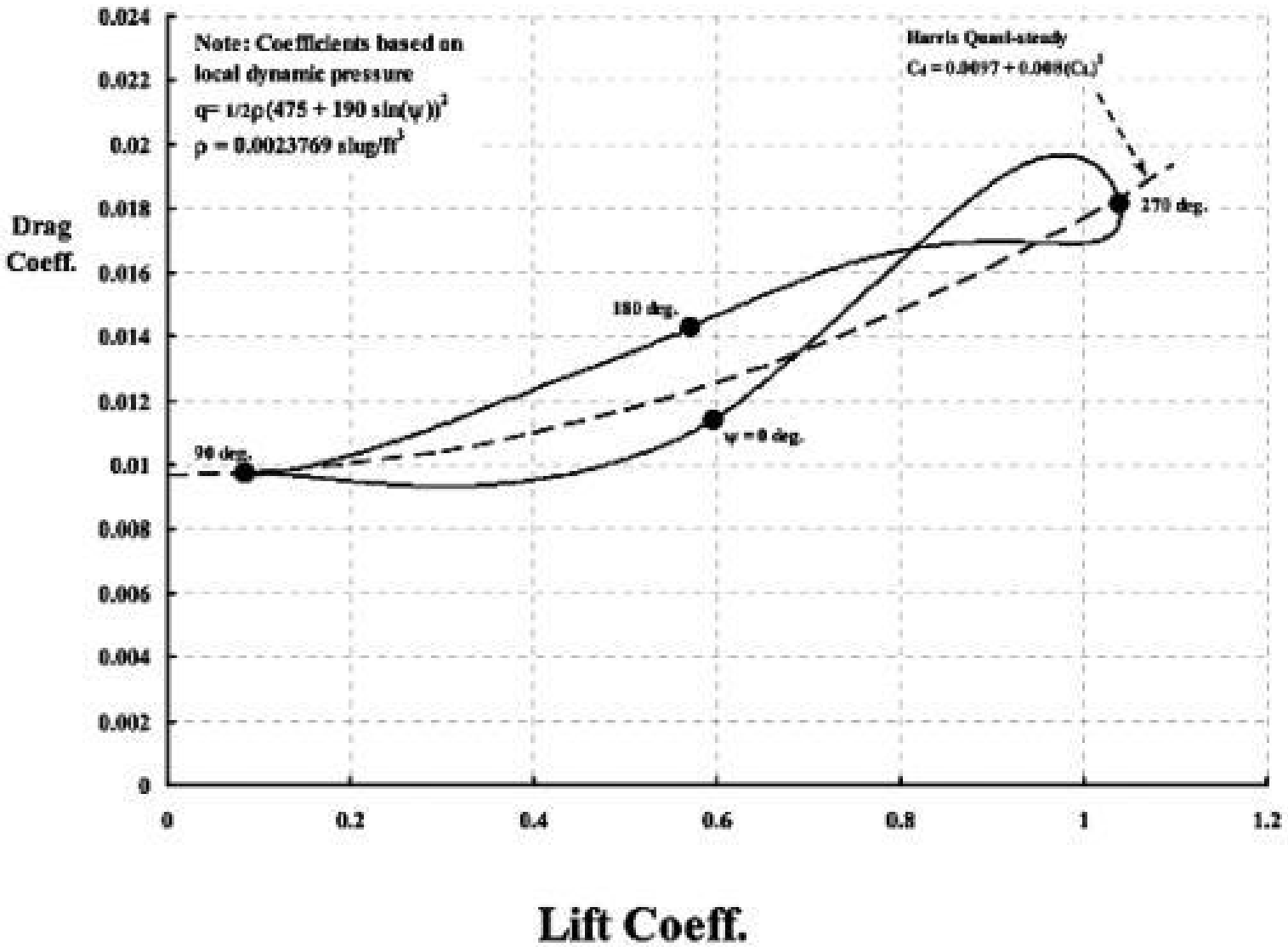

Fig. B-17. Hysteresis loops in drag coefficient versus lift coefficient due to unsteady aerodynamics according to the Navier–Stokes equation for the example chosen.

The influence of unsteady motion on elemental drag is quite substantial as Fig. B-17 shows . Not only are the hysteresis loops large, but the average drag coefficient for one oscillation cycle is greater than what a quasi-steady airfoil experiences . This is a factor in computing profile power of rotor systems.

Closing Remarks

An understanding of airfoil aerodynamics began in the 1750s when Euler developed a very basic fluid dynamics equation; since then numerous outstanding individuals—more than one can imagine—have contributed to this process. In addition, the CFD solutions of the Navier–Stokes equation have reduced a dependency on wind tunnel testing. Nevertheless, the fundamentals provided

in this appendix should be beneficial to the uninitiated.

Another purpose of this appendix is to provide a basis for calculating blade elastic twisting, which is the subject of Appendix D.

APPENDIX C

BASIC DYNAMICS AND GROUND RESONANCE

The purpose of this appendix is to provide an analytical sense of ground resonance. This was the phenomena that destroyed a Kellett XR-2 autogyro (see Fig. 2-1

1) and became a serious consideration when the lead-lag hinge was introduced.

Without some basic understanding of dynamics, a ground resonance analysis is not one of the easier engineering problems to explain, derive the dynamic equations for, or obtain solutions to the equations once they are written.[1] However, George Townson, in his excellent book containing both history and engineering features of autogyros,[2] presents the clearest illustration of the ground resonance phenomena that I have ever seen. His illustration (from page 149 of his book) was reproduce in this volume on page 33 . In Fig. C-1 of this appendix, I have included the first three parts of Townson's illustration as a starting point for the discussion that follows.

Ground resonance is basically a multi-degree-of-freedom vibration problem with damping included. Two degrees of freedom are the rotorcraft rocking and pitching on its landing gear. Since springs and shock absorbers were standard equipment for all autogyros just for hard landings, these two

degrees of freedom were well damped. The other degrees of freedom come from blade lead-lag motion. One degree of freedom is written for each blade. The motions of rotorcraft rocking and pitching, with the addition of each blade leading and lagging, have the potential to couple together such that one motion can feed all the other degrees of freedom. The pioneers found out that blade motion definitely needed additional mechanical damping. Without damping in all degrees of freedom, there can be real problems.

Fortunately the theory to predict stability boundaries for ground resonance was in place when practical helicopters began to evolve.[3]

BASIC DYNAMICS

Introduction

A shortcut in analyzing ground resonance can be taken as Fig. C-2 suggests. It is the translation of the rotor hub that is the

dominate aircraft coordinate in most basic studies . How the translation occurs is rather secondary . The actual rocking motion (which could be describe by an angle) and all of the dimensions and masses implied by Fig. C-2 only lead to a natural rocking frequency (ω_{ac}) of the aircraft while sitting on the ground. This frequency has the units of radians per second.

---

[1] I learned dynamics from J. P. Den Hartog's *Mechanical Vibrations*, McGraw-Hill Book Co., Inc., New York, 4th Ed., 1956. His explanations and solutions are the easiest to understand that I have found. [2] G. Townson, *AUTOGIRO—The Story of the Windmill Plane*, Aero Publishers, Inc., Fallbrook, Calif., 1985. [3] Robert Coleman and Arnold Feingold, *Theory of Self-Excited Mechanical Oscillations of Helicopter Rotors with Hinged Blades*, NACA Report No. 1351, 1958.

APPENDIX C

It should be obvious that an autogyro landing gear leg uses both a spring and damper just like car suspensions use springs and shock absorbers . These components allow the aircraft to rock when a force is applied at the hub. Fig. C-2 shows a simple schematic of what could be the Kellett XR-2 autogyro rolled to starboard because of a lateral force applied at the hub. In rolling to starboard, the hub translates along the Y-axis until the landing gear spring forces and dampers provide a countering force.

Static Calibration

The complete aircraft could be statically calibrated with a tabulation of deflection (y) for successively larger force (F). This data would be plotted as a curve of F versus y. The slope of this F versus y curve defines the spring

constant of the autogyro. This spring constant is denoted by the letter (k), which is defined as k = F/y and is expressed in pounds per foot.

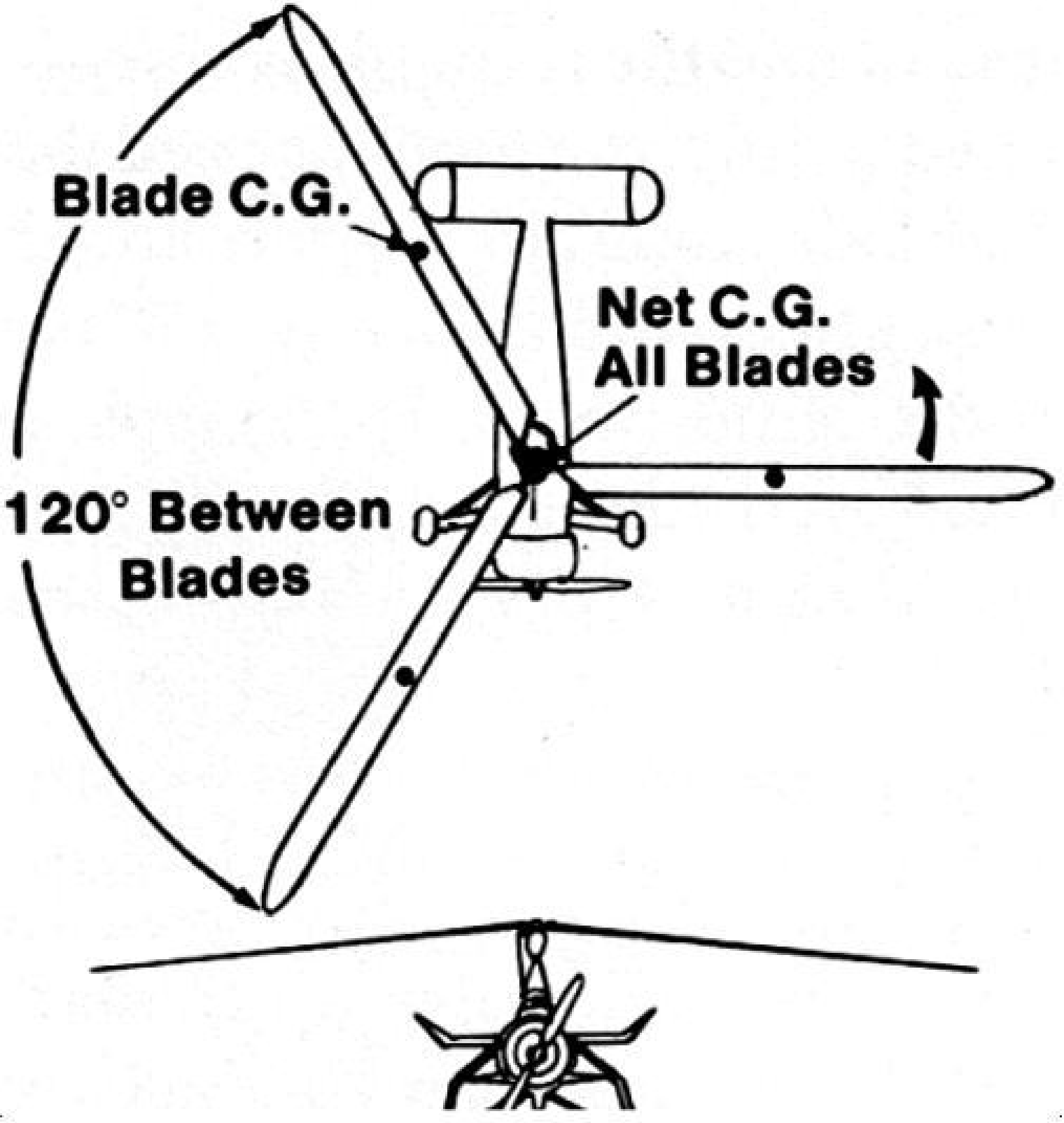

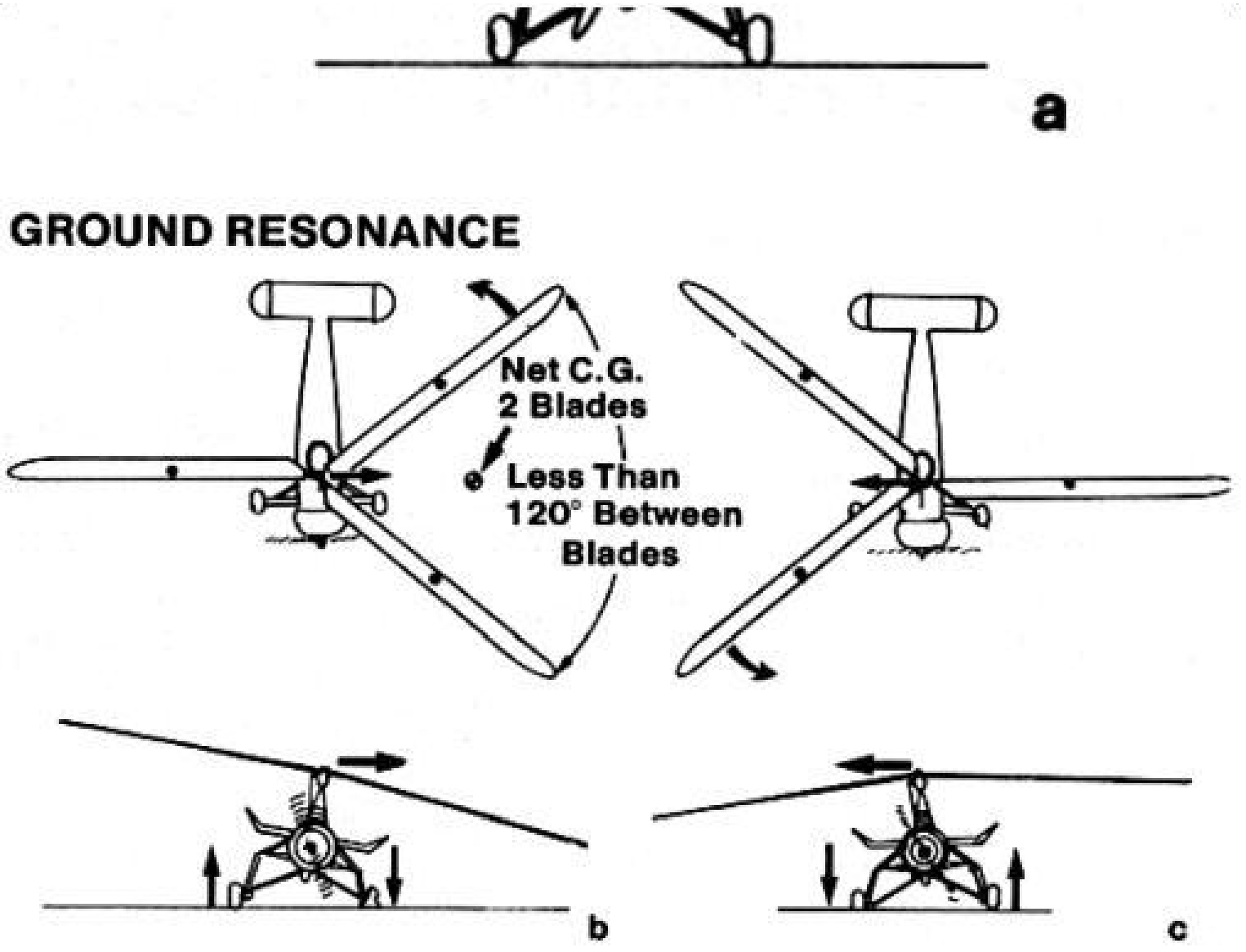

Fig. C-1. De-patterned blades in the lead-lag plane create a potentially destructive force that can lead to ground resonance.

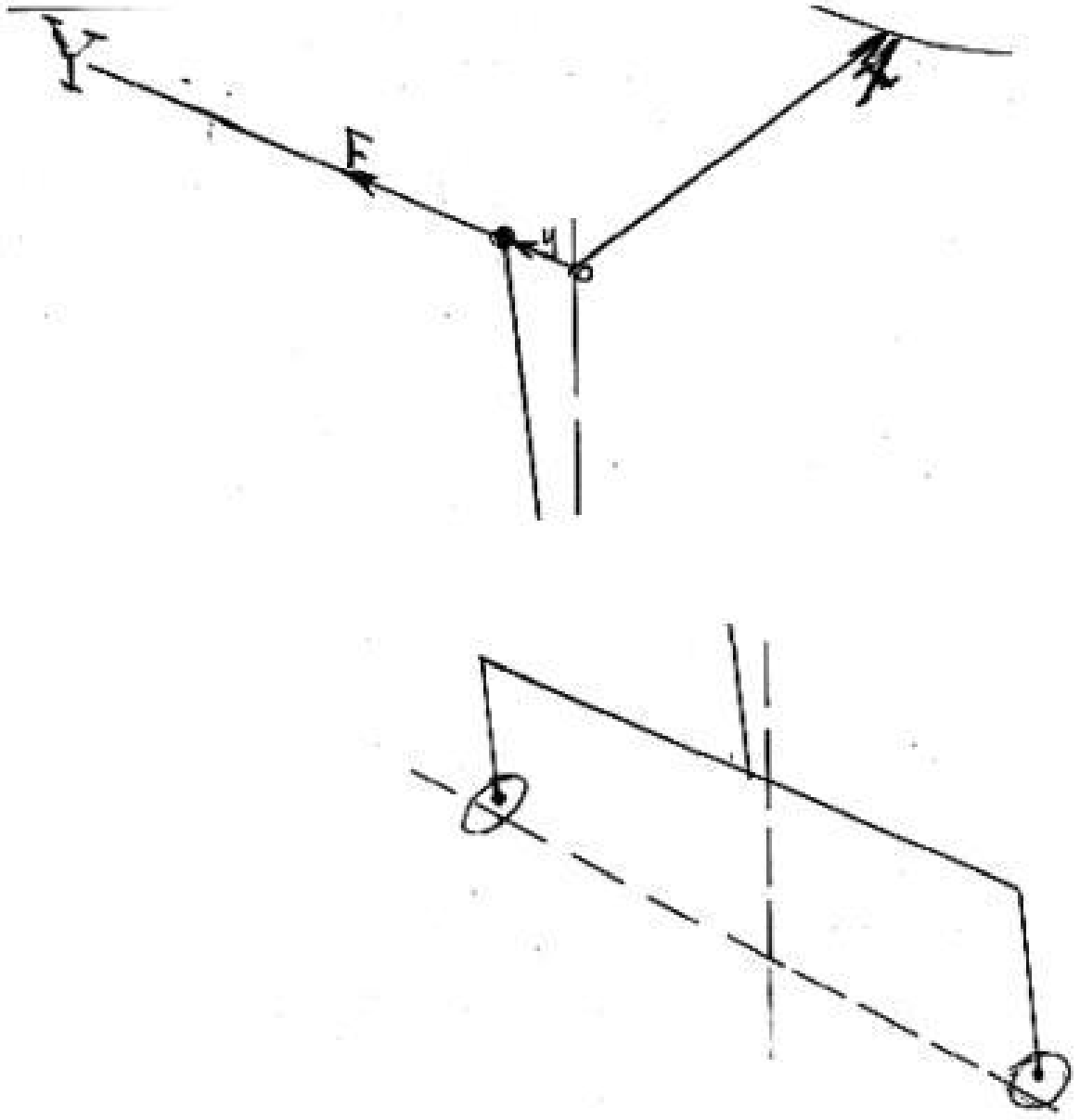

Fig. C-2. Autogyro rocking leads to hub translation.

APPENDIX C

Dynamic Calibration

Since the landing gear assembly includes a shock absorber (i.e., a damper), the aircraft has a damping coefficient denoted here by the letter (c). The landing gear damping creates a force proportional to velocity, and therefore the damping constant has the units of pounds per foot per second. The complete autogyro damping constant can also be found by experiment. Suppose the hub force (F) in Fig. C-2 rocks the autogyro so that the hub is deflected an amount (y_o), and then the force is suddenly released. The expected result is that the autogyro would rock over to the port side, then back to starboard, and then stop in the upright position. This is the exact parallel of standing on a car bumper and then jumping off—a test to see if the shock absorbers are still good because the car does not continue to bounce up and down.

Basic Theory of Dynamics

Both the static and dynamic experiments suggested above can be summed up with one mathematical equation. This very fundamental differential equation is:

$$(1) \qquad m\frac{d^2y}{dt^2} = F - c\frac{dy}{dt} - ky \qquad \text{or}$$

$$m\frac{d^2y}{dt^2} + c\frac{dy}{dt} + ky = F\,.$$

The first experiment calibrates the aircraft on its landing gear by slowly increasing the force (F) and recording values of (y). Since the calibration is a static experiment, there is no velocity ($dy/dt = 0$) or acceleration ($d^2y/dt^2 = 0$), and so it follows that the autogyro spring constant is $k = F/y$.

The second experiment is not static because the force is suddenly released, and the resulting oscillation is recorded by some

instrument. This instrument would record the deflection (y) and time (t). Since this second experiment occurs with the force (F) being zero, the fundamental equation is rewritten as

$$(2) \qquad m\frac{d^2y}{dt^2}+c\frac{dy}{dt}+ky=0,$$

which is a second order, ordinary, differential equation. The experiment begins at time (t) equal zero with an initial deflection of $y_{(t\,=\,0)} = y_0$ and zero velocity (i.e., $dy/dt = 0$), and has the solution

(3)

$$y_{(t)} = y_0\left(e^{-\frac{c}{2m}t}\right)\left[\cos\left(t\sqrt{\frac{k}{m}-\frac{c^2}{4m^2}}\right)\right] = y_0\left(e^{-\frac{c}{2m}t}\right)\left[\cos(\omega t)\right].$$

Theory Application—Case 1

Now imagine this experiment where only autogyro lateral rocking is of concern. That is, there can be no autogyro pitching because the machine is locked in such a way that the hub cannot move along the X-axis in Fig . C-2 . Assume the static experiment has established that an 8,000-pound force acting at the hub (say 13 feet above the ground) will tilt the autogyro so

that the hub moves one-half foot to starboard along the Y-axis. This means that the system has a spring constant of $k = F/y = 16{,}000$ pounds per foot. For illustration purposes, assume that the weight of the autogyro acts as an apparent mass at the hub so that $m = 1{,}470/32.17$ slugs.

Suppose this experiment is conducted in two parts. For the first part of this vibration experiment, *disconnect* the shock absorbers so that there is no damping, which means the damping constant (c) is zero. Next, apply an 8,000-pound force at the hub in the positive Y-axis direction so that the hub is set at an initial deflection (y_0) of $y_0 = 0.5$ feet. Now, abruptly release the 8,000 pounds. The autogyro will rock from starboard to port and back again such that the hub translates, following Eq. (3), as

(4)

$$y_{(t)} = 0.5\left[\cos\left(t\sqrt{\left(\frac{16,000}{1,470}\right)32.17}\right)\right] = 0.5\cos(18.71t).$$

This result, graphed in Fig. C-3 as the light dashed line, implies that the vibration will continue indefinitely. In fact, some slight

amount of damping will exist in the real world, and the vibration will, of course, eventually die out.

For the second part of this vibration experiment, *reconnect* the shock absorbers, which, I will assume, create a damping coefficient (c) at the hub of about 228 pounds per foot per second.[4] With these values (i.e., k = 16,000 lbs/ft, m = 45.695 slugs, c = 228.47 lbs/fps, and $y_0 = 0.5$ ft), Eq. (3) becomes

$$(5) \qquad y_{(t)} = 0.5\left(e^{-2.5t}\right)\cos\left(18.5445t\right).$$

This result, graphed in Fig. C-3 as the heavy solid line, implies that the vibration will decrease in amplitude with increasing oscillation time. This experimental data, recorded for example by an oscillograph, can be used to obtain two key properties about the aircraft.

The first property is the damped natural

frequency, which is, from Eq. (3),

$$(6) \qquad \omega = \sqrt{\frac{k}{m} - \frac{c^2}{4m^2}} \, .$$

Notice in Fig. C-3 that the points A, B, and C occur as a vibration cycle is completed. That is, cos (ωt) starts at zero time where the cosine is unity and finishes 360 degrees (or 2π radians) later when $\omega t = 2\pi$ and the cosine again equals unity. This is one cycle and amounts to one revolution. The time to complete a cycle is called a period (T). In this example, Fig. C-3 shows that the period is about $T = 0.34$ seconds. That is, the time between points B and A is 0.34 seconds and the time between points C and B is 0.34 seconds. The rule is that $\omega T = 2\pi$, which means from Eq.(6), that

[4] The value of c = 228.47 lbs per ft/sec chosen for this example is perhaps 2 to 5 times lower than practice would dictate. A more general estimate would be that c

$= \sqrt{mk}$.

336

APPENDIX C

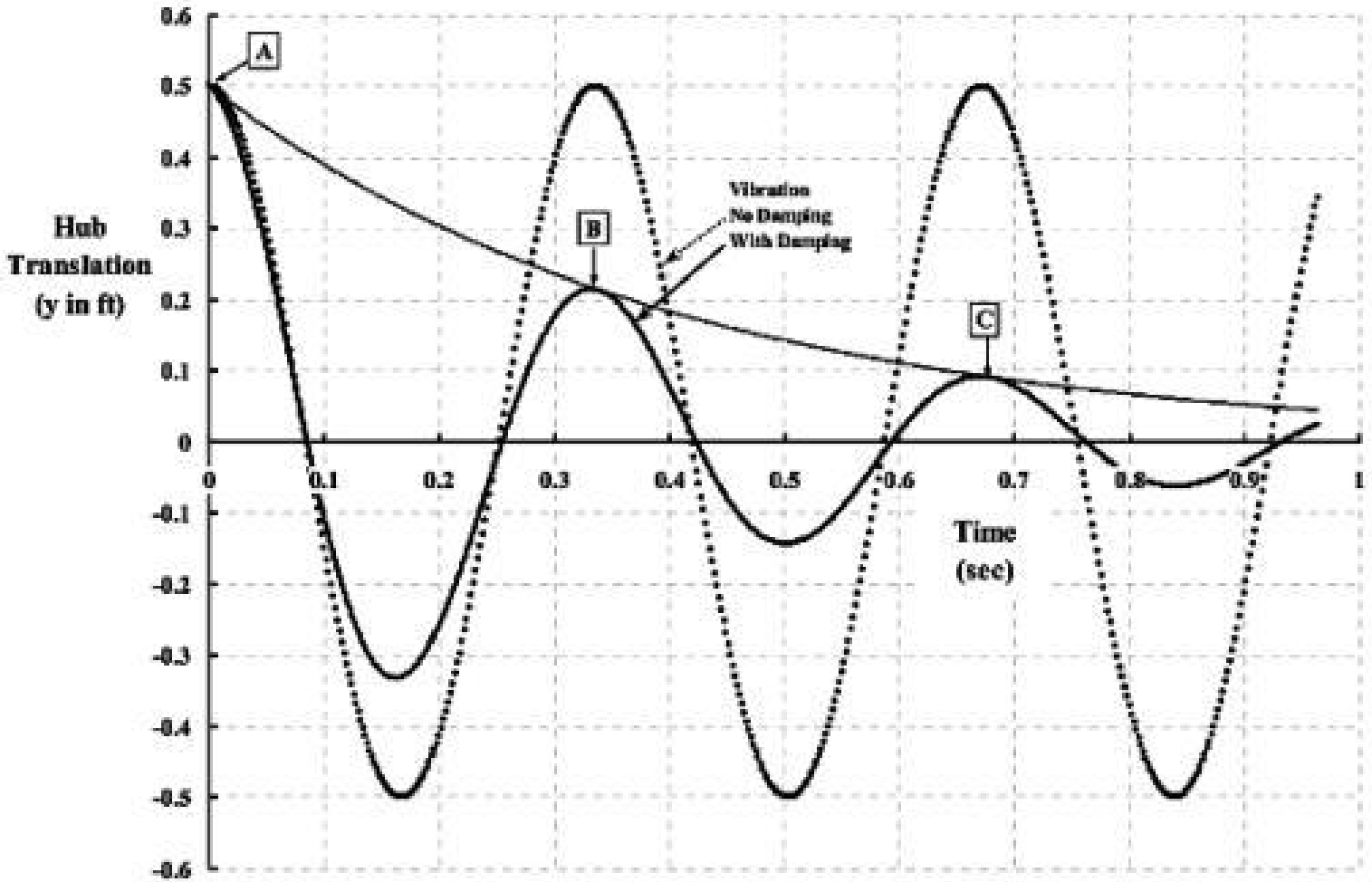

Fig. C-3. Autogyro rocking leads to hub translation.

(7) $$\omega = \sqrt{\frac{k}{m} - \frac{c^2}{4m^2}} = \frac{2\pi}{T}.$$

An oscillograph trace (such as shown in Fig. C-3, particularly when stretched out) can give a very accurate value of the period (T) when care is taken. This, in turn, means that $k/m - (c/2m)^2$ is known because

(8) $$\frac{k}{m} - \frac{c^2}{4m^2} = \left(\frac{2\pi}{T}\right)^2.$$

The second property is the successive reduction in amplitude you see in the waveform in Fig. C-3 as you follow the heavy solid line. This amplitude reduction of point B over point A and point C over B yields the parameter (c/2m). This is done from experimental data by measuring the amplitudes at the beginning and end of a cycle. Consider the

ratio of amplitudes at points A and B . At point A, t = 0, and at point B, t = T. At both points, the cosine in Eq. (5) is 1 .0 . Therefore, you have

$$(9) \qquad \frac{y_B}{y_A} = \frac{y_0\left(e^{-\frac{c}{2m}T}\right)}{y_0} = e^{-\frac{c}{2m}T}$$

APPENDIX C

and, by taking the natural logarithm of both sides, the property (c/2m) is immediately obtained as

$$(10) \qquad \frac{c}{2m} = -\frac{1}{T}\ln\frac{y_B}{y_A} = -\frac{1}{T}\ln\frac{y_C}{y_B}.$$

Having the experimental values of period (T) and (c/2m), it follows from Eq. (8) that

$$(11) \qquad \frac{k}{m} = \left(\frac{2\pi}{T}\right)^2 + \left(\frac{c}{2m}\right)^2 .$$

Recall now that the static test established the system spring constant (k) so that the apparent mass (m) and damping constant (c) are found directly as

$$(12) \qquad m = \frac{k}{(k/m)} \quad \text{and} \quad c = \left(\frac{c}{2m}\right) 2m .$$

Theory Application—Case 2, Constant Rotor Speed

The experiments of Case 1 were conducted with the hub not turning, but now

consider a case where the hub is turning. Imagine an experiment where a weight is added to the hub. A weight of mass (m_w) is attached to the end of a weightless rod that is (e) feet long, the other end being solidly bolted to the hub. As the hub begins to rotate, an unbalance will occur. This unbalance will rock the autogyro, and the hub will translate along the Y-axis. Keep in mind that there will be no autogyro pitching because the machine is locked in such a way that the hub cannot move along the X-axis. This experimental situation is shown in Fig. C-4, which constitutes a top view of Fig. C-2.

Equation (1) can now be used to describe the vibration of the system with an unbalance weight. Thus,

$$(13) \qquad m_h \frac{d^2 y_h}{dt^2} + c\frac{dy_h}{dt} + ky_h = F = -m_w \frac{d^2 y_w}{dt^2} .$$

At time (t) equals zero, let the hub be at rest ($y_h = 0$), and let the weightless rod (e) and added mass (m_w) be aligned with the X-axis as Fig. C-4 shows. Now assume some time has passed; the weightless rod has rotated through the angle (ψ), the hub has translated to $y_{(t)} = y_h$, and the added mass has moved to

$$y_w = y_h + e\sin(\psi). \tag{14}$$

Equation (13) requires the second derivative of displacement with respect to time. Velocity, the first derivative, is

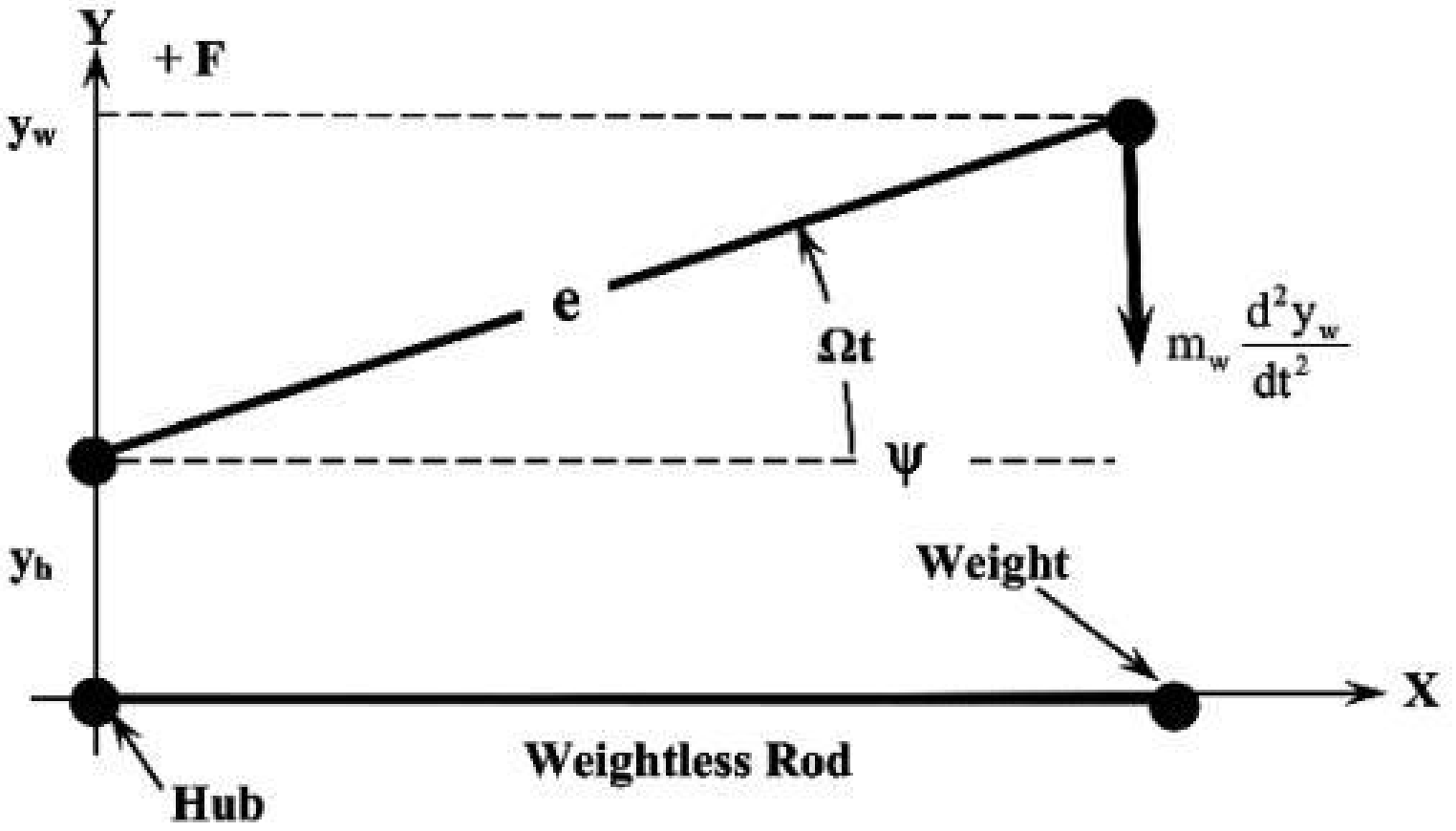

Fig. C-4. A top-view of Fig. C-2.

(15) $$\frac{dy_w}{dt} = \frac{dy_h}{dt} + e\cos(\psi)\left[\frac{d\psi}{dt}\right],$$

and acceleration, the second derivative of displacement, is (16)

$$\frac{d^2y_w}{dt^2}=\frac{d^2y_h}{dt^2}+e\cos(\psi)\left[\frac{d^2\psi}{dt^2}\right]-e\sin(\psi)\left[\frac{d\psi}{dt}\right]^2.$$

The basic dynamics equation that I intend to examine in this appendix is obtained by substituting Eq. (16) into Eq. (13), which yields

(17)

$$(m_h+m_w)\frac{d^2y_h}{dt^2}+c\frac{dy_h}{dt}+ky_h=m_we\sin(\psi)\left[\frac{d\psi}{dt}\right]^2-m_we\cos(\psi)\left[\frac{d^2\psi}{dt^2}\right].$$

Notice that no restriction has been placed on the rotational angle (ψ), which for rotorcraft problems is generally referred to as the azimuth angle.

Typically, the most common problem examined in textbooks on dynamics is the case where the rotational speed (a frequency in strict dynamic terms) is constant. That is, $d\psi/dt$ is constant, and therefore azimuth (ψ) equals a

constant times time. For purposes of this appendix, I have chosen a rotorcraft notation where if $d\psi/dt$ is constant, then $d\psi/dt = \Omega$ and $d^2\psi/dt^2 = d\Omega/dt = 0$. The rotational speed ($\Omega$) has the units of radians per second, and therefore the rotational angle can be written as $\psi = \Omega t$. With this basic understanding in mind, consider the behavior of the weight and hub shown in Fig. C-4 when the rotor speed is constant.

APPENDIX C

When the rotor speed (Ω) is constant and letting $m = m_h + m_w$, then Eq. (17) becomes

$$(18) \qquad m\frac{d^2y_h}{dt^2} + c\frac{dy_h}{dt} + ky_h = m_w e\Omega^2 \sin(\Omega t)$$

IF Ω = constant

which is solved quite easily. Using classical

theory, you immediately have (19)

$$y_h = \frac{\left(m_w e \Omega^2\right)}{\left(k - m\Omega^2\right)^2 + (c\Omega)^2}\left[\left(k - m\Omega^2\right)\sin(\Omega t) - (c\Omega)\cos(\Omega t)\right]$$

or, when using a phase angle form, which can be used to illuminate the vibration amplitude (20)

$$y_h = \frac{\left(m_w e \Omega^2\right)}{\sqrt{\left(k - m\Omega^2\right)^2 + (c\Omega)^2}}\left\{\sin\left[\Omega t - \arctan\left(\frac{c\Omega}{k - m\Omega^2}\right)\right]\right\}.$$

From this solution for displacement, you immediately have the hub acceleration, a very important result in most practical engineering experiences

(21)

$$\frac{d^2 y_h}{dt^2} = \left[\frac{\left(m_w e \Omega^2\right)}{\sqrt{\left(k - m\Omega^2\right)^2 + (c\Omega)^2}}\right](-\Omega^2)\left\{\sin\left[\Omega t - \arctan\left(\frac{c\Omega}{k - m\Omega^2}\right)\right]\right\}.$$

These results can be used in a very practical way. Think of starting up an autogyro rotor with the prespin gearing used on late model Cierva, Pitcairn, and Kellett machines, which were designed for jump takeoff. Assume from the preceding discussion that the autogyro with the added weight on the end of the weightless rod is described as shown in Table C-1.

Using Eq. (19) and the configuration from Table C-1, the result of this rotor startup calculation is the hub motion time history shown in Fig. C-5 . This calculation treated the constant rotor speed problem as a sequence of quasi-steady conditions to give the graphical appearance of an infinitely slow rotor startup. You will notice immediately that before reaching the operating rotor speed of 25 radians per second (about 240 rpm), the hub translation experiences a resonance at a

rotor speed of about 19 radians per second. If 25 radians per second is taken as 100-percent rotor speed, then the worst of the resonance occurs at about 76 percent of design rotor speed.

Table C-1. Assumed Autogyro Configuration

Parameter	Symbol	Unit	Value
Mass	$m = m_h + m_w$	slug	45.695
Damping coefficient	c	lbs/fps	228.47
Spring stiffness coefficient	k	lbs/ft	16,000
Added mass	m_w	slug	5.2844
Weightless rod length	e	ft	2.5

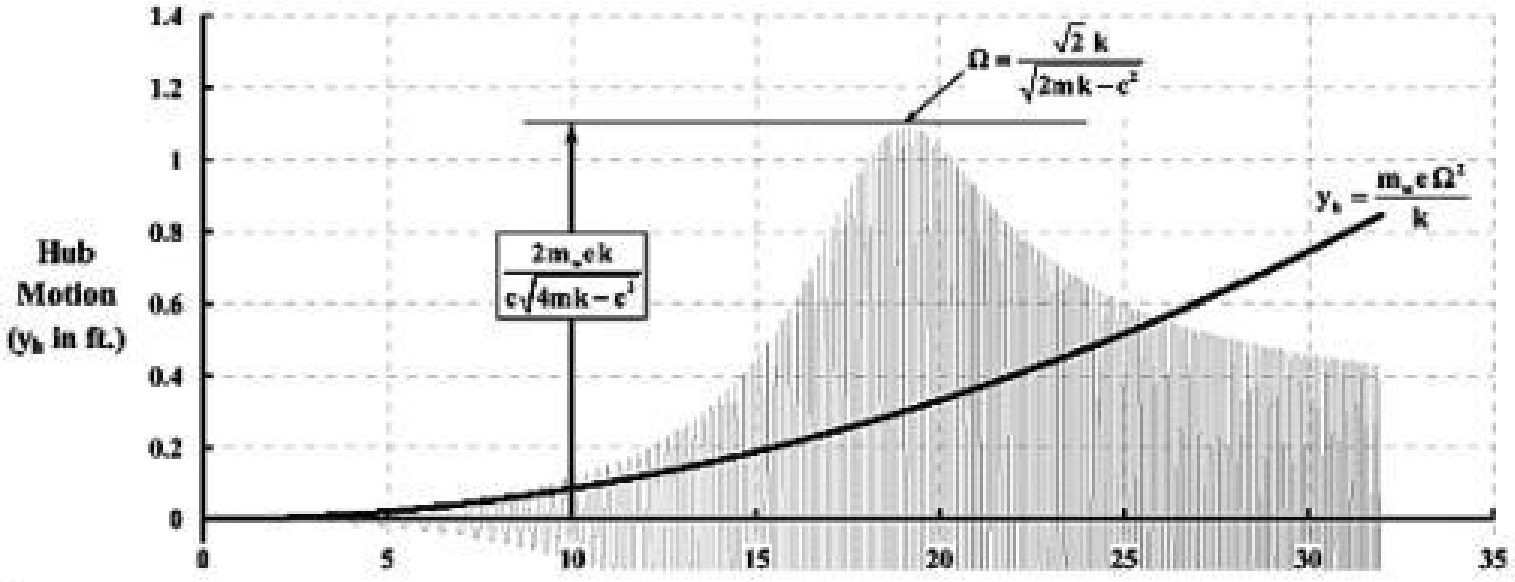

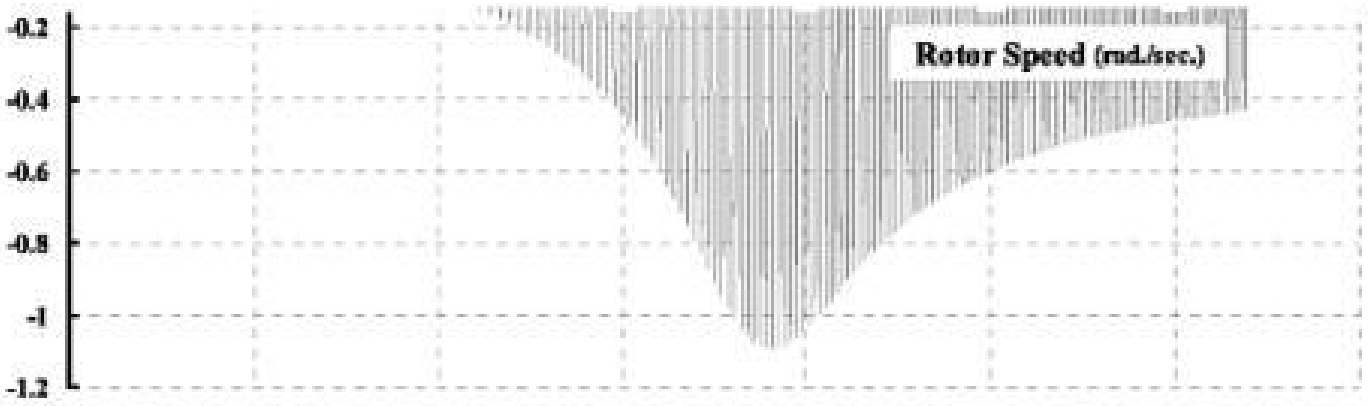

Fig. C-5. Possible resonance vibration during a rotor startup.

The heavy line in Fig. C-5 represents the maximum hub displacement if the *spring force was the only force* resisting the unbalance weight applied force. That is, from Eq. (18), the maximum hub displacement would be

$$y_h = \frac{m_w e \Omega^2}{k} \sin\left(\frac{\pi}{2}\right) \tag{22}$$

IF Ω = constant .

Notice that up to a rotor speed of about 26 radians per second, the dynamic system amplifies the applied unbalance rotating force. However, beyond 26 radians per second rotor speed, the dynamic system attenuates the response.

The fact that a resonance is possible should come as no surprise. Equation (20) presents the fact quite clearly. The question is simply, "What rotor speed will cause the maximum value of hub deflection (y_h)?" To begin with, no matter what the time (t) is in Eq. (20), the maximum hub displacement will occur when

$$\left[\Omega t - \arctan\left(\frac{c\Omega}{k - m\Omega^2}\right)\right] = \pm\pi/2 \quad \rightarrow$$

$$\sin(\pm\pi/2) = \pm 1.0 .$$

Therefore, the question becomes, "What value of rotor speed (Ω) makes the lead coefficient in Eq. (20) a maximum?" The usual mathematical steps to find the maximum of a function show that when

APPENDIX C

$$(23) \qquad \Omega = \frac{\sqrt{2}\ k}{\sqrt{2mk - c^2}}$$

the largest vibratory amplitude of hub displacement will occur. With values for this example from Table C-1, $\Omega = 19$ radians per second. The magnitude of this hub deflection will be

(24) $$\text{Maximum } y_h = \pm \frac{2 m_w e k}{c\sqrt{4mk - c^2}}.$$

Notice immediately that this result says that if there is no damping (i.e., $c = 0$), then the hub motion will be $\pm \infty$. Fortunately, with values for this example, maximum $y_h = \pm 1.092$ feet.

This example leads to very severe vibration. You can see this by approximated hub maximum acceleration (d^2y_h/dt^2) from Eqs. (23) and (24) as

calculating an

(25)

$$\text{Maximum } \frac{d^2 y_h}{dt^2} = \pm \frac{2 m_w e k}{c\sqrt{4mk - c^2}} \Omega^2 = \pm \frac{4 m_w e k^3}{c\left(2mk - c^2\right)\sqrt{4mk - c^2}}.$$

In this example, the maximum hub acceleration is 396 feet-per-second squared, which is slightly over 12 times the acceleration of gravity ($g = 32.17$ ft/sec^2). While the hub in this

example is some 13 feet above the ground, the pilot is perhaps 7 feet above the ground, so he would be feeling on the order of 7/13 times 12 g's or about 6.6 g's. The pilot would find this vibration level—to put it mildly—beyond intolerable.

Using such an extreme example makes three points. The first is that you now have some appreciation of dynamic technology. The second point is to always be on the lookout for resonance possibilities. The third point is that simple vibrations of the sort discussed above should never create more that 0.005 g's at any rotor speed. Pilots and passengers, radios, and other electronics, etc., are very sensitive to vibration.

Theory Application—Case 3, Varying Rotor Speed

In the rotorcraft world of dynamics, there is considerable danger in assuming that rotor speed is constant. This is particularly apparent for the situation when a pilot is bringing a rotor up to speed. To begin with, after the engine is started, a rotor clutch may be used to start the rotor turning, which could introduce a "jerk" into the system. After that, the rotor may well be brought up to speed in some nonlinear fashion. For this example then, I will assume a reasonable rotor startup where the instantaneous rotor speed is

$$\frac{d\psi}{dt} = \Omega_f \left[\frac{3}{2}\left(\frac{t}{T}\right)^2 - \frac{1}{2}\left(\frac{t}{T}\right)^6 \right] \tag{26}$$

where (Ω_f) is the final, constant rotor speed to be obtained in a time of (T) seconds. Since the rotor hub azimuth angle (ψ) is the integral of rotor speed, it follows from Eq. (26) that

APPENDIX C

(27) $$\psi = \int_0^t \frac{d\psi}{dt} dt = \Omega_f T \left[\frac{1}{2}\left(\frac{t}{T}\right)^3 - \frac{1}{14}\left(\frac{t}{T}\right)^7 \right]$$

and the acceleration is simply the second derivative with respect to time, so that

(28) $$\frac{d^2\psi}{dt^2} = \frac{\Omega_f}{T}\left[3\left(\frac{t}{T}\right) - 3\left(\frac{t}{T}\right)^5 \right].$$

Notice that I have carefully selected an approximation so that at time (t) equals zero, the instantaneous rotor speed is zero; and when time (t) equals the final time (T), the rotor speed equals the final rotor speed (Ω_f).

In the following study, I have assumed the rotor will reach a final rotor speed of

RPM_f = 230 rpm (Ω_f = 24 radians per second) in 60 seconds (T = 60 seconds). This input numerically defines ψ, $d\psi/dt$, and $d^2\psi/dt^2$ using Eqs. (27), (26), and (28) respectively. The basic differential equation (Eq. 17) repeated here for convenience, as

(29)

$$(m_h + m_w)\frac{d^2y_h}{dt^2} + c\frac{dy_h}{dt} + ky_h = m_w e \sin(\psi)\left[\frac{d\psi}{dt}\right]^2 - m_w e \cos(\psi)\left[\frac{d^2\psi}{dt^2}\right]$$

can now be solved using the configuration defined by Table C-1.

The solution of Eq. (29) is not easily obtained in simple closed form as in the case where a constant rotor speed was assumed. Therefore, I must interrupt this discussion to show one way of solving Eq. (29) given ψ, $d\psi/dt$, and $d^2\psi/dt^2$ from Eqs. (27), (26), and (28) respectively, with $\Omega_f = 24$ radians per second and T = 60 seconds.

Dynamists, by profession, are superb applied mathematicians. When faced with a

problem like Eq. (29), they seem to intuitively know that a solution in terms of elementary functions[5] is likely to be quite involved and of doubtful practical use. They most frequently turn instead to some numerical integration scheme. Today, applied mathematics software such as Mathematica and MathCad have tools quite capable of solving Eq. (29) in the blink of an

eye. But in "the old days" (before digital computers), I depended on some applied mathematics book[6] to construct a tailored numerical integration scheme that few of us—working together as human calculators—would solve with slide rules, pencils, and paper.

In 1991 Dewey Hodges, a professor at the Georgia Institute of Technology in Atlanta, Georgia, sent me a numerical integration approach that I have found very useful over the last 20 years. His method (a) is quite simple, (b) is very accurate, (c) minimizes numerically introduced damping, (d) is well suited to programming with spreadsheet tools like Microsoft® Excel®, and (e) allows

time-varying damper and spring terms . It goes like this:

---

[5] Things like sin(x) and ln(x) are rather common, and I would call them elementary functions. [6] William Milne, *Numerical Solution of Differential Equations*, John Wiley & Sons, Inc., New York, 1953.

APPENDIX C

$$\left(\frac{dy}{dt}\right)_{N+1} = \left[\frac{1-\omega^2(\Delta t/2)^2}{1+\omega^2(\Delta t/2)^2}\right]\left(\frac{dy}{dt}\right)_N - \left[\frac{\omega^2(\Delta t)}{1+\omega^2(\Delta t/2)^2}\right](y)_N + \left[\frac{(\Delta t)/m}{1+\omega^2(\Delta t/2)^2}\right]\left\{F_{(t)} - c_{(t)}\left(\frac{dy}{dt}\right) - k_{(t)}(y)\right\}_N \tag{30}$$

and

$$(y)_{N+1} = \left[\frac{\Delta t}{1+\omega^2(\Delta t/2)^2}\right]\left(\frac{dy}{dt}\right)_N + \left[\frac{1-\omega^2(\Delta t/2)^2}{1+\omega^2(\Delta t/2)^2}\right](y)_N + \left[\frac{(\Delta t)^2/2m}{1+\omega^2(\Delta t/2)^2}\right]\left\{F_{(t)} - c_{(t)}\left(\frac{dy}{dt}\right) - k_{(t)}(y)\right\}_N \tag{31}$$

Initially Dewey suggested that $k_{(t)}$ should be of the form $k_o + k_{(t)}$ so that $\omega = \sqrt{k_o / m}$. In recent discussions, Dewey could think of no reason that the frequency could not vary with time. This is an important point when studying rotor blade lead-lag motion, where ω_ξ equals a constant times rotor speed (Ω).

As applied to Eq. (29), where the mass, damper, and spring coefficients are constant, the numerical integration proceeds as follows:

$$(32)\qquad \left(\frac{dy}{dt}\right)_{N+1} = A_1\left(\frac{dy}{dt}\right)_N - A_2(y)_N + A_3\left\{F_{(t)} - c\left(\frac{dy}{dt}\right)\right\}_N$$

$$(y)_{N+1} = A_4\left(\frac{dy}{dt}\right)_N + A_5(y)_N + A_6\left\{F_{(t)} - c\left(\frac{dy}{dt}\right)\right\}_N$$

where the constants (i.e., A_1 through A_6) are as observed in Eqs. (30) and (31) and calculated using Table C-1, which gives $\omega = \sqrt{k_0 / m}$ or ω = 18.7122863344901 0 radians per second and the damping constant c = 228.47 pounds per foot per second. The constants A_1 through A_6 in Eq. (32) are immediately at hand as provided by Table C-2.

The force is, of course, from Eq. (29)

(33)

$$F_{(t)} = m_w e \sin(\psi)\left[\frac{d\psi}{dt}\right]^2 - m_w e \cos(\psi)\left[\frac{d^2\psi}{dt^2}\right]$$

where

(34)

$$\psi = \left(\frac{\Omega_r}{2T^2}\right)t^3 - \left(\frac{\Omega_r}{14T^6}\right)t^7,\ \frac{d\psi}{dt} = \left(\frac{3\Omega_r}{2T^2}\right)t^2 - \left(\frac{\Omega_r}{2T^6}\right)t^6,\ \frac{d^2\psi}{dt^2} = \left(\frac{3\Omega_r}{T^2}\right)t - \left(\frac{3\Omega_r}{T^6}\right)t^5.$$

Table C-2. Constants A_1 Through A_6

A1	+0.99982494049432500000		A4	+0.00099991247024716200000
A2	-0.35011901135076100000		A5	+0.99982494049432500000000
A3	+0.00002188243820942260		A6	+0.00000010942176870748 30

APPENDIX C

To set up Hodges' numerical integration, I will use the configuration described in Table C-1 and a time increment (Δt) of 0.001 seconds. The solution begins by

stating the initial conditions at time equals zero, which corresponds to N = 0. That is, $y_{N=0} = \text{input}$ and $(dy/dt)_{N=0} = \text{input}$.

A simple calculator (like a Microsoft® Excel® spreadsheet) makes short work of this computation using Eqs. (32), (33), and (34), and advancing time in very small steps. Given a column of $t_{N+1} = t_N + \Delta t$, and a second column of acceleration as $d^2\psi/dt^2$ radians-per-second squared, the third column calculates the instantaneous rotor speed as $(d\psi/dt)_N$. The fourth column calculates the time-varying azimuth angle as $\psi_N = 0.2t_N^2$, and a few more columns give a time history of hub motion (y_h) as the rotor comes up to speed.

The hub motion obtained by numerical integration during rotor startup with the unbalanced weight configuration of Fig. C-4 is shown in Fig. C-6. With increasing rotor speed, the resonance appears at a time (t) of about 48 seconds. At this moment

in time, the instantaneous rotor speed is just under 20 radians per second or about 190 revolutions per minute . The final rotor speed (24 radians per second) is reached in 60 seconds . There is little practical difference between this result and the quasi-steady result shown in Fig. C-5.

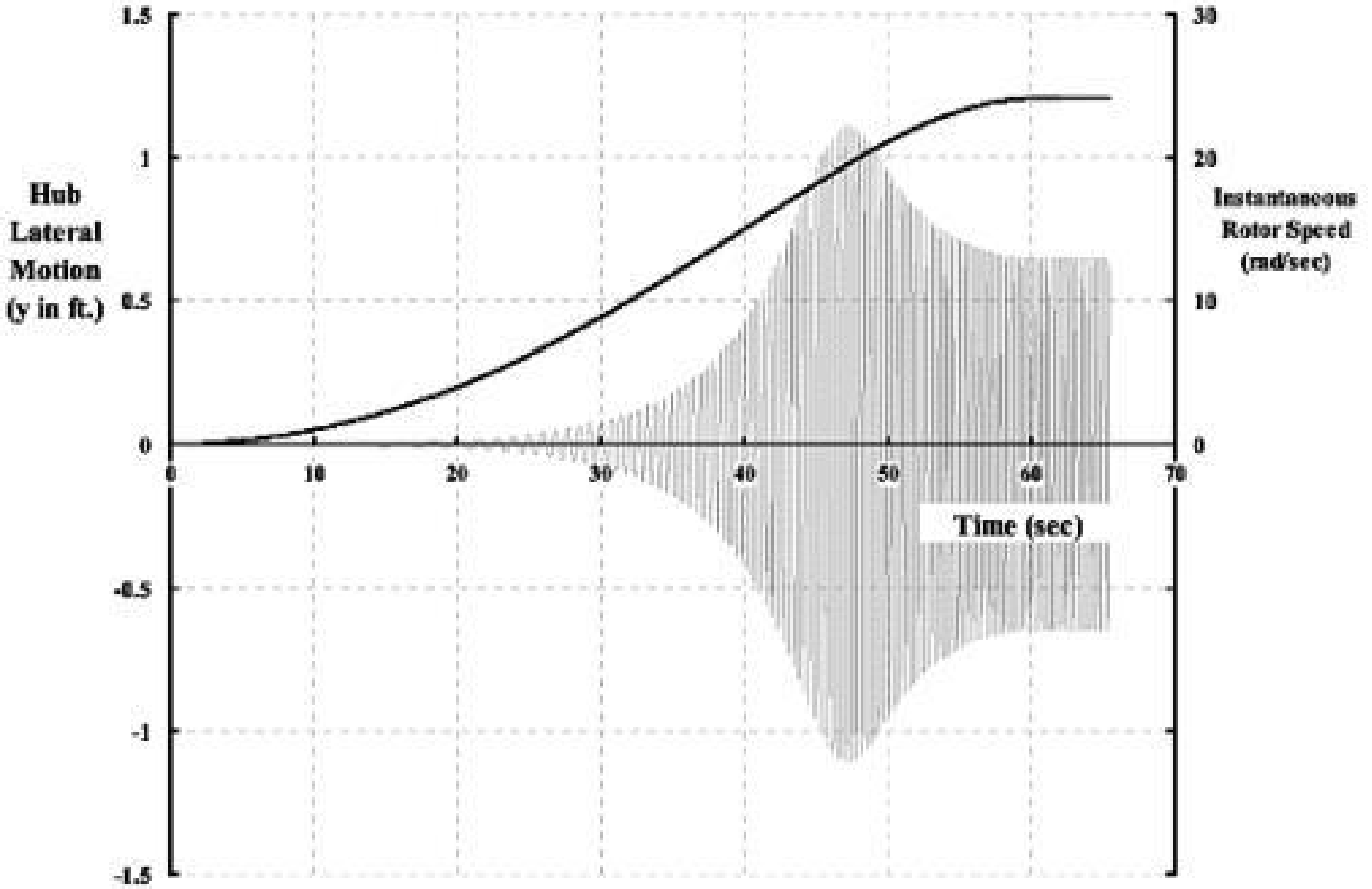

Fig. C-6. Hub motion during rotor startup

with an unbalanced weight.

APPENDIX C

Closing Remarks

The preceding paragraphs may well be considered "old hat" to many readers. On the other hand, those without an intimate daily use of these dynamics fundamentals may well find them useful. The Dewey Hodges' numerical integration scheme should be of considerable value to anyone wanting to obtain differential equation solutions using spreadsheet calculating tools. At any rate, the first half of Appendix C provides (in my view) a minimum discussion about vibration and the mathematics of dynamics that are required to examine ground resonance.

Now let me continue with a discussion of the ground resonance phenomena that destroyed the Kellett XR-2 autogyro in nearly the blink of an eye.

APPENDIX C

GROUND RESONANCE

Introduction

Technical literature tackles the ground resonance problem from many aspects . The basic objective has been to define stability and instability boundaries. These boundaries are quite different for a two-bladed rotor and rotors with three or more blades, all configurations having a lead-lag hinge or behaving as if they have a lag hinge. Occasionally one hears the statement that multi-bladed rotors behave differently than two-bladed rotors.[7] All of the

results I am aware of assume that rotor speed is constant. Therefore, let me first show you the analysis with a series of constant rotor speeds (Ω) and then with a normal rotor startup.

Basic Theory

The basics of ground resonance can be examined rather simply by adding *one blade* to the hub and using the weight from Fig. C-4 as a counterweight. This configuration is shown in Fig. C-7 . The blade is attached to the lead-lag hinge, and a viscous damper bridges across the hinge. The lead-lag hinge is located outward from the hub a distance (e) . The blade has uniform mass distribution so the blade center of gravity is located a distance (r_{cg}) from the lead-lag hinge . Therefore, the blade center of gravity is located a distance ($e + r_{cg}$) from the centerline of rotation *when* the lead-lag angle (ξ) is zero . The counterweight is mounted to what could be a lead-lag hinge for a second

blade and, therefore, at the same distance (e) from the centerline of rotation.

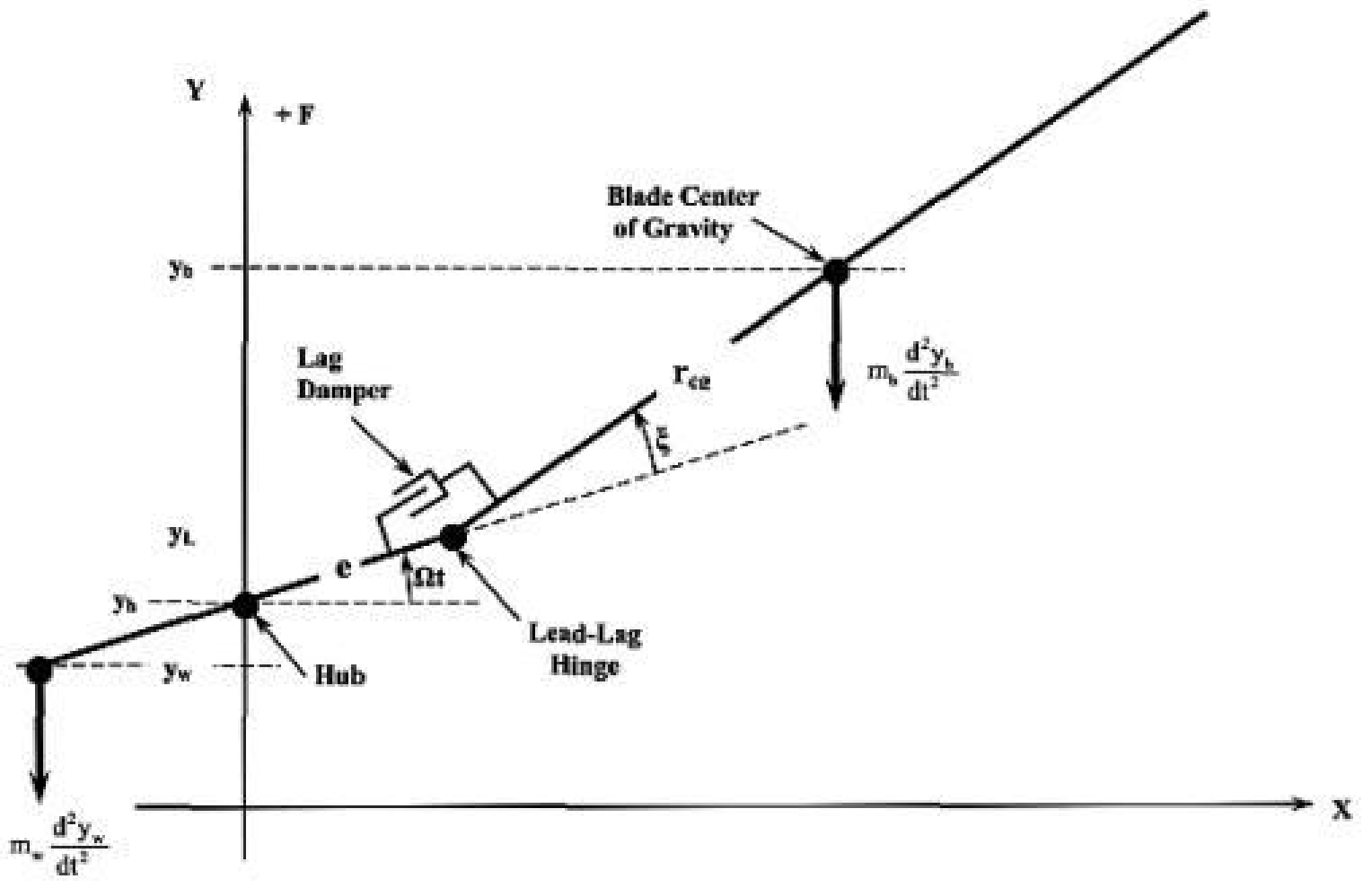

Fig. C-7. A counterbalanced one-bladed rotor system.

[7] I have always thought that the classification *multi* included a two-bladed rotor.

APPENDIX C

The equations of motion for this case, guided by Fig. C-7, require first adding the blade mass (m_b) times its acceleration (d^2y_b/dt^2) to Eq. (13) which gives

(35)

$$m_h \frac{d^2y_h}{dt^2} + c\frac{dy_h}{dt} + ky_h = F = -m_w \frac{d^2y_w}{dt^2} - m_b \frac{d^2y_b}{dt^2}.$$

However, in addition to this hub vibration equation, the blade lead-lag motion must also be taken into account. The equation from which lead-lag motion (ξ) is obtained comes by solving

(36)

$$I_b \frac{d^2\xi}{dt^2} + c_b \frac{d\xi}{dt} + I_b\omega_b^2\xi = -\left(m_b r_{cg} \frac{d^2y_h}{dt^2}\right)\cos(\psi + \xi)$$

where (I_b) is the second moment of inertia of the blade in slug-feet squared, and (c_b) is a

viscous lag damper constant in foot-pounds per radians per second. The inplane natural frequency (ω_b) of the blade in radians per second is frequently approximated as

$$\omega_b = \Omega\sqrt{\frac{3}{2}\left(\frac{e}{R-e}\right)}. \tag{37}$$

Notice immediately in Eq. (36) that the lead-lag motion is dependent on the hub acceleration (d^2y_h/dt^2). However, the hub motion is dependent on the lead-lag angular displacement (ξ) itself. The interaction (more precisely, the coupling) between the two motions occurs because

$$y_w = y_h + e\sin(\psi+180^\circ) = y_h - e\sin(\psi) \tag{38}$$

$$y_b = y_h + e\sin(\psi) + r_{cg}\sin(\psi+\xi)$$

It is the second derivative of these two displacements (y_w and y_b) with respect to time that is required. Thus, for the counterbalance weight, the acceleration required by Eq. (35) is

(39)

$$\frac{d^2y_w}{dt^2} = \frac{d^2y_h}{dt^2} + e\sin(\psi)\left[\frac{d\psi}{dt}\right]^2 - e\cos(\psi)\left[\frac{d^2\psi}{dt^2}\right].$$

The blade acceleration (d^2y_b/dt^2) required by Eq. (35)—while a somewhat longer expression because of the lead-lag terms—is simply

(40)

$$\frac{d^2y_b}{dt^2} = \frac{d^2y_h}{dt^2} - e\sin(\psi)\left[\frac{d\psi}{dt}\right]^2 + e\cos(\psi)\left[\frac{d^2\psi}{dt^2}\right] - r_{cg}\sin(\psi+\xi)\left[\frac{d(\psi+\xi)}{dt}\right]^2 + r_{cg}\cos(\psi+\xi)\left[\frac{d^2(\psi+\xi)}{dt^2}\right].$$

Case 1. One Blade, Counterbalanced, at Several Rotor Speeds

Imagine the pilot starting the rotor up with the blade in the lead position shown in Fig. C-7, and suppose neither the pilot nor the ground crew are aware (for whatever reason)

that the blade-lag damper has locked up and is holding the blade in the lead position. Finally, assume that at some rotor speed the lag damper breaks free and lead-lag motion is allowed in

the normal operating manner. The small question is, "Will the pilot sense a vibration due to the locked-up blade, get worried, and shut the engine down?" The bigger question is, "If he accepts the warning vibration, stops increasing rotor speed ($d\psi/dt$ becomes constant at $d\psi/dt = \Omega$) to investigate, and then the lag damper breaks free, what are the resulting blade lead-lag and hub motions?"

Let me answer the small question first. Consider a normal startup with the blade in a

locked position with a lead angle (ξ_0) of, say, 0.01 radian, which is just over one-half degree. With a fixed lead angle, no angular velocity or acceleration can occur, which means that $d\xi/dt = 0$ and $d^2\xi/dt^2 = 0$. Now I will again assume a quasi-steady increase in rotor speed so that at each rotor speed where data might be taken, $d^2\psi/dt^2 = 0$. Finally, let me also assume that the lead-lag angle is small for this case, so that

(41)

$$\sin(\Omega t + \xi) = \sin(\Omega t)\cos\xi + \cos(\Omega t)\sin\xi \approx \sin(\Omega t) + \xi\cos(\Omega t)$$
$$\cos(\Omega t + \xi) = \cos(\Omega t)\cos\xi - \sin(\Omega t)\sin\xi \approx \cos(\Omega t) - \xi\sin(\Omega t)$$

Now comes the four steps where considerable care must be taken. First, substitute the weight and blade acceleration equations [Eqs. (39) and (40) respectively] into the hub motion equation, Eq. (35). Second, simplify this result using the small angle assumption given by Eq. (41), and set $d\psi/dt = \Omega$ and $d^2\psi/dt^2 = 0$. Third, rearrange the results of step two to see what further simplification can be made. Fourth,

make the further simplifications.

To proceed then, from the first step you have:

$$m_h \frac{d^2 y_h}{dt^2} + c\frac{dy_h}{dt} + ky_h = -m_w \left\{ \frac{d^2 y_h}{dt^2} + e\sin(\psi)\left[\frac{d\psi}{dt}\right]^2 - e\cos(\psi)\left[\frac{d^2\psi}{dt^2}\right] \right\}$$

(42)

$$-m_b \begin{Bmatrix} \frac{d^2 y_h}{dt^2} - e\sin(\psi)\left[\frac{d\psi}{dt}\right]^2 + e\cos(\psi)\left[\frac{d^2\psi}{dt^2}\right] \\ -r_{cg}\sin(\psi+\xi)\left[\frac{d\psi}{dt} + \frac{d\xi}{dt}\right]^2 \\ +r_{cg}\cos(\psi+\xi)\left[\frac{d^2\psi}{dt^2} + \frac{d^2\xi}{dt^2}\right] \end{Bmatrix}.$$

Then from the second step (i.e., simplification with assumptions), you obtain

$$m_h \frac{d^2 y_h}{dt^2} + c\frac{dy_h}{dt} + ky_h = -m_w \left\{ \frac{d^2 y_h}{dt^2} + e\sin(\psi)[\Omega]^2 \right\}$$

(43)

$$-m_b \begin{Bmatrix} \frac{d^2 y_h}{dt^2} - e\sin(\psi)[\Omega]^2 \\ -r_{cg}\left[\sin(\psi) + \xi\cos(\psi)\right][\Omega]^2 \end{Bmatrix}.$$

APPENDIX C

The third step is taken because you see that some rearrangement can be made. So

(44)

$$m_h \frac{d^2 y_h}{dt^2} + c\frac{dy_h}{dt} + k y_h = -(m_w + m_b)\frac{d^2 y_h}{dt^2} - m_w e\Omega^2 \sin(\psi)$$

.

$$+ m_b (e + r_{cg})\Omega^2 \sin(\psi) + m_b r_{cg}\xi\Omega^2 \cos(\psi)$$

Now you can see that both the counterbalance mass and blade mass times the hub acceleration should be moved to the left side of Eq. (44). Furthermore, since the centrifugal force of the counterbalance weight equals the centrifugal force of the blade, these two forces cancel out. That is,

$$\left[-m_w e\Omega^2 \sin(\psi) + m_b\left(e + r_{cg}\right)\Omega^2 \sin(\psi)\right] = 0.$$

Finally, because the blade is locked at a lead angle, ξ must be replaced with ξ_0. With these finishing touches, you see that the hub is shaken by the relatively small unbalance caused by the blade being locked in the lead position (ξ_0). Therefore, the hub motion of the locked-blade system is described quite familiarly as

(45)

$$\left(m_h + m_w + m_b\right)\frac{d^2 y_h}{dt^2} + c\frac{dy_h}{dt} + k y_h = \left(m_b r_{cg} \xi_0 \Omega^2\right)\cos(\psi).$$

Now define $m_h + m_w + m_b = m$ and recognize that with a constant rotor speed ($\psi = \Omega t$), the solution to Eq. (45) is

(46)

$$y_h = \frac{\left(m_b r_{cg} \xi_0 \Omega^2\right)}{\left(k - m\Omega^2\right)^2 + (c\Omega)^2}\left[\left(k - m\Omega^2\right)\cos(\Omega t) + (c\Omega)\sin(\Omega t)\right],$$

or in phase angle form, which illuminates the vibration's amplitude, you have (47)

$$y_h = \frac{\left(m_b r_{cg} \xi_0 \Omega^2\right)}{\sqrt{\left(k - m\Omega^2\right)^2 + (c\Omega)^2}} \left\{ \cos\left[\Omega t - \arctan\left(\frac{c\Omega}{k - m\Omega^2} \right) \right] \right\}.$$

As the pilot brings the rotor slowly up to speed, the unbalance will begin to vibrate the hub, rock the machine, and shake the pilot. The maximum amplitude of hub acceleration will vary with rotor speed as you learned from Basic Dynamics. That is,

(48) $$\text{Max.} \frac{d^2 y_h}{dt^2} = \pm \left[\frac{\left(m_b r_{cg} \xi_0\right)\Omega^2}{\sqrt{\left(k - m\Omega^2\right)^2 + (c\Omega)^2}} \right] \Omega^2.$$

To numerically study the situation, use the physical properties of the system provided in Table C-3 and, since this is a practical problem under discussion, let me express rotor speed (Ω) not in radians per second, but in revolutions per minute (RPM $= 30\Omega/\pi$). Furthermore, I will measure hub acceleration not in

dividing d^2y_h/dt^2 by 32.17 ft/sec^2.

feet-per-second squared, but in g's, which means

APPENDIX C

Table C-3. Physical Properties

Autogyro Properties	Symbol	Value	Units
Aircraft weight	GW	1,900	lbs
Blade radius	R	21.25	ft
Hub height above the ground	H_{hub}	13.0	ft
Pilot height above the ground	H_{pilot}	7.0	ft
Landing gear spread	x_{lg}	12.0	ft
Apparent autogyro spring stiffness at the hub	k	16,000.0	lbs/ft
Apparent autogyro weight at hub	W_h	1,300.0	lbs
Apparent autogyro mass at the hub	m_h	40.410320	slugs
Apparent damping coefficient of the autogyro	c	228.470	lbs/fps
Blade Properties			
Weight	w_b	40.0	lbs
Mass	m_b	1.2433945	slugs
Spanwise center of gravity	r_{cg}	9.3750	ft
Centrifugal force	CF_b	9,228.3	lbs
Lead-lag hinge location	e	2.50	ft
Lag frequency per rev	ω_ζ/Ω	0.20000	per rev
Running mass (m_b) outboard of lag hinge	$\Delta m_b/\Delta r$	0.066314372	slugs/ft
Lag moment of inertia	I_ζ	211.7656201	slug-ft^2
Lag damper coefficient	c_ζ	15.00	ft-lbs per rad/sec
Counterweight Properties			
Weight	W_w	190.0	lbs
Mass	m_w	5.9061237	slugs
Radial location	e	2.50	ft
Counterweight centrifugal force	CF_w	9,228.3	lbs

The maximum acceleration of the hub (and what the pilot feels sitting well below the rotor) varies with RPM as shown in Fig. C-8 when the blade-lag damper remains locked up at the lead angle (ξ_0) of 0.01 radians, which is only 0.57 degrees. Because the aircraft is assumed to be rocking about a point on the ground (see Fig. C-2), pilot acceleration equals 7/13 times hub acceleration.

The smaller question was, "Will the pilot sense a vibration due to the locked-up blade, get worried, and shut the engine down?" I would suggest, based on Fig. C-8, that autogyro engineers and pilots in this pioneering era would have accepted this maximum vibration level at the cockpit and would not have been unduly alarmed.

Now consider the bigger question, "If the pilot accepts the warning vibration, but stops increasing rotor speed to investigate (i.e., Ω becomes a constant), and then the locked-up blade breaks free, what are the resulting blade lead-lag and hub motions?" To answer this question, imagine that during the Kellett XR-2 test (of over-speeding the rotor for jump takeoff), ground resonance was encountered with this sequence of events:

a. The rotor speed for jump takeoff has been

determined to be 230 rpm.

APPENDIX C

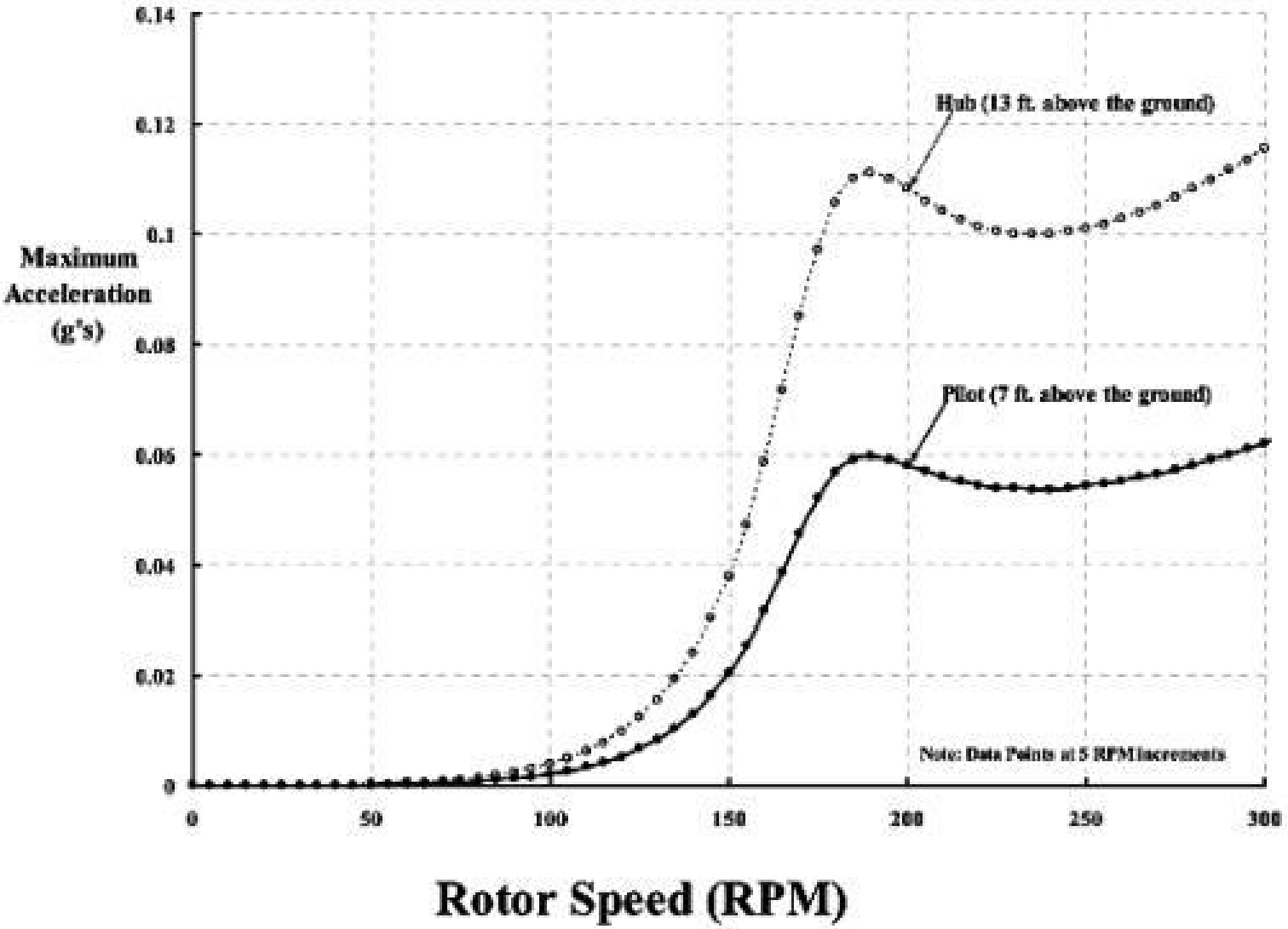

Fig. C-8. Vibration caused by a blade not being exactly counterbalanced.

b. The engineers and the pilot agree to run the rotor up from 0 to 230 rpm, taking data in 5-rpm steps.

c. Data taken at each step shows cockpit accelerations that follow Fig. C-8.

d. Everyone has become comfortable because whatever was causing the vibration to increase up to 0.06 g's at 190 rpm has stopped and, at higher RPM points, the vibration even appears to be decreasing.

d. When the test objective of 230 rpm is reached and the pilot is holding at a constant 230 rpm, the lag damper, for one reason or another, unlocks and *completely fails to provide damping.*

e. Lead-lag motion begins—*with a zero value for the blade damping constant* ($c_b = 0$).

f. And, in well under 15 seconds, the Kellett XR-2 is destroyed. The blade lead-lag motion precipitating the destruction is shown in Fig. C-9 and the resulting hub acceleration in Fig. C-10. The reason I show destruction within 15 seconds is because the hub force is so great that the autogyro structure that supports the rotor is likely to be ripped off the top of the fuselage. The maximum magnitude of this force is

(49)

$$\text{Max. } F = ma = \left(\frac{W_h + W_w + W_b}{g} \right) \frac{d^2 y_h}{dt^2} = (W_h + W_w + W_b) \left(\frac{d^2 y_h / dt^2}{g} \right).$$

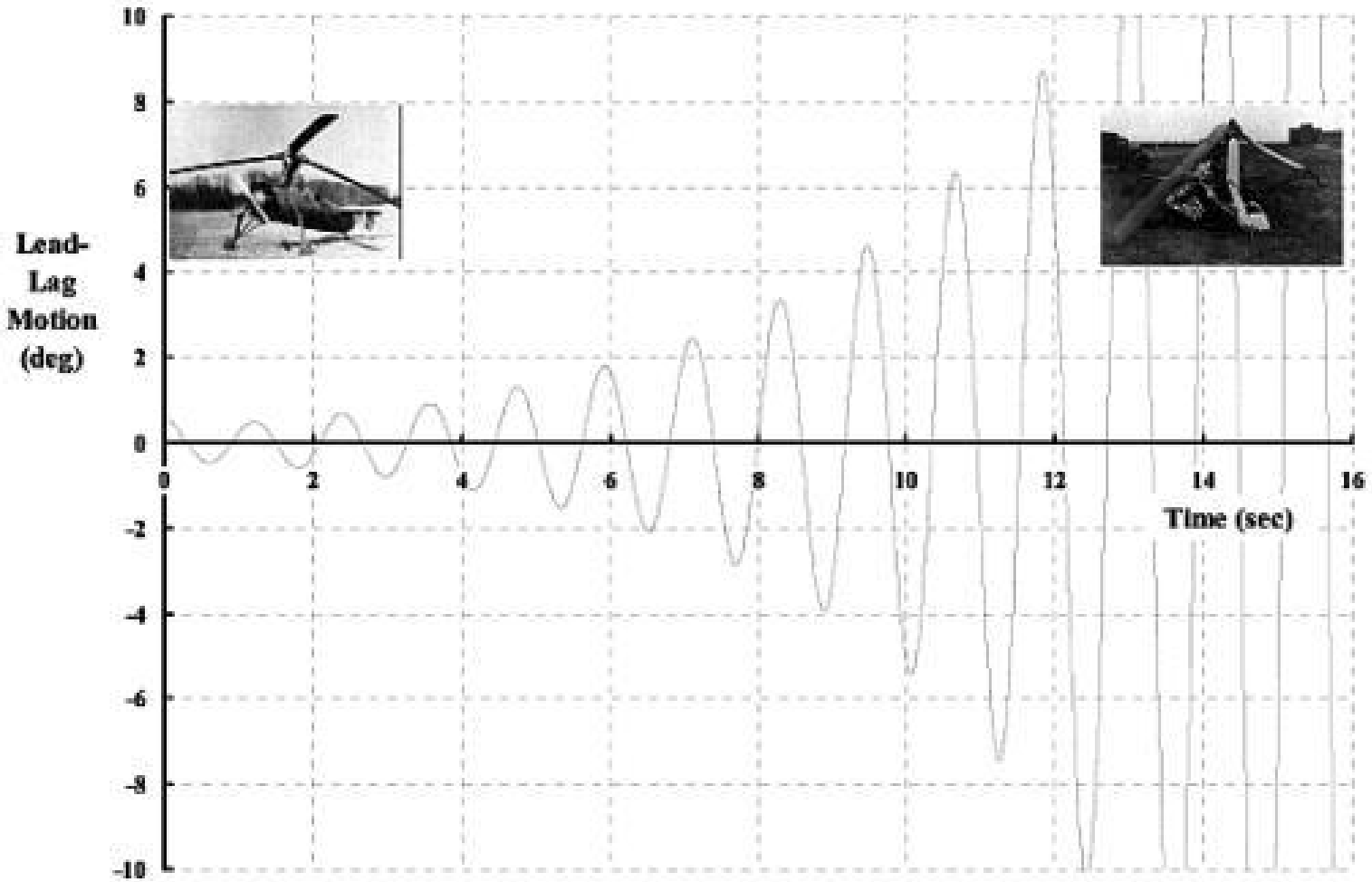

Fig. C-9. Rapid divergence of blade motion during ground resonance.

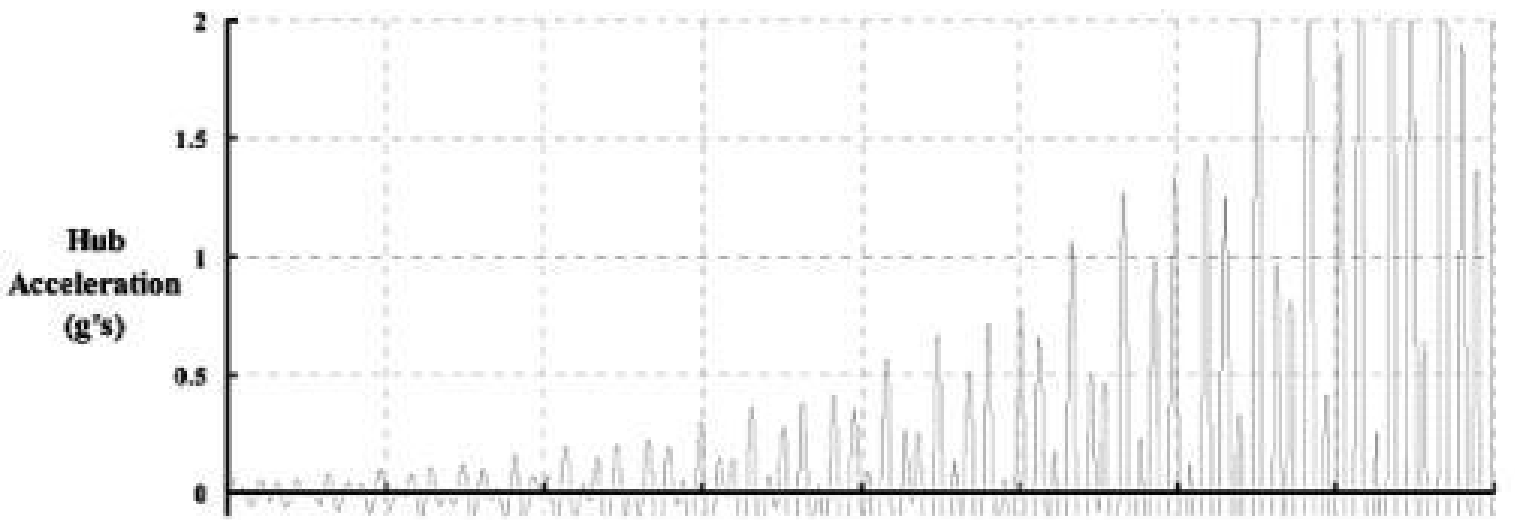

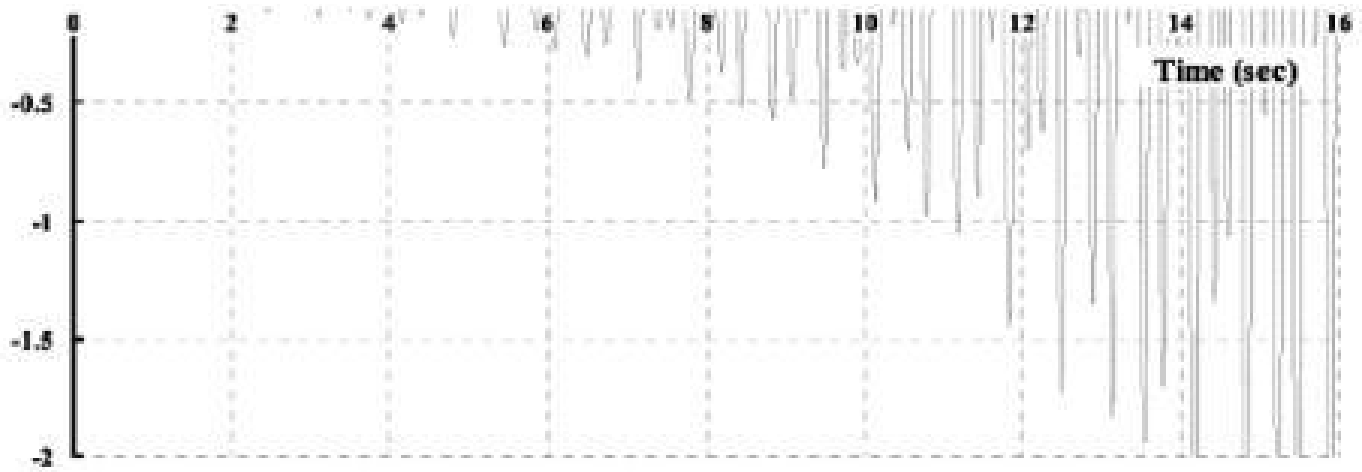

Fig. C-10. Rapid buildup in hub vibration during ground resonance.

APPENDIX C

From Table C-3, the total weight being vibrated is 1,530 pounds, and if the maximum acceleration is 10 g's, the vibratory force has an amplitude of ±15,300 pounds. It is not hard to argue that the machine came apart in under 1 1 seconds because of 1,530 pounds of force.

Now, let me explain how the time histories displayed in Fig. C-9 and Fig. C- 10 were

obtained. I started the time history assuming that at time (t) equals zero the rotor speed was constant at 230 rpm, so $d\psi/dt = \Omega = 24.086$ radians per second, $d^2\psi/dt^2 = 0$, and $\psi = \Omega t$.

Making no small angle assumptions, the general hub motion equation, Eq. (42), and lead-lag equation, Eq. (36), become

(50)

$$(m_h + m_w + m_b)\frac{d^2y_h}{dt^2} + c\frac{dy_h}{dt} + ky_h = -m_w e\Omega^2 \sin(\Omega t) + m_b e\Omega^2 \sin(\Omega t)$$

and

$$+ m_b r_{cg}\left[\Omega + \frac{d\xi}{dt}\right]^2 \sin(\Omega t + \xi) - m_b r_{cg}\left[\frac{d^2\xi}{dt^2}\right]\cos(\Omega t + \xi)$$

(51)

$$I_b \frac{d^2\xi}{dt^2} + c_b \frac{d\xi}{dt} + I_b \omega_b^2 \xi = -\left(m_b r_{cg} \frac{d^2 y_h}{dt^2} \right) \cos(\Omega t + \xi) .$$

The calculation was rather simple using the previously discussed Dewey Hodges' numerical integrator to solve the two equations. The Hodges' solver was set up using a Microsoft® Excel® spreadsheet. The initial conditions came from the locked-blade solution so that at zero time (t), the blade lead-lag angle was at $\xi_0 = 0.01$ radians, and the hub displacement (y_h) was zero. The hub velocity ($dy_h/dt = -0.18$ ft/sec) and acceleration ($d^2y_h/dt^2 = 0.00562$ ft/sec^2) corresponded to the beginning of a cycle when $y_h = 0$ at 230 rpm. The first spreadsheet row set the initial conditions. The second and following rows computed lead-lag angle first, and then hub displacement, velocity, and acceleration.

The preceding example leads to a very important question dealing with the amount of lead-lag damping required for at least neutral

stability. Neutral stability means the oscillation will continue indefinitely, neither growing in amplitude nor subsiding. For the results shown in Fig. C-9 and Fig. C-10, I selected a rotor speed of 230 rpm and assumed that the lag damper completely failed. In reality, the blade might have unlocked at any rotor speed. Therefore, the amount of damping required to avoid autogyro destruction at all rotor speeds is of considerable interest. Figure C-11 shows the amount of damping required to ensure at least neutral stability as a function of rotor speed. These results were calculated using the configuration data from Table C-3.

There is a somewhat general rule of thumb as to what rotor speed will definitely cause ground resonance if the system is under damped. The basis for this rule is well explained by Bramwell.[8] In equation form, the rule is that when:

$$\Omega - \omega_b = \omega_h \quad \rightarrow \quad \Omega = \omega_h + \omega_b \tag{52}$$

there is the potential for ground resonance. That is, if the sum of aircraft natural frequency (ω_h) and blade lead-lag frequency (ω_b) equals the rotor speed (Ω), then there is an ensured

---

[8] A.R.S. Bramwell, *Helicopter Dynamics*, John Wiley & Sons, New York, 1976, pp. 379–382.

APPENDIX C

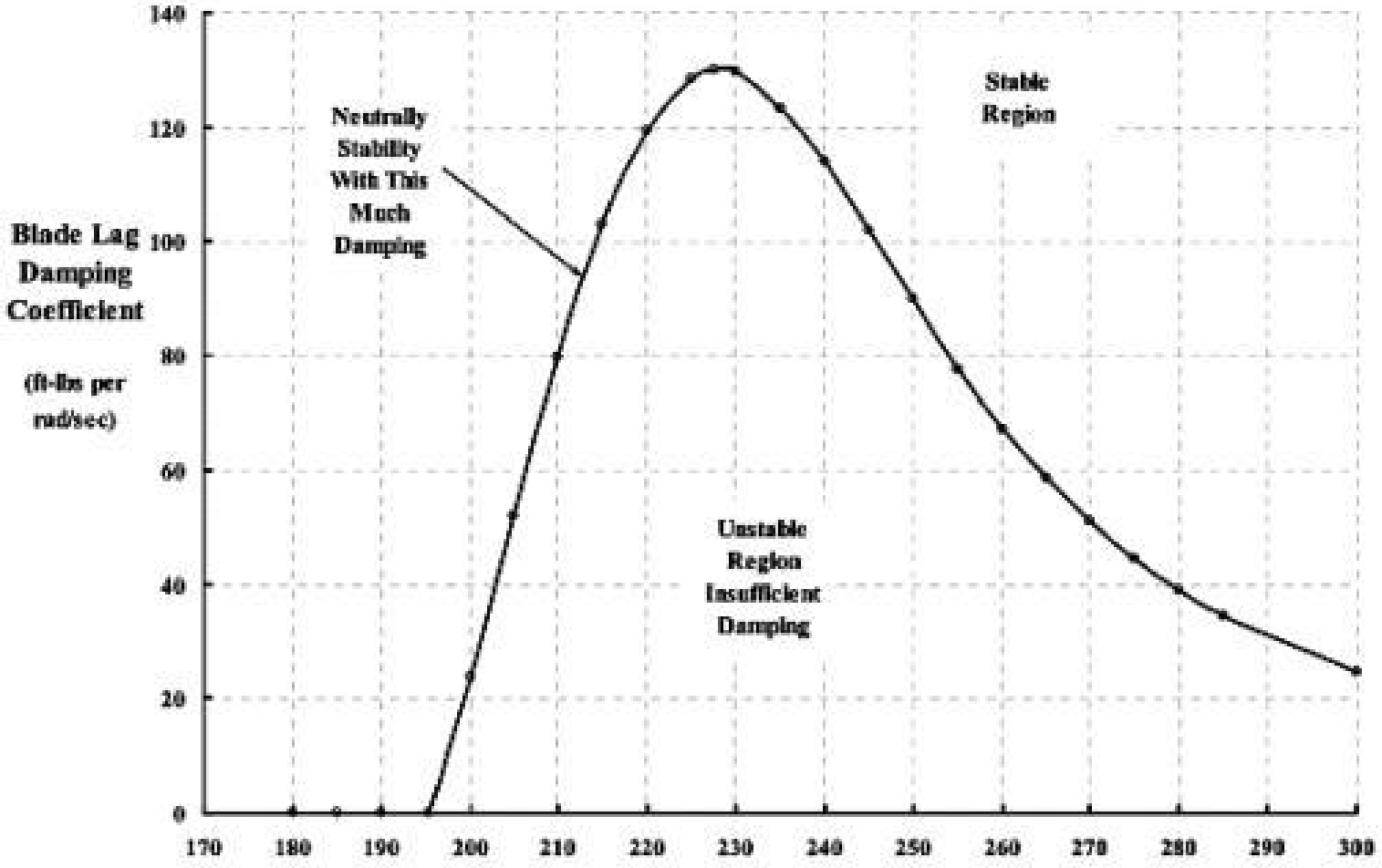

Fig. C-11. Lag damping required for neutral stability of ground resonance.

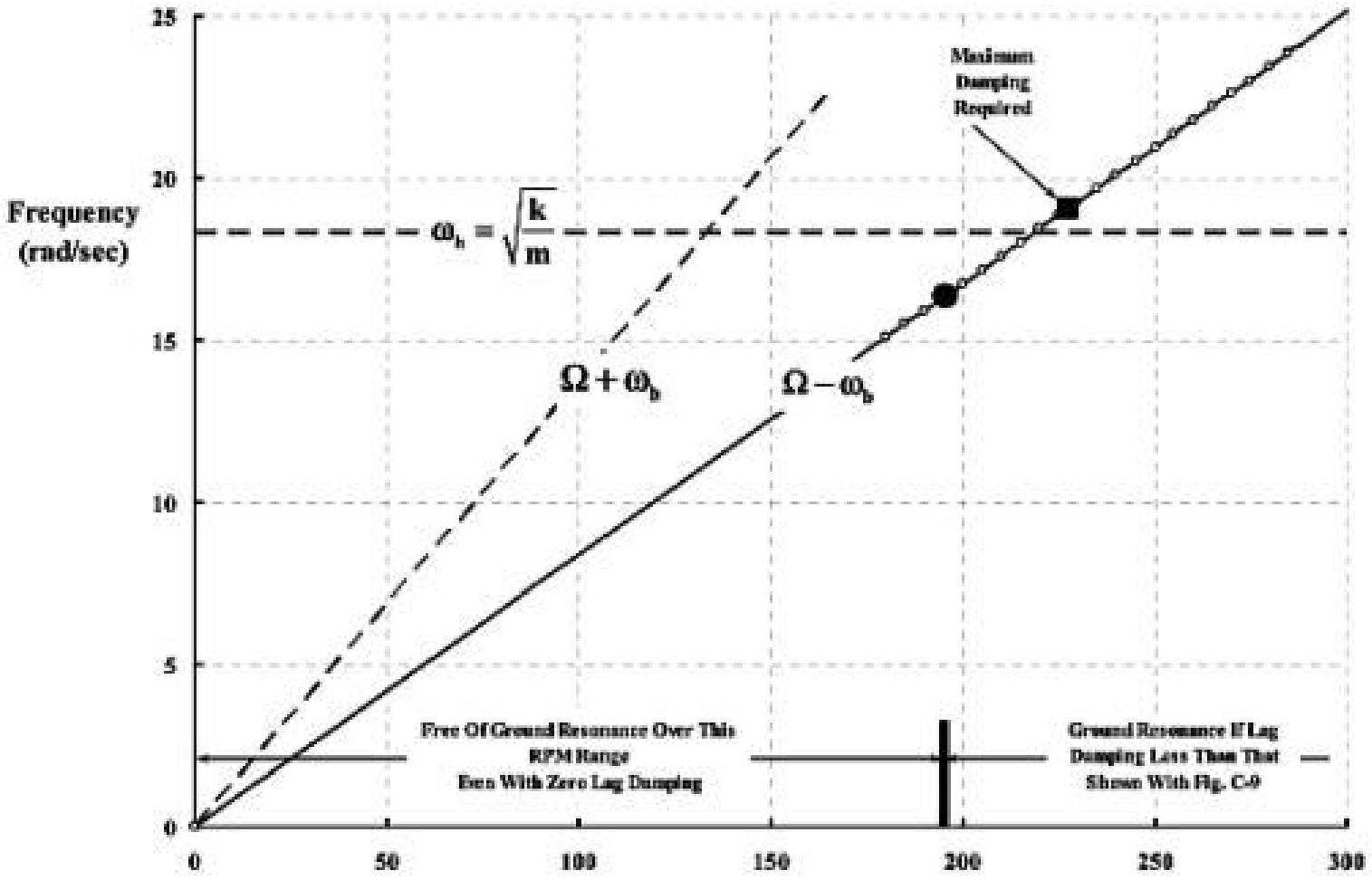

Fig. C-12. Two branches of the coupled blade-hub vibration problem.

potential for ground resonance. As Fig. C-12

shows, this rule is approximately correct, but should be considered rather optimistic. The potential for ground resonance actually begins at a lower rotor speed than Eq. (52) suggests. Only a very thorough dynamic analysis offers some assurance that a rotorcraft design will be safe from the destruction that will occur if ground resonance is encountered. Lastly, as you will note in Fig. C-12, there is a second branch of lead-lag motion that can occur. This second branch involves lead-lag motion at a frequency of $\Omega + \omega_b$, and this blade motion can coalesce with the hub natural frequency. That is, there is potential for a forced vibration resonance when

$$(53) \qquad \Omega + \omega_b = \omega_h \quad \rightarrow \quad \Omega = \omega_h - \omega_b \, .$$

Advanced dynamics study has determined that a ground resonance situation cannot occur in this branch of the blade-hub vibration problem.

Case 2. One Blade, Counterbalanced, with Rotor Speed Acceleration

The preceding paragraphs examined just the ground resonance branch (i.e., the $\Omega - \omega_b$ line) shown in Fig. C-1 2 . This solution branch is associated with the vibration mode controlled by the blade lead-lag motion, which can create such large forces that the whole machine can be shaken to bits in a matter of seconds—*if there is insufficient damping.* There is, in fact, a second solution branch (i.e., the $\Omega + \omega_b$ line) shown in Fig. C-12 where the vibration is controlled by the hub motion, and the blade lead-lag motion is a simple forcing function akin to the problem examined in Fig. C-4 . In both solution branches there is the possibility of a resonance, but it is only the $\Omega - \omega_b$ branch that is of real concern. I have used a rotor startup example so you can see both solution branches and

associated potential resonances.

For this case, I will again assume that the pilot starts the rotor up following Eq. (34), which is repeated here as

(34)

$$\psi = \left(\frac{\Omega_f}{2T^2}\right)t^3 - \left(\frac{\Omega_f}{14T^6}\right)t^7,\ \frac{d\psi}{dt} = \left(\frac{3\Omega_f}{2T^2}\right)t^2 - \left(\frac{\Omega_f}{2T^6}\right)t^6,\ \frac{d^2\psi}{dt^2} = \left(\frac{3\Omega_f}{T^2}\right)t - \left(\frac{3\Omega_f}{T^6}\right)t^5.$$

With a final rotor speed (Ω_f) of 230 rpm (times $\pi/30$ to get radians per second) reached in T = 50 seconds, the displacement (ψ), velocity ($d\psi/dt$), and acceleration ($d^2\psi/dt^2$) describe a reasonable rotor startup model for the solution of the hub motion equation given earlier as

$$(m_h + m_w + m_b)\frac{d^2y_h}{dt^2} + c\frac{dy_h}{dt} + ky_h = \left\{m_w e\cos(\psi)\left[\frac{d^2\psi}{dt^2}\right] - m_w e\sin(\psi)\left[\frac{d\psi}{dt}\right]^2\right\}$$

(54)

$$+\left\{\begin{array}{l} m_b e \sin(\psi)\left[\frac{d\psi}{dt}\right]^2 - m_b e \cos(\psi)\left[\frac{d^2\psi}{dt^2}\right] \\ m_b r_{cg} \sin(\psi+\xi)\left[\frac{d\psi}{dt}+\frac{d\xi}{dt}\right]^2 \\ -m_b r_{cg} \cos(\psi+\xi)\left[\frac{d^2\psi}{dt^2}+\frac{d^2\xi}{dt^2}\right] \end{array}\right\}.$$

APPENDIX C

Of course, the blade lead-lag equation does not change, so, to repeat,

(55)

$$I_b \frac{d^2\xi}{dt^2} + c_b \frac{d\xi}{dt} + I_b \omega_b^2 \xi = -\left(m_b r_{cg} \frac{d^2 y_h}{dt^2}\right)\cos(\psi+\xi).$$

Again, the actual calculation was rather simple using the previously discussed Hodges' numerical integrator to solve the two coupled equations, (54) and (55). The solver was set up using a Microsoft® Excel® spreadsheet. The initial conditions required by the two

equations were simply that the blade was against the lead stop (i.e., $\xi_0 = +5$ degrees) and the rotor was at rest ($y_h = dy_h/dt = d^2y_h/dt^2 = 0$). Of course, time (t) began at zero. The configuration again followed Table C-3, and I set the blade-lag damper (c_b) to a nominal value of 60 foot-pounds per radian per second. This is enough damping to bring the rotor blade to nearly a straight-out position at relatively low rotor speed; but not enough damping to avoid ground resonance. The results of this calculation are shown in Fig. C-13 and Fig. C-14.

As you can see from Fig. C-13, the blade started from a lead stop position of 5 degrees, which can often be a quite normal

position after shutting down from the previous flight. The lag damper value of 60 foot-pounds per radian per second is sufficient to damp the oscillating blade motion to a straight-out position ($\xi = 0$ degrees) in about 35 seconds. (In reality, a more realistic value of lag damping would be about 200 to 250 foot-pounds per radian per second in which case the lead-lag position becomes zero in about 20 seconds. However, with a higher blade-lag damping constant, the time histories show no deflections in blade or hub motion after 1 5 seconds, and my example would be less interesting.)

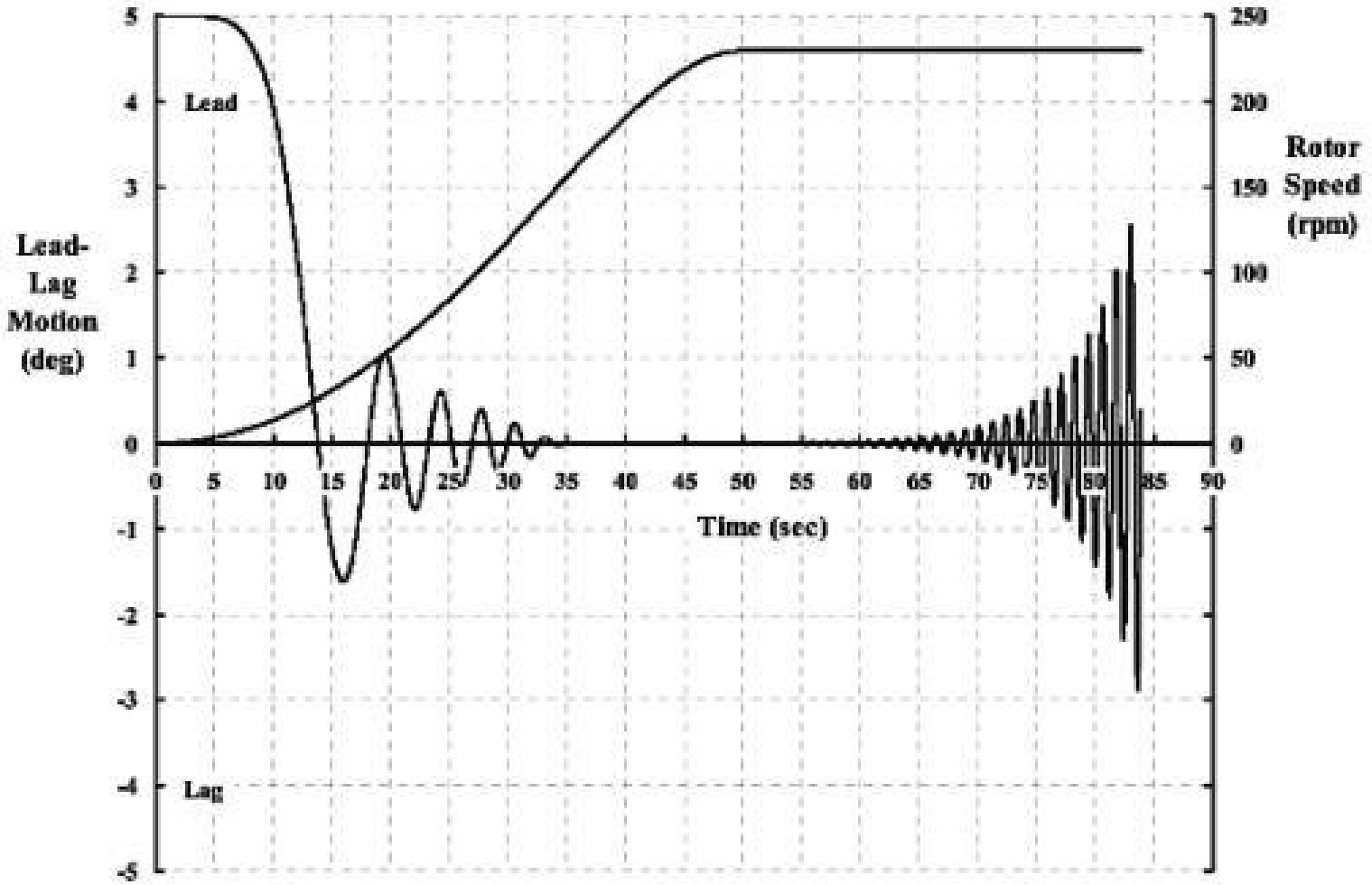

Fig. C-13. Blade motion during rotor startup.

APPENDIX C

Notice that the blade motion is virtually zero at 35 seconds. In fact, there is a very small vibratory amplitude of under ±0.01 degree between 25 and 35 seconds that is

sufficient to excite hub motion at the ω_h frequency intersection with the lead-lag motion frequency of $\Omega + \omega_b$ shown in Fig. C-12. The resulting forced hub vibration is visible in Fig. C-14. Obviously, the ordinate scale in Fig. C-13 obscures this information. This residual lead-lag motion serves as enough excitation to create the beginnings of ground resonance around 50 seconds into the rotor startup where the final rotor speed of 230 rpm is reached. (From Fig. C-11, at least 130 foot-pounds per radian per second of lag damping is required just for neutral stability of blade lead-lag motion, so my choice of c_b equal to 60 foot-pounds per radian per second has ensured that ground resonance will occur.)

It is the hub vibration time history during this rotor startup example that shows both solution branches (i.e., $\Omega + \omega_b$ and $\Omega - \omega_b$) of this dynamics problem. Figure C-14 shows the time history of hub acceleration in units of

gravity. You can immediately see that a damped resonance is passed through in the 25- to 35-second period after rotor startup is begun. This is associated with the ω_h frequency intersection with the lead-lag, $\Omega + \omega_b$ frequency in Fig. C-12. However, with the small amount of lag damping and the landing gear shock absorber damping, the hub acceleration is not greater than $\pm$ 0.2 g's. The pilot, located well below the hub, would probably feel only about $\pm$ 0.1 g's and not be unduly alarmed. He would quite naturally be satisfied that the final rotor speed of 230 rpm had been achieved without incident. By 60 seconds into the startup, I would think the test pilot would become aware of a new and growing vibration, but by then—without prior experience—it would be too late. The destruction of the machine would be inevitable.

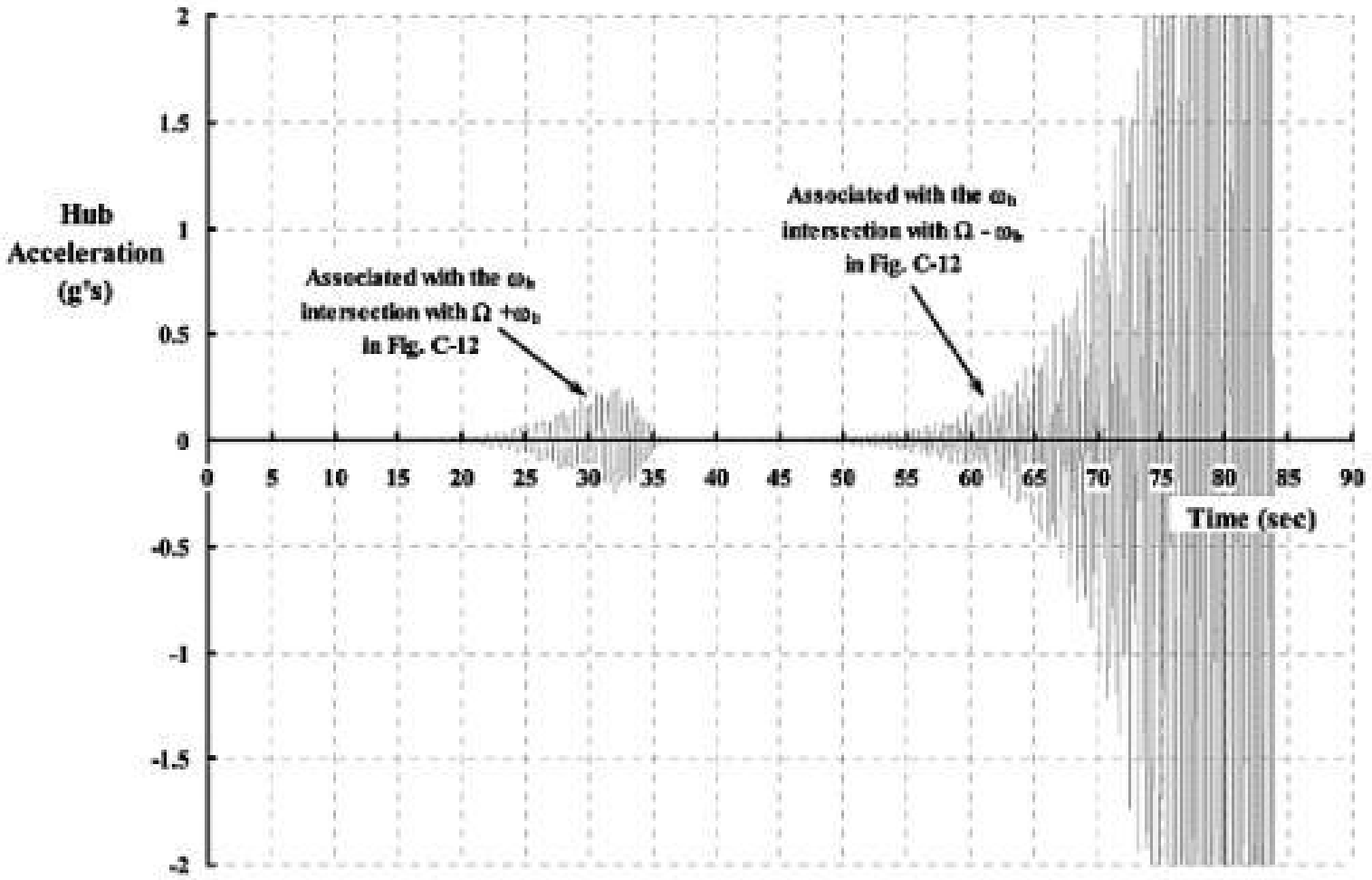

Fig. C-14. Hub vibration during rotor startup.

Case 3. Three Blades at Several Rotor

Speeds

As a concluding example to this discussion about ground resonance, I have chosen a classic ground resonance problem. In this case, the rotor system has three *absolutely identical* blades, which are described in Table C-3 . The rotor speed is fixed at a constant RPM. The objective is to establish the amount of damping required for neutral stability at each of several RPMs in order to make a comparison with Fig. C-11.

Before presenting the results of this case, it is very important to appreciate that as more blades are added, each blade will have its own dynamic equation. Thus, the degrees of freedom increase from the two degrees (y_h and ξ) suggested by Fig . C-5 . Some mathematical simplification is obtained by assuming that all blades, regardless of the number, are *absolutely* identical . However, in real life, this

perfection has yet to be achieved. It is common manufacturing practice to balance all blades against a master blade. This practice yields blades of equal weight and gives some assurance that the spanwise center of gravity is within tolerance. However, I am not aware of any production process that checks a blade's second moment of inertia $\left(I_b = \int_e^R r^2 dm\right)$ against a master blade. And finally, in the field operation, blade deterioration does not occur equally. Perhaps the worst that can happen is that blade-lag dampers and landing gear shock absorbers degrade, and even fail, which is an extremely dangerous matter.

The equations of motion for this case, guided by Fig. C-7, require replacing the counterbalance weight with two blades. This yields a rotor system where blade one becomes the master blade, which is indexed in azimuth

to $\psi_1 = \Omega t$ since rotor speed (Ω) is assumed constant. Blade two is placed 120 degrees ahead of master blade one, and blade three is placed 240 degrees ahead of the master blade. Thus, each blade has its individual displacement of

$$y_{b1} = y_h + e_1 \sin(\Omega t) + r_{cg1} \sin(\Omega t + \xi_1)$$

(56)

$$y_{b2} = y_h + e_2 \sin\left(\Omega t + \frac{2\pi}{3}\right) + r_{cg2} \sin\left(\Omega t + \frac{2\pi}{3} + \xi_2\right)$$

$$y_{b3} = y_h + e_3 \sin\left(\Omega t + \frac{4\pi}{3}\right) + r_{cg3} \sin\left(\Omega t + \frac{4\pi}{3} + \xi_3\right)$$

Now the hub equation accounting for all three blades is

(57)

$$(m_h + m_{b1} + m_{b2} + m_{b3})\frac{d^2y_h}{dt^2} + c\frac{dy_h}{dt} + ky_h = F_{b1} + F_{b2} + F_{b3}$$

where the force is computed individually for each blade (should they not be absolutely identical) from

APPENDIX C

$$F_{b1} = m_{b1}e_1\Omega^2 \sin(\Omega t) - m_{b1}r_{cg1}\left\{\cos(\Omega t)\frac{d^2\xi_1}{dt^2} - \sin(\Omega t)\left[\Omega + \frac{d\xi_1}{dt}\right]^2\right\}$$

(58)

$$F_{b2} = m_{b2}e_2\Omega^2 \sin\left(\Omega t + \frac{2\pi}{3}\right) - m_{b2}r_{cg2}\left\{\cos\left(\Omega t + \frac{2\pi}{3} + \xi_2\right)\frac{d^2\xi_2}{dt^2} - \sin\left(\Omega t + \frac{2\pi}{3} + \xi_2\right)\left[\Omega + \frac{d\xi_2}{dt}\right]^2\right\}$$

$$F_{b3} = m_{b3} e_3 \Omega^2 \sin\left(\Omega t + \frac{4\pi}{3}\right) - m_{b3} r_{cg3} \left\{ \cos\left(\Omega t + \frac{4\pi}{3} + \xi_3\right) \frac{d^2\xi_3}{dt^2} - \sin\left(\Omega t + \frac{4\pi}{3} + \xi_3\right) \left[\Omega + \frac{d\xi_3}{dt}\right]^2 \right\}$$

As noted above, each blade must have its own dynamics equation. I have purposely written the three blade lead-lag equations so that ground resonance with dissimilar blades might be studied at some later date. However, for this introduction, all blades are absolutely identical. Thus

$$I_{b1} \frac{d^2\xi_1}{dt^2} + c_{b1} \frac{d\xi_1}{dt} + I_{b1} \omega_{b1}^2 \xi_1 = -\left(m_{b1} r_{cg1} \frac{d^2 y_h}{dt^2} \right) \cos(\Omega t + \xi_1)$$

(59)

$$I_{b2} \frac{d^2\xi_2}{dt^2} + c_{b2} \frac{d\xi_2}{dt} + I_{b2} \omega_{b2}^2 \xi_2 = -\left(m_{b2} r_{cg2} \frac{d^2 y_h}{dt^2} \right) \cos\left(\Omega t + \frac{2\pi}{3} + \xi_2\right).$$

$$I_{b3}\frac{d^2\xi_3}{dt^2}+c_{b3}\frac{d\xi_3}{dt}+I_{b3}\omega_{b3}^2\xi_3=-\left(m_{b3}r_{cg3}\frac{d^2y_h}{dt^2}\right)\cos\left(\Omega t+\frac{4\pi}{3}+\xi_3\right)$$

The calculation was rather simple using the previously discussed Dewey Hodges' numerical integrator to solve the four equations: The Hodges' solver was set up using a Microsoft® Excel® spreadsheet, which now, admittedly, required many columns. The initial conditions came from the earlier locked-blade solution for one blade so that at zero time (t), the initial

blade lead-lag angle for all three blades was at $\xi_0 = 0.05$ radians, and the hub displacement (y_h) was zero. The hub velocity ($dy_h/dt = -0.18$ ft/sec) and acceleration ($d^2y_h/dt^2 = 0.00562$ ft/sec^2) corresponded to the beginning of a cycle when $y_h = 0$ at 230 rpm.

Figures C-15 and C-16 summarize the neutral stability boundaries for ground resonance of a three-bladed autogyro with lead-lag hinges and lead-lag dampers . The example is, perhaps, what might have been seen by the Kellett engineering department before testing began on the XR-2 autogyro—if the

theory had been developed. Unfortunately for the XR-2, a problem was not foreseen as the pioneers focused on rotor over-speed for jump takeoff and, just as unfortunately, no theory was available.

A comparison of Fig. C-15 to Fig. C-11 shows a very similar trend. The big difference is that each blade in the three-bladed set now needs more than four times the lag damper value required by just one blade that is counterbalanced.

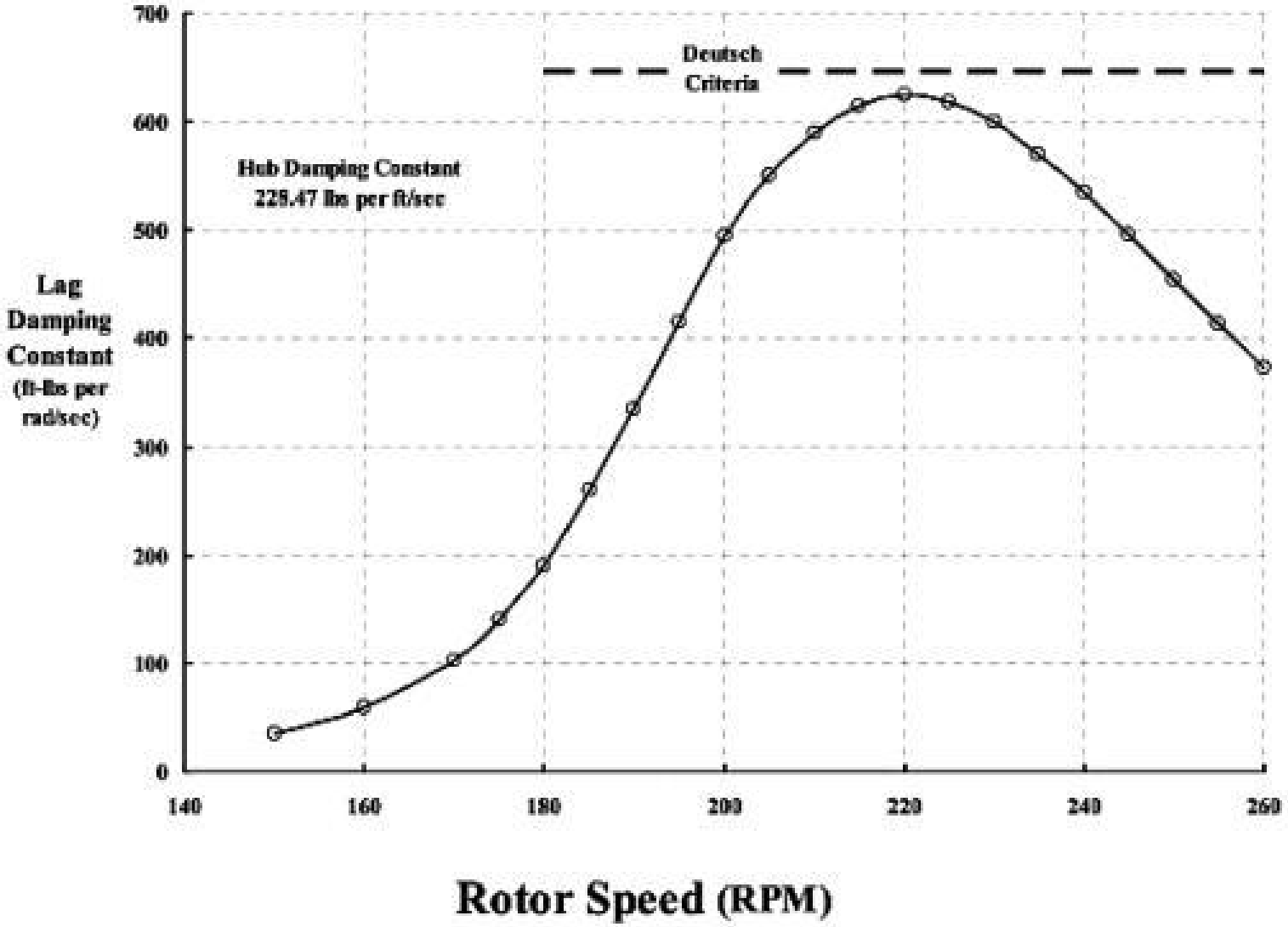

Fig. C-15. Damping required for neutral stability of ground resonance with a three-bladed rotor.

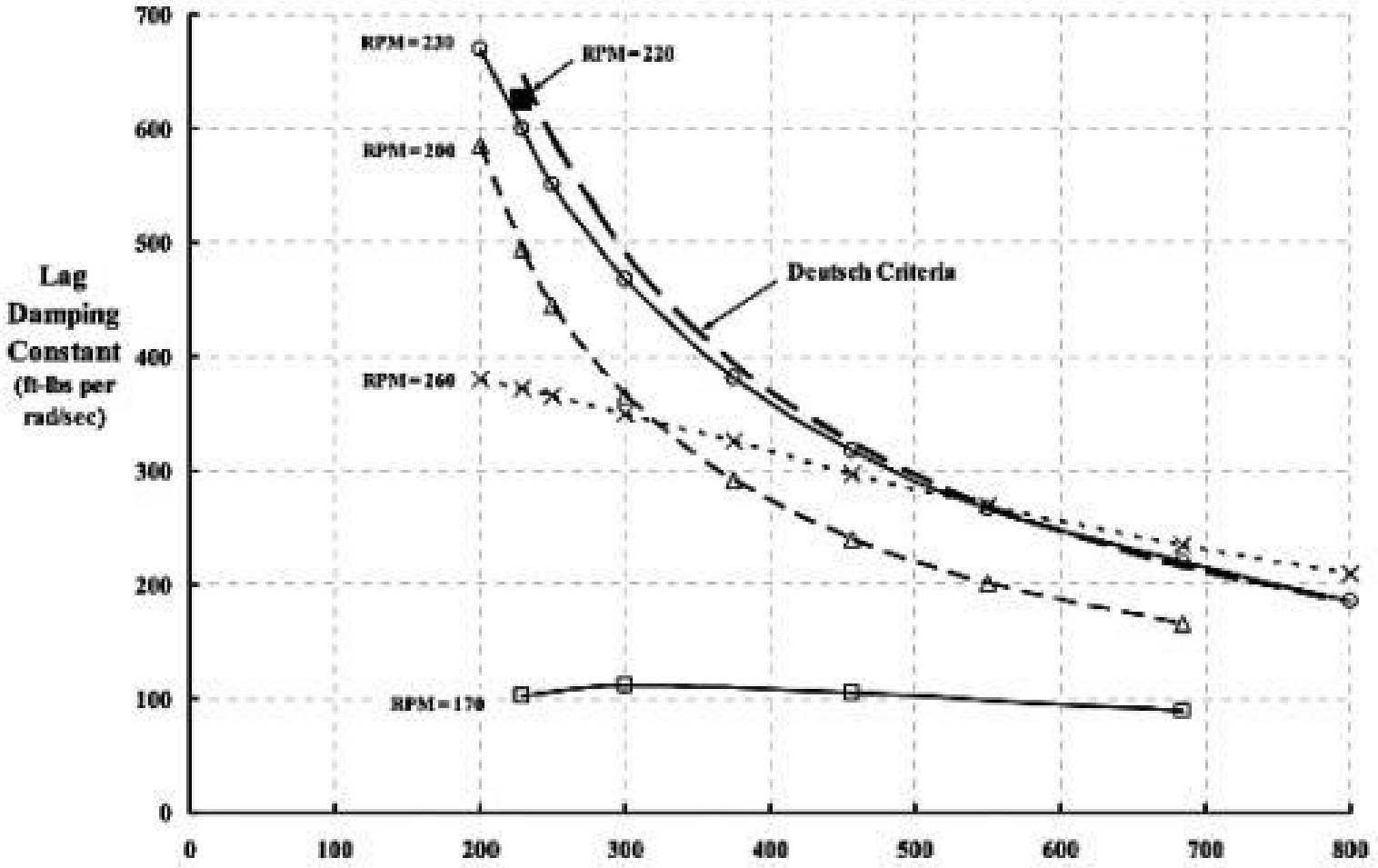

Fig. C-16. Required combinations of hub- and blade-lag damping to ensure neutral stability of ground resonance with a three-bladed rotor.

Figure C-16 is particularly informative. Two points are immediately apparent. First, there are unique sets of damping coefficients (i.e., blade and landing gear) at any given rotor speed that define a neutral stability boundary. Second, there is a very small range in rotor speed that captures the very maximum of lag and hub damping required for neutral stability; about 220 to 230 rpm for this configuration defined in Table C-3 . This general trend exhibited in Fig. C-16 means that serious design attention must be given to landing gear design details and blade-root-end configuration details to say nothing about the rotor speed operating range.

Finally, I have added a most practical design criteria (labeled Deutsch Criteria) to both Figs. C-16 and C-17. Mr. M. L. Deutsch published some of his work in the Journal of the Aeronautical Sciences, Volume 13, Number 5, in May 1946.[9] At that time, he was a member of the Engineering Division of the Army Air Force Air Technical Service Command located

at Wright Field in Dayton, Ohio. Deutsch's ground resonance criteria, now rather well known, is simplicity itself. The approximation for the maximum required lag damping for any given hub damping, so that at least neutral stability is obtained, is calculated from

$$(60)\quad \text{Lag damping constant} = \frac{\frac{b}{4}\left(\omega_h^2\right)\left[\frac{1-\left(\omega_\xi/\Omega\right)^2}{\omega_\xi/\Omega}\right]\left(\text{Blade first moment of inertia}\right)^2}{\text{Hub damping constant}}$$

where (b) is the number of blades (being three or more). The hub natural frequency (ω_h) in radians per second is equal to $\sqrt{k/m}$, and the blade inplane natural frequency ratio (ω_ξ/Ω) on a per-rev basis can be approximated as $\sqrt{\frac{3}{2}\left(\frac{e}{R-e}\right)}$, which is unitless. The blade first moment of inertia is calculated as $\int_e^R r\left(\frac{dm_b}{dr}\right)dr$, which, for a blade having a uniform mass distribution as in my example, becomes ($m_b\, r_{cg}$)

in slug-feet.

Closing Remarks

The first point to make in conclusion is that good engineering practice requires that more system damping than the minimum required for neutral stability, is mandatory. Suppose, for example, that one of two landing gear shock absorbers fails. Or what about the case of operating from ice—the list of "what ifs" is nearly endless.

---

[9] Wayne Johnson (NASA Ames Research Center), who patiently watched over me on parts of this appendix, brought Deutsch's work to my attention. Wayne sent me a PDF copy of Deutsch's paper. I had my memory jogged when I saw the paper. It was a copy of the Journal paper that Robert (Bob) Lowey (then Chief of Dynamics at Vertol Aircraft Corp.) gave me to read in 1957 in response to my asking if he would tell me all about ground resonance, a new term in my apprenticeship.

APPENDIX C

Secondly, it seems that this particular incidence of the Kellett XR-2 destruction due to ground resonance[10] opened a door to comprehensive rotorcraft dynamics. The question of a similar type of instability with the aircraft flying was asked. Then, as ever-improved helicopters came on the scene, questions about drive-system coupled to rotor-system behavior arose. Then blade flapping-motion coupling to blade lead-lag-motion was studied in considerable detail.

Both the autogyro in its era and now the helicopter are multi-degree-of-freedom machines. By multi, I mean between two and at least one hundred. The odds of some previously unknown instability striking current and future rotorcraft without warning are, in my opinion, very high. I do, however, expect that prominent dynamic engineers will debate me on

this somewhat pessimistic view.

---

[10] Mr. Deutsch writes in his Memorandum Report MLD:fb1:51 dated January 23, 1943, titled *Theory of Mechanical Instability of Rotors* that: "Ground resonance has been one of the major problems retarding the development of rotary wing aircraft. Several aircraft have been either destroyed or seriously damaged on the ground during rev-up (e.g. the XR-2). It was believed, at first, that this phenomena might be a result of coupled aerodynamic and mechanical forces affected by the proximity of the ground. However, it has been understood for some time that a purely mechanical system can exhibit – to a very high degree of approximation – the type of instabilities observed in actual rotary wing aircraft."

APPENDIX D

CONTROL LOADS

By the end of the autogyro era, our pioneers had learned a great deal about blade twisting and control loads. In this appendix, I want to discuss control loads in the three parts that I consider to be of particular importance.

Control Loads: Part I—The Basics

In my opinion, the 1932 blade feathering system of E. Burke Wilford (see Fig. 2-35) and the addition of the pitch change mechanism by Raoul Hafner in 1937 (see Figs. 2-39, 2-40, 2-41, and 2-43) were major steps toward developing today's rotor systems. A schematic drawing of what may be considered today's control system is repeated here as Fig. D-1 . This configuration is a quite adequate schematic from which several key points about control loads can be made.

To begin with, all of the torsional moments (M_T) that the blade can produce are resisted by a pitch link force (PLL) acting at a moment arm provided by the pitch arm. This moment arm is of length (d). That is,

$$(1) \qquad PLL(d) = M_T \qquad \text{or} \quad PLL = \frac{M_T}{d}$$

where the blade torsional moment is in units of foot-pounds, the moment arm is in units of feet, and the pitch link load is in units of pounds.

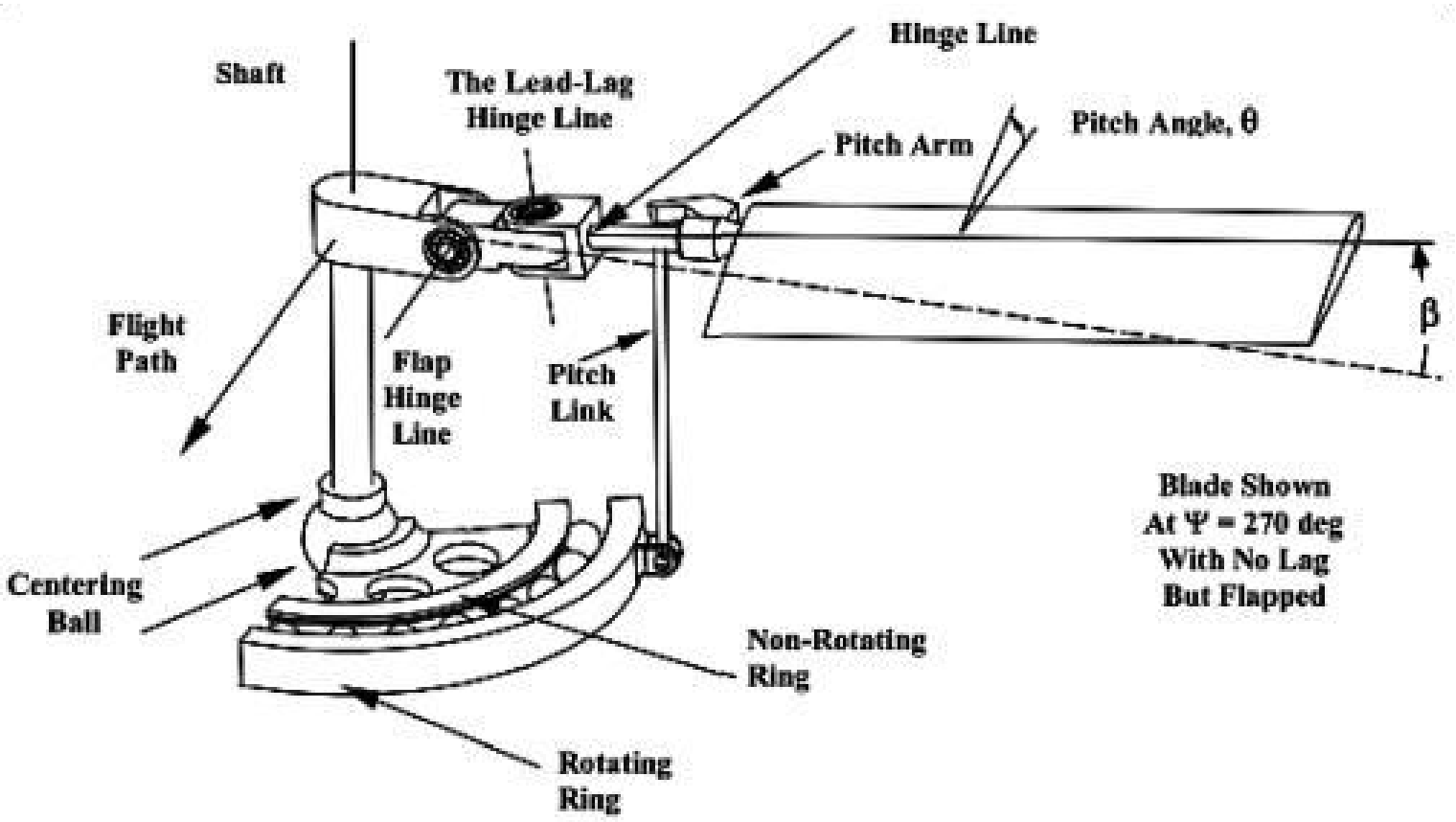

Fig. D-1. Blade feathering and a modern swashplate gave the pilot complete control. The assembly, including swashplate actuators, is frequently referred to as the upper controls; cockpit controls are the lower controls.

APPENDIX D

To help in this discussion, consider a line drawing in top view of the control system as shown in Fig. D-2 . The blade feathers about an axis positioned at the azimuth angle (ψ), which is measured from the X-axis. The X-axis forms the fore and aft plane of the machine. The pitch arm ends (point D) in a ball joint. A pitch link connects point D to the rotating ring below in a nearly vertical line going into the paper. The bottom end of the pitch link ties to a ball joint that is solidly attached to the rotating ring. The rotating ring has a radius (r_{PL}), so the moment arm (d) is approximately equal to r_{PL} times the sine of the angle (Δ).

The rotating assembly is held in space by the nonrotating ring. This is the swashplate assembly, which is basically a ball bearing. The

nonrotating ring is attached to a slider with a centering ball . Control of the swashplate is obtained through three actuators located at points A, B, and C. The tilt of the swashplate in space depends on the individual lengths of the actuators. The bottom of the actuators are attached to some part of the airframe, commonly the transmission in a helicopter. Both ends of each actuator end in ball joints . I have positioned the swashplate actuators (points A, B, and C) in a quite arbitrary way; that is, they need not be inside the pitch link radius (point D) nor located at the azithmuths shown.

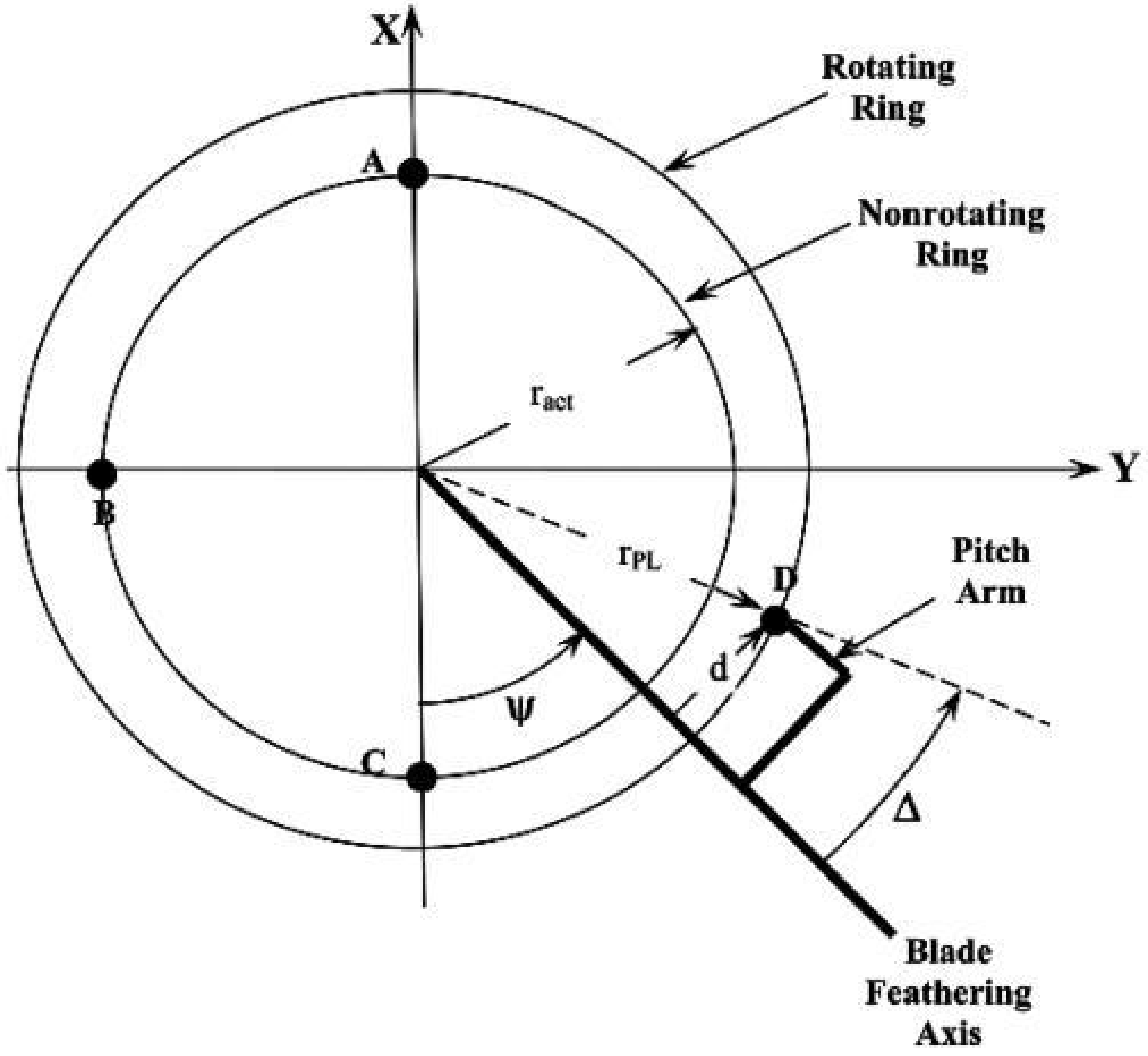

Fig. D-2. Schematic of the upper controls.

APPENDIX D

Now with the mechanical design layout of Fig. D-2, think about calculating the load in a pitch link and the three swashplate control actuators. Assume that the *torsional moment at the root* ($M_{T\psi}$) of one blade can be represented by a Fourier series of the form

(2) $$M_{T\psi} = M_0 + M_{1S}\sin\psi + M_{1C}\cos\psi + M_{2S}\sin 2\psi + M_{2C}\cos 2\psi + \text{etc.}$$

where a leading-edge-up pitching moment is a positive moment with the units of foot-pounds. Then the associated pitch link load is

(3)

$$PLL_\psi = \frac{M_{T\psi}}{d} = \frac{1}{d}\left(M_0 + M_{1S}\sin\psi + M_{1C}\cos\psi + M_{2S}\sin 2\psi + M_{2C}\cos 2\psi + \text{etc.}\right).$$

Since the pitch link is shown at an advanced angle (Δ) relative to the blade feathering axis, the pitch link will be in tension (which I will assume is the positive sign convention) when the torsional moment is positive (i.e., nose up). Now the pitch link load creates a moment about
the nonrotating X-axis and Y-axis system.
down moment in the amount of

$$M_Y = -PLL_\psi \left[r_{PL} \cos(\psi + \Delta) \right] \tag{4}$$

and the moment about the X-axis is

$$M_X = -PLL_\psi \left[r_{PL} \sin(\psi + \Delta) \right]. \tag{5}$$

Let me interject here that there

For the moment about the Y-axis, this is a nose-

is an important characteristic of rotary wing

trigonometry that you should be aware of. The pitch link load of Eq. (3) is transferred from the rotating system to the nonrotating system by multiplying by a cosine function or a sine

function as Eqs . (4) and (5) respectively require. Furthermore, to get the total contribution to M_Y and M_X of two, three, or four or more blades, additional trigonometry is involved. It is possible to complete the trigonometry in longhand as was done in the autogyro era. So let me refer you to Gessow and Myers[1] who include, near the end of their book, some very handy tables that show some quite simple results.

To continue then, these two moments (M_Y and M_X) in the fixed system are reacted by the approximately vertical forces (i.e., in or out of the paper) at actuator points A, B, and C, which are at a radius (r_{act}). Figure D-2 shows these actuator points in the simplest geometric positions. That is, the moment about the Y-axis must be resisted by an upward force at point A and a downward force at point C. This puts the actuator at point A in compression and the actuator at point C in tension. A sign convention for actuator loads must now be chosen. Let me choose tension as the positive sign convention for *all* actuator loads. Together

these two actuators (A and C) produce a couple (i.e., $F_A = -F_C$) having the moment

$$(6) \qquad \left(F_A - F_C\right) r_{act} = -2F_C r_{act} = M_Y = -PLL_\psi \left[r_{PL} \cos\left(\psi + \Delta\right)\right].$$

In like manner, the moment about the X-axis puts the actuator at point C in compression, which is negative load, so you have

[1] Alfred Gessow and Garry Myers, *Aerodynamics of the Helicopter*, Frederick Ungar Publishing Co., New York, 3rd Printing, 1952, pp. 316–319.

APPENDIX D

$$(7) \qquad F_B r_{act} = M_X = -PLL_\psi \left[r_{PL} \sin\left(\psi + \Delta\right)\right].$$

The preceding discussion accounts for

fixed-system actuator loads from *one* blade and can be summarized as

$$F_C = \left(\frac{r_{PL}}{2r_{act}}\right) PLL_\psi \left[\cos(\psi + \Delta)\right] = -F_A$$

(8)

$$F_B = -\left(\frac{r_{PL}}{r_{act}}\right) PLL_\psi \left[r_{PL} \sin(\psi + \Delta)\right]$$

I will show you the actuator loading for three blades after quantifying three important torsional moments.

Control Loads: Part II—Three Important Torsional Moments

In the discussion of control loads for the Raoul Hafner autogyro (see paragraph 2.7.5) you have read that he designed the blades so that two key assumptions could be made . These assumptions, in his words, were that:

"The blades produce no [torsional] moments about their longitudinal [spanwise] or pitch change axes due to (a) aerodynamic forces, because the blades are fitted with aerofoil sections, the centre of pressures of which lie always on a straight line coinciding with the pitch change axis; and (b) weight and centrifugal forces,

because the centre of gravity of each blade lies also in this [pitch change] axis."

(Hafner made an implied assumption that the line of shear centers of every blade element also is coincident with the pitch change axis.[2]) Following those assumptions here means that blade feathering causes a torsional moment. The second torsional moment will come from the pitching moment coefficient ($C_{M¼c}$) . The third torsional moment comes from unsteady aerodynamics, which was discussed in Appendix B . Let me consider these three moments in order and later offer numerical results using the Hafner A.R. III autogyro as an example.

Blade Feathering. Suppose that the blade pitch angle (θ), at any radius station ($x = r/R$) and azimuth position (ψ), is described simply as

$$\theta_{x,\psi} = \theta_o + x\theta_t - B_{1C}\sin\psi - A_{1C}\cos\psi \tag{9}$$

then a pitch link is loaded by a moment

associated with the blade retention components and by the feathering inertia of the blade. That is,

---

[2] The shear center is a point about which a section of a beam twists. It can be found experimentally by applying a perpendicular force at successive chordwise points and finding the point where the force only bends the beam and does not twist the beam at all. The test would be done by hanging a blade by a clamped root end and applying the force at several span and chordwise points. Early rotor blades were built up on a main spar that was circular. To the first approximation, the center of the circular spar was the shear center. For a main spar that is a C-section to which the rest of the airfoil is attached, it is quite likely that the shear center is, in fact, very near the leading edge of the airfoil. Thus, a blade might feather about the pitch change axis, but twist elastically about a different axis.

(10)

$$M_{T\psi} = -K_\theta\left(\theta_o - B_{1C}\sin\psi - A_{1C}\cos\psi\right) + \int_r^R \left(-I_\theta \frac{\partial^2\theta}{\partial t^2} - I_\theta\Omega^2\theta\right) dr .$$

The first moment in Eq. (10) comes from the tie rod that Hafner used. In modern designs, such a component is called a tension-torsion (T-T) strap assembly. The blade is retained against centrifugal force, but the T-T strap assembly has a relatively low torsional rigidity (GJ in pound-feet^2) and is relatively easy to twist. The second moment in Eq. (10) is due to the blade's resistance to being feathered in a once-per-revolution manner (i.e., 1/rev).

The second moment in Eq. (10) deserves some discussion. To begin with, the moment of inertia in pitch is denoted as (I_θ) and has the units of slug-feet^2 per foot. This moment can be rearranged by assuming that rotor speed times time is azimuth ($\psi = \Omega t$) and defining ($dr = R dx$). Thus, the total blade length can create a root torsional moment ($M_{inertia}$ in foot-pounds) amounting to

(11)

$$M_{inertia} = \int_{r=0}^{R} \left(-I_\theta \frac{\partial^2 \theta}{\partial t^2} - I_\theta \Omega^2 \theta \right) dr = \int_0^1 \left(-I_\theta \Omega^2 \frac{\partial^2 \theta_{x,\psi}}{\partial \psi^2} - I_\theta \Omega^2 \theta_{x,\psi} \right) R dx .$$

Now make the assumption that the blade has a very high torsional rigidity (GJ) so that no elastic twisting (θ_e) need be accounted for. Furthermore, assume that the pitch moment of inertia (I_θ) is constant from the blade root to its tip. Then Eq. (9) and its second derivative can be substituted into Eq. (11) with the result that

$$M_{inertia} = -I_\theta \Omega^2 R \int_0^1 \left(\frac{\partial^2 \theta_{x,\psi}}{\partial \psi^2} + \theta_{x,\psi} \right) dx$$

(12)

$$= -I_\theta \Omega^2 R \int_0^1 \left[(B_{1C} \sin\psi + A_{1C} \cos\psi) + (\theta_o + x\theta_t - B_{1C} \sin\psi - A_{1C} \cos\psi) \right] dx$$

$$= -I_\theta \Omega^2 R \int_0^1 (\theta_o + x\theta_t) dx$$

$$= -I_\theta \Omega^2 R \left(\theta_o + \frac{1}{2}\theta_t \right)$$

Notice immediately from this result that it takes no root-end moment to feather the blade at once-per-revolution, which is to say that the torsional natural frequency of the blade is exactly 1/rev. Secondly, if the blade has a built-in twist (θ_t) that is negative (i.e., washout) then there is some root-end pitch angle (θ_o) that leads to a zero root moment, and no pitch link force is needed for this equilibrium position.

The proceeding discussion leads to the root torsional moment from one blade that a pitch link must resist. To summarize then, the first root torsional moment is

(13)

$$M_{T\psi} = -K_\theta\left(\theta_o - B_{1C}\sin\psi - A_{1C}\cos\psi\right) - I_\theta\Omega^2 R\left(\theta_o + \frac{1}{2}\theta_t\right).$$

[3] Wayne Johnson gives a complete discussion of the blade torsion problem in his book *Helicopter Theory*, Princeton University Press, Princeton, N.J., 1980, pp. 403–408.

APPENDIX D

A subtlety—not immediately apparent in Eq. (13) or Hafner's design shown in Fig. 2-43—is that the end fittings of a tension-torsion strap can be designed so that the steady value of the root torsion moment is zero. Thus, an untwisted T-T strap can place the blade at the nominal root-collective-pitch angle (θ_o) best suited for cruise flight. This can, for an unboosted (i.e., no power steering) actuator system, reduce pilot workload.

Airfoil Steady Pitching Moment. You will recall that Cierva sought to improve Autogiro performance by using a cambered airfoil. Hafner chose a symmetrical airfoil, which, theoretically, has a zero-airfoil pitching moment coefficient. However, in the rotorcraft world, there can be a significant difference between theory and a manufactured blade. This real-life possibility must admit to a nonzero moment coefficient ($C_{M\ ¼\ c}$). Therefore, a blade element torsional moment can exist of magnitude

$$\frac{dM}{dr} = \left(\frac{1}{2}\rho V_t^2\right)\left(x + \mu \sin\psi\right)^2 c^2 C_{Ml/4c} \tag{14}$$

and the integration of this moment over the blade length (r = 0 to r = R) gives

(15)

$$M_{T\psi} = \left(\frac{1}{2}\rho V_t^2\right)\left(c^2 R C_{M1/4c}\right)\left(\frac{1}{3} + \frac{\mu^2}{2} + \mu\sin\psi - \frac{\mu^2}{2}\cos 2\psi\right).$$

Airfoil Unsteady Pitching Moment. When an airfoil is oscillating in angle of attack about the 1/4-chord point in an unsteady relative wind, there arises an unsteady pitching moment.

When this airfoil is one of many in a rotor blade that is rigid and can only flap and feather, Johnson[4] points out that care must be taken in bookkeeping flapping and feathering. From Johnson's Engineering Note,[4] he recommends that the pitching motion about the 1/4-chord point of the airfoil ($b = c/2$ and $a = -1/2$) be calculated as

$$(16)\qquad \frac{dM_{x\rho}}{dr} = \frac{\pi\rho c^2}{4}\left\{\begin{array}{l}\left(\frac{c}{2}\right)\left(-\frac{1}{2}\right)\left[\frac{d}{dt}(U_T\theta + U_P)\right] - \frac{1}{2}\left(\frac{c}{2}\right)U_T\left(\frac{d\theta}{dt} + \Omega\beta\right) \\ -\left(\frac{c}{2}\right)^2\left[\frac{1}{8} + \left(-\frac{1}{2}\right)^2\right]\left[\frac{d}{dt}\left(\frac{d\theta}{dt} + \Omega\beta\right)\right]\end{array}\right\}.$$

Given that the rotor blade is rotating at constant RPM, derivatives with respect to time can be replaced with $\Omega\, d()/d\psi$, and then Eq. (16) can be factored and simplified to read as

(17)

$$\frac{dM_{xp}}{dr} = -\frac{\pi\rho c^3\Omega}{16}\left\{\left[\frac{d}{d\psi}(U_T\theta + U_P)\right] + U_T\left(\frac{d\theta}{d\psi} + \beta\right) + \frac{3c\Omega}{8}\left[\frac{d}{d\psi}\left(\frac{d\theta}{d\psi} + \beta\right)\right]\right\}$$

from which it follows from the derivatives that

(18)

$$\frac{dM_{xp}}{dr} = -\frac{\pi\rho c^3\Omega}{16}\left\{\theta\frac{dU_T}{d\psi} + 2U_T\frac{d\theta}{d\psi} + \frac{dU_P}{d\psi} + U_T\beta + \frac{3c\Omega}{8}\left(\frac{d^2\theta}{d\psi^2} + \frac{d\beta}{d\psi}\right)\right\}$$

---

[4] Wayne Johnson, *Application of Unsteady Airfoil Theory to Rotary Wings*, AIAA J. of Aircraft, vol. 17, no. 4, April 1980.

APPENDIX D

where

$$U_T = \Omega R\left(x + \mu\sin\psi\right) \rightarrow$$

$$\frac{dU_T}{d\psi} = \Omega R \mu \cos\psi$$

$$\theta = \theta_0 + x\theta_t - B_{1C}\sin\psi - A_{1C}\cos\psi \rightarrow \frac{d\theta}{d\psi} = -B_{1C}\cos\psi + A_{1C}\sin\psi$$

$$\frac{d^2\theta}{d\psi^2} = B_{1C}\sin\psi + A_{1C}\cos\psi$$

(19)

$$U_P = \Omega R\left(\lambda_{hp} - x\frac{d\beta}{d\psi} - \mu\beta\cos\psi\right) \rightarrow$$

$$\frac{dU_P}{d\psi} = \Omega R\left(-x\frac{d^2\beta}{d\psi^2} + \mu\beta\sin\psi - \mu\frac{d\beta}{d\psi}\cos\psi\right)$$

$$\beta = \beta_0 - a_{1S}\cos\psi - b_{1S}\sin\psi \rightarrow$$

$$\frac{d\beta}{d\psi} = a_{1S}\sin\psi - b_{1S}\cos\psi$$

$$\frac{d^2\beta}{d\psi^2} = a_{1S}\cos\psi + b_{1S}\sin\psi$$

The blade-root-end pitching moment is obtained by substituting Eq. (19) into Eq. (18) and then integrating over the blade length from r = 0 to r = R. The results are that the root-blade pitching moment (M_ψ) in foot-pounds varies with blade azimuth as

$$M_\psi = \frac{\pi \rho c^3 V_t^2}{16} \left\{ \begin{aligned} &\frac{\mu}{2}(b_{1S} - A_{1C}) - \frac{1}{2}\beta_0 + \left[(b_{1S} - A_{1C}) - 2\mu\beta_0 - \frac{3c}{8R}(a_{1S} + B_{1C}) \right] \sin\psi \\ &+ \left[(a_{1S} + B_{1C}) + \frac{3c}{8R}(b_{1S} - A_{1C}) - \mu\left(\theta_0 + \tfrac{1}{2}\theta_t\right) \right] \cos\psi \\ &+ \frac{3\mu}{2}(a_{1S} + B_{1C}) \sin 2\psi - \frac{3\mu}{2}(b_{1S} - A_{1C}) \cos 2\psi \end{aligned} \right\} \tag{20}$$

In applying Eq. (16) to the rotor problem, the rotor tip-path-plane coordinate system must be used. In the tip-path-plane coordinate system, the fundamental thrust and feathering equations, as given by Harris[5] for uniform induced velocity, are

(21)

$$\frac{2C_T}{\sigma a}=\left(\frac{1}{2}+\frac{\mu^2}{4}\right)\lambda_{tpp}+\left(\frac{1}{3}+\frac{\mu^2}{2}-\frac{4\mu^3}{9\pi}\right)\theta_0+\left(\frac{1}{4}+\frac{\mu^2}{4}-\frac{\mu^4}{32}\right)\theta_t-\left(\frac{\mu}{2}+\frac{\mu^3}{8}\right)(B_{1C}+a_{1S}),$$

---

[5] F. D. Harris, *Rotary Wing Aerodynamics–Historical Perspective and Important Issues*, National Specialist's Meeting on Aerodynamic and Aeroacoustics sponsored by the American Helicopter Society Southwest Region, Arlington, Tex., 1987.

APPENDIX D

(22)

$$(B_{1C}+a_{1S})=\frac{\left(2\mu+\frac{\mu^3}{2}\right)\lambda_{tpp}+\left(\frac{8\mu}{3}+\frac{32\mu^4}{45\pi}\right)\theta_0+\left(2\mu+\frac{\mu^5}{12}\right)\theta_t}{1+\frac{3\mu^2}{2}-\frac{5\mu^4}{24}},$$

$$(23) \qquad (b_{1S} - A_{1C}) = \frac{\frac{4\mu}{3}\left(1+\frac{4\mu^3}{15\pi}\right)\beta_0}{1+\frac{\mu^2}{2}-\frac{\mu^4}{24}}.$$

Control Loads: Part III—A Numerical Example

A review of Part II shows that blade-root torsional moments include—as a minimum—steady terms, once-per-revolution terms (i.e., sin ψ and cos ψ), and two-per-revolution terms (i.e., sin 2ψ and cos 2ψ). Let me use the Hafner A.R. III autogyro (see sections 2.7.4 and 2.75) as a configuration to obtain some numerical and graphical results. Table D-1 provides the necessary configuration data. Given these aircraft properties, the three root torsional moments for one blade are:

1. Blade feathering

$$M_{\psi} = -(3.529 + 1.497) + 3.676 \sin\psi - 2.110 \cos\psi .$$

2. Airfoil steady pitching moment, $C_{M\ 1/4c} = -0.005$ (as manufactured)

$$M_{\psi} = -1.350 - 1.150 \sin\psi - 0.095 \cos 2\psi$$

.

3. Airfoil unsteady pitching moment

$$M_{\psi} = -0.2779 - 0.1603 \sin\psi + 0.3243 \cos\psi + 0.2337 \sin 2\psi - 0.1341 \cos 2\psi .$$

The total of these three contributors to root torsional moments for one blade is: (24) Total $M_{T\psi} = -6.6539 + 2.3657 \sin\psi - 1.7857 \cos\psi + 0.2337 \sin 2\psi - 0.2291 \cos 2\psi$. Then, using Eq. (1) with a pitch link offset (d) of 0.75 feet, the results of the pitch link load of one blade is shown in Fig. D-3.

Now consider a three-blade rotor

system where each blade has the root torsional moment given by Eq. (24), which sets values in Eq. (2) for M_0, M_{1S}, M_{1C}, M_{2S}, and M_{2C}. Let the blades be numbered 1, 2, and 3 with an azimuthal spacing of 120 degrees, and let blade 1 be the master blade. Then blade 2 is located at an azimuthal angle of $\psi + 2\pi/3$, and blade 3 is located at $\psi + 4\pi/3$. The pitch link load for blade 1 will be

(25)

$$\text{Blade 1 PLL}_{\psi} = \frac{1}{d}\left[M_0 + M_{1S}\sin\psi + M_{1C}\cos\psi + M_{2S}\sin 2\psi + M_{2C}\cos 2\psi\right].$$

APPENDIX D

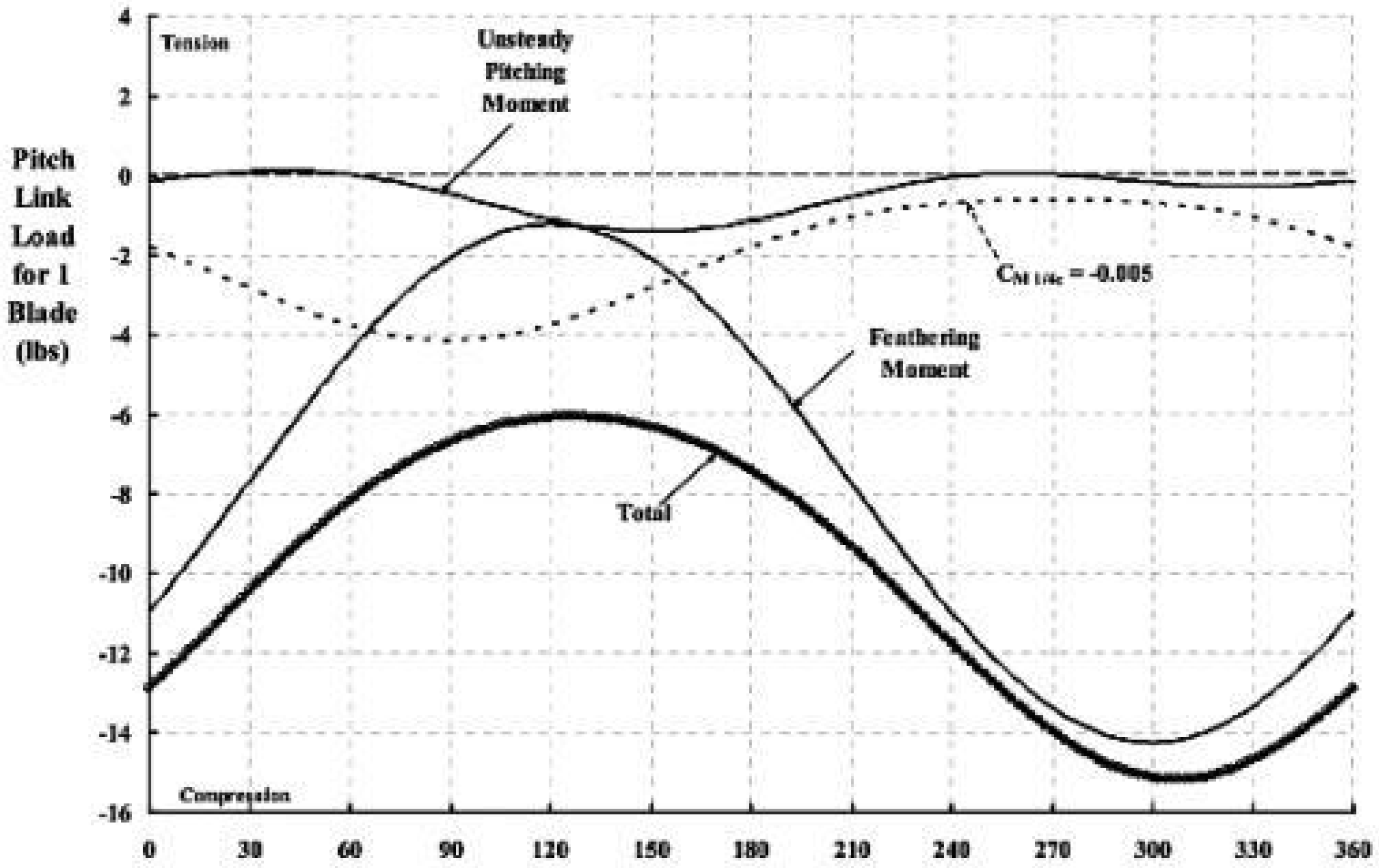

Fig. D-3. Steady, 1/rev, 2/rev, etc., torsional moments create pitch link loads. In a similar manner, the pitch link load of blade 2 is keyed to the azimuth angle of the master blade by replacing ψ with $\psi + 2\pi/3$ so that

(26)

$$\text{Blade 2 PLL}_{\psi} = \frac{1}{d}\left[\begin{array}{l} M_0 + M_{1S}\sin(\psi + 2\pi/3) + M_{1C}\cos(\psi + 2\pi/3) \\ + M_{2S}\sin 2(\psi + 2\pi/3) + M_{2C}\cos 2(\psi + 2\pi/3) \end{array}\right]$$

and for blade 3

(27)

$$\text{Blade 3 PLL}_{\psi} = \frac{1}{d}\left[\begin{array}{l} M_0 + M_{1S}\sin(\psi + 4\pi/3) + M_{1C}\cos(\psi + 4\pi/3) \\ + M_{2S}\sin 2(\psi + 4\pi/3) + M_{2C}\cos 2(\psi + 4\pi/3) \end{array}\right].$$

The three pitch link loads, which are in the rotating system, transfer their loads to the nonrotating system as moments about the Y-axis and X-axis according to Eqs. (4) and (5). Thus,

(28)

$$\begin{aligned} M_Y = &-\text{Blade 1 PLL}_{\psi}\left[r_{PL}\cos(\psi + \Delta)\right] - \text{Blade 2 PLL}_{\psi}\left[r_{PL}\cos(\psi + 2\pi/3 + \Delta)\right] \\ &- \text{Blade 3 PLL}_{\psi}\left[r_{PL}\cos(\psi + 4\pi/3 + \Delta)\right] \end{aligned}$$

and the moment about the X-axis is

(29)

$$\begin{aligned} M_X = &-\text{Blade 1 PLL}_{\psi}\left[r_{PL}\sin(\psi + \Delta)\right] - \text{Blade 2 PLL}_{\psi}\left[r_{PL}\sin(\psi + 2\pi/3 + \Delta)\right] \\ &- \text{Blade 3 PLL}_{\psi}\left[r_{PL}\sin(\psi + 4\pi/3 + \Delta)\right] \end{aligned}.$$

and the results are shown in Fig. D-4.

APPENDIX D

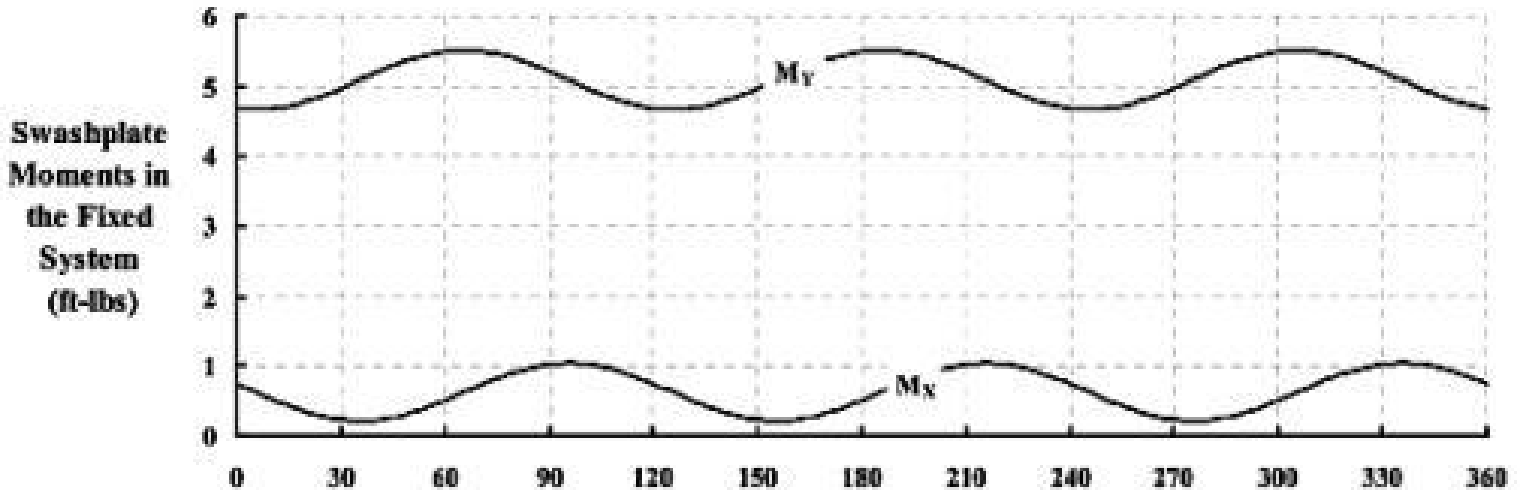

Fig. D-4. For a three-bladed rotor, once-per-rev pitch link loads become a steady moment in the fixed system. Two-per-rev loads become three-per-rev moments.

Table D-1. Approximate Hafner A.R. III Autogyro Properties

Parameter	Symbol	Value	Units	Comments
Flight speed	V	153	ft/sec	115 mph
Density	ρ	0.002378	slug/ft^3	Sea level standard
Tip speed	V_t	464	ft/sec	270 rpm
Thrust	T	900	lbs	Gross weight
Radius	R	16.41	ft	A = 846 ft^2
Chord	c	0.4071	ft	
No. of blades	b	3	nd	
Solidity	σ	0.02369	nd	
Advance ratio	μ_{tpp}	0.3305	nd	Tip-path plane
Inflow ratio	λ_{tpp}	+0.032	nd	Tip-path plane
Collective pitch	θ_0	0.06671	rad	
Blade twist	θ_t	0.00	rad	
Longitudinal flapping	a_{1S}	0.00	rad	Zero pitching moment
Lateral flapping	b_{1S}	0.00	rad	Zero rolling moment
T-T strap stiffness	K_θ	52.9	ft-lbs/rad	Hafner data
Torsional 2nd inertia	I_θ	0.00171	slug-ft^2	Harris estimate
Pitch link moment arm	d	0.65	ft	Fig. 2-41
Pitch link lead angle	Δ	60	deg	Fig. 2-41
Pitch link radius	r_{PL}	0.75	ft	Fig. 2-41
Actuator radius	r_{act}	0.75	ft	Fig. 2-41
Actuator locations				Fig. D-2
Airfoil properties				
Lift-curve slope	a	5.73	per radian	
Pitching moment	$CM_{1/4c}$	0.00	nd	Symmetrical airfoil
Pitching moment	$CM_{1/4c}$	–0.005	nd	As manufactured
Calculations				
Thrust coefficient	C_T	0.002078	nd	Eq. (21), T = 900 lbs
Longitudinal feathering	$a_{1S} + B_{1C}$	0.06949	rad	Eq. (22)
Lateral feathering	$b_{1S} - A_{1C}$	0.03988	rad	Eq. (23), β_o = 5.45 deg

APPENDIX D

Notice in Fig. D-4 that there are very little vibratory moments in the swashplate nonrotating system. What little there is comes from the 2/rev unsteady pitching moment and from any 2/rev caused by manufactured blades not having perfectly "symmetrical" airfoils . In Hafner's rotor control system, the pilot had direct control of the swashplate (he called it a spider) with a rather long control stick. The mechanical advantage offered by the long control stick would have reduced pilot workload to the bare minimum.

Recall that Hafner told the Royal Aeronautical Society members that "the variation of incidence is achieved by a separate control linkage which enables the rotor to be controlled by light loads on the control column, which, as is shown in the mathematical analysis of control and as has been proved in flight, is free from all parasite loads and vibrations." I

suggest— based on Fig. D-4—that Hafner was absolutely correct in his description.

The final step, from the swashplate moments of Fig. D-4 to the actuator loads at points A, B, and C shown on Fig. D-2, is rather simple. By following Eqs. (6) and (7) you have the loads as shown in Fig. D-5.

It is, of course, incomplete to neglect the steady actuator loads that arise because of the steady pitch link loads. These steady pitch link loads appear in Eqs. (25), (26), and (27) as

$$\text{(30)} \qquad \text{Steady PLL} = \frac{1}{d}[M_0].$$

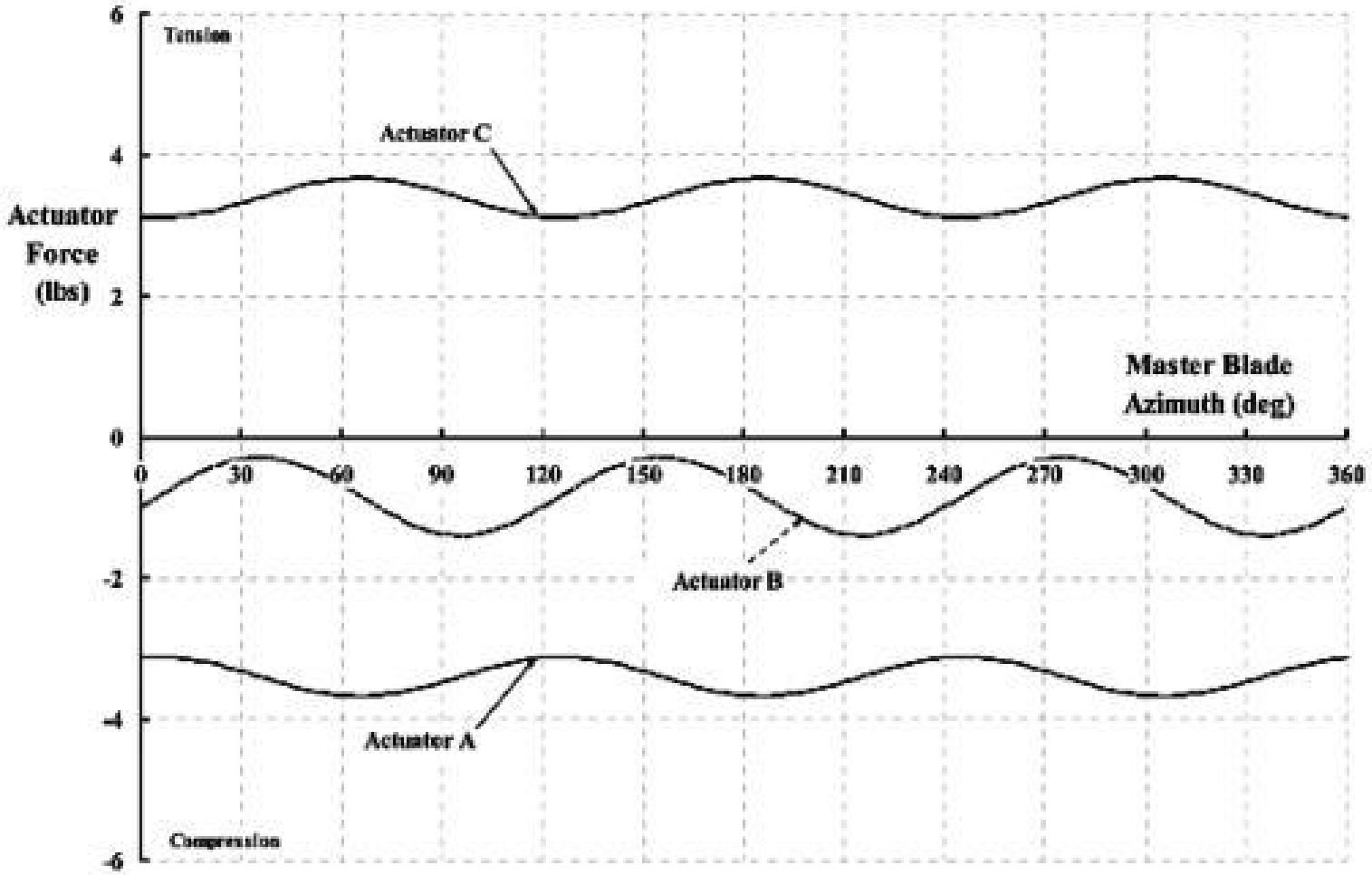

Fig. D-5. Actuator loads for a Hafner-type three-bladed rotor system.

APPENDIX D

Since there are three blades, the steady pitch

link loads act together to try and raise or depress the swashplate assembly up or down the rotor shaft (see Fig. D-1). (Because the pitch links are spaced in 120-degree-azimuth increments, their steady forces create no moment about either the nonrotating X-axis or Y-axis.) Any swashplate movement up or down the rotor shaft is resisted by the collective force of the three actuators . Therefore, there is a total vertical force (F_V) with *three* blades of

$$(31) \qquad F_V = -\frac{3}{d}[M_0]$$

which is shared among the three actuators. Fig. D-2 shows that the vertical force would be split between actuators at points A and C. The actuator at point B would support none of the vertical force (F_V)—*with the particular actuator locations I chose.*

You will recall that Hafner gave the

pilot a "lift lever" to collectively set the blades to a desired pitch angle (θ_0) and resist the vertical force (F_V) . That lever became the collective pitch control in modern helicopters.

Closing Remarks

In Hafner's paper about his gyroplane (see reference 74), he does not address the more general problem of blade element torsional moments that, when summed over the length of the blade, can create pitch link loads at all harmonics. To alert you to how complicated the blade torsion problem can be, consider Fig. D-6, which contains only a few of the multitude of terms to be included.

Because the blade is flexible, airfoil forces and moments that might be reasonably located at the 1/4-chord point of a blade element are, in fact, displaced from the

feathering axis both vertically (Z) and inplane (X) because of blade flapping, lead lagging, and bending, both inplane and out of plane. Furthermore, the blade element center of gravity can contribute torsional moments due to mass times acceleration forces . To top it off, the shear center of a blade element is most likely not located at the blade element center of gravity. Unfortunately, it is not within the scope of this volume to quantify all the terms that contribute to pitch link and actuator loads. However, Fig. D-6 offers a hint as to the complexity inherent in the blade torsion problem.

When you compare Fig. D-6 to Hafner's assumptions, which were, to repeat,

"The blades produce no [torsional] moments about their longitudinal [spanwise] or pitch change axes due to

(a) aerodynamic forces, because the blades are fitted with aerofoil sections, the centre of pressures of

which lie always on a straight line coinciding with the pitch change axis; and

(b) weight and centrifugal forces, because the centre of gravity of each blade lies also in this [pitch change] axis."

376

APPENDIX D

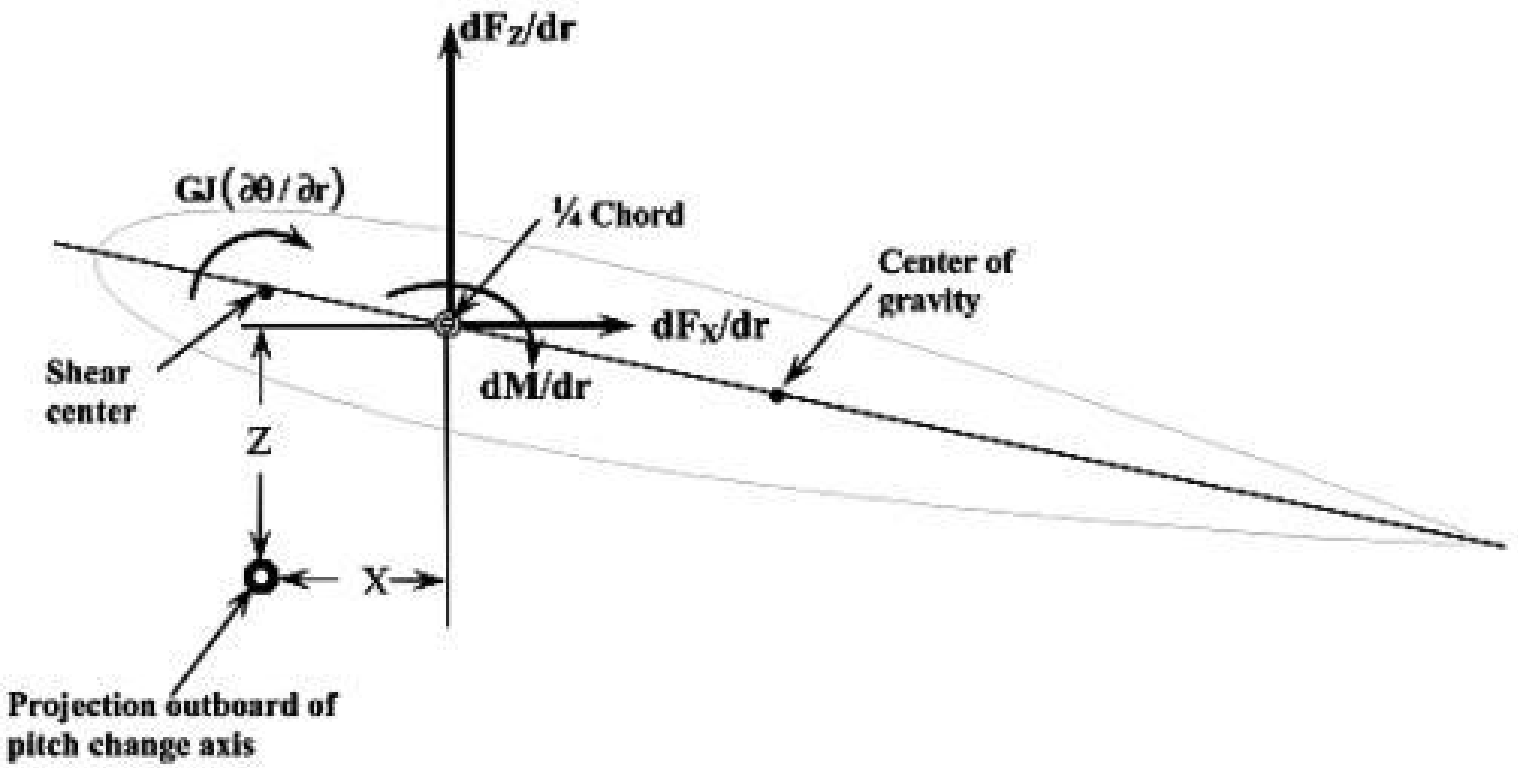

Fig. D-6. A few force and moment terms that must be included to accurately account for

elastic torsional deflection, blade element pitch angle, blade-root-end moments,
pitch link loads, and actuator loads.

you can appreciate that he made every effort to minimize moments assuming a blade did not bend flapwise (Z) or chordwise (X). Furthermore, he chose a symmetrical airfoil so that aerodynamic pitching moment (dM/dr) could be assumed zero.

Analyses that could capture *all* of the aerodynamics, dynamics, and mechanical features that contribute to accurate prediction of control loads *throughout* the flight envelope of *any* rotorcraft only began to emerge in the 21st century as I will discuss in Volume II—Helicopters. This capability has come some 70 years after Raoul Hafner's A.R. III was publically demonstrated at the Royal Aeronautical Society garden party on May 9th,

1937.

APPENDIX E

AUTOGYRO ERA ROTOR TRIM AND PERFORMANCE EQUATIONS

All through the 1930s, the theory of how to calculate rotor trim and performance steadily improved. By 1937, Wheatley, at the N.A.C.A. in the United States, had published his last rotorcraft contribution, and Lock, Beavan, Owen, and others in Great Britain had the prospect of World War II to face. Their ground-breaking work was carried on by a translation of work by G. Sissingh,[1] and by F. J. Bailey, Jr. who worked at the N.A.C.A Langley Research Center.[2,3] Bailey's NACA Report No. 716 is particularly interesting because he includes a sentence in the introduction stating:

"The form in which these expressions have been presented is unsatisfactory for practical engineering calculations, chiefly because the expressions have not been reduced to terms of the two basic parameters: inflow velocity and blade pitch."

The "expressions" Bailey was referring to were those that Wheatley had published in NACA Reports No. 487 and 591 . As to being "unsatisfactory," I would have to agree because several times early in my apprenticeship, I made all the computations Wheatley required with a slide rule, pencil, and paper. One could not be sure of the answers without a parallel check by a fellow sitting close by.

In early 2007, Dr. William Warmbrodt, Chief of the Aeromechanics Branch at NASA Ames Research Center, put me to work studying rotor performance at high advance ratio (at least up to $\mu = 1$). That work, published as NASA/CR–2008-215370, dealt with a correlation of the most advanced rotor trim and

performance theories with available experimental data. During that effort, I began to wonder if we were—today—really doing any better than what Wheatley, Bailey, and others had done in their era. To pursue that evaluation, I carefully re- derived all of the pioneer's equations using MathCad software and then performed a check by creating an EXCEL® spreadsheet to batch process any group of inputs corresponding to experimental data. Of course, I compared my developed equations to all the earlier work and found, not surprisingly, some differences.[4] These differences were primarily in how higher harmonic flapping terms are computed and in my including all powers of advance ratio.

---

[1] G. Sissingh, *Contribution to the Aerodynamics of Rotating-Wing Aircraft*, NACA Report No. 921, 1937.
[2] F. J. Bailey Jr., *A Study of the Torque Equilibrium of an Autogiro Rotor*, NACA Report No. 623, 1938.
[3] F . J. Bailey Jr., *A Simplified Theoretical Method of Determining the Characteristics of a Lifting Rotor in For- ward Flight*, NACA Report No. 716, March 17, 1941.
[4] In 2006, Ray Prouty told me this story that John Wheatley told to him about NACA Report No. 487. Both Ray and John worked at Lockheed then. As the story goes, somebody at the Bureau of Standards had derived some of Wheatley's equations and found an "error." (As Ray

tells it, the error was a numerical coefficient buried deep within one equation and that John thought the fellow had too much time on his hands). When this somebody brought the matter to Wheatley's attention by letter, John replied that he had re-derived that portion of his work twice and got different values of the coefficient himself. So he, John, was quite prepared to leave the published work untouched particularly since it was in widespread use.

APPENDIX E

To provide *some* progress after seven decades, I included elastic twisting and a simple nonuniform induced velocity function attributable to Glauert (see R&M 1111). The basic assumptions, parameter, symbols, and equations I used parallel Wheatley and Bailey. My definitions and symbols are:

$$\theta := \theta o + x \cdot \theta t - B1c \cdot \sin(\psi) - A1c \cdot \cos(\psi) +$$

$$x \cdot \theta e1s \cdot \sin(\psi) + x \cdot \theta e1c \cdot \cos(\psi)$$

$$\beta := \beta o - a1s \cdot \cos(\psi) - b1s \cdot \sin(\psi)$$

$$- a2s \cdot \cos(2 \cdot \psi) - b2s \cdot \sin(2 \cdot \psi) \quad UT$$

$$= x + \mu \cdot \sin(\psi)$$

$$UP := \lambda s + \lambda 1 \cdot x \cdot \cos(\psi) - x \cdot d\beta d\psi$$

$$\mu \cdot \beta \cdot \cos(\psi)$$

There are a few key points in the above definitions worth noting.

First, in the blade angle (θ) equation, all of the elastic blade twisting is included as a *linear variation* between the root and tip and based on the tip deflections ($\theta e1s$) and ($\theta e1c$), which only accounts for once-per-revolution twisting motion. The second harmonic elastic twisting is not negligible, but I was not prepared to carry the derivations to that level. The steady elastic twist can be included as part of the geometric twist (θt).

Second, in the blade flapping (β) equation, the expressions for the higher harmonic flapping coefficients (a2s and b2s) I used differ substantially from what our pioneers used. Lock and Wheatley, for example, assumed a Fourier-series solution to the blade flapping

equation. This approach leads to inner harmonic coupling, which requires a solution matrix of some magnitude. I, instead, took a page each out of books by Bramwell[5] and Johnson[6] that say the net work over a cycle must be zero. Adhering to this principle allows all higher harmonic flapping to be directly expressed in the primary parameters.

Third, in the out-of-plane velocity (UP) equation, I included a triangular inflow distribution of induced velocity ($\lambda 1$) in the fore and aft plane.

Finally, I followed Bailey's approach of collecting intermediate steps and output parameters in terms of the inflow ratio (λs).

This approach leads to a quadratic equation in inflow ratio, which, when solved, defines the rotor system angle of attack for autorotation. This is particularly handy for autogyro performance as Bailey suggested.

The equations and numerical example which follow should allow you to create any computer code you like—then you can take the same trip back in time that I did. I have laid out what follows in four parts, which are:

Part I. The fundamental equations that have been integrated

Part II. The input parameters (including values for the sample case)

Part III. The order in which parameters are calculated, which serves as an outline

Part IV. The several pages of equations that

perform the calculations

---

[5] A. R. S. Bramwell, *Helicopter Dynamics*, John Wiley & Sons, New York, 1976. [6] Wayne Johnson, *Helicopter Theory*, Princeton University Press, New Jersey, 1980.

APPENDIX E

Part I. The fundamental equations that have been integrated

$$CT := \frac{\sigma \cdot a}{2} \cdot \frac{1}{2 \cdot \pi} \cdot \int_{0}^{2 \cdot \pi}$$

$$\int_{0}^{B} UT^2 \cdot \left(\theta + \frac{UP}{UT} \right) dx\, d\psi - \frac{\sigma \cdot a}{2} \cdot \frac{2}{2 \cdot \pi} \cdot \int_{\pi}^{2 \cdot \pi}$$

$$\int_{0}^{-\mu \cdot \sin(\psi)} UT^2 \cdot \left(\theta + \frac{UP}{UT} \right) dx\, d\psi$$

$$CQa := \frac{\sigma \cdot a}{2} \cdot \left| -1 \cdot \frac{1}{2 \cdot \pi} \cdot \int_{\pi}^{\pi} \int_{B}^{B} \left[UT^2 \cdot \left(\theta + \frac{UP}{UT} \right) \cdot \frac{UP}{UT} \right] \cdot x \, dx \, d\psi - \frac{1}{2 \cdot \pi} \cdot \int_{0}^{2 \cdot \pi} \right.$$

$$\left| \int_{0}^{0} \int_{0}^{0} \left[UT^2 \cdot \left(\theta + \frac{UP}{UT} \right) \cdot \frac{UP}{UT} \right] dx \, d\psi \right.$$

$$\left. + \frac{1}{2 \cdot \pi} \cdot \int_{\pi}^{2 \cdot \pi} \int_{0}^{-\mu \cdot \sin(\psi)} \left[UT^2 \cdot \left(\theta + \frac{UP}{UT} \right) \cdot \frac{UP}{UT} \right] dx \, d\psi \right|$$

$$CQd := \frac{\sigma \cdot Cdo}{2} \cdot \left(\frac{1}{2 \cdot \pi} \cdot \int_{0}^{2 \cdot \pi} \int_{0}^{1} UT^2 \cdot x \, dx \, d\psi - \frac{2}{2 \cdot \pi} \cdot \int_{\pi}^{2 \cdot \pi} \int_{0}^{-\mu \cdot \sin(\psi)} \right.$$

$$\left. + \frac{\sigma \cdot \delta 1}{2} \cdot \frac{1}{2 \cdot \pi} \cdot \left| \int_{0}^{2 \cdot \pi} \int_{0}^{1} UT^2 \cdot \left(\theta + \frac{UP}{UT} \right) \cdot x \, dx \, d\psi \right| \ldots \right.$$

$$\left| \int_{-\mu \cdot \sin(\psi)}^{B} \left[UT^2 \cdot \left(\theta + \frac{UP}{UT} \right) \cdot \frac{UP}{UT} \right] \cdot x \, dx \, d\psi \ldots \right|$$

$$UT^2 \cdot x \, dx \, d\psi \Big| \ \ldots$$

$$+ \frac{\sigma \cdot \delta 2}{2} \cdot \left[\frac{1}{2 \cdot \pi} \cdot \int_{0}^{2 \cdot \pi} \int_{0}^{1} UT^2 \cdot \left(\theta + \right. \right.$$

$$CHa := \frac{\sigma \cdot a}{2} \cdot \left| -1 \cdot \frac{1}{2 \cdot \pi} \cdot \int_{0}^{\pi} \int_{0}^{B} \left[UT^2 \cdot \left(\theta + \right. \right. \right.$$

$$\left. \left. \left. \frac{UP}{UT} \right)^2 \cdot x \, dx \, d\psi - \frac{2}{2 \cdot \pi} \cdot \int_{\pi}^{2 \cdot \pi} \int_{0}^{-\mu \cdot \sin(\psi)} UT^2 \cdot \left(\theta + \frac{UP}{UT} \right)^2 \cdot x \, dx \, d\psi \right] \right.$$

$$\left. \frac{UP}{UT} \right) \Big] \cdot \left(\beta \cdot \cos(\psi) + \frac{UP}{UT} \cdot \sin(\psi) \right) dx \, d\psi \ \ldots \Big|$$

$$+0-\frac{1}{2\cdot\pi}\cdot\int_{-\pi}^{2\cdot\pi}\int_{-\mu\cdot\sin(\psi)}^{B}\left[UT^2\cdot\left(\theta+\frac{UP}{UT}\right)\right]\cdot\left(\beta\cdot\cos(\psi)+\frac{UP}{UT}\cdot\sin(\psi)\right)dx\,d\psi\ldots$$

$$+\frac{1}{2\cdot\pi}\cdot\left[\int_{-\pi}^{2\cdot\pi}\int_{0}^{\mu\cdot\sin(\psi)}\left[UT^2\cdot\left(\theta+\frac{UP}{UT}\right)\right]\cdot\left(\beta\cdot\cos(\psi)+\frac{UP}{UT}\cdot\sin(\psi)\right)dx\,d\psi\right]$$

APPENDIX E

$$CHd=\frac{\sigma\cdot Cdo}{2}\cdot\left(\frac{1}{2\cdot\pi}\cdot\int_{0}^{2\cdot\pi}\int_{0}^{1}UT^2\cdot\sin(\psi)\,dx\,d\psi-\frac{2}{2\cdot\pi}\cdot\int_{\pi}^{2\cdot\pi}\right.$$

$$+\frac{\sigma\cdot\delta1}{2}\cdot\frac{1}{2\cdot\pi}\cdot\left[\int_{}^{2\cdot\pi}\int_{}^{1}UT^2\cdot\left(\theta+\frac{UP}{UT}\right)\cdot\sin(\psi)\,dx\,d\psi\right]\ldots$$

$$+\frac{\sigma\cdot\delta2}{2}\cdot\left[\frac{1}{2\cdot\pi}\cdot\left[\int_{0}^{2\cdot\pi}\int_{0}^{1}UT^2\cdot\left(\theta+\frac{UP}{UT}\right)^2\cdot\sin(\psi)\,dx\,d\psi\ldots\right.\right.$$

$$\int_0^0 \int_0^{-\mu\cdot\sin(\psi)} UT^2\cdot\sin(\psi)\,dx\,d\psi \ \ldots$$

$$+0-\frac{2}{2\cdot\pi}\cdot\left[\int_{\pi}^{2\cdot\pi}\int_{0}^{-\mu\cdot\sin(\psi)} UT^2\cdot\left(\theta+\frac{UP}{UT}\right)^2\cdot\sin(\psi)\,dx\,d\psi\right]$$

$$CYa=\frac{\sigma\cdot a}{2}\cdot\left[-1\cdot\frac{1}{2\cdot\pi}\cdot\int_{0}^{\pi}\int_{0}^{B}\left[UT^2\cdot\left(\theta+\frac{UP}{UT}\right)\right]\cdot\left(\beta\cdot\sin(\psi)-\frac{UP}{UT}\cdot\cos(\psi)\right)dx\,d\psi \ \ldots\right.$$

$$\left.+0-\frac{1}{2\cdot\pi}\cdot\int_{\pi}^{2\cdot\pi}\int_{-\mu\cdot\sin(\psi)}^{B}\left[UT^2\cdot\left(\theta+\frac{UP}{UT}\right)\right]\cdot\left(\beta\cdot\sin(\psi)-\frac{UP}{UT}\cdot\cos(\psi)\right)dx\,d\psi \ \ldots\right.$$

$$\left.+\frac{1}{2\cdot\pi}\cdot\left[\int_{\pi}^{2\cdot\pi}\int_{0}^{-\mu\cdot\sin(\psi)}\left[UT^2\cdot\left(\theta+\frac{UP}{UT}\right)\right]\cdot\left(\beta\cdot\sin(\psi)-\frac{UP}{UT}\cdot\cos(\psi)\right)dx\,d\psi\right]\right]$$

$$CYd = \frac{\sigma \cdot Cdo}{2} \cdot \left| \frac{1}{2 \cdot \pi} \cdot \int_0^{2 \cdot \pi} \int_0^{1} -1 \cdot \left(UT^2 \cdot \cos(\psi) \right) dx\, d\psi - \frac{2}{2 \cdot \pi} \cdot \int_{\pi}^{2 \cdot \pi} \right.$$

$$+ \frac{\sigma \cdot \delta 1}{2} \cdot \frac{1}{2 \cdot \pi} \cdot \left[\int_0^{2 \cdot \pi} \int_0^{1} -1 \cdot \left[UT^2 \cdot \left(\frac{UP}{UT} + \theta \right) \right] \cdot \cos(\psi)\, dx\, d\psi \right| \ldots$$

$$+ \frac{\sigma \cdot \delta 2}{2} \cdot \left| \frac{1}{2 \cdot \pi} \cdot \int_0^{2 \cdot \pi} \int_0^{1} -1 \cdot \left[UT^2 \cdot \left(\frac{UP}{UT} + \theta \right)^2 \right] \cdot \cos(\psi)\, dx\, d\psi \ldots \right.$$

$$\int_0^{-\mu \cdot \sin(\psi)} -1 \cdot \left(UT^2 \cdot \cos(\psi) \right) dx\, d\psi \Bigg| \ldots$$

$$\Bigg| + 0 \quad - \frac{2}{2 \cdot \pi} \cdot \int_0^{2 \cdot \pi} \int_0^{-\mu \cdot \sin(\psi)}$$

$$-1\cdot\left[UT^2\cdot\left(\frac{UP}{UT}+\theta\right)^2\right]\cdot\cos(\psi)\,dx\,d\psi$$

$$\pi \qquad 0$$

382

APPENDIX E

Part II. The input parameters (including values for the sample case)

Parameter	Symbol	Sample Case	Units	Comments
Advance ratio	μ	0.70	na	$V\cos\alpha_s/V_t$
Uniform inflow ratio	λs	0.0130	na	$(V\sin\alpha_s - v)/V_t$
Nonuniform inflow ratio	$\lambda 1$	–0.007287534590767	na	$(-Kv)/V_t$
Lock number	γ	19.2	na	$\rho acR^4/I_b$
Tip loss factor	B	0.97	na	r/R
Solidity	σ	0.0976	na	$bc/\pi R$
Airfoil lift-curve slope	a	5.73	per radian	
Airfoil drag polar				
Minimum drag coefficient	Cdo	0.0120	na	
Drag rise with Cl	$\delta 1$	–0.0216	na	
Drag rise with Cl^2	$\delta 2$	0.0400	na	
Root collective	θo	$1.9\pi/180$	radian	
Twist	θt	$-1.0\pi/180$	radian	
Longitudinal cyclic	B1c	$-2.0\pi/180$	radian	
Lateral cyclic	A1c	$1.0\pi/180$	radian	
Elastic twist (sine)	$\theta e1s$	$-1.0\pi/180$	radian	
Elastic twist (cosine)	$\theta e1c$	$1.0\pi/180$	radian	

Part III. The order in which parameters are calculated, which serves as an outline

1. Calculate βo, a1s, b1s, a2s, and b2s to use in all calculations
2. Calculate Thrust Coefficient, CT
3. Calculate Accelerating Torque Coefficient, CQa
4. Calculate Decelerating Torque

Coefficient, CQd (per Bailey NACA Report No. 716)

5. Calculate Total Torque Coefficient, CQ

6. Calculate Inflow Ratio for Autorotation

7. Calculate Accelerating H-Force Coefficient, CHa, due to Cl and inflow

8. Check CHa due to Cl and inflow from $CHa := \frac{-1 \cdot (CT \cdot \lambda s + CQa)}{}$

9. Calculate H-Force Coefficient, CHd, due to Cd μ

10. Calculate Total H-Force Coefficient, CH

11. Calculate Y-Force Coefficient, CYa, due to CL (Y-Force positive to $\psi = 90^{\circ}$)

12. Calculate Y-Force, CYd, due to Cd

13. Calculate Total Y-Force Coefficient, CY

14. Calculate Shaft Angle of Attack, α_S, positive nose-up

15. Repeat input (angles now in degrees)

16. Summarize output

APPENDIX E

Part IV. The several pages of equations that perform the calculations

These equations have been copied directly from MathCad and pasted in this document. This has, I hope, avoided any typographical errors that might have occurred were I to have entered the equations in some

equation editor software. MathCad uses := for equations to be calculated and entry values. It uses a conventional = for computed values of an equation. A number of intermediate calculations are made before the final parameter is calculated as you can see from the calculation of (b2s) below. The final calculation of a parameter is in large type, as you see for (b2s) below.

1. Calculate βo, a1s, b1s, a2s, and b2s to use in all calculations

$$M0 := \left(B^4 + \frac{1}{6}\cdot\mu^4\right)\cdot\left(B^4 - \frac{1}{2}\cdot B^2\cdot\mu^2 + \frac{7}{24}\cdot\mu^4\right) - \left(\frac{2}{3}\cdot B^3\cdot\mu - \frac{88}{315\cdot\pi}\cdot\mu^4\right)\cdot\left(\frac{2}{3}\cdot B^3\cdot\mu - \frac{64}{45\cdot\pi}\cdot\mu^4\right)$$

$$M0 = 0.542330515448621$$

$$M1 := \left(\frac{8}{15\cdot\pi}\cdot\mu^3\right)\cdot\left(B^4 - \frac{1}{2}\cdot B^2\cdot\mu^2 + \frac{7}{24}\cdot\mu^4\right) - \left(\frac{2}{3}\cdot B^3\cdot\mu - \frac{88}{315\cdot\pi}\cdot\mu^4\right)\cdot\left(2\cdot B^2\cdot\mu - \frac{1}{2}\cdot\mu^3\right)$$

$$M1 = -0.421327574886569$$

M2

$$= \left(\frac{1}{2}\cdot B^2\cdot\mu^2 - \frac{1}{12}\cdot\mu^4\right)\cdot\left(B^4 - \frac{1}{2}\cdot B^2\cdot\mu^2 + \frac{7}{24}\cdot\mu^4\right) - \left(\frac{2}{3}\cdot B^3\cdot\mu - \frac{88}{315\cdot\pi}\cdot\mu^4\right)\cdot\left(\frac{8}{3}\cdot B^3\cdot\mu + \frac{32}{45\cdot\pi}\cdot\mu^4\right)$$

$$M2 = -0.558644204651302$$

M3

$$= \left(\frac{1}{3}\cdot B^3\cdot\mu^2 - \frac{32}{315\cdot\pi}\cdot\mu^5\right)\cdot\left(B^4 - \frac{1}{2}\cdot B^2\cdot\mu^2 + \frac{7}{24}\cdot\mu^4\right) - \left(\frac{2}{3}\cdot B^3\cdot\mu - \frac{88}{315\cdot\pi}\cdot\mu^4\right)\cdot\left(2\cdot B^4\cdot\mu + \frac{1}{12}\cdot\mu^5\right)$$

$$M3 = -0.402978977618712$$

$$M4 := \left(\frac{2}{3}\cdot B^3\cdot\mu - \frac{88}{315\cdot\pi}\cdot\mu^4\right)\cdot\left(B^4 + \frac{3}{2}\cdot B^2\cdot\mu^2 - \frac{5}{24}\cdot\mu^4\right)$$

$$\left(\frac{2}{3}\cdot B^3\cdot\mu + \frac{16}{63\cdot\pi}\cdot\mu^4\right)\cdot\left(B^4 - \frac{1}{2}\cdot B^2\cdot\mu^2 + \frac{7}{24}\cdot\mu^4\right)$$

$$M4 = 0.294929302420598$$

M5

$$= \left(B^4 - \frac{1}{2}\cdot B^2\cdot\mu^2 + \frac{7}{24}\cdot\mu^4\right)\cdot\left(\frac{1}{2}\cdot B^4\cdot\mu + \frac{1}{32}\cdot\mu^5\right) - \left(\frac{2}{3}\cdot B^3\cdot\mu - \frac{88}{315\cdot\pi}\cdot\mu^4\right)\cdot\left(\frac{4}{5}\cdot B^5 + B^3\cdot\mu^2 - \frac{128}{525\cdot\pi}\cdot\mu^5\right)$$

$$M5 = -0.225189212027 64$$

$$c1 := \frac{M1}{M0} \qquad c1 = -0.776883400223281$$

$$k1 := \frac{M2\cdot\theta o + M3\cdot\theta t + M4\cdot B1c + M5\cdot\theta e1s}{M0}$$

$$k1 = -0.032925890146846$$

$$b2s := c1\cdot\lambda s + k1 \qquad b2s$$

$= -0.043025374349748$

384

$$c2 := \frac{\left(2\cdot B^2\cdot\mu - \frac{1}{2}\cdot\mu^3\right) - \left(\frac{2}{3}\cdot B^3\cdot\mu - \frac{64}{45\cdot\pi}\cdot\mu^4\right)\cdot c1}{B^4 - \frac{1}{2}\cdot B^2\cdot\mu^2 + \frac{7}{24}\cdot\mu^4}$$

$c2 = 1.920804850449535$

$$\left(\frac{8}{3}\cdot B^3\cdot\mu + \frac{32}{45\cdot\pi}\cdot\mu^4\right)\cdot\theta o + \left(2\cdot B^4\cdot\mu + \frac{1}{12}\cdot\mu^5\right)\cdot\theta t - \left(B^4 + \frac{3}{2}\cdot B^2\cdot\mu^2 -\right.$$

$$k2 := \frac{\left. + \left(\frac{4}{5}\cdot B^5 + B^3\cdot\mu^2 - \frac{128}{525\cdot\pi}\cdot\mu^5\right)\cdot\theta e1s\right.}{B^4 - \frac{1}{2}\cdot B^2\cdot\mu^2 + \frac{7}{24}\cdot\mu^4}$$

$k2 = 0.111195718630495$

APPENDIX E

$$\left(\frac{5}{24}\cdot\mu^4\right)\cdot B1c - \left(\frac{2}{3}\cdot B^3\cdot\mu - \frac{64}{45\cdot\pi}\cdot\mu^4\right)\cdot k1 \ldots$$

$$a1s := c2\cdot\lambda s + k2$$

$$a1s = 0.136166181686339 \quad c3$$

$$= \frac{\gamma}{2}\cdot\left[\left(\left(B^3 + \frac{2}{3\cdot\pi}\cdot\mu^3\right)\cdot\frac{1}{3} + \left(B^2\cdot\mu^2 - \frac{1}{2}\cdot\mu^4\right)\cdot\frac{1}{8}\right)\cdot c1 \left(\frac{2}{15\cdot\pi}\cdot\mu^4\right)\cdot c2\right]$$

$$c3 = 3.02348303009608$$

$$k3 := \frac{\gamma}{2}\cdot\left[\left(\left(B^4 + B^2\cdot\mu^2 - \frac{1}{8}\cdot\mu^4\right)\cdot\frac{\theta o}{4} + \left(B^5 + \frac{5}{6}\cdot B^3\cdot\mu^2 \frac{8}{45\cdot\pi}\cdot\mu^5\right)\cdot\frac{\theta t}{5}\right) + \left(B^2\cdot\mu^2 - \frac{1}{2}\cdot\mu^4\right)\cdot\frac{1}{8}\cdot k1 - \left(B^3\cdot\mu + \frac{4}{15\cdot\pi}\cdot\mu^4\right)\cdot\frac{B1c}{3} + \left(\frac{2}{15\cdot\pi}\cdot\mu^4\right)\cdot k2 + \left(\frac{1}{4}\cdot B^4\cdot\mu + \frac{1}{96}\cdot\mu^5\right)\cdot\theta e1s$$

$k3 = 0.10860836153735 3$

$$\beta o := c3 \cdot \lambda s + k3$$

$$\beta o = 0.14791364092860 2$$

$$N0 := \left(B^4 + \frac{1}{12}\cdot\mu^4\right)\cdot\left(B^4 + \frac{1}{2}\cdot B^2\cdot\mu^2 - \frac{1}{24}\cdot\mu^4\right) - \left(\frac{2}{3}\cdot B^3\cdot\mu + \frac{32}{315\cdot\pi}\cdot\mu^4\right)\cdot\left(\frac{2}{3}\cdot B^3\cdot\mu - \frac{16}{45\cdot\pi}\cdot\mu^4\right)$$

$N0 = 0.82816538423059$

$N1$

$$= \left(\frac{2}{3}\cdot B^3\cdot\mu + \frac{32}{315\cdot\pi}\cdot\mu^4\right)\cdot\left(\frac{4}{3}\cdot B^3\cdot\mu + \frac{16}{45\cdot\pi}\cdot\mu^4\right) - \left(B^4 + \frac{1}{2}\cdot B^2\cdot\mu^2 - \frac{1}{24}\cdot\mu^4\right)\cdot\left(\frac{1}{2}\cdot B^2\cdot\mu^2 - \frac{1}{12}\cdot\mu^4\right)$$

$$N1 = 0.14841750363409 4$$

$$N2 := \left(B^4 + \frac{1}{2}\cdot B^2\cdot\mu^2 - \frac{1}{24}\cdot\mu^4\right)\cdot\left(\frac{1}{3}\cdot B^3\cdot\mu -$$

$$N2 = -0.16136619305292 3$$

$$N3 := \left(B^4 + \frac{1}{2}\cdot B^2\cdot\mu^2 - \frac{1}{24}\cdot\mu^4\right)\cdot\left(\frac{1}{2}\cdot B^4\cdot\mu + \right.$$

$$N3 = -0.017063134116859$$

$$\left.\frac{32}{315\cdot\pi}\cdot\mu^4\right) - \left(\frac{2}{3}\cdot B^3\cdot\mu + \frac{32}{315\cdot\pi}\cdot\mu^4\right)\cdot\left(B^4 + \frac{1}{24}\cdot\mu^4\right)$$

$$\left.\frac{1}{96}\cdot\mu^5\right) - \left(\frac{2}{3}\cdot B^3\cdot\mu + \frac{32}{315\cdot\pi}\cdot\mu^4\right)\cdot\left(\frac{4}{5}\cdot B^5 + \frac{1}{3}\cdot B^3\cdot\mu^2 - \frac{64}{1575\cdot\pi}\cdot\mu^5\right)$$

APPENDIX E

$$c4 := \frac{N1\cdot c3}{N0}$$

$$c4 = 0.541845641162371$$

$$k4 := \frac{N1\cdot(k3) + (N2)\cdot\lambda1 + (N3)\cdot\theta e1c}{}$$

N0

$k4 = 0.020524325285051$

$$a2s := c4 \cdot \lambda s + k4$$

$$a2s = 0.027568318620162$$

$$c5 := \frac{\left(\frac{4}{3}\cdot B^3\cdot\mu + \frac{16}{45\cdot\pi}\cdot\mu^4\right)\cdot c3 + \left(\frac{2}{3}\cdot B^3\cdot\mu - \frac{16}{45\cdot\pi}\cdot\mu^4\right)\cdot c4}{B^4 + \frac{1}{2}\cdot B^2\cdot\mu^2 - \frac{1}{24}\cdot\mu^4}$$

$c5 = 2.59873326749403$

$$k5 := \frac{\left[\left(\frac{4}{3}\cdot B^3\cdot\mu + \frac{16}{45\cdot\pi}\cdot\mu^4\right)\cdot k3 - \left(B^4 + \frac{1}{24}\cdot\mu^4\right)\cdot\lambda 1 + \left(B^4 + \frac{1}{2}\cdot B^2\cdot\mu^2 - \frac{1}{24}\cdot\mu^4\right)\cdot A1c\right.}{B^4 + \frac{1}{2}\cdot B^2\cdot\mu^2 - \frac{1}{24}\cdot\mu^4}$$
$$\frac{\left. + \left(\frac{2}{3}\cdot B^3\cdot\mu - \frac{16}{45\cdot\pi}\cdot\mu^4\right)\cdot k4 - \left(\frac{4}{5}\cdot B^5 + \frac{1}{3}\cdot B^3\cdot\mu^2 - \frac{64}{1575\pi}\cdot\mu^5\right)\cdot\theta e1c\right]}{}$$

$k5 = 0.103925113983945$

$$b1s := c5 \cdot \lambda s + k5$$

$$b1s = 0.137708646461368$$

2. Calculate Thrust Coefficient, CT

$$T1 := \left(\frac{1}{2}\cdot B^2 + \frac{1}{4}\cdot\mu^2\right) + \left(\frac{1}{4}\cdot B\cdot\mu^2 \right.$$

$$\left.\frac{8}{15\cdot\pi}\cdot\mu^3\right)\cdot c1 + \left(\frac{1}{8}\cdot\mu^3\right)\cdot c2$$

$$T1 = 0.628228860960388$$

$$T2 := \left(\frac{1}{3}\cdot B^3 + \frac{1}{2}\cdot B\cdot\mu^2 - \frac{4}{9\cdot\pi}\cdot\mu^3\right)\cdot\theta o + \left(\frac{1}{4}\cdot B^4 + \frac{1}{4}\cdot B^2\cdot\mu^2 \right.$$

$$\left.\frac{1}{32}\cdot\mu^4\right)\cdot\theta t - \left(\frac{1}{2}\cdot B^2\cdot\mu + \frac{1}{8}\cdot\mu^3\right)\cdot B1c \ldots$$

$$+ \left(\frac{1}{4}\cdot B\cdot\mu^2 - \frac{8}{15\cdot\pi}\cdot\mu^3\right)\cdot k1 + \left(\frac{1}{8}\cdot\mu^3\right)\cdot k2 + \left(\frac{1}{3}\cdot B^3\cdot\mu + \frac{4}{45\cdot\pi}\cdot\mu^4\right)\cdot\theta e1s$$

$$T2 = 0.022545430221145$$

$$CT := \frac{\sigma\cdot a}{2}\cdot(T1\cdot\lambda s + T2)$$

$$CT = 0.008587925651381$$

386

APPENDIX E

3. Calculate Accelerating Torque, CQa

$$A1 := \left(\frac{1}{2}\cdot B^2 - \frac{1}{4}\cdot \mu^2\right) + \left(\frac{1}{2}\cdot B^2\cdot \mu - \frac{3}{8}\cdot \mu^3\right)\cdot c2 + \left(\frac{8}{5\cdot \pi}\cdot \mu^3\right)\cdot c1$$

$$A1 = 0.597723756350029$$

A2

$$= \left(\frac{1}{3}\cdot B^3 + \frac{2}{9\cdot \pi}\cdot \mu^3\right)\cdot \theta o + \left(\frac{1}{4}\cdot B^4 + \frac{1}{32}\cdot \mu^4\right)\cdot \theta t + \left(\frac{1}{2}\cdot B^2\cdot \mu - \frac{3}{8}\cdot \mu^3\right)\cdot k2 \ldots$$
$$+ \left(\frac{8}{5\cdot \pi}\cdot \mu^3\right)\cdot k1 - \left(\frac{1}{4}\cdot B^2\cdot \mu - \frac{1}{16}\cdot \mu^3\right)\cdot B1c + \left(\frac{1}{6}\cdot B^3\cdot \mu - \frac{4}{45\cdot \pi}\cdot \mu^4\right)\cdot \theta e1s$$

$$A2 = 0.026722839863594$$

$$A3 := \left(\frac{1}{8}\cdot B^2\cdot \mu^2 - \frac{1}{16}\cdot \mu^4\right)\cdot c1\cdot \theta o + \left(\frac{2}{15\cdot \pi}\cdot \mu^4\right)\cdot c2\cdot \theta o$$

$$A3 = -0.00044901903045 1$$

$$A4 := \left(\frac{1}{8}\cdot B^2\cdot\mu^2 - \frac{1}{16}\cdot\mu^4\right)\cdot k1\cdot\theta o + \left(\frac{2}{15\cdot\pi}\cdot\mu^4\right)\cdot k2\cdot\theta o$$

$$A4 = -0.000008964376402$$

$$A5 := \left(\frac{1}{12}\cdot B^3\cdot\mu^2 - \frac{32}{315\cdot\pi}\cdot\mu^5\right)\cdot c1\cdot\theta t + \left(\frac{1}{48}\cdot\mu^5\right)\cdot c2\cdot\theta t$$

$$A5 = 0.000314241300393$$

$$A6 := \left(\frac{1}{12}\cdot B^3\cdot\mu^2 - \frac{32}{315\cdot\pi}\cdot\mu^5\right)\cdot k1\cdot\theta t + \left(\frac{1}{48}\cdot\mu^5\right)\cdot k2\cdot\theta t$$

$$A6 = 0.000011497770935$$

$$A7 := \left(\frac{1}{8}\cdot B^4 + \frac{3}{16}\cdot B^2\cdot\mu^2 - \frac{29}{192}\cdot\mu^4\right)\cdot c2^2 + \left(\frac{1}{6}\cdot B^3\cdot\mu + \frac{56}{45\cdot\pi}\cdot\mu^4\right)\cdot c1\cdot c2 \quad A7 = 0.29260799957433$$

$$A8 := \left(\frac{1}{4}\cdot B^4 + \frac{3}{8}\cdot B^2\cdot\mu^2 - \frac{29}{96}\cdot\mu^4\right)\cdot c2\cdot k2 + \left(\frac{1}{8}\cdot B^4 - \frac{1}{16}\cdot B^2\cdot\mu^2 + \frac{7}{192}\cdot\mu^4\right)\cdot B1c\cdot c2 \ldots + \left(\frac{1}{6}\cdot B^3\cdot\mu + \frac{56}{45\cdot\pi}\cdot\mu^4\right)\cdot(c1\cdot k2 + k1\cdot c2) - \left(\frac{1}{10}\cdot B^5 - \frac{1}{24}\cdot B^3\cdot\mu^2 + \frac{92}{1575\cdot\pi}\cdot\mu^5\right)\cdot\theta e1s\cdot c2$$

$$A8 = 0.034827654259352$$

A9

$$= \left(\frac{1}{8}\cdot B^4 + \frac{3}{16}\cdot B^2\cdot\mu^2 - \frac{29}{192}\cdot\mu^4\right)\cdot k2^2 + \left(\frac{1}{8}\cdot B^4 - \frac{1}{16}\cdot B^2\cdot\mu^2 + \frac{7}{192}\cdot\mu^4\right)\cdot B1c\cdot k2 \ldots$$

$$+ \left(\frac{1}{6}\cdot B^3\cdot\mu + \frac{56}{45\cdot\pi}\cdot\mu^4\right)\cdot k1\cdot k2 - \left(\frac{1}{10}\cdot B^5 - \frac{1}{24}\cdot B^3\cdot\mu^2 + \frac{92}{1575\cdot\pi}\cdot\mu^5\right)\cdot\theta e1s\cdot k2 \quad A9 = 0.001035569893085$$

APPENDIX E

$$A10 := \left(\frac{1}{8}\cdot B^4 + \frac{1}{16}\cdot B^2\cdot\mu^2 - \frac{1}{192}\cdot\mu^4\right)\cdot c5^2 - \left(\frac{1}{3}\cdot B^3\cdot\mu + \frac{4}{45\cdot\pi}\cdot\mu^4\right)\cdot c3\cdot c5 - \left(\frac{1}{6}\cdot B^3\cdot\mu - \frac{4}{45\cdot\pi}\cdot\mu^4\right)\cdot c4\cdot c5 \quad A10 =$$

$$-0.933498451064171$$

A11

$$= \left(\frac{1}{4}\cdot B^4 + \frac{1}{8}\cdot B^2\cdot\mu^2 - \frac{1}{96}\cdot\mu^4\right)\cdot c5\cdot k5 - \left(\frac{1}{3}\cdot B^3\cdot\mu + \frac{4}{45\cdot\pi}\cdot\mu^4\right)\cdot(c3\cdot k5 + k3\cdot c5) \ldots$$

$$+0 - \left(\frac{1}{6}\cdot B^3\cdot\mu - \frac{4}{45\cdot\pi}\cdot\mu^4\right)\cdot(c4\cdot k5 + k4\cdot c5) + \left(\frac{1}{4}\cdot B^4 + \frac{1}{96}\cdot\mu^4\right)\cdot\lambda1\cdot c5$$

$$+0 - \left(\frac{1}{8}\cdot B^4 + \frac{1}{16}\cdot B^2\cdot\mu^2 - \frac{1}{192}\cdot\mu^4\right)\cdot A1c\cdot c5 + \left(\frac{1}{10}\cdot B^5 + \frac{1}{24}\cdot B^3\cdot\mu^2 - \frac{8}{1575\cdot\pi}\cdot\mu^5\right)\cdot\theta e1c\cdot c5$$

$$A11 = -0.073120778920482$$

$$A12 := \left(\frac{1}{8}\cdot B^4 + \frac{1}{16}\cdot B^2\cdot\mu^2 - \frac{1}{192}\cdot\mu^4\right)\cdot k5^2 - \left(\frac{1}{3}\cdot B^3\cdot\mu + \right.$$

$$\left.\frac{4}{45\cdot\pi}\cdot\mu^4\right)\cdot k3\cdot k5 - \left(\frac{1}{6}\cdot B^3\cdot\mu - \frac{4}{45\cdot\pi}\cdot\mu^4\right)\cdot k4\cdot k5 \ldots$$

$$+\left(\frac{1}{4}\cdot B^4 + \frac{1}{96}\cdot\mu^4\right)\cdot\lambda1\cdot k5 - \left(\frac{1}{8}\cdot B^4 + \frac{1}{16}\cdot B^2\cdot\mu^2 - \frac{1}{192}\cdot\mu^4\right)\cdot A1c\cdot k5 \ldots$$

$$+\left(\frac{1}{10}\cdot B^5 + \frac{1}{24}\cdot B^3\cdot\mu^2 - \frac{8}{1575\cdot\pi}\cdot\mu^5\right)\cdot\theta e1c\cdot k5$$

$$A12 = -0.001431248082753$$

$$A13 := \left(\frac{1}{4}\cdot B^2\cdot\mu^2 - \frac{1}{16}\cdot\mu^4\right)\cdot c3^2 - \left(\frac{1}{4}\cdot B^2\cdot\mu^2 - \frac{1}{6}\cdot\mu^4\right)\cdot c4\cdot c3$$

$$A13 = 0.793198255860955$$

$$A14 := \left(\frac{1}{2}\cdot B^2\cdot\mu^2 - \frac{1}{8}\cdot\mu^4\right)\cdot c3\cdot k3 - \left(\frac{1}{4}\cdot B^2\cdot\mu^2 - \frac{1}{6}\cdot\mu^4\right)\cdot(c4\cdot k3 + k4\cdot c3) \ldots$$
$$+ \left(\frac{1}{6}\cdot B^3\cdot\mu + \frac{2}{45\cdot\pi}\cdot\mu^4\right)\cdot A1c\cdot c3 - \left(\frac{1}{3}\cdot B^3\cdot\mu - \frac{8}{45\cdot\pi}\cdot\mu^4\right)\cdot\lambda1\cdot c3 - \left(\frac{1}{8}\cdot B^4\cdot\mu + \frac{1}{192}\cdot\mu^5\right)\cdot\theta e1c\cdot c3$$

$A14 = 0.062801733980362$

$$A15 := \left(\frac{1}{4}\cdot B^2\cdot\mu^2 - \frac{1}{16}\cdot\mu^4\right)\cdot k3^2 - \left(\frac{1}{4}\cdot B^2\cdot\mu^2 - \frac{1}{6}\cdot\mu^4\right)\cdot k4\cdot k3 \ldots$$
$$+ \left(\frac{1}{6}\cdot B^3\cdot\mu + \frac{2}{45\cdot\pi}\cdot\mu^4\right)\cdot A1c\cdot k3 - \left(\frac{1}{3}\cdot B^3\cdot\mu - \frac{8}{45\cdot\pi}\cdot\mu^4\right)\cdot\lambda1\cdot k3 - \left(\frac{1}{8}\cdot B^4\cdot\mu + \frac{1}{192}\cdot\mu^5\right)\cdot\theta e1c\cdot k3$$

$A15 = 0.00123242642384$

$$A16 := \left(\frac{1}{6}\cdot B^3\cdot\mu - \frac{88}{315\cdot\pi}\cdot\mu^4\right)\cdot\lambda1\cdot c4$$

$A16 = -0.00033614537052$

$A17$

$$= \left(\frac{1}{8}\cdot B^4 - \frac{1}{64}\cdot\mu^4\right)\cdot\lambda1^2 - \left(\frac{1}{8}\cdot B^4 + \frac{1}{192}\cdot\mu^4\right)\cdot A1c\cdot\lambda1 + \left(\frac{1}{6}\cdot B^3\cdot\mu - \frac{88}{315\cdot\pi}\cdot\mu^4\right)\cdot\lambda1\cdot k4 \ldots$$

$$+ \left(\frac{1}{10}\cdot B^5 + \frac{4}{525\cdot\pi}\cdot\mu^5\right)\cdot\theta e1c\cdot\lambda1$$

$A17 = -0.000003794843514$

$$A18 := \left(\frac{1}{2}\cdot B^4 + \frac{1}{8}\cdot B^2\cdot\mu^2 - \frac{25}{192}\cdot\mu^4\right)\cdot c4^2$$

$$A18 = 0.137700818005821$$

$$A19 := \left(B^4 + \frac{1}{4}\cdot B^2\cdot\mu^2 - \frac{25}{96}\cdot\mu^4\right)\cdot c4\cdot k4 + \left(\frac{1}{12}\cdot B^3\cdot\mu - \frac{2}{45\cdot\pi}\cdot\mu^4\right)\cdot A1c\cdot c4 -$$

$$A19 = 0.010547237964583$$

$$A20 := \left(\frac{1}{2}\cdot B^4 + \frac{1}{8}\cdot B^2\cdot\mu^2 - \frac{25}{192}\cdot\mu^4\right)\cdot k4^2 + \left(\frac{1}{12}\cdot B^3\cdot\mu - \frac{2}{45\cdot\pi}\cdot\mu^4\right)\cdot A1c\cdot k4$$

$$A20 = 0.000201943073982$$

$$A2S := A18\cdot\lambda s^2 + A19\cdot\lambda s + A20 \qquad A2S = 0.000362328605764$$

$$A21 := \left(\frac{1}{2}\cdot B^4 + \frac{1}{8}\cdot B^2\cdot\mu^2 - \frac{59}{192}\cdot\mu^4\right)\cdot c1^2$$

$$A21 = 0.257410609783993$$

$$A22 := \left(B^4 + \frac{1}{4}\cdot B^2\cdot\mu^2 - \frac{59}{96}\cdot\mu^4\right)\cdot c1\cdot k1 + \left(\frac{1}{12}\cdot B^3\cdot\mu -$$

$$A22 = 0.022437551769387$$

$$A23 := \left(\frac{1}{2}\cdot B^4 + \frac{1}{8}\cdot B^2\cdot\mu^2 - \frac{59}{192}\cdot\mu^4\right)\cdot k1^2 + \left(\frac{1}{12}\cdot B^3\cdot\mu\right.$$

$$A23 = 0.000488578663 63$$

$$A24 := A13 + A1 + A7 + A21 + A18 + A10$$

APPENDIX E

$$\left(\frac{1}{16}\cdot B^4\cdot\mu - \frac{5}{768}\cdot\mu^5\right)\cdot\theta e1c\cdot c4$$

$$- \left(\frac{1}{16}\cdot B^4\cdot\mu - \frac{5}{768}\cdot\mu^5\right)\cdot\theta e1c\cdot k4$$

$$\frac{8}{45\cdot\pi}\cdot\mu^4\right)\cdot B1c\cdot c1 - \left(\frac{1}{16}\cdot B^4\cdot\mu - \frac{23}{768}\cdot\mu^5\right)\cdot\theta e1s\cdot c1$$

$$- \frac{8}{45\cdot\pi}\cdot\mu^4\right)\cdot B1c\cdot k1 - \left(\frac{1}{16}\cdot B^4\cdot\mu - \frac{23}{768}\cdot\mu^5\right)\cdot\theta e1s\cdot k1$$

$$A24 = 1.145142988510958$$

$$A25 := A3 + A14 + A11 + A8 + A5 + A22 + A2 + A16 +$$

A19 $A25 = 0.083745315816218$ $A26 := A9 + A15 + A20 + A4 + A17 + A6 + A12 + A23$ $A26 = 0.001526008522803$

$$CQa := -1 \cdot \frac{\sigma \cdot a}{2} \cdot \left(A24 \cdot \lambda s^2 + A25 \cdot \lambda s + A26 \right)$$

$$CQa = -0.000785247608898$$

4. Calculate Decelerating Torque, CQd (per Bailey NACA TR 716)

$$D0 := 1 + \mu^2 - \frac{1}{8} \cdot \mu^4 \qquad D0 = 1.4599875$$

$$CQCdo := \frac{\sigma \cdot Cdo}{8} \cdot (D0)$$

$$CQCdo = 0.00021374217$$

$$D1 := \frac{1}{3} + \left(\frac{1}{8} \cdot \mu^2 \right) \cdot c1 \qquad D1 = 0.285749225069657$$

D2

$$= \left(\frac{1}{4} + \frac{1}{4}\cdot\mu^2\right)\cdot\theta o + \left(\frac{1}{5} + \frac{1}{6}\cdot\mu^2\right)\cdot\theta t + \left(\frac{1}{8}\cdot\mu^2\right)\cdot k1 - \left(\frac{1}{3}\cdot\mu\right)\cdot B1c + \left(\frac{1}{4}\cdot\mu\right)\cdot\theta e1s$$

$$D2 = 0.010510389934695$$

$$CQ\delta 1 := \frac{\sigma\cdot\delta 1}{2}\cdot(D1\cdot\lambda s + D2)$$

$$D3 := \left(\frac{1}{2} - \frac{1}{4}\cdot\mu^2\right) + \left(\frac{1}{2}\cdot\mu - \frac{3}{8}\cdot\mu^3\right)\cdot c2 + \left(\frac{8}{5\cdot\pi}\cdot\mu^3\right)\cdot c1$$

$$D3 = 0.667005604681578$$

$$D4 := \left(\frac{2}{3} + \frac{4}{9\cdot\pi}\cdot\mu^3\right)\cdot\theta o + \left(\frac{1}{2}\cdot\mu - \frac{3}{8}\cdot\mu^3\right)\cdot k2 + \left(\frac{1}{2} + \frac{1}{16}\cdot\mu^4\right)\cdot\theta t + \left(\frac{1}{3}\cdot\mu - \frac{8}{45\cdot\pi}\cdot\mu^4\right)\cdot\theta e1s$$

$$D4 = 0.040477649727351$$

$$D5 := \left(\frac{4}{15\cdot\pi}\cdot\mu^4\right)\cdot c2\cdot\theta o + \left(\frac{1}{4}\cdot\mu^2 - \frac{1}{8}\cdot\mu^4\right)\cdot c1\cdot\theta o$$

$$D5 = -0.001084551607357$$

$$CQ\delta 1 = -0.000014994424883$$

$$\left(\frac{8}{5\cdot\pi}\cdot\mu^3\right)\cdot k1 - \left(\frac{1}{2}\cdot\mu - \frac{1}{8}\cdot\mu^3\right)\cdot B1c \ldots$$

$$D6 := \left(\frac{1}{4} + \frac{1}{4}\cdot\mu^2 - \frac{1}{32}\cdot\mu^4\right)\cdot\theta o^2 + \left(\frac{1}{4}\cdot\mu^2 - \frac{1}{8}\cdot\mu^4\right)\cdot k1\cdot\theta o$$

$$\left(\frac{2}{3}\cdot\mu + \frac{8}{45\cdot\pi}\cdot\mu^4\right)\cdot B1c\cdot\theta o \ldots$$

$$+\left(\frac{2}{5} + \frac{1}{3}\cdot\mu^2 - \frac{16}{225\cdot\pi}\cdot\mu^5\right)\cdot\theta t\cdot\theta o + \left(\frac{4}{15\cdot\pi}\cdot\mu^4\right)\cdot k2\cdot\theta o + \left(\frac{1}{2}\cdot\mu + \frac{1}{48}\cdot\mu^5\right)\cdot\theta e1s\cdot\theta o$$

$$D6 = 0.000403020328445$$

$$D7 := \left(\frac{1}{6}\cdot\mu^2 - \frac{64}{315\cdot\pi}\cdot\mu^5\right)\cdot c1\cdot\theta t + \left(\frac{1}{24}\cdot\mu^5\right)\cdot c2\cdot\theta t$$

$$D7 = 0.000725182624363$$

$$D8 := \left(\frac{1}{6} + \frac{1}{8}\cdot\mu^2 - \frac{1}{192}\cdot\mu^6\right)\cdot\theta t^2 + \left(\frac{1}{6}\cdot\mu^2\right.$$

$$\left.\frac{64}{315\cdot\pi}\cdot\mu^5\right)\cdot k1\cdot\theta t + \left(\frac{1}{24}\cdot\mu^5\right)\cdot k2\cdot\theta t \ldots$$

$$+0-\left(\frac{1}{2}\cdot\mu+\frac{1}{48}\cdot\mu^{5}\right)\cdot B1c\cdot\theta t+\left(\frac{2}{5}\cdot\mu+\frac{16}{525\cdot\pi}\cdot\mu^{6}\right)\cdot\theta e1s\cdot\theta t$$

$$D8=-0.000033390251961$$

$$D9:=\left(\frac{1}{6}\cdot\mu+\frac{56}{45\cdot\pi}\cdot\mu^{4}\right)\cdot c1\cdot c2+\left(\frac{1}{8}+\frac{3}{16}\cdot\mu^{2}-\frac{29}{192}\cdot\mu^{4}\right)\cdot c2^{2}$$

$$D9=0.350339463220244$$

APPENDIX E

$$D10:=\left(\frac{1}{4}+\frac{3}{8}\cdot\mu^{2}-\frac{29}{96}\cdot\mu^{4}\right)\cdot k2\cdot c2+\left(\frac{1}{6}\cdot\mu+\right.$$

$$\left.\frac{56}{45\cdot\pi}\cdot\mu^{4}\right)\cdot k1\cdot c2+\left(\frac{1}{6}\cdot\mu+\frac{56}{45\cdot\pi}\cdot\mu^{4}\right)\cdot c1\cdot k2\ldots$$

$$+\left(\frac{1}{4}-\frac{1}{8}\cdot\mu^{2}+\frac{7}{96}\cdot\mu^{4}\right)\cdot B1c\cdot c2-\left(\frac{1}{5}-\frac{1}{12}\cdot\mu^{2}+\frac{184}{1575\cdot\pi}\cdot\mu^{5}\right)\cdot\theta e1s\cdot c2$$

$$D10=0.037179490667527$$

$$D11 := \left(\frac{1}{8} + \frac{3}{16}\cdot\mu^2 - \frac{29}{192}\cdot\mu^4\right)\cdot k2^2 + \left(\frac{1}{4} - \frac{1}{8}\cdot\mu^2 + \frac{7}{96}\cdot\mu^4\right)\cdot B1c\cdot k2 \ldots$$
$$+ \left(\frac{1}{6}\cdot\mu + \frac{56}{45\cdot\pi}\cdot\mu^4\right)\cdot k1\cdot k2 - \left(\frac{1}{5} - \frac{1}{12}\cdot\mu^2 + \frac{184}{1575\pi}\cdot\mu^5\right)\cdot\theta e1s\cdot k2$$

$$D11 = 0.00097824427905 6$$

$$D12 := \left(\frac{1}{8} + \frac{1}{16}\cdot\mu^2 - \frac{1}{192}\cdot\mu^4\right)\cdot c5^2 - \left(\frac{1}{6}\cdot\mu - \frac{4}{45\cdot\pi}\cdot\mu^4\right)\cdot c4\cdot c5 - \left(\frac{1}{3}\cdot\mu + \frac{4}{45\cdot\pi}\cdot\mu^4\right)\cdot c3\cdot c5$$

$$D12 = -0.99888929340172 2$$

$$D13 := \left(\frac{1}{4} + \frac{1}{8}\cdot\mu^2 - \frac{1}{96}\cdot\mu^4\right)\cdot k5\cdot c5 - \left(\frac{1}{6}\cdot\mu - \frac{4}{45\cdot\pi}\cdot\mu^4\right)\cdot k4\cdot c5$$
$$\left(\frac{1}{6}\cdot\mu - \frac{4}{45\cdot\pi}\cdot\mu^4\right)\cdot c4\cdot k5 \ldots$$
$$+ \left(\frac{1}{4} + \frac{1}{96}\cdot\mu^4\right)\cdot\lambda1\cdot c5 - \left(\frac{1}{4} + \frac{1}{8}\cdot\mu^2 - \frac{1}{96}\cdot\mu^4\right)\cdot A1c\cdot c5 - \left(\frac{\mu}{3} + \frac{4}{45\cdot\pi}\cdot\mu^4\right)\cdot k3\cdot c5 \ldots$$
$$+ 0 - \left(\frac{\mu}{3} + \frac{4}{45\cdot\pi}\cdot\mu^4\right)\cdot c3\cdot k5 + \left(\frac{1}{5} + \frac{1}{12}\cdot\mu^2 - \frac{16}{1575\pi}\cdot\mu^5\right)\cdot\theta e1c\cdot c5$$

$$D13 = -0.07977551683312 3$$

$$D14 := \left(\frac{1}{8} + \frac{1}{16}\cdot\mu^2 - \frac{1}{192}\cdot\mu^4\right)\cdot k5^2 + \left(\frac{1}{4} + \frac{1}{96}\cdot\mu^4\right)\cdot\lambda1\cdot k5 - \left(\frac{1}{3}\cdot\mu + \frac{4}{45\cdot\pi}\cdot\mu^4\right)\cdot k3\cdot k5 - \left(\frac{1}{6}\cdot\mu - \frac{4}{45\cdot\pi}\cdot\mu^4\right)\cdot k4\cdot k5 \ldots$$
$$+ 0 - \left(\frac{1}{4} + \frac{1}{8}\cdot\mu^2 - \frac{1}{96}\cdot\mu^4\right)\cdot A1c\cdot k5 + \left(\frac{1}{5} + \frac{1}{12}\cdot\mu^2 - \frac{16}{1575\pi}\cdot\mu^5\right)\cdot\theta e1c\cdot k5$$

D14 = 0.001592798981

$$D15 := \left(\frac{1}{4}\cdot\mu^2 - \frac{1}{16}\cdot\mu^4\right)\cdot c3^2 - \left(\frac{1}{4}\cdot\mu^2 - \frac{1}{6}\cdot\mu^4\right)\cdot c4\cdot c3$$

$$D15 = 0.847519465037623$$

$$D16 := \left(\frac{1}{2}\cdot\mu^2 - \frac{1}{8}\cdot\mu^4\right)\cdot k3\cdot c3 - \left(\frac{1}{3}\cdot\mu - \frac{8}{45\cdot\pi}\cdot\mu^4\right)\cdot\lambda 1\cdot c3 + \left(\frac{1}{3}\cdot\mu + \frac{4}{45\cdot\pi}\cdot\mu^4\right)\cdot A1c\cdot c3 \ldots$$
$$+0 - \left(\frac{1}{4}\cdot\mu^2 - \frac{1}{6}\cdot\mu^4\right)\cdot k4\cdot c3 - \left(\frac{1}{4}\cdot\mu^2 - \frac{1}{6}\cdot\mu^4\right)\cdot c4\cdot k3 - \left(\frac{1}{4}\cdot\mu + \frac{1}{96}\cdot\mu^5\right)\cdot\theta e1c\cdot c3$$

$$D16 = 0.068810250513425$$

$$D17 := \left(\frac{1}{4}\cdot\mu^2 - \frac{1}{16}\cdot\mu^4\right)\cdot k3^2 + \left(\frac{\mu}{3} + \frac{4}{45\cdot\pi}\cdot\mu^4\right)\cdot A1c\cdot k3 - \left(\frac{1}{4}\cdot\mu^2 - \frac{1}{6}\cdot\mu^4\right)\cdot k4\cdot k3 \ldots$$
$$+0 - \left(\frac{\mu}{3} - \frac{8}{45\cdot\pi}\cdot\mu^4\right)\cdot\lambda 1\cdot k3 - \left(\frac{1}{4}\cdot\mu + \frac{1}{96}\cdot\mu^5\right)\cdot\theta e1c\cdot k3$$

$$D17 = 0.001378167972134$$

APPENDIX E

$$D18 := \left(\frac{1}{2} + \frac{1}{8}\cdot\mu^2 - \frac{25}{192}\cdot\mu^4\right)\cdot c4^2$$

$$D18 = 0.155602427515047$$

$$D19 := \left(\frac{1}{6}\cdot\mu - \frac{88}{315\cdot\pi}\cdot\mu^4\right)\cdot\lambda1\cdot c4 + \left(\frac{1}{6}\cdot\mu - \frac{4}{45\cdot\pi}\cdot\mu^4\right)\cdot A1c\cdot c4 \ldots$$

$$+ \left(1 + \frac{1}{4}\cdot\mu^2 - \frac{25}{96}\cdot\mu^4\right)\cdot k4\cdot c4 - \left(\frac{1}{8}\cdot\mu - \frac{5}{384}\cdot\mu^5\right)\cdot\theta e1c\cdot c4$$

$$D19 = 0.011643891219549$$

$$D20 := \left(\frac{1}{2} + \frac{1}{8}\cdot\mu^2 - \frac{25}{192}\cdot\mu^4\right)\cdot k4^2 + \left(\frac{1}{6}\cdot\mu - \frac{88}{315\cdot\pi}\cdot\mu^4\right)\cdot\lambda1\cdot k4 \ldots$$

$$+ \left(\frac{1}{6}\cdot\mu - \frac{4}{45\cdot\pi}\cdot\mu^4\right)\cdot A1c\cdot k4 - \left(\frac{1}{8}\cdot\mu - \frac{5}{384}\cdot\mu^5\right)\cdot\theta e1c\cdot k4$$

$$D20 = 0.000217797757309$$

$$D21 := \left(\frac{1}{2} + \frac{1}{8}\cdot\mu^2 - \frac{59}{192}\cdot\mu^4\right)\cdot c1^2$$

$$D21 = 0.294211014530486$$

$$D22 := \left(\frac{1}{6}\cdot\mu - \frac{16}{45\cdot\pi}\cdot\mu^4\right)\cdot B1c\cdot c1 + \left(1 + \frac{1}{4}\cdot\mu^2 - \frac{59}{96}\cdot\mu^4\right)\cdot k1\cdot c1$$

$$D22 = 0.026315483963901$$

$$D23 := \left(\frac{1}{2} + \frac{1}{8}\cdot\mu^2 - \frac{59}{192}\cdot\mu^4\right)\cdot k1^2 + \left(\frac{1}{6}\cdot\mu - \frac{16}{45\cdot\pi}\cdot\mu^4\right)\cdot B1c\cdot k1 -$$

$$D23 = 0.000586831067933$$

$$D24 := \left(\frac{1}{8} + \frac{1}{16}\cdot\mu^2 - \frac{1}{192}\cdot\mu^4\right)\cdot A1c^2 - \left(\frac{1}{4} + \frac{1}{96}\cdot\mu^4\right)\cdot\lambda1\cdot A1c -$$

$$D24 = 0.000005944658361$$

$$- \left(\frac{1}{8}\cdot\mu - \frac{23}{384}\cdot\mu^5\right)\cdot\theta e1s\cdot c1$$

$$- \left(\frac{1}{8}\cdot\mu - \frac{23}{384}\cdot\mu^5\right)\cdot\theta e1s\cdot k1$$

$$\left(\frac{1}{5} + \frac{1}{12}\cdot\mu^2 - \frac{16}{1575\cdot\pi}\cdot\mu^5\right)\cdot\theta e1c\cdot A1c$$

$$D25 := \left(\frac{1}{8} + \frac{3}{16}\cdot\mu^2 - \frac{5}{192}\cdot\mu^4\right)\cdot B1c^2 - \left(\frac{1}{5} + \frac{1}{4}\cdot\mu^2 - \frac{32}{525\cdot\pi}\cdot\mu^5\right)\cdot\theta e1s\cdot B1c$$

$$D25 = 0.000062145391563$$

$$D26 := \left(\frac{1}{8} - \frac{1}{64}\cdot\mu^4\right)\cdot\lambda 1^2 + \left(\frac{1}{5} + \frac{8}{525\cdot\pi}\cdot\mu^5\right)\cdot\theta e1c\cdot\lambda 1 \ldots$$
$$+\left(\frac{1}{12} + \frac{1}{32}\cdot\mu^2 - \frac{1}{1536}\cdot\mu^6\right)\cdot\theta e1c^2 + \left(\frac{1}{12} + \frac{3}{32}\cdot\mu^2 -$$

$$D26 = 0.00005013802977$$

$$D27 := D21 + D18 + D15 + D3 + D12 + D9$$

$$D28 := D5 + D16 + D22 + D19 + D4 + D13 + D10 + D7$$

$$D29 := D20 + D17 + D26 + D6 + D11 + D8 + D23 + D25$$

392

$$\frac{7}{1536}\cdot\mu^6\Bigg)\cdot\theta e1s^2$$

$$D27 = 1.315788681583257$$

$$D28 = 0.104291880275636$$

$+ D14 + D24 \qquad D29 = 0.00205610025161$

APPENDIX E

$$CQ\delta 2 := \frac{\sigma \cdot \delta 2}{2} \cdot \left(D27 \cdot \lambda s^2 + D28 \cdot \lambda s + D29 \right)$$

$$CQ\delta 2 = 0.000070940813416$$

$$D30 := \left(\frac{\sigma \cdot \delta 2}{2} \right) \cdot D27 \qquad D30 = 0.025684195064505$$

$$D31 := \left(\frac{\sigma \cdot \delta 1}{2} \right) \cdot D1 + \frac{1}{2} \cdot \sigma \cdot \delta 2 \cdot D28$$

$$D31 = 0.001734574959819$$

$$D32 := \left(\frac{\sigma \cdot Cdo}{8} \right) \cdot D0 + \left(\frac{\sigma \cdot \delta 1}{2} \right) \cdot D2 + \left(\frac{\sigma \cdot \delta 2}{2} \right) \cdot D29$$

$$D32 = 0.000242798455089$$

$$CQd := D30 \cdot \lambda s^2 + D31 \cdot \lambda s + D32$$

$$CQd = 0.000269688558533$$

5. Calculate Total Torque, CQ

$$CQ := \left[D30 - \left(\frac{\sigma \cdot a}{2}\right) \cdot A24\right] \cdot \lambda s^2 + \left[D31 - \left(\frac{\sigma \cdot a}{2}\right) \cdot A25\right] \cdot \lambda s + \left[D32 - \left(\frac{\sigma \cdot a}{2}\right) \cdot A26\right]$$

$$CQ = -0.000515559050365$$

6. Calculate Inflow for Autorotation (may be applicable)

$$F := \left(D30 - \frac{1}{2} \cdot \sigma \cdot a \cdot A24\right) \qquad F = -0.294525267954883$$

$$D := \left(D31 - \frac{1}{2} \cdot \sigma \cdot a \cdot A25\right) \qquad D = -0.021682625229975$$

$$H := \left(D32 - \frac{1}{2} \cdot \sigma \cdot a \cdot A26\right) \qquad H = -0.000183910152091$$

$$CheckCQ := F \cdot \lambda s^2 + D \cdot \lambda s + H \qquad CheckCQ =$$

0.000515559050365

$$\lambda sRootONE := \frac{1}{2 \cdot F} \cdot \left(-D + \sqrt{D^2 - 4 \cdot F \cdot H} \right)$$

$$\lambda sRootONE = -0.063837329578679$$

$$\lambda sRootTWO := \frac{1}{2 \cdot F} \cdot \left(-D - \sqrt{D^2 - 4 \cdot F \cdot H} \right)$$

$$\lambda sRootTWO = -0.009781566961283$$

7. Calculate Accelerating H-Force, CHa

H1

$$= \left(\frac{1}{2} \cdot \mu \right) \cdot \lambda s^2 - \left(\frac{1}{2} \cdot B \cdot \mu - \frac{2}{3 \cdot \pi} \cdot \mu^2 \right) \cdot \theta o \cdot \lambda s - \left(\frac{1}{4} \cdot B^2 \cdot \mu - \frac{1}{16} \cdot \mu^3 \right) \cdot \theta t \cdot \lambda s + \left(\frac{1}{4} \cdot B^2 + \frac{3}{16} \cdot \mu^2 \right) \cdot B1c \cdot \lambda s \ldots$$
$$+ \left(\frac{3}{4} \cdot B^2 - \frac{9}{16} \cdot \mu^2 \right) \cdot a1s \cdot \lambda s - \left(\frac{1}{4} \cdot B \cdot \mu - \frac{12}{5 \cdot \pi} \cdot \mu^2 \right) \cdot b2s \cdot \lambda s - \left(\frac{1}{6} \cdot B^3 + \frac{8}{45 \cdot \pi} \cdot \mu^3 \right) \cdot \theta e1s \cdot \lambda s$$

H1 = 0.000409126548125

$$H2 := \left(\frac{1}{3} \cdot B^3 + \frac{2}{9 \cdot \pi} \cdot \mu^3 \right) \cdot a1s \cdot \theta o + \left(\frac{3}{8} \cdot B^2 \cdot \mu - \frac{5}{48} \cdot \mu^3 \right) \cdot b2s \cdot \theta o$$

$H2 = 0.001181845724661$

$$H3 := \left(\frac{1}{4}\cdot B^4 + \frac{1}{32}\cdot \mu^4\right)\cdot a1s\cdot \theta t + \left(\frac{1}{4}\cdot B^3\cdot \mu - \frac{16}{105}\cdot\frac{\mu^4}{\pi}\right)\cdot b2s\cdot \theta t$$

$H3 = -0.000432624523905$

$$H4 := \left(\frac{1}{4}\cdot B^2\cdot \mu - \frac{3}{16}\cdot \mu^3\right)\cdot a1s^2 - \left(\frac{1}{4}\cdot B^2\cdot \mu - \frac{1}{16}\cdot \mu^3\right)\cdot B1c\cdot a1s -$$

$$+ \left(\frac{1}{6}\cdot B^3\cdot \mu - \frac{4}{45}\cdot\frac{\mu^4}{\pi}\right)\cdot \theta e1s\cdot a1s$$

$H4 = 0.002642035801963$

$$H5 := \left(\frac{1}{4}\cdot B^3 + \frac{2}{21}\cdot\frac{\mu^3}{\pi}\right)\cdot a2s\cdot b1s - \left(\frac{1}{6}\cdot B^3 + \frac{2}{45}\cdot\frac{\mu^3}{\pi}\right)\cdot \beta o\cdot b1s -$$

$H5 = -0.002253792891716$

$$- \left(\frac{1}{4}\cdot B^3 - \frac{164}{105}\cdot\frac{\mu^3}{\pi}\right)\cdot b2s\cdot a1s \ \ldots$$

$$\left(\frac{1}{16}\cdot B^2\cdot\mu-\frac{1}{96}\cdot\mu^3\right)\cdot\lambda 1\cdot b1s$$

$$H6:=\left(\frac{1}{4}\cdot B^2\cdot\mu-\frac{1}{16}\cdot\mu^3\right)\cdot\beta o^2+\left(\frac{1}{6}\cdot B^3+\frac{2}{45}\cdot\frac{\mu^3}{\pi}\right)\cdot A1c\cdot\beta o-\left(\frac{1}{6}\cdot B^3-\frac{2}{9}\cdot\frac{\mu^3}{\pi}\right)\cdot\lambda 1\cdot\beta o$$
$$+0-\left(\frac{1}{2}\cdot B^2\cdot\mu-\frac{5}{24}\cdot\mu^3\right)\cdot a2s\cdot\beta o-\left(\frac{1}{8}\cdot B^4+\frac{1}{192}\cdot\mu^4\right)\cdot\theta e1c\cdot\beta o$$

$$H6=0.00236080274585$$

$$H7:=\left(\frac{1}{8}\cdot B^2\cdot\mu-\frac{11}{64}\cdot\mu^3\right)\cdot a2s^2-\left(\frac{1}{4}\cdot B^3+\frac{2}{21}\cdot\frac{\mu^3}{\pi}\right)\cdot A1c\cdot a2s$$

$$\left(\frac{3}{16}\cdot B^4+\frac{3}{256}\cdot\mu^4\right)\cdot\theta e1c\cdot a2s\quad H7=-0.000015799961115$$

$$H8:=\left(\frac{1}{8}\cdot B^2\cdot\mu-\frac{25}{64}\cdot\mu^3\right)\cdot b2s^2-\left(\frac{1}{4}\cdot B^3+\frac{32}{105}\cdot\frac{\mu^3}{\pi}\right)\cdot b2s\cdot B1c+\left(\frac{3}{16}\cdot B^4+\frac{35}{768}\cdot\mu^4\right)\cdot b2s\cdot\theta e1s$$

$$H8=-0.00035540979829 5$$

$$H9 := \left(\frac{1}{16}\cdot B^2\cdot\mu - \frac{1}{96}\cdot\mu^3\right)\cdot A1c\cdot\lambda 1 + \left(\frac{5}{12}\cdot B^3 - \frac{118}{315}\cdot\frac{\mu^3}{\pi}\right)\cdot a2s\cdot\lambda 1 - \left(\frac{1}{24}\cdot B^3\cdot\mu - \frac{4}{315}\cdot\frac{\mu^4}{\pi}\right)\cdot\theta e1c\cdot\lambda 1 - \left(\frac{1}{48}\cdot\mu^3\right)\cdot\lambda 1^2$$

$$H9 = -0.000070081855597$$

$$CHa := \frac{\sigma\cdot a}{2}\cdot(H1 + H2 + H3 + H4 + H5 + H6 + H7 + H8 + H9)$$

$$CHa = 0.000962292250614$$

8. Derive CHa due to C1 and inflow from CHa

$$= \frac{-1\cdot(CT\cdot\lambda s + CQa)}{\mu}$$

$$CHaCheck := \frac{-1\cdot(CT\cdot\lambda s + CQa)}{\mu}$$

CHaCheck = 0.000962922506 14

Double Check $\mu \cdot CHa + (CT \cdot \lambda s + CQa) = 0$

9. Calculate CHd due to Cd

$$CHCdo := \frac{\sigma \cdot Cdo}{8} \cdot \left(2 \cdot \mu + \frac{1}{2} \cdot \mu^3\right)$$

CHCdo = 0.0002300676

$$CH\delta 1 := \sigma \cdot \delta 1 \cdot \left[\left(\frac{1}{4} \cdot \mu\right) \cdot \lambda s + \left(\frac{1}{4} \cdot \mu\right) \cdot \theta o + \left(\frac{1}{6} \cdot \mu\right) \cdot \theta t - \left(\frac{3}{16} \cdot \mu^2\right) \cdot B1c \ldots \right.$$
$$\left. + \left(\frac{1}{16} \cdot \mu^2\right) \cdot a1s - \left(\frac{1}{16} \cdot \mu\right) \cdot b2s - \frac{1}{12} \cdot B1c - \frac{1}{12} \cdot a1s + \left(\frac{1}{16} + \frac{3}{32} \cdot \mu^2\right) \cdot \theta e1s\right.$$

CHδ1 = −0.000010478826666

$$H10 := \left(\frac{1}{2} \cdot \mu\right) \cdot \lambda s^2 - \left(\frac{1}{2} - \frac{5}{8} \cdot \mu^2\right) \cdot a1s \cdot \lambda s + \left(\frac{1}{2} \cdot \mu - \frac{1}{8} \cdot \mu^3\right) \cdot \theta t \cdot \lambda s + \left(\mu - \frac{4}{3 \cdot \pi} \cdot \mu^2\right) \cdot \theta o \cdot \lambda s$$
$$+ \left(\frac{1}{2} \cdot \mu - \frac{8}{3 \cdot \pi} \cdot \mu^2\right) \cdot b2s \cdot \lambda s - \left(\frac{1}{2} + \frac{3}{8} \cdot \mu^2\right) \cdot B1c \cdot \lambda s + \left(\frac{1}{3} + \frac{16}{45 \cdot \pi} \cdot \mu^3\right) \cdot \theta e1s \cdot \lambda s$$

$$H10 = 0.000121323401491$$

$$H11 := \left(\frac{1}{2}\cdot\mu + \frac{1}{8}\cdot\mu^3\right)\cdot\theta o^2 + \left(\frac{2}{3}\cdot\mu + \frac{8}{45\cdot\pi}\cdot\mu^4\right)\cdot\theta t\cdot\theta o - \left(\frac{1}{3} - \frac{1}{4}\cdot\mu^2 + \frac{28}{45\cdot\pi}\cdot\mu^3\right)\cdot a1s\cdot\theta o \ldots$$
$$+0 - \left(\frac{1}{4}\cdot\mu - \frac{7}{24}\cdot\mu^3\right)\cdot b2s\cdot\theta o - \left(\frac{1}{3} + \frac{3}{4}\cdot\mu^2 - \frac{32}{45\cdot\pi}\cdot\mu^3\right)\cdot B1c\cdot\theta o + \left(\frac{1}{4} - \frac{5}{96}\cdot\mu^4 + \frac{3}{8}\cdot\mu^2\right)\cdot\theta e1s\cdot\theta o$$

$$H11 = -0.000520165431 29$$

$$H12 := \left(\frac{1}{4}\cdot\mu + \frac{1}{96}\cdot\mu^5\right)\cdot\theta t^2 - \left(\frac{1}{4} - \frac{1}{8}\cdot\mu^2 + \frac{7}{96}\cdot\mu^4\right)\cdot a1s\cdot\theta t - \left(\frac{1}{6}\cdot\mu - \frac{16}{45\cdot\pi}\cdot\mu^4\right)\cdot b2s\cdot\theta t$$
$$+0 - \left(\frac{1}{4} + \frac{3}{8}\cdot\mu^2 - \frac{5}{96}\cdot\mu^4\right)\cdot B1c\cdot\theta t + \left(\frac{1}{5} + \frac{1}{4}\cdot\mu^2 - \frac{32}{525\cdot\pi}\cdot\mu^5\right)\cdot\theta e1s\cdot\theta t$$

$$H12 = 0.000317427243898$$

APPENDIX E

$$H13 := \left(\frac{1}{8}\cdot\mu^3\right)\cdot\beta o^2 + \left(\frac{1}{2}\cdot\mu - \frac{1}{4}\cdot\mu^3\right)\cdot a2s\cdot\beta o - \left(\frac{1}{4}\cdot\mu^2 - \frac{4}{15\cdot\pi}\cdot\mu^3\right)\cdot b1s\cdot\beta o \ldots$$

$$+\left(\frac{1}{4}\cdot\mu^2-\frac{4}{15\cdot\pi}\cdot\mu^3\right)\cdot A1c\cdot\beta o-\left(\frac{4}{15\cdot\pi}\cdot\mu^3\right)\cdot\lambda 1\cdot\beta o+\left(\frac{1}{48}\cdot\mu^4-\frac{1}{8}\cdot\mu^2\right)\cdot\theta e1c\cdot\beta o$$

$$H13=0.00024067204983 4$$

$$H14:=\left(\frac{1}{3}+\frac{1}{4}\cdot\mu^2-\frac{584}{315\cdot\pi}\cdot\mu^3\right)\cdot b2s\cdot a1s-\left(\frac{1}{8}\cdot\mu-\frac{11}{48}\cdot\mu^3\right)\cdot a1s^2\ \ldots$$

$$+\left(\frac{1}{4}\cdot\mu-\frac{1}{6}\cdot\mu^3\right)\cdot B1c\cdot a1s-\left(\frac{1}{6}\cdot\mu-\frac{64}{315\cdot\pi}\cdot\mu^4\right)\cdot\theta e1s\cdot a1s$$

$$H14=-0.00196931801469 8$$

$$H15:=\left(\frac{1}{8}\cdot\mu+\frac{1}{48}\cdot\mu^3\right)\cdot b1s^2-\left(\frac{1}{3}+\frac{52}{315\cdot\pi}\cdot\mu^3\right)\cdot a2s\cdot b1s+\left(\frac{1}{8}\cdot\mu-\frac{1}{48}\cdot\mu^3\right)\cdot\lambda 1\cdot b1s-\left(\frac{1}{4}\cdot\mu+\frac{1}{24}\cdot\mu^3\right)\cdot A1c\cdot b1s\ \ldots$$

$$+\left(\frac{1}{6}\cdot\mu+\frac{8}{315\cdot\pi}\cdot\mu^4\right)\cdot\theta e1c\cdot b1s$$

$$H15=0.00021041637036 6$$

$$H16:=\left(\frac{43}{96}\cdot\mu^3\right)\cdot b2s^2+\left(\frac{17}{96}\cdot\mu^3\right)\cdot a2s^2$$

$$H16=0.00033057007047 5$$

$$H17:=\left(\frac{3}{8}\cdot\mu+\frac{5}{48}\cdot\mu^3\right)\cdot B1c^2+\left(\frac{1}{3}-\frac{1}{4}\cdot\mu^2\right.$$

$$\frac{256}{315\cdot\pi}\cdot\mu^3\Big)\cdot b2s\cdot B1c \ldots$$

$$+\left(\frac{1}{8}\cdot\mu+\frac{1}{48}\cdot\mu^3\right)\cdot A1c^2+\left(\frac{1}{3}+\frac{52}{315\cdot\pi}\cdot\mu^3\right)\cdot a2s\cdot A1c$$

$$H17 = 0.001011177876538$$

$$H18 := \left(\frac{1}{48}\cdot\mu^3\right)\cdot\lambda1^2-\left(\frac{1}{3}-\frac{116}{315\cdot\pi}\cdot\mu^3\right)\cdot a2s\cdot\lambda1-\left(\frac{1}{8}\cdot\mu\right.$$

$$\left.\frac{1}{48}\cdot\mu^3\right)\cdot A1c\cdot\lambda1$$

$$H18 = 0.000069490620782$$

$$H19 := \left(\frac{1}{12}\cdot\mu-\frac{8}{315\cdot\pi}\cdot\mu^4\right)\cdot\theta e1c\cdot\lambda1-\left(\frac{1}{6}\cdot\mu+\frac{8}{315\cdot\pi}\cdot\mu^4\right)\cdot\theta e1c\cdot A1c-\left(\frac{16}{105\cdot\pi}\cdot\mu^4+\frac{1}{2}\cdot\mu\right)\cdot\theta e1s\cdot B1c \ldots$$
$$+\left(\frac{3}{16}\cdot\mu+\frac{7}{768}\cdot\mu^5\right)\cdot\theta e1s^2+\left(\frac{1}{16}\cdot\mu+\frac{1}{768}\cdot\mu^5\right)\cdot\theta e1c^2 \ldots$$
$$+0-\left(\frac{1}{4}-\frac{1}{8}\cdot\mu^2+\frac{5}{48}\cdot\mu^4\right)\cdot\theta e1s\cdot b2s-\left(\frac{1}{4}+\frac{1}{48}\cdot\mu^4\right)\cdot\theta e1c\cdot a2s$$

$$H19 = -0.00049300484576$$

$$CH\delta2$$

$$=\frac{\sigma\cdot\delta2}{2}\cdot(H10+H11+H12+H13+H14+H15+H16+H17+H18+H19)$$

$$CH\delta2 = -0.000013301136051$$

$$CHd := CHCdo + CH\delta1 + CH\delta2$$

$$CHd = 0.000206287637283$$

10. Calculate Total CH

$$CH := CHa + CHd$$

$$CH = 0.00116857988789 7$$

11. Calculate CYa due to CL (Y-force positive to ψ = 90 deg)

$$Y1 = \left(\frac{3}{4}\cdot B^2 + \frac{5}{16}\cdot\mu^2\right)\cdot b1s\cdot\lambda s - \left(\frac{3}{2}\cdot B\cdot\mu - \frac{2}{\pi}\cdot\mu^2\right)\cdot\beta o\cdot\lambda s + \left(\frac{1}{4}\cdot B\cdot\mu - \frac{14}{15\cdot\pi}\cdot\mu^2\right)\cdot a2s\cdot\lambda s \ ...$$

$$+\left(\frac{1}{2}\cdot B^2-\frac{1}{8}\cdot\mu^2\right)\cdot\lambda 1\cdot\lambda s-\left(\frac{1}{4}\cdot B^2+\frac{1}{16}\cdot\mu^2\right)\cdot A1c\cdot\lambda s+\left(\frac{1}{6}\cdot B^3+\frac{2}{45\cdot\pi}\cdot\mu^3\right)\cdot\theta e1c\cdot\lambda s$$

$Y1 = 0.0001240057117 33$

$$Y2 := \left(\frac{1}{3}\cdot B^3+\frac{1}{2}\cdot B\cdot\mu^2-\frac{4}{9\cdot\pi}\cdot\mu^3\right)\cdot b1s\cdot\theta o-\left(\frac{3}{4}\cdot B^2\cdot\mu-\frac{3}{16}\cdot\mu^3\right)\cdot\beta o\cdot\theta o$$

$$+0-\left(\frac{3}{8}\cdot B^2\cdot\mu+\frac{1}{24}\cdot\mu^3\right)\cdot a2s\cdot\theta o+\left(\frac{1}{6}\cdot B^3+\frac{2}{45\cdot\pi}\cdot\mu^3\right)\cdot\lambda 1\cdot\theta o$$

$Y2 = -0.0007622551504 36$

$$Y3 := \left(\frac{1}{4}\cdot B^4+\frac{1}{4}\cdot B^2\cdot\mu^2-\frac{1}{32}\cdot\mu^4\right)\cdot b1s\cdot\theta t-\left(\frac{1}{2}\cdot B^3\cdot\mu+\frac{2}{15\cdot\pi}\cdot\mu^4\right)\cdot\beta o\cdot\theta t \ldots$$

$$+0-\left(\frac{1}{4}\cdot B^3\cdot\mu+\frac{2}{105\cdot\pi}\cdot\mu^4\right)\cdot a2s\cdot\theta t+\left(\frac{1}{8}\cdot B^4+\frac{1}{192}\cdot\mu^4\right)\cdot\lambda 1\cdot\theta t$$

$Y3 = 0.0001518048759 9$

$$Y4 := \left(\frac{1}{6}\cdot B^3-B\cdot\mu^2+\frac{68}{45\cdot\pi}\cdot\mu^3\right)\cdot a1s\cdot\beta o-\left(\frac{1}{2}\cdot B^2\cdot\mu+\frac{11}{24}\cdot\mu^3\right)\cdot b2s\cdot\beta o$$

$$+\left(\frac{1}{6}\cdot B^3+\frac{1}{2}\cdot B\cdot\mu^2-\frac{22}{45\cdot\pi}\cdot\mu^3\right)\cdot B1c\cdot\beta o-\left(\frac{1}{8}\cdot B^4+\frac{1}{4}\cdot B^2\cdot\mu^2-\frac{7}{192}\cdot\mu^4\right)\cdot\theta e1s\cdot\beta o$$

$$Y4=-0.001266285819158$$

$$Y5:=\left(\frac{1}{4}\cdot B^2\cdot\mu+\frac{3}{16}\cdot\mu^3\right)\cdot a1s\cdot b1s+\left(\frac{1}{4}\cdot B^3+\frac{1}{2}\cdot B\cdot\mu^2-\frac{116}{105\cdot\pi}\cdot\mu^3\right)\cdot a2s\cdot a1s$$

$$+\left(\frac{7}{16}\cdot B^2\cdot\mu-\frac{11}{96}\cdot\mu^3\right)\cdot\lambda1\cdot a1s-\left(\frac{1}{4}\cdot B^2\cdot\mu\right.$$

$$\left.\frac{1}{16}\cdot\mu^3\right)\cdot A1c\cdot a1s+\left(\frac{1}{6}\cdot B^3\cdot\mu+\frac{2}{45\cdot\pi}\cdot\mu^4\right)\cdot\theta e1c\cdot a1s$$

$$Y5=0.005161236802228$$

$$Y6:=\left(\frac{1}{4}\cdot B^3+\frac{1}{2}\cdot B\cdot\mu^2-\frac{16}{21\cdot\pi}\cdot\mu^3\right)\cdot b2s\cdot b1s-\left(\frac{1}{2}\cdot B^2\cdot\mu+\frac{1}{8}\cdot\mu^3\right)\cdot B1c\cdot b1s+$$

$$Y6=-0.001006158164124$$

$$Y7:=\left(\frac{7}{32}\cdot\mu^3\right)\cdot b2s\cdot a2s+\left(\frac{1}{4}\cdot B^3+\frac{1}{4}\cdot B\cdot\mu^2-\frac{6}{35\cdot\pi}\cdot\mu^3\right)\cdot B1c\cdot a2s-\left(\frac{3}{16}\cdot B^4-\right.$$

$$Y7=-0.000298358384238$$

$$\left(\frac{1}{3}\cdot B^3\cdot\mu+\frac{4}{45\cdot\pi}\cdot\mu^4\right)\cdot\theta e1s\cdot b1s$$

$$+\left(\frac{1}{8}\cdot B^2\cdot\mu^2-\frac{7}{768}\cdot\mu^4\right)\cdot\theta e1s\cdot a2s$$

APPENDIX E

$$Y8:=\left(\frac{5}{12}\cdot B^3+\frac{104}{315\cdot\pi}\cdot\mu^3\right)\cdot\lambda1\cdot b2s-\left(\frac{1}{4}\cdot B^3+\frac{1}{4}\cdot B\cdot\mu^2-\frac{8}{35\cdot\pi}\cdot\mu^3\right)\cdot A1c\cdot b2s$$
$$+\left(\frac{3}{16}\cdot B^4+\frac{1}{8}\cdot B^2\cdot\mu^2-\frac{13}{768}\cdot\mu^4\right)\cdot\theta e1c\cdot b2s$$

$$Y8=0.000207494277531$$

$$Y9:=\left(\frac{1}{24}\cdot B^3\cdot\mu-\frac{4}{315\cdot\pi}\cdot\mu^4\right)\cdot\theta e1s\cdot\lambda1-\left(\frac{1}{16}\cdot\mu\cdot B^2-\frac{1}{96}\cdot\mu^3\right)\cdot B1c\cdot\lambda1$$

$$Y9=-0.000006300274309$$

$$CYa:=\frac{\sigma\cdot a}{2}\cdot(Y1+Y4+Y2+Y3+Y5+Y6+Y7+Y8+Y9)$$

$$CYa=0.000644584735924$$

12. Calculate CYd due to Cd

$$CYCdo := 0$$

$$CY\delta l$$

$$= \frac{\sigma \cdot \delta l}{2} \cdot \left[\left(\frac{1}{6} + \frac{1}{8} \cdot \mu^2 \right) \cdot A1c - \left(\frac{1}{6} + \frac{1}{8} \cdot \mu^2 \right) \cdot b1s - \left(\frac{1}{8} + \frac{1}{16} \cdot \mu^2 \right) \cdot \theta e1c + \left(\frac{1}{4} \cdot \mu \right) \cdot \beta o + \left(\frac{1}{8} \cdot \mu \right) \cdot a2s - \frac{1}{6} \cdot \lambda 1 \right]$$

$$CY\delta l = 0.00000645796793$$

$$Y10 = \left(\frac{1}{2} + \frac{1}{8} \cdot \mu^2 \right) \cdot b1s \cdot \lambda s - \left(\mu - \frac{4}{3 \cdot \pi} \cdot \mu^2 \right) \cdot \beta o \cdot \lambda s + \left(\frac{1}{2} \cdot \mu - \frac{4}{3 \cdot \pi} \cdot \mu^2 \right) \cdot a2s \cdot \lambda s - \left(\frac{1}{2} + \frac{1}{16} \cdot \mu^2 \right) \cdot A1c \cdot \lambda s \ldots$$
$$+ \left(\frac{1}{2} - \frac{1}{8} \cdot \mu^2 \right) \cdot \lambda 1 \cdot \lambda s + \left(\frac{1}{3} + \frac{2}{45 \cdot \pi} \cdot \mu^3 \right) \cdot \theta e1c \cdot \lambda s$$

$$Y10 = 0.000024304101028$$

$$Y11 = \left(\frac{1}{3} + \frac{1}{4} \cdot \mu^2 - \frac{4}{45 \cdot \pi} \cdot \mu^3 \right) \cdot \theta o \cdot b1s - \left(\frac{1}{2} \cdot \mu + \frac{1}{16} \cdot \mu^3 \right) \cdot \theta o \cdot \beta o - \left(\frac{1}{4} \cdot \mu - \frac{1}{24} \cdot \mu^3 \right) \cdot \theta o \cdot a2s$$

$$+ 0 - \left(\frac{1}{3} + \frac{1}{4} \cdot \mu^2 - \frac{8}{45 \cdot \pi} \cdot \mu^3 \right) \cdot \theta o \cdot A1c + \left(\frac{1}{3} + \frac{2}{45 \cdot \pi} \cdot \mu^3 \right) \cdot \theta o \cdot \lambda 1 + \left(\frac{1}{4} + \frac{1}{8} \cdot \mu^2 - \frac{1}{96} \cdot \mu^4 \right) \cdot \theta o \cdot \theta e1c$$

$$Y11 = -0.0000871568235 4$$

$$Y12 = \left(\frac{1}{4} + \frac{1}{8} \cdot \mu^2 - \frac{1}{192} \cdot \mu^4 \right) \cdot \theta t \cdot b1s - \left(\frac{1}{3} \cdot \mu + \frac{2}{45 \cdot \pi} \cdot \mu^4 \right) \cdot \theta t \cdot \beta o - \left(\frac{1}{6} \cdot \mu - \frac{2}{45 \cdot \pi} \cdot \mu^4 \right) \cdot \theta t \cdot a2s \ldots$$
$$+ 0 - \left(\frac{1}{4} + \frac{1}{8} \cdot \mu^2 - \frac{1}{96} \cdot \mu^4 \right) \cdot \theta t \cdot A1c + \left(\frac{1}{4} + \frac{1}{192} \cdot \mu^4 \right) \cdot \theta t \cdot \lambda 1 + \left(\frac{1}{5} + \frac{1}{12} \cdot \mu^2 - \frac{16}{1575 \cdot \pi} \cdot \mu^5 \right) \cdot \theta t \cdot \theta e1c$$

$$Y12 = -0.000026625155014$$

$$Y13 = \left(\frac{1}{4} \cdot \mu^2 - \frac{2}{15 \cdot \pi} \cdot \mu^3 \right) \cdot \beta o \cdot B1c - \left(\frac{3}{4} \cdot \mu^2 - \frac{16}{15 \cdot \pi} \cdot \mu^3 \right) \cdot \beta o \cdot a1s - \left(\frac{1}{2} \cdot \mu + \frac{1}{4} \cdot \mu^3 \right) \cdot \beta o \cdot b2s - \left(\frac{1}{8} \cdot \mu^2 - \frac{1}{96} \cdot \mu^4 \right) \cdot \theta e1s \cdot \beta o$$

$$Y13 = -0.00268870559 7424$$

$$Y14 = \left(\frac{1}{4}\cdot\mu + \frac{1}{12}\cdot\mu^3\right)\cdot a1s\cdot b1s + \left(\frac{1}{3} + \frac{1}{2}\cdot\mu^2 - \frac{368}{315\cdot\pi}\cdot\mu^3\right)\cdot a1s\cdot a2s -$$

$$+ \left(\frac{3}{8}\cdot\mu - \frac{5}{48}\cdot\mu^3\right)\cdot a1s\cdot\lambda 1 + \left(\frac{1}{6}\cdot\mu + \frac{2}{63\cdot\pi}\cdot\mu^4\right)\cdot a1s\cdot\theta e1c$$

$$Y14 = 0.005117767180249$$

$$Y15 = \left(\frac{1}{3} + \frac{1}{4}\cdot\mu^2 - \frac{16}{63\cdot\pi}\cdot\mu^3\right)\cdot b1s\cdot b2s - \left(\frac{1}{4}\cdot\mu + \frac{1}{48}\cdot\mu^3\right)\cdot b1s\cdot B1c +$$

$$Y15 = -0.001943681093466$$

APPENDIX E

$$\left(\frac{1}{4}\cdot\mu + \frac{1}{24}\cdot\mu^3\right)\cdot a1s\cdot A1c \ \ldots$$

$$\left(\frac{1}{6}\cdot\mu + \frac{4}{315\cdot\pi}\cdot\mu^4\right)\cdot b1s\cdot\theta e1s$$

$$Y16 = \left(\frac{1}{3} + \frac{26}{315\cdot\pi}\cdot\mu^3\right)\cdot a2s\cdot B1c - \left(\frac{1}{4} + \frac{1}{96}\cdot\mu^4\right)\cdot a2s\cdot\theta e1s + \left(\frac{13}{48}\cdot\mu^3\right)\cdot b2s\cdot a2s$$

$$Y16 = -0.000318138388903$$

$$Y17 := \left(\frac{1}{3} + \frac{88}{315\cdot\pi}\cdot\mu^3\right)\cdot b2s\cdot\lambda 1 - \left(\frac{1}{3} + \frac{1}{4}\cdot\mu^2 - \frac{8}{63\cdot\pi}\cdot\mu^3\right)\cdot b2s\cdot A1c + \left(\frac{1}{4} + \frac{1}{8}\cdot\mu^2 - \frac{1}{96}\cdot\mu^4\right)\cdot b2s\cdot\theta e1c$$

$$Y17 = 0.000214119551942$$

$$Y18 := \left(\frac{1}{12}\cdot\mu - \frac{4}{315\cdot\pi}\cdot\mu^4\right)\cdot\lambda 1\cdot\theta e1s - \left(\frac{1}{8}\cdot\mu - \frac{1}{96}\cdot\mu^3\right)\cdot\lambda 1\cdot B1c$$

$$Y18 = -0.000014053554352$$

$$Y19 := \left(\frac{1}{4}\cdot\mu + \frac{1}{24}\cdot\mu^3\right)\cdot A1c\cdot B1c - \left(\frac{1}{6}\cdot\mu + \frac{8}{315\cdot\pi}\cdot\mu^4\right)\cdot A1c\cdot\theta e1s - \left(\frac{1}{6}\cdot\mu + \frac{8}{315\cdot\pi}\cdot\mu^4\right)\cdot B1c\cdot\theta e1c \ldots$$

$$+ \left(\frac{1}{8}\cdot\mu + \frac{1}{384}\cdot\mu^5\right)\cdot\theta e1s\cdot\theta e1c$$

$$Y19 = -0.000033720559476$$

$$CY\delta 2 := \left(-1\cdot\frac{\sigma\cdot\delta 2}{2}\right)\cdot(Y10 + Y11 + Y12 + Y13 + Y14 + Y15 + Y16 + Y17 + Y18 + Y19)$$

$$CY\delta 2 = -0.000004765020584$$

$$CYd := CYCdo + CY\delta 1 +$$

$$CYd = -0.000004119223791$$

13. Calculate Total CY

$$CY := CYa + CYd$$

$CY\delta 2$

$$CY = 0.000640465512133$$

APPENDIX E

14. Calculate Shaft Angle of Attack (radians)

$$\alpha s := \operatorname{atan}\left(\frac{\lambda s}{\mu} + \frac{1}{2}\cdot\frac{CT}{\mu\cdot\sqrt{\mu^2 + \lambda s^2}}\right)$$

$$\alpha s = 0.027326303405535$$

15. Repeat Input (angles now in degrees)

$\mu = 0.7$ $\lambda s = 0.013$ $\lambda 1 = -0.007287534590767$

$\gamma = 19.2$ $B = 0.97$ $\sigma = 0.0976$

$a = 5.73$

$\theta o \cdot \frac{180}{\pi} = 1.9$ $\theta t \cdot \frac{180}{\pi} = -1$ $B1c \cdot \frac{180}{\pi} = -2$ $A1c \cdot \frac{180}{\pi} = 1$

$Cdo = 0.012$ $\delta 1 = -0.0216$ $\delta 2 = 0.4$

16. Summarize Output

$\beta o \cdot \frac{180}{\pi} = 8.474827357622401$ $a1s \cdot \frac{180}{\pi} = 7.801747523038808$

$a2s \cdot \frac{180}{\pi} = 1.579548305207202$

$$\theta e1s \cdot \frac{180}{\pi} = -1 \qquad \theta e1c \cdot \frac{180}{\pi} = 1$$

$$b1s \cdot \frac{180}{\pi} = 7.890124244695535$$

$$b2s \cdot \frac{180}{\pi} = -2.465172362211013$$

$$CT = 0.008587925651381 \qquad CH = 0.001168579887897$$
$$CY = 0.000640465512133$$

$$CQ = -0.000515559050365$$

$$\alpha s \cdot \frac{180}{\pi} = 1.565681854831141$$

$$RotorCL := CT \cdot \cos(\alpha s) - CH \cdot \sin(\alpha s)$$

$$RotorCD := CT \cdot \sin(\alpha s) + CH \cdot \cos(\alpha s)$$

$$\text{RotorCY} := \text{CY}$$

$$\text{AirplaneCL} := \frac{2}{\mu^2} \cdot (\text{RotorCL})$$

$$\text{AirplaneCD} := \frac{2}{\mu^2} \cdot (\text{RotorCD})$$

$$\text{AirplaneCY} := 2 \cdot \frac{\text{CY}}{\mu^2}$$

400

$$\text{RotorCL} = 0.008552790439016$$

$$\text{RotorCD} = 0.001402790666605$$

$$\text{RotorCY} = 0.000640465512133$$

AirplaneCL = 0.034909348730678

AirplaneCD = 0.005725676190225

AirplaneCY = 0.002614144947481

APPENDIX F
EXCERPTS FROM PROCEEDINGS OF [FIRST] ROTATING WING MEETING

PROCEEDINGS

OF

ROTATING WING

AIRCRAFT MEETING

Sponsored by

Philadelphia Chapter, Institute of the Aeronautical Sciences -

held at

The Franklin Institute,

Philadelphia, Penna.

October 28 and

29, 1938

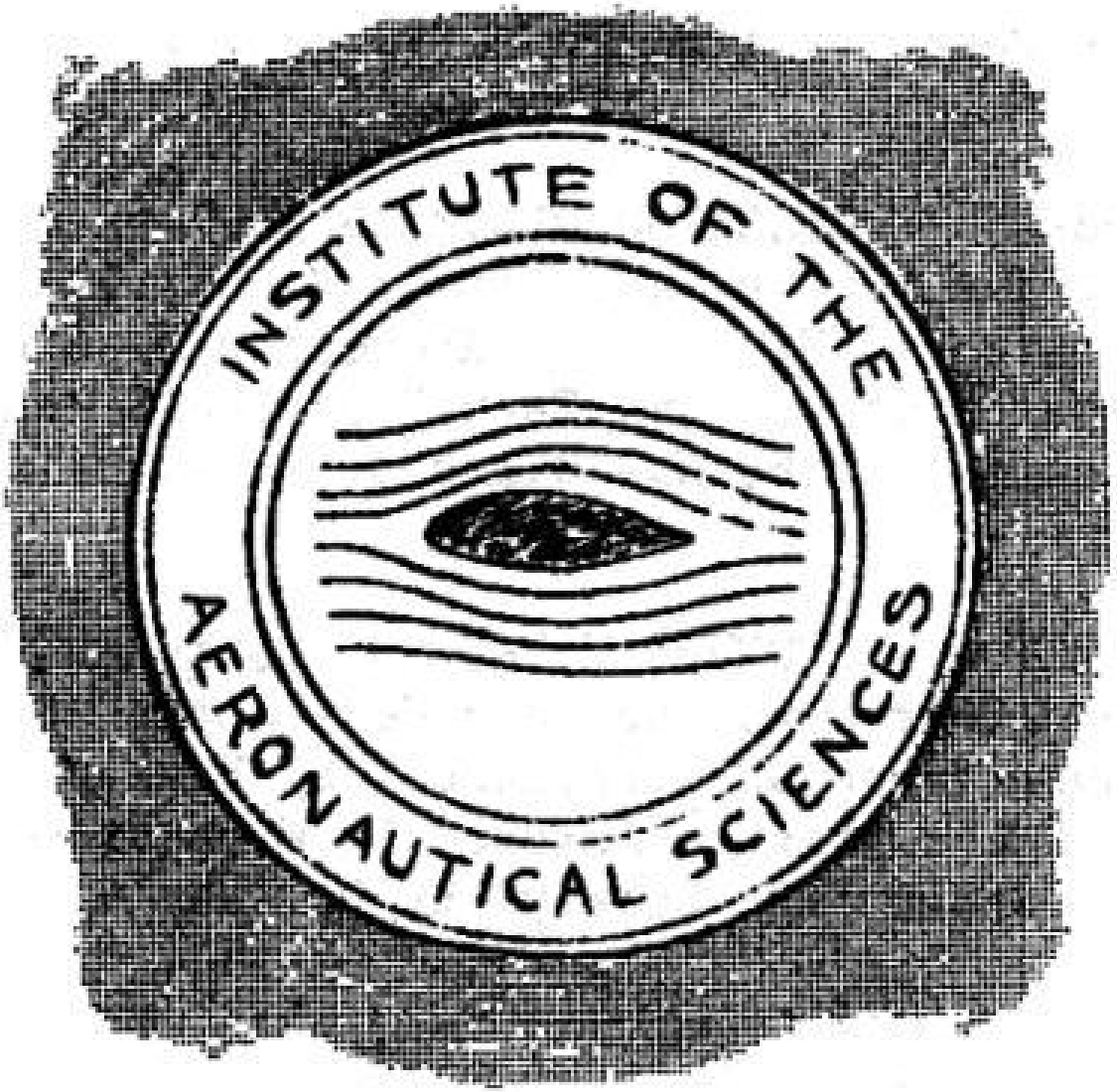

APPENDIX F

INDEX

APPENDIX F

AIRCRAFT MEETING

Sponsored by

PHILADELPHIA CHAPTER
INSTITUTE of the AERONAUTICAL SCIENCES

Friday and Saturday, October 28 and 29, 1938
Lecture Hall, THE FRANKLIN INSTITUTE
Benjamin Franklin Parkway at 20th Street
Philadelphia

This Rotating Wing Aircraft Meeting

was the first free discussion in this field of science open to all engineers in the aircraft industry. A complete two day program was arranged and a series of papers presented by experts and pioneers thoroughly acquainted with the various problems in this branch of the aeronautical sciences. The scope of the meetings cover Uses, Developments and Relation to the Future of Heavier-than-Aircraft.

The Philadelphia Chapter is grateful to the Franklin Institute and the Aero Club of Pennsylvania for their help and cooperation extended for meetings.

All delegates were invited to attend special lecture at regu- lar meeting of The Franklin Institute on Thursday, October 27th, at 8:15 P.M.

"PRINCIPLES OF ROTARY AIRCRAFT"
by Dr. Alexander Klemin, Professor,
Daniel Guggenheim School of
Aeronautics, New York University.

For the regular meetings all delegates and visitors assembled in the Hall of Aviation of the Franklin Institute. It was rather fitting that registration take place in this large hall devoted to a splendid collection of aviation exhibits and particularly in view of the fact, hanging from the ceiling is the first autogiro built in this country.

Mr. E. Burke Wilford, President of the Philadelphia Chapter acknowledges his gratefulness to the committee consisting of

Agnew E. Larsen

W. Laurence LePage
Richard H. Prewitt
James G. Ray
Ralph H. McClarren, Secretary

APPENDIX F

FRIDAY, OCTOBER 28, 1938

INTRODUCTION by E. BURKE WILFORD, Chairman

Gentlemen, I want to welcome you all here in the name of the Philadelphia Branch of Institute of Aeronautical Sciences, and to say that we appreciate the co-operation which the Institute of Aeronautical Sciences has given us in organizing this meeting.

As this is probably the first rotary wing aircraft conference occurring in the world, we hope to make a little history here, and the only way that we can do that is for everyone to say what he thinks. Don't be afraid of hurting anybody's feelings, or departing from the conventional procedure. That's what this meeting is for, and we hope that it will be the start of a real boom in the rotary wing aircraft industry. We hope to see that within the next ten years, there will be at least 10,000 men working in this industry. To all you young men that are here, why, this is the line to work in, because it is going places.

I want to introduce Mr. Ralph H. McClarren, who has only spent about the last two months working on this meeting, and we ap- preciate the fact that the Franklin Institute is allowing him to assist us, and he will open the meeting with a general dis- cussion of rotary wing aircraft.

"Review of Rotating Wing Aircraft,"
Ralph H. McClarren, The Franklin Institute.

Mr. Chairman, Members of the Institute of Aeronautical Sciences and Guests -- The title of my paper, assigned to me for this meeting was, "Review of Rotating Wing Aircraft". Any of you who were so fortunate as to be present last night and hear the most excellent paper presented by Dr. Alexander Klemin, of New York University, would realize that it would be hopeless for me to attempt, in the eleven minutes that I have left, to give you any comprehensive review of rotating wing aircraft. I hope that Dr. Klemin's paper will be published, and if so, we will try to supply most of you who have registered here, with copies of that paper when it is published.

I have a few little demonstrations that I would like to make. When we

think of rotating wing aircraft, or, in fact, when we think of anything, we try to go back to nature to find some example in nature of the methods or scientific machines that man has developed, to see if we can find an example. We don't have to go very far for rotating wing aircraft. Here is a little maple seed model, of course larger than the maple seed itself, but let's see what it does. (Demonstration) The maple seed spins as it falls to the ground. That is really a

rotating wing aircraft, and the autogiro, gyroplane, converta- plane, and so on, vary but little in principle of rotation from this little maple seed.

The Australian hunters were rather clever, and they developed this form of rotating wing aircraft,-- the boomerang. (Demonstration) Of course, if you missed the bird on your first shot, you get your weapon back again to take another crack at it. The boomerang is really a rotating wing aircraft.

Then we have the helicopter, which we are going to demonstrate on the principle of the jump-off autogiro. Let's assume that this is the rotor of a jump-off giro, and we place it on the spool, decreasing the angle of incidence, of course, so we don't take off when we first spin it, then put a little bit of power into it, and up it goes. (Demonstration) So you say that even little Chinese toys that were developed about a thousand years ago show that there is really nothing new in the world, and it's just how we put them together.

Take the actual autogiro. I am indebted for this model to Mr. Paul Stanley, of the Autogiro Company of America. He made this

many years ago, and wondered what happened to it. Well, I can tell Paul now that I have had it for the last three and one-half years. This demonstrates very nicely the auto-rota- tion of rotors on rotating wing aircraft. Just move it through the air a little bit, and it spins around, whether I walk along with it, or whether I just wave it back and forth. (Demonstration) Of course, the minute you stop motion, it will stop turning.

Let's go back a little bit, to the beginning of the 16th cen- tury. Lenardo da Vinci was one of those versatile chaps, scientist as well as artist, that delved into the problem of flight, and he developed probably one of the first machines to imitate the bird method of flight. Here we have a model ornithopter. (Demonstration) That is one way to conquer this problem of vertical flight, not by rotating, but by flap- ping wings.

I have a few motion pictures that I would like to show you, of a real hovering flier, one that I don't think we will ever equal in control and maneuverability and in flight character- istics, but I think we might use as our goal the control and maneuverability of little humming bird in flight. (Moving pictures shown.) There you see him in his natural flight. This picture was taken with an ordinary camera. His wings go back and forth about fifty times a second. Dr. Harold E. Edgerton, of the Massachusetts Institute of Technology, develop- ed a special highspeed camera, taking 1200 pictures to the sec- ond, and being interested in slowing down the motion of these rapidly moving things to where he might observe them, he took some pictures of this little fellow in flight. You can really

APPENDIX F

see how the little humming bird moves his wings. Those wings operate on a sculling principle. That is, he reverses the incidence of the wing on each stroke. Forward, it has one in- cidence, positive, and when he comes to the backward stroke, he flops the wing over, moves it back, doing that a hundred times a second. That is why he can keep his body about vertical, and he can hover and fly stationary in the air. I think he will back away from his perch in a moment, showing you that he can also fly backward, as well as forward. There is a good example of backward flight.

We ask ourselves this question: Why is it that the humming bird can fly in this remarkable manner? Let's look at it from a scientific point of view. The muscle weight in a humming bird is 55% of the weight of his body. That is the answer. Man's muscle weight is only 8% of his body, so how in the world can we expect a man, with so little muscle, to flap wings, as Lenardo da Vinci proposed, and many others up until we had the practical fixed wing aeroplane and successful helicopter?

You notice how the tail moves there, stabilizing or controlling his flight. I believe that is a good example of a goal for the rotating wing aircraft fliers to try to reach.

I have a few more models here that I would like to show. We use some of this equipment in the Franklin Institute traveling air show. This particular one is what we call an endurance type of flier, and I think a good example of fixed wing flight. (Demonstration)

Then we have another very interesting fixed wing flier, the soaring type of glider, or slow flier, large aspect ratio wing, and he makes a pretty nice flight, as you let him go. Just to bring in a little variation as to these various types of fixed wing aircraft that depend upon forward motion to sustain them in the air, to create enough lift to keep them up. (Demonstration)

Here is a little model that I had hoped to

have completed to actually demonstrate to you vertical flight, -- not like the autogiro or the gyroplane, all types of which you will hear of later on, but this helicopter type. The model contains all the essential principles of a single rotor helicopter, -- the rotor to be power driven. There is a torque reaction to counteract, so we would rev this prop up a little bit or change the pitch of it, to counteract the torque. When we want to go forward, we change the pitch, and have both props turning, use them to help our forward propulsion, tilt the rotor, and also use the forward component or sine angle, Theta, to help in the forward propulsion.

There is another little trick we might do that the model doesn't show. To effectively use these two little propellors for forward propulsion, we could put a small wing on one side of the fuselage, another wing or slot wing effect on the other side, aft, and then in forward flight, there would be enough

5.

enough speed and enough lifting force on those, to counteract the torque caused by the power put into the rotor. We had hoped to have this flying, and I am sorry it wasn't finished in time.

I have a short demonstration to make using what might be called a wind tunnel. In my work here and in the traveling air show, to make things evident and easier to understand, we generate a visible stream of air. This is accomplished by placing a few pieces of dry ice into luke-warm water, which produces a stream of vapor that makes it possible for us to see the direction of flow. (Demonstration) To demonstrate this physical air flow, that is, to demonstrate something in it, I have a model rotor. You might say this is the Herrick rotor, because it can rotate either way; it is a

symmetrical section fore and aft of the vertical center line. I will place this rotor in the wind stream, turn on the fan, that produces a stream of air through the tunnel. Of course, the wing will not rotate unless we start it, and that is true of all auto-rotating rotors. But as soon as we give it a little start, it continues to rotate as long as air moves thru it. You can now see the general effect in the air flow above the rotor. Pulling the air stream down a bit, we would say, with the wing, that the wing was stalled through here, but that is not true with the rotor, because it turns, the blades turn at a high enough speed so that you don't stall, that is, the individual section, except on a portion of the down-wind blade. You can't see the detailed flow pattern; close observation, however allows one to study the individual flow characteristic on the up-wind blade. Now I am going to move it over to the down-wind blade, and you notice how much freer the air moves through this portion of the rotor. Of course, that is under- standable when we take our velocity vectors through the disc of the individual blade elements.

Here is a very interesting thing, though, that I would like to point out in particular. Many people like to say that the rotor is similar to a wing, particularly at the low angles of flight. I am going to step up the speed just a bit, and we will place our rotor at a low angle of attack. Now, you will notice that we are unable to get much air to flow through the disc, especially on the up-wind blade. But as we increase the angle, we change from that down force characteristic to another one at the high angles, where we merely block the flow of air rather than having a down-flow characteristic. (Indicating) And that transition point is the one in which the aeronautical engineer has to make his best guess when developing the theory of rotor operation.

There is a lot more that I might point out, but my time is just a few minutes gone, and we would like to start the regular session promptly.

APPENDIX F

APPENDIX I

by

Ralph H. McClarren, AeE.

The Franklin Institute

Following the adjournment of the meetings on Saturday morning many of the delegates had luncheon together and later availed themselves of an opportunity to see some very interesting Flight Demonstrations at the Philadelphia Airport. About 70% of the 242 total registered at the meetings saw John M. Miller put a Kellett KD-1 autogiro through its paces. He produced some spectacular flying from the direct-control, wingless Autogiro, making very quick take-offs, almost vertical climbs, practically hovering against the wing and landing without rolling a wheel.

Also, a fine demonstration of Crop Dusting was made by George Townson, flying one of the Giro Associates Pitcairn Model P.C.A. -2 Autogiros. It exemplified the use of rotating wing aircraft in the important field of agriculture.

Keen appreciation was expressed by many of those attending the meetings and all agreed that every effort should be made to have such a meeting a yearly affair. It is understood that a rotary wing aircraft meeting will be held this year in September at the Daniel Guggenheim School of Aeronautics, New York University in connection with the International Aircraft Congress at the N. Y. World Fair.

The officials of The Franklin Institute hope that suitable arrangements can be made to again hold such a meeting in Philadelphia and extend a cordial invitation to all in the aircraft industry.

APPENDIX G

NORMAL MODES AND FREQUENCIES

In the late 1950s, while working at the Vertol Aircraft Company located in Morton, Pennsylvania, I was told to get familiar with the flapwise bending moment equation for a rotating blade.[1] I became entranced with Fig. G-1, bowled over by Eq. (1), and quite doubtful that I could find a solution. My apprenticeship up to then only included the "facts" that blades were rigid and flapped, and that I could calculate all the rotor performance with just these ground rules. The book *Aeroelasticity*,[2] and specifically pages 95 through 98 that show how to solve Eq. (1), became a bible for the rest of my career.

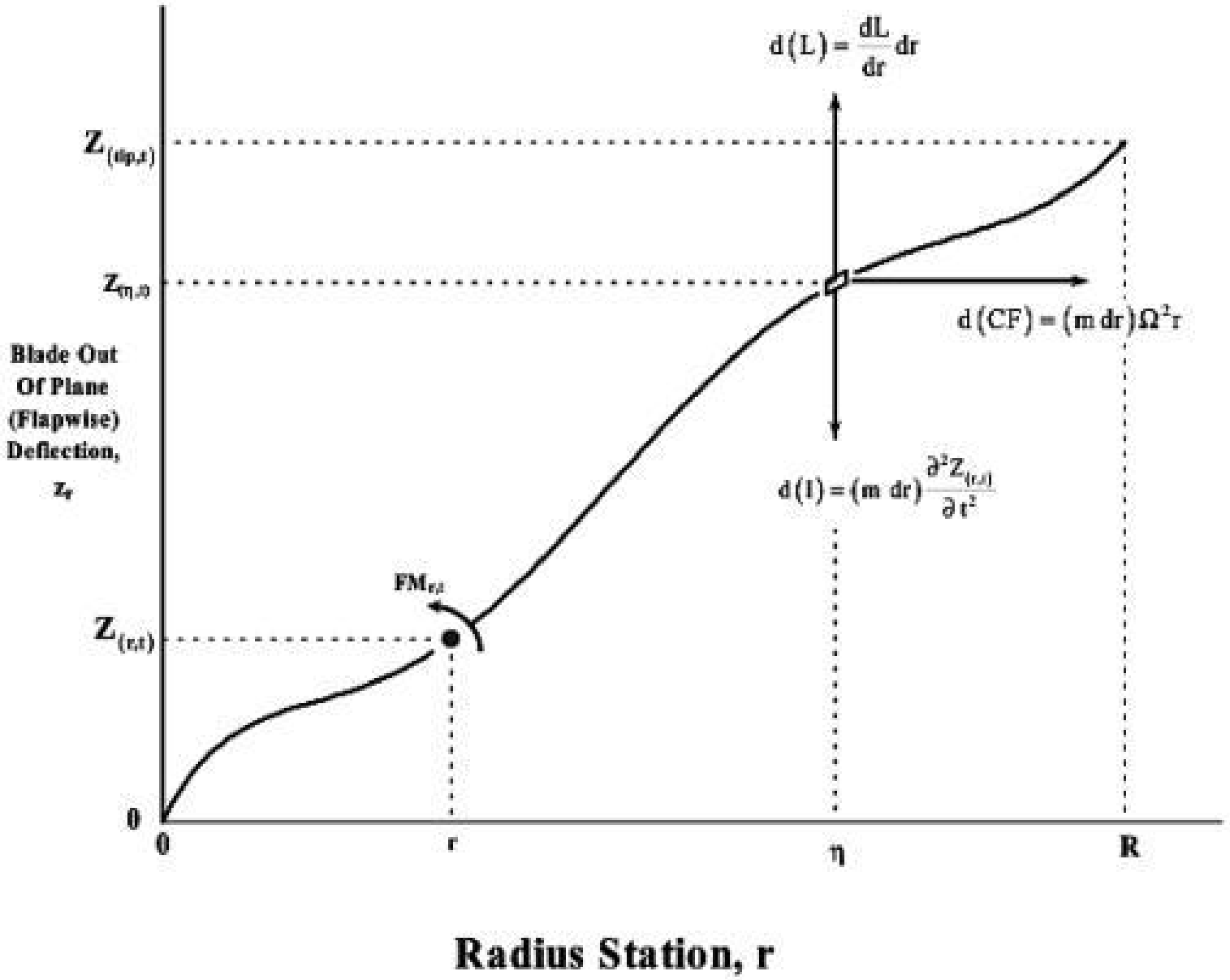

Fig. G-1. Flapwise forces and bending moment on a rotating rotor blade.

---

[1] I thought of myself as an aerodynamics engineer and was bent on learning my trade. My boss then was Joe Mallen and he said, "Go to the library, check out Bisplinghoff's book on Aeroelasticity, and learn the first

100 pages." Joe was my first mentor and later became Boeing Helicopter Division manager. I owe him a great deal; certainly more than I can thank him for.

[2] Raymond L. Bisplinghoff, Holt Ashley, and Robert L. Halfman, *Aeroelasticity,* 2nd Ed., Addison–Wesley Publishing Co., Reading, Mass., 1955.

APPENDIX G

$$\text{Flapwise } M_{r,t} = \left(EI_{flap}\right)_r \left(\frac{\partial^2 Z_{r,t}}{\partial r^2}\right) \tag{1}$$

$$= \int_r^R (\eta - r)\, d\left(L_{\eta,t}\right) - \int_r^R \left(Z_{\eta,t} - Z_{r,t}\right) d\left(CF_{\eta,t}\right) - \int_r^R (\eta - r)\, d\left(I_{\eta,t}\right)$$

The solution to Eq. (1) begins by differentiating it twice with respect to radius (r). For a uniform mass and stiffness beam (i.e., m is constant from root to tip in the units slugs per foot, and EL_{flap} is constant in units of pounds-feet^2), the result is

(2)

$$EI\frac{\partial^4 Z_{(r,t)}}{\partial r^4}-\frac{m\Omega^2}{2}\left\{\frac{\partial}{\partial r}\left[\left(R^2-r^2\right)\frac{\partial Z_{(r,t)}}{\partial r}\right]\right\}+m\frac{\partial^2 Z_{(r,t)}}{\partial t^2}=\frac{\partial\left(L_{r,t}\right)}{\partial r}.$$

This is a fourth-order partial differential equation, which can be separated into two, ordinary differential equations. One equation accounts for the radial deflection of the blade, and the other accounts for blade behavior with time. The separation is done by first nondimensionalizing by radius (R) so $x = r/R$ and defining the rotational azimuth of the blade as $\psi = \Omega t$, where the rotational speed (Ω) is constant. Next, the assumption is made that an infinite series of the following form is reasonable:

$$Z_{r,t}=R\sum_{m=1}^{\infty} z_{m,x}\left(\frac{Z_{tip}}{R}\right)_{m,t}$$

(3)

$$= R\left\{\left[z_x\left(\frac{Z_{tip}}{R}\right)_t\right]_{m=1} + \left[z_x\left(\frac{Z_{tip}}{R}\right)_t\right]_{m=2} + \left[z_x\left(\frac{Z_{tip}}{R}\right)_t\right]_{m=3} + \cdots\cdots\right\}$$

Substituting Eq. (3) into Eq. (2) results in a radial deflection (z_x) equation and a blade-tip deflection (Z_{tip}/R) equation that is time dependent. Both equations are dimensionless because of the substitutions that $x = r/R$ and $\psi = \Omega t$. The summation operator in Eq. (3) says that the result depends on an infinite sum of radial times time functions . The two equations *that must be solved for each vibration mode (m) in the summation* are, for the radial behavior

(4)

$$\frac{d^4 z_{(x)}}{dx^4} - \frac{1}{2}\left(\frac{m\Omega^2 R^4}{EI}\right)\left\{\frac{d}{dx}\left[\left(1-x^2\right)\frac{d^2 z_{(x)}}{dx}\right]\right\} - \left(\frac{m\omega_n^2 R^4}{EI}\right) z_{(x)} = 0$$

and, for the time behavior

(5)

$$\frac{d^2\left(Z_{tip}/R\right)}{d\psi^2}+\left(\frac{\omega_n}{\Omega}\right)^2\left(\frac{Z_{tip}}{R}\right)=\frac{1}{mR^2\Omega^2\int_0^1\left(z_{(x)}\right)^2dx}\int_0^1 z_{(x)}\frac{dL_{(x,\psi)}}{dx}dx\,.$$

Notice that radial deflection must be obtained first from Eq. (4) before the time equation can be solved. This is because the right-hand side of Eq. (5) contains integrals of the deflection. The solution of Eq. (4) gives the normal modes (i.e., radial deflections) and associated frequencies for the rotating uniform beam—the blade . It is customary to scale the mode shapes so that, at the blade tip where x = 1, the deflected shape (z_x) gives $z_{x=1}$ exactly to unity.

The mode shape equation, Eq. (4), requires boundary conditions. A blade with a flapping hinge is classified as a pin-free beam. This means that the root boundary conditions (i.e., the pinned end where the flapping hinge is located) are that at $x = 0$, $z_{(x)} = 0$, and $d^2z_{(x)}/dx^2 = 0$. The free end of the beam is the blade tip at which $x = 1$, and both moment ($d^2z_{(x)}/dx^2$) and shear ($d^3z_{(x)}/dx^3$) are zero. Autogyro blades fall in this classification.

This appendix gives the solution to Eq. (4), which I have used in this volume about autogyros. I chose to recast this normal modes and associated frequencies equation to illuminate two key parameters upon which the solution depends. That is, I defined

$$g = \frac{m\Omega^2 R^4}{EI} \qquad \text{and} \qquad f = \frac{m\omega_n^2 R^4}{EI}$$

so that the normal modes and frequencies equation to be solved becomes (6)

$$\frac{d^4 z_{(x)}}{dx^4} - \frac{1}{2}(g)\left\{\frac{d}{dx}\left[\left(1-x^2\right)\frac{d^2 z_{(x)}}{dx}\right]\right\} - (f)\, z_{(x)} = 0 .$$

Both g and f have no units, so Eq. (6) is completely nondimensional.

I took the simple Frobenius solution approach, which is a power series method. The assumption is that

(7) $$z_{(x)} = A_1 \sum_{n=1}^{\infty} K_n x^n + A_3 \sum_{n=1}^{\infty} M_n x^n .$$

First, the three derivatives are easily obtained and substituted into Eq. (6). Next, the expansion is collected in a K series and an M series. Then the coefficients of each x^m are set to zero. Finally, the recursion formulas for the K and M series are created. The result for the K series is

(8)

$$K_n = \left[f - \frac{g}{2}(n-4)(n-3) \right] \left[\frac{1}{n(n-1)(n-2)(n-3)} \right] K_{(n-4)} + \frac{g}{2} \left[\frac{1}{n(n-1)} \right] K_{(n-2)}$$

where n proceeds as n = 5, 7, 9, etc., and K_1 =

1 and $K_3 = 0$. Similarly, for the M series, the result is

(9)

$$M_n = \left[f - \frac{g}{2}(n-4)(n-3) \right] \left[\frac{1}{n(n-1)(n-2)(n-3)} \right] M_{(n-4)} + \frac{g}{2} \left[\frac{1}{n(n-1)} \right] M_{(n-2)}$$

where n proceeds as n = 5, 7, 9, etc., and $M_1 = 0$ and $M_3 = 1/6$. Notice that both series have exactly the same mathematical form. The difference between the two is the first coefficient values, K_1, K_3 and M_1, M_3 . Both series behave as hyperbolic sine functions.

The coefficients A_1 and A_3 required by Eq. (7) are given by

APPENDIX G

$$\sum_{n=1}^{N} n(n-1)M_n$$

(10) A_1

$$= \frac{}{\sum_{n=1}^{N} K_n \sum_{n=1}^{N} n(n-1)M_n - \sum_{n=1}^{N} M_n \sum_{n=1}^{N} n(n-1)K_n}$$

and

$$-1\sum_{n=1}^{N} n(n-1)K_n$$

(11) A_3

$$= \frac{}{\sum_{n=1}^{N} K_n \sum_{n=1}^{N} n(n-1)M_n - \sum_{n=1}^{N} M_n \sum_{n=1}^{N} n(n-1)K_n}.$$

The final key to the solution is the transcendental equation, which says that for any value of $g = \frac{m\Omega^2 R^4}{EI}$ there is a corresponding value of $f = \frac{m\omega_n^2 R^4}{EI}$ such that

$$\sum_{n=1}^{N}(n-1)(n-2)K_n\sum_{n=1}^{N}n(n-1)(n-2)M_n-\sum_{n=1}^{N}n(n-1)(n-2)K_n\sum_{n=1}^{N}n(n-1)M_n=0. \quad (12)$$

The computational process is quite straightforward and can be carried out using a spreadsheet program such as Microsoft® Excel®. For a given value of g, various values of f must be selected. With each value of f, the K and M series are constructed using Eqs. (8) and (9). Then the transcendental equation is tested for a value of f that gives zero . The value of f that makes Eq. (12) zero leads to the natural frequency for that particular mode. This step defines the exact values of K_n and M_n for that mode. Finally, the lead coefficients, A_1 and A_3, are calculated with Eqs. (10) and (11).

I set the whole problem up in Excel® and used the goal seeking tool to find the

f value for any selected g value that made the transcendental equation zero. One example of the behavior of the transcendental equation is shown in Fig. G-2, which was obtained with g = 600. Notice that the transcendental equation crosses zero at successive values of the parameter (f). Each crossing of zero defines a mode frequency and, therefore, a solution to Eq. (6) . For this result, I obtained satisfactory convergence of the mode shapes and frequencies using K and M series created as n = 5, 7, 9, on up to n = 139.

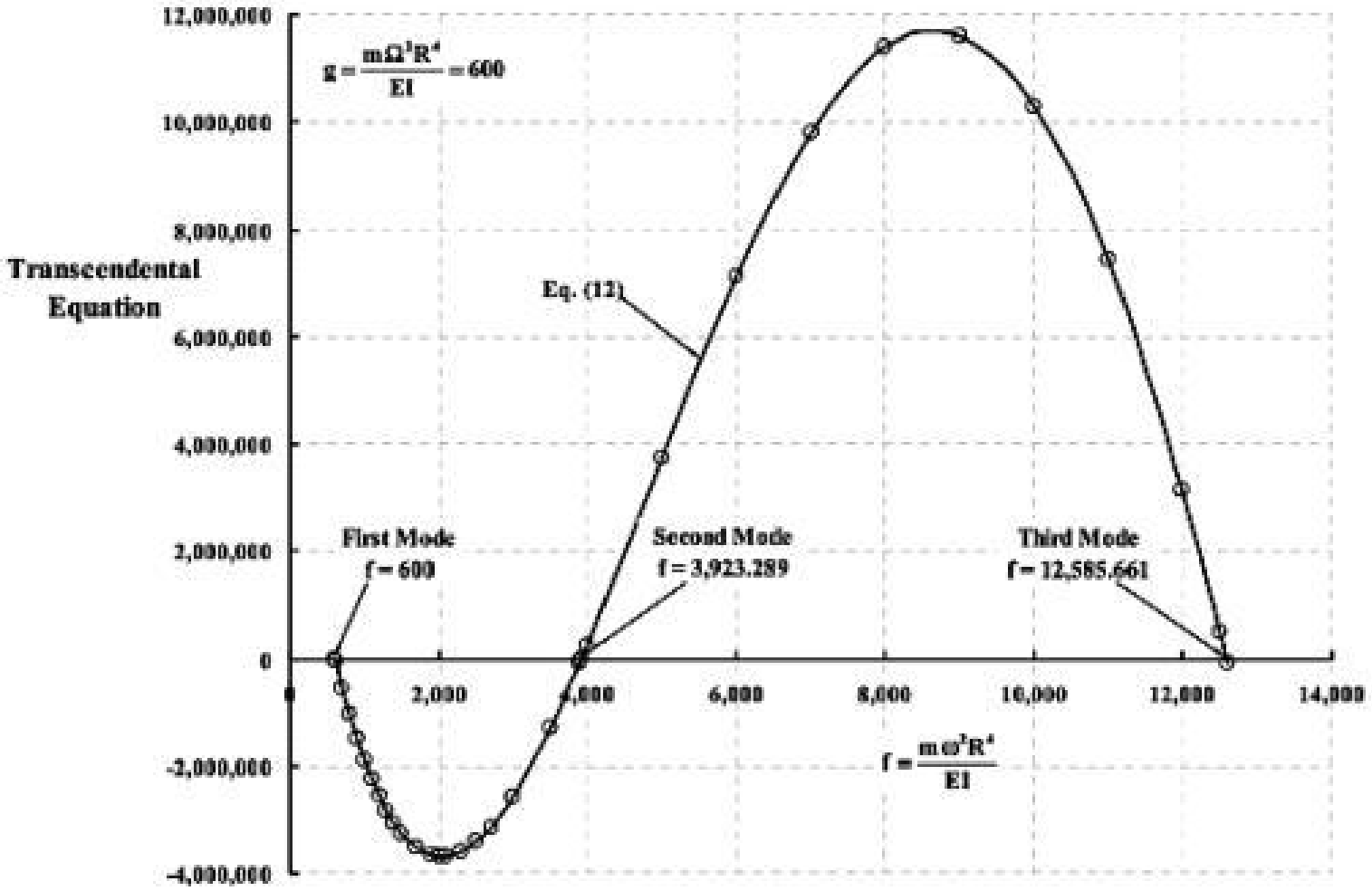

Fig. G-2. Transcendental equation.

APPENDIX H

FLAP BENDING MOMENT

EQUATION SOLVED BY FINITE DIFFERENCE METHOD

This appendix shows one way to solve the rotating beam out-of-plane response to simple blade-element lift. The solution approach is one that could have been done in the autogyro era—if the pioneers had decided to spend the resources . I have include this appendix because it is a special piece of work that was just plain fun. But first, a little background.

While at Bell Helicopter Textron,[1] I sent a memo, dated August 24, 1987, to the technology department and computer support staff that said, in part:

On Enclosures A, B and C I have written out the simple equation for flap bending. I would like to see this equation solved without using normal

modes. Hopefully, there is a "canned" partial differential equation solver that can be used.

As you know, I believe future rotor analysis will become finite element based rather than normal mode based. This does not mean I see the Myklestad/C-81 analysis disappearing because knowledge of blade natural frequencies, for example, will always be important. However, when I read a paper such as the one included at the end of this memo,[2] I begin to think the structural representation of the blade by "simple modal equations" may not be worth the trouble. And, therefore, a more direct approach of feeding the rotor design group's tabulated blade properties into a finite element analysis could easily yield more correct results. The big question to me is one of absolute accuracy as a function of total turn-around time.

Please make sure the staff understands that I am not advocating discarding C-8 1. What I want is to lay the foundation to a new, finite element approach that will grow as computer power grows and that can incorporate CFD progress. Perhaps in ten years the C-81/COPTER approach will be used in

preliminary design of rotor systems and the finite element approach will be used for detailed design.

On October 15, 1987 I received a memo back from Mark Dreier (then a Senior Computing Project Engineer working in the Scientific Systems department) that showed a finite difference solution that worked like a charm.[3] It was a beautiful piece of work that I hold in high regard

---

[1] At that time I reported to Bob Lynn, Senior Vice President for Engineering, as the Deputy for Technology and
Advanced Development.

[2] K. B . Subrahmanyam, et al., *Nonlinear Vibration and Stability of Rotating, Pretwisted, Preconed Blades Including Coriolis Effects*, AIAA J. of Aircraft, vol. 24, no. 5, 1987, pp. 342 –352.

[3] My first encounter with numerical solutions in rotorcraft problems came when we began using the N.A.C.A. method in the late 1950s. This groundbreaking analysis was developed by Alfred Gessow and Almer Crim and published in January 1955. The report, NACA

TN 3366, is titled *A Method for Studying the Transient Blade- Flapping Behavior of Lifting Rotors at Extreme Operating Conditions*. The method numerically solved the rigid blade-flapping, ordinary differential equation with real airfoil properties. Mark Dreier's extension allowed flap bending to occur with the fourth order, partial differential equation.

APPENDIX H

After retiring from Bell in January of 1991, I decided in 1992–1993 to "program" Mark's solution method in Microsoft® Excel® as part of my research about autogyros that has culminated in this volume . It took about a month of very enjoyable spare time. The solution approach that follows is Mark's memo in my words and nomenclature.

From Appendix G, you learned about the flap

bending equation, which is

$$\text{Flapwise } M_{r,t} = \left(EI_{flap}\right)_r \left(\frac{\partial^2 Z_{r,t}}{\partial r^2}\right) \quad (1)$$

$$= \int_r^R (\eta - r)\, d\left(L_{\eta,t}\right) - \int_r^R \left(Z_{\eta,t} - Z_{r,t}\right) d\left(CF_{\eta,t}\right) - \int_r^R (\eta - r)\, d\left(I_{\eta,t}\right)$$

This solution to Eq. (1) begins by differentiating it twice with respect to radius (r).[4,5] For a uniform mass and stiffness beam (i.e., m is constant from root to tip in the units slugs per foot and EL_{flap} is constant in units of pounds-feet^2). The second step is done by nondimensionalizing by radius (R) so $x = r/R$ and defining the rotational azimuth of the blade as $\psi = \Omega t$, where the rotational speed (Ω) is constant. The last step is to scale out-of-plane deflection by rotor radius (R) so that $z = Z/R$. The results of these steps is the partial differential equation:

(2)

$$\frac{EI}{m\Omega^2R^4}\frac{\partial^4 z_{(x,\psi)}}{\partial x^4}-\frac{\left(1-x^2\right)}{2}\frac{\partial^2 z_{(x,\psi)}}{\partial x^2}+x\frac{\partial z_{(x,\psi)}}{\partial x}+\frac{\partial^2 z_{(x,\psi)}}{\partial \psi^2}=\frac{1}{m\Omega^2R^2}\frac{\partial\left(L_{x,\psi}\right)}{\partial x}.$$

This equation is fourth order in space ($x = r/R$) and second order in azimuth (ψ) (i.e., time). Again, the equation applies to a blade with uniform mass and stiffness, and rotating at a constant tip speed of $V_t = \Omega R$.

The airload—the right-hand side of Eq. (2)—is expanded with a very simple representation as

(3)
$$\frac{1}{m\Omega^2R^2}\frac{\partial\left(L_{x,\psi}\right)}{\partial x}=\frac{\gamma}{6}\left\{\begin{array}{l}\left(x+\mu\sin\psi\right)^2\left(\theta_o+x\theta_t-B_{1C}\sin\psi-A_{1C}\cos\psi\right)+\left(x+\mu\sin\psi\right)\lambda_{hp}\\ -\left(x+\mu\sin\psi\right)\dfrac{\partial z_{(x,\psi)}}{\partial\psi}-\mu\cos\psi\left(x+\mu\sin\psi\right)\dfrac{\partial z_{(x,\psi)}}{\partial x}\end{array}\right\}.$$

Damping Term

Spring Term

which follows previous models and symbols discussed in this volume. The Lock number (γ) is defined as $\rho acR^4/I_b$.

[4] It is entirely feasible to solve this differential-integral equation directly. This was demonstrated by Joe Stuart in his paper titled *A Tabular Method of Propeller Blade Stress Analysis*. This paper was presented at the Power Plants and Propeller Session of the Eleventh Annual Meeting of the Institute of the Aeronautical Sciences, New York, Jan. 25–29, 1943 . The work was later published in the J. of the Aeronautical Sciences, vol. 10, no. 4, pp. 115–118, April 1943. This approach easily accommodates nonuniform blade geometry and structural properties.

[5] The paper *The Bending of Rotor Blades* by Al Flax published in the J. of the Aeronautical Sciences, vol. 14, no. 1, Jan. 1947 provides a rather comprehensive review of several solution approaches.

APPENDIX H

My Excel® solution approach begins by assigning columns to blade segments that go from i = –2, i = – 1, i = 0, i = +1, etc, on up to

i_{max} = tip, i_{max+1} i_{max+2} . I used a segment length of $\Delta x = 0.05$. This means that 21 columns are used for the blade, 2 more columns are used for root boundary conditions and 2 more are used for the tip boundary conditions, which makes a total of 25 columns. Then 25 rows were used to construct 25 equations (shown shortly) in 25 unknowns. Each equation, constructed based on the current azimuth (n), is used to predict the deflection at the next azimuth (n+1) . This gives the time marching portion of the solution. This is a relatively simple matrix algebra game.

The 25 equations in 25 radial points are created using finite difference approximations for all derivatives of the deflection. The approximations must be tagged with a space counter (i) and an azimuth counter (n). I have made the space counter a subscript and the azimuth counter a superscript. On this basis, any one of the 25 equations is found from:

(4) $$(K_4)z_{i-2}^{n+1} - (K_7)z_{i-1}^{n+1}$$
$$+(K_6 + K_1)z_i^{n+1} - (K_5)z_{i+1}^{n+1} + (K_4)z_{i+2}^{n+1} = RHS$$

where the right-hand side (RHS) is

(5) $$RHS = F_i^n - (K_4)z_{i+2}^n + (K_5)z_{i+1}^n + (K_6 - K_2)z_i^n$$
$$+(K_7)z_{i-1}^n - (K_4)z_{i-2}^n - K_3 z_i^{n-1}.$$

The coefficients (K_1 through K_8) are obtained from the input data, the radial station (x_i), and azimuth (ψ_n) with which Eq. (4) is identified. Thus,

$$K_1 = \frac{1}{(\Delta\psi)^2} + \left\{\frac{\frac{\gamma}{6}(x + \mu\sin\psi)}{2(\Delta\psi)}\right\}_i^n$$

$$K_2 = \frac{2}{(\Delta\psi)^2}$$

$$K_3 = \frac{1}{(\Delta\psi)^2} - \left\{\frac{\frac{\gamma}{6}(x + \mu\sin\psi)}{2(\Delta\psi)}\right\}_i^n$$

(6)

$$K_4 = \frac{EI/m\Omega^2R^4}{2(\Delta x)^4}$$

$$K_5 = 2\frac{EI/m\Omega^2R^4}{(\Delta x)^4} + \left\{\frac{1-x^2}{4(\Delta x)^2} - \frac{1}{4(\Delta x)}\left[x + \frac{\gamma}{6}(\mu\cos\psi)(x+\mu\sin\psi)\right]\right\}_i^n$$

$$K_6 = 3\frac{EI/m\Omega^2R^4}{(\Delta x)^4} + \left\{\frac{1-x^2}{2(\Delta x)^2}\right\}_i^n$$

$$K_7 = 2\frac{EI/m\Omega^2R^4}{(\Delta x)^4} + \left\{\frac{1-x^2}{4(\Delta x)^2} + \frac{1}{4(\Delta x)}\left[x + \frac{\gamma}{6}(\mu\cos\psi)(x+\mu\sin\psi)\right]\right\}_i^n$$

Note that actually only K_2 and K_4 are constants; K_1, K_3, K_4, K_5, K_6, and K_7 all depend on the radial station counter (i) and azimuth counter (n) under calculation. The forcing function (F_i^n) required by Eq. (5) is calculated as

(7) $$F_i^n = \frac{\gamma}{6}\left\{(x+\mu\sin\psi)^2(\theta_o + x\theta_t - B_{1C}\sin\psi - A_{1C}\cos\psi) + (x+\mu\sin\psi)\lambda_{hp}\right\}_i^n \cdot$$

APPENDIX H

The solution of 25 equations in 25 unknowns (i.e., x_{i-2} through x_{imax+2}) was accomplished in Excel®[6] by creating a K matrix. A sample of this matrix in Excel® form is shown in Table H-1 . The calculations at azimuth counter (n) are used to calculate the radial deflection at azimuth counter (n+1). In matrix algebra shorthand notation, the operation is written as

$$Z_i^{n+1} = \left[K^n\right]^{-1} (RHS)_i^n . \quad (8)$$

In Excel® this operation is performed by creating (from the Insert menu) the function named MMULT(MINVERSE(C60:AA84),AC60:AC84). The MINVERSE function inverts the K^n matrix to give $[K^n]^{-1}$, and the MMULT function does the multiplication that Eq. (8) requires. As I set the problem up, the K matrix occupied the cells from column C, row 60, to column AA,

row 84. The RHS occupied the cells in column AC, row 60 to row 84. I put the results for deflection at azimuth n+1 in cells occupying column AF, row 60 to row 84.

The solution of Eq. (4) at the 25 radial stations required a Macro to advance azimuth in steps of $\Delta\psi = 2$ degrees starting at $\psi = 0$. The initial deflection was set to zero (i.e., a straight line from root to tip) . The slope, curvature, and azimuth derivatives were all zero. The analysis then proceeds to march around the azimuth solving 25 equations in 25 unknowns at each azimuth using trailing azimuth data to calculate deflection at the new azimuth. Both deflection at azimuth counters (n-1) and (n) are saved, but progressively overwritten in preparation for the next time step . The blade motion converges quite rapidly because of the damping, and I found that the fourth revolution repeated results from the third revolution within engineering accuracy.

Given the deflection at every blade radial station and any given azimuth, the following important derivatives were calculated as

$$z_{(x,\psi)} = z_i^n$$

$$\frac{\partial z_{(x,\psi)}}{\partial x} = \frac{\partial z_i^n}{\partial x} = \frac{z_{i+1}^n - z_{i-1}^n}{2(\Delta x)}$$

(9)

$$\frac{\partial^2 z_{(x,\psi)}}{\partial x^2} = \frac{\partial^2 z_i^n}{\partial x^2} = \frac{z_{i+1}^n - 2z_i^n + z_{i-1}^n}{(\Delta x)^2}$$

$$\frac{\partial^3 z_{(x,\psi)}}{\partial x^3} = \frac{\partial^3 z_i^n}{\partial x^3} = \frac{z_{i+2}^n - 2z_{i+1}^n + 2z_{i-1}^n - z_{i-2}^n}{2(\Delta x)^3}$$

$$\frac{\partial^4 z_{(x,\psi)}}{\partial x^4} = \frac{\partial^4 z_i^n}{\partial x^4} = \frac{z_{i+2}^n - 4z_{i+1}^n + 6z_i^n - 4z_{i-1}^n + z_{i-2}^n}{(\Delta x)^4}$$

[6] The whole problem can, of course, be solved using a FORTRAN code or any one of a number of mathematical software applications on the market.

Table H-1. The K Matrix

Radial Station (r/b)	-0.2	-0.05	0	0.05	0.1	0.15	0.2	0.25	0.3	0.35	0.4	0.45	0.5	0.55	0.6	0.65	0.7	0.75	0.8	0.85	0.9	0.95	1.0	1.05	1.1
Radial Counter	i = -2	i = -1	i = 0	i = 1	i = 2	i = 3	i = 4	i = 5	i = 6	i = 7	i = 8	i = 9	i = 10	i = 11	i = 12	i = 13	i = 14	i = 15	i = 16	i = 17	i = 18	i = 19	i = 20	i = 21	i = 22
Eq. 1 (i = 2)	1	-4	6	-4	1	0	0	0	0	0	0	0	0	0	0	0	0	0	0	0	0	0	0	0	0
Eq. 2 (i = 1)	0	1	-2	1	0	0	0	0	0	0	0	0	0	0	0	0	0	0	0	0	0	0	0	0	0
Eq. 3 (i = 0)	0	0	1	0	0	0	0	0	0	0	0	0	0	0	0	0	0	0	0	0	0	0	0	0	0
Eq. 4 (i = 1)	0	K4	-K7	K6+K2	-K5	K4	0	0	0	0	0	0	0	0	0	0	0	0	0	0	0	0	0	0	0
Eq. 5 (i = 2)	0	0	K4	-K7	K6+K2	-K5	K4	0	0	0	0	0	0	0	0	0	0	0	0	0	0	0	0	0	0
Eq. 6 (i = 3)	0	0	0	K4	-K7	K6+K1	-K5	K4	0	0	0	0	0	0	0	0	0	0	0	0	0	0	0	0	0
Eq. 7 (i = 4)	0	0	0	0	K4	-K7	K6+K1	-K5	K4	0	0	0	0	0	0	0	0	0	0	0	0	0	0	0	0
Eq. 8 (i = 5)	0	0	0	0	0	K4	-K7	K6+K1	-K5	K4	0	0	0	0	0	0	0	0	0	0	0	0	0	0	0
Eq. 9 (i = 6)	0	0	0	0	0	0	K4	-K7	K6+K1	-K5	K4	0	0	0	0	0	0	0	0	0	0	0	0	0	0
Eq. 10 (i = 7)	0	0	0	0	0	0	0	K4	-K7	K6+K1	-K5	K4	0	0	0	0	0	0	0	0	0	0	0	0	0
Eq. 11 (i = 8)	0	0	0	0	0	0	0	0	K4	-K7	K6+K1	-K5	K4	0	0	0	0	0	0	0	0	0	0	0	0
Eq. 12 (i = 9)	0	0	0	0	0	0	0	0	0	K4	-K7	K6+K1	-K5	K4	0	0	0	0	0	0	0	0	0	0	0
Eq. 13 (i = 10)	0	0	0	0	0	0	0	0	0	0	K4	-K7	K6+K1	-K5	K4	0	0	0	0	0	0	0	0	0	0
Eq. 14 (i = 11)	0	0	0	0	0	0	0	0	0	0	0	K4	-K7	K6+K1	-K5	K4	0	0	0	0	0	0	0	0	0
Eq. 15 (i = 12)	0	0	0	0	0	0	0	0	0	0	0	0	K4	-K7	K6+K1	-K5	K4	0	0	0	0	0	0	0	0
Eq. 16 (i = 13)	0	0	0	0	0	0	0	0	0	0	0	0	0	K4	-K7	K6+K1	-K5	K4	0	0	0	0	0	0	0
Eq. 17 (i = 14)	0	0	0	0	0	0	0	0	0	0	0	0	0	0	K4	-K7	K6+K1	-K5	K4	0	0	0	0	0	0
Eq. 18 (i = 15)	0	0	0	0	0	0	0	0	0	0	0	0	0	0	0	K4	-K7	K6+K1	-K5	K4	0	0	0	0	0
Eq. 19 (i = 16)	0	0	0	0	0	0	0	0	0	0	0	0	0	0	0	0	K4	-K7	K6+K1	-K5	K4	0	0	0	0
Eq. 20 (i = 17)	0	0	0	0	0	0	0	0	0	0	0	0	0	0	0	0	0	K4	-K7	K6+K1	-K5	K4	0	0	0
Eq. 21 (i = 18)	0	0	0	0	0	0	0	0	0	0	0	0	0	0	0	0	0	0	K4	-K7	K6+K1	-K5	K4	0	0
Eq. 22 (i = 19)	0	0	0	0	0	0	0	0	0	0	0	0	0	0	0	0	0	0	0	K4	-K7	K6+K1	-K5	K4	0
Eq. 23 (i = 20)	0	0	0	0	0	0	0	0	0	0	0	0	0	0	0	0	0	0	0	0	K4	-K7	K6+K1	-K5	K4
Eq. 24 (i = 21)	0	0	0	0	0	0	0	0	0	0	0	0	0	0	0	0	0	0	0	0	0	1	-2	1	0
Eq. 25 (i = 22)	0	0	0	0	0	0	0	0	0	0	0	0	0	0	0	0	0	0	0	0	-1	2	-1	-2	1

Note: The sum K6 + K1 forms the diagonal of this matrix. Even though K4 and –K7 and –K5 and K4 are placed in adjoining cells on the same row, all coefficients are calculate using the same radial

station (i.e., x_i) as the K6 + K1 sum.

APPENDIX H

Sample Case 1. Analysis Versus CH-34 Wind Tunnel Test

Mark and I had a check case for the analysis he created. The check case was for a Sikorsky CH-34 rotor. This rotor was tested in the NASA Ames 40- by 80-foot wind tunnel in September 1964 . The primary data became available when Jack Rabbott (et al.) published *A*

Presentation of Measured and Calculated Full-Scale Rotor Blade Aerodynamic and Structural Loads in July 1966 as USAAVLBS TR 66-31.[7] The 56-foot-diameter rotor had one

of its 4 blades heavily instrumented (for the time) . This blade had strain gages for loads and pressure taps for airfoil data. The full-span trailing-edge tab on the instrumented blade had zero deflection for spanwise stations r/R = 0.25, 0.40, 0.55, 0.75, and 0.95; the trim tab was deflected upward 4 degrees over stations r/R = 0.85 and 0.90. Two-dimensional airfoil data was available.[8] The flapping and lagging hinges were coincident and offset from the center of rotation by one foot. The check case had the input provided here in Table H-2, and note that the flapping hinge offset was zero.

Table H-2. Input for Sample Case 1 (V = 110 kts, αS = –5 deg, thrust = 8,250 lbs)

Configuration and Test Parameters	Symbol	Value	Units
Radius	R	28.0	ft
Chord	c	1.366666	ft
Root cutout	x_c	0.20	nd
Blades	b	4	nd
Tip speed	V_t	650	ft/sec
Blade flap inertia	I_b	1,360	slug-ft^2
Flap hinge offset	r_β	0.0	ft
Density	ρ	0.002378	slug/ft^3
Hub plane angle of attack	α_{hp}	–5.0	deg (nose down)
Forward speed	V	110	knots
Blade running weight	w_b	0.50	lb/in.
Blade flap stiffness	EI_f	15,000,000.0	lb-in.^{2}
Collective pitch	θ_0	14.0(π/180)	radians
Twist	θ_t	–8.0(π/180)	radians
Longitudinal cyclic	B_{1C}	6.0(π/180)	radians
Lateral cyclic	A_{1C}	2.4(π/180)	radians
Calculated Input Parameters	**Symbol**	**Value**	**Units**
Advance ratio	μ_{hp}	0.2847431	nd
Inflow ratio	λ_{hp}	–0.03153197	nd
Lock number (x = 0 to 0.20)	γ_c	0.0	nd
Lock number (x = 0.2 to 1.0)	γ	8.417	nd
$EI_f/m_b\Omega^2R^4$	none	0.001687682	nd

[7] The rotor was first tested in flight; data from that experiment was published by James Scheiman and titled *Tabulation of Helicopter Rotor-Blade Differential Pressures, Stresses, and Motions as Measured in Flight*, as NASA/TM–X-952 in March 1964.

[8] Anon.: *Two-Dimensional Wind-Tunnel Tests of an H-34 Main Rotor Airfoil Section.* TREC Tech. Rep. 60-53 (Contract DA 44-177-TC-657), U.S. Army

APPENDIX H

Table H-3. Fourier Flapwise Stress Coefficients ($V = 110$ kts, $\alpha_S = -5$ deg, $T = 8{,}250$ lbs)

	x = 0.375		x = 0.45		x = 0.65		x = 0.80	
N	Cosine	Sine	Cosine	Sine	Cosine	Sine	Cosine	Sine
0	–243		–395		–881		–1555	
1	–811	942	–899	1060	–1105	1297	–470	701
2	124	–571	191	–565	586	–459	590	–266
3	–140	–204	–133	–259	94	–474	181	–515
4	–39	–72	–12	–51	171	–1	325	–27
5	67	–38	60	–55	–14	37	–68	119
6	–11	–25	15	2	30	66	–71	23
7	29	–6	–9	2	–51	17	13	4
8	30	19	28	7	–21	–24	–13	11
9	4	30	–16	28	0	–27	27	26
10	–7	1	–22	8	17	–4	0	3

The test data used in the comparison between the finite difference analysis and test

came from reconstituted flapwise stress waveforms from Fourier coefficients provided by Rabbott as Table XXVIIIa on page 126 of USAAVLBS TR 66-3 1 . This table of experimental data reduced to Fourier coefficients is shown here as Table H-3.

The finite difference solution provided the nondimensional curvature derivative $\left(\partial^2 z_{x,\psi}/\partial x^2\right)$. This derivative was converted to CH-34 flapwise bending stress in pounds per

square inch according to
(10)

$$\text{Flap Stress}_{x,\psi} = \frac{\text{Flap } M_{x,\psi}\left(\frac{t/2}{c}\right)c}{I_{\text{Flap}}} = \frac{\left(\frac{t/2}{c}\right)c}{I_{\text{Flap}}}\left(\frac{EI_{\text{Flap}}}{R}\frac{\partial^2 z_{x,\psi}}{\partial x^2}\right)$$

$$= \frac{tE}{2R}\left(\frac{\partial^2 z_{x,\psi}}{\partial x^2}\right) = \frac{(1.95\text{in})\left(10\times10^6\ \text{lb}-\text{ft}^2\right)}{2(336)}\left(\frac{\partial^2 z_{x,\psi}}{\partial x^2}\right)$$

in order to show the waveform comparisons in Figs. H-1 through H-4.

The comparisons, a "correlation" if you prefer, is what I imagine could have been produced in the autogyro era. In fact, the actual waveforms probably would have been of

secondary interest to Cierva. What he wanted was some confidence that the magnitude[9] of the flapwise bending stress was approximately correct. This

vibratory

vibratory

magnitude comparison, shown in Fig. H-5, indicates that this simple finite difference analysis with a simple airload overpredicts the actual measured flapwise stresses by a safe margin. It is worth noting that a jump in airloads due to the absence of an airfoil (i.e., a root cutout) causes a distortion in the radial flapwise vibratory stress distribution.

[9] The vibratory magnitude is frequently referred to as (1) peak-to-peak divided by two, or (2) one-half peak-to-peak. In either case, the steady stress is often of little interest.

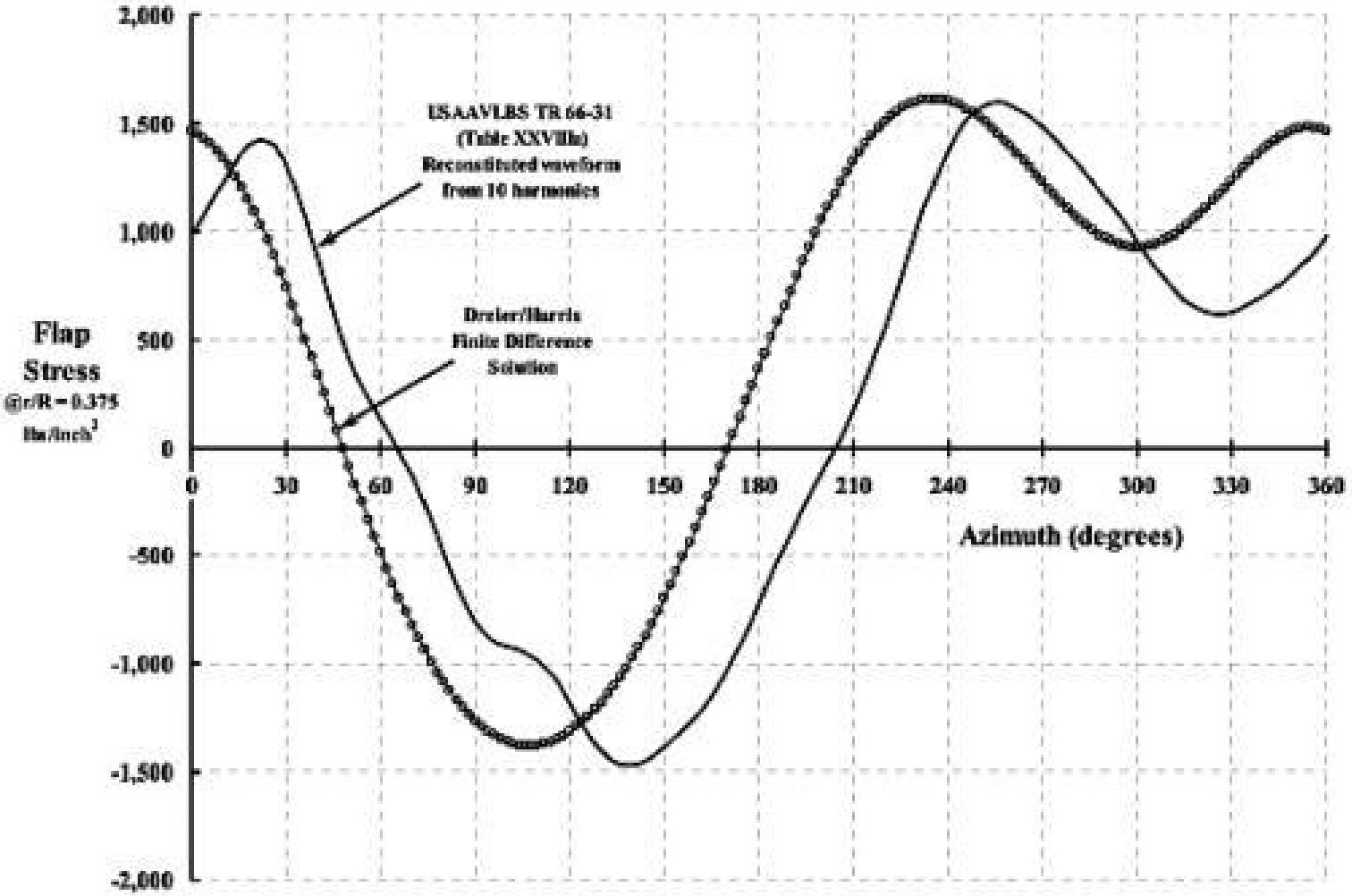

Fig. H-1. Prediction of flapwise stress at x = 0.375 R versus CH-34 test.

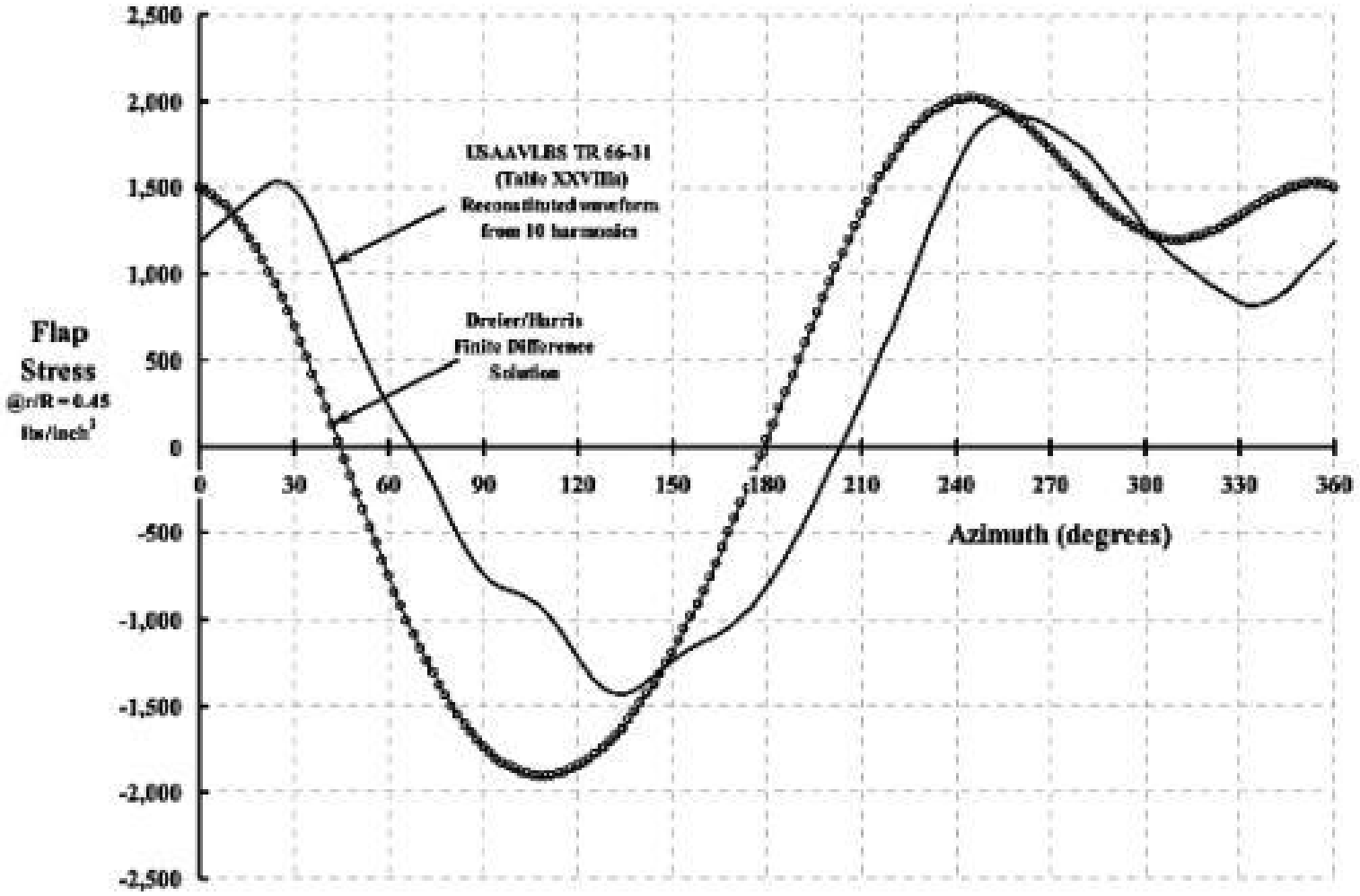

Fig. H-2. Prediction of flapwise stress at x = 0.45 R versus CH-34 test. 422

APPENDIX H

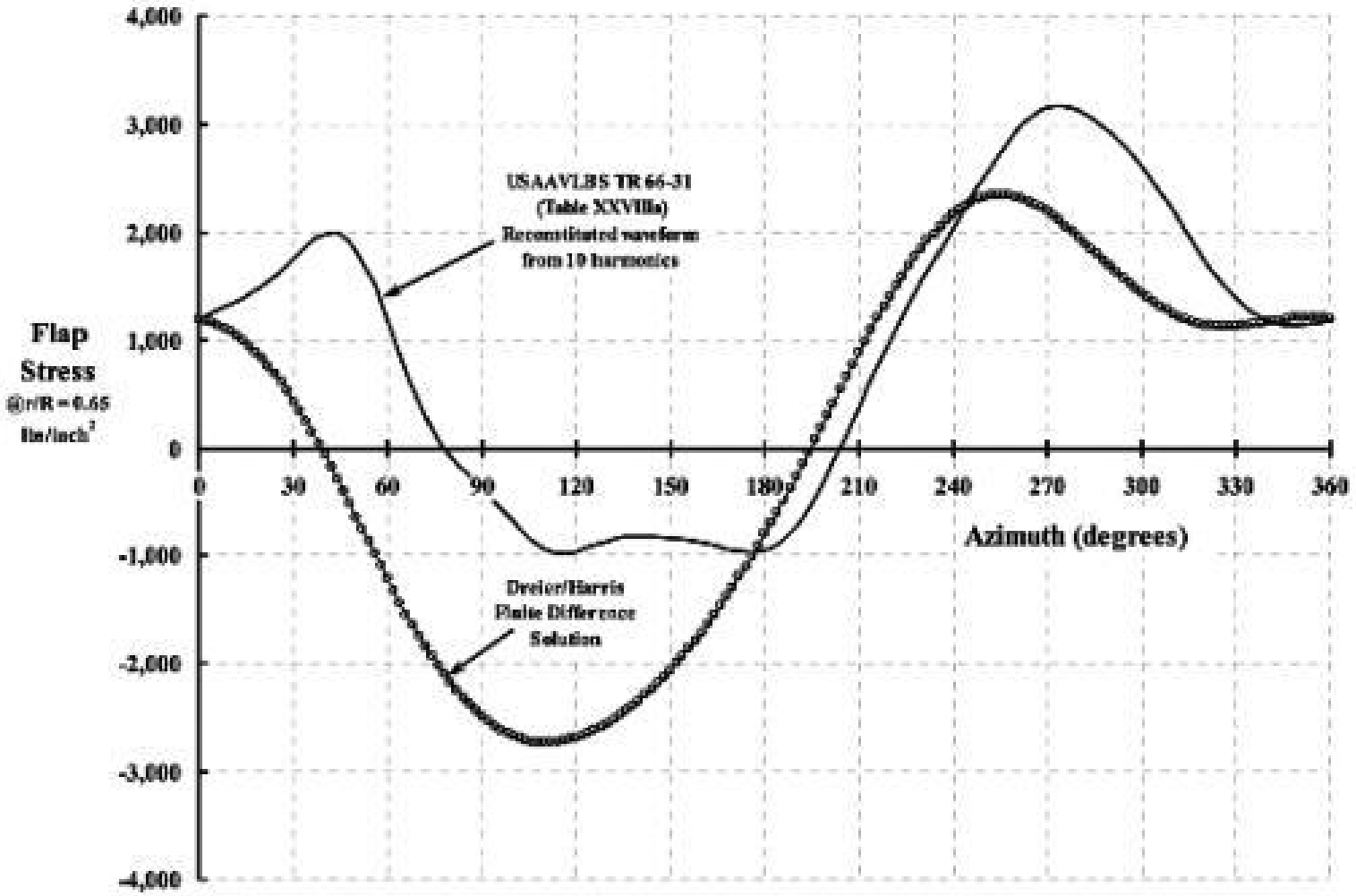

Fig. H-3. Prediction of flapwise stress at x = 0.65 R versus CH-34 test.

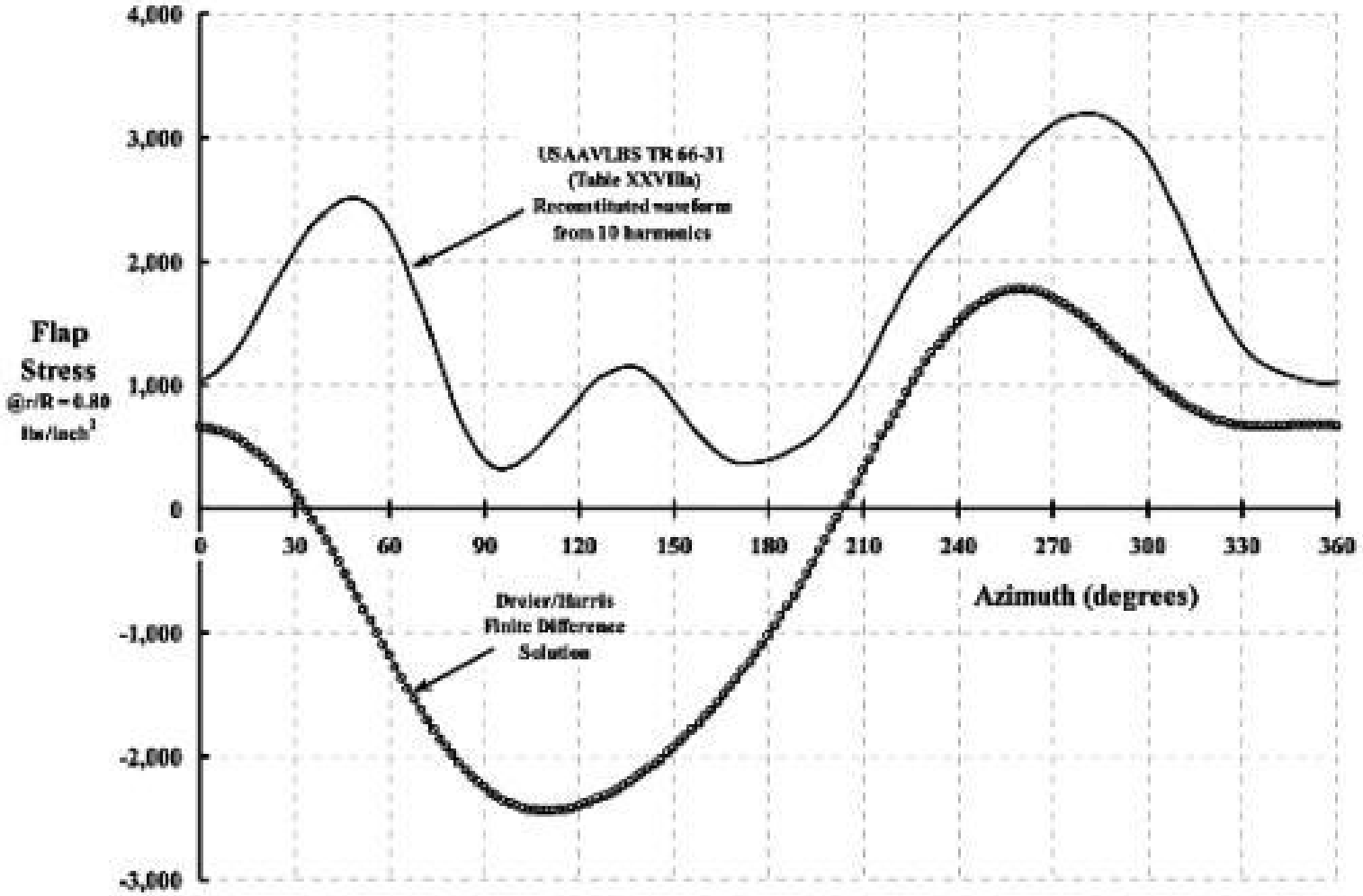

Fig. H-4. Prediction of flapwise stress at x = 0.80 R versus CH-34 test.

APPENDIX H

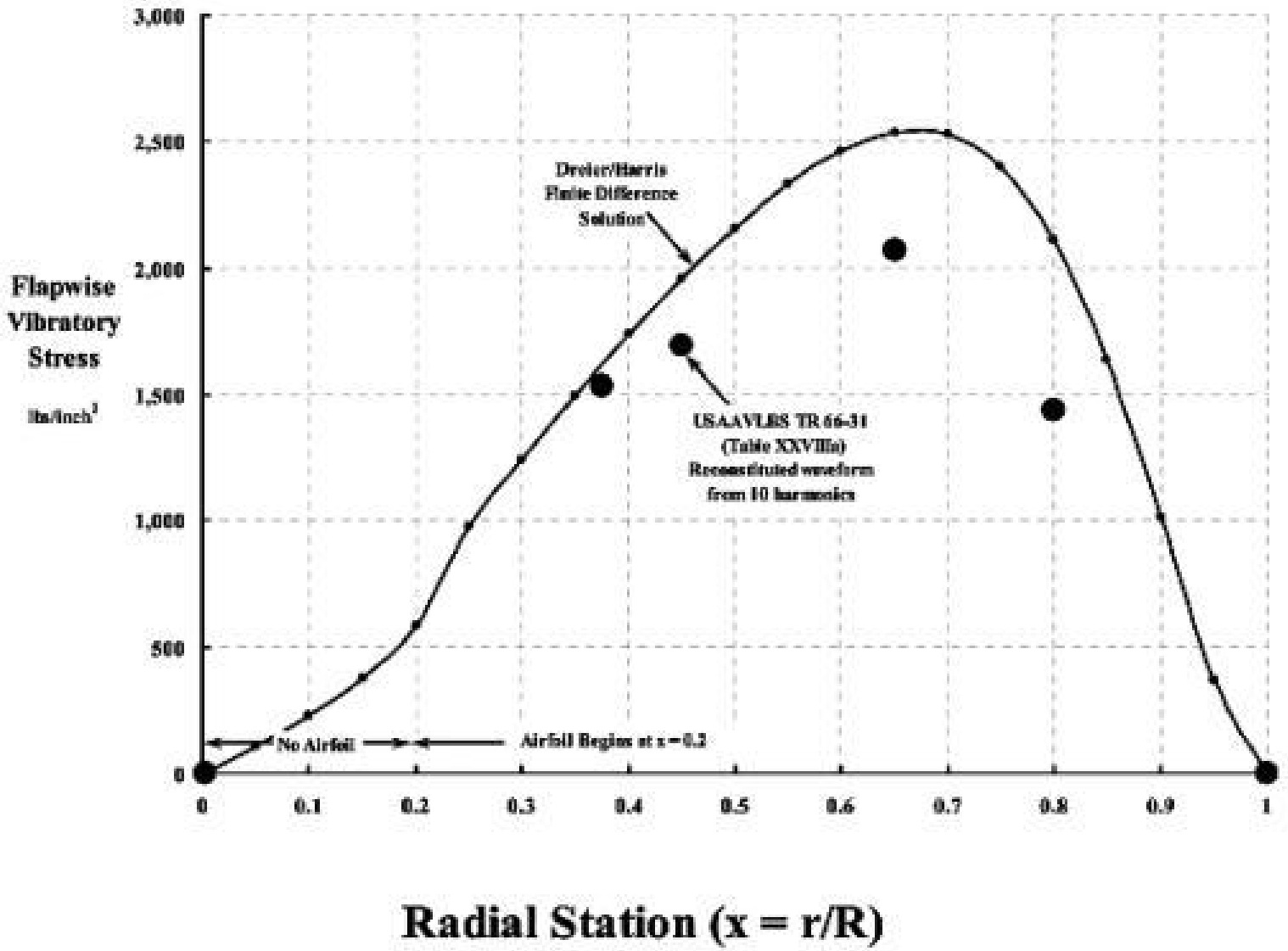

Fig. H-5. Vibratory flapwise stress prediction by finite difference using simple airloads

appears conservative in this comparison (CH-34 at V = 110 kts, α_S = –5 deg, and

T = 8,250 lbs).

Sample Case 2. Finite Difference Analysis Versus Exact Result

The comparison shown in Figs . H- 1 through H-4 points out a significant difference in phase angle as well as waveform shape. The differences are, based on knowledge today, caused by an inaccurate airload. In short, Eq. (7) is quite inadequate . These differences will be discussed further in Volume II, Helicopters.

The question can be asked, of course, if the waveform differences between test and analysis might not be caused by the finite difference solution being inaccurate. Fortunately, there was an exact solution to Eq. (2) available with which to test the accuracy of the finite difference method.[10] This test case was constructed in an inverse manner; in a problem that requires solving for acceleration given mass and force (i.e., a = F/m), it is sometimes more informative to specify the acceleration desired and solve for the force and mass required to produce the desired acceleration.[11]

[10] Franklin D. Harris, *The Rotor Blade Flap Bending Problem—An Analytical Test Case*, J. of the American Helicopter Society, vol. 37, no. 4, pp. 64–67, Oct. 1992.

[11] A.R.S. Bramwell provides a very good example of specifying a helicopter hovering maneuver that is desired and then solving backward for the control motion that the pilot must provide. He is discussing the influence of hinge offset on roll control. See *Helicopter Dynamics*, John Wiley & Sons, New York, 1976, p. 243.

APPENDIX H

The application of this inverse thinking in this appendix goes like this:

From Eqs . (2), (3), and (7), the spring and damper terms in the elemental lift can be moved to the structural side of the equation. This exposes the basic forcing function (F) . The

result of this rearrangement is

(11)

$$F_i^n = \frac{EI}{m\Omega^2 R^4}\frac{\partial^4 z_{(x,\psi)}}{\partial x^4} - \frac{\left(1-x^2\right)}{2}\frac{\partial^2 z_{(x,\psi)}}{\partial x^2} + x\frac{\partial z_{(x,\psi)}}{\partial x} + \frac{\partial^2 z_{(x,\psi)}}{\partial \psi^2}$$

$$+\frac{\gamma}{6}\left\{(x+\mu\sin\psi)\frac{\partial z_{(x,\psi)}}{\partial \psi} + \mu\cos\psi(x+\mu\sin\psi)\frac{\partial z_{(x,\psi)}}{\partial x}\right\}$$

Damping Term

Spring Term

Now constants of $EI/m\Omega^2R^4 = 1/600$, $\gamma = 8$, and $\mu = 2/7$ can be selected and a specified deflection can be defined such as

$$Z := (\cos(0\cdot\psi))\cdot\left(\frac{1}{20}\cdot x - \frac{8}{90}\cdot x^{10} + \frac{16}{110}\cdot x^{11} - \frac{8}{132}\cdot x^{12}\right)$$

$$+\sin(1\cdot\psi)\cdot\left(\frac{1}{16}\cdot x - \frac{4}{60}\cdot x^5 + \frac{8}{90}\cdot x^6 - \frac{4}{126}\cdot x^7\right) + (\cos(1\cdot\psi))\cdot\left(\frac{1}{80}\cdot x + \frac{9}{160}\cdot x^5 - \frac{18}{240}\cdot x^6 + \frac{9}{336}\cdot x^7\right) \ldots$$

$$+\sin(2\cdot\psi)\cdot\left(-\frac{1}{300}\cdot x + \frac{1}{40}\cdot x^5 - \frac{1}{30}\cdot x^6 + \frac{1}{84}\cdot x^7\right) + (\cos(2\cdot\psi))\cdot\left(-\frac{1}{570}\cdot x - \frac{1}{30}\cdot x^7 + \frac{1}{20}\cdot x^8 - \frac{7}{360}\cdot x^9\right) \ldots$$

$$+\sin(3\cdot\psi)\cdot\left(-\frac{1}{1680}\cdot x + \frac{1}{32}\cdot x^8 - \frac{7}{144}\cdot x^9 + \frac{7}{360}\cdot x^{10}\right) + (\cos(3\cdot\psi))\cdot\left(-\frac{1}{6640}\cdot x - \frac{1}{108}\cdot x^{10} + \frac{1}{66}\cdot x^{11} - \frac{5}{792}\cdot x^{12}\right) \ldots$$

$$+\sin(4\cdot\psi)\cdot 0 + (\cos(4\cdot\psi))\cdot\left(\frac{1}{9900}\cdot x - \frac{7}{330}\cdot x^{11} + \frac{7}{198}\cdot x^{12} - \frac{7}{468}\cdot x^{13}\right)$$

Then derivatives can be taken and the force (F) required by Eq. (11) is obtained by careful use of algebra (which I did using MathCad symbolic software) . This is the essence of the AHS Journal paper referenced in footnote 1 0 of this appendix.

The resulting expression from the preceding arithmetic created a forcing function (F) that I used in place of the CH-34 example, Eq. (7), and then the finite difference analysis was rerun. The resulting comparisons to exact values (of the finite difference predictions of root slope, tip slope, tip deflection, and curvature at the 0.65R radial station) are shown in Figs . H-6, H-7, and H-8 . Note that finite difference results are shown as symbols at 2-degree azimuth increments while the exact results are shown as a continuous line. It is more than an aside to say that the blade flapping angle (Fig. H-6), which is generally measured

at the root, *is not representative of actual blade motion outboard of the root* and certainly not representative of tip motion.

These comparative results confirm that the structural response to an airload can be accurately predicted even with a quite simple structural analysis that solves the fourth order, partial differential equation. The problem the pioneers faced was that predicted airloads—available during and well beyond the autogyro era—were totally incorrect. This situation was not—in my opinion—corrected until the 21st century began as you will learn in Volume II, Helicopters.

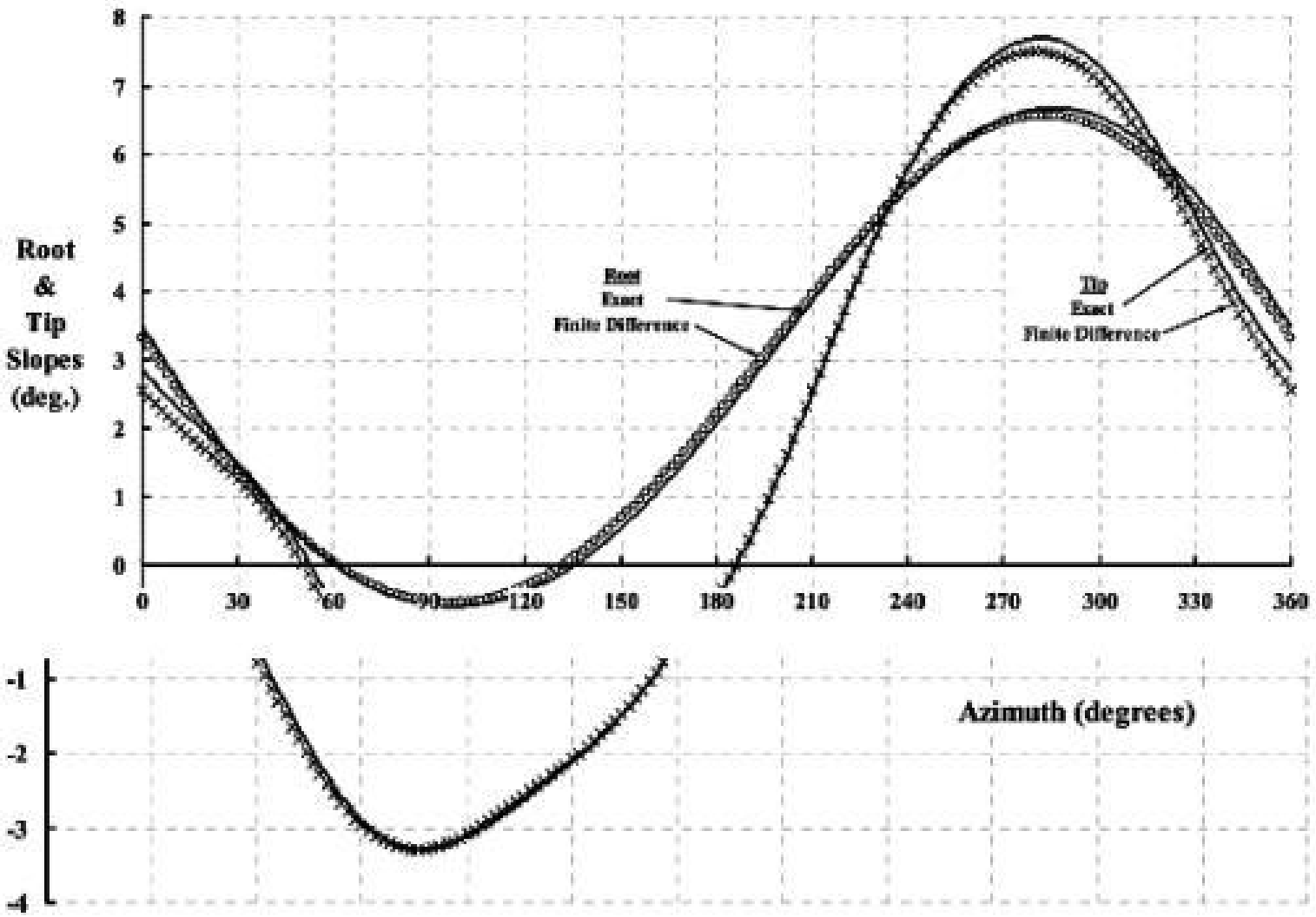

Fig. H-6. Accurate blade slopes can be predicted given accurate airloads.

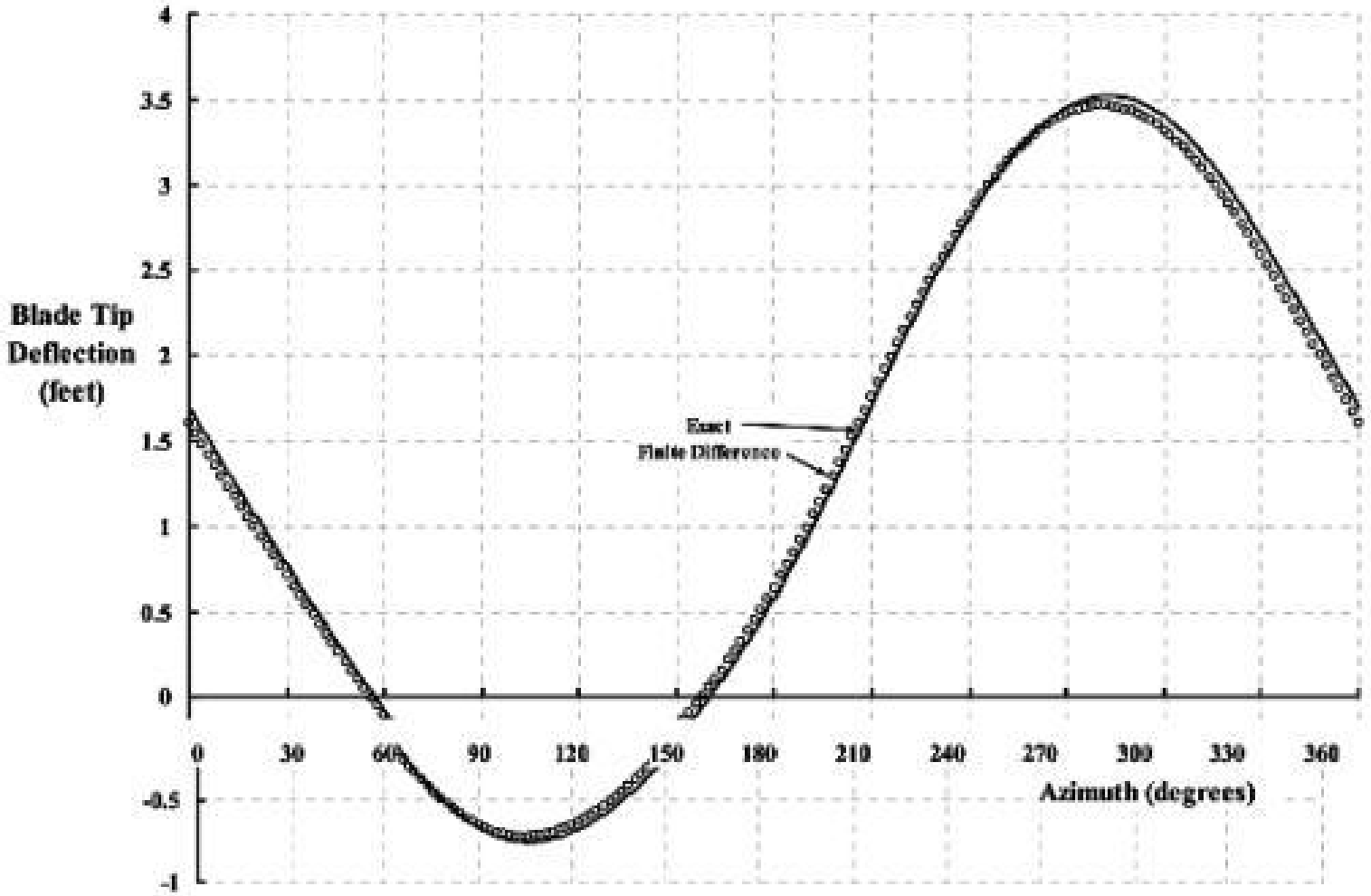

Fig. H-7. Accurate blade-tip deflection can be predicted given accurate airloads.

APPENDIX H

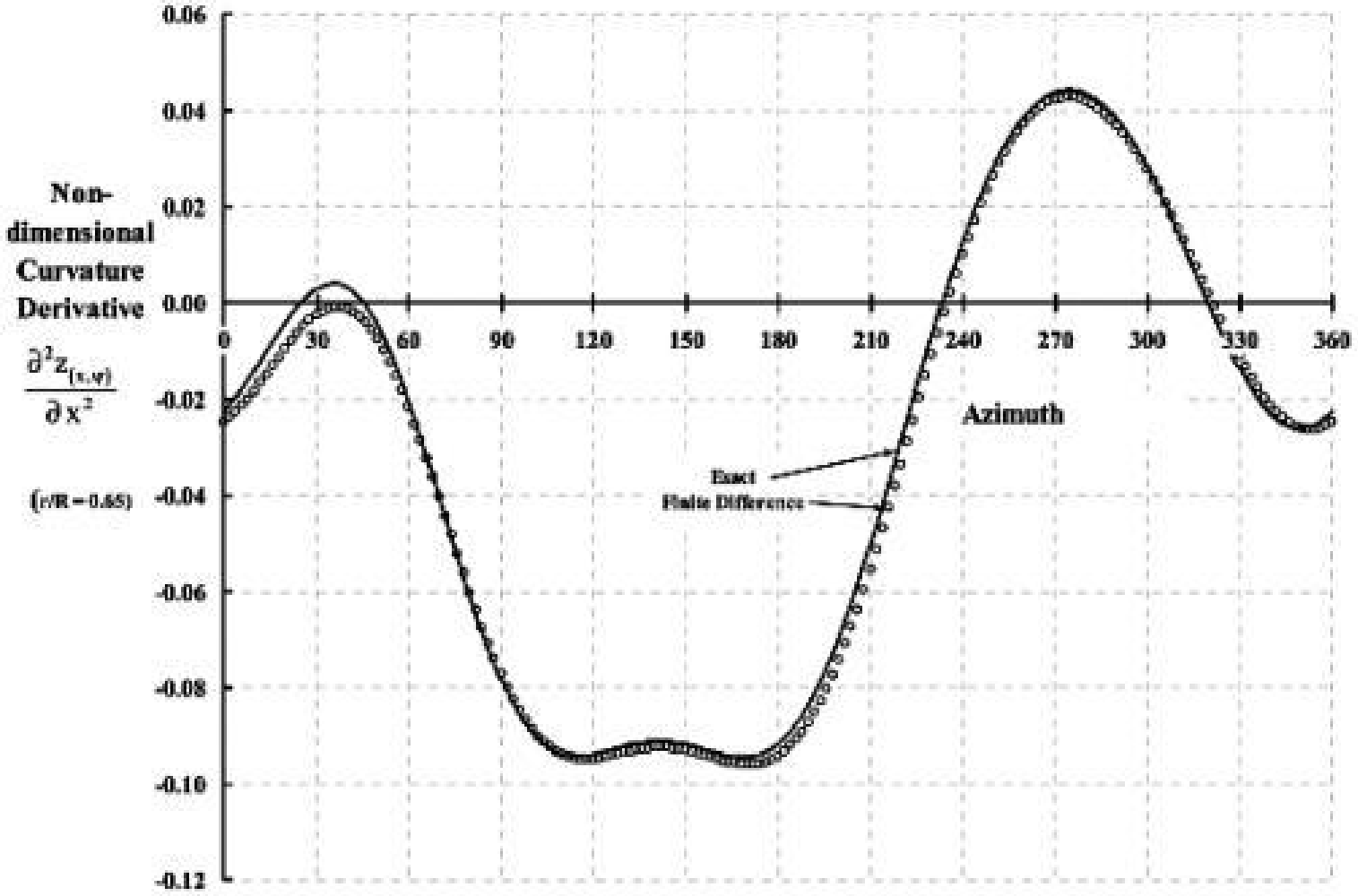

Fig. H-8. Accurate blade loads can be predicted given accurate airloads.

APPENDIX I
INDUCED VELOCITY IN

PARTIAL-POWER DESCENT

During and well beyond the autogyro era, the rotorcraft industry used the Glauert assumption to calculate the uniform induced velocity (v or v_i or $v_{Glauert}$) created by the wake of a lifting rotor. This hypothesis took the form of a quartic equation as shown in Eqs. (2.258) through (2.260), which resulted in

(2.261)

$$\left(\frac{v}{v_h}\right)^4 - \left[2\frac{V_{FP}}{v_h}\sin\alpha_{tpp}\right]\left(\frac{v}{v_h}\right)^3 + \left(\frac{V_{FP}}{v_h}\right)^2\left(\frac{v}{v_h}\right)^2 - 1 = 0 .$$

Figure I-1 repeats the graphical form that results from solving the Glauert equation.

There was little the industry could do to theoretically challenge the Glauert assumption until the digital computer came along. Experimentally, however, Walter Castles and Robin Gray obtained data[1] leading to empirical results for vertical descent. This comparison was shown in Fig. 2-101, which

indicated a significant difference between test results and the Glauert theory.

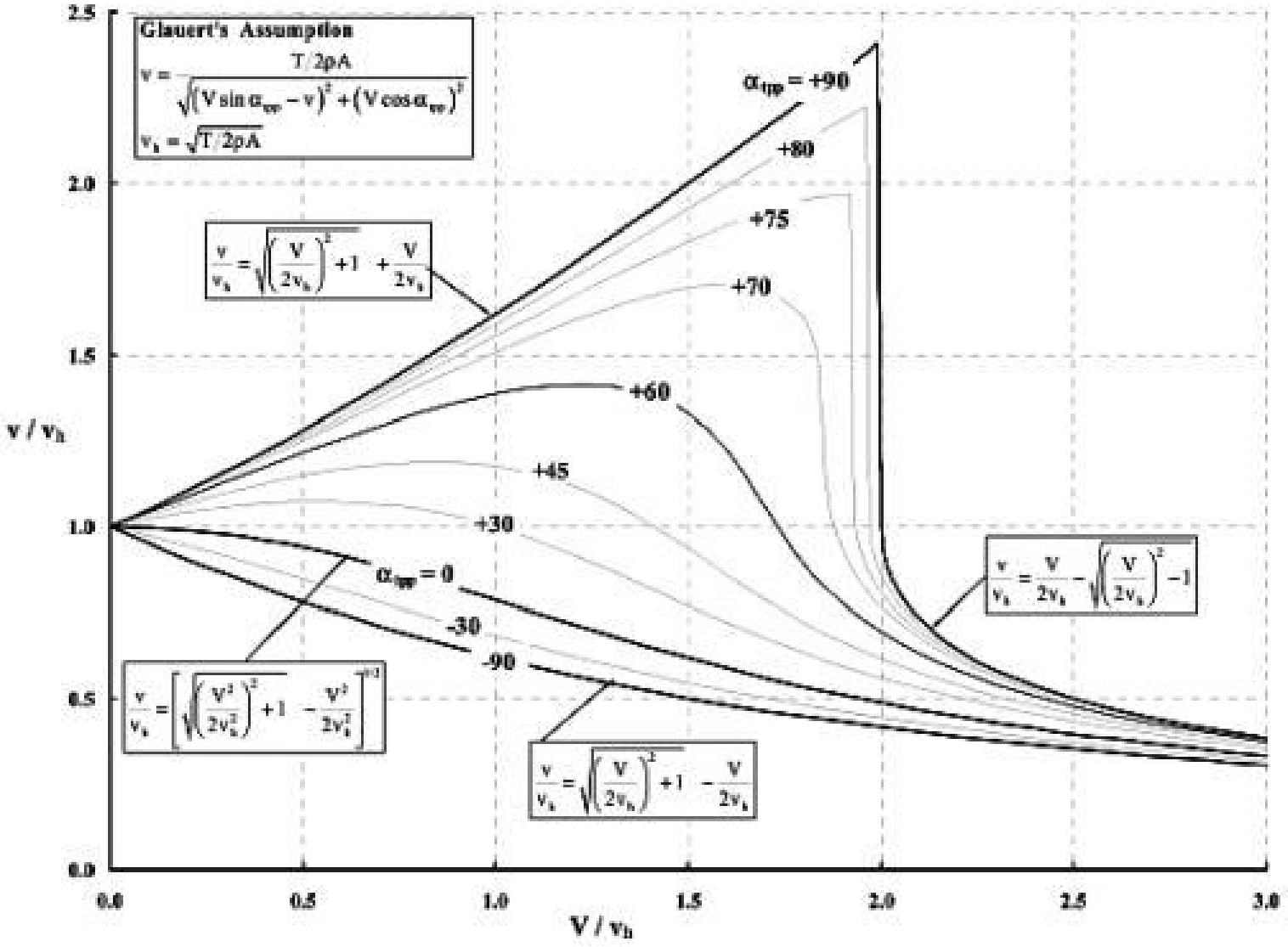

Fig. I-1. The Glauert assumption for rotor-induced velocity.

---

[1] Walter Castles and Robin Gray, *Empirical Relation Between Induced Velocity, Thrust, and Rate of Descent of a Helicopter Rotor as Determined by Wind-Tunnel Tests of Four Model Rotors,*

APPENDIX I

Over the years, two things have bothered me about Fig. I-1. The first bothersome thing is that I never really stopped to solve the quartic equation for the useful root. The second bothersome thing is that no testing comparable to the vertical descent experiment by Castles and Gray has been published for partial-power descents at tip-path plane angles of attack between 0 and 90 degrees.[2] This appendix—to some extent—removes these two bothersome things.

Solution of the Glauert Quartic

The ratio of induced velocity (v) to ideal hover-induced velocity (v_h) depends on the ratio of the flight path velocity (V_{FP}) to ideal hover-induced velocity, and the tip-path

plane angle of attack (α_{tpp} in radians). Suppose, for shorthand purposes, that

$$\bar{v} = \frac{v}{v_h}, \quad \bar{V} = \frac{V_{FP}}{v_h} \quad \text{and} \quad v_h = \sqrt{\frac{T}{2\rho(\pi R^2)}}$$

then Eq. (2.261) becomes $\bar{v}^4 - (2\sin\alpha_{tpp}\bar{V})\bar{v}^3 + (\bar{V}^2)\bar{v}^2 - 1 = 0$, and the applicable root is computed as follows:

$$G = \bar{V}^8\cos^2\alpha_{tpp} - \bar{V}^4 - 18\bar{V}^4\cos^2\alpha_{tpp} + 27\bar{V}^4\cos^4\alpha_{tpp} + 16$$

$$F = \bar{V}^2\left(\frac{\bar{V}^4 - 18 + 54\cos^2\alpha_{tpp}}{1,728}\right)$$

$$H = \frac{\sqrt{3}}{288}\sqrt{|G|}$$

$$A = \sqrt[3]{F + H}$$

$$B = \sqrt[3]{F - H}$$

$$C = \frac{\bar{V}^2 \left(3\cos^2 \alpha_{tpp} - 1\right)}{12}$$

$$D = \sqrt{\left[2\sqrt{(A+B)^2 + C(A+B) + C^2 - 3AB}\right] - (A+B+2C)}$$

$$\bar{v} = D + \frac{\bar{V}}{2}\sin \alpha_{tpp} - \sqrt{(A+B) - C}$$

Note that when the tip-path plane angle of attack equals exactly 90 degrees, the induced velocity ratio is calculated more directly with the equations shown in Fig. I-1 . A straight, vertical line connects the two solution branches at $V_{FP}/v_h = 2.0$.

---

[2] That is not to say an effort has not been made. See for example:

a. Washizu, K. et al., *Experiments on a Model Helicopter Rotor Operating in the Vortex Ring State*, J. of

Aircraft, vol. 3, no. 3, May–June 1966, pp. 225–230.

b. Washizu, K. et al., *Experimental Study on the Unsteady Aerodynamics of a Tandem Rotor Operating in the Vortex Ring State,* Proceedings of the 22nd Annual National Forum, American Helicopter Society, May 1966, pp. 215–220.

c. McLemore, H. C. and Canon, M. D., *Aerodynamic Investigation of a Four-Bladed Propeller Operating Through an Angle-of-Attack Range From 0° to 180°,* NACA TN No. 3228, 1954.

d. Sheridan, P. F. et al., *Math Modeling for Helicopter Simulation of Low Speed, Low Altitude, and Steeply Descending Flight,* NASA CR 166385, July 1982.

APPENDIX I

Application of the Glauert Assumption in Partial-Power-Descent Angles

Castles and Gray reported their experimental results in NACA TN 2474. These

tests dealt solely with vertical descent. The experimental data was provided in both tabulated and graphical forms. One of the rotor sets tested was a 6-foot-diameter rotor with constant chord, untwisted blades . Two graphs for this model are reproduced here as Figs. I-2 and I-3 . From these data, Castles and Gray solved the simple thrust equation

$$(1) \qquad \frac{2C_T}{\sigma a} = \frac{1}{2}\left(\frac{V_{FP}}{V_t} - \frac{v}{V_t}\right) + \frac{1}{3}\theta_{0.75R}$$

backwards for induced velocity (v) using the experimental data for blade loading (C_T/σ), collective pitch at the ¾-radius station ($\theta_{0.75R}$) in radians, vertical descent velocity (V_{FP}) in feet per second, and tip speed (V_t) in feet per second. In solving backwards for the induced velocity, they calculated (for the NACA 0015 airfoil per Table VIII of their report) that the

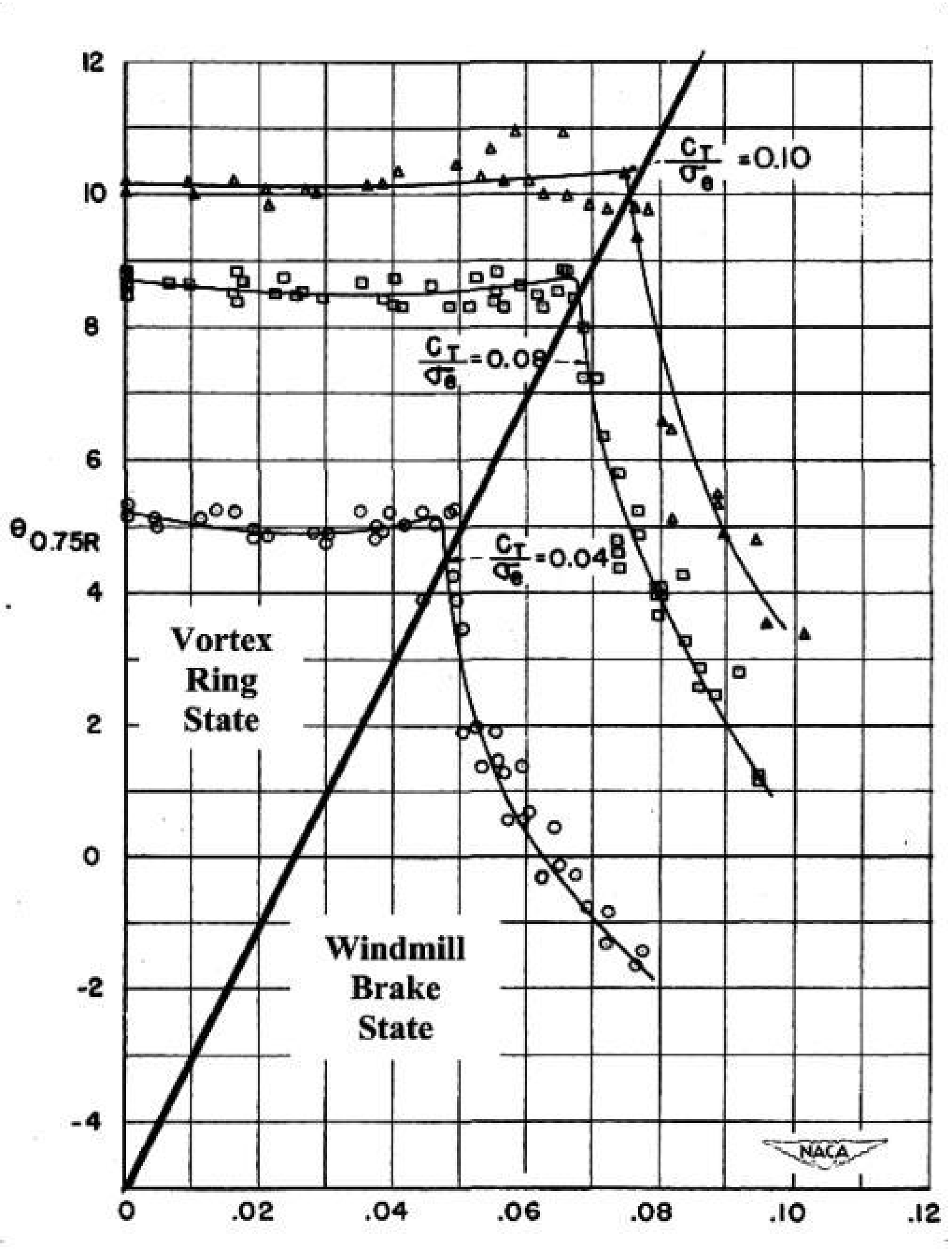
12
10
8
6
4
2
0
-2
-4
θ 0.75R
$\frac{C_T}{\sigma_e}$ =0.10
$\frac{C_T}{\sigma_e}$ =0.08
$\frac{C_T}{\sigma_e}$ =0.04
Vortex Ring State
Windmill Brake State
NACA
0
.02
.04
.06
.08
.10
.12

Figure 4.- Blade angles for 6-foot-diameter rotor with untwisted blades.

constant-chord,

Fig. I-2. Experimental data establishing the vortex ring and windmill brake states for a rotor operating in vertical descent.

APPENDIX I

airfoil lift-curve slope ($dC_l/d\alpha = a$) was a = 5.95 per radian for testing conducted at 1,200 rpm ($RN_{0.75R}$ = 256,000, Vt = 377 ft/sec^2) and a = 6.07 per radian for the rotor speed of 1,600 rpm ($RN_{0.75R}$ = 341,000, Vt = 502 ft/sec^2).[3] Castles and Gray determined that torsional moments would twist the blade so that root collective-pitch measurements would not be representative of blade angle at the ¾-radius station. The correction they applied for the 6-foot-diameter rotor with constant chord, untwisted blades were

$\theta_{0.75R} = 0.820\ (\theta_{root})$ at 1,600 rpm

$\theta_{0.75R} = 0.890\ (\theta_{root})$ at 1,200 rpm.

From the experimental data they obtained and

the engineering calculations (i.e., a and $\theta_{0.75R}$) they made, they obtained comparative results to the assumption made by Glauert. This comparison is shown in Fig. 2-101 of this volume.

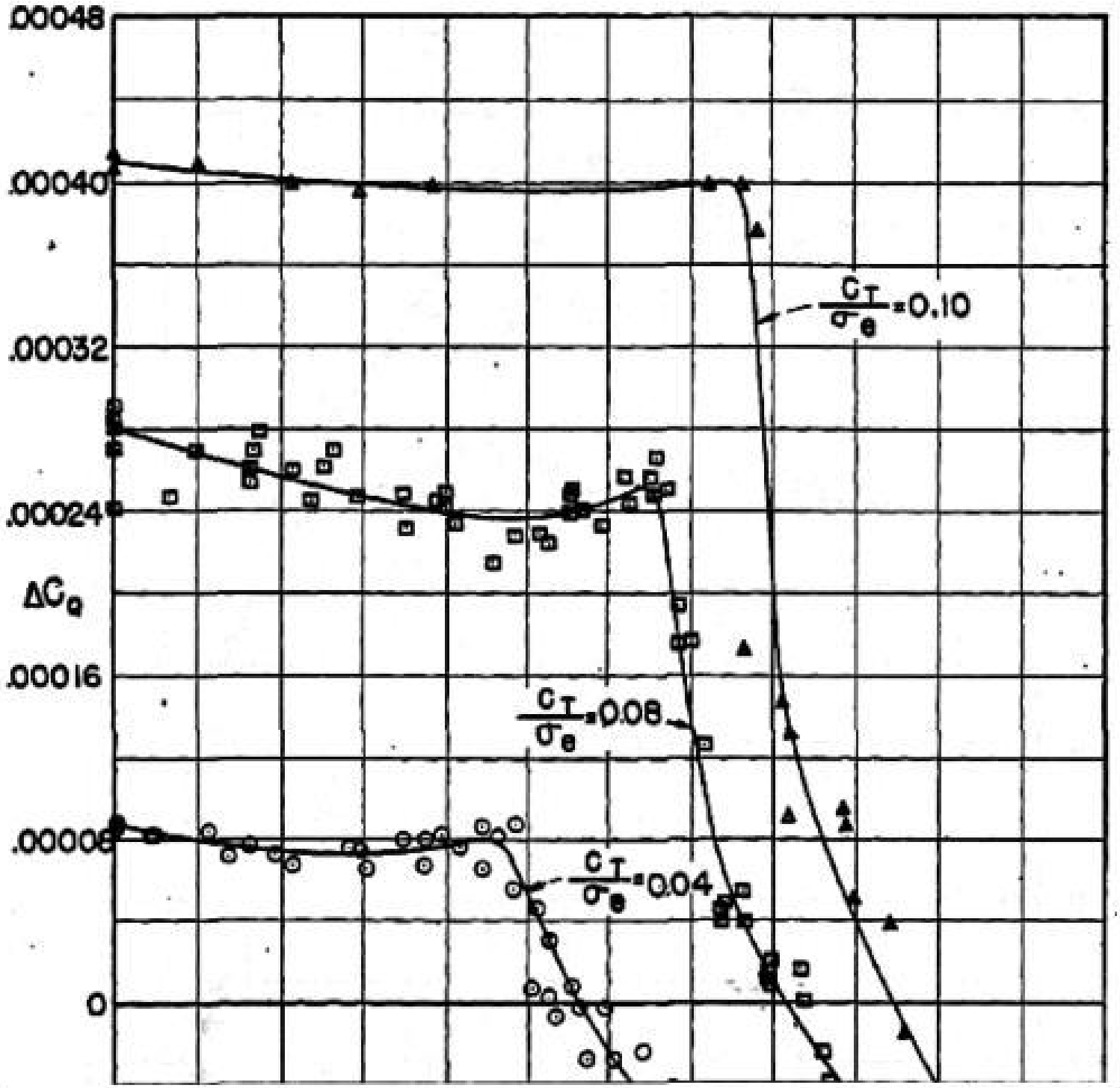

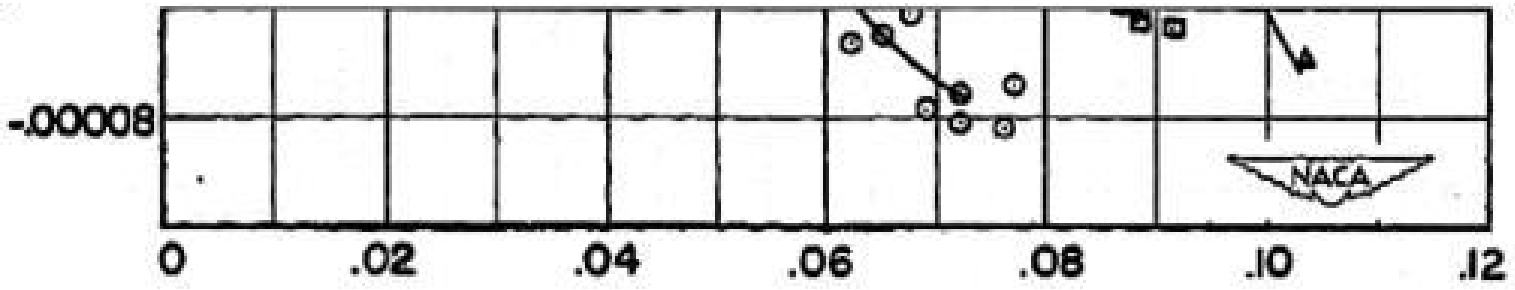

Figure 8.- Variation of torque

V/ΩR

coefficient for 6-foot-diameter rotor

with constant-chord, untwisted blades.

Fig. I-3. Behavior of rotor power in vertical descent.

[3] These lift-curve slopes correspond to the incompressible slope (a = 5.73 per radian) corrected for Mach number at the ¾-radius station using Prandtl–Glauert theory $\left(a = 5.73 / \sqrt{1 - M^2}\right)$.

APPENDIX I

There is a very important observation made by Castles and Gray in the middle of page 10 of their NACA TN 2474 report. They wrote:

At the larger rates of power-on descent the

thrust and torque fluctuated in an irregular manner. An attempt was made in each such case to read the average values.[My italics]

This is the key characteristic of what is known today as the vortex ring state. It is, therefore, to be expected that mean values of thrust and torque may be found that somewhat follow the theory Glauert assumed. However, the magnitude of force and moment fluctuations about the mean values are of much more practical importance to the control and stability of all rotorcraft in partial-power descent.

Given this background, the question I raise is this, "What are the mean and fluctuating values of forces and moments for an isolated rotor at descent angles less than vertical?" Suppose, for example, the Castles and Gray 6-foot-diameter rotor with constant chord, untwisted blades had been tested at other

tip-path plane angles of attack, such as 0, 30, 45, and 60 degrees. In my opinion, a real gap in rotorcraft technology results from a very controlled

experiment that has not been carefully documented in the six decades since Castles and Gray published NACA TN 2474.[4]

This appendix can, however, take a small step towards answering the preceding question. A prediction of mean thrust and torque at several partial-power-descent angles of attack is made using the Glauert theory and following the Castles and Gray test procedure. This prediction, using the Glauert assumption according to Eq. (2.261) with an empirical correction, and the geometry provided in Table I-1, is shown in Figs. I-4 and I-5.

Table I-1. Model Rotor Configuration for Partial-Power-Descent Study

Parameter	Symbol	Value	Unit	Comments
Blade number	b	3	nd	
Radius	R	36.0	inches	
Chord	c	1.884955592	inches	Constant
Solidity	σ	0.05	nd	
Twist	θ_t	0.00	degrees	Untwisted
Root cutout	x_c	0.135	of R	
Flapping hinge offset	e_β	0.0	of R	Blade straight out
Lagging hinge offset	e_ζ	0.0	of R	Blade straight out
Stiffnesses	EI, GJ	Rigid	na	No elastic deflections
Lock number	γ	Infinite	nd	No coning
Aifoil lift-curve slope	a	6.05	per radian	No stall, Mach no. corrected
Airfoil minimum drag coefficient	δ_0	0.013	nd	Author's guess
Airfoil drag rise with $(\alpha_{BE})^2$	δ_2	1.25	per radian^2	No stall
Tip speed		502.6548246	fps	
Density		0.0023769	slug/ft^3	Sea level standard

[4] It can be argued, of course, that so many experimental and production helicopters have flown throughout this region with only minor troubles (other than mapping out the "dead man's" regions and understanding power settling or settling with power) that there is no reason to bother with further study.

APPENDIX I

The predictions assume a propeller-type

model rotor hub with three, very stiff blades. A control system provides collective pitch, as well as lateral and longitudinal cyclic pitch, so that *mean* rotor hub moments can be brought to zero at each test point.

A prediction of collective pitch at the ¾-radius station for a mean $C_T/\sigma = 0.08$ thrust coefficient ($C_T = T/\rho A V_t^2$) is given in Fig. I-4. This prediction was made using Eqs. (2.47) and (2.49) to solve for collective pitch at the ¾-radius station and several flight path velocities (V_{FP}) holding descent angle of attack (α_{hp}) constant. That is, from Eq. (2.49) you have

(2)

$$\frac{2C_T}{\sigma a} = \frac{1}{2}\lambda_{hp} + \frac{1}{3}\left(1 + \frac{3}{2}\mu_{hp}^2\right)\theta_o - \frac{1}{2}\mu_{hp}B_{1C}$$

and, from Eq. (2.47) with zero longitudinal

flapping (a_{1S})—so hub pitching moment is zero— you have

$$(3) \qquad B_{1C} = \frac{2\mu_{hp}\lambda_{hp} + \frac{8}{3}\mu_{hp}\theta_o}{1+\frac{3}{2}\mu_{hp}^2}.$$

Then substituting (B_{1C}) from Eq. (3) into Eq. (2) yields

$$(4) \qquad \theta_{0.75R} = \frac{1}{\left(1-\mu_{hp}^2+\frac{9}{4}\mu_{hp}^4\right)}\left[\frac{6C_T}{\sigma a}\left(1+\frac{3}{2}\mu_{hp}^2\right)-\frac{3}{2}\left(\frac{V_{FP}}{V_t}\sin\alpha_{hp}-\frac{K_i v_{Glauert}}{V_t}\right)\left(1-\frac{1}{2}\mu_{hp}^2\right)\right].$$

Notice in this result that the inflow ratio (λ_{hp}) now contains an empirical factor (K_i) times the Glauert induced velocity. I have used this factor to make the ¾-radius-station collective-pitch angle agree with the Castles and Gray value at hover where $V_{FP}/V_t = 0$. This factor then remains constant for all descent points.

A prediction of the rotor torque (i.e., power) coefficient ($C_Q = Q/\rho A V_t^2 R$) less the profile torque coefficient $\sigma\delta_0\left(1+\mu_{hp}^2\right)/8$ is shown in Fig. I-5. This prediction was made following Eq. (2.48) as

$$\Delta C_Q = C_Q - \frac{\sigma\delta_0}{8}\left(1+\mu_{hp}^2\right)$$

(5)

$$= \sigma\delta_2\left[\left(\frac{1}{2}+\frac{5}{4}\mu_{hp}^2\right)\lambda_{hp}^2+\left(\frac{2}{3}+\frac{8}{3}\mu_{hp}^2\right)\lambda_{hp}\theta_{0.75R}+\left(\frac{1}{4}+\frac{41}{36}\mu_{hp}^2\right)\theta_{0.75R}^2\right],$$

$$-\frac{\sigma a}{4}\left[\lambda_{hp}^2+\frac{2}{3}\theta_o\lambda_{hp}-\frac{1}{2}\mu_{hp}\lambda_{hp}B_{1C}\right]$$

which assumes there can be no rolling moment if lateral flapping (a_{1C}) is zero. Furthermore, if coning (β_o) is zero, no lateral cyclic (A_{1C}) is required according to Eq. (2.46). Both of these assumptions only apply if the induced velocity is uniform over the rotor disc.

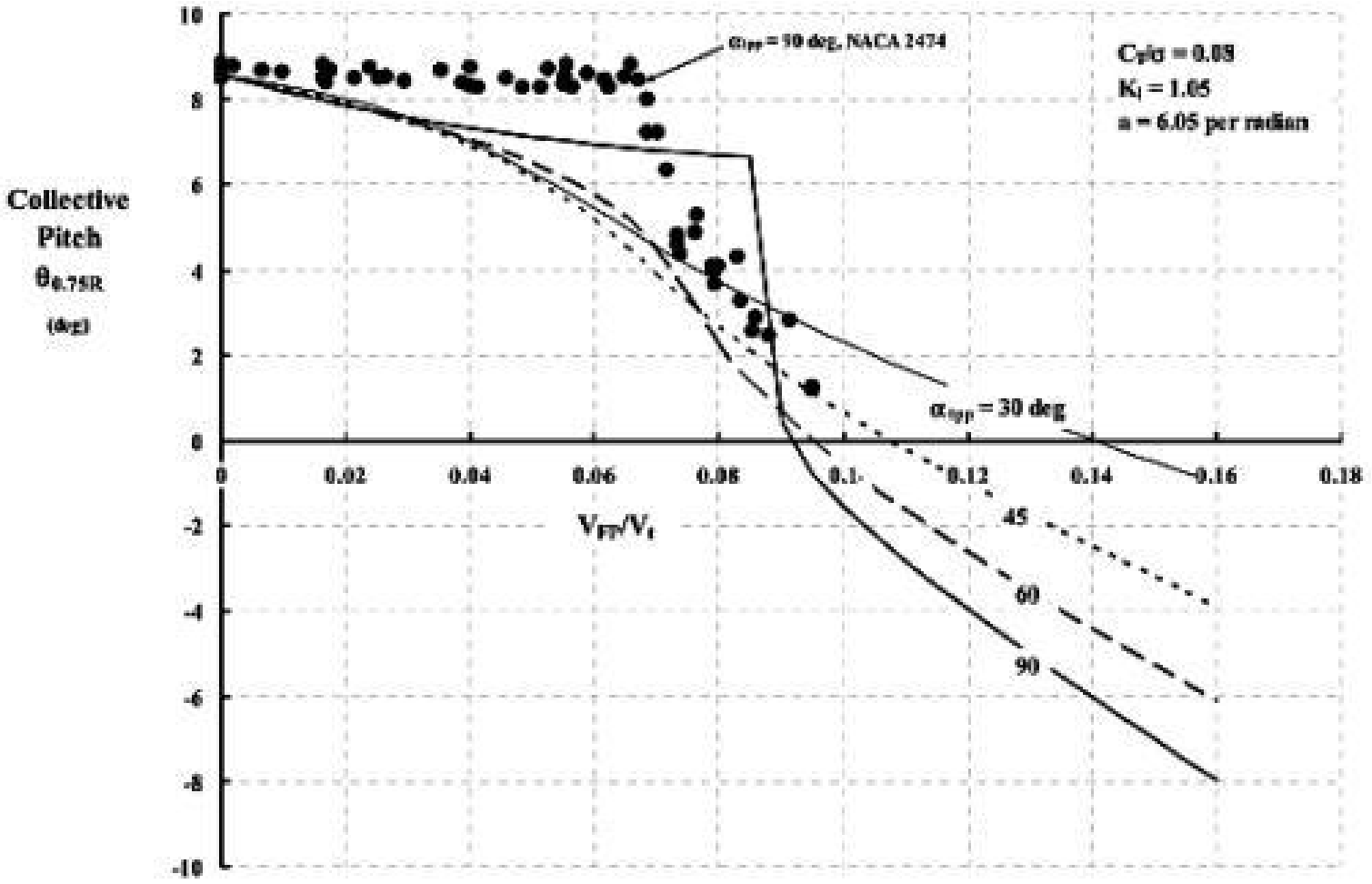

Fig. I-4. Prediction of blade angle to maintain constant thrust for descent angles other than vertical.

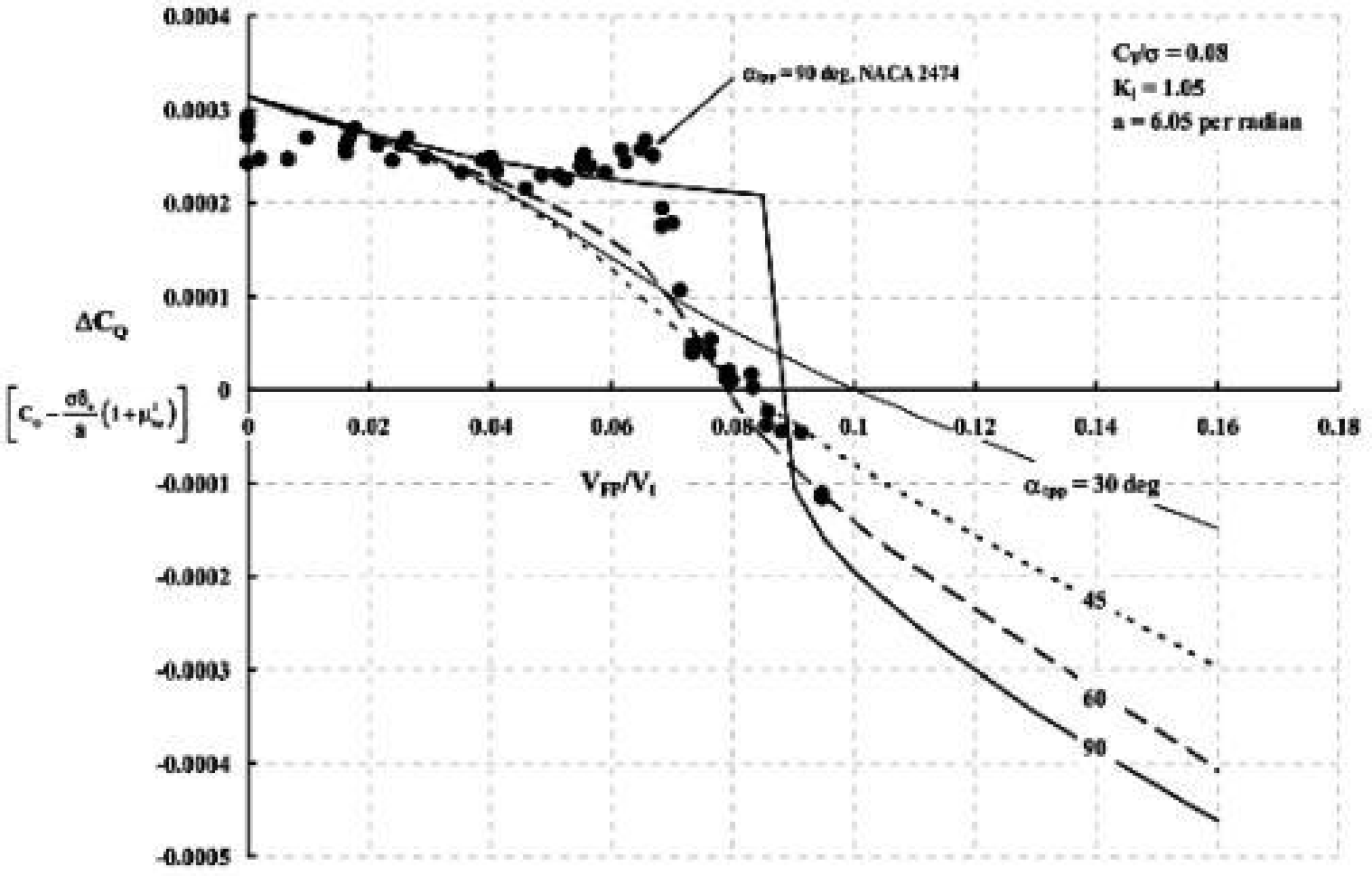

Fig. I-5. Prediction of ΔC_Q to maintain constant thrust for descent angles other than vertical.

APPENDIX I

Closing Remarks

In looking closely at the preceding figures, it is important to note that the vortex ring state extends from near-zero rates of descent up to the point where an abrupt change in the data trends occur. This change varies with the rotor blade loading coefficient (C_T/σ) as Figs. I-2 and I-3 show for vertical descent. What is not so clear is where the vortex ring region is for tip-path-plane angle of attacks less than 90 degrees. Furthermore, it is by no means clear what definition(s) might be used for the vortex ring state.

The one report that provides at least some thrust data (but only in graphical form and with no corresponding power data) at several descent angles came when Paul Yaggy and Ken Mort published *Wind Tunnel Tests of Two VTOL Propellers in Descent* as NASA/TN–D- 1766 in 1963. I suggest that, as a minimum, the advanced theories today be

compared to this 1960s-era data.

Finally, keep in mind that autogyros never flew (or fly today) in the vortex ring region. By definition, the autogyro rotor is always operating at a zero-torque coefficient, which is autorotation. This requires the rotor to operate beyond a V_{FP}/v_h of 2.0 following the Glauert theory. This region is commonly called the windmill brake state. Fig. I-5 shows that— ignoring the minimum torque coefficient—the flight path velocity ratioed to tip speed of at least 0.08 in vertical descent is required to obtain $\Delta C_Q = 0$. Accounting for a minimum torque coefficient for this model rotor of approximately 0.0001 means that autorotative vertical descent would occur at V_{FP}/V_t = 0.09, and V_{FP}/V_t could reach 0.14 for a descent angle of 30 degrees—if the Glauert assumption were correct.

APPENDIX J

MINIMUM PROFILE POWER, H-FORCE, TORQUE, Y-FORCE, AND THRUST

The airfoil at any given blade element of a rotor blade has a minimum drag coefficient (C_{do}) . At the very least, this airfoil drag coefficient must equate to a skin friction drag. However, there is also some form drag (i.e., pressure drag). This blade element drag is classically resolved in a specified direction, summed over the rotor blade span, and then averaged over a blade revolution to give a force at the hub. Based on this integration using a value of C_{do} that is constant over the whole rotor disc, minimum values of profile power coefficient (C_{Po}), H-force coefficient (C_{Ho}), Y-force coefficient (C_{Yo}), torque coefficient

(C_{Qo}), and thrust coefficient (C_{To}) can be defined and calculated. The fundamental relationship that connects four of these coefficients is

(1) $$P_o = \Omega Q_o + (V\cos|\alpha|)H_o + (V\sin|\alpha|)T_o .$$

To avoid any confusion about the sign convention of angle of attack (α) *in this appendix*, I have used the absolute value of angle of attack as you will notice in Eq. (1).

In rotor coefficient notation [i.e., divide Eq. (1) through by $\rho A V_t^3$] you have

(2) $$C_{P_o} = C_{Q_o} + \mu C_{H_o} + \lambda C_{T_o}$$

where advance ratio (μ) is defined as $V\cos|\alpha|/V_t$, and inflow ratio (λ) is taken as $V\sin|\alpha|/V_t$. Airspeed (V) is the reference forward flight speed, and the rotor tip speed is ($V_t = \Omega R$). The angle of attack (α) is

frequently referenced to the rotor shaft, which is perhaps more correctly the angle between the plane perpendicular to the shaft and the airspeed. Thus, when angle of attack is zero, the rotor is in edgewise flight. When $|\alpha| = 90$ degrees, the rotor is in axial flight and is generally called a propeller.

The following paragraphs summarize the classical theory for the five coefficients.

Profile Power

As you know, Cierva and then Glauert (R&M 1111) were the first to state that (in my notation)

$$C_{Po} = \frac{\sigma C_{do}}{8} P_{(\mu,\lambda)}$$

(3) where

$$P_{(\mu,\lambda)} = \frac{1}{2\pi}\int_0^{2\pi}\int_0^1 4\left[(x+\mu\sin\psi)^2+(\mu\cos\psi)^2+\lambda^2\right]^{3/2} dx\, d\psi.$$

$$= \frac{1}{2\pi}\int_0^{2\pi}\int_0^1 4\left[x^2+2x\mu\sin\psi+\mu^2+\lambda^2\right]^{3/2} dx\, d\psi$$

The assumptions associated with this fundamental problem are (1) the blades are constant chord, untwisted, and have no root cutout, and (2) the blade element drag coefficient is constant over the disc.

I found it convenient to let $JJ = \mu^2 + \lambda^2 = (V/V_t)^2$ in all of the equations that follow.

The integration of Eq. (3) falls in the elliptic integral world, but less exact and simpler approximations are available. Using the

software called MathCad, I found that integrating with respect to radius first (which is exact) and then approximating the azimuthal averaging gives

$$P_{(\mu,\lambda)} = \sqrt{1+JJ}\left[1+\frac{5}{2}JJ+\frac{3}{8}\mu^2\frac{4+7JJ+4JJ^2}{(1+JJ)^2}-\frac{9}{16}\frac{\mu^4}{(1+JJ)}\right] + \left(\frac{3}{2}\lambda^4+\frac{3}{2}\lambda^2\mu^2+\frac{9}{16}\mu^4\right)\ln\left(\frac{1+\sqrt{1+JJ}}{\sqrt{JJ}}\right) \quad (4)$$

In the special case where $\lambda = 0$ and $\mu < 0.4$, the proceeding lengthy expression reduces to (5)

$$P_{(\mu<0.4,\lambda=0)} = 1+\frac{9}{2}\mu^2+\frac{3}{16}\mu^4\left[5+3\ln\left(\frac{2}{\mu}\right)\right]+\frac{35}{64}\mu^6 \approx 1+\frac{9}{2}\mu^2$$

which confirms the approximations that both Cierva and Glauert obtained.

When the rotor is in edgewise flight ($\lambda = 0$) at high advance ratios on the order of $\mu > 1.5$ on up to $\mu = \infty$, Eq. (4) has the very useful and

quite adequate approximation that

(6) $$P_{(\mu>1.5,\lambda=0)} = 3\mu + 4\mu^3 .$$

In fact, Eq. (6) is the asymptotic behavior of the profile power function $P_{(\mu,\lambda=0)}$.

The propeller case is defined by $\alpha = -90$ degrees (or + 90 degrees) so $\mu = 0$ and the flow ratio (λ) becomes V/V_t because I have used the absolute value of angle of attack. For the propeller case, Eq. (3) has the exact solution of

(7)

$$P_{(\mu=0,\lambda)} = \left(1+\frac{5}{2}\lambda^2\right)\sqrt{1+\lambda^2} + \frac{3}{2}\lambda^4 \ln\left[\frac{1+\sqrt{1+\lambda^2}}{\lambda}\right].$$

At high propeller advance ratio on the order of $\lambda > 1.5$ up to $\lambda = \infty$, Eq. (7) has the quite adequate approximation for engineering purposes of

$$P_{(\mu=0,\lambda>1.5)} = \frac{3}{10\lambda} + 2\lambda + 4\lambda^3, \quad (8)$$

which has the identical asymptotic behavior of the rotor profile power function. That is, both Eqs. (6) and (8) behave as $4(V/V_t)^3$ in the final limit where tip speed goes to zero.

The reason for this equality is rather easy to understand. In the limit where either rotor advance ratio or propeller inflow ratio is infinite, the shaft rotational speed (Ω) is zero. In either case the profile power is, from Eq. (1), either VH_o or VT_o. In either case the force (i.e., H_o or T_o) is total blade area times drag coefficient times dynamic pressure. The rotor case represents a stopped rotor. The propeller case represents a set of feathered blades.

H–Force

In the general rotor case, there is an H-force acting perpendicular to the shaft and in the downwind direction. This force in rotor notation is

$$C_{Ho} = \frac{\sigma C_{do}}{8} H_{(\mu,\lambda)}$$

(9) where

$$H_{(\mu,\lambda)} = \frac{1}{2\pi}\int_0^{2\pi}\int_0^1 4\left[x^2 + 2x\mu\sin\psi + \mu^2 + \lambda^2\right]\sin(\psi+\Lambda)\,dx\,d\psi$$

$$= \frac{1}{2\pi}\int_0^{2\pi}\int_0^1 4\left[x^2 + 2x\mu\sin\psi + \mu^2 + \lambda^2\right](\sin\psi\cos\Lambda + \cos\psi\sin\Lambda)\,dx\,d\psi$$

Now the sine and cosine of the sweep angle (Λ) are simply

(10) $$\sin\Lambda = \frac{\mu\cos\psi}{\sqrt{x^2 + 2x\mu\sin\psi + \mu^2 + \lambda^2}}$$

$$\cos\Lambda = \frac{x + \mu\sin\psi}{\sqrt{x^2 + 2x\mu\sin\psi + \mu^2 + \lambda^2}}$$

so that

(11)

$$H_{(\mu,\lambda)} = \frac{1}{2\pi}\int_0^{2\pi}\int_0^1 4\left[x^2 + 2x\mu\sin\psi + \mu^2 + \lambda^2\right]^{1/2}\left[x\sin\psi + \mu\right]dx\,d\psi$$

and the approximation to the H-force integral is

(12)

$$H_{(\mu,\lambda)} = \sqrt{1+JJ}\left[3\mu + \frac{1}{4}\mu^3\frac{JJ-1}{(1+JJ)^2}\right] + \left(\mu\lambda^2 + \frac{3}{4}\mu^3\right)\ln\left(\frac{1+\sqrt{1+JJ}}{\sqrt{JJ}}\right).$$

In the special case where $\lambda = 0$ and $\mu < 0.4$, this lengthy expression reduces to (13)

$$H_{(\mu<0.4,\lambda=0)} = 3\mu + \frac{1}{4}\mu^3\left[5 + 3\ln\left(\frac{2}{\mu}\right)\right] + \frac{7}{16}\mu^5.$$

APPENDIX J

Another interesting case occurs when $\lambda = 0$ and μ approaches infinity. In this case, the rotor approaches a stopped rotor in edgewise flight. The H-force in this case is the drag of nonrotating blades, and at high advance ratios on the order of $\mu > 1.5$ on up to $\mu = \infty$, Eq. (12) has the very useful approximation that

(14) $$H_{(\mu>1.5,\lambda=0)} = 1 + 4\mu^2 .$$

In fact Eq. (14) is the asymptotic behavior of the H-force function, $H_{(\mu,\lambda=0)}$.

This minimum H-force component of rotor drag can be expressed in the form of drag (D) divided by dynamic pressure (q). Since

(15) $$D = H_o = \rho\left(\pi R^2\right) V_t^2 \frac{\sigma C_{do}}{8} H_{(\mu>1.5,\lambda=0)}$$

it follows that the equivalent parasite drag (f_e = D/q) is

$$\frac{D}{q}=\frac{H_o}{q}=\frac{\rho(\pi R^2)V_t^2}{\frac{1}{2}\rho V^2}\left(\frac{bcR}{\pi R^2}\right)\frac{C_{do}}{8}H_{(\mu>1.5,\lambda=0)}$$

(16)

$$=(bcR)C_{do}\frac{H_{(\mu>1.5,\lambda=0)}}{4\mu^2}=(bcR)C_{do}\left(1+\frac{1}{4\mu^2}\right)$$

Keep in mind that some sort of propulsive device must be used to drag the edgewise rotor through the air. This 100-percent-efficient device requires power equal to VD. In the special case where $\mu = 0$, which is the propeller case, the exact solution of Eq. (11) is (17) $H_{(\mu=0,\lambda)} \equiv 0$.

Y–Force

In the general rotor case, there is a Y-force acting perpendicular to the shaft and perpendicular to the free-stream velocity. This Y-force is positive towards the right wing tip when the rotor rotation is counterclockwise as viewed from above. This force in rotor notation is

$$C_{Yo}=\frac{\sigma C_{do}}{8}Y_{(\mu,\lambda)}$$

(18) where

$$Y_{(\mu,\lambda)} = \frac{1}{2\pi}\int_0^{2\pi}\int_0^1 4\left[x^2 + 2x\mu\sin\psi + \mu^2 + \lambda^2\right]\cos(\psi + \Lambda)\,dx\,d\psi$$

$$= \frac{1}{2\pi}\int_0^{2\pi}\int_0^1 4\left[x^2 + 2x\mu\sin\psi + \mu^2 + \lambda^2\right][\cos\psi\cos\Lambda - \sin\psi\sin\Lambda]\,dx\,d\psi$$

Substituting the sine and cosine of the sweep angle (Λ) relationships from Eq. (10) yields

(19)

$$Y_{(\mu,\lambda)} = \frac{1}{2\pi}\int_0^{2\pi}\int_0^1 4\left[x^2 + 2x\mu\sin\psi + \mu^2 + \lambda^2\right]^{1/2}[x\cos\psi]\,dx\,d\psi$$

from which it follows that for all advance ratios and all inflow ratios, (20) $Y_{(\mu,\lambda)} \equiv 0$.

Torque

In the general rotor case, a torque must

be applied to the shaft to maintain rotor speed. This torque might be obtained from an engine if the rotor is not in autorotation (or the propeller is not windmilling). The required torque in rotor notation is

$$C_{Qo} = \frac{\sigma C_{do}}{8} Q_{(\mu,\lambda)} \tag{21}$$

$$\text{where } Q_{(\mu,\lambda)} = \frac{1}{2\pi}\int_0^{2\pi}\int_0^1 4\left[x^2 + 2x\mu\sin\psi + \mu^2 + \lambda^2\right]^{1/2}(x + \mu\sin\psi)\,x\,dx\,d\psi$$

and the approximation to this torque integral is

(22)

$$Q_{(\mu,\lambda)} = \sqrt{1+JJ}\left[1 + \frac{1}{2}JJ + \frac{1}{8}\mu^2\frac{4 + JJ - 4JJ^2}{(1+JJ)^2} + \frac{3}{16}\frac{\mu^4}{(1+JJ)}\right] - \left(\frac{1}{2}\lambda^4 + \frac{1}{2}\lambda^2\mu^2 + \frac{3}{16}\mu^4\right)\ln\left(\frac{1+\sqrt{1+JJ}}{\sqrt{JJ}}\right)$$

In the special case where $\lambda = 0$ and $\mu < 0.4$, this lengthy expression reduces to (23)

$$Q_{(\mu<0.4,\lambda=0)} = 1+\frac{3}{2}\mu^2-\frac{1}{16}\mu^4\left[5+3\ln\left(\frac{2}{\mu}\right)\right]+\frac{7}{64}\mu^6.$$

In the special helicopter rotor case where $\lambda = 0$ and advance ratio approaches infinity (24)

$Q_{(\mu>1.5,\lambda=0)} \rightarrow 2\mu$.

Note that C_{Qo} goes to infinity as advance ratio approaches infinity, but, in fact, the actual torque goes to zero for the stopped rotor or propeller. You can see this by writing (25)

$$Q_o = \rho\left(\pi R^2\right)V_t^2 R\left(\frac{\sigma C_{do}}{8}\right)Q_{(\mu>1.5,\lambda=0)} = \rho\left(bcR\right)RC_{do}\left(\frac{VV_t}{4}\right).$$

This last result applies equally well to a feathered propeller because, as the tip speed goes to zero, the torque goes to zero.

In the special case where $\mu = 0$, which is the propeller, the *exact solution* to Eq. (21) is

APPENDIX J

(26)

$$Q_{(\mu=0,\lambda)} = \frac{1}{2}\left(2+\lambda^2\right)\sqrt{1+\lambda^2} - \frac{1}{2}\lambda^4 \ln\left(\frac{1+\sqrt{1+\lambda^2}}{\lambda}\right).$$

At high propeller advance ratio on the order of $\lambda > 1.5$ on up to $\lambda = \infty$, Eq. (26) has the very useful and quite adequate approximation of

(27) $$Q_{(\mu=0,\lambda>1.5)} = \frac{2}{5\lambda} + \frac{4}{3}\lambda.$$

Thrust

In the general rotor case, when there is an inflow (i.e., λ is not zero), there is a component of minimum blade element drag in the shaft axial direction. This force is a

negative thrust (a drag if you prefer) and is given by

(28) $$C_{To} = \frac{\sigma C_{do}}{8} T_{(\mu,\lambda)} \quad \text{where}$$

$$T_{(\mu,\lambda)} = \frac{\lambda}{2\pi} \int_0^{2\pi} \int_0^1 4\left[x^2 + 2x\mu \sin\psi + \mu^2 + \lambda^2 \right]^{1/2} dx\, d\psi$$

and the approximation to the thrust integral is

(29)

$$T_{(\mu,\lambda)} = \lambda\sqrt{1+JJ}\left[2 + \frac{1}{2}\mu^2 \frac{1+2JJ}{(1+JJ)^2} \right] + \lambda\left(2\lambda^2 + \mu^2\right) \ln\left(\frac{1+\sqrt{1+JJ}}{\sqrt{JJ}} \right).$$

Obviously, if inflow is zero then C_{To} is zero. But, in the special case when $\mu = 0$, which corresponds to a propeller, then the *exact solution* to Eq. (28) is

(30)

$$T_{(\mu=0,\lambda)} = 2\lambda\sqrt{1+\lambda^2} + 2\lambda^3 \ln\left(\frac{1+\sqrt{1+\lambda^2}}{\lambda}\right).$$

At high propeller advance ratio on the order of $\lambda > 1.5$ up to $\lambda = \infty$, Eq. (7) has the approximation that

(31) $$T_{(\mu=0,\lambda>1.5)} = \frac{2}{3} - \frac{1}{10\lambda^2} + 4\lambda^2$$

It is of interest to see how the drag of the feathered propeller is approached as the shaft rotational speed approaches zero. In this progression towards the limit, the equivalent parasite drag (f_e) form is

(32)

$$\frac{D}{q} = \frac{T_o}{q} = \frac{\rho(\pi R^2)V_t^2}{\frac{1}{2}\rho V^2}\left(\frac{bcR}{\pi R^2}\right)\frac{C_{do}}{8}T_{(\mu=0,\lambda\to\infty)} = (bcR)C_{do}\left(1+\frac{1}{6\lambda^2}-\frac{1}{40\lambda^4}\right).$$

Equivalent Drag in Edgewise Flight

It can be very helpful to express the minimum profile power from Eq. (3) as an equivalent parasite drag area (i.e., D/q) parameter. That is

$$\frac{D/q}{(bcR)C_{do}} = \frac{P_0/qV}{(bcR)C_{do}} = \frac{1}{4\mu^3} P_{(\mu,\lambda=0)} . \tag{33}$$

This form shows that in the limit of infinite advance ratio when the rotor is stopped, the minimum drag area parameter is

$$\frac{D/q}{(bcR)C_{do}} = 1 . \tag{34}$$

The variation of this equivalent drag area parameter with advance ratio is illustrated with Fig. J-1 and, in an enlarged view, with Fig. J-2.

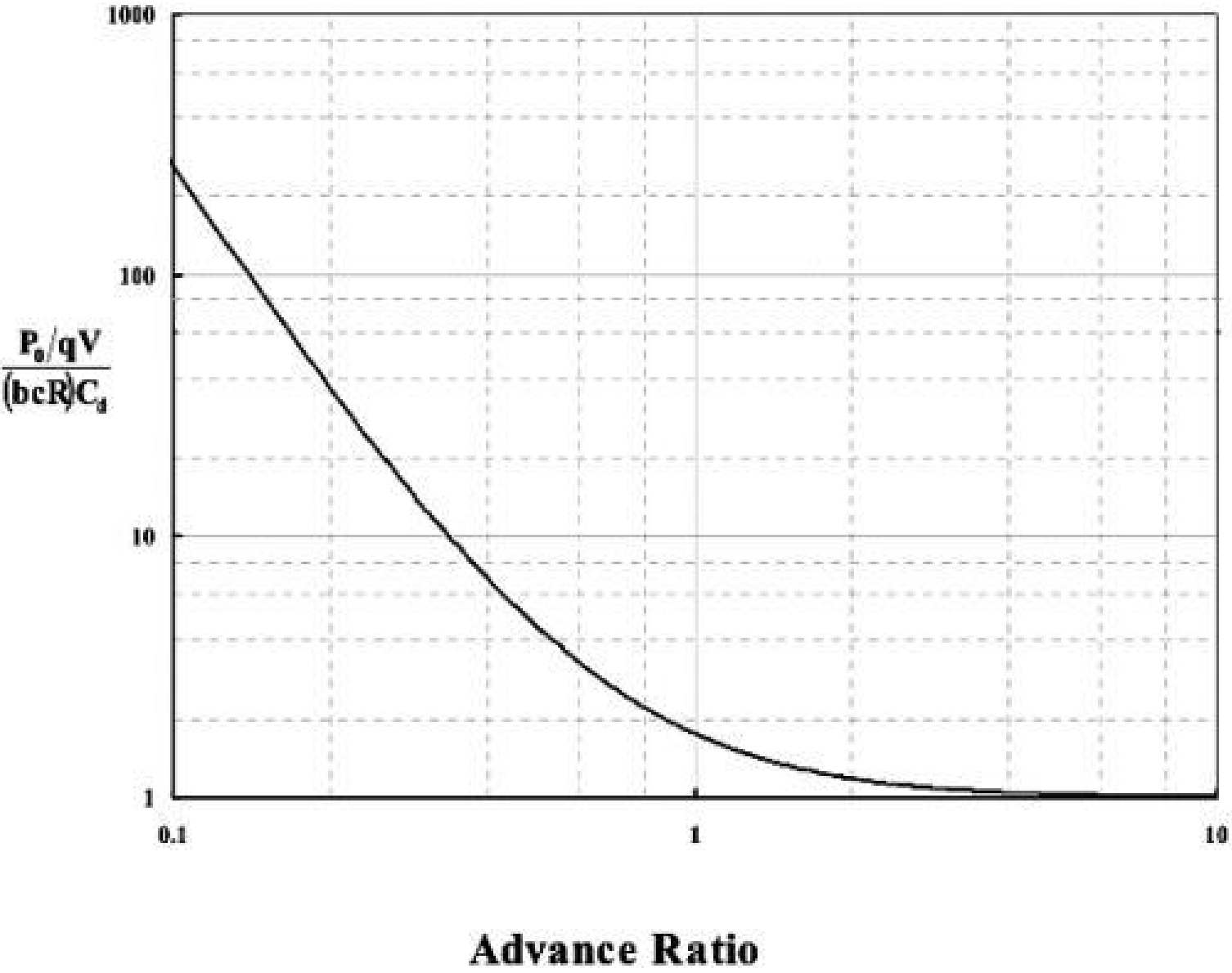

Fig. J-1. Equivalent drag decreases with advance ratio. The limit is the drag of stopped blades.

APPENDIX J

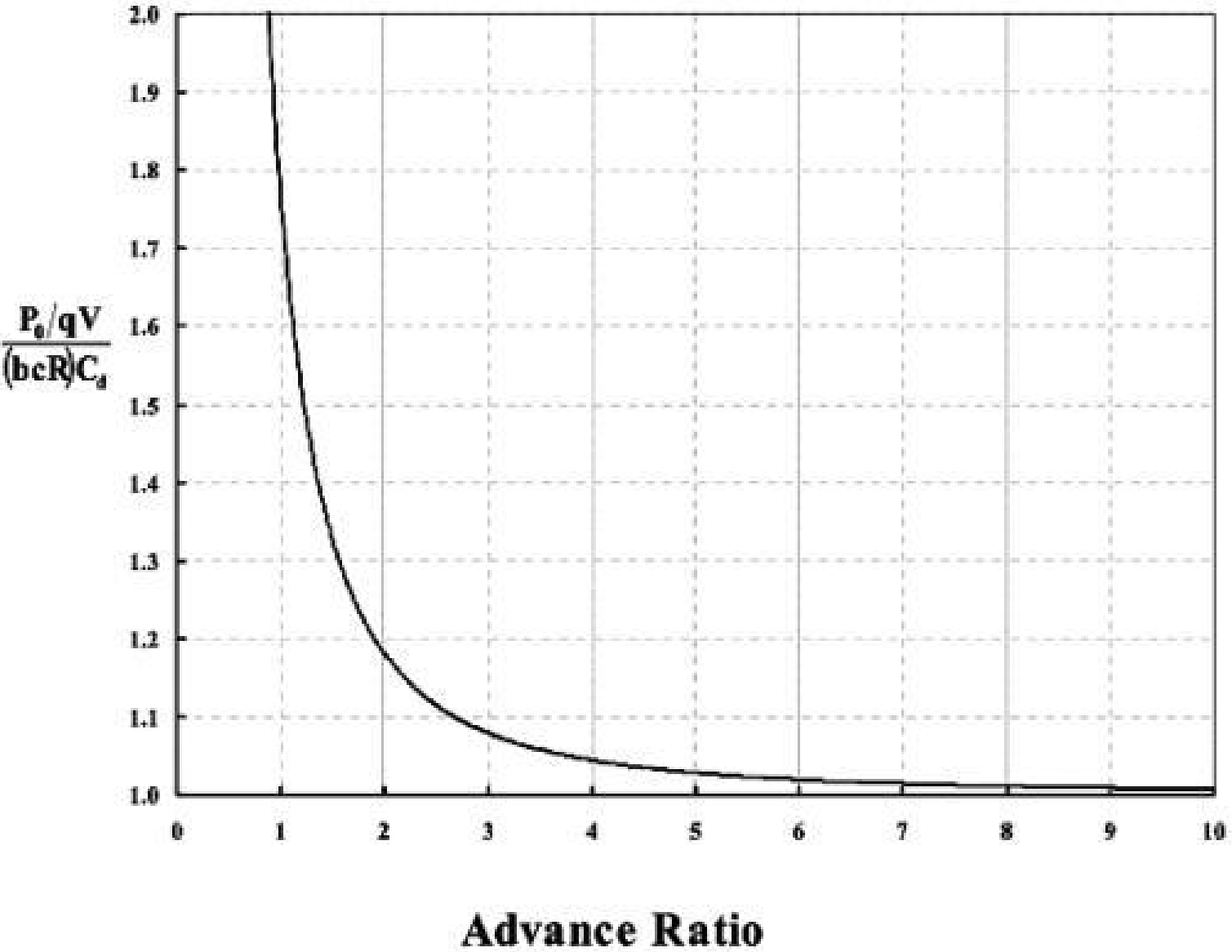

Fig. J-2. There is relatively clear indication of diminishing return to high advance ratio.

A Proof

The preceding results are connected by the fundamental, total energy per unit time equation, which is

(35) $$P_o = \Omega Q_o + (V\cos|\alpha|)H_o + (V\sin|\alpha|)T_o,$$

and in rotor coefficient notation (i.e., after dividing through by $\rho A V_t^3$) you have (36) $$C_{P_o} = C_{Q_o} + \mu C_{H_o} + \lambda C_{T_o}.$$

A simple "proof" of the above relationship can be seen by using the approximation equations for the edgewise flying rotor, Eqs. (23) and (13), which are the series expansions from the preceding paragraphs. Thus, when $\lambda = 0$ and $\mu < 0.4$,

$$C_{P_o} = C_{Q_o} + \mu C_{H_o} = \frac{\sigma C_{do}}{8} Q_{(\mu,\lambda=0)} + \frac{\sigma C_{do}}{8} \mu H_{(\mu,\lambda=0)}$$

(37)

$$= \frac{\sigma C_{do}}{8}\left\{1+\frac{3}{2}\mu^2 - \frac{1}{16}\mu^4\left[5+3\ln\left(\frac{2}{\mu}\right)\right]+\frac{7}{64}\mu^6\right\} + \frac{\sigma C_{do}}{8}\left\{\mu\left[3\mu+\frac{1}{4}\mu^3\left[5+3\ln\left(\frac{2}{\mu}\right)\right]+\frac{7}{16}\mu^5\right]\right\},$$

$$= \frac{\sigma C_{do}}{8}\left\{1+\left(\frac{3}{2}+3\right)\mu^2+\left(-\frac{1}{16}+\frac{1}{4}\right)\mu^4\left[5+3\ln\left(\frac{2}{\mu}\right)\right]+\left(\frac{7}{64}+\frac{7}{16}\right)\mu^6\right\}$$

$$= \frac{\sigma C_{do}}{8}\left\{1+\frac{9}{2}\mu^2+\frac{3}{16}\mu^4\left[5+3\ln\left(\frac{2}{\mu}\right)\right]+\frac{35}{64}\mu^6\right\}$$

and you can see by inspection that Eq. (5) has been reproduced.

Azimuth Integrals

For the sake of completeness, the azimuthal averaging approximations I used were

(38)

$$I0 = \frac{1}{2\pi}\int_0^{2\pi} \sqrt{1+2\mu\sin\psi+JJ}\; d\psi \approx \sqrt{1+JJ} - \frac{1}{2}\mu^2\left[\frac{1}{2(1+JJ)^{3/2}}\right]$$

(39) $$I1 = \frac{1}{2\pi}\int_0^{2\pi} \sin\psi\sqrt{1+2\mu\sin\psi+JJ}$$

$$d\psi \approx \frac{1}{2}\mu\left[\frac{1}{\sqrt{1+JJ}}\right]$$

(40)

$$I2 = \frac{1}{2\pi}\int_0^{2\pi} (\sin\psi)^2 \sqrt{1+2\mu\sin\psi+JJ}\; d\psi \approx \frac{1}{2}\sqrt{1+JJ}$$

(41)

$$I3 = \frac{1}{2\pi}\int_0^{2\pi} (\sin\psi)^3 \sqrt{1+2\mu\sin\psi+JJ}\; d\psi \approx \frac{3}{8}\mu\left[\frac{1}{\sqrt{1+JJ}}\right]$$

(42)

$$I4 = \frac{1}{2\pi}\int_0^{2\pi} (\sin\psi)^4 \sqrt{1+2\mu\sin\psi+JJ}\; d\psi \approx \frac{3}{8}\sqrt{1+JJ}$$

(43)

$$L0 = \frac{1}{2\pi}\int_0^{2\pi} \ln\left(\frac{\sqrt{1+2\mu\sin\psi+JJ}+1+\mu\sin\psi}{\sqrt{JJ}+\mu\sin\psi}\right) d\psi \approx \ln\left(\frac{\sqrt{1+JJ}+1}{\sqrt{JJ}}\right)$$

(44)

$$L2 = \frac{1}{2\pi}\int_0^{2\pi} (\sin\psi)^2 \ln\left(\frac{\sqrt{1+2\mu\sin\psi+JJ}+1+\mu\sin\psi}{\sqrt{JJ}+\mu\sin\psi}\right) d\psi \approx \frac{1}{2}\ln\left(\frac{\sqrt{1+JJ}+1}{\sqrt{JJ}}\right)$$

(45)

$$L4 = \frac{1}{2\pi}\int_0^{2\pi} (\sin\psi)^4 \ln\left(\frac{\sqrt{1+2\mu\sin\psi+JJ}+1+\mu\sin\psi}{\sqrt{JJ}+\mu\sin\psi}\right) d\psi \approx \frac{3}{8}\ln\left(\frac{\sqrt{1+JJ}+1}{\sqrt{JJ}}\right)$$

The use of these approximations leads to numerical results that are, at most, 1.1 percent in error with the MathCad numerical integrations. The greatest error is when $\mu = \lambda = 1.0$.

APPENDIX K

AIR MINISTRY MANUALS FOR THE ROTA GYROPLANE

This appendix provides a few key publications by the Air Ministry of Great Britain applicable to the Royal Air Force fleet (RAF) of Cierva C.30 Autogiros. To the RAF, the Cierva C.30 was designated as the ROTA Gyroplane and was powered by the CIVET I reciprocating piston engine. The civil version of this engine was the Genet Major MK. IA. I have included these manuals because they are, in my view, of great historical significance and have resided in the RAF Museum Library for far too long. The rotorcraft industry (myself included) must express our most grateful appreciation to Miss Mary Jane Millare, Office Administrator of the Department

of Research and Information Services at the Royal Air Force Museum in London. At my request, she tracked down the original manuals and got me a copy.

The manuals captured in this appendix are organized in four publications . The first publication (pages 448 to 490) provides a general description of the aircraft with quite detailed dimensions in several areas . The document is a First Edition and is dated December 1934. Chapter IX, which begins on page 475, gives some special flying notes that are of particular interest.

The second publication (pages 491 to 5 12) provides quite specific maintenance procedures to be followed in order to keep a ROTA in safe flying condition. This document is also dated December 1934. I have added two amendments (pages 513 to 517) to the maintenance manual dated June 1936 and May

1938 respectively.

The third publication (pages 5 1 8 to 529) is a flight training manual for the ROTA. This document is titled "Notes on the Handling of the ROTA Gyroplane in the Air and Upon the Ground." The few pages are packed with very clear instructions. The weight statement on page 527 gives the weight empty of a ROTA as 1,228 pounds and the maximum all-up weight as 1,800 pounds.

The fourth publication (pages 530 to 561) is a collection of modifications that the Air Ministry published. The airspeed restriction of 130 mph (because of the inability to recover from a dive at higher speeds) was removed July 20, 1935 (see page 542). Blade life was set at 75 hours by modification A.P. 1490/P.5 as seen on page 549.

APPENDIX K

AIR MINISTRY

THE

FOR OFFICIAL USE ONLY

AIR PUBLICATION 1490

Volume 1

1st Edition, December, 1934

ROTA GYROPLANE

CIVET

448

I AERO-ENGINE

Promulgated for the information
and guidance of all concerned.
By Command of the Air Council,
C. LL. BULLOCK.

CONTENTS

Axles and radius rods
Oleo leg
Brakes

CHAPTER III

Tail Unit:-

General
Horizontal fin
Vertical fin
Tail wheel

CHAPTER IV

The Rotor:-

General
34A Classification of rotor blades — Rotor blade
Rotor blade friction damper
Pylon structure & top joint
34B Method of balancing rotor blades — Rotor hub
Mechanical startor
Quick-release lever

Revolutions indicator

CHAPTER V

Controls:-

General

APPENDIX K

Para.

1

5322

31
32

33
34
34a
35
34b
36

37
38
40
41

42
43

APPENDIX K

CHAPTER V (Contd.)

Controls:- (Contd.)

Bias control
Wheel brake and clutch and rotor
Ground steering bars

CHAPTER VI

Engine Installation:-

General
Fuel tank

Equipment - Flying:-

Air speed indicator
58 Altimeter
59 Cross level
60 Compass
61

Equipment - Miscellaneous:-

Fire extinguisher
62 Parachutes
63

CHAPTER VIII

Rigging, Assembly and Various Adjustments:-

Rigging fuselage
64
Fuselage routine check
65
Engine mounting and engine
66
Undercarriage
68
Checking oil level in oleo leg
69

Adjustment of clutches

87

450

CHAPTER VIII (Contd.)

Dismantling:-

Fuel tank
Contents gauge
Oil tank
Rotor head
Friction clutch housing
Airscrew and hub
Replacing airscrew and hub

CHAPTER IX

Special Flying Notes:-

Engine starting procedure
Ground handling
Starting up rotor - normal conditions
Starting up rotor - wind velocity over 25 m.p.h.
Hints on starting
General flying
Gliding
Hovering with engine on
Vertical descent

APPENDIX K

Para

ABCDEFGHIJKLMNOPQRSTUVWXYZ
abcdefghijklmnopqrstuvwxyz
0123456789

ABCDEFGHIJKLMNOPQRSTUVWXYZ
abcdefghijklmnopqrstuvwxyz
0123456789

APPENDIX K

A.L.3
5

Fig. 11

30387-1

452

LIST OF ILLUSTRATIONS

---oOo---

APPENDIX K

LEADING PARTICULARS

Duty _____ Communications

Type _____ Two-seater single-engined gyroplane

Main dimensions

(Gyroplane in rigging position)

Diameter of rotor disc

Span of tail plane

Length overall

Height overall

Rotor hub, range of movement

Incidence of rotor blade

Incidence of tail plane

Areas

Tail plane
Upturned tip (Both)
Upper fin
Lower fin
Rotor blades (Each)
Rotor blades (Total of 3 per gyroplane)

Undercarriage

Track

Engine

Type

Airscrew

Type
Drg. No.

Tankage

Fuel tank
Oil tank

Note to Official Users.

Air Ministry Orders and Volume II Leaflets as issued from time to time will effect the subject matter of this publication. It should be understood that Amendment Lists are not always issued to bring the publication into line with the Orders or Leaflets and it is for holders of this book to arrange the necessary linking-up.

Where an Order or Leaflet contradicts any portion of this publication, an Amendment List will generally be issued, but when this is not done the Order or Leaflet must be taken as the overriding authority.

30?

37 ft. 0 in.
10 ft. 2 in.
19 ft. 8 in.
10 ft. 10 in.
$2\frac{1}{2}^{o}$ forward

$7\frac{1}{2}^{o}$ aft
5^{o} right hand
3^{o} left hand
2^{o} 40'
$+1\frac{1}{2}^{o}$ to $+2^{o}$

15.6 sq. ft.
8.55 sq. ft.
12.9 sq. ft.
3.38 sq. ft.
15.6 sq. ft.
46.8 sq. ft.

9 ft. 5 in.

Civet I

Fairey-Reed metal
95193/A/X2

23 galls.

(3.3 galls. oil
(1 gall. air

A.L.3
6

APPENDIX K

INTRODUCTION

1. The Rota is a two-seater gyroplane fitted with a Civet I engine and is intended as a Communications Gyroplane. It is mainly of metal construction although the tail plane is built up with spruce spars and ribs. The oleo undercarriage is of the split axle type and a tail wheel is fitted.

CHAPTER I - FUSELAGE

General

2. The fuselage structure, with the exception of the engine mounting, is constructed of steel tube to B.S. Specification T.45, with butt welded joints, wire bracing being employed in the top and bottom panels aft of the cockpits. The structure may be considered as three separate assemblies, - engine mounting, centre portion at cockpits and rear portion, the centre and rear portions being welded together to form the fuselage structure proper.

Engine mounting

3. This is built up as a complete unit and is detachable as such from the fuselage. The ring is a 12 s.w.g. mild steel angle sec- tion and is attached to the fuselage by eight struts. At the fuse- lage end the eight struts are bolted in pairs to four lugs provided in the ends of the top and bottom longerons by special H.T.S. bolts. The front end of the struts are bolted to the outer side of the engine ring with mild steel bolts.

4. The struts are mild steel tubes reinforced at each end with external sleeves and web plates. Eight lugs are provided on the engine ring to receive the dowels on the forward portion of the cowling, and four lugs to take the cowling formers.

Centre portion

5. The centre portion of the fuselage from the engine mounting attachments to the aft end of the second cockpit is constructed of mild steel tubes to B.S. Specification T.45. The joints consist of plain butt welds. The side and bottom bays are cross braced with tubes and no wire bracing is fitted in this portion of the structure.

6. All three bays in the top longerons are open, the first bay accomodates the fuel tank and clutch gear and the second and third bays form the two cockpits. A cross tube welded to the diagonal side and bulkhead struts forms a mounting for the fuel tank and clutch mechanism.

7. A fireproof bulkhead consisting of a sandwich of asbestos between 24 S.W.G. aluminium sheets is clipped to the first bulkhead of the fuselage. It is reinforced to carry the oil tank which is situated in the engine mounting bay.

8. Brackets are welded to the top longerons for bolting on the deck, and further brackets are provided on the bottom longerons for the attachment of the floors,
cockpit.
and side members of sliding door in front 30387-1
2.

APPENDIX K

9. The four sockets to take the pylon struts are located at the four corners of the front cockpit, and are formed by an extension of the fuselage side struts with a distance tube welded in, and are welded integral with the top longeron. Outrigger struts are also welded to the top and bottom longerons at the front end of the fuselage on either side to form the attachment for the oleo leg. Sockets are welded to the underside of the bottom longerons, for the attachment of the axles and radius rods.

10. On the port side of the frame at the front cockpit, the top longeron is cut away to accommodate a large door which gives easy access to the cockpit between the pylon struts. A special bracing is made in the side frame at this point to allow for the longeron being cut away.

Rear portion

11. The rear portion of the fuselage is constructed of mild steel tubes to B.S. Specification T.45 and the top and bottom panels are wire braced. The wire bracing is of the loop type, the wire being passed round a pair of corner tubes and the ends joined by a turnbuckle. The body of the turnbuckle is stamped from mild steel plate, the two ends being held together by a ferrule and the other end formed

to be a snug fit for the spherical seated nut which is provided with flats to take a 3/16 in. jaw spanner and four 1/8 in. tommy bar holes through which a locking wire is passed after adjustment has been made. The mild steel eye is threaded 4 mm. metric. The wires are 14 S.W.G. H.T.S. and are attached to the turnbuckles by bending into a loop secured by an oval wire ferrule, the free end of the wire being bent back over the ferrule. Fibre pads are fitted at all wire crossings.

12. At the rear portion of the frame, upper and lower vertical fins, constructed of small diameter tubes, are welded integral with the fuselage. The front end of each fin is attached to wooden fairing formers. At the end of the fuselage proper, lugs are provided on the top and bottom longerons for the attachment of the tail wheel telescopic leg.

Datum points

13. The datum points for longitudinal levelling of the fuselage consist of small tubes welded to fuselage vertical members, and will be found projecting through the fabric of the port rear portion of the frame.

Floor

14. The flooring, which extends over the two cockpits, is constructed of plywood stiffened at the edges and also longitudinally and transversely by spruce members. It is made in three sections and bolted to small plates, which are welded into the corners formed by the bottom longeron and cross tubes.

Seats

15. The seats are practically identical in construction except for differences in the method of mounting and are not adjustable. The seat itself is welded up from sheet aluminium and takes the standard seat type parachute. Safety belts are fitted in each cockpit. The front one is secured by Italian hemp cords to the joints on the top longeron immediately aft of the seat, but in the rear cockpit, the cords run to the second joint aft of the seat and are connected by a tensioned elastic cord. This latter is to prevent the belt, when not in use, from fouling the brake and rotor controls. The front seat has clips riveted on to its front face, which pick up a tube running across the fuselage and attached to the side fuselage members. On the back of the seat are riveted brackets which belt on to lugs on the top cross strut between the two cockpits. The rear seat sits in a well cut out of the top of the locker, and is bolted to the latter and the floor, 303P7-1

APPENDIX K

through a tongue which is riveted to the front face of the seat. The seat is also fastened to a top cross member of the fuselage in a similar manner to the front seat.

Cowling

16. The aluminium cowling extends from the engine mounting ring to the front bulkhead of the front cockpit. At the engine ring the panels are provided with dowels, which sit in lugs on the ring, and, at all other places, with spring turnbuttons. The panels are independently detachable.

Decking

17. The decking is constructed of plywood and spruce, and extends from the cowling to the rear bulkhead of the rear cockpit and finishes flush with the top longerons. The latter have small lugs welded on, to which the decking is bolted.

Fairing and locker

18. The remainder of the body exterior consists of doped fabric on a framework of plywood and spruce formers which are clipped to the top and bottom longerons, and spruce longitudinal stringers. Eyeletted duralumin lacing strips are fitted along the bottom longeron, the front cockpit door, and at the juncture with the cowling, but these are subsequently doped down, and no open joint is discernible in the fabric covering the whole of the

body, the decking and the fins. Low down in the fabric, on the starboard side of the rear cockpit, is a door giving access to the locker, on which, it has been previously noted, the rear seat is mounted. The similarly situated door in the port side is for the inspection of brake and rotor clutch control levers.

Arrangement of cockpits

19. In general, it has been arranged that only the actual handles of the various controls are in the cockpits, while the rest of the control runs between the fuselage proper and the fairing. A map case, various pipes and labels etc. are also mounted in the fairing. On the right

hand side of the rear cockpit,

stowage box.

30387-1

10

456

on top of the locker, is a small

3

APPENDIX K

CHAPTER II - UNDERCARRIAGE

General

20. The undercarriage is of the divided axle type with an oleo leg to the bottom outer joints of the outrigger structure, and axles and radius rods running to shackles on the bottom longeron. Palmer low pressure air wheels, type 431/B. (480 m m x 180 m m) and 7 in. diameter Bendix brakes are fitted.

Axles and radius rods

21. The axle tubes, which are of nickel chrome steel, are pinned and sweated into the wheel hub forging. This forging has a flange to which the brake torque plate is bolted, and integral lugs for the oleo leg attachment. The eyebolt through these lugs to secure the oleo leg, also serves the radius rod, which is to B.S. Specification T.45. The upper ends of the tubes are fitted with fork-ended sockets secured with ferrules and tie rods. The axles and radius rods have wooden tail fairings bound on with glued fabric.

Oleo leg

22. The oleo legs are of the coil spring and hydraulic loading type. The oil alone would, under suitable loading, allow a gradual movement of the leg over its whole range, but the main spring limits the range of movement and forms a cushion to take the static load or when taxying. When the leg is fully extended, as on assembly, there is no load in the main spring. When a landing is made, the energy of the moving mass of the gyroplane is absorbed in compressing the main spring and in forcing oil at high pressure through small orifices. The energy taken up by the spring, lessened by frictioned losses, forms the potential energy for the recoil which is again damped by oil flow. The leg consists of two tubes, the top one acting as a piston in the bottom one. The outside joint is maintained oil-tight by a gland nut and packing. The piston tube has a male-ended socket and the cylinder tube a female- ended socket. These sockets are sweated in position and secured with grub screws. No universal block is fitted at these joints as they transmit the brake torque when the engine is being run-up on the ground.

23. A socket made from a steel forging is sweated and secured with grub screws to the top of the bottom cylinder tube. This socket is tapped to receive the gland nut, which also acts as a stop to the leg when fully extended. A stop collar is fitted to the piston tube for this purpose. A filler cap is fitted on the bottom tube for filling the leg with oil.

24. At the bottom end of the top tube is fitted the piston and valve unit. The actual duralumin piston which is secured by grub screws to the tube, has two brass piston rings of the constant pressure type and is tapped to receive the piston end cap, which acts as the abutment for the main spring and also the clack valve. The piston incorporates a spring loaded poppet valve, which is set to lift at a load of 75 lb.

25. The whole of the piston and valve unit is immersed in the oil and, on landing, the oil is forced under pressure through three radiused leak holes in the clack valve. Under a heavy landing this would not dissipate the energy quickly enough, and so, at a predeter- mined pressure, the valve lifts and passes oil through the orifice around its stem until the pressure has dropped. After the leg has compressed 4 in. the main spring comes into action and movement continues until the spring goes solid after a further 3 in. travel on oil and spring. The total range of the leg is thus 7 in. On the recoil, the clack valve lifts from its seat, and allows the oil to flow back

APPENDIX K

quickly through twelve holes which it had previously covered, drilled in the piston. This flow and reflow of the oil will continue until all the stored up energy of the gyroplane's descent, has been absorbed by the work done by forcing the oil through the orifices, assisted by frictional losses.

26. The fairings are made from 20 S.W.G. aluminium sheet, with reinforced ends. They are attached with screws to the top and bottom sockets respectively and the bottom fairing is, in addition, attached to the stop socket. When checking the oil level the top fairing has to be slipped down until the filler cap is exposed through an opening in the wall of the lower fairing.

Brakes

27. The brakes are of the two shoe type in 7 in. diameter drums and are operated by a hand lever in the rear cockpit,. The cable enters the torque plate and connects to the cam lever by a shackle. The adjustable link, which connects the two shoes, consists of a bar, in the middle of which is a serrated disc, one end of the bar being screwed left hand and the other end right hand. The length of the link is adjusted by rotating the serrated disc by means of a screw-driver inserted through the hole in the torque plate, after turning open the torque plate. The brake lever and a rotor clutch lever are mounted in a position convenient to the pi- lot's left hand on a quadrant on the rear cockpit floor, the brake lever being the inner. It

is provided with a ratchet and the brakes can be locked on. The brakes are applied by cables simultaneously on each wheel and cannot be applied differentially. Their purpose is purely for the function of holding the gyroplane stationary on the ground whilst the rotors are being run from the engine, and they are not intended for checking any forward run after landing.

APPENDIX K

CHAPTER III - TAIL UNIT

General.

28. The tail unit is of unconventional design compared with a normal aeroplane, in that it has no surfaces which are movable in flight. There are two vertical fins and a horizontal fin characterised by up-turned tips. A steerable tail wheel is fitted in a Dowty fork and oleo leg.

Horizontal fin.

29. The horizontal fin is constructed almost completely of wood, the only metal parts being the tubes for the leading and trailing edges and various clips. The two spars are of spruce, the ribs of plywood and spruce, and the N-type drag bracing consists of spruce members to the top and bottom faces of the spars. The tips are at 45° to the main horizontal fin and are constructed in a similar manner to it, the spars of the tips being "tongued" into the main spars. The rib section on the left hand half of the main fin is inverted, to provide a reversed moment to that of the airscrew. In the trailing edges of the two halves and also the tips are adjustable trimming flaps. They are hinged to the main portions and further connected with an adjustable link and strap. On the top surface of the left hand half and on the bottom surface of the right hand, incidence blocks will be found projecting through the fabric. The front spar is attached to the fuselage by two male lugs which pick up female lugs welded on to the top longerons. At the rear spar, female lugs pick up eyebolts which are screwed into lugs projecting from the side of the longeron and locked with nuts. By adjusting these eyebolts, the rear spar will rotate about the pins securing the front spar and alteration to the angle of incidence of the horizontal fin will be made.

30. The horizontal fin is braced by four adjustable raking struts, i.e., two each side. They are bolted together to a fitting on the bottom longeron and, from there, run upwards and outwards, one to each spar. The struts are of steel tube, the bottom end being flattened and bent to a lug, whilst the top has a screwed plug which receives an eyebolt and thus allows the length of the strut to be adjusted.

Vertical fins.

31. There are two vertical stabilising fins,

the main one and a

much smaller one underneath the body. They are constructed entirely from mild steel tube and are welded integral with the fuselage. To the trailing edge of the main vertical fin, a trimmer is fitted on two hinge clips. A bolt running through these hinge clips is tightened to lock the trimmer by friction.

Tail wheel.

32. The tail wheel is a Palmer No.448(270 mm. x 100 mm.) and is fitted to a fork and oleo leg. The top of the oleo leg has an internal socket with a male-ended lug which is bolted into a bracket welded to the fuselage cross member. The bottom attachment is by means of a socket which encircles the oleo tube and picks up two eyebolts which are bolted to the bottom longeron. The bottom tube of the oleo leg is free to rotate inside the top tube and carries a lever which is connected with cables to the steering bar in the cockpit. Check cables are fitted from the lever to the fuselage to prevent excessive wheel movement.

APPENDIX K

CHAPTER IV - THE ROTOR

General

33. The rotor is of the three blade type with direct control from either cockpit. The blades are aerofoils and supply all the lift necess- necessary

to keep the gyroplane in the air, but do not play any part in inducing forward velocity, which is obtained in the usual manner by air- screw thrust from a tractor engine. The initial rotation of the rotor is by shaft drive from the engine, but this is merely to get sufficient revolutions to enable the gyroplane to take off and, is in no way for use in flight. Once energised, the rotor maintains its rotation by aero- dynamic action. In flight the attitude of the blades is decided by the action of combined lift and centrifugal force, and normally the blades cone slightly upwards in their rotation, but it is quite impossible for them to fold up or cone above a certain angle. Even when all forward motion has been lost, there are still forces acting on the rotor blades which keep them moving at a high speed, and although the gyroplane drops on an even keel, its rate of descent is not high enough to involve danger. The rotor is also the sole directional control, any desired manoeuvre being effected by tilting the rotor head by means of the control column. On the ground, the rotor blades may be unpinned and folded back along the longitudinal axis, to reduce the overall width when it is desired to house the gryoplane.

Rotor blade

34. The rotor blades have a single spar consisting of a 1½ in. x 14 s.w.g. nickel chrome steel tube (Specification D.T.D.54 A), which, at the inner end, is sweated and secured with ferrules and tie rods to a large fork end. Spruce ribs at 3½ in. pitch are threaded on to the spar, secured with ferrules and tie rods, and then the whole covered with a plywood skin. The rotor tip consists of a block of shaped balsa wood; which is recessed to fit inside the plywood skin and then

glued and secured with woodscrews. The whole is then covered with fabric and

Classification of rotor blades

34A. Owing to manufacturing differences the weight of the rotor blades varies slightly, as also does the position of the centre of gravity along the blade. When finished the rotor blades are balanced, classified into Class "A", "B", "C", "D", etc. and marked at the inner end accordingly. It is essential that only rotor blades of the same class are used on a particular gyroplane.

NOTE:-

It should be understood that the classification refers only to the weight (W), see Fig. 11. In all other respects such as method of construction, dimensions, etc. the different classes of rotor blades are alike.

34B. Each particular gyroplane is supplied with three rotor blades of the same class and spare or replacement rotor blades should be requisitioned only of the same class as the ones originally supplied.

34C. Before assembling a new rotor blade, the existing rotor blades should be checked for balance (weight W) and adjusted, together with the new rotor blade, to give the same value for (W). This precaution is necessary owing to additional fabric and extra coats of dope on rotor blades which have been in service for any length of time, probably causing a variation in the value (W).

Method of balancing rotor blades

34D. Set up the rotor blade with the knife-edge of the balancing block on a hard flat surface. Support the outer end of the rotor blade at a point exactly 16ft. -6 in. from centre of fulcrum pin on a weighing machine (see Fig. 11). The balance weights, which are positioned beneath a tear-off patch at the outer tip, should then be adjusted to give the value (W) as given in the column for the particular class of rotor blade to which it belongs.

NOTE:- See Vol.2, Part III, of this publication, Chapter 5, para. 2.

bolts are of large diameter and are mounted on Hoffman needle bearings (4). The end play for both these bolts should not exceed 0.002 in., and, if it is found that this clearance is exceeded, shims may be added to take up the excess. On the T-headed bolt (3) is carried the rotor hub complete, which is secured by retaining nut (15).

Rotor hub

37. This consists of a base plate (13) to which is bolted a manganese bronze casting (5) with bolts which also pick up the housing (6) for ball races (22) and (19). These ball races receive the hub axle (7), which is secured with the retaining nut (8). The spur wheel (9) for the revolution

drive is secured to the hub axle and retaining nut. The main crown wheel (10) is bolted to the hub axle. The inside of the crown wheel is machined out to form a brake drum and inside it is fitted a conventional type of two shoe internal expanding brake (11); it is not, however, of the servo or self-energising type as this would be too fierce and subject the pylon structure to rather high torque load. To the hub axle are pinned the three rotor links (12).

Mechanical starter

38. The drive for the mechanical starter unit is taken from the rear end of the engine through a special crankshaft extension with a splined end. A short transmission shaft, free to slide on the spline on the crank- shaft extension, carries the power into the main clutch, which is mounted on a cross strut in the first fuselage bay and braced back to the longerons with struts. This clutch is of the dry, single plate type, the driving plate being an aluminium casting bolted to the driving shaft and lined with ferodo, whilst the driven plate is machined from a mild steel bar rein- forced with welded steel webs. The driven plate is free to slide along a splined shaft and is pressed against the driving plate by means of two cams which bear directly on to one face of a single thrust bearing, the other face being held against the driven plate. One concentric coil spring forces the two plates apart as soon as the load is taken off. In this respect the

clutch design is the reverse of normal motor car practice. At the back end of the clutch is a gear box containing two bevel gears, which con- stitute the first speed reduction in the ratio 1.5 to 1. The vertical transmission shaft from the clutch to the rotor head is free to move in a splined fitting at the lower end and has two universal couplings of the Mollart ball and claw socket type. A special shear pin is driven through the shaft and coupling at the bottom end and is designed to shear at about $1\frac{1}{4}$ times the normal load thus putting a limit to the load which can be put on the rotor structure.

39. At the top of the vertical transmission shaft, the drive is trans- ferred to a bevel pinion, which gears with the main crown wheel and so turns the rotor. The ratio of this final drive in the transmission is 5.3 to 1. The pinion is contained in a cast aluminium housing which is bolted to the front of the manganese bronze seating (5) in fig. 2, and also incorporates an automatic dog-clutch. The operation of both the friction clutch and rotor brake is by bowden cable from a single lever in the rear cockpit. The lever is designed to operate one of two quadrants: by depressing the lever and engaging it in the near side quadrant the clutch is operated and a similar operation but engaging the offside quadrant operates the rotor brake; thus only one of these units can be operated at a time and the clutch cannot be engaged with the rotor brake on and vice- versa. Attached to the operating levers of the friction clutch are two strong return springs, which operate the dog-clutch. With the friction clutch disengaged the initial tension in these springs is sufficient to tension a small bowden cable and free the dog-clutch against the pull of a

light spring. When the friction clutch is operated, the first movement of the levers relieves the tension in the dog-clutch bowden cable and the light spring immediately engages the dog clutch before the main clutch is fully engaged.

APPENDIX K

Quick-release lever

40. On the left hand vertical member behind the front seat and in the rear cockpit, is mounted the quick release lever for the wheel brakes and clutch and rotor brake controls. The lever is connected by a rod to the quadrant in which the control levers are mounted on the floor, and when the lever is pushed forward it releases the wheel brakes and rotor clutch or brake by disengaging their ratchets. On the rear instrument board is a spring loaded clip for the control column and with this is incorporated a locking lever. From this locking lever to the quick release lever is a bowden cable which operates a plunger stop on the quick release gear. This stop is so arranged that when the control column is locked, the quick release gear is also locked, i.e. the con- trol column must be

unlocked before the quick release lever can be operated to free the wheel brakes and clutch. Furthermore, until the quick release lever has been pulled back, the wheel brakes and rotor brake or clutch cannot be engaged.

Rotor revolution indicator

41. A rotor revolution indicator is fitted to the instrument board in each cockpit. A flexible drive is taken from the rotor hub to a gear box (ratio 1:1) which is clipped to two fuselage side members in the front cockpit and from it a flexible drive is taken to each instrument.

APPENDIX K

CHAPTER V - CONTROLS

General.

42. The main controls consisting of a control column and engine controls are duplicated in each cockpit and the gyroplane may be flown from either. In addition, a tail wheel steering bar and fuel cock con-

trol is fitted in each cockpit. The wheel brake control, the rotor clutch and brake control and the two bias controls are fitted in the rear cockpit only.

Control column:

43. The flying controls consist merely of an inverted control column hinged universally on a cross bar, which is mounted on the rear struts of the pylon structure. Above this hinge the control column is continued and coupled to a short stiff lever by means of a ball joint. This short lever is attached directly to the base of the rotor hub, below the lateral and longitudinal hinges. Therefore, when the control column is moved by the pilot in the cockpit, it turns about the universal hinge, pushes the ball joint in the opposite direction, and so tilts the rotor hub. On examining the ball joint it will be found that the ball is surrounded by a bronze cap which screws on to a hollow socket, fitted in the end of the control column. Inside this

socket, a floating cup-shaped bearing with a thick rubber washer beneath it, supports the end of the ball. This device gives minimum friction and no play when the bronze cap is screwed down the correct amount. The cap is then locked in position, by a thin nut below it.

44. A few inches below the ball joint the universal hinge is situated, and at this point the control column is hinged on a pin between the jaws of a fork which allows it to move in a fore and aft direction. The shaft of this fork is fitted into a cross-bar and free to turn. The whole of this unit can also rotate about the axis of the cross bar and is attached to the pylon struts by two large clips to which are welded screwed studs, the plain portion of these studs forming a bearing inside the cross bar, the threaded portion screwing into bronze bushes that are riveted inside it. Therefore, to adjust the lateral position of the universal hinge all that is necessary is to rotate this unit, and owing to the action of the screws the whole will move to the right or left, as the case may be. Actually, the cross bar is designed to turn slightly with the controls, in order to compensate for the rise and fall of the ball joint due to the movement of the hub. After long service, slight play may develop at the control column ball joint; this can be rectified by giving the bronze

cap half a turn or so to take up the slackness. If this does not cure it or the cap appears to be badly worn, it should be renewed. To do this it will be necessary to take out the bolts at the bottom of the top control lever and withdraw the ball, before the cap can be taken off. The floating bearing and the rubber washer beneath it should, if necessary, be replaced at the same time.

Bias control.

45. Just below the rotor head and inside the head fairing, it will be noticed that there are four coil springs attached to the top control lever, by means of a socket that is flanged up at right angles, so that the pull from the springs acts on the centre of the ball joint. These constitute the control bias, and their use is to centralise the control column and alter the trim of the gyroplane for all conditions of flight. A large U-shaped welded tube bracket is bolted to the rear pylon struts, and a short cross tube is mounted between the two front struts to take the other ends of the four springs with four trunnions as the points of attachment. Into each of these trunnions is fitted the screwed shaft of a forked eyebolt to which is pinned the eye end of each spring.

APPENDIX K

To increase the tension on any of these springs, draw the eyebolt outwards with the nut on the back of the trunnion and then lock up with the lock nut provided. Each of these springs is given initial tension to give the pilot a control "feel". This tension is also variable from the cockpit during flight by rotating the trunnion a few degrees in either direction. The arrangement is simply a short length of tube sliding over one of the tubes comprising the U-bracket and free to turn; the sleeve for the lateral bias being on the starboard side of the U-bracket and on the front cross strut for the longitudinal bias. To one end of these tubes are welded web plates carrying the trunnions and to the other end is welded a short plate lever. Control cables run from these levers down the rear pylon strut on the starboard side in fair-lead tubes, guided at the bottom to the separate controls in the rear cockpit, by small pulleys.

46. The lateral bias is operated from the rear cockpit by a handwheel on the starboard side of the instrument board and the gyroplane is made to turn to the right when the handwheel is turned to the left i.e. in an anti-clockwise direction. Very fine adjustment can be obtained from this control, it being possible to turn the handwheel through approximately 36 turns. This applies tension on the control cable through a screwed spindle that is pulled backwards by the female shaft of the handwheel. A thrust race is

incorporated to prevent the mechan- ism becoming stiff when under load. A lever acting on a ratchet in a quadrant on the starboard side of the rear pilot forms the longitudinal bias control and when pulled backwards, tensions the control cable, thus making the gyroplane become tail heavy and vice-versa. The ratchet has a series of inverted serrations, which are engaged by a pawl in the centre of the lever and operated from a press button on top of the handle. Wheel brake and clutch and rotor brake control

47. Mounted on the floor on the port side of the rear cockpit is a quadrant with two levers. The ~~outer lever~~ operates the cables for the wheel brakes (see para. 27). The ~~inner lever~~ operates either the rotor brake or the two clutches (see para. 39).

inner lever, which is the longer of the two and nearest the port bearer for the seat.

Ground steering bars.

outer lever, nearest the inspection door, on the port side of the fuselage.

A.L. 1

48. The ground steering bars are identical in construction and the foot pedals are adjustable to suit varying leg lengths. Each bar is mounted on a pedestal made from an aluminium spinning, which is bolted to the floor. Heel rubbing plates are also screwed to the floor to avoid undue wear. The right hand halves of the bars are connected with a steel tubular strut and the central spindle of the rear bar carries a lever which is attached with cables to the lever on the tail wheel.

APPENDIX K

CHAPTER VI - ENGINE INSTALLATION

General

49. The power unit is a Civet I air-cooled radial engine of 140 B.H.P. at 2200 R.P.M. (153 B.H.P. at 2420 R.P.M.). The fuel supply is entirely by gravity and is carried in a 23 gallon tank immediately behind the bulkhead.

Fuel tank

50. The fuel tank of 23 gallons capacity rests on the first top cross strut of the fuselage and on a cross tube connecting the fuselage side diagonals. The tank is held down to the top longerons by two steel straps, which are adjustable in length. The tank is constructed of 18 s.w.g. aluminium sheet (B.S.Specification L.16), welded and anodised, and is fitted with a standard filler cap and a Simms' type contents gauge. A sorbo packing is inserted between the tank and fire-proof bulkhead to locate it against end creep and prevent chafing.

Fuel system

51. The feed pipes from the bottom of the two halves of the tank (the latter is cut away in the centre to clear the clutch) are led into a tee-piece which is connected to a Vickers cock. From the cock one feed pipe is led into the standard type filter and then to the engine. All the above pipes are Superflexit tubing. A Ki-gass priming pump is mounted on the left hand lower engine mounting strut; it is fed by a copper tube from an elbow in the top of the filter. The Vickers cock can be operated by means of a torque shaft from either cockpit.

Oil tank

52. The oil tank is welded up from 18 s.w.g. aluminium sheet, its capacity being 3.3 gallons of oil and 1 gallon air. The filler is on the left hand side and incorporates a graduated dip rod by which the amount of oil contained in the tank is readily ascertained. A drain plug, vent pipe, thermometer flange and return and feed connections are fitted, - the last named incorporating an internal stack pipe. The tank is mounted on the front face of the fireproof bulkhead by two steel straps, which are adjustable in length.

Oil system

53. The circulation of oil is maintained by the engine pumps. The feed and return pipes are both Superflexit tube. Copper pipes 1/4 in. od. x 20 s.w.g. are led from the pressure connection on the engine, and from the temperature connection on the tank to their respective instruments in the rear cockpit.

Engine controls

54. The throttle and mixture control levers are mounted on fuse- lage members on the port side. The control lever assemblies are similar in both cockpits, the quadrants and levers are light alloy castings and integral lugs on the levers ensure that the mixture control is closed with the throttle. The quadrant is bolted to the fuselage and the spindles are concentric, the mixture spindle being between the throttle spindle and the quadrant and using them both as bearings. The hand levers are attached to the spindles with bolts which engage slots in the spindle.

55. The outer levers are attached to the spindles by a similar bolt in the case of the mixture lever and a split taper pin for the throttle lever. The outer levers in the front cockpit are connected with adjustable rods to the corresponding levers in the rear cockpit.

APPENDIX K

Additional rods, which are also adjustable in length, from the front cockpit levers, pass through sliding glands in the fireproof bulkhead and operate levers on concentric horizontal countershafts, which are mounted on the lower side engine mounting struts. The mounting clips incorporate a leather lined adjustable friction bearing. Additional levers on the countershafts operate the carburettor by means of adjustable rods.

Engine speed indicator

56. An engine speed indicator is fitted to the rear cockpit, and

driven direct from the engine with a flexible drive.

Exhaust manifold

57. The exhaust manifold is in two portions attached by a flanged joint at the top and terminates in a single short vertical tail pipe.

APPENDIX K

CHAPTER VII - EQUIPMENT

Flying Equipment

Air speed indicator

58. The pressure head tubes are welded into a streamlined tube

which is clipped at the bottom of the right hand outrigger tube, running from the outer joint to the top longeron, and they are parallel to the fuselage datum line. The $\frac{5}{16}$ in. aluminium connecting tubes pass up the inside tail fairing of this outrigger tube to two T-pieces, from which connections are taken to the front and rear airspeed indicators on the instrument boards.

Altimeters

59. Altimeters are fitted to the instrument board in both cockpits.

Cross level

60. A cross level is fitted to the rear board only.

Compass

61. A compass (Type P.6, Stores ref.6A/0.367) is fitted in the rear cockpit to a base plate which is clipped to the vee bulkhead bracing struts behind the rear seat.

Equipment

Fire extinguisher

62. A fire extinguisher, methyl bromide No.3, is mounted to the right hand fuselage diagonal member in the rear cockpit, close to the seat. The nozzle of the extinguisher fits into a coupling on the bracket, from which a pipe line is taken forward and through the fireproof bulkhead, terminating in a nozzle directed to spray on the carburettor. When the fire extinguisher is to be used in this manner for dealing with a carburettor it is to be operated by a hand lever acting against the extinguisher knob, the safety catch being first turned aside out of engagement. For use by hand the extinguisher can be removed from the bracket and operated in the usual manner.

Parachutes

63. Both seats are arranged to take the seat-type Irving parachute.

APPENDIX K

CHAPTER VIII - RIGGING, ASSEMBLY & VARIOUS ADJUSTMENTS

Rigging fuselage.

64. The fuselage should be supported on trestles, one at the jacking points on the front bottom fuselage cross member and one at the tail wheel. Special packing blocks will be required at the rear, to enable the lower fin to clear the trestle, and at the front to clear the fireproof bulkhead and axles, if in position. The position of the rear jacking points will be found marked on the fairing. The fuselage may be checked for rigging position, transversely by straightedge and level across the longerons in the rear cockpit, using the under side of the tubes, and longitudinally across the datum points which will be found projecting through the rear fairing on the left hand side.

Routine check.

65. Owing to the welded tube type of construction of the fuselage, the frame is so stiff that no rigging operations by altering wire tensions may be carried out. The fuselage structure should be examined periodically, for which purpose the covering must be unlaced and all joints and members carefully examined. The cross bracing wires should be checked, and, if necessary, adjusted to an even tension; care must be taken that the wires are normal to the attachment tubes, other- wise a slight movement and consequent slackening of the wire may take place in service.

Engine mounting and engine.

66. Raise the engine mounting and support it while the tubular struts are being secured to the fuselage attachments. The struts are fixed to the engine ring and fuselage by special bolts. Suitable lifting tackle, capable of dealing with a load of about a ton, should now be prepared, and a sling attached to the lifting eyebolt on the engine. The engine can then be bolted into the mounting. Before releasing the sling, a weight should be attached to the tail end of the fuselage to prevent any tendency for it to tip up on its nose.

67. After the engine has been secured to the mounting, the following operations should be carried out:-

(i) Fit the exhaust manifold.

(ii) Fit the carburettor and connect up the engine controls.

(iii) Complete the ignition system wiring.

(iv) Connect up oil and fuel pipes.

(v) Thoroughly check the installation.

(vi) Fit engine cowling.

Undercarriage.

68. The points of attachment for the shackles of the axles and radius rods will be found on the bottom longerons, and the attachments can be made without any difficulty. The oleo legs can now be fitted by attaching the lug at the top and bottom to the jaws on the outrigger joint and the axle socket respectively. Finally, liberally grease the axles and fit the wheels. Care must be taken to ensure that the axle caps and all pins are securely fitted and that split pins, where required, are in position.

APPENDIX K

Checking oil level in oleo leg.

69. It will be necessary to verify the oil level in the oleo leg at intervals, and this may be carried out with the legs supporting the gyroplane, i.e. it is not necessary to "jack up." The screws securing the top fairing should be removed and the fairing slid down the leg to expose the filler cap. A mixture of 70% treated castor oil, Stores Ref. 34 A/5 or 34 A/45, and 30% paraffin should be used, and the leg filled until it overflows from the filler cap.

Adjusting wheel brakes.

70. The routine adjustment for wear on the brake shoes should be carried out by means of the adjustable link, as follows:-

(i) Jack up both wheels and see that the hand brake lever is in the off position with the ratchet in the last notch of the quadrant.

(ii) Expand the shoes until the brakes just grip by rotating the serrated disc on the adjustable link by a screw driver, inserted through the slot in the torque plate, rotating the disc so that the serrations nearest the hand move downwards.

(iii) Slacken off the adjustment until the wheels will just move freely.

The bowden operating cables are adjustable at either end, and, in addition, further adjustment can be effected by moving the actuating lever on the serrated cam spindle.

Tyre pressure.

71. The tyres should be kept inflated to 20 lb. per sq. in. and must be checked by gauge, as a visual check is liable to be misleading.

Lubrication of wheel hubs.

72. Care must be taken not to over lubricate the wheel hubs, as excess lubricant will be thrown outwards on to the brake drums and reduce the effectiveness of the brakes.

Preparation of new wheels.

73. New wheels drawn from Stores will be found to have the brake drums coated on the inside with grease and this should be carefully wiped off before the wheels are fitted. Care must also be taken to see that there is 1/16 in. clearance all round between the wheel and the brake casing. If required, steel shims can be fitted on the axle before fitting the wheel to give this clearance.

Removal of undercarriage.

74. The gyroplane should be supported on trestles as already described (see para. 62) and the rear of gyroplane tied down to a weight on the floor. The brake cables should be disconnected at the top of the axle and then the bolts at the axle and radius rod attachments to fuse- lage and at the oleo leg universal blocks may be knocked out and the two units removed separately.

Tail unit.

75. The horizontal fin and its integral up-turned tips are secured by four lugs on the under side of the spars to fittings on the top longeron. The incidence is variable by adjusting the eyebolt at the rear attachment and should be set from $+1\frac{1}{2}^{o}$ to $+2^{o}$. Incidence blocks for this purpose will be found projecting through the fabric on the top surface of the left hand and the bottom surface of the right hand portion.

APPENDIX K

The horizontal fin is stayed by four struts which are all adjustable for length. The two struts on each side are bolted to a common fitting on the bottom longeron, from which they run upwards and outwards, one to each spar, to projecting lugs on the under surface. The strut lengths should be adjusted until the front and rear spars are horizontal laterally, when checked with a spirit level.

Checking oil level in tail wheel oleo leg.

76. This is the same procedure as for the main oleo legs. Remove plug in the leg and fill slowly with oil of the same composition until it overflows.

Tyre pressure for tail wheel.

77. The tyre should be kept inflated to 30 lb. per sq. in. and must be checked by gauge.

Rotor blades.

78. The attachment of rotor blade to the rotor link, including the friction damper assembly, has been described in para. 35. The articulating pin, which secures the link to the rotor hub, runs in special Hoffman needle bearings and is secured with a special washer and greaser bolt. The square ended stop pin is then inserted with its washers and bolt and the latter locked with wire to the greaser bolt in the articulating pin. The latter and the link pin securing the rotor blade should be well greased on assembly and the grease chambers filled by the grease gun before the gyroplane is flown. The lubricant to be used is Texaco Marfak Grease No.2.

Checking friction damper.

79. After the three blades have been assembled the "pull off" of the friction dampers on each should be checked as follows:-

Put on rotor brake and lock the control column. Set the rotor to be checked in line with the fuselage, in such a position that the total movement of the blade is equally divided on each side of the centre line of gyroplane. Next place a piece of tape round the rotor blade across the centre of the oblong recess where the balance weights are fixed, i.e. about 12 inches from the tip. The tape should be tied so that the hooked end of the spring balance supplied with the tool kit can be attached. Now move the blade over to the left to the extent of its free movement and attach the tape from the trailing edge to the spring balance which is tied or secured in any convenient manner. It will facilitate the operation now if another person will steady the rotor by taking hold of one of the other two blades. The blade being checked is gently pulled to the right and the reading on the spring balance noted. With the blade extended to the right until up against the stop, the operation should be reversed with the tape pulling off the leading edge. It will usually be found that the two readings vary slightly and the friction damper should be adjusted until the mean of the two readings is consistent at approximately 12 lb. and then locked.

Adjusting friction damper (see fig. 1)

80. Loosen the lock nut on the top of the damper and adjust by turning the bottom nut to the right to increase the pressure and to the left to decrease it. When the correct pressure has been obtained, secure the adjustment by means of the lock nut above the adjusting nut.

Changing a rotor blade.

81. The rotor blades are divided into three categories by their weight. The weight class of any blade is identified by one of the letters "A", "B" or "C" appearing at the end of the serial number printed

APPENDIX K

"Folding the rotor blades

81A. When the rotor blades are being folded with the control column locked in its catch on the instrument board there is a considerable load tending to pull the column out of engagement, and should the column be freed through the inadvertent release of the catch some injury may result to the occupant of the cockpit; it is therefore imperative that the column is not so locked whilst the operation of folding the blades is being performed. The blades should be supported when folded so that they do not damage the tail unit. This may be effected by means of slings from the hangar roof or by planks placed across trestles situated on each side of the fuselage."

on the in
be mainta
category
the same,
81.A.
Adjusting

82.
universal
position
and also

adjustments, of course, alter the flying position of the column. To bring it to the left, it is necessary to take out the hinge fork pin securing the column and turn the fork in a clock-wise direction towards the left.

One complete turn will give a shift of approximately 1 inch at the hands.

Should less movement be required, the fork can be removed, the cross bar

given half a turn and the fork and shims replaced exactly as before.

It will be found on some gyroplanes that shims are fitted between the

hinge fork and the bearing on the cross shaft. These shims vary the

ratio between the diving and climbing control and should on no account

be touched. In case the control is ever taken down and the correct

shimming forgotten it should be remembered that a shim between the fork

and the bearing will give more diving control.

Adjustment of fore and aft bias.

83. The initial adjustment of the bias is made with the blades taken off the hub. The control column should be unlocked and the lever for the fore and aft bias placed centrally in the quadrant. In this position the lever on the cross tube carrying the eyebolt of the front longitudinal spring should also be central. Now push the control column forward, and adjust the rear spring so that its full length is taken up without any tension. Adjust the front spring on its eyebolt until the tension is sufficient to hold the control column at a distance of 12 in. from the fuselage cross tube immediately below the dashboard. The compensating spring on the longitudinal bias control in the cockpit should now be adjusted by pulling the hand lever fully back and attaching the spring with a small initial tension.

Adjustment of lateral bias.

The handwheel should be set in its central position, that is,

18 turns from either way and the lever on the right hand side of the U-bracket should then also be central. Push the control column hard over to the right and in this position the left hand spring should be adjusted to have a small initial tension. Leave the control column free and adjust the right hand spring with its eyebolt until the control column takes up a position about 1.5 in. to the right of the centre line of gyroplane.

85. The two above positions for the control column are the initial ground settings and further adjustments can be made in flight. Further, as is the case with all springs, those forming the bias will, no doubt, become "tired" in time and some readjustment will be necessary. It should be remembered in making these adjustments that nose heaviness can be corrected by putting more tension on the front spring. If the "feal" of the controls is too light, heaviness can be added by adding an equal tension to opposite springs. The two bias control cables may, in time, stretch a little. For the lateral bias, an adjusting screw is fitted in the centre of the screwed spindle; and the slot may be reached with an ordinary screw driver inserted down the bore of the hand-wheel. To tighten the cable, the screw driver should be turned to the left. For the longitudinal control, the link plate inserted between the cable and the hand lever has a series of holes drilled in it, by which any slack may be taken up.

A.L.2. 3

APPENDIX K

Changing a rotor drive shaft

86. If at any time the vertical driving shaft from the engine friction clutch to the rotor dog clutch is dismantled or a new one fitted, the following precautions should be observed:-

(i) The corresponding fork members or ears on the two joints must be in the same plane, as otherwise, the transmission will not be uniform, resulting in a very uneven velocity and overheating at the ball joints.

(ii) In assembling component parts of transmission shafts, it is absolutely imperative that these should be co-related one to the other, "0" to "0" as marked.

Adjustment of clutches

87. The clutch lever handle in the quadrant on the floor in the rear cockpit should be engaged in the third notch in the ratchet and then the bowden cable for the dog clutch adjusted until the dogs are just meshing. This may be ascertained by the fact that, when turned by hand, the shaft is free to move in one direction only. The clutch control handle should be pulled up to the sixth notch and the friction clutch cable adjusted until it is impossible to turn the shaft by hand, thus indicating that the clutch plates are fully engaged. In addition to this, the cable operating the dog clutch should be slack. The bowden cable controls are adjustable by means of adjusting screws at either end.

Fuel tank

88. The fuel tank is removed by removing the top cowling over it, the two feed pipes and undoing the straps which secure it to the top longeron.

Contents gauge

89. This can be removed after freeing the flange at the top. When replacing the gauge care must be taken that the guide tube for the float is properly located in the hole in the bridge piece on the tank bottom.

Oil tank

90. To remove the oil tank the following is the sequence of operations:-

(i) Remove the port and starboard side panels of the engine cowling.

(ii) Disconnect feed, return, thermometer and drain connections at oil tank, the petrol filter with its pipes to elbow on bulkhead and to carburettor.

(iii) Remove engine controls cross shaft.

(iv) Unlock tank strap and remove sideways.

To dismantle rotor head (see fig. 2)

91. The following is the sequence of operations:-

(i) Remove the three rotor blades and their links. To do this,

cut the locking wire at the horizontal link pins, remove the studs and special washers in the ends of the stop pins (14) the greaser bolt and washer for the horizontal articulating pin, and knock out the latter with

472

APPENDIX K

(xv) Cut the brass locking wire, unscrew stud securing revolution indicator drive spur wheel and remove the latter. Note: On assembly, it may be necessary to adjust the head of the stud until the hole for locking wire lines up with the holes in the spur wheel. Remove locking screw (18) and unscrew retaining nut (8) with special 3-prong spanner. This will gradually press out the single ball race (19) and the retaining nut can then be screwed right off. The hub axle can then be extracted with an extractor tool. It must not be hammered out, as this method is liable to damage the ball races. This will free the langite sealing washer (20). On re-assembling, this item should be coated with graphite and grease. The ball race (22) and the distance piece (21) can now be pressed out with an extractor tool. On re-assembling, the housing (6) and ball races should be packed in grease, and it is essential that the

retaining nut is tight.

A special spanner is provided for this purpose. If replacements have been made, the unit should be assembled without the mounting plate (5) and the gap between the housing (6) and the base plate (13) checked with feeler strips. The unit can then be stripped and the distance piece (21) adjusted in thickness until the ball races are locked.

(xvi) The bevel gear (10) can be stripped from the stub axle (7) by removing the twelve bolts, nuts and split pins.

When re-assembling, the process should be reversed. It should be noted that the above is for a complete detailed stripping down, and, in many cases, it will be found convenient to leave various items (e.g. the drain plug and pinion) in place. The grease to be used for packing ball races, rotor hub and articulating pins, etc. is Texaco Marfak Grease No.2.

Friction clutch housing

92. (i) Remove bowden cable by slacking off and clearing nipples from swivelling bracket.

(ii) Disconnect both horizontal and vertical driving shafts from "Hardy" couplings and universal joints.

(iii) Disconnect securing bolts holding housing to frame members and remove clutch.

Airscrew and hub

93. A special spanner is supplied in the engine tool kit for this purpose, which fits over the airscrew locking nut. On examination an inner stub piece will be observed, and on the spanner being forced right home, this stub presses in the serrated locking device which secures the locking nut in position, thus freeing it. Whilst the spanner is held in this position give the handle a sharp blow with a hammer, thus freeing the locking nut on the crankshaft. Still pressing the spanner inwards, unscrew the locking nut in an anti-clockwise direction off the crankshaft, this action at the same time releasing both halves of the front cone. The airscrew and hub are now free to be withdrawn from the engine, but it will be found, most probably, that the hub is still tight on the airscrew, but if tapped at the back by hand it will free itself and the hub slide off.

Replacing airscrew and hub

94. Careful examination of the splines on the crankshaft will show that two form a master spline by means of a small peg joining them together, and a similar inspection of the inner surface of the airscrew hub will also reveal a master spline formed by a

spline having been machined away. The lining up of these two master splines will ensure that the airscrew hub is always fixed in the same position, and will allow it to slide freely on the crankshaft.

T/S APPENDIX

The correct procedure is as follows:-

(i)

Replace rear split cone on crankshaft, making sure that its jaws engage the dogs on the crankshaft lock-nut.

(ii) Place hub and airscrew, in accordance with the above instructions, on the crankshaft.

(iii) Replace the two halves of the front cone on the flange of the lock-nut and insert on the crankshaft as a unit.

22

APPENDIX K

CHAPTER IX - SPECIAL FLYING NOTES

Engine starting procedure

85. When starting up the engine the following instruction will serve as a guide to the amount of priming required. The number of Ki-gass pump strokes quoted are full strokes of the pump after the fuel has commenced to enter the cylinders. Standing beside the engine the fuel can be heard entering the cylinders.

(i) When starting from cold - 8 strokes.

(ii) When engine is warm - 4 strokes.

(iii) When engine is hot - 2 strokes.

but if engine fails to start, open throttle wide and blow out two complete turns.

(iv) When engine is hot and day

temperature is also high, do not use Ki-gass but give two or three pumps on throttle lever when sucking in.

Ground handling and taxying

96. The control column must be locked in its crutch, the quick release set, and the rotor brake on, when stationary or taxying. It is not advisable to have a rotor blade immediately over either the nose or tail. The fore and aft bias control lever should be approximately mid-way or slightly forward. The gyroplane is taxied entirely by the throttle and the steering bars controlling the tail wheel. The wheel brakes must not be used while the gyro- plane is moving (see para.27). If the wind is very strong avoid taxying into it except at a very slow rate.

Starting up rotor - normal conditions

97. (i) Head into wind.

(ii) Set fore and aft bias about $\frac{2}{3}$ down.

(iii) Lock wheel brakes hard on.

(iv) Open throttle slightly.

(v) Release rotor brake.

(vi) Move rotor control lever inwards towards seat and slowly engage it. The more gently the clutch is let in, the smoother becomes the initial rotation of the rotor. This smooth engagement can easily be checked by watching the tips of the blades. If the clutch is let in fiercely it is possible that the engine may be stopped, but more important is the fact that the rotor pylon is unduly stressed. Finally, pull the clutch lever up as far as it will go, otherwise the clutch will slip.

(vii) Slowly open throttle.

(viii) When rotor revolution indicator shows 120 r.p.m. release the catch holding the control column in its crutch but continue to hold the control column forward. At this stage the engine revolutions should be 960 and the rotor 120, i.e. a ratio of 8 to 1, and this shows the clutch is fully engaged.

APPENDIX K

(ix) . Open throttle slowly until rotor shows 180 r.p.m. little or no wind this can be increased to 200 or 210 r.p.m).

(In

(x) Release quick release lever, thus freeing wheel brakes and clutch. Keep control column forward.

(xi) Open throttle fully, wait two seconds, and ease control column back until the gyroplane lifts off front wheels first and until an air speed of from 20 to 25 m.p.h. is reached. During the take-off keep a firm pressure on the right steering pedal, to correct a tendency to swing left.

(xii) When clear of the ground ease control column forward.

The best climb is 55 m.p.h. with normal load and 65 m.p.h. with full load.

(xiii) When well away from the ground, the quick release should be re-set.

Starting up rotor - wind velocity over 25 m.p.h.

98. (i) Turn about 100° to wind, with wind on starboard side.

(ii) Engage wheel brakes and clutch as before and get rotor spinning to about 100 to 110 r.p.m.

(iii) Release wheel brakes and clutch by the hand levers (leaving quick release engaged) and swing into wind on the throttle and tail wheel control, leaving engine about 1,100 r.p.m.

(iv) Put on wheel brakes and engage clutch rapidly.

(v) Run up rotor to 175 r.p.m. (no more) and then carry on as before.

Should the wind be very gusty or variable, be ready to slip quick release and take off even slightly before 175 rotor r.p.m.

Hints on starting

99. (i) If the clutch slips and the throttle is opened too fast with the rotor spinning, throttle back at once. There is a danger of the tail rising and the gyroplane nosing over.

(ii) If, for any reason, the quick

release fails to work the wheel brakes and clutch can be thrown out independently.

(iii) Rotor revolutions will drop anything up to 30 to 40 r.p.m. especially in a calm, but will build up as the gyroplane moves forward. They should, however, not be allowed to drop below about 150 r.p.m.

Table of approximate rotor and engine revolutions for any given wind speed

Wind		Rotor revs.
Engine revs.	0 - 10 m.p.h.	200 or a little over
(solo 195)		1,600
	10 - 15 m.p.h.	190
1,520		
	15 - 20 m.p.h.	185
1,480		
	20 - 25 m.p.h.	180
1,440		
	25 - 30 m.p.h.	175
1,400		

APPENDIX K

General flying

100. The gyroplane responds to controls in the same way as a normal aeroplane. If the control column pulls either right or left, this may be corrected by use of the lateral bias. Absence of rudder will not be noticed but a change in direction, particularly at high speeds, will be apparent if the tail wheel is put hard over. At slower speeds of 20 - 40 m.p.h. a slight lag will be noticed in the fore and aft control, which may be a little disconcerting until one is used to it. Slow flying should be practised at a reasonable height before attempting it near the ground, and a point should also be made of doing this practice into the wind, as the effects of the latter are very noticeable. Try out the effect of opening and closing the throttle suddenly, as this may prove disconcerting if using engine during a landing. Full use should be made of the fore and aft bias to get the best "feel" on control. If nose heavy the trimming lever should be set back slightly, and if tail heavy, it should be set forward. Each gyroplane will vary slightly, owing to varying adjustments on the bias springs.

101. If a "swaying" or vibration is felt on the ground, when starting up rotor, it is usually due to the friction dampers being set unevenly. It will tend to smooth out when the rotor revolutions approach 100-120 r.p.m, and the blades become stabilised. If it does not, the rotor should be stopped and the friction dampers checked over. This same defect will produce a slight "once per revolution" pulsation on the control column in flight. If a noise like a machine gun is heard from the rotor head, when the engine is throttled back, it is a sign that the dog clutch is out of adjustment and that the dogs are rubbing. Another cause of pulsation can be due to slackness in fore-and-aft ball joint, or the lateral pin of control column, and a feeling of "looseness" will be experienced when handling the control column. Usually, however, a pulsation felt on

the control column will be due to the rotor blades being out of static balance. This may be due to one blade getting slightly damaged or being re-doped excessively. Another cause of slackness is play in the lateral and longitudinal rocking pins at the pylon head.

Gliding

102. The gyroplane has a final glide with normal load, of 45 m.p.h. plus wind speed and gliding turns can be executed in the normal manner.

Hovering with engine on

103. This is accomplished by running the engine at about 2000 r.p.m. and easing the control column slowly back. Note an object on the ground and continue to ease back the control column until the object appears stationary. This manoeuvre should also be practised into wind at a reasonable height. The position of the nose in relation to the ground will vary with the wind strength.

Vertical descent

104. The engine should be throttled down and the control column eased slowly back until an object sighted on the ground appears to remain in the same relative position. The rate of vertical descent then remains constant at about 16 - 18 ft. per second. It is not possible to judge a vertical descent by the relationship between the nose of the gyroplane and the horizon, as this depends upon the strength of the wind. Vertical descent should not be exaggerated in a calm. The fore and aft trimming bias can be used to advantage in both hover- ing and vertical descent.

APPENDIX K

Approaching to land and landing

105. Until one is accustomed to the gyroplane

it is as well to approach very much like a normal aeroplane. Later on the vertical descent can be used as a means of losing height in a plane just behind the intended landing mark, until about 70 ft. from the ground. The control column is then eased forward until an indicated gliding speed of about 40 m.p.h. is attained and the landing carried out in the usual manner by easing the control column back and finally touching the ground slightly tail first. A landing made in this manner, with a little forward speed, eases the gyroplane as a whole from excessive shock and the landing run is barely noticeable. When landing the
feet should be kept braced on the steering bar to hold the tail wheel steady.

After landing

106. (i) Put control column forward and lock in crutch.

(ii) When stationary turn to port until about 120° to wind.

(iii) Apply rotor brake gently and stop rotor.

(iv) Do not taxy until rotor is at rest.

When landing in a strong wind, the gyroplane should have a definite forward speed and a "dead stop" landing must not be attempted. Inadvertent

application of rotor brake or clutch

107. The rotor brake or clutch should not be applied in the air, but if they are applied in error, no serious results are likely to happen. The rotor brake has been designed to avoid being too fierce in action, and it should be adjusted so that its application will result in a positive but gradual deceleration, so that any undue torsion on the rotor structure is avoided. If the rotor brake is applied in flight, the gyroplane will tend to turn to the starboard, but there is no marked loss in rotor r.p.m. If the gyroplane is taken off the ground with the clutch engaged it will swerve to port, the take-off run will be shortened and the initial rate of climb improved, but the engine r.p.m. will be down. If the engine should fail in these circumstances, the dog-clutch of the mechanical drive will over-ride, and the rotor will free-wheel at its normal rate of rotation. It will be obvious that, although mechanical failure will not take place when the clutch or rotor brake is applied in the air, there is an element of risk attached when the pilot is a novice, especially when taking off, and care should be taken to avoid their misapplication.

Ballasting

108. No provision is made for ballasting.

Setting tail trimming flaps (see fig.10)

flaps:-

The following is the average setting of the tail trimming

High speed trim (A.1.- down slightly.
(A.2 - up slightly.

Torque trim (B.1 - up slightly.
(B.2 - down slightly.

Slow speed trimmer C - slightly right.

478

APPENDIX K

Having C central, A.1 down and A.2 up about 15°, B.1 and B.2 neutral, proceed as follows:-

(1) Trimming tail as a whole. Flying with C.G. in average position, tail incidence must be set to make the gyroplane slightly tail heavy, when opening throttle at any speed. If too tail heavy, increase incidence and vice-versa. Approximate angle of incidence $+1\frac{1}{2}^{o}$ to $+2^{o}$.

(ii) Engine torque correction at slow speeds. The incidence of each side should be made equal by adjusting the struts. Fly at 35 -

40 m.p.h. at full throttle and adjust both bias springs to fly "hands off." Throttle back slowly and release control column. The gyroplane should continue to be well trimmed laterally. If, after throttling back, there is a tendency to turn right, the engine torque is over corrected and the horizontal fin should be adjusted to decrease in- cidence on the starboard and increase it on the port side, and vice- versa. Fine adjustment is by means of the torque flaps B.1 and B.2.

(iii) High speed trimming. If there is a tendency to turn right at high speed, adjust A.1 down slightly and A.2 up slightly, and vice- versa. This adjustment is fine and even a slight amount will have quite a large "rudder action."

(iv) slow speed trimming. If there is a tendency to turn left at slow speed with engine on, adjust the vertical fin flap C slightly right and vice-versa. Refer back to (ii), try this at high speed and adjust B.1 and B.2 so that the gyroplane flies level at all speeds, ignoring any slight turn (if there is any). The gyroplane should tilt slightly to port after throttling back.

(v) Centralising control column. All the above adjustments are made without regard to the control column position. When the tail trimming has been corrected to the satisfaction of the

pilot, the
position of the control column may be corrected.

APPENDIX K

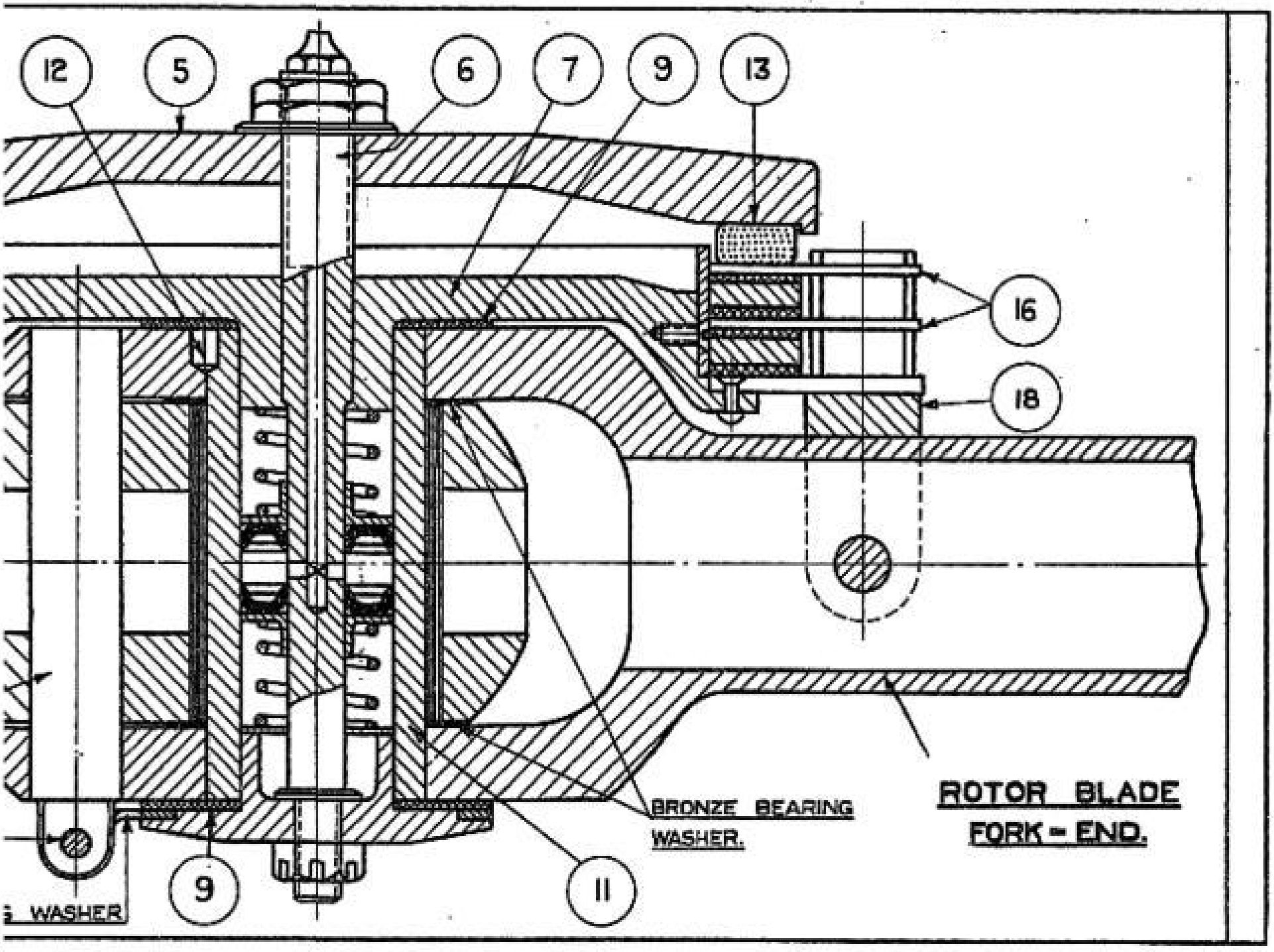
12
5
6
7
9
13
16
18
BRONZE BEARING WASHER.
ROTOR BLADE FORK - END.
9
11
WASHER

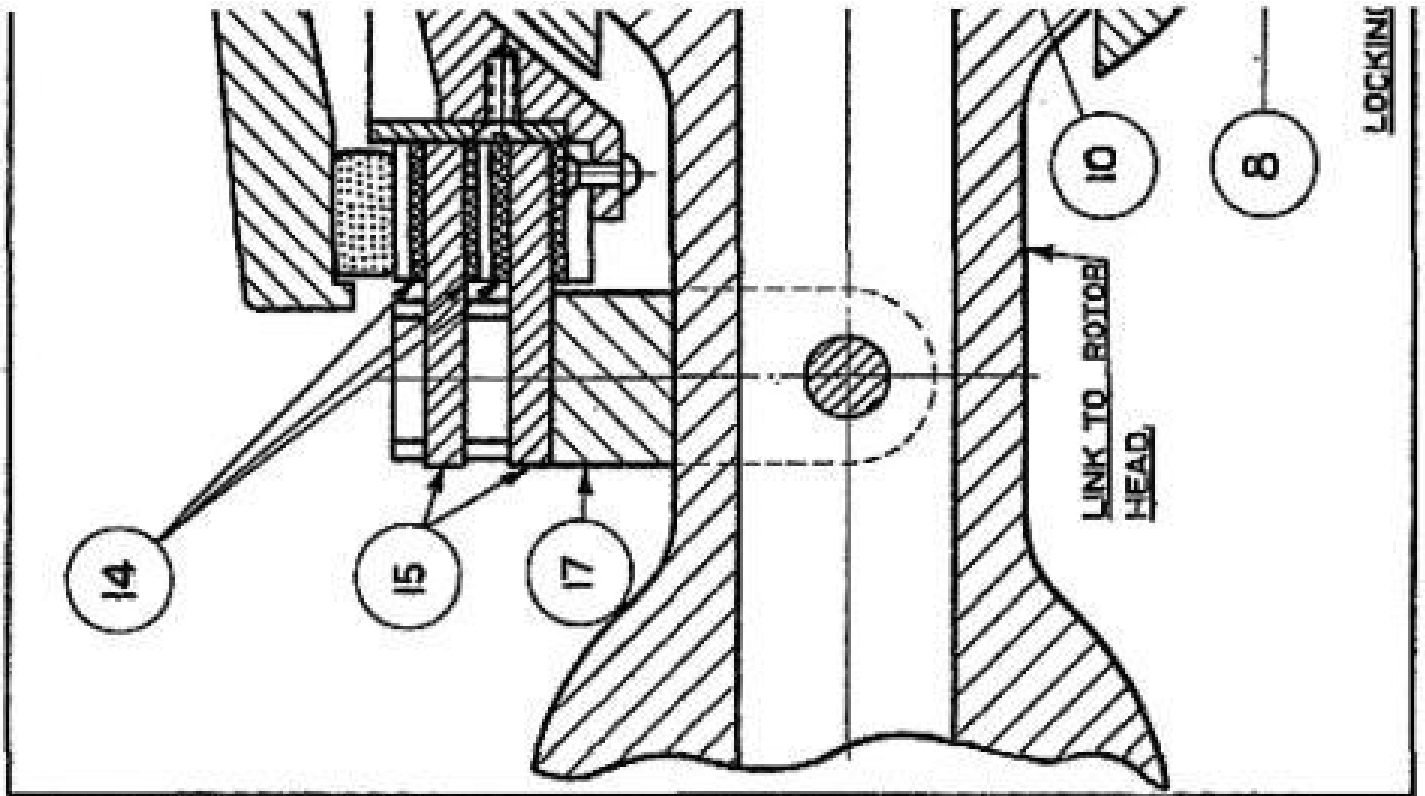

FRICTION DAMPER FOR ROTOR BLADE | FIG. I.

APPENDIX K

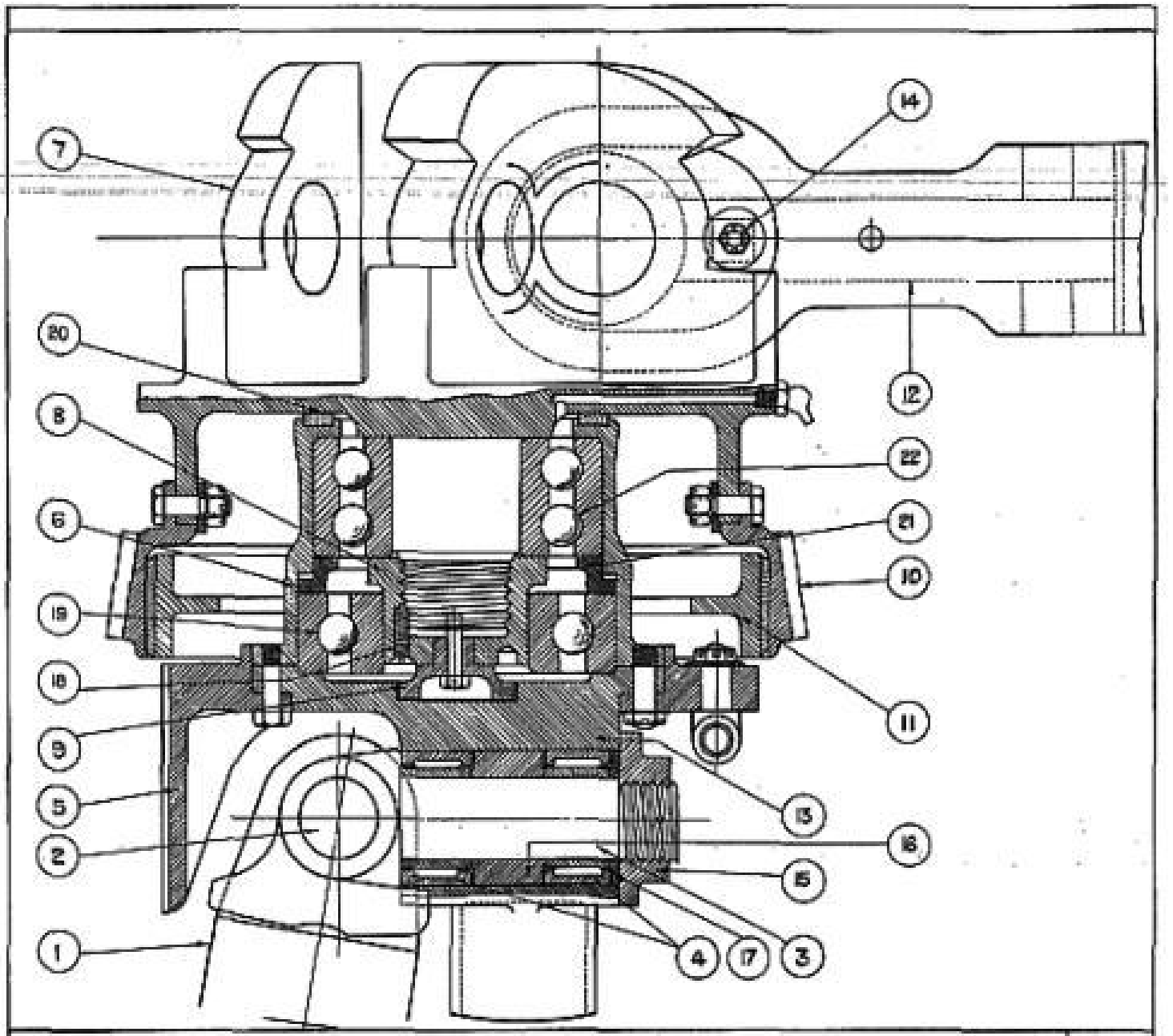

PYLON STRUCTURE AND TOP JOINT. FIG. 2.

APPENDIX K

APPENDIX K

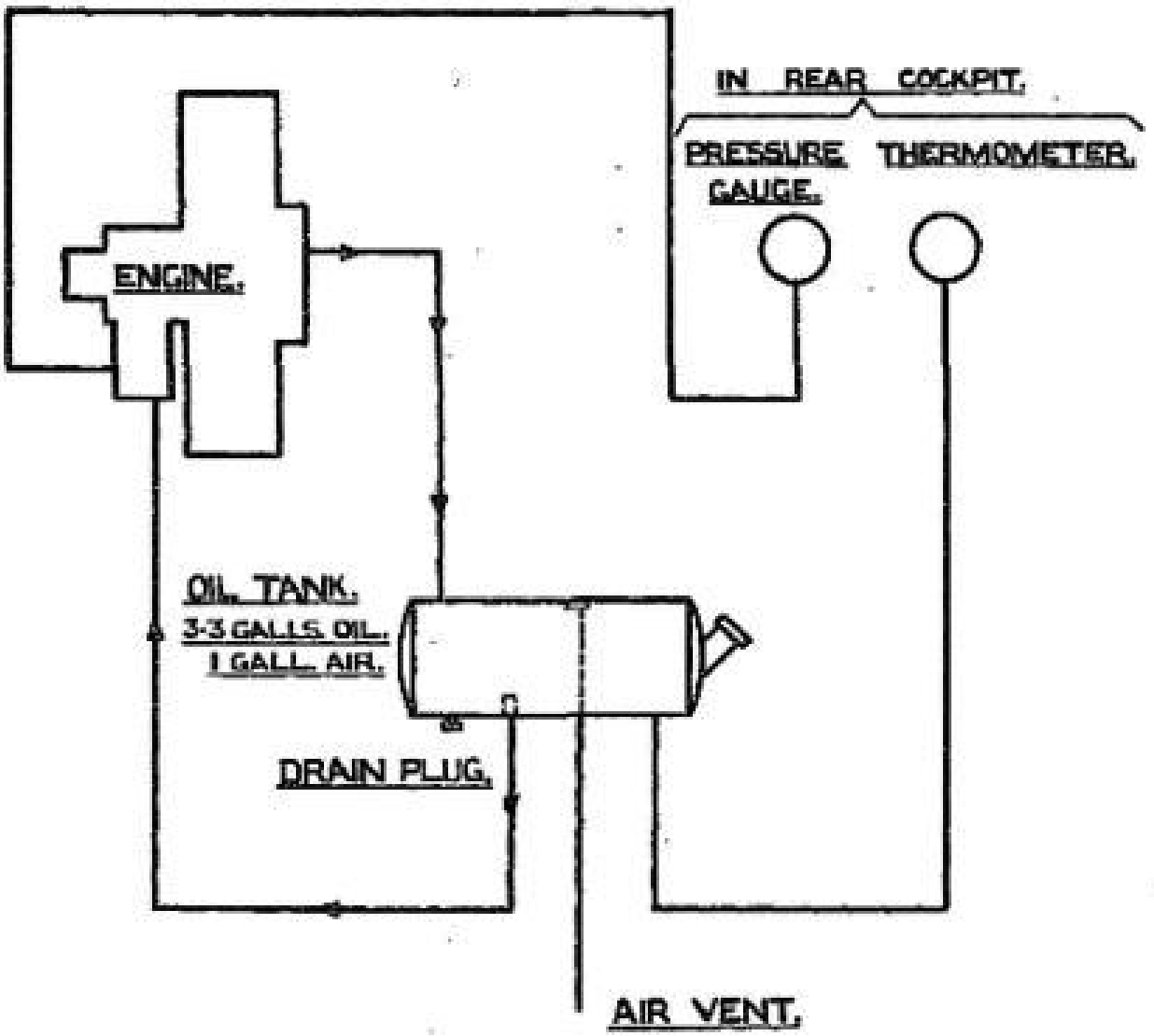
IN REAR COCKPIT.
PRESSURE GAUGE.
THERMOMETER.
ENGINE.
OIL TANK.
3-3 GALLS. OIL.
1 GALL. AIR.
DRAIN PLUG.
AIR VENT.

DIAGRAM OF OIL SYSTEM.	FIG. 4.

APPENDIX K

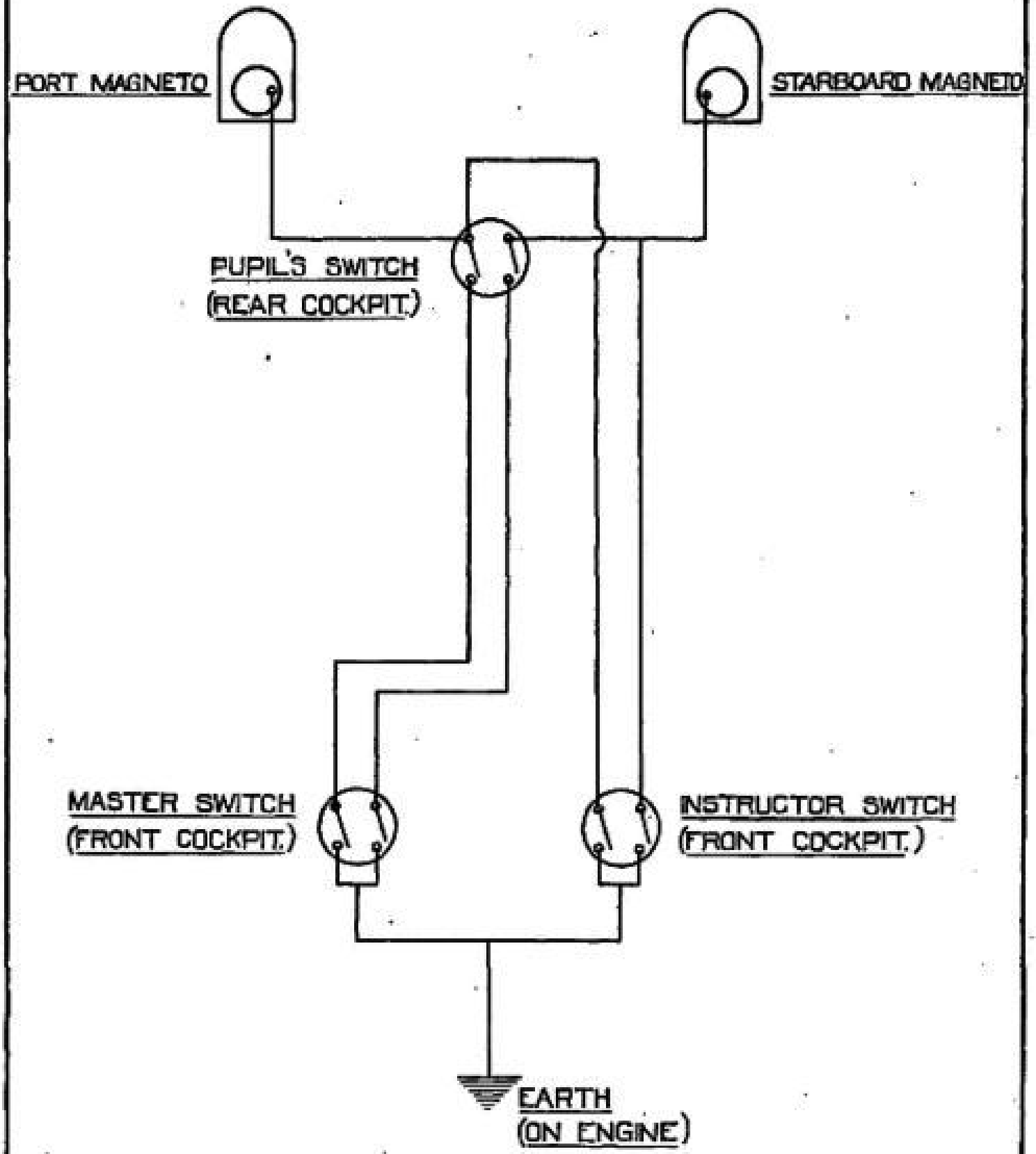
PORT MAGNETO
STARBOARD MAGNETO
PUPIL'S SWITCH
(REAR COCKPIT.)
MASTER SWITCH
(FRONT COCKPIT.)
INSTRUCTOR SWITCH
(FRONT COCKPIT.)
EARTH
(ON ENGINE)

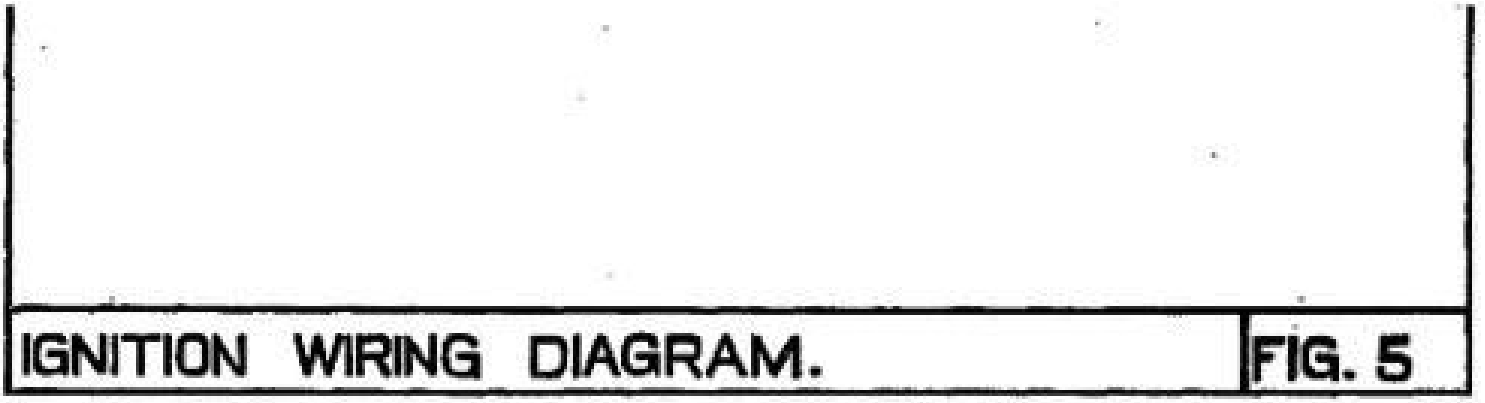

APPENDIX K

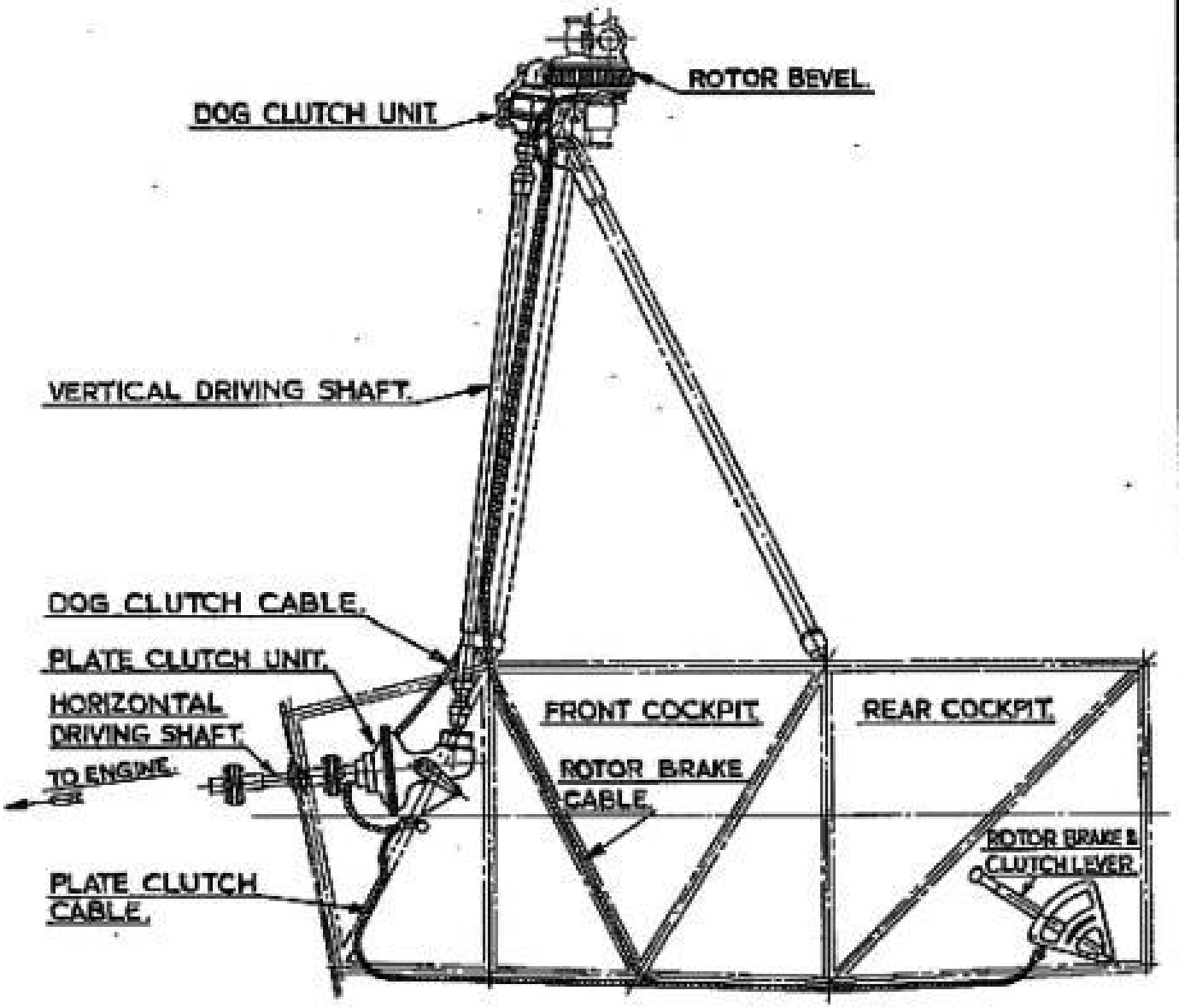
ROTOR BEVEL.
DOG CLUTCH UNIT.
VERTICAL DRIVING SHAFT.
DOG CLUTCH CABLE.
PLATE CLUTCH UNIT.
HORIZONTAL DRIVING SHAFT.
TO ENGINE.
FRONT COCKPIT.
REAR COCKPIT.
ROTOR BRAKE CABLE.
ROTOR BRAKE & CLUTCH LEVER.
PLATE CLUTCH CABLE.

MECHANICAL STARTER.	FIG. 6.

APPENDIX K

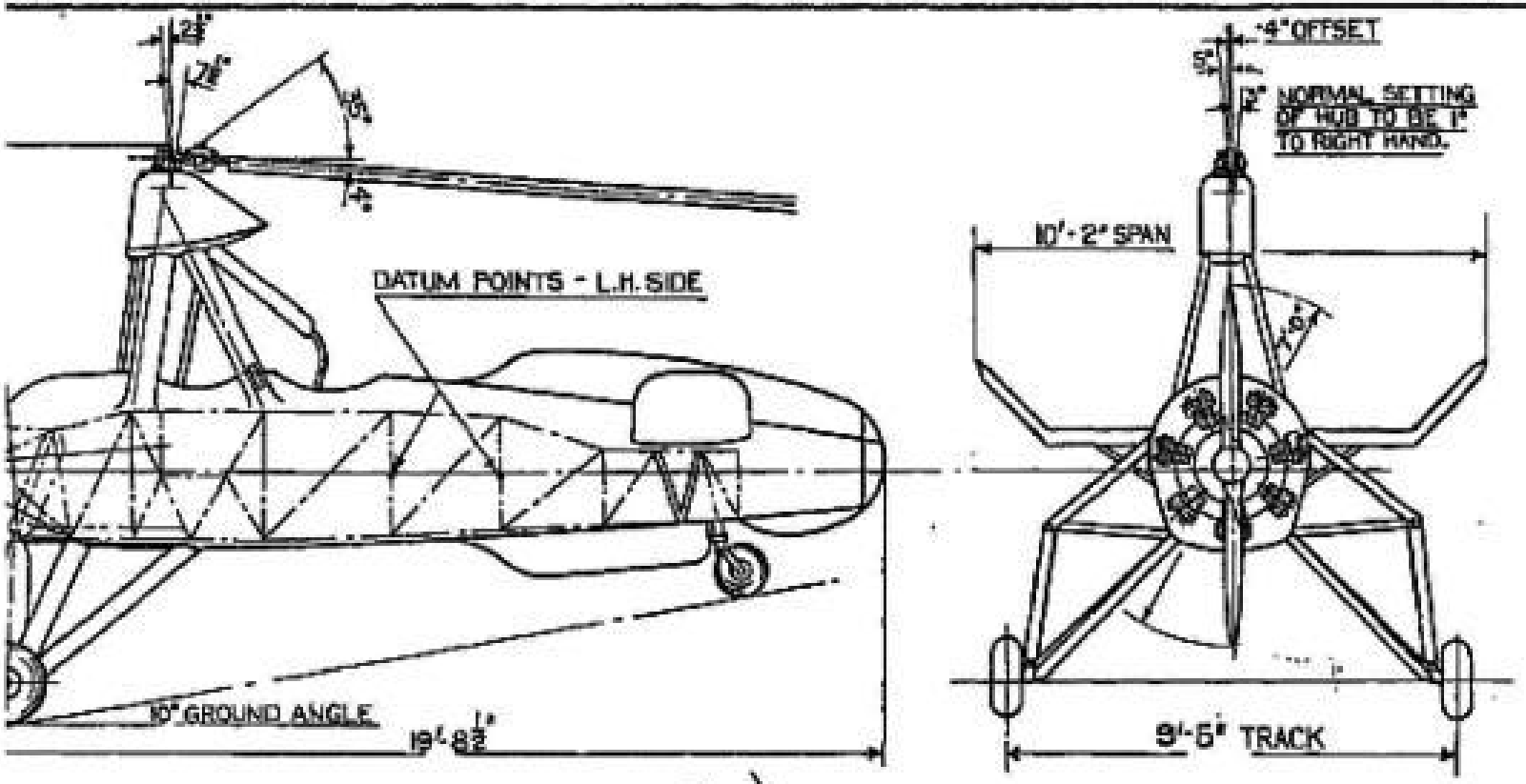

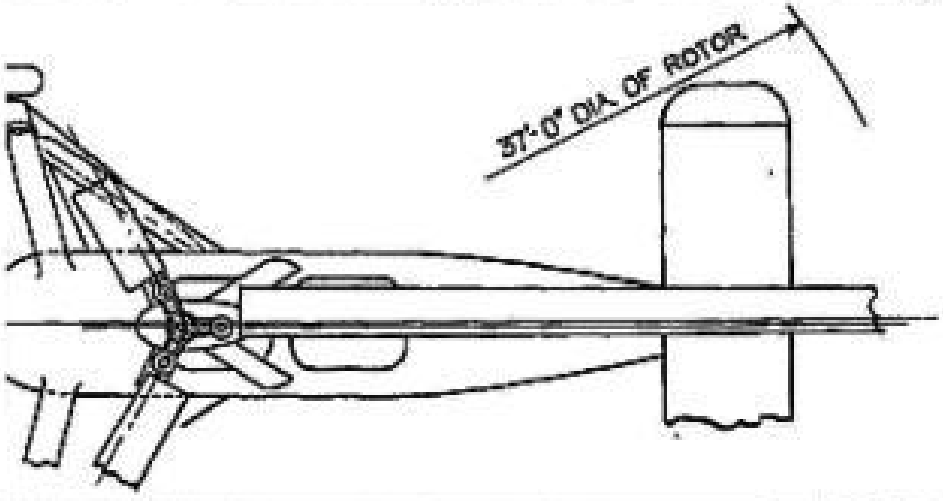

INCIDENCE OF TAIL PLANE +½° TO +2°

INCIDENCE OF ROTOR BLADE 2°·40'

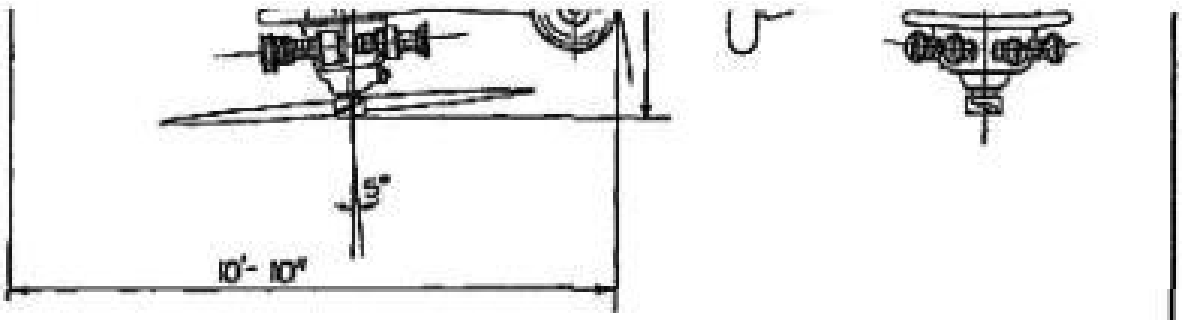

RIGGING DATA | FIG. 7.

APPENDIX K

NOTE:-

(I) THE CORRESPONDING FORK MEMBERS OR EARS ON THE TWO JOINTS MUST BE IN THE SAME PLANE, AS OTHERWISE, THE TRANSMISSION WILL NOT BE UNIFORM RESULTING IN A VERY UNEVEN VELOCITY AND OVERHEATING AT THE BALL JOINTS.

(II) IN ASSEMBLING COMPONENT PARTS OF TRANSMISSION SHAFTS, IT IS ABSOLUTELY IMPERATIVE THAT THESE SHOULD BE CO-RELATED ONE TO THE OTHER "O" TO "O", AS MARKED.

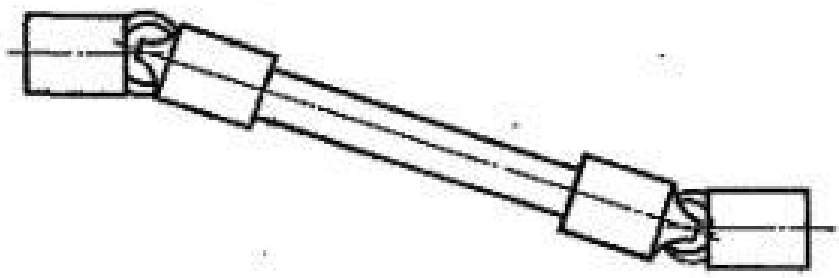

CORRECT.

(ILLUSTRATION I.)

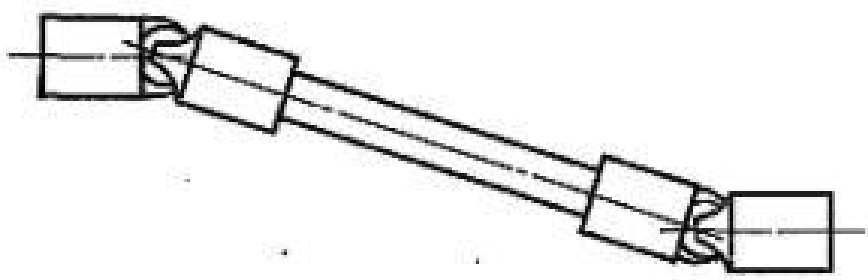

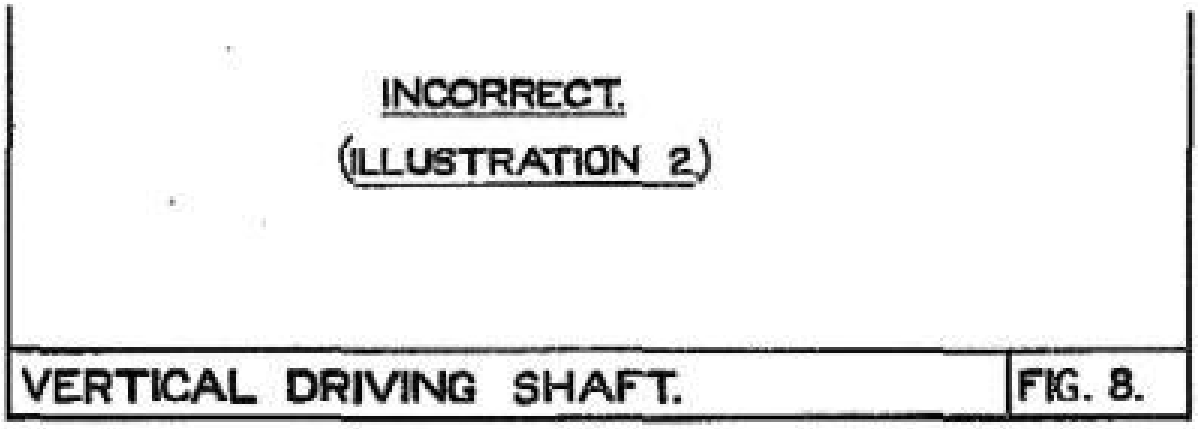

APPENDIX K

LUBRICATING DIAGRAM.

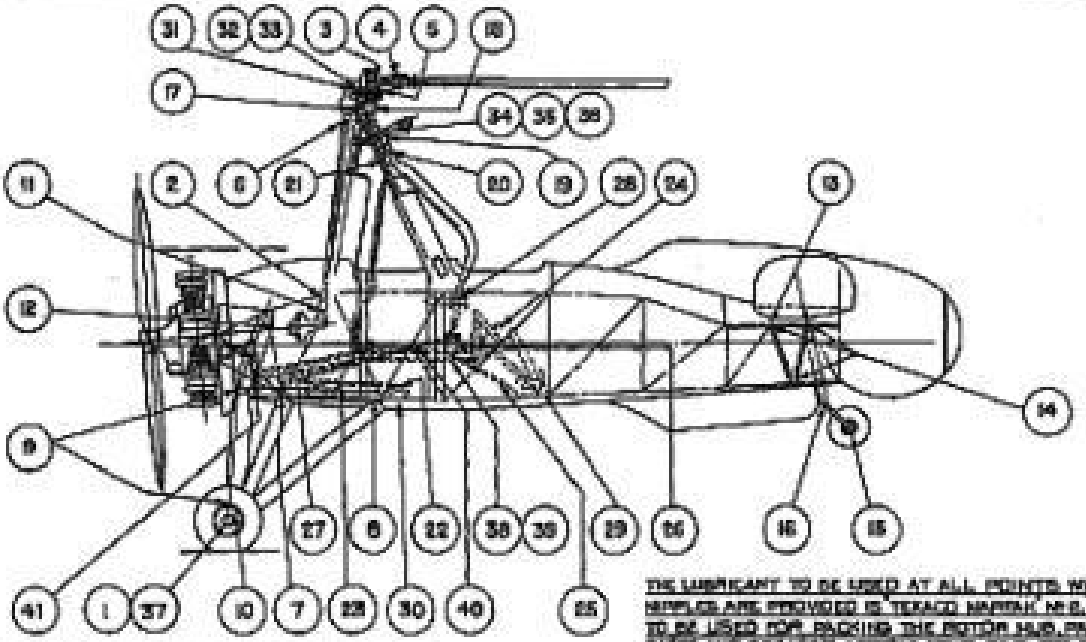

THE ITEMS MARKED * HAVE GREASE NIPPLES FITTED FOR THE USE OF A GREASE GUN.

THE LUBRICANT TO BE USED AT ALL POINTS WHERE GREASE NIPPLES ARE PROVIDED IS TEXACO MARFAK NO.0. IT IS ALSO TO BE USED FOR PACKING THE ROTOR HUB, PACKING THE BALL RACES AND GREASING ARTICULATING PINS ETC. THROUGHOUT THE ROTOR SYSTEM WHEN RE-ASSEMBLING AFTER REMANTLING. IN ALL OTHER CASES, THE TYPES OF LUBRICANT ARE LAID DOWN IN SP/RRA/0 6/P.

* (1) MAIN WHEEL BUSHES.
* (2) BOTTOM BALL JOINT (VERTICAL SHAFT)
* (3) HORIZONTAL ARTICULATING PINS.
* (4) VERTICAL ARTICULATING PINS.
* (5) ROTOR HUB AXLE.
* (6) TOP BALL JOINT (VERTICAL SHAFT)
* (7) AXLE SHACKLE BOLTS.
* (8) RADIUS ROD SHACKLE BOLTS.
* (9) GUIDE LEG TOP & BOTTOM BOLTS.
(10) RADIUS ROD BOTTOM BOLTS.
* (11) SPLINES AT BOTTOM OF VERTICAL SHAFT.
(12) BUSH IN BULKHEAD FOR CLUTCH DRIVE.
(13)
(14)
* (15) TAIL WHEEL BUSHES.
(16) PINS FOR TAIL WHEEL LEVER.
* (17) LONGITUDINAL HINGE PIN.
* (18) LATERAL HINGE PIN.
* (19) BALL JOINT AT TOP OF CONTROL COLUMN.
* (20) HINGE FORK PIN.
* (21) BALL SOCKET FOR HINGE FORK.
* (22) REAR STEERING BAR PIVOT PIN.
(23) PINS IN STEERING BAR CONNECTING ROD.
(24) FORK & ART BIAS GEAR PINS IN CABLE & SPRING.
(25) PINS IN CONNECTING ROD (QUICK RELEASE TO QUADRANT)
(26) BUSH & SPINDLE OF QUICK RELEASE GEAR.
* (27) FRONT STEERING BAR PIVOT PIN.
(28) LATERAL BIAS GEAR & PINS IN CABLE.
(29) QUADRANT RATCHETS & PINS.
(30) PINS IN STEERING BAR LEVER.
* (31) DOG CLUTCH HOUSING.
(32) PIN IN ROTOR BRAKE LEVER.
(33) PIN IN DOG CLUTCH LEVER.
(34) PINS FOR BIAS STRINGS.
(35) BEARINGS FOR BIAS LEVERS.
(36) PINS FOR BIAS CONTROL CABLES.
(37) WHEEL BRAKE GEAR INSIDE DRUM.
(38) ENGINE CONTROL PINS & BULKHEAD GUIDES.
* (39) ENGINE CONTROL QUADRANT BEARINGS.
(40) FUEL COCK CONTROL PINS & BEARINGS.
(41) ENGINE CONTROL COUNTERSHAFT BEARINGS.

FIG. 9.

APPENDIX K

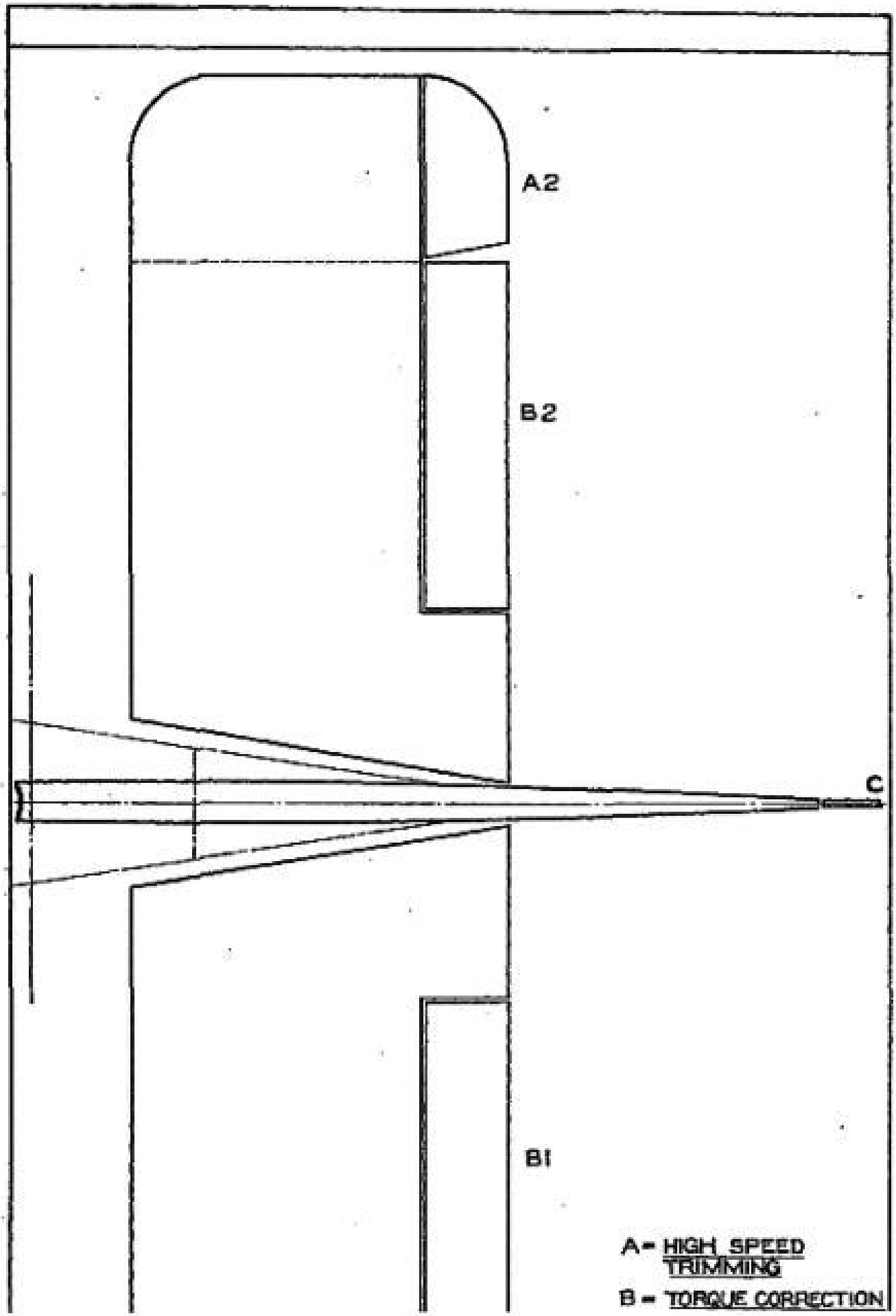
A2
B2
C
B1
A= HIGH SPEED TRIMMING
B= TORQUE CORRECTION

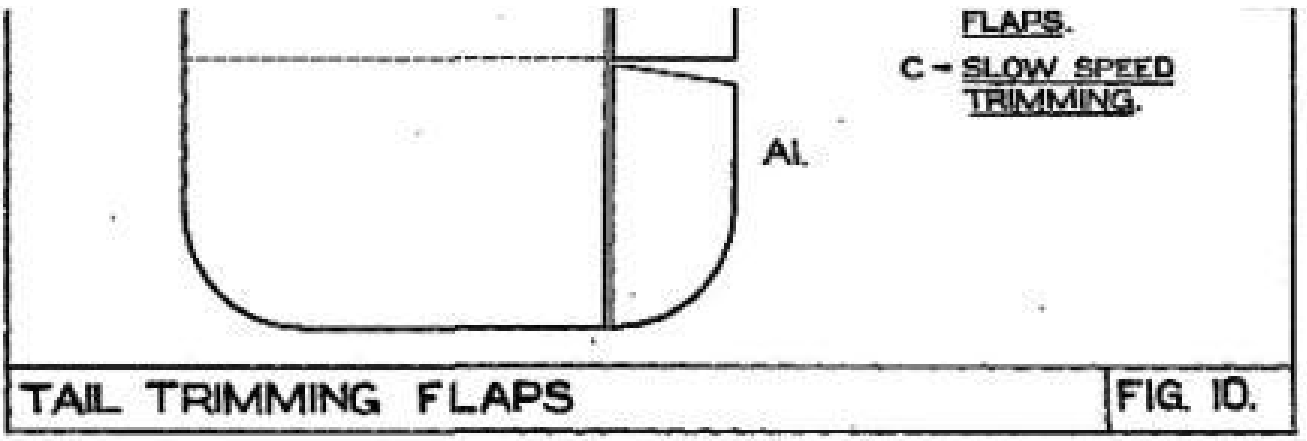

TAIL TRIMMING FLAPS | FIG. 10.

APPENDIX K

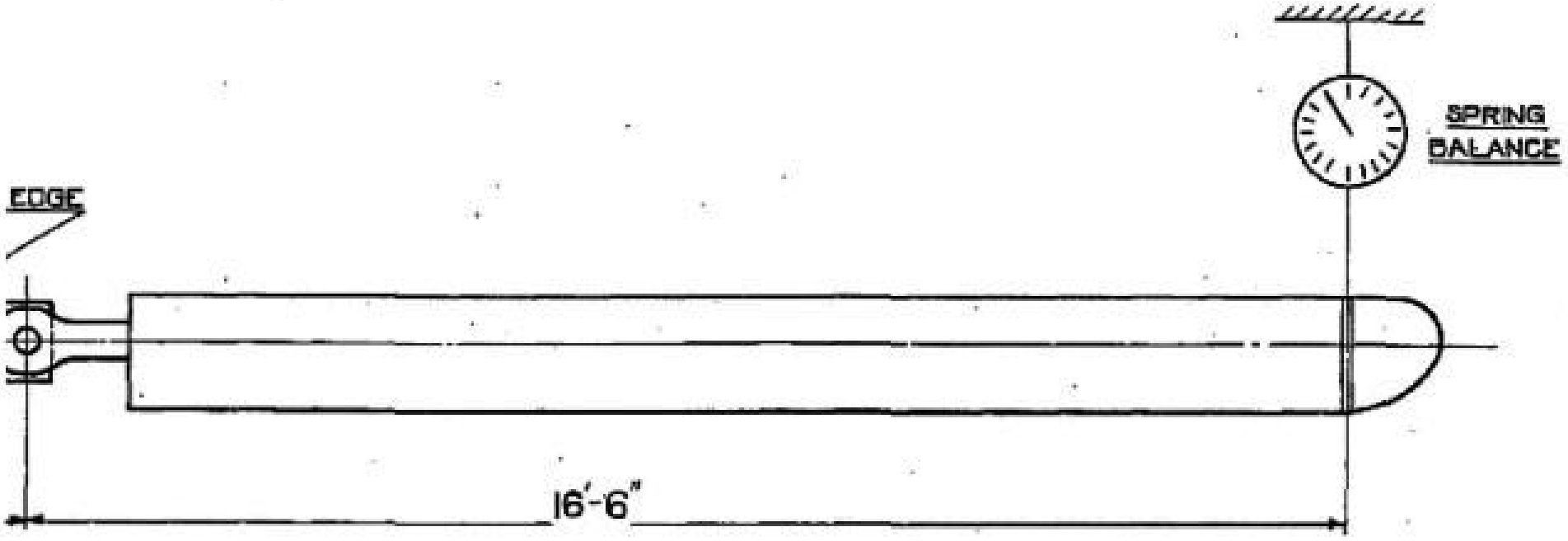

CLASS OF BLADE	W
CLASS 'A'	19LB. 8OZ.
CLASS 'B'	20LB. 2OZ.
CLASS 'C'	20LB. 12OZ.
CLASS 'D'	21LB. 6OZ.

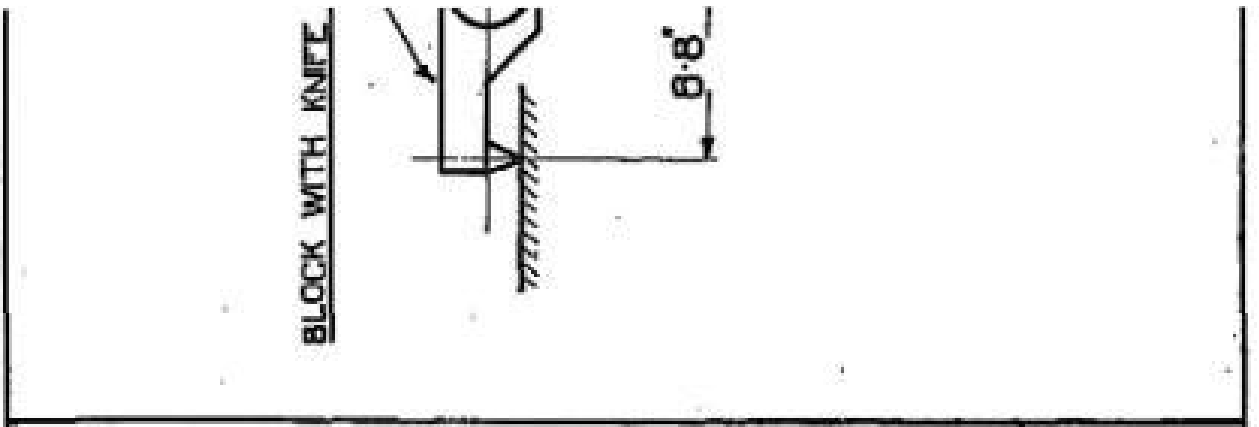

CLASSIFICATION & BALANCE OF ROTOR BLADES | FIG. 11

490

APPENDIX K

FOR OFFICIAL USE ONLY

AIR PUBLICATION 1490
(Volume II)
December, 1934

nto

PART 2

MAINTENANCE

SCHEDULE [No. 42]
ROTA WITH CIVET I
ENGINE

Note: RAF called the Genet Major MK. IA a CIVET I. See Brooks pg 189

This schedule is issued in accordance with

King's Regulations & Air Council

AIR MINISTRY

Instructions, para. 669.

491

APPENDIX K

2

MAINTENANCE SCHEDULE

1. This schedule describes the technical detail of the maintenance and shows the routine which is considered to be necessary in normal circumstances. It is not to be interpreted as absolving any persons concerned from the responsibility of acquainting themselves with or acting upon any circumstances indicating the necessity for additional work.

2. For purposes of convenient reference, the aeroplane is divided into a number of assembly groups, each having the distinguishing reference letters given below :—

Airframe

Uc. Undercarriage.
Co. Cockpits.
Fu. Fuselage.
Ta. Tail unit.
Pl. Rotor.
Ge. General.

Ig. Ignition.
Pe. Fuel system.
Ol. Oil system.
Cy. Cylinders.
As. Airscrew.
Cn. Controls.
St. Doping and starting.
Ge. General.

3. The principal feature of maintenance consists of adequate periodical inspection, the frequency of which will depend upon the nature of the assembly group and its duty.

4. The details of the inspections are given in progressive form, and for any period, the complete detail will be obtained by adding the corresponding detail for all the shorter periods.

5. The sequence of operations is to be followed as far as possible,

and where the inspections are spread over the allowable periods the appropriate tradesman is responsible that no operation is missed.

6. It is desirable, but not essential, that the hours at which periodical inspections are due should be made to correspond with the flying hours of the airframe, engine, etc., e.g., that 10-hour inspections should occur at 10, 20, 30, 40, etc., hours, that 20-hour inspections should occur at 20, 40, 60, 80, etc., hours ; and that the 40-hour inspections should occur at 40, 80 and 120 hours.

7.

Amendments.—Amendments may be deletions from or additions to the schedule. They may be circulated generally by the Air Ministry or they may be made locally as the result of accumulated experience or to meet peculiar local conditions. They are to be added in red ink on the schedule (and on the drawings), and are to be numbered in their proper sequence. Where a deletion is made, the existing number is to be cut out; it is not to be used to represent alternative work. Where an addition is made, it is to be numbered by means of a letter suffix to the number immediately preceding (e.g., P1.29.a, etc.). The Air Ministry is to be notified in April of each year through the usual channels of all amendments found necessary, together with the reasons for their adoption. This will make it possible to circulate information to other units concerned and will ensure that subsequent reprints of the schedule embody the results of accumulated maintenance experience.

MAINTENANCE SCHEDULE FOR ROTA

WITH CIVET I ENGINE

AIRFRAME

INSPECTION BETWEEN FLIGHTS

Group.
Ref.

Note.—The details of this inspection need not be entered on the Aircraft Maintenance Form.

1. See any reports on the Aircraft Maintenance Form.

2. Inspect the undercarriage for damage and see that the tyre pressures appear normal.

3.

Examine the pressure head for damage.

4. Examine the rotor blades at the tips and the leading edges for wear to the fabric, thinness of dope, or damage.

5. See that the rotor will turn easily without any A.P.1490, signs of " picking-up " or binding. For this Vol. I, operation it will be necessary to ensure that para. 40. the rotor brake and clutch are disengaged.

6. Examine each rotor blade in turn for freedom of movement in a vertical plane.

7. Examine the tail wheel for damage and see that the tyre pressure appears normal.

8. Examine the safety pins of the Sutton safety A.P.1182/
belt, in each cockpit, for distortion or fracture. B.3.

9. See that all loose articles and the locker lid K.R. &
are properly secured.
A.C.I., para. 704.

10. Report to the next pilot before he "takes off."

INSPECTION DAILY. (D.I.A.)

Notes.—See any reports on the Aircraft Maintenance Form.

The lubricant to be used at all points where A.M.O. grease nipples are provided is Texaco Marfak N.545/34. No. 2. It is also to be used for packing the rotor hub, packing the ball races and greasing articulating pins, etc., throughout the

rotor system, when reassembling after dismantling.

In all other cases the types of lubricant to be used are laid down in A.P.1464/D.68.

Details of the aeroplane are given in A.P.1490, Volume I, 1st Edition.

5

Group.
Ref.

Undercarriage. (Uc.1/4.)

Uc.1. See that the undercarriage attachments are secure.

Uc.2. See that the wheels are properly secured.

Uc.3. See that the tyre pressures

appear normal and
examine the tyres for cuts and other damage. Uc.4. Check the functioning of the oleo leg by
rocking the aeroplane.

Cockpit, rear. (Co.1/11.)

Co.1. See that the steering bar can be operated
without excessive backlash.
Co.2. Operate the control column both transversely A.P.1490,
and longitudinally and see that full and free Vol. I,
travel is obtainable without backlash. para. 43. Co.3.
Check the action of the fore and aft bias control
gear and see that it moves freely.
Co.4. Check the action of the lateral bias control

gear and see that it moves freely.

Co.5. See that the fire extinguisher is properly secured in its fitting.

Co.6. Inspect the safety belt and its anchorages for security.

Co.7. See that the windscreen is secure.

Cockpit, front.

Co.8. See that the steering bar can be operated without excessive backlash.

Co.9. Operate the control column both transversely and longitudinally and see that full and free movement is obtainable without backlash ; in particular at attachment to the rear control column.

Co.10. Inspect the safety belt and its anchorages for security. Co.11.

See that the windscreen is secure.

Fuselage. (Fu.1.)

Fu.1. See that the fabric covering and fabric lacing are undamaged.

APPENDIX K

6

Group. Ref.

Tail Unit. (Ta.1/5.)

Ta.1.

Inspect the top and bottom vertical fins, and the horizontal fin and tips for external damage.

Ta.2. Inspect the bracing struts of the horizontal fin for damage.

Ta.3. See that the tail wheel is properly secured.

Ta.4. See that the tail wheel tyre pressure appears normal and examine the tyre for cuts or other damage.

Ta.5. Check the functioning of the tail oleo leg by lifting or rocking the aeroplane.

Rotor. (Pl.1/6.)

Pl.1. Inspect the tips and leading edges of the rotor blade for damage, wear of fabric or thinness

of dope.

Pl.2.

See that the rotor will turn easily without any sign of " picking-up " or binding. For this, it will be necessary to ensure that the rotor brake and clutch are disengaged. A.P.1490, Vol. I, para.40.

Pl.3. Examine each rotor blade in turn for freedom of movement in a vertical plane.

Pl.4.

Inspect and lubricate vertical and horizontal articulating pins.

Note.—Tecalemit nipples are fitted. A.P.1490, Vol. I, fig. 9, refs. 3 & 4.

Pl.5. Lubricate the rotor hub axle.

A.P.1490, Vol. I, fig. 9,

Note.—A Tecalemit nipple is fitted.

ref.

Pl.6.

5. Check the setting for the friction dampers (the " pull-off ") for each rotor blade. A.P.1490, Vol. I, para. 77.

General. (Ge.1/4.)

Ge.1. See that all cowling panels and inspection doors are undamaged and securely fastened.

Note.—Turnbuttons should all be in the line of flight.

Ge.2. See that all loose articles are properly secured. K.R. & A.C.I., para. 704.

Group Ref.

General. (Ge.1/4)—*cont.*

Ge.3. Keep the aeroplane and cockpits clean.

Ge.4. Make the necessary entries on the Aircraft Maintenance Form. K.R. & A.C.I., paras. 669 & 671.

INSPECTION EVERY 10 HOURS. (10 I.A.)

Undercarriage. (Uc.21/25.)

Uc.21. Lubricate the shackle bolts at the fuselage A.P.1490,

ends of the axles and radius rods

and see that Vol. I,
they are securely locked.
Note.—Tecalemit nipples are fitted.
fig. 9,
refs. 7 & 8.

Uc.22. Lubricate the bolts at both ends of the oleo A.P.1490,
leg and see that they are securely locked.
Note.—Tecalemit nipples are fitted.
Vol. I,
fig. 9,
ref. 9.

Uc.23. Lubricate the bolts at the bottom end of the A.P.1490,
radius rod and see that they are securely Vol. 5,
locked.
fig. 9,
ref. 10.

Uc.24. See that all axle, radius rod and oleo leg
fairings are secure.

Uc.25. Lubricate the wheel bushes.

A.P.1490,

Note.—Tecalemit nipples are fitted. It will be necessary to remove the wheel fairing disc to obtain access. Vol. I, fig. 9. ref. 1.

Cockpits. (Co.21/26.)

Note.—The following inspection should be carried out in the rear cockpit.

Co.21. Operate the brake lever to ensure correct functioning of brake control.

Co.22. Operate the rotor brake and then the rotor clutch lever to ensure their correct functioning. A.P.1490, Vol. I, para. 85.

Co.23. Check the operation of the quick release lever by locking on the wheel brake lever and either the rotor brake or clutch lever, and ascertaining that it releases them. Also check that, with the control column locked in its

crutch, the quick release lever is locked.

Co.24. Inspect the four seat attachment points for security and damage.

APPENDIX K

Group.
Ref.

Cockpits. (Co.21/26)—*cont.*

The following inspection should be carried out in the front cockpit.

Co.25. Lubricate the bottom universal ball joint on A.P.1490, the vertical transmission shaft.

Vol. I,

Note.—A Tecalemit nipple is fitted. Access is obtained by removing the clutch cover. fig. 9, ref. 2.

Co.26. Inspect the four seat attachment points for security and damage.

Fuselage. (Fu.21/24.)

Fu.21. Lubricate the splines at the bottom of the A.P.1490, vertical transmission shaft.

Vol. I,

Note.—A Tecalemit nipple is fitted. Access fig. 9, is obtained by removing the top cowl panel. ref. 11.

Fu.22.

Inspect the top and bottom attachments of the tail wheel oleo leg to the top and bottom longerons and see that they are secure.

Note.—Access is obtained

through an in-
spection door at the end of the fuselage.

Fu.23. Check the correct relationship between the A.P.1490,
friction clutch and the dog clutch.
Ensure Vol. I,
that the dog clutch engages before the friction para. 85.
clutch.

Note.—Access to the control quadrant is
obtained through a door in the fairing on the
left-hand side of the rear cockpit.

Fu.24. Lubricate the gland in the bulkhead for the A.P.1490,
clutch drive.
Vol. I,
fig. 9, ref. 12.

Tail Unit. (Ta.21/27.)

Ta.21. Inspect the four points of attachment of the horizontal fin to the fuselage for security.

Ta.22. Inspect the horizontal fin stay tube attachments to the horizontal fin and fuselage for security.

Ta.23. Lubricate the tail wheel bushes. A.P.1490, Vol. I, fig. 9, ref. 15.

Note.—A Tecalemit nipple is fitted.

Ta.24. Examine tail wheel check cables for damage.

Group.
Ref.

Tail Unit. (Ta.21/27)—*cont.*

Ta.25.

Inspect and lubricate the pins at the tail A.P.1490,
wheel lever and examine the external run of Vol. I,
cable for corrosion and fraying
where they fig. 9,
pass through fairleads.
ref. 16.

Ta.26. Inspect the trimmers on the horizontal fin
and tips for damage and security.

Ta.27. Inspect the vertical fin trimmer attachments
for damage and security.

Rotor. (Pl.21/29.)

Note.—It will be necessary to remove rotor head fairing for these inspections.

Pl.21. Inspect the attachments of the pylon struts to fuselage and rotor head for security.

Pl.22. Inspect the attachments of the control columns for security.

Pl.23. Inspect for security and lubricate each side A.P.1490, the longitudinal hinge pin. Inspect for any Vol. I, backlash or wear. The clearance between para. 36, the nut and hub must not exceed ·002 in. fig. 9, Check with a feeler gauge. ref. 17.

Note.—A Tecalemit nipple is fitted on each side.

Pl.24. Inspect for security and lubricate the lateral A.P.1490,
hinge pin. Inspect for any backlash or wear. Vol. I,
The clearance between the nut and hub must para. 36,
not exceed ·002 in. Check with a feeler fig. 9,
gauge.
ref. 18.

Note.—A Tecalemit nipple is fitted on the
right-hand side.

Pl.25. Lubricate the ball joint at the top of the A.P.1490,
control column.
Vol. I,

Note.—A Tecalemit nipple is fitted. fig. 9,

ref. 19.

Pl.26. Inspect for security and lubricate the hinge A.P.1490,
fork pin for the control column.
Vol. I,
Note.—A Tecalemit nipple is
fitted. fig. 9,
ref. 20.

Pl.27. Inspect for security and lubricate the ball A.P.1490,
socket for the fork on the cross shaft.
Vol. I,
Note.—A Tecalemit nipple is fitted.
fig. 9,
ref. 21.

APPENDIX K

10

Group.

Ref.

Rotor. (Pl.21/29)—*cont.*

Pl.28. Inspect for security, damage or wear, the four bias springs and their anchorages.

Pl.29. Lubricate the top universal and ball joints on A.P.1490, the vertical transmission shaft. Vol. I, *Note.*—Tecalemit nipples are fitted. ref. 6.

INSPECTION EVERY 20 HOURS. (20 I.A.)

Undercarriage. (Uc.31/33.)

Uc.31. Check the oil content of the oleo leg. A.P.1490, *Note.*—See the instructions on

the oleo leg Vol. I,
fairing.

para. 67. Uc.32. Check the tyre pressures by gauge.

Note.—The correct pressure is 20 lb. per
square inch.

Uc.33. Try the brakes for simultaneous operation and
ensure that the shoes are not rubbing when
the brake lever is released.

Cockpit. (Co.31/40.)

The following inspections should be carried
out in the rear cockpit.

Co.31. Inspect the steering bar for security and A.P.1490,
lubricate the pivot pin.
Vol. I,

Note.—A Tecalemit nipple is fitted.

fig. 9,
ref. 22.

Co.32. Inspect for security and lubricate the connecting rod at the joint between the front and rear steering bars. A.P.1490, Vol. I, fig. 9, ref. 23.

Co.33. Inspect the fore and aft bias lever and spring for security and lubricate the pins. A.P.1490, Vol. I, Examine the cable splice and shackle for security and lubricate the pin. fig. 9, ref. 24.

Co.34. Examine the cable for wear and fraying, especially where it runs over the pulley. Lubricate the pin through the pulley. A.P.1490, Vol. I, fig. 9, ref. 24.

Co.35. Inspect the connecting rod from the quick A.P.1490,
release lever to the brake and the
rotor control Vol. I,
quadrant for damage and lubricate the pins. fig. 9,
ref. 25.

500

APPENDIX K

11

Group.
Ref.

Cockpit. (Co.31/40)—*cont.*

Co.36.

Inspect for security and take up any slack in A.P.1490,
the Bowden cable from the quick release lever Vol. I,
to the control column crutch.
Lubricate the fig. 9,
slide and spindle of the quick release gear. ref. 26.
Inspect the control column locking crutch

and the clip for security.

The following inspections should be carried out in the front cockpit.

Co.37.

Inspect the steering bar for security. Lubricate the steering bar pivot pin. *Note.*—A Tecalemit nipple is fitted.	Lubri-	A.P.1490, Vol. I, fig. 9, ref. 27.

Co.38.	Inspect for security and lubricate the connecting rod at the joint between the front and rear steering bars.	A.P.1490, Vol. I, fig. 9, ref. 23.

Co.39.	Inspect for security and lubricate the lateral bias gear mounted at the front of the rear instrument board on the right-hand side. Inspect the cable for wear and fraying, especially where it runs over the two pulleys. Lubricate the pins through the pulleys.	A.P.1490, Vol. I, fig. 9, ref. 28.

Co.40. Inspect for security the attachments of the
Bowden cables to the clutch lever.

Fuselage. (Fu.31/34.)

Fu.31. Inspect the wheel brake, rotor clutch and A.P.1490,
brake control quadrant for security and lubri- Vol. I,
cate the ratchet gear and all pins. Inspect for fig. 9,
security and take up any slack in the Bowden ref. 29.
cables at the quadrant.
Note.—Access is through a door in the
fairing on the left-hand side of the rear
cockpit.

Fu.32.

Inspect the rear steering bar attachment bolts A.P.1490,
for security. Inspect the cable splices, pins, Vol. I,
and shackles for wear, damage
and security fig. 9,
and lubricate the pins.
ref. 30.

Inspect and take up any slack in the Bowden cables.

Note.—Access is by a door in the fairing
under the cockpit.

Group.

Fuselage. (Fu.31/34)—*cont.*

Ref. Fu.33. Inspect the front steering

bar attachments for security.

Note.—Access is through a door in the fairing under the cockpit.

Fu.34. Check the air speed indicator pipe lines for leaks. A.P.1275, Vol. I, chap II, para. 27.

Tail Unit. (Ta.31/35.)

Ta.31. Check the correct oil content of the tail wheel oleo leg. A.P.1490, Vol. I,

Note.—See the instructions on the leg. para. 74.

Ta.32. Check the tyre pressure by gauge.

Note.—The correct pressure is 30 lb. per square inch.

Ta.33. Inspect the tail wheel lever for damage and security.

Ta.34. See that the bolts securing the tail wheel are secure.

Ta.35. Inspect the tail wheel fork for damage and security.

Rotor. (Pl.31/38.)

Pl.31.

Inspect the pylon strut attachments to the fuselage and rotor head for corrosion and see that they are secure and properly locked.

Pl.32. Inspect for wear, damage and security the A.P.1490,
friction damper plates and discs, studs and Vol. I,
spigot for each blade.
para. 35,
Note.—The grease well is to be filled with fig. 1.
lubricant when replacing.

Pl.33. Lubricate the dog clutch. A.P.1490,
Note.—A Tecalemit nipple is fitted. Vol. I,
fig. 9, ref. 31.

Pl.34. Inspect the rotor brake Bowden cable for A.P.1490,
security and take up any slack. See that the Vol. I,
brake shoes are not rubbing when the brake fig. 9,
lever is released. Lubricate the

pin at the ref. 32.

lever and see that it is secure.

502

13

Group.
Ref.

Rotor. (Pl.31/38)—*cont.*

Pl.35. Inspect the dog clutch Bowden cable for A.P.1490,

security and take up any slack. Lubricate Vol. I,

the pin at the lever and see that it is secure. fig. 9,

ref. 32.

Pl.36.

Inspect for security and lubricate the pins securing the four bias springs. A.P.1490, Vol. I, fig. 9, ref. 34.

Pl.37. Lubricate the bearings of the levers actuating the fore and aft and lateral bias springs. A.P.1490, Vol. I, fig. 9, ref. 35.

Note.—Oil holes are provided.

Pl.38. Inspect for stretch or fraying the control cables for bias spring levers. A.P.1490, Vol. I, fig. 9, ref. 36.

Examine cable splices and pins for wear, damage and security, and lubricate the pins.

INSPECTION EVERY 40 HOURS. (40 I.A.)

Undercarriage. (Uc.61/64.)

Uc.61. Remove the wheels and inspect the axle stub A.P.1490,
for damage.
Vol. I,
para. 72.

Uc.62. Examine the brake linings for wear and cracks A.P.1490,
and lubricate the working parts of the brake Vol. I,
gear in the drum very sparingly.
para. 70,
fig. 9,
ref. 37.

Uc.63. Examine the bearings and see that the wheels
are replaced securely and with the nut and split
pin in position.

Uc.64. See that there is no excessive slackness of the wheels on the axle stub. Check that there is no side play on the wheels.

Fuselage. (Fu.61.)

Fu.61. Inspect the engine ring, struts and attachment fittings at the fuselage, including all bolts, for security.

Note.—The cowling must be removed.

Group.
Ref.

Tail Unit. (Ta.61/64.)

Ta.61.
Remove the tail wheel and inspect the axle for damage. A.P.1490, Vol. I, para. 62.

Ta.62.

Examine the bearings and see that the wheel is replaced securely with the nuts and split pin in position.

Ta.63. See that there is no excessive slackness of the wheel on the axle.

Ta.64. Inspect the horizontal and vertical fins externally for signs of internal damage.

Rotor. (Pl.61/63.)

Pl.61. Inspect for wear the horizontal and vertical A.P.1490,

articulating link pins for each blade. Check Vol. I,
that with the blade removed the rotor link paras. 34

will just drop by its own weight and that there & 76.

is no " play " in any of the pins. Check that

no " picking-up " has taken place between

the jaws of the rotor head and the fork end

on the rotor blade.

Note.—This only applies to the earlier

gyroplanes, as on later types a bronze wearing

washer is fitted at these points. In carrying

out the inspection special care should be taken

when driving out the pins holding the rotor blade to the rotor head.

Pl.62. Check the movements of the rotor head and A.P.1490, inspect for any signs of " play." Vol. I, fig. 7.

Pl.63. Inspect each rotor blade externally for any sign of internal damage to the ribs, leading and trailing edges or of the attachments of the tip or the fork at the root.

INSPECTION EVERY 120 HOURS. (120 I.A.)

Fuselage. (Fu.101/103.)

Fu.101. Remove or fold back the fuselage fabric and A.P.1464/
inspect the fuselage members for bowing, D.29.
damage and corrosion, and check the security
of the fairing and decking clips on the longeron.

15

Group.
Ref.

Fuselage. (Fu.101/103)—*cont.*

Fu.102. Check the tension of all bracing wires and the
locking of stringers.
Note.—Before any

adjustments are made,

the aeroplane must be put into the rigging position.

Fu.103. Dismantle the clutch and examine the plates for wear, damage or security. The plates should be dry and any signs of grease removed. They are to be packed with grease and the ball races lubricated, avoiding excess of lubricant. For this inspection the fuel tank must be removed. A.P.1490, Vol. I, paras. 86 & 90.

Rotor. (Pl.101/103.) Pl.101.

Inspect the pylon struts for any signs of bowing.

A.P.1464/ D.29.

Pl.102.

Dismantle the rotor head and inspect for wear, damage and security. A.P.1490, Vol. I, para. 89.

Pl.103.

Inspect the rotor blades for any signs of bowing and check the weights to ensure they are still in static balance.

General. (Ge.101.)

Ge.101. Carry out a check on the rigging of the complete aeroplane. A.P.1490, Vol. I, fig. 7.

505

APPENDIX K

INSPECTION BETWEEN

Group.

FLIGHTS

Note.—The details of this inspection need not be entered on the Aircraft Maintenance Form.

Ref.

1. See any reports on the Aireraft Maintenance Form.

2. See that the switches are " off."

3. Inspect the airscrew for damage.

4. Make a general examination of the fuel and oil systems for obvious leaks.

A.P.1490, Vol. I,

para. 49.

5. Replenish the fuel and oil tanks if necessary A.P.1464/
and see that the filler caps are properly secured. G.24.

A.P.957, para. 52.

6. See that no cowling panels appear loose or
cracked.

7. Report to the next pilot before he "takes off"
and state the approximate amount of fuel and
oil in the tanks.

INSPECTION DAILY. (D.I.E.)

Note.—See any reports on the Aircraft

Maintenance Form.

Ignition. (Ig.1/2.)

Ig.1. Inspect the switches for correct mechanical A.P.1490, functioning and see that they are "off." Vol. I, fig. 5.

Ig.2. See that all H.T. leads and sparking plug connections are secure and the plugs undamaged.

Fuel System. (Pe.1.)

Pe.1. Inspect the unions and pipe lines for leaks. A.P.1490, Vol. I, para. 49.

17

Group.
Ref.

Oil System. (Ol.1.)

Ol.1.

Inspect the pipe lines and unions for security and for leaks, particularly on the suction side of the pressure pump. A.P.1490, Vol. I, para. 51.

Cylinders. (Cy.1/4.)

Cy.1.

See that the sparking plug and other cylinder joints are tight.

Cy.2. Inspect the valve springs for fractures and the rocker arms for damage.

Cy.3. Check (without feelers) for excessive valve clearance.

Cy.4. Inspect the exhaust manifold for security.

Airscrew. (As.1.)

As.1. See that the airscrew hub is tight upon the airscrew shaft.

Note.—After initial attachment the air-screw should be examined for tightness at the end of each of the first one or

two flights.

Controls. (Cn.1.)

Cn.1. Test the throttle and mixture controls from both cockpits for freedom of movement.

General. (Ge.1/5.)

Ge.1. Remove oil and dirt.

Ge.2. Replenish the fuel and oil tanks if necessary, A.P.1490, and see that the filler caps are firmly secured. Vol. I, *Note.*—The fuel filler is in the centre of the paras. 48 top aluminium panel aft of the bulkhead. & 50. Access to the oil filler is through a hand A.P.957, hole on the left-hand side aluminium panel in para. 52. front of the bulkhead. A.P.129,

para. 167.

Ge.3. See that no tools or rag are left lying on the engine. Ge.4. Inspect the engine cowling for security.

Note.—All turnbuttons must be in the line of flight.

Ge.5. Make the necessary entries on the Aircraft K.R. & Maintenance Form.

A.C.I., paras. 669 & 671.

APPENDIX K

INSPECTION EVERY 10

HOURS. (10. I.E.)

Group.

Ref.

Fuel System. (Pe.21/23.)

Pe.21. Remove and clean the filter on the bulkhead.

Note.—When the filter is dismantled, see that the gauze is not damaged ; and do not use rag for cleaning. Ensure that the filter is locked when it is reassembled.

Pe.22. Check for flooding of the carburettor under the pressure of the normal working head of fuel.

Pe.23. Inspect the tank for security and leaks.

Oil System. (Ol.21/23.)

Ol.21. Remove and clean the scavenge pump filter. Ol.22. Remove and clean the

pressure filter.

Note.—When the filters are dismantled see that the gauze is not damaged and do not use rag for cleaning. Ensure that the filter base is locked when it is reassembled.

Ol.23. Inspect the tank for security and leaks.

Cylinders. (Cy.21/25.)

Cy.21.

Inspect for wear at the rocker sockets and their enclosed steel thrust pads and at the corresponding ends of the tappet rods.

Cy.22. Inspect the steel striking pins at the valve ends of the rocker arms for wear.

Cy.23.

Check the valve clearances with feelers.

Cy.24. See that the locking ring on each cylinder is tight ; avoid overtightening the bottom ring, which may deform the cylinder or crack the ring.

Note.—After initial attachment the rings should be checked up at the end of each of the first one or two flights.

Cy.25.

Inspect exhaust manifold for excessive burning or cracks.

Airscrew. (As.21.)

As.21. See that the hub bolts are secure and properly locked with the tab washers.

19

Group.

Ref.

Controls. (Cn.21/24.)

Cn.21. Examine the connecting rods of the throttle A.P.1490,

and mixture controls and see that they are secure; lubricate the pivot points, fork ends and fireproof bulkhead slides. Vol. I, fig. 9, ref. 38.

Note.—On the left-hand side of the fuselage. Cn.22. Lubricate the bearings of the engine control A.P.1490,

hand-levers.

Vol. I,

Note.—On the left-hand side of

the fuselage. fig. 9,
Tecalemit nipples are fitted.

ref. 39. Cn.23. Inspect for security and lubricate the bearings, A.P.1490,
fork ends and pins of the fuel cock control. Vol. I,
Note.—On the right-hand side of the fuse- fig. 9,
lage.

ref. 40. Cn.24. Inspect for security and lubricate the bearings A.P.1490,
of the engine control countershafts.
Note.—On the lower side struts engine mounting.

INSPECTION EVERY 20 HOURS.

Ignition. (Ig.31/35.)

Ig.31. Remove and clean the sparking plugs.

Vol. I,
of the fig. 9,
ref. 41.
(20 I.E.)
Re-set A.P.1464/

the gaps and test the plugs at a pressure of 100 lb. per square inch. B.12.

Note.—Graphite should be used on the screw threads when refitting the plugs. Ig.32. Check the gap between the magneto contact breaker points and see that the rocker arm

is free and that the points are securely locked.

Note.—When carrying out this check see

that the rocker arm is riding on the highest

point of the cam, and apply finger pressure

to ensure that the contact breaker is home

in its housing.

Ig.33. Clean and examine the distributor and con-

tact breaker covers for cracks, and see that

Ig.34.

the connections to each are tight.

Inspect the runs of the H.T. cables for

damage; the cables must not be tightly

stretched.

Ig.35. See that the run of the L.T. cables is free

from oil, that it is secure against fire in any part of the airframe, and that it is not in contact with any parts likely to become hot.

APPENDIX K

Group.
Ref.

Fuel System. (Pe.31/33.)

Pe.31. Break the pipe connection at the carburettor and check that the fuel flow is not restricted. Pe.32. Inspect the superflexit between the tank and A.P.1464/ filter and the filter and the engine

for kinking D.59.
or damage.

Pe.33. Remove the jet well plugs of the carburettor A.P.1464/
and flush out the wells.
C.15.

Oil System. (Ol.31/33.)

Ol.31. Inspect the superflexit feed and return pipes
from the tank to the engine for kinking or
damage.

Ol.32. See that all pipes are secure and test the A.P.1490,
metal connections with an approved spanner. Vol. I,
fig. 4.

Ol.33. Examine the oil gauge and thermometer lines
for security and damage.

Cylinders. (Cy.31/32.)

Cy.31. Inspect the push rod return springs for fracture.

Cy.32. Check the compression of each cylinder.

Airscrew. (As.31.)

As.31. Check the airscrew for track.

Controls. (Cn.31.)

Cn.31. Inspect the controls for wear and for excessive play in the connecting rods, and check the settings of the throttle and mixture control levers.

Doping and Starting. (St.31.)

St.31. Uncouple the pipe connections and check the

flow of fuel from the priming pump ; then
check the pipe line for leaks.

Note.—On the starboard lower engine
mounting strut, remove the cowl panel for
access to the pump connections.

General. (Ge.31.)

Ge.31. Check the engine bolts at the cone mounting
for security.

21

INSPECTION EVERY 40

Group.

HOURS. (40 I.E.)

Ref.

Ignition. (Ig.61.)

Ig.61. Lubricate the magnetos. (B.T.H. S.G.7–1.)

Fuel System. (Pe.61.)

Pe.61. See that the fuel pipes are adequately sup- A.P.1490,
ported against
vibration with packing between Vol. I,
the clips and the pipes. Also see that they fig. 3.
are not touching any parts of the aeroplane
in a manner likely to cause wear.

Oil System. (Ol.61.)

Ol.61. Drain the oil from the system, flush out the A.P.1490, tank and pipe lines and refill with fresh oil. Vol. I,

Note.—The tank should be drained when fig. 4.
the oil is hot.

A.P.1464/
C.20.

Cylinders. (Cy.61/63.)

Cy.61. Lubricate the steel thrust pads in the rocker sockets and the corresponding ends of the tappet rods.

Cy.62. Lubricate the rocker arm bearings.

Cy.63. See that the holding down nuts of the rocker arm brackets are tight.

Airscrew. (As.61/62.)

As.61. Inspect the splines in the hub and on the airscrew shaft for signs of wear. A.P.1490, Vol. I, para. 91.

As.62. Inspect the front and rear hub centring cones on the airscrew shaft, and the hollow flanged plug in the end of the shaft.

INSPECTION EVERY 120 HOURS. (120 I.E.)

Ignition. (Ig.101.)

Ig.101. Check the L.T. leads for continuity and serviceability.

APPENDIX K

22

Group.
Ref.

Fuel System. (Pe.101.)

Pe.101. Drain the fuel tank, and if necessary clean the A.P.1490, interior.

Vol. I, *Note.*—The tank should be removed. para. 86.

Oil System. (Ol.101.)

Ol.101. Calibrate the transmitting thermometer. A.P.1275/

D.2.

(24230) Wt. 27671/1294 375 2/35 Hw.

512

G.371

APPENDIX K

AIR PUBLICATION 1490 (VOLUME II), PART 2

Maintenance Amendment List 1 June 1936

Maintenance Amendment

List 2 May 1938

513

APPENDIX K

AIR MINISTRY

FOR OFFICIAL USE ONLY

Amendment List No. 1
to
AIR PUBLICATION 1490

MAINTENANCE SCHEDULE No. 42.—ROTA WITH CIVET I ENGINE

(1) Page 3. Para. 7, lines 10–15. *Delete* "The Air Ministry" to end of paragraph and *substitute* :—

"The procedure for the co-ordination of aeroplane maintenance and maintenance schedules is laid down in A.M.O. A.232/35."

(2) Page 6. *Add* at end of clause Pl.1. :—" and see that the eyelet drain holes are free from any obstruction ".

Add ref. " A.P. 1490/P.2 ".

(3) Page 10. Clause Pl.29. *Delete ref.* and *substitute*

" A.P. 1490, Vol. I, fig. 9 ".

(4) Page 10. Clause Uc.32. *Add ref.* " A.P. 1490, Vol. I, para. 71 ".

(5) Page 12. Clause Fu.34. *Delete ref.* and *substitute* " A.P. 1275/B.9 ".

(6) Page 12. Clause Ta.32. *Add ref.* " A.P. 1490, Vol. I, para. 77 ".

(7) Page 17. **Airscrew.** *Delete* " **(As.1)** " and *substitute*

" **(As.1/2)** ".

(8) Page 17.

Delete clause As.1 and *substitute* :—

" As.1. Test the airscrew for tightness of the K.R. & boss on the shaft.

A.C.I., *Note*.—For these tests the airscrew must para. be gripped above the red band. After 715 (4). initial attachment the airscrew should be examined for tightness at the end of each of the first two or three

flights.

As.2. Examine the airscrew for damage and A.P. ' deep scratches and the blade sheets for 1464/ signs of fracture in the region of the D.17. identification marks ".

(9) Page 17. Clause Ge.2, *ref.* *Delete* "A.P. 129, para.167 "
and *substitute* " A.P. 1464/G.24 ".

(10) Page 18. **Fuel System.** *Delete* " **(Pe.21/23)** " and
substitute " **(Pe.21/22)** ".

514

APPENDIX K

2

(11) Page 18. *Delete* clause Pe.22.
(12) Page 18. *Renumber* clause Pe.23 as

Pe.22. (13) Page 19.

Ignition. *Delete* **" (Ig.31/35) "** and *substitute* **" (Ig.31/34) ".**

(14) Page 19. Clause Ig.31. *Delete ref.* and *substitute* " A.P. 1464/B.47 ".

(15) Page 19. *Delete* clause Ig.34 and *substitute* :—

" Ig.34. Inspect the H.T. and L.T. ignition A.P.
cables for serviceability ".
1464/
C.27.

(16) Page 19. *Delete* clause Ig.35.

(17) Page 20. Clause Pe.32. *Delete ref.* and *substitute* " A.P. 1464/D.84 ".

(18) Page 20. *Delete* clause As.31 and *substitute* :—

" As.31. Remove the spinner nose cap and A.P.
examine the front side of the blade sheet
1464/ within the boss blocks for signs of
fracture". D.17.

(19) Page 21. **Airscrew.** *Delete* " **(As.61/62)** " and *substitute*

" **(As.61)** ".

(20) Page 21. *Delete* clauses As.61 and As.62 and *substitute* :

" As.61. Remove the airscrew from the hub A.P.
and the spinner from the airscrew and 1464/
examine for signs of fracture both sides
D17. and both edges of the blade sheet in the region normally covered by the spinner ".

(21) Page 21. **Ignition.** *Delete* " **(Ig.101)** " and *substitute* " **(Ig.101/102)** ".

(22) Page 21. *Delete* clause Ig.101 and *substitute* :—

" Ig.101. Check the gap between the brush
and segments of the distributor and see that the vent holes are clear.
Ig.102. Check the L.T. leads for continuity ". A.P.

1464/
C.27.

(23) Page 22. **Fuel System.** *Delete* "**(Pe.101)**" and

substitute "**(Pe.101/102)**".

(24) Page 22. After clause Pe.101 *insert* new clause :—

"Pe.102. Examine the flexible pipe between A.P. the fuel filter and the carburettor for date 1464/ of manufacture and replace, if necessary". D.84.

(25) Page 22. Clause Ol.101. *Delete ref.* and *substitute*

"A.P. 1275/D.6".

(26) Page 22. After clause Ol.101 *insert* new assembly group :—

"**Airscrew (As.101).**

As.101. Dismantle the airscrew, clean the A.P. parts and examine for defects". 1464/

D.17.

(32427) Wt. 14102/432 450 7/36 Hw G.371

FOR OFFICIAL USE ONLY

AL 3 1-4

AIR MINISTRY

MAINTENANCE

Amendment List No. 2
to
AIR PUBLICATION 1490
(VOLUME II), PART 2
May, 1938

SCHEDULE No. 42.—ROTA WITH CIVET I ENGINE

---

(27) Cover, lines 11–13. *Delete* " This schedule..... para. 669 ".

(28) Remove

and destroy pages 2 and 3, and attached new pages 2 and 3.

substitute

(29) Page 4. **INSPECTION BETWEEN FLIGHTS,** note,

lines 1 and 2. *Delete* " need not " and *substitute* " are not to ".

(30) Page 6. Clause Pl.6, ref. *Delete* " para. 77 " and *substitute* " para. 35 ".

(31) Page 7. *Delete* clause Ge.4 and *substitute* ;—

" Ge.4. Make the necessary entries and sign A.P. the aeroplane maintenance form ". 1574, paras. 68–101.

(32) Page 15. *Delete* clause Pl.102 and *substitute* ;—

" Pl.102. Dismantle the rotor head and A.P.

inspect for wear and damage, paying par-
1490, ticular attention to the T-piece for
the Vol. I control hinge ".
para.89, A.P. 1490/

D.1. (33) Page 16. **INSPECTION BETWEEN FLIGHTS,** note, lines 1 and 2. *Delete* " need not " and *substitute* " are not to ".

(34) Page 16. Clause 5, ref. After " G.24 " *add* " and G.62 ".

(35) Page 16. Clause Ig.1. *Add* to *ref.* " A.P.1095/J.14 ".

(36) Page 17. Clause Ge.2. *Add* to ref. " and G.62 ".

(37) Page 17. *Delete* clause Ge.5 and *substitute* :—

" Ge.5 Make the necessary entries and sign A.P. the aeroplane maintenance form ".

(38) Page 19. *Delete* clause Ig.31 and *substitute* ;—

" Ig.31. Remove and clean the sparking plugs. Reset the gaps and test ".

(39) Page 19. Clause Ig.32, line 3. After " the points are " *insert* " clean, free from oil and not pitted. The points are to be ". *Add* ref. " A.P. 1374/C.6 ".

(40) Page 21. **Ignition.** *Delete* "**(Ig.61/63)**". "**(Ig.61)**" and *substitute*

(41) Page 21. After clause Ig.61 *insert* new clauses :—

"Ig.62. Lubricate the contact breaker and A.P. cam group. 1374/ D.7.

Ig.63. Clean the central brush of the magneto. See that the holder is clean and that the brush has free movement.

Note.—This is the brush of the hand-starting magneto lead connection".

FOR OFFICIAL USE ONLY

AIR MINISTRY **AIR PUBLICATION 1568**

July 1936

NOTES ON THE HANDLING OF THE ROTA GYROPLANE IN THE AIR AND UPON THE GROUND

These notes should be read in conjunction with A.P. 1490, Vol. I. They are intended to amplify that publication, for the guidance of pilots of the C.30 Autogiro.

The contents are arranged in normal sequence of training.

For ease of reference, certain parts of A.P. 1490, Vol. I, have been included with alterations to suit the context.

Promulgated for the information and guidance of all concerned.

By Command of the Air Council,

DONALD BANKS.

APPENDIX K

CONTENTS

APPENDIX K

1. Checking the Friction Dampers

The "pull-off" of the friction dampers on each blade should be checked as follows:-

Put on the rotor brake and lock the control column. Set the blade to be checked in line with, and directly over, the centre line of the fuselage. Next place a loop of tape round the rotor blade tip across the centre of the

recess where the balance weights are housed. Hook the spring balance to the loop, and move the blade over to the left to the extent of its free movement - an assistant is required to hold one of the other blades steady. Next, pull the blade being checked gently to the right and note the reading on the spring balance. With the blade extended to the right until up against the stop, the operation should be reversed with the tape pulling from the leading edge. The readings may vary slightly; the friction damper should be adjusted until the mean of the two readings is consistent at approximately 12-lb, and then locked. To adjust the friction damper, loosen the lock nut on the top of the damper and adjust by turning the bottom nut to the right to increase the pressure, and to the left to decrease it. When the correct pressure has been obtained, secure the adjustment by means of the lock nut above the adjusting nut. Repeat this process with each blade.

2. Engine Starting

The airscrew swinging drill laid down in A.P.129 (Flying Training Manual, Part I) is to be followed under normal circumstances when starting up the engine. If, however, there is no one available to assist when starting up, the following procedure should be followed:-

(i) Place the Rota tail to wind; wheel chocks are not required.

(ii) Put on the wheel brakes.

(iii) Turn on the fuel cock.

(iv) Switch off all switches.

(v) Turn on the dope cock and pump the primer four times if the engine is cold, twice if slightly warm, and not at all if the engine is hot.

(vi) Turn off the dope cock and screw the primer home.

(vii) Spin the airscrew over with both hands to suck in until it is considered that sufficient mixture has entered the cylinders. Care must be taken to avoid being struck by the airscrew and gloves should be worn to avoid cuts from the trailing edge.

(viii) Switch on the front switches and the left, or outboard, switch in the rear cockpit, set the throttle slightly open.

(ix)

Swing the airscrew with a follow through movement and step clear.

(x) When the engine starts, switch on the remaining switch in the rear cockpit, and adjust the throttle so that the engine "ticks over" at 600 r.p.m.

(xi) Should the engine fail to fire and the cause be considered to be too rich a mixture, turn the switches off, open the throttle and blow out by turning the airscrew backwards. Care must be taken to avoid being struck by the airscrew should it bounce off compression.

APPENDIX K

3. Taxying

Before taxying, place one blade forward, and slightly to the right of the engine. In this position there is less tendency for the blades to soar against the wind. Taxy slowly at all times as rough ground, or excessive speed, will cause bending stresses in the blades greater than those encountered in flight. If the wind is in excess of 20 m.p.h. do not taxy into wind as this will cause the windward blade to soar and strain against its stop. When it is necessary to taxy while the blades are revolving, (e.g. avoiding a landing aircraft) make sure that the rotor brake is fully OFF or the Rota will tend to swing to the right. The wheel brakes, of a necessity being extremely positive in their action, should not be used to stop the Rota running. If it is necessary to employ them in order to prevent running down hill, or to avoid an obstacle, the brake lever should be worked on and off with a very gentle touch, at the same time moving the tail wheel from side to side. This causes the brakes to have a more gentle action in arresting the aircraft. The control column should always be locked when taxying, whether the rotor is stationary or, for some special reason, revolving slowly. Whenever the control column is locked the fore and aft bins control lever must be set

fully forward to release the strain on the locking mechanism. It is also advisable to keep the right hand resting on the control column, as a twisting movement, caused by travelling over rough ground, may allow the control column to become unfastened and swing back into the pilot's face. In order to preserve clear vision of the taxy path, it is necessary to turn slightly from side to side. Since each wheel can be seen and the wide range of the tail wheel allows of very free turning, it is easy to taxy accurately in close proximity to ground obstacles. This is made the more easy if the pilot unfastens the belt and adopts a half standing attitude; a clear view can then be obtained while still re- taining control of the tail wheel bar.

4. The Take-off - Normal

To take-off in normal wind conditions, the following sequence should be adopted:-

(i) Having taxied into position, move forward slightly until the tail wheel bar is straight and the Rota is facing squarely into wind.

(ii) Apply the wheel brakes fully by pulling up the lever as far as

it will go: a strong pull is required.

(iii) Place the fore and aft bias lever a little forward of the half-way mark.

(iv) Run the engine up to 2,000 r.p.m., testing each magneto at 1,200 r.p.m.

(v) Allow the engine to settle down to 950 r.p.m.

(vi) Take off the rotor brake and pull up the clutch lever very slowly at the same time watching a blade tip. Just before the blade begins to move a click will be heard as the dog clutch comes into mesh. By watching the rotor blades as the clutch lever is pulled up the initial acceleration of the rotor can be made smooth, When rotation becomes too fast to watch, the engagement should contimue notch by notch by a steadily increasing pull on the lever until the clutch is fully home. By keeping the thumb clear of the

ratchet button the engagement of each notch can be heard.

APPENDIX K

(vii) Open the throttle progressively, but very slowly, at the same time observing that the rotor and the engine r.p.m. counters are increasing their reading in sympathy. Should the rotor r.p.m. counter be lagging slightly, force the clutch lever into one more notch on the ratchet. This will overcome the tendency for the clutch to slip. (As the engine is turning eight times to one revolution of the rotor system, marks at sympathetic intervals should be made on

the two r.p.m. counters to facilitate the quick checking of clutch slip). If a swaying or vibration is felt when running up the rotor, it is usually due to the friction dampers being set unevenly. It will tend to smooth out when approaching 120 r.p.m., at which rate the blades should become balanced. If the pulsation does not smooth out the rotor should be stopped and the friction dampers checked over again.

(viii) At 120 rotor r.p.m. unclamp the control column and hold it forward.

(ix)

Continue opening the throttle slowly until the desired rate of rotor r.p.m. is reached (normal wind 185 - 190.)

(x) Operate the quick release, open the throttle fully and, keeping the tail straight, hold the control column forward for about three seconds until the Rota has gathered way (a little right "rudder" is required at the

commencement of the take-off to counteract the tendency to swing to the left). If, on gaining the required rotor revolutions, the quick release does not function, the Rota may be taken off by releasing the clutch and brake levers, in that order.

If this method is adopted, care must be taken that the rotor revolutions are not allowed to die down below the minimum necessary.

(xi) Ease the control column fully back straight and centrally, hold it there until the front wheels rise from the ground.

When the Rota has taken off, the nose will be pointing upwards at a steep angle; the control column should be eased forward slightly to prevent the nose from continuing to rise and to allow the airspeed to increase. The initial climb should be made at 45 to 50 m.p.h. followed by a steady climb at 60 m.p.h. using 2150 engine r.p.m. The fore and aft bias lever should be adjusted to

facilitate this.

(xii) The quick release should be reset after taking off. If this is not done it will be found that the rotor brake and the wheel brakes are not operative after the landing. The control column clamp should be left in the unclamped position when in the air; it can easily be reset immediately after landing.

(xiii) Whenever there is a good run for the take-off, 190 rotor r.p.m. is sufficient for calm conditions. 180 rotor r.p.m. is required for wind strengths of 15 m.p.h. and for every increase of wind strength of 5 m.p.h. the rotor speed may be decreased by 5 r.p.m. It is better to take a longer run for the take-off than to over-accelerate the rotor in strong wind conditions. However strong the wind, the minimum rate should not be less than 165 r.p.m. The Rota

522

APPENDIX K

will take-off readily if the control column is eased back in the early stages of the run. A longer take-off will result if the control column is held too far forward or for too long.

(xiv) To get accustomed to having no rudder it is found to be an advantage to remove the feet from the tail wheel bar when the aircraft leaves the ground.

5.

The Take-off in Strong Wind (exceeding 20 m.p.h.)

(i) When taxying into position for a take-off in strong wind conditions do not face the wind, or the

windward blades will soar. Taxy slowly down, or down and across wind.

(ii) Face the Rota 100° to the left of the wind direction and apply the wheel brakes.

(iii) After testing the engine, engage the clutch and run the rotor up to 120 rotor r.p.m.

(iv) Leaving the control column clamped, disengage the clutch and the wheel brake levers by hand, allow the engine to run at about 1100 r.p.m. and turn to the right into wind.

(v) Put on the wheel brakes and engage the clutch smoothly but fairly quickly.

(vi) Carry on as for a normal take-off but disengage the quick release at about 175 rotor r.p.m.

(vii) To avoid ballooning in a strong wind take-off, the control column should not be eased back quite so far as in a normal take-off, and greater speed is necessary for the initial climb.

(viii) A turn down wind should not be attempted at a low altitude until full speed is reached, as at slow speeds the resultant loss in height is relatively greater in strong wind than in normal wind conditions. This applies in greater measure to a right hand turn than in one to the left.

6. Normal Flying

The Rota handles best at medium speeds, therefore, after taking off, the engine should be throttled down to approximately 2,000 r.p.m. or less. An increase of engine r.p.m. can then be used to assist in turns. It will be found that a variation of engine r.p.m. is necessary for comfortable and easy flight. Also, the fore and aft bias lever should be worked so that the control column is light to move at all times. The lateral bias lever is not very effective; once set it may be left unaltered.

7. High Speed Flying

The Rota will perform all normal manoeuvres at high speed. It is, however, draughty and uncomfortable to fly, the control column being very heavy to move and the aircraft reluctant to alter course. Diving at high speed should not be attempted until thoroughly practised on the type.

8. Turns with Engine

When turning to the left there is a marked tendency for the nose to drop; this must be counteracted by a backward movement of the

APPENDIX K

control column. This may be facilitated by an adjustment of the fore and aft bias lever before, or during, the turn. When turning to the right the nose tends to rise; in holding the control column forward to

counteract this there is a slight tendency for the aircraft to over-bank. This makes it difficult to execute a neat turn when turning down a strong wind. Increased engine power should be used to avoid loss of height when near the ground.

9. The Climbing Turn

The climbing turn is a strong feature of the Rota's perform- ance; it may be carried out equally effectively either to the left or to the right. It is, however, more comfortable to climb to the right, as once the Rota is placed at the correct angle of climb and bank for a right handed climbing turn it tends to remain in that position as long as a little forward speed is maintained.

10. Hovering

The Rota will not hover in still air, but it is possible to remain over the same piece of ground, when facing the wind, by bringing the nose up and increasing the engine r.p.m. as the Rota sinks. The aircraft will lose height, and a distinct lag is noticeable before this movement can be arrested. It is therefore necessary to open up the engine and ease the control column forward and so anticipate this effect. When attempting to hover into wind, forward speed should be gained before turning down wind. Though the Rota is in full control, a marked loss of height will occur, and the time lag in recovering from a slow down wind turn is more noticeable at very slow speeds.

11. Gliding

The Rota is capable of various gliding angles ranging from a semi-stalled descent, approaching the vertical, to a gliding angle of 1 in 7 at 65 m.p.h. Therefore, by employing a method of sinking and gliding alternately, it is possible to make accurate approaches from varying heights without recourse to gliding turns or an application of engine. In order to allow for the time lag when sinking with little forward speed, the air speed should not be allowed to drop below the correct pre-landing speed of 40 m.p.h. when below 150 feet from the ground. When sinking vertically, or nearly so, care must be taken to avoid stopping the engine. There is little forward speed to assist the airscrew in turning, and insufficient air enters the carburet- tor intake, therefore the engine should be set so as to tick over audibly when coming in to land, or when throttling down during a flight. Should the engine stop, the airscrew cannot be restarted by diving from normal heights. Owing to the time lag in recovering from a dive the Rota should not be dived near the ground. When gliding down to land it is best to manoeuvre into a position facing the wind and as nearly over the desired landing point as will allow a view of it.

Then, by easing the control column back, height may be lost in nearly vertical descent. When doing this, the aircraft should be turned slightly from side to side so that clear vision below may be maintained. When sinking with no forward speed the Rota must not be allowed to slide backwards at a low altitude as a stall may result.

12. Stalling

Gentle stalls should be practised at a safe height. To do this, throttle down the engine and slowly ease the control column back, in the fore and aft line, until an angle of approximately 45° is reached and all forward speed is lost; the Rota will begin to slide backwards, the nose will drop and spin round to the right. Control is regained when the Rota has faced about 180° from the original direction. The

loss in height increases with the steepness of the angle of entry into the stall. Stalling from an angle approaching the vertical should not be attempted as the Rota will execute a side loop

with great loss of height and recovery may prove extremely difficult.

The reason that the Rota usually twists righthanded from the stall is thought to be due, firstly to the collapse of torque correction when stalled, and, secondly to the tendency for the fuselage to follow the direction of rotation of the blades. That the Rota should be reluctant to emerge from a steep dive is thought to be due to a change in the centre of pressure on the aerofoil section of the rotor blade, possibly caused by the essential flexibility of this unit. When practising manoeuvres, or operating the various controls of Rota aircraft, manual strength must not be despised; indeed, a marked firmness is necessary in most phases of gyroflight.

13. Landing - Normal

On approaching to land at a normal gliding speed of 40 m.p.h.,
the tail wheel bar must be held in the central position with the feet,
and the Rota must be headed directly into wind, the fore and aft bias
lever should be set back and when at about 10 feet above the ground, the
control column should be eased back slowly and centrally until nearly
all forward speed is lost and the Rota lands

tail wheel first on an even keel. On landing, the control column must be pushed forward centrally so that the lift from the rotor may be reduced and the rotor may spin horizontally. If an immediate take-off is not desired, the control column should be clamped and the Rota turned to the left through an angle of at least 100°. The rotor brake may then be applied as soon as the blades begin to slow their rate of turning. The blades should be finally arrested so that one blade is forward, and slightly to the right, of the engine. This is the normal taxying position.

14. Landing with Engine

If it is desired to land gently without forward speed, the engine r.p.m. must be increased as the nose is brought up until the Rota drops with the tail wheel touching the ground. An application of full engine power is necessary to lower the Rota gently to the ground. With practice, this form of "Power Descent" can be carried out from any height the chief point to remember being to keep some reserve throttle as the ground gets nearer so as to be able to check the rate of descent during the final flattening out. The "Power Descent" is useful when landing in confined spaces or in

close proximity to trees or buildings. As the Rota has no fixed wing, other than the differential tail unit to counteract engine torque, it must be remembered that a sudden increase of engine power will cause the Rota to twist to the right, and a sudden cessation of engine power will cause an equal twist to the left. This may be disconcerting when near the ground, but it is easily obviated by gentle use of the throttle, or counteracted by means of banking in anticipation of the movement. If drift becomes apparent as the Rota is landing, the pilot should not attempt to correct it, but by increasing the attitude of the rotor head the landing can be carried out without any forward speed. Though drifting noticeably, a safe landing can be made in this manner.

15. Landing in Strong Wind

Should the wind strength exceed 25 m.p.h., the point selected for a landing should be up wind of the place where it is desired to park the Rota. It should also be clear of buildings and trees, as these obstacles may create differences in wind strength and direction that may not be apparent until the Rota is about to touch down. To avoid ballooning near the ground the approach should be made with engine,

APPENDIX K

followed by a three point landing with increased forward speed. As soon as possible after landing, the Rota should be turned down wind to the left. After a bad landing, a burst of engine will tend to smooth out any oscillation in the head. In the event of the necessity to land without engine in a strong wind, the landing should be made with sufficient speed to enable the Rota to turn left as soon as it has landed. If there is insufficient way on the Rota to do this, the pilot should jump out after landing and turn the Rota down wind by hand.

16. Landing on Rough Ground

Rough ground should, if possible, be avoided when landing. The wide undercarriage when coming in contact with ground irregulari- ties at the moment of landing may cause a swing to either side which, once commenced, cannot be corrected. To avoid this, a landing on rough ground should be made tail wheel first, and without forward speed.

Landing on the side of a hill, or downhill, should be avoided, but a safe landing can be carried out against a gentle uphill slope.

Hilly ground should not be selected for a landing as, even if the landing presents little difficulty, the ensuing take-off will be impaired.

17. Parking

Bearing in mind the necessity for turning to the left after landing, and the desirability of taxying down wind, a final landing should be made up wind of the chosen parking place. The Rota should be parked facing down wind with the wheel brakes on. If the wind is blowing strongly and the shelter is poor, the rotor brake should be released so that the blades may revolve freely. Before leaving the Rota, the fuel cock and all switches should be turned off and the airscrew turned until the bottom exhaust valve is open. Should it be considered necessary to picket the Rota, it should be lashed to screw pickets from the handles at each side of the tail, and from each front wheel axle. If the Rota is to be left in darkness, a lamp should be placed so as to reveal the rotating blades, otherwise injury may be caused to personnel approaching the aircraft.

18. Slow Flying

Slow flying is useful when making detailed examination of ground features, or when flying in mist, or fog. Until thoroughly practised, slow flying should be carried out only into wind. The method lies in adopting alternately an attitude of stalling and slight forward flight. The nose should be kept well above the horizon and the throttle worked so as to prevent the Rota either sinking or climbing. Controlled turns can be made at very slow speeds, but the engine speed should be increased when turning down wind near the ground. The time lag in the Rota's response to the engine and to the control column should be anticipated when approaching obstacles or when about to make a turn. When flying slowly near the ground a reserve of engine power should be kept in hand so that speed may be picked up without losing height.

19. Load

The performance of the Rota is regulated primarily by its all up weight. Endurance, therefore, should be sacrificed to load. The Rota responds the more readily to the controls when flown as a single seater, and for all flights other than long cross country flights a maximum of 15 gallons of petrol will suffice. When it is necessary to take a passenger on a long flight, fuel quantities must be reduced should the pilot and passenger weigh more than 326 lb. together.

APPENDIX K

The maximum all-up weight is made up as follows:-

Normal loading

Tare weight	1,228 lb.
Fuel (23 galls)	172.5 lb.
Oil (3.3 galls)	33.
Two parachutes	40.
	1,473.5 lb.

Maximum all up weight -

1,800 lb.	
1,473.5	
	326.5

The Rota pilot must therefore know his own weight, the weight of his passenger, and of any luggage or equipment that is to be carried, fuel load being adjusted to ensure against exceeding 1,800 lb. all up weight.

20. Bad Weather

Heavy rain or hail should be avoided, since they rapidly cause damage to the fabric of the leading edges of the blades, in view of the unprotected nature of the blades, and the speed at which they travel. The speed of the tips is in excess of 200 m.p.h. Flight in clouds or in mist, when no view of the ground can be gained, should not be carried out until thoroughly practised on the type. Flying accurately by compass in clouds is difficult; the Rota is reluctant to make small changes in direction and inclines towards a curved rather than a straight path.

21. Trimming the Rota

Looking at the tail from the rear of the Rota, four flaps may be seen at the trailing edge of the tail plane. Reading from left to right these are A1, B1, B2 and A2, the vertical flap at the extremity of the fin being "C". The following is a normal setting for flaps:-

(i) For high speed trimming - A1 down slightly, A2 up slightly. (ii) For torque correction - B1 up slightly, B2 down slightly.

(iii) For slow speed trim - "C" slightly to the right.

(iv) The tail incidence must be set to make the Rota slightly tail heavy when opening the throttle at any speed. If tail heavy, increase incidence and vice versa.

Approximate angle of incidence plus $1\frac{1}{2}^{o}$ to plus 2^{o}.

(v)

Engine torque correction at slow speeds

The incidence of each side should be made equal by adjusting the struts. Fly at 35 to 40 m.p.h. at full throttle and adjust both bias springs to fly "hands off". Throttle back slowly and release control column. The Rota should continue to be well trimmed laterally. If, after throttling

back, there is a tendency to turn right, the engine torque
is over-corrected and the horizontal fin should be adjusted
to decrease incidence on the right, and increase it on the
left side, and vice versa. Fine adjustment is by means of
the torque flaps B1 and B2.

APPENDIX K

(vi) High speed trimming

If there is a tendency to turn right at high speeds
adjust A1 down slightly and A2 up slightly, and vice versa.
This adjustment is fine, and even a slight amount will have
quite a large "rudder action."

(vii) Slow speed trimming

If there is a tendency to turn left at slow speed with engine on, adjust the vertical fin, flap "C", slightly right, and vice versa. Refer back to (v), try this at high speed and adjust B1 and B2 so that the Rota flies level at all speeds, ignoring any slight turn (if there is any). The Rota should tilt slightly to the left after throttling back.

(viii) Centralising control column

All the above adjustments are made without regard to the control column position. When the tail trimming has been corrected to the satisfaction of the pilot, the position of the control column may be corrected. The control column pivots about a hinged fork which is mounted universally on a cross bar bolted across the rear pylon struts. The position of the hinged fork is adjustable laterally along the cross bar, and also in a fore and aft direction by the insertion of shims; these adjustments, of course, alter the flying position of the column.

Elementary theory of the working of the rotor system in flight

The Rota is airborne by rotating wings of conventional aero-foil section; these wings, or blades, are hinged at a common axis so that they may move, within limits, both in the horizontal and in the flapping plane. This articulation overcomes the gyroscopic action associated with a rigidly mounted rotating system. While the lift forces tend to raise the revolving blades, centrifugal force controls them in equilibrium. This position of equilibrium is known as the CONING angle. The rotor system is said to be a stable surface, and gives pendular stability in a vertical descent. When descending vertically, or nearly so, the coning angle of each blade is equally disposed about the hub; when flying forwards the coning angle of the blade approaching the front increases and that of the retreating blade decreases. In effect, this is a flapping movement and is due to the advancing blade having a greater relative speed than the one which is retreating. In this manner the blades automatically adjust themselves to differences in airflow. Were

the blades unable to flap, the Rota would yield to the greater lift upon the left hand side and would tend to roll to the right. As the advancing blade is free to rise as it moves forward, it presents less effective incidence at the greater resultant air speed than the retreating blade, which is descending at greater effective incidence at less resultant speed. This eliminates dissymetry of lift. (Note - The blades do not form a true "cone" excepting in a vertical descent in still air). The rate of rotation of the rotor varies according to load and speed of the aircraft. It will decrease as the forward speed of the rotor drops, and will increase as the speed rises. The rate of rotation may vary throughout the Rota's speed range by as much as 20 per cent. As in a fixed wing aircraft the loading increases with the rate of turn. As the loading increases, so the rotor automatically speeds up, and thus compensates for the increased load. The lift imparted by the rotor system being independent of forward speed, the degree of stability and control remains unchanged. When lightly laden the normal rate of rotation lies between 170 r.p.m. at minimum and 210 r.p.m. at

maximum speed. With full load the rotational speeds shew an increase

528

APPENDIX K

of 10 r.p.m. throughout the range. The rate of rotation is seldom constant during flight. The lift and centrifugal forces, holding the rotor in a state of equilibrium, immediately counteract distur- bance by a proportional increase or decrease in the rate of rotation of the blades. This, combined with the flexibility of the rotor system, has the effect of assisting keel in bumpy weather.

the aircraft to keep an even

APPENDIX K

Part 1 General Orders and Modifications

Part 2 Maintenance Schedule

Part 3 Instructions for Repair

ROTA AEROPLANE

Promulgated for information and guidance and

necessary action.

By Command of the Air Council,

C. L. Bullock

AIR MINISTRY

530

APPENDIX K

FOR OFFICIAL USE ONLY

Air Publication 1490 (Volume II)

January, 1936

INDEX OF LEAFLETS FOR

ROTA

This index contains all relevant leaflets issued during 1935, and should be inserted in place of the manuscript index

previously in use.

Log Book No.	Mod. No.	Leaflet No.	Title.
1	—	P.1	Transmission clutch rotor starter gear—Coupling—Strengthened.
2	179	B.1	Oleo leg—Locking of gland body to outer tube.
3	—	J.1	Sutton harness replaced by safety belt.
—	—	P.2	Rotor blades—Maintenance.
4	—	J.2	Notice stating limit of speed during dive—Removal.
5	—	P.3	Rotor blades—Removal of the cuff.
—	—	B.2	Tail wheel tyre—Inflation.
—	—	B.3	Tail wheel equipment.
6	—	P.4	Airscrews — Duralumin — Location bolts — Elastic stop nuts—Introduction.

Manuscript entries in continuation should not be made on this page, but should commence on a new Form 2095.

(30407)—32 Wt. 33232/2392 250 4.36 Hw. G.371

APPENDIX K

FOR OFFICIAL USE ONLY

Air Publication 1490

(Volume II)

January, 1937

INDEX OF LEAFLETS FOR ROTA

This index contains all relevant leaflets issued during 1936, and should be inserted in place of the manuscript index previously in use.

Log Book No.	Mod. No.	Leaflet No.	Title.

—	—	Z.1	Modification.
—	—	Z.2	Modification.
—	—	P.5	Rotor blades—Flying life limited.
—	—	F.1	Ignition circuit—Master switch in front cockpit—Position.
7	2	P.6	Clutch and rotor brake control quadrants—Improved.

Manuscript entries in continuation should not be made on this page, but should commence on a new Form 2095.

(35647)—84 Wt. 32942/1887 250 3/37

Hw. G.371

APPENDIX K

FOR OFFICIAL USE ONLY

Air Publication 1490 (Volume II) *January*, 1939.

INDEX OF LEAFLETS FOR ROTA

This index contains all relevant leaflets issued during 1938, and should be inserted in place of the manuscript index previously in use.

Log Book No.	Mod. No.	Leaflet No.	Title.
10	15	P.8	Friction dampers, extended—New type.

Manuscript entries in continuation should not be made on this page, but should commence on a new Form 2095.

(3558–25) Wt. 8033/4612 250 4/39 W.C. & S. (Gp. 395)

APPENDIX K

Rota—Oleo Leg—Locking of Gland Body to Outer Tube

LOG BOOK NO. 2. (ALTERATION NO. ROTA/179.)

(Class II.)

(370282/34.—9.3.35.)

1. To provide a definite locking of the oleo gland body, which is screwed in the top end of the outer tube, two 4 B.A. screws are to be fitted on aeroplanes numbers K.4231 to K.4236 inclusive.

2. The following is the sequence of operations, *see* Drg. No. A.P. 1490/B.1/35 :—

(i) Extract the four screws at the top end of the upper oleo leg fairing.

(ii) Slide the top fairing down over the bottom fairing so that the gland nut C and gland body A are fully exposed.

(iii) Drill and tap two holes for the locking screws, Part No. 30K.1366.

(iv) Screw in the locking screw, Part No. 30K.1366, and lock in position with wire, brass (Stores Ref. 30B/325).

(v) Replace the top fairing in position and secure with set screws as before.

3. The undermentioned parts are required and are available at No. 3 Stores Depôt :—

Stores Ref.	*Part No.*
26H/—	30K.1366

24968—12) Wt. 8040/6020 500

534

Nomenclature.	*No. off.*	*Class of Store.*
Screws, locking	4	C

3/35 Hw. (Gp. 377)

APPENDIX K

— TOP —

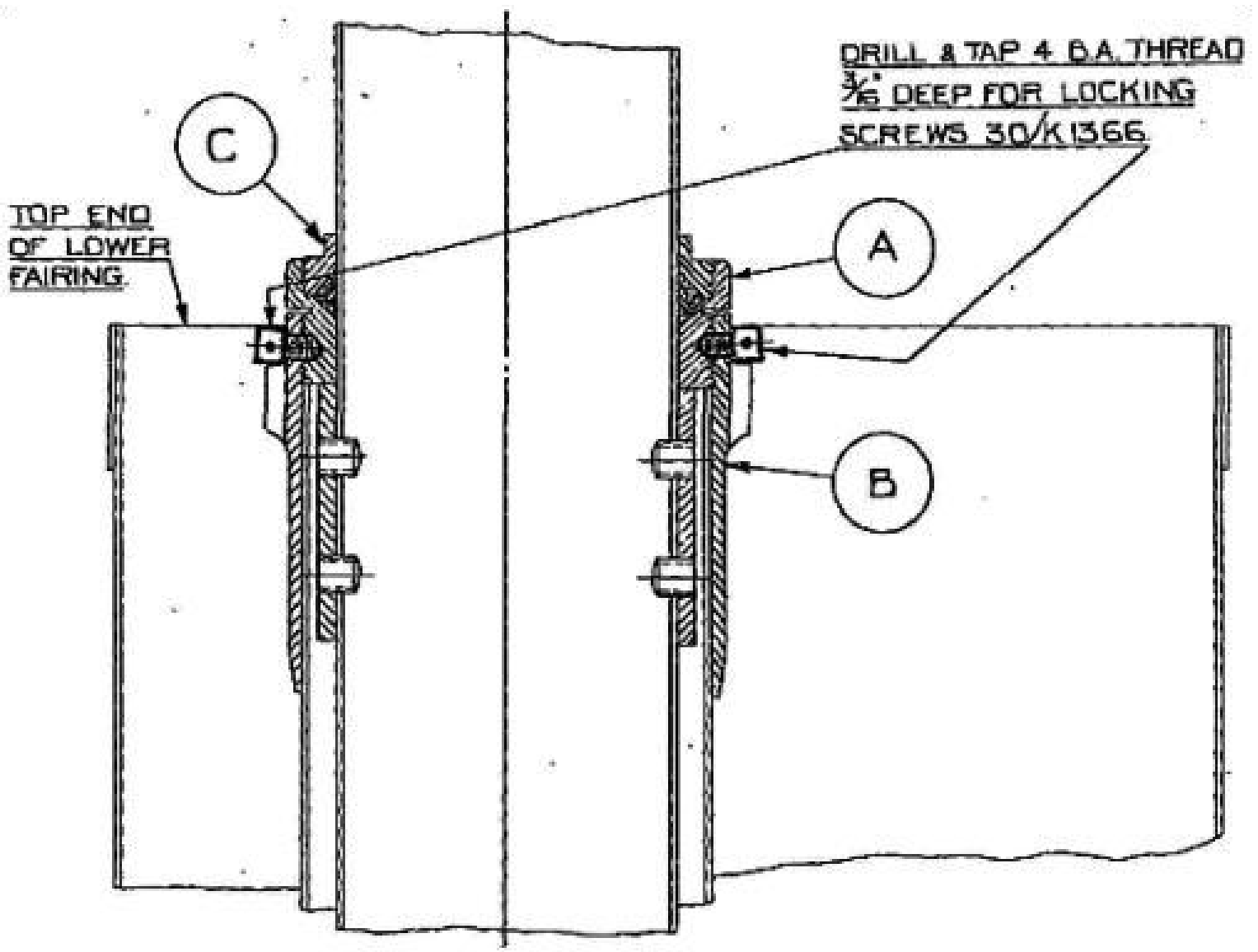

20 G. LOCKING WIRE PASSED

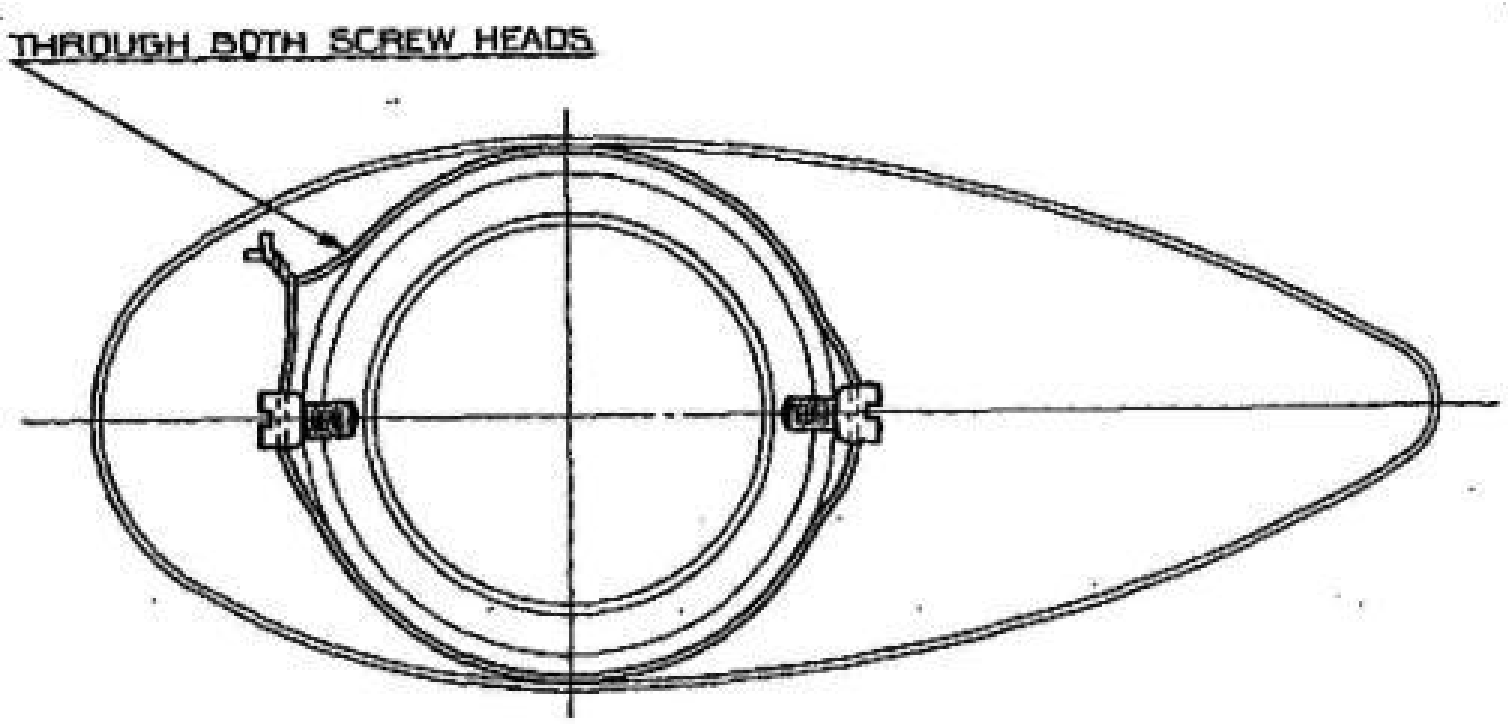

SECTION THRO' LOCKING SCREWS.

DRG. Nº A.P 1490/B.1/35.

APPENDIX K

A.P.

1490/B.2

Rota—Tail Wheel Tyre—Inflation

(442165/35.—26.10.35.)

1. To facilitate inflation of the tail wheel tyre, an extension piece for the tyre inflation valve has been introduced.

2. The extension piece is to be screwed direct on to the tyre valve, after removal of the cap.

3. The undermentioned part is required and is available at No. 3 Stores Depôt :—

Stores Ref.	*Nomenclature.*
	Valves, tyre, aeroplane :—
	Type 5850 :—
27A/1113	Extension piece.

No. off.

2 per flight
or
2 for each four gyroplanes on charge
or
2 per unit if less than four gyroplanes on charge.

(28181—88) Wt. 8104/6022 250 10/35 Hw. .(Gp. 877)

APPENDIX K

A.P. 1490/B.3

Rota—Tail Wheel Equipment

(374863/34.—26.10.35.)

1. When existing stocks of tail wheels and corresponding covers outer and tubes inner are

exhausted, a new type tail wheel equipment will be issued.

2. This equipment will ensure a path to earth of a resistance not exceeding 20,000 ohms, and when fitted will make the use of the earthing chains unnecessary.

3. Details of the new wheels, covers outer and tubes inner, are as follows :—

Stores Ref.	*Nomenclature.*
	Wheels aeroplane :—
	Patt. G :—
27A/1100	Full low pressure, type A.H.O.1249, 4 in. × 3½ in.
27A/1101	Covers outer, 4 in. × 3½ in. (non-insulating).
27A/1102	Tubes inner, 4 in. × 3½ in. ... ...

No. off.	*Class of Store.*
1	B
1	B
1	B.

(28181—92) Wt. 8104/6022 250 10/35 Hw. Gp. 377)

APPENDIX K

A.P. 1490/D.1

Rota—Control Hinges—T Piece—Improved

LOG BOOK NO. 8. (MOD. NO. ROTA/13.)

(Class I.)

(600109/37.—11.3.37.)

1. This modification introduces an improved design of T piece for the control hinge.

2. The following is the sequence of operations :-

(i) Dismantle the rotor head in accordance with the instructions given in Air Publication 1490, vol. I, para. 91, part I to XIII. The outer race of the bearing at the aft end of the pin need not be removed. All needles must be retained.

(ii) Fit the new central distance piece, Part No. 4/J.792 and the new needle race, modified to Part No. 3/J.792, taking care that the

chamfering is on the outside edge. Arrangements for chamfering should be made with the No. 3 Equipment Depôt, quoting Air Ministry letter 303397/34/E.1 dated 13th November, 1936.

(iii) Fit the new T piece, Part No. 2/J.792 and adjust the thickness of the distance washer, Part No. 24/J.610 until the required clearance is obtained between the nut, Part No. 7/J.612 and the hub. Shims may be used if required.

(iv) Fit the nut, Part No. 7/J.612 and lock with split pin, Part No. A.G.S.784/21.

(v) Assemble the rotor head in the reverse manner to which it was dismantled.

3. The undermentioned parts are required and are available at No. 3 Equipment Depôt :—

Stores Ref.	*Part No.*	*Nomenclature.*	*No. off.*	*Class of Store.*
26H/5654	1/J.792	T piece, group ...	...	1
B 28/5045	A.G.S./784/21	Pin, split	... ...	1
C 28/5046	A.G.S./784/22	Pin, split	... ...	1
C				

4. Parts rendered redundant by the incorporation of this modification are to be disposed of in accordance with current authorised procedure.

(36107—39) Wt. 8063/6010 250 3/37 Hw. (Gp. 377)

APPENDIX K

A.P. 1490/F.1

Rota—Ignition Circuit—Master Switch in Front Cockpit—Position

(544872/36.—15.8.36.)

1. The master switch in the front cockpit must be kept permanently in the IN position. This gives control of the ignition from either of the ignition switches, front cockpit or rear cockpit.

2. The system must be treated in these circumstances as the usual dual control arrangement, the pilot operating the switch in whichever cockpit he is occupying, the other switch being normally at ON.

(33125—25) Wt. 8063/6010 250 8/36 Hw. (Gp. 377)

APPENDIX K

Air Publication 1490
(Vol. II)
J.1

Rota—Sutton Harness replaced by Safety Belt

Log Book No. 3.

(370283/34.—9.3.35.)

1. The Sutton harness in aeroplanes numbers K.4231 to K.4236 inclusive is to be replaced by belts, safety, standard type (Stores Ref. 6F/4).

2. The following is the sequence of operations, *see* Drg. No. A.P. 1490/J.1/35.

(i) Remove the Sutton harness, leaving the attachment fittings in position.

(ii) Fit eyebolts complete with rings, Part No. 4.Z.935, through the existing distance tube at joints immediately aft of the front seat.

(iii) Fasten the belt by No. 4 line looped through the rings.

(iv) Fit the clips complete with rings, Part No. 3.Z.935, on the cross member immediately aft of the rear seat at 18 in. centres.

(v) Fasten the belt by No. 4 line passed through the rings and looped round the bracing tubes at top joint of the second bay aft of the rear seat.

(vi) Connect the two lines securing the separate halves of the rear belt by a length of ¼ in. dia. elastic cord (Stores Ref. 32C/50) lashed to each line approximately 12 in. from the point of attachment to the belt. This cord should have a free length of 8 in. Its function is to lift the belt, quick release, catch clear of the brake and clutch control when the belt is not in use.

3. The undermentioned parts are required and

are available at No . 3 Stores Depôt :—

Class Stores Ref.	*Part No.*
26H/—	3.Z.935
26H/—	4.Z.935

(24968—13) Wt. 8040/6020 500 3/35

540

Nomenclature	*No. off.*	*of Store.*
Clip, complete	2	C
Eyebolt, complete ...	2	C

Hw. (Gp. 377)

APPENDIX K

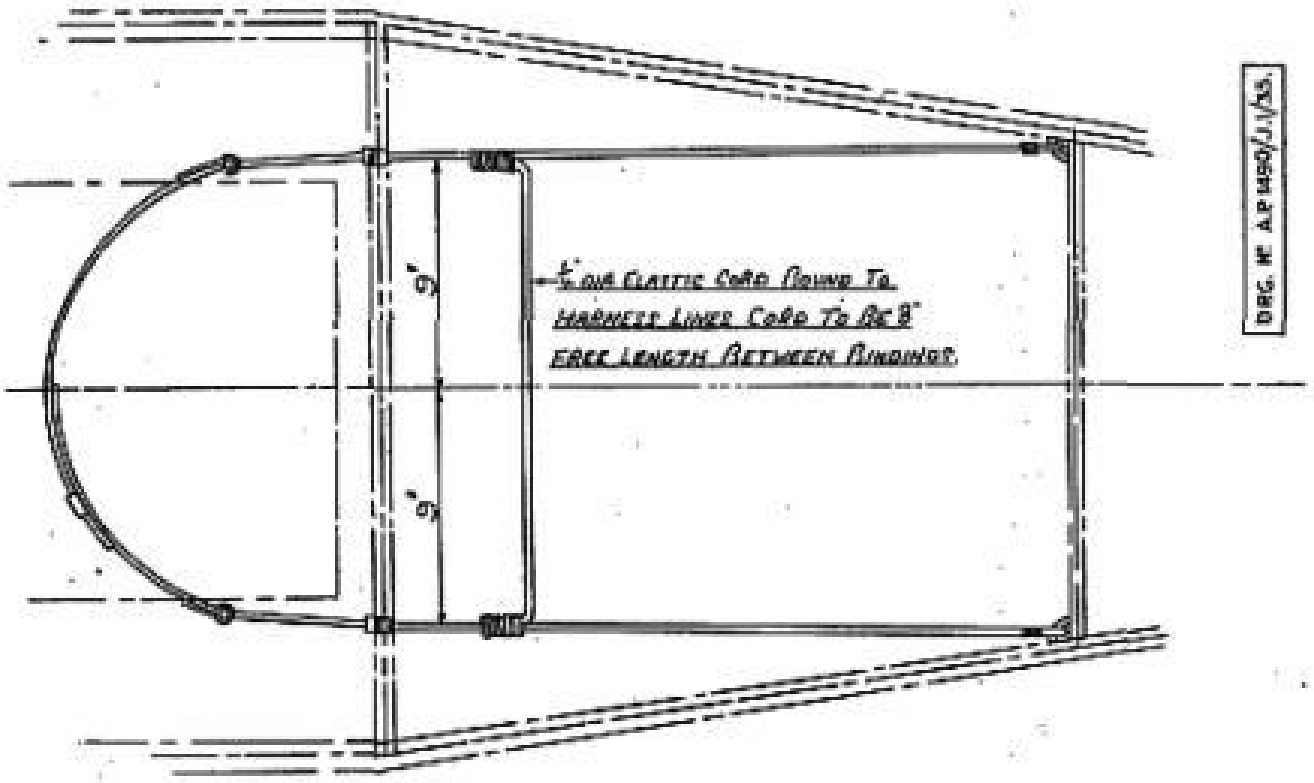

DRG. Nº A.P 1450/J.J/55.

APPENDIX K

A. M. I. D. A.P. 1490/J.2

MEMORANDUM

COPY

Rota—Notice stating limit of Speed during Dive—Removal

Loc. Book No. 4.

(Class II.)

(414963/35.—20.7.35.)

The notice, fitted to the instrument board in the front cockpit, which states that the diving speed is limited to 130 m.p.h., is to be removed.

(28825—78) Wt. 8104/6022 250 7/35

Hw. (Gp. 377)

542

APPENDIX K

Rota—Transmission Clutch Rotor Starter Gear—Coupling—Strengthened

LOG BOOK NO. 1.

(Class II.)

(364696/34.—14.2.35.)

1. The clutch coupling, Part No. 7 T.541, is to be replaced by a stronger coupling, Part No. 8 T.546.

2. The following is the sequence of operations, *see* Drg. No. A.P. 1490/P.1/35 :—

(i) Remove the cowling over the tank.

(ii) Remove the fuel tank by unfastening straps that secure it to top longeron and disconnecting the two feed pipes.

(iii) Remove the guard over the transmission shaft if fitted.

(iv) Remove the Hardy discs.

(v) Remove the taper bolts securing the socket on the clutch shaft and withdraw the socket from the shaft.

(vi) Fit the new socket, opening out the holes to suit the holes in the clutch shaft.

(vii) Refit the taper bolts and secure, using new washer, Part No. A.G.S.160/C, with the hole opened out to $\frac{1}{4}$ in. dia.

(viii) Re-assemble in the reverse order.

3. The undermentioned

Stores Depôt :—

Stores Ref.	*Part No.*
26H/—	8 T.546

part is required and is available at No. 3

Nomenclature.	*No. off.*	*Class of Store.*
Socket for flexible coupling	1	C

(24547—60) Wt.8040/6020 500 2/35 Hw. (Gp. 377)

543 APPENDIX K

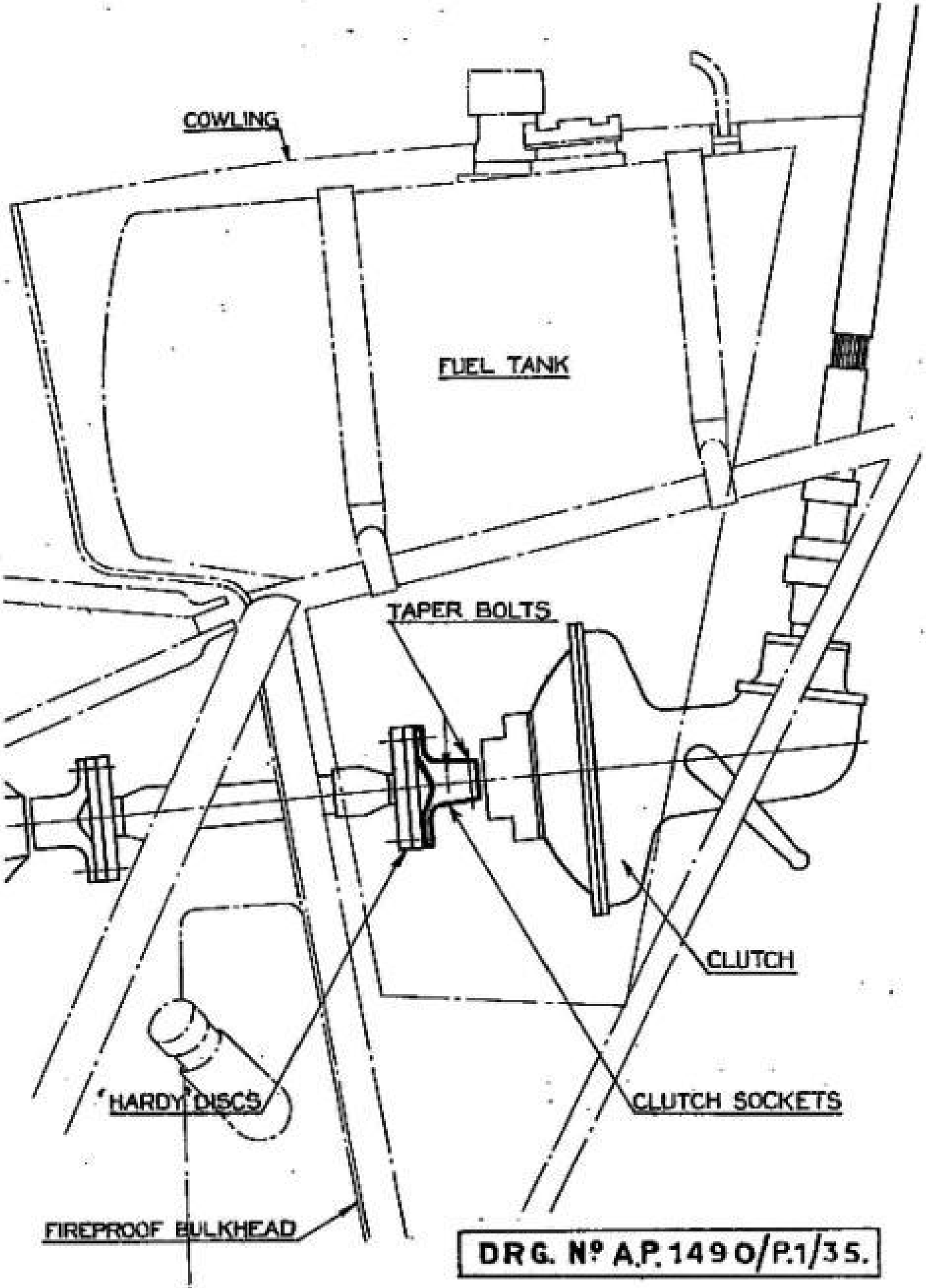

DRG. Nº A.P. 1490/P.1/35.

APPENDIX K

Air Publication 1490
(Vol. II)
P.2

Rota—Rotor-Blades—Maintenance

(411078/35.—31.5.35.)

1. The eyelet drain-holes, near the root and at the tip of the rotor blades, at the trailing edge, are to be kept open and free from any obstruc- tion such as fabric or dope which may be used in repairs.

2. Under the centrifugal force generated by the revolving blades, the pressure of air entrapped in the blade, through the drain-hole at the tip being obstructed, is sufficient to burst open the plywood at the tip and cause serious damage which may render the gyroplane unstable and, in certain circumstances, beyond control.

(25986—147) Wt. 8104/6022 250 5/35 Hw. (Gp. 377)

APPENDIX K

A.P. 1490/P.3

Rota—Rotor blades—Removal of the Cuff

Log Book No. 5.

(Class III.)

(440978/35.—21.9.35.)

1. Failures due to the cuff or fairing-piece at the root of the blades, either splitting or lifting at the junction with the blade itself, have been experienced. As the cuff is of little aerodynamic value, and it is prone to these defects, it is to be removed as follows :—

(i) Slit the cuff open with a chisel, or sharp knife, beginning near the inner end, and cut outwards carefully, until the innermost rib of the blade is encountered. When this has been located, cut the cuff off all round the inner face of this rib.

(ii) Dope a fabric patch over the exposed end of the rib to cover the lightening holes. Care must be taken to see that all three patches for a set of three blades are the same dimensions to maintain correct balance.

(iii) Paint on the blade the maker's number and identification marks as stencilled on the cuff, in order that they may be available for reference at any future date.

(27795—74) Wt. 8104/6022 250 9/35

Hw. (Cp. 377)

APPENDIX K

A.P. 1490/P.4

Rota—Airscrews—Duralumin—Location Bolts—Elastic Stop Nuts—Introduction

Log Book No. 6.

(Class II.)

(395159/35.—23.11.35.)

1.

When the next inspection is made in accordance with A.P. 1464/D.17, para. 7, the existing location bolts, nuts and washers are to be replaced in serviceable airscrews by new bolts, elastic stop nuts and washers. The washers as shown in Drg. No. A.P. 1490/P.4/35 are to be manufactured from Part No. A.G.S.160E.

2. The undermentioned parts are required and are available at No. 3 Stores Depôt :—

Stores Ref.	*Part No.*	*Nomenclature.*	*No. off.*	*Class of Store.*
28/136	A.1.G.30	Bolt, steel, mild $\frac{5}{16}$ in. B.S.F. by 3 in.		
26H/—	F.S.90/5 Ref. G.P.	Elastic stop nut		
26H/—	—	Washer, steel (to be manufactured from Part No. A.G.S.160E).		

(28662—61) Wt. 8104/6022 250 11/35 Hw. (Gp. 377)

4 C

4 C

8 C

APPENDIX K

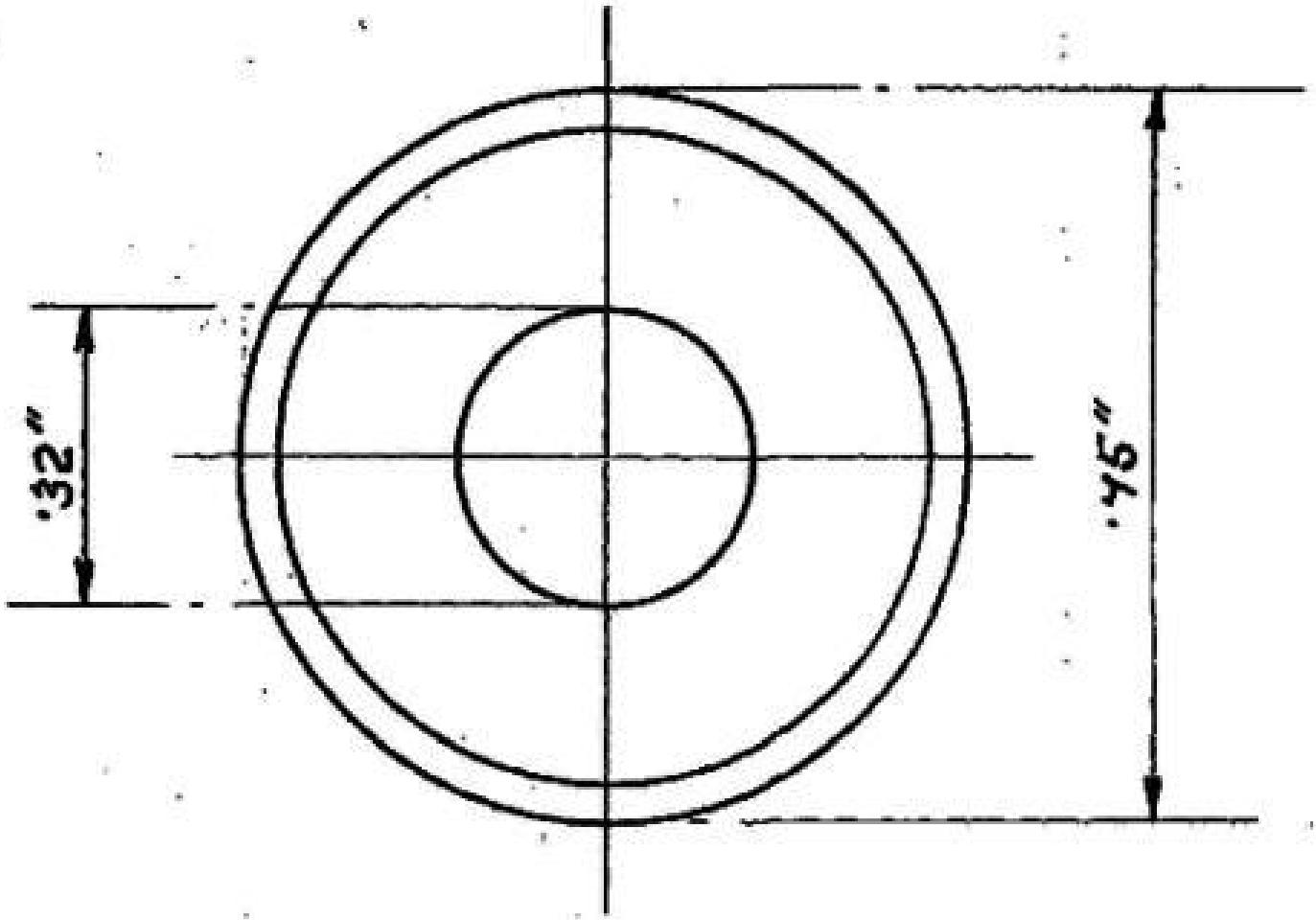

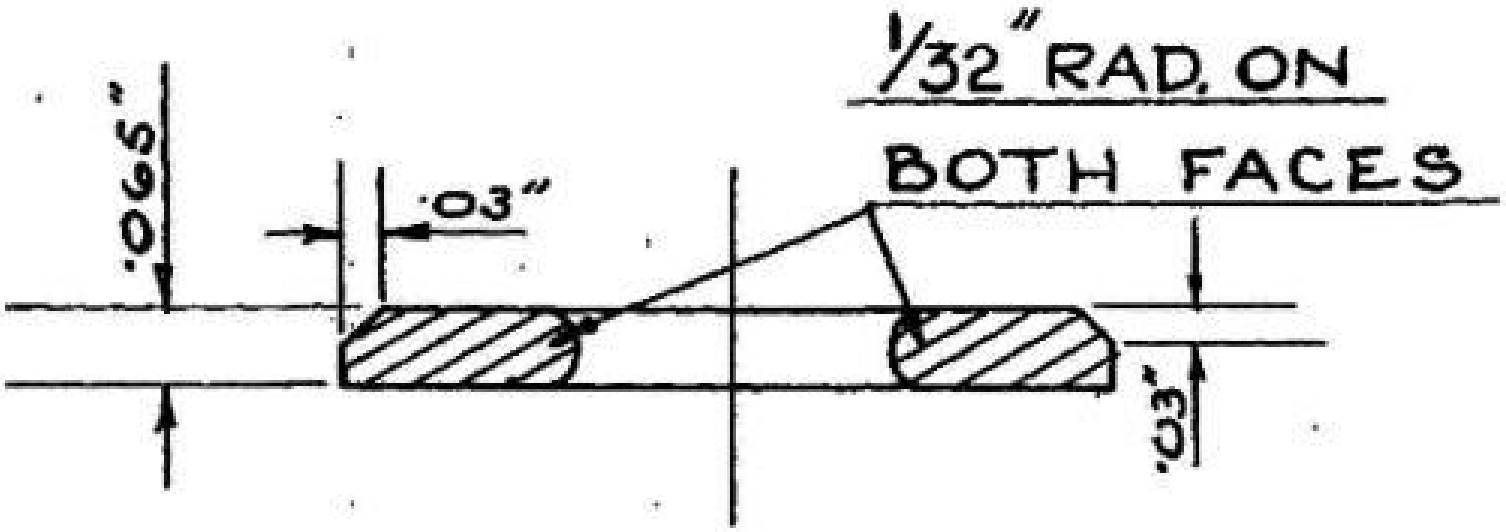

MADE FROM A.G.S.160.E

548

DRG. Nº A.P. 1490/P.4/35.

APPENDIX K

A.P. 1490/P.5

Rota—Rotor Blades—Flying Life Limited

(526255/36.—26.6.36.)

1. The flying life of each rotor blade is to be limited to 75 hours in all, and on completion of this period the blade is to be surveyed locally and reduced to produce.

2. When a blade which has rendered flying service is fitted to a gyro- plane, the number of hours the blade has been flown is to be entered against that particular blade in the chronological section of the log book of the gyroplane to which the blade is fitted.

3. It is necessary, therefore, when both serviceable and repairable blades are dismantled from gyroplanes, that a durable label recording the flying hours already rendered be prepared and securely attached to each blade. This label is to remain with the blade until the flying hours entered on it are recorded, on fitment of the blade to a gyroplane, in the appropriate log book.

4. Spare blades, or sets of blades, issued by No. 3 Stores Depôt are to be labelled to show the flying hours already rendered by the blades. A "Nil" label is to be attached where appropriate.

5. If a unit is doubtful as to the flying hours rendered by any blade, or blades, the matter is to be reported for investigation to the Secretary, Air Ministry.

(32164—105) Wt. 8063/6010 250 6/36 Hw. (Gp. 377)

APPENDIX K

A.P.

1490/P.6

Rota—Clutch and Rotor Brake Control Quadrants—Improved

Log Book No. 7. (Mod. No. Rota/2.)

(Class V.)

(512733/36.—5.11.36.)

1. To improve the wearing properties of the packing plates attached to the inner quadrants of the clutch and rotor brake control unit, new packing plates in high tensile steel, B.S. specification S.2 are to be fitted. These plates are to be riveted to the existing quadrants, Part No. 7.T.530 and 8.T.530, replacing the present packing plates, Part No. 7D and 8D/T.530.

2. The following is the sequence of operations :—

(i) Remove the inspection door situated on the port side of the gyroplane, adjacent to the left hand side of the rear seat, which gives access to the clutch, rotor and wheel brake control unit, by detaching the hinges. Open the fabric covering, *see* Drg. No. A.P. 1490/P.6/36, sheet 1. Remove the wooden former situated immediately below the inspection door by detaching it from the body fairing and the bottom longeron.

(ii) Remove the three mounting bolts on the fuselage frame, Part No. A1/E.18, A1/E.18 and A1/E.16, the anchorage bolt, Part No. A1/E.12 and 2 B.A. steadying bolt, Part No. A1/C.12, on the locker.

(iii) Detach the quick release rod at the top end, by removing the $\frac{1}{16}$ in. split pin, Part No. 3 A.G.S.784 and the $\frac{7}{32}$ in. dia. solid pin, Part No.

C5/SP4, securing it to the lever, Part No. 4.T.566.

(iv) Detach the clutch and the rotor brake control cables by the following method :—

Remove the cable guard plates, Part No. 22.T.530, which are attached to the inner quadrants by 4 B.A. bolts. Release the tension in the cables by slackening off the cable stops. Release the cable nipples from their sockets on the inner quadrants, thus freeing the cables.

(v) Detach the wheel brake control cable by the following method :—

Release the tension in the cable by slackening off the cable stop, mounted on the underside of the control unit. Remove the two inspection covers situated on the underside of the fuselage, immediately below the front seat. This gives access to the forward connection of the brake cable, and the linkage can be disconnected by removing a $\frac{1}{16}$ in. split pin, Part No. 3.A.G.S.784, and a $\frac{3}{16}$ in. dia. solid pin, Part No. B.11/SP4. The cable being freed will permit the control unit to be moved bodily forward, thus making it possible to release the cable from the wheel brake lever by removing the $\frac{1}{16}$ in. split pin, Part No. 3.A.G.S.784, and $\frac{1}{4}$ in. dia. solid pin, Part No. D6/SP4 securing the link.

(vi) Remove the control unit bodily from the gyroplane.

(vii) Remove the sliding pin, Part No. 22.T.556,

to which the quick release device, quadrants, springs, distance tubes and ratchets are attached. Remove the two $\frac{1}{2}$ in. dia. mounting bolts, Part No. A1/E.50, and the two 2 B.A. guiding bolts, Part No. A1/C6, and bushes, Part No. 12.T.530. The inner quadrants are now free.

.2

(viii) Embody the modification to the inner quadrant as follows :—

(*a*) Remove by filing the weld securing the packing plate to quadrant, *see* Drg. No. A.P. 1490/P.6/36, sheet 2.

(*b*) Remove the packing plate with a small chisel.

(*c*) Dress the quadrant, file up.

(*d*) Position the modified packing plate. File the packing

plate to suit the profile of the quadrant. Using the packing plate as a template locate the rivet holes on the quadrant. Drill the quadrant, morse No. 41 to suit $\frac{3}{32}$ in. dia. mild steel rivets, in position as shown in the drawing.

(*e*) Rivet the packing plate in position, using $\frac{3}{32}$ in. dia. mild steel rivets and forming the heads as shown in the drawing.

(ix) Reassemble the control unit.

(x) Check the rotor brake and clutch control lever for alignment and for correct engagement with the modified inner quadrants.

(xi) Fit the control unit in the gyroplane by the following procedure :—

(*a*) Connect up the wheel brake control cable.

(*b*) Connect up the clutch and rotor brake control cables.

(*c*) Replace the cable guards on the quadrants.

(*d*) Install the mounting bolts and secure the control unit in the correct position.

(*e*) Connect up the quick release device.

(xii) Adjust the clutch, rotor and wheel brake control cables by use of the cable stops. Adjust the quick release device.

(xiii) Check the control cable circuits throughout. Check the controls, clutch, rotor and wheel brake, quick release device, for

smooth and correct operation.

(xiv) Refit the wooden former, securing it to the bottom longeron and the body fairing.

(xv) Lace up and repair the fabric covering in an approved manner.

3. The undermentioned parts are required and are available at No. 3 Stores Depôt :—

Stores Ref.	*Part No.*	*Nomenclature.*	*No. off.*	*Class of Store.*
26H/—	65/T.556	Plate, packing ...	1	C
26H/—	67/T.556	Plate, packing ...	1	C

(34271—26) Wt. 8063/6010 250 11/36 Hw. (Gp.377)

APPENDIX K

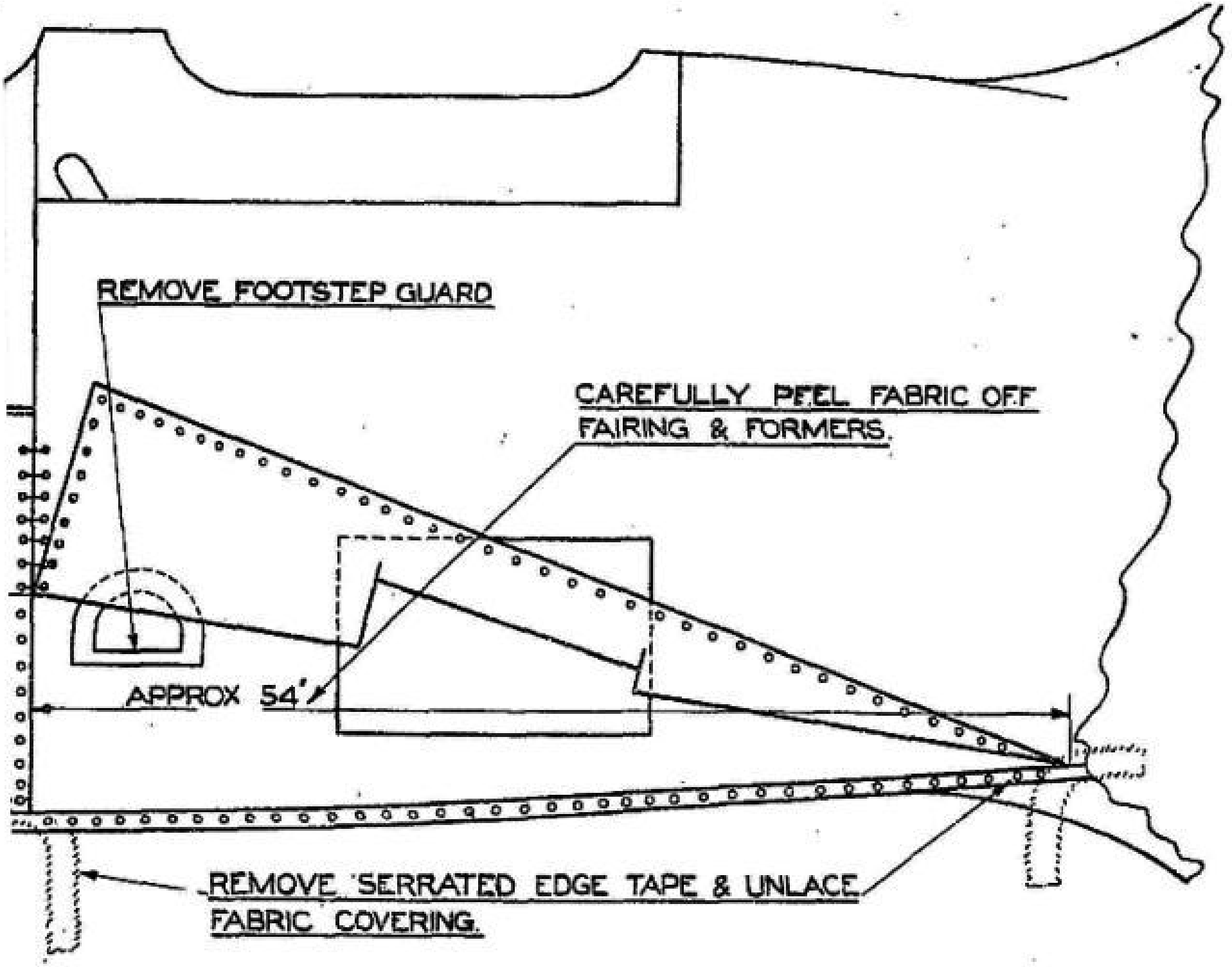
REMOVE FOOTSTEP GUARD
CAREFULLY PEEL FABRIC OFF FAIRING & FORMERS.
APPROX 54"
REMOVE SERRATED EDGE TAPE & UNLACE FABRIC COVERING.

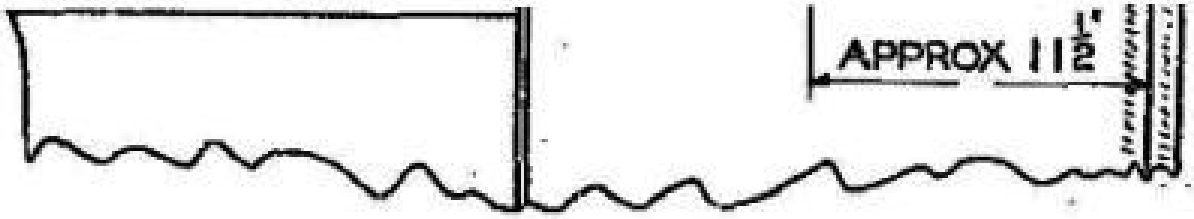

SKETCH SHOWING THE NECESSARY

AMOUNT OF UNLACING TO CARRY OUT MODIFICATION.

(E696) 8063, E50, 11/36, Gp 521/CR R ED

DRG. Nº A.P. 1490./ P.6./36.
SHEET 1

552

APPENDIX K

EXISTING PACKING PLATE & WELD REMOVED IN REGION OF NEW PACKING PLATE.

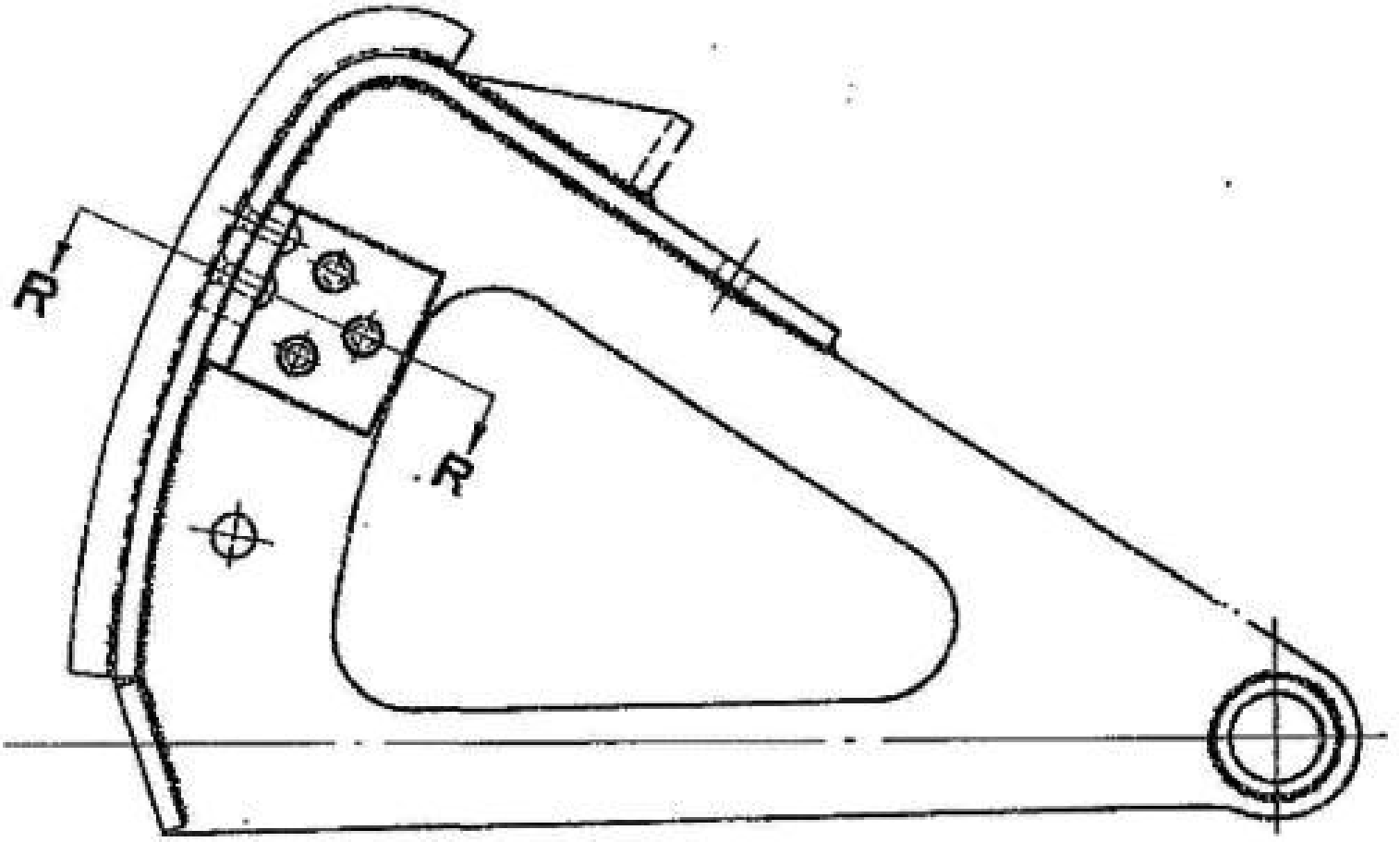

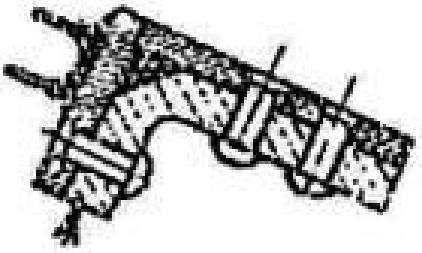

SECTION RR.

FILE TO SUIT PROFILE
OF QUADRANT.

SKETCH SHOWING PACKING

PLATE

65 OR 67/T. 556 RIVETED IN POSITION ON INNER QUADRANT.

DRG. Nº A.P. 1490. / P.6. / 36. SHEET 2.

553

APPENDIX K

A.P. 1490/P.7

Rota—Pawl Springs for Brake Lever and Clutch and Rotor Brake Lever—Strengthened

Log Book No. 9. (Mod. No.

(Class II.)

(585822/36.—26.5.37.)

1. This modification introduces a strengthened type of pawl spring in the brake lever and the clutch and rotor brake lever.

2. The following is the sequence of operations :—

(i) Unscrew the locking piece, Part No. 8T.556, from the push rod,

Part No. 10T.556 in the brake lever and also from Part No. 42T.548

in the clutch and rotor brake lever, at the top of the levers.

(ii) Unscrew the press stud, Part No. 7T.556, from the push rod.

(iii) Remove the spring, Part No. 12T.556.

(iv) Fit new spring, Part No. 69T.556.

(v) Refit press stud and locking piece.

3. The undermentioned parts are required and are available at No. 3 Equipment Depôt :—

Stores Ref.	*Part No.*

Nomenclature.	*No. off.*	*Class of Store.*		
26H/5669	69T.556	Spring	...	...
...	2	B		

4. Parts rendered redundant by the incorporation of this modification are to be disposed of in accordance with current authorised procedure.

(36914—58) Wt. 8035/4506 250 6/37

Hw. (Gp. 377)

APPENDIX K

1

A.P. 1490/P.8

Rota—Friction Dampers, Extended—New Type

Log Book No. 10. (Mod. No. Rota/15.)

(Class II.)

(604212/37.—14.1.38.)

1. This modification introduces new extended friction dampers to relieve the local bending stresses set up by the anchorage of the present type friction dampers.

2. The sequence of operations is as follows :—

(i) Remove the rotor blades and their links by the following procedure :—

(*a*) Cut the locking wire that secures the link stop pin bolt and the greaser bolt, in the horizontal articulation pin.

(*b*) Remove the link stop pin bolts, Part No. A.1/C.4, and the special washers, Part No. 53/J.610.

(*c*) Remove the greaser bolt, Part No. 20/J.610, in the end of the articulation pin, by relieving the tab washer ; also remove the attached washer, Part No. 21/J.610.

(*d*) Knock out the horizontal articulation pin, Part No. 17/J.610, with the special drift that is supplied in the tool kit, and the blades complete with drag links and friction dampers are free.

(*e*) Secure the inner portion of the needle bearings with a piece of soft wire, as it is quite free to fall out and the needles are very troublesome to replace.

(ii) Support the blades on felt-covered benches or trestles and proceed as if to dismantle the friction dampers in the following sequence :—

(*a*) Release the two locking nuts, Part No. 14/J.555, and remove the washer, Part No. A.G.S.160/H.

(*b*) Remove the cap, Part No. 6/J.611, covering the friction dampers.

(*c*) Remove the rubber washer, Part No. 17/J.611.

(*d*) Remove the friction damper plates, Part No. 19/J.1388 and 18/J.1388, also the ferodo discs, Part No. 30/J.611.

(*e*) Remove the spigot, Part No. 3/J.1388, to which is riveted the plate, Part No. 14/J.1388.

(iii) Remove the packing block on the adaptor, Part No. 8/J.1388,

by releasing the split pin, Part No. A.G.S.784/12, slotted nut, Part

No. A.1/J.S., and bolt, Part No. 27/J.1388. These last three items

are to be scrapped.

(iv) Fit new items, bolt, Part No. 41/J.778, saddle washers, Part

No. 42/J.778, nut, Part No. A.1/J.S., and split pin, Part No.

A.G.S.784/3, in the hole which was previously used for securing the

packing block on the adaptor.

(v) Release the plate, Part No. 14/J.1388, from the spigot, Part

No. 3/J.1388, by removing the rivets. The snap heads of the rivets

are to be filed off and the rivets themselves punched out.

(vi) Fit new type base plate, Part No. J.779, to the spigot, Part No. 3/J.1388, in the following manner :—

(*a*) Remove from the spigot any burrs round the rivet holes.

(*b*) Clean and then position new base plate on the spigot as

shown in Drg. A.P. 1490/P.8/38.

APPENDIX K

(*c*) Drill the base plate through rivet holes in the spigot and countersink holes on the top face of the base plate.

(*d*) Remove any burrs on the base plate caused by drilling.

(*e*) Rivet the base plate to the spigot, using $\frac{1}{8}$ in. dia. countersunk head × $\frac{3}{8}$ in. long dural rivets, Part No. A.G.S.259/18, snap heads being formed on spigot bottom face. The countersunk head of the rivet must be flush with the base plate to ensure smooth operation of the dampers.

(vii) Fit to the base plate, inner bracket, Part No. 3/J.778, with bolts, Part No. 11 and 12/J.778, and nuts, Part No. A.1/E.T. The bolts to be riveted over the nuts.

(viii) Fit to the base plate, pressure pad, Part No. 7/J.778, using nuts, Part No. A.1/E.T.

(ix) Fit the block on the spar tube, assemble by the following procedure :—

(*a*) Mark out the position of the holes to be cut in the blade.

(*b*) Carefully cut out the holes with a sharp penknife.

(*c*) Clean the spar locally in the way of the block.

(*d*) Fit the block, Part No. 5/J.788, on the pressure pad, Part No. 7/J.778.

(*e*) Fit the top plate, Part No. 4/J.778, on the block, Part No. 5/J.778, with bolts, Part No. A.1/B.4, and lock the heads with 18 s.w.g. tinned soft iron locking wire.

(x) Fit the base plate complete with spigot and block, on the blade and spindle of the friction damper and proceed to assemble friction damper plates, ferodo discs, rubber washer, cap, washer and locking nuts. The face of the spigot in contact with the friction plates is to be smeared with graphite.

(xi) Position the block, Part No. 5/J.778, centrally about the pressure pad and then fit the bottom cap, Part No. 6/J.778, with bolts, Part No. A.G.S.749/4/G, locking the heads of the bolts with 18 s.w.g. tinned soft iron locking wire. This block and cap must be a tight fit on the spar tube, to prevent rotation during flight.

(xii) Assemble the rotor blades and their links to the rotor hub axle by fitting the horizontal articulation pins, special washers, tab washers, greaser bolts and link stop pin bolts. Lock with 18 s.w.g. tinned soft iron wire.

(xiii) Adjust and check the friction damper by the procedure laid down in Air Publication 1490, Vol. I, Chapter VIII, para. 79 and 80.

(xiv) Dope on serrated edge patches, Part No. 50/J.778, over the holes in the rotor blade.

3. The undermentioned drawing is required :—

Drg. No. J.778, assembly of extended friction damper.

4. The undermentioned parts are required and are available at No. 3 Equipment Depôt :—

Stores Ref.	*Part No.*	*Nomenclature.*	*No. off.*	*Class of Store.*
26H/5668	1/J.779	Base-plate	3	C
26H/5658	5/J.778	Block	3	C
26H/5660	41/J.778	Bolt	3	C
26H/5659	11/J.778	Bolt	6	C
26H/5661	3/J.778	Bracket	3	C
26H/5662	6/J.778	Cap	3	C
26H/5663	7/J.778	Pad	3	C
26H/5664	4/J.778	Plate	3	C
26H/5665	12/J.778	Screw	3	C
26H/5666	42/J.778	Washer	6	C

5. The undermentioned A.G.S. parts are also required :—

Stores Ref.	*Part No.*	*Nomenclature.*	*No. off.*	*Class of Store.*
28/3	A.1/B.4	Bolt	12	C 28/—
A.G.S.749/4/G	Bolt		6	

C					
28/776	A.1/E.T.			Nut, lock	...
28/772	A.1/J.S.			Nut, slotted	...
... 15	C	28/5032		A.G.S.784/3	
... 3	C	28/1670		A.G.S.259/18	
Pin, split	...	...	3	C	
Rivet ...	...	...	36	C	

6. The undermentioned parts are to be made up locally as required :—

Stores Ref.	*Part No.*	*Nomenclature.*	*No. off.*	*Class of Store.*
32B/147	50/J.778			
30A/1038	—			
Patch fabric ...	...		6	C
Wire, locking, 18 s.w.g.			as reqd.	C

7. Parts rendered redundant by the incorporation of the modification are to be disposed of in accordance with current authorised procedure.

(40205—28) Wt. 8035/4506 250 1/38 Hw. (Gp. 377)

APPENDIX K

A.P. 1490/Z.1

Rota—Modification

(471409/35.—21.1.36.)

The following modification has been approved from 1st November, 1935, to 30th November, 1935 :—

Mod No.	*Description.*
Rota/3	Removal of rotor blade cuffs

(29578–50) Wt. 8104/6022 250 1/36 Hw. (Gp. 377)

Extent of application.	*Whether order is being issued.*
B.	Yes.

APPENDIX K

A.P. 1490/Z.2

Rota—Modification

(471409/35.—5.2.36.)

The following modification has been approved from 1st December, 1935, to 31st December, 1935 :—

Mod. No.	*Description.*
Rota/2.	Improved design clutch and rotor brake control quadrants.

(29578—160) Wt. 8104/6022 250 1/36 Hw. (Gp. 377)

Extent of application.	*Whether order is being issued.*
B.	Yes.

APPENDIX K

A.P. 1490/Z.3

Rota—Modification

(471409/35.—30.1.37.)

The following modification has been 1936, to 31st December, 1936 :—

approved from 1st December,

Mod. No.	*Description.*
Rota/13	Introduction of improved T piece for control hinges.

(35120—79) Wt. 8063/6010 250 1/37 Hw. (Gp. 377)

Extent of application.	*Whether order is being issued.*
B	Yes

APPENDIX K

A.P.

1490/Z.4

Rota—Modifications

(471409/35.—9.4.37.)

The following modifications have been approved from 1st February, 1937, to 28th February, 1937.

Mod. No.	*Description.*
Rota/14	Introduction of pawl spring for brake and clutch levers.
Rota/15	Introduction of pawl spring for brake and clutch lever.

(36405—19) Wt. 8035/4506 250 4/37 Hw. (Gp. 377)

Extent of application.	*Whether order is being issued.*
B	Yes
B	Yes

INDEX

INDEX

INDEX

National Aeronautics and
Space Administration

Ames Research Center
Moffett Field, California 94035-1000

Prepared for Mantech Technologies, Inc.
under NASA Contract NNA07BB01C
Subcontract 200703.NNA07BB01C
Task Order 01C-38

ISBN 978-0-615-47845-6